Cadre structurel, déformations et exhumation des Schistes du Santa Marta : accumulation et histoire de déformation d'un terrain caraïbe au nord de la Sierra Nevada de Santa Marta

Alejandro Piraquive

Communauté
UNIVERSITÉ Grenoble Alpes

Departamento de Geociencias
Facultad de Ciencias
Sede Bogotá

UNIVERSIDAD NACIONAL DE COLOMBIA

THÈSE

Pour obtenir le grade de

DOCTEUR EN SCIENCES DE LA TERRE DE LA COMMUNAUTE UNIVERSITE GRENOBLE ALPES

préparée dans le cadre d'une cotutelle *entre la Communauté Université Grenoble Alpes* et l'Universidad Nacional de Colombia

Spécialité : **Doctorat TUE/Sciences de la Terre el Univers, Environnement**

Arrêté ministériel : le 6 janvier 2005 - 7 août 2006
Présentée par

« Alejandro PIRAQUIVE »

Thèse dirigée par **« Matthias BERNET »**
codirigée par **« Andreas KAMMER »**
préparée au sein des **Laboratoires ISTerre et Departament des Geosciences**
dans **les Écoles Doctorales de l'Université Grenoble Alpes et Universidad Nacional de Colombia**

CADRE STRUCTUREL, DÉFORMATIONS ET EXHUMATION DES SCHISTES DU SANTA MARTA: ACCUMULATION, ET HISTOIRE DE DÉFORMATION D'UN TERRAIN CARAÏBE AU NORD DE LA SIERRA NEVADA DE SANTA MARTA

Thèse soutenue publiquement le **« 20 de Fevrier de 2017»**, devant le jury composé de :

M, Etienne, JAILLARD
DR1, IRD ISTerre, Université de Grenoble, France (Président)
M, Brian, HORTON
Prof., University of Texas, USA (Rapporteur)
M, Richard, SPIKINGS
Dr., Université de Genève, Suisse (Rapporteur)
M, Cesar, VINASCO
Prof., Universidad Nacional de Colombia, Medellín, Colombie (Rapporteur)
M, Matthias, BERNET
Dr., ISTerre, Université de Grenoble, France (Co-Directeur de thèse)
M, Andreas, KAMMER
Prof., UNAL, Bogotá, Colombie (Co-Directeur de thèse)

Cadre structurel, déformations et exhumation des Schistes du Santa Marta: accumulation, et histoire de déformation d'un terrain Caraïbe au nord de la Sierra Nevada de Santa Marta

Marco estructural deformaciones y exhumación de los Esquistos de Santa Marta : la acreción e historia de deformación de un terreno Caribeño al norte de la Sierra Nevada de Santa Marta

Alejandro Piraquive Bermúdez

Universidad Nacional de Colombia
Facultad de Ciencias, Departamento de Geociencias
Bogotá, Colombia

Año 2016

Marco estructural deformaciones y exhumación de los Esquistos de Santa Marta : la acreción e historia de deformación de un terreno Caribeño al norte de la Sierra Nevada de Santa Marta

Structural Framework, deformation and exhumation of the Santa Marta Schists: accretion and deformational history of a Caribbean Terrane at the north of the Sierra Nevada de Santa Marta

Alejandro Piraquive Bermúdez

Tesis presentada como requisito parcial para optar al titulo Ph. D.
Doctor en Geociencias

Director:
Profesor Andreas Kammer
Co-director:
Profesor Matthias Bernet

Línea de Investigación:
Geología estructural, Tectonica y Geodinámica
Grupo de Investigación:
Grupo de Geología Estructural y Fracturas

Universidad Nacional de Colombia
Facultad de Ciencias, Departamento de Geociencias
Bogotá, Colombia
2017

Cadre structurel, déformations et exhumation des Schistes du Santa Marta: accumulation, et histoire de déformation d'un terrain Caraïbe au nord de la Sierra Nevada de Santa Marta

Structural Framework, deformation and exhumation of the Santa Marta Schists: accretion and deformational history of a Caribbean Terrane at the north of the Sierra Nevada de Santa Marta

Thèse

Présentée par
Alejandro Piraquive Bermúdez
pour l'obtention du grade de

Docteur ès Sciences
de l'Université Grenoble Alpes

Encadrant :
Professeur Matthias Bernet
Co-encadrant :
Professeur Andreas Kammer

Géologie structurale, Tectonique et Geodynamique
Equipé de Recherche :
Tectonique, reliefs et bassins (TRB)

Université Grenoble Alpes
Ecole Doctorale, ISTERRE
Grenoble, France
2017

To see a world in a grain of sand and a heaven in a wild flower, hold infinity in the palm of your hand and eternity in an hour.

William Blake

Je laisse Sisyphe au bas de la montagne ! On retrouve toujours son fardeau. Mais Sisyphe enseigne la fidélité supérieure qui nie les dieux et soulève les rochers. Lui aussi juge que tout est bien. Cet univers désormais sans maître ne lui paraît ni stérile ni futile. Chacun des grains de cette pierre, chaque éclat minéral de cette montagne pleine de nuit, à lui seul, forme un monde. La lutte elle-même vers les sommets suffit à remplir un coeur d'homme. Il faut imaginer Sisyphe heureux.

Le Mythe du Sisyphe
Albert Camus

Thesis Abstract

The Sierra Nevada de Santa Marta (SNSM) is perhaps the most complex crustal massif in the Northern Andes. Its unique situation as an isolated triangular massif segmented from the continuity of the 7000 km long Andes as the last standing mountain before the domains of the younger Caribbean plate, places the SNSM as an island separated from all surrounding mountain ranges of the continental margin. A prominent relief characterizes this mountain reaching the highest altitude in the entire Caribbean realm at 5750 m, and defines, the SNSM as the highest coastal mountain range in the world. For this reason, the SNSM is a unique geological feature that embraces an outstanding biodiversity from its coral reefs in the Caribbean Sea passing through heavily vegetated tropical rainforests, high cloud forests, and moorlands, until its magnificent summit capped by glaciers. Such an extraordinary place is inhabited by humans since at least 6000 years ago. These people are: the Arhuaco, Wiwa, Kogi and Kankuamo had called the Sierra Nevada de Santa Marta, as "The Heart" of the World: *Gonawindúa, "This ancestral name refers in the ancient inhabitants cosmogony to the most important peak in the Sierra Nevada de Santa Marta, which in the moment that the spiritual world transcended into the material world was the first element that emerged for remind us of our tasks, is the subsistence of everything, Gonawindúa is where our sense of responsibility, our physical and material sense, intelligence, wisdom and strength are codified and kept*."

Beyond its historical and mystic background, the SNSM hides an equally fascinating geological history as well. One of the most interesting topics to address when studying the evolution of this massif resides in the correlations between the Northern Andes, Central American and Mexican blocks because the SNSM not only possesses a complex geometry, but a prolific assembly of igneous and metamorphic rocks with ages that range from the Mesoproterozoic to the Eocene, and collateral sediments and volcanoclastic deposits from Devonian to Miocene times. By its position on the northwestern margin of South America the study of the SNSM provides the opportunity to resolve important questions on the evolution of super-continental cycles since Grenvillian times through the Neoproterozoic Pan-African orogeny, the late Paleozoic Ouachitan-Appalachian orogeny that led to Pangæa assembly, and Triassic Pangæa break-up followed by the Jurassic Central Atlantic Rift and more recently by the start of the Caribbean plate accretion/subduction since the Late Cretaceous against northwestern South America, which was one of the most important factors operating during the Andean orogeny. In the SNSM, rocks from all the previously described Wilson cycles are preserved. During these vast periods, the

SNSM massif occupied the outboard position in an accretionary margin of NW Gondwana and in this position accumulated remnants of the collisional and orogenic episodes, which are preserved as low to high metamorphic grade crustal slivers, separated by sutures.

Figure 1. Satellite imagery from the Northern Andes of Colombia, the center of the image focuses on the traingular massif of the Sierra Nevada de Santa Marta. The gray box indicates the studied area. Taken from http://server.arcgisonline.com/arcgis/rest/services/ESRI_Imagery_World_2D/MapServer.

Pioneer expeditions shed light on the geology of the Sierra Nevada de Santa Marta. The classic work of Gansser, 1955, advanced in a first reconnaissance of the rocks that integrate the massif and produced a first geological map accompanied by petrological and structural observations. About 20 years later MacDonald et al., 1971; Macdonald and Hurley, 1969; Tschanz et al., 1974, 1969 updated a first full inventory of the geology of the Sierra Nevada de Santa Marta, even performing radiometric K/Ar dating

that permitted for the first time to investigate thermal processes that affected the rocks. Recently several studies have attempted to reconstruct the geological history of this massif, relying on the foundations provided by Tschanz et al., 1969, these works had outlined the palaeogeographic implications of the SNSM through different epochs and gradually augmented the resolution on mapping, geochemistry and isotopic geology (Bayona et al., 2010; Cardona et al., 2010b, 2010c, 2011, 2011a; Cordani et al., 2005; Doolan, 1970; Duque, 2009; Ordóñez et al., 2002; Restrepo-Pace et al., 1997; Villagómez et al., 2011b; Zuluaga and Stowell, 2012), however, most of the SNSM remains unknown for geologists.

In this investigation I attempt to unravel the geological history of the Sierra Nevada de Santa Marta Massif using the most advanced geochronological, thermochronological geochemical and isotopic techniques that allowed gathering a significant amount of new data to add to the existent database on the SNSM. Although given the intrinsically complex geologic history these analyses were only conducted after several months of fieldwork, in which a detailed geological and metamorphic map was constructed and sample collection was performed following the procedures and techniques in modern structural geology (Fossen, 2010; Ramsay and Huber, 1987).

Our results include a reevaluated geological map 1:25000, in which I define 4 new stratigraphic units, accompanied by two crustal-scale cross sections of 320 km length that dissect the massif, and 8 parallel cross sections at the NW corner of the SNSM metamorphic belt. The geochemical and isotopic dataset includes: i) 17 igneous and metamorphic rocks and 6 detrital samples dated by laser-ablation induced-coupled-plasma mass-spectrometry (LA-ICP-MS), U-Pb zircon geochronology that resulted in 2790 new dates and in-situ trace element analyses, ii) 16 igneous and metamorphic rocks that yielded 31 new thermochronometric ages as follows: 12 zircon fission track ages, 11 Apatite fission track ages and 7 (U-Th)/He in apatite ages, iii) Whole rock geochemistry from 10 samples and iv) Microprobe mineral chemistry in spot analyses and x-ray maps from 4 samples that yielded zoned and peritectic garnet. These data were acquired from the units of the northwestern metamorphic suite of the SNSM massif. With these data we investigated i) The units that conform the SNSM metamorphic belts, their chronological and stratigraphic relationships from the Precambrian to the Eocene; ii) The time span and P-T conditions of a late Paleozoic-early Mezosoic metamorphic event (Chapter 1), iii) The timing of igneous activity accretion and exhumation of oceanic and continental terranes during the Late Cretaceous to late Miocene. iv) A mechanism for explaining how this exhumation occurred under a collisional regime by a climate influenced process at elevated erosion and thermal gradients (Chapter 2); v) The late processes of denudation and sedimentation controlled by tectonics in two marginal basins since the early Miocene under decreased erosion rates and thermal gradients (Chapter 3).

Chapter 1. Convergence between Laurentia and Gondwana eventually led to collision and formation of Pangæa during the late Paleozoic. This long lasting plate interaction generated HT-HP rocks, which characterize a large part of the northwest portion of the Sierra Nevada de Santa Marta Massif (SNSM) in the Northern Andes of Colombia, where a tilted metamorphic lower crustal section is preserved. Field and petrological observations coupled with zircon U-Pb LA-ICP-MS geochronologic data from 17 new samples of igneous and metamorphic rocks together with whole rock and trace element geochemistry are used for reconstructing the tectonic evolution of this strongly remobilized crustal section juxtaposed onto low-grade metamorphic sequences during the late Paleozoic. The metamorphic evolution was investigated by means of several geothermobarometers (Grt+Bt, Hbl+Grt, Hbl+Pl+Qtz, GASP and Ti-in-Zr) for obtaining reliable estimates on *P-T* conditions during at least two metamorphic phases identified by their mineral paragenesis. Our results provide new constraints for palaeogeographic reconstructions between Laurentia and Gondwana during middle Permian to Early Jurassic times. This reconstruction is defined by the interaction of the NW margin of Gondwana with Central American and Mexican terranes during Pangæa amalgamation. An evolutionary scenario for this supercontinental cycle is proposed in several phases defined by arc inception, timing of metamorphism, and late exhumation of lower crustal segments. The closure of the Rheic Ocean (ca. 290 Ma) marks the start of interaction of crustal blocks during Pangæa assembly that caused 1) post-collisional anatectic melts at ca. 278±0.5 Ma and maximum crustal thickening, 2) Barrovian type metamorphism peak *P-T* conditions (13 kb, 840ºC) at ≈ 254 Ma followed by 3) slab retreat and delamination, 4) orogenic collapse, 5) thermal weakening, crustal extension and underplating of mafic crust that caused *LP-HT* metamorphism (5.6 kb, 550ºC) at ≈ 225 Ma marking a rifting phase. These processes were accompanied by the infilling of a back-arc basin that accumulated at least 2000 m of carbonate and volcanoclastic sediments provided by the surrounding basement highs. By ~216 Ma most of the conjugated margin was removed by drifting, but remnants of this Permian arc are still preserved in Oaxaquia and Acatlán complexes and the Maya block. The crustal attenuation responsible for rifting and drift contributed to an eventual isostatic rebound of the subducted Pacific slab that reactivated arc activity during the Jurassic. By this time, the arc migrated into a continent-ward position, and the former back-arc basin

turned into a fore-arc depocenter accumulating at least an additional burden of ≈ 5000 m of volcanoclastic deposits. Our new reconstruction defines an age span of 60 Myr from the Alleghenides collision to Pangæa break-up at this portion of the Northern Andes.

Chapter 2. New low-temperature thermochronological data from the Precambrian, Permian-to Jurassic, Late Cretaceous and Paleocene-Eocene rocks that make up the northern metamorphic belt of the Sierra Nevada de Santa Marta (SNSM) of the Northern Andes of Colombia reveal exhumation trends in this part of the continental margin during Paleocene to Miocene times. Our analysis involves apatite and zircon fission tracks, as well as apatite (U-Th)/He dating, which allowed to constrain the thermal histories (~240 ºC – ~60ºC) of an inverted crustal sequence that exposes greenschist to granulite facies metamorphic rocks. Temperature-time paths evidence that cooling occurred diachronously in the massif through the activation of NW verging thrusts with the onset of rapid erosional exhumation after collision and TTG series pluton emplacement under an initially high geothermal gradient of 40ºC/km. In this regime, the massif exhumed at elevated rates ~0.9 km/Myr during 50-45 Ma. These rates incremented to 2 km/Myr for the interval 45-40 Ma with a decreasing geothermal gradient of 30ºC/km, reaching the highest rates of 2.7 km/Myr during 37-35 Myr. We interpret the exhumation of this inverted lower crustal sequence because of coupling of ductile extrusion of a thickened continental crust and surface denudation. Post-Eocene exhumation events show subsequent cooling under a decreased exhumation rates of ~0.2 km/Myr at ca. 25 Ma, related to the start of a composite transpressive-transtensive regime in the southern Caribbean plate boundary as a result of changes in convergence between the Caribbean and South American plates. This reorganization led to the activation of the NW trending Santa Marta - Bucaramanga (SMBF) and E-W trending Oca (OF) faults. These faults contributed to the partitioning of a subsequent oblique convergence and transferred strain from the Caribbean Plate into the Santander Massif, the Eastern Cordillera of Colombia, the Perijá Range, and the Merida Andes until the late Miocene. We interpret that this new tectonic regime inhibited further NW thrust propagation and caused a NE tilting of the SNSM massif due to extensional activity of the SMBF coupled with the tectonic drag caused by the transit of the Caribbean plate These processes resulted in attenuated exhumation rates of ~0.09 km/Myr that persisted until the late Miocene during the SNSM thermal re-equilibration.

Chapter 3. Geo-thermochronologic data from sedimentary rocks, coupled with

stratigraphic analyses, unravel an early Neogene exhumation of the Sierra Nevada de Santa Marta massif (SNSM). This fault-bounded triangular block in the northern Andes of Colombia, exposes Precambrian to Paleozoic metamorphic rocks and suites of a Triassic-Jurassic magmatic arc. We compare the Neogene basin fills of two marginal basins, a western one located along the Santa Marta-Bucaramanga fault (SMBF) and the northern one occupying the southern margin of the Oca fault. The western sequence consists of gravitational conglomeratic deposits ≈ 1200 m that define a progradational Gilbert-type delta emanating from a scarp coinciding with the SMBF. By its stratigraphic and structural position this sequence compares to the northern transgressive sequence. Provenance analyses of representative sections of these two sequences, evidence a sourcing from the underlying basement. This finding is in concordance with zircon U-Pb age spectra that lack pre-Grenvillian and Ordovician signals of coeval sediments of the Magdalena basin, demonstrating, that they were deposited in a local basins disconnected to the trunk system of the proto-Magdalena river. In order to reconcile the different organization of the two marginal basins we propose a regional-scale tilting of the SNSM towards the northeast during the early Neogene. This model takes account of the coeval progradational sedimentary cycle at the fault-bounded western flank and the transgressive onlapping of the northern conglomerates on a tilted surface during an overall exhumation of the massif.

Bayona, G., Jiménez, G., Silva, C., Cardona, A., Montes, C., Roncancio, J., Cordani, U., 2010. Paleomagnetic data and K–Ar ages from Mesozoic units of the Santa Marta massif: A preliminary interpretation for block rotation and translations. J. South Am. Earth Sci. 29, 817–831. doi:10.1016/j.jsames.2009.10.005

Cardona, A., Valencia, V., Bayona, G., Duque, J., Ducea, M., Gehrels, G., Jaramillo, C., Montes, C., Ojeda, G., Ruiz, J., 2011. Early-subduction-related orogeny in the northern Andes: Turonian to Eocene magmatic and provenance record in the Santa Marta Massif and Rancheria Basin, northern Colombia. Terra Nova 23, 26–34. doi:10.1111/j.1365-3121.2010.00979.x

Cardona, A., Valencia, V., Bustamante, C., García-Casco, A., Ojeda, G., Ruiz, J., Saldarriaga, M., Weber, M., 2010a. Tectonomagmatic setting and provenance of the Santa Marta Schists, northern Colombia: Insights on the growth and approach of Cretaceous Caribbean oceanic terranes to the South American continent. J. South Am. Earth Sci., Sierra Nevada de Santa Marta and Adjacent Basins 29, 784–804. doi:10.1016/j.jsames.2009.08.012

Cardona, A., Valencia, V., Garzón, A., Montes, C., Ojeda, G., Ruiz, J., Weber, M., 2010b. Permian to Triassic I to S-type magmatic switch in the northeast Sierra Nevada de Santa Marta and adjacent regions, Colombian Caribbean: Tectonic setting and implications within Pangæa paleogeography. J. South Am. Earth Sci., Sierra Nevada de Santa Marta and Adjacent Basins 29, 772–783. doi:10.1016/j.jsames.2009.12.005

Cardona, A., Valencia, V., Weber, M., Duque, J., Montes, C., Ojeda, G., Reiners, P., Domanik, K., Nicolescu, S., Villagómez, D., 2011a. Transient Cenozoic tectonic stages in the southern margin of the Caribbean plate: U-Th/He thermochronological constraints from Eocene plutonic rocks in the Santa Marta massif and Serranía de Jarara, northern Colombia. Geol. Acta 9, 445–469. doi:10.1344/105.000001739

Cordani, U.G., Cardona, A., Jimenez, D.M., Liu, D., Nutman, A.P., 2005. Geochronology of Proterozoic basement inliers in the Colombian Andes: tectonic history of remnants of a fragmented Grenville belt. Geol. Soc. Lond. Spec. Publ. 246, 329–346. doi:10.1144/GSL.SP.2005.246.01.13

Doolan, B., 1970. Structure and metamorphism of the Santa Marta Area Colombia, South America [microform] / [WWW Document]. URL

https://www.researchgate.net/publication/34351494_Structure_and_metamorphism_of_the_Santa_Marta_Area_Colombia_South_America_microform (accessed 7.20.16).

Duque, T., 2009. Geocronología (U/Pb y 40Ar/39Ar) y geoquímica de los intrusivos paleógenos de la Sierra Nevada de Santa Marta y sus relaciones con la tectónica del Caribe y el arco magmático circun-caribeñ.

Fossen, H., 2010. Structural Geology. Cambridge University Press.

Gansser, A., 1955. Contribución a la geología y petrografía de la Sierra Nevada de Santa Marta (Colombia, Suramérica). Traducido de Gansser, A., 1955. Ein Beitrag zur Geologie und Petrographie der Sierra Nevada de Santa Marta (Kolumbien, Sudamerika):

MacDonald, W.D., Doolan, B.L., Cordani, U.G., 1971. Cretaceous-Early Tertiary Metamorphic K-Ar Age Values from the South Caribbean. Geol. Soc. Am. Bull. 82, 1381–1388. doi:10.1130/0016-7606(1971)82[1381:CTMKAV]2.0.CO;2

Macdonald, W.D., Hurley, P.M., 1969. Precambrian Gneisses from Northern Colombia, South America. Geol. Soc. Am. Bull. 80, 1867. doi:10.1130/0016-7606(1969)80[1867:PGFNCS]2.0.CO;2

Ordóñez, O., Pimentel, M., Moraes, R., 2002. GRANULITAS DE LOS MANGOS, UN FRAGMENTO GRENVILLIANO EN LA PARTE ORIENTAL DE LA SIERRA NEVADA DE SANTA MARTA. Rev. Acad. Colomb. Cienc. Exactas Físicas Nat. 0370-3908 26, 169–179.

Ramsay, J.G., Huber, M.I., 1987. The Techniques of Modern Structural Geology. Academic Press.

Restrepo-Pace, P., Ruiz, J., Gehrels, G., Cosca, M., 1997. Geochronology and Nd isotopic data of Grenville-age rocks in the Colombian Andes: new constraints for Late Proterozoic-Early Paleozoic paleocontinental reconstructions of the Americas. Earth Planet. Sci. Lett. 427–441. doi:10.1016/S0012-821X(97)00091-5

Tschanz, C., Jimeno, A., Cruz, J., 1969. Geology of the Sierra Nevada de Santa Marta area, Colombia. Informe interno 1829. INGEOMINAS Bogotá Prelim. Rep. 288pLinks.

Tschanz, C., Marvin, R.F., B, J.C., Mehnert, H.H., Cebula, G.T., 1974. Geologic Evolution of the Sierra Nevada de Santa Marta, Northeastern Colombia. Geol. Soc. Am. Bull. 85, 273–284. doi:10.1130/0016-7606(1974)85<273:GEOTSN>2.0.CO;2

Villagómez, D., Spikings, R., Mora, A., Guzmán, G., Ojeda, G., Cortés, E., van der Lelij, R., 2011. Vertical tectonics at a continental crust-oceanic plateau plate boundary zone: Fission track thermochronology of the Sierra Nevada de Santa Marta, Colombia. Tectonics 30, TC4004. doi:10.1029/2010TC002835

Zuluaga, C., Stowell, H., 2012. Late Cretaceous–Paleocene metamorphic evolution of the Sierra Nevada de Santa Marta: Implications for Caribbean geodynamic evolution. J. South Am. Earth Sci. 34, 1–9. doi:10.1016/j.jsames.2011.10.001

Resumen

La Sierra Nevada de Santa Marta (SNSM) es quizás al macizo cortical más complejo encontrado en los Andes del Norte. Su situación es única pues se trata de un macizo triangular aislado, segmentado de la continuidad de 7000 km de longitud de los Andes como la ultima montaña antes de los dominios de la placa Caribe más joven. Estas circunstancias particulares ubican a la SNSM como una isla separada de todas las cadenas montañosas circundantes del margen continental. Un relieve prominente caracteriza a esta montaña alcanzando la mayor altitud del Caribe a 5750 msnm y define la SNSM como la mayor elevación costera del mundo. Por esta razón es un elemento geológico único que involucra una excepcional biodiversidad desde sus arrecifes de coral en el Mar Caribe pasando a través de selvas tropicales lluviosas, bosques altos de niebla, y páramos, hasta su magnifica cumbre cubierta de nieve. Este lugar extraordinario ha sido habitado por seres humanos desde hace al menos 6000 años, estos pobladores los: Arhuacos, Wiwa, Kogi y Kankuamo han llamado a la Sierra Nevada de Santa Marta, "el corazón" del mundo: *Gonawindúa, "Este nombre ancestral se refiere en su cosmogonía al pico mas importante de la Sierra Nevada de Santa Marta, el cual en el momento que el mundo espiritual trascendió hacia el mundo material fue el primer elemento que emergió para recordarnos de nuestras tareas, es el sostén de todo, Gonawindúa es donde nuestro sentido de responsabilidad , nuestro sentido físico y material, nuestra inteligencia, sabiduría y fuerza son codificadas y mantenidas.*

Mas allá de su trasfondo histórico y místico, la Sierra Nevada de Santa Marta también oculta una historia geológica igualmente fascinante. Uno de los temas mas interesantes a estudiar durante la evolución de este macizo, reside en las correlaciones existentes con los Andes del Norte, y los bloques de Centro América y México, debido a que la SNSM no solo posee una geometría compleja, pero también un prolífico ensamblaje de rocas ígneas y metamórficas con edades que varían desde el Mesoproterozoico hasta el Eoceno, así como series sedimentarias y depósitos volcano-clásticos desde el Devónico hasta el Mioceno Superior. Por su posición en el margen noroccidental de Suramérica el estudio de la SNSM nos da la oportunidad de resolver importantes preguntas acerca de la evolución de los ciclos súper-continentales desde la época del orógeno Grenvillian, a través de la orogenia Neoproterozoica Brasiliana/Pan Africana, la orogenia Ouachita-Appalachia del Paleozoico tardío que culmino con la aglutinación de Pangæa, y la posterior separación de Pangæa seguida por el *rift* Jurásico que marco la apertura del Océano Atlántico central, y mas recientemente durante el Cretácico Superior el inicio de la

interacción de la placa del Caribe y el Noroccidente de Suramérica, el cual fue uno de los factores mas importantes operando durante la orogenia Andina.

En la Sierra Nevada de Santa Marta rocas pertenecientes a todos los ciclos de Wilson descritos previamente se encuentran preservadas. Durante estos vastos periodos de tiempo el macizo de la SNSM ocupo una posición frontal en un margen acrecional del NW de Gondwana y en esta posición acumuló remanentes de episodios orogénicos y colisionales, los cuales se encuentran preservados como, escamas corticales de rocas metamórficas de bajo a alto grado, separadas por suturas.

Expediciones pioneras dieron las primeras observaciones de la geología de la Sierra Nevada de Santa Marta, el trabajo clásico de Gansser, 1955, avanzó en el primer reconocimiento sistemático de las rocas que integran el macizo y produjo el primer mapa geológico acompañado de observaciones petrológicas y estructurales. Cerca de 20 años mas tarde MacDonald et al., 1971, MacDonald and Hurley, 1969; Tschanz et al., 1974, 1969 realizaron una actualización completa de la geología de la Sierra Nevada de Santa Marta, e incluso llevaron a cabo dataciones K/Ar lo cual permitió por primera vez investigar los procesos termales que afectaron a estas rocas. Recientemente varios estudios han intentado realizar una reconstrucción la historia geológica del macizo de la SNSM, apoyándose en las bases cimentadas por Tschanz et al., 1969, estos trabajos han delineado las implicaciones paleogeograficas de la SNSM a través de diferentes épocas y día a día han aumentado la resolución en cartografía, geoquímica y geología isotópica (Bayona et al., 2010; Cardona et al., 2011, 2010b, 2010c, 2011a; Cordani et al., 2005; Doolan, 1970; Duque, 2009; Ordóñez et al., 2002; Restrepo-Pace et al., 1997; Villagómez et al., 2011b; Zuluaga and Stowell, 2012). Sin embargo la mayor parte de la SNSM continua siendo un territorio desconocido para los geólogos y otros visitantes extranjeros, y durante mi experiencia trabajando en el área, no fue posible alcanzar varias locaciones enigmáticas que deberán esperar por futuras exploraciones.

En esta investigación he intentado revelar la historia geológica de la Sierra Nevada de Santa Marta utilizando las técnicas isotópicas, geocronológicas, termocronológicas y geoquímicas mas avanzadas, las cuales permitieron adquirir una cantidad significativa de nuevos datos que hemos añadido a la base de datos existente en la SNSM. Aunque dada la historia geológica intrínsecamente compleja estos análisis fueron conducidos únicamente después de varios meses de trabajo de campo, durante los cuales un nuevo mapa geológico y metamórfico fue construido y la colección de muestras fue realizada siguiendo los procedimientos y técnicas modernas en geología estructural (Fossen, 2010; Ramsay and Huber, 1987).

Nuestros resultados incluyen un mapa geológico reevaluado a escala 1:25000, el cual incluye la definición de cuatro nuevas unidades estratigráficas acompañado por dos secciones estructurales a escala cortical de 320 km de longitud que atraviesan el macizo y 8 secciones seriadas en la esquina NW del cinturón metamórfico de la SNSM. la base de datos geoquímica e isotópica incluye: i) 17 muestras de rocas ígneas y metamórficas y 6 muestras detríticas datadas por geocronología de U-Pb en zircones mediante espectrometría de masa por plasma inducido por ablación con láser (LA-ICP-MS), cuyos resultados suman 2790 edades nuevas y análisis de elementos traza in-situ, ii) 16 rocas ígneas y metamórficas que resultaron en 31 nuevas edades termocronológicas de la siguiente manera: 12 edades de trazas de fisión en zircones, 11 edades de trazas de fisión en apatitos y 7 edades (U-Th)/He en apatitos, iii) Geoquímica de roca total se realizó en 10 muestras y finalmente iv) Análisis de la química mineral en granates zonados y peritécticos en 4 secciones delgadas se realizaron utilizando la microsonda electrónica. Estos datos fueron adquiridos de las unidades de la serie metamórfica del cinturón noroccidental de la SNSM, y de rocas sedimentarias en cuencas adyacentes al macizo. Con estos datos hemos investigado: i) Las unidades que conforman los cinturones metamórficos de la SNSM, y su relaciones cronológicas y estratigráficas desde el Precámbrico hasta el Eoceno, ii) el intervalo de tiempo y condiciones P-T de un evento metamórfico Paleozoico tardío a Mesozoico temprano (Capítulo 1), iii) la temporalidad de actividad ígnea, acreción y exhumación de terrenos oceánicos y continentales durante el Cretácico Tardío hasta el Mioceno Tardío, iv) un mecanismo para explicar como esta exhumación ocurrió durante un régimen colisional debido a procesos influenciados por el clima a elevados gradientes termales y tasas de erosión (Capítulo 2), v) los procesos tardíos de denudación y sedimentación controlados por tectónica en dos cuencas marginales desde el Mioceno Inferior bajo gradientes geotérmicos y tasas de erosión decrecientes (Capítulo 3).

Capítulo 1. La convergencia entre Laurencia y Gondwana eventualmente culminó con la colisión y posterior aglutinación de Pangæa durante el Paleozoico Tardío. Durante la temporalmente extensa interacción de estas placas tectónicas, rocas de alta presión y alta temperatura fueron originadas (HP-HT), dichas rocas caracterizan una gran parte de la porción noroccidental del macizo de la Sierra Nevada de Santa Marta (SNSM) en los Andes del norte de Colombia, donde una sección imbricada de la corteza inferior se encuentra preservada. Observaciones de campo y petrología acopladas junto con geocronología de zircones (LA-ICP-MS) de 17 nuevas muestras de rocas ígneas y metamórficas junto con geoquímica de roca total y mediciones de elementos traza en zircones fueron usadas para reconstruir la evolución tectónica de esta sección cortical fuertemente removilizada, yuxtapuesta

sobre rocas metamórficas de bajo grado durante el Paleozoico Tardío. La evolución metamórfica fue investigada utilizando diferentes termobarómetros (Grt-Bt, Hbl+Grt, Hbl+Pl+Qtz, GAS y Ti-in-Zr) con el fin de obtener estimaciones confiables de las condiciones de P-T durante al menos dos fases metamórficas identificadas por su paragenesis mineral. Nuestros resultados proporcionan nuevos constreñimientos para las reconstrucciones paleogeográficas entre Laurencia y Gondwana durante el Pérmico medio y hasta el Jurásico Temprano. Esta reconstrucción se define por la interacción del margen NW de Gondwana con los terrenos Centro-Americanos y Mexicanos durante la formación de Pangæa. Un escenario evolutivo para este ciclo supercontinental se propone en diferentes fases definidas por el inicio de un arco, el tiempo de metamorfismo, y exhumación tardía de segmentos de la corteza inferior. El cierre del Océano Reico (ca. 290 Ma) marca el inicio de la interacción de los diferentes bloques corticales durante la formación de Pangæa que causó: 1) fundidos anatécticos post-colisionales ca. 278 ± 0.5 Ma acompañados de un máximo engrosamiento cortical, 2) metamorfismo de tipo Barrovian con condiciones *P-T* máximas de (13 kb, 840ºC) en ≈254 Ma seguido por 3) retroceso del segmento de placa subducido y delaminación cortical, 4) colapso orogénico, 5) debilitamiento térmico, extensión cortical y *underplating* de corteza máfica en la base de la corteza continental que causó metamorfismo *LP-HT* en condiciones (5.6 kb, 550ºC) a ≈ 225 Ma marcando el comienzo de una fase de *rift*. Estos procesos fueron acompañados por el relleno de una cuenca sedimentaria de tras-arco que acumuló al menos 2000m de sedimentos calcáreos y volcano-clásticos suministrados por los altos de basamento circundantes. En ~216 Ma la mayor parte del margen conjugado fue removida, pero los remanentes de este arco Pérmico aun se encuentran preservados en los complejos Oaxaca y Acatlán, y en el Bloque Maya. La atenuación cortical responsable del proceso de *rifting* y posterior deriva contribuyo a un eventual rebote isostático del segmento de placa del Pacifico subducido que reinicio la actividad del arco durante el Jurásico. Para esta época el arco migró hacia el interior del continente, y la previa cuenca de tras-arco se redefinió como una depocentro de ante-arco el cual acumuló una carga adicional de ≈ 5000 m de depósitos volcano-clásticos. Nuestra nueva reconstrucción define un rango de tiempo de 60 Ma desde la colisión de los Alleghenides, hasta la separación de Pangæa para este sector de los Andes del norte.

Capítulo 2. Nuevos datos termocronológicos de baja temperatura de rocas del Precámbrico, Pérmico a Jurásico, Cretácico Tardío y Paleoceno-Eoceno las cuales componen el cinturón metamórfico noroccidental de la sierra Nevada de Santa

Marta (SNSM) en los Andes del norte de Colombia revelan las tendencias de exhumación en esta parte del margen continental durante el intervalo Paleoceno-Mioceno. Nuestros análisis involucran trazas de fisión en zircones y apatitos y dataciones (U-Th)/He en apatitos, las cuales permitieron establecer historias termales (~240 ºC – ~60ºC) de una secuencia cortical invertida que expone rocas metamórficas desde facies esquistos verdes hasta granulita. Las trayectorias de temperatura-tiempo evidencian que el enfriamiento ocurrió de manera diacrónica en el macizo a través de la activación de fallas de cabalgamiento con vergencia NW con el inicio de una rápida exhumación erosional posterior a la colisión y el emplazamiento de plutones de la serie TTG bajo un gradiente geotérmico inicialmente alto de 40ºC/km. Bajo este régimen el macizo se exhumo a tasas ~0.9 km/Myr durante 50-45 Ma. Estas tasas se incrementaron a 2 km/Myr para el intervalo 45-40 Ma con un gradiente geotérmico en disminución de 30ºC/km, alcanzando los mayores valores de 2.7 km7Myr entre 37-35 Myr. Interpretamos la exhumación de esta secuencia de corteza inferior invertida como resultado del acoplamiento de la extrusión dúctil de una corteza continental engrosada junto con denudación superficial. Los eventos de exhumación post-Eoceno muestran un enfriamiento posterior y un decrecimiento de las tasas de exhumación hasta valores de ~0.2 km/Myr para ca. 25 Ma, esta variación se relaciona al inicio de un régimen compuesto transpresivo-transtensivo en el límite sur de la placa del Caribe como resultado de cambios en la convergencia entre las placas del Caribe y Sur América. Esta reorganización condujo a la activación de la falla de Santa Marta-Bucaramanga (SMBF) de rumbo NW y de la falla de Oca de rumbo E-W. Estas fallas asumieron la convergencia particionada y transfirieron deformación desde la placa del Caribe hacia el Macizo de Santander, la Cordillera Oriental de Colombia, la Serranía del Perijá, y los Andes de Mérida hasta el Mioceno Tardío. Interpretamos que este nuevo régimen tectónico inhibió la propagación de cabalgamientos convergencia NW y fue la causa de un basculamiento en dirección NE del macizo de la SNSM debido a la actividad extensional de la SMBF en conjunción con el arrastre tectónico producido por la placa del Caribe. Estos procesos resultaron en tasas de exhumación disminuidas de ~0.09 km/Myr que persistieron hasta el Mioceno Tardío durante la re-equilibración termal de la SNSM

Capítulo 3. Datos geo-termocronológicos provenientes de rocas sedimentarias junto con análisis estratigráficos, revelan una exhumación del macizo de la Sierra Nevada de Santa Marta (SNSM) durante el Neógeno temprano. este bloque triangular delimitado por fallas en los Andes del norte de

Colombia, expone rocas metamórficas Precámbricas a Paleozoicas, y restos de un arco magmático Triásico-Jurásico. En este trabajo comparamos el relleno de cuencas Neógenas de dos cuencas marginales, una occidental localizada junto a la falla de Santa Marta-Bucaramanga (SMBF) y una cuenca norte ocupando el margen sur de la falla de Oca.

La secuencia del occidente consiste de depósitos gravitacionales de conglomerados de hasta ≈ 1200 m de espesor que definen un delta tipo Gilbert progradacional emanando de un escarpe que coincide con la SMBF. Debido a su posición estructural y estratigráfica esta secuencia se compara a una secuencia transgresiva en la cuenca norte. Análisis de proveniencia de dos secciones representativas de estas dos secuencias, evidencian una fuente derivada del basamento subyacente. Este hallazgo es concordante con el espectro de edades U-Pb en circones que carece de señales pre-Grenvillianas y Ordovícicas de sedimentos coetáneos de la cuenca del Magdalena, demostrando, que estos sedimentos fueron depositados en cuencas locales desconectadas del eje del sistema fluvial del proto-Magdalena. Con el fin de reconciliar la diferente organización de las dos cuencas marginales proponemos un basculamiento de escala regional de la SNSM hacia el noreste durante el Neógeno temprano. Este modelo considera la contemporaneidad entre un ciclo progradacional en el flanco occidental delimitado por una falla y un traspaso transgresivo de los conglomerados de la cuenca norte en una superficie inclinada durante una exhumación generalizada del macizo.

Bayona, G., Jiménez, G., Silva, C., Cardona, A., Montes, C., Roncancio, J., Cordani, U., 2010. Paleomagnetic data and K–Ar ages from Mesozoic units of the Santa Marta massif: A preliminary interpretation for block rotation and translations. J. South Am. Earth Sci. 29, 817–831. doi:10.1016/j.jsames.2009.10.005

Cardona, A., Valencia, V., Bayona, G., Duque, J., Ducea, M., Gehrels, G., Jaramillo, C., Montes, C., Ojeda, G., Ruiz, J., 2011. Early-subduction-related orogeny in the northern Andes: Turonian to Eocene magmatic and provenance record in the Santa Marta Massif and Rancheria Basin, northern Colombia. Terra Nova 23, 26–34. doi:10.1111/j.1365-3121.2010.00979.x

Cardona, A., Valencia, V., Bustamante, C., García-Casco, A., Ojeda, G., Ruiz, J., Saldarriaga, M., Weber, M., 2010a. Tectonomagmatic setting and provenance of the Santa Marta Schists, northern Colombia: Insights on the growth and approach of Cretaceous Caribbean oceanic terranes to the South American continent. J. South Am. Earth Sci., Sierra Nevada de Santa Marta and Adjacent Basins 29, 784–804. doi:10.1016/j.jsames.2009.08.012

Cardona, A., Valencia, V., Garzón, A., Montes, C., Ojeda, G., Ruiz, J., Weber, M., 2010b. Permian to Triassic I to S-type magmatic switch in the northeast Sierra Nevada de Santa Marta and adjacent regions, Colombian Caribbean: Tectonic setting and implications within Pangæa paleogeography. J. South Am. Earth Sci., Sierra Nevada de Santa Marta and Adjacent Basins 29, 772–783. doi:10.1016/j.jsames.2009.12.005

Cardona, A., Valencia, V., Weber, M., Duque, J., Montes, C., Ojeda, G., Reiners, P., Domanik, K., Nicolescu, S., Villagómez, D., 2011a. Transient Cenozoic tectonic stages in the southern margin of the Caribbean plate: U-Th/He thermochronological constraints from Eocene plutonic rocks in the Santa Marta massif and Serranía de Jarara, northern Colombia. Geol. Acta 9, 445–469. doi:10.1344/105.000001739

Cordani, U.G., Cardona, A., Jimenez, D.M., Liu, D., Nutman, A.P., 2005. Geochronology of Proterozoic basement inliers in the Colombian Andes: tectonic history of remnants of a

fragmented Grenville belt. Geol. Soc. Lond. Spec. Publ. 246, 329–346. doi:10.1144/GSL.SP.2005.246.01.13

Doolan, B., 1970. Structure and metamorphism of the Santa Marta Area Colombia, South America [microform] / [WWW Document]. URL https://www.researchgate.net/publication/34351494_Structure_and_metamorphism_of_the_Santa_Marta_Area_Colombia_South_America_microform (accessed 7.20.16).

Duque, T., 2009. Geocronología (U/Pb y 40Ar/39Ar) y geoquímica de los intrusivos paleógenos de la Sierra Nevada de Santa Marta y sus relaciones con la tectónica del Caribe y el arco magmático circun-caribeñ.

Fossen, H., 2010. Structural Geology. Cambridge University Press.

Gansser, A., 1955. Contribución a la geología y petrografía de la Sierra Nevada de Santa Marta (Colombia, Suramérica). Traducido de Gansser, A., 1955. Ein Beitrag zur Geologie und Petrographie der Sierra Nevada de Santa Marta (Kolumbien, Sudamerika):

MacDonald, W.D., Doolan, B.L., Cordani, U.G., 1971. Cretaceous-Early Tertiary Metamorphic K-Ar Age Values from the South Caribbean. Geol. Soc. Am. Bull. 82, 1381–1388. doi:10.1130/0016-7606(1971)82[1381:CTMKAV]2.0.CO;2

Macdonald, W.D., Hurley, P.M., 1969. Precambrian Gneisses from Northern Colombia, South America. Geol. Soc. Am. Bull. 80, 1867. doi:10.1130/0016-7606(1969)80[1867:PGFNCS]2.0.CO;2

Ordóñez, O., Pimentel, M., Moraes, R., 2002. GRANULITAS DE LOS MANGOS, UN FRAGMENTO GRENVILLIANO EN LA PARTE ORIENTAL DE LA SIERRA NEVADA DE SANTA MARTA. Rev. Acad. Colomb. Cienc. Exactas Físicas Nat. 0370-3908 26, 169–179.

Ramsay, J.G., Huber, M.I., 1987. The Techniques of Modern Structural Geology. Academic Press.

Restrepo-Pace, P., Ruiz, J., Gehrels, G., Cosca, M., 1997. Geochronology and Nd isotopic data of Grenville-age rocks in the Colombian Andes: new constraints for Late Proterozoic-Early Paleozoic paleocontinental reconstructions of the Americas. Earth Planet. Sci. Lett. 427–441. doi:10.1016/S0012-821X(97)00091-5

Tschanz, C., Jimeno, A., Cruz, J., 1969. Geology of the Sierra Nevada de Santa Marta area, Colombia. Informe interno 1829. INGEOMINAS Bogotá Prelim. Rep. 288pLinks.

Tschanz, C., Marvin, R.F., B, J.C., Mehnert, H.H., Cebula, G.T., 1974. Geologic Evolution of the Sierra Nevada de Santa Marta, Northeastern Colombia. Geol. Soc. Am. Bull. 85, 273–284. doi:10.1130/0016-7606(1974)85<273:GEOTSN>2.0.CO;2

Villagómez, D., Spikings, R., Mora, A., Guzmán, G., Ojeda, G., Cortés, E., van der Lelij, R., 2011. Vertical tectonics at a continental crust-oceanic plateau plate boundary zone: Fission track thermochronology of the Sierra Nevada de Santa Marta, Colombia. Tectonics 30, TC4004. doi:10.1029/2010TC002835

Zuluaga, C., Stowell, H., 2012. Late Cretaceous–Paleocene metamorphic evolution of the Sierra Nevada de Santa Marta: Implications for Caribbean geodynamic evolution. J. South Am. Earth Sci. 34, 1–9. doi:10.1016/j.jsames.2011.10.001

Résumé de la thèse

La Sierra Nevada de Santa Marta (SNSM) est peut-être le massif de la croûte terrestre le plus complexe trouvé dans les Andes du Nord. Sa situation unique comme un massif triangulaire isolé séparé de la continuité de 7000 km de long de la chaîne des Andes, et comme le dernier massif avant les domaines de la plaque Caraïbes plus jeune, place la SNSM comme une île séparée de toutes les chaînes de montagnes environnantes de la marge continentale. Un relief important caractérise cette montagne qui atteint l'altitude la plus élevée dans tout le domaine des Caraïbes à 5750 m, et fait de la SNSM la plus grande chaîne de montagnes côtières du monde. Pour cette raison, la SNSM est un objet géologique unique qui comprend une biodiversité exceptionnelle depuis ses récifs coralliens dans la mer des Caraïbes, passant des forêts tropicales humides, aux forêts de nuage d'altitude puis aux bruyères, jusqu'à son magnifique sommet couronné de glaciers. Un tel endroit extraordinaire est habité par les humains depuis 6000 ans. Ces peuples les Arhuaco, Wiwa, Kogi et Kankuamos avaient appelé la Sierra Nevada de Santa Marta, comme "Le Coeur" du Monde: *Gonawindúa, «Ce nom ancestral fait référence dans leur cosmogonie au pic le plus important de la Sierra Nevada de Santa Marta, qui quand le monde spirituel a transcendé le monde matériel, a été le premier élément qui* a *émergé pour nous rappeler nos tâches, qu'il est le pilier de tout, Gonawindúa est le lieu où notre sens de la responsabilité, notre sentiment physique et matériel, notre intelligence, notre sagesse et notre force sont codifiés et conservés.* "

Au-delà du contexte historique et mystique la SNSM cache une histoire géologique également fascinante. L'un des sujets les plus intéressants à aborder au moment de l'étude de l'évolution du ce massif réside dans ses corrélations avec les Andes du Nord, d'Amérique centrale et des blocs Mexicains, puisque la SNSM non seulement possède une géométrie complexe, mais un ensemble prolifique de roches ignées et métamorphiques, dont les âges varient du Mésoprotérozoïque à l'Eocène, comprenant des sédiments et les dépôts volcanoclastiques depuis le Dévonien jusqu'au Miocène. En raison de sa position sur la marge nord-ouest de l'Amérique du Sud, l'étude de la SNSM nous donne l'occasion de résoudre des questions importantes sur l'évolution des cycles continentaux depuis l'époque de l'orogène Grenvillien, en passant par les orogènes Neoprotérozoïque-Pan-Africain, Ouachitan-Appalaches du Paléozoïque tardif, qui ont conduit à l'assemblage de la Pangaea, puis à la fragmentation de la Pangaea, suivie par le Rift au Jurassique de l'Atlantique central, et plus récemment, depuis le Crétacé supérieur, par le début de l'accrétion / subduction de la plaque des Caraïbes contre le nord-ouest de Amérique du Sud, qui a été l'un des moteurs les plus importants de l'orogenèse Andine-Alpine.

Dans la SNSM, des roches de tous les cycles de Wilson décrits précédemment sont conservées. Pendant ces vastes périodes de temps, la SNSM occupait une position externe sur la marge d'accrétion du NW du Gondwana et a donc accumulé des témoins des épisodes collisionnels et orogéniques, qui sont conservés comme écailles crustales de roches métamorphiques de bas à haut grade, séparées par des sutures. Pionier dans les expéditions explorant la géologie de la SNSM, le travail classique de Ganser (1955), effectua la première identification systématique des roches constituant ce massif et produisit la première carte géologique accompagnées d'observations pétrographiques et structurales. Près de 20 ans plus tard, MacDonald et al. (1971), Macdonald et Hurley (1969), Tschanz et al. (1974, 1969) réalisèrent une mise à jour complète de la géologie de la Sierra Nevada de Santa Marta, effectuèrent même des datations radiométriques K/Ar qui permirent pour la première fois d'étudier les processus thermiques qui affectèrent ces roches. Récemment, plusieurs études ont tenté de reconstituer l'histoire géologique du la SNSM, en s'appuyant sur les travaux fondamentaux de Tschanz et al. (1969), et ont exposé les implications paléogéographiques de l'évolution de la SNSM à travers les âges, et jour après jour, ont augmenté la résolution de la cartographie, de la géochimie et de la géologie isotopique (Bayona et al., 2010; Cardona et al., 2011, 2010b, 2010c, 2011a; Cordani et al., 2005; Doolan, 1970; Duke 2009; Ordóñez et al., 2002; Restrepo Pace et al., 1997; Villagomez et al., 2011b; Zuluaga et Stowell, 2012). Cependant, la plus grande partie de la SNSM reste inconnue des géologues et d'autres visiteurs étrangers, et au cours de mon expérience de travail dans la région, je ne pus pas atteindre certaines zones énigmatiques qui attendent de nouvelles recherches.

Dans cette enquête, je tenté de démêler l'histoire géologique de la Sierra Nevada de Santa Marta Massif utilisant les techniques les plus avancées en géochronologie, thermochronologie, géochimie et géochimie isotopique, techniques qui ont permis de recueillir une quantité importante de nouvelles données qui s'ajoutent à la base de données existante sur la SNSM. Mais compte tenu de l'histoire géologique intrinsèquement complexe, ces analyses n'ont été réalisées qu'après plusieurs mois de travail sur le terrain, au cours desquels une carte géologique et métamorphique détaillée a été construite et la collecte des échantillons a été réalisée suivant les procédures et techniques modernes de la géologie structurale (Fossen, 2010; Ramsay et Huber, 1987). Nos résultats comprennent une carte géologique révisée au 1:25 000, comprenant la définition de quatre nouvelles unités stratigraphiques, accompagnée de deux sections crustales de 320 km de long traversant le massif, et 8 coupes sériées de l'angle nord-ouest de le ceinture métamorphique de la SNSM. L'ensemble des données géochimiques et isotopiques comprend: i) 17 échantillons de roches ignées et métamorphiques et six échantillons de roches détritiques datées par U-Pb sur zircon par ablation laser induite par couplage plasma spectrométrie de masse (LA-ICP-MS), qui ont abouti à 2790 nouveaux âges et analyses in-situ d'élément-traces, ii) 16 roches ignées et métamorphiques qui ont donné 31 nouveaux âges thermochronometriques:

12 âges par traces de fission sur zircon, 11 âges par traces de fission sur apatites et 7 âges (U-Th)/He sur apatites, iii) Géochimie de la roche totale de 10 échantillons et finalement iv) analyses à la microsonde sur quatre lames minces de grenats zonées et péritectiques pour analyser leur chimie minérale.

Ces données ont été données acquises sur les unités du complexe métamorphique de la bordure nord-ouest de la SNSM et de roches sédimentaires voisines du massif. Avec ces données, nous avons étudié i) Les unités qui constituent la ceinture métamorphique nord-occidentale de la SNSM, et leurs relations chronologiques et stratigraphiques du Précambrien à l'Eocène; ii) L'intervalle de temps et les conditions P-T de l'événement métamorphique Paléozoïque tardif à Mésozoïque précoce (chapitre 1), iii) La chronologie de l'activité magmatique, des accrétions et de l'exhumation des terrains océaniques et continentaux au Crétacé supérieur et jusqu'à la fin du Miocène, iv) Un mécanisme pour expliquer comment l'exhumation a eu lieu sous un régime collisionnel influencé par un climat à forts gradients thermiques et par des taux d'érosion élevés (chapitre 2); v) Les processus tardifs de dénudation et de sédimentation contrôlés par la tectonique dans deux bassins sédimentaires depuis le Miocène inférieur soumis à des taux d'érosion et des gradients thermiques décroissants (chapitre 3).

Chapitre 1. La convergence entre Laurentia et Gondwana a finalement conduit à la collision et à la formation de la Pangée au Paléozoïque supérieur. De ces longues interactions de plaques, a résulté la création de roches de Haute Pression (HP) et de Haute Température (HT), qui caractérisent une grande partie du nord-ouest de la Sierra Nevada de Santa Marta Massif (SNSM) dans les Andes du Nord de la Colombie, où une section imbriquée de croûte inférieure est préservée.

Les observations de terrain et l'étude pétrographique, couplées aux âges U-Pb (LA-ICP-MS) sur zircon de 17 nouveaux échantillons de roches ignées et métamorphiques et l'analyse des élément-traces sur zircons et de la géochimie sur roche totale sont utilisés pour la reconstruction de l'évolution tectonique de cette section crustale fortement remobilisée, charriée sur des séquences métamorphiques de bas grade à la fin du Paléozoïque. L'évolution métamorphique a été étudiée au moyen de plusieurs thermobaromètres (Grt + Bt, Hbl + Grt, Hbl + Pl + Qtz, GASP et Ti-in-Zr) pour obtenir des estimations fiables sur les conditions *P-T* pendant au moins deux phases métamorphiques identifiés par leurs paragenèses minérales.

Nos résultats fournissent de nouvelles contraintes pour les reconstructions paléogéographiques entre Laurentia et Gondwana au Permien moyen et jusqu'au début du Jurassique. Cette reconstruction est définie par l'interaction de la marge nord-ouest de Gondwana avec les terrains

d'Amérique centrale et du Mexique acuels lors de la formation de la Pangaea.

Un scénario évolutif pour ce cycle supercontinental est proposé en plusieurs phases comprenant la création d'un arc, l'épisode métamorphique, et l'exhumation tardive des segments de la croûte inférieure.

La fermeture de l'océan Rhéique (ca. 290 Ma) marque le début de l'interaction des blocs crustaux lors de l'assemblage de la Pangaea, qui provoqua 1) une fusion anatectic post-collisionnelle et un épaississement maximal de la croûte vers 278 ± 0.5 Ma, 2) un métamorphisme de type Barrovian culminant à 13 kb et 840 ° C, vers 254 Ma, suivie par 3) le retrait de la plaque subduite et sa délamination, 4) un effondrement orogénique 5) affaiblissement thermique, extension crustale et sous-placage de croûte mafique qui a causé un métamorphisme *LP-HT* (5,6 kb, 550) vers 225 Ma, marquant le début d'une phase de rifting.

Ces processus sont associés au remplissage d'un bassin d'arrière-arc dans lequel se sont accumulés au moins 2000 m de sédiments carbonatés et volcanoclastiques fournis par les massifs de socles exhumés.

Vers 216 Ma la plus grande partie de la marge conjuguée a été retiré, mais les restes de cet arc Permien sont encore conservés dans les complexes Oaxaca et Acatlán et dans le bloc Maya. L'amincissement cortical responsable du rifting et la dérive qui a suivi a contribué au rebond isostatique de la plaque Pacifique subduite qui a réactivé l'arc magmatique au Jurassique. A cette époque, l'arc a migré vers le continent, et l'ancien bassin d'arrière-arc passa en position d'avant-arc dans lequel se sont accumulés ≈ 5000 m de dépôts volcano-clastiques. Cette nouvelle reconstitution établit une durée de 60 Myr d'âge entre la collision de les Alleghenides et l'éclatement du Pangaea dans cette partie des Andes du Nord.

Chapitre 2. De nouvelles données thermochronologiques à basse température sur des roches du Précambrien, Permien à Jurassique, Crétacé supérieur et Paléocène-Eocène qui forment la ceinture métamorphique nord-occidentale de la SNSM des Andes du Nord de la Colombie révèlent les tendances à l'exhumation de cette partie de la marge continentale entre le Paléocène et le Miocène. Nos analyses comprennent des traces de fission sur apatites et zircons et des âges (U-Th)/He sur apatite, qui ont permis de contraindre l'histoire thermique (~ 240°C - ~ 60°C) d'une séquence crustale inversée qui expose des roches métamorphiques de faciès schistes verts à granulite.

Les trajets température-temps prouvent que ce refroidissement est diachrone dans le massif en raison de l'activation de chevauchements vers le NW, avec le début d'une exhumation rapide liée à l'érosion après collision, et l'intrusion de plutons de la série TTG sous gradient géothermique initialement élevé de 40°C / km.

Dans ce régime, le massif a été exhumée à des taux élevés ~ 0.9 km/Myr de 50 à 45 Ma ; ce taux augmenta à 2 km/Myr pour l'intervalle 45-40 Ma avec un gradient géothermique diminuant à 30°C/km, et atteignit les taux les plus élevés pendant 2.7km/Myr de 37 à 35 Myr.

Nous interprétons l'exhumation de cette séquence de croûte inférieure inversée comme liée à l'association de l'extrusion ductile d'une croûte continentale épaissie et de la dénudation du surface. Les événements d'exhumation post-éocènes montrent une diminution des taux de refroidissement et d'exhumation à ~ 0.2 km/Myr vers 25 Ma, en rapport avec le début d'un régime composite de transpression-transtension à la limite sud de la plaque Caraïbes en raison d'un changement de la convergence entre les plaques Caraïbes et Amérique du Sud. Cette réorganisation a conduit à l'activation de la Faille Santa Marta-Bucaramanga (SMBF) de direction NW et de la faille de Oca de direction E-W.

Ces failles ont accommodé le partitionnement de la convergence et ont transféré la déformation depuis la plaque Caraïbe vers le Massif de Santander, la Cordillère orientale de Colombie, la Serranía de Perija, et les Andes de Merida jusqu'à la fin du Miocène.

Nous proposons que ce nouveau régime tectonique a inhibé la propagation vers le NW de chevauchements et a provoqué le basculement vers le NE de la SNSM en raison de l'activité distensive de la SMBF, associée à l'arrachement tectonique causé par le transit de la plaque Caraïbes. Ces processus ont entraîné des taux d'exhumation réduits de ~ 0.09 km/Myr qui ont persisté jusqu'à la fin du Miocène, lors de la rééquilibration thermique de la SNSM.

Chapitre 3. Geo-thermochronologie de roches sédimentaires avec analyses stratigraphiques, révèlent une exhumation du massif de la Sierra Nevada de Santa Marta (SNSM) au début du Néogène. Ce bloc triangulaire délimité par des failles dans les Andes du nord de la Colombie, exposée roches métamorphiques du Précambrien et Paléozoïque et reste d'un Trias-Jurassique arc magmatique. Dans cet article, nous comparons les bassins Néogène remplissent deux bassins marginaux, localisés ouest le long de la faille de Santa Marta-Bucaramanga (SMBF) et occupant le nord du bassin de la la marge sud de la faille de Oca.

La séquence de l'Ouest est constituée de dépôts de conglomérats de gravité jusqu'à une épaisseur ≈ 1200 m définissant un delta type Gilbert progradante émanant d'un escarpement qui correspond à la SMBF. En raison de sa position structurale et stratigraphique cette séquence est comparée à une séquence de transgression dans le bassin nord. Analyse de provenance des deux sections de ces deux séquences montrent une source dérivée du socle sous-jacent.

Ce résultat est cohérent avec le spectre des âges zircons U-Pb dépourvus de signaux pré-Grenvillienne et Ordovicien des sédiments contemporains dans la bassin de Magdalena, montrant que ces sédiments ont été déposés dans les bassins versants locaux déconnectés de l'axe du système fluvial proto - Magdalena. Afin de concilier l'organisation différente des deux bassins marginaux nous proposons une inclinaison a échelle régionale de la SNSM vers le nord-est au début du Néogène. Ce modèle tient compte de la contemporanéité entre un cycle progradante sur le flanc ouest délimitée par un faille et un conglomérats transgressive transfert du bassin nord dans une surface inclinée pendant exhumation généralisée du massif.

Bayona, G., Jiménez, G., Silva, C., Cardona, A., Montes, C., Roncancio, J., Cordani, U., 2010. Paleomagnetic data and K–Ar ages from Mesozoic units of the Santa Marta massif: A preliminary interpretation for block rotation and translations. J. South Am. Earth Sci. 29, 817–831. doi:10.1016/j.jsames.2009.10.005

Cardona, A., Valencia, V., Bayona, G., Duque, J., Ducea, M., Gehrels, G., Jaramillo, C., Montes, C., Ojeda, G., Ruiz, J., 2011. Early-subduction-related orogeny in the northern Andes: Turonian to Eocene magmatic and provenance record in the Santa Marta Massif and Rancheria Basin, northern Colombia. Terra Nova 23, 26–34. doi:10.1111/j.1365-3121.2010.00979.x

Cardona, A., Valencia, V., Bustamante, C., García-Casco, A., Ojeda, G., Ruiz, J., Saldarriaga, M., Weber, M., 2010a. Tectonomagmatic setting and provenance of the Santa Marta Schists, northern Colombia: Insights on the growth and approach of Cretaceous Caribbean oceanic terranes to the South American continent. J. South Am. Earth Sci., Sierra Nevada de Santa Marta and Adjacent Basins 29, 784–804. doi:10.1016/j.jsames.2009.08.012

Cardona, A., Valencia, V., Garzón, A., Montes, C., Ojeda, G., Ruiz, J., Weber, M., 2010b. Permian to Triassic I to S-type magmatic switch in the northeast Sierra Nevada de Santa Marta and adjacent regions, Colombian Caribbean: Tectonic setting and implications within Pangæa paleogeography. J. South Am. Earth Sci., Sierra Nevada de Santa Marta and Adjacent Basins 29, 772–783. doi:10.1016/j.jsames.2009.12.005

Cardona, A., Valencia, V., Weber, M., Duque, J., Montes, C., Ojeda, G., Reiners, P., Domanik, K., Nicolescu, S., Villagómez, D., 2011a. Transient Cenozoic tectonic stages in the southern margin of the Caribbean plate: U-Th/He thermochronological constraints from Eocene plutonic rocks in the Santa Marta massif and Serranía de Jarara, northern Colombia. Geol. Acta 9, 445–469. doi:10.1344/105.000001739

Cordani, U.G., Cardona, A., Jimenez, D.M., Liu, D., Nutman, A.P., 2005. Geochronology of Proterozoic basement inliers in the Colombian Andes: tectonic history of remnants of a fragmented Grenville belt. Geol. Soc. Lond. Spec. Publ. 246, 329–346. doi:10.1144/GSL.SP.2005.246.01.13

Doolan, B., 1970. Structure and metamorphism of the Santa Marta Area Colombia, South America [microform] / [WWW Document]. URL https://www.researchgate.net/publication/34351494_Structure_and_metamorphism_of_the_Santa_Marta_Area_Colombia_South_America_microform (accessed 7.20.16).

Duque, T., 2009. Geocronología (U/Pb y 40Ar/39Ar) y geoquímica de los intrusivos paleógenos de la Sierra Nevada de Santa Marta y sus relaciones con la tectónica del Caribe y el arco magmático circun-caribeñ.

Fossen, H., 2010. Structural Geology. Cambridge University Press.

Gansser, A., 1955. Contribución a la geología y petrografía de la Sierra Nevada de Santa Marta (Colombia, Suramérica). Traducido de Gansser, A., 1955. Ein Beitrag zur Geologie und Petrographie der Sierra Nevada de Santa Marta (Kolumbien, Sudamerika):

MacDonald, W.D., Doolan, B.L., Cordani, U.G., 1971. Cretaceous-Early Tertiary Metamorphic K-Ar Age Values from the South Caribbean. Geol. Soc. Am. Bull. 82, 1381–1388. doi:10.1130/0016-7606(1971)82[1381:CTMKAV]2.0.CO;2

Macdonald, W.D., Hurley, P.M., 1969. Precambrian Gneisses from Northern Colombia, South America. Geol. Soc. Am. Bull. 80, 1867. doi:10.1130/0016-7606(1969)80[1867:PGFNCS]2.0.CO;2

Ordóñez, O., Pimentel, M., Moraes, R., 2002. GRANULITAS DE LOS MANGOS, UN FRAGMENTO GRENVILLIANO EN LA PARTE ORIENTAL DE LA SIERRA NEVADA DE SANTA MARTA. Rev. Acad. Colomb. Cienc. Exactas Físicas Nat. 0370-3908 26, 169–179.

Ramsay, J.G., Huber, M.I., 1987. The Techniques of Modern Structural Geology. Academic Press.

Restrepo-Pace, P., Ruiz, J., Gehrels, G., Cosca, M., 1997. Geochronology and Nd isotopic data of Grenville-age rocks in the Colombian Andes: new constraints for Late Proterozoic-Early Paleozoic paleocontinental reconstructions of the Americas. Earth Planet. Sci. Lett. 427–441. doi:10.1016/S0012-821X(97)00091-5

Tschanz, C., Jimeno, A., Cruz, J., 1969. Geology of the Sierra Nevada de Santa Marta area, Colombia. Informe interno 1829. INGEOMINAS Bogotá Prelim. Rep. 288pLinks.

Tschanz, C., Marvin, R.F., B, J.C., Mehnert, H.H., Cebula, G.T., 1974. Geologic Evolution of the Sierra Nevada de Santa Marta, Northeastern Colombia. Geol. Soc. Am. Bull. 85, 273–284. doi:10.1130/0016-7606(1974)85<273:GEOTSN>2.0.CO;2

Villagómez, D., Spikings, R., Mora, A., Guzmán, G., Ojeda, G., Cortés, E., van der Lelij, R., 2011. Vertical tectonics at a continental crust-oceanic plateau plate boundary zone: Fission track thermochronology of the Sierra Nevada de Santa Marta, Colombia. Tectonics 30, TC4004. doi:10.1029/2010TC002835

Zuluaga, C., Stowell, H., 2012. Late Cretaceous–Paleocene metamorphic evolution of the Sierra Nevada de Santa Marta: Implications for Caribbean geodynamic evolution. J. South Am. Earth Sci. 34, 1–9. doi:10.1016/j.jsames.2

Contents

Figures List

INTRODUCTION

CHAPTER 1

CHAPTER 2

CHAPTER 3

OVERALL CONCLUSIONS

INTRODUCTION

Evolution of orogens is defined by events that may involve igneous activity, metamorphism, surface uplift, and exhumation coupled with erosion and coeval sedimentation processes. The different stages of evolution can be deciphered by the integration of a growing number of geophysical and geological techniques including: field observation to mantle geophysics through metamorphic petrology, sedimentology, geochemistry, thermochronology, numerical and analogue modeling and others on various spatial and temporal scales that may reveal the transient stages of an orogen (Rolland et al., 2012).

The orogenic stages may involve a “juvenile” stage of crustal thickening and synchronous or late metamorphism that may vary in metamorphic degree depending of a given geological configuration, time span, and kinematic constraints. During this stage, maximum crustal thickening is achieved, and most of the high temperature process act during mineral phase equilibration until a metamorphic peak is reached.

The onset of exhumation marks another fundamental process in the evolution of orogens and is defined by the onset of erosion that acts over a newly exposed mountain range causing the activation of sedimentary cycles which will transport minerals to new basins or depocenters in which the removed material will accumulate to form syn-orogenic sedimentary rocks.

These orogenic stages can coexist at any given moment and overlap in their histories, depending mostly on the timing of igneous activity, metamorphism and exhumation, which are controlled by plate tectonic-scale processes, as changes in plate convergence

magnitude and direction, crustal thermal regimes and external influences to the system like plume-induced anomalies that increase thermal gradients and crustal production.

During orogenesis, an accretionary margin will evolve from an orogenic wedge to a continental plateau, if the mass flux related to tectonic accretion dominates over the redistribution caused by erosion. Crustal thickening enhances radiogenic heat production and conduction overcomes advection. Such processes may involve the increase of geothermal gradients and crustal melting. Lower crustal weakening will induce lateral flow and therefore, vertical growth of the wedge range is replaced by a rectangular continental plateau geometry indicating that the orogenic belt cannot sustain topographic gradients anymore. Orogenic plateaus can sustain steady state equilibrium for several tens of millions of years if accretion is balanced by gravity driven flow (Vanderhaeghe, 2012).

In a long-lived orogenic plateau maintaining steady state conditions of growth and maximum thickness, a transition to crustal thinning is influenced by lithospheric-scale boundary condition modifications such as plate convergence reorganization, and subduction failure.

Subduction can fail by either thickening of the oceanic plateau by accretion, or thickening of the continental plateau, or a combination on different time scales of these processes. Another external factor to consider is a redistribution of the geoid highs by mantle plume activity, which may influence an extensional regime under a thickened continental crust (Murphy and Nance, 2013). Under these circumstances, an orogen will tend to thin by its gravitational potential, and thus reach a stage of

gravitational collapse in which late crustal attenuation will increase geothermal gradients until finally rifting and opening of new oceans may occur.

During orogenic evolution, the generation of crust due to magmatism generates zircons that constitute an accessory mineral in the majority of upper crustal rocks, and by their endurance under extreme thermobarometric conditions, are ideal for studying the igneous and metamorphic evolution of an orogen. At the same time the crust is consumed along subduction zones, in many cases disappearing by tectonic erosion, the remnants of an eroded crust are incorporated in the accretionary wedge. A positive feedback of oceanic crustal thickness may enhance exhumation of the continental plateau, particularly observed in several parts of the Andean margin (Spikings and Simpson, 2014). Another consequence of the increment of the thickness of the subducted plate is a late subduction failure (Stern, 2011). During these interactions between the oceanic-continental plates, the activation of sedimentary cycles reflects the changes between exhumation and plate geodynamics. Therefore it is possible to quantify the time span and magnitude, temperature and pressure conditions of these events by studying zircons, apatites and garnet among other mineral species, found both in-situ and recycled from their sources and accumulated in sedimentary basins adjacent to the orogenic belt.

The Andes form a 7000 km long orogenic belt on the western margin of South America (Fig. 1). The current scenario is defined by the subduction of the oceanic Pacific plate, under the cold lithosphere of the South American plate. The interaction of the Pacific, South American and Caribbean Plates controls the structure of the Andes, which in the Neogene led to the individualization of the North Andean block, as a response of plate

reconfiguration kinematics during the rupture of the Pacific Farallon plate originating the Cocos and Nazca plates.

In this work, my aim is to study the tectonic history of the northern Andes focused on the Sierra Nevada de Santa Marta (SNSM) massif, the highest topographic relief of the Colombian Andes. This massif occupies a northwestern position within the Maracaibo Block (Figs. 2, 3 & 4) and is composed by the amalgamation of igneous and metamorphic rocks from different ages; my approach is directed to establish an orogenic evolution of the SNSM massif by a combination of isotopic and geochemistry analyses in detrital and bedrock minerals. In the following sections, I will describe briefly the main geological features from the Northern Andes of Colombia.

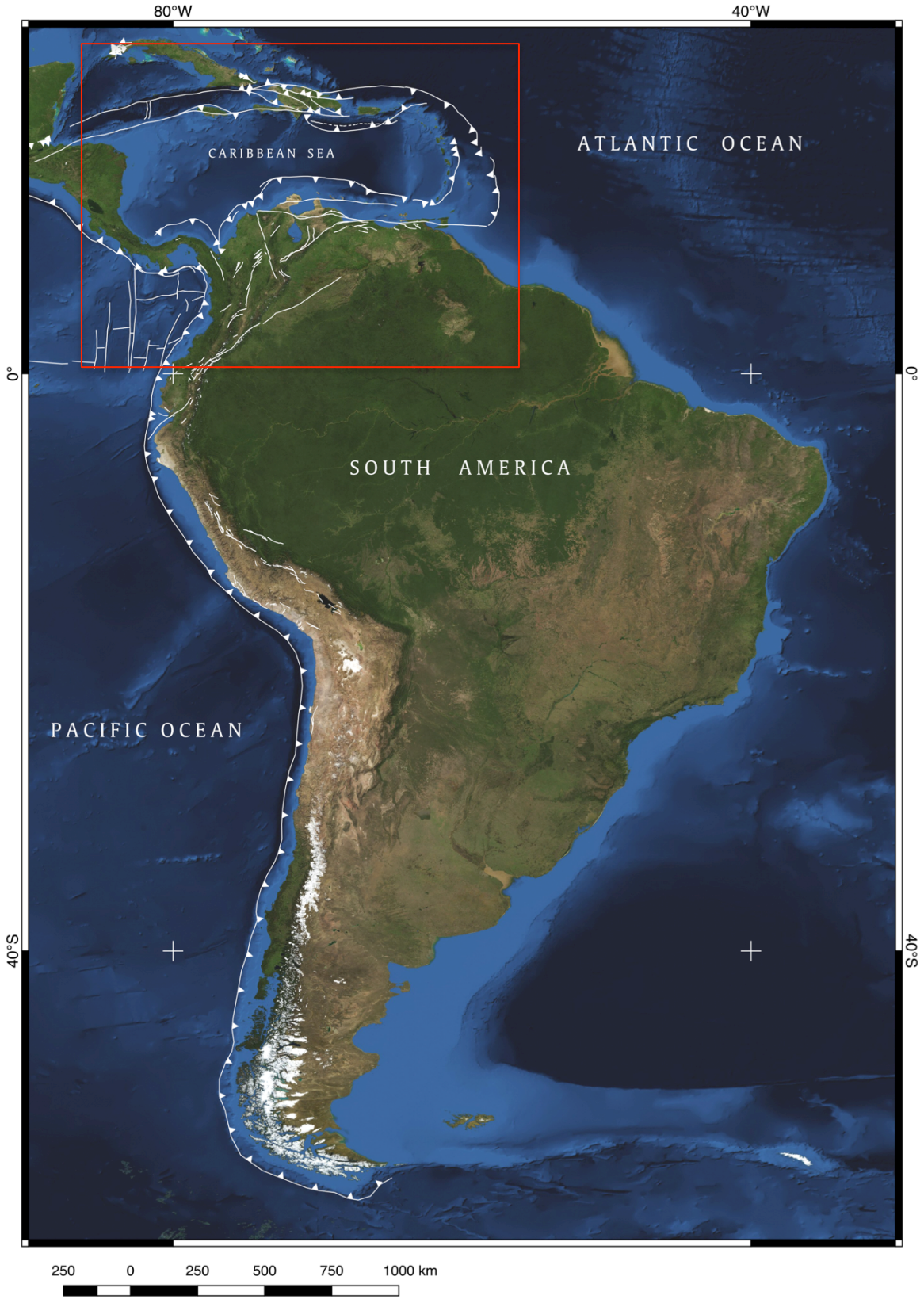

Figure 1. South America and main plate boundaries. Taken from http://server.arcgisonline.com/arcgis/rest/services/ESRI_Imagery_World_2D/.

Northern Andean Block

The Colombian Caribbean margin consists of a group of individualized tectonic blocks that represent an atypical section of the Andean margin because of its transpressive plate-tectonic configuration. In this context, the Northern Andean block can be divided into several tectonic terranes separated from the rest of the Andes through a main frontal thrust system denominated the Borde Llanero fault system that bounds the deformation front to the east against the Guyana shield (Fig. 2 & 3). From southwestern Colombia, the mountain ranges of the Colombian Cordilleras trend NE (Fig. 2). The Central and the Eastern Cordillera are separated by the Upper and Lower Magdalena basin, which reaches its major depth near the Caribbean margin, filled with Mesozoic and Cenozoic sediments. To the west of the Lower Magdalena basin is the accretional Sinú-San Jacinto fold belt (Fig. 2).

The Lower Magdalena basin resulted from a Paleocene rotational basin, separating the Sierra Nevada de Santa Marta massif (SNSM) from the foothills of the Central Cordillera and the San Lucas range (Fig. 2). The Lower Magdalena basin is attributed to transtensional tectonics, in which normal faults perpendicular to the margin were responsible for block rotation and translation of the SNSM block to its current position (Bernal-Olaya et al., 2015; Flinch, 2003; MacDonald and Opdyke, 1972; Montes et al., 2010).

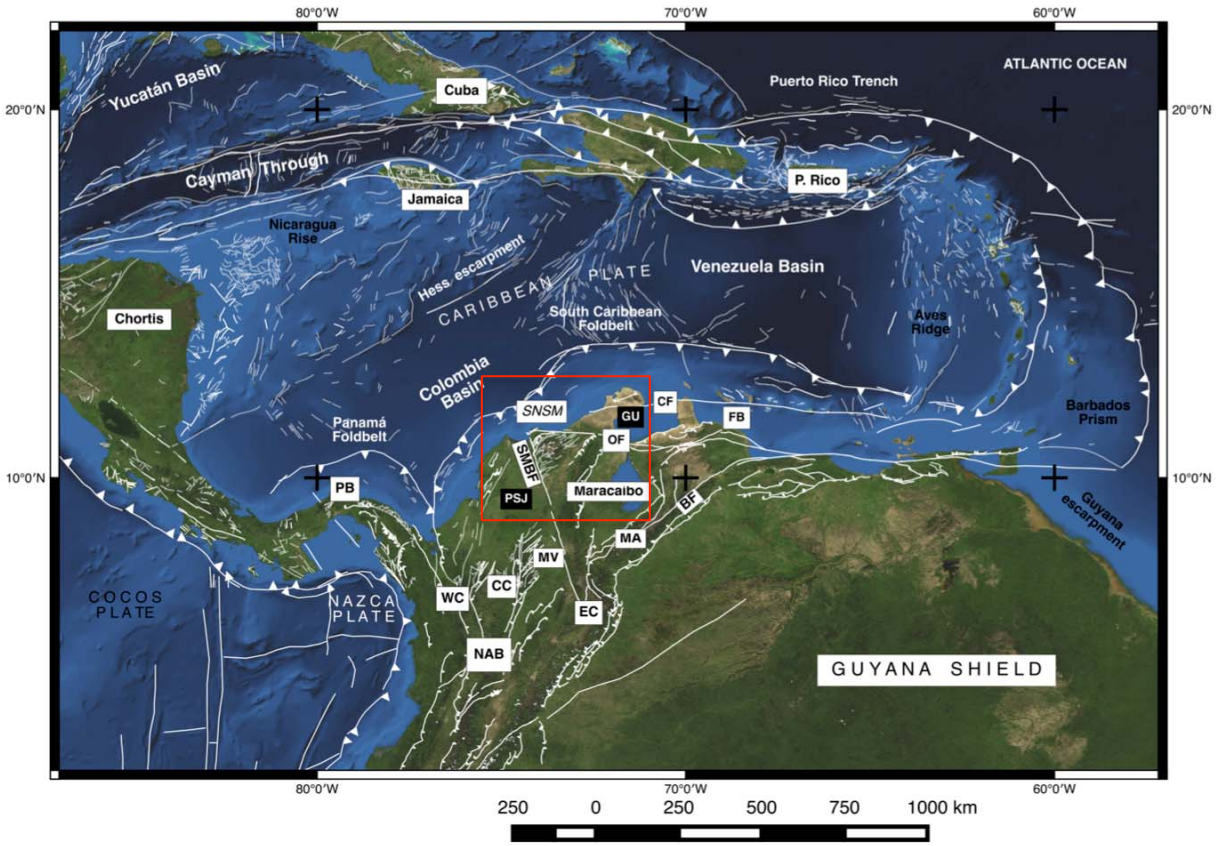

Figure 2. Regional tectonic map of the Caribbean realm showing the most relevant geological features intervening in the plate boundary configuration. (Veloza et al., 2012). Elements of the North Andean Block (NAB): Maracaibo block, SNSM: Sierra Nevada de Santa Marta, OF: Oca Fault, CF: Cuisa Fault, SMBF: Santa Marta-Bucaramanga Fault, GU: Guajira Basin, PSJ: Plato-San Jorge Basin MA: Mérida Andes, BF: Boconó Fault, FB: Falcon Basin, WC: Western Cordillera, CC: Central Cordillera, EC: Eastern Cordillera, MV: Magdalena Valley, PB: Panamá Block. Satellite imagery taken from: http://server.arcgisonline.com/arcgis/rest/services/ESRI_Imagery_World_2D/.

Grenvillian inliers in the NW margin of South America

The easternmost morphotectonic province in the Colombian Andes corresponds to a Precambrian belt of granulites, gneisses and anorthosites (Fig. 3), derived from igneous and volcanoclastic protoliths, which chronologically can be traced up to the Grenvillian orogeny, locally defined as the Putumayo orogeny (Cardona et al., 2006; Kroonenberg, 1982; Ordóñez et al., 2002). The Putumayo orogeny was the consequence of the

collision between Amazonia and the Sveconorwergian province in Baltica during the early Neoproterozoic (Ibanez-Mejia et al., 2011).

These Precambrian inliers are denominated as the Chibcha terrane and are restricted to the east of the Otú-Pericos-Palestina fault system (Feininger, 1970; Ordóñez, 1999; Vinasco et al., 2006). They crop out in the San Lucas Range, the Santander Massif, the Guajira Peninsula, and the SNSM (Fig. 2 & 3), and constitute Grenvillian remnants that had undergone at least three metamorphic episodes (Cardona et al., 2010a).

The Precambrian rocks of the Santander Massif are intruded by Ordovician to Silurian plutons (Van Der Lelij, 2013), corresponding to a magmatic arc that fringed Gondwana. Remnants of this arc can be found in the Central Cordillera were they had been defined as the Anacona suspect terrane (Fig. 3; Martens et al., 2014). Ordovician-Silurian plutons are elusive or absent in the Guajira peninsula and SNSM, although zircons of this age interval are commonly reworked through orogenic recycling and partial melting into younger plutons as well as into the medium-grade metamorphic units of the SNSM (Cardona et al., 2010b, 2010c).

Permo-Triassic Tahamí Terrane

The central morphotectonic province of the Colombian Andes corresponds to a suite of Paleozoic meta-sedimentary and meta-igneous rocks denominated the Tahamí terrane, which includes Permian orthogneisses affected by partial melting during the Triassic (Cochrane et al., 2014a; Vinasco et al., 2006). The Tahamí terrane includes the Central

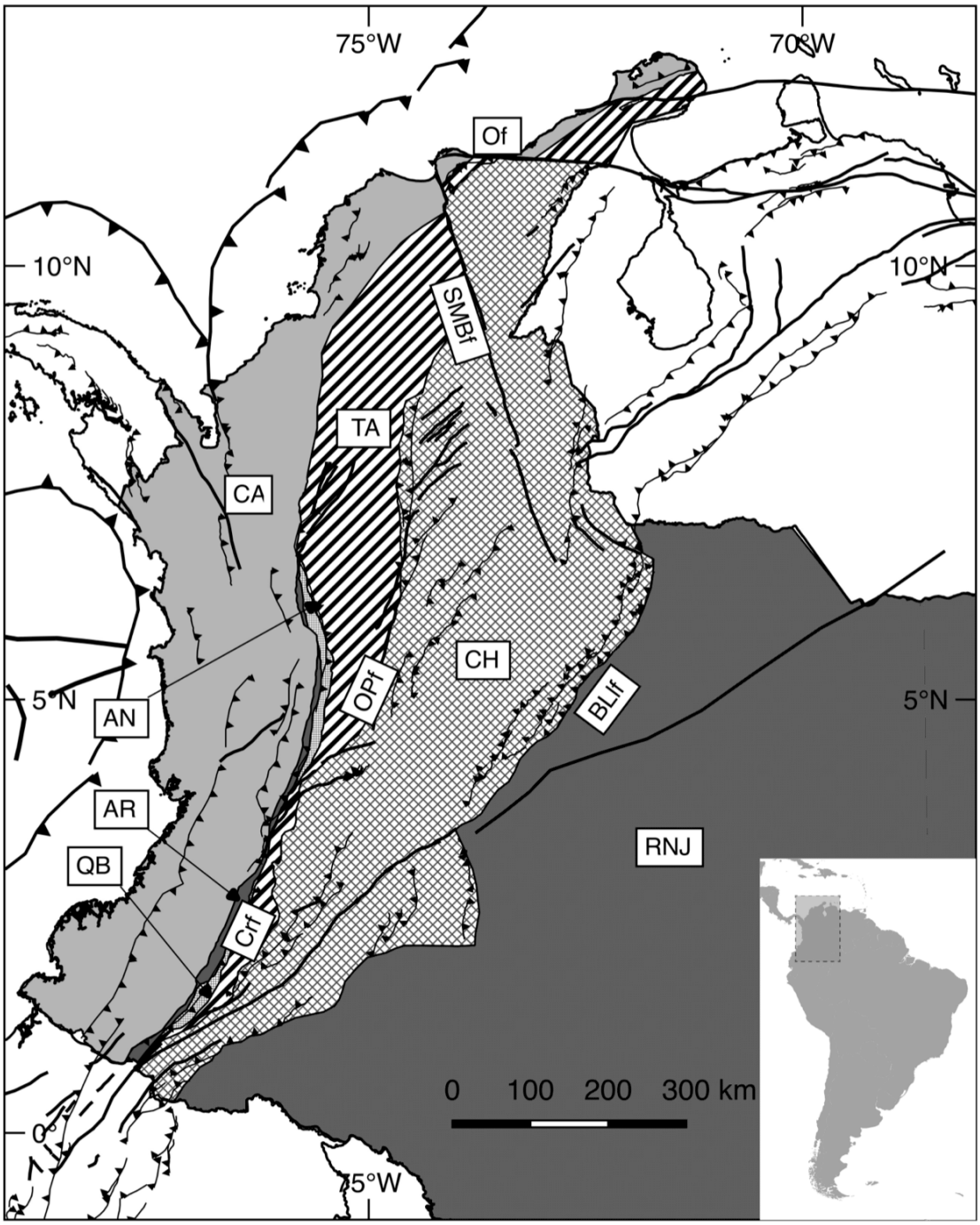

Figure 3. Simplified terrane map of Colombia after Colombian Geological survey (Gomez et al., 2015). Terrane names: RNJ: Rio Negro Juruena Province; CH: Chibcha terrane; TA: Tahamí terrane; AN: Anacona terrane; QB: Quebradagrande terrane; AR: Arquía Terrane; CA: Caribe Terrane; OPf: Otú-Pericos fault; SMBf: Santa Marta-Bucaramanga fault; CRf: Cauca Romeral fault; Of: Oca fault; BLlf: Borde Llanero fault.

Cordillera of Colombia (Ordóñez Carmona and Pimentel, 2002; Restrepo et al., 2011; Spikings et al., 2015; Villagómez et al., 2011a; Villagómez and Spikings, 2013; Vinasco et al., 2006), the northernmost part of the Sierra Nevada de Santa Marta Massif (Cardona et al., 2010c), and the Guajira Peninsula (Fig. 3). Furthermore, it corresponds to the remnant of a Peri-Gondwana arc composed of meta-igneous and metasedimentary rocks that host anatectic melts. The Tahamí terrane can be correlated with other exposures of Permian to Triassic meta-sedimentary and meta-igneous rocks in the Andes, such as the Loja (Aspden and Litherland, 1992), and the Amotape or El Oro Complex (Chew et al., 2007; Riel et al., 2013), the late Paleozoic sediments and metaluminous to peraluminous intrusive rocks of the early Paleozoic Marañon Complex in Peru (Chew et al., 2007; Mišković et al., 2009) and the Chiapas massif in southern Mexico (Weber et al., 2007).

The remnants of the Permo-Triassic metamorphic belt in the SNSM are on their NW margin capped by a sequence of meta-igneous and meta-pelitic units with a Caribbean affinity (Doolan, 1970; MacDonald et al., 1971; Tschanz et al., 1969, 1974). Recent geochemical and geochronological studies (Cardona et al., 2010b, 2010c; Cordani et al., 2005) allowed establishing the accretion of the Caribbean plateau and related arcs at least since the Turonian (Cardona et al., 2011).

Paleomagnetic and geochronological data from the Cesar Ranchería basin (Bayona et al., 2006; Nova et al., 2013), and seismic stratigraphy and zircon U-Pb geochronology in well core samples from the metamorphic basement of the Lower Magdalena valley at the Plató-San Jorge depocenter (Fig. 1; Montes et al., 2010) shed light on the Cenozoic clockwise rotation of the SNSM to its current position, and permitted as well to stablish a co-genetic relationship between the Central Cordillera and the SNSM basement,

where Permo-Triassic granitoids are slightly deformed at the Plató-San Jorge basin, whereas orthogneisses of the same age in the SNSM are mylonitic. From all this it was concluded that the SNSM was segmented from a former continuous margin that was composed of a Permo-Triassic arc (Cardona et al., 2010c; Montes et al., 2005, 2010).

Late Cretaceous-Paleogene Caribe Terrane

The youngest morphotectonic province of the Colombian Andes is defined as the Caribe Terrane (Fig. 3). the Caribe Terrane is located in the western margin of the Colombian Andes and comprises the oceanic and volcanic sequences accreted throuhg the Romeral Suture to the pre–existent Permo-Triassic terranes of the continental margin, these terranes were separated from the rocks of the continental margin through a major suture known as the Cauca-Romeral fault (Fig. 3).

The origin of Caribbean plate is widely discussed, between a pacific realm or a segmentation and incorporation between Cocos and Nazca plates, against cratonic South America. The main boundary of this scene can be reconstructed up to Late Cretaceous ages were an active subduction process began related to Thethys closure, evidenced from the marine sequences with an important basaltic input which acted until lower Paleocene times. The accretion of an oceanic plateau during the campanian defined as the CLIP (Hoernle et al., 2004; Kerr et al., 1997; Villagómez and Spikings, 2013; Whattam and Stern, 2015), yields major implication on the origin and late evolution of the Caribbean Plate.

Models for Caribbean evolution involve the development of this proto Caribbean oceanic floor and its accretion against continental South America, which is defined by a

preexistent Jurassic volcanic arc and basin emplaced on older Paleozoic sedimentary and low to medium grade metamorphic rocks of the Tahamí terrane, which overly unconformably the Precambrian basement of the Chibcha terrane.

The Caribbean Colombian Margin is configured by two belts that define the continental slope intensely deformed and mountain areas in its continental portion. The first is commonly addressed as the *South Caribbean Deformed Belt (SCDB)*, which is constituted by sediments from Oligocene times to the present. The marginal high is conformed by the South American Plate Basement Cretaceous to Cenozoic platform sediments. At the Sierra Nevada de Santa Marta massif (SNSM) (Fig. 4) this structural high exhibits its major development and is composed by three provinces (Tschanz et al., 1974): 1) the south eastern flank (Sierra Nevada Province) comprises a Jurassic magmatic-volcanic arc that grew over a Grenvillian basement (Cardona et al., 2010a; Restrepo-Pace et al., 1997). 2) The intermediate Sevilla province consists of Neoproterozoic gneisses intruded by Permian to Triassic syntectonic granitoids (Cardona et al., 2010c). 3), and the Santa Marta province to the northwest consists of Triassic-Cretaceous greenschists associated with amphibolites and orthogneisses (Doolan, 1970).

In order to understand the tectonic relationships it is crucial to investigate the origin and structural style of the oceanic unit, that conforms the Santa Marta belts (Tschanz et al., 1974): the sub-units of the schists and amphibolites of Santa Marta had been object of an exhaustive geochemical and isotopic research that includes results on the provenance obtained by zircon U-Pb dating (Cardona et al., 2010b). As a set these units are characterized by an increase in the metamorphic degree from NW to SE including a low-grade sequence of metavulcanites and metapelites with MORB signature (Fm.

Concha) to the schists and amphibolites of a medium to high-pressure grade in an internal structural position (San Lorenzo Schists). For the Metavulcanites a zircon age of 82 Ma was obtained (Cardona et al., 2010b). The zircons from a continental source are scarce. For the most internal units of San Lorenzo and Rodadero (amphibolites, amphibole schists) the youngest reworked zircons showed Middle Triassic ca. ≈235 Ma and Middle Jurassic ca. ≈157 ages. At these units, zircon populations include an age spectrum since the Mesoproterozoic and therefore show an affinity with the continental basement. Compared with the situation at the Guajira Peninsula, these sequences do not include continental slope derived deposits (Weber et al., 2010). In contrast, the continental basement to the east of the Santa Marta belts exposes in an intrusive contact with Jurassic extrusive rocks, low deformed platform sediments from the Albian (Fig. 4 & 5). The lack of continental slope sediments implies a tectonic hiatus that would be explained by tectonic erosion of these marine sequences typical of the Guajira Peninsula.

For the Subduction event switched subduction polarity situations can be assumed, which are combined, although supposing an allocthonous origin for the Caribbean plate. A coherent synthesis for the study area assumes a subduction of the continental plate and an oceanic-transitional plate or proto-Caribbean under the Caribbean plate. A late stage of subduction failure in consequence is followed by an accretionary event for an epoch prior or coeval with the metamorphic peak. This evolution concludes with a subduction polarity reversal since the Late Cretaceous linked with the current scenario (Pindell et al., 2005; van der Lelij et al., 2010).

The main interest in the studied area resides in the tectonic relationship between units that belong originally to the domain of the Caribbean plate (Santa Marta schists) and

the continental basement of the Sevilla Metamorphic Belt (Fig. 5). For the contact between these two provinces, a suture has been speculated, but its nature and tectonic meaning is still matter of debate. The problematic of the study area can be compiled in two main questions: 1) what mechanisms juxtaposed these tectonic units? And 2) what is the cause of Cenozoic uplift of the SNSM?

Aspden, J.A., Litherland, M., 1992. The geology and Mesozoic collisional history of the Cordillera Real, Ecuador. Tectonophysics 205, 187–204. doi:10.1016/0040-1951(92)90426-7

Bayona, G., Rapalini, A., Costanzo-Alvarez, V., 2006. Paleomagnetism in Mesozoic rocks of the Northern Andes and its Implications in Mesozoic Tectonics of Northwestern South America. Earth Planets Space 58, 1255–1272. doi:10.1186/BF03352621

Bernal-Olaya, R., Mann, P., Escalona, A., 2015. Tectonostratigraphic Evolution of the Lower Magdalena Basin, Colombia: An Example of an Underfilled to Overfilled Forearc Basin. Presented at the GCAGS.

Cardona, A., Chew, D., Valencia, V., Bayona, G., Mišković, A., Ibañez-Mejía, M., 2010a. Grenvillian remnants in the Northern Andes: Rodinian and Phanerozoic paleogeographic perspectives. J. South Am. Earth Sci., The Grenville Orogen in Central and South America 29, 92–104. doi:10.1016/j.jsames.2009.07.011

Cardona, A., Valencia, V., Bustamante, C., García-Casco, A., Ojeda, G., Ruiz, J., Saldarriaga, M., Weber, M., 2010b. Tectonomagmatic setting and provenance of the Santa Marta Schists, northern Colombia: Insights on the growth and approach of Cretaceous Caribbean oceanic terranes to the South American continent. J. South Am. Earth Sci., Sierra Nevada de Santa Marta and Adjacent Basins 29, 784–804. doi:10.1016/j.jsames.2009.08.012

Cardona, A., Valencia, V., Garzón, A., Montes, C., Ojeda, G., Ruiz, J., Weber, M., 2010c. Permian to Triassic I to S-type magmatic switch in the northeast Sierra Nevada de Santa Marta and adjacent regions, Colombian Caribbean: Tectonic setting and implications within Pangæa paleogeography. J. South Am. Earth Sci., Sierra Nevada de Santa Marta and Adjacent Basins 29, 772–783. doi:10.1016/j.jsames.2009.12.005

Cardona, A., Valencia, V., Bayona, G., Duque, J., Ducea, M., Gehrels, G., Jaramillo, C., Montes, C., Ojeda, G., Ruiz, J., 2011. Early-subduction-related orogeny in the northern Andes: Turonian to Eocene magmatic and provenance record in the Santa Marta Massif and

Rancheria Basin, northern Colombia. Terra Nova 23, 26–34. doi:10.1111/j.1365-3121.2010.00979.x

Cardona, A., Cordani, U.G., MacDonald, W.D., 2006. Tectonic correlations of pre-Mesozoic crust from the northern termination of the Colombian Andes, Caribbean region. J. South Am. Earth Sci. 21, 337–354. doi:10.1016/j.jsames.2006.07.009

Chew, D.M., Schaltegger, U., Kosler, J., Whitehouse, M.J., Gutjahr, M., Spikings, R.A., Miskovic, A., 2007. U-Pb geochronologic evidence for the evolution of the Gondwanan margin of the north-central Andes. Geol. Soc. Am. Bull. 119, 697–711. doi:10.1130/B26080.1

Cochrane, R., Spikings, R., Gerdes, A., Ulianov, A., Mora, A., Villagómez, D., Putlitz, B., Chiaradia, M., 2014a. Permo-Triassic anatexis, continental rifting and the disassembly of western Pangæa. Lithos 190–191, 383–402. doi:10.1016/j.lithos.2013.12.020

Cordani, U.G., Cardona, A., Jimenez, D.M., Liu, D., Nutman, A.P., 2005. Geochronology of Proterozoic basement inliers in the Colombian Andes: tectonic history of remnants of a fragmented Grenville belt. Geol. Soc. Lond. Spec. Publ. 246, 329–346. doi:10.1144/GSL.SP.2005.246.01.13

Doolan, B., 1970. Structure and metamorphism of the Santa Marta Area Colombia, South America [microform] / [WWW Document]. URL https://www.researchgate.net/publication/34351494_Structure_and_metamorphism_of_the_Santa_Marta_Area_Colombia_South_America_microform (accessed 7.20.16).

Feininger, T., 1970. The Palestina Fault, Colombia. GSA Bull. 81, 1201–1216. doi:10.1130/0016-7606(1970)81[1201:TPFC]2.0.CO;2

Flinch, J.F., 2003. Structural Evolution of the Sinu-Lower Magdalena Area (Northern Colombia) 776–796.

Gómez, J., Nivia, Á, Montes, N.E., Almanza, M.F., Alcárcel, F.A. & Madrid, C.A. 2015. Notas explicativas: Mapa Geológico de Colombia. En: Gómez, J. & Almanza, M.F. (Editores), Compilando la geología de Colombia: Una visión a 2015. Servicio Geológico Colombiano, Publicaciones Geológicas Especiales 33, p. 9–33. Bogotá.

Hoernle, K., Hauff, F., Bogaard, P. van den, 2004. 70 m.y. history (139–69 Ma) for the Caribbean large igneous province. Geology 32, 697. doi:10.1130/G20574.1

Ibanez-Mejia, M., Ruiz, J., Valencia, V., Cardona, A., Gehrels, G., Mora, A., 2011. The Putumayo Orogen of Amazonia and its implications for Rodinia reconstructions: New U–Pb geochronological insights into the Proterozoic tectonic evolution of northwestern South America. Precambrian Res. 191, 58–77. doi:10.1016/j.precamres.2011.09.005

Kerr, A.C., Tarney, J., Marriner, G.F., Nivia, A., Saunders, A.D., 1997. The Caribbean-Colombian Cretaceous Igneous Province: The Internal Anatomy of an Oceanic Plateau, in:

J.honey, J., Coffin, M.F. (Eds.), Large Igneous Provinces: Continental, Oceanic, and Planetary Flood Volcanism. American Geophysical Union, pp. 123–144.

Kroonenberg, S.B., 1982. A Grenvillian granulite belt in the Colombian Andes and its relation to the Guiana shield. Geol Mijnb. 61 1982 325-333.

MacDonald, W.D., Doolan, B.L., Cordani, U.G., 1971. Cretaceous-Early Tertiary Metamorphic K-Ar Age Values from the South Caribbean. Geol. Soc. Am. Bull. 82, 1381–1388. doi:10.1130/0016-7606(1971)82[1381:CTMKAV]2.0.CO;2

MacDonald, W.D., Opdyke, N.D., 1972. Tectonic rotations suggested by paleomagnetic results from northern Colombia, South America. J. Geophys. Res. 77, 5720–5730. doi:10.1029/JB077i029p05720

Martens, U., Restrepo, J.J., Ordóñez-Carmona, O., Correa-Martínez, A.M., 2014. The Tahamí and Anacona Terranes of the Colombian Andes: Missing Links between the South American and Mexican Gondwana Margins. J. Geol. 122, 507–530. doi:10.1086/677177

Mišković, A., Spikings, R.A., Chew, D.M., Košler, J., Ulianov, A., Schaltegger, U., 2009. Tectonomagmatic evolution of Western Amazonia: Geochemical characterization and zircon U-Pb geochronologic constraints from the Peruvian Eastern Cordilleran granitoids. Geol. Soc. Am. Bull. 121, 1298–1324. doi:10.1130/B26488.1

Montes, C., Guzman, G., Bayona, G., Cardona, A., Valencia, V., Jaramillo, C., 2010. Clockwise rotation of the Santa Marta massif and simultaneous Paleogene to Neogene deformation of the Plato-San Jorge and Cesar-Ranchería basins. J. South Am. Earth Sci., Sierra Nevada de Santa Marta and Adjacent Basins 29, 832–848. doi:10.1016/j.jsames.2009.07.010

Montes, C., Hatcher, R.D., Restrepo-Pace, P.A., 2005. Tectonic reconstruction of the northern Andean blocks: Oblique convergence and rotations derived from the kinematics of the Piedras–Girardot area, Colombia. Tectonophysics 399, 221–250. doi:10.1016/j.tecto.2004.12.024

Murphy, J.B., Nance, R.D., 2013. Speculations on the mechanisms for the formation and breakup of supercontinents. Geosci. Front. 4, 185–194. doi:10.1016/j.gsf.2012.07.005

Nance, R.D., Gutiérrez-Alonso, G., Keppie, J.D., Linnemann, U., Murphy, J.B., Quesada, C., Strachan, R.A., Woodcock, N.H., 2012. A brief history of the Rheic Ocean. Geosci. Front. 3, 125–135. doi:10.1016/j.gsf.2011.11.008

Nance, R.D., Gutiérrez-Alonso, G., Keppie, J.D., Linnemann, U., Murphy, J.B., Quesada, C., Strachan, R.A., Woodcock, N.H., 2010. Evolution of the Rheic Ocean. Gondwana Res., The Rheic Ocean: Palaeozoic Evolution from Gondwana and Laurussia to Pangæa 17, 194–222. doi:10.1016/j.gr.2009.08.001

Nova, G., Montaño, P., Bayona, G., Rapalini, A., Montes, C., 2013. Paleomagnetismo en rocas del Júrasico y Cretácico inferior en el flanco occidental de la Serranía del Perijá; contribuciones a la evolución tectónica del NW de Suramérica. Bol. Geol. 34.

Ordóñez, O., Pimentel, M., Moraes, R., 2002. GRANULITAS DE LOS MANGOS, UN FRAGMENTO GRENVILLIANO EN LA PARTE ORIENTAL DE LA SIERRA NEVADA DE SANTA MARTA. Rev. Acad. Colomb. Cienc. Exactas Físicas Nat. 0370-3908 26, 169–179.

Ordóñez, O., 1999. ROCAS GRENVILLIANAS EN LA REGIÓN DE PUERTO BERRIO - ANTIOQUIA.

Pindell, J., Kennan, L., Maresch, W.V., Stanek, K.-P., Draper, G., Higgs, R., 2005. Plate-kinematics and crustal dynamics of circum-Caribbean arc-continent interactions: Tectonic controls on basin development in Proto-Caribbean margins. Geol. Soc. Am. Spec. Pap. 394, 7–52. doi:10.1130/0-8137-2394-9.7

Pindell, J.L., 1985. Alleghenian reconstruction and subsequent evolution of the Gulf of Mexico, Bahamas, and Proto-Caribbean. Tectonics 4, 1–39. doi:10.1029/TC004i001p00001

Restrepo-Pace, P., Ruiz, J., Gehrels, G., Cosca, M., 1997. Geochronology and Nd isotopic data of Grenville-age rocks in the Colombian Andes: new constraints for Late Proterozoic-Early Paleozoic paleocontinental reconstructions of the Americas. Earth Planet. Sci. Lett. 427–441. doi:10.1016/S0012-821X(97)00091-5

Riel, N., Guillot, S., Jaillard, E., Martelat, J.-E., Paquette, J.-L., Schwartz, S., Goncalves, P., Duclaux, G., Thebaud, N., Lanari, P., Janots, E., Yuquilema, J., 2013. Metamorphic and geochronogical study of the Triassic El Oro metamorphic complex, Ecuador: Implications for high-temperature metamorphism in a forearc zone. Lithos 156–159, 41–68. doi:10.1016/j.lithos.2012.10.005

Rolland, Y., Lardeaux, J.-M., Jolivet, L., 2012. Deciphering orogenic evolution. J. Geodyn. 56–57, 1–6. doi:10.1016/j.jog.2011.09.004

Spikings, R., Simpson, G., 2014. Rock uplift and exhumation of continental margins by the collision, accretion, and subduction of buoyant and topographically prominent oceanic crust. Tectonics 33, 2013TC003425. doi:10.1002/2013TC003425

Stern, C.R., 2011. Subduction erosion: Rates, mechanisms, and its role in arc magmatism and the evolution of the continental crust and mantle. Gondwana Res. 20, 284–308. doi:10.1016/j.gr.2011.03.006

Tschanz, C., Marvin, R.F., B, J.C., Mehnert, H.H., Cebula, G.T., 1974. Geologic Evolution of the Sierra Nevada de Santa Marta, Northeastern Colombia. Geol. Soc. Am. Bull. 85, 273–284. doi:10.1130/0016-7606(1974)85<273:GEOTSN>2.0.CO;2

Van Der Lelij, R., 2013. Reconstructing north-western Gondwana with implications for the evolution of the Iapetus and Rheic Oceans: a geochronological, thermochronological and geochemical study. University of Geneva.

Van der Lelij, R., Spikings, R.A., Kerr, A.C., Kounov, A., Cosca, M., Chew, D., Villagomez, D., 2010. Thermochronology and tectonics of the Leeward Antilles: Evolution of the southern Caribbean Plate boundary zone. Tectonics 29, TC6003. doi:10.1029/2009TC002654

Vanderhaeghe, O., 2012. The thermal–mechanical evolution of crustal orogenic belts at convergent plate boundaries: A reappraisal of the orogenic cycle. J. Geodyn. 56–57, 124–145. doi:10.1016/j.jog.2011.10.004

Veloza, G., Styron, R., Taylor, M., Mora, A., 2012. Open-source archive of active faults for northwest South America. GSA Today 22, 4–10. doi:10.1130/GSAT-G156A.1

Vinasco, C.J., Cordani, U.G., González, H., Weber, M., Pelaez, C., 2006. Geochronological, isotopic, and geochemical data from Permo-Triassic granitic gneisses and granitoids of the Colombian Central Andes. J. South Am. Earth Sci., Tectonic evolution of the Colombian Andes 21, 355–371. doi:10.1016/j.jsames.2006.07.007

Villagómez, D., Spikings, R., 2013. Thermochronology and tectonics of the Central and Western Cordilleras of Colombia: Early Cretaceous–Tertiary evolution of the Northern Andes. Lithos 160–161, 228–249. doi:10.1016/j.lithos.2012.12.008

Villagómez, D., Spikings, R., Magna, T., Kammer, A., Winkler, W., Beltrán, A., 2011. Geochronology, geochemistry and tectonic evolution of the Western and Central cordilleras of Colombia. Lithos 125, 875–896. doi:10.1016/j.lithos.2011.05.003

Weber, B., Iriondo, A., Premo, W.R., Hecht, L., Schaaf, P., 2007. New insights into the history and origin of the southern Maya block, SE México: U–Pb–SHRIMP zircon geochronology from metamorphic rocks of the Chiapas massif. Int. J. Earth Sci. 96, 253–269. doi:10.1007/s00531-006-0093-7

Weber, M., Cardona, A., Valencia, V., García-Casco, A., Tobón, M., Zapata, S., 2010. U/Pb detrital zircon provenance from Late Cretaceous metamorphic units of the Guajira Peninsula, Colombia: Tectonic implications on the collision between the Caribbean arc and the South American margin. J. South Am. Earth Sci., Sierra Nevada de Santa Marta and Adjacent Basins 29, 805–816. doi:10.1016/j.jsames.2009.10.004

Whattam, S.A., Stern, R.J., 2015. Late Cretaceous plume-induced subduction initiation along the southern margin of the Caribbean and NW South America: The first documented example with implications for the onset of plate tectonics. Gondwana Res. 27, 38–63. doi:10.1016/j.gr.2014.07.011

Objectives

The main objective of this dissertation is to unravel the tectonometamorphic history of the northwestern corner of the Sierra Nevada de Santa Marta massif (SNSM). During the late Paleozoic to Neogene, investigating igneous and metamorphic bedrock from the massif and the Neogene sediment series preserved on the flanks of this mountain range. In order to achieve this main objective, I:

1. studied the deformation of the schists in the northwestern corner of the SNSM massif from microtectonics to map scale, for determining the mechanisms of accretion and late exhumation of these units by means of integrating geochronology and thermochronology.

2. examined the conditions that led to a Late Cretaceous to early Paleogene subduction failure, between the South American plate and the Great Caribbean arc in the study area, and identified deformational phases for collisional tectonics, proposing a new evolutionary model.

3. identified the evolution phases of the basement of the continental margin by U-Pb dating of zircons from igneous and metamorphic rocks.

4. constrained the peak metamorphic conditions (P-T) undergone by the units of the Inner Santa Marta Metamorphic belt, in order to define their geodynamic implications in a chronological context, by analyzing mineral chemistry of paragenesis.

5. evaluated the timing and spatial distribution of magmatic and metamorphic events during the Alleghanian, and Andean orogenies. The occurrence and importance of rift,

subduction, and collision-related volcanism is evaluated by investigation of the age and chemistry of zircons and bulk rock compositions.

6. examined the exhumation history of different tectonic provinces using apatite and zircon fission-track coupled with apatite (U-Th)/He thermochronology.

7. evaluated the widely accepted Caribbean tectonomagmatic origin for the low to medium metamorphic grade units of the SNSM, their stratigraphic context, boundaries and its implications in the geodynamic evolution of northwestern SNSM.

8. investigated the detrital zircon provenance in Neogene sediment series for establishing a chronology on the exhumation of the massif.

Thesis Outline

Structural Framework, deformation and exhumation of the Santa Marta Schists: accretion and deformational history of a Caribbean Terrane at the north of the Sierra Nevada de Santa Marta

The methods and results of this work, along with interpretations and conclusions of this dissertation are presented in three chapters, which cover the proposed objectives of research. The geological context of the evolution of the SNSM is explained in each chapter as needed. I choose to present each chapter as an independent research article with individual discussion, conclusions and references. Currently this thesis includes two articles to be submitted (Chapter 1, Chapter 2), and one article under review for publication in the Geological Society of America Bulletin (Chapter 3). A regional description of the crustal remnants of the continental margin and their provenance, metamorphism and chronological relations during the orogenic cycle that led to Pangæa formation and late break-up is presented in Chapter 1. A thermochronological study constraining the early Cenozoic exhumation of the northwestern SNSM in the context of Caribbean plate subduction and collision against South America and later onset of strike-slip tectonics is discussed in Chapter 2. Finally, a combined structural and sedimentary geology investigation aimed at reconstructing the tectonic and exhumation history of the SNSM during the early Neogene is discussed in chapter 3. A conclusion chapter after Chapter 3 summarizes the main contributions of this dissertation, which was done under joint supervision between the Universidad Nacional de Colombia at Bogotá, Colombia and the Université Grenoble Alpes at Grenoble, France.

CHAPTER 1

Permo-Triassic evolution in the Sierra Nevada de Santa Marta, from the Alleghenides collision to Pangæa break-up

Alejandro Piraquive[1,2], Andreas Kammer[2], Albrecht Von Quadt[3], Matthias Bernet[1]

1. Institut des Sciences de la Terre, Université Grenoble Alpes, CNRS 1381, rue de la Piscine, 38058 Grenoble Cedex 9, France.
2.. Grupo de Investigación en Geologia Estructural y Fracturas Universidad Nacional de Colombia. apartado Aéreo, 14490 Bogotá, Colombia.
3. Department of Earth Sciences, Institute of Geochemistry and Petrology, ETH Zentrum, Clausiusstrasse 25, 8092 Zurich, Switzerland

Abstract

Convergence between Laurentia and Gondwana eventually led to the consolidation of Pangaea during the late Paleozoic. This long lasting plate interaction gave rise to belts of HT-HP rocks, which characterize a large part of the northwest portion of the Sierra Nevada de Santa Marta Massif (SNSM) in the Northern Andes of Colombia, where a tilted metamorphic lower crustal section is preserved. Field and petrological observations coupled with zircon U-Pb LA-ICP-MS geochronologic data from 17 samples of igneous and metamorphic rocks, together with whole rock and trace element geochemistry, are used for reconstructing the evolution of this strongly remobilized crustal section that was juxtaposed against a low-grade metamorphic terrane during the late Paleozoic. The metamorphic evolution is asserted by means of several geothermobarometers and yields (Grt+Bt, Hbl+Grt, Hbl+Pl+Qtz, GASP and Ti-in-Zr) and can be tracked by P-T conditions, allowing the differentiation of at least two metamorphic phases identified by their mineral paragenesis. Our results provide new constraints for the palaeogeographic reconstruction of the relative position of Laurentia and Gondwana during the middle Permian to Early Jurassic. This reconstruction is defined by the interaction of the NW margin of Gondwana with Central American and Mexican terranes during Pangaea amalgamation. An evolutionary scenario for this supercontinental cycle is proposed in several phases defined by arc inception, timing of metamorphism, and late exhumation of lower crustal segments. The closure of the Rheic Ocean (ca. 290 Ma) marks the start of interaction of crustal blocks during Pangaea assembly that caused 1) post-collisional anatectic melts at ca. 278±0.5

Ma and maximum crustal thickening, 2) Barrovian type metamorphism peak *P-T* conditions (13 kb, 840ºC) at ≈ 254 Ma followed by 3) slab retreat and delamination, 4) orogenic collapse, 5) thermal weakening, crustal extension and underplating of mafic crust that caused *HT-LP* metamorphism (5.6 kb, 550ºC) at ≈ 225 Ma marking a rifting phase. These processes were accompanied by the infilling of a back-arc basin that accumulated at least 2000 m of volcanoclastic sediments provided by the adjacent arc, and towards the basement highs fringed by carbonate platforms. By ~216 Ma most of the conjugated margin was removed, but remnants of this Permian arc are still preserved in the Oaxaquia, Acatlán, and the Maya blocks. The crustal attenuation responsible for rifting and drift contributed to an eventual isostatic rebound of the subducted Pacific slab that reactivated arc activity during the Jurassic. By this time, the arc migrated into a continent-ward position, and the former back-arc basin turned into a fore-arc depocenter accumulating at least an additional burden of ≈ 5000 m of volcanoclastic deposits. This evolutionary scheme comprises an age span of 60 Myr from the Alleghenides collision to Pangaea break-up at this portion of the Northern Andes.

Key words: Lower crustal sequence, Peri-Gondwana correlations, Barrovian metamorphism, Pangaea, U-Pb Geochronology, P-T paths.

1. INTRODUCTION

Paleogeographic reconstructions and geodynamic models support the closure of the Rheic Ocean from Carboniferous to Permian times. The Rheic Ocean closure in eastern Pangæa was almost complete during the Mississippian with the onset of the Variscan orogeny (Franke, 2006; Nance et al., 2012). In western Pangæa, the closure of the Rheic Ocean and onset of crustal thickening occurred during the middle Permian. Because of this long lasting deformation during Pangæa formation, the Variscan-Appalachian-Ouachitan-Marathon and Huastecan mountain ranges constituted a continuous but diachronous late Paleozoic mountain belt, referred to as the Alleghenides (Pindell and Dewey, 1982; Pindell, 1985).

In the northwestern South American Andes (Fig. 1), remnants of the late stages of amalgamation of this colossal mountain belt are preserved in isolated blocks, in which

Precambrian Gondwanan inliers are juxtaposed against Permo-Triassic meta-igneous and meta-sedimentary rocks probably related to an accreted arc. However, little is known about the geodynamic evolution of these blocks and how they came to interact during two major phases of this supercontinental cycle: 1) timing of metamorphism and igneous activity involved during arc collision, crustal thickening, metamorphic peak, thermal re-equilibration and 2) late post-orogenic collapse crustal attenuation, rifting and drifting, which culminated in Pangæa break-up.

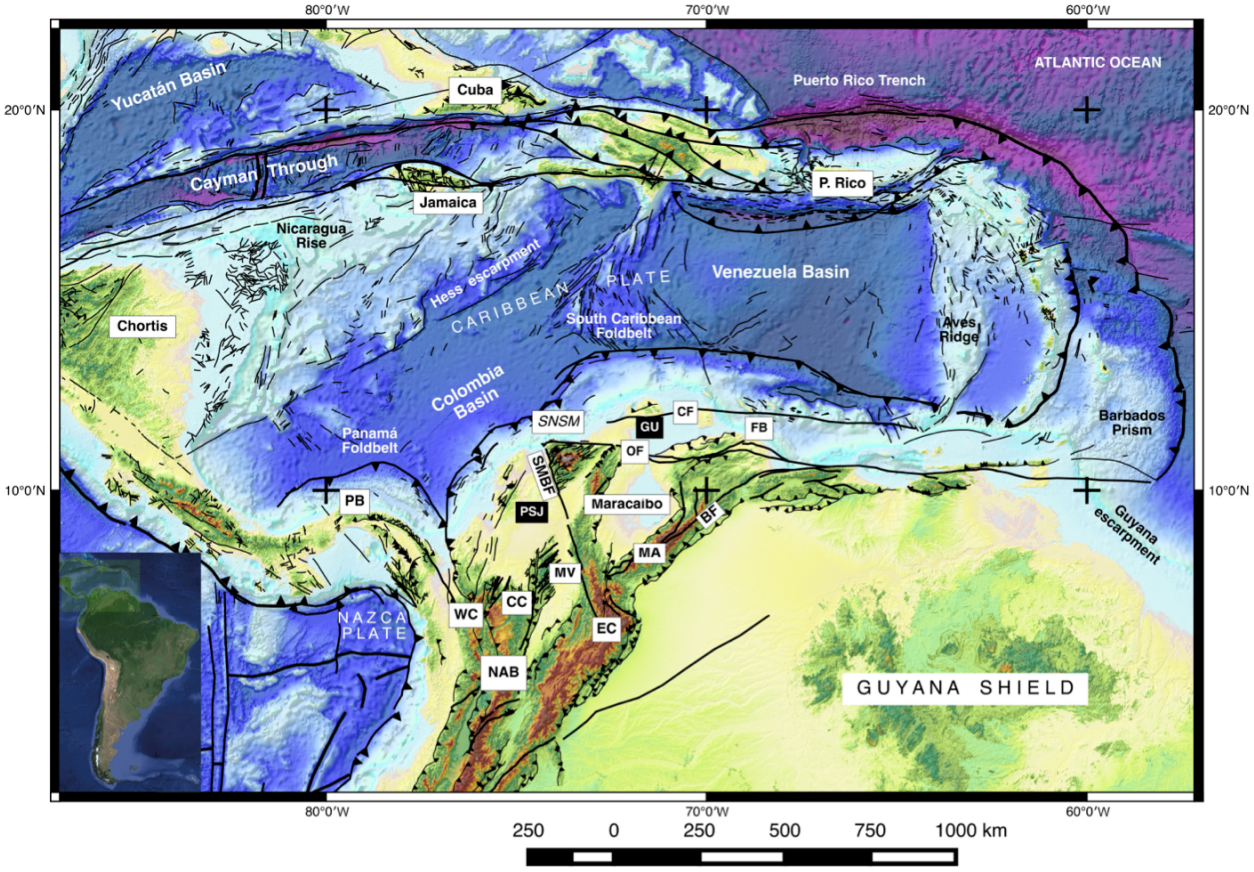

Figure 1. Regional tectonic map of the Caribbean realm showing the most relevant geological features intervening in the plate boundary configuration. After (Veloza et al., 2012). Elements of the North Andean Block (NAB): Maracaibo block, SNSM: Sierra Nevada de Santa Marta, OF: Oca Fault, CF: Cuisa Fault, SMBF: Santa Marta-Bucaramanga Fault, GU: Guajira Basin, PSJ: Plato-San Jorge Basin MA: Mérida Andes, BF: Boconó Fault, FB: Falcon Basin, WC: Western Cordillera, CC: Central Cordillera, EC: Eastern Cordillera, MV: Magdalena Valley, PB: Panamá Block.

This study presents new field, petrological, geochronological, and geochemical data, as well as thermobarometric estimates from an inverted lower crustal section of the Sierra Nevada de Santa Marta Massif in the Northern Andes of Colombia. The lithology of the Sierra Nevada de Santa Marta holds evidence of an orogenic cycle were the accretion of allochthonous terranes to NW Gondwana played a major role during Pangæa assembly. These new data provide constraints on the timing of igneous activity, the metamorphic peak during Pangæa assembly, and the later fragmentation of Western Pangæa within the western Tethys supercontinental cycle, which led to decompression and crustal thinning.

Here, we focus on the HT-HP Permo-Triassic units associated with the Inner Santa Marta Metamorphic belt, and Permian to lower Jurassic meta-sedimentary rocks of a fore-arc basin associated with the two-stage evolution of a colliding Permian arc and later arc migration into the continental domain (Fig. 2 & 3). Our aims are: 1) to redefine the stratigraphy of the provinces that make up the Sierra Nevada de Santa Marta: the Sevilla Metamorphic Belt, the Inner Santa Marta Metamorphic belt, and the Outer Santa Marta Metamorphic belt, 2) To constrain the age of the metamorphic events that occurred along the continental margin during crustal thickening that led to thermal re-equilibration during the Pangæa assembly. 3) To estimate the P-T conditions operating during the metamorphic phases, and 4) to propose a kinematic model for the tectonic evolution of the NW margin of Gondwana from the early Permian to the lower Jurassic, including terrane accretion, HT-HP metamorphism, and late decompression during extension coeval with deposition of volcanoclastic rocks in a fore-arc basin.

2. GEOLOGICAL SETTING

2.1 The Massif of the Sierra Nevada de Santa Marta

The SNSM integrates, along with the Mérida Andes, the Perijá range, and the Santander Massif, the Maracaibo block. The triangular outline of this block relates to two intracontinental border faults composed of the sinistral Santa Marta-Bucaramanga on its western side and the dextral Oca-Ancón fault on its northern side. Since the Pliocene, the Maracaibo block is separated, additionally, from stable South America by the dextral Boconó fault. The Santa Marta-Bucaramanga and Oca faults meet at the western tip of the SNSM without extending into the continental slope of the Caribbean basin, suggesting they are limited to the continental crust and accommodated a northwest-directed escape, supposing a basal detachment, as envisioned by an "orogenic float" model (Audemard & Audemard, 2002).

Along with the Mérida Andes, the Perijá range, and the Santander Massif it integrates the Maracaibo block that is separated, in turn, from stable South America by the Boconó fault (Fig. 1). In the Maracaibo block, the SNSM occupies the most NW position and is separated from the Perijá range (PR) by the Cesar-Ranchería basin, which is filled with Cretaceous to Neogene marine to continental sediments that rest unconformably above a basement that varies between Precambrian granulites to Jurassic volcanoclastic and sedimentary rocks. The massifs that belong to the Maracaibo block like the SNSM and PR are fragmented as a consequence of a complex tectonic history resulting from a Jurassic Pacific slab rollback, crustal extension, and late Cenozoic

transpressive tectonics. Within these massifs the record of Jurassic back-arc tectonics is preserved. Extensional tectonics gave origin to the Central Atlantic Magmatic Province (CAMP), which followed the orogenic collapse of the Ouachita-Appalachian-Variscan mountain range during Early Triassic Pangaea break-up. The supercontinental cycle transition from the Alleghanian orogenic mountain building and collapse to Pangæa rifting to drifting can be studied in the NW metamorphic belt of the SNSM massif, where a thick sequence of Permian to Cretaceous meta-pelites and meta-volcanic rocks are juxtaposed against Precambrian basement through an upper Paleozoic suture zone (Fig. 2 & 3).

In its internal part, the crustal organization of the SNSM approximates a continent-ward dipping monocline that bends, on meeting the Caribbean crust at its western tip, into a steeply NW-dipping attitude. Above this bend, Caribbean extrusive-intrusive sequences are obducted onto crustal units of continental affinity.

By its well-defined structural setting the SNSM exposes a complex crustal profile, comprising a suite of highly mobilized high-grade sequences at its northwestern corner or base, followed by an undisturbed Meso-proterozoic basement, overlain, in turn, by unmetamorphosed Jurassic extrusive-intrusive sequences, that are capped by Cretaceous platform sediments.

These successions have been grouped into morphotectonic provinces, according to metamorphic grade and age, deformation style and lithological associations (Tschanz et al., 1974). The southwestern Sierra Nevada Province comprises a basement composed of the meso-proterozoic Mangos Granulite, which is succeded, above a major hiatus, by Lower Jurassic volcanic and volcanoclastic sequences and plutons of a Jurassic arc. This province is separated from the Sevilla Belt by the Sevilla Lineament,

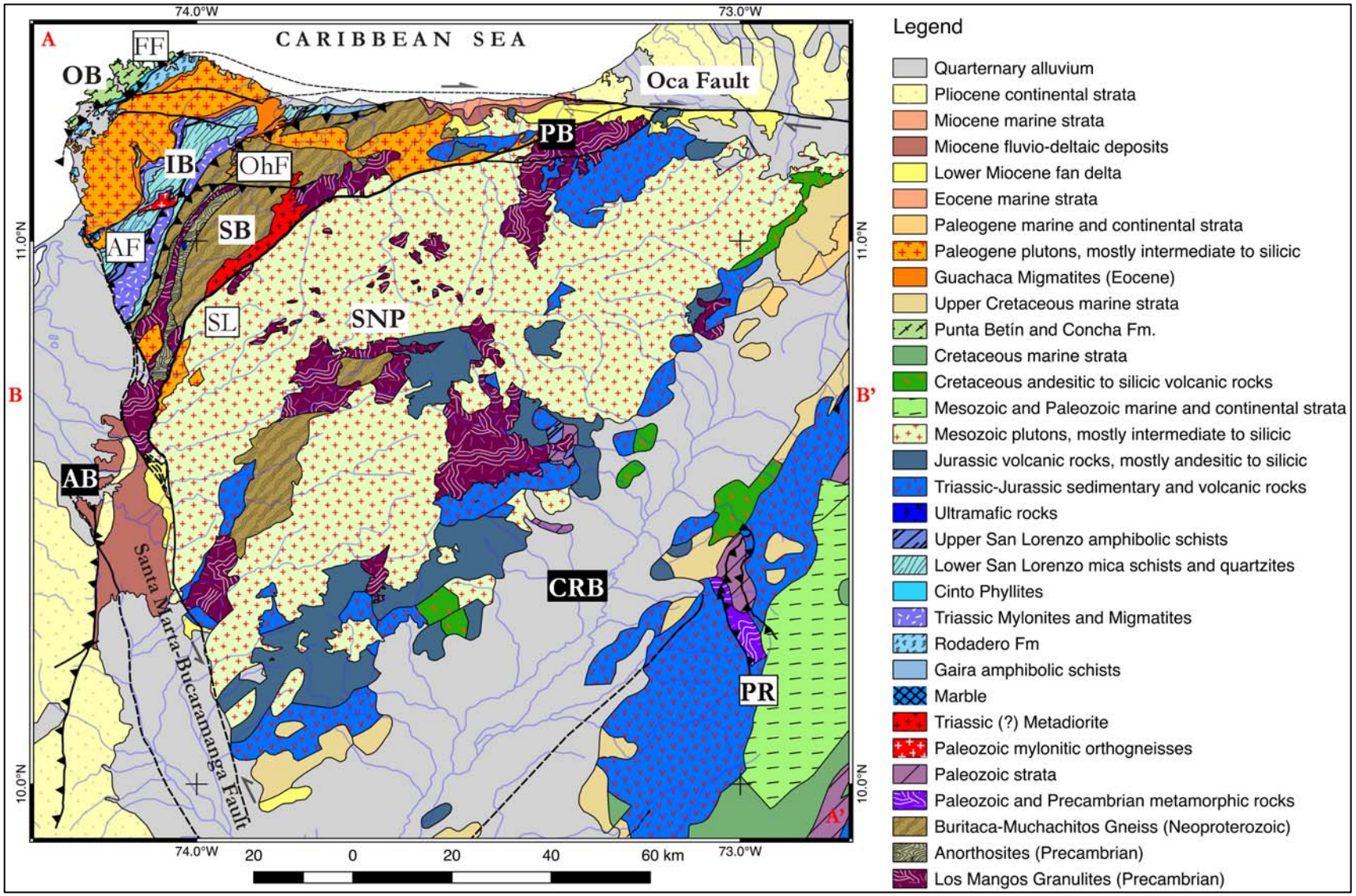

Figure 2 Geological Map of the Sierra Nevada de Santa Marta Massif. SNP: Sierra Nevada Province, SB: Sevilla Belt, IB: Inner Santa Marta Metamorphic Belt, OB: Outer Santa Marta Metamorphic Belt. AB: Aracataca Basin, PB: Palomino Basin, CRB: Cesar Rancheria Basin. Faults: SL: Sevilla Lineament, OhF: Orihueca Fault, AF: Aguja Fault, FF: Florin Fault. Updated from Ingeominas (2007a).

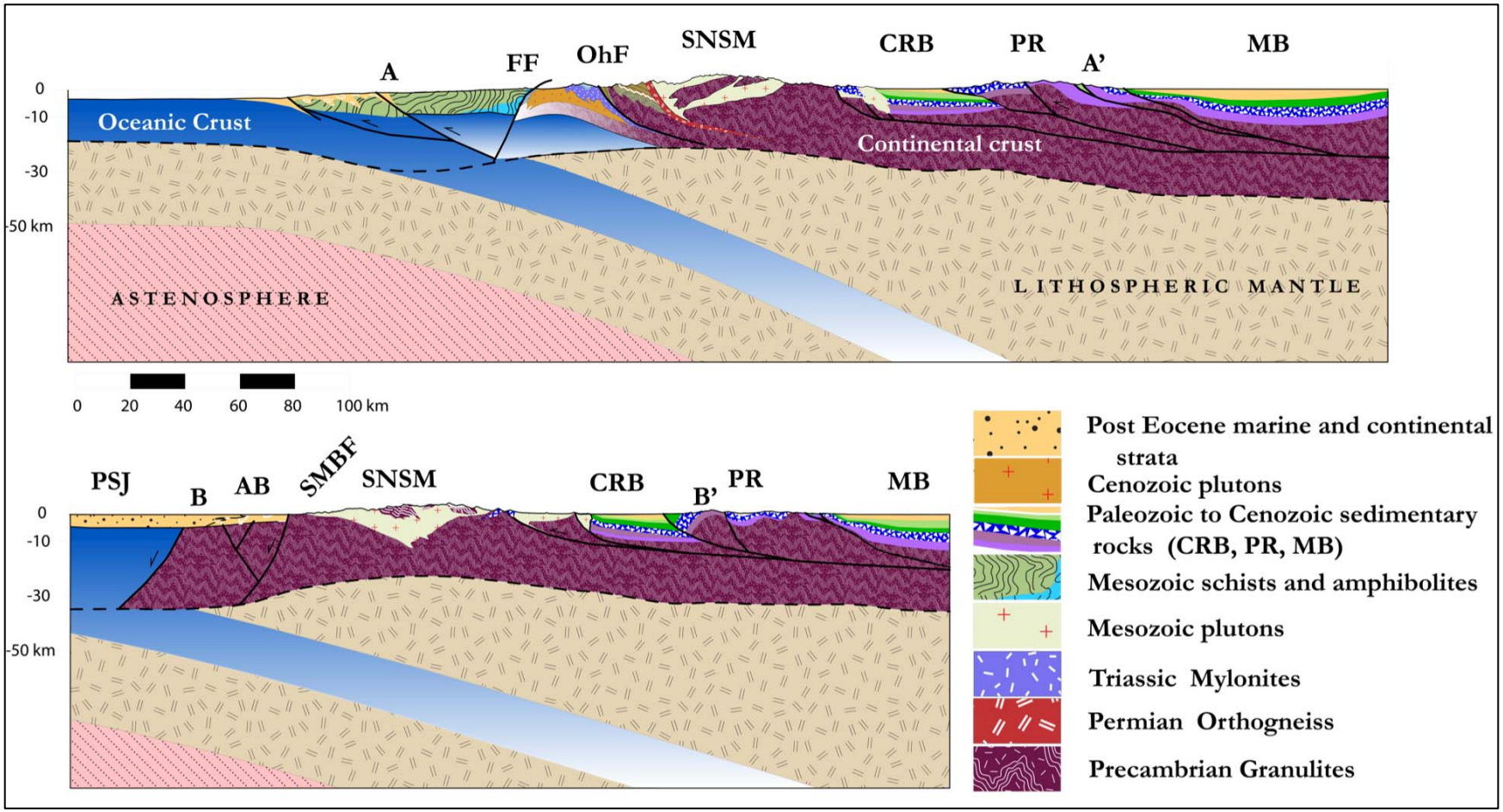

Figure 3. Regional cross sections of the SNSM, locations in fig 2 labeled y letters A-A' and B-B'. AB: Aracataca Basin, PB: Palomino Basin, MB: Maracaibo Basin, PSJ: Plató-San Jorge Basin, CrB: Cesar Rancheria Basin, SMBF: Santa Marta Bucaramanga Fault, SP: Serranía del Perijá, AF: Aguja Fault, OhF: Orihueca Fault, FF: Florin Fault. Moho depth is the dashed line (ca. 16-25 km) constrained from inversion of gravity, magnetic data and integration with seismological data (Camargo, 2014; Sanchez and Mann, 2015).

that is intruded by elongated stocks of inferred late Paleozoic, Early Jurassic and Eocene ages (Tschanz et al., 1974; Cardona et al., 2010), attesting thus to repeated periods of magmatic activity.

The Sierra Nevada Province (Tschanz et al., 1974; Cardona et al., 2010) bounded to the northwest by the Sevilla Lineament is relatable to the Sunsas-Putumayo province that was juxtaposed against the South American Craton, during the amalgamation of Rodinia (Ibanez-Mejia et al., 2011). Several metamorphic episodes affected the NW part of Gondwana, with a major Neoproterozoic HT-HP metamorphic event (Ordóñez et al., 2002; Restrepo-Pace et al., 1997). These Precambrian granulitic and gneissic terranes compose the NW part of Gondwana and were isolated from other continental blocks by the Iapetus Ocean between Laurussia and Gondwana, and subsequently by the Rheic Ocean (Nance et al., 2012).

Most of the Sierra Nevada Province is extensively affected by Jurassic arc plutons and covered by Triassic and Jurassic volcanic deposits (Fig.s 2 & 3), which are more evident on the SE flank of the massif in the vicinity of the Cesar-Rancheria basin, where bi-modal volcanic flows and associated felsic batholiths alternate with siliciclastic and carbonate sequences.

The Sevilla Metamorphic Belt (SB), albeit of its lithologic diversity, has not been differentiated into tectonic units. The SB contains medium to high-grade metamorphic mafic gneisses of a supposed Paleozoic age (Cardona et al., 2006; Tschanz et al., 1974; Zuluaga and Stowell, 2012).

The metamorphic assemblage at the northwestern corner of the SNSM composes the Santa Marta province (Tschanz et al., 1974) and can be subdivided into two metamorphic belts, which are separated by the Eocene Santa Marta Batholith (SMB).

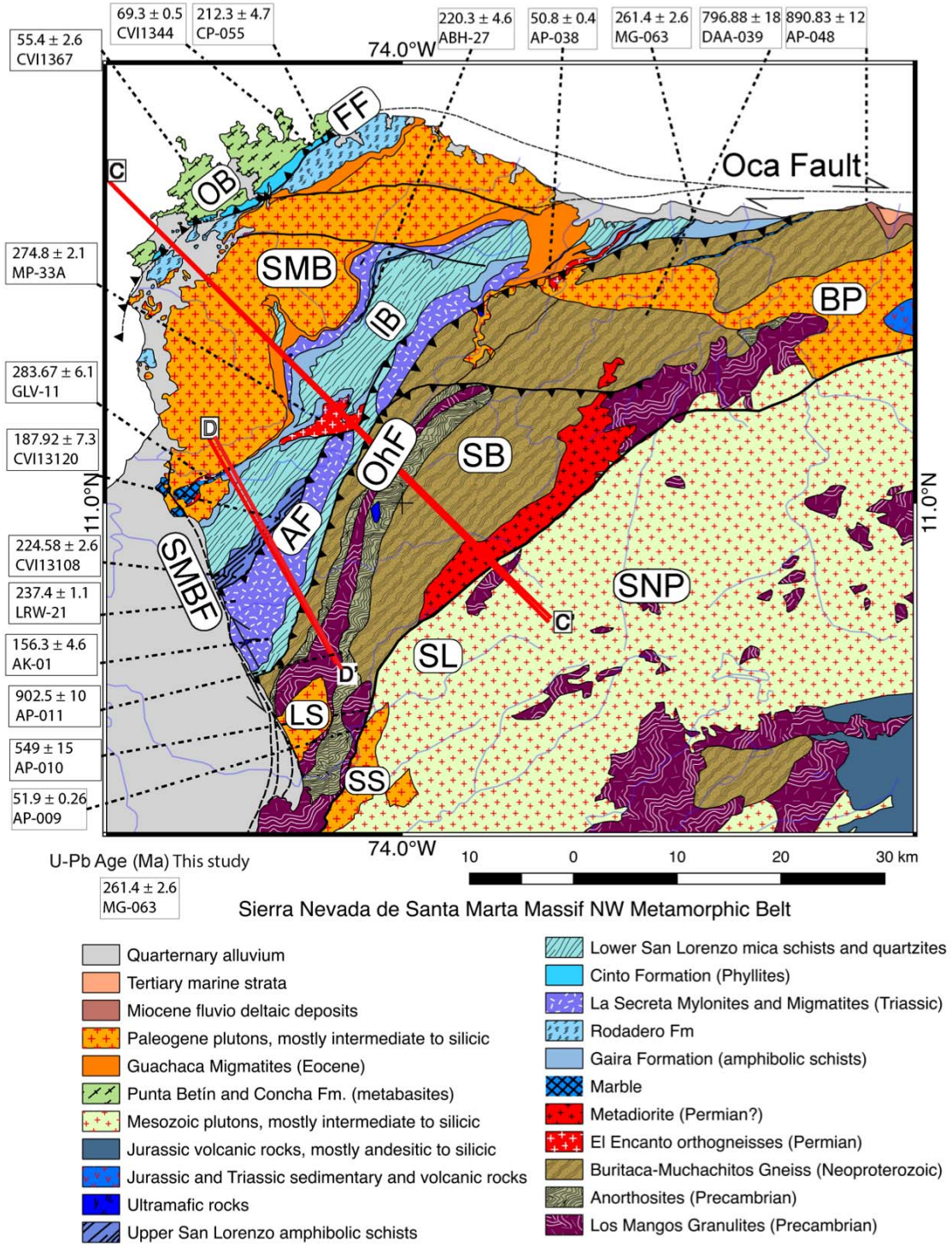

Figure 4. Geological Map of the Sierra Nevada de Santa Marta Massif (SNSM). C-C' and D-D' locates cross sections of figures 5 & 6. OB: Outer Santa Marta Metamorphic Belt, SMB: Santa Marta Batholith, IB: Inner Santa Marta Metamorphic Belt, SB: Sevilla Metamorphic Belt, SNP: Sierra Nevada Province, SL: Sevilla Lineament BP: Buritaca Pluton, SS: Sevilla Stock, LS: Latal Stock, SMBF: Santa Marta Bucaramanga Fault, AF: Aguja Fault, OhF: Orihueca Fault, FF: Florin Fault.

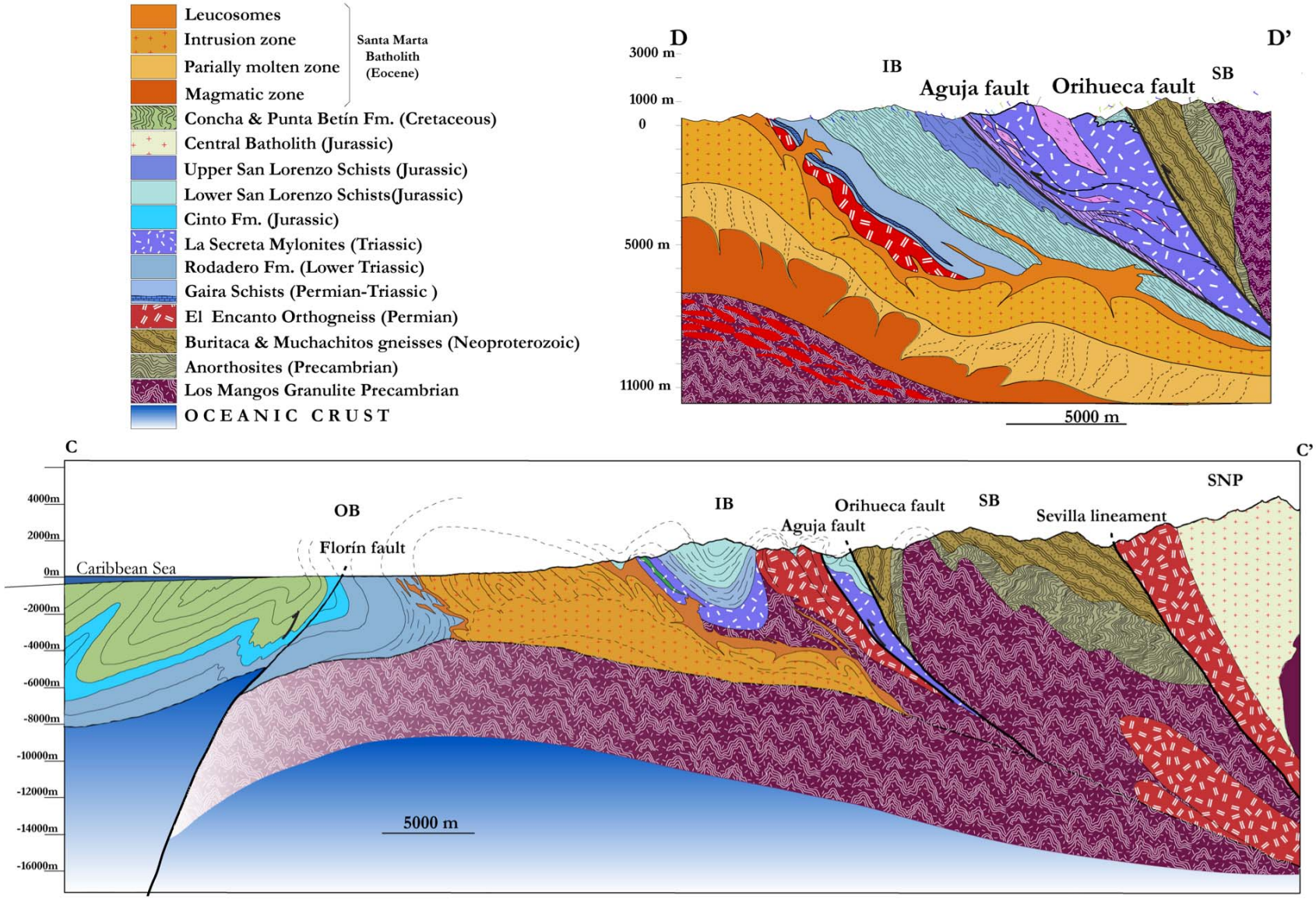

Figure 5. Sections C-C' and D-D' illustrating the structural style of the SNSM. OB: Outer Santa Marta Metamorphic Belt, IB: Inner Santa Marta Metamorphic Belt, SB: Sevilla Metamorphic Belt, SNP: Sierra Nevada Province.

The inner Santa Marta Metamorphic Belt (IB; Figs. 2 & 4) contains epidote-amphibolite to high amphibolite facies rocks from the Gaira and San Lorenzo schists and mylonites that overly Permian granitoids and are in turn intruded by Cretaceous-Paleogene granitoids. The Outer Santa Marta Metamorphic Belt (OB; Fig. 2) is defined by greenschist to epidote amphibolite facies meta-pelites and meta-volcanic rocks of Jurassic-Cretaceous age from the Rodadero, Cinto, Punta Betín and Concha formations that constitute the NW verging overturned flank of an antiform (Doolan, 1970), nucleated by the SMB (Figs. 3 & 5).

3. METHODS

3.1 LA-ICP-MS U–Pb Geochronology

Tracing the timing of metamorphism and igneous activity of the morphotectonic provinces of the SNSM was attempted by LA-ICP-MS U-Pb dating. U-Pb dating was done in conjunction with the morphological analysis of zircon crystals with cathodoluminescence imagery. Coherence of results was checked by integrating age data with other geologic information, such as field relationships, mineral paragenesis, and stratigraphy.

Zircon U-Pb ages were obtained for 17 samples. Zircons were extracted using conventional mineral separation techniques, including rock crushing, sieving (250-60 µm fraction), and mineral concentration was carried out by means of heavy liquid and magnetic separation. Detrital zircons (50 to 200 grains per sample) were manually picked, selecting clean, crack and inclusion-free grains. Subsequently polished grain epoxy mounts were coated with graphite and imaged at the Institute of Geochemistry

and Petrology of the ETH at Zürich, Switzerland using a Vega ©Tescan MV2300VP SEM, to create a detailed set of panchromatic cathode-luminescence images. Laser ablation spots were selected, in both grain cores and rims.

LA-ICP-MS were carried in zircons ablated with a NewWave UP-193nm Ar-F excimer ablation system coupled to a PerkinElmer PE SCIEX Elan 6100 ICP-MS to measure Pb/U and Pb isotopic ratios. The following parameters were applied during this process: 30 µm diameter beam size, 10 Hz repetition rate, 30–45 second signal and a beam intensity of 2.2–2.5 J/cm^2. Reproducibility of U-Pb data was monitored by measurements of GEMOC GJ-1 CA-ID-TIMS ^{206}Pb–^{238}U age of 608.5 ± 0.4 Ma (Jackson et al., 2004), used as a primary standard. The external reference standards Plešovice 337.13 ± 0.37 Ma (Sláma et al., 2008), and TEMORA 1 416.75±0.24 Ma (Black et al., 2003), were used to calibrate and monitor fractionation and consistency in the measured U–Pb dates. Ages were calculated using LAMTRACE (Jackson, 2008). Additional data reduction details are given by Ulianov et al. (2012). Statistical analyses of zircon data were performed using Isoplot 3.71 (Ludwig, 2003). All discordant (> 1–3%) analyses of magmatic zircons were discarded. Only zircons with concordance greater than 90% were accepted and plotted. Analytical results are presented in Table A1, Trace element compositions are presented in Table A2. Zircon trace element data obtained by LA-ICP-MS U-Pb were normalized to primitive mantle (McDonough and Sun, 1995).

3.2 Microprobe analyses

Mineral chemistry has been studied by microprobe analysis on thin-sections, using a JEOL JXA-8230 microprobe at the ISTerre, Université Grenoble Alpes, with 15 kV acceleration potential and 10 nA beam current. Representative analyses of minerals are presented in Table A3. Acquisition of the garnet x-ray maps was done on the same microprobe with 15 kV acceleration potential, 100 nA beam current and 300 ms counting time.

3.3 Whole rock geochemistry

Whole-rock analyses were performed at the ALS LTDA labs facilities in Medellin, Colombia and are presented in Table A4. Concentrations of major oxides and trace elements were determined by atomic emission spectroscopy (ICP-AES) and inductively coupled plasma – mass spectrometry (ICP-MS) respectively in accordance with the following procedure: A prepared sample (0.200 g) is added to ($LiBO_2$ /Li_2 B_4 O_7) lithium metaborate/lithium tetraborate flux (0.90 g), mixed and fused in a furnace at 1000°C. The resulting melt is then cooled and dissolved in 100 ml of 4% nitric acid/2% hydrochloric acid. This solution is then analyzed by ICP-AES and the results are corrected for spectral inter-element interferences. Oxide concentration is calculated from the determined elemental concentration and the result is reported in that format.

If required, the total oxide content is determined from the ICP analyte concentrations and loss on Ignition (L.O.I.) values. A prepared sample (1.0 g) is placed in an oven at

1000°C for one hour, cooled and then weighed. The percent loss on ignition is calculated from the difference in weight.

We analyzed our results with Ancomp (Röhr, 1997), a DOS program that compares bulk rock analyses finding the most similar values in a database of 3591 analyses of igneous, sedimentary and pyroclastic rocks. We complemented this dataset by compiling published geochemical data from the Northern Andes (Bosch et al., 2002; Bustamante et al., 2012; Cardona et al., 2010b, 2010c; Cochrane et al., 2014a, 2014b, 2014b; Colmenares, 2007; John et al., 2010; López et al., 2014; Mamani et al., 2010; Riel et al., 2013; Spikings et al., 2015; Villagómez et al., 2011a; Vinasco et al., 2006) in order to increase statistical confidence. The output table is included as Table A5 with major oxide composition of analyzed samples and a list of the ten samples whose composition are the most similar. The results are calculated in both: absolute difference of wt% and log wt% oxides for comparison. Protolith discrimination diagrams are used for evaluating data in a petrographic and field context to obtain a coherent and reliable discrimination of the protoliths of the metamorphic rocks studied in the SNSM.

4. RESULTS

4.1 Field relationships, petrography and mineralogy

4.1.1 Sevilla Metamorphic Belt

The Sevilla Metamorphic Belt SB is a strongly deformed NE-SW striking, and NW verging gneissic complex, some 20 km thick and 75 km long (Figs. 2, 3, 4 &5). The SB is genetically related with the high-grade metamorphic rocks of the Sierra Nevada

Province. It consists of amphibole and quartz-feldspathic gneisses rich in hornblende, biotite, pyroxene, and amethyst, these gneisses commonly exhibith cataclastic textures (Muchachitos and Buritaca gneiss suites), interdigitaded with undifferentiated amphibolites, mica-schists, quartzites, diopside marbles and ultramafic pockets (Tschanz et al., 1974). These metamorphic rocks had predominantly vulcano-sedimentary protoliths that experienced high amphibolite to granulite facies metamorphism.

The NE boundary of the SB with the IB has not been clearly defined, and we therefore propose that the high-grade Muchachitos and Buritaca gneiss, should be grouped into the SB, these high-grade units nucleate an antiform and expose the lower crust. The SB is separated from the SNP by the Sevilla lineament, granulites are common at the SNP and mostly intruded by Jurassic felsic plutons. The Sevilla Belt and Inner Santa Marta Belt are separated by The Orihueca fault that thrusts the high-grade complexes of the SB onto the medium-grade complexes (Figs. 5 & 6) of the IB (El Encanto orthogneisses, la Secreta Mylonites, and San lorenzo and Gaira Schists). This limit is proposed regarding all the available field and geochronological data. Chronologic relationships will be discussed in detail in section (5.1).

4.1.2 Inner Santa Marta Metamorphic Belt

The Inner Santa Marta Metamorphic belt is the morphotectonic province that shows the most prolific lithologies in the entire SNSM, with metamorphic grade ranging from greenschist to high amphibolite facies. The older unit of orthogneisses underlies this suit of paraschists. Internally, the IB is further subdivided by the Aguja fault that

separates medium grade garnet-sillimanite bearing mylonites to the SE from mica-amphibole-epidote schists to the NW (Figs. 5 & 6).

El Encanto Orthogneiss

The El Encanto Orthogneiss outcrops are isolated and show lobular and elliptical shapes. The typical texture of these granitoids is coarse-grained with bands composed of amphiboles and plagioclase. Mineral lineation is strongly developed in some locations with L-type tectonic fabrics, with a NE attitude almost parallel to the strike of the regional foliation, which shows ductile deformation in quartz veins arranged in ptygmatic folds (Fig. 7d).

The contact with paraschists is of a non-intrusive nature and clearly suggests that the orthogneisses are the oldest unit underlying the paraschists of the Gaira and San Lorenzo formations. Discrete outcrops of El Encanto Orthogneiss occur in the Valencia creek in the northern foothills of the SNSM (Cardona et al., 2010c), were it had been described but not formaly named. New outcrops of this unit have been identified in the Encanto creek, about 10 km to the SW of the Valencia creek, in an intrusive contact with nebulitic diatexites from Eocene migmatization. Furthermore, outcrops exist close to Minca in the very core of the IB at Jueves Santo and Viernes Santo creeks (Figs. 4 & 5). There is a discordant contact with amphibolite, mica schists, and mylonites rich in biotite and garnet. In the vicinity of the Cienaga Marble quarry near the Córdoba River, the El Encanto orthogneiss is in contact with dark green amphibolites of the Gaira schist unit (Figs. 5 & 6).

La Secreta Mylonites

A 45 km long and 3-6 km wide belt of mylonites is present in the hanging wall of the Aguja fault. The mylonites dip in a SE direction that follows the Aguja fault plane attitude. This strongly tectonized basement overrides metasedimentary sequences of the Gaira hornblende schists and San Lorenzo mica schists, and in turn is thrusted by Precambrian gneisses through the Orihueca fault (Figs. 5 & 6). The best exposure of these mylonites is found at La Secreta Creek on the western flank of the SNSM (Fig. 7b). Previously, the mylonite belt was included in the SB together with the Buritaca gneiss, and drawn a very diffuse NW boundary on the SNSM map of Tschanz et al. (1974).

Towards the SE boundary of the IB, Hbl, gneisses acquire a migmatitic appearance, as they display layers or lenses of leucocratic segregations set into a relatively homogeneous micaceous matrix. Where leuco- and mesosome produce a relatively continuous banding these migmatite-like rocks obtain a stromatic structure.

Lens-like leucosome segregations and mineral aggregates confer to these gneisses a phlebitic or ophthalmitic structure. Flow structures around felsic mineral aggregates and lenses of mafic fragments are associated with strain shadows related to these competent parts and attest to deformations that accompanied these segregation processes.

Foliation trends parallel to lithologic boundaries and major faults in the IB and dips SE. Subhorizontal to moderately inclined mineral aggregate lineations are ubiquitous in gneisses containing plagioclase porphyroblasts, that constitute the mesosome of this rock association. A top to NE dextral shear sense was locally deduced from, mineral fish, C-bands, strain shadows and mantled feldspar porphyroclasts that define a stair-stepped array and deformation bands.

Mylonitized gneiss can be subdivided into garnet-biotite schists derived from pelites and amphibolites of a probable vulcano-sedimentary origin. These medium grade mylonites show recrystallized quartz with undulate extinction, red biotite fish deviates of the mylonitic foliation around garnet porphyroblasts formed in strain shadows (Figs. 6 & 7c).

The mylonitic zone typically consists of biotite-amphibole gneiss with plagioclase and garnet forming porphyroblasts. Schists include phenocrysts of up to 2 cm of garnet embedded in a biotite matrix, the restite consists of amphibolite (Fig. 7a).

Biotite schist paragenesis consists of Bt+Grt+Qtz+Pl. The amphibole gneiss paragenesis is Hbl+Grt+Pl+Bt+Qtz+Czo+Sph. Amphibole crystals are brown in their core and grade to green with undulated pleochroism at the rim. Close to the Aguja fault, high-grade mylonite paragenesis consists of Sil+Grt+Bt+Qz+Pl+Or+Ms. Kinematic markers such as folds formed in strain shadows, porphyroblasts with stepped wings, and shearbands flanking boudins indicate a dextral shear sense (Figs. 7c). The remobilization under amphibolite facies conditions produced simple shear constriction, which is evidenced by a subhorizontal lineation. Leucocratic bands of Qtz+Pl+Grt are parallel to foliation and evidence a sub-solidus segregation remobilization, resulting in a phlebitic to stromatic metatexite texture. Sheath folds are common in shear zones (Fig. 7b).

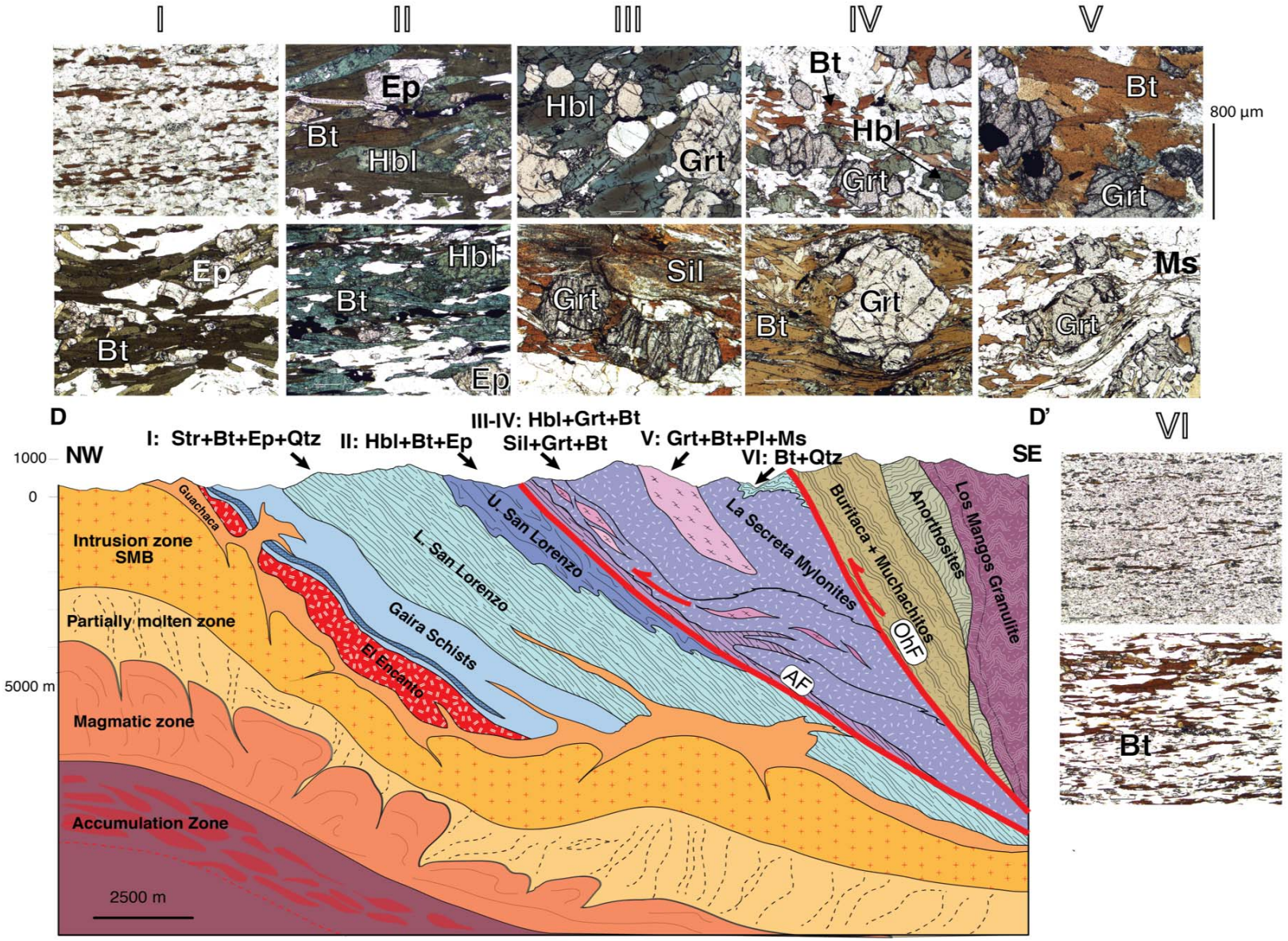

Figure 6. Aguja Creek cross section, unit labels according to the Figure 2. AF: Aguja fault, OhF: Orihueca fault. Top petrographic slides show paragenesis labeled in roman numbers on top of images and with its corresponding location at section, mineral abbreviations are indicated. I: Lower San Lorenzo Schists, II: Upper San Lorenzo Schists, III+IV+V: La Secreta Mylonites, VI: San Lorenzo Schists (quartzites) . The magmatic zones at the SMB are adapted after Vanderhaeghe (2009).

Gaira Schists

The Gaira schists defined by Tschanz et al., (1974), consists mainly of dark green amphibolites and schists, including marble levels, biotite and graphite schists and ultramafic rocks. Although in the OB the Gaira Schist has been divided into several different units (Doolan, 1970), for the IB the original definition is preserved. Amphibolite foliation resembles original sedimentary layering of the protoliths and is common to find minor interlayering of muscovite-biotite schists and a thick marble level at the base, and intercalations with schists whithin the unit.

Gaira schists are unconformably overlain by the metapelitic San Lorenzo schists. At the lower contact with la Secreta Mylonites Bt+Grt+Pl mylonitic schists locally show stromatic metatexite textures.

For the Gaira schists an approximate thickness of ≈ 2000 m of amphibolites interbedded with marble layers and biotite schist is estimated (Figs. 5 & 6). However, the Gaira schists can easily double this thickness when including the mylonitic schists with low partial melting (metatexties) in the lower part of the schists. The mylonites are intruded by the SMB that originated diatexites that include mostly amphibolite restites as paleosomes and xenoliths. The lower contact of the Gaira Schists with El Encanto Orthogneiss is non-intrusive and indicates deposition of the volcanoclastic protoliths unconformably above a pre-existing crystalline unit.

Lower San Lorenzo Schists

The Lower San Lorenzo Schists includes all the pelitic schists where quartzites and Bt+Ms schists are predominant, we distinguish the underlying amphibolite unit with marble content as the Gaira Schists, and the upper hornblende schist unit as the Upper San Lorenzo Schists. Our criterion for such a division is the marked difference in composition represented by amphibole occurrence. The pelitic composition of the protolih is evidenced in the presence of aluminosilicates (Sil+Ky) in the Bt+Ms schists (Zuluaga and Stowell, 2012), and St+Grt in the graphite schists at the base. The Lower San Lorenzo Schists crops out along the road towards La Tagua, capping the San Lorenzo High (Figs. 4 & 5). This unit is also exposed in the Aguja creek and on the road north of the Aguja creek. This area was included originally in the Gaira Schists by Tschanz et al., (1974).

New outcrop localities of the San Lorenzo Schists were found at the hanging wall of the Aguja fault, and in the vicinity of the Orihueca fault, where quartzites are thrusted by the Buritaca gneiss (Figs. 3, 4 & 5), quartzites overlay the La Secreta Mylonites dipping towards the SE, extending along strike 27 km and 1.5 km (Fig. 4). Stratigraphic relationships are very complex and interpretation of the units is mainly based on geochronological data of Cardona et al. (2010b), as well as new zircon U-Pb data described in detail in section (4.3). The top of the quartzites abuts against the Orihueca fault (Fig. 3, 4 & 5) in contact directly with amethyst bearing amphibolite gneisses of the Buritaca Gneiss. Interestingly, both units show overlapping folds with parallel orientations that crosscut contacts, indicating that deformation occurred after the coupling of the two units (Fig. 7h & i). Detailed mapping is necessary to establish if an

amphibolite unit exists at the base of the unit, or if the metapelitic sequence rests directly over mylonites and migmatites of the La Secreta Mylonites.

On a regional scope, at the base of the Lower San Lorenzo Formation muscovite-biotite, quartzite schists, and quartzites, are the most common lithotypes with subordinated amphibolite schists. The average paragenesis consists of Bt+Grt+Ep+Ms+Qzt+Pl+Sil+Ky+Sph. However, aluminosilicates are subordinate. Quartzites are gray to brown, containing Qzt+Pl+Bt+Ms, with a paragneisses similar to fine grained schists with high quartz content. Biotite crystals are mostly red and locally green due to metasomatism. Quartzites are interbedded with mica schists and graphite schists that contain Grt+St+Qtz and carbonate segregation veins parallel to S1. The Bt+Ep+Pl+Qtz schists in the middle part of the Lower San Lorenzo Schists (Figs. 5 & 6) exhibit a very strong subvertical L-type tectonic lineation fabric, which is easily recognizable in the Aguja Creek, indicating a lengthening shear orthogonal to the foliation strike (Fig. 7e & g). Schists and quartzites locally present meta-andesite sills with phenocrysts in a matrix in a porphyritic relict texture. These sills contain relict Hbl, which is absent in the other lithotypes. Along with ductile deformation of boudinage in some locations, kink bands are developed within the platy minerals. Homogeneous quartzite beds are common in the middle part of the unit.

Upper San Lorenzo Schists

The best exposure so far of the Upper San Lorenzo Schists is at the tributaries that feed the Aguja Creek from SE to NW (Fig. 4). In this section, the unit is composed of hornblende schists, amphibole schists, biotite-muscovite schists interbedded with rare quartzite beds, in contrast to the more metapelitic character of the Lower San Lorenzo

Schists. The lower part of the schists exhibits the development of boudinage coeval with a very persistent mineral elongation lineation. The contact with the Lower San Lorenzo Schists is marked by the occurrence of staurolite and aluminosilicates. The paragenesis of the Upper San Lorenzo Schists consists of Hbl+Bt+Ep+Pl+Qtz+Sph. Biotite is predominantly green, and is found with Hbl+Ep (Fig. 6). Feldspars exhibit a myrmekitic texture and epidote prophyroblasts are rather common. La Secreta Mylonites is thrusted onto the Upper San Lorenzo epidote-hornblende schists through the Aguja fault (Figs. 5 & 6). Both units show very different deformation styles and metamorphic grades (Fig. 7e & f).

Guachaca Migmatites

Migmatites were caused by the intrusion of the Santa Marta Batholith granitoid suite into the units of the IB and the OB. The broad NE-SW oriented migmatite zone intrudes a sequence of mica and amphibole schists from the Gaira Schists. The best exposures on the N flank of the SNSM are located in the Guachaca River, El Encanto and El Rumbon creeks and in the central part of the IB, in the vicinity of Minca at Pozo Azul. The migmatites are always exposed in contact with the lower part of the Gaira Schists. At the Piedras River location, migmatization involved marble beds and caused skarn type contact metamorphism. To the SW the exposition of the migmatite zone is discrete and the SMB intrudes a thick sequence of marble from the Gaira Schists, with frequent mica-schist, amphibolite and orthogneiss xenoliths.

Migmatites are classified as nebulitic diatexites and are present in the border zone of the SMB. These rocks show schlieren and nebulitic textures, and eventually grade into a zone showing meso-metric leucosomes and syn-migmatitic foliation. In the more

distal parts of the pluton, clusters of granitic tabular dikes and sills crosscut the Gaira Schists in the Cinto creek at the OB. This phenomenon is observed around most of the Paleogene plutons, were they intrude the more fertile low-and medium-grade metamorphic rocks, but it is absent at the contact between the Paleogene plutons and the high-grade metamorphic gneisses of the SB, in which case a hornblendite zone marks the contact instead.

4.1.3 Outer Santa Marta Metamorphic Belt

The Outer Santa Marta Metamorphic belt (OB) consists of a sequence of mainly greenschist to epidote-amphibolite facies rocks, cropping out with a regional SE dip direction. This metamorphic suite is limited to the Southeast by the SMB and internally divided into at least two tectonic blocks by the Florin fault (Figs. 4 & 5). The metamorphic suite is grouped as the Santa Marta Schists (Tschanz et al., 1974), but can be subdivided as the Concha, Punta Betín, Cinto and Rodadero formations, based on lithological affinities and metamorphic grade (Doolan, 1970; MacDonald et al., 1971).

Rodadero Formation

The Rodadero Formation (Doolan, 1970) corresponds to S0 layered amphibolites and amphibolic schists with Hbl+Pl+Di+Bt+Ep+Czo, alternated with of quartz-feldspathic Grt+Bt+Ms schists. Inherited isoclinal folds with vertical axes show two distinctive mineral lineations, NE verging dextral faults sub-perpendicular to the foliation, and NW verging normal faults that cut in a low angle the foliation affect dikes and the host

rock. A main characteristic of this unit is that is commonly affected by felsic dikes that cut trough foliation in an oblique angle and quartz segregations parallel to S1, these melts are genetically related with the Santa Marta Batholith.The Rodadero and Cinto formations constitute the NW verging overturned flank of an antiform, which is nucleated by the SMB. Thermobarometry studies of the Rodadero Formation indicate pressures of 7.6 -9.5 Kb and temperatures of 565-665ºC in amphibole composition is concordant with Dalradian type metamorphic belt (Bustamante et al., 2009), in contrast to 5.5 Kb and 529ºC for the Cinto Formation phyllites (Cardona 2008b). The stratigraphic relationship between the two formations has therefore been interpreted as a tectonic contact through the Florin fault, because of the structural relationships and the inverse metamorphic grade.

Cinto Formation

The Cinto Formation is about 700 m thick and dips to the SE, internally the Cinto formation presents ESE verging folds. Differently from the Concha and Punta Betín formations it includes quartzites, graphite phyllites, and psephites containing Qtz+Grt+Ms+Bt. Several psephite levels with pebble-sized porphyroclasts. The layered phyllites contain regularly dissected hinges of isoclinal folds and quartz lenses parallel to S1. Graphite schists are frequently interbedded with phyllites that show relicts of cross-bedding in the more siliceous beds that indicate an overturned position.

Concha and Punta Betín formations

The phyllite units at the NW tip of the SNSM consist mainly of an array of folded slivers of oceanic crust derived material that varies in metamorphic grade from zeolite facies through greenschist facies in the coastal range (Concha Formation meta-volcanic rocks), and grade into the amphibolite facies schists of the Punta Betín Formation. Protholits of these units have a mixed oceanic and island arc signature (Cardona et al., 2010b). The base of the sequence is composed of volcanoclastic breccias with copper and calcopyrite and sulphide nodules interdigitaded with Chl+Act carbonate schists, graphite schist, quartz-phyllites, derived from pelites and tuffs of basaltic to andesitic composition (Bustamante et al., 2009) and subordinated meta-gabbros (Hbl+Pl), and andesites in dykes and sills. The presence of syn-depositional folds, slumps and relict olistostroms with lenticular geometries and an oblique cleavage evidence slope deposits associated with tectonic activity. Towards the top of the Punta Betín Formation meta-gabbros, tuffs and basalts are interbedded with exhalative siliceous deposits. Although intensely folded the Punta Betín Formation preserves a regional SE dip. In the Actinolite schists, the main metamorphic foliation S1 cuts S0 in a low angle, but with the same strike. S1 exhibits a penetrative cleavage that defines a crenulation lineation L2. L2 crosscuts in an angle of 70º an inherited L1 lineation parallel to the regional shortening. L1 is associated to a first deformation phase of lengthened fabric preserved in hinges. L2 was produced in a second phase related to strike slip tectonics (Fig. 7j, k & l). Kinematic indicators in meta-gabbros in the upper part of the Punta Betín Formation close to the contact with the Cinto Formation evidence oblique shortening.

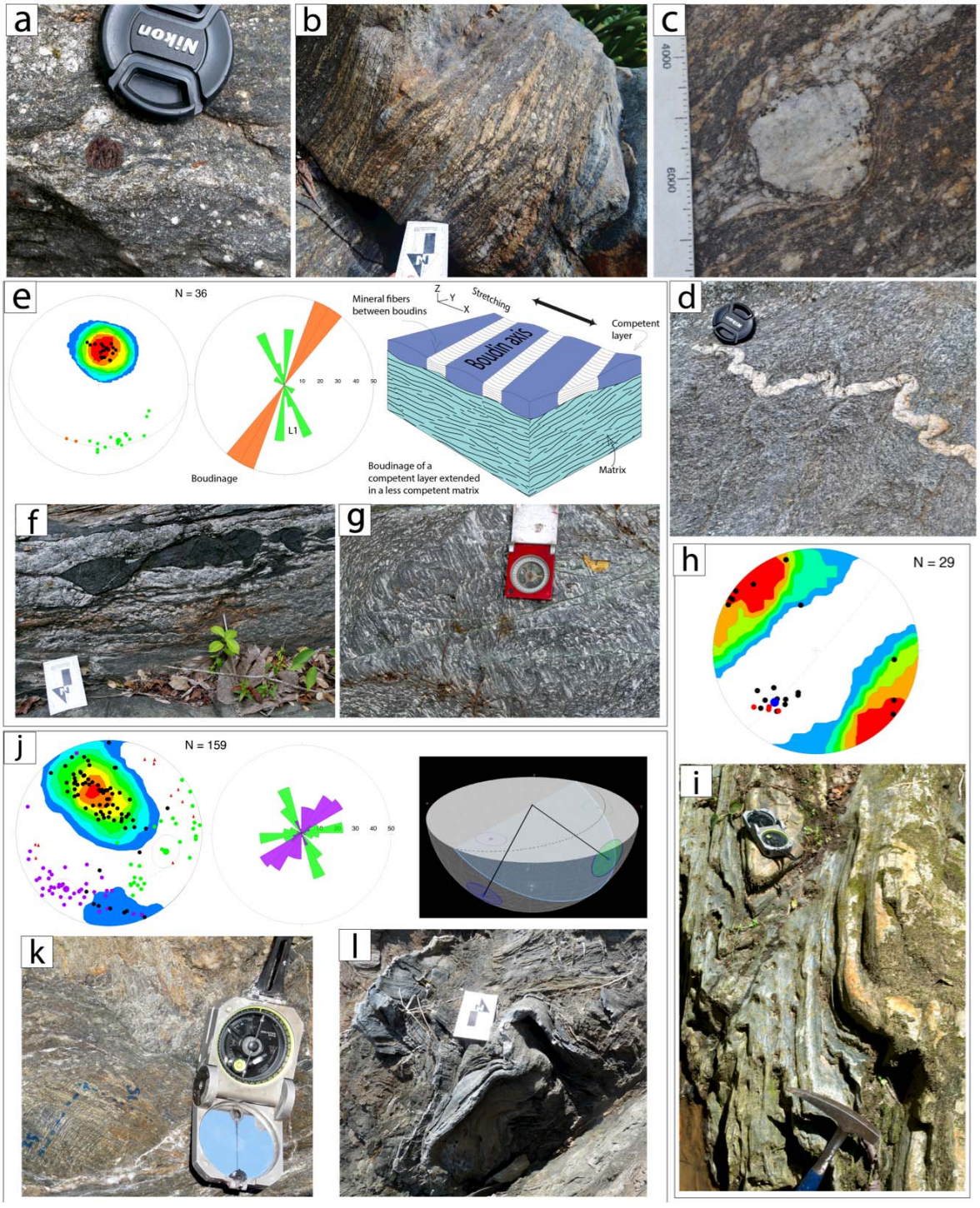

Figure 7. Main structural features of the low to medium metamorphic grade units at the SNSM . La Secreta Mylonites a) Garnet porphyroblast embedded in a Bt+Pl+Qtz matrix, b) stromatic migmatite-like structure with discontinuous leucosome segregations in an amphibolite facies Bt+Grt mylonite. c) Feldspar prophyroblast with pressure shadows showing a weak stair-stepping that indicate a dextral shear sense. d) Hbl + Pl Encanto orthogneiss; vein is affected

by ptygmatic fold. e) Stereographic projection (lower hemisphere) of foliation poles (black, contoured) and a N to northwest trending L_1 mineral aggregate lineations (green) in mica schists of the Lower San Lorenzo Schists with corresponding rose diagram with mineral aggregate lineation (green petals) and stretching direction of boudins (orange petals); inset shows boudinaged competent layer with x-direction oriented parallel to mineral lineation. f) Mafic boudin set off at shear bands and embedded within a Qzt+Pl matrix indicates a sinistral shear; Upper San Lorenzo Schists; g) L-type tectonite from the Lower San Lorenzo Schists, stretching lineation corresponds to L_1, mineral association consists of Bt+Pl+Qz; h) Stereographic projetion (lower hemisphere) of foliation poles contoured; and fold axis plunging SW of quartzites and amphibolites located NE of the Orihueca fault, i) subvertical folds at the Santa Clara creek, this deformation is found in the hanging walll and footwall of the Orihueca fault affecting the Precambrian and Jurassic units supposing that the deformation that originated this folds ocurred after coupling of the tectonic blocks of the Sevilla Metamorphic Belt and the IB; j) Compilation of poles to the foliation at the OB, L1 in green is the oldest lineation from a first folding phase, L2 transversal to the foliation is related to an overprinted deformation. k) photograph showing the interception of L1 and L2 (Concha Formation); l) Asymmetric fold with an superposed event of sinistral transpression related to L2 (Concha Formation).

4.2 Whole rock geochemistry

We included whole rock geochemistry analysis from nine samples that were also analysed by zircon U-Pb dating (Tabe A4). These samples were selected from the morphotectonic provinces described above. We focused on rare Earth elements (REE) as well as the relatively immobile High Field Strength (HFS) and transition elements (Ti, Zr, Hf, Nb, Th, Ta, Y, Cr, P, Ni, Sc). Classified at protolith discrimination diagrams (Fig. 8) based on major oxide ratios, and major oxides vs Cr.

4.2.1 High-grade metamorphic rocks from the Sevilla Metamorphic Belt

Major oxide and trace element data were acquired from a mafic migmatite from the Buritaca Gneiss (AP-010) that belongs to the lower calc-alkaline to tholeitic series (Irvine and Baragar, 1971). The REE chondrite normalized plot shows a flat slope (Fig.

9e). Primitive mantle normalized multi element analysis of this sample shows a negative Th anomaly.

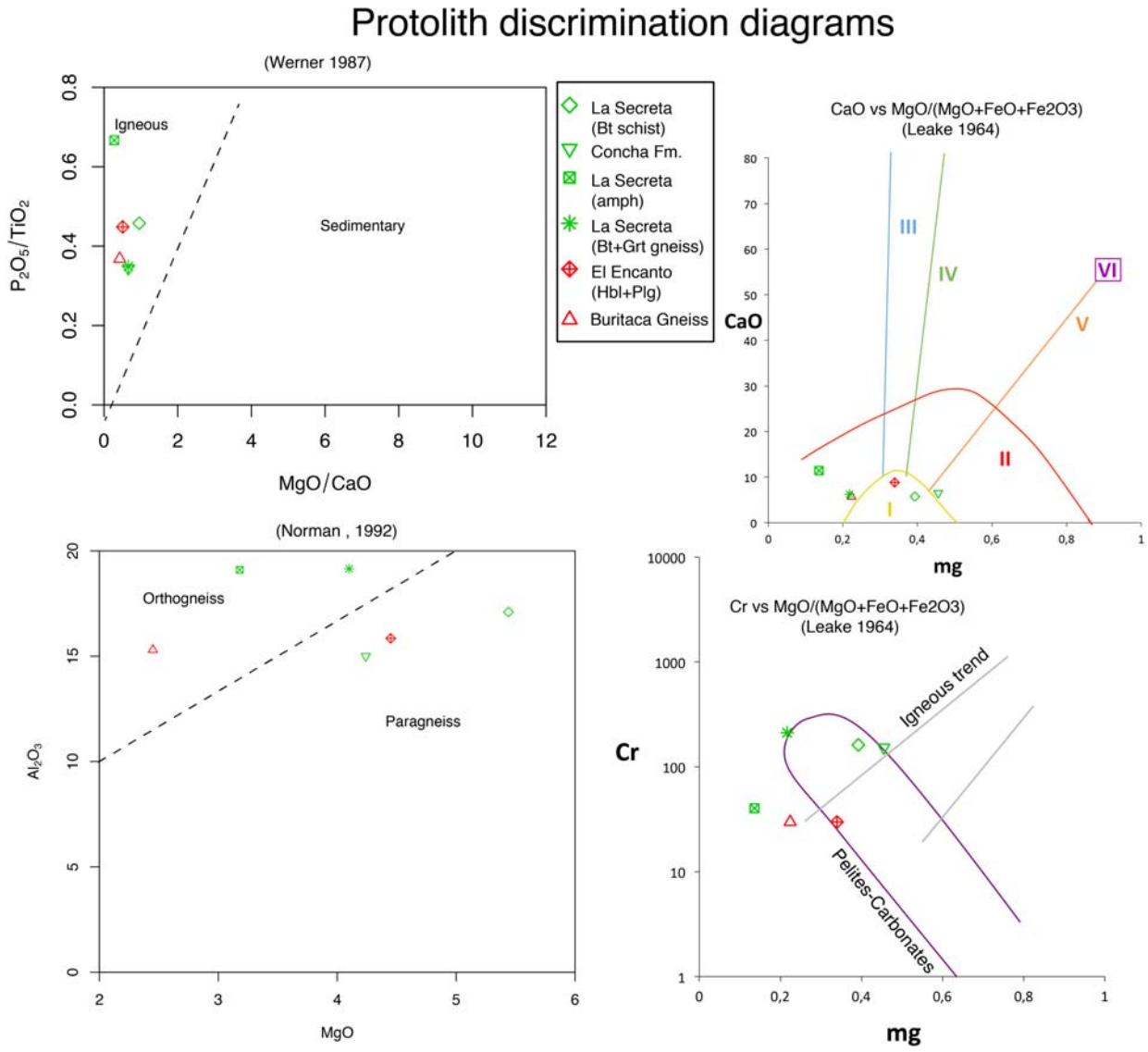

Figure 8. Protholith discrimination diagrams. (top left) discrimination between igneous and sedimentary provenance (Werner, 1987); (top righ) Diagram that shows the origin of mafic rocks based on Niggli's numbers (Leake, 1964), c =CaO; mg=MgO/ (MgO+FeO+Fe_2O_3) for amphibolites and amphibolic gneisses, I. pelites, II. Igneous rocks, III. Calcareous rocks, IV. Mixing zone between limestone and pelites, V. Mixing zone between pelites and dolomites, VI. dolomites.; (Bottom left) Al_2O_3 Vs MgO (wt%) (Norman et al., 1992); (bottom right) Diagram that shows the igneous trend for amphibolites and mafic schists (Evans and Leake, 1960), Cr= Chrome; mg=MgO/ (MgO+FeO+Fe_2O_3).

4.2.2 Amphibolite-grade rocks from the IB

Four samples from the IB, which include two garnet bearing mylonites, one garnet biotite schist, and one orthogneiss were analyzed obtaining major oxide and trace element data. Samples garnet amphibolites from the La Secreta Mylonites belong in the tholeitic field, Bt schists from la Secreta Mylonites and sample Hbl+Pl granitoid from el Encanto Orthogneiss correspond to the calc-alkaline series (Irvine and Baragar, 1971), and is classified as an orthogneiss indicated by trace element composition and high Y content as a calc–alkaline gabbro (Fig. 8).

Garnet amphibolites, plot in the field of ultrabasic rocks (Bas et al., 1986; Cox, 1979). Biotite-garnet schists according to the protolith discrimination diagrams corresponds to a volcanoclastic protolith, probably a basaltic tuff or siltstone with an important terrigenous component. Mylonites Pl+Gr+Bt is compositionally a gabbroid (Bas et al, 1986), this corresponds with a protolith discrimination that shows a mixed igneous to pelitic protolith for this sample.

The primitive mantle normalized multi element plot (McDonough and Sun, 1995) of Bt+Grt+Pl schists shows a flat to negative slope with negative Ta, Ti, Eu, Nb, and Sr anomalies. Garnet amphibolites and garnet plagioclase metaigneous sample LRW-21 show a flat profile (Fig. 9). In the mafic orthogneisses (El Encanto) Th/Ta vs Yb and Th/Hf vs Ta/Hf ratios are compatible with an active continental margin environment (ACM) (Schandl and Gorton, 2002). Garnet amphibolites correspond to the boundary between a within plate volcanic zone (WPVZ) field and ACM. Bt+Grt+Pl achists and Pl+Grt+Bt gneisses plot in the WPVZ field (Fig. 9).

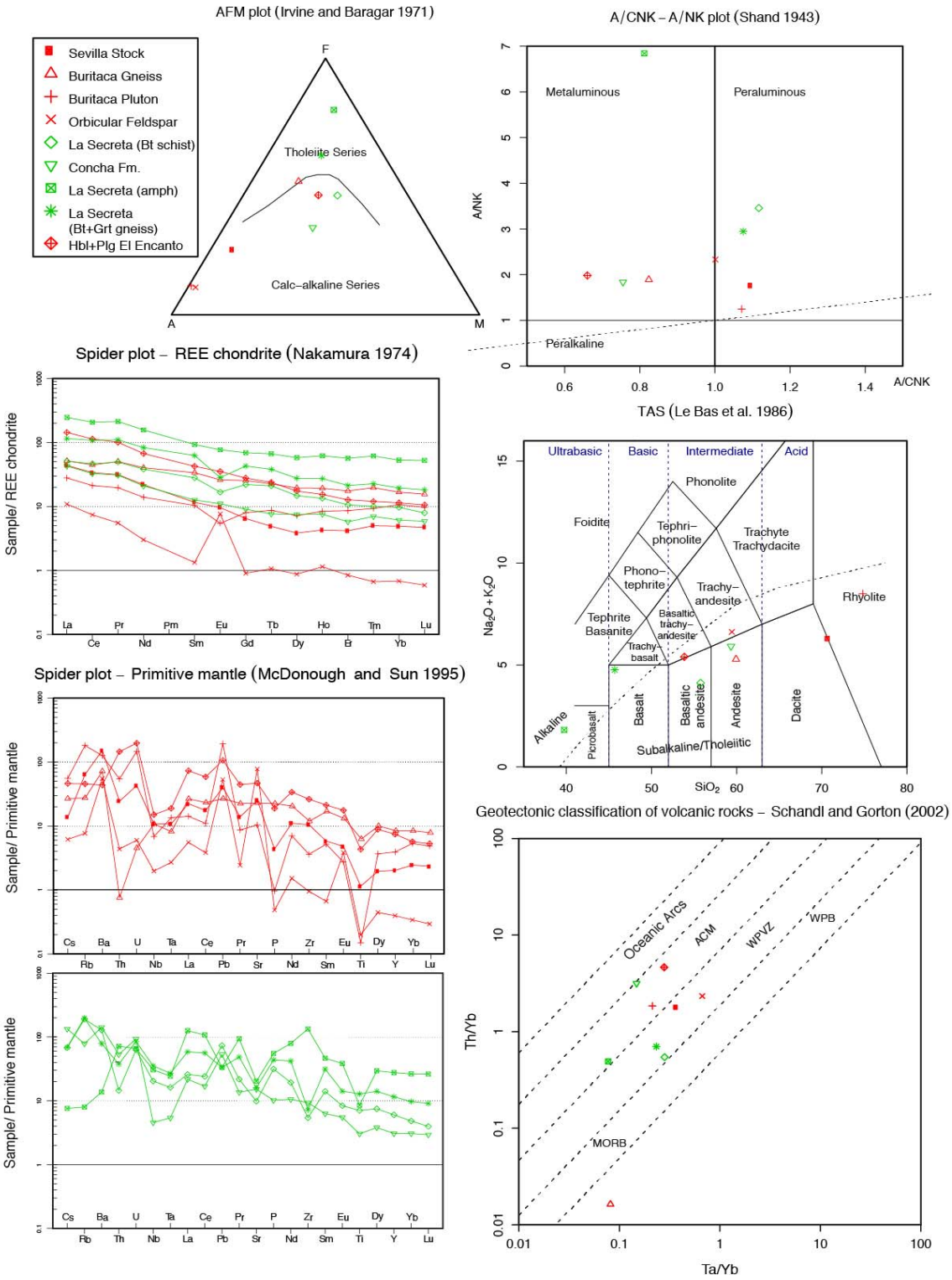

Figure 9. Whole rock geochemistry: Green represents metavolcanic rocks and red samples are related to granitoids(a) AFM diagram (Irvine and Baragar, 1971); (b) A/CNK- A/NK plot (Shand, 1943); (c) TAS diagram (Bas et al., 1986); (d) Geotectonic classsification of volcanic rocks (Schandl and Gorton, 2002); (e) REE diagrams normalized to chondrite (Nakamura, 1974) and Primitive Mantle (McDonough and Sun, 1995).

4.2.3 Greenschists from the OB

Major element oxide and trace element data of the lower greenschist facies porphyritic meta-andesite point to a calc-alkaline series protolith. Th/Ta vs Yb ratios indicate an ACM to oceanic arc environment (Schandl and Gorton, 2002).

Primitive mantle and chondrite normalized multi-element plots of this sample show a negative slope with negative Ta-Ti and Nb anomalies (Fig. 9e).

4.2.4 Granitoids associated with the Santa Marta Batholith

Three samples from Eocene granitoids were analyzed. Samples AP-009 and AP-038 correspond to the Sevilla Stock rocks and the Guachaca Migmatites respectively. Sample CJJ-91 is a decimetric orbicular feldspar collected in the central part of the SMB. The Guachaca Migmatite is a very acid granitic intrusion whereas the Sevilla Stock rock resides on the boundary between granite and granodiorite. The orbicular feldspar shows an intermediate dioritic composition (Fig. 9).

Trace element compositions of the Guachaca migmatites and the Sevilla Stock revealed negative Ta, Ti, Nb, and Sr anomalies. The negative Ti anomaly was significantly more pronounced in migmatites. The orbicular feldspar shows a strong positive Eu anomaly, which was not observed in the other two granitoids.

4.3 Zircon Morphology

When it comes to discussing zircons from metamorphic rocks, it is very important to make a distinction between zircons that grew as result of a metamorphic reaction (=

“metamorphic zircons”), and zircons that crystallized from magma and recrystallized during thermal overprints (= “metamorphosed zircons”) in a regional metamorphic context, or because of magma recycling. In the SNSM, we found both metamorphosed and metamorphic crystals along with magmatic zircons. By studying their morphologies and combined core-rim age data, we gained information on the tectonic history of this complex area. Magmatic zircons are mostly euhedral translucent and prismatic with oscillatory zonning. In contrast metamorphic zircons tend to be rounded subhedral, with more complex zonning patterns that include, thick rims, patchy and convolute zonning, and collapsed cores. Although crystals are mostly colourless, as a main feature of the SNSM the Precambrian zircons present a purple hue whereas some Permian zircons present a yellowish hue. The specific traits of the crystals found at the different samples are briefly described in the following paragraphs.

Cathodoluminescence imagery analysis revealed core-rim relations that allow defining at least two episodes of rim growth in metamorphosed zircons, around inherited cores of Precambrian and Paleozoic ages (Fig. 10).

Zircons from the SB samples are subhedral, sub-rounded to sub-angular, and their color varies between translucent to purple and faintly yellow. These Precambrian crystals from high-grade metamorphic granulites, amphibolic and quartz-feldspathic gneisses, have a larger size (>250 um) in contrast to their younger Permian-Jurassic counterparts. Purple zircons are mostly older than the translucent ones and can be associated with a 1200-1300 Ma age peak. Samples with dominant populations younger than 1200 Ma mostly yield translucent to slightly yellowish crystals, with purplish faint xenomorphic cores.

Inner textures show characteristic recrystallization under high-grade metamorphic conditions, with rims that commonly are brighter and thicker, evidencing a homogeneous composition. Xenomorphic cores occur frequently and present dark purple colors. Inherited cores sometimes show fracturing at the outer rims. Precambrian crystals found in detrital samples (Chapter 3) show the same traits, but the purple colored population is more abundant and again it corresponds to crystals older than 1200 Ma.

Zircons from orthogneisses are euhedral, angular, and prismatic, with oscillatory zoning and sharp edges, with packed, closely spaced rims attesting to a continuous stable growth. Crystals vary between translucent to yellowish colored, and are mostly clean and inclusion free (Fig. 10d). The crystal population is unimodal in terms of morphology and age, average size of the crystals is around 200 µm.

Mylonite zircons are neoformed irregular subhedral to anehdral crystals sub-rounded to sub-angular, and colorless. The typical sub-rounded to multifaceted metamorphic morphology evidence highly reabsorbed shapes, irregular concentric zoning with chaotic texture with local aspects of flow and overprint of new recrystallization (Fig. 10 j & k).

Zircons from the Permian-Jurassic meta-pelites and meta-basites in the IB and the OB show a bimodal distribution with three distinctive populations. The first population is made of typical subrounded metamorphic zircons of Precambrian age and magmatic Ordovician-Jurassic zircons recycled from plutons. The second population found at the metamorphic units, has translucent to yellow Permian euhedral to subhedral crystals. A third population is made of Jurassic tabular prismatic euhedral translucent crystals. Zoning is oscillatory in magmatic crystals and with the core-rim structures common

for high-grade metamorphic granulites and gneisses (Fig. 10 f, l, m & p). Within the metapelitic units a distinctive population of rounded zircons with Precambrian cores and subrounded Permian rims, thicker and brighter than the cores, can be observed with a maximum lower Permian depositional age (Fig. 10e & i), and is seldom found in the younger metapelite units (Fig. 10a).

Crystals from the meta-basites of the OB are mainly euhedral to subhedral, tabular prismatic and acicular, prismatic, colorless, inclusion free and with grain sizes of up to 100 µm (Fig. 10 g & q). These magmatic zircons are always smaller than all the other observed populations.

The Eocene Sevilla Stock contains translucent prismatic, inclusion free zircon crystals with oscillatory zoning in the outer rims, and inherited Precambrian cores with the typical metamorphic texture of Precambrian zircons (Fig. 10n). Zircons from the Guachaca Migmatites are subhedral, showing extensive damage and fracturing with a disturbed oscillatory zoning, abundant inclusions, collapsed cores, and patchy zoning (Fig. 10o).

4.4 Zircon U-Pb Geochronology

Results from 17 samples from the metamorphic units of the NW corner of the SNSM are presented here. One sample from a granitoid of the southern SB, four samples from high-grade metamorphic gneisses of the SB, and eight samples from meta-pelites, mica and amphibole schists, orthogneisses, and granitoids from the IB. Additionally three samples from psephites and meta-basites of the OB, and finally one leucosome

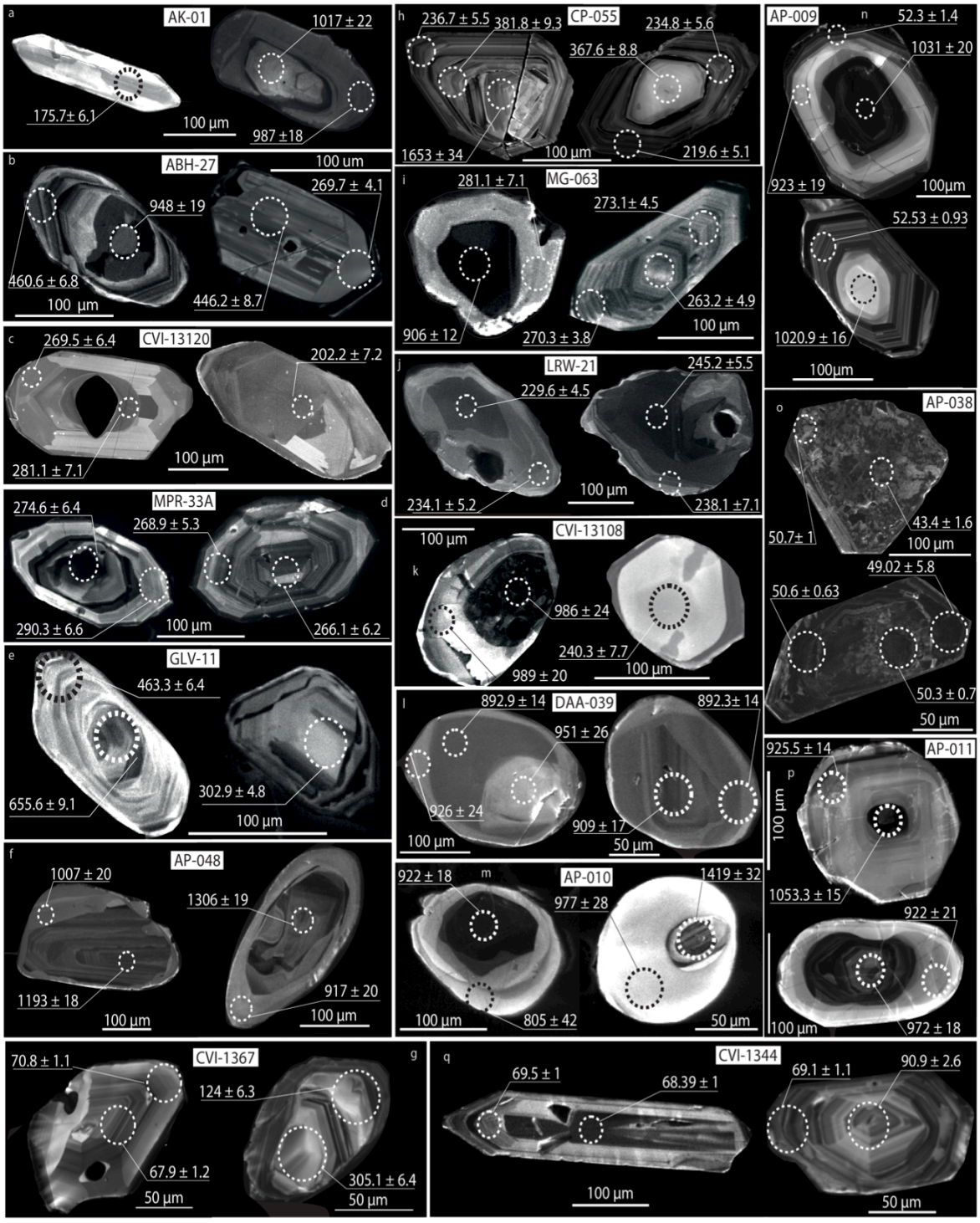

Figure 10. Panchromatic cathodoluminescence imagery of zircons analyzed in this study. a- Lower San Lorenzo Schists, b- Lower San Lorenzo Schists, c- Upper San Lorenzo Schists, d- El Encanto Orthogneiss, e- Gaira Schists, f- Muchachitos Gneiss, g- Concha Formation, h- Cinto Formation, i- Gaira Schist, j & k - La Secreta Mylonites, l & m- Buritaca Gneiss, n- Sevilla Stock, o- Guachaca Migmatite, p- Muchachitos Gneiss, q- Cinto Formation (dike). Dashed circles ablation size diameter is 30 µm.

from the southern SMB. Sample locations and general description is summarized in figures 4 & 5 and table A1, geochronological data are shown in figures 10 to 16.

4.4.1 Sevilla Metamorphic Belt (SB)

Four samples from the amphibolite gneisses within the SB yield concordant 970 Ma ages (Fig. 11 & 12). The Muchachitos Gneiss (Samples AP-048, DAA-039) yields an age spectrum between 900-1300 Ma, and 800-1080 Ma respectivelly with a rim recrystallization episode close to 944 ± 36 Ma. and youngest grain an ages of ca. 890 ± 12 Ma and ca. 796 ± 18 Ma (Fig. 11 & 12).

The Buritaca Gneiss (Samples AP-011, AP-010) showed simillar age trends with an age spectrum between 900-1300 Ma, and a rim recrystallization event at 955 ± 24 Ma. (Fig. 11 & 12) and the youngest crystal at ca. 902.5 ± 10 Ma for the rocks that did not suffered migmatization. However, mafic migmatites from this unit showed a younger overprint with a population of ca. 797-898 Ma distinguished in cores and rims and concordant zircons between 549-772 Ma ages found at cores and rims, the age ca. 549±15 Ma corresponds to a rim and belongs to the youngest of the Precambrian populations identified in this study. Younger veinlets in migmatites provide Phanerozoic crystals with Permian-Jurassic ages ca. 199.8-258.1 Ma (Fig. 11 & 12).

Zircons from the Sevilla Stock show recrystallization at ca. 51.9 ± 0.3 Ma with inherited Precambrian cores (800-1400 Ma) and some 900-1100 Ma rims. A discrete 180-200 Ma population and four Permian crystals completes the sample signature (Fig. 15 & 16).

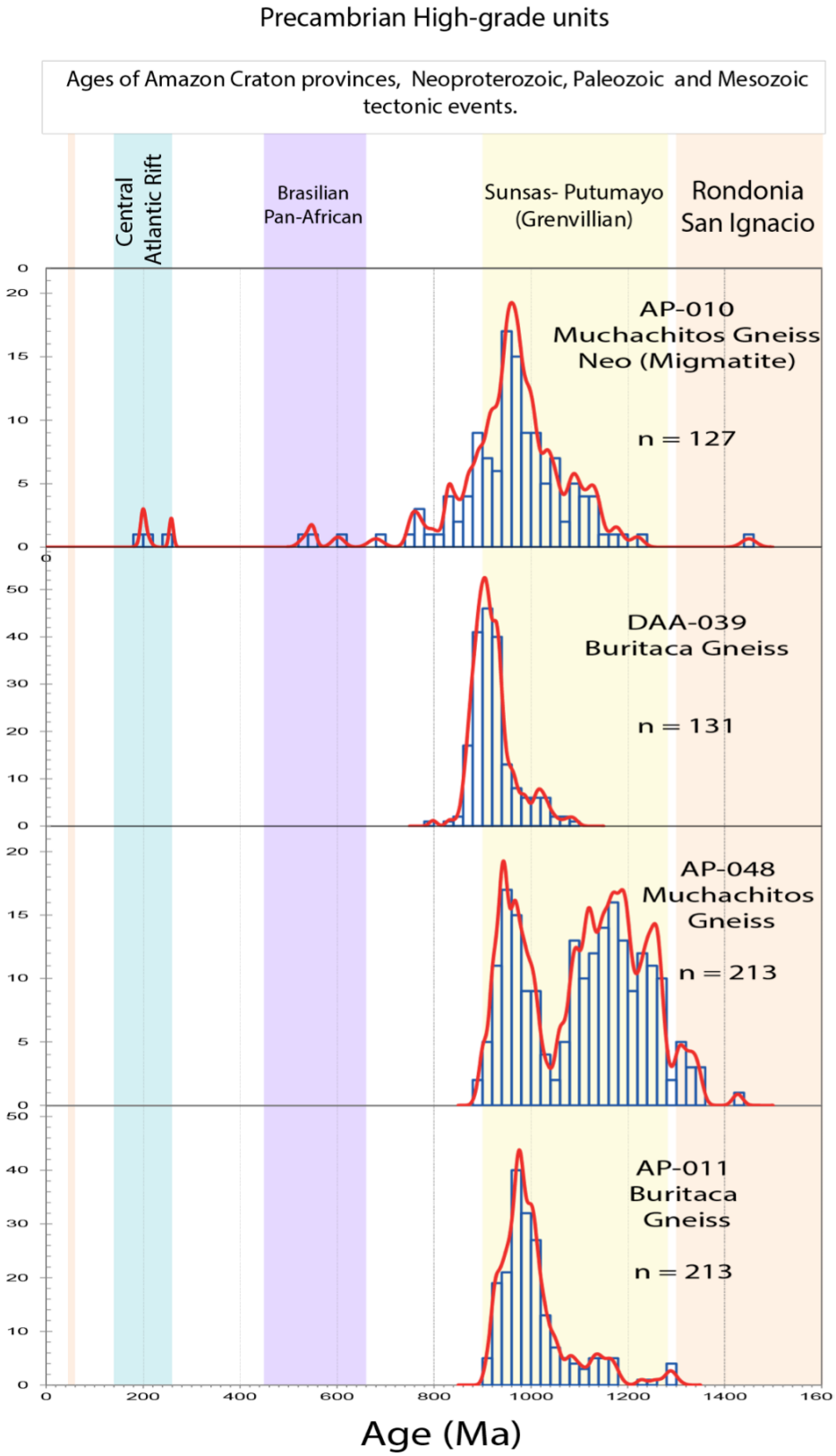

Figure 11. Zircon U-Pb LA-ICP-MS probability density plots obtained from the Precambrian units of the Sevilla Metamorphic Belt.

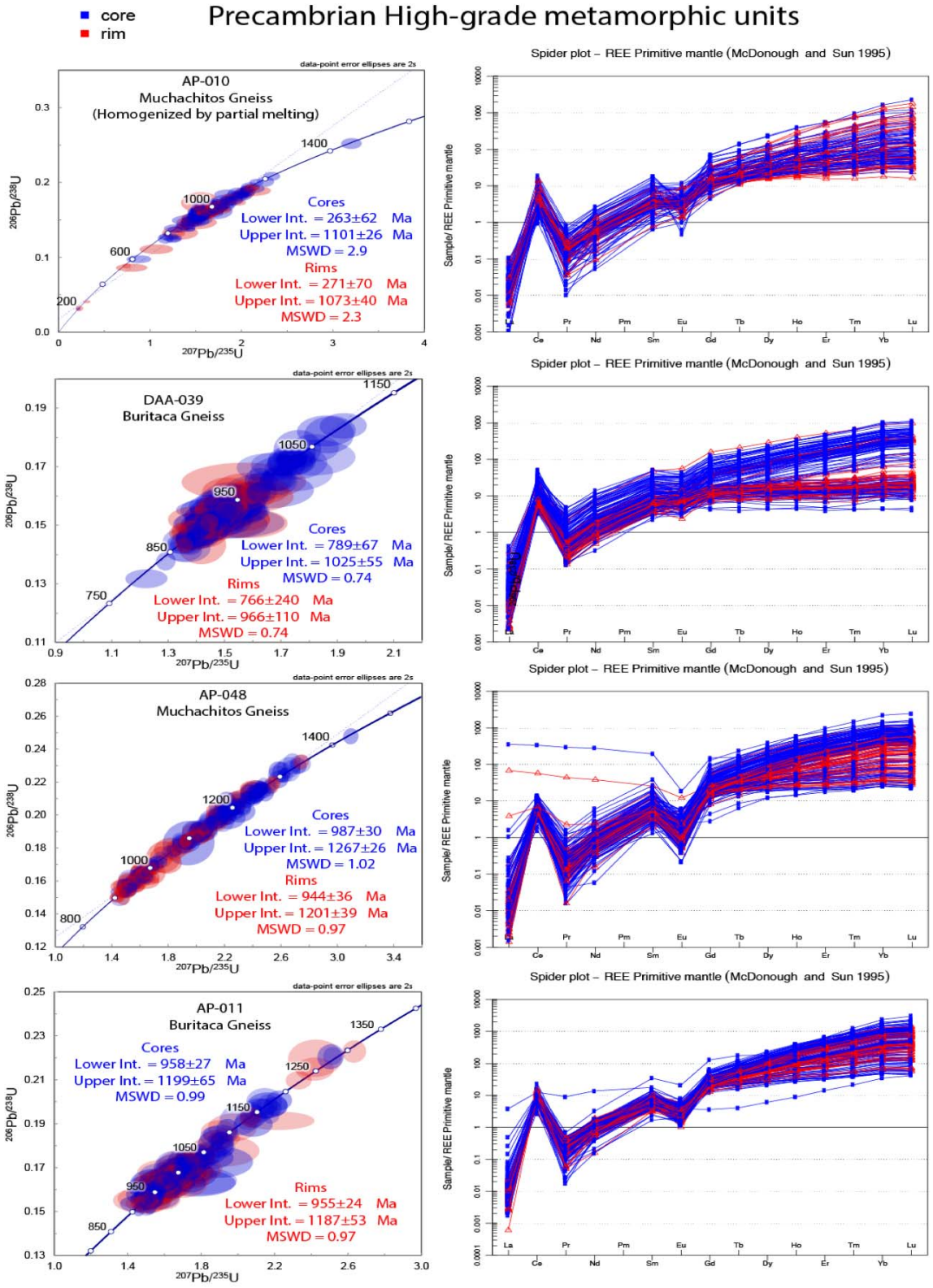

Figure 12. Concordia plots (left) and trace element composition of zircons from the Precambrian units of the Sevilla Metamorphic Belt south of the Orihueca fault.

4.2 Inner Santa Marta Metamorphic Belt (IB)

Eight samples from the SE dipping IB were analyzed. Sample MPR-33A from el Encanto Orthogneiss has an age of 274.8 ± 2.1 Ma, and mica-schist sample GLV-11 yields an age of 283.67 ± 6.1 Ma. Sample MG-063 from the Gaira Schists has an age of 261.46 ± 2.6 Ma. El Encanto Orthogneiss sample MPR-33A shows a discrete Pan-African/Brasiliano age population of 543±14 Ma, an late Pennsylvanian age population between 302-310 Ma, and a dominant Cisuralian to Guadalupian age population between 292-270 Ma (Fig. 13 & 14). Garnet-mica schist sample GLV-11 shows an early Paleozoic population of 284-463 Ma of four crystals. The Permian age is present in a recrystallized rim over a Carboniferous core. Other age populations in this sample include a Pan-African/Brasiliano 522-655 Ma population, a Neoproterozoic population at 900-1200 Ma and a Paleoproterozoic population at 1500-1770 Ma. One zircon yielded an age of 2235 ± 58 Ma (Fig. 13 & 14). Mica schist from sample MG-063 contains age populations at around 950 Ma, 655-850 Ma, and 270 Ma. One zircon yielded an Ordovician age of ca. 468.9 ± 7.1 Ma. In this sample, metamorphic rounded zircons with Precambrian cores and bright homogeneous rims of Permian age are frequent (Fig. 10, 13 & 14). Sample LRW-21 Pl+Grt+Bt from La Secreta Mylonites shows an age range between 230-250 Ma with growth of cores and rims, and a weighted average age of 237.4 ± 1.1 Ma. Bt+Grt+Pl schist sample CVI13108 from La Secreta Mylonites shows an age spectrum of 224 to 1300 Ma, with the youngest crystal age of 224.58 ± 3 Ma, and most cores and rims between 225-250 Ma. Nonetheless, an early Permian age population of 270-285 Ma and a Precambrian inherited population of 1000-1300 Ma were also detected (Fig. 13 & 14). Quartzitic schists sample ABH-27 from the Lower

San Lorenzo Schists contains zircons with Neoproterozoic 563-1189 Ma inherited cores, and Middle Ordovician to middle Carboniferous rim overgrowths and external Triassic rims c.a. 220-243 Ma. Sample CVI-13120 from Bt+Ep schists from the upper San Lorenzo Schists showed a Jurassic age of 187.92 ± 7.6 Ma. In contrast, sample AK-01 from a paraschist of the Lower San Lorenzo unit showed two main age trends with a 1000-1400 Ma population, and a concordant Jurassic 184.96 ± 0.78 Ma population. Leucosome AP-038 from the Guachaca Migmatites yields an age of ca. 50.8 ± 0.4 Ma. This sample contains few inherited Permian and Precambrian zircons (Fig. 15 & 16). Eocene zircons are extensively damaged, and they have inclusions and collapsed cores (Fig. 10o).

4.4.3 The Outer Santa Marta Metamorphic Belt (OB)

Three samples were analyzed from the OB. Sample CVI1367 a meta-andesite of the Concha Formation at the OB yields a lower Paleocene age of 55.4 ± 2.6 Ma. In the hanging wall of the SE verging Florin fault, CP-055 psephite from the Cinto Formation yields a Triassic age of 212 ± 4.7 Ma product of magmatic overgrowth, this sample contains Pan African/Brasiliano zircons at ca. 611- 505 Ma, Devonian to Carboniferous zircons between 402-310 Ma and few Permian grains at 254.1 ± 5.9 Ma and 280.4 ± 6.6 Ma. At the margins of the SMB, the basal part of the Rodadero Formation is affected by migmatization that grades into granitoids, which are also intruding the Cinto Formation phyllites as leucocratic dikes (sample CVI1344) and yield a Maastrichtian age of 69 ± 0.5 Ma ages. One sample of the Eocene Sevilla Stock hosted between the Precambrian Buritaca gneiss and the Triassic to Jurassic western batholith border zone was analyzed (Fig. 15 & 16).

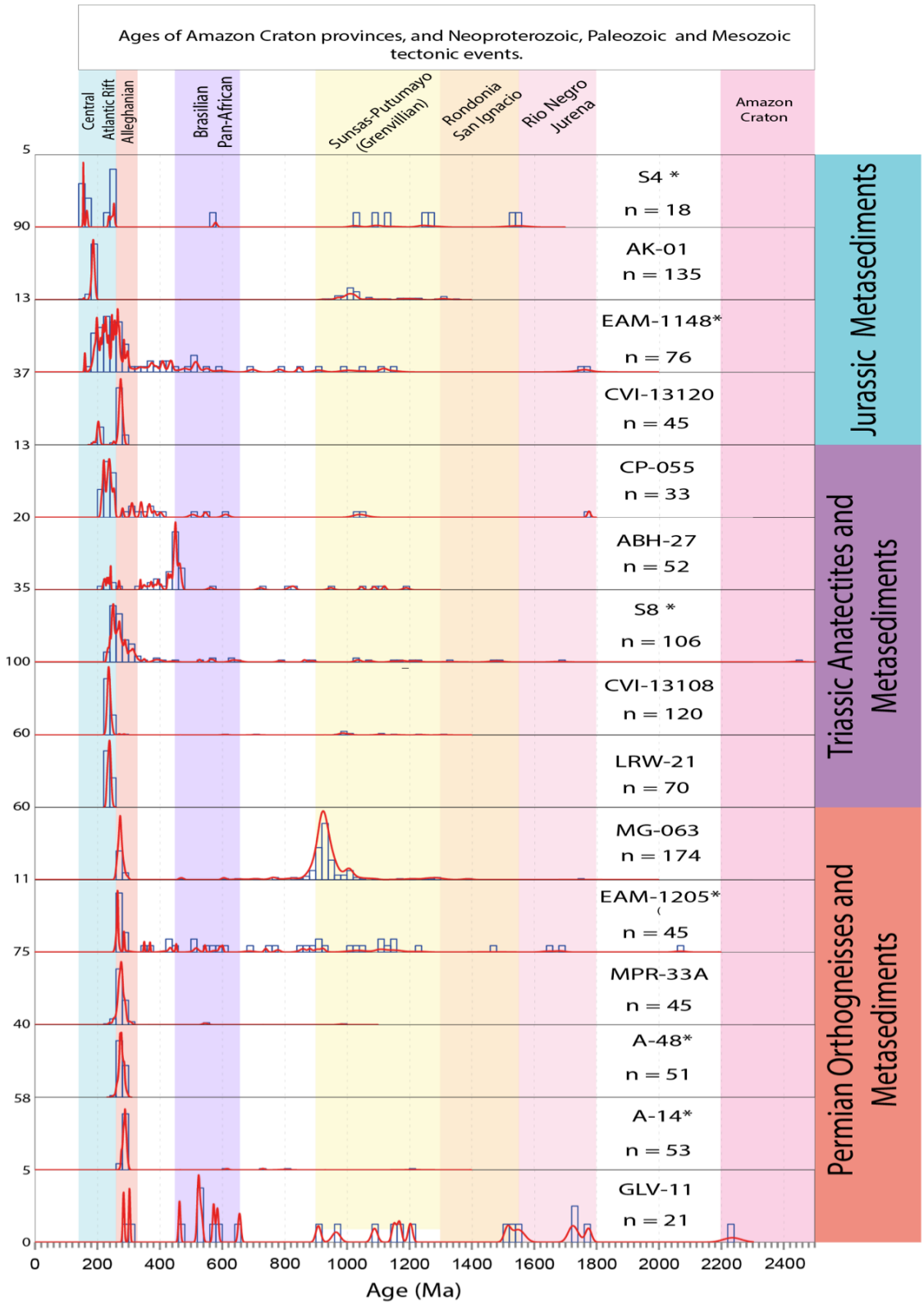

Figure 13. Zircon U-Pb LA-ICP-MS probability density plots obtained from the Permian to Jurassic metasedimentary and metaigneous units of the IB. Data sets labeled by asterisk are taken from (Cardona et al., 2010b, 2010c).

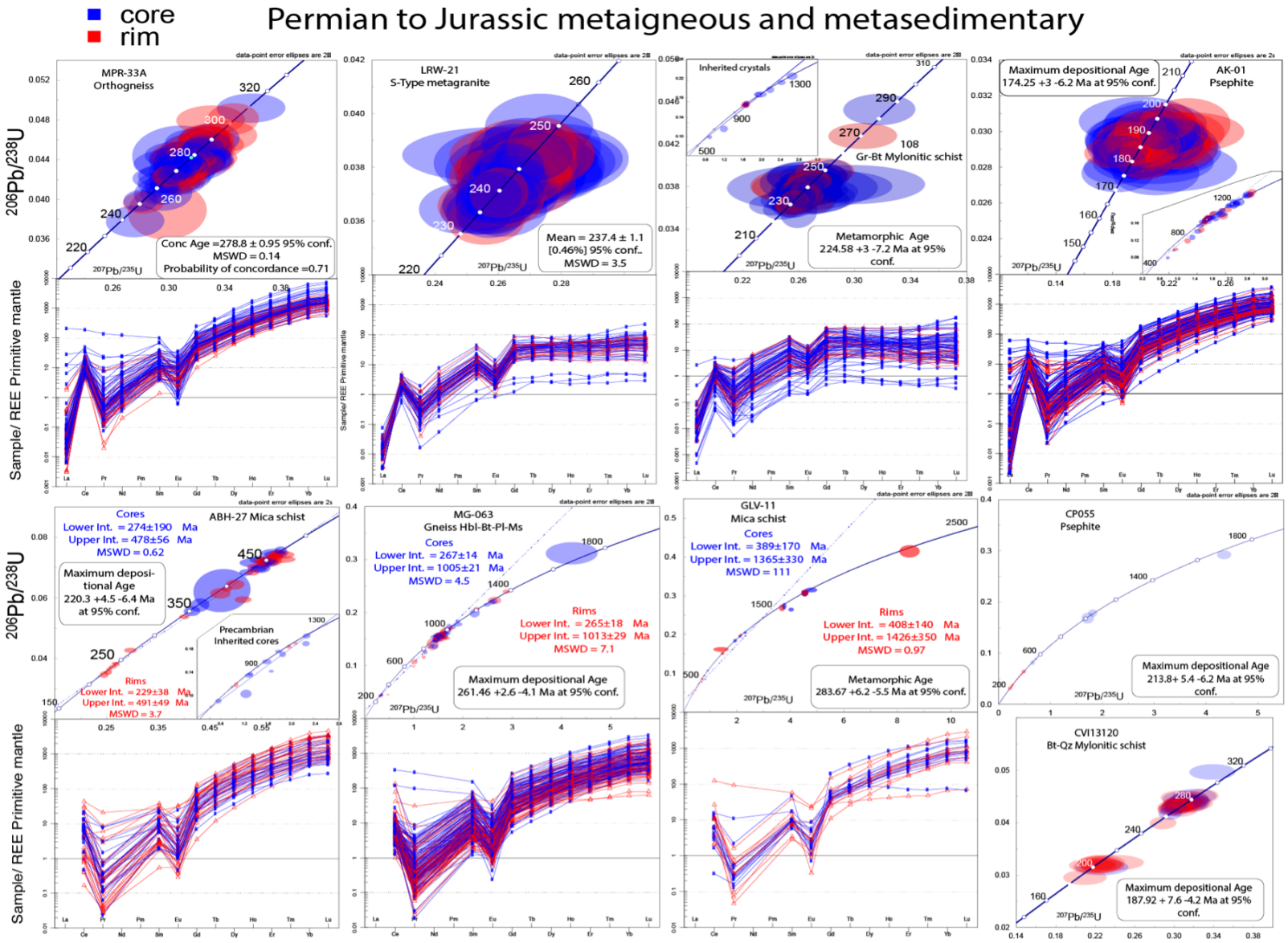

Figure 14. Concordia plots and trace element composition of zircons from the Permo- Triassic metaigneous and metasedimentary units of the IB.

4.5 Trace Elements in Zircon

REE composition in zircon reveals the original conditions in which zircons grew associated either with a magmatic or metamorphic origin. This discrimination must be done based on zircon morphology and host rock context, which is fundamental for defining a coherent history for a given set of crystals. As zircon is a common accessory mineral in the continental crust, and due to its relatively high crystallization temperature, it is obvious that its formation history is linked to other phases during magmatism or metamorphism, if temperatures are high enough for allowing phase re-equilibration and zircon recrystallization. It has been shown that under epidote-amphibolite facies zircon recrystallization does not occur (Lancelot et al., 1983), but at high amphibolite facies conditions (600-650ºC) zircon can recrystallize (Peucat et al., 1985). For the metamorphic units of the SNSM we had obtained a simillar T-t trend, with episodes of zircon crystalization during metamorphism, and coeval magmatism. At higher temperatures (650-1000ºC), zircon can be totally reabsorbed and reset with no appreciable Pb-loss (Mezger and Krogstad, 1997). For this reason analyzing REE content in magmatic and metamorphic zircon is fundamental for defining the conditions under which recrystallization occurred. HREE content in zircon can evidence if recrystallization took place under a sub-solidus environment with limited supply of trace elements, considering the concurrent growth of feldspars and garnet in a closed system (Murali et al., 1983, Rubatto, 2002; Schaltegger et al., 1999). Garnet crystallization produces depletion on HREE in the reactive bulk and in consequence HREE patterns in zircon that grew under these conditions tend to be flat.

4.5.1 Sevilla Metamorphic Belt

The REE content in zircons from the Precambrian units of the SB is defined by a very clear compositional trend, in which cores are enriched in HREE, whereas rims are depleted in HREE (Fig. 12).

Sample AP-011 from the Buritaca Gneiss shows enriched cores, which exhibit higher HREE values (Lu_n/Sm_n = 5 – 1221, av. 126.8) than the depleted rims (Lu_n/Sm_n = 4 – 288, av. 91.7). A negative Eu anomaly is present (Eu/Eu* 0.05-0.61, av. 0.25). Th/U ratios are high with values of 0.56 av. at cores and 0.5 av. at rims.

Quartz amphibole cataclastic gneisses from Sample AP-048 (Muchachitos Gneiss) exhibit a negative Eu anomaly (Eu/Eu* 0.05-0.95, av. 0.15), with a HREE depletion trend towards the rims (Lu_n/Sm_n = 4.5 –184, av. 56.3), and slightly higher values in the cores (Lu_n/Sm_n = 4 –396, av. 92.12). As a general trend, cores younger than 980 Ma have Lu_n/Sm_n values lower than 20. Th/U ratios are high with values of 0.22 av. for the cores and 0.18 av. for the rims.

Sample DAA-39 quartz-feldsphatic gneiss form the Buritaca Gneiss shows a compositional trend in cores and rims with a gap that separates a flat profile for rims and younger cores, from a steeper profile for the eldest cores. HRRE element content declines from (Lu_n/Sm_n = 1.4 –104, av. 18) in the cores to (Lu_n/Sm_n = 1.5 – 45, av. 8.7) in the rims. Th/U ratios are high and present values of 0.62 av. in the cores and 0.36 av. at the rims. Differently from the other samples, the Eu anomaly is less pronounced (Eu/Eu* 0.2-1.7, av. 0.75),

For sample AP-010, a mafic migmatitic gneiss, HREE is very similar in cores (Lu_n/Sm_n = 4 – 416, av. 50.6) and rims (Lu_n/Sm_n = 5 – 320, av. 59). This minor rim enrichment

shows some melt rejuvenation due to recrystallization in a melt. Th/U ratios show high values of about 0.26 av. for the cores and 0.27 av. for the rims. A negative Eu anomaly is present (Eu/Eu* 0.017-1.6, av. 0.5),

The Eocene Sevilla Stock shows high Y content (830 - 5200 ppm, av 1800 ppm), typical of magmatic zircons (Rubatto, 2002). This pluton shows an inverse REE profile in comparison to the Precambrian units (Fig. 16). At the Eocene Sevilla Stock core and rim populations are sharply separated. Most of the rims are Eocene and the inherited cores are Precambrian. The general trend shows a high enrichment in HREE in all the Eocene population with (Lu_n /Sm_n = 137 – 5700, av. 805), whereas Precambrian cores and rims show (Lu_n /Sm_n = 1.9 – 550, av. 108). A negative Eu anomaly is present, and significantly lower in Eocene zircons (Eu/Eu* 0.43-1,1 av. 0,62) than in Precambrian zircons (Eu/Eu* 0.038-0,915 av. 0,3). Th/U ratios are on average 0.36 for older population and 0.12 av. for the young crystals.

4.5.2 Inner Santa Marta Metamorphic Belt

Permian El Encanto Orthogneiss show an extremely high Y content (550 -7750 ppm, av 1900 ppm), values that are common in magmatic zircons. This is coherent with magmatic crystal morphologies. HREE elements describe a homogeneous compositional trend between cores and rims (Fig. 14), with relatively high values (Lu_n /Sm_n = 21– 729, av. 168) in the cores and (Lu_n /Sm_n = 34– 264, av. 159) in the rims. A negative Eu anomaly evidences classic magmatic zircon growth during feldspar crystallization (Eu/Eu* 0.02-0.6, av. 0.3). Th/U ratios are high 0.8 av, and in this case are interpreted as related to a magmatic origin.

Sample GLV-11 from the Gaira Schists shows very high age variability with Precambrian and early Paleozoic crystals in very few grains (n= 20). For this reason, it would be inaccurate to try to establish trace element compositional trends. The observation of the latest recrystallization event in this sample is recorded in a single rim age of 284 ± 5.2 Ma. The rim has low HREE, Lu_n/Sm_n = 6.66, and high Th/U ratio 0.8. Mica-schist sample MG-063 contains a Precambrian population that shares the same trace element signature as observed in the Precambrian Muchachitos Gneiss. The secondary Permian population shows (Lu_n /Sm_n = 43– 419, av. 145), and high Th/U ratios av. 0.75. Samples from the La Secreta Mylonites show the most distinctive HREE profile with a general depletion in cores and rims, compared to the other lithologies analyzed in the SNSM (Fig. 11). For example, the mylonitic Pl+Grt+Bt schists sample LRW-21 shows (Lu_n /Sm_n = 1– 12, av. 5) in the cores and (Lu_n /Sm_n = 2.3– 8.2, av. 5,25) in the rims. The negative Eu anomaly shows values of (Eu/Eu* 0.15-1.2, av. 0.26) in the rims and (Eu/Eu* 0.13-1.04, av. 0.26). Th/U ratios show a general 0.22 av. in the cores 0.20 av. in the rims. Bt+Grt schist sample CVI-13108 contains some relevant Precambrian inheritance, with a trace element content that is almost equal to the HREE indexes obtained for the Precambrian units of the SB. Metamorphic zircons (Fig. 14) with depleted HRRE contents in the cores of (Lu_n /Sm_n = 0.3– 48, av. 6) and (Lu_n /Sm_n = 0.3 – 7, av. 2.08) in the rims. This ratio shows flat to negative HREE profiles. The negative Eu anomaly (Eu/Eu* 0.15-1.7, av. 0.43) is concurrent and does not variate significantly from core to rim. Th/U ratios are in the range of 0.15 -0.17 from core to rim. In sample ABH-27 from the Lower San Lorenzo Schists the HREE distribution of the early Paleozoic zircons shows values in the cores of (Lu_n /Sm_n = 31– 732, av. 185) and (Lu_n /Sm_n = 42– 623, av. 337) in the rims. In addition, it shows a negative Eu

anomaly (Eu/Eu* 0.032-0.996, av. 0.43), Th/U ratios of 0.012-1.8, av. 0.45, and high Y content (281-4400 ppm). Permo-Triassic rims present high HREE values (Lu_n/Sm_n = 44– 1185, av. 436.5), but low Th/U ratios of 0.0086 -0.0349 The youngest analyzed metasedimentary sample AK-01, from the San Lorenzo Schists yields two distinctive populations (Fig. 14). The Precambrian zircons show trace element compositions, and Th/U ratios akin to the Buritaca Gneiss. The Jurassic population shows high Y contents (135-4240 ppm), and elevated HREE contents (Lu_n/Sm_n = 25– 581, av. 113) with a minor rim enrichment (Lu_n/Sm_n = 37– 263, av. 128). The negative Eu anomaly is typical of these magmatic zircons (Eu/Eu* av 0.28), along with high Th/U ratios 0.83 av. in the cores and 0.95 av. in the rims. At the Eocene granitic leucosome associated to the SMB intruded in the Gaira Schists amphibolites zircons show high HREE concentrations (Lu_n/Sm_n = 16– 380, av. 127). This sample presents the highest Y values from all the analyzed samples (936 -28000 ppm) (Fig. 16). The negative Eu anomaly of these migmatitic crystals is (Eu/Eu* av. 0.2). Th/U ratios are relatively low (0.0126 – 1.5, av 0.14).

4.5.3 Outer Santa Marta Metamorphic Belt

Zircons for both metavolcanic samples CVI-1367 and CVI1344 present high Y contents (400-6000 ppm) (Fig. 13). For sample CVI-1367, the HREE are enriched progressively from cores (Lu_n/Sm_n = 65– 559, av. 245) to rims (Lu_n/Sm_n = 159– 433, av. 270), Th/U ratios are on average 0.5, and a negative Eu anomaly (Eu/Eu* av 0.5) is observed. Sample CVI-1344 shows HRRE values ranging from cores (Lu_n/Sm_n = 10– 355, av. 214) to rims (Lu_n/Sm_n = 88– 363, av. 228). Th/U ratios are in the range of 0.3 av., and a negative Eu anomaly (Eu/Eu* av 0.3).

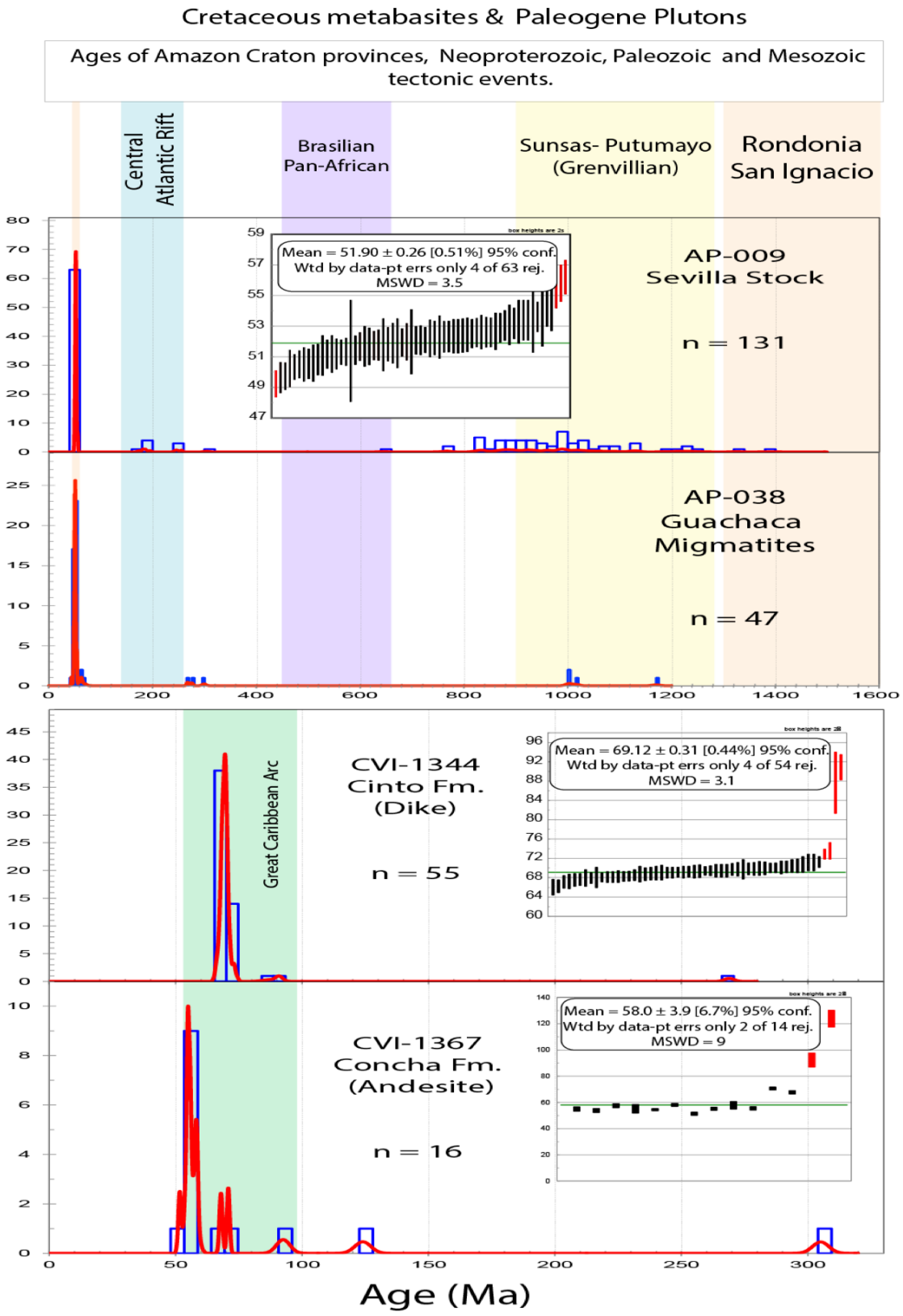

Figure 15. Zircon U-Pb LA-ICP-MS probability density plots obtained from the Cretaceous to Eocene metabasites and granitoids of the OB and SB.

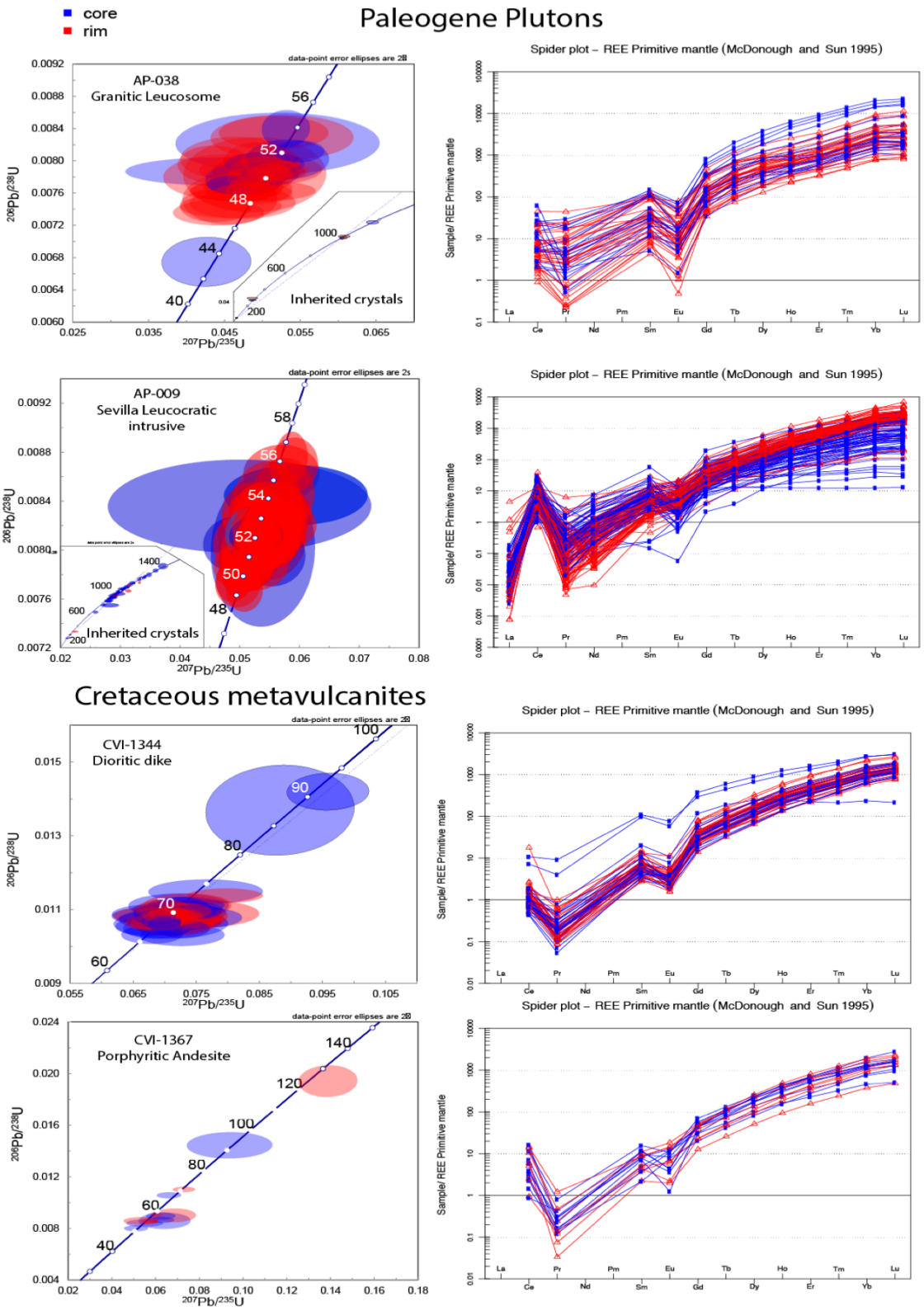

Figure 16. Concordia plots (left) and trace element composition (right) of zircons from the Cretaceous to Eocene metabasites and granitoids of the OB and SB.

4.6 Mineral Chemistry

Representative microprobe analyses of garnet, biotite, plagioclase, hornblende from three samples of the La Secreta Mylonites, are presented in table A2. Garnet exhibits high chemical variations from core to rim observed in weak to a strong zoning (Fig. 17 & 18). From major oxides, mole fractions were calculated into the structural formula for separating the end-member compositions ($X_{Alm} X_{Prp} X_{Sps} X_{Gr}$). Each end-member was plotted in a compositional profile for visualizing Mg, Fe and Mn contents within cores and rims of the crystals (Fig. 18). The garnet amphibolite sample presents weak zoning CVI-1388 and the X_{Alm} content ranges from 0.55 to 0.65, enriched in the rim, the X_{Prp} content from 0.09 to 0.12 depleted in the rim, the X_{Grs} content from 0.01 to 0.03, and the X_{Sps} content from 0.01 to 0.04 enriched in the rims. Minor zoning is evidenced in x-ray maps by a rim Mn enrichment and Mg depletion. Fe shows as well a minor increase towards the rim.

At the transitional zone to the Bt+Grt schist strong zoning can be observed in the compositional profiles with X_{Alm} content ranging from 0.45 to 0.68, showing enrichment in the rim. X_{Prp} values vary from 0.12 to 0.31 with core enrichement, the compositional variation in the X_{Alm}, X_{Prp} end-members is abrupt and coincides with zoning observed in back-scattered images (Fig. 17) and x-ray compositional maps (Fig. 18), the X_{Grs} content varies from 0.09 to 0.2 higher at core, and X_{Sps} from 0.01 to 0.09 enriched in the rim.

Bt+Ms+Grt schist showed an X_{Alm} content ranging 0.65 to 0.72, with a minor enrichment towards the rim, X_{Prp} from 0.1 to 0.12 with rim enrichment, X_{Grs} content from 0.03-0.13, and X_{Sps} from 0.04 to 0.15 depleted in the rim. The compositional

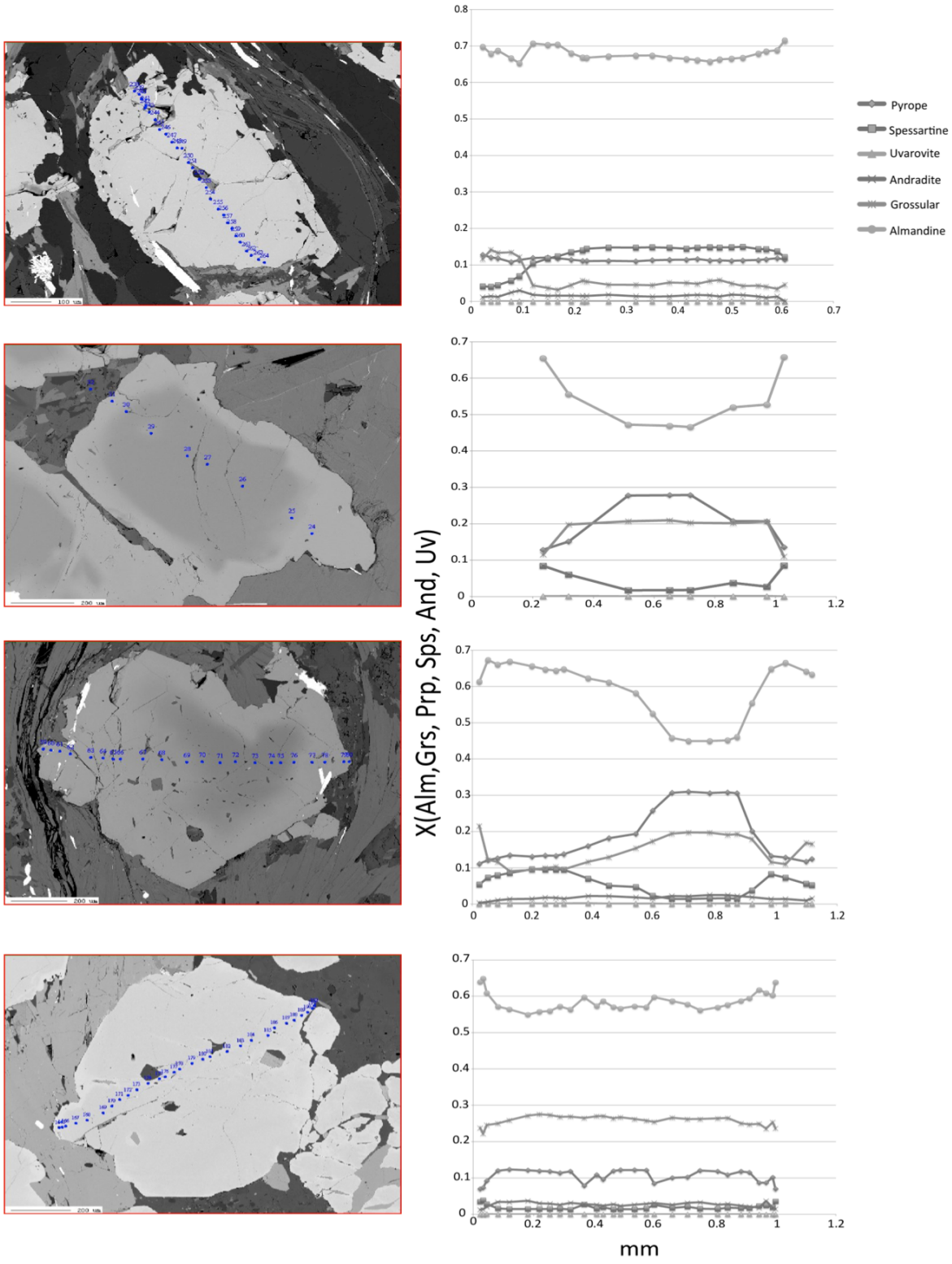

Figure 17. (a) Garnet compositional profile, sample CVI-1388. (b) Garnet compositional profile, sample CVI-13108. (c) Garnet compositional profile, sample CVI-13108. (d) Garnet compositional profile, sample CVI-1385, note strong zoning and garnet Mn enrichment towards rims.

profile is asymmetric, and the rim shows inclusions. A Mn x-ray map shows core enrichment for this element differently from Fe and Mg, which remained constant (Fig. 17 & 18). Major differences between X_{Alm} and X_{Prp} reflect differences in MgO/(MgO+FeO) bulk compositions.

Representative analyses of biotite in Bt+Grt+Pl schists show X_{mg} values of 0.6 to 0.645 typically of intermediate to magnesium biotites. Biotite crystals are not zoned and mostly homogeneous.

Hornblende crystals from Hbl+Grt+Pl+Qtz sample CVI-1388 are zoned. This can be observed in thin section, like a marked color variation from brown in the cores to bluish-green in the rims (Fig. 6). This mineralogical variation corresponds to compositional trends of the end-members and is related to an increasing Ti content. In consequence of the increment in metamorphic grade, in this case describing a decrease of Ti to the crystal borders and therefore a prograde reaction for hornblende. End-member X_{Mg} varies between 0.34-0.41 with higher values in the crystal cores. X_{Fe} varies between 0.59-0.66 with higher values in crystal rims, and with Al enrichment and Mg depletion in hornblende crystal borders. In the same sample, garnet shows a discrete zoning in rims with a minor Fe and Mn increase and Mg depletion in Mg.

Alternative evidence of this retrograde path for Garnets from Hbl+Grt+Bt+Pl+Qtz amphibolites and in Bt+Grt+Qtz+Pl schists is addressed with garnet geochemical discrimination diagrams (Mange and Morton, 2007; Wright, 1938). Based on approximately 544000 analytical spots measured by x-ray map standardization, it can be demonstrated that the garnet rims crystallized in biotite schists under lower amphibolite facies metamorphic conditions, whereas the cores crystallized under high amphibolite facies conditions (Fig. 19a-c).

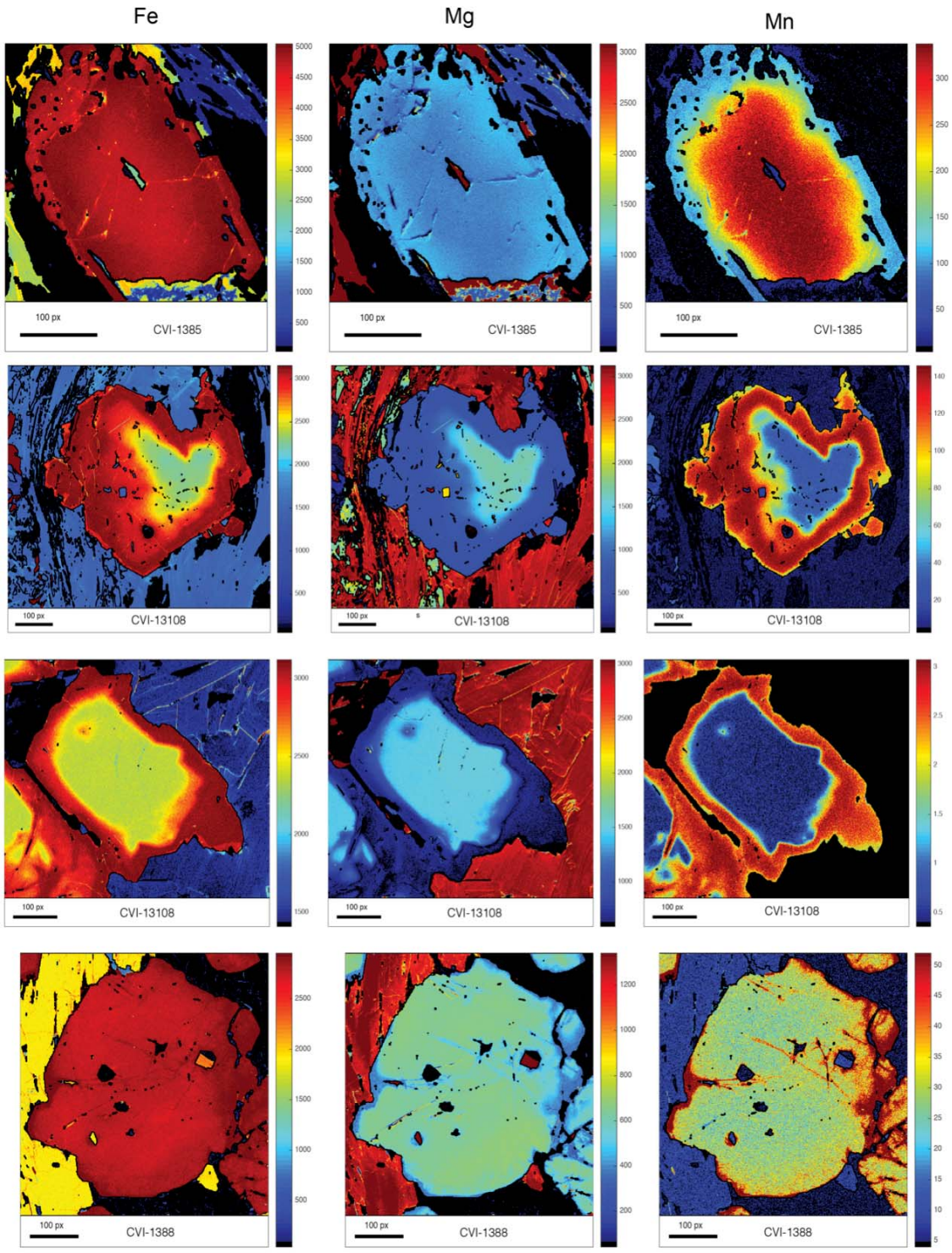

Figure 18. Mn, Mg and Fe X-ray maps from Hbl+Grt+Pl amphibolite (CVI-1388) (bottom), Bt+Grt+Pl schist (CVI-13108) (center) and Bt+Ms+Grt+Qtz+Pl+Chl CVI-1385 (top), collected adjacent to the Aguja fault. Observe compositional zoning varying, being more intense at the Bt+Grt Schists (CVI-13108), with higher values of Fe and Mn at rims, and a decrease of Mg in the rim, this strong zoning is related to retrograde metamorphism.

In contrast Bt+Ms+Grt+Qtz+Pl+Chl schist shows a prograde path in the biotite schist field (Fig. 19d), and a decrease of Mn from core to rim, as it would be expected for a continuous fractionation growth process (Hollister, 1966; Tracy et al., 1976).

4.7 Thermobarometry

Thermobarometry of the Lower–Middle Triassic La Secreta Mylonites has been performed on three samples combining different approaches of quantifying raw x-ray electron microprobe data using internal standards, and including empirical and semi-empirical geothermobarometers from the literature, using XMapTools, a MATLAB based GUI program. We used for samples CVI-13108 and CVI-1385 garnet and biotite geothermometers (Bhattacharya et al., 1992), and for sample CVI-1388 the Hbl+Grt geothermometers (Ravna, 2000) and Hbl+Pl+Qtz geothermobarometers (Lanari et al., 2014). This first approach was complemented by calculations on pressure and temperature using the Garnet-Al_2SiO_5-Plagioclase (GASP) geobarometer for metapelites (Ghent, 1976; Holdaway, 2001). Results of both methods are compared for estimating pressure-temperature conditions of mineral crystallization in this metamorphic suite.

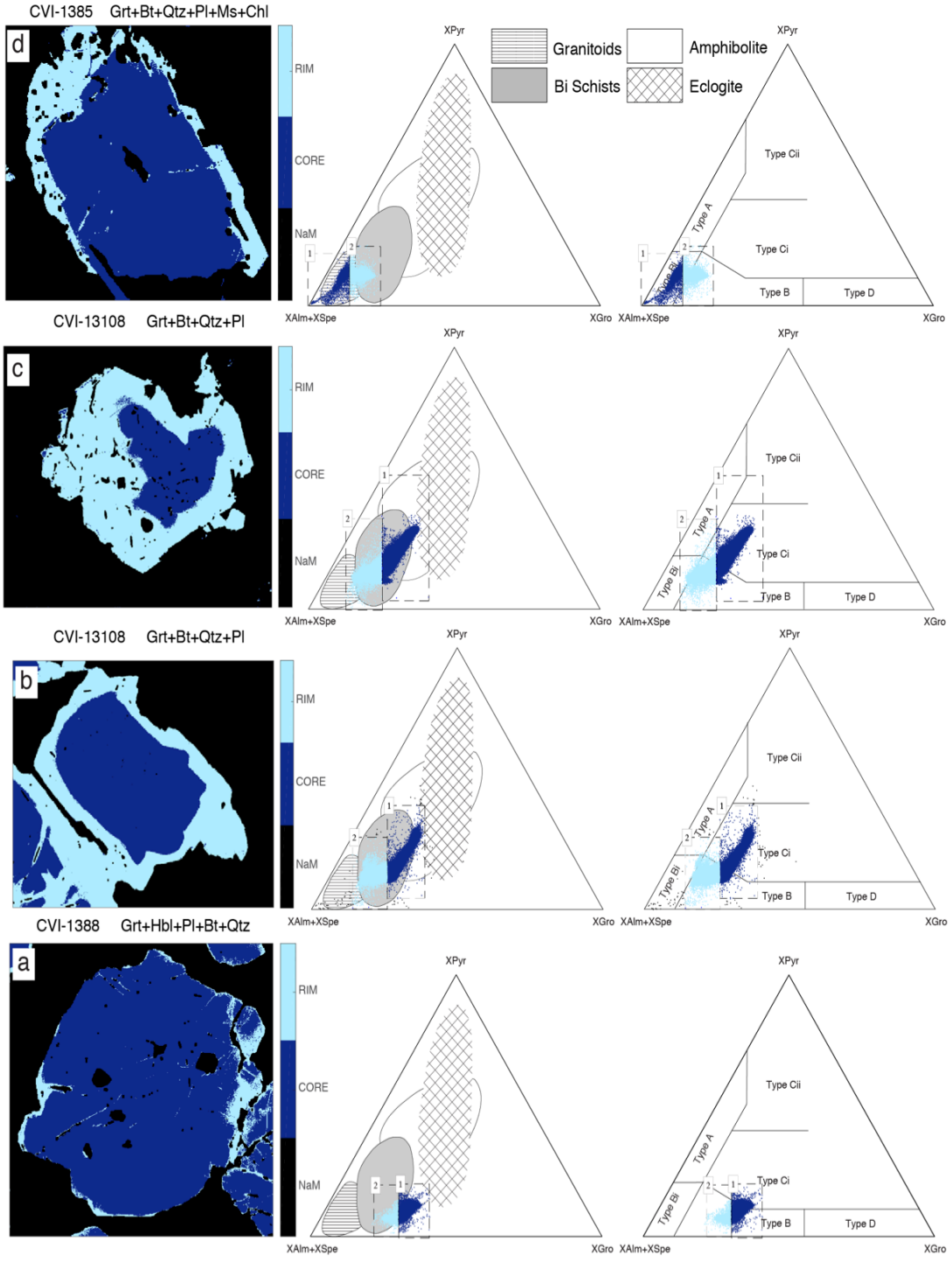

Figure 19. Retrograde zonation is evidenced in lower metamorphic degree towards the rims in samples CVI-1388 a), CVI-13108 b & c), in contrast sample CVI-1385 d), shows a prograde zoning. Samples reside within the amphibolite and biotite schists fields.
Garnet composition discrimination diagrams (left) image, extract form the Grt maskfile generated in XMapTools® (Lanari et al., 2014) showing core and rim selected areas for each crystal, each pixel from the maskfile is plotted in the triangular diagrams according end-member composition, tones indicate

compositional ranges pertaining to the crystal core and rim. (Center) Ternary discrimination diagram after (Wright, 1938), legend of the fields in in the top center of the figure; (right) ternary discrimination diagram after (Mange and Morton, 2007). A — mainly from high-grade granulite-facies metasediments or charnockites and intermediate felsic igneous rocks, B — amphibolite-facies metasedimentary rocks, Bi — intermediate to felsic igneous rocks, Ci — mainly from high-grade mafic rocks, Cii — ultramafics with high Mg (pyroxenites and peridotites), D — metasomatic rocks, very low-grade metamafic rocks and ultrahigh temperature metamorphosed calc-silicate granulites.

4.7.1 La Secreta Mylonites - Garnet Amphiblolites

Metamorphic temperatures of garnet amphibolite sample CVI-1388 were estimated using the Hbl+Grt geothermometer by Ravna (2000), with values ranging from 530-570 ºC for the rims and 771-835 ºC for the cores. In both cases, we had chosen 20 spots from core to rim in an Hbl+Grt assemblage.

Our second calculation involved the geothermobarometer Hbl+Pl+Qz (Lanari et al., 2014) resulting in values of 660 ºC- 750 ºC for Hbl crystal cores and at crystal borders respectively, in the vicinity of the Grt+Hbl interaction. Pressure for this assemblage was calculated with 10.2 - 11 kb for crystal cores and 11.6 - 12.1 Kb at crystal borders of Hbl+Grt and Hbl+Plg mineral pairs. Peak conditions for hornblende crystallization were 750 º C and 12.5 kb (Fig. 20) based on 11000 data points measured by x-ray map standardization on 15 amphibole spot measurements and seven feldspar spot measurements (Table A3). Thermobarometry results evidence contemporaneous Gr+Hbl growth during prograde metamorphism as temperature and pressure values increase from hornblende cores to borders (Fig 20). Garnet crystals show a similar behavior with increasing T values towards the border of the crystals. Retrograde rims in garnet are discrete (Fig 21b), indicating that garnet amphibolites experienced a less intense retrograde metamorphism.

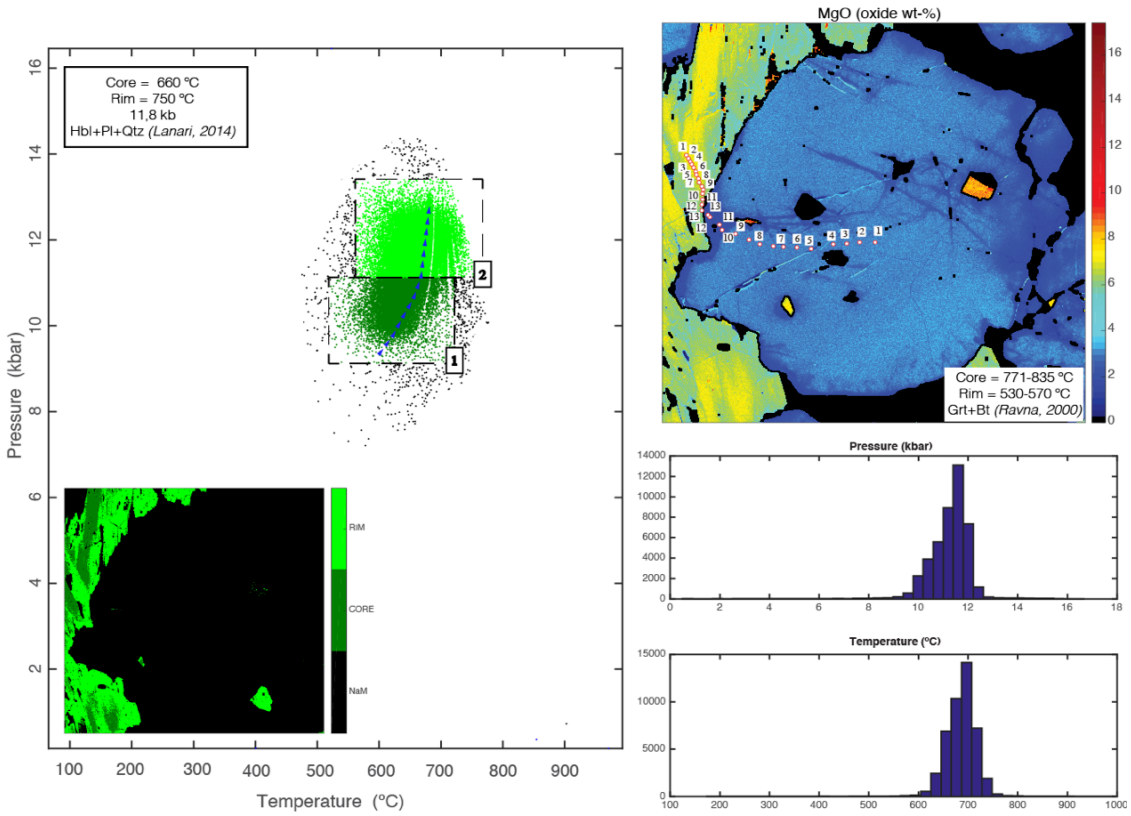

Figure 20. P-T paths for sample CVI-1388 showing (left) calculation for the Hbl+Pl+Qtz and pairs, green shaded Hbl crystal evidences a prograde growth with increasing conditions of P and T from core to rim, peak at = 750ºC and 11. 8 kb. T and P probability density plots. (top right) the Grt+Hbl thermometer was calculated using 13 paired spots measured from core to rim, peak T conditions for Grt are 771-835 ºC, note incipient zoning with lower temperature range between 530-570ºC, describing a retrograde path.

4.7.2 La Secreta Mylonites - Biotite-Garnet schists

Up section mylonites with Grt+Bt+Pl+Qz paragenesis geothermometry was calculated using the calibration by Bhattacharya et al. (1992) based on the exchange equilibria with relative large entropy change considering the reaction:

$$Bt_{Fe} + Grt_{mg} = Grt_{Fe} + Bt_{mg}$$

Measurements were made in spot couplets of Grt+Bt from crystal centers to borders. The results show temperatures from 512ºC to 830ºC. With a first prograde growth from the center of the crystal from 781-832ºC, and after this peak with temperature decreasing progressively towards the rim where the measured values are between 513-536ºC (Fig 20). This change depends on the compositional zoning occurring as a gentle transition or a sharp boundary. In either case, the temperature response is a gradual temperature decrease or a 200ºC gap between core and rim respectively.

An additional approach is Ti-in-biotite thermometer of Henry (2005), which allows estimating an average 600ºC ±12ºC within a range of 510-630ºC ± 12ºC. However, this result should be addressed carefully because this geothermometer is recommended to be applied to ilmenite or rutile-bearing, graphitic, peraluminous metapelites, and for this sample graphite is absent, which could lead to underestimating the peak temperature by about 80ºC.

Thermometry in sample CVI-1385, with a Bt+Ms+Grt+Pl+Qtz paragenesis, showed lower *T* conditions with values between 300-475ºC ± 12ºC with the Ti-in-Biotite thermometer, with the highest values in Bt inclusions inside Grt. The results of this thermometer are again underestimated by 50ºC ± 12ºC, because of the absence of graphite and ilmenite.

Garnet thermometry showed homogeneous values from core to rim ranging from 497-560 ºC, with a T increase towards the rim in contrast to the samples described above. Coexistence of muscovite and light red to transparent pleochroic biotite support this assumption.

For samples CVI-13108 and CVI-1385, we determined pressure values using the GASP geobarometer (Ghent, 1976; Holdaway, 2001), calculating molar fraction from the

major oxide composition obtained in core to rim spot couplets measured in x-ray maps and considering sillimanite as aluminosilicate results are summarized in (Fig. 21).

4.7.3 Ti-in zircon thermometry

Trace element measurements in zircon provide Ti concentrations for each spot ablated. The Ti-in zircon thermometer is a powerful petrological tool. Recent studies have demonstrated that most zircons cluster strongly at ≈ 700ºC (Watson, 2005), in plutonic rocks however this apparently fixed temperature can decrease depending on the presence of near-water saturated conditions (Harrison et al., 2007). Experimental and natural results define a linear dependence of equilibrium Ti content (expressed in ppm by weight) upon reciprocal temperature (Watson et al., 2006). This is expressed by the relations:

1) $$\mathrm{Log\ (Ti_{zircon})} = (6.01\pm0.03) - (5080\pm30)/T(\mathrm{K})$$

2) $$T\,(^{\circ}\mathrm{C})_{\mathrm{zircon}} = (5080\pm30)/((6.01\pm0.03)-\mathrm{Log(Ti)})$$

Results on La Secreta Mylonites samples showed an average Triassic zircon *T* of 730-800±10 ºC, with an average of 745ºC which is within the range of *T* predicted by the thermobarometric systems Bt+Grt, Hbl+Grt. Inherited Grenvillian zircons showed values between 820-1110ºC. (Table A2).

El Encanto Orthogneiss yielded slightly lower temperatures between 600-850 ºC, with an average value of ≈ 685ºC. Eocene intrusive rocks show a temperature range similar

to an average zircon crystallization temperature of 683ºC. Precambrian cores preserve the original thermal signature of 820ºC. Rocks from the Precambrian basement show values between 850-1200ºC, attesting for a higher thermal regime during their crystallization.

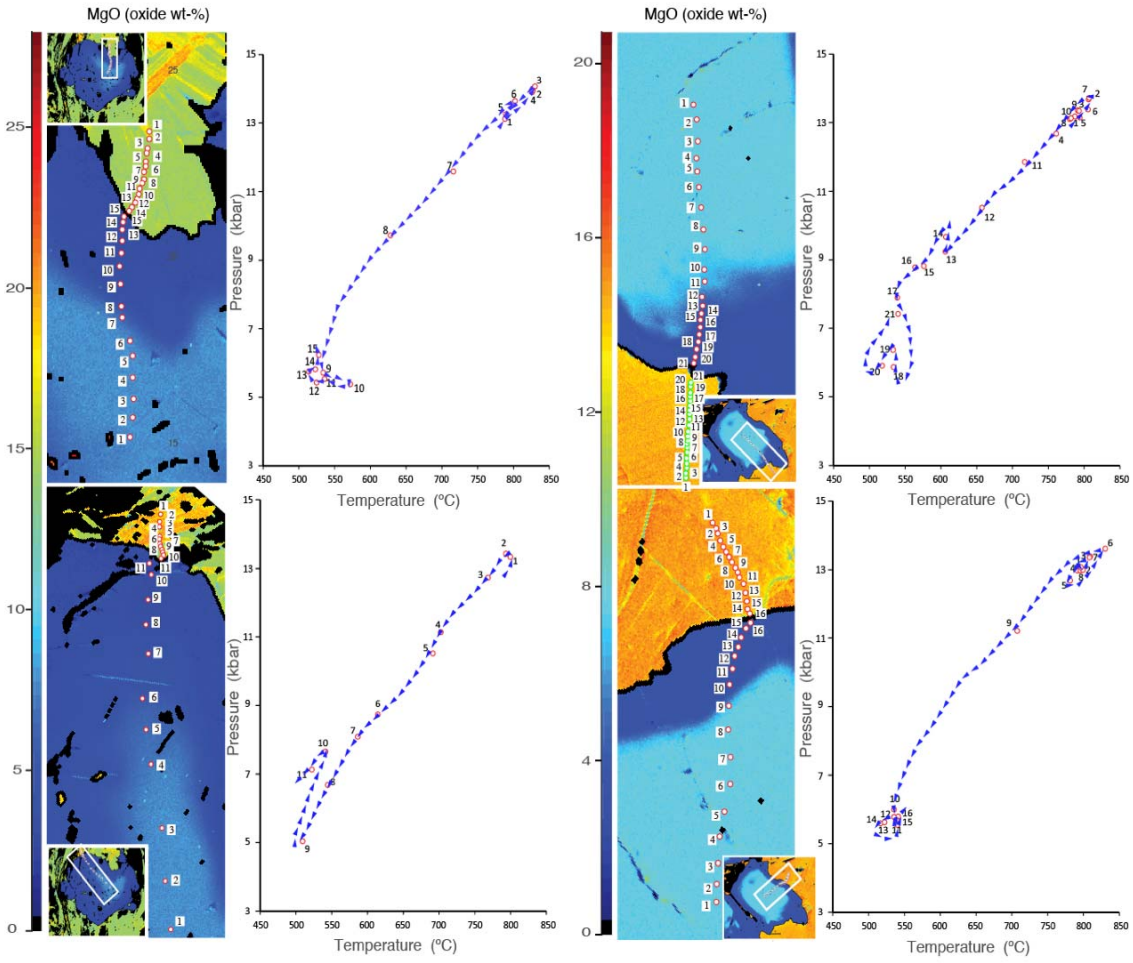

Figure 21. P-T paths calculated for sample CVI-13108 in four Grt+Bt core to rim profiles within two different crystals, each profile has between 15 to 20 measured spot couplets. Extracted major oxide compositions are used for calculating P-T conditions using the GASP geobarometer ant the thermometry calibration by (Bhattacharya et al., 1992), results are plotted in the P Vs T diagrams at the right of each measurement, an initial prograde phase reaches metamorphic peak around 830ºC and 14kb, and is followed by cooling and decompression down to 530ºC and 5.5 kb.

5. DISCUSSION

5.1 Geochronological implications for the SNSM

Originally the SNSM has been subdivided into different tectonic provinces: 1) the Sierra Nevada Province SNP, 2) the Sevilla Metamorphic Belt or SB, 3) the Inner Santa Marta Metamorphic Belt IB, and 4) the Outer Santa Marta Metamorphic Belt OB (Tschanz et al., 1974). Our results help to redefine the extent of these provinces in a litho-chronostratigraphic context (Fig. 22).

Zircons recovered from the samples can be classified either as magmatic or metamorphic. Most of the samples exhibit a mixture between these two types of crystals. The rounded and larger crystals with subrounded shapes and thick outer rims are associated with inheritance from older sources.

Zircons commonly present overgrowths that may be related to metamorphic episodes. The first metamorphic episode corresponds to early Neoproterozoic ages and is found in all Precambrian samples 900-790 Ma. The second episode of middle Permian age was identified in the Gaira and San Lorenzo schists as a magmatic reworking of crystals ca. 270-260 Ma. A third metamorphic episode was identified in La Secreta Mylonites, related to crystallization of zircon under high-amphibolite facies, with very low inheritance and two disctintive populations at 250-220 Ma (Fig. 22).

We found that there is a significant age variation from the Sierra Nevada Province and the SB. Zircon U-Pb data show that the presumed Paleozoic Buritaca and Muchachitos cataclastic gneisses to the north of the Sevilla Lineament present Neoproterozoic age

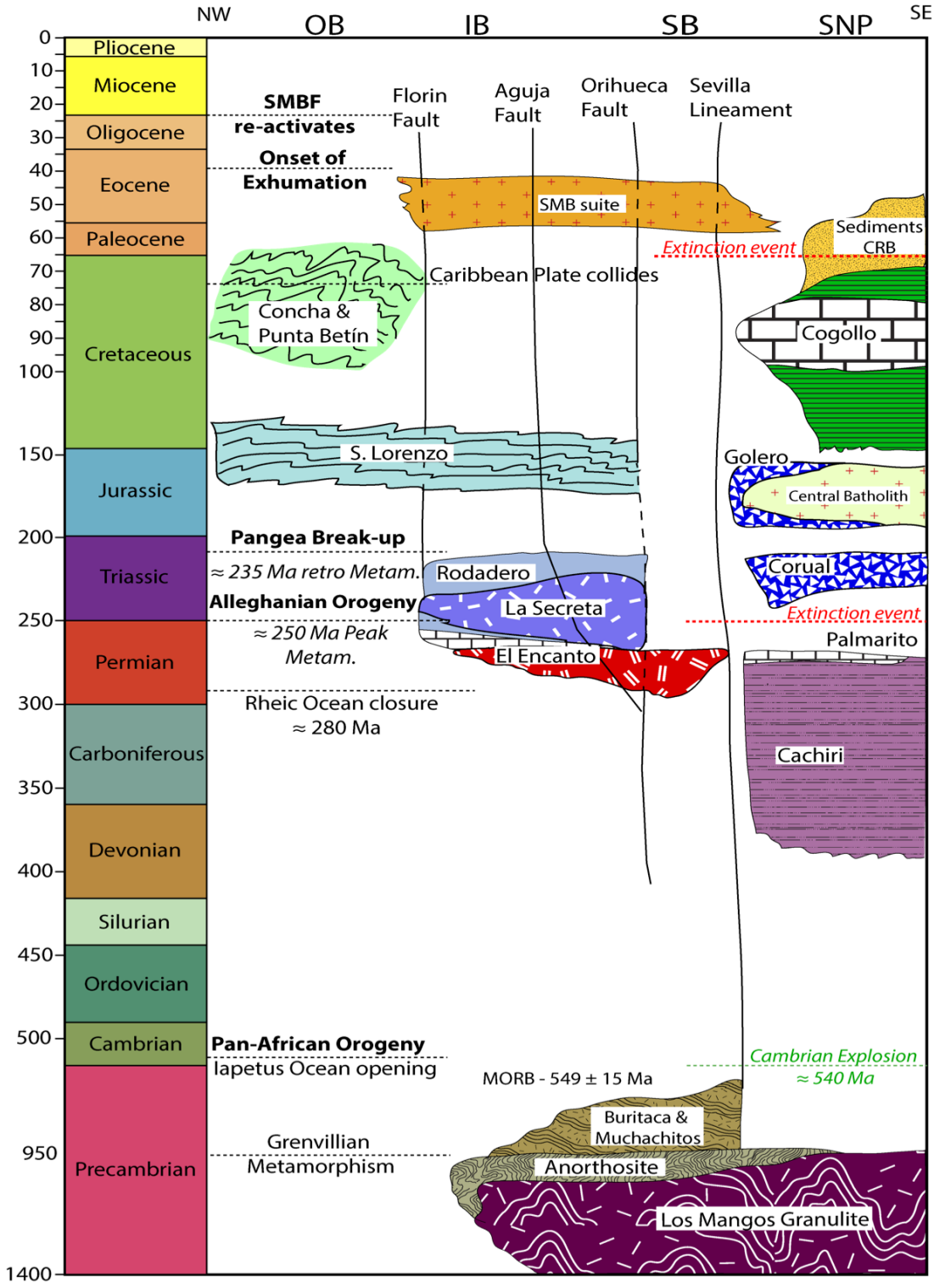

Figure 22. Stratigraphic summary of the Sierra Nevada Province, Sevilla Belt, Inner Santa Marta Metamorphic Belt, and Outer Santa Marta Metamorphic Belt according to the field relationships and stratigraphy section. Major tectonic events, geochronological significant ages, and massive extinctions are indicated.

populations with a spectrum from 790-1350 Ma recrystallized at ca. 980 Ma. Including a late generation of MORB oceanic crust aged 549±15 Ma at late Neoproterozoic-Cambrian, evidencing that these gneisses are probably remnants of the opening of the Iapetus Ocean after Rodinia break up at this part of the Proto-Andean margin (Fig. 23), although slightly younger these ages, are closer to the Dibulla Gneiss and Los Mangos Granulite ages (Cardona et al., 2010a; Cordani et al., 2005; Ordóñez et al., 2002; Restrepo-Pace et al., 1997) than they are to the previously suspected Paleozoic age (Tschanz et al., 1974). Late Neoproterozoic ages found in these units are correlative with autochthonous rocks from the Proto-Andean margin of South America related to anorogenic magmatism within the southern Appalachians, during the initiation of the Neoproterozoic active margin (Chew et al., 2007, 2008; Mišković et al., 2009). Previous U-Pb zircon ages (Cardona et al., 2006; Cordani et al., 2005) (Neoproterozoic cores, Permian rims) as well as Jurassic ca. 147 Ma K/Ar ages of the SB (Tschanz et al., 1974), evidence at least two major thermal events. The first thermal event can be linked to the intrusion of Permian metaluminous granitoids in the Gondwana basement. The second thermal event may relate to Jurassic pluton emplacement at around 147 ±6 Ma (Tschanz et al., 1974). Later thermal disturbances associated with the Caribbean arc accretion are recorded in the AFT and ZFT systems (Villagómez et al., 2011b).

Regarding our age data we propose that the Orihueca fault is the limit between the SB and IB, separating the Neoproterozoic gneisses from the Permian-Triassic and Jurassic schists that post-date, in turn, the intrusion of the El Encanto orthogneiss, which proves a continental-arc derived affinity during the late Paleozoic. This faulted contact is sharp and is marked by the juxtaposition of amethyst bearing amphibole gneisses with a zircon U-Pb age of ca. 902 Ma against quartzites with a Middle Jurassic

maximum depositional age of 174.2 ± 6 Ma. These meta-sediments overlie the La Secreta Mylonites (Figs. 6 & 22).

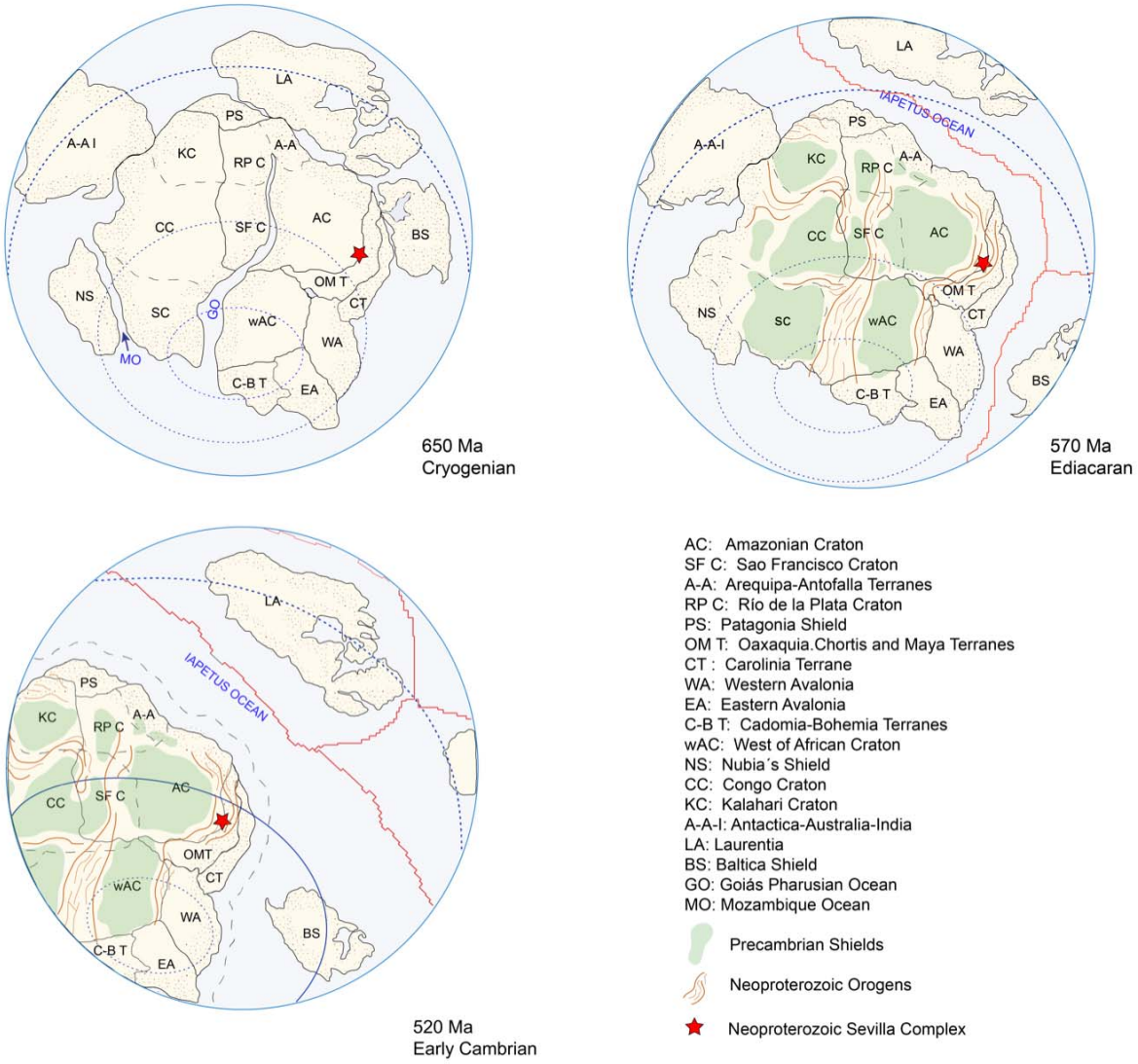

Figure 23. Palaeogeographic reconstruction at the Neoproterozoic- Cambrian transition ≈ 650 - 520 Ma. The closure of the Goiás Pharusian and Mozambique Oceans led to Gondwana assembly, and the subsequent Brazilian- Pan African Orogeny, zircons at the Sevilla Metamorphic Belt attest a Grenvillian and Pan African sources (see Fig. 7), this reconstruction is modified after (Chicangana and Kammer, 2016a, 2016b; Cordani et al., 2013; Ganade de Araujo et al., 2014; Nance et al., 2014).

The El Encanto Orthogneiss can be correlated with the mylonitic orthogneisses of the Valencia creek with zircon U-Pb ages of 264.9 ± 4 Ma, 276.5 Ma ± 1.8 and 288.1 ±4.5 Ma (Cardona et al., 2010c).

El Encanto Orthogneiss of Permian age underlying the Gaira and San Lorenzo Schists is in contradiction to the widely accepted view that the IB is of Caribbean origin (Cardona et al., 2010b; MacDonald et al., 1971; Tschanz et al., 1969; Zuluaga and Stowell, 2012). The geochronologic evidence in this case favors the affinity of the IB to Gondwana and precludes a Caribbean origin of this province. The Permian granitoids intrude the Precambrian units at the Sierra Nevada Province at the Perijá Range and Mérida Andes (Macdonald and Hurley, 1969, van der Lelij et al., 2016).

Zircons recovered from the Gaira Schists showed maximum depositional ages of ca. 283.67± 6.1 (sample GLV-11) and 261.46 ±2.6 (sample MG-063). Both meta-sedimentary rocks with lower Permian maximum depositional ages are interbedded with marble layers and amphibolites. We presume that it is possible that the age of the marbles included into the Gaira schists is Permian. For the San Lorenzo Schists, maximum depositional ages range between 188.3 ±7.3 in the footwall of the Aguja fault, and to 174.2 ± 6 Ma adjacent to the Orihueca Fault.

These ages do not allow constraining a stratigraphic age but a range between Late Triassic and Middle Jurassic for the deposition of the protolith. Towards the base of the San Lorenzo Schists the maximum depositional ages are slightly older (220.33 ±4.6 Ma), and the Precambrian inheritance is minimal as Permian and Ordovician sources are the most relevant sources for these sediments. These extensive age components suggest that deeper levels of the circum-Pangaean orogen were already exhumed and eroded. We assume that sedimentation took place during the Jurassic rifting phase due

to the fact that meta-sedimentary units rest in a non-intrusive contact over Permian orthogneisses. In this scenario, the Aguja fault controlled sedimentation (Figs. 24 & 25).

In the OB we identified meta-sediments represented by the clastic Cinto Formation (CP-055) with a maximum depositional age of ca. 213.33 ± 4.7 Ma. The affinity of this unit to the continental margin is evident by the prolific content in zircon populations that includes a complete Triassic record, and with Permian, Carboniferous and early Paleozoic crystals attesting to continuous erosion from a continental source.

The widely recognized upper Cretaceous Caribbean arc inception led to accretion of oceanic island arc terranes recognized in the OB with an overall age of ca. 82 Ma (Cardona et al., 2010b). The accretion of this arc is documented on the continental margin at least since ca. 92 Ma by dikes that intruded the Jurassic meta-sediments of the IB (Cardona et al., 2011).

All samples that yield this upper cretaceous signature correspond to the Concha and Punta Betín formations. These low-grade metamorphic units are related to the Caribbean arc. Coeval with arc collision this metamorphic suite underwent metamorphism during the upper Cretaceous. In the IB during metamorphism hornblende schists retrogressed to greenschist facies rocks (Bustamante et al., 2009; Tschanz et al., 1974; Zuluaga and Stowell, 2012).

The magmatism affected extensively the Precambrian basement of the SB: the Latal, Buritaca and Sevilla plutons yield crystallization ages of 55.5 ± 0.65 Ma, 65.1 ±0.9 Ma, and 51± 0.26 Ma respectively. Dioritic dikes intrude the OB, and yield a Paleocene age of ca. 62 Ma, followed by the emplacement of the SMB between 58-50 Ma (Duque, 2009), whereas in the northern greenschist from Concha Formation porphyritic

andesites crystallized at 55.4 ± 2.6 My and record volcanic arc. This age span defines the duration of the Caribbean arc plutonism whose thermal overprint annealed ZFT and AFT systems (Villagómez et al., 2011b). The SMB and coeval plutons (Latal, Buritaca and Sevilla stocks) I-type plutons resulted from collisional tectonics between the Caribbean plate and NW South America (Cardona et al., 2011). Eocene plutonism thermal overprint caused migmatization of the remobilized Permo-Triassic rocks of the IB, the leucosomes associated to this episode yield Lower Eocene ages ca. 50.8 ± 0.4 Ma. Migmatization represents the culmination of the post-collisional magmatic activity marked by cooling and middle Eocene exhumation of the SNSM massif that had persisted until the present day.

5.2 Concluding remarks on zircon trace elements and mineral chemistry

We found relationships between variations in REE content, sample age and structural position in many samples. In several cases, it is common to observe HREE depletion in crystal rims. Precambrian samples indicate a metamorphic crystallization event in a sub-solidus medium with a clear HREE depleting towards 980 Ma, either in cores or in rims. The compositional change occurs in a clockwise rotation from a steep to a flat HREE profile (Fig. 12).

Negative Eu anomaly in Precambrian zircons indicates feldspars grew coeval with zircon and during metamorphism. Trace element content along with textural and field observations within the IB defines the magmatic origin for a Permian arc located on the margin of the SNSM massif. Permian aged rims in zircon commonly cover

Precambrian cores, attesting for a metamorphic recrystallization induced by partial melting of the basement. Eocene granitoids intruded the Precambrian crust causing zircon recrystallization; the melt provided a high amount of HREE to the newly formed zircons and rims around older cores.

Eocene migmatites yield high HREE values, and plutonic rocks of the same age from the Sevilla Stock showed HREE concentrations 10 times lower. The decrease in concentration of HREE elements from core to rim in the Guachaca Migmatites is related to garnet crystallization, whereas garnet in the Sevilla Stock rocks is absent.

The Th/U ratio in zircons has been traditionally used for discriminating between magmatic (Th/U >0.01) and metamorphic (Th/U <0.01) zircons. Our results however show that at the SNSM, Eocene magmatic zircons commonly have Th/U ratios <0.01(Table A1). Instead many zircons from metapelites and mylonites yield Th/U ratios >0.01 and evidence that Th/U ratios by themselves are not useful for discriminating if a zircon has a magmatic or metamorphic origin. This paradox can be explained for solid-state recrystallized zircons typically inherit the Th/U characteristics of its parents (Möller, 2004; Möller et al., 2003). Combining of Th/U ratios, the Lu_n /Sm_n ratio and Y content and core-rim variations allows better to discriminate between zircons that grew in the presence of a melt or otherwise in a sub-solidus environment with depleted HREE. The Y content in magmatic zircons is an order of magnitude higher than in metamorphic zircons (Table A2). There is not a specific marker for a zircon to be magmatic or metamorphic based on trace element composition, because several other factors, such as the coeval growth of phases retaining Th, U or REE influence the final REE composition in zircon.

The chemical profiles of samples CVI-13108 and CVI-1388 (Fig. 20) show the characteristics of garnets that had undergone homogenization and retrograde zoning, with a core-to-rim increase in Mn and decrease in Mg (Tuccillo et al., 1990). Mn increase in the rims in Bt+Grt schists and Hbl+Grt+Bt+Pl+Qtz amphibolites corresponds to a retrograde diffusional effect driven by cooling during interaction with an aqueous phase (Tracy et al., 1976). In normal prograde zonned garnets, Mn profiles are typically bell-shaped, Mn depletion is related to the higher Mn fractionation factor in contrast to Fe, and Mg, as Mn in the rest of the rock is depleted during a continuous growth process (Hollister, 1966; Tracy et al., 1976).

Thermometry of the Grt+Hbl and Grt+Bt pairs show similar *P-T* estimates for amphibolites and mica schists for both cores and rims, which gives a reliable *P-T* path for the thermal evolution of this unit. A two-phase metamorphic event was identified in the La Secreta Mylonites in the hanging wall of the Aguja fault. The metamorphic paragenesis varies from Grt+Hbl+Pl amphibolites at the base to Grt+Bt+Ms+Pl+Qtz to the upper part of the suite, passing from the sillimanite zone to the Grt+Bt zone. Temperature and pressure estimates derived from zoned garnet in amphibolites and mica schists indicate a two-stage evolution with pro-grade peak temperatures of 770-830ºC and pressures of 11.66-14 kb, and retrograde temperatures between 510-550ºC and pressures between 5-7 kb (Fig 20 & 21).

Hbl+Pl+Qtz thermobarometry of garnet amphibolites indicates a temperature of 80ºC and a pressure of 1.2 kb below the calculated peak metamorphic conditions shown above. This difference can be related to disequilibrium between the phases due to transient thermal perturbation or a late-stage re-equilibration of the phases at conditions different from maximum *P-T* conditions, thus reflecting final equilibration

during a retrograde stage. Under the described HP-HT range zircons are prone to recrystallize in a sub-solid phase as result of the metamorphism (Peucat et al., 1985; Rubatto, 2002; Sawyer and Barnes, 1988). Garnet zoning is therefore the product of continuous reactions in the presence of an aqueous fluid, which can be related either to an external source or to prograde dehydration fluids unable to escape (Tracy et al., 1976).

Therefore, zircon crystallization between 250-220 Ma is coeval with garnet growth, the two age peaks date metamorphic ages and can be related to the two metamorphic phases identified in garnet crystals. This process occurred under a sub-solidus remobilization product of dynamic metamorphism during crustal thickening of the first phase (11.7 kb), and subsequently by crustal attenuation and sub-solidus melting under lower *P-T* conditions (500ºC -5.6 kb).

The high temperatures of 770-830ºC and pressures of 12 kb reached by these rocks are consequence of crustal thickening and subsequent thermal relaxation and shearing, which is not compatible with an arc-subduction setting, as it has been postulated before (Cardona et al., 2010c). The absence of HP-LT assembly also precludes a subduction context, because *P-T* trajectories evidence an isothermal decompression and not an isobaric cooling, as it would be expected from subduction. Examples of subduction HP-LT assemblages due to underplated mafic crust that validate a subduction context are further to the south in the Central Cordillera of Colombia and the El Oro Metamorphic Complex in Ecuador (Bustamante et al., 2012; Riel et al., 2013). Former P-T paths obtained from IB rocks were interpreted in a subduction context during the Caribbean accretion (Zuluaga and Stowell, 2012). Such P-T paths

should be reconsidered in the light of the new geochronological data presented in this study that preclude a Caribbean origin for this particular area.

5.3 Pangaea Assembly during Alleghanian Orogeny

Based on our results we aim to discuss in a regional scope an evolutionary scenario for this part of the Proto-Andean margin from the late Paleozoic, describing the tectonic phases related with episodes of metamorphic and magmatic zircon crystallization. Boundary conditions were constrained from several geothermobaromethers and evaluated along with the geochronological data.

290-250 Ma

The Permo-Triassic Tahamí (Vinasco et al. 2006) terrane was accreted onto the NW margin of Gondwana during collision. The convergent zone changed into a dextral shear zone that culminated with the Pangaea assembly and the closure of the Rheic Ocean. Following the Rheic Ocean closure during the Laurentia collision with NW Gondwana at ca. 310 Ma (Cardona et al., 2016), crustal thickening reached its maximum over a time span of 10-15 Myr, causing the formation of collisional anatectic melts in the continental crust during the early Permian at around 290-280 Ma (Figs. 24 & 25).

The Cisuralian orthogneisses and mylonites in the SNSM, at around 278 ±0.5 Ma are only present in the NW metamorphic belt. Rocks of an equivalent age have been recognized in the Central Cordillera of Colombia as crustal anatectites originating from the Laurentia-Gondwana collision (Cochrane et al., 2014a; Vinasco et al., 2006). Permian granitoids that present inliers of metasedimentary rocks of equivalent age

have been recognized as far as the southern Maya block in the Chiapas Massif (Weber et al., 2007). Mexican and Colombian orthogneisses share a compressional origin that differs from other Permian granitoids found further to the south of the Andes interpreted as being the result of lithospheric thinning (Mišković et al., 2009; Sempere et al., 2002).

Zircon age and trace element core-rim relations prove that the principal Permian arc plutons intruded and recycled Gondwana crust as suggested by Cochrane et al. (2014a). In the SNSM the post collisional crystallization occurred at ca. 278 ± 0.5 Ma, and later high-grade metamorphism at ca. 250 Ma. Inheritance of zircons with Grenvillian U-Pb ages evidences a continuous magmatic arc through the Central Cordillera, the Perijá Range and the Merida Andes existed with a highly similar tectonic history to coeval granitoids northeastern Mexico (Weber et al., 2007).

Furthermore, during Permian times calcareous reefs fringed the arc and shallow marine sediments deposited in a nascent back-arc basin (Fig. 24 & 25). Remnants of these basin deposits are found on the E flank of the SNSM, the Perija Range, the Santander Massif, and the Merida Andes (Cardona et al., 2016; Langenheim, 1959; Laya and Tucker, 2012; Patarroyo, 2001; Villarroel and Mojica, 1987).

Geochronology and detailed mapping shows that an extensive area mapped homogeneously as mylonitic orthogneisses in the Valencia creek (Cardona et al., 2010c) is in fact a sequence consisting of meta-sediments, metabasites and meta-igneous rocks evidenced by the occurrence of marble seams and layered amphibolites. We propose to include within the Gaira Schists the undifferentiated amphibole schists that crop out in the northern part of the SNSM, where marble beds are frequent as well as interbedded with amphibolites and biotite schists.

In this context, the SNSM displays the record of a Permian arc and basin, which underwent a period of collisional magmatism between 300-280 Ma during Laurentia-Gondwana collision in the Ouachita-Alleghanian orogenic episode. The accretion of the so-called "Tahamí" terrane in the NW of Gondwana constituted the basement of the Central Cordillera (Vinasco et al., 2006), this interaction was responsible for an orogeny whose climax was the Pangaea amalgamation followed by Barrovian metamorphism. The final stage of this orogenic phase was marked by the onset of Pacific subduction during the Early Triassic beneath the recently formed Pangaea supercontinent (Figs. 24 & 25).

5.4 Post-Orogenic Collapse and metamorphism during Pangaea Break-Up

250-225 Ma

Pangæa agglutination at this part of the proto-Andean margin is marked by post-collisional anatectic melting at ca. 278 ±0.5 Ma. This magmatism was followed 30 Myr later by *P-T* peak metamorphic conditions at ca. 250 Ma. This implies that the early Triassic peak metamorphism occurred several tens of million years after the deformation phases that were responsible for crustal thickening.

Between 240-230 Myr isothermal decompression was triggered by crustal extension that caused zircon recrystallization (Figs. 10, 13, 14, 24 & 25). The mechanism for extension can be explained by delamination of the slab of the overriding plate that causes plate decoupling, trench retreat and decrease on the convergence rates (Gorczyk et al., 2007). In this context, crustal delamination influenced a transition from compression to extension, given that crustal delamination triggers extension in

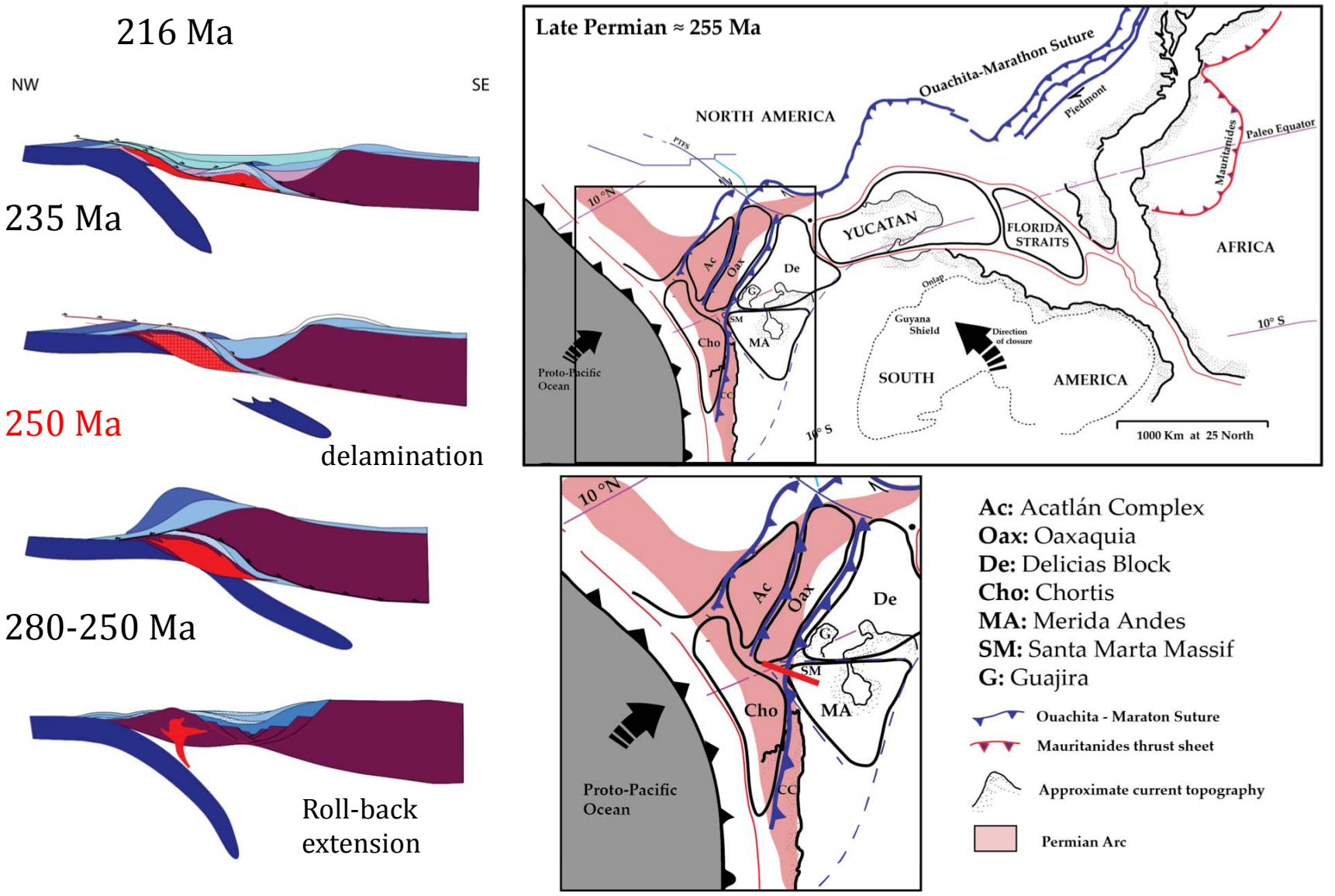

Figure 24. a) Schematic multi-stage evolution for the conjugate NW Gondwana margin and related arcs during Laurentia-Gondwana interaction. b) Palaeogeographic reconstruction of Pangaea late Permian ≈ 250 Ma, Gondwana and Laurentia are assembled entraining the Mexican- Central American Blocks in which a Permian arc is emplaced, modified after (Pindell, 1985; Van Der Lelij, 2013; Weber et al., 2007)

convergent orogens (Houseman and Molnar, 2001). It has been shown that continued extension causes partial melting of the crust and remobilization that can last for a range of 10 My (Ashworth and Brown, 1990; England and Richardson, 1977; Stüwe, 2007). Extension as well enhances the geothermal gradient, for this particular case documented during retrograde HT-LP metamorphism by an isothermal decompression that lasted between 240-225 Myr. Coeval with thermal weakening and extension occurred the formation back-arc marginal basins in half-graben systems filled with shallow marine carbonates, volcanic deposits and clastic sediments from the erosion of exhumed Precambrian basement (Fig. 24a). The geochemical composition of the La Secreta Mylonites allowed identifying volcanoclastic and mafic protoliths for this unit, which is coherent with Triassic mafic magmatism associated with an attenuated crust. For instance, based on matching 3591 analyses from the Ancomp database, the Bt+Grt+Pl schist sample CVI-13108 is comparable with the chemical composition of the middle to upper Triassic volcanoclastic Los Indios and Corual formations that crops out on the southeastern flank of the SNSM (Tschanz et al., 1969) (Table A5).

In contrast, the garnet amphibolite samples from La Secreta Mylonites (CVI-1388, LRW-21) shows a very dominant gabbroid-basaltic trend in the field of ultrabasic rocks (Bas et al., 1986). Further calibration with the Ancomp database hints at olivine-gabbro, gabbro, norite, diabas or a mafic volcaniclastic rock as protolith. The protolith database evaluation allows defining spilite or pillow lavas as protolith. Furthermore, the common occurrence of ultramafic pockets due to hyperextension within La Secreta Mylonites provides additional evidence for a tectonic extensional regime.

The continuous extensional process that permitted the onset of mafic magmatism induced an increase in the thermal gradient along with decompression. Isothermal

decompression was the main cause for retrograde metamorphism that affected the lower crustal sequences of the Alleghenides orogen as observed in the garnet retrograde zoning in metapelites, which for the proposed model, would fit a thermal re-equilibration of a thinned lithosphere. Ti-in-zircon thermometry demonstrated that metamorphic zircon grew within the P-T conditions estimated from the mineral paragenesis Grt+Bt, Hbl+Grt+Pl of the previously described samples from La Secreta Mylonites. These results bracket the period from 250-220 Ma for the Triassic metamorphism followed by the onset of magmatism during the upper Triassic that reworked the basement of the IB.

Kinematic indicators attest to a dextral shear (Fig. 7a, b) and in this case crustal extrusion more likely occurred by dextral strike slip tectonics during the Appalachian-Ouachitas Orogeny between about 315-273 Ma (Sacks and Secor, 1990). This tectonic segregation is coeval with the dynamic metamorphism (Sawyer and Barnes, 1988), and in consequence produced the mylonitic fabric c.a. ≈ 240 Ma. Crustal thickening lasted at least for 20 Myr until metamorphic peak conditions and thermal re-equilibration were reached. After the metamorphic peak, orogenic collapse led to crustal extension, and continued Pacific subduction caused the development of a continental arc from the Early Triassic to the Late Jurassic. Remnants of this arc are well preserved in the SE flank of the SNSM, where the rift had its major extension and thick volcanoclastic sequences developed in a back-arc basin, which were later affected by intra-plate arc magmatism (Figs. 24 & 25). *P-T* trajectories indicate that deformation and metamorphism of the second metamorphic phase occurred simultaneously.

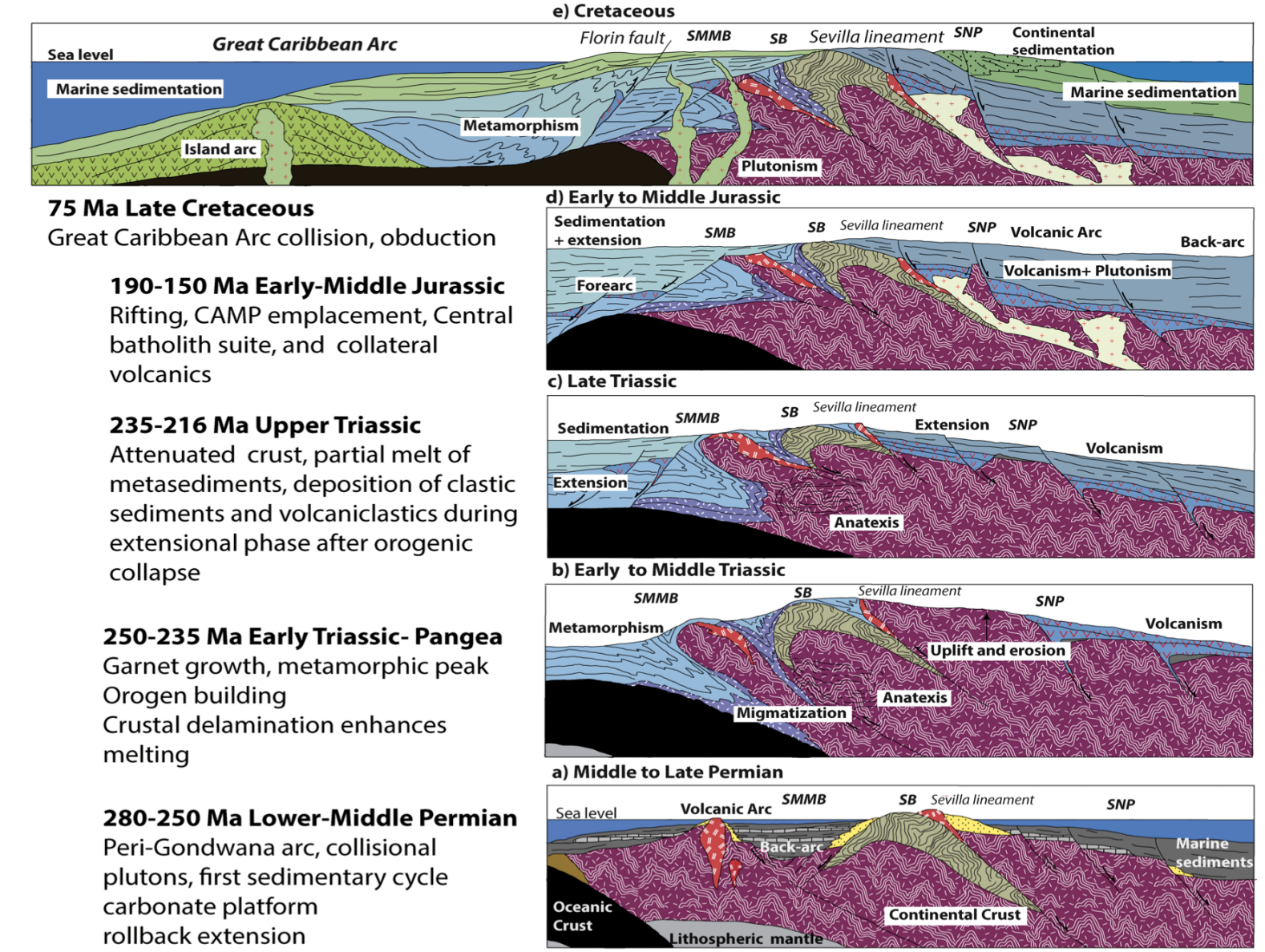

Figure 25. a) Schematic not-to-scale multi-stage tectono-metamorphic evolution for the SNSM massif since Late Permian to Late Cretaceous times, involving metamorphism, anatexia, and sedimentation cycles.

During the Triassic onset of rifting, magmatism evolved from intra plate to oceanic during Pangaea break-up. This process advanced in a rift that gave origin to the Atlantic Ocean (Cochrane et al., 2014a). Emerged Paleozoic and Precambrian massifs acted as source areas for the sediments that filled the growing rift basins. This is clearly evidenced by zircon populations that show a regional episode of arc plutonism during the Early Jurassic. This plutonic episode is distributed along the Andes and defines the drifting between the Central Cordillera to the south and the Chortis-Mexico block in North and Central America (Pindell and Kennan, 2009) (Fig 24b).

6. CONCLUSIONS

1) The gneissic units of the Sevilla Metamorphic Belt showed late Neoproterozoic ages, precluding an allocthonous origin for the SB and a Permian origin for the Sevilla lineament (Tschanz et al., 1974). Units correlatable with the Central Cordillera basament (Tahamí Terrane) are found instead in the metamorphic suites of La Secreta Mylonites and El Encanto Orthogneiss at the IB that are the continuation of the Permo-Triassic basement of the Lower Magdalena Valley. The Sevilla Metamorphic Belt units are a remnant of a late Neoproterozoic arc related to an ocean that existed between Laurentia and Amazonia during early Rodinia break-up and the later Brazilian/Pan-African orogeny that led to Gondwana assembly. This is evidenced in the ages of the gneisses of the Sevilla Metamorphic Belt of 890.83±12, 796±18 that are too young to be related with the Grenvillian orogeny. The Sevilla lineament therefore is a suture that suffered normal reactivation as suspected by (Tschanz et al., 1974) during Triassic-

Jurassic rifting and facilitated pluton emplacement, this major structural feature played as well a fundamental role during the Cenozoic evolution of the SNSM.

2) We document collisional plutonism that caused partial melting of the continental crust at ca. 278 ± 0.5 Ma and our prograde metamorphic event (D1) at ca. 250 Ma that may reflect the delayed thermal response of a crustal thickenning. This first tectonic cycle was linked to the closure of the Rheic Ocean that juxtaposed the Permian arc to the Neoproterozoic Pan-African units of the SB at the NW margin of Gondwana. Collisional Permian granitoids with Triassic metamorphic overprint are found in Oaxaquia, Acatlán and Maya blocks, and the Central cordillera of Colombia. These plutons confirm the existence of a late-Carboniferous-Permian magmatism that connected the Ouachita fold belt with the Oaxaquia terrane at the Central Pangæa Mountains, magmatism extended from southern North America through Central America and northern South America.

3) During collision prograde Hbl growth in an anti-clockwise P-T-t path, defines the Alleghanian-Ouachitan belt in NW Gondwana as an example of an evolving orogen that experienced metamorphic peak after crustal thickening. This is documented by an early high-pressure event (11 Kb ≈ 35km depth Hbl+Pl+Qtz), and the influence of a non-constrained tectonic overpressure due to dextral shear.

4) The rocks reached their thermal metamorphic peak at 830ºC and 13 kb at ca. 250 Ma, at this moment zircon metamorphic growth took place. We interpret this phase as result of collisional processes of the Central Pangaean Orogen or Alleghenides.

5) Metamorphism at ca. 250 Ma has so far been regarded as independent of the Alleghanian-Ouachitan orogeny, because its age was not linked to Pangaea amalgamation and closure of the Rheic Ocean at around 300-280 Ma for this part of

Gondwana but rather to terrane accretion or a different orogenic event. However, this assumption underestimates the fact that the timing of crustal thickening and thermal re-equilibration can post-date collision, and that metamorphic peak conditions are reached several tens of millions of years after crustal thickening occurred (Stüwe, 2007). For this reason we postulate a continued single metamorphic event that reached its metamorphic peak ca. 40 Myr after the Laurentia-Gondwana collision, with at least 10 Myr for crustal thickening and 30 Myr until thermal re-equilibration occurred at peak *P-T* conditions. Understanding this equilibration as the moment at which mineral paragenesis crystallize. This long lasting coupling between Laurentia and Gondwana is related as well to oblique top to NE dextral shear acting during Pangaea amalgamation.

6) After the thermal peak conditions were reached the thickened crust created enough potential energy to hamper the convergence rate between the Pacific plate and the Pangaea supercontinent, which led to slab retreat and later delamination of the lower crust. As recently documented the removal of a lithospheric root causes a rapid increase in the topographic relief and onset of erosion of a previously thickened crust (Duretz and Gerya, 2013; Stüwe, 2007). The erosional cycle lasted for several million years as recorded by the Permian-Triassic clastic back-arc basin deposits, which register maximum depositional ages of ca. 260 Ma in the SNSM. The metamorphic age of the Chiapas massif at ca. 257 Ma (Weber et al., 2007) provides a temporal limit for the duration of the Pangaea formation.

7) A retrograde phase of isothermal decompression is recorded on garnet rims enriched in Mn with an episode of zircon recrystallization at ca. 240 Ma evidencing thinning and thermal weakening of the crust. The geochemical signature of garnet

amphibolites, which points to ultrabasic protoliths, evidences the onset of mafic magmatism following the pronounced crustal attenuation with deformation occurring coeval with metamorphism as evidenced by sheared zircon crystals of this age.

8) Zircon recrystallization persisted between 240–225 Ma at HT-LP conditions indicating a progressive thinning of continental crust during rifting and break-up of western Pangaea. During this process, mafic magma generation persisted at least until ca. 220 Ma. By about 216 Ma the removal of the conjugate margin suppressed most of the Permian arc remnants from NW Gondwana isolating remnants of this arc in the Mexican and Central American terranes from the continental margin. The continuation of Pacific plate subduction reactivated by slab break-off and isostatic rebound caused the arc to migrate continent-ward, and the former back-arc Permian basin occupied a fore-arc position fed by an emerging Jurassic arc. The basin fill of back-arc volcanoclastic deposits is recorded in the Gaira Schists and the volcanoclastic San Lorenzo Schists. This sedimentary cycle remained active during the Jurassic.

7. REFERENCES

Ashworth, J.R., Brown, M., 1990. High-temperature Metamorphism and Crustal Anatexis. Springer Science & Business Media.

Bas, M.J.L., Maitre, R.W.L., Streckeisen, A., Zanettin, B., IUGS Subcommission on the Systematics of Igneous Rocks, 1986. A Chemical Classification of Volcanic Rocks Based on the Total Alkali-Silica Diagram. J. Petrol. 27, 745–750. doi:10.1093/petrology/27.3.745

Bhattacharya, A., Mohanty, L., Maji, A., Sen, S.K., Raith, M., 1992. Non-ideal mixing in the phlogopite-annite binary: constraints from experimental data on Mg?Fe partitioning and a reformulation of the biotite-garnet geothermometer. Contrib. Mineral. Petrol. 111, 87–93. doi:10.1007/BF00296580

Bosch, D., Gabriele, P., Lapierre, H., Malfere, J.-L., Jaillard, E., 2002. Geodynamic significance of the Raspas Metamorphic Complex (SW Ecuador): geochemical and isotopic constraints. Tectonophysics 345, 83–102. doi:10.1016/S0040-1951(01)00207-4

Bustamante, A., Juliani, C., Essene, E.J., Hall, C.M., Hyppolito, T., 2012. Geochemical constraints on blueschist- and amphibolite-facies rocks of the Central Cordillera of Colombia: the Andean Barragan region. Int. Geol. Rev. 54, 1013–1030. doi:10.1080/00206814.2011.594226

Bustamante, C., Cardona, A., Saldarriaga, M., García-Casco, A., Valencia, V., Weber, M., 2009. Metamorfismo de los esquistos verdes y anfibolitas pertenecientes a los esquistos de santa marta, sierra nevada de santa marta (colombia): ¿registro de la colisión entre el arco caribe y la margen suramericana? Bol. Cienc. Tierra Núm 25 2009 07-26 0120-3630.

Camargo, S., 2014. Estructura litosférica asociada a la Sierra Nevada de Santa Marta a partir de datos de gravimetría, magnetometría y sismología.

Cardona, A., Chew, D., Valencia, V., Bayona, G., Mišković, A., Ibañez-Mejía, M., 2010a. Grenvillian remnants in the Northern Andes: Rodinian and Phanerozoic paleogeographic perspectives. J. South Am. Earth Sci., The Grenville Orogen in Central and South America 29, 92–104. doi:10.1016/j.jsames.2009.07.011

Cardona, A., Cordani, U.G., MacDonald, W.D., 2006. Tectonic correlations of pre-Mesozoic crust from the northern termination of the Colombian Andes, Caribbean region. J. South Am. Earth Sci. 21, 337–354. doi:10.1016/j.jsames.2006.07.009

Cardona, A., Valencia, V.A., Lotero, A., Villafañez, Y., Bayona, G., 2016. Provenance of middle to late Palaeozoic sediments in the northeastern Colombian Andes: implications for Pangæa reconstruction. Int. Geol. Rev. 58, 1914–1939. doi:10.1080/00206814.2016.1190948

Cardona, A., Valencia, V., Bayona, G., Duque, J., Ducea, M., Gehrels, G., Jaramillo, C., Montes, C., Ojeda, G., Ruiz, J., 2011. Early-subduction-related orogeny in the northern Andes: Turonian to Eocene magmatic and provenance record in the Santa Marta Massif and Rancheria Basin, northern Colombia. Terra Nova 23, 26–34. doi:10.1111/j.1365-3121.2010.00979.x

Cardona, A., Valencia, V., Bustamante, C., García-Casco, A., Ojeda, G., Ruiz, J., Saldarriaga, M., Weber, M., 2010b. Tectonomagmatic setting and provenance of the Santa Marta Schists, northern Colombia: Insights on the growth and approach of Cretaceous Caribbean oceanic terranes to the South American continent. J. South Am. Earth Sci., Sierra Nevada de Santa Marta and Adjacent Basins 29, 784–804. doi:10.1016/j.jsames.2009.08.012

Cardona, A., Valencia, V., Garzón, A., Montes, C., Ojeda, G., Ruiz, J., Weber, M., 2010c. Permian to Triassic I to S-type magmatic switch in the northeast Sierra Nevada de Santa Marta and adjacent regions, Colombian Caribbean: Tectonic setting and implications within Pangæa paleogeography. J. South Am. Earth Sci., Sierra Nevada de Santa Marta and Adjacent Basins 29, 772–783. doi:10.1016/j.jsames.2009.12.005

Chemenda, A.I., Mattauer, M., Bokun, A.N., 1996. Continental subduction and a mechanism for exhumation of high-pressure metamorphic rocks: new modelling and field data from Oman. Earth Planet. Sci. Lett. 143, 173–182. doi:10.1016/0012-821X(96)00123-9

Chew, D., Magna, T., Kirkland, C., Miskovic, A., Cardona, A., Spikings, R., Schaltegger, U., 2008. Detrital zircon fingerprint of the Proto-Andes: Evidence for a Neoproterozoic active margin? Precambrian Res. 167, 186–200. doi:10.1016/j.precamres.2008.08.002

Chew, D.M., Schaltegger, U., Kosler, J., Whitehouse, M.J., Gutjahr, M., Spikings, R.A., Miskovic, A., 2007. U-Pb geochronologic evidence for the evolution of the Gondwanan margin of the north-central Andes. Geol. Soc. Am. Bull. 119, 697–711. doi:10.1130/B26080.1

Chicangana, G., Kammer, A., 2016a. Evolución tectónica de la Cordillera Oriental de Colombia. 1. Del Océano Iapeto a la Pangæa: una visión preliminar. Segunda parte: Evolución Geodinámica. Geol. Colomb. 38, 75–88.

Chicangana, G., Kammer, A., 2016b. Evolución tectónica de la cordillera oriental de Colombia. Desde la apertura del océano Iapeto hasta la conformación de la Pangæa: una visión preliminar. Primera Parte: aspectos geológicos. Geol. Colomb. 38, 65–74.

Cochrane, R., Spikings, R., Gerdes, A., Ulianov, A., Mora, A., Villagómez, D., Putlitz, B., Chiaradia, M., 2014a. Permo-Triassic anatexis, continental rifting and the disassembly of western Pangæa. Lithos 190–191, 383–402. doi:10.1016/j.lithos.2013.12.020

Cochrane, R., Spikings, R., Gerdes, A., Winkler, W., Ulianov, A., Mora, A., Chiaradia, M., 2014b. Distinguishing between in-situ and accretionary growth of continents along active margins. Lithos 202-203, 382–394. doi:10.1016/j.lithos.2014.05.031

Colmenares, F., 2007. Evolución Geohistorica de la Sierra Nevada de Santa Marta (Internal report No. PS 025-06). INGEOMINAS.

Cordani, U.G., Pimentel, M.M., Araújo, C.E.G. de, Fuck, R.A., 2013. The significance of the Transbrasiliano-Kandi tectonic corridor for the amalgamation of West Gondwana. Braz. J. Geol. 43, 583–597. doi:10.5327/Z2317-48892013000300012

Cordani, U.G., Cardona, A., Jimenez, D.M., Liu, D., Nutman, A.P., 2005. Geochronology of Proterozoic basement inliers in the Colombian Andes: tectonic history of remnants of a fragmented Grenville belt. Geol. Soc. Lond. Spec. Publ. 246, 329–346. doi:10.1144/GSL.SP.2005.246.01.13

Cox, K., 1979. The interpretation of igneous rocks. Chapman and Hall, London.

Doolan, B., 1970. Structure and metamorphism of the Santa Marta Area Colombia, South America [microform] / [WWW Document]. URL https://www.researchgate.net/publication/34351494_Structure_and_metamorphism_of_the_Santa_Marta_Area_Colombia_South_America_microform (accessed 7.20.16).

Duque, T., 2009. Geocronología (U/Pb y 40Ar/39Ar) y geoquímica de los intrusivos paleógenos de la Sierra Nevada de Santa Marta y sus relaciones con la tectónica del Caribe y el arco magmático circun-caribeñ.

Duretz, T., Gerya, T.V., 2013. Slab detachment during continental collision: Influence of crustal rheology and interaction with lithospheric delamination. Tectonophysics 602, 124–140. doi:10.1016/j.tecto.2012.12.024

England, P.C., Richardson, S.W., 1977. The influence of erosion upon the mineral fades of rocks from different metamorphic environments. J. Geol. Soc. 134, 201–213. doi:10.1144/gsjgs.134.2.0201

Forero, A., 1967. Notas preliminares sobre la estratigrafía del Paleozoico en el Norte de los Andes de Colombia.

Franke, W., 2006. The Variscan orogen in Central Europe: construction and collapse. Geol. Soc. Lond. Mem. 32, 333–343. doi:10.1144/GSL.MEM.2006.032.01.20

Ganade de Araujo, C.E., Rubatto, D., Hermann, J., Cordani, U.G., Caby, R., Basei, M.A.S., 2014. Ediacaran 2,500-km-long synchronous deep continental subduction in the West Gondwana Orogen. Nat. Commun. 5, 5198. doi:10.1038/ncomms6198

Gansser, A., 1955. Contribución a la geología y petrografía de la Sierra Nevada de Santa Marta (Colombia, Suramérica). Traducido de Gansser, A., 1955. Ein Beitrag zur Geologie und Petrographie der Sierra Nevada de Santa Marta (Kolumbien, Sudamerika):

Ghent, E.D., 1976. Plagioclase-garnet-Al 2 SiO 5 -quartz; a potential geobarometer-geothermometer. Am. Mineral. 61, 710–714.

Gorczyk, W., Willner, A.P., Gerya, T.V., Connolly, J.A.D., Burg, J.-P., 2007. Physical controls of magmatic productivity at Pacific-type convergent margins: Numerical modelling. Phys. Earth Planet. Inter. 163, 209–232. doi:10.1016/j.pepi.2007.05.010

Henry, D.J., 2005. The Ti-saturation surface for low-to-medium pressure metapelitic biotites: Implications for geothermometry and Ti-substitution mechanisms. Am. Mineral. 90, 316–328. doi:10.2138/am.2005.1498

Holdaway, M.J., 2001. Recalibration of the GASP geobarometer in light of recent garnet and plagioclase activity models and versions of the garnet-biotite geothermometer. Am. Mineral. 86, 1117–1129. doi:10.2138/am-2001-1001

Hollister, L.S., 1966. Garnet Zoning: An Interpretation Based on the Rayleigh Fractionation Model. Science 154, 1647–1651. doi:10.1126/science.154.3757.1647

Ibanez-Mejia, M., Ruiz, J., Valencia, V., Cardona, A., Gehrels, G., Mora, A., 2011. The Putumayo Orogen of Amazonia and its implications for Rodinia reconstructions: New U–Pb

geochronological insights into the Proterozoic tectonic evolution of northwestern South America. Precambrian Res. 191, 58–77. doi:10.1016/j.precamres.2011.09.005
Irvine, T.N., Baragar, W.R.A., 1971. A Guide to the Chemical Classification of the Common Volcanic Rocks. Can. J. Earth Sci. 8, 523–548. doi:10.1139/e71-055
John, T., Scherer, E.E., Schenk, V., Herms, P., Halama, R., Garbe-Schönberg, D., 2010. Subducted seamounts in an eclogite-facies ophiolite sequence: the Andean Raspas Complex, SW Ecuador. Contrib. Mineral. Petrol. 159, 265–284. doi:10.1007/s00410-009-0427-0
Lanari, P., Vidal, O., De Andrade, V., Dubacq, B., Lewin, E., Grosch, E.G., Schwartz, S., 2014. XMapTools: A MATLAB©-based program for electron microprobe X-ray image processing and geothermobarometry. Comput. Geosci. 62, 227–240. doi:10.1016/j.cageo.2013.08.010
Lancelot, J.R., Boullier, A.M., Maluski, H., Ducrot, J., 1983. Deformation and related radiochronology in a late Pan-African mylonitic shear zone, adrar des Iforas (Mali). Contrib. Mineral. Petrol. 82, 312–326. doi:10.1007/BF00399709
Langenheim, J.H., 1959. Preliminary Notes on Plant Fossils from Late Paleozoic and Early Mesozoic Rocks in the Cordillera Oriental of Colombia. Bol. Geol. 3.
Laya, J.C., Tucker, M.E., 2012. Facies analysis and depositional environments of Permian carbonates of the Venezuelan Andes: Palaeogeographic implications for Northern Gondwana. Palaeogeogr. Palaeoclimatol. Palaeoecol. 331–332, 1–26. doi:10.1016/j.palaeo.2012.02.011
MacDonald, W.D., Doolan, B.L., Cordani, U.G., 1971. Cretaceous-Early Tertiary Metamorphic K-Ar Age Values from the South Caribbean. Geol. Soc. Am. Bull. 82, 1381–1388. doi:10.1130/0016-7606(1971)82[1381:CTMKAV]2.0.CO;2
Macdonald, W.D., Hurley, P.M., 1969. Precambrian Gneisses from Northern Colombia, South America. Geol. Soc. Am. Bull. 80, 1867. doi:10.1130/0016-7606(1969)80[1867:PGFNCS]2.0.CO;2
Mamani, M., Worner, G., Sempere, T., 2010. Geochemical variations in igneous rocks of the Central Andean orocline (13 S to 18 S): Tracing crustal thickening and magma generation through time and space. Geol. Soc. Am. Bull. 122, 162–182. doi:10.1130/B26538.1
Mange, M.A., Morton, A.C., 2007. Chapter 13 Geochemistry of Heavy Minerals, in: Developments in Sedimentology. Elsevier, pp. 345–391.
Mateus, D. 2014 Análisis petrológico y geoquímico de las rocas expuestas al costado noroccidental de la sierra nevada de santa marta- sector río guachaca, río don diego. Bsc Thesis, Universidad Nacional de Colombia -Bogotá.
McDonough, W.F., Sun, S. -s., 1995. The composition of the Earth. Chem. Geol. 120, 223–253. doi:10.1016/0009-2541(94)00140-4
Mezger, K., Krogstad, E.J., 1997. Interpretation of discordant U-Pb zircon ages: An evaluation. J. Metamorph. Geol. 15, 127–140. doi:10.1111/j.1525-1314.1997.00008.x
Mišković, A., Spikings, R.A., Chew, D.M., Košler, J., Ulianov, A., Schaltegger, U., 2009. Tectonomagmatic evolution of Western Amazonia: Geochemical characterization and zircon U-Pb geochronologic constraints from the Peruvian Eastern Cordilleran granitoids. Geol. Soc. Am. Bull. 121, 1298–1324. doi:10.1130/B26488.1
Möller, A., 2004. Advances in Zircon Geochronology: Understanding Zircon Growth and Modification During Metamorphism. AGU Spring Meet. Abstr.
Möller, A., ÓBrien, P.J., Kennedy, A., Kröner, A., 2003. The Use and Abuse of Th-U Ratios in the Interpretation of Zircon, in: EGS - AGU - EUG Joint Assembly. Presented at the EGS - AGU - EUG Joint Assembly.
Murali, A.V., Parthasarathy, R., Mahadevan, T.M., Das, M.S., 1983. Trace element characteristics, REE patterns and partition coefficients of zircons from different geological environments—A case study on Indian zircons. Geochim. Cosmochim. Acta 47, 2047–2052. doi:10.1016/0016-7037(83)90220-X

Nance, R.D., Gutiérrez-Alonso, G., Keppie, J.D., Linnemann, U., Murphy, J.B., Quesada, C., Strachan, R.A., Woodcock, N.H., 2012. A brief history of the Rheic Ocean. Geosci. Front. 3, 125–135. doi:10.1016/j.gsf.2011.11.008

Nance, R.D., Murphy, J.B., Santosh, M., 2014. The supercontinent cycle: A retrospective essay. Gondwana Res. 25, 4–29. doi:10.1016/j.gr.2012.12.026

Ordóñez, O., Pimentel, M., Moraes, R., 2002. GRANULITAS DE LOS MANGOS, UN FRAGMENTO GRENVILLIANO EN LA PARTE ORIENTAL DE LA SIERRA NEVADA DE SANTA MARTA. Rev. Acad. Colomb. Cienc. Exactas Físicas Nat. 0370-3908 26, 169–179.

Patarroyo, P., 2001. Perrinites sp. en las sedimentitas del Pérmico de la Formación Diamante en cercanías de Bucaramanga (Santander - Colombia), in: Geologia Colombiana. Presented at the VII Congreso Colombiano de Geologia.

Peccerillo, A., Taylor, S.R., 1976. Geochemistry of eocene calc-alkaline volcanic rocks from the Kastamonu area, Northern Turkey. Contrib. Mineral. Petrol. 58, 63–81. doi:10.1007/BF00384745

Peucat, J.J., Tisserant, D., Caby, R., Clauer, N., 1985. Resistance of zircons to U–Pb resetting in a prograde metamorphic sequence of Caledonian age in East Greenland. Can. J. Earth Sci. 22, 330–338. doi:10.1139/e85-033

Pindell, J., Dewey, J.F., 1982. Permo-Triassic reconstruction of western Pangæa and the evolution of the Gulf of Mexico/Caribbean region. Tectonics 1, 179–211. doi:10.1029/TC001i002p00179

Pindell, J.L., 1985. Alleghenian reconstruction and subsequent evolution of the Gulf of Mexico, Bahamas, and Proto-Caribbean. Tectonics 4, 1–39. doi:10.1029/TC004i001p00001

Pindell, J.L., Kennan, L., 2009. Tectonic evolution of the Gulf of Mexico, Caribbean and northern South America in the mantle reference frame: an update. Geol. Soc. Lond. Spec. Publ. 328, 1–55. doi:10.1144/SP328.1

Radelli, L., 1962. Acerca de la geología de la Serranía de Perijá entre Codazzi y Villanueva (Magdalena-Guajira, Colombia). Geol. Colomb. 1, 23–42.

Ravna, E.K., 2000. Distribution of Fe2+ and Mg between coexisting garnet and hornblende in synthetic and natural systems: an empirical calibration of the garnet–hornblende Fe–Mg geothermometer. Lithos 53, 265–277. doi:10.1016/S0024-4937(00)00029-3

Restrepo-Pace, P., Ruiz, J., Gehrels, G., Cosca, M., 1997. Geochronology and Nd isotopic data of Grenville-age rocks in the Colombian Andes: new constraints for Late Proterozoic-Early Paleozoic paleocontinental reconstructions of the Americas. Earth Planet. Sci. Lett. 427–441. doi:10.1016/S0012-821X(97)00091-5

Riel, N., Guillot, S., Jaillard, E., Martelat, J.-E., Paquette, J.-L., Schwartz, S., Goncalves, P., Duclaux, G., Thebaud, N., Lanari, P., Janots, E., Yuquilema, J., 2013. Metamorphic and geochronogical study of the Triassic El Oro metamorphic complex, Ecuador: Implications for high-temperature metamorphism in a forearc zone. Lithos 156–159, 41–68. doi:10.1016/j.lithos.2012.10.005

Röhr, C., 1997. Ancomp - a computer program for metamorphic petrology that compares bulk rock analyses and finds out the most similiar ones from a database [WWW Document]. URL http://www.oberrheingraben.de/Ancomp/ancomp.html (accessed 11.3.16).

Rubatto, D., 2002. Zircon trace element geochemistry: partitioning with garnet and the link between U–Pb ages and metamorphism. Chem. Geol. 184, 123–138. doi:10.1016/S0009-2541(01)00355-2

Sanchez, J., Mann, P., 2015. Integrated Structural and Basinal Analysis of the Cesar–Rancheria Basin, Colombia: Implications for its Tectonic History and Petroleum Systems, in: Bartolini, C., Mann, P. (Eds.), Memoir 108: Petroleum Geology and Potential of the Colombian Caribbean Margin. AAPG

Sawyer, E. w., Barnes, S.-J., 1988. Temporal and compositional differences between subsolidus and anatectic migmatite leucosomes from the Quetico metasedimentary belt, Canada. J. Metamorph. Geol. 6, 437–450. doi:10.1111/j.1525-1314.1988.tb00432.x

Schaltegger, U., Fanning, C.M., Günther, D., Maurin, J.C., Schulmann, K., Gebauer, D., 1999. Growth, annealing and recrystallization of zircon and preservation of monazite in high-grade metamorphism: conventional and in-situ U-Pb isotope, cathodoluminescence and microchemical evidence. Contrib. Mineral. Petrol. 134, 186–201. doi:10.1007/s004100050478

Schandl, E.S., Gorton, M.P., 2002. APPLICATION OF HIGH FIELD STRENGTH ELEMENTSTO DISCRIMINATE TECTONIC SETTINGS IN VMS ENVIRONMENTS. Econ. Geol. 97, 629–642. doi:10.2113/gsecongeo.97.3.629

Spikings, R., Cochrane, R., Villagomez, D., Van der Lelij, R., Vallejo, C., Winkler, W., Beate, B., 2015. The geological history of northwestern South America: from Pangæa to the early collision of the Caribbean Large Igneous Province (290–75 Ma). Gondwana Res. 27, 95–139. doi:10.1016/j.gr.2014.06.004

Stüwe, K., 2007. Geodynamics of the Lithosphere: An Introduction. Springer Science & Business Media.

Tracy, R.J., Robinson, P., Thompson, A.B., 1976. Garnet composition and zoning in the determination of temperature and pressure of metamorphism, central Massachusetts. Am. Mineral. 61, 762–775.

Tschanz, C., Jimeno, A., Cruz, J., 1969. Geology of the Sierra Nevada de Santa Marta area, Colombia. Informe interno 1829. INGEOMINAS Bogotá Prelim. Rep. 288pLinks.

Tschanz, C., Marvin, R.F., B, J.C., Mehnert, H.H., Cebula, G.T., 1974. Geologic Evolution of the Sierra Nevada de Santa Marta, Northeastern Colombia. Geol. Soc. Am. Bull. 85, 273–284. doi:10.1130/0016-7606(1974)85<273:GEOTSN>2.0.CO;2

Van der Lelij, R., Spikings, R., Ulianov, A., Chiaradia, M., Mora, A., 2016. Palaeozoic to Early Jurassic history of the northwestern corner of Gondwana, and implications for the evolution of the Iapetus, Rheic and Pacific Oceans. Gondwana Res. 31, 271–294. doi:10.1016/j.gr.2015.01.011

Van der Lelij, R., 2013. Reconstructing north-western Gondwana with implications for the evolution of the Iapetus and Rheic Oceans: a geochronological, thermochronological and geochemical study. University of Geneva.

Vanderhaeghe, O., 2009. Migmatites, granites and orogeny: Flow modes of partially-molten rocks and magmas associated with melt/solid segregation in orogenic belts. Tectonophysics, Hot orogens 477, 119–134. doi:10.1016/j.tecto.2009.06.021

Veloza, G., Styron, R., Taylor, M., Mora, A., 2012. Open-source archive of active faults for northwest South America. GSA Today 22, 4–10. doi:10.1130/GSAT-G156A.1

Villagómez, D., Spikings, R., 2013. Thermochronology and tectonics of the Central and Western Cordilleras of Colombia: Early Cretaceous–Tertiary evolution of the Northern Andes. Lithos 160–161, 228–249. doi:10.1016/j.lithos.2012.12.008

Villagómez, D., Spikings, R., Magna, T., Kammer, A., Winkler, W., Beltrán, A., 2011. Geochronology, geochemistry and tectonic evolution of the Western and Central cordilleras of Colombia. Lithos 125, 875–896. doi:10.1016/j.lithos.2011.05.003

Villarroel, C., Mojica, J., 1987. El Paleozoico Superior (Carbonífero-Pérmico) sedimentario de Colombia: Afloramientos conocidos y características generales. Geol. Colomb. 16, 81–87.

Vinasco, C.J., Cordani, U.G., González, H., Weber, M., Pelaez, C., 2006. Geochronological, isotopic, and geochemical data from Permo-Triassic granitic gneisses and granitoids of the Colombian Central Andes. J. South Am. Earth Sci., Tectonic evolution of the Colombian Andes 21, 355–371. doi:10.1016/j.jsames.2006.07.007

Weber, B., Iriondo, A., Premo, W.R., Hecht, L., Schaaf, P., 2007. New insights into the history and origin of the southern Maya block, SE México: U–Pb–SHRIMP zircon geochronology

from metamorphic rocks of the Chiapas massif. Int. J. Earth Sci. 96, 253–269. doi:10.1007/s00531-006-0093-7
Wright, W.I., 1938. The composition and occurrence of garnets. Am. Mineral. 436–449.
Zuluaga, C., Stowell, H., 2012. Late Cretaceous–Paleocene metamorphic evolution of the Sierra Nevada de Santa Marta: Implications for Caribbean geodynamic evolution. J. South Am. Earth Sci. 34, 1–9. doi:10.1016/j.jsames.2011.10.001

CHAPTER 2

Cenozoic exhumation of the Sierra Nevada de Santa Marta: From a collisional margin to a transpressive boundary

Alejandro Piraquive[1,2], Matthias Bernet[1], Andreas Kammer[2], Maria Giuditta Fellin[3]

1. Institut des Sciences de la Terre, Université Grenoble Alpes, CNRS 1381, rue de la Piscine, 38058 Grenoble Cedex 9, France.
2.. Grupo de Investigación en Geologia Estructural y Fracturas Universidad Nacional de Colombia. apartado Aéreo, 14490 Bogotá, Colombia.
3. Department of Earth Sciences, Institute of Geochemistry and Petrology, ETH Zentrum, Clausiusstrasse 25, 8092 Zurich, Switzerland

Abstract

New low-temperature thermochronological data from the Precambrian, Permian-to Jurassic, Late Cretaceous and Paleocene-Eocene rocks that make up the northern metamorphic belt of the Sierra Nevada de Santa Marta (SNSM) of the Northern Andes of Colombia reveal exhumation trends in this part of the continental margin during Paleocene to Miocene times. Our analysis involves apatite and zircon fission track, as well as apatite (U-Th)/He dating, which allowed to constrain the thermal histories (~240 ºC – ~60ºC) of an inverted crustal sequence that exposes greenschist to granulite facies metamorphic rocks. Temperature-time paths evidence that cooling occurred diachronously in the massif through the activation of NW verging thrusts with the onset of rapid erosional exhumation after collision and TTG series pluton emplacement under an initially high geothermal gradient of 40ºC/km. In this regime the massif exhumed at elevated rates ~0.9 km/Myr during 50-45 Ma. These rates incremented to 2 km/Myr for the interval 45-40 Ma with a decreasing geothermal gradient of 30ºC/km, reaching the highest rates of 2.7km during 37-35 Myr. We interpret the exhumation of this inverted lower crustal sequence because of coupling of ductile extrusion of a thickened continental crust and surface denudation. Post-Eocene exhumation events show subsequent cooling under a decreased exhumation rates of ~0.2 km/Myr at ca. 25 Ma, related to the start of a composite transpressive-transtensive regime in the southern Caribbean plate boundary as a result of changes in convergence between the Caribbean and South American plates. This reorganization led to the activation of the NW trending Santa Marta - Bucaramanga (SMBF) and E-W trending Oca (OF) faults. These faults contributed to the partitioning of a subsequent oblique convergence and transferred strain from the Caribbean Plate into the Santander Massif, the Eastern Cordillera of Colombia, the Perijá Range, and the Merida Andes until the late Miocene. We interpret that this new tectonic regime inhibited further NW thrust propagation and caused a NE tilting of the SNSM massif due to extensional activity of the SMBF coupled with the

tectonic drag caused by the transit of the Caribbean plate These processes resulted in attenuated exhumation rates of ~0.09 km/Myr that persisted until the late Miocene during the SNSM thermal re-equilibration.

Key words: Northern Andean block, low temperature thermochronology, collisional plutonism, lower crustal channel

1. INTRODUCTION

Bedrock thermochronological studies play a major role in elucidating evolutionary trends in mountain building around the globe. Recent thermochronological studies in the Northern Andes revealed the influence of tectonic process coupled with climatic influence during the growth of this mountain belt (Bermúdez et al., 2010, 2011, 2013; Michalak et al., 2016; Mora et al., 2008, 2010, Parra et al., 2009, 2010; Restrepo et al., 2009; Spikings and Simpson, 2014; van der Lelij et al., 2010, 2016; Villagómez et al., 2011b; Villagómez and Spikings, 2013; Whipple, 2009). Nevertheless, it is still matter of debate if exhumation is strongly dependent on climate-induced erosion or if it is mostly controlled by tectonics (Molnar and England, 1990; Montgomery et al., 2001; Raymo and Ruddiman, 1992; Reiners et al., 2003; Whipple, 2009). This problem has intrigued geologists for decades, and it seems that every specific geological problem must be addressed under the light of sedimentological and petrographic evidences and a well–constrained structural context.

At the current location of the Northern-Andean block the Caribbean-South American boundary presents a transpressive situation (Cardona et al., 2011a; Kennan and Pindell, 2009; Taboada et al., 2000). A major question remain on the evolution of the Sierra Nevada de Santa Marta massif (SNSM): 1) What is the mechanism or

mechanisms that operated during the uplifting phases experienced by SNSM during the Cenozoic?

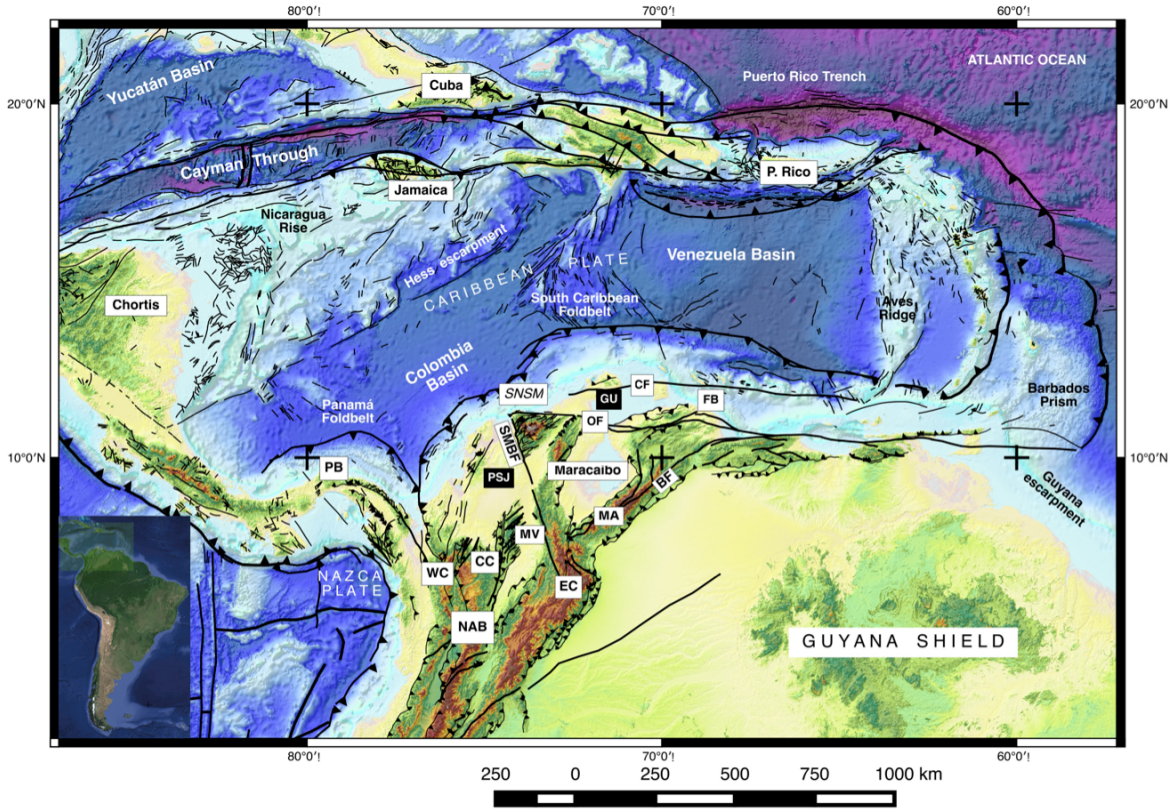

Figure 1. Regional tectonic map of the Caribbean realm showing the most relevant geological features intervening in the plate boundary configuration. after (Veloza et al., 2012). Elements of the North Andean Block (NAB): Maracaibo block, SNSM: Sierra Nevada de Santa Marta, OF: Oca Fault, CF: Cuisa Fault, SMBF: Santa Marta-Bucaramanga Fault, GU: Guajira Basin, PSJ: Plato-San Jorge Basin MA: Mérida Andes, BF: Boconó Fault, FB: Falcon Basin, WC: Western Cordillera, CC: Central Cordillera, EC: Eastern Cordillera, MV: Magdalena Valley, PB: Panamá Block.

In this paper we present a new low-temperature thermochronology dataset for the SNSM massif, which we combine with previously published apatite fission-track (AFT) data of Villagómez et al., 2011b, and apatite (U-Th)/He by Cardona et al., 2011a

Our aims are 1) to constrain erosion rates during a first phase of rapid post-magmatic cooling 2) to identify the major role played by thrust faults during lower crustal extrusion, 3) to evaluate the magnitude of exhumation of three different tectonic

blocks separated by master faults that are inherited reactivated sutures, 4) to evaluate new and pre-existent thermochronological data in order to asses a tectonic model for Eocene-Miocene exhumation of the metamorphic complexes, and 5) to establish regional correlations between the SNSM, the Merida Andes and the Eastern Cordillera of Colombia.

2. TECTONIC SETTING

The interaction between the Caribbean and South American plates can be traced to Campanian times, and is directly related with the Caribbean Large Igneous Province (CLIP) accretion into the western margin of South America (Kerr et al., 1997; Spikings et al., 2015; Villagómez et al., 2011a). The orogenic evolution of the Northern Andes during the Cenozoic is the result of a complex interaction between the Caribbean, Nazca, Cocos and South American plates (Fig. 1). The transit of the Caribbean plate from the Pacific around the NW corner of South America constituted a major event that is recorded at least since Late Cretaceous (Campanian) times, when the old crust of the Pacific plate was incorporated in a juvenile crust of the nascent Caribbean plate. Between 139-69 Myr the CLIP, an oceanic plateau, formed above the Galapagos Plume by the interaction of multiple oceanic intraplate igneous structures (Hoernle et al., 2004; Kerr et al., 1997). The origin of this plateau has been attributed to the rise of an asthenospheric plume that induced subduction at its margins, which later evolved into the Great Caribbean Arc and the Central American Volcanic arc systems during the Late Cretaceous (Whattam and Stern, 2015). The CLIP approached NW South America

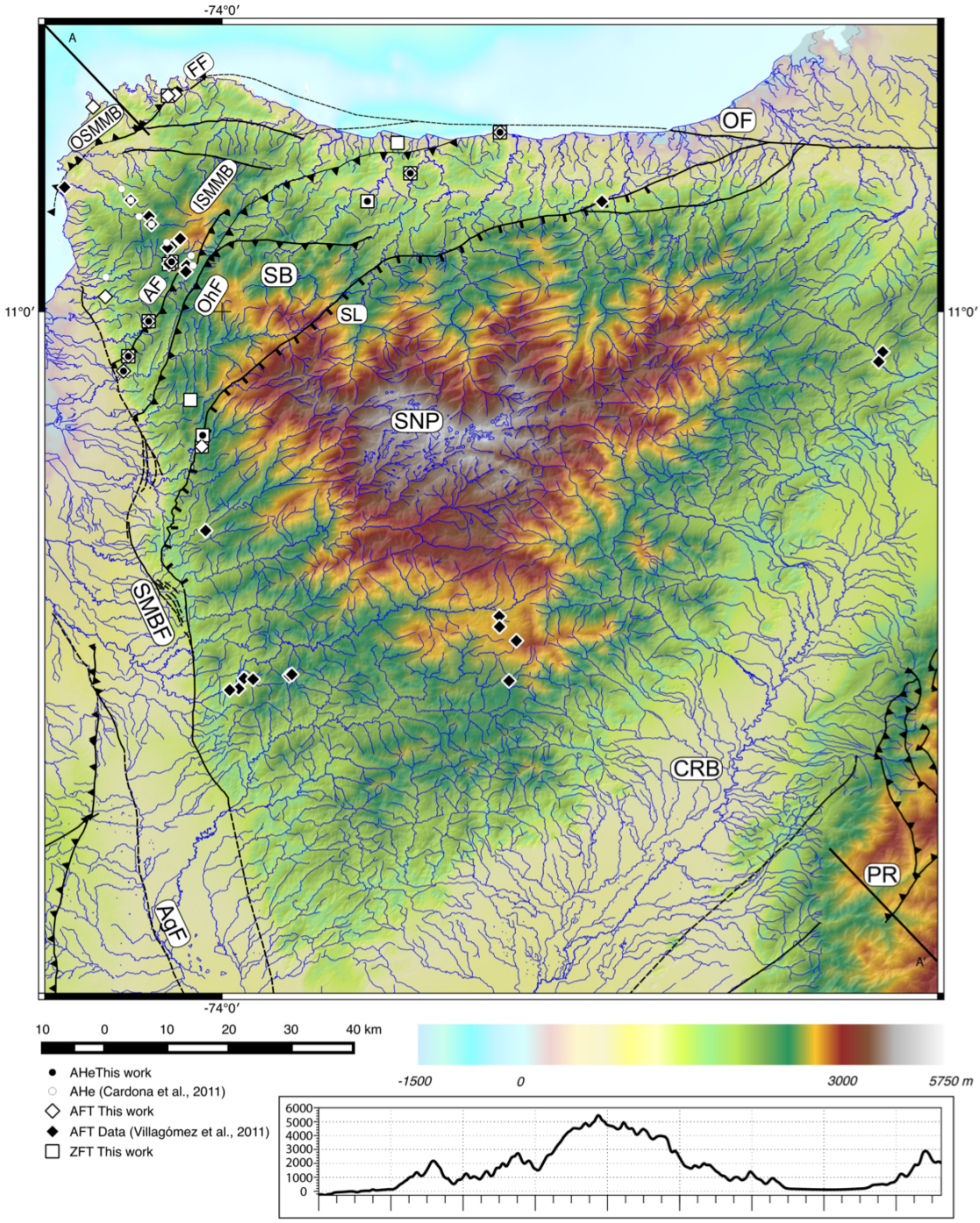

Figure 2. Digital elevation map (DEM) of the Sierra Nevada de Santa Marta Massif, including sample localities from previous studies and the new acquired samples. Major structural elements are indicated: OB:Outer Santa Marta Metamorphic Belt, IB: Innner Santa Marta Metamorphic Belt, SB: Sevilla Metamorphic Belt, SL: Sevilla Lineament, SNP: Sierra Nevada Province, SMBF: Santa Marta Bucaramanga Fault, OF: Oca Fault, AF: Aguja Fault, OhF: Orihueca Fault, FF: Florin Fault, CRB: Cesar Ranchería Basin, PR: Perija Range, AgF: Algarrobo Fault. the black thick lines at the corners indicate the trace of the topographic profile at the bottom.

and its marginal arcs collided against the continental margin during Late Cretaceous-Paleogene times. Remnants of this collision can be traced along Ecuador the Western Cordillera of Colombia, the SNSM massif, the Guajira Peninsula, and the Leeward Antilles (Cardona et al., 2010; Duque-Caro, 1979; Jaillard et al., 2009; Spikings et al., 2015; Vallejo et al., 2009; van der Lelij et al., 2010; Villagómez et al., 2011a) The collision of this massive arc involved obduction and accretion of the oceanic arc into the continental crust. Interaction of the Caribbean plate with the South American plate caused fragmentation of the continental margin at the northern Andes as plate coupling increased with the advance of the Caribbean plate towards the E. The initiation of a low-angle SE dipping subduction zone resulted in the development of a magmatic arc along NW South America during Paleocene-Eocene times (Kennan and Pindell, 2009). Magmatism manifests in felsic plutons that were emplaced in the oceanic plate, as the Parashi Stock and the Mandé Batholith in the Guajira Peninsula and the Western Cordillera respectively (Cardona et al., 2011a, 2014; Duque, 2009; Villagómez et al., 2011a; Weber et al., 2010). In the SNSM massif, the Eocene plutons were emplaced in a transitional crust, and within the Precambrian basement producing wide migmatite zones.

The SNSM massif, with 5775 m elevation is the highest mountain in the Caribbean realm (Fig. 2), is an isolated tectonic block. Mainly an assemblage of Precambrian to Late Paleozoic metamorphic rocks, Jurassic-Cretaceous granitoids, and remnants of Caribbean plate metabasites constitutes this remarkable topographic element. These arc-units were obducted onto tilted Permo-Triassic lower crustal rocks. The different units have been grouped in four major morphotectonic provinces: 1) the Sierra Nevada Province (SNP) that corresponds to Precambrian granulites, anorthosites and gneisses

related to the Grenvillian-Sunsas-Putumayo orogenic belt with nested Jurassic to Cretaceous plutons (Cardona et al., 2006; Cordani et al., 2005; Ibanez-Mejia et al., 2011; Kroonenberg, 1982; Ordóñez et al., 2002; Tschanz et al., 1974), 2) the Sevilla Metamorphic Belt (SB) composed by Neoproterozoic gneisses probably associated with the Pan-African episode (Chapter 1), 3) The Inner Santa Marta Metamorphic belt (IB) composed of, Permian orthogneisses, Triassic mylonites and Jurassic metapelites (Chapter 1), 4) The Outer Santa Marta Metamorphic belt (OB) at the northwestern corner of the SNSM composed of accreted Caribbean metavolcanic rocks as supported by all geochronological data available (Cardona et al., 2010); (Chapter 1).

Internally the relations between the provinces that conform the SNSM massif are very complex and involve a Grenvillian basement of the Sierra Nevada Province (SNP) amalgamated to the late Neoproterozoic complex of the SB through an elusive structure known as the Sevilla lineament (SL). The SB thrusts over the Permo-Triassic (IB) through a major shear zone denominated the Orihueca fault (OhF). Internally to the IB a thrust fault exposes a mylonite belt of Triassic age and is named as the Aguja fault. At the northernmost tip of the massif, an accreted Caribbean oceanic sliver (OB) is thrusted along the Florin fault (FF) onto the continental margin. Paleocene-Eocene plutonism affected all provinces, and great volumes of granite were emplaced in the Santa Marta Batholith (SMB), the Buritaca Pluton (BP), the Latal Stock (LS), and the Sevilla Stock (SS) (Fig. 3).

In this context, the Paleocene-Eocene plutonic episode is extremely relevant because its thermal overprint is recorded in low- and high-temperature thermochronological systems. This thermal event masked most of the pre-Caribbean thermal events that

took place on the continental margin. During the late Eocene cessation of plutonism was directly linked to Caribbean slab flattening (Bernal-Olaya et al., 2015).

During the Eocene- Miocene, the SNSM was dragged along the continental margin to its current position as a consequence of the tectonic force exerted by the continuous convergence between the Caribbean plate and South America (Ayala et al., 2012; Bayona et al., 2010). The clockwise rotation of the SNSM led to the opening of the Lower- Magdalena valley basin until Oligocene times, when convergence was partitioned. Then the current boundaries of the SNSM were established, the Santa Marta-Bucaramanga fault on the western flank and the Oca fault on the northern flank of the massif (Bernal-Olaya et al., 2015; Flinch, 2003; Flinch and Castillo, 2015; Montes et al., 2010).

Accretion of the Great Caribbean arc against northwestern South America highly influenced the end of subduction (Vence, 2008). To the east of the Guajira Peninsula, the Leeward Antilles underwent rotation during their transit around the northwestern corner of South America at ca. 45 Ma. Contemporaneously the basement was exhumed next to the continental margin (van der Lelij et al., 2010), and the Great Caribbean arc was segmented along major extensional faults, creating basins that received up to 3000 m of sediments. This process marked the final stages of the accretion of the Great Caribbean arc (Gorney et al., 2007).

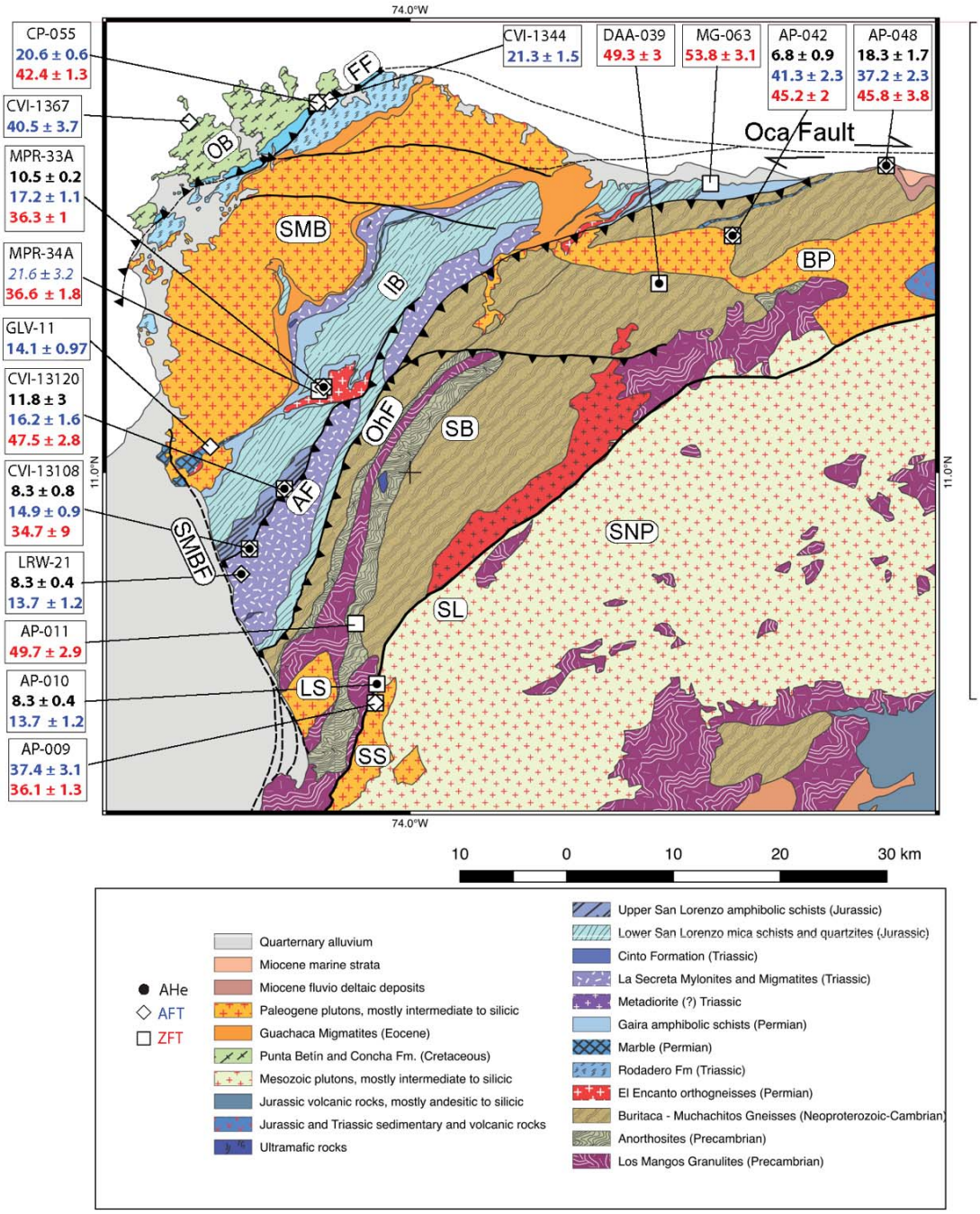

Figure 3. Geological Map of the NW metamorphic belt of the Sierra Nevada de Santa Marta Massif (SNSM) with location of samples analyzed in this study, color labels represent each thermochronometic system. OB:Outer Santa Marta Metamorphic Belt, SMB: Santa Marta Batholith, IB: Innner Santa Marta Metamorphic Belt, SB: Sevilla Metamorphic Belt, SNP: Sierra Nevada Province, BP: Buritaca Pluton, SS: Sevilla Stock, SL: Sevilla Lineament, LS: Latal Stock, SMBF: Santa Marta Bucaramanga Fault, AF: Aguja Fault, OhF: Orihueca Fault, FF: Florin Fault.

The Santa Marta-Bucaramanga fault (SMBF) separates the crystalline basement of the SNSM from the Oligocene-Miocene Lower Magdalena basin to the west (Bernal-Olaya et al., 2015; Montes et al., 2010; Tschanz et al., 1974; Villagómez et al., 2011b). The SMBF is a long-lived major discontinuity that extends more than 500 km, and connects the Southern Caribbean plate boundary with the Santander Massif in the Eastern Cordillera of Colombia (Fig. 1). The Santa Marta Bucaramanga fault was active during the Early Jurassic rifting episode, accommodating an important amount of right lateral displacement, and was reactivated during the Neogene (Kammer and Sánchez, 2006). During reactivation it accommodated strain from the Caribbean plate into the North-Andean block driving the surface uplift and exhumation of the Eastern Cordillera since the Miocene, with a major pulse during the Pliocene (Cortés et al., 2005; Parra et al., 2009). Implying that the SMBF is perhaps the most relevant structure that controlled the evolution of the Northern Andes from the Early Jurassic to the late Pliocene. Previous thermochronological studies on the SNSM had shown six time intervals in which the SNSM exhumed at elevated rates 0.2 -0.7 km/Myr, in response to the collision of the Caribbean plateau with northwestern South America, subsequent underthrusting of the Caribbean plate, and late propagation of NW verging thrust faults (Villagómez et al., 2011b). In the following sections, we present our thermochronological data, combined with data from previous studies, in the context of the redefined tectonic provinces that make-up the SNSM, and its exhumation histories constrained from middle Eocene to late Miocene times.

3. METHODS

3.1 Bedrock fission-track thermochronology

3.1.1 Zircon fission track

Zircons of the 125-250 µm fraction, were mounted in Teflon® sheets, with at least two mounts per sample. Zircons were polished to expose internal grain surfaces and etched in a NaOH-KOH solution at 228°C. Etching time varied between 20-60 hours in order to revel countable tracks in at least 100 grains per sample. Samples were irradiated together with Fish Canyon Tuff and Buluk Tuff zircon age standards and IRMM541 dosimeter glasses.

3.1.2 Apatite fission track

Apatite crystals were mounted in epoxy, polished and etched in 5.5 M HNO_3 at 21°C for 20 s and covered with muscovite detectors. The samples were irradiated together with Fish Canyon Tuff and Durango Tuff age standards and IRMM540R dosimeter glasses. Both apatite ad zircon samples were irradiated at the FRM II research reactor at Münich, Germany.

3.1.3 (U-Th)/He in Apatites

Crystals separated from the metamorphic and igneous rocks of the SNSM were prepared for (U-Th)/He analysis at the Institute of Geochemistry and Petrology at ETH Zürich. The objective was to obtain euhedral, inclusion free, colorless crystals without fractures Selected apatite crystals were photographed, measured and wrapped in Pt foil. Apatites were first analyzed for ^{4}He by degassing in a static vacuum using a diode laser heating to temperatures around 1000°C, and using a sector field mass

spectrometer equipped with a Baur-Signer ion source. Gases were pre-cleaned with liquid nitrogen traps and zirconium-vanadium-iron getters (SAES, St707). Net signal intensities were interpolated to the inlet time of the gas into the mass spectrometer, and then compared to the corresponding mean signal from reference gas aliquots of known absolute amounts analyzed by the same procedure. The degassed apatites were retrieved, dissolved in HNO_3 at ~90°C for 1 hour, spiked with ^{233}U, ^{230}Th, and ^{149}Sm, and analyzed on an ElementXR ICP-Mass spectrometer for ^{238}U, ^{232}Th, and ^{147}Sm.

4. RESULTS

In this section, results from ZFT, AFT and (U-Th)/He analyses obtained from samples of the distinctive lithologies of the northwestern corner of the SNSM are presented. Our aim was to perform these analyses on all the same samples analyzed with the U-Pb LA-ICP-MS method for Chapter-1. Nevertheless, because of several different factors, such as U content and/or grain quality for example not all of these samples could be analyzed. In some cases, zircons were scarce and only served for U-Pb dating. Apatites in most of the metamorphic rocks were severely damaged and fractured, and presented low U content. Regardless of these inherent complications, we were able to obtain 31 thermochronological ages (Fig. 3, supplementary Tables A1, A2, and A3). The results are presented here according to structural position of the sampled rock within the different lithotectonic units of the SNSM massif. Two-sigma analytical errors are reported in this study.

4.2 Sevilla Metamorphic Belt (SB)

Five samples from the high-grade metamorphic gneisses of the Buritaca and Muchachitos gneiss suite and one sample of the Eocene Sevilla Stock at the SB in the hanging wall of the Orihueca fault were selected for obtaining zircon and apatite ages (Fig. 3). Fission track ages are quite similar along the SB in both AFT and ZFT systems. Apatite yield was low, so only two samples were triple dated by ZFT, AFT and AHe; two samples were double dated by ZFT and AHe and one sample was double dated by ZFT, AFT. (Fig. 3, 4 & 5).

4.2.1 ZFT

Quartz-feldspathic gneiss sample AP-048 from the northwestern most part of the unit at sea level next to the Oca fault has an age of 45.8 ±3.8 Ma, whereas amphibole gneiss sample DAA-039 yields an age of 49.3 ±3 Ma. For the Buritaca Pluton a cooling age of 45.2 ±2 was obtained. Amphibole gneiss sample AP-011, from the western flank of the SNSM has a ZFT cooling of 49.7 ± 2.9 Ma, and 45.3 ±1.9 Ma for mafic gneiss sample AP-010. The Sevilla Stock sample AP-009 presented a slightly younger cooling age of 36.1 ±1.3 Ma.

4.2.2 AFT

Sample AP-048 has a pooled age of 37.2 ±2.3 Ma, and was the only sample of Precambrian rock that could be analyzed with the apatite fission-track method, as crystals from the remaining samples were highly damaged, or presented to many flaws for counting. The Sevilla Stock sample AP-009 has an age of 37.4 ±3.1, which is

almost identical to its ZFT age. The Buritaca Pluton tonalite has a cooling age of. 41.3 ±2.3 Ma.

4.2.3 Apatite (U-Th)/He

Sample AP-048 has an average age of 18.3±1.7 Ma replicated from five grains, whereas sample AP-010 from the western flank of the SNSM yields an age of 13.6 ±0.9 Ma. at one grain. The Eocene Buritaca Pluton yields a younger age of 6.8 ± 0.89 Ma replicated from five grains.

4.3 Inner Santa Marta Metamorphic Belt (IB)

Zircons and apatites were separated from seven samples (Fig 4 & 5) from the meta-igneous and metasedimentary rocks of the IB, either in the hanging wall or the footwall of the Aguja fault (Fig. 3). From these samples, two belong to the La Secreta Mylonites unit, one to the El Encanto Orthogneiss, three to the Gaira Schists, and one to the Upper San Lorenzo Schists.

4.3.1 ZFT

Sample MPR-33A from the El Encanto Orthogneiss yield a cooling age of 36.3 ±1 Ma. Sample MPR-34A from the Gaira Schists yields a cooling age of 36.6 ± 1.8 Ma. Sample CVI-13120 of the Upper San Lorenzo Schists in the footwall of the Aguja fault yields an age of 47.5 ± 2.8 Ma. Sample CVI-13108 Bt+Grt+Pl schist from the hanging wall of the Aguja fault yields a cooling age of 34.7 ±1.9 Ma.. Sample MG-063 from the Gaira Schists from the northern flank of the SNSM yields a cooling age of 53.8 ± 3.1Ma.

4.3.2 AFT

El Encanto Orthogneiss sample MPR-33A yields a cooling age of 17.2±1.1 Ma, whereas sample GLV-11 from the Gaira Schists yields an age of 14.1±0.97 Ma. Sample CVI-13120 from Upper San Lorenzo Schists shows a cooling age of 16.2±1.6 Ma. In the hanging wall of the Aguja fault at La Secreta Mylonites sample CVI-13108 shows a cooling age of 14.96 ± 0.9 Ma, and sample LRW-21 yields a similar age of 13.7 ± 1.2Ma.

4.2.3 Apatite (U-Th)/He

From the IB apatites were recovered from four samples. Sample MPR-33A from the El Encanto Orthogneiss has an age of 10.5 ±0.2 Ma replicated from five grains. Sample CVI-13120 from Upper San Lorenzo Schists yields a cooling age of 11.8 ± 3 Ma replicated from three grains. Samples LRW-21 and CVI-13108 from La Secreta Mylonites yield identical cooling ages of 8.3 ± 0.4 Ma and 8.3 ± 0.8 Ma respectively replicated from five grains.

4.4 Outer Santa Marta Metamorphic Belt (OB)

Zircon and apatite grains were separated from three samples of low-grade metamorphic rocks from the OB. Two of the samples are from the Cinto Formation and one sample from to the Concha Formation (Fig. 3). In the units of the OB apatite and zircon content is very scarce. For this reason there were not enough apatite crystals for (U-Th)/He dating, and only one of the samples yielded enough zircons for fission track analysis (Fig. 4 &5).

4.4.1 ZFT

Sample CP-055, from the Cinto Formation has a cooling age of 42.4 ± 1.3 Ma.

4.3.2 AFT

Sample CP-055 from the Cinto Formation yields a cooling age of 20.6 ± 0.66 Ma, and sample CVI-1344 from the most external part of the SNSM massif yields a cooling age of 40.5 ± 3.7 Ma,

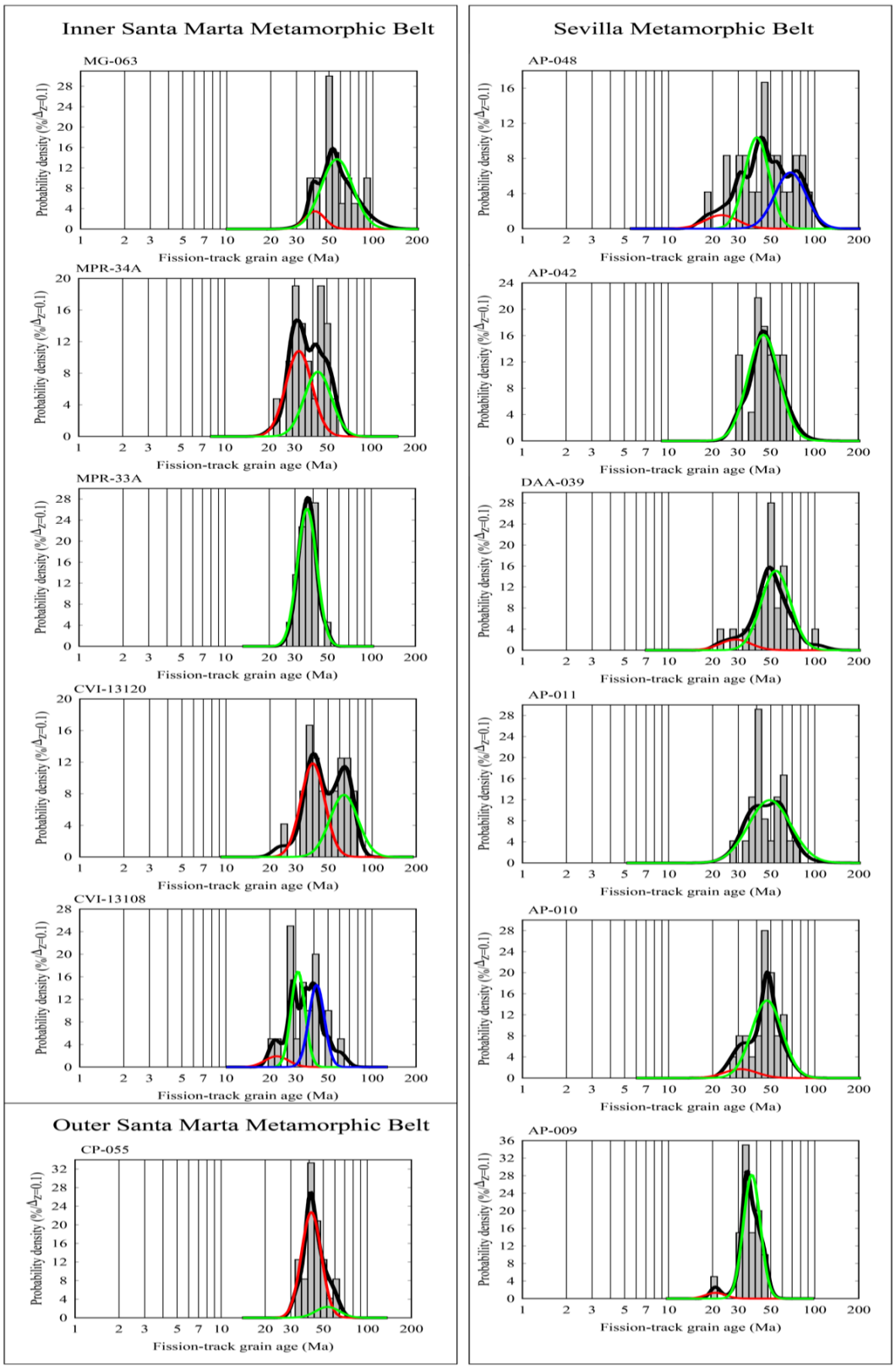

Figure 4. Bedrock ZFT data from the SNSM, probability density plots elaborated with Binomfit (Ehlers et al. 2005; Stewart & Brandon 2004).

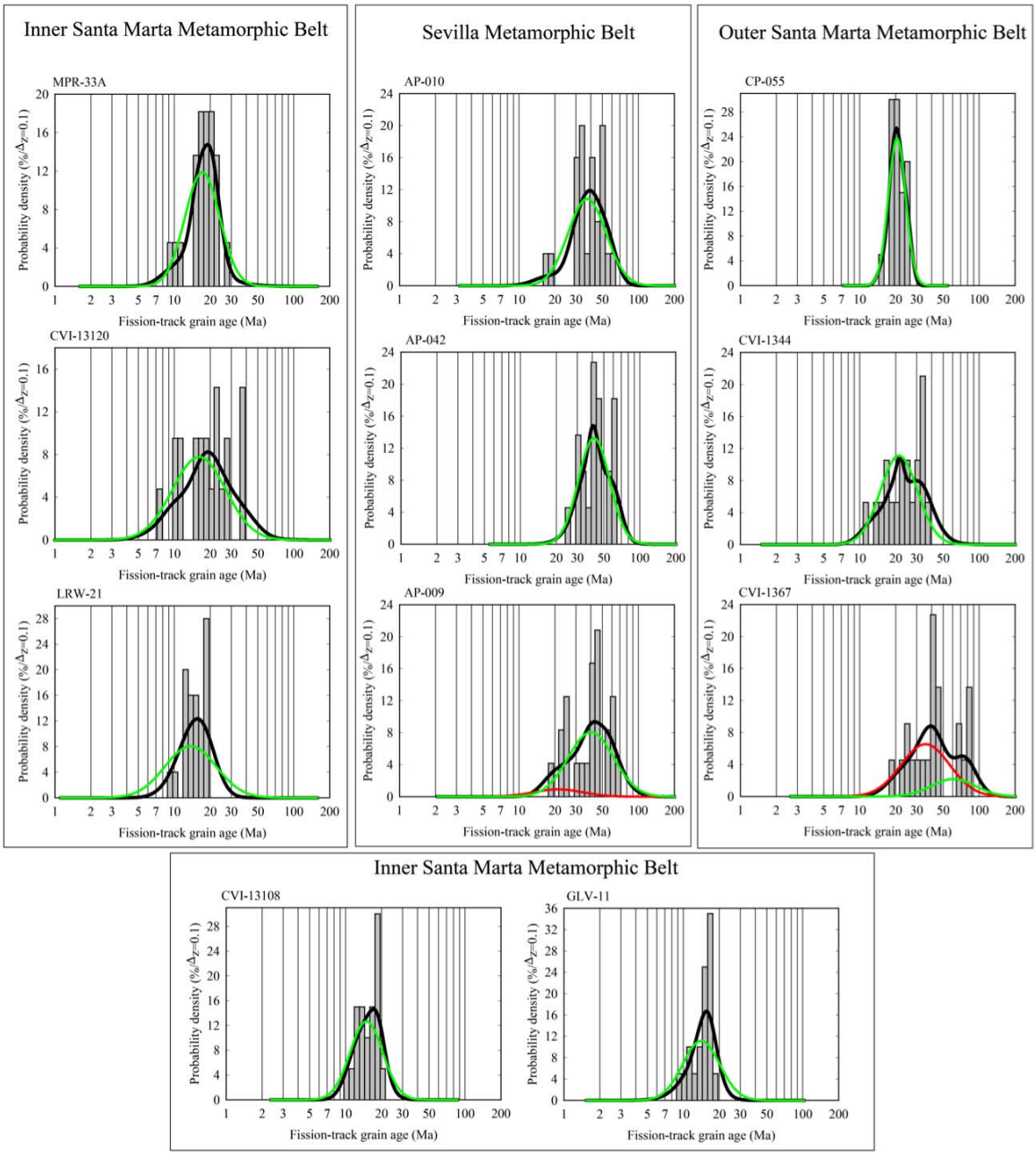

Figure 5. Bedrock AFT data from data from the SNSM, probability density plots elaborated with Binomfit (Ehlers et al. 2005; Stewart & Brandon 2004).

5. DISCUSSION

5.1 Accretion of Caribbean Terranes and onset of magmatism

The beginning of exhumation in the SNSM corresponds the later stages of diachronic accretion of the Caribbean Plateau to the Pacific margin of the South American plate between 65 and 58 Ma (Villagómez et al., 2011b). Zircon U-Pb ages of 69.3 ±0.5 Ma for the first dikes intrusions in metamorphic rocks of the OB and the youngest ages ca. 55.4 ±2.6 Ma for andesitic arc volcanism (Chapter 1) along with crystallization ages for the SMB and associated plutons between 65-49 Ma (Duque, 2009). It shows that arc accretion and pluton emplacement occurred contemporaneously in a time span of ≈ 15 Ma.

Paleogene plutonism affected the OB, the IB, the SB and the SNP. For this reason the AHe, AFT and ZFT systems were regionally reset and annealed in the SNSM in the vicinity of the Paleocene-Eocene plutons

During the late stages of Caribbean and South American plate convergence, the intrusion of the Santa Marta Batholith occurred within the upper plate and transitional crust. Pluton emplacement continued until about 50 Ma and rocks cooled at fast rates of 97-80 ºC/Myr until about 48 Ma (Duque, 2009). The thermal overprint produced by the Eocene plutons caused migmatization and skarns in the metapelitic Permian-Jurassic rocks. The Precambrian basement of the Sevilla Belt and Sierra Nevada Provinces was affected by mafic magmatism producing hornblendite clusters around plutons. P-T conditions for the pluton emplacement estimated from Al-in-amphibole content, yield values of 4.9± 0.6 kb and 6.4±0.6 kb (Cardona et al., 2011a), indicating at

least 16.6 -21.8 km depth with an ΔP of 0.2493 b/Km assuming an average crustal density of 3.0 g/cm^2 given the geological context of the SNSM massif. For the Buritaca Pluton, thermobarometry analyses performed on sample AP-042 (Mateus, 2014) with the Qtz+Hbl+Bt+Pl calibration yield P-T conditions of 3.18 kb and 762ºC for an approximated depth of 10.8 km (Chapter 2).

5.2 Erosion rates

Thermal histories had been modeled recently for the SNSM (Villagómez et al., 2011b) using apatite fission track length using the HeFTy program of Ketcham (2005). We constructed thermal paths for our samples (Fig. 6 & 7) for three thermochronological systems (ZFT, AFT, AHe). Erosion rates, closure depths and cooling rates were calculated with the Age2Edot program of Brandon (see Ehlers et al., 2005; Willett and Brandon, 2013), using a geothermal gradient, the current surface temperature and cooling ages. We defined closure temperature depending on cooling rates for the different low-temperature thermochronometers (Ehlers, 2005).

Recent estimates on the geothermal gradient for the SNSM obtained from the geothermal map of Colombia and from curie depth values (CDP) revealed a thermal gradient in the range of 12-18 ºC/km (Vargas et al., 2009, 2015). Nonetheless, thermal gradients during the Eocene should have been higher in consequence of the Paleocene-Eocene island to continental arc. Given its tonalite-trondhjemite-granodiorite (TTG) series character, the SMB required a high thermal gradient during emplacement ≈ 40ºC/km (Duque, 2009). Furthermore, the different plutons (SMB, SS, and BP) intruded at different crustal depths. In this context the Cenozoic paleo-thermal gradients estimated for the SNSM, which have been estimated between 20-

40ºC (Cardona et al., 2011a; Ceron-Abril, 2008; Mendoza and Ojeda, 2006; Villagómez et al., 2011b), should be analyzed carefully for calculating cooling rates regarding the timing and depth of magmatism according to temperature paths (Fig. 6). During pluton emplacement a gradient of 62ºC/km is assumed, whereas during post magmatic cooling the geothermal gradient decreased progressively to about 20ºC/km. It is very important to acknowledge that cooling occurred diachronously across the SNSM. First at the Buritaca Pluton in the north and subsequently in the plutons of the SMB with later cooling of the Sevilla Stock in the south-western flank of the SNSM (Fig. 6), this cooling trend is the consequence of plutons of the same age intruded at different depths with even 8 km of difference in intrusion depth between the northern and western flanks of the SNSM.

For this reason, geothermal gradients used for calculating erosion rates take into account the magmatic activity and its influence at least until ca. 45 Ma at the northern flank of the SNSM (Buritaca Pluton), and 37 Ma at the western flank of the SNSM (Sevilla Stock) as constrained by ZFT.

After assigning a geothermal gradient according to the chronological and structural context, we estimated erosion rates as a linear function on the change in temperature ΔT vs change in time Δt. For a given sample in this way defining a cooling rate for a particular interval of time, this is for example the amount of time in Ma for a particle to travel from the isotherm of closure temperature for zircon U-Pb crystallization ≈ 700ºC calculated from Ti-in-Zr thermometry (Chapter 1), until the ZFT closure temperature ≈ 350ºC, such elevated temperature corresponds to fully reset zircons with zero radiation damage and is applied to the Eocene plutons samples.

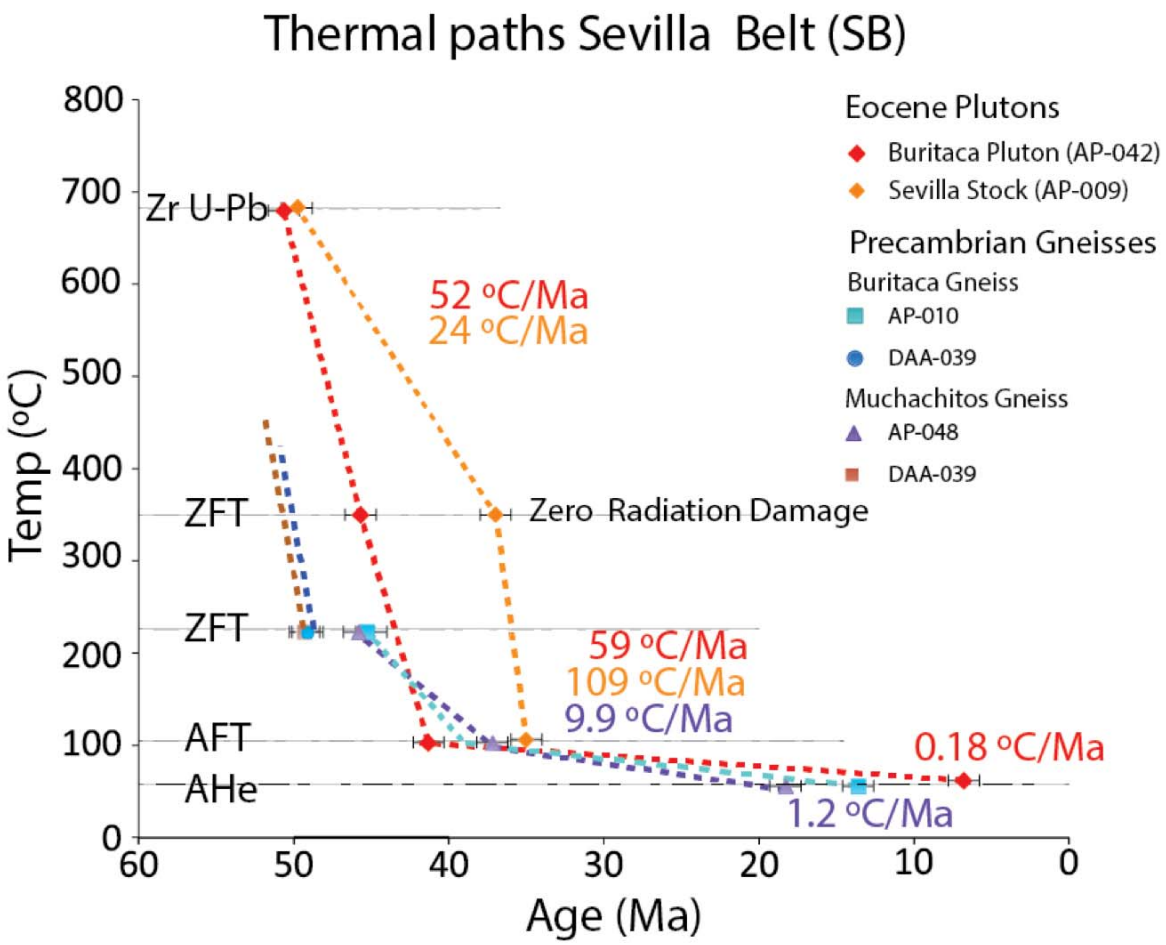

Figure 6. Temperature-time Paths of the Sevilla Metamorphic Belt (SB), constructed with ZFT, AFT and (U-Th)/He cooling ages.

Post magmatic cooling at the Sevilla Belt occurred, between 50-45 Ma at rates of ≈ 0.8 km/Myr, and cooling rates of about 52ºC/Myr documented for the Buritaca Pluton estimated from ΔT/Δt.

Thermobarometry estimates that the pluton intruded at 10.8 km depth (Mateus, 2014) at 50.7 Ma and cooled at elevated rates of 52ºC/Ma until reaching closure temperature of 342 ºC at ≈ 5.52 km which is the calculated closure depth for the ZFT system for a T_c of 342 ºC, considering zero radiation damage zircon occurring at 44.9 Ma. This accounts for an exhumation rate of 0.9 km/Myr estimated from ΔZ/ΔT. These very

similar results indicate that initial post magmatic cooling was highly influenced by exhumation. Erosion rates increased to 2 km/Myr between 45 - 40 Myr, during the establishment of a decreasing geothermal gradient (≈30ºC/km) as evidenced by the increase of cooling rates to 59 ºC/Ma. The last cooling phase is recorded between 40-5 Ma estimated on AHe data with a stable geothermal gradient of 20ºC/km and low erosion rates ≈ 0,01 km/Myr (Fig. 6).

On the western flank of the SNSM the Sevilla Stock shows fast cooling interval between 49.8- 37 Ma with values of 0.4 km/Myr and cooling rates of 24 ºC/Myr, related to a latest stages of Eocene plutonism. These values are coherent with rates of 0.73 km/Myr estimated for the SMB between ca. 50-41 Ma (Cardona et al., 2011a). The Sevilla Stock cooled at a very high rate of 109ºC/km, ≈ 12Ma after crystallization, we interpret that this rapid cooling was driven by erosional exhumation between 37-35 Myr at an increasing rate of 2.7 km/Myr. Differently from the other units of the Sevilla Metamorphic Belt (Fig. 6), this rate evidences the onset of intense erosive process at this part of the SNSM. The Precambrian Muchachitos gneiss hosting the Buritaca Pluton presented cooling rates of 10ºC/Myr between 46-37 Ma, which can be transferred into erosion rates about 0.32 km/Myr during that period. The Buritaca Pluton shares a similar thermal history, showing a significant decrease in cooling rate after this epoch and reaching erosion rates of 0.03 km/Myr (Fig. 6). The Buritaca Gneiss at the western flank of the SNSM shares a similar thermal path with respect to the previously described Muchachitos Gneiss and with erosion rates of 0.14 km/Myr at ca. 45.8 Ma and 0.08 km/Myr after 45.8 Ma that had persisted until the present.

Permian, Triassic and Jurassic meta-igneous and metasedimentary rocks from the IB evidence as a general trend younger cooling ages in all systems. For these rocks we

assumed a geothermal gradient decreasing from 30 to 20ºC/km. The exhumation of the IB postdates the middle Eocene major cooling event that led to exhumation recorded as an unconformity, this is corroborated by their time-temperature path that describes an independent history from the Eocene plutons and the Sevilla Belt rocks.

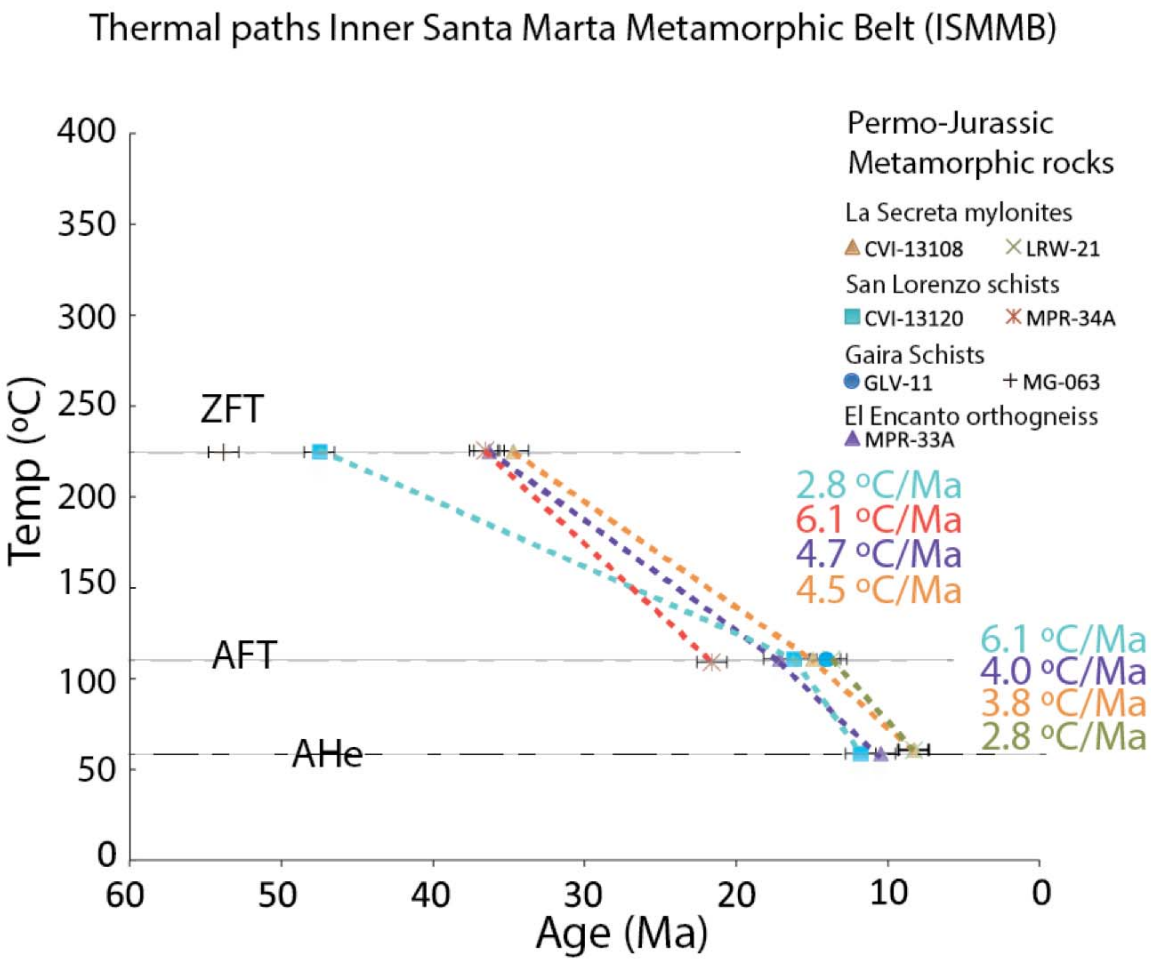

Figure 7. Temperature-time Paths of the Inner Sant Marta Metamorphic Belt (IB), constructed with ZFT, AFT and (U-Th)/He cooling ages.

Between 37-13 Ma all samples from the IB cooled at rates between 3-6ºC/Myr, exhuming with erosion rates ranging from 0.09-0.2 km/Ma (Fig. 7). From this group

two samples presented older ZFT ages of 47.5 and 53.8 Ma and showed the slowest cooling rates. The last exhumation phase is recorded in the AHe system between 12-8 Ma with a minor increase in exhumation rates between 0.14-0.3 km/My. Meta-volcanic rocks of the OB cooled at rates of 4ºC/Myr between 42-20 Ma, with exhumation rates estimated at ≈ 0.15 km/Myr

Our results show that a first phase of rapid cooling and erosion followed the pluton emplacement, this phase occurred between 50-45 Ma in the northern SNSM at rates of 0.8 km/Myr, and later in the western SNSM between 45-35 M at rates of 0.4 km/Myr (Fig. 6). A second exhumation phase evidences its erosional influence by the increase in cooling and therefore in erosion rates. At the northern SNSM with values of 2 km/Myr during 45-40 Myr whereas at the western SNSM rates reached 2.7 km/Myr during 37-35 Myr defining diachronous elevated rates for the middle Eocene. A third phase of exhumation took place between 32-19 Ma with decreased exhumation rates between 0.09-0.2 km/Myr. The last exhumation pulse occurred between 17-8 Ma as constrained by apatite (U-Th)/He data, and with slow cooling at a slower exhumation at 0.09 -0.03 km/Myr in the northern SNSM massif, in contrast with more elevated erosion rates in the western SNSM of 0.14-0.3 km/Myr (Fig. 7). In synthesis, our results based on three thermochronological systems reveal that during the first phase of exhumation of the SNSM relatively high exhumation rates dominated at the –Sevilla Belt. This phase occurred immediately after post-magmatic cooling for ~10 Myr in both the northern and western flanks of the SNSM diachronously with a time difference of about 8 Myr. This difference in time may be related to intrusion depths, as zircon crystallization ages of Eocene plutons are coeval throughout the SNSM. Because thermal histories are similar, we propose that the rapid cooling and

exhumation in the SNSM between 50-35 Ma should be considered as a single phase of post magmatic and exhumational cooling, rather than two independent phases.

5.3 Exhumation driven by crustal channel flow

Accelerated exhumation under high geothermal gradients may have occurred during the formation of a low-viscosity mid crustal channel, in which intruding pods at different depths were fed from a thickened continental crust (Beaumont et al., 2001, 2004; Grujic, 2006), during pluton emplacement, the flow of partially-molten rocks corresponds to lateral channel flow. Such flow may have led eventually to exhumation of migmatites and granites by extrusion along the edges of the orogenic wedge (Vanderhaeghe, 2009). The subducting buoyant Caribbean crust may have favored doming triggered by an underthrust ramp with exhumation of the dome at 1.1 km/Myr. Channel flow is favored by the current structural configuration of the SNSM in which a lower crustal section that preserves greenschist to granulite facies rocks in an inverted position occupies the NW corner of the massif (Fig. 8). Similar configurations of inverted crustal sections hosting granitoids and migmatites are a common feature of channel flow as documented in the High Himalayas (Godin et al., 2006; Jamieson et al., 2004). The “inversion” of the sequence may be syn-metamorphic or post-metamorphic and was most likely caused by ductile shear during strong plate coupling (Hubbard, 1996). As other documented inverted crustal sections, the SNSM is separated by two major shears zones: the lower shear zone with a thrust-sense kinematic is the Orihueca fault, and the upper shear zone dominated by normal-sense kinematics is the Sevilla lineament (Fig. 8).

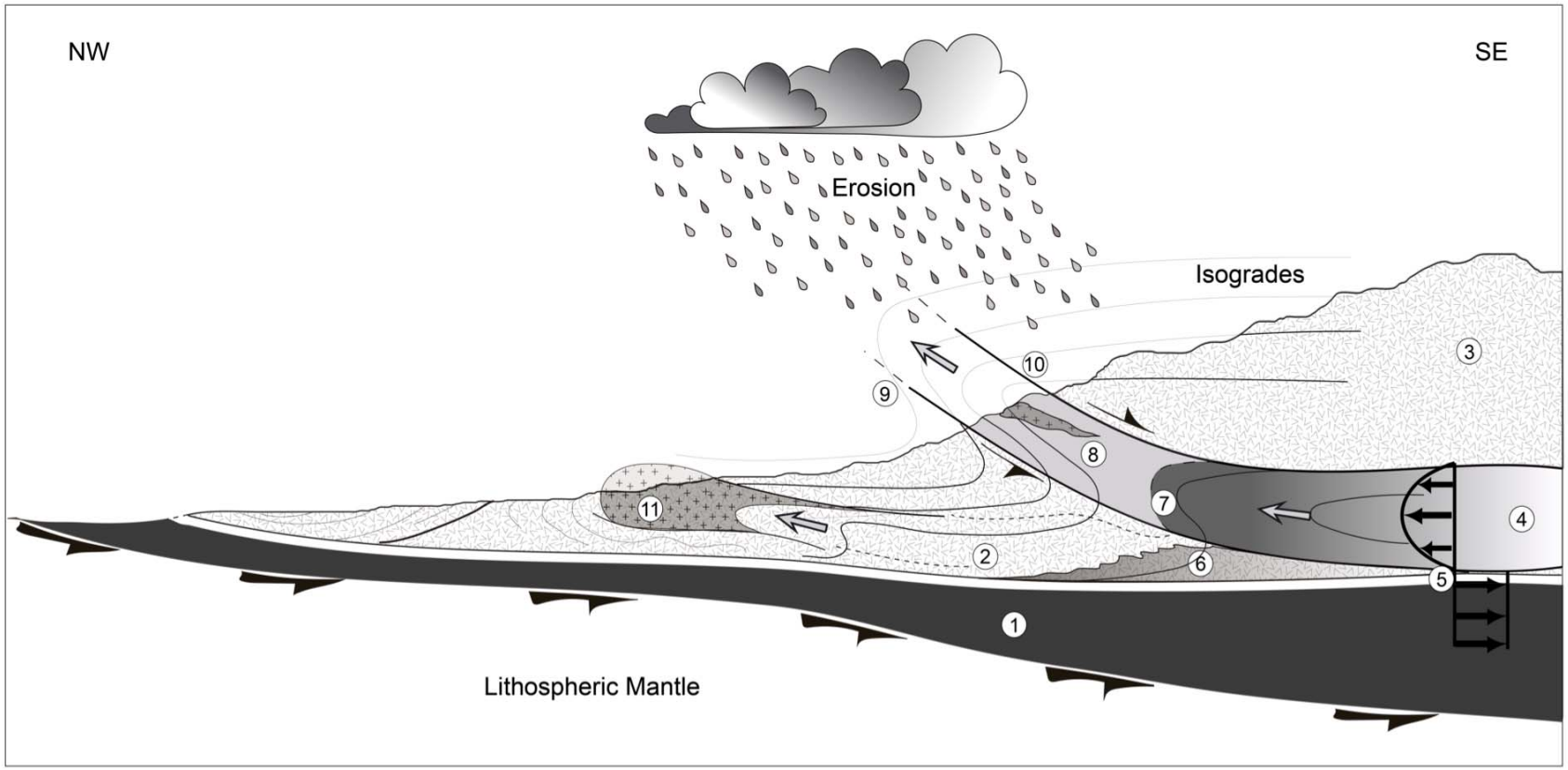

1. Lower crust
2. Mid-crust
3. Upper crust
4. Weak crustal channel
5. Schematic velocity profile during return channel flow
6. Isotherm wich partial melt starts (750°C)
7. Rheological tip of the channel: at lower termperatures
8. Extruding crustal block (palaeo-channel)
9. Lower shear zone of the extruding crustal block (dominantly thrust-sense kinematics)
10. Upper shear zone of the extruding crustal block (dominantly normal sense kinematics)
11. Intrusion zone

Figure 8. Schematic diagram of kinematic relationship between channel flow and extrusion of a lower crustal channel, applied to the crustal section of the SNSM. Modified from (Godin et al., 2006), in this representation the crustal channel would correspond to the Sevilla Metamorphic Belt bounded by major shear zones, granitoids hosted in the channel and migrated into te upper plate may correspond to Paleocene-Eocene plutons. Erosion enhances lower crustal extrusion.

5.4 Exhumation along major faults

Our data complements the existing SNSM thermochronological database, including a complete new dataset for the SB. The new data shows that the tectonic blocks of the northwestern metamorphic belt have different thermal histories. The boundaries between these tectonic blocks are the Orihueca fault and the Sevilla lineament, and at the tip of the SNSM the Florin fault separates the continental margin sequences from accreted Caribbean slivers (Fig. 9).

After the high-temperature phase of pluton crystallization, post magmatic cooling lasted from 48-35 Ma (Duque, 2009). This cooling age trend is observed in ZFT system in the SB, where the Precambrian rocks cooled around 45-50 Ma below about 350º C, The Sevilla Stock to the SE of the Sevilla lineament shows a much younger cooling age ca. 36.1 ± 1.3, its cataclastic texture may indicate a syn-tectonic exhumation driven by the Sevilla Lineament.

Elevation profiles validate different thermal histories for the hanging wall and the footwall of the Orihueca fault (Fig. 10). Middle Eocene AFT cooling ages in the hanging wall are juxtaposed against early Miocene AFT cooling ages in the footwall of the Orihueca fault, evidencing that the advancing thrust front was located at this structure, this also evidences that the Miocene exhumation involved the two fault blocks that exhumed as a whole. ZFT, AFT and AHe cooling ages in the IB vary between 33-8 Myr, and are slightly younger than ZFT-AFT ages in the OB ca. 42-20 Ma. These values indicate that after the post-magmatic cooling exhumation in the NW part of the SNSM, the fault blocks were individualized at the middle Eocene.

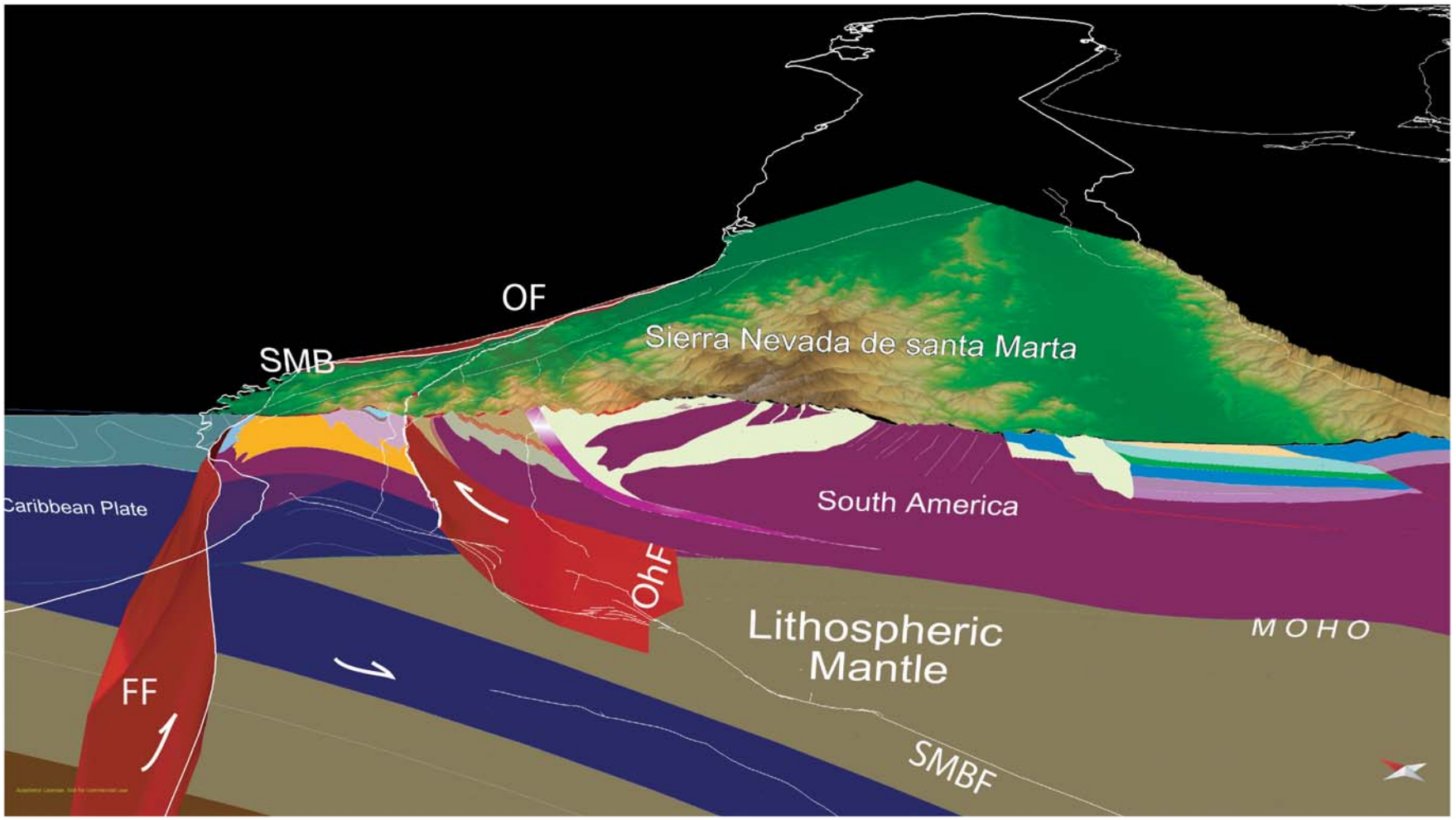

Figure 9. 3D model of the Sierra Nevada de Santa Marta massif, cross section trace corresponds to the topographic profile presented in Fig. 2. OF: Oca Fault, SMBF: santa Marta Bucaramanga Fault, SMB: Santa Marta Batholith, FF:Florin fault and OhF: Orihueca fault geometries were constructed from serial cross sections, the Sevilla Lineament is indicated as a highlighted polygon in the cross section due the lack of structural data, Moho depth is incorpored in the model from (Camargo, 2014), north direction towrds the upper left corner of the render.

In contrast exhumation at the SE flank of the SNSM was already active since upper Paleocene corresponding with coeval deposits at the Cesar-Rancheria basin (Bayona et al., 2011; Montes et al., 2010; Villagómez et al., 2011b), this means that exhumation migrated from continent interior to the active margin.

Exhumation of Caribbean crustal slivers can be traced up to 40 Ma in the hanging wall of the Florin fault in the OB according to ZFT ages. At the OB during 40-20 Myr the metavolcanic rocks obducted the continental crust, by the Florin fault with a constant exhumation rate ≈ 0.12 km/Myr, attesting for continuous accretion-obduction that lasted at least until the early Miocene. These ZFT ages ca. 40 Ma overlap the most intense period of Orihueca fault activity and showed a similar age trend as the IB, implying that Florin fault activity was coeval with IB doming and exhumation. The Florin fault activity postdates the activity of the Orihueca fault and the Sevilla lineament, and predates the activity of the Aguja fault.

Relief increased as consequence of slip through NW verging thrust faults, active since the late Paleocene this process led to erosional exhumation. The major structure involved during this process was the Orihueca fault, which is responsible for at least 11 km of vertical rock exhumation towards the Caribbean since the early Eocene (ca. 50.7 Ma), from the calculated depth of intrusion of sample AP-042 (Mateus, 2014). In the SNP the Sevilla lineament may have acted as a normal shear zone along which at least 6 km of rock were exhumed since the middle Eocene at a rate of about 1.17 km/Myr, evidenced by almost equal cooling ages in the ZFT and AFT systems. Most of the rock was eroded and transported into the Baja Guajira basin, which was displaced by the Oca fault 65 km to the west (Tschanz et al., 1974). Some sediment may have reached the Caribbean Sea, where it was recycled back into the accretionary wedge,

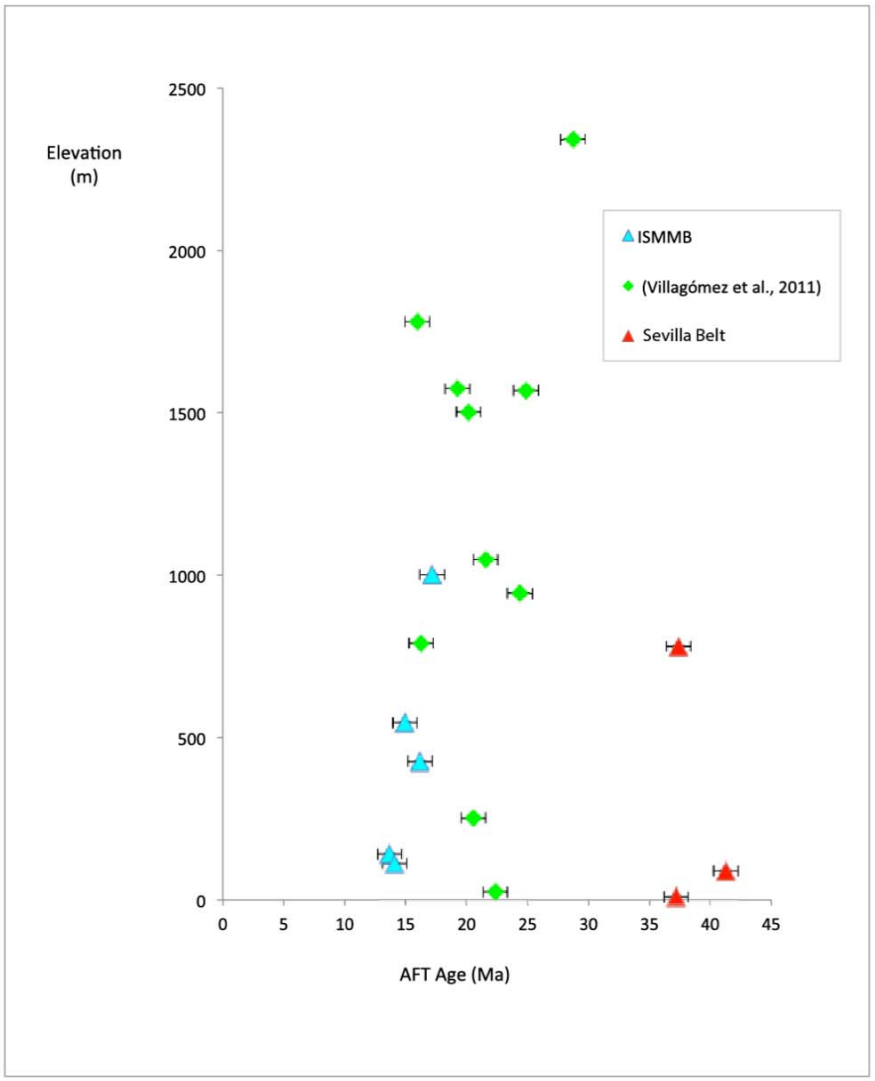

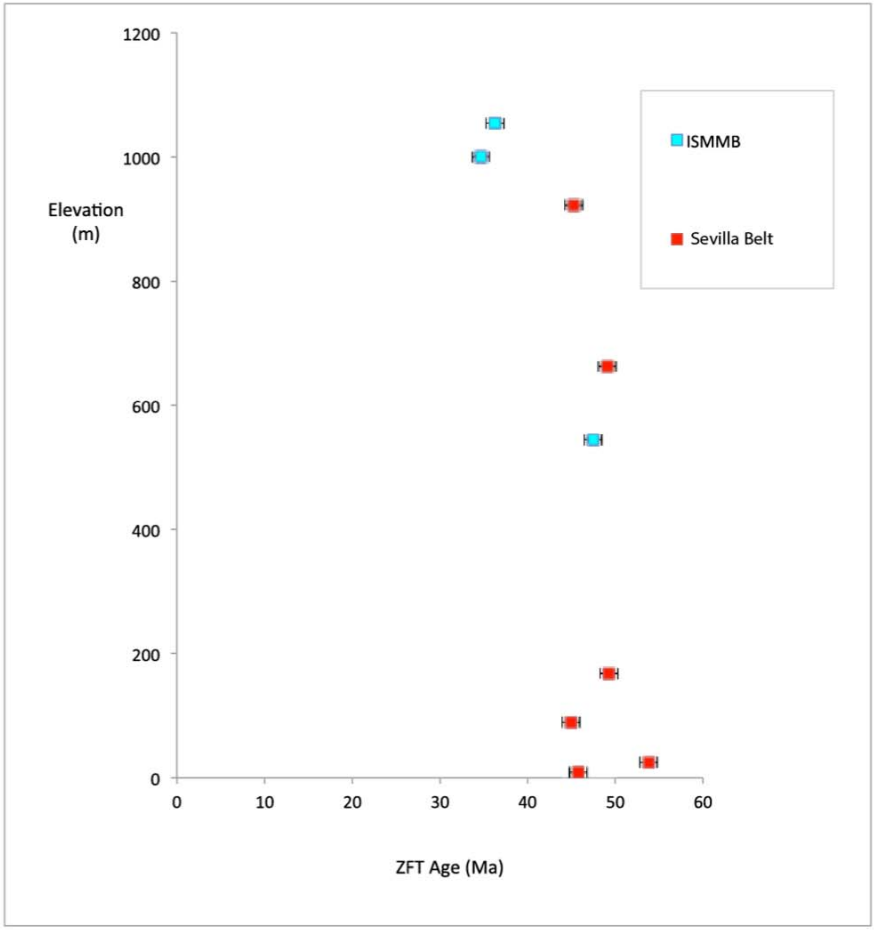

Figure 10. AFT and ZFT elevation profiles from samples of the IB and the Sevilla Metamorphic Belt.

either by tectonic accretion or by sediment accumulation on the shelf and basin slope, contributing to increasing the relief of the oceanic plate. This process worked until a significant decrease in slab angle led to the Oligocene activation of the Oca and Santa Marta - Bucaramanga faults. The SMBF is a transfer fault that accomodate strain differences between the Lower Magdalena and the SNSM massifl. The SMBF contributed to an enhanced exhumation on the western flank of the SNSM, as evidenced by younger AFT ages towards the fault trace. The youngest age is 13.7 ± 1.2 Ma. The regional pattern of AFT, and ZFT cooling ages suggests a regional tilting of the SNSM towards the NE as a consequence of increased subsidence at the SMBF hanging wall (Fig. 11).

At the same time the onset of sinistral displacement on the SMBF during the late Oligocene was coeval with a decrease in thrust advance towards the Caribbean. The increased amount of slip assumed by the reactivated Santa Marta-Bucaramanga and Oca faults was recorded in the adjacent clastic basins of Aracataca and Palomino in thick clastic sequences that evidence unroofing of the Precambrian basement since the late Oligocene (Piraquive et al., 2016, Chapter 3). From late Eocene-Oligocene times on exhumation rates decreased progressively to ~0.2 km/Myr to a steady-state equilibrium, which culminated with the transference of slip from the Orihueca fault to the Aguja fault, which acted as a splay on the advance of the deformation front. In the late stages of deformation, the obducting Caribbean plate impeded the advance of the thrust front.

5.5 Implications on the evolution of the Nor-Andean Block

Since the Paleocene the southeastern flank of the SNSM was exhumed, sourcing sediments to the newly formed Cesar-Rancheria basin. At the start of exhumation, the cover of the SNSM was the first material eroded. In a regional, basin-wide drainage system fed by the Cretaceous sedimentary cover exposed in low-amplitude topography and developed a mixed siliciclastic-carbonate platform in the shelf areas, with a major sediment contribution from the craton, as evidenced by a dominant population of Paleoproterozoic zircons (Ayala et al., 2012). During the late Paleocene, unroofing of the Permo-Triassic metamorphic basement from the Central Cordillera and Perija Range started to contribute to the clastic sediments.

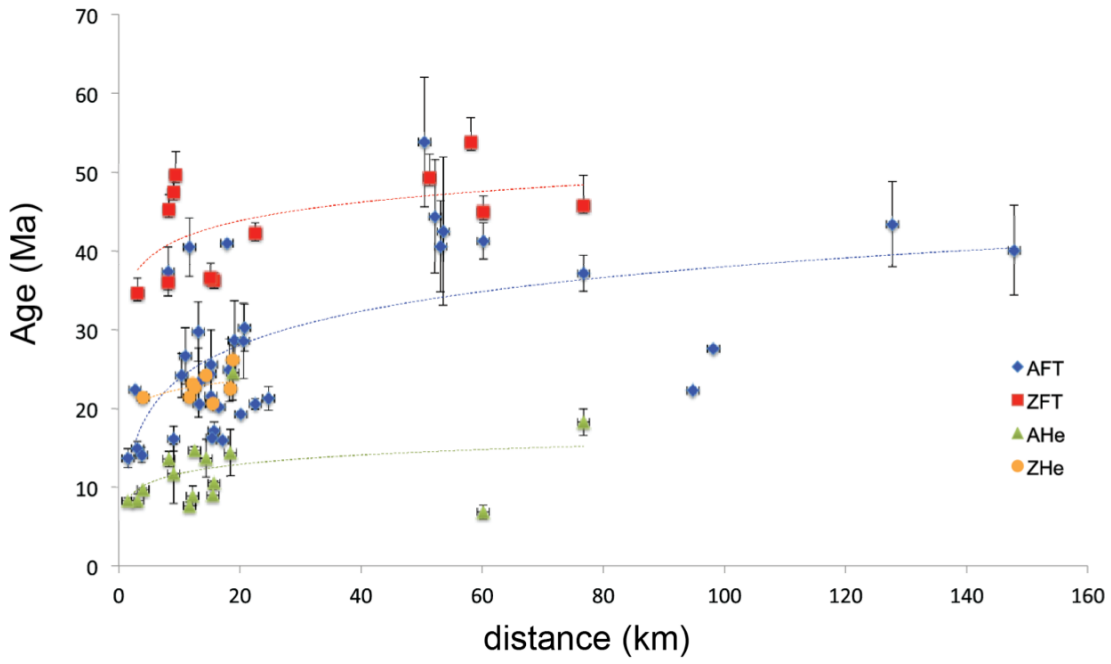

Figure 11. AFT, ZFT, AHe, ZHe thermochronometric ages obtained in this study and compiled with previous data (Cardona et al., 2011a; Villagómez et al., 2011), n= 64. Data are plotted relative to the linear distance from the Santa Marta Bucaramanga fault (SMBF), at the Sierra Nevada de Santa Marta massif (SNSM). All distances were measured as normal lines to the mapped SMBF, uncertainties are 2σ errors, and the dashed lines show the age trend towards the SMBF.

Evidence of Paleogene sedimentation is preserved as well on the western margin of the SNSM in the Lower Magdalena basin, recording arc-continent collision and basin opening. In this area, the main sediment sources areas were the upper Cretaceous volcanic arc and a continental margin composed upper Paleozoic to Triassic metamorphic rocks (Cardona et al., 2012). Minor contributions of Permo-Triassic zircons found in the Catatumbo, Cesar-Rancheria and NW Maracaibo basins since the Mid-Paleocene are related to sources in the Perijá Range and Santander Massif (Ayala et al., 2012). An important shift in provenance occurred during the middle Eocene, when the Precambrian basement of the SNSM, the Perija Range, the Merida Andes, and the Santander Massif exhumed and supplied Grenvillian zircons to the Cesar Rancheria, Catatumbo and Maracaibo basins. These mountain belts became the main sediment source areas, diminishing cratonic input because of the topographic configuration that individualized these basins (Bayona et al., 2007; Montes et al., 2010; van der Lelij et al., 2016; Villagómez et al., 2011b).

High middle Eocene exhumation rates (1.1 km/Myr) in the SNSM caused the removal of at least 9 km of upper crustal rocks that contributed to the filling of the adjacent sedimentary basins. The onset of exhumation was probably a consequence of Caribbean slab flattening and strong plate coupling that led to surface uplift of the Eastern Cordillera of Colombia (Caballero et al., 2010). The magnitude of regional exhumation during the late Eocene- late Oligocene is recorded in the Cenozoic strata of the Middle Magdalena basin and the Eastern Cordillera (Horton et al., 2010a, 2010b; Mora et al., 2010; Nie et al., 2010). The mechanism that triggered this accelerated exhumation during the middle Eocene is closely related to strain transfer between the

Caribbean plate and the Eastern Cordillera, through reactivation of the SMBF, which accommodated significant subsidence during the Oligocene favoring carbonate platform development at marginal highs (Arjona, El Cicuco, El Dificil) (Duque-Caro, 1979; Montes et al., 2010).

The reorganization of the Nazca, Caribbean and South American plates with a change in convergence direction from an E-W during the Paleocene to NW-SE during the Oligocene was responsible for the strain transfer (Cortés et al., 2005). The Paleocene-late Eocene shift in the regional stress field can be observed in fracture patterns, kinematic markers and structural styles in the Eastern Cordillera of Colombia, coeval with the middle Eocene unconformity. The mid-Eocene unconformity coincides with the episode of the highest rates of exhumation (0.8 - 1.2 km/Myr) in the SNSM.

The early indentation of the Panama block at ca. ~ 23-25 Ma against western South America (Farris et al., 2011; Montes et al., 2012) induced a pulse of surface uplift and exhumation. This led to doming and exhumation of the SMB in the IB. The last pulse of exhumation recorded in the IB, about 2 km to the NE of the SMBF, is related to the activity of the Aguja fault. (U-Th)/He ages of 8.3 ±0.8 for the IB attest that this pulse of exhumation continued at least until the late Miocene with erosion rates of 0.14-0.18 km/Myr. The onset of exhumation of the Merida Andes at ca. 14 Ma was due to Boconó fault activation (Bermúdez et al., 2010, 2011; Javadi et al., 2011). This exhumation persisted at high rates of about 1.5 km/Myr from 14 -4 Ma and at 0.4 km/Myr from 4 Ma to the present for the Sierra Nevada block. Whereas the El Carmen block, to the north of the Bocono fault was exhumed at 1.5 km/Myr since about 2 Ma until the present (Kon et al. 1984; Bermudez et al. 2011). Simultaneously elevated erosion rates on the eastern flank of the Eastern Cordillera started during the late Pliocene (Mora et

al., 2008, 2010; Parra et al., 2009). Evidence of late Pliocene exhumation in the SNSM is absent, and its elevated topography may be the consequence of a very recent surface uplift triggered by mantle upwelling (Ceron-Abril, 2008; Villagómez et al., 2011b). We favor this hypothesis considering the orogenic float model (Monod et al., 2010), given that inversion of gravity and magnetic data constrain crustal thickness to only 25 km and doming under the SNSM (Camargo, 2014). Rapid mantle upwelling beneath the SNSM could be a consequence of late Pliocene convective removal of the SNSM underthrusted Caribbean slab causing isostatic rebound, which may explain the high topography. Convective removal can occur much more rapidly than mountain building, over 1-10 Myr (Houseman and Molnar, 2001). The removal of the dense root probably caused 1-3 km of surface uplift (England and Houseman, 1989; Platt and England, 1994).

7. CONCLUSIONS

1) The history of exhumation of the SNSM has been complemented with new low-temperature thermochronological data, which has allowed to calculate cooling rates and determine exhumation rates a for the Sevilla Metamorphic Belt (SB). Our data show that this province presents an independent cooling history from the thermal histories presented in the SNP and IB (Cardona et al., 2011a; Villagómez et al., 2011b).

2) Paleocene-Eocene plutonism was produced by collision between the South American and Caribbean plates. Although, previous studies tried do define a geochemical character for these plutons, the results were ambiguous (Cardona et al., 2011a; Duque, 2009; Tschanz et al., 1974). Field relationships as well as thermal

history models support a thickened continental crust origin. Intrusion depth of the SMB batholith has been constrained between 15-20 km. Emplacement occurred during subduction failure, which was a consequence of an abnormally thick oceanic crust of the Caribbean plate (Stern, 2002). During convergence and plate coupling part of the Caribbean plate was obducted onto the South American plate margin through the Florin fault. The onset of extrusion of crustal slivers is calculated after ca. 40 Ma by ZFT.

3) Widespread Paleocene-Eocene plutonism affected the Precambrian basement of the Sevilla Metamorphic Belt. In this tectonic block, exhumation occurred diachronusly, with ZFT cooling ages 10 Myr older at the Buritaca pluton with respect to the Sevilla Stock. Exhumation of the SB occurred at rates that increased from 0.8 – to 2 km/Myr on the northern flank of the SNSM, between 50-42 Ma. On the western flank of the SNSM, exhumation took place between 49-35 Ma, with rates that increased from 0.4 to 2.7 km/Myr.

4) The SNSM exhibits an inverted metamorphic sequence, in which the SB occupies a position between the Sierra Nevada Province and the IB. The SB is separated from the adjacent blocks by two major shear zones: the Orihueca fault and the Sevilla lineament, with thrust and normal components respectively. This structural configuration and the elevated exhumation rates make the SB a possible example of crustal channel flow during the middle-Eocene In this model the SB was extruded as a weakened viscous crustal channel between major faults, with focused exhumation in a narrow zone. In such channel partial melting occurs commonly in the core of the channel and in the marginal thrust zones. Therefore, we interpret that the Paleocene plutons of the Latal Stock (LS) and Sevilla Stock (SS) are a consequence of lower crustal

extrusion. This model satisfies the conditions in which an extruded narrow zone of lower crustal rocks bounded by faults, incorporating deformed granitoids of a more recent age, overlies younger rocks of a lower metamorphic grade.

5) Elevated exhumation rates during the middle Eocene are related to collision of the Caribbean plate against South America. This collision induced I-type plutonism because of crustal thickenning of radiogenic pelites and subsequent exhumation of the lower crust under a high geothermal gradient ≈ 62ºC/km. Subduction failure due to strong plate coupling led to reactivation of mid crustal structures of the continental margin and strain transfer from the Caribbean plate to the South American plate along the SMBF causing surface uplifting and exhumation of the SNSM, the Perijá Range and the Eastern Cordillera of Colombia.

6) The Santa Marta-Bucaramanga fault caused tilting of the SNSM towards the NE during the Miocene as evidenced by younger thermochronological ages close to the fault trace. This tilting may be related to subsidence of the SMBF hanging wall coupled with the tectonic drag produced by the Caribbean plate during its eastward motion.

7) An overall change in convergence during the Oligocene caused a decrease in exhumation rates. Slip was transferred from the Sevilla fault to the Santa Marta-Bucaramanga fault, and exhumation rates decreased to 0.09 km/My, at the same time plutonism ended and geothermal gradients decreased. With this scenario of a partitioned convergence strike slip faults started because of the eastward motion of the Caribbean plate, generating subsidence along the Santa Marta-Bucaramanga and Oca faults.

8) The last pulse of surface uplift triggered by the indentation of the Panama Block at ca. 23 Ma influenced renewed thrusting that persisted on the Aguja fault until about 8

Ma. In the already established transpressive regime the SNSM may had reached its maximum thickness. The current lack of isostatic compensation and absence of younger cooling ages at the surface may be related to a very recent episode of convective removal of the crustal root that resulted in accelerated exhumation of the massif during the late Pliocene.

8. REFERENCES

Ayala, R.C., Bayona, G., Cardona, A., Ojeda, C., Montenegro, O.C., Montes, C., Valencia, V., Jaramillo, C., 2012. The paleogene synorogenic succession in the northwestern Maracaibo block: Tracking intraplate uplifts and changes in sediment delivery systems. J. South Am. Earth Sci., Tectonic and climatic shaping of the northern Andes and southern Caribbean margin 39, 93–111. doi:10.1016/j.jsames.2012.04.005

Bayona, G., Jiménez, G., Silva, C., Cardona, A., Montes, C., Roncancio, J., Cordani, U., 2010. Paleomagnetic data and K–Ar ages from Mesozoic units of the Santa Marta massif: A preliminary interpretation for block rotation and translations. J. South Am. Earth Sci. 29, 817–831. doi:10.1016/j.jsames.2009.10.005

Bayona, G., Montes, C., Cardona, A., Jaramillo, C., Ojeda, G., Valencia, V., Ayala-Calvo, C., 2011. Intraplate subsidence and basin filling adjacent to an oceanic arc–continent collision: a case from the southern Caribbean-South America plate margin. Basin Res. 23, 403–422. doi:10.1111/j.1365-2117.2010.00495.x

Bayona, G., Ochoa, F.L., Cardona, A., Jaramillo, C., Montes, C., Tchegliakova, N., 2007. Procesos orogénicos del Paleoceno para la cuenca de Ranchería (Guajira, Colombia) y áreas adyacentes definidos por análisis de procedencia. Geol. Colomb. 32, 21–46.

Beaumont, C., Jamieson, R.A., Nguyen, M.H., Lee, B., 2001. Himalayan tectonics explained by extrusion of a low-viscosity crustal channel coupled to focused surface denudation. Nature 414, 738–742. doi:10.1038/414738a

Beaumont, C., Jamieson, R.A., Nguyen, M.H., Medvedev, S., 2004. Crustal channel flows: 1. Numerical models with applications to the tectonics of the Himalayan-Tibetan orogen: HIMALAYAN-TIBETAN CRUSTAL CHANNEL FLOWS. J. Geophys. Res. Solid Earth 109. doi:10.1029/2003JB002809

Bermúdez, M.A., Kohn, B.P., van der Beek, P.A., Bernet, M., O'Sullivan, P.B., Shagam, R., 2010. Spatial and temporal patterns of exhumation across the Venezuelan Andes: Implications for Cenozoic Caribbean geodynamics. Tectonics 29, TC5009. doi:10.1029/2009TC002635

Bermudez, M.A., van der Beek, P., Bernet, M., 2011. Asynchronous Miocene-Pliocene exhumation of the central Venezuelan Andes. Geology 39, 139–142. doi:10.1130/G31582.1

Bermudez, M.A., van der Beek, P.A., Bernet, M., 2013. Strong tectonic and weak climatic control on exhumation rates in the Venezuelan Andes. Lithosphere 5, 3–16. doi:10.1130/L212.1

Bernal-Olaya, R., Mann, P., Escalona, A., 2015. Tectonostratigraphic Evolution of the Lower Magdalena Basin, Colombia: An Example of an Underfilled to Overfilled Forearc Basin. Presented at the GCAGS.

Caballero, V., Parra, M., Bohorquez, A.R.M., 2010. LEVANTAMIENTO DE LA CORDILLERA ORIENTAL DE COLOMBIA DURANTE EL EOCENO TARDÍO – OLIGOCENO TEMPRANO: PROVENIENCIA SEDIMENTARIA EN EL SINCLINAL DE NUEVO MUNDO, CUENCA VALLE MEDIO DEL MAGDALENA. Bol. Geol. 32.

Camargo, S., 2014. Estructura litosférica asociada a la Sierra Nevada de Santa Marta a partir de datos de gravimetría, magnetometría y sismología.

Cardona, A., Cordani, U.G., MacDonald, W.D., 2006. Tectonic correlations of pre-Mesozoic crust from the northern termination of the Colombian Andes, Caribbean region. J. South Am. Earth Sci. 21, 337–354. doi:10.1016/j.jsames.2006.07.009

Cardona, A., Montes, C., Ayala, C., Bustamante, C., Hoyos, N., Montenegro, O., Ojeda, C., Niño, H., Ramirez, V., Valencia, V., Rincón, D., Vervoort, J., Zapata, S., 2012. From arc-continent collision to continuous convergence, clues from Paleogene conglomerates along the southern Caribbean–South America plate boundary. Tectonophysics 580, 58–87. doi:10.1016/j.tecto.2012.08.039

Cardona, A., Valencia, V., Bayona, G., Duque, J., Ducea, M., Gehrels, G., Jaramillo, C., Montes, C., Ojeda, G., Ruiz, J., 2011. Early-subduction-related orogeny in the northern Andes: Turonian to Eocene magmatic and provenance record in the Santa Marta Massif and Rancheria Basin, northern Colombia. Terra Nova 23, 26–34. doi:10.1111/j.1365-3121.2010.00979.x

Cardona, A., Valencia, V., Bustamante, C., García-Casco, A., Ojeda, G., Ruiz, J., Saldarriaga, M., Weber, M., 2010. Tectonomagmatic setting and provenance of the Santa Marta Schists, northern Colombia: Insights on the growth and approach of Cretaceous Caribbean oceanic terranes to the South American continent. J. South Am. Earth Sci., Sierra Nevada de Santa Marta and Adjacent Basins 29, 784–804. doi:10.1016/j.jsames.2009.08.012

Cardona, A., Valencia, V., Weber, M., Duque, J., Montes, C., Ojeda, G., Reiners, P., Domanik, K., Nicolescu, S., Villagómez, D., 2011a. Transient Cenozoic tectonic stages in the southern margin of the Caribbean plate: U-Th/He thermochronological constraints from Eocene plutonic rocks in the Santa Marta massif and Serranía de Jarara, northern Colombia. Geol. Acta 9, 445–469. doi:10.1344/105.000001739

Cardona, A., Weber, M., Valencia, V., Bustamante, C., Montes, C., Cordani, U., Muñoz, C.M., 2014. Geochronology and geochemistry of the Parashi granitoid, NE Colombia: Tectonic implication of short-lived Early Eocene plutonism along the SE Caribbean margin. J. South Am. Earth Sci. 50, 75–92. doi:10.1016/j.jsames.2013.12.006

Ceron-Abril, J.F., 2008. Crustal structure of the Colombian Caribbean basin and margins.

Cordani, U.G., Cardona, A., Jimenez, D.M., Liu, D., Nutman, A.P., 2005. Geochronology of Proterozoic basement inliers in the Colombian Andes: tectonic history of remnants of a fragmented Grenville belt. Geol. Soc. Lond. Spec. Publ. 246, 329–346. doi:10.1144/GSL.SP.2005.246.01.13

Cortés, M., Angelier, J., Colletta, B., 2005. Paleostress evolution of the northern Andes (Eastern Cordillera of Colombia): Implications on plate kinematics of the South Caribbean region: PALEOSTRESS EVOLUTION OF THE NORTHERN ANDES. Tectonics 24, n/a-n/a. doi:10.1029/2003TC001551

Duque, T., 2009. Geocronología (U/Pb y 40Ar/39Ar) y geoquímica de los intrusivos paleógenos de la Sierra Nevada de Santa Marta y sus relaciones con la tectónica del Caribe y el arco magmático circun-caribeñ.

Duque-Caro, H., 1979. Major structural elements and evolution of northwestern Colombia. Geol. Geophys. Investig. Cont. Margins AAPG Mem. 29, 329–351.

Ehlers, T.A., 2005. Computational Tools for Low-Temperature Thermochronometer Interpretation. Rev. Mineral. Geochem. 58, 589–622. doi:10.2138/rmg.2005.58.22
England, P., Houseman, G., 1989. Extension during continental convergence, with application to the Tibetan Plateau. J. Geophys. Res. 94, 17561. doi:10.1029/JB094iB12p17561
Farris, D.W., Jaramillo, C., Bayona, G., Restrepo-Moreno, S.A., Montes, C., Cardona, A., Mora, A., Speakman, R.J., Glascock, M.D., Valencia, V., 2011. Fracturing of the Panamanian Isthmus during initial collision with South America. Geology 39, 1007–1010. doi:10.1130/G32237.1
Flinch, J.F., 2003. Structural Evolution of the Sinu-Lower Magdalena Area (Northern Colombia) 776–796.
Flinch, J.F., Castillo, V., 2015. Record and Constraints of the Eastward Advance of the Caribbean Plate in Northern South America.
Godin, L., Grujic, D., Law, R.D., Searle, M.P., 2006. Channel flow, ductile extrusion and exhumation in continental collision zones: an introduction. Geol. Soc. Lond. Spec. Publ. 268, 1–23. doi:10.1144/GSL.SP.2006.268.01.01
Gorney, D., Escalona, A., Mann, P., Magnani, M.B., BOLIVAR Study Group, 2007. Chronology of Cenozoic tectonic events in western Venezuela and the Leeward Antilles based on integration of offshore seismic reflection data and on-land geology. AAPG Bull. 91, 653–684. doi:10.1306/11280606002
Grujic, D., 2006. Channel flow and continental collision tectonics: an overview. Geol. Soc. Lond. Spec. Publ. 268, 25–37. doi:10.1144/GSL.SP.2006.268.01.02
Hoernle, K., Hauff, F., Bogaard, P. van den, 2004. 70 m.y. history (139–69 Ma) for the Caribbean large igneous province. Geology 32, 697. doi:10.1130/G20574.1
Horton, Parra, M., Saylor, J., Nie, J., Mora, A., Torres, V., Stockli, D., Strecker, M., 2010a. Resolving uplift of the northern Andes using detrital zircon age signatures. GSA Today 4–10. doi:10.1130/GSATG76A.1
Horton, Saylor, J.E., Nie, J., Mora, A., Parra, M., Reyes-Harker, A., Stockli, D.F., 2010b. Linking sedimentation in the northern Andes to basement configuration, Mesozoic extension, and Cenozoic shortening: Evidence from detrital zircon U-Pb ages, Eastern Cordillera, Colombia. Geol. Soc. Am. Bull. 122, 1423–1442. doi:10.1130/B30118.1
Houseman, G., Molnar, P., 2001. Mechanisms of lithospheric rejuvenation associated with continental orogeny. Geol. Soc. Lond. Spec. Publ. 184, 13–38. doi:10.1144/GSL.SP.2001.184.01.02
Hubbard, M.S., 1996. Ductile Shear as a Cause of Inverted Metamorphism: Example from the Nepal Himalaya. J. Geol. 104, 493–499. doi:10.1086/629842
Ibanez-Mejia, M., Ruiz, J., Valencia, V., Cardona, A., Gehrels, G., Mora, A., 2011. The Putumayo Orogen of Amazonia and its implications for Rodinia reconstructions: New U–Pb geochronological insights into the Proterozoic tectonic evolution of northwestern South America. Precambrian Res. 191, 58–77. doi:10.1016/j.precamres.2011.09.005
Jaillard, E., Lapierre, H., Ordonez, M., Alava, J.T., Amortegui, A., Vanmelle, J., 2009. Accreted oceanic terranes in Ecuador: southern edge of the Caribbean Plate? Geol. Soc. Lond. Spec. Publ. 328, 469–485.
Jamieson, R.A., Beaumont, C., Medvedev, S., Nguyen, M.H., 2004. Crustal channel flows: 2. Numerical models with implications for metamorphism in the Himalayan-Tibetan orogen: CHANNEL FLOWS AND HIMALAYAN METAMORPHISM. J. Geophys. Res. Solid Earth 109. doi:10.1029/2003JB002811
Javadi, H.R., Foroutan, M., Ashtiani, M.E., Urbina, J.A., Saidi, A., Faridi, M., 2011. Tectonics changes in NW South American Plate and their effect on the movement pattern of the Boconó Fault System during the Mérida Andes evolution. J. South Am. Earth Sci. 32, 14–29. doi:10.1016/j.jsames.2011.04.008
Kammer, A., Sánchez, J., 2006. Early Jurassic rift structures associated with the Soapaga and Boyacá faults of the Eastern Cordillera, Colombia: Sedimentological inferences and

regional implications. J. South Am. Earth Sci., Tectonic evolution of the Colombian Andes 21, 412–422. doi:10.1016/j.jsames.2006.07.006
Kennan, L., Pindell, J.L., 2009. Dextral shear, terrane accretion and basin formation in the Northern Andes: best explained by interaction with a Pacific-derived Caribbean Plate? Geol. Soc. Lond. Spec. Publ. 328, 487–531.
Kerr, A.C., Tarney, J., Marriner, G.F., Nivia, A., Saunders, A.D., 1997. The Caribbean-Colombian Cretaceous Igneous Province: The Internal Anatomy of an Oceanic Plateau, in: J.honey, J., Coffin, M.F. (Eds.), Large Igneous Provinces: Continental, Oceanic, and Planetary Flood Volcanism. American Geophysical Union, pp. 123–144.
Ketcham, R.A., 2005. Forward and Inverse Modeling of Low-Temperature Thermochronometry Data. Rev. Mineral. Geochem. 58, 275–314. doi:10.2138/rmg.2005.58.11
Kroonenberg, S.B., 1982. A Grenvillian granulite belt in the Colombian Andes and its relation to the Guiana shield. Geol Mijnb. 61 1982 325-333.
Mendoza, L.C.L., Ojeda, G.Y., 2006. Heat flow in the colombian caribbean from the bottom simulating reflector (BSR). CTF - Cienc. Tecnol. Futuro 3, 29–39.
Michalak, M.J., Hall, S.R., Farber, D.L., Audin, L., Hourigan, J.K., 2016. (U-Th)/He thermochronology records late Miocene accelerated cooling in the north-central Peruvian Andes. Lithosphere 8, 103–115. doi:10.1130/L485.1
Molnar, P., England, P., 1990. Late Cenozoic uplift of mountain ranges and global climate change: chicken or egg? Nature 346, 29–34. doi:10.1038/346029a0
Monod, B., Dhont, D., Hervouët, Y., 2010. Orogenic float of the Venezuelan Andes. Tectonophysics 490, 123–135. doi:10.1016/j.tecto.2010.04.036
Montes, C., Bayona, G., Cardona, A., Buchs, D.M., Silva, C.A., Morón, S., Hoyos, N., Ramírez, D.A., Jaramillo, C.A., Valencia, V., 2012. Arc-continent collision and orocline formation: Closing of the Central American seaway: CLOSING OF THE CENTRAL AMERICAN SEAWAY. J. Geophys. Res. Solid Earth 117, n/a-n/a. doi:10.1029/2011JB008959
Montes, C., Guzman, G., Bayona, G., Cardona, A., Valencia, V., Jaramillo, C., 2010. Clockwise rotation of the Santa Marta massif and simultaneous Paleogene to Neogene deformation of the Plato-San Jorge and Cesar-Ranchería basins. J. South Am. Earth Sci., Sierra Nevada de Santa Marta and Adjacent Basins 29, 832–848. doi:10.1016/j.jsames.2009.07.010
Montgomery, D.R., Balco, G., Willett, S.D., 2001. Climate, tectonics, and the morphology of the Andes. Geology 29, 579. doi:10.1130/0091-7613(2001)029<0579:CTATMO>2.0.CO;2
Mora, A., Horton, B.K., Mesa, A., Rubiano, J., Ketcham, R.A., Parra, M., Blanco, V., Garcia, D., Stockli, D.F., 2010. Migration of Cenozoic deformation in the Eastern Cordillera of Colombia interpreted from fission track results and structural relationships: Implications for petroleum systems. AAPG Bull. 94, 1543–1580. doi:10.1306/01051009111
Mora, A., Parra, M., Strecker, M.R., Sobel, E.R., Hooghiemstra, H., Torres, V., Jaramillo, J.V., 2008. Climatic forcing of asymmetric orogenic evolution in the Eastern Cordillera of Colombia. Geol. Soc. Am. Bull. 120, 930–949. doi:10.1130/B26186.1
Nie, J., Horton, B.K., Mora, A., Saylor, J.E., Housh, T.B., Rubiano, J., Naranjo, J., 2010. Tracking exhumation of Andean ranges bounding the Middle Magdalena Valley Basin, Colombia. Geology 38, 451–454. doi:10.1130/G30775.1
Ordóñez, O., Pimentel, M., Moraes, R., 2002. GRANULITAS DE LOS MANGOS, UN FRAGMENTO GRENVILLIANO EN LA PARTE ORIENTAL DE LA SIERRA NEVADA DE SANTA MARTA. Rev. Acad. Colomb. Cienc. Exactas Físicas Nat. 0370-3908 26, 169–179.
Parra, M., Mora, A., Jaramillo, C., Torres, V., Zeilinger, G., Strecker, M.R., 2010. Tectonic controls on Cenozoic foreland basin development in the north-eastern Andes, Colombia. Basin Res. doi:10.1111/j.1365-2117.2009.00459.x
Parra, M., Mora, A., Sobel, E.R., Strecker, M.R., González, R., 2009. Episodic orogenic front migration in the northern Andes: Constraints from low-temperature

thermochronology in the Eastern Cordillera, Colombia: OROGEN-FRONT MIGRATION, COLOMBIAN ANDES. Tectonics 28, n/a-n/a. doi:10.1029/2008TC002423
Platt, J.P., England, P.C., 1994. Convective removal of lithosphere beneath mountain belts; thermal and mechanical consequences. Am. J. Sci. 294, 307–336. doi:10.2475/ajs.294.3.307
Raymo, M.E., Ruddiman, W.F., 1992. Tectonic forcing of late Cenozoic climate. Nature 359, 117–122. doi:10.1038/359117a0
Reiners, P.W., Ehlers, T.A., Mitchell, S.G., Montgomery, D.R., 2003. Coupled spatial variations in precipitation and long-term erosion rates across the Washington Cascades. Nature 426, 645–647. doi:10.1038/nature02111
Restrepo, S., Foster, D., Stockli, D., Parra, M, Sanchez, L., 2009. Long-term erosion and exhumation of the "Altiplano Antioqueño", Northern Andes (Colombia) from apatite (U–Th)/He thermochronology. Earth Planet. Sci. Lett. 278, 1–12. doi:10.1016/j.epsl.2008.09.037
Spikings, R., Cochrane, R., Villagomez, D., Van der Lelij, R., Vallejo, C., Winkler, W., Beate, B., 2015. The geological history of northwestern South America: from Pangæa to the early collision of the Caribbean Large Igneous Province (290–75 Ma). Gondwana Res. 27, 95–139. doi:10.1016/j.gr.2014.06.004
Spikings, R., Simpson, G., 2014. Rock uplift and exhumation of continental margins by the collision, accretion, and subduction of buoyant and topographically prominent oceanic crust. Tectonics 33, 2013TC003425. doi:10.1002/2013TC003425
Stern, R.J., 2002. Subduction zones. Rev. Geophys. 40. doi:10.1029/2001RG000108
Taboada, A., Rivera, L.A., Fuenzalida, A., Cisternas, A., Philip, H., Bijwaard, H., Olaya, J., Rivera, C., 2000. Geodynamics of the northern Andes: Subductions and intracontinental deformation (Colombia). Tectonics 19, 787–813. doi:10.1029/2000TC900004
Tschanz, C., Marvin, R.F., B, J.C., Mehnert, H.H., Cebula, G.T., 1974. Geologic Evolution of the Sierra Nevada de Santa Marta, Northeastern Colombia. Geol. Soc. Am. Bull. 85, 273–284. doi:10.1130/0016-7606(1974)85<273:GEOTSN>2.0.CO;2
Vallejo, C., Winkler, W., Spikings, R.A., Luzieux, L., Heller, F., Bussy, F., 2009. Mode and timing of terrane accretion in the forearc of the Andes in Ecuador. Geol. Soc. Am. Mem. 204, 197–216. doi:10.1130/2009.1204(09)
Van der Lelij, R., Spikings, R., Mora, A., 2016. Thermochronology and tectonics of the Mérida Andes and the Santander Massif, NW South America. Lithos 248–251, 220–239. doi:10.1016/j.lithos.2016.01.006
Van der Lelij, R., Spikings, R.A., Kerr, A.C., Kounov, A., Cosca, M., Chew, D., Villagomez, D., 2010. Thermochronology and tectonics of the Leeward Antilles: Evolution of the southern Caribbean Plate boundary zone. Tectonics 29, TC6003. doi:10.1029/2009TC002654
Vanderhaeghe, O., 2009. Migmatites, granites and orogeny: Flow modes of partially-molten rocks and magmas associated with melt/solid segregation in orogenic belts. Tectonophysics, Hot orogens 477, 119–134. doi:10.1016/j.tecto.2009.06.021
Vargas, C., J., Alfaro, C., Briceño, L.A., Alvarado, I., Quintero, W., 2009. Mapa Geotérmico De Colombia - 2009. Presented at the 10th Simposio Bolivariano - Exploracion Petrolera en las Cuencas Subandinas.
Vargas, C.A., Idarraga-Garcia, J., Salazar, J.M., 2015. Curie Point Depths in Northwestern South America and the Southwestern Caribbean Sea 179–200. doi:DOI:10.1306/13531936M1083642
Veloza, G., Styron, R., Taylor, M., Mora, A., 2012. Open-source archive of active faults for northwest South America. GSA Today 22, 4–10. doi:10.1130/GSAT-G156A.1
Vence, E., 2008. Abstract: Along-Strike Continuity of Caribbean Tectonic Terranes and Their Controls on Source and Reservoir Rocks Offshore Colombia and ; #90063 (2007) [WWW Document]. URL

http://www.searchanddiscovery.com/abstracts/html/2007/annual/abstracts/lbVence.htm (accessed 7.20.16).
Villagómez, D., Spikings, R., 2013. Thermochronology and tectonics of the Central and Western Cordilleras of Colombia: Early Cretaceous–Tertiary evolution of the Northern Andes. Lithos 160–161, 228–249. doi:10.1016/j.lithos.2012.12.008
Villagómez, D., Spikings, R., Magna, T., Kammer, A., Winkler, W., Beltrán, A., 2011a. Geochronology, geochemistry and tectonic evolution of the Western and Central cordilleras of Colombia. Lithos 125, 875–896. doi:10.1016/j.lithos.2011.05.003
Villagómez, D., Spikings, R., Mora, A., Guzmán, G., Ojeda, G., Cortés, E., van der Lelij, R., 2011b. Vertical tectonics at a continental crust-oceanic plateau plate boundary zone: Fission track thermochronology of the Sierra Nevada de Santa Marta, Colombia. Tectonics 30, TC4004. doi:10.1029/2010TC002835
Weber, M., Cardona, A., Valencia, V., García-Casco, A., Tobón, M., Zapata, S., 2010. U/Pb detrital zircon provenance from Late Cretaceous metamorphic units of the Guajira Peninsula, Colombia: Tectonic implications on the collision between the Caribbean arc and the South American margin. J. South Am. Earth Sci., Sierra Nevada de Santa Marta and Adjacent Basins 29, 805–816. doi:10.1016/j.jsames.2009.10.004
Whattam, S.A., Stern, R.J., 2015. Late Cretaceous plume-induced subduction initiation along the southern margin of the Caribbean and NW South America: The first documented example with implications for the onset of plate tectonics. Gondwana Res. 27, 38–63. doi:10.1016/j.gr.2014.07.011
Whipple, K.X., 2009. The influence of climate on the tectonic evolution of mountain belts. Nat. Geosci. 2, 97–104. doi:10.1038/ngeo413
Willett, S.D., Brandon, M.T., 2013. Some analytical methods for converting thermochronometric age to erosion rate: AGE TO EROSION RATE. Geochem. Geophys. Geosystems 14, 209–222. doi:10.1029/2012GC00427

CHAPTER 3

Early Neogene unroofing of the Sierra Nevada de Santa Marta determined from detrital geo-thermochronology and the petrology of clastic basin sediments

Alejandro Piraquive[1,2†], Edna Pinzón[2], Andreas Kammer[2], Matthias Bernet[1], Albrecht von Quadt[3]

1. Institut des Sciences de la Terre, Université Grenoble Alpes, 1381, rue de la Piscine, 38400 Saint –Martin D'Hères. alejandro.piraquive-bermudez@univ-grenoble-alpes.fr, matthias.bernet@univ-grenoble-alpes.fr
2. Grupo de Investigación en Geologia Estructural y Fracturas Universidad Nacional de Colombia. apartado Aéreo, 14490 Bogotá, Colombia. apiraquiveb@unal.edu.co, edmpinzonro@unal.edu.co, akammer@unal.edu.co
3. Department of Earth Sciences, Institute of Geochemistry and Petrology, ETH Zentrum, Clausiusstrasse 25, 8092 Zurich, Switzerland albrecht.vonquadt@erdw.ethz.ch

Abstract

Geo-thermochronologic data from sedimentary rocks, coupled with stratigraphic analyses, unravel an early Neogene exhumation of the Sierra Nevada de Santa Marta massif (SNSM). This fault-bounded triangular block in the northern Andes of Colombia exposes Precambrian to Paleozoic metamorphic rocks and suites of a Triassic-Jurassic magmatic arc. We compare the Neogene basin fills of two marginal basins, a western one located along the Santa Marta-Bucaramanga fault (SMBF) and the northern one occupying the southern margin of the Oca fault. The western sequence consists of gravitational conglomeratic deposits ≈ 1200 m that define a progradational Gilbert-type delta emanating from a scarp coinciding with the SMBF. By its stratigraphic and structural position this sequence compares to the northern transgressive sequence. Provenance analyses of representative sections of these two sequences, evidence a sourcing from the underlying basement. This finding is in concordance with zircon U-Pb age spectra that lack pre-Grenvillian and Ordovician signals of coeval sediments of the Magdalena basin, demonstrating, that they were deposited in a local basins disconnected to the trunk system of the proto-Magdalena river. In order to reconcile the different organization of the two marginal basins we propose a regional-scale tilting of the SNSM towards the northeast during the early Neogene. This model takes account of the coeval progradational sedimentary cycle at the fault-bounded western flank and the transgressive onlapping of the northern conglomerates on a tilted surface during an overall exhumation of the massif.

Key words: Santa Marta Massif, Marginal basins, Neogene tectonics, Gilbert-type delta, Santa Marta-Bucaramanga fault

1. INTRODUCTION

The northwest corner of South America is divided into the Northern Andean block which, on its turn, is subdivided into a number of micro-blocks as a result of the continued interaction between the South American, Caribbean and Nazca plates that record various Cretaceous to Cenozoic contractional events. Although, fault-bounded morphotectonic provinces (Fig. 1) readily define the assemblage of the individual micro-blocks, controversy exists about tracing kinematic limits between the North Andean block (or continental South America) and adjacent oceanic plates. Velocity gradients deduced from Regional Global Positioning of the Central and South America Project (CASA) (Trenkamp et al., 2002) argue for diffuse limits that emerged as a result of a transpressive stress regime between the Caribbean plate and South America (Fig. 1). Inherited sutures and present plate boundaries are partly concealed by the mountain ranges of the North Andean block, that comprise the Eastern, Central and Western Cordilleras, the Sinú folded belt, the Sierra Nevada de Santa Marta (SNSM) and the Guajira massifs in Colombia, and the Perijá Range and Merida Andes in Venezuela and the Neogene basin fill of the LMV (Fig.1).

During the Maastrichtian-Paleocene a juvenile Caribbean plateau with associated marginal island arcs collided against the NW corner of South America, (Ayala et al., 2012; Bayona et al., 2011; Cardona et al., 2011a, 2012; Higgs, 2009; Pindell et al., 2005; Pindell and Kennan, 2009; Spikings et al., 2015; Villagómez et al., 2011), juxtaposing oceanic crustal slivers against the continental margin. This accretion was followed by a post-collisional Eocene plutonic event, marking the closure of a Cretaceous-Paleogene subduction cycle. During the Oligocene-Miocene the onset of a transpressive regime

led to the opening of the Plato-San Jorge basin to the west and the separation of the Sierra Nevada de Santa Marta massif from the Central Cordillera, as the continental margin became fragmented along the Santa Marta - Bucaramanga fault (Duque-Caro Mora-Bohórquez et al., 2017, Montes et al., 2010) and the drainage of the Magdalena River originally communicating with into the Maracaibo basin became diverted to its present site

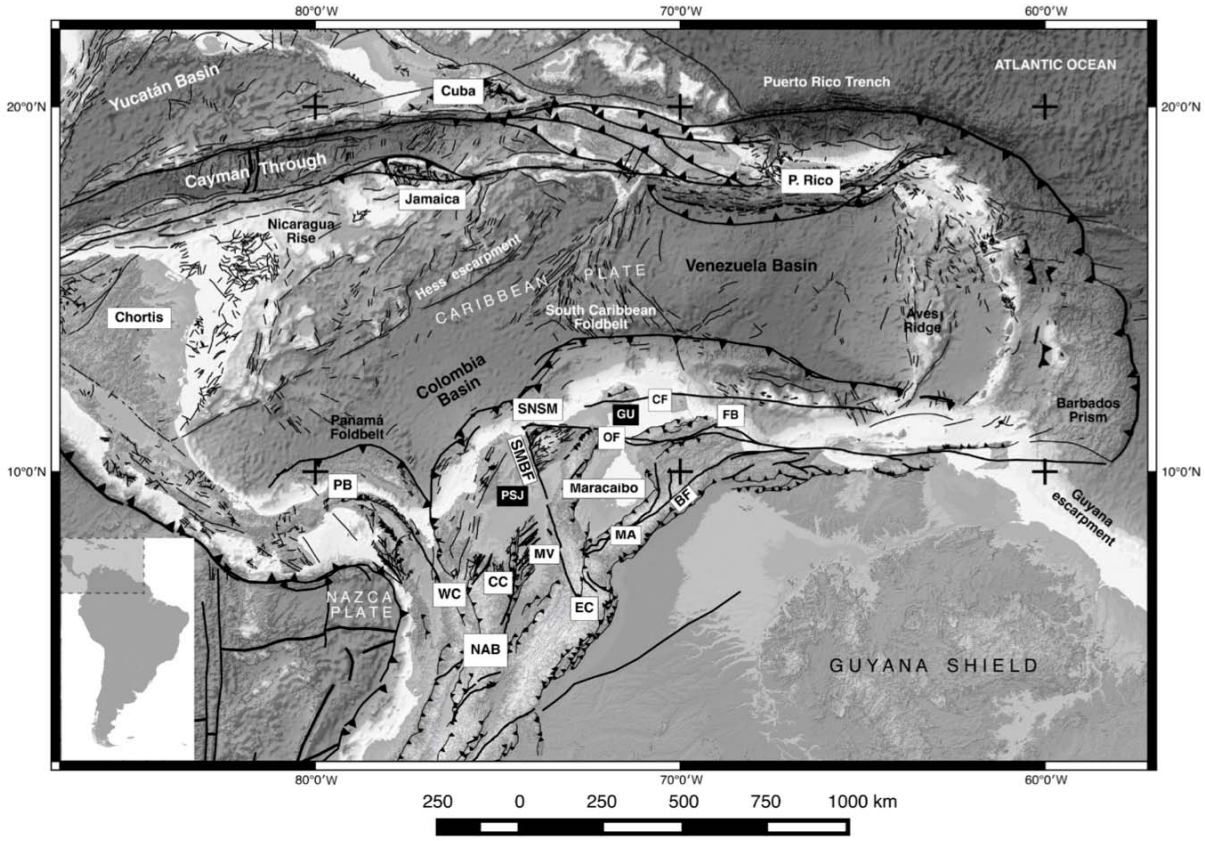

Figure 1. Regional tectonic map of the Caribbean realm showing the most relevant geological features intervening in the plate boundary configuration. after (Veloza et al. 2012). Elements of the North Andean Block (NAB): Maracaibo block, SNSM: Sierra Nevada de Santa Marta, OF: Oca Fault, CF: Cuisa Fault, SMBF: Santa Marta-Bucaramanga Fault, GU: Guajira Basin, PSJ: Plato-San Jorge Basin MA: Mérida Andes, BF: Boconó Fault, FB: Falcon Basin, WC: Western Cordillera, CC: Central Cordillera, EC: Eastern Cordillera, MV: Magdalena Valley, PB: Panamá Block.

Recent bedrock thermochronological studies demonstrated an early Eocene to early Miocene exhumation of the SNSM, with youngest cooling ages (25-16 Ma) located to the NW and older ages (50-40 Ma) located to the SE of the SNSM (Villagómez et al., 2011). This asymmetric age distribution may be attributed to an enhanced exhumation at the Santa Marta – Bucaramanga fault in the course of a separation of the SNSM from its co-terminal western Central Cordillera, as the collisional impact of the Caribbean plate induced a clockwise rotation of the continental margin (Montes et al., 2010). A coeval accumulation of a Cenozoic marine sedimentary pile of ≈ 8 km in the Plato San Jorge basin supports this scenario (Duque-Caro, 1979). This predominantly extensional regime gave rise to fault bounded marginal basins and persisted up to the middle Miocene, when the stress regime became transpressive and the Oca fault assumed its strike-slip displacement (Audemard and Audemard, 2002). The late stages of the tectonic evolution of the SNSM are recorded in the basins surrounding the massif.

This study focuses on the Oligocene-Miocene sedimentary fill of the fault-bounded sub-basins located in the footwall block of the Santa Marta-Bucaramanga fault associated with the Plato-San Jorge basin and the hanging wall block of the Oca fault at the Guajira basin. We defined these marginal fault related basins as the Aracataca basin at the western foothills of the SNSM, and the Palomino basin along the northern foothills of the SNSM respectively.

We analysed the late exhumation history of the SNSM using the most proximal Neogene sediments found in the Aracataca and Palomino basins. The studied Cenozoic clastic sedimentary successions in both basins consist mainly of conglomeratic fan delta deposits that are interbedded with marine to transitional sandstones at their

base and at their top. Compositional changes and age data record relevant stages of a Paleogene exhumation of the SNSM.

Our methodological approach is based on the determination of sediment provenance, relating compositional data with bedrock units of a mainly Jurassic arc assemblage of the SNSM. This compositional analysis is performed by heavy mineral counts in sandstones and pebble variations in the conglomeratic sequence. These results are combined with U-Pb ages measured in detrital zircon, and fission-track cooling ages from apatites and zircons.

The integration of stratigraphic and geochronological data helps constraining the timing of deformation phases that led to the exhumation of basement rocks that form the footwall of the Santa Marta-Bucaramanga fault and NW-verging thrust slices of the interior of the massif.

2. TECTONIC SETTING

The Caribbean continental margin of South America was shaped/constituted itself during a Cretaceous to Paleogene subduction cycle and a subsequent collisional event (Audemard and Audemard, 2002; Cardona et al., 2011b, 2012; van der Lelij et al., 2010; Villagómez et al., 2011). During Cretaceous subduction of the Farallones plate, the convergence was not partitioned, as strike-slip displacements are absent until the Paleogene (Acosta et al., 2007; Cortés et al., 2005; Kennan and Pindell, 2009; Vence, 2008). The Paleocene-Oligocene collisional phase, however, entailed a strike-slip reactivation of margin-parallel faults, as the North-Andean block rotated into its present position (Nova et al., 2013; Vence, 2008), culminating in the late Miocene to

Pliocene with the activation of the Boconó fault of the Merida Andes (Bermúdez et al., 2010; Egbue and Kellogg, 2010; Javadi et al., 2011). In this tectonic environment, upper crustal heterogeneities caused the formation of minor tectonic blocks during Paleogene-Neogene transpression. Contrary to the presence of directional faults that form sharp boundaries (Motagua fault, Cayman trough, Puerto Rico trench) on the northern edge of the Caribbean plate (Fig. 1), deformation on the southern edge of the Caribbean plate is widely distributed along crustal heterogeneities of the different mountain chains (Pennington, 1981; Taboada et al., 2000).

The northern edge of the South American plate in the Colombian Andes is segmented by the Santa Marta-Bucaramanga fault, between the N-S striking Andean Cordilleras and the Maracaibo block (Fig. 1). The Santa Marta-Bucaramanga fault originated during the early Mesozoic continental break-up (Kammer and Sánchez, 2006), and subsequently decoupled the structural evolution of the Central Cordillera and the Maracaibo block (Figs. 1, 2, 3.). The Western Andean domain still preserves the tectonic frame of an arrested Pre-Campanian subduction setting with the Romeral suture separating continental and oceanic terrains. However, in the Eastern block of the Santa Marta-Bucaramanga fault, the triangular SNSM massif and the isolated Perijá Range formed as response to the early subduction of the Caribbean plate during the Paleogene (Ayala et al., 2012; Bayona et al., 2011; Cardona et al., 2011a; Monod et al., 2010).

2.1 Sierra Nevada de Santa Marta massif

The SNSM constitutes a remarkably elevated massif along the South-Caribbean margin with the Bolivar peak reaching an altitude of 5775 m. This triangular block displays the structural array of a monocline, with its northwestern corner exposing an imbricated lower crustal section, capped by nested Jurassic plutons and correlative volcanic sequences forming its southwestern flank (Tschanz et al., 1974). On its western side it is limited by the normal-sinistral Santa Marta-Bucaramanga fault, which produced a structural relief of >7000 m between the basement of the SNSM and the basement of the Lower Magdalena basin (LMB), and accumulated as much as 45 km of left lateral displacement since the Oligocene (Montes et al., 2010) (Fig. 2 & 3). At its northwestern corner, an obducted contact of the Caribbean plate can be inferred (Doolan, 1970). On its northern side the contact of the Caribbean and South American plates is cut by the right-lateral Oca fault (Fig. 2).

The juxtaposition of the South American and Caribbean plates sustains the idea of a delaminated crustal section “floating” on the Caribbean plate (Audemard and Audemard, 2002) this exceptionally thick crustal section forms the upper crust of a continent-ward dipping main suture that is underlain by strongly sheared platform sediments and transitional basement rocks of the lower crust. The lower crustal section incorporates low to high-grade metamorphic units, the Sierra Nevada Province and the Sevilla Metamorphic Belt composed of Precambrian granulites, anorthosites and gneisses (Cardona et al., 2010a; Cordani et al., 2005; Kroonenberg, 1982; Ordóñez et al., 2002; Restrepo-Pace et al., 1997), the Inner Santa Marta Metamorphic Belt that is composed of a Permian mylonitic belt (Cardona et al., 2010c) of orthogneisses and

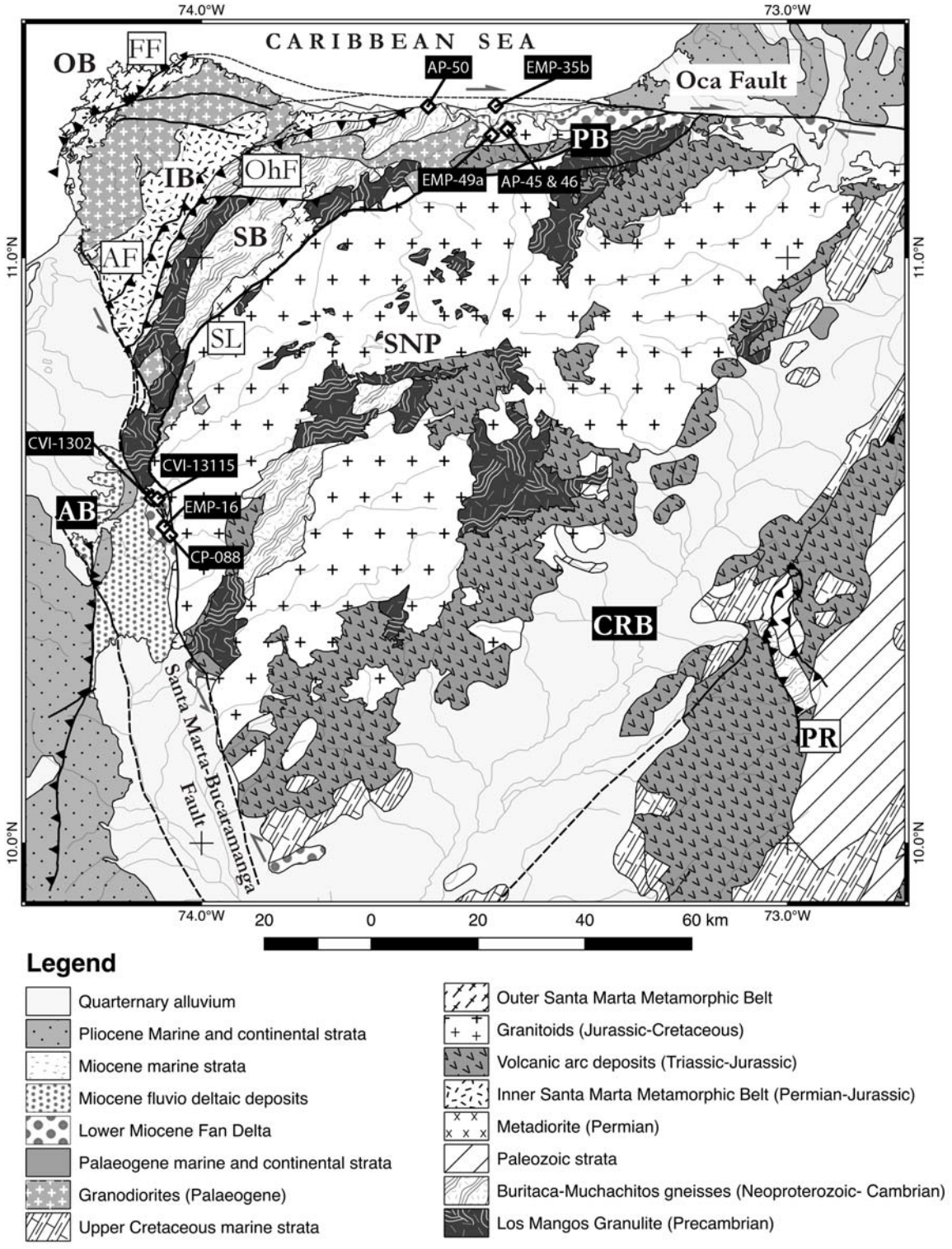

Figure 2. Geological Map of the Sierra Nevada de Santa Marta Massif (SNSM) and sampling sites. SNP: Sierra Nevada Province, SB: Sevilla Belt, IB: Inner Santa Marta Metamorphic Belt, OB: Outer Santa Marta Metamorphic Belt, AB: Aracataca Basin, PB: Palomino Basin, CRB: Cesar Rancheria Basin, AF: Aguja Fault, OhF: Orihueca Fault, FF: Florin Fault, SL: Sevilla Lineament, PR: Perijá Range.

meta-sedimentary rocks, a Triassic to Lower Cretaceous sequence of high amphibolite facies meta-sedimentary rocks and S-type granites (Zuluaga and Stowell, 2012), and the Outer Santa Marta Metamorphic Belt, a phyllite belt that is related to oblique accretion of oceanic crust composed of low-grade metamorphic schists, meta-conglomerates, and Upper Cretaceous-Paleogene meta-basites (Cardona et al., 2010b; Doolan, 1970; MacDonald et al., 1971). These units were subject to surface uplift and erosion as a consequence of collisional tectonics along the continental margin since the Paleogene.

3. STRATIGRAPHY OF THE ARACATACA AND PALOMINO MARGINAL BASINS

3.1 Aracataca Marginal basin (Western SNSM)

The Cenozoic Aracataca basin, forms a narrow depositional fill along the western flank of the SNSM (Fig. 2), and is reported to record marine to lagoonal and continental depositional conditions (Tschanz et al., 1969). Considering this setting, the Santa Marta-Bucaramanga is likely to have controlled its subsidence, as its elevated eastern block contains the Precambrian Mangos granulite and the Jurassic acid to intermediate plutonic and volcanic arc assemblage, which essentially sourced the basement fill (see below). A compilation of the stratigraphy is given in (Table. 1).

We divide the stratigraphic profile of the Aracataca basin, into a lower shaley to conglomeratic unit with a marine fossils, informally designated as Macaraquilla

conglomerate (Hernandez et al., 2003) and an upper unit of sandstones and conglomerates formerly attributed to a fluvial to transitional molasses facies of a Miocene age (Tschanz et al., 1969). This eminently conglomeratic sequence is succeeded by interbedded sandstones, marls and mudstones of the Zambrano Formation which yielded pollen of a lower Pliocene age (Hernandez et al., 2003). Upper Pliocene deposits are defined as the informal Guamachito conglomerate unit, which towards the west of Aracataca decreases in grain size and give rise to the "Unidad Arenosa de Fundación" (Table. 1).

3.2 Palomino Marginal Basin (Northern SNSM)

In the southern footwall of the Oca fault a fining-upward sequence rests unconformably on Pre-Cretaceous basement rocks. In the Palomino basin along the road from Santa Marta to Riohacha, the outcrops preserve a Miocene conglomeratic succession defined as molasse facies (Tschanz et al., 1969). The conglomeratic facies rests directly over the crystalline basement with no remnants of pebbly mudstones and associated marine deposits. The sedimentary succession of pebble conglomerates ends against the Oca fault, fine grained Upper Miocene – Pliocene sequences are preserved north of the Oca fault. (Tschanz et al., 1969).

TABLE 1. STRATIGRAPHIC NOMENCLATURE FOR THE CENOZOIC SEDIMENTARY ROCKS AT THE ARACATACA BASIN

<table>
<tr><th></th><th>AGE</th><th>TSCHANZ et al. (1969)</th><th>HERNANDEZ, (2003)</th><th>COLMENARES, (2007)</th><th>THIS WORK</th></tr>
<tr><td>Q.</td><td>PLEISTOCENE</td><td rowspan="3">Upper Tertiary sedimentary rocks</td><td>Unidad arenosa de Fundación</td><td></td><td>Unidad arenosa de Fundación</td></tr>
<tr><td rowspan="3">NEOGENE</td><td>PLIOCENE</td><td>Guamachito Conglomerates</td><td>Guamachito Conglomerates</td><td>Guamachito Conglomerates</td></tr>
<tr><td rowspan="2">MIOCENE</td><td>Zambrano Formation</td><td>Zambrano Formation</td><td>Zambrano Formation</td></tr>
<tr><td>Miocene sedimentary rocks</td><td rowspan="3"></td><td>Miocene sedimentary rocks</td><td></td></tr>
<tr><td rowspan="3">PALEOGENE</td><td>OLIGOCENE</td><td></td><td rowspan="3"></td><td rowspan="2">Aracataca Conglomerates</td></tr>
<tr><td>EOCENE</td><td>Eocene Sedmentary rocks</td><td rowspan="2"></td></tr>
<tr><td>PALEOCENE</td><td></td><td>Macaraquilla Conglomerates</td><td>Macaraquilla Conglomerates</td></tr>
</table>

An appraisal of the two sedimentary basins clearly needs the precision of a biostratigraphic frame, a task still to be performed. Our argument for an Oligocene to early Miocene stratigraphic age of the Aracataca conglomerates is based on the regional framework of the Lower Magdalena basin and the Paleogene evolution of its sub-basins, as documented by their subsidence histories (Bernal-Olaya et al., 2015; Flinch and Castillo, 2015). These data are fit the frame of exhumation ages (Villagómez et al., 2011) of the Santa Marta Massif reasonably well.

A well-constrained subsidence history has been elaborated recently for the Plato sub-basin (Bernal-Olaya, 2015), which constitutes one of the well-evolved depocenters to the W of the study area. Burial plots document two phases of subsidence. A first late Paleogene/early Neogene depositional phase was initiated along faults oriented perpendicularly to the continental margin (Bernal-Olaya, 2015; Montes et al., 2010).

Subsidence plots constrain this rift re-related basin evolution to the middle Oligocene until the late Miocene age. Among the graben-bounding faults, the Santa Marta-Bucaramanga fault and subsidiary strands form a western basin margin and control the NNW-striking depocenter of the Arjona sub-basin (Bernal-Olaya et al. 2015), which connects further north to Aracataca sub-basin.

A second subsidence phase spans the middle Miocene to Pliocene and concludes with the deposition of deep-water shales of the Tubará Formation (Flinch, 2003). Subsidence was accommodated without rifting.

A late Paleogene exhumation phase of the western border of the SNSM massif has been documented by fission track-data by Villagómez et al. (2011), who evidenced a principal exhumation interval of 29 to 26 Ma estimating exhumation rates of 0.6 to 0.7 km/Ma. Considering the proximal depositional setting for the Aracataca conglomerates with respect to a mountain front located at the SMBF, the time lag between denudation, transport and deposition could below our very approximate time frame and amount to just a few million years, as alluded for a gravelly-dominated depositional settings of a similar tectonic environment (Jones et al., 2014). Such a largely synchronous interplay between exhumation and deposition may be presumed for the late Oligocene exhumation of the western flank of the SNSM and the largely coeval rifting of the Lower Magdalena Valley (LMV), which most likely triggered the accumulation of the Aracataca conglomerates.

4. METHODS

4.1 Clast Counting

Along the two stratigraphic sections conglomerate clast counts were performed at 13 locations shown in Fig. 3 & 4. Clast counting was intended at least to have one representative count for each conglomeratic facies associations. An average of 100 clasts (range between 60 up to 200 clasts) with sizes varying from very coarse pebbles (>3 cm) to boulders were counted using the ribbon method (Howard, 1993). Conglomerates are commonly matrix-supported poorly sorted and highly immature. Clasts were classified into plutonic, volcanic, metamorphic, sedimentary and minor abundances of gabbroic and ultramafic related clasts. Within the discrimination twelve specific litho-types were defined according to macroscopic compositions, results are summarized in Fig. 6.

4.2 LA-ICP-MS U–Pb Geochronology

Zircon U-Pb ages were obtained from 6 samples, using LA-ICP-MS analyses. Zircons were extracted from samples using conventional mineral separation technique including rock crushing, sieving (250-60 µm fraction), and concentration with heavy liquid and magnetic separation techniques. Detrital zircons (50 to 200 grains per sample) were randomly picked, selecting clean, crack and inclusion-free grains. Subsequently polished grain epoxy mounts were coated with graphite and imaged at

the Geosciences Department of the Université de Lausanne using a Vega ©Tescan MV2300VP SEM, to create a detailed set of panchromatic cathodoluminescence images. Laser ablation spots were selected, in both grain cores and rims.

LA-ICP-MS analyses and data processing were carried out at the Institute of Geochemistry and Petrology at ETH Zürich, Switzerland. Zircons were ablated with a NewWave UP-193nm Ar-F excimer ablation system coupled to a PerkinElmer PE SCIEX Elan 6100 ICP-MS to measure Pb/U and Pb isotopic ratios. The following parameters were applied during this process: 30 µm diameter beam size, 10 Hz repetition rate, 30–45 second signal and a beam intensity of 2.2–2.5 J/cm^2. Reproducibility of U/Pb data was monitored by measurements of GEMOC GJ-1 CA-ID-TIMS ^{206}Pb–^{238}U age of 608.5 ± 0.4 Ma; (Jackson et al., 2004) used as a primary standard. The external reference standards Plešovice 337.13 ± 0.37 Ma (Sláma et al., 2008), and TEMORA 1 416.75±0.24 Ma, (Black et al., 2003), were used to calibrate and monitor fractionation and consistency in the measured U–Pb dates. Ages were calculated using LAMTRACE (Jackson, 2008). Additional data reduction details are given by Ulianov et al, (2012). Statistical analyses of zircon data were performed using Isoplot 3.71 (Ludwig, 2003). All discordant (> 1–3%) analyses of magmatic zircons were discarded. Only zircons with concordance greater than 90% were accepted and plotted. Statistical interpretation of the results, regarding to discordance, maximum depositional ages and selection of the best age were done considering a threshold of 1.5 Ga given the change in chronometric power, the details on these proceedings are explained in Spencer et al. (2016).

4.3 Detrital fission-track thermochronology

Zircons of the 125-250 µm fraction from eight samples, mounted in Teflon® sheets, with at least two mounts per sample. Zircons were polished to expose an internal surface and etched in a NaOH-KOH solution at 228°C. Etching time varied between 20-60 hours in order to reveal countable tracks in at least 100 grains per sample. Samples were irradiated together with Fish Canyon Tuff and Buluk Tuff zircon age standards and IRMM541 dosimeter glasses.

Apatite crystals of 4 samples were mounted in epoxy, polished and etched in 5.5 M HNO_3 at 21°C for 20 s and covered with muscovite detectors. The samples were irradiated together with Fish Canyon Tuff and Durango Tuff age standards and IRMM540R dosimeter glasses. Both apatite and zircon samples were irradiated at the FRM II research reactor at Munich, Germany. A summary of the dated samples and analytical details as zeta calibration, grain number and U content are presented in Table A2, Probability density plots for selected examples are shown on figures 9 & 10.

5. RESULTS

5.1 Stratigraphy

In this section, we present a summary of the lithofacies of two representative sections of the Aracataca and Palomino basins, which we measured along the Rio Aracataca and the Rio Negro respectively (Fig. 3 & 4).

The analysed deltaic deposits are mainly conglomeratic, commonly with presence of calcareous cement, gravels that can be monomict but in general, a polymict composition is dominant especially towards the top. The detailed analysis and classification of the sedimentary rocks (Boggs, 2009; Folk, 1980; Pettijohn, 1980) led to the definition of 19 different facies, associated in four different assemblages. For the facies definition, we rely on the fluvial system classification defined by (Miall, 1978, 2006).

This stratigraphic scheme allowed defining the presence of four facies assemblages in the Aracataca basin and three facies assemblages in the Palomino basin. Depositional processes attest for major differences between two delta systems that are coeval but respond to different genetic process.

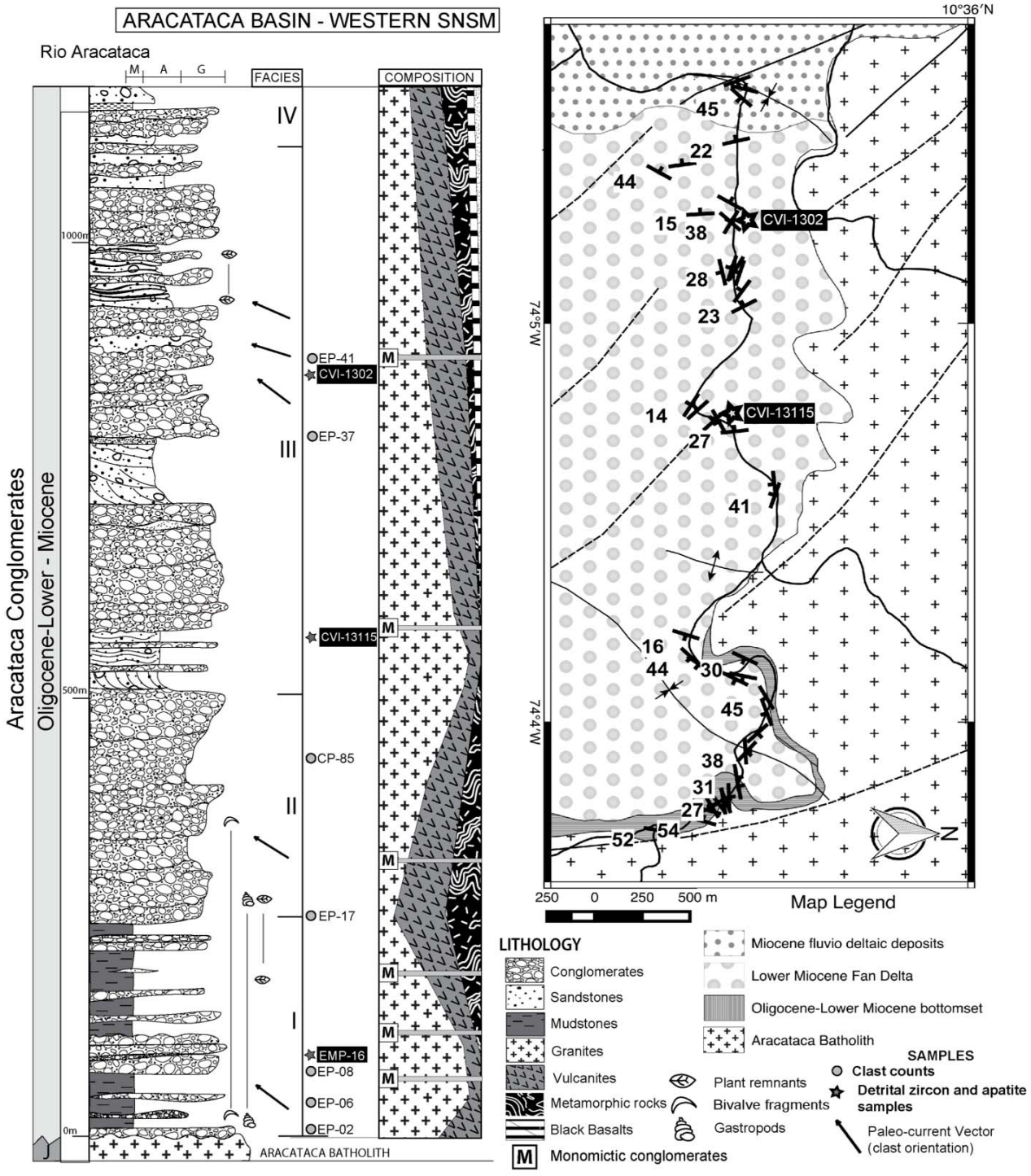

Figure 3. Stratigraphic column of the sedimentary successions at the Rio Aracataca with compositional variations of clast counts. Right: location map of the Rio Aracataca section. Facies associations are described in detail in Table. 2.

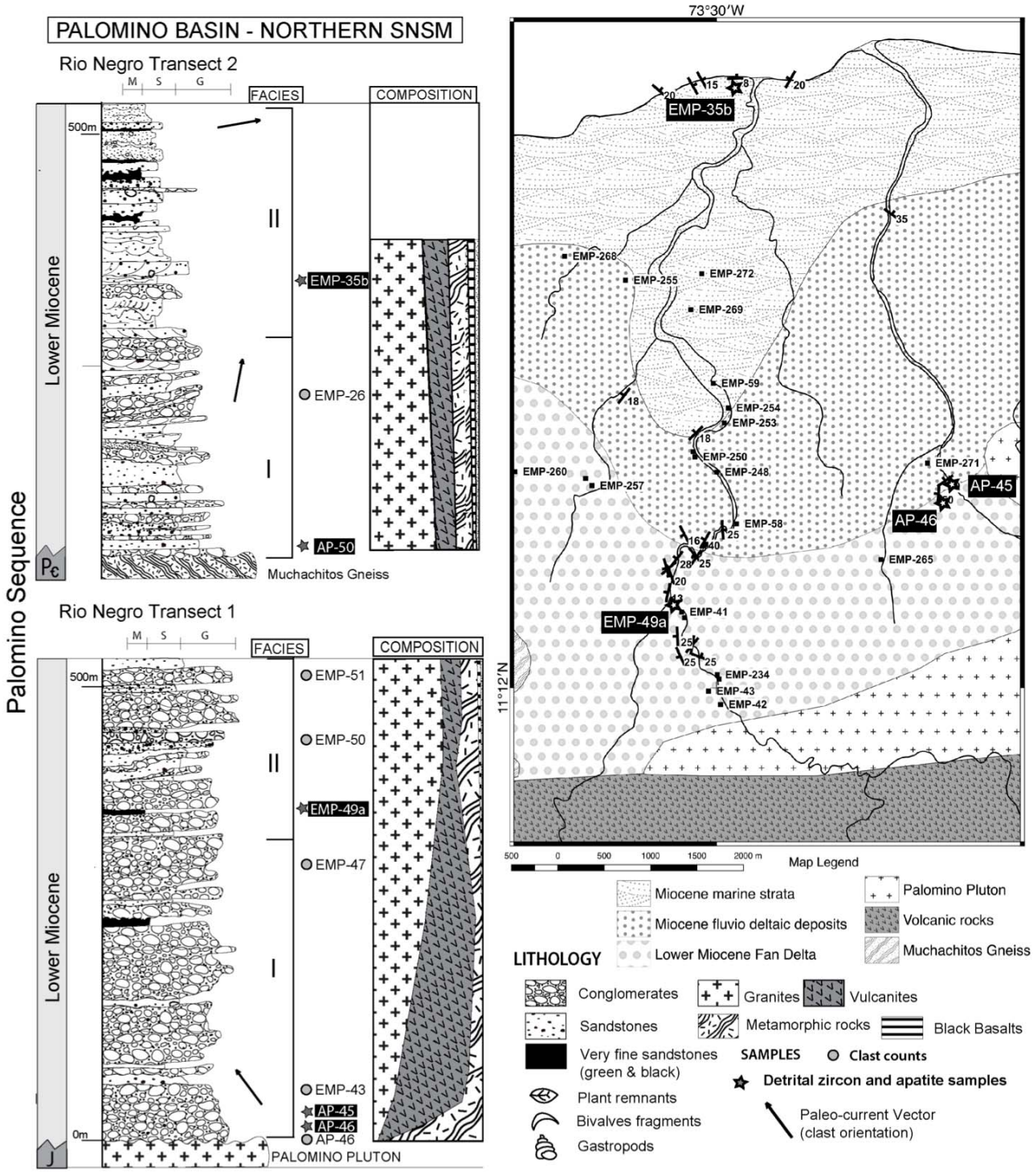

Figure 4. Stratigraphic column of the sedimentary succession at the Rio Negro and at the Palomino basin with compositional variations from clast counts. Right: location map of the Rio Negro section. Facies associations are described in detail in Table. 3.

5.1.1 Aracataca Conglomerates

Along the Aracataca River we measured a composite section of 1200 m of a mainly conglomeratic succession, which include fossil-bearing mudstones at its base. Based on lithological criteria and facies analysis we divide this profile into four sequences, numbered from base to top and labeled by interpretative names for ease of description (Fig. 3, Table 2). Sequence I consists of mud- to siltstones, alternating with discrete conglomeratic lenses. Sequences II and III are characterized by a predominance of tabular conglomeratic beds, which form amalgamated in sequence II and separated by sandy layers in sequence III. Sequence IV displays conglomeratic beds in discontinuous lenses and channel-like bedforms, which interfinger with sandy units and are separated by muddy beds. We base our facies analyses on the classification Miall (1978) proposed for fluvial deposits.

Our provenance study depicts trends in compositional variation of the gravel fraction. These variations may be divided into a two-fold scheme, according to the contribution of the local substratum, the Aracataca Batholith that belongs to the Central Batholith suite, and a wider bedrock spectrum of the southwestern flank of the SNSM. Thus, monomict conglomerates exclusively consist of granitic components of the Aracataca batholith, while polymict conglomerates include acid and basic volcanic clasts, supplemented by granulitic rock fragments of the Los Mangos unit.

Sequence I starts with a basal polymict pebble-boulder conglomerate, 20 m thick, composed of stacked beds, each distinguished by a characteristic clast size (facies *Ia*). Up-section, muddy to silty beds with calcareous intercalations denotes the extent of this unit. They alternate with lenses and mound-like accumulations of debris flows

with boulders of granite and micritic limestone (Figure 5-a) and enclose solitary boulders and monomict lenses of angular granitic clasts (facies *A-IIb*), which are virtually devoid of matrix, but locally intermingled with shell fragments. Overlying laminated silt- and mudstones smooth out rugged surfaces of these breccia-like conglomerates and mark a steady background sedimentation.

The base of sequence II is traced by the appearance of a first thick tabular conglomerate bed that overlies a basal mud layer in sharp contact (facies *A-IIa*). Large cobble-sized clasts show a bed-parallel orientation and a tendency of a reverse grading in the lower part of this bed (Figure 5-b), displaying thereby characteristics of a non-cohesive debris flow (Nemec & Steel, 1984) or a concentrated particle flow (Mulder & Alexander, 2001). Other similar beds contain solitary granitic boulders embedded along their base or floating in cobble conglomerates (facies *A-IIb*). Where defining closely packed lenses, they display an *a(p)a(i)* imbrication with their long axes dipping in a southeastern upflow direction. Other interfaces of debrites contain pockets of polymict cobbles, which are angular and highly disorganized. Occasionally, these conglomeratic layers are superseded by laminated medium-grained and coarse, massive sandstone (facies *A-IIIa*). Throughout this sequence, conglomeratic beds are intermittently separated by thin beds of silt- and mudstones, which contain lenses of monomict breccias, as described for unit I. Their presence defines the extent of sequence II.

Amalgamated debrites prevail in the lower part of sequence III and may be separated into distinct m-scaled flow units, according to particular clast size and sandy matrix content (Figure 5-c). Further up-section, flow units are capped by thin to medium-sized sandstone beds. These sandy layers are laminar to massive (facies *A-IIIa*) and

display water-escape structures, as evidenced by sheared sandy flames intruded into overlying conglomerates, patchy granular pockets within the sandstone and conglomeratic pillars or dikes emanating from underlying debris flows (nomenclature adopted from Postma, 1983). These debrites include in their upper part outsized granite boulders, which are aligned close to or may drape the very interface to the overlying sandy layer, displaying imbricate arrays, where closely packed (figure 5-d). Outsized clasts may also be present in the overlying sandy layers, suggesting an emplacement mechanism related to their common interface.

Within sequence III, matrix-supported polymict conglomerates compose a distinct facies, as they define channel fills with an abundant sand- to granule-sized matrix (facies *A-IIIb*).

Sequence IV is composed of discontinuous beds of pebble-cobble conglomerate, both clast- and matrix-supported, which form channel-shaped lenses up to 3m thick and display no distinct or a normal grading (facies *A-IVa*). Clasts are rounded and display an *a(t)b(i)* imbrication. They alternate and interfinger with trough-cross stratified sand beds that display conglomeratic base lags (facies *A-IVb*). This assemblage is subdivided by thin to medium beds of massive mudstone, which are variably scoured by channel-shaped bedforms (facies *A-IVc*).

Interpretation

Our facies inventory combines diagnostic characteristics of the three principal architectural elements of a Gilbert-type delta that defines, from base to top, a progradational succession. Sequence 1 constitutes a bottom- or toeset, sequences 2

and 3 a lower and upper foreset assemblage of a delta slope and sequence 4 a topset of a delta plane. We base our arguments mainly on the facies distribution, as detailed in table 2.

Mud- and silt-stones of facies with embedded conglomerate lenses and outsized boulders (facies *A-Ia* and *A-IIIb*) define a bottomset within the reach of debris slides and falls of a nearby delta slope. Our measured section (Fig. 3) illustrates a decrease of muddy lithologies topwards, which supports a progradational change from distal bottom- to proximal toeset. By their composition and textural maturity, debris flow units comprise two distinct classes. Monomict breccias are derived from the local bedrock of the Aracataca granite and are texturally highly immature, as they encompass granule- to boulder-sized rock fragments within a same bed. This lack of sorting and their disordered fabric (akin to an open-work fabric; Gobo et al., 2014) suggest an origin by debris fall from cliffs of a contiguous topographic scarp. Their intermingling with little fragmented marine fossil shells and boulders of calcareous beds (Fig. 5-a) points to the existence of a subaqueous platform or delta plain which they must have crossed during their avalanching. Considering an elevated sediment supply for the progradational setting of a fan delta, the formation of calcareous beds is atypical and may be restricted to minor transgressional cycles, as documented for a Paleogene clastic fan-delta of the northeastern Ebro basin (López-Blanco et al., 2000). Isolated outsized clasts embedded within mudstones attest to the presence of a pronounced delta slope, which contributed to their separation from smaller-sized clasts, according to a high momentum imparted by their fall or down-slope tumbling (Nemec, 1990).

Polymict conglomerates, on the other hand, are texturally more mature and represent hyperconcentrated flows. By their inverse grading in basal divisions, they document an incipient sorting of bigger clasts by dispersive pressure (Lowe, 1982; Mulder & Alexander, 2001). In the lower part of sequence 2 these beds represent homogeneous units enriched in a sandy matrix and lack, as a distinctive feature, scoured contacts even overlying soft muddy beds (figure 5-b). These relations point to a reduced basal drag of relatively impermeable flow units, and may be associated to an emplacement by hydroplaning (Mohrig et al., 1998). In contrast to these compact plugs, lenses of polymict cobble-boulder conglomerates, which by their disordered fabric and textural immaturity resemble debris fall deposits, may have been derived by the extraction of the sandy matrix of a "leaky" debris flow within a gravel-rich front of a debris flow (Nemec, 1990), from which gravels may have detached and formed debris fall deposits in front of a parental debris flow (Sohn, 2000).

Amalgamated conglomeratic units of segment 2 may represent multiphase debris flows deposited under different rheological regimes (Sohn, 2000). Basal divisions of inversely graded, thin-bedded pebbly sandstones and conglomerates may be attributed to a flow regime of traction carpets, while normally graded upper conglomeratic divisions may have accumulated by the fall-out of particles initially supported by a turbiditic suspension mechanism (Figure 6-c; Sohn, 1997, 2000). The segregation of conglomeratic and sandy layers becomes distinctly bipartite in segment 3 with a basal conglomeratic traction carpet (or inertia layer; Postma et al., 1988) separated from an overlying sandy turbidite layer by a sharp interface. These debrite-turbidite couplets contain outsized clasts reaching the fraction of boulders that align close to the top of conglomeratic beds or at the very interface to overlying sandy

layers. This situation closely relates to the experimental findings of Postma et al. (1988) and their conceptual model of a laminar inertia flow capable of supporting large clasts and a segregating upper turbulent layer. The trapped outsized clasts of figure (5-d) may thus have slid close to the interface of a conglomeratic laminar and sandy turbulent flow unit. In contrast to other deltaic foreset sequences, secondary reworking of the depositional units is subordinate and can only be inferred from an isolated channel-shaped bedform with the matrix-rich conglomerate that composes facies *A-IIIb*.

Conglomeratic and sandy deposits of sequence 4 display channel-like bedforms and may be associated to a distributary delta plain. Intervening muddy layers are likely to represent floodplain deposits. The lack of pedogenic horizons supposes a subaquatic environment and suggests that sea-level rise outpaced depositional aggradation.

Summarizing, the depositional environment of a Gilbert-type delta may be constrained by its three basic architectural elements and a progradational setting. The bottomset contains outrunners of outsized clasts and debris-fall deposits, signaling the proximity of a delta front. Distal conglomeratic units intercalated with muddy layers of the bottom- to toeset consist of little differentiated, matrix-rich debris flows. These conglomeratic deposits become increasingly differentiated into composite basal conglomeratic inertia and overlying sandy turbidity flow units. The presence of outsized clasts at clear-cut interfaces attests to elevated grain-support mechanisms in the proximal foreset setting of facies assemblage 3. Delta plain deposits of sequence 4, finally, may be assigned to a topset.

Ubiquitous outsized clasts point to a steep foreset gradient and pose the question about a tectonically active catchment area. For polymict conglomerates, gross

compositional trends of sequences 1 and 2 record a gradual increase in input of the Precambrian Mangos Granulite suite and gneiss components of the southern Sevilla Metamorphic Belt. The exclusion of metasedimentary components of the Inner Santa Marta Metamorphic Belt restricts the catchment area to the central and southern part of the SNSM. Compositional variations of the gravel spectrum are minor, presupposing that the drainage system maintained a similar structural position since its onset, as might be expected for the gradual denudation of a topographic scarp at an active fault. This relatively uniform contribution is punctuated by the monomict input of the of the Aracataca batholtih, which must have constituted both fault scarp and hillslopes of an incised valley. These findings support a localized uplift at the western flank of the SNSM, for which Villagómez et al. (2011) modeled a time span of 29 Ma to 25 Ma, based on AFT data.

TABLE 2. SUMMARY OF FACIES AND FACIES ASSEMBLAGES FOR THE ARACATACA BASIN

ARACATACA BASIN - WESTERN SNSM				
Facies assemblage	**Code***	**Description**	**Inferred depositional process**	**Interpreted environment**
A-IVc	**Fm**	Massive mud- to siltstone layer with sand dikes	Overbank deposit	Gravelly to sandy braid-plain constituting the topset of a Gilbert-type delta
A-IVb	**Sm-t**	Medium- to coarse-grained sandstone, filling scours or forming planar beds; scoured surfaces are draped by pebbly lag.	Isolated channel fill or crevasse splay on flood plain	
A-IVa	**Gh-t**	Pebble-cobble conglomerate in lenses, 0.8m to 3m thick. Components are well-sorted, rounded and sand- to clast-supported. Beds tend to be normally graded , display a scoured base (Gt) or are interdigitized with sandstone (Gh). Cobbles display an *a(t)b(i)* imbrication.	Channelized hyperconcentrated mass flow	
A-IIIb	**Gmt**	Pebble-cobble conglomerate in lenses with an erosional base, uniformly dispersed rounded components or angular fragments, sand-supported.	Channel-fill of a cohesive (?) debris-slide associated to an erosional scar (Postma, 1984; Nemec 1990)	Slide-scar in the foreset domai of a Gilbert-type delta
A-IIIa	**Sh-m**	Laminated medium-grained sandstone grading upwards into massive coarse-grained sandstone with interspersed pebbles and cobbles.	River-generated hyperpycnal flow descending from a delta brink, *or:* grain flow associated to the turbulent layer of a descending laminar inertia-flow of a debris avalanche (Postma et al., 1988)	Foreset domain of a Gilbert-typ delta
A-IIb	**Gmb**	Lenses, pockets or horizons of outsized boulders with diameters up to 2m, gravel-supported, composed of granite.	Boulders derived from a delta brink zone or from canyon walls of an incised valley by debris-fall avalanches	Boulder accumulation in the fo to bottomset domain of a Gilbe type delta
A-IIa	**Gms**	Pebble-cobble conglomerate in tabular beds, 0.8m to 1.5m thick. Clasts are subangular to rounded, sand- to gravel-supported, poorly to regularly sorted. Beds display a coarse-tail inverse grading in their lower part. Cobbles are oriented parallel to bedding or imbricated, exhibiting an *a(p)* or *a(p)a(i)* fabric.	Cohesionless debris flow with sheared basal part. Inverse coarse-tail grading due to the forced upward movement of larger clasts (Lowe, 1982).	Foreset of a Gilbert-type delta
A-Ia	**Fsm**	Laminated mud- and siltstone with calcareous lenses; contain shells and shell fragments of molluscs shells and gasteropods. Associated with lenses of monomict breccia conglomerates and outsized granite boulders (facies IIb).	Suspension fall-out of turbidity flow *or* of an homopycnal river outflow (Colella, 1987)	Toe- to bottomset of a Gilbert-type delta

*Facies code modified from (Miall,1978)

5.1.2 Palomino Conglomerates

This conglomeratic to sandy sequence forms an isolated strip to the south of the Oca fault. In an internal or southern position it involves facies associations that comprise hyperconcentrated mass flows of a braid plain that grade, northwards, into sandy sequences associated to flood plain and siliciclastic shoreface deposits. It overlies the Muchachitos Gneiss of the Sevilla Metamorphic Belt (Tschanz et al., 1974), a quartz monzonite of a probable Jurassic age, which has been mapped as the Palomino Stock (Tschanz et al., 1974) and a Late Jurassic volcanic suite. Further toward the hinterland, the basement exposes the Precambrian Mangos Granulite and igneous to volcanic suites of the Sierra Nevada Province constitute the present exposure level (Tschanz et al., 1974).

We discuss this sequence by means of a southern conglomeratic and a northern sandy section, each one resting unconformably on the Jurassic igneous or Late Paleozoic metamorphic basement of the Sevilla Metamorphic Belt (Palomino stock and Muchachitos Gneiss; Fig. 4). Their comparable structural position above a pre-Cretaceous basement suggests that their particular facies associations belong to an equivalent systems tract, which comprise three laterally equivalent sequences and are associated to (1) a gravelly braidplain, (2) a sandy floodplain and (3) a shoreface environment. These sequences are mapped as facies belts (figure 4), according to the predominance of conglomeratic, sandy and sandy to muddy alternations.

We label facies according to the classification of Miall (1978c, complemented by Miall 2006), combining some gravelly and sandy facies of similar bedforms into one category for simplification.

Sequence 1 is composed of pebble-cobble conglomerates and includes subordinately intercalations of sandy and muddy beds (Table 3). Pebble-cobble conglomerates form units up to 4 m thick (facies *P-Ia*, Table 3). They display a sand- to gravel-supported fabric with an ill to moderately sorted clast assemblage. Scoured bases and internal reactivation surfaces may be draped by cobbles and outsized boulders (Fig. 5-e). Discontinuous sand lenses subdivide conglomeratic beds into individual flow units. Major bedforms with erosive bases grade upwards into pebbly sandstones, which display trough-shaped laminations of channel fills (Fig. 5-e). Toward the internal part of this braidplain belt (or sequence 1) channel-shaped bedforms comprise stacked units. At the transition to the sandy facies belt (or sequence 2), isolated conglomeratic lenses increasingly interfinger with sandstones and form thin intercalations within sandy beds.

Facies *P-Ib* consists of gravel- to sand-supported, well-sorted and rounded pebble-cobble conglomerates, with oriented pebbles displaying an *a(t)b(i)* imbrication. These m-sized units are subdivided by thin sandstone beds with sharp contacts.

Facies *P-Ic* is made up of pebbly sandstones and pebble conglomerates with angular components arranged in foresets that abut against underlying beds at a sharp, non-tangential contact.

In sequence 2 conglomerates are still present, though subordinate. Facies *P-IIa* consists of ill- to well-sorted and angular to rounded pebble-cobble conglomerates, with a sand-supported texture. Bedforms are tabular and display a scoured base. In pebbly stringers and thin beds granule and pebble-sized clasts are disorganized. Facies *P-IIb* contains laminar coarse-grained sandstones, overlain by massive sandstone. Facies *P-IIc* consists of massive sandstones making up channel fills. Facies *P-IId* is represented

by normally graded silt- to mudstone beds, the latter displaying a bluish-grey tone and evolving from the silty substrate by a normal gradation.

Sequence 3 is composed of sandy units up to 4 m thick embedded within massive bluish-grey mudstones of variable thickness (facies *P-IIIa* and *P-IIIb*). Basal contacts of the sandy units are sharp and planar or shaped by open scours. Fluidization is evident by flame structures that, in an advanced stage, may disrupt even thick beds. Internally, sandstone units display amalgamated sets of cross-stratification with bi- or multi-directional flow directions. Interwoven laminae between coarse- and medium-grained cross-sets argue for aggradation under bi-polar currents. Muddy beds, on their turn, are massive and devoid of fossil remnants and trace fossils. By their gently inclined laminae and bi- (or multi- polar) cross-sets the low-angle cross stratification of sandy units bears a resemblance to a hummocky cross stratification (HCS). Where basal laminae abut against underlying mudstone, these bedforms may derive from migrating dunes.

Interpretation

Conglomeratic channel and sandy flood plain are the principal components of the *gravelly braidplain facies association* of sequence 1. Stacked channels are aligned in a southern continuation of an embayment delineated by the facies belts of sequences 2 and 3 (Fig. 4) that may designate the axis of a fluvial trunk system. Within this environment, bedforms of facies *P-Ib* are interpreted as longitudinal bars and those of facies *P-Ic* as straight-crested dunes, considering a deposition of relatively well-sorted gravel by avalanching along foresets. Occasionally, conglomeratic beds associated to

longitudinal bars and transverse bedforms overly dark muddy layers, which we group into the sandy flood plain facies *P-IId*. By their dark color and their lack of pedogenetic features, these muddy layers may indicate a subaqueous depositional environment.

In the *sandy flood plain facies association* of sequence 2 matrix-rich conglomerates of facies *P-IIa* are interpreted as cohesionless debris flows, on account of their high and variable proportion of sandy matrix and their strongly disorganized pebbles, whose occasional unstable position may indicate a cohesive, in-situ freezing of a mass flow (Lowe, 1982; Rasmussen, 2000). The laminar sandstones of facies *P-IIb* may record flashes of minor sheet floods. The bluish-grey color of the tabular mudstones of facies *P-IId* suggests again a subaqueous sedimentation by suspension fall-out. This interpretation is corroborated by their lateral transition into mottled sand- to siltstones, which overly the Palomino Pluton at the eastern margin of the mapped sandplain belt (AP-46, Fig. 4). These reddish sand- and silt-stones include pedogenic structures, like mudcracks, coated nodules and carbonized rootlets, advocating a subaerial exposure.

Coarse-grained sandstones with HCS and large-scale wave ripples or dunes characterize the *shoreface facies association* of sequence 3. Gradual changes between these structures have been attributed to textural changes from fine- to coarse-grained sandstones (Bourgeois & Leithold, 1984; Leckie, 1988) and characterize oscillating to unidirectional flow conditions of a lower shoreface (Leckie, 1988; Duke et al., 1991). The lack of fossil remains points to a high-energy, near-shore environment (Bourgeois & Leithold, 1984). In this facies belt well-sorted conglomerates with a shape-preferred selection diagnostic of a beachface facies (Bluck, 2010) are absent, a circumstance that could be attributed to a low preservation potential of this type of deposit in a wave- to

storm-dominated siliciclastic coast (Bourgeois & Leithold, 1984). The key features of these depositional environments should be based on a low-gradient braidplain to coastal setting dominated by basinal storm- and wave-driven processes. If our interpretation of an embayment of the coastline at a major river trunk is correct, we should discard the existence of a delta and refer to this coastal configuration as a small-scaled estuary of a transgressive setting (Dalrymple & Choi, 2007). A transgressive frame is indicated, further, by the superposition of sandplain over braidplain and shoreface over sandplain facies associations, as documented by the two logs presented in figure 4.

TABLE 3. SUMMARY OF FACIES AND FACIES ASSEMBLAGES FOR THE PALOMINO BASIN

PALOMINO BASIN - NORTHERN SNSM

Facies assemblage	Code*	Description	Inferred depositional process	Interpreted environment
P-IIIb	**Fm**	Massive mudstone layers	Suspension sedimentation	Middle to lower shoreface, below fair-weather wave base
P-IIIa	**St/Sp**	Well-sorted coarse sand, grouped into low-angle sets of trough or planar cross stratfication constituting units 1 m to 4 m thick. Major bedforms and the base of the units are erosive and contain pebbly lags. Foresets indicate bi- or multidirectional currents. Sand units affected by fluidization.	Wave-worked tractional transportation of sand at middle to lower shoreface conditions and migration of predominantly sinuous bedforms or formation of rip channels	
P-IId	**Fm**	Massive silt- to mudstone in tabular beds	Suspension sedimentation	Sandy flood plains with channels representing cut-and-fill events and
P-IIc	**Sm**	Medium- to coarse-grained sand in isolated channel fills	Sands emplaced by cut-and-fill processes during flood	
P-IIb	**Sh, Sm**	Coarse laminar sandstone, grading into massive	Flashy overbank floods	
P-IIa	**Gh, Gm**	Pebble conglomerate in tabular beds with scoured bases or thin non-erosive conglomerate layers, clast or sand-supported, grading into pebbly sandstone. Disk-shaped clasts tend to be oriented parallel or at high angles to bedding.	Hyperconcentrated gravel or cohesionless debris flow emplaced on flood plain. Clasts oriented at a high angle to bedding attest to rapid frictional freezing.	
P-Ic	**Gp, Sp**	Pebbly sandstone with moderately inclined foresets (<30^{o}) that form sharp angles with an unscoured base. Foreset laminae are graded.	Straight-crested dunes, associated to transverse bedforms	Gravelly channel fills of a sub-aqueous(?) braidplain. - Major units may be composed of stacked channel units along a structural depression or less confined flow conduits, that interfinger with a sandy flood plain of facies association II.
P-Ib	**Gh, Sm**	Pebble-cobble conglomerates in tabular, ungraded units, with rounded, relatively well-sorted clasts, which are sand- to gravel-supported. Disk-shaped clasts are oriented parallel to bedding or display, where closely packed, an a(t)b(i) imbrication. Beds have an unscoured base and are overlain by sandstone with sharp contacts.	Longitudinal bar of braided stream formed by bedload transport	
P-Ia	**Gh-t, Sm-t**	Pebble-cobble conglomerates with rounded, relatively well-sorted clasts, sand- to gravel-supported, forming lenses and channel fills 0.8 m to 4 m thick. Their scoured base may be draped with outsized clasts. Units are stacked or form individual channel fills. Minor channels fills are ungraded, major channel fills fine upward, grading into gravelly sandstone. Isolated conglomerate lenses interfinger with sandstone. Closely packed cobbles display an a(t)b(i) fabric.	Channelized hyperconcentrated gravel flows defining stacked patterns or relatively isolated shallow channels, when alternating with sandy beds.	

*Facies code modified from Miall (1978c, 2006)

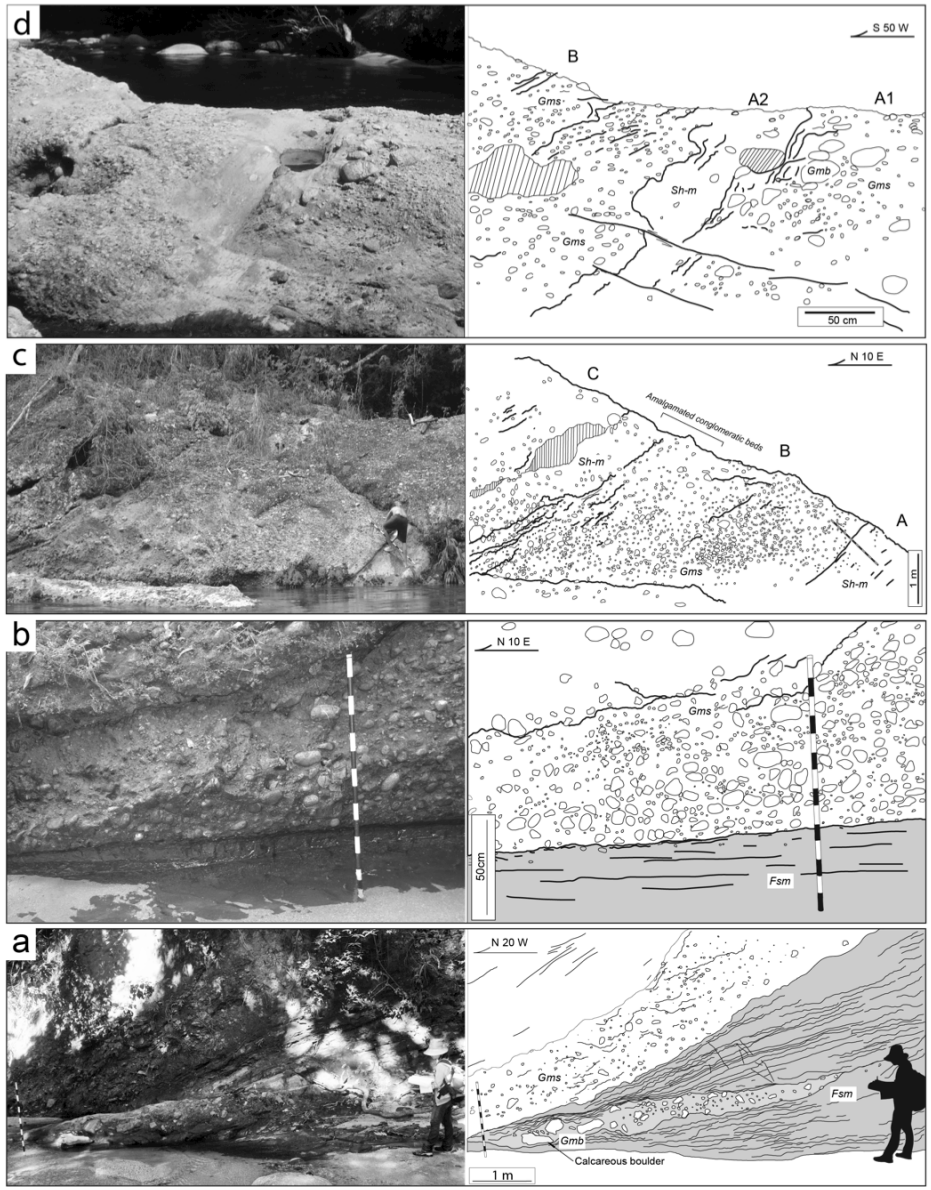
d
S 50 W
B
A2
A1
Gms
Gmb
Sh-m
Gms
Gms
50 cm
c
N 10 E
C
Amalgamated conglomeratic beds
B
Sh-m
A
Gms
Sh-m
1 m
b
N 10 E
Gms
50cm
Fsm
a
N 20 W
Gms
Fsm
Gmb
Calcareous boulder
1 m

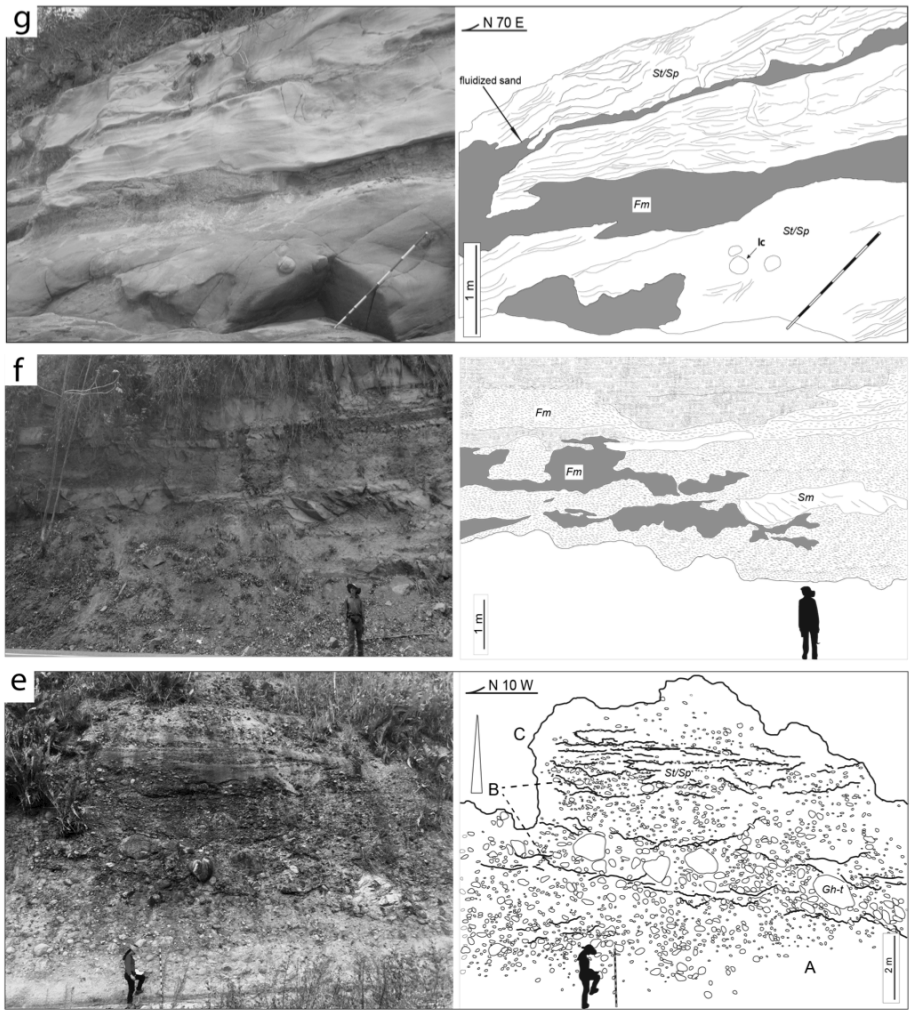
g
N 70 E
fluidized sand
St/Sp
Fm
St/Sp
Ic
1 m
f
Fm
Fm
Sm
1 m
e
N 10 W
C
B
St/Sp
Gh-f
A
2 m

Figure 5.
Left:
Figures from the Aracataca section (facies refer to Table 2.):
a) Facies *A-Ia* and *A-IIb*, bottomset of a Gilbert-type delta: Lens of debris flow embedded within mud-and siltstone. Boulders are concentrated at the head of this mound-like accumulation (termination to the left) and consist of granite and micritic limestone. The boulders are variously tilted with respect to bedding and, according to the muddy matrix, point to a cohesive flow rheology. For scale, refer to the Jacob staff with dm-scaled divisions.
b) Facies *A-IIa*, lower foreset of a Gilbert-like delta: Polymict pebble-cobble conglomerate with sub-rounded clasts, displaying a tendency of a coarse-tail inverse grading at its base and a normal grading in its upper half. Contact to underlying mudstone is planar. Imbricated and closely packed cobbles may display an *a(p)a(i)* fabric (basal domain to the right of the Jacob staff). Flow direction is to the right.
c) Facies *A-IIa*, lower to upper foreset of a Gilbert-like delta: Three amalgamated conglomerate beds may be differentiated by textural criteria, such as clast size and orientation that vary from disordered to bed-parallel and may be imbricated. Despite of patchy clast-size variations parallel to bedding, units A to C display some contrasting trends of an internal organization: unit B sets in with a sand-supported pebble conglomerate and grades into a coarser, clast-supported cobble-pebble conglomerate. Pebbly sandstones form a top-most division and are loosely stratified, attesting to frictional aggradation. A similar stratified pebbly sandstone forms the top of unit A. The cobble conglomerate of unit C sets in with boulder-sized clasts and displays a highly disordered fabric. The scale is given by the Jacob staff (1.4 m). Label units A, B, C; indicate tendency for normal/reverse grading; flow direction.
d) Facies *A-IIa* and *A-IIIa*, upper foreset of a Gilbert-like delta: A thick unit of pebble-cobble conglomeratic (unit A1) is capped by a pebbly sandstone (unit A2) (center of figure). Outsized angular granite cobbles and boulders drape or are closely aligned to this lithological boundary. In the central upper part, this interface steps up to a stratigraphically higher horizon and marks the termination of a row of imbricated boulders (center-right of figure). Flow direction is to the left.
Right:
Figures from the Río Negro section (facies refer to Table 3.):
e) Facies *P-Ia* and *P-IIIa*, channel fill of braidplain: A crudely stratified conglomeratic unit A is cut by a densely packed unit B that, on its turn, grades into a stratified pebbly sandstone (unit C). Units B and C are interpreted to define a channel fill. Outsized boulders mark the erosive base of unit A.
f) Facies *P-IIc* and *P-IId*, sandy floodplain: Scoured sandy beds alternate with tabular strata of siltstone and gray mudstone. To the right-hand side of the center, a sandstone forms asymmetric channel fills within a muddy substrate.
g) Facies *P-IIIa* and *P-IIIb*, middle to lower shoreface: Sandy cross-stratified units alternate with thin beds of gray mudstone. The coarse- to medium-sized sandstone displays low-angle, tangential foresets, which may abut against underlying muddy beds. Foresets indicate bi- or multidirectional currents. Sandy units are strongly distorted and partially homogenized by fluidization.

5.2 Clast Counting

Thirteen clast counts were performed in Rio Aracataca and Rio Negro sections, at the western and northern foothills of the SNSM respectively; results are summarized in Figures 3, 4 & 6 and location of clast counts in Table 4. The conglomerates are mainly matrix to clast supported, with clast sizes ranging from granules to boulders. Many of the pebbles are sub-rounded, and clast variety increases up-section in both of the basins with twelve different litho-types identified.

Plutonic clasts: From granites through sienogranites and granodiorites, with high contents of plagioclase, quartz, biotite, and hornblende and alkaline feldspar is present in a lower proportion. Granodiorites are in fact the most abundant population of clasts in both basins, being at 100% of clast counts at the base of the sequence of the Rio Aracataca section where this litho-type decreases topwards to a proportion between 30%-50%. In the Rio Negro section, granites and sienogranites are present at 20%-50% of the counts throughout the whole section.

Volcanic clasts: Are the second major component represented by a suite of multi-coloured basalts (red, green, black) and spilites that vary widely in texture (aphanitic, porphyritic, amigdular). In the Rio Negro section, the presence of andesites and rhyolites is common; in the Rio Aracataca, basalts are dominant over more acid volcanic rocks. Volcanic clasts constitute between 20%-40% of the composition, and its contribution increases to the top in both basins.

TABLE 4. SUMMARY OF CLAST COUNT ANALYSIS, AND LOCATIONS

Clast/station	EP-02	EP-06	EP-08	EP-17	CP-085	EP-37	EP-41	AP-46	EMP-43	EMP-47	EMP-50	EMP-51	EMP-26
Lat (ºN)	10º35'06"	10º35'14"	10º35'15"	10º35'21"	10º35'19"	10º35'20"	10º35'18"	11º13'07"	11º11'58"	11º12'14"	11º12'39"	11º12'41"	11º15'44"
Long (ºW)	74º03'16"	74º03'18"	74º03'21"	74º03'47"	74º04'28"	74º04'53"	74º05'06"	73º28'41"	73º30'02"	73º30'08"	73º30'16"	73º30'17"	73º35'25"
Granite	118	119	70	13	45	83	21	N.D.	21	46	42	60	16
Rhyolite	N.D.	N.D.	N.D.	N.D.	N.D.	N.D.	N.D.	N.D.	17	19	4	6	N.D.
Andesite	N.D.	N.D.	N.D.	N.D.	N.D.	N.D.	N.D.	N.D.	10	3	5	N.D.	7
Red Basalt	31	N.D.	1	9	5	26	14	1	2	1	N.D.	N.D.	8
Green Basalt	N.D.	N.D.	N.D.	16	8	32	42	N.D.	2	8	3	5	N.D.
Black Basalt	51	N.D.	2	22	20	23	27	6	4	9	4	6	24
Gabbro	N.D.	N.D.	N.D.	2	N.D.	2	5	N.D.	1	1	3	3	N.D.
Volcanic Breccia	N.D.	N.D.	N.D.	N.D.	N.D.	N.D.	N.D.	N.D.	N.D.	2	N.D.	8	N.D.
Gneiss	N.D.	N.D.	N.D.	5	13	N.D.	13	122	N.D.	2	13	5	7
Quartzite	N.D.	N.D.	N.D.	10	N.D.	N.D.	10	N.D.	1	N.D.	1	N.D.	N.D.
Sandstones	N.D.	N.D.	N.D.	1	N.D.	N.D.	2	N.D.	N.D.	N.D.	N.D.	3	N.D.
Mudstones	N.D.	N.D.	N.D.	N.D.	N.D.	N.D.	N.D.	N.D.	N.D.	N.D.	N.D.	1	2

Metamorphic clasts: Are characterized by amphibolite gneisses, leucocratic gneisses bearing blue quartz, anorthosites, granulites, and a minor contribution of quartzites. In the Rio Aracataca section, these litho-types appear after sequence I (Fig. 3) and account for up to 30% of the clasts. In contrast in the Rio Negro section the base of the sequence consists of oligomictic conglomerates from facies *P-Ia* with leucocratic gneisses as the main component (90%), decreasing to the top to 20% and quartzites (5%).

Sedimentary clasts: Mainly reworked sandstones and rare mudstones. Carbonate clasts are common in sequence I at the Aracataca River, facies *Fsm* from facies assemblage Ia and often contain macrofossils. The presence of 1%-4% of sedimentary clasts coincides with the occurrence of metamorphic clasts.

Ultramafic clasts: These clasts appear at the same locations as the metamorphic and sedimentary clasts. This litho-type (3%-5%) is

represented mainly by dark green gabbros and volcanic breccias, which locally may represent up to 10% of the counts.

5.3 Heavy Mineral Analysis

The heavy mineral spectra found in the SNSM Neogene sedimentary rocks includes garnet, chlorite, amphibole, pyroxene, rutile, muscovite, biotite, andalusite, sphene, tourmaline, epidote, and opaque minerals such as ilmenite and pyrite (Table. 5). The Aracataca conglomerates samples CVI1302, CVI13115 contain rutile, pyroxenes, and garnet. Green augite-aegirine clinopyroxenes are present in all samples. Amphiboles are present in the form of green and brown hornblende. Garnet is also present, but is much more abundant in the Palomino basin in samples AP-45 and AP-46, whereas in the Aracataca basin garnet occurs as a minor component. Sphene and rutile are found in both basins and rutile content is observed to increase in samples towards the top of the Rio Aracataca section.

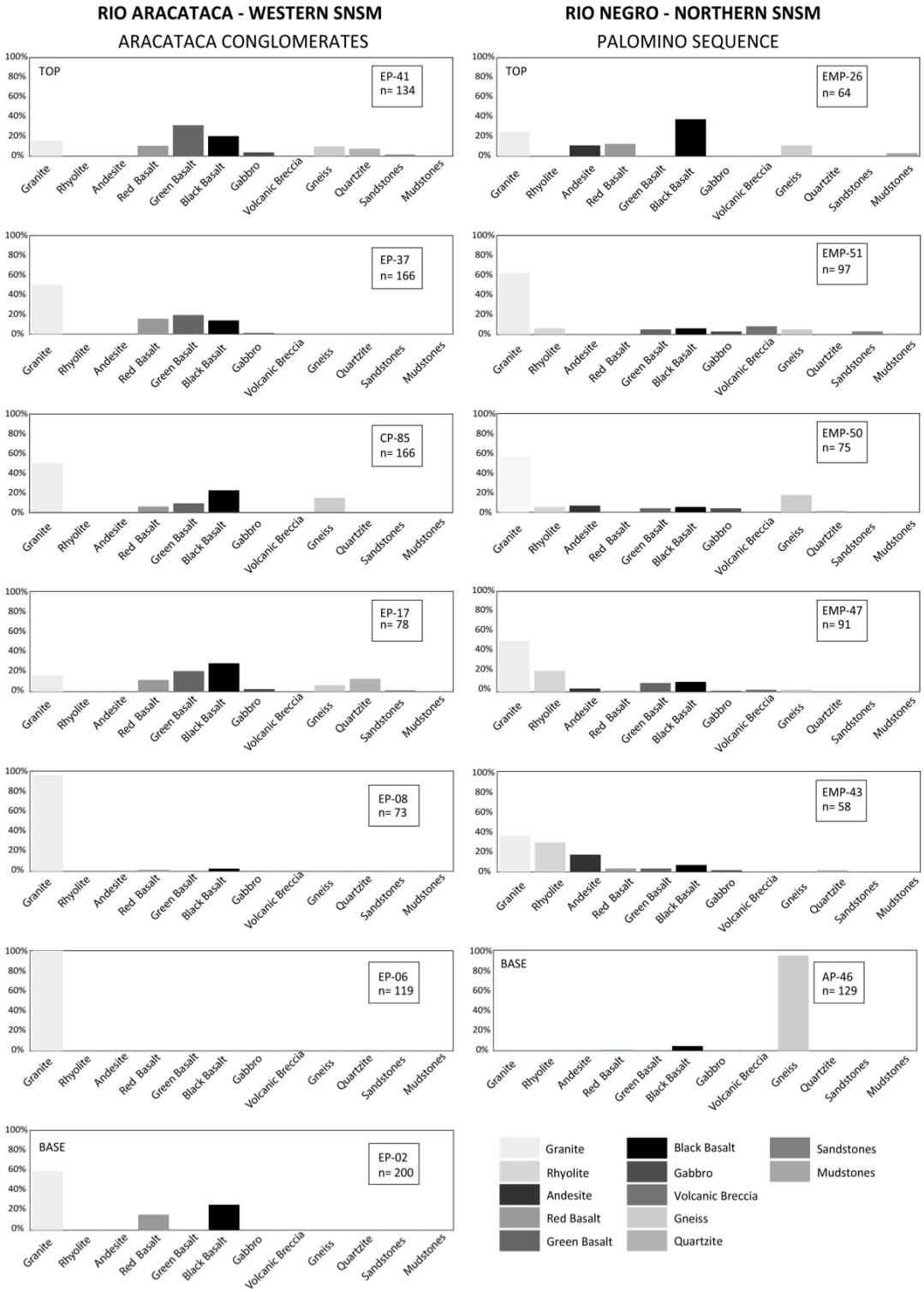

Figure 6. Clast counts from The SNSM Cenozoic Aracataca and Palomino basins at the Negro and Aracataca rivers, respectively, counts were done following the ribbon method (Howard, 1993).

TABLE 5. LOCATION, DESCRIPTION, DIAGNOSTIC MINERALS, ZIRCON MORPHOLOGY, AND AGES OF SAMPLES ANALYZED BY U-Pb LA-ICP-MS

Sample Code	Coordinates Lat (ºN)	Long (ºW)	Description	Diagnostic Minerals*	Zircon Morphology and CL Zoning	Age Core	Age Rim
				Post-Oligocene Sediments			
CVI1302	10º35'18"	74º05'06"	Coarse grained sandstone matrix, of medium pebble polimictic conglomerates with abundant clasts of igneous and metamorphic rocks, rounded to subrounded	Zr, Rt, Ap, Chl, Aeg, Hbn, Bio, Plag	Angular to subangular, subhedral and tabular prismatic, purple brown translucent, irregular edges, with inclusions, showing xenocrystic cores in metamorphic grains and rim growth by recrystallization,	803 -1434 Ma	889-1295 Ma
CVI13115	10º35'15"	74º04'30"	Silica cemented grey conglomeratic sandstone, well sorted, subrounded grains	Rt, Zr, Hbn, Chl, Str, Aeg, Gr,	Angular to subangular, subhedral and tabular prismatic and xenomorphic, purple brown translucent, irregular edges, with inclusions, showing xenocrystic cores in metamorphic grains and rim growth by recrystallization; magmatic grains are translucent, euhedral and tabular prismatic, with regular zonning and convolute zoning	986-1182 Ma 116.5-135.6 Ma	881 -1324 Ma 126.1-193.3 Ma
EMP-16	10º32'21"	74º03'50"	Conglomeratic sandstone	Zr, Gr, Ep, Ap, Str, Aeg, Hbn	Subangular to subrounded, subhedral and tabular prismatic and xenomorphic, purple brown translucent, irregular edges, with inclusions, showing xenocrystic cores in metamorphic grains and rim growth by recrystallization; magmatic grains are translucent, euhedral and tabular prismatic, with regular zonning and convolute zoning	944-1507 Ma 592 Ma 179.5-205.8 Ma	955-1365 Ma 181.5-185.5 Ma
CP088	10º31'33"	74º03'13"	White conglomeratic quartzsandstones, angular-subangular, regular sorted with lithics, very friable highly porous, probably from fluvial coastal deposits	Zr, Rt, Chl, Aeg, Hbn, Bio	mainly subrounded and some subangular, subhedral prismatic, purple and brownish, translucent, irregular edges, with inclusions, showing xenocrystic cores in metamorphic grains and rim growth by recrystallization, magmatic grains present are translucent, euhedral and tabular prismatic and showed no recrystallization	997-1359 Ma 132.7-189.5 Ma	904-1398 Ma 127.9-197.6 Ma
AP-045	11º13'12"	73º28'39"	medium to coarse grained sandstone matrix from a coarse pebble polimictic conglomerate, with abundant gneissic and granitic clasts and also a minor maphic fraction	Zr, Gr, Hbn, Chl, Ap, Aeg, , Ep, Str, Rt	Rounded to subangular, subhedral fewer prismatic, purple, translucent and yellowish, seldom inclusions, some grains exibith xenocrystic cores and rim growht by recrystallization, magmatic grains are translucent and more prismatic, euhedral with oscillatory zoning	897-1300 Ma 189.2 - 258.6 Ma	888 - 1241 Ma 191.2 -265.8 Ma
EMP-49A	11º12'33"	73º30'17"	Sub-lithic green coarse sandstone	Gr, Chl, Hbn, Str, Aeg,	Subangular to subrounded, subhedral and tabular prismatic and xenomorphic, purple brown translucent, irregular edges, with inclusions, showing xenocrystic cores in metamorphic grains and rim growth by recrystallization; magmatic grains are translucent, euhedral and tabular prismatic, with regular zonning and convolute zoning	850-1259 Ma 178.2-192.7 Ma	945-1132 Ma 180.2-198.9 Ma

*Mineral abbreviations Aeg = Aegirine, Ap= Apatite, Bio= Biotite, Chl= Chlorite, Gr=Garnet, Hbn= Hornblende, Rt= Rutile, Str= Staurolite, Tre= Tremolite, Zr= Zircon

5.4 Detrital Zircon U-Pb Dating Results of the Conglomerate Matrix

Four samples were collected in the western foothills of the SNSM from outcrops along the Rio Aracataca, and outcrops at the adjacent Río Piedras and the Macaraquilla Creek. The analysed samples are located into the Aracataca stratigraphic section (Fig. 3). Additionally, two more samples were collected from outcrops in the northern foothills of the SNSM in the Negro and Ancho rivers at the Palomino basin that are located in the Rio Negro stratigraphic section (Fig. 4). We collected the sandy matrix of the conglomeratic facies. The detrital samples contain a major amount of euhedral and tabular prismatic magmatic zircons with classical oscillatory zoning patterns. Metamorphic zircons are mostly purple, brownish or translucent, and show more complex growth zoning with local intermediate reabsorption, sector and patchy zoning (Fig. 7). U-Pb ages range from 1450 to 116 Ma, with two main peaks at 1000 Ma and 200 Ma (Fig. 8). The main age population corresponds to the 1000 Ma peak, which is present in all samples, independently of stratigraphic position in the western and northern basins (Fig. 8). The Lower Jurassic to Lower Cretaceous ages between 200 and 116 Ma are the second major population of zircons of the conglomerates. This population significantly decreases up-section and Precambrian ages become dominant. In the Aracataca basin, samples CP088 and CVI13115 are similar, with core ages mainly from 950 to 1360 Ma and a minor population of zircons with Mesozoic (190 to 130 Ma) crystallization ages. One zircon with a discordant Meso-Archean core age of 2970 Ma was also detected.

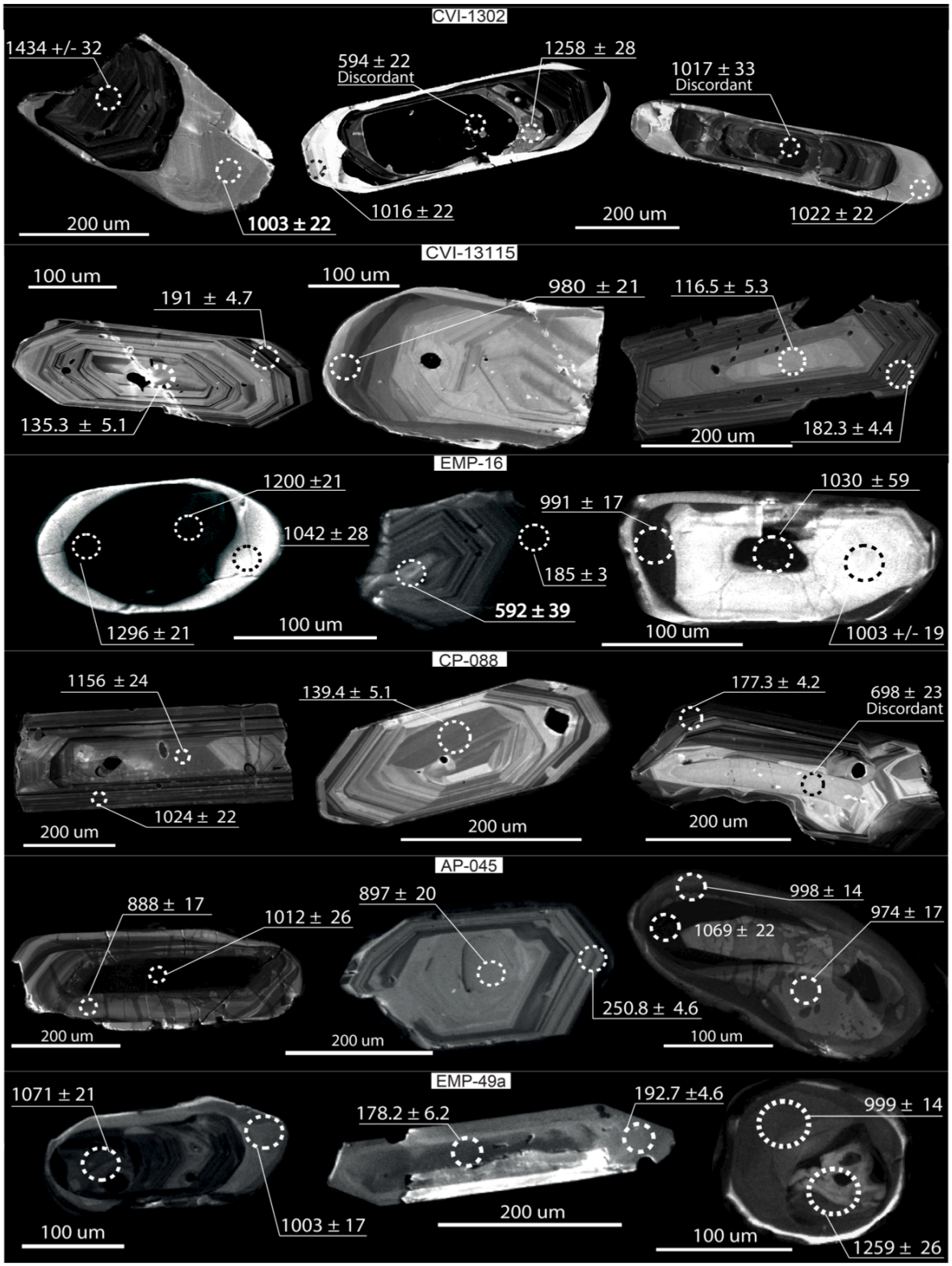

Figure 7. Panchromatic cathodoluminescence imagery of zircons analysed in this study, there are representative crystals for each sample labelled at the top with the name of sample. A high variability of crystals is observed with different age distributions showing two main distinctive populations. Circles correspond to the ablation spot.

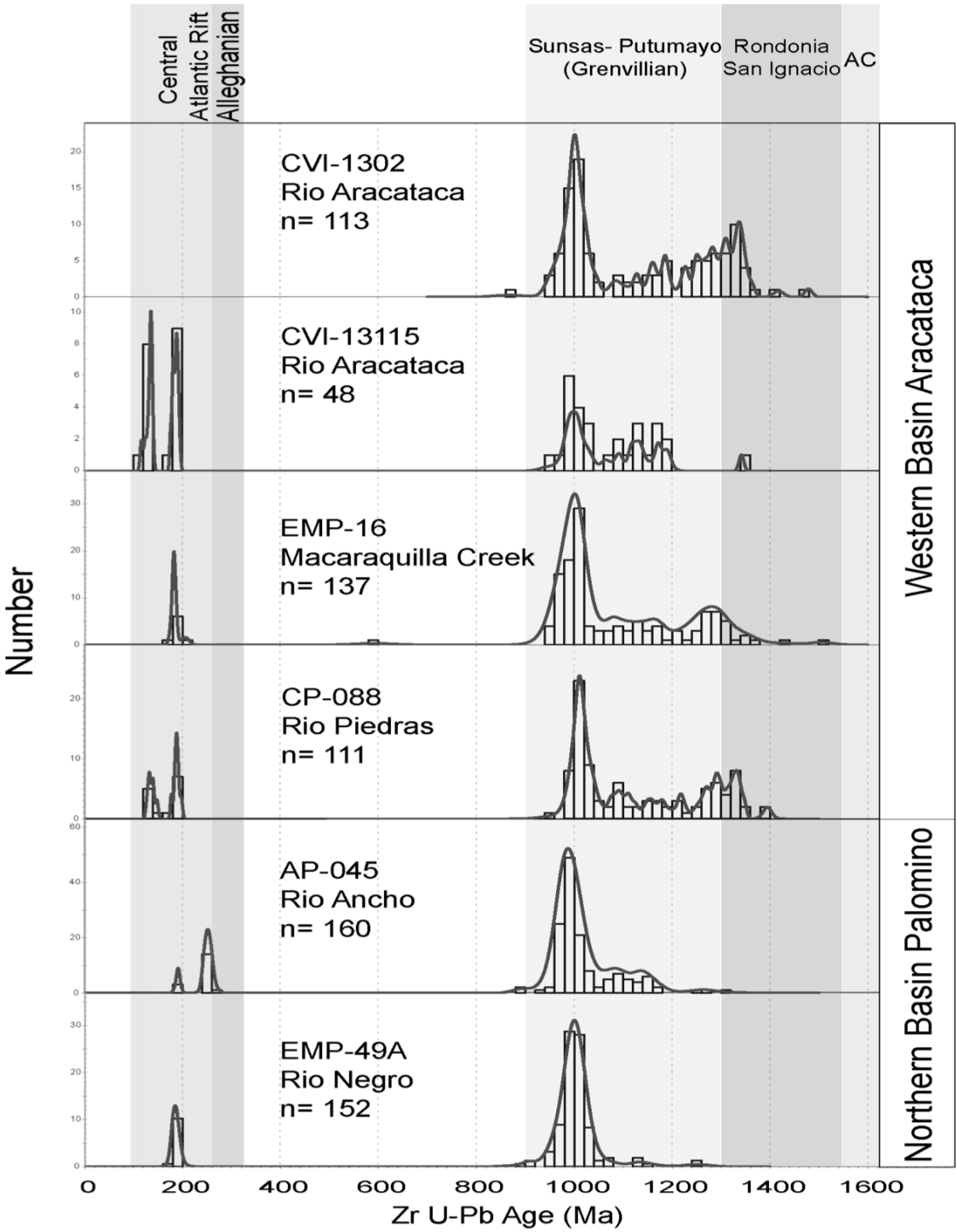

Figure 8. Detrital zircon U-Pb LA-ICP-MS probability density plots obtained from the Post-Eocene sediments of the western and northern foothills of the Sierra Nevada de Santa (Aracataca and Palomino basins), data are organized from base to top for each basin, there is still not a precise stratigraphic correlation between basins due the lack of fauna in the coarser deposits, however zircon populations are intimately related implying the same sources supplied with sediments both basins, with an older signature in the Aracataca basin at the western border of the SNSM massif.

Zircons from sample CVI1302 have ages older than 800 Ma, with peaks at 1100 Ma, 1200 Ma, and 1320 Ma, similar to sample EMP-16. Samples AP-45 and EMP-49a from the northern basin show nearly equal age trends with the most significant 1000 Ma peak in both samples and lesser populations of Jurassic and Triassic peaks in sample AP-45. The only significant difference between age populations from samples of the Aracataca and Palomino basins is the presence of a 1300 Ma age peak in the Aracataca basin (Fig. 8).

5.5 Detrital Fission Track Thermochronology

5.5.1 Zircon fission-track results

Zircon fission-track ages were determined for 751 crystals in eight samples from the western and northern foothills of the SNSM. In the Aracataca basin, samples CVI-1302 and CP-088, show a fixed major peak age of 103 ± 5.5 Ma, sample EMP-16 shows a peak of 107 ± 7.2 Ma; with a secondary age population of 52-74 Ma A minor younger peak at 29-33 Ma is present in samples CVI-1302 and CP-088, but is absent in sample EMP-16, which was collected closer to the base of the stratigraphic section. Sample EMP-16 yields as well an older age component of 158 ± 27 Ma. In the Palomino basin, the fission-track age distributions are characterized by a major moving peak between 94-132 Ma present in all samples that rejuvenates topwards. A second moving peak population ranging from 55-80 Ma is also present (Fig. 9). The pre-orogenic signature is defined by ages between 155-170 Ma, and an older population of 250± 30 Ma peak.

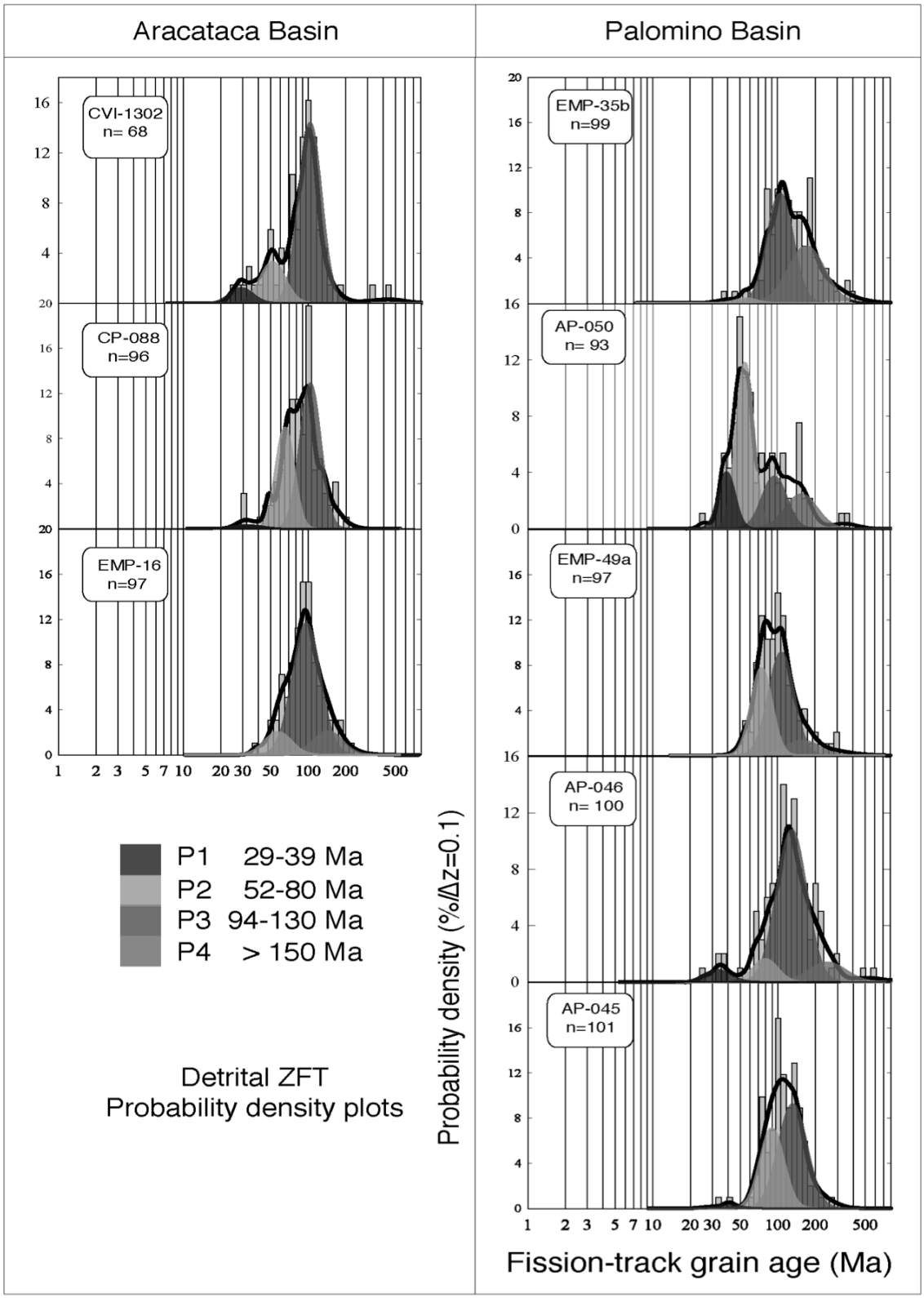

Figure 9. Detrital ZFT data from Aracataca and Palomino basins, probability density plots elaborated with Binomfit (Ehlers et al. 2005; Stewart & Brandon 2004).

The youngest age population was found at samples AP-45, AP-46 and AP-50 and consists of a 33-49 Ma peak. In synthesis, the main age populations for the Aracataca and Palomino basins are defined as an older P4 at 150 Ma, P3 at 94-130 Ma, P2 at 52-80 Ma and P1, the youngest at 29-39 Ma. Probability density plots of all samples are presented in Fig. 9.

5.5.2 Apatite fission-track results

Apatite fission-track ages were obtained for 153 crystals in four samples; CVI1302 and EMP-16 from the Aracataca basin, and form samples AP-45 and EMP-49 from the Palomino basin. In general, other processed samples contained few apatites and in several cases, samples were discarded due to the low quality of crystals, fractures, and inclusions. Three age populations were identified in both basins, and these populations are discriminated as follows with P1 at 19-25 Ma, P2 at 25-35 Ma and P3 at 42-60 Ma. Similarly, to the ZFT peaks, the AFT peaks are becoming younger up-section (Fig. 10).

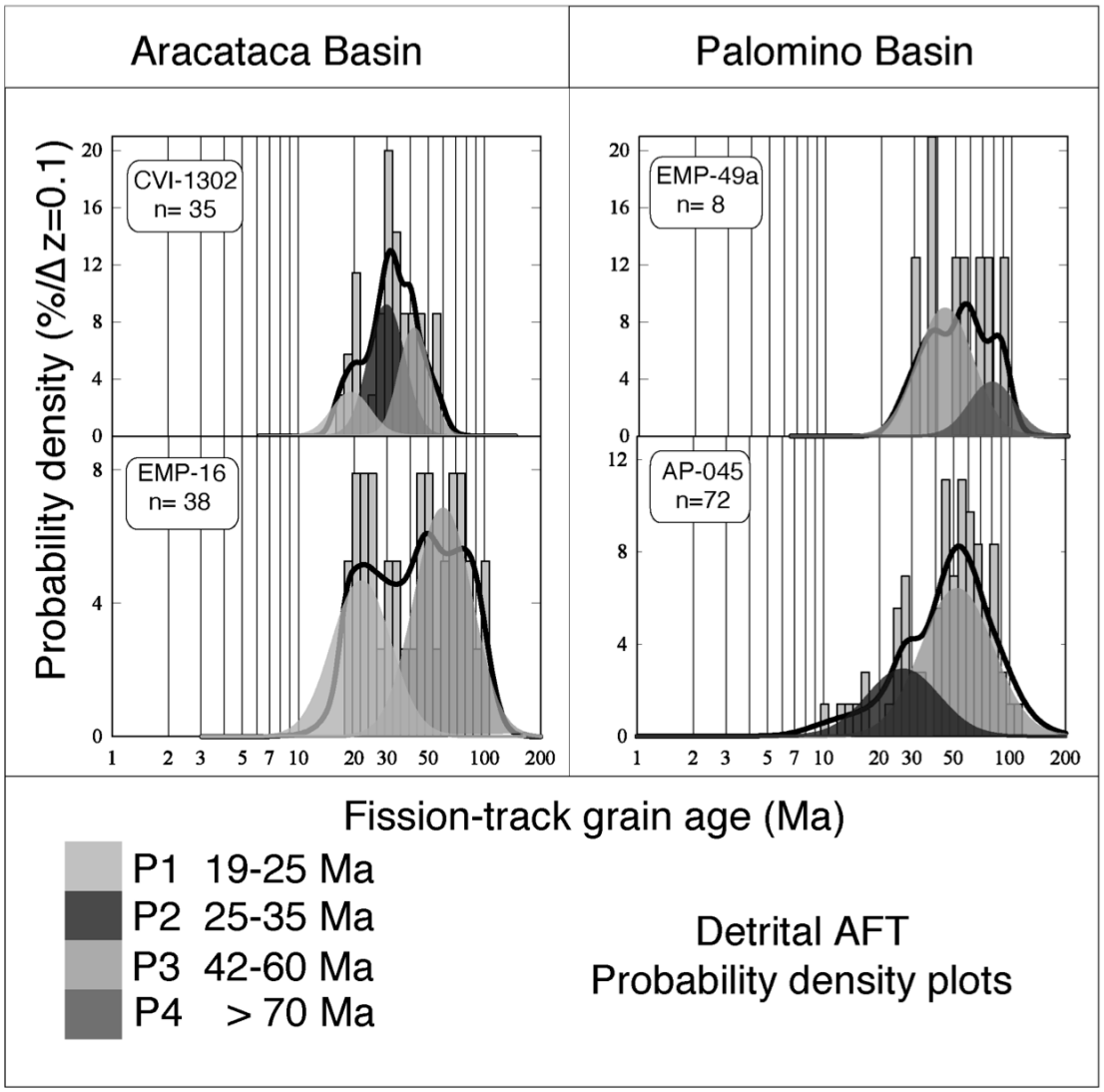

Figure 10. Detrital AFT data from data from Aracataca and Palomino basins, probability density plots elaborated with Binomfit (Ehlers et al. 2005; Stewart & Brandon 2004).

6. DISCUSSION

6.1 Sediment Provenance

There are two main zircon U-Pb age populations in the detrital zircons from the Neogene sedimentary rocks of the Aracataca and Palomino basins. Proterozoic ages

correspond to a widespread population around 850 to 1400 Ma which is found in the SNSM and the Alta Guajira massifs high-grade metamorphic rocks (Weber et al., 2010), which were reworked in Neogene sediments. This population can be related to the Grenvillian belt in the northern Andes (Cardona et al., 2010a; Restrepo-Pace et al., 1997).

Zircon populations from the conglomerates matrix are strictly dominated by the Precambrian U-Pb signal, even if the granitic and volcanic clasts are more abundant. The main sources for the Neogene sediments in the Aracataca and Palomino basins, were the Los Mangos Granulite from the SNP, and the Muchachitos and Buritaca gneisses from the SB, as the detrital zircon U-Pb age spectra are clearly related to the reworking of the Precambrian basement older than ≈ 850 Ma. The main zircon U-Pb age population between 900-1150 Ma, which can be found in all samples, corresponds to inherited Grenvillian zircons (Cordani et al., 2005), from the Sunsas-Putumayo province (Ibanez-Mejia et al., 2011).

The older populations of 1300-1600 Ma point to a source in the Rondonia San Ignacio Province in the Amazon Craton. This composite Proterozoic signature has been detected in the Precambrian inliers of the Northern Andes (Cardona et al., 2010a, 2006; Cordani et al., 2005) as well as in the post-Permian metamorphic rocks of the SNSM, the Alta Guajira, and in Cenozoic sediments of the Leeward Antilles (Cardona et al., 2010c; Weber et al., 2010; Zapata et al., 2014). Jurassic and Cretaceous zircons are related to volcanoclastic deposits and arc granodiorites and sienograntes. These zircons indicate the constant erosion of the Central Batholith of the SNSM as well as the associated Jurassic plutonic and volcanic units. In the top-most samples, the Precambrian ages became the dominant population.

The deposition in a Gilbert-type delta system, which traversed the Santa Marta – Bucaramanga fault in the western basin, developed since the late Oligocene. The bottomset segment with an input of mainly granodiorites is related to the Aracataca Batholith, part of the Central Batholith suite. The foresets shows a mixture of Precambrian and Upper Jurassic to Lower Cretaceous ages.

Zircons found at the Neogene sedimentary rocks of the Aracataca and Palomino basins are subrounded to subangular and the presence of unstable heavy minerals indicates a relatively short sediment transport distance from the source area. Rutile presence is also characteristic of high-grade regionally metamorphosed terrains (Force, 1980), which is supported by the fact that conglomerates are highly immature and contain at least ten different litho-types that include high-grade metamorphic and ultramafic rocks.

The provenance information derived from the zircon fission-track maximum relative ages suggests that the main sedimentary source area was the core of the SNSM massif. ZFT and AFT ages are younger in the Aracataca basin in comparison to the Palomino basin, suggesting that the sediments of the western limb of the SNSM were derived from a more deeply exhumed lower crustal source (Fig. 11).

Provenance on the Aracataca and Palomino basins shows that during the Oligocene - Miocene, sediments were sourced from the SNP, and evidence that the Santa Marta Batholith, and Buritaca pluton, although exhumed during the Miocene did not contributed as a sources for the Oligocene-Miocene sediments, probably due to the development of a drainage system with a NE-SW and N-S trend, controlled by the main structures (i.e. Orihueca fault, Aguja Fault, Sevilla Lineament). This would explain

the Miocene exhumation of the Eocene batholiths and the absence of Paleocene-Eocene zircons in both basins.

The Buritaca Pluton yields an early Miocene AFT age for this unit of 22.3 ± 3.1 Ma (Villagómez et al., 2011), and is cut by N-S drainages, but in the sedimentary rocks of Palomino basin, there is no record of Paleogene zircons, therefore is possible to constrain the deposition of the sediments in this basin maximum the middle Miocene (≈ 16 Ma), with a lag time of 5 Myr constrained from an exhumation rate of 0.8km/Myr (Villagómez et al., 2011) and a surface temperature of 30ºC. Sediments deposited after the unroofing of the Buritaca pluton containing Eocene zircons are probably bypassed offshore in the late Miocene-Pliocene deposits (Vence, 2008).

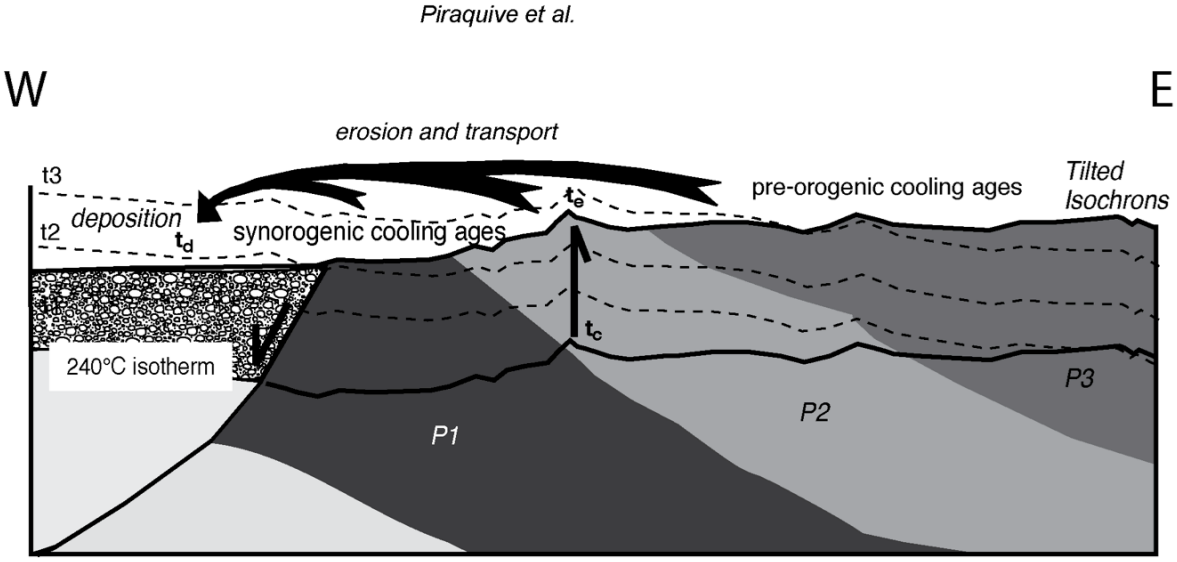

Figure 11. Schematic cross section showing the sources for the ZFT age populations found at the Aracataca Basin, The Santa Marta-Bucaramanga fault activity controls exhumation and isochrone tilting. Modified from (Bernet et al. 2006).

6.2 Regional Stratigraphic Correlations

Lower Miocene sedimentary rocks found either in the Aracataca and the Palomino basins correspond to proximal fan delta systems that developed during the first pulse of surface uplift of the SNSM during the late Oligocene. The clockwise rotation of the SNSM towards the east led to the development of an extensional phase defining the Lower Magdalena basin as a rotational basin linked to the advance of the Caribbean plate (Bayona et al., 2010; Montes et al., 2010). The record of the first tectonic pulse of the Santa Marta-Bucaramanga fault, are the basal deposits of the Aracataca border basin in the proximity of the SNSM massif. At the western edge of the Plato-San Jorge basin, the Romeral suture separated the continental basement of South America from the Caribbean intra-oceanic crust that hosted volcanic arcs and accreted during the Paleocene. The accretion of terranes evolved into I-type plutonism during the Eocene, which gave a characteristically mixed oceanic arc-basement zircon U-Pb age signal in the Paleogene sediments from the San Jacinto belt (Cardona et al., 2012). Towards the SNSM the detrital zircon U-Pb ages became dominated strictly by the continental crust basement signature, with the start of sedimentation in the late Oligocene, sediments in the Aracataca and Palomino basins record a late Oligocene activation of the Santa Marta- Bucaramanga and Oca faults, as the North-Andean block indented against the Caribbean plate. Coarse sediments derived from the SNSM massif, were deposited as growth strata along the active faults. The coarse facies are typical of hyperconcentrate flows, being the product of rapid slope instabilities. During the Miocene, in the Plato-San Jorge basin, the Lower Magdalena basin, and the San Jacinto basin, distal deposits of mudstones, siltstones, and carbonate facies were deposited in a low-energy

environment, coeval with the conglomerates of the Aracataca and Palomino basins (Fig. 12).

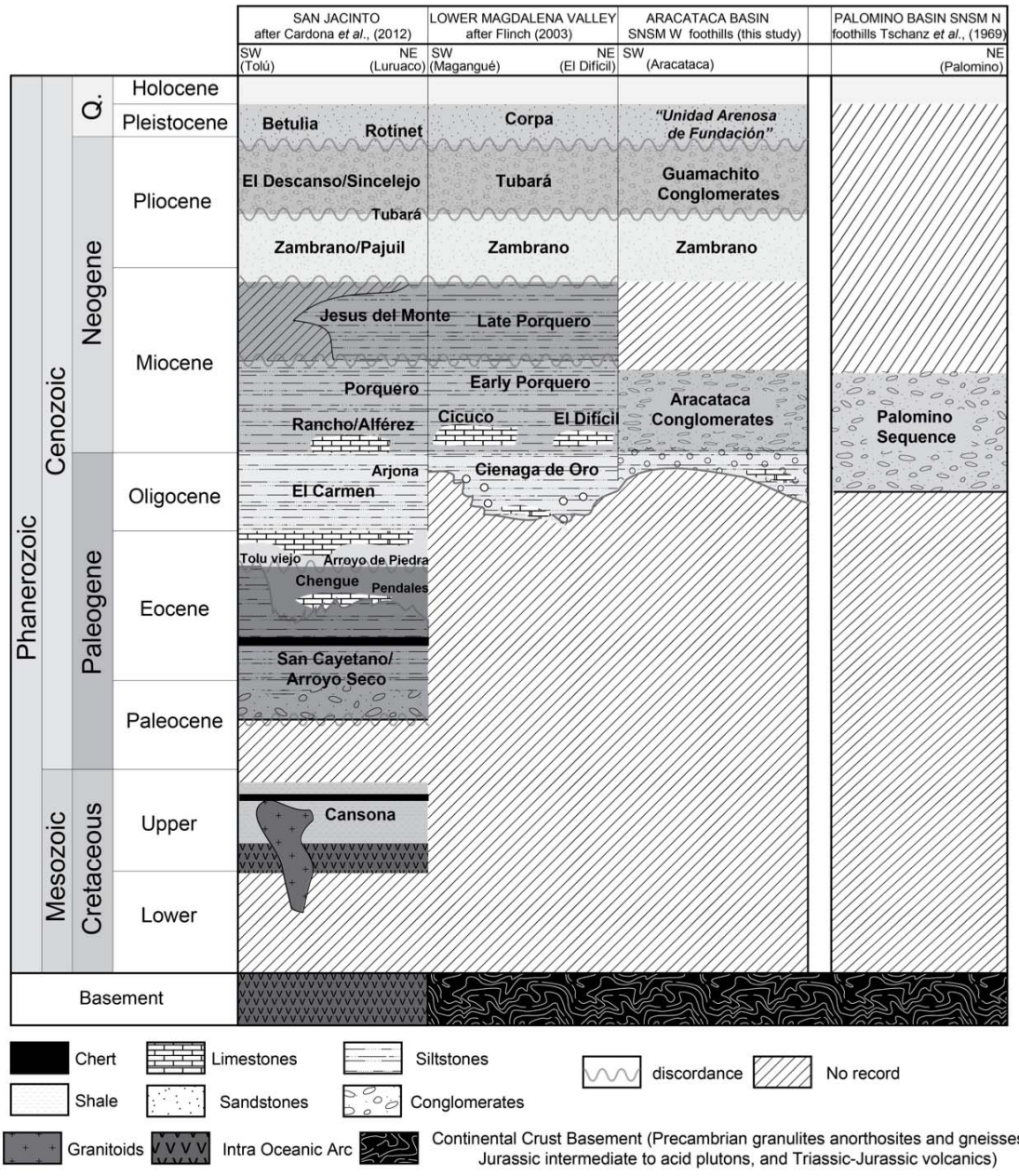

Figure 12. Stratigraphic correlation chart from the Plato-San Jorge basin, the adjacent Lower Magdalena Valley and San Jacinto belt; as well as the Guajira basin in the N foothillls of the SNSM. Modified from (Cardona et al., 2012; Duque-Caro, 1979; Flinch, 2003; Tschanz et al., 1969).

The Santa Marta Batholith, the Palomino Pluton, Sevilla, Latal, and Buritaca Stocks (Fig. 2) share Paleocene-Eocene zircon U-Pb ages and are outcropping closely to both the Aracataca, and Palomino basins. Paleogene zircon U-Pb ages are not found within the Neogene sedimentary rocks of Aracataca and Palomino basins, suggesting that by Oligocene-Miocene times, the Paleogene intrusive rocks were not yet exhumed to the surface, and therefore did not acted as sources. Although, Paleocene deposits of the Cesar-Ranchería basin (Fig. 2) contain a distinctive population of Paleocene zircons (Bayona et al., 2011), we discard a direct supply of these crystals from the plutons in the NW part of the SNSM, given that thermochronological data of Villagómez et al. (2011) and Duque (2009) evidence exhumation of the Eocene Buritaca stock and Santa Marta Batholith plutons during the Miocene. Accordingly, the Palomino conglomerates lack of corresponding quartzdioritic and tonalitic components of this Paleogene intrusive suite. The sediments from the Paleocene Cerrejón and the Eocene Tabaco Formation in the CRB are derived from Precambrian and Permo-Triassic source rocks (290-220 Ma) with a younger Cretaceous-Paleocene zircon U-Pb age signature (90-65Ma), nevertheless they do not necessarily support exhumation of the NW corner of the SNSM during the Paleocene (Bayona et al., 2011; Montes et al., 2005), neither erosion of the plutons of the Paleogene arc in the NW corner of the Massif at the Santa Marta Metamorphic belts (Cardona et al., 2011), instead thermochronological AFT ages record Paleocene-Eocene exhumation at the SE flank of the SNSM in the Sierra Nevada Province, adjacent to the Cesar-Ranchería basin (Villagómez et al., 2011). In consequence, the older exhumation of the SE flank of the SNSM would have created topography that may have acted both as a barrier for sediment derived from the NW part of the SNSM, and as a source for the CRB.

Zircon U-Pb ages from the lower Eocene Misoa Formation, and Cerrejón and Tabaco Formations from the Cesar-Rancehría basin, indeed overlap with zircon U-Pb ages of plutons in the Santa Marta Metamorphic Belts at the NW corner of the massif, but erosion of these source rocks during the Paleocene seems unlikely of the Miocene cooling histories documented for these igneous rocks (Villagómez et al., 2011). In this context the Late Cretaceous-Paleogene zircon U-Pb populations in the Cesar-Ranchería basin (56-70 Ma) are most likely related to a volcanic source found further to the east, as evidenced by tuffs within the Misoa Formation of the Maracaibo basin, coeval with the Eocene Tabaco Formation (Bayona et al., 2011). Paleocurrent directions measured in the Cerrejón Formation show an E to SE trend (Bayona et al., 2011), given that the SNSM has rotated clockwise by about 30º after the Eocene according to Montes et al. (2010), paleocurrent directions result in E to NE flow directions for the Cerrejón Formation, which in turn are coherent with an E-NE sediment dispersal direction during the early-mid Paleocene 65-58 Ma as documented by Ayala et al. (2012). In this epoch the Precambrian, Permian-Triassic and Cretaceous zircons found at the Cerrejón and Tabaco Formations from the Cesar-Ranchería basin may not be exclusively derived from the SNSM and could also be supplied by the rocks of the Proto-Perijá Range that yield as well Permian to Jurassic granitoids (Martin, 1968), and the Central Cordillera (Mora-Bohórquez et al., 2017), regarding that at Paleocene times the SNSM, Perijá ranges and Central Cordillera were exhumed (Ayala et al., 2012; Shagam et al., 1984; Villagómez et al., 2011; Villagómez and Spikings, 2013), with the major exhumation of the Perijá Range during the Oligocene (Shagam et al., 1984). Other sources probably supplied Paleocene zircons to the Cesar-Ranchería basin. Such sources can be related to Paleocene volcanism, and plutons of the Guajira Peninsula (Cardona et al., 2014), the

Central Cordillera and the Eastern Cordillera. Alternatively a plutonic source of Paleocene zircons found at the Cerrejón and Tabaco formations could be related to unmapped and undated Paleocene plutons (i.e. Atánquez Laccolith, Tschanz et al., 1969) located within the Sierra Nevada Province. This alternative would agree with Paleocene-Eocene exhumation of this province and would correlate with the unstable metamorphic minerals found at the Tabaco and Cerrejón formations indicative of short sediment transport (Bayona et al., 2007). Adjacent to the Cesar-Ranchería basin the onset of a NE directed drainage system occurred during the Paleogene incising the newly formed topography and precluding a connection with the drainage systems, in the NW of the SNSM. The interpretation of a disconnected NW-SE drainage of the SNSM is validated by the zircon U-Pb ages found in the Sinú San Jacinto Belt (Fig. 13), in which Precambrian and Permian-Triassic source rocks are dominant along with the youngest arc derived material from the Late Cretaceous, 71.3± 1.3 Ma and 68.7 ± 1.4 Ma (Cardona et al., 2012), without Paleocene-Eocene zircons record in the sediments. Instead of a Paleocene tilting towards the SE which would have generated an inclined topography towards the Cesar-Ranchería basin and an extensive NW-SE drainage system feeding a clastic wedge, the distribution of U-Pb and detrital thermochronologic ages in Oligocene-Miocene sedimentary rocks in the Aracataca and Palomino basins indicates that the SNSM was tilted during Oligocene-Miocene exhumation towards the NE, with an increasing relief in the western limb of the SNSM controlled by the Santa Marta Bucaramanga fault, whose activation was contemporaneous with the dextral Oca fault and the onset of transpressive tectonics.

The Oligocene-Miocene progradational deposits of the Aracataca conglomerates coeval with the transgressive deposits of the Palomino conglomerates during exhumation can

be explained by tilting of a block bounded by normal faults (Leeder and Gawthorpe, 1987). For the NE tilting, we presume a fulcrum that separates elevated from subsided segments of a ramp. In this block, two basins are opposed by a drainage divide correspondent to the uplifted crest of the domino-block (Fig. 13): a fault scarp prefiguring a steep slope (drainage basin of Aracataca conglomerates) and ramp of a gentle inclination (Palomino sub-basin). The latter is not fault-controlled: This mechanism provides a simple kinematic explanation for a contemporaneous uplift and subsidence; only valid for a thick crustal block. This block can be delimitated by the Sevilla Lineament and involves the Sierra Nevada Province.

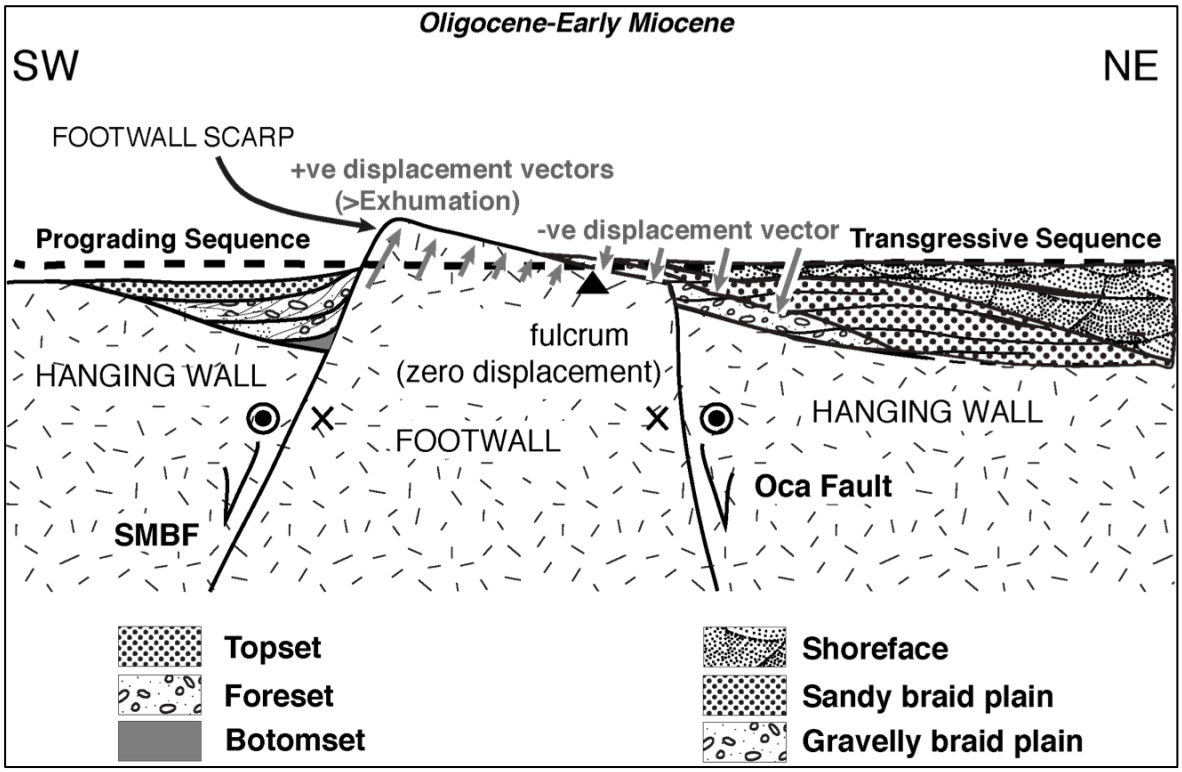

Figure. 13 Conceptual model not to scale, depicting tectonic slopes associated with a simple tilt block/half-graben, involving a fault-bounded syn-extensional clastic wedge, as the case of the Aracataca basin gravel rich fan-delta, at the Santa Marta-Bucaramanga fault, and its counterpart deposited on a gently inclined slope dominated by estuarine deposits of the Palomino basin, modified after (Henstra et al., 2016; Leeder and Gawthorpe, 1987; Ravnås and Steel, 1998).

6.3 Tectonic Implications for the Caribbean Realm

Transition in the Caribbean plate subduction angle from 30º to a shallower dipping subduction between 4º-8º occurred between the late Eocene and middle Miocene (Bernal-Olaya et al., 2015). Since the late Eocene a relevant change in the subduction regime is evidenced by a gradual cessation of arc-plutonism and late cooling, which during the Oligocene-Miocene is defined by a gently inclined slab dipping less than 30º. The establishment of a shallower dipping slab 4º-8º since the middle Miocene is related to the subsequent underthrusting of a thickened Caribbean crust under NW South America responsible for the Santa Marta-Bucaramanga fault reactivation (Kammer and Sánchez, 2006; Villagómez et al., 2011) and accumulation of left lateral slip, as the Caribbean plate moved to the East during the late Miocene. In response to the rigid coupling of oceanic and continental lithospheres, the Santa Marta-Bucaramanga fault slip was prevented and in the interior of the SNSM massif, Early Mesozoic sutures became reactivated as NW verging thrusts (Villagómez et al., 2011) (Fig. 14).

The sedimentary rocks of the SNSM basins attest basement exhumation, which was controlled mainly by block tectonics at the NW corner of the SNSM massif, driven by the normal-sinistral slip of the Santa Marta - Bucaramanga fault (Villagómez et al., 2011).

Zircon provenance evidences that the fan–delta systems and estuaries sourced by the Sierra Nevada de Santa Marta massif remained isolated from the main trunk system of the proto- Magdalena paleochannel (Fig. 15). The proto-delta was controlled by the

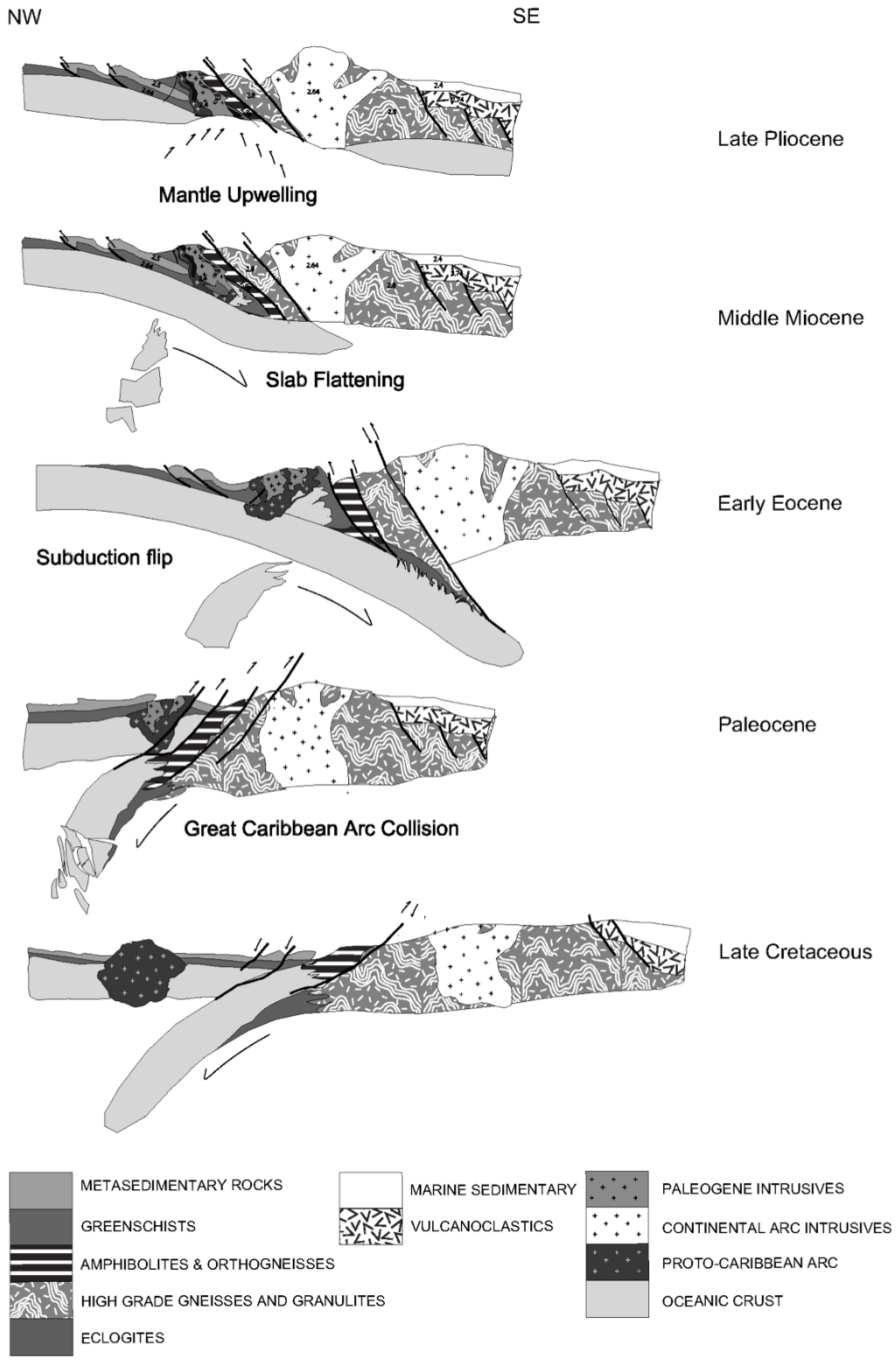

Figure 14. Schematic multi-stage evolution for the Caribbean-South American Margin, in the sense of cross section A-A' Fig 3. During first stages Proto-Caribbean arc approaches to South America; in the late Eocene slab flattening is responsible for the reactivation of crustal structures as the Santa Marta-Bucaramanga Fault.

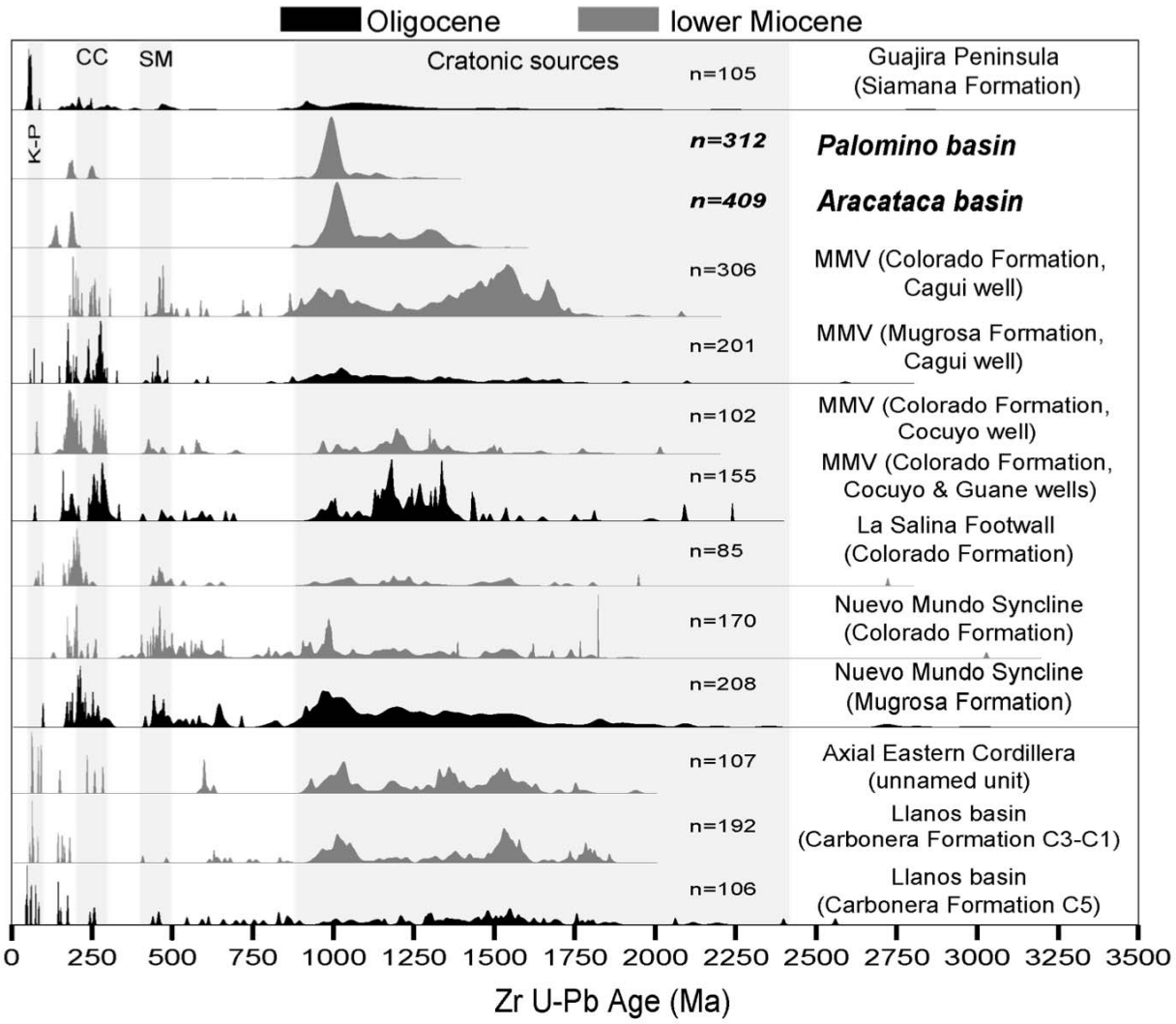

Figure 15. Comparative plots of detrital zircon U-Pb age spectra for Oligocene - lower Miocene sedimentary rocks from the Guajira Peninsula (Zapata et al., 2010), the Middle Magdalena Valley (Caballero et al., 2013; Horton et al., 2015), the axial Eastern Cordillera and Llanos basin (Horton et al., 2010b, 2010a), and the Aracataca and Palomino basins from this study. Diagnostic age populations are delimited by grey shaded zones, SM: Santander Massif, CC: Central Cordillera, K-P: Cretaceous-Paleogene volcanic-plutonic arc.

Santa Marta Bucaramanga fault activity at the southern boundary of the Lower Magdalena basin (Bernal-Olaya et al., 2015). These new findings improve greatly paleogeographic reconstructions by this epoch and allow to precise timing between

fault activity and the onset of sedimentation in the Lower Magdalena basin and the sourcing of sediments from the Eastern Cordillera, the Central Cordillera, the Santander Massif, the Perijá Range, and the SNSM (Ayala et al., 2012; Caballero et al., 2013; Horton et al., 201b, 2015; Zapata et al., 2010).

The Miocene activity of the Orihueca fault marks a tectonic pulse driven by a significant variation in convergence rate between the Caribbean and South-American plates, and the shift from collision to transpression produced the increased NW verging thrusting in the interior of the SNSM (Fig. 14), culminating in the displacement shift from normal to dextral-slip of the Oca fault, that segmented the Guajira basin from the North-Andean margin in the Pliocene and displaced it to its current location about 55 km to the east (Kellogg, 1984; Tschanz et al., 1974).

The sediments of the SNSM basins attest basement exhumation, which was controlled mainly by block tectonics at the NW corner of the SNSM massif, driven by the normal-sinistral slip of the Santa Marta - Bucaramanga fault (Villagómez et al., 2011). The Miocene activity of the Orihueca fault marks the onset of a tectonic pulse driven by a significant variation in convergence rate between the Caribbean and South-American plates, and the shift from collision to transpression that produced the increased NW verging thrusting in the interior of the SNSM, culminating in the displacement shift from normal to dextral-slip of the Oca fault.

Other evidence of this episode can be observed in the Leeward Antilles (van der Lelij et al., 2010; Zapata et al., 2014) where oblique displacements occurred diachronously, and also in the Venezuelan Andes when transpression was accommodated by vertical tectonics and caused a rapid exhumation through the Boconó fault in the Pliocene (Bermúdez et al., 2010).

7. CONCLUSIONS

1) Post-Oligocene sedimentary rocks found in the Aracataca basin show a major input from Precambrian source rocks from the SNP. This major input is the consequence of the unroofing of the basement that was accelerated since the deposition of the Aracataca conglomerates foresets. The shift in composition of the clasts means that the Aracataca conglomerates are growth strata that evidence both extension tectonics along the Santa Marta - Bucaramanga fault since the Upper Oligocene and exhumation of the massif through the Orihueca fault that occurred at least since the Lower Miocene supported by AFT and ZFT cooling ages.

2) The abundance of the Precambrian source is related to an exhumation due to extensional tectonics at the Santa Marta - Bucaramanga fault and a subsequent activation of NW verging thrusts at the interior of the SNSM.

3) The Precambrian sources are derived from inherited Grenvillian terranes that passed through the apatite partial annealing zone approximately since 25-20 Ma, and were lately exhumed and affected by surface erosion.

4) The sudden change from muddy oligomictic conglomerates and siltstones to a coarser facies in the sediments attests to a steepening slope in the source areas, which led to debris flow into Gilbert-type delta environment during the transition from a shallow marine to a more fluvial dominated environment. The facies change is as well related to an increase in erosion and therefore probably also in exhumation rates.

5) Provenance analysis of the basin sediments clearly shows that the clastic material was derived by erosion of the SNSM Precambrian inliers, and that Permo-Triassic, and Late-Cretaceous accreted terrains at the NW corner of the SNSM did not contributed to

sediments, as these tectonic blocks were not yet exhumed during Oligocene-Miocene times.

6) The major shift in provenance between the bottomset and foresets of the Aracataca conglomerates is related to exhumation of the massif during increasing displacement along the Santa Marta – Bucaramanga fault, which occurred between the late Oligocene and early Miocene. The increase in the variety of source rock lithologies registered in the stratigraphic record is evidence for unroofing of the Precambrian basement and the Central Batholith.

7) Detrital thermochronologic ages from the Aracataca basin are evidence for the Santa Marta-Bucaramanga fault being responsible for the increase of relief in the western flank of the SNSM massif, as it acted coeval with the NW verging Orihueca fault and Oca fault. In the Palomino basin extensional faulting started since the Late Eocene-Oligocene with the onset of a dextral strike-slip since the Miocene in consequence of the coupling of the South American crust and the Caribbean crust. This caused faster exhumation of the western flank of the SNSM massif, exhuming lower crustal levels that acted as sources for the Miocene sequences that yield the oldest zircon U-Pb ages and younger detrital ZFT and AFT ages.

8. ACKNOWLEDGMENTS

This research was funded by COLCIENCIAS, in the frame of the project “Evolución Tectónica del margen Caribeño Colombiano” which provided the resources for fieldwork, and sample analysis. This project was also supported by BQR Sud grant from ISTerre, Universite Grenoble Alpes, Mélanie Balvay at ISTerre is thanked for help with fission-track sample preparation. Geochronological analyses were done at the facilities of the ETH institute of Petrology and Geochemistry in Zurich; Marcel Guillong carefully explained data reduction procedures. Alejandro Beltran provided his knowledge on the methods for U-Pb sample preparation, and discussions on the significance of geochronological data, Pierre Vonlanthene aided us with cathodluminiscense imagery at the UNIL. And finally the authors want to acknowledge the students of the field courses in geology of the UNAL from the years 2013-2014, which explored with us the different creeks and outcrops inland and on the shores of the Sierra Nevada de Santa Marta Massif, and were involved in the development of a more precise map. Camilo Montes and an anonymous person are thanked by their detailed reviews and comments in a previous manuscript contribution.

9. REFERENCES

Audemard, F.E., Audemard, F.A., 2002. Structure of the Mérida Andes, Venezuela: relations with the South America–Caribbean geodynamic interaction. Tectonophysics 345, 1–26. doi:10.1016/S0040-1951(01)00218-9

Acosta, J., Velandia, F., Osorio, J., Lonergan, L., Mora, H., 2007. Strike-slip deformation within the Colombian Andes. Geol. Soc. Lond. Spec. Publ. 272, 303–319. doi:10.1144/GSL.SP.2007.272.01.16

Ayala, R.C., Bayona, G., Cardona, A., Ojeda, C., Montenegro, O.C., Montes, C., Valencia, V., Jaramillo, C., 2012. The Paleogene synorogenic succession in the northwestern Maracaibo block: Tracking intraplate uplifts and changes in sediment delivery systems. J. South Am. Earth Sci., Tectonic and climatic shaping of the northern Andes and southern Caribbean margin 39, 93–111. doi:10.1016/j.jsames.2012.04.005

Bayona, G., Montes, C., Cardona, A., Jaramillo, C., Ojeda, G., Valencia, V., Ayala-Calvo, C., 2011. Intraplate subsidence and basin filling adjacent to an oceanic arc–continent collision: a case from the southern Caribbean-South America plate margin. Basin Res. 23, 403–422. doi:10.1111/j.1365-2117.2010.00495.x

Bayona, G., Ochoa, F.L., Cardona, A., Jaramillo, C., Montes, C., Tchegliakova, N., 2007. Procesos orogénicos del Paleoceno para la cuenca de Ranchería (Guajira, Colombia) y áreas adyacentes definidos por análisis de procedencia. Geol. Colomb. 32, 21–46.

Bermúdez, M.A., Kohn, B.P., van der Beek, P.A., Bernet, M., O'Sullivan, P.B., Shagam, R., 2010. Spatial and temporal patterns of exhumation across the Venezuelan Andes: Implications for Cenozoic Caribbean geodynamics. Tectonics 29, TC5009. doi:10.1029/2009TC002635

Bernal-Olaya, R., Mann, P., Escalona, A., 2015. Tectonostratigraphic Evolution of the Lower Magdalena Basin, Colombia: An Example of an Underfilled to Overfilled Forearc Basin. Basin, in C. Bartolini and P. Mann, eds., Petroleum geology and potential of the Colombian Caribbean Margin: AAPG Memoir 108, p. 345–398.

Bernet, M., van der Beek, P., Pik, R., Huyghe, P., Mugnier, J.-L., Labrin, E., Szulc, A., 2006. Miocene to Recent exhumation of the central Himalaya determined from combined detrital zircon fission-track and U/Pb analysis of Siwalik sediments, western Nepal. Basin Res. 18, 393–412. doi:10.1111/j.1365-2117.2006.00303.x

Black, L.P., Kamo, S.L., Allen, C.M., Aleinikoff, J.N., Davis, D.W., Korsch, R.J., Foudoulis, C., 2003. TEMORA 1: a new zircon standard for Phanerozoic U–Pb geochronology. Chem. Geol. 200, 155–170. doi:10.1016/S0009-2541(03)00165-7

Bluck, 2010, Structure of gravel beaches and their relationship to tidal range. Sedimentology (2011) 58, 994–1006 doi: 10.1111/j.1365-3091.2010.01192.x

Boggs, S., 2009. Petrology of Sedimentary Rocks. Cambridge University Press.

Brandon, M.T., Roden-Tice, M.K., Garver, J.I., 1998. Late Cenozoic exhumation of the Cascadia accretionary wedge in the Olympic Mountains, northwest Washington State. Geol. Soc. Am. Bull. 110, 985–1009. doi:10.1130/0016-7606(1998)110<0985:LCEOTC>2.3.CO;2

Caballero, V., Mora, A., Quintero, I., Blanco, V., Parra, M., Rojas, L.E., Lopez, C., Sánchez, N., Horton, B.K., Stockli, D., Duddy, I., 2013. Tectonic controls on sedimentation in an intermontane hinterland basin adjacent to inversion structures: the Nuevo Mundo syncline, Middle Magdalena Valley, Colombia. Geol. Soc. Lond. Spec. Publ. 377, 315–342. doi:10.1144/SP377.12

Camargo, S., 2014. Estructura litosférica asociada a la Sierra Nevada de Santa Marta a partir de datos de gravimetría, magnetometría y sismología. Poster session presented at the Latin-American and Caribbean seismological commision LACSC-2014, Bogotá 23-25 July 2014.

Cardona, A., Chew, D., Valencia, V.A., Bayona, G., Mišković, A., Ibañez-Mejía, M., 2010a. Grenvillian remnants in the Northern Andes: Rodinian and Phanerozoic Paleogeographic perspectives. J. South Am. Earth Sci., The Grenville Orogen in Central and South America 29, 92–104. doi:10.1016/j.jsames.2009.07.011

Cardona, A., Cordani, U.G., MacDonald, W.D., 2006. Tectonic correlations of pre-Mesozoic crust from the northern termination of the Colombian Andes, Caribbean region. J. South Am. Earth Sci. 21, 337–354. doi:10.1016/j.jsames.2006.07.009

Cardona, A., Montes, C., Ayala, C., Bustamante, C., Hoyos, N., Montenegro, O., Ojeda, C., Niño, H., Ramirez, V., Valencia, V., Rincón, D., Vervoort, J., Zapata, S., 2012. From arc-continent collision to continuous convergence, clues from Paleogene conglomerates along the southern Caribbean–South America plate boundary. Tectonophysics 580, 58–87. doi:10.1016/j.tecto.2012.08.039

Cardona, A., Valencia, V., Bayona, G., Duque, J., Ducea, M., Gehrels, G., Jaramillo, C., Montes, C., Ojeda, G., Ruiz, J., 2011a. Early-subduction-related orogeny in the northern Andes: Turonian to Eocene magmatic and provenance record in the Santa Marta Massif and Rancheria Basin, northern Colombia. Terra Nova 23, 26–34. doi:10.1111/j.1365-3121.2010.00979.x

Cardona, A., Valencia, V., Bustamante, C., García-Casco, A., Ojeda, G., Ruiz, J., Saldarriaga, M., Weber, M., 2010b. Tectonomagmatic setting and provenance of the Santa Marta Schists, northern Colombia: Insights on the growth and approach of Cretaceous Caribbean oceanic terranes to the South American continent. J. South Am. Earth Sci., Sierra Nevada de Santa Marta and Adjacent Basins 29, 784–804. doi:10.1016/j.jsames.2009.08.012

Cardona, A., Valencia, V., Garzón, A., Montes, C., Ojeda, G., Ruiz, J., Weber, M., 2010c. Permian to Triassic I to S-type magmatic switch in the northeast Sierra Nevada de Santa Marta and adjacent regions, Colombian Caribbean: Tectonic setting and implications within Pangæa Paleogeography. J. South Am. Earth Sci., Sierra Nevada de Santa Marta and Adjacent Basins 29, 772–783. doi:10.1016/j.jsames.2009.12.005

Cardona, A., Valencia, V., Weber, M., Duque, J., Montes, C., Ojeda, G., Reiners, P., Domanik, K., Nicolescu, S., Villagómez, D., 2011b. Transient Cenozoic tectonic stages in the southern margin of the Caribbean plate: U-Th/He thermochronological constraints from Eocene plutonic rocks in the Santa Marta massif and Serranía de Jarara, northern Colombia. Geol. Acta 9, 445–469. doi:10.1344/105.000001739

Colella, A., 1988. Fault-controlled marine Gilbert-type fan deltas. Geology 16, 1031–1034. doi:10.1130/0091-7613(1988)016<1031:FCMGTF>2.3.CO;2

Colmenares, F., 2007. Evolución Geohistorica de la Sierra Nevada de Santa Marta (Internal report No. PS 025-06). INGEOMINAS.

Cordani, U.G., Cardona, A., Jimenez, D.M., Liu, D., Nutman, A.P., 2005. Geochronology of Proterozoic basement inliers in the Colombian Andes: tectonic history of remnants of a fragmented Grenville belt. Geol. Soc. Lond. Spec. Publ. 246, 329–346. doi:10.1144/GSL.SP.2005.246.01.13

Cortés, M., Angelier, J., Colletta, B., 2005. Paleostress evolution of the northern Andes (Eastern Cordillera of Colombia): Implications on plate kinematics of the South Caribbean region: PALEOSTRESS EVOLUTION OF THE NORTHERN ANDES. Tectonics 24, n/a-n/a. doi:10.1029/2003TC001551

Dalrymple, R.W., Choi, K., 2007. Morphologic and facies trends through the fluvial–marine transition in tide-dominated depositional systems: A schematic framework for environmental and sequence-stratigraphic interpretation. Earth-Sci. Rev. 81, 135–174. doi:10.1016/j.earscirev.2006.10.002

Doolan, B., 1970. Structure and metamorphism of the Santa Marta Area Colombia, South America [microform] / [WWW Document]. URL https://www.researchgate.net/publication/34351494_Structure_and_metamorphism_of_the_Santa_Marta_Area_Colombia_South_America_microform (accessed 7.20.16).

Duque-Caro, H., 1979. Major structural elements and evolution of northwestern Colombia. Geol. Geophys. Investig. Cont. Margins AAPG Mem. 29, 329–351.
Duke, W.L., Arnott, R.W.C., Cheel, R.J., 1991. Shelf sandstones and hummocky cross-stratification: New insights on a stormy debate. Geology 19, 625. doi:10.1130/0091-7613(1991)019<0625:SSAHCS>2.3.CO;2
Egbue, O., Kellogg, J., 2010. Pleistocene to Present North Andean "escape." Tectonophysics 489, 248–257. doi:10.1016/j.tecto.2010.04.021
Ehlers, T.A., 2005. Crustal Thermal Processes and the Interpretation of Thermochronometer Data. Rev. Mineral. Geochem. 58, 315–350. doi:10.2138/rmg.2005.58.12
Falk, P.D. and Dorsey, R.J. (1998) Rapid development of gravelly high-density turbidity currents in marine Gilberttype fan deltas, Lorento Basin, Baja California Sur, Mexico. Sedimentology, 45, 331-349.
Flinch, J.F., Castillo, V., 2015. Record and Constraints of the Eastward Advance of the Caribbean Plate in Northern South America.
Flinch, J.F., 2003. Structural Evolution of the Sinu-Lower Magdalena Area (Northern Colombia). AAPG Mem. 79, 776–796.
Folk, R. L, 1980, Petrology of sedimentary rocks: Austin,TX,Hemphill's,170p.
Force, E.R., 1980. The provenance of rutile. Journal of Sedimentary Research. Vol 50, Issue 2, pp 485–488. doi:10.1306/212F7A31-2B24-11D7-8648000102C1865D
Ghibaudo, G., 1992. Subaqueous sediment gravity flow deposits: practical criteria for their field description and classification. Sedimentology 39, 423–454. doi:10.1111/j.1365-3091.1992.tb02126.x
Gobo, K., Ghinassi, M., Nemec, W., 2015. Gilbert-type deltas recording short-term base-level changes: Delta-brink morphodynamics and related foreset facies. Sedimentology 62, 1923–1949. doi:10.1111/sed.12212
Gobo, K., Ghinassi, M., Nemec, W., 2014. Reciprocal Changes In Foreset To Bottomset Facies In A Gilbert-Type Delta: Response To Short-Term Changes In Base Level. J. Sediment. Res. 84, 1079–1095. doi:10.2110/jsr.2014.83
Hernandez, M., Maldonado, I., Gonzáles, J., Martínez, H., Clavijo, J., Reyes, G., 2003. Geología de las planchas 25 Fundación, 32 Monterrubio y 39 El Difícil. Escala 1:100.000. Memoria explicativa. Versión año 2003.
Henstra, G.A., Grundvag, S.-A., Johannessen, E.P., Kristensen, T.B., Midtkandal, I., Nystuen, J.P., Rotevatn, A., Surlyk, F., Sæther, T., Jørgen, W., 2016. Depositional processes and stratigraphic architecture within a coarse-grained rift-margin turbidite system: The Wollaston Forland Group, east Greenland. Mar. Pet. Geol. 76, 187–209. doi:10.1016/j.marpetgeo.2016.05.018
Higgs, R., 2009. Caribbean-South America oblique collision model revised. Geol. Soc. Lond. Spec. Publ. 328, 613–657. doi:10.1144/SP328.25
Horton, B.K., Anderson, V.J., Caballero, V., Saylor, J.E., Nie, J., Parra, M., Mora, A., 2015. Application of detrital zircon U-Pb geochronology to surface and subsurface correlations of provenance, paleodrainage, and tectonics of the Middle Magdalena Valley Basin of Colombia. Geosphere 11, 1790–1811. doi:10.1130/GES01251.1
Horton, Parra, M., Saylor, J., Nie, J., Mora, A., Torres, V., Stockli, D., Strecker, M., 2010a. Resolving uplift of the northern Andes using detrital zircon age signatures. GSA Today 4–10. doi:10.1130/GSATG76A.1
Horton, Saylor, J.E., Nie, J., Mora, A., Parra, M., Reyes-Harker, A., Stockli, D.F., 2010b. Linking sedimentation in the northern Andes to basement configuration, Mesozoic extension, and Cenozoic shortening: Evidence from detrital zircon U-Pb ages, Eastern Cordillera, Colombia. Geol. Soc. Am. Bull. 122, 1423–1442. doi:10.1130/B30118.1
Howard, J.L., 1993. The statistics of counting clasts in rudites: a review, with examples from the upper Paleogene of southern California, USA. Sedimentology 40, 157–174. doi:10.1111/j.1365-3091.1993.tb01759.x

Ibanez-Mejia, M., Ruiz, J., Valencia, V., Cardona, A., Gehrels, G., Mora, A., 2011. The Putumayo Orogen of Amazonia and its implications for Rodinia reconstructions: New U–Pb geochronological insights into the Proterozoic tectonic evolution of northwestern South America. Precambrian Res. 191, 58–77. doi:10.1016/j.precamres.2011.09.005

Ingeominas (2007a), Geologic Map of the Sierra Nevada de Santa Marta, scale 1:200,000, Ingeominas-Invemar-Ecopetrol-ICP-Geosearch, Ltda.,Bogota.

Jackson, S.E., 2008. , in: LAMTRACE Data Reduction Software for LA-ICP-MS. In: Sylvester P. (ed.), Laser Ablation-ICP-Mass Spectrometry in the Earth Sciences: Current Practices and Outstanding Issues. Mineralogical Association of Canada Short Course Series. Mineralogical Association of Canada, pp. 305–307.

Jackson, S.E., Pearson, N.J., Griffin, W.L., Belousova, E.A., 2004. The application of laser ablation-inductively coupled plasma-mass spectrometry to in situ {U}–{Pb} zircon geochronology. Chem. Geol. 211, 47–69. doi:10.1016/j.chemgeo.2004.06.017

Javadi, H.R., Foroutan, M., Ashtiani, M.E., Urbina, J.A., Saidi, A., Faridi, M., 2011. Tectonics changes in NW South American Plate and their effect on the movement pattern of the Boconó Fault System during the Mérida Andes evolution. J. South Am. Earth Sci. 32, 14–29. doi:10.1016/j.jsames.2011.04.008

Jones, M.A., Heller, P.L., Roca, E., Garcés, M., Cabrera, L., 2004. Time lag of syntectonic sedimentation across an alluvial basin: theory and example from the Ebro Basin, Spain. Basin Res. 16, 489–506. doi:10.1111/j.1365-2117.2004.00244.x

Kammer, A., Sánchez, J., 2006. Early Jurassic rift structures associated with the Soapaga and Boyacá faults of the Eastern Cordillera, Colombia: Sedimentological inferences and regional implications. J. South Am. Earth Sci., Tectonic evolution of the Colombian Andes 21, 412–422. doi:10.1016/j.jsames.2006.07.006

Kellogg, J.N., 1984. Cenozoic Tectonic History of the Sierra de Perija, Venezuela- Colombia, and Adjacent Basins. Geol. Soc. Am. Mem. 162, 239.

Kennan, L., Pindell, J.L., 2009. Dextral shear, terrane accretion and basin formation in the Northern Andes: best explained by interaction with a Pacific-derived Caribbean Plate? Geol. Soc. Lond. Spec. Publ. 328, 487–531.

Kroonenberg, S.B., 1982. A Grenvillian granulite belt in the Colombian Andes and its relation to the Guiana shield. Geol Mijnb. 61 1982 325-333.

Leithold, E.L., Bourgeois, J., 1984. Characteristics of coarse-grained sequences deposited in nearshore, wave-dominated environments—examples from the Miocene of south-west Oregon. Sedimentology 31, 749–775.

Leckie, D., 1988. Wave-formed, coarse-grained ripples and their relationship to hummocky cross-stratification. J. Sediment. Res. 58, 607–622. doi:10.1306/212F8E04-2B24-11D7-8648000102C1865D

Leeder, M.R., Gawthorpe, R.L., 1987. Sedimentary models for extensional tilt-block/half-graben basins. Geol. Soc. Lond. Spec. Publ. 28, 139–152. doi:10.1144/GSL.SP.1987.028.01.11

Lowe, D.R., 1982. Sediment gravity flows; II, Depositional models with special reference to the deposits of high-density turbidity currents. J. Sediment. Res. 52, 279–297. doi:10.1306/212F7F31-2B24-11D7-8648000102C1865D.

López-Blanco, M., Piña, J., Marzo, M., 2000. Anatomy of regressive tracts in a regressive sequence set: Vilomara unit, Sant Llorenç del Munt, Ebro Basin, NE Spain. Sediment. Geol. 138, 143–159. doi:10.1016/S0037-0738(00)00147-0

Ludwig, K.R.., 2003. User's Manual for Isoplot 3.00: a Geochronological Toolkit for Microsoft Excel. [Kenneth R. Ludwig?], Berkeley CA.

MacDonald, W.D., Doolan, B.L., Cordani, U.G., 1971. Cretaceous-Early Tertiary Metamorphic K-Ar Age Values from the South Caribbean. Geol. Soc. Am. Bull. 82, 1381–1388. doi:10.1130/0016-7606(1971)82[1381:CTMKAV]2.0.CO;2

Martin B., C. (1968) Edades isotópicas de rocas venezolanas. *Bol. Geol., Caracas*, 9 (19): 356-380.

Merren A. Jones, Paul L. Heller, Eduard Roca, Miguel Garcés and Lluís Cabrera, 2004. Time lag of syntectonic sedimentation across an alluvial basin: theory and example from the Ebro Basin,Spain. Basin Research (2004) 16, 467–488, doi: 10.1111/j.1365-2117.2004.00244.x

Miall, A.D., 2006. The Geology of Fluvial Deposits. Springer Berlin Heidelberg, Berlin, Heidelberg.

Miall, A., 2014. Fluvial Depositional Systems. Springer International Publishing, Cham.

Miall, A.D., 1985. Architectural-element analysis: A new method of facies analysis applied to fluvial deposits. Earth-Sci. Rev. 22, 261–308. doi:10.1016/0012-8252(85)90001-7

Miall, A.D. 1978. Lithofacies types and vertical profile models in braided river deposits: A summary. In A.D. Miall (Ed.), Fluvial Sedimentology. Canadian Society of Petroleum Geologists, Memoir 5, p. 597-604.

Middleton, G.V., 1993, Sediment deposition from turbidity currents: Annual Review of Earth and Planetary Sciences, v. 21, p. 89–114, doi: 10.1146 /annurev.ea.21.050193.000513.

Mohrig, D., Whipple, K.X., Hondzo, M., Ellis, C. and Parker, G., 1998. Hydroplaning of subaqueous debris flows. Bull. Geol. Soc. Am., 110, 387–394.

Monod, B., Dhont, D., Hervouët, Y., 2010. Orogenic float of the Venezuelan Andes. Tectonophysics 490, 123–135. doi:10.1016/j.tecto.2010.04.036

Montes, C., Bayona, G., Jaramillo, C., Ojeda, G., Molina, M., Herrera, F., 2005, Uplift of the Sierra Nevada de Santa Marta and Subsidence in the Cesar-Rancheria Valley: Rigid-Beam Pivot Model. In: Extended Abstracts, Sixth International Symposium of Andean Geodynamics, pp. 520-523.

Montes, C., Guzman, G., Bayona, G., Cardona, A., Valencia, V., Jaramillo, C., 2010. Clockwise rotation of the Santa Marta massif and simultaneous Paleogene to Neogene deformation of the Plato-San Jorge and Cesar-Ranchería basins. J. South Am. Earth Sci., Sierra Nevada de Santa Marta and Adjacent Basins 29, 832–848. doi:10.1016/j.jsames.2009.07.010

Mora-Bohórquez, J.A., Ibánez-Mejia, M., Oncken, O., de Freitas, M., Vélez, V., Mesa, A., Serna, L., 2017. Structure and age of the Lower Magdalena Valley basin basement, northern Colombia: New reflection-seismic and U-Pb-Hf insights into the termination of the central andes against the Caribbean basin. J. South Am. Earth Sci. 74, 1–26. doi:10.1016/j.jsames.2017.01.001

Mulder, T. and Alexander, J., 2001. The physical character of subaqueous sedimentary density flows and their deposits. Sedimentology, 48, 269–299.

Nemec, W., 1990. Aspects of Sediment Movement on Steep Delta Slopes, in: Coarse-Grained Deltas, Special Publication Number 10 of the International Association of Sedimentologists. Blackwell Publishing Ltd, Oxford, UK.

Nemec, W. and Steel, R.J. (1984) Alluvial and coastal conglomerates: their significant features and some comments on gravelly mass-flow deposits. In: Sedimentology of Gravels and Conglomerates (Eds E.H. Koster and R.J. Steel), Can. Soc. Petrol. Geol. Memoir, 10, 1–31.

Nova, G., Montaño, P., Bayona, G., Rapalini, A., Montes, C., 2013. Paleomagnetismo en rocas del Júrasico y Cretácico inferior en el flanco occidental de la Serranía del Perijá; contribuciones a la evolución tectónica del NW de Suramérica. Bol. Geol. 34.

Ordóñez, O., Pimentel, M., Moraes, R., 2002. GRANULITAS DE LOS MANGOS, UN FRAGMENTO GRENVILLIANO EN LA PARTE ORIENTAL DE LA SIERRA NEVADA DE SANTA MARTA. Rev. Acad. Colomb. Cienc. Exactas Físicas Nat. 0370-3908 26, 169–179.

Pennington, W.D., 1981. Subduction of the Eastern Panama Basin and seismotectonics of northwestern South America. J. Geophys. Res. Solid Earth 86, 10753–10770. doi:10.1029/JB086iB11p10753

Pettijohn, F., 1980. Rocas sedimentarias, Eudeba manuales. Editorial Universitaria de Buenos Aires, Buenos Aires.

Pindell, J., Kennan, L., Maresch, W.V., Stanek, K.-P., Draper, G., Higgs, R., 2005. Plate-kinematics and crustal dynamics of circum-Caribbean arc-continent interactions: Tectonic controls on basin development in Proto-Caribbean margins. Geol. Soc. Am. Spec. Pap. 394, 7–52. doi:10.1130/0-8137-2394-9.7

Pindell, J.L., Kennan, L., 2009. Tectonic evolution of the Gulf of Mexico, Caribbean and northern South America in the mantle reference frame: an update. Geol. Soc. Lond. Spec. Publ. 328, 1–55. doi:10.1144/SP328.1

Pinzón, E., 2014. Caracterización litológica y sedimentológica de una unidad conglomerática en cercanías de Aracataca y su significado para el levantañiento de la Sierra Nevada de Santa Marta (SNSM). Universidad Nacional de Colombia sede Bogotá, Bogotá.

Postma, G., Nemec, W., Kleinspehn, K.L., 1988. Large floating clasts in turbidites: a mechanism for their emplacement. Sediment. Geol. 58, 47–61. doi:10.1016/0037-0738(88)90005-X

Postma, G., 1986. Classification for sediment gravity-flow deposits based on flow conditions during sedimentation. Geology 14, 291–294. doi:10.1130/0091-7613(1986)14<291:CFSGDB>2.0.CO;2

Postma, G., 1984. Mass-Flow Conglomerates in a Submarine Canyon: Abrioja Fan-Delta, Pliocene, Southeast Spain 237–258.

Postma, G., 1983. Water escape structures in the context of a depositional model of a mass flow dominated conglomeratic fan-delta (Abrioja Formation, Pliocene, Almeria Basin, SE Spain). Sedimentology 30, 91–103. doi:10.1111/j.1365-3091.1983.tb00652.x

Powers, M.C., 1953. A new roundness scale for sedimentary particles. J. Sediment. Res. 23, 117–119. doi:10.1306/D4269567-2B26-11D7-8648000102C1865D

Restrepo-Pace, P., Ruiz, J., Gehrels, G., Cosca, M., 1997. Geochronology and Nd isotopic data of Grenville-age rocks in the Colombian Andes: new constraints for Late Proterozoic-Early Paleozoic Paleocontinental reconstructions of the Americas. Earth Planet. Sci. Lett. 427–441. doi:10.1016/S0012-821X(97)00091-5

Ravnås, R., Steel, J., 1998. Architecture of Marine Rift-Basin Successions. AAPG Bull. 82, 110–146.

Sanchez, J., Mann, P., 2015. Integrated Structural and Basinal Analysis of the Cesar–Rancheria Basin, Colombia: Implications for its Tectonic History and Petroleum Systems, in: Bartolini, C., Mann, P. (Eds.), Memoir 108: Petroleum Geology and Potential of the Colombian Caribbean Margin. AAPG.

Sláma, J., Košler, J., Condon, D.J., Crowley, J.L., Gerdes, A., Hanchar, J.M., Horstwood, M.S.A., Morris, G.A., Nasdala, L., Norberg, N., Schaltegger, U., Schoene, B., Tubrett, M.N., Whitehouse, M.J., 2008. Plešovice zircon — A new natural reference material for U–Pb and Hf isotopic microanalysis. Chem. Geol. 249, 1–35. doi:10.1016/j.chemgeo.2007.11.005

Shagam, R., Kohn, B.P., Banks, P.O., Dasch, L.E., Vargas, R., Rodríguez, G.I., Pimentel, N., 1984. Tectonic implications of Cretaceous-Pliocene fission-track ages from rocks of the circum-Maracaiho Basin region of western Venezuela and eastern Colombia, in: Geological Society of America Memoirs. Geological Society of America, pp. 385–412. doi:10.1130/MEM162-p385

Sohn, Y.K., 2000b. Depositional processes of submarine debris flows in the Miocene fan deltas, Pohang Basin, SE Korea with special reference to flow transformation. J. Sediment. Res., 70, 491–503.

Sohn, Y.K., 1997. On traction-carpet sedimentation. J. Sediment. Res., 67, 502–509.

Spencer, C.J., Kirkland, C.L., Taylor, R.J.M., 2016. Strategies towards statistically robust interpretations of in situ U–Pb zircon geochronology. Geosci. Front. 7, 581–589. doi:10.1016/j.gsf.2015.11.006

Spikings, R., Cochrane, R., Villagomez, D., Van der Lelij, R., Vallejo, C., Winkler, W., Beate, B., 2015. The geological history of northwestern South America: from Pangæa to the early

collision of the Caribbean Large Igneous Province (290–75 Ma). Gondwana Res. 27, 95–139. doi:10.1016/j.gr.2014.06.004

Stewart, R.J., Brandon, M.T., 2004. Detrital-zircon fission-track ages for the "Hoh Formation": Implications for late Cenozoic evolution of the Cascadia subduction wedge. Geol. Soc. Am. Bull. 116, 60–75. doi:10.1130/B22101.1

Taboada, A., Rivera, L.A., Fuenzalida, A., Cisternas, A., Philip, H., Bijwaard, H., Olaya, J., Rivera, C., 2000. Geodynamics of the northern Andes: Subductions and intracontinental deformation (Colombia). Tectonics 19, 787–813. doi:10.1029/2000TC900004

Trenkamp, R., Kellogg, J.N., Freymueller, J.T., Mora, H.P., 2002. Wide plate margin deformation, southern Central America and northwestern South America, CASA GPS observations. J. South Am. Earth Sci. 15, 157–171. doi:10.1016/S0895-9811(02)00018-4

Tschanz, C., Jimeno, A., Cruz, J., 1969. Geology of the Sierra Nevada de Santa Marta area, Colombia. Informe interno 1829. INGEOMINAS Bogotá Prelim. Rep. 288pLinks.

Tschanz, C., Marvin, R.F., B, J.C., Mehnert, H.H., Cebula, G.T., 1974. Geologic Evolution of the Sierra Nevada de Santa Marta, Northeastern Colombia. Geol. Soc. Am. Bull. 85, 273–284. doi:10.1130/0016-7606(1974)85<273:GEOTSN>2.0.CO;2

Ulianov, A., Müntener, O., Schaltegger, U., Bussy, F., 2012. The data treatment dependent variability of {U}–{Pb} zircon ages obtained using mono-collector, sector field, laser ablation {ICPMS}. J. Anal. At. Spectrom. 27, 663. doi:10.1039/c2ja10358c

Van der Lelij, R., Spikings, R.A., Kerr, A.C., Kounov, A., Cosca, M., Chew, D., Villagomez, D., 2010. Thermochronology and tectonics of the Leeward Antilles: Evolution of the southern Caribbean Plate boundary zone. Tectonics 29, TC6003. doi:10.1029/2009TC002654

Vence, E., 2008. Abstract: Along-Strike Continuity of Caribbean Tectonic Terranes and Their Controls on Source and Reservoir Rocks Offshore Colombia and ; #90063 (2007) [WWW Document]. URL http://www.searchanddiscovery.com/abstracts/html/2007/annual/abstracts/lbVence.htm (accessed 7.20.16).

Villagómez, D., Spikings, R., 2013. Thermochronology and tectonics of the Central and Western Cordilleras of Colombia: Early Cretaceous–Tertiary evolution of the Northern Andes. Lithos 160–161, 228–249. doi:10.1016/j.lithos.2012.12.008

Villagómez, D., Spikings, R., Mora, A., Guzmán, G., Ojeda, G., Cortés, E., van der Lelij, R., 2011. Vertical tectonics at a continental crust-oceanic plateau plate boundary zone: Fission track thermochronology of the Sierra Nevada de Santa Marta, Colombia. Tectonics 30, TC4004. doi:10.1029/2010TC002835

Weber, M., Cardona, A., Valencia, V., García-Casco, A., Tobón, M., Zapata, S., 2010. U/Pb detrital zircon provenance from late cretaceous metamorphic units of the Guajira Peninsula, Colombia: Tectonic implications on the collision between the Caribbean arc and the South American margin. J. South Am. Earth Sci. 29, 805–816. doi:10.1016/j.jsames.2009.10.004

Zapata, S., Cardona, A., Montes, C., Valencia, V., Vervoort, J., Reiners, P., 2014. Provenance of the Eocene Soebi Blanco formation, Bonaire, Leeward Antilles: Correlations with post-Eocene tectonic evolution of northern South America. J. South Am. Earth Sci. 52, 179–193. doi:10.1016/j.jsames.2014.02.009

Zapata, S., Weber, M., Cardona, A., Valencia, V., Guzmán, G., Tobón, M., 2010. Provenance of Oligocene conglomerates and associated sandstones from the Siamaná Formation, Serrania de Jarara, Guajira, Colombia: Implication on Oligocene Caribbean-South America tectonics. Bol. Cienc. Tierra 27, 7–24.

Zuluaga, C., Stowell, H., 2012. Late Cretaceous–Paleocene metamorphic evolution of the Sierra Nevada de Santa Marta: Implications for Caribbean geodynamic evolution. J. South Am. Earth Sci. 34, 1–9. doi:10.1016/j.jsames.2011.10.001

OVERALL CONCLUSIONS

At The Sierra Nevada de Santa Marta massif I had found evidences that this part of the Andean margin has acted as an accretionary margin throughout its history, and that the rocks that form the SNSM preserve the record of at least three orogenic cycles that involve processes of crustal thickening, orogenic wedge growth, thermal equilibration, crustal weakening and late orogenic collapse due plate kinematic reconfiguration (Fig. 1). In this dissertation, I integrated several geochronological and thermochronological techniques to construct a scenario on P-T-t-d paths during the evolution of the SNSM; during the Phanerozoic.

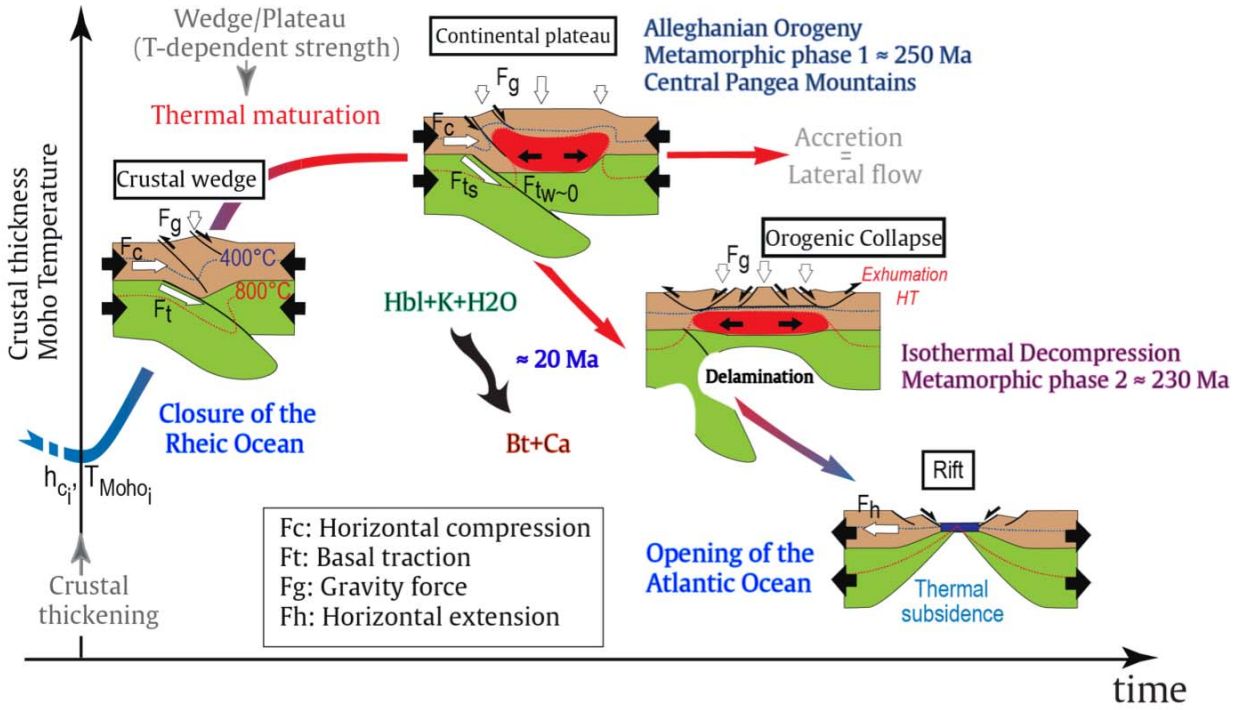

Figure 1. Sketch of a Thermal-Mechanical evolutive scenario of the crust at plate boundaries and the crustal tectonic cycle. Illustrated by the evolution of crustal thickness and Moho temperature as a function of time. The first stage of the thermal–mechanical evolution of the crust at convergent plate boundaries is characterized by the development of a crustal wedge under a low-geothermal gradient dominated by subduction. Thermal maturation of the crustal wedge is responsible for the weakening of the lower crust, which leads to the

wedge/plateau transition. At this stage, the basal traction force decomposes into Ftw beneath the plateau and Fts along its edges. A steady state is reached if accretion is balanced by gravity-driven lateral flow of the weakened crust. A modification of the lithospheric-scale dynamics boundary condition causes the switch from crustal thickening to thinning and the mode of crustal extension ranges from metamorphic core complex to rift as a function of the rheologic state of the crust. Crustal thinning is associated with isothermal decompression and is followed by thermal subsidence. Taken from (Vanderhaeghe, 2012).
My interpretation is that at the Sierra Nevada de Santa Marta this evolutionary trend occurred during three orogenic cycles, at the end of Neoproterozoic, In the middle Permian - Upper Triassic, and during the Late Cretaceous - Miocene. During these interactions, lower crustal delamination and slab retreat played a major role influencing the modification of lithospheric-scale dynamics boundary conditions i.e. Oligocene plate reorganization, caused a transition from lower crustal extrusion to extension through reactivated faults.

In Chapter 1, I presented a tectonic history of the SNSM massif that includes its evolution during the supercontinental cycle of Pangæa amalgamation and disassembly.

A secondary topic of interest discussed briefly in Chapter 1, derived from our results is related to the geochronological implications of previous interactions of the continental margin related to the opening of the Iapetus Ocean during Rodinia disassembly and the subsequent Brazilian/Pan-African orogeny. Although the new evidences found in this study at the high metamorphic grade units of the Sevilla Metamorphic Belt suggest a palaeogeographic context for the Iapetus opening at this part of the Proto-Andean margin. It, is necessary to continue with deeper and extended analyses on this particular topic since most of the mapping and sample collection on the late Neoproterozoic to early Paleozoic units at the SNSM remains to be done (Fig. 2).

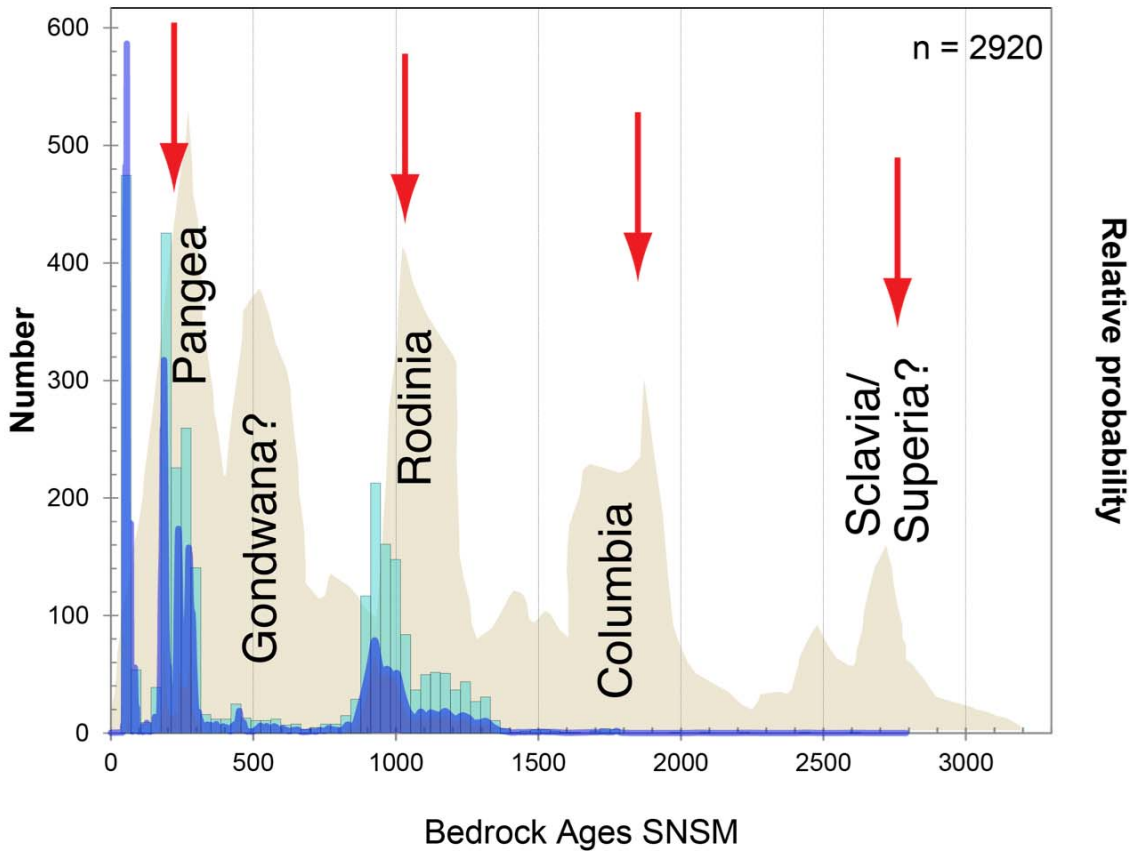

Figure 2. Comparison of all U-Pb data previously published and from this work of bedrock samples from the SNSM massif represented by the blue curve and bins, the red arrows indicate the orogenic peaks recognized by Runcorn, (1962) brown shade in the background corresponds to the spectra of U-Pb ages compiled by (Hawkesworth et al., 2010). Although minor, a Neoproterozoic-Paleozoic population is present and may indicate sampling bias or either orogenic quiescence. There are two major currents on the interpretation of age peaks: one is related with crustal growth driven by mantle convection and the second to preservation of the continental crust due supercontinent assembly, within this discussion U-Pb peaks may correspond to periods of accelerated crustal growth (Arndt, 2013), and detrital zircon populations may act as a measure of the intensity of continental arc magmatism (McKenzie et al., 2016). Modified after (Nance et al., 2014).

My results in Chapter 1 redefine the morphotectonic provinces of the SNSM (Tschanz et al., 1974) based in geochronology and petrology. This new considerations have a high impact in the palaeogeographic models discussed for Pangæa assembly (Fig. 3) in

the Proto-Andean margin, and geodynamics of the South American and Pacific plates, in which I had reevaluated the role played by the Pacific plate in the arc inception and the subduction of a juvenile oceanic crust of the Rheic Ocean during Pangæa Assembly. Interaction of Laurentia and Gondwana resulting from a dextral oblique collision between their irregular margins caused the closure of the Rheic Ocean, and led to continental arc magmatism that extended from the current Peruvian Andes to the Southern North America Maya block including the Colombian Andes and the Sierra Nevada de Santa Marta Massif.

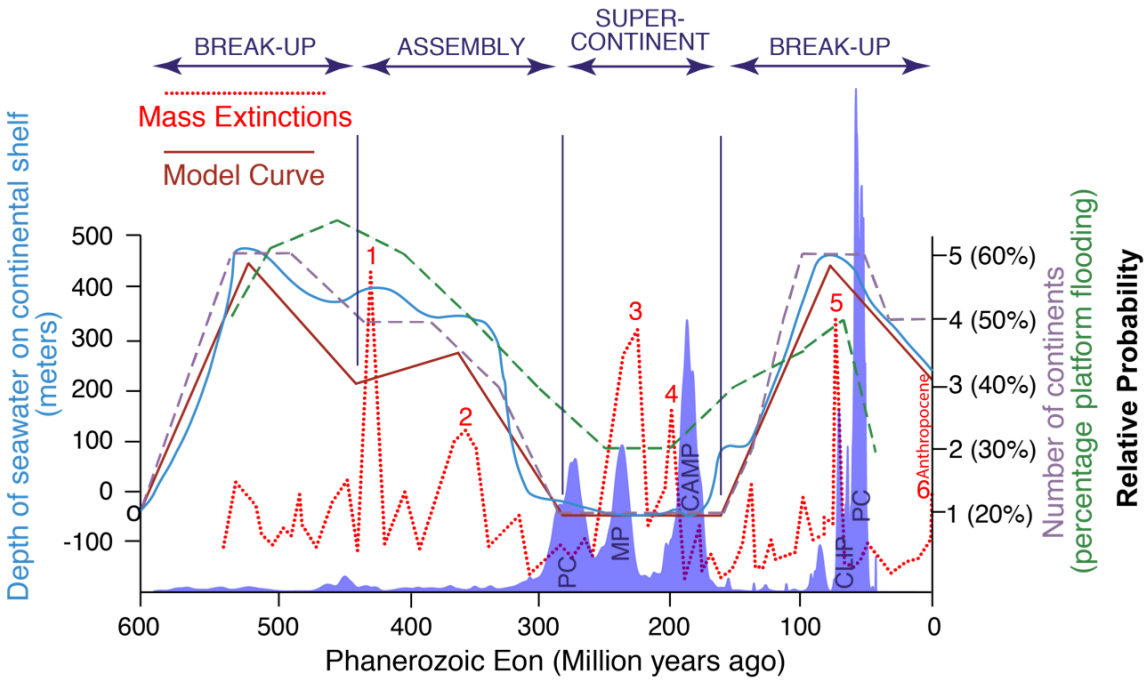

Figure 3. Spectra of U-Pb data from the SNSM massif illustrates periods of crustal growth associated to tectonic events PC: Post collisional I-type magmatism, MP: Metamorphic peak, CAMP: Central Atlantic Magmatic Province, CLIP: Caribbean Large Igneous Province. Blue curve represents variation in sea level, purple dashed line represents the number of continents and green dashed curve depicts amount of flooding of shallow shelves by seawater for the last 600 Ma. Stages of supercontinent are indicated in this case for Pangæa. Modified after (Condie, 2011; Hawkesworth et al., 2010; Nance et al., 2014). Massive extinction curve in red reproduced from the University of California Museum of Paleontology's Understanding Evolution (http://evolution.berkeley.edu).

The youngest arc magmatism of this episode is early Permian 290-280 Ma in western Pangæa and is associated with collision tectonics (Weber et al., 2007), and found further to the south of the Andes interpreted as being the result of lithospheric thinning (Mišković et al., 2009; Sempere et al., 2002). In East Pangæa Permian magmatism is associated to a Post-Variscan extensional regime (Beltrando et al., 2010; Beltrán-Triviño et al., 2016; Franke, 2006; Friedl et al., 2004; Letsch et al., 2015; Nance et al., 2012, 2010). This diachronous closure was controlled by a north oblique convergence in Europe in the early Carboniferous as Gondwana collided with southern Baltica, and a late Carboniferous-early Permian dextral transpressive convergence between Gondwana and Laurentia that originated the Appalachian-Ouachitan orogen. In Western Pangæa approximately 30 Myr after the ca. 280 Ma magmatism, peak conditions of Barrovian metamorphism were reached along the assembled margin (ca. 250 Ma), 10 Myr later orogenic collapse of the Appalachian-Ouachitan orogen led to crustal thinning and isothermal decompression during the Triassic. This was the beginning of Western Pangæa disassembly and is recorded at this part of the Proto-Andean margin in zoned garnet and metamorphic zircon and in-situ rim overgrowths.

We also point out the relevance of the late Paleozoic tectonics during Pangæa amalgamation and the regional correlations of the Permo-Triassic terranes in the Colombian Andes, with the Inner Santa Marta Metamorphic belt were rocks of this epoch have been recognized and studied by geochronology and thermobarometry. It had revealed the metamorphic conditions (P-T) during a time span of 60 Ma that shifted between two phases, that constrain Pangæa amalgamation in a first collisional phase with a prograde path and a second phase of isothermal decompression. It attests

for crustal thinning and orogenic collapse prior Pangæa disassembly by rifting and subsequent drifting during the Late Triassic ca. 216 Ma.

Finally, the correlation between the depletion of trace element concentrations in zircons and coeval crystallization of garnet provides a reliable estimate of the age of metamorphism that rather is defined as a time span.

Chapter 2 explored the geodynamic constraints that operated during the Late Cretaceous Caribbean Plate interaction against the South American plate. In this scenario, we had discussed the mechanisms for terrane accretion, collisional plutonism and high-elevated geothermal gradients and the later events that correspond to major plate reorganization during the Oligocene in Chapter 3.

In Chapter 2, we animate this discussion in the context of the Caribbean plate origin, which is debated, between a pacific realm or a segmentation and incorporation between Cocos and Nazca plates, against cratonic South America. The main boundary of this scene can be reconstructed up to Late Cretaceous ages, when is widely recognized, an active subduction process related to Thethys closure, is evidenced from the marine sequences with a important basaltic input acting until early Paleocene. Such marine deposits and its arc related deep basaltic sequences are most known as the CLIP.

The thermal overprint produced by the CLIP accretion annealed the fission track systems preserving exclusively the last orogenic event since the Eocene.

Models for Caribbean plate evolution involve the development of this proto Caribbean oceanic floor and its accretion against a continental South America. The main interest in Chapter 2 resides in the tectonic relationship between units that belong originally to the domain of the Caribbean plate (Santa Marta schists) and the continental basement

of the Inner Santa Marta Metamorphic Belt. For the contact between these two provinces, a suture has been discovered in the field and confirmed by geochronological data. Our results showed that this inherited discontinuities favor renewed thrusting and shear as the case of the Orihueca fault and the Sevilla lineament, and even can conduct crustal channeling exhuming the lower crust.

A major breakthrough of this work is the complete redefinition of the extent of the Caribbean accreted oceanic crust at the SNSM massif, which is confined only to the NW corner of the massif, as proven by geochronological data and field observations, metamorphic degree, deformations, and paragenesis. The metapelitic and metavolcanic sequences formerly associated to the Caribbean arc are underlain by ca. 280 Ma orthogneisses, implying a clear affinity with the continental margin in contradiction with the widely accepted Caribbean origin for these units. This new concept has major consequences in the magnitude of the subducted Caribbean slab; allowing understanding this process at the continental margin of the SNSM as a collision governed tectonics.

Collision and subduction failure are highly influenced by the consumption of a thickened oceanic crust composed by the plateau basaltic rocks and a thick sedimentary sequence of at least 6000 m, which is to be found at the Guajira Peninsula and the Western Cordillera of Colombia, but that was eroded by subduction at the portion of the continental margin that corresponds to the SNSM massif.

Collision favored a high temperature regime for the SNSM during the Cenozoic, and lower crustal weakening as well as increase on relief and hence accelerated exhumation rates at least until thermal maturity and crustal thickening.

It is likely that the SNSM had experienced these processes during its orogenic history with periods of crustal thickening and orogenic building followed by orogenic collapse and extension, and crustal delamination, as documented in this work this may had occurred during Pangæa amalgamation and during CLIP accretion.

In the most recent part of its history described at Chapter 3, strong plate coupling reactivated mid-crustal structures that controlled exhumation during the transient stages of the Caribbean plate towards the East. The Santa Marta Bucaramanga fault, a major fault inherited from Jurassic rift, suffered a normal sinistral strike slip activation due the establishment of a partitioned convergence between the Caribbean Plate and the Nor-Andean block. This process created enough subsidence for accommodating sediments and redistributed strain onto the continental margin causing the uplift and late exhumation of the Eastern Cordillera, the Santander Massif and the Merida Andes.

The perspectives for a future work on the SNSM involve a major expedition for acquiring samples from several elusive areas as the peaks of the glacial zones that may hold keys for the Neoproterozoic-Paleozoic history of the massif. It is clear that most of the research has been done in the vicinity to the most populated areas, and although it seems that the remnants of an Ordovician arc present further to the SE in the Merida Andes, Santander Massif, and Central Cordillera (Anacona terrane) is absent in the SNSM. This assumption has yet to be demonstrated, the relevance of these investigations is related with the regional correlations of the proto-Andean margin. In this same workflow it is fundamental to construct a more precise time frame for the metamorphic episodes, for which is necessary to perform geochronological dating in minerals as garnet, monazite, and mica using techniques as Lu-Hf and oxygen isotopes in mica by TIMS.

The author recommends as well investigating the active sediments integrating thermo-geochronology, further research needs a detailed hydrographic analysis and sampling on the river catchments for studying the erosive processes acting during the Neogene, this research may be aided by cosmogenic nuclide dating.

Arndt, N.T., 2013. The Formation and Evolution of the Continental Crust. Geochem. Perspect. 2, 405–405.

Beltrando, M., Rubatto, D., Manatschal, G., 2010. From passive margins to orogens: The link between ocean-continent transition zones and (ultra)high-pressure metamorphism. Geology 38, 559–562. doi:10.1130/G30768.1

Beltrán-Triviño, A., Winkler, W., von Quadt, A., Gallhofer, D., 2016. Triassic magmatism on the transition from Variscan to Alpine cycles: evidence from U–Pb, Hf, and geochemistry of detrital minerals. Swiss J. Geosci. doi:10.1007/s00015-016-0234-3

Condie, K.C., 2011. The Supercontinent Cycle, in: Earth as an Evolving Planetary System. Elsevier, pp. 317–355.

Franke, W., 2006. The Variscan orogen in Central Europe: construction and collapse. Geol. Soc. Lond. Mem. 32, 333–343. doi:10.1144/GSL.MEM.2006.032.01.20

Friedl, G., Finger, F., Paquette, J.-L., von Quadt, A., McNaughton, N.J., Fletcher, I.R., 2004. Pre-Variscan geological events in the Austrian part of the Bohemian Massif deduced from U–Pb zircon ages. Int. J. Earth Sci. 93, 802–823. doi:10.1007/s00531-004-0420-9

Hawkesworth, C.J., Dhuime, B., Pietranik, A.B., Cawood, P.A., Kemp, A.I.S., Storey, C.D., 2010. The generation and evolution of the continental crust. J. Geol. Soc. 167, 229–248. doi:10.1144/0016-76492009-072

Letsch, D., Winkler, W., Quadt, A. von, Gallhofer, D., 2015. The volcano-sedimentary evolution of a post-Variscan intramontane basin in the Swiss Alps (Glarus Verrucano) as revealed by zircon U–Pb age dating and Hf isotope geochemistry. Int. J. Earth Sci. 104, 123–145. doi:10.1007/s00531-014-1055-0

Mišković, A., Spikings, R.A., Chew, D.M., Košler, J., Ulianov, A., Schaltegger, U., 2009. Tectonomagmatic evolution of Western Amazonia: Geochemical characterization and zircon U-Pb geochronologic constraints from the Peruvian Eastern Cordilleran granitoids. Geol. Soc. Am. Bull. 121, 1298–1324. doi:10.1130/B26488.1

Nance, R.D., Gutiérrez-Alonso, G., Keppie, J.D., Linnemann, U., Murphy, J.B., Quesada, C., Strachan, R.A., Woodcock, N.H., 2012. A brief history of the Rheic Ocean. Geosci. Front. 3, 125–135. doi:10.1016/j.gsf.2011.11.008

Nance, R.D., Gutiérrez-Alonso, G., Keppie, J.D., Linnemann, U., Murphy, J.B., Quesada, C., Strachan, R.A., Woodcock, N.H., 2010. Evolution of the Rheic Ocean. Gondwana Res., The Rheic Ocean: Palaeozoic Evolution from Gondwana and Laurussia to Pangæa 17, 194–222. doi:10.1016/j.gr.2009.08.001

Nance, R.D., Murphy, J.B., Santosh, M., 2014. The supercontinent cycle: A retrospective essay. Gondwana Res. 25, 4–29. doi:10.1016/j.gr.2012.12.026

Runcorn, S.K., 1962. Convection Currents in the Earth's Mantle. Nature 195, 1248–1249. doi:10.1038/1951248a0

Sempere, T., Carlier, G., Soler, P., Fornari, M., Carlotto, V., Jacay, J., Arispe, O., Néraudeau, D., Cárdenas, J., Rosas, S., Jiménez, N., 2002. Late Permian–Middle Jurassic lithospheric thinning in Peru and Bolivia, and its bearing on Andean-age tectonics. Tectonophysics 345, 153–181. doi:10.1016/S0040-1951(01)00211-6

Vanderhaeghe, O., 2012. The thermal–mechanical evolution of crustal orogenic belts at convergent plate boundaries: A reappraisal of the orogenic cycle. J. Geodyn. 56–57, 124–145. doi:10.1016/j.jog.2011.10.004

Weber, B., Iriondo, A., Premo, W.R., Hecht, L., Schaaf, P., 2007. New insights into the history and origin of the southern Maya block, SE México: U–Pb–SHRIMP zircon geochronology from metamorphic rocks of the Chiapas massif. Int. J. Earth Sci. 96, 253–269. doi:10.1007/s00531-006-0093-7

ACKNOWLEDGMENTS

We started with this project on the Evolution of the Colombian Caribbean Margin in the 2011, since then there have been so many people that had contributed to the completion of this thesis. I have to say that I feel an enormous gratitude for having the opportunity to study the Sierra Nevada de Santa Marta and met among its inhabitants, generous and hard-working people that show the best of Colombians. I consider that this is one of the most amazing and magic places on the planet, and that possess a huge relevance in the cultural and historical backgrounds of the Colombian people as well as a biosphere reserve declared by UNESCO in 1979.

This research was funded by COLCIENCIAS, in the frame of the project "Evolución Tectónica del margen Caribeño Colombiano" which provided the resources for fieldwork, and sample analysis. This project was also supported by BQR Sud grant from ISTerre, Universite Grenoble Alpes. Geochronological analyses were done at the facilities of the ETH institute of Petrology and Geochemistry in Zurich. Midland Valley provided us Move ® Academic license for the construction of structural sections and 3D models presented in the chapters.

I had worked with Professor Andreas Kammer during my bachelor and master's at the Eastern Cordillera of Colombia, and suddenly one day we were redirecting our efforts to a new adventure: the Sierra Nevada de Santa Marta massif, the pioneers in this endeavor were Prof. Jean Francois Stephan director from the Institut national des Sciences de l'Universe (INSU - CNRS) and Dr Thomas Maurin from Geoazur at the Université Sophia Antípolis, together we enjoyed excellent journeys on field and shared good times in Santa Marta either at the Aracataca river, or the Tayrona park,

this first field trip ultimately induced me to start my PhD. These first explorations reveled an incredibly complex geology for us in that time and from the beginning, I felt that I seriously wanted to pursuit a research project in this area.

I want to thank Prof. Kammer for always guiding me along all this years, thanks for all the adventures and experiences, in the jungle, deserts and glaciers in all this places were we took a look of the rocks, sometimes with great efforts, but every time with great rewards!!

In the winter of 2012 our collaboration led to a stage at Nice, my deepest feelings of gratitude are directed to Michel Manetti who was the first person that introduced me to mineral separation techniques, and gave me some nice geological souvenirs from Corsica that remain as favorite samples from my collection. Moreover, with Prof. Bernard Mercier de Lepinay and Flore Barat we discussed very interesting aims in the Northern Andes. At Geneva Diego Villagómez received and helped me in mounting apatites with great patience and expertise, even with his multiple responsibilities, he separated some time for this purpose.

I first met Prof. Matthias Bernet in 2012 and since our first reunion, he showed great interest in our investigations on the Caribbean realm, from there we started a cooperation the ultimately led to a cotutelle convention between the Universidad Nacional de Colombia and the Université Grenoble Alpes, thank you so much for your help during all the stages of this work and your commitment, every time I was worried you made me feel confident to keep working and advancing, for you intervention it was possible to me to apply to Grenoble, where I found fantastic research possibilities and also adventures in the Alps were I had enjoyed most of my stage. Thanks to the fellows of ISTerre, Melanie and François who helped me in mounting and separating

minerals and the students Nathalie, Margarita, Thibaud, Clara, Gonzalo, Latifa, Ahmed, Cyril, Camille, Franz and Ellie for sharing a short but very nice time at Grenoble.

I want to express my gratitude especially to my friend Alejandro Beltrán, who encouraged me to enter to the world of U-Pb zircon geochronology, and also was with me in all my journeys to Zürich, day and night working, studying, cooking, and having some beers in time–to-time, thanks for your constant company and help. To the people of ETH Zürich especially Dr Albrecht Von Quadt who supported me in doing the U-Pb zircon dating, Marcel Guillong who taught me how to reduce and evaluate geochronological data, and Dr Giuditta Fellin who taught me the techniques on AHe dating, thank you all so much for your collaboration and guidance, I will always remember my stage in ETH as an incredible scientific experience.

To my companions form the Structural Geology Group at Universidad Nacional de Colombia my most sincere thanks, for helping me in the field and in the office with discussions, models, drawings interpretations and many good times together, to Miguel, Christian, Fabio, Jose and Carlos. And specially to Edna who was with me along my whole PhD doing her Master's, in the field and crushing rocks in the lab, counting fission tracks and picking zircons, thank you so much for your company and your help, and your beautiful way of being, your support and enthusiasm made everything better.

To the students and professors from the Geology department Universidad Nacional de Colombia who participated at the field campaigns on the Sierra Nevada de Santa Marta thank you for your hard work and countless field excursions in which we attempted to discover the geology in the Sierra Nevada, specially to Prof. Gustavo Sarmiento which participated in our first attempts to constrain palynological ages for the Neogene sediments we studied. Thank you for your notes drawings discussions and samples all

the material we gathered constitutes an archive for future geologists, and all of us contributed to build a new Geological map.

I want do dedicate this work to my friends Sebastían and Tomás, your departure in 2016 was a very difficult moment, and it grieves me so to write this particular line, but you must know that you belong in my memories, and I'll remember you.

Finally I want to thank my family for their support during my studies, Lucero Alejandro and Daniela, your thrust and love gave me all the energy and inspiration that I needed to finally get to this point since the start of this adventure many years ago and write this final words: thanks forever I love you all.

APPENDIX CHAPTER 1

TABLE A1. U, Pb AND Th ISOTOPIC DATA OBTAINED USING THE LA-ICP-MS METHOD

I.D.	Isotopic Ratios								Isotopic Ages								Parts per million (ppm)		
	$^{207}Pb/^{235}U$	±2σ	$^{206}Pb/^{238}U$	±2σ	Pb^{207}/Pb^{206}	±2σ	$^{208}Pb/^{232}U$	±2σ	$^{235}U/^{207}Pb$	±2σ	$^{238}U/^{206}Pb$	±2σ	$^{232}U/^{208}Pb$	±2σ	Pb^{207}/Pb^{206}	±2σ	^{238}U	^{232}Th	Th/U
AP-009																			
AP_09_1	1.433	0.036	0.1389	0.0022	0.0756	0.0019	0.0416	0.0041	902	15	**838.5**	13	824	80	1078	51	88.8	26.2	0.2950
AP_09_2	1.791	0.038	0.1762	0.0033	0.07389	0.0011	0.04775	0.0038	1042	14	**1046**	18	943	73	1038	29	1905	517	0.2714
AP_09_3	0.0541	0.0035	0.00811	0.00015	0.0481	0.003	0.00214	0.00039	53.4	3.4	**52.1**	0.95	43.2	7.9	100	120	266	28.5	0.1071
AP_09_4	0.201	0.017	0.02734	0.001	0.0501	0.0059	0.00947	0.0012	186	14	**173.9**	6.5	191	25	190	240	83.6	39.6	0.4737
AP_09_5	1.611	0.057	0.1659	0.003	0.0705	0.0026	0.0479	0.0047	972	22	**989**	17	945	90	938	75	30.7	13.92	0.4534
AP_09_6	1.718	0.048	0.1713	0.0027	0.0729	0.0021	0.0483	0.0048	1014	18	**1020.9**	16	953	92	1019	56	56.6	12.17	0.2150
AP_09_7	0.0523	0.0027	0.00818	0.00015	0.0462	0.0024	0.00298	0.00047	51.5	2.6	**52.53**	0.93	60.2	9.6	31	100	282.2	29.04	0.1029
AP_09_8	1.557	0.017	0.1604	0.0024	0.07035	0.00084	0.0464	0.0038	953.3	6.9	**959.1**	13	916	73	938	25	2170	83.2	0.0383
AP_09_9	0.0522	0.0028	0.00787	0.00015	0.0477	0.0026	0.00262	0.00048	51.6	2.7	**50.55**	0.97	53	9.6	110	110	401.1	37.1	0.0925
AP_09_10	0.0521	0.0025	0.00787	0.00014	0.0481	0.0024	0.00222	0.00022	51.5	2.4	**50.52**	0.89	48.5	4.5	109	100	545	242.1	0.4442
AP_09_11	0.0528	0.0037	0.008118	0.00013	0.0471	0.0033	0.00251	0.00031	52.2	3.5	**52.12**	0.83	50.6	6.3	70	130	213.9	92.9	0.4343
AP_09_12	0.0545	0.0039	0.00815	0.00016	0.0487	0.0034	0.00308	0.00039	53.8	3.7	**52.34**	1	62.1	7.9	120	140	232	41.41	0.1785
AP_09_13	2.2	0.031	0.1925	0.0029	0.08317	0.0012	0.0576	0.0047	1182.2	10	**1134.6**	16	1132	90	1272	27	332.3	202.1	0.6082
AP_09_14	0.0521	0.0042	0.0083	0.00021	0.0447	0.0034	0.00308	0.00046	51.5	4	**54.7**	1.4	62.1	9.2	-30	140	346.4	50.7	0.1464
AP_09_15	1.352	0.058	0.1364	0.0029	0.071	0.0025	0.0432	0.0035	868	25	**824**	17	855	69	955	72	281	137.6	0.4897
AP_09_16	0.0539	0.0071	0.008	0.00051	0.0477	0.0045	0.00242	0.0003	53.3	6.8	**51.4**	3.3	49	16	170	230	335	47.8	0.1427
AP_09_17	0.057	0.0052	0.00863	0.00019	0.0493	0.0045	0.00262	0.00048	56.9	4.8	**55.4**	1.2	53	9.7	170	170	128	29.6	0.2313
AP_09_18	1.851	0.06	0.1798	0.0039	0.0751	0.0021	0.0526	0.0046	1065	22	**1065**	21	1036	88	1062	57	49.3	27.5	0.5578
AP_09_19	0.1978	0.0071	0.03089	0.00073	0.0466	0.0018	0.0105	0.0031	183.3	6	**196.1**	4.6	210	63	36	79	320	16.43	0.0513
AP_09_20	1.514	0.025	0.1561	0.003	0.07062	0.00096	0.0453	0.0038	936	10	**935**	17	896	73	946	28	2361	190.2	0.0806
AP_09_21	2.472	0.061	0.2152	0.0053	0.08319	0.0013	0.062	0.0053	1263	18	**1256**	28	1215	100	1273	30	310	71.4	0.2303
AP_09_22	0.0524	0.0048	0.00789	0.00018	0.0477	0.0047	0.00272	0.00033	51.8	4.7	**50.6**	1.2	55	6.6	50	200	219	83.9	0.3831
AP_09_23	1.91	0.035	0.1836	0.0032	0.0751	0.0013	0.0529	0.0048	1086	13	**1086**	18	1042	91	1070	34	212.4	22.59	0.1064
AP_09_24	2.657	0.064	0.2275	0.0046	0.0838	0.0017	0.0682	0.006	1315	18	**1324**	23	1333	110	1299	41	109.9	28.4	0.2584
AP_09_25	0.0501	0.0037	0.00805	0.0002	0.0452	0.0037	0.00201	0.00046	50.5	3.2	**51.7**	1.3	40.5	9.3	-10	150	203	26.8	0.1320
AP_09_26	0.0571	0.0041	0.00829	0.00016	0.0505	0.0039	0.0028	0.00035	56.3	3.9	**53.2**	1	56.6	7	200	160	572	118	0.2063
AP_09_27	1.717	0.029	0.1708	0.0029	0.0732	0.0013	0.0514	0.0042	1014.3	11	**1016**	16	1014	81	1018	35	287	81.8	0.2850
AP_09_28	0.0524	0.0024	0.00811	0.00014	0.0471	0.0022	0.00257	0.00043	51.9	2.3	**52.09**	0.91	51.9	8.6	68	92	452	29.32	0.0649
AP_09_29	0.0499	0.0049	0.00805	0.00019	0.0436	0.0039	0.0024	0.00052	50.2	4.6	**51.7**	1.2	48.4	11	-40	170	93.7	26.9	0.2871
AP_09_30	2.373	0.033	0.2116	0.0032	0.08128	0.001	0.06301	0.005	1234.2	10	**1237**	17	1235	96	1230	26	453	201	0.4437
AP_09_31	0.0548	0.0051	0.00808	0.00026	0.0495	0.0052	0.00363	0.00096	54.2	4.9	**51.8**	1.7	73	19	170	220	486.8	41.7	0.0857
AP_09_32	1.465	0.059	0.1521	0.0041	0.0705	0.0029	0.041	0.0052	915	24	**912**	23	810	100	933	84	45.5	6.52	0.1433
AP_09_33	2.86	0.11	0.2405	0.0072	0.0879	0.0026	0.0633	0.0066	1380	26	**1389**	38	1240	120	1378	56	84.1	25.75	0.3062
AP_09_34	0.0521	0.0026	0.00806	0.00015	0.0473	0.0023	0.00243	0.00041	51.5	2.5	**51.74**	0.94	49.1	8.3	75	98	395	34.66	0.0877
AP_09_35	0.0571	0.0047	0.0082	0.00017	0.0504	0.004	0.00272	0.00051	56.3	4.5	**52.62**	1.1	54.9	10	200	160	226.6	38.4	0.1695
AP_09_36	0.0554	0.0048	0.00816	0.00018	0.0496	0.0043	0.00212	0.00053	54.7	4.6	**52.36**	1.1	43	11	190	180	234.7	17.99	0.0767
AP_09_37	0.0552	0.0052	0.00831	0.00021	0.0496	0.0049	0.0045	0.0011	54.5	5	**53.4**	1.3	91	22	160	190	269	16.2	0.0602
AP_09_38	1.55	0.037	0.158	0.003	0.0711	0.0017	0.0475	0.005	950	15	**946**	17	936	97	954	48	84.8	8.29	0.0978
AP_09_39	0.0529	0.0033	0.00827	0.0002	0.0466	0.0033	0.00255	0.00075	52.3	3.2	**53.1**	1.3	52	15	50	140	485	14.15	0.0292
AP_09_40	0.0529	0.0037	0.00821	0.00018	0.047	0.0034	0.0035	0.0014	52.3	3.5	**52.68**	1.2	70	27	60	140	355	7.9	0.0223
AP_09_41	0.0553	0.003	0.00817	0.00016	0.0502	0.0029	0.00272	0.00069	54.6	2.9	**52.45**	1.1	55	14	190	120	376	21.77	0.0579
AP_09_42	0.242	0.041	0.02932	0.00069	0.06	0.0099	0.0094	0.0015	219	34	**186.3**	4.3	188	30	550	370	46.4	27.5	0.5927
AP_09_43	2.207	0.049	0.2021	0.0043	0.0792	0.0014	0.0586	0.0057	1183	16	**1186**	23	1150	110	1177	35	419	57.8	0.1379
AP_09_44	0.0594	0.0098	0.00845	0.0002	0.0512	0.0088	0.0028	0.0013	58.5	9.4	**54.3**	1.3	56	26	220	340	182.1	14.37	0.0789
AP_09_45	1.758	0.065	0.1741	0.0034	0.072	0.0025	0.0527	0.01	1028	24	**1034**	19	1030	200	989	73	31.1	1.662	0.0534
AP_09_46	0.0549	0.0044	0.00809	0.0002	0.0497	0.0041	0.00241	0.00066	54.2	4.2	**51.9**	1.3	49	13	160	160	280.7	24.27	0.0865
AP_09_47	0.0587	0.0022	0.00876	0.00017	0.048	0.0021	0.00236	0.00025	57.9	2.1	**56.21**	1.1	47.7	5	102	90	662	204	0.3082
AP_09_48	0.266	0.034	0.0386	0.0011	0.0499	0.0058	0.0152	0.0024	238	27	**244.4**	7	305	47	170	230	28.62	14.63	0.5112
AP_09_49	1.509	0.052	0.1501	0.0026	0.0726	0.0024	0.0453	0.0042	934	21	**901.7**	14	895	81	1002	66	572.4	410	0.7163
AP_09_50	0.121	0.07	0.01081	0.001	0.078	0.041	0.009	0.0095	114	63	**69.3**	6.4	180	190	900	1100	59	2.8	0.0475
AP_09_51	0.235	0.026	0.0284	0.0012	0.0601	0.0076	0.009	0.0013	214	21	**180.6**	7.8	181	26	570	290	34.9	38	1.0888
AP_09_52	0.0543	0.0028	0.007997	0.00014	0.0501	0.0024	0.00258	0.00032	53.6	2.7	**51.34**	0.89	52	6.4	180	110	434.2	84.3	0.1942
AP_09_53	0.22	0.021	0.03072	0.00095	0.0517	0.0051	0.009	0.0033	201	18	**195.1**	5.9	181	66	240	200	66.4	5.5	0.0828
AP_09_54	0.0508	0.0042	0.00787	0.00017	0.0475	0.0039	0.00241	0.00055	50.2	4.1	**50.52**	1.1	49	11	80	160	229	24.3	0.1061
AP_09_55	0.0543	0.0047	0.00807	0.00018	0.0493	0.0044	0.00194	0.00036	53.6	4.5	**51.84**	1.1	39.2	7.2	140	170	250.4	37.39	0.1493
AP_09_56	0.0591	0.0033	0.0087	0.00018	0.0488	0.0029	0.00323	0.00064	58.3	3.2	**55.81**	1.2	65	13	130	120	313	27.4	0.0875
AP_09_57	1.673	0.029	0.1679	0.0031	0.07311	0.001	0.0437	0.0037	998.3	11	**1000**	17	864	71	1016	29	1227	112.1	0.0914
AP_09_58	1.493	0.033	0.1541	0.0026	0.0713	0.0014	0.0437	0.0036	929	13	**923.6**	14	863	69	963	40	179	90.93	0.5080
AP_09_59	0.0551	0.003	0.00806	0.00016	0.0499	0.0029	0.00264	0.00037	54.5	2.9	**51.78**	1	53.3	7.4	180	120	298	46.12	0.1548
AP_09_60	1.623	0.02	0.1608	0.0025	0.07317	0.00099	0.045	0.0037	979.1	7.8	**961.3**	14	890	71	1018	27	1829	301.4	0.1648
AP_09_61	1.676	0.022	0.1654	0.0026	0.07329	0.00092	0.0463	0.0044	999.4	8.5	**986.9**	15	914	85	1025	27	1500	20.2	0.0135
AP_09_62	0.0506	0.0031	0.00798	0.00019	0.045	0.0029	0.00264	0.00043	50	3	**51.2**	1.2	53.3	8.7	-20	120	295.4	31.4	0.1063
AP_09_63	1.302	0.048	0.1382	0.0043	0.0681	0.002	0.0403	0.004	846	21	**834**	24	798	78	870	61	140.6	48.7	0.3464
AP_09_64	0.0535	0.0019	0.00824	0.00015	0.0466	0.0016	0.00235	0.00048	52.9	1.8	**52.91**	0.94	47.4	9.6	33	71	737	17.5	0.0237
AP_09_65	1.226	0.035	0.1266	0.0025	0.069	0.0017	0.0376	0.0033	812	16	**768**	14	746	64	898	52	435	208.7	0.4798
AP_09_66	0.273	0.02	0.0391	0.0011	0.0497	0.0038	0.006	0.01	244	16	**247.4**	6.9	110	210	170	150	32.7	0.609	0.0186
AP_09_67	0.0493	0.0093	0.00889	0.00027	0.1201	0.0084	0.0196	0.0025	141.1	8.3	**57**	1.7	393	50	1990	150	278.8	23.25	0.0834
AP_09_68	0.0569	0.0031	0.00832	0.0002	0.0497	0.003	0.00362	0.00075	56.2	2.9	**53.4**	1.3	73	15	170	130	441	20	0.0454
AP_09_69	1.689	0.069	0.1726	0.0041	0.0709	0.003	0.054	0.013	1005	26	**1026**	23	1060	240	945	89	16.52	0.865	0.0524
AP_09_70	1.428	0.052	0.1448	0.0033	0.0717	0.0033	0.0393	0.0067	900	22	**872**	18	780	130	975	94	181.2	56.6	0.3124
AP_09_71	1.527	0.026	0.1563	0.0023	0.0711	0.0012	0.0468	0.0038	943	9.8	**936.4**	13	923	74	958	35	529	229	0.4329
AP_09_72	0.0706	0.0083	0.00808	0.00024	0.0644	0.0043	0.0075	0.0015	69.2	7.9	**51.9**	1.6	152	30	740	140	329	19.4	0.0590
AP_09_73	0.204	0.053	0.0291	0.0013	0.049	0.012	0.027	0.021	186	45	**185.2**	7.9	530	420	130	450	20.7	0.723	0.0349
AP_09_74	2.355	0.039	0.2086	0.0034	0.08153	0.0013	0.0594	0.0049	1229	12	**1221**	18	1167	93	1239	33	276	73.3	0.2656
AP_09_75	0.532	0.017	0.0629	0.0017	0.0613	0.0012	0.0185	0.003	433	11	**393**	10	371	59	647	42	1240	14.99	0.0121
AP_09_76	0.0499	0.0023	0.00783	0.00018	0.0462	0.002	0.00306	0.00079	49.4	2.3	**50.26**	1.2	62	16	30	85	553	31.5	0.0570
AP_09_77	0.0559	0.0033	0.00805	0.00014	0.0505	0.0029	0.00268	0.00031	55.2	3.2	**51.68**	0.92	54	6.3	230	120	258.3	89.2	0.3453
AP_09_78	1.409	0.033	0.1474	0.003	0.0694	0.0015	0.0461	0.0041	892	14	**886**	17	911	78	916	43	218.2	32.8	0.1503
AP_09_79	0.0533	0.0021	0.0082	0.00015	0.0469	0.0018	0.00231	0.00037	52.7	2.1	**52.62**	0.98	46.6	7.5	57	76	894	46.6	0.0521
AP_09_80	1.938	0.062	0.1856	0.0046	0.0753	0.0021	0.0531	0.0047	1098	23	**1097**	25	1045	90	1073	56	139.5	80.8	0.5792
AP_09_81	0.414	0.074	0.0482	0.0018	0.062	0.01	0.0211	0.0035	350	53	**304**	11	422	70	640	370	78.6	13	0.1654
AP_09_82	2.287	0.067	0.2064	0.0036	0.0802	0.0022	0.0616	0.0059	1206	21	**1209**	19	1208	110	1202	46	46	14.26	0.3100
AP_09_83	1.711	0.04	0.1666	0.0031	0.0738	0.0018	0.0475	0.0048	1012	15	**993**	17	938	93	1050	45	92.2	15.36	0.1666
AP_09_84	0.0746	0.0095	0.00822	0.00034	0.0659	0.0076	0.0064	0.0014	72.9	9	**52.7**	2.2	129	29	740	240	180.6	28.2	0.1561
AP_09_85	0.1498	0.0094	0.00878	0.0002	0.1256	0.0075	0.0529	0.0049	141.6	8.3	**56.3**	1.3	1042	95	2054	94	1018	35.5	0.0349
AP_09_86	1.626	0.044	0.1646	0.0029	0.0719	0.0019	0.0449	0.0045	979	17	**982**	16	888	87	975	55	46.1	11.8	0.2560
AP_09_87	0.0539	0.0021	0.00797	0.00014	0.0495	0.0018	0.00208	0.00049	53.3	2	**51.19**	0.93	58.2	9.9	157	80	837.8	57.8	0.0705
AP_09_88	0.284	0.012	0.04052	0.00069	0.0509	0.0022	0.01334	0.0014	253.2	9.8	**256**	4.3	268	28	224	92	98.9	28.11	0.2842
AP_09_89	0.982	0.06	0.1053	0.0034	0.0662	0.0018	0.0396	0.005	694	30	**645**	20	784	97	812	56	93.6	31.19	0.3332
AP_09_90	0.0511	0.0018	0.00784	0.00013	0.047	0.0017	0.00259	0.00039	50.6	1.7	**50.35**	0.83	52.2	7.9	63	75	1040	57.8	0.0556
AP_09_91	0.0536	0.0026	0.0082	0.00015	0.0476	0.0026	0.00278	0.0006	53	2.5	**52.62**	0.95	56	12	110	110	378	18.9	0.0500
AP_09_92	1.63	0.15	0.1587	0.0044	0.0742	0.0078	0.042	0.019	975	58	**957**	28	950	430	1000	220	25.25	1.16	0.0459
AP_09_93	1.777	0.042	0.1735	0.0036	0.07489	0.0012	0.0473	0.007	1041	14	**1031**	20	940	140	1065	33	2334	12.42	0.0053
AP_09_94	1.565	0.044	0.154	0.0035	0.0738	0.0028	0.0538	0.0079	956	18	**923**	19	1060	150	1059	61	66.4	19.14	0.2883
AP_09_95	0.0707	0.0077	0.00815	0.00022	0.0627	0.0055	0.0227	0.0068	69.2	7.1	**52.3**	1.4	450	130	660	150	5130	85.2	0.0166
AP_09_96	0.0508	0.0025	0.007669	0.00014	0.0484	0.0026	0.00262	0.0003	50.3	2.4	**49.25**	0.87	52.8	6	140	110	583	116.1	0.1991
AP_09_97	1.38	0.21	0.1253	0.0049	0.08	0.01	0.064	0.017	875	88	**761**	28	1250	330	1260	200	9.35	1.25	0.1337
AP_09_98	0.0574	0.0042	0.00846	0.00024	0.0494	0.0037	0.00332	0.00079	56.6	4.1	**54.3**	1.6	65	16	150	150	243	19.74	0.0812
AP_09_99	0.028	0.028	0.17	0.0027	0.07328	0.0012	0.04913	0.0039	1011.5	11	**1012.1**	15	969	76	1024	34	219	484	2.2100
AP_09_100	0.0537	0.0024	0.00819	0.00015	0.048	0.0024	0.00249	0.00055	53.1	2.3	**52.59**	0.94	50	11	104	100	388	16.61	0.0428
AP_09_101	1.384	0.046	0.1376	0.0038	0.0747	0.0024	0.0414	0.0036	882	20	**831**	22	820	69	1056	64	219.9	71.6	0.3256
AP_09_102	1.462	0.063	0.148	0.0023	0.0714	0.0033	0.0429	0.0046	915	26	**889.9**	13	849	85	966	96	641.2	205.4	0.3203
AP_09_103	0.0712	0.0052	0.00774	0.00015	0.0649	0.004	0.0066	0.0011	69.8	4.9	**49.73**	0.98	133	23	750	130	1532	118.4	0.0773
AP_09_104	1.668	0.031	0.1644	0.0027	0.0737	0.0013	0.0506	0.0044	998	11	**981**	15	997	85	1036	35	192.7	32.63	0.1693
AP_09_105	0.0515	0.0032	0.00813	0.00018	0.0462	0.003	0.00255	0.00038	51	3.1	**52.21**	1.2	51.4	7.7	30	120	176.7	59.2	0.3350
AP_09_106	0.0545	0.005	0.00832	0.00033	0.0459	0.0036	0.00283	0.00059	53.8	4.8	**53.4**	2.1	57	12	10	140	193	27.8	0.1440
AP_09_107	1.872	0.051	0.1787	0.0039	0.0758	0.0017	0.0458	0.0038	1071	18	**1060**	21	905	74	1088	45	141.3	85.2	0.6030
AP_09_108	0.0608	0.0041	0.00804	0.00017	0.055	0.0034	0.00374	0.0006	59.9	3.9	**51.63**	1.1	75	12	430	120	459	64.7	0.1410
AP_09_109	0.0548	0.0035	0.00815	0.00016	0.0488	0.0031	0.0029	0.00073	54.1	3.4	**52.32**	1	58	15	110	130	292	12.63	0.0433
AP_09_110	1.367	0.054	0.1442	0.0026	0.0693	0.0025	0.0489	0.005	874	23	**869**	15	966	96	904	75	273.1	73.5	0.2691
AP_09_111	1.603	0.031	0.1618	0.003	0.0723	0.0013	0.051	0.0044	971	12	**967**	16	1006	84	992	38	127.9	34.3	0.2682
AP_09_112	1.344	0.028	0.1426	0.0024	0.0686	0.0014	0.0428	0.004	865	12	**859.5**	14	847	77	885	43	257	70.2	0.2732
AP_09_113	1.895	0.067	0.1675	0.0035	0.0829	0.038	0.0771	0.011	1078	24	**998**	19	1500	210	1257	88	51.5	12.51	0.2429
AP_09_114	0.0497	0.0031	0.00773	0.00016	0.0461	0.0027	0.0025	0.00039	49.2	3	**49.66**	1	50.4	7.8	30	110	236	49.1	0.2081
AP_09_115	2.008	0.068	0.1912	0.0042	0.0764	0.0023	0.062	0.0087	1117	23	**1128**	23	1240	170	1114	65	34.1	4.24	0.1243
AP_09_116	0.0541	0.0024	0.00808	0.00015	0.048	0.0022	0.00216	0.00043	53.4	2.3	**51.9**	0.96	43.5	8.7	110	94	642	25.7	0.0400
AP_09_117	0.0523	0.0013	0.00801	0.00015	0.0474	0.0014	0.00236	0.00033	51.8	1.3	**51.45**	0.93	47.6	6.6	68	62	911	59.1	0.0649
AP_09_118	1.457	0.095	0.1524	0.0054	0.0682	0.0036	0.0459	0.0092	909	39	**914**	30	900	180	890	130	13.76	2.47	0.1795
AP_09_119	2.039	0.039	0.1908	0.003	0.0775	0.0014	0.0554	0.0045	1128	13	**1126**	16	1090	86	1138	37	261	219.3	0.8402
AP_09_120	0.0489	0.0023	0.007747	0.00014	0.0465	0.0021	0.0022	0.00038	48.4	2.2	**49.75**	0.88	44.4	7.6	40	88	480	51.9	0.1081
AP_09_121	0.0544	0.0045	0.0081	0.00018	0.0487	0.0038	0.00272	0.00058	53.8	4.3	**51.99**	1.2	55	12	120	150	199.8	34.7	0.1737
AP_09_122	1.489	0.043	0.1533	0.0026	0.0712	0.0021	0.044	0.0037	924	18	**919**	15	869	72	960	59	50.7	42.17	0.8318
AP_09_123	0.0556	0.0039	0.00816	0.00018	0.0496	0.0036	0.00254	0.00079	54.9	3.8	**52.36**	1.1	51	16	210	140	162.2	11.59	0.0719
AP_09_124	1.395	0.031	0.1461	0.0024	0.0698	0.0015	0.043	0.0036	886	13	**878.9**	14	850	70	918	46	119.2	59.1	0.4958
AP_09_125	1.501	0.07	0.1487	0.0039	0.0731	0.0035	0.0428	0.0056	930	29	**894**	22	847	110	1012	99	141.9	33.8	0.2382
AP_09_126	0.0531	0.0032	0.00809	0.00014	0.0465	0.0026	0.0021	0.00053	52.5	3.1	**51.95**	0.91	42	11	80	120	377	15.5	0.0411
AP_09_127	1.279	0.048	0.138	0.0025	0.0665	0.0021	0.0401	0.004	836	21	**833**	14	795	78	840	76	276	96.4	0.3493
AP_09_128	1.377	0.054	0.1453	0.0028	0.0695	0.0023	0.0443	0.0038	878	23	**875**	16	876	74	920	72	70.1	42.8	0.6106
AP_09_129	0.052	0.0017	0.007992	0.00012	0.047	0.0015	0.00251	0.00026	51.5	1.6	**51.32**	0.8	50.6	5.3	60	63	1128	142.6	0.1264
AP_09_130	0.0908	0.0062	0.00812	0.00018	0.0812	0.0049	0.0202	0.0029	88.2	5.8	**52.12**	1.1	405	56	1200	120

AP-010 - 42	1.07	0.15	0.1112	0.0051	0.0697	0.0098	0.045	0.0092	730	70	**680**	**30**	890	180	850	270	18.73	3.06	0.1634
AP-010 - 43	1.966	0.086	0.1815	0.0047	0.0785	0.002	0.0557	0.0042	1103	29	**1075**	**26**	1095	80	1155	52	329.6	192.6	0.5843
AP-010 - 44	1.29	0.11	0.139	0.0044	0.0678	0.0058	0.057	0.013	836	50	**839**	**25**	1110	240	800	190	16.7	2.3	0.1377
AP-010 - 45	2.072	0.071	0.189	0.0063	0.0798	0.0017	0.0574	0.0099	1139	23	**1116**	**34**	1130	190	1189	43	443	7.68	0.0173
AP-010 - 46	1.49	0.12	0.1538	0.005	0.0707	0.0068	0.04	0.012	924	51	**922**	**28**	790	220	920	200	25.48	3.04	0.1193
AP-010 - 47	3.61	0.14	0.2463	0.0062	0.1063	0.002	0.0724	0.0055	1549	31	**1419**	**32**	1412	100	1732	34	394	146	0.3706
AP-010 - 48	1.72	0.14	0.1637	0.005	0.0764	0.0056	0.0445	0.0098	1007	53	**977**	**28**	870	190	1050	150	11.91	1.5	0.1259
AP-010 - 49	1.542	0.072	0.1531	0.0036	0.0722	0.0027	0.0506	0.0065	945	28	**918**	**20**	1000	130	1003	85	51.4	11.75	0.2286
AP-010 - 50	1.626	0.091	0.1588	0.0052	0.0744	0.0032	0.0569	0.0089	977	35	**950**	**29**	1110	170	1033	88	26.56	4.8	0.1802
AP-010 - 51	1.665	0.047	0.1589	0.0031	0.076	0.001	0.0509	0.0055	995	18	**951**	**17**	1002	110	1093	27	338	9.48	0.0280
AP-010 - 52	0.8	0.14	0.0865	0.0043	0.066	0.01	0.0184	0.0096	587	82	**535**	**25**	370	190	740	330	17.8	3.27	0.1837
AP-010 - 53	1.699	0.045	0.163	0.0034	0.0754	0.0011	0.0479	0.0042	1007.6	17	**973**	**19**	944	81	1075	29	673	20.4	0.0303
AP-010 - 54	1.5	0.082	0.1553	0.0041	0.0702	0.0034	0.048	0.0065	925	34	**930**	**23**	940	130	925	94	20.9	3.67	0.1756
AP-010 - 55	1.56	0.12	0.1587	0.0046	0.0702	0.0046	0.0478	0.01	943	48	**949**	**26**	940	190	900	150	9.58	1.222	0.1276
AP-010 - 56	2.05	0.066	0.1874	0.0049	0.0794	0.0021	0.0552	0.0042	1132	22	**1107**	**27**	1086	81	1180	55	345.9	153.4	0.4435
AP-010 - 57	1.66	0.14	0.168	0.0053	0.0724	0.0063	0.074	0.014	978	56	**1000**	**29**	1490	280	900	190	9.6	1.194	0.1244
AP-010 - 58	1.386	0.083	0.143	0.0046	0.0703	0.0033	0.0407	0.0049	881	35	**861**	**26**	805	95	923	98	95.5	30.1	0.3152
AP-010 - 59	0.228	0.032	0.0321	0.0029	0.0521	0.0054	0.01153	0.0014	207	26	**204**	**18**	232	28	280	220	304	87	0.2862
AP-010 - 60	1.443	0.041	0.1374	0.0025	0.0763	0.0012	0.0422	0.0045	906	17	**829.6**	**14**	834	86	1099	31	567	14.8	0.0261
AP-010 - 61	2.025	0.095	0.1852	0.0054	0.0795	0.0031	0.0553	0.005	1122	32	**1095**	**29**	1086	96	1172	81	54.7	37.4	0.6837
AP-010 - 62	1.448	0.04	0.145	0.0029	0.07256	0.00083	0.0441	0.0035	909	17	**873**	**16**	871	68	1000	23	1970	64.1	0.0325
AP-010 - 63	2.14	0.15	0.1893	0.0054	0.0826	0.0061	0.0642	0.0085	1150	50	**1117**	**29**	1250	160	1190	140	11.31	3.53	0.3121
AP-010 - 64	1.7	0.12	0.1672	0.0058	0.0739	0.0045	0.0509	0.0096	999	43	**996**	**32**	990	180	990	120	11.28	1.64	0.1454
AP-010 - 65	1.707	0.078	0.1677	0.0051	0.0748	0.0023	0.0529	0.0093	1014	27	**999**	**28**	1030	180	1050	63	28.6	2.6	0.0909
AP-010 - 66	2.02	0.061	0.1838	0.0039	0.0799	0.0011	0.0563	0.0042	1122	21	**1087**	**21**	1108	81	1193	28	389	166.1	0.4270
AP-010 - 67	1.6	0.13	0.1626	0.0057	0.0714	0.005	0.046	0.011	958	51	**971**	**32**	910	200	940	130	10.08	1.467	0.1455
AP-010 - 68	1.581	0.05	0.1537	0.0033	0.0747	0.0013	0.0462	0.0048	962	20	**922**	**18**	911	92	1057	34	479	18.4	0.0384
AP-010 - 69	1.33	0.16	0.133	0.0074	0.0727	0.0089	0.054	0.015	853	69	**805**	**42**	1060	290	970	250	19.9	5.79	0.2910
AP-010 - 70	2.091	0.064	0.1922	0.0043	0.079	0.0013	0.0707	0.0077	1145	21	**1133**	**23**	1380	140	1169	33	330	36.9	0.1118
AP-010 - 71	0.216	0.018	0.0315	0.0016	0.0501	0.0036	0.016	0.011	198	15	**199.8**	**9.8**	320	210	190	150	102.7	2.46	0.0240
AP-010 - 72	1.701	0.057	0.1644	0.0049	0.0754	0.0016	0.0484	0.0072	1008	21	**981**	**27**	950	140	1077	42	786	13.11	0.0167
AP-010 - 73	1.58	0.13	0.1612	0.0056	0.0716	0.0056	0.067	0.016	950	52	**963**	**31**	1280	300	880	170	9.42	1.087	0.1154
AP-010 - 74	1.963	0.092	0.1856	0.0064	0.0768	0.0021	0.054	0.0048	1099	33	**1097**	**35**	1062	92	1120	51	88	26.7	0.3034
AP-010 - 75	1.65	0.13	0.1619	0.0048	0.0745	0.006	0.057	0.012	990	47	**967**	**27**	1110	230	1010	150	9.61	1.065	0.1108
AP-010 - 76	1.669	0.11	0.1679	0.0059	0.0724	0.0038	0.0356	0.0077	989	39	**1000**	**32**	700	150	982	98	11.02	1.67	0.1515
AP-010 - 77	1.547	0.088	0.1531	0.004	0.0734	0.0041	0.0445	0.0062	948	35	**919**	**22**	880	120	1020	110	167	43.7	0.2617
AP-010 - 78	1.446	0.096	0.1478	0.0042	0.0715	0.0047	0.049	0.012	901	40	**888**	**23**	960	230	910	140	10.8	1.43	0.1324
AP-010 - 79	1.48	0.11	0.1492	0.0051	0.0728	0.0055	0.057	0.013	913	45	**896**	**29**	1100	240	930	150	11.1	1.53	0.1378
AP-010 - 80	1.739	0.09	0.1662	0.0044	0.0767	0.004	0.0564	0.0074	1026	37	**991**	**24**	1110	140	1080	110	20.78	3.88	0.1867
AP-010 - 81	1.172	0.071	0.1254	0.0054	0.0679	0.0043	0.0353	0.0043	787	33	**762**	**31**	701	84	860	130	381	16.9	0.0444
AP-010 - 82	1.574	0.086	0.1588	0.0043	0.0725	0.0042	0.0477	0.0063	955	34	**949**	**24**	940	120	950	120	17.7	4.5	0.2542
AP-010 - 83	1.59	0.11	0.1636	0.0045	0.0709	0.0045	0.0531	0.0088	959	43	**976**	**25**	1040	170	890	140	13.41	2.24	0.1670
AP-010 - 84	1.55	0.11	0.1596	0.0049	0.0708	0.0046	0.0532	0.0095	941	44	**954**	**27**	1040	180	890	140	12.71	2.15	0.1692
AP-010 - 85	1.597	0.043	0.156	0.0031	0.07441	0.00099	0.047	0.0041	968.4	17	**935**	**17**	928	78	1050	27	779	23.9	0.0307
AP-010 - 86	1.267	0.096	0.1316	0.004	0.0682	0.0037	0.0433	0.0066	826	43	**797**	**23**	850	130	890	140	31.2	6.11	0.1958
AP-010 - 87	2.163	0.063	0.2	0.004	0.0787	0.0015	0.0607	0.0057	1168	20	**1175**	**22**	1190	110	1159	38	149.1	15.46	0.1037
AP-010 - 88	0.88	0.11	0.0978	0.0042	0.0654	0.0072	0.027	0.012	637	62	**602**	**25**	540	230	730	260	16.83	2.32	0.1378
AP-010 - 89	1.6	0.13	0.1649	0.0056	0.0718	0.0069	0.068	0.014	957	53	**983**	**31**	1320	270	860	200	11.16	1.34	0.1201
AP-010 - 90	1.388	0.094	0.141	0.0034	0.0711	0.0044	0.047	0.011	876	41	**850**	**19**	920	200	900	140	16.2	1.87	0.1154
AP-010 - 91	1.859	0.069	0.1711	0.0041	0.0791	0.0019	0.0607	0.0055	1064	25	**1018**	**23**	1190	97	1167	47	90	26	0.2889
AP-010 - 92	1.405	0.073	0.1438	0.0042	0.0713	0.0036	0.0411	0.0059	888	32	**866**	**24**	810	110	940	110	34.1	9.75	0.2859
AP-010 - 93	2.332	0.075	0.2084	0.0047	0.0814	0.0015	0.0679	0.0061	1220	23	**1220**	**25**	1327	110	1225	37	209	23.2	0.1110
AP-010 - 94	0.657	0.064	0.0654	0.0021	0.0731	0.0068	0.04	0.011	507	38	**408**	**13**	780	220	930	190	20.4	2.04	0.1000
AP-010 - 95	1.96	0.063	0.1835	0.0042	0.0778	0.0015	0.055	0.0041	1101	22	**1086**	**23**	1082	79	1139	37	511	454	0.8885
AP-010 - 96	1.55	0.17	0.174	0.011	0.0654	0.0079	0.053	0.018	945	72	**1035**	**60**	1040	350	730	280	13.2	2.08	0.1576
AP-010 - 97	1.65	0.13	0.1623	0.0053	0.0735	0.0046	0.0463	0.0086	977	50	**969**	**30**	910	170	970	140	11.32	1.84	0.1625
AP-010 - 98	1.251	0.082	0.1253	0.0039	0.0711	0.0039	0.0428	0.0043	821	37	**761**	**23**	847	84	980	140	70	42	0.6000
AP-010 - 99	1.759	0.079	0.1735	0.004	0.0737	0.0025	0.0511	0.0075	1027	29	**1031**	**22**	1000	140	1016	69	53.6	3.64	0.0679
AP-010 - 100	1.556	0.1	0.154	0.0043	0.0735	0.0044	0.0629	0.011	945	41	**923**	**24**	1220	200	980	130	15.49	1.791	0.1156
AP-010 - 101	1.85	0.14	0.1765	0.0063	0.0762	0.0049	0.063	0.011	1051	49	**1047**	**35**	1230	210	1040	140	12.18	2.11	0.1732
AP-010 - 102	1.499	0.074	0.1515	0.0042	0.0731	0.0036	0.0444	0.0077	933	33	**909**	**24**	870	150	982	99	21.26	2.81	0.1322
AP-010 - 103	1.666	0.1	0.1631	0.0046	0.0744	0.0042	0.053	0.013	988	41	**973**	**26**	1030	240	1000	120	10.73	1.467	0.1367
AP-010 - 104	1.84	0.11	0.1844	0.0051	0.0726	0.0036	0.0539	0.0043	1053	39	**1090**	**28**	1061	82	970	100	24	61.7	2.5708
AP-010 - 105	1.346	0.069	0.1379	0.0039	0.071	0.0035	0.0413	0.0035	864	31	**833**	**22**	818	68	940	110	113.4	25.6	0.2257
AP-010 - 106	1.597	0.1	0.1659	0.0054	0.0701	0.0039	0.054	0.011	961	40	**989**	**30**	1110	220	890	120	11.85	1.509	0.1273
AP-010 - 107	2.062	0.06	0.1904	0.0038	0.0787	0.0014	0.05728	0.0041	1136	20	**1124**	**20**	1126	78	1162	36	390	341	0.8744
AP-010 - 108	1.718	0.099	0.1648	0.0041	0.0752	0.0043	0.0518	0.0067	1010	36	**983**	**23**	1020	130	1040	110	20	3.69	0.1845
AP-010 - 109	1.849	0.064	0.1778	0.004	0.0752	0.0015	0.0515	0.0044	1061	23	**1055**	**22**	1015	85	1069	42	87.4	35.13	0.4019
AP-010 - 110	1.256	0.068	0.1239	0.0033	0.0742	0.0041	0.0405	0.0069	822	31	**753**	**19**	800	130	1000	120	18.85	2.56	0.1358
AP-010 - 111	2.264	0.077	0.2012	0.0054	0.0819	0.0016	0.0591	0.0048	1200	24	**1181**	**29**	1161	92	1241	39	180	86.3	0.4794
AP-010 - 112	1.412	0.068	0.1393	0.004	0.0729	0.0021	0.0435	0.0043	891	28	**840**	**22**	861	82	1002	57	153	31.6	0.2065
AP-010 - 113	1.72	0.15	0.162	0.0088	0.0776	0.0058	0.0494	0.0056	1015	57	**968**	**49**	974	110	1130	150	88.6	131.7	1.4865
AP-010 - 114	1.816	0.066	0.1742	0.0044	0.0758	0.0019	0.0514	0.0042	1049	24	**1035**	**24**	1013	81	1082	49	159	91	0.5723
AP-010 - 115	2.096	0.081	0.1944	0.0048	0.0785	0.0022	0.0588	0.0048	1145	26	**1145**	**26**	1154	92	1148	53	67.9	42	0.6186
AP-010 - 116	1.587	0.066	0.1599	0.0037	0.0724	0.0027	0.0503	0.0055	963	26	**956**	**21**	990	110	976	79	40	7.89	0.1973
AP-010 - 117	1.61	0.11	0.1591	0.0053	0.074	0.0048	0.0533	0.0078	965	44	**951**	**30**	1050	150	980	150	17.47	4.05	0.2318
AP-010 - 118	1.67	0.15	0.1716	0.0056	0.0708	0.0057	0.0548	0.0063	989	57	**1021**	**31**	1078	120	900	170	19.94	11.41	0.5722
AP-010 - 119	1.896	0.057	0.1751	0.0044	0.0793	0.0012	0.0606	0.0045	1079	20	**1040**	**24**	1188	86	1178	30	548	189.5	0.3458
AP-010 - 120	1.768	0.089	0.1684	0.0058	0.0767	0.0035	0.048	0.0043	1031	32	**1003**	**32**	947	82	1092	99	44.9	33.2	0.7394
AP-010 - 121	38	2.8	0.301	0.019	0.899	0.046	18.1	4.4	3696	71	**1692**	**93**	5.50E+04	4.90E+03	5190	100	1.345	0.065	0.0483
AP-010 - 122	1.62	0.15	0.1593	0.0055	0.0756	0.0067	0.054	0.012	973	61	**952**	**31**	1040	230	980	190	8.78	1.208	0.1376
AP-010 - 123	1.815	0.052	0.1761	0.004	0.075	0.0014	0.0516	0.0059	1050	19	**1045**	**22**	1015	110	1065	37	229	9.35	0.0408
AP-010 - 124	1.65	0.11	0.1658	0.005	0.073	0.0051	0.059	0.013	982	43	**994**	**25**	1150	250	950	140	9.52	1.19	0.1250
AP-010 - 125	1.48	0.1	0.1525	0.0059	0.0709	0.0054	0.057	0.015	915	43	**914**	**33**	1110	290	900	150	14.74	1.94	0.1316
AP-010 - 126	0.311	0.034	0.0409	0.0014	0.055	0.0053	0.0149	0.0046	271	26	**258.1**	**8.7**	297	91	340	190	26.2	2.46	0.0939
AP-010 - 127	3.204	0.092	0.2524	0.0059	0.093	0.0019	0.0768	0.0062	1457	22	**1450**	**30**	1493	120	1482	38	64.1	27.6	0.4306
AP-010 - 128	0.746	0.038	0.0888	0.0026	0.0612	0.0024	0.0353	0.0059	566	22	**549**	**15**	700	110	640	81	122.7	11.48	0.0936
AP-010 - 129	1.864	0.069	0.1782	0.006	0.0762	0.0019	0.0557	0.0053	1068	24	**1056**	**33**	1095	100	1097	49	267	20.58	0.0771
AP-010 - 130	1.49	0.054	0.1485	0.0035	0.073	0.0014	0.0441	0.0043	926	22	**892**	**20**	871	84	1011	38	405.4	31.34	0.0773
AP-011																			
AP_011_1	1.767	0.087	0.1748	0.0041	0.0724	0.0036	0.0507	0.0051	1029	32	**1038**	**22**	998	97	990	110	17.99	8.59	0.4775
AP_011_2	1.69	0.12	0.1703	0.0052	0.0737	0.0061	0.0501	0.0082	1005	48	**1013**	**29**	980	160	1020	170	10.24	2.66	0.2598
AP_011_3	1.513	0.065	0.1559	0.0042	0.071	0.0027	0.0472	0.0046	939	25	**934**	**19**	932	89	982	77	43	22.5	0.5233
AP_011_4	1.642	0.05	0.1657	0.003	0.0725	0.0024	0.0457	0.0045	988	19	**989**	**17**	902	87	1011	66	35.8	14.2	0.3966
AP_011_5	1.641	0.057	0.1676	0.0032	0.0705	0.0022	0.0508	0.0045	985	22	**999**	**17**	1002	87	944	67	40.7	32	0.7862
AP_011_6	2.085	0.06	0.1936	0.0043	0.0767	0.002	0.055	0.0046	1142	20	**1140**	**23**	1082	88	1113	49	47.2	36.84	0.7805
AP_011_7	2.01	0.33	0.1651	0.007	0.084	0.013	0.075	0.014	1100	110	**985**	**39**	1450	260	1330	370	7.66	1.88	0.2454
AP_011_8	1.56	0.1	0.1584	0.0036	0.0716	0.0049	0.047	0.0051	946	41	**948**	**20**	928	99	960	130	13.46	7.61	0.5654
AP_011_9	1.608	0.076	0.1654	0.0044	0.0714	0.0034	0.0501	0.0066	978	27	**987**	**24**	990	130	951	99	16.13	8.15	0.5053
AP_011_10	1.607	0.041	0.1619	0.0033	0.0718	0.002	0.0511	0.0044	972	16	**967**	**18**	1006	84	972	57	53.3	28.1	0.5272
AP_011_11	1.713	0.085	0.1705	0.0045	0.0722	0.0036	0.0514	0.0051	1009	32	**1015**	**25**	1013	98	1019	99	16.06	12.85	0.8001
AP_011_12	1.7	0.11	0.163	0.0054	0.0777	0.0053	0.0564	0.01	1011	44	**973**	**30**	1100	200	1100	140	9.39	2.56	0.2726
AP_011_13	1.601	0.044	0.1648	0.0031	0.071	0.002	05	0.0044	970	17	**983**	**17**	986	84	951	59	79.1	59.3	0.7497
AP_011_14	1.589	0.079	0.1555	0.0038	0.0742	0.0042	0.0491	0.0064	970	32	**932**	**21**	967	120	1020	120	20.53	6.68	0.3254
AP_011_15	1.766	0.093	0.1735	0.0042	0.0735	0.004	0.0547	0.0057	1027	35	**1031**	**23**	1075	110	1060	110	15.79	6.93	0.4389
AP_011_16	1.595	0.051	0.1619	0.0032	0.0712	0.0024	0.0482	0.0039	974	21	**967**	**18**	952	76	959	72	39.28	88.4	2.2505
AP_011_17	1.731	0.1	0.1723	0.0038	0.0724	0.0042	0.0518	0.0056	1019	36	**1025**	**21**	1019	110	990	120	11.34	7.4	0.6526
AP_011_18	1.78	0.11	0.1694	0.0048	0.076	0.0045	0.0527	0.0069	1032	41	**1008**	**26**	1040	130	1080	110	13.05	3.8	0.2912
AP_011_19	1.767	0.056	0.173	0.0052	0.074	0.0018	0.0532	0.0051	1033	21	**1029**	**28**	1047	98	1055	60	66.6	47.6	0.7147
AP_011_20	1.55	0.084	0.1602	0.004	0.0702	0.0036	0.0525	0.008	946	33	**957**	**22**	1030	150	910	110	12.29	3.462	0.2817
AP_011_21	2.42	0.12	0.2199	0.0069	0.0791	0.0039	0.0615	0.0051	1256	32	**1281**	**37**	1205	97	1164	99	31.2	26.5	0.8494
AP_011_22	1.92	0.16	0.1777	0.0058	0.0783	0.0058	0.0527	0.008	1081	54	**1054**	**32**	1040	150	1130	150	15.24	8.43	0.5531
AP_011_23	1.67	0.047	0.1685	0.0031	0.072	0.002	0.04914	0.004	998	17	**1004**	**17**	970	77	985	55	58.8	125	2.1259
AP_011_24	1.611	0.059	0.1632	0.0035	0.0718	0.0023	0.0513	0.0053	973	23	**975**	**20**	1011	100	970	67	32.26	16.06	0.4978
AP_011_25	1.821	0.041	0.1768	0.0031	0.0746	0.002	0.0547	0.0046	1055	14	**1050**	**17**	1077	89	1050	53	51.3	43.4	0.8460
AP_011_26	1.907	0.079	0.1852	0.0035	0.0734	0.0025	0.0542	0.0048	1081	28	**1095**	**19**	1067	92	1028	67	53.7	43.8	0.8156
AP_011_27	1.604	0.057	0.1633	0.0029	0.071	0.0023	0.0482	0.0044	969	23	**975**	**16**	951	86	956	71	30.7	21.4	0.6971
AP_011_28	1.865	0.092	0.1745	0.004	0.0777	0.0043	0.0515	0.0057	1069	31	**1037**	**22**	1015	110	1140	110	15.9	9.24	0.5811
AP_011_29	1.71	0.055	0.1692	0.0037	0.0737	0.0022	0.052	0.0047	1013	20	**1007**	**21**	1024	89	1032	58	58.8	35.7	0.6071
AP_011_30	2.151	0.072	0.197	0.0036	0.0792	0.0027	0.0579	0.0059	1166	22	**1159**	**19**	1137	110	1171	69	28.6	11.7	0.4091
AP_011_31	1.6	0.12	0.1683	0.0045	0.0691	0.0052	0.0488	0.0063	976	47	**1002**	**25**	961	120	920	150	9.25	4.56	0.4930
AP_011_32	1.78	0.17	0.1631	0.005	0.0798	0.0081	0.0576	0.01	1056	61	**973**	**28**	1130	200	1220	200	7.92	1.71	0.2159
AP_011_33	1.62	0.1	0.1642	0.0039	0.0717	0.0046	0.0488	0.0074	971	40	**980**	**21**	960	140	970	140	9.61	2.606	0.2712
AP_011_34	1.708	0.08	0.171	0.0067	0.0723	0.0024	0.0494	0.0058	1016	32	**1017**	**37**	974	110	1000	63	40.6	15.71	0.3869
AP_011_35	1.494	0.051	0.1533	0.003	0.0709	0.0029	0.0476	0.0045	930	22	**919**	**17**	940	86	953	80	44.9	25.1	0.5590
AP_011_36	1.643	0.071	0.1659	0.0037	0.0722	0.0034	0.0451	0.0053	988	26	**989**	**21**	903	110	1013	99	13.5	4.17	0.3089
AP_011_37	1.571	0.091	0.1562	0.0041	0.0724	0.0042	0.0424	0.0051	971	31	**940**	**22**	839	99	990	110	11.81	6.04	0.5114
AP_011_38	1.514	0.095	0.1614	0.0043	0.0702	0.0045	0.0512	0.007	941	39	**964**	**24**	1010	140	900	130	9.68	2.57	0.2655
AP_011_39	1.488	0.079	0.158	0.0039	0.0686	0.0038	0.0463	0.0046	922	32	**946**	**22**	914	88	880	120	31.4	20.9	0.6656
AP_011_40	1.453	0.078	0.1536	0.0031	0.0689	0.0038	0.0434	0.0055	917	29	**921**	**17**	858	110	910	110	19.69	12.55	0.6374
AP_011_41	1.532	0.088	0.1561	0.0012	0.07	0.0039	0.0489	0.0047	942	36	**935**	**18**	964	90	940	120	15.95	10.58	0.6633
AP_011_42	1.676	0.031	0.1663	0.003	0.07295	0.001	0.0494	0.0041	999	12	**992**	**17**	974	79	1015	30	691	63.6	0.0920
AP_011_43	1.519	0.039	0.1553	0.0025	0.0725	0.0019	0.0509	0.0052	937	16	**930.4**	**14**	1002	100	1004	59	211	11.5	0.0545
AP_011_44	1.72	0.12	0.1678	0.005	0.0748	0.0051	0.0474	0.0062	1014	44	**1004**	**27**	934	120	1050	140	8.56	3.61	0.4217
AP_011_45	1.471	0.051	0.1542	0.0026	0.0703	0.0023	0.0454	0.0039	920	20	**924.3**	**14**	897	76	925	69	37.4	20.18	0.5396
AP_011_46	1.461	0.027	0.151	0.0025	0.07024	0.0011	0.04626	0.0037	914	11	**906.5**	**14**	914	72	933	34	370	235.1	0.6354
AP_011_47	1.48	0.13	0.1553	0.0048	0.0692	0.007	0.05263	0.0042	921	54	**931**	**27**	1037	81	890	200	33.43	21.56	0.6330
AP_011_48	2.667

AP_011_107	3.15	0.21	0.182	0.0039	0.1258	0.0085	0.1187	0.013	1443	52	**1078**	**22**	2260	240	2050	120	9.47	4.17	0.4403
AP_011_108	1.524	0.03	0.1525	0.003	0.07289	0.0009	0.0453	0.0038	940	12	**915**	**17**	896	74	1010	25	1156	202	0.1747
AP_011_109	1.854	0.042	0.1753	0.0032	0.07698	0.0012	0.0526	0.0043	1064	15	**1041**	**18**	1036	83	1119	32	632	115	0.1800
AP_011_110	2.22	0.16	0.1915	0.0034	0.0844	0.0057	0.0606	0.0064	1184	50	**1129**	**18**	1189	120	1290	130	25.43	15.63	0.6146
AP_011_111	1.519	0.019	0.1562	0.0024	0.0708	0.00085	0.046	0.0038	937.7	7.6	**935.3**	**13**	910	73	951	25	1808	110.9	0.0613
AP_011_112	1.61	0.11	0.161	0.0041	0.0719	0.0047	0.0538	0.007	980	39	**962**	**23**	1060	130	1010	140	12.94	5.99	0.4629
AP_011_113	1.545	0.044	0.1577	0.0034	0.07152	0.0012	0.0565	0.005	948	18	**944**	**19**	1110	96	972	34	668	44.6	0.0668
AP_011_114	2.084	0.087	0.1898	0.0046	0.0787	0.0032	0.0542	0.0048	1141	29	**1125**	**23**	1067	93	1168	82	44	39.4	0.8955
AP_011_115	1.63	0.053	0.1601	0.0032	0.0734	0.0022	0.0481	0.0044	983	21	**957**	**18**	950	84	1023	63	35.2	15.88	0.4511
AP_011_116	1.9	0.15	0.1725	0.0057	0.0793	0.0059	0.0571	0.0087	1073	53	**1026**	**31**	1120	170	1130	150	12.74	3.28	0.2575
AP_011_117	1.663	0.052	0.1676	0.0034	0.0725	0.0022	0.0478	0.0041	993	19	**999**	**19**	943	80	988	60	35.1	22.86	0.6513
AP_011_118	2.46	0.26	0.1849	0.0083	0.0949	0.0079	0.0702	0.01	1270	83	**1093**	**45**	1378	190	1540	180	11.33	7.11	0.6275
AP_011_119	1.942	0.049	0.1873	0.0041	0.0745	0.0018	0.0545	0.0047	1094	17	**1107**	**22**	1073	89	1063	49	45.8	59.6	1.3013
AP_011_120	2.54	0.18	0.235	0.0075	0.0775	0.0052	0.0594	0.0096	1279	52	**1372**	**44**	1160	180	1120	130	28.7	11.78	0.4105
AP_011_121	1.565	0.077	0.1578	0.0043	0.072	0.0039	0.0412	0.0044	957	31	**944**	**24**	815	86	980	110	13.5	11.09	0.8215
AP_011_122	2.16	0.09	0.1984	0.0048	0.0788	0.0033	0.0612	0.0058	1169	30	**1166**	**26**	1200	110	1172	90	15.82	10.32	0.6523
AP_011_123	1.594	0.038	0.1634	0.0027	0.0707	0.0017	0.0504	0.0044	967	15	**975.5**	**15**	994	85	957	46	68.2	40.9	0.5997
AP_011_124	1.558	0.048	0.1608	0.0029	0.0711	0.0022	0.0468	0.0039	958	19	**961**	**19**	924	75	966	60	62.9	37.7	0.5994
AP_011_125	2.01	0.14	0.189	0.0057	0.0773	0.0056	0.0551	0.0055	1122	45	**1115**	**31**	1083	100	1070	150	7.8	3.65	0.4679
AP_011_126	1.661	0.077	0.1678	0.0057	0.0712	0.0019	0.0533	0.005	999	29	**999**	**32**	1048	96	954	55	90	23.7	0.2633
AP_011_127	1.734	0.053	0.1676	0.0027	0.0749	0.0022	0.0491	0.0041	1020	20	**998.9**	**15**	968	79	1058	60	102.1	132.6	1.2987
AP_011_128	1.527	0.069	0.1526	0.0024	0.0723	0.0032	0.0448	0.0042	946	27	**915.5**	**14**	885	81	995	91	29.79	13.54	0.4545
AP_011_129	1.578	0.075	0.1595	0.0034	0.0698	0.0033	0.0487	0.0046	967	29	**954**	**19**	960	89	948	100	18.7	11.86	0.6342
AP_011_130	1.582	0.06	0.1629	0.0031	0.0691	0.0025	0.0517	0.005	960	24	**975**	**18**	1019	95	895	79	21.2	11.5	0.5425
AP_011_131	1.67	0.068	0.1638	0.0031	0.0734	0.0028	0.0496	0.0054	994	26	**978**	**17**	977	100	1004	80	19.8	6.39	0.3227
AP_011_132	1.581	0.069	0.163	0.0032	0.0705	0.0032	0.0479	0.0041	964	28	**973**	**18**	946	78	964	95	20.33	44.7	2.1987
AP_011_133	1.801	0.026	0.1775	0.0027	0.07334	0.0011	0.0462	0.0039	1045.6	9.4	**1053.3**	**15**	913	75	1022	30	548	61.5	0.1122
AP_011_134	1.522	0.036	0.1544	0.0026	0.0719	0.0018	0.0475	0.0045	940	15	**925.5**	**14**	938	88	984	51	81	18.91	0.2335
AP_011_135	1.6	0.044	0.1624	0.0034	0.0716	0.0017	0.0468	0.004	969	17	**970**	**19**	924	77	968	47	109	69.9	0.6413
AP_011_136	1.72	0.052	0.1728	0.0034	0.0735	0.0023	0.0527	0.0045	1021	20	**1027**	**19**	1037	87	1024	66	27.2	31.19	1.1467
AP_011_137	2.01	0.088	0.1919	0.0057	0.0774	0.0021	0.0587	0.0058	1114	30	**1131**	**31**	1163	120	1122	55	40.3	26.3	0.6526
AP_011_138	1.652	0.043	0.1683	0.0028	0.0715	0.002	0.0479	0.0046	990	17	**1003**	**16**	945	88	964	57	82.84	33.92	0.4095
AP_011_139	1.67	0.094	0.1662	0.0038	0.0727	0.0044	0.0502	0.0072	990	37	**991**	**21**	990	140	1010	110	11.02	3.03	0.2750
AP_011_140	1.8	0.16	0.164	0.0051	0.0799	0.0073	0.0698	0.0087	1052	55	**979**	**29**	1360	160	1190	170	14.91	4.58	0.3072
AP_011_141	1.507	0.02	0.1545	0.0026	0.07078	0.0011	0.0497	0.0042	933.1	8.1	**925.9**	**14**	979	82	950	30	593	64.6	0.1089
AP_011_142	1.608	0.063	0.1631	0.0032	0.0711	0.0025	0.0487	0.0051	970	24	**974**	**18**	961	98	956	75	25.9	14.06	0.5429
AP_011_143	2.066	0.047	0.193	0.0038	0.07711	0.0012	0.0627	0.0057	1136	16	**1138**	**21**	1228	110	1122	31	300	14.67	0.0489
AP_011_144	1.545	0.043	0.1563	0.0039	0.0715	0.0019	0.0456	0.0041	948	17	**936**	**22**	901	79	968	56	66.9	98	1.4649
AP_011_145	2.182	0.038	0.1941	0.0032	0.08178	0.0011	0.058	0.0047	1177	11	**1143**	**17**	1139	90	1239	27	497	153	0.3078
AP_011_146	1.52	0.058	0.1594	0.0027	0.0685	0.0027	0.0469	0.0044	939	23	**953**	**15**	927	84	902	82	28.48	16.91	0.5938
AP_011_147	1.646	0.077	0.1606	0.0031	0.0751	0.0039	0.0466	0.0047	984	30	**960**	**17**	920	92	1030	110	12.72	8.43	0.6627
AP_011_148	1.542	0.092	0.1627	0.0041	0.0667	0.0043	0.0509	0.0071	958	37	**971**	**23**	1000	140	900	130	15.76	5.67	0.3598
AP_011_149	2.079	0.048	0.1948	0.0042	0.0775	0.0021	0.0556	0.0048	1141	16	**1147**	**23**	1092	92	1127	53	45.8	41.5	0.9061
AP_011_150	1.636	0.056	0.1644	0.0039	0.0727	0.0027	0.0502	0.0048	986	23	**981**	**22**	989	93	1000	74	30.1	13.61	0.4522
AP_011_151	1.673	0.063	0.168	0.0037	0.0725	0.0026	0.0493	0.0045	996	24	**1001**	**20**	972	86	993	73	49.7	29.2	0.5875
AP_011_152	1.696	0.039	0.171	0.0032	0.0723	0.0014	0.05044	0.004	1008	15	**1017**	**18**	995	78	998	38	73.3	169.9	2.3179
AP_011_153	1.659	0.086	0.1697	0.0037	0.0698	0.0039	0.0476	0.0062	987	33	**1010**	**20**	938	120	930	110	12.12	6.52	0.5380
AP_011_154	1.502	0.054	0.1589	0.0028	0.0691	0.0027	0.0509	0.0045	929	22	**951**	**16**	1003	87	891	81	27.7	18.8	0.6787
AP_011_155	1.639	0.076	0.1645	0.0037	0.0705	0.0028	0.0509	0.0055	981	29	**981**	**21**	1003	110	971	83	13.65	9.22	0.6755
AP_011_156	2.145	0.079	0.2004	0.0048	0.0785	0.0023	0.0564	0.0048	1164	25	**1177**	**26**	1109	91	1166	58	52.7	60.1	1.1404
AP_011_157	1.673	0.056	0.1703	0.0031	0.0723	0.0026	0.0496	0.0049	1005	24	**1013**	**17**	978	93	1001	72	17.18	7.87	0.4581
AP_011_158	1.504	0.042	0.1527	0.0037	0.0718	0.0016	0.0501	0.0049	931	17	**916**	**21**	988	94	976	45	490	50.9	0.1039
AP_011_159	1.55	0.1	0.1646	0.0042	0.0701	0.0046	0.0493	0.0071	945	40	**982**	**24**	970	140	910	140	15.9	5.48	0.3447
AP_011_160	1.584	0.056	0.1577	0.0031	0.0721	0.0026	0.0474	0.0046	962	22	**944**	**17**	935	89	973	74	27.9	10.16	0.3642
AP_011_161	1.54	0.1	0.1639	0.0044	0.0696	0.0049	0.0556	0.0087	938	40	**978**	**25**	1090	170	850	140	10.11	3.01	0.2977
AP_011_162	1.649	0.051	0.1648	0.0034	0.0726	0.002	0.0512	0.0047	990	19	**983**	**19**	1008	90	993	57	37.3	18.44	0.4944
AP_011_163	1.724	0.046	0.1711	0.0034	0.0728	0.002	0.0498	0.0043	1016	17	**1018**	**19**	983	83	1008	55	43	31.8	0.7395
AP_011_164	1.894	0.078	0.1867	0.0041	0.0731	0.0028	0.0549	0.0056	1080	28	**1103**	**22**	1078	110	1023	85	18.04	7.67	0.4252
AP_011_165	1.635	0.024	0.1646	0.0026	0.07178	0.00089	0.0589	0.0051	983.4	9.2	**982.4**	**14**	1157	97	979	25	1303	25.8	0.0198
AP_011_166	1.77	0.11	0.1689	0.0041	0.0745	0.0049	0.0491	0.0077	1044	38	**1006**	**22**	960	150	1140	140	10.52	2.77	0.2633
AP_011_167	1.582	0.025	0.1623	0.0026	0.07078	0.0011	0.0463	0.0038	962.9	9.7	**969.6**	**14**	914	73	949	31	341	101.1	0.2965
AP_011_168	1.6	0.076	0.1586	0.0036	0.0726	0.0033	0.048	0.0043	966	30	**949**	**20**	946	82	1021	89	18.19	18.66	1.0258
AP_011_169	1.555	0.04	0.1608	0.0027	0.0702	0.0016	0.0482	0.004	951	16	**961**	**15**	951	77	929	47	97.1	64.5	0.6643
AP_011_170	1.611	0.026	0.1663	0.0031	0.07018	0.00084	0.0468	0.0038	974.1	10	**992**	**17**	924	74	938	25	1060	85.7	0.0808
AP_011_171	1.521	0.04	0.1577	0.0028	0.07	0.0019	0.0477	0.0039	940	17	**944**	**16**	941	76	926	56	46.43	49.7	1.0704
AP_011_172	1.568	0.078	0.1619	0.0038	0.0726	0.004	0.0541	0.0066	958	32	**967**	**21**	1062	130	1000	120	13.87	4.2	0.3028
AP_011_173	1.634	0.056	0.1676	0.0044	0.0703	0.0018	0.0462	0.004	981	21	**999**	**24**	914	77	938	50	55.7	28.35	0.5090
AP_011_174	1.693	0.039	0.1678	0.0034	0.0725	0.0012	0.0481	0.0047	1005	15	**1000**	**19**	949	91	999	34	787	27.7	0.0352
AP_011_175	2.162	0.046	0.1987	0.0038	0.07874	0.0013	0.0537	0.0044	1170	15	**1168**	**20**	1057	85	1164	32	245.4	52.6	0.2143
AP_011_176	1.51	0.1	0.1541	0.0037	0.0725	0.0063	0.053	0.009	930	41	**924**	**21**	1040	170	1020	160	23.41	7.81	0.3336
AP_011_177	2.39	0.32	0.179	0.013	0.096	0.011	0.134	0.047	1231	97	**1088**	**48**	2520	840	1530	200	6.17	1.56	0.2528
AP_011_178	1.759	0.049	0.1762	0.003	0.0735	0.0023	0.0499	0.0046	1029	18	**1046**	**17**	984	88	1025	65	33.6	22.95	0.6830
AP_011_179	1.67	0.13	0.1671	0.0042	0.0722	0.0053	0.0565	0.01	992	50	**996**	**23**	1100	190	940	160	7.89	1.71	0.2167
AP_011_180	1.664	0.088	0.1724	0.0044	0.0703	0.0035	0.0418	0.0062	989	34	**1025**	**24**	830	120	940	110	9.11	2.09	0.2294
AP_011_181	1.6	0.1	0.1596	0.0035	0.0743	0.0048	0.0523	0.0068	970	42	**954**	**19**	1030	130	1020	130	8.92	2.46	0.2758
AP_011_182	1.506	0.039	0.1555	0.0028	0.0708	0.0021	0.044	0.0038	932	16	**932**	**16**	869	73	939	60	58.9	45.9	0.7793
AP_011_183	1.705	0.086	0.1662	0.0042	0.0764	0.0034	0.0447	0.0067	1016	30	**994**	**24**	880	130	1095	88	9.88	2.84	0.2874
AP_011_184	1.573	0.048	0.163	0.003	0.0697	0.0022	0.0463	0.004	961	18	**973**	**16**	914	77	917	65	37.1	30.9	0.8329
AP_011_185	1.709	0.047	0.1725	0.0034	0.0712	0.002	0.0511	0.0045	1011	17	**1026**	**19**	1006	85	979	63	55.4	40.1	0.7238
AP_011_186	1.488	0.02	0.1545	0.0024	0.06984	0.001	0.04653	0.0038	925.3	8.1	**926**	**13**	919	73	922	30	405	112.4	0.2775
AP_011_187	1.702	0.027	0.1687	0.0029	0.07376	0.0011	0.0505	0.0042	1010.2	10	**1005**	**16**	997	80	1033	31	175.2	89.4	0.5103
AP_011_188	1.6	0.11	0.1674	0.004	0.0702	0.0045	0.0446	0.0053	969	42	**998**	**22**	880	100	870	130	12.4	6.76	0.5452
AP_011_189	1.874	0.064	0.1842	0.0038	0.0753	0.0025	0.0536	0.0051	1074	24	**1090**	**21**	1055	98	1064	65	25.4	12.45	0.4902
AP_011_190	1.72	0.078	0.1686	0.0032	0.0739	0.0034	0.0527	0.0053	1012	29	**1004**	**18**	1036	100	1025	89	25.64	14.63	0.5706
AP_011_191	1.643	0.057	0.165	0.0032	0.072	0.0026	0.0517	0.0053	988	22	**984**	**18**	1017	100	992	74	23.5	8.11	0.3451
AP_011_192	1.551	0.076	0.1581	0.0036	0.0715	0.0038	0.0453	0.0068	952	31	**946**	**20**	890	130	1000	110	11.02	3.234	0.2935
AP_011_193	2.33	0.058	0.2099	0.0034	0.0809	0.002	0.0614	0.0051	1222	17	**1228**	**18**	1204	97	1212	48	48.8	32.1	0.6578
AP_011_194	1.915	0.052	0.1788	0.0036	0.0774	0.0023	0.0518	0.0053	1088	19	**1060**	**19**	1019	100	1134	57	30.7	12.36	0.4026
AP_011_195	1.682	0.093	0.1721	0.0047	0.0704	0.0043	0.0574	0.009	1008	37	**1023**	**26**	1120	180	930	130	8.12	1.89	0.2328
AP_011_196	2	0.13	0.1606	0.0026	0.0907	0.0058	0.0859	0.0073	1106	42	**960.2**	**15**	1666	140	1390	120	570	39	0.0684
AP_011_197	1.677	0.056	0.1693	0.0036	0.0722	0.0023	0.0525	0.0052	1004	22	**1008**	**20**	1033	99	997	67	42	17.36	0.4133
AP_011_198	1.647	0.083	0.1644	0.0047	0.0737	0.0045	0.0575	0.0083	989	31	**981**	**26**	1130	160	1020	130	9.88	2.44	0.2470
AP_011_199	1.637	0.08	0.1651	0.0039	0.0726	0.0026	0.0487	0.0045	982	31	**985**	**22**	960	86	1014	81	45	26.5	0.5889
AP_011_200	2.518	0.042	0.221	0.0033	0.0833	0.0015	0.0625	0.0051	1277	12	**1287**	**18**	1226	96	1273	35	131	114.6	0.8748
AP_011_201	2.06	0.061	0.1917	0.0036	0.0779	0.002	0.0569	0.0047	1133	20	**1130**	**19**	1117	91	1136	52	49.1	41.2	0.8390
AP_011_202	1.619	0.035	0.1627	0.0033	0.0728	0.0018	0.0477	0.0039	977	14	**972**	**18**	942	76	1007	51	498	118.1	0.2371
AP_011_203	1.507	0.072	0.1537	0.0038	0.0713	0.0033	0.047	0.0048	932	29	**922**	**21**	929	93	958	95	97.4	57.6	0.5914
AP_011_204	1.936	0.04	0.1792	0.0032	0.0789	0.0012	0.0552	0.0046	1093	14	**1062**	**17**	1087	89	1168	31	509	120.1	0.2360
AP_011_205	1.685	0.089	0.1693	0.0035	0.0714	0.004	0.0489	0.0064	1002	35	**1008**	**19**	963	120	960	120	11.15	2.85	0.2556
AP-048																			
AP-048 - 1	2.271	0.042	0.2038	0.0034	0.08067	0.0013	0.0577	0.0047	1203	13	**1196**	**18**	1133	90	1211	31	295	125.6	0.4258
AP-048 - 2	2.013	0.032	0.1853	0.0028	0.07865	0.0012	0.0514	0.0042	1119.6	11	**1095.9**	**15**	1012	81	1162	30	514	97.6	0.1899
AP-048 - 3	1.921	0.033	0.1842	0.003	0.0758	0.0014	0.0517	0.0043	1088	11	**1090**	**17**	1018	83	1092	39	127.7	39.8	0.3117
AP-048 - 4	1.625	0.058	0.1641	0.0039	0.0725	0.002	0.0485	0.0056	977	23	**979**	**22**	985	110	991	56	67.5	7.97	0.1181
AP-048 - 5	2.169	0.064	0.2005	0.0041	0.0795	0.0021	0.0532	0.0056	1174	19	**1178**	**22**	1047	110	1180	52	54.6	10.22	0.1872
AP-048 - 6	2.226	0.041	0.2034	0.0034	0.07934	0.0012	0.0565	0.0048	1189	13	**1193**	**18**	1111	92	1179	30	190	64.3	0.3384
AP-048 - 7	1.635	0.058	0.1692	0.0035	0.0702	0.0021	0.0475	0.0054	982	22	**1007**	**20**	937	100	928	62	61.2	8.01	0.1309
AP-048 - 8	1.705	0.032	0.1695	0.0029	0.0729	0.0013	0.0494	0.0041	1012	13	**1009**	**16**	974	79	1009	35	234	75	0.3205
AP-048 - 9	2.354	0.068	0.1981	0.0048	0.0871	0.0022	0.0714	0.0074	1228	21	**1165**	**26**	1394	140	1360	48	179	23.5	0.1313
AP-048 - 10	1.648	0.025	0.1655	0.0025	0.07237	0.001	0.0487	0.0043	988.4	9.7	**987.4**	**14**	961	83	999	27	699	31.7	0.0454
AP-048 - 11	1.672	0.041	0.1674	0.003	0.0722	0.0015	0.0456	0.0065	999	15	**1000**	**16**	900	130	993	42	60.8	4.01	0.0660
AP-048 - 12	2.157	0.048	0.1962	0.0037	0.0806	0.0015	0.0575	0.0049	1167	15	**1155**	**20**	1130	93	1210	36	436	166.4	0.3817
AP-048 - 13	2.432	0.027	0.2132	0.0031	0.08286	0.0011	0.0603	0.0049	1252	8	**1245.6**	**16**	1184	94	1265	26	757	95.3	0.1259
AP-048 - 14	2.333	0.066	0.212	0.003	0.0799	0.0021	0.0657	0.0083	1224	19	**1239.6**	**16**	1280	160	1195	54	55	5.63	0.1024
AP-048 - 15	2.288	0.054	0.2054	0.0044	0.08088	0.0013	0.0635	0.0055	1207	17	**1204**	**23**	1244	100	1217	30	202	28.7	0.1421
AP-048 - 16	2.403	0.072	0.2149	0.0043	0.0821	0.0024	0.0652	0.0061	1249	20	**1255**	**23**	1276	120	1247	58	38.8	10.2	0.2629
AP-048 - 17	2.39	0.11	0.2087	0.0065	0.0827	0.0029	0.0634	0.008	1237	32	**1222**	**34**	1240	150	1259	69	50.84	12.11	0.2382
AP-048 - 18	1.858	0.026	0.1787	0.0029	0.07544	0.0011	0.055	0.0046	1065.9	9.2	**1060**	**16**	1081	88	1079	29	309.6	52.5	0.1696
AP-048 - 19	2.279	0.047	0.2054	0.0039	0.08131	0.0013	0.0588	0.0048	1205	15	**1204**	**21**	1155	91	1228	31	295.2	109	0.3692
AP-048 - 20	1.608	0.051	0.1617	0.0035	0.0729	0.002	0.0451	0.0049	972	20	**966**	**20**	891	95	1000	57	64.4	8.43	0.1309
AP-048 - 21	1.749	0.042	0.174	0.0031	0.0726	0.0016	0.052	0.0048	1026	15	**1034**	**17**	1024	93	1012	49	195.2	28.25	0.1447
AP-048 - 22	1.958	0.058	0.1856	0.0032	0.0763	0.0023	0.0509	0.0053	1102	19	**1098**	**17**	1003	100	1112	55	43.9	8.31	0.1893
AP-048 - 23	2.414	0.046	0.2107	0.0042	0.08375	0.0011	0.0575	0.005	1246	14	**1232**	**22**	1130	95	1286	26	888	90.4	0.1018
AP-048 - 24	1.6	0.059	0.164	0.0033	0.0703	0.0022	0.0478	0.0082	968	23	**979**	**18**	940	160	936	62	49.2	2.99	0.0608
AP-048 - 25	2.064	0.044	0.1943	0.0033	0.0767	0.0015	0.0571	0.0048	1136	15	**1145**	**18**	1122	92	1115	41	154	39.2	0.2545
AP-048 - 26	1.926	0.043	0.1838	0.0033	0.0754	0.0016	0.0545	0.0054	1090	15	**1088**	**18**	1073	100	1079	43	260	79.6	0.3062
AP-048 - 27	1.667	0.062	0.1621	0.0035	0.0751	0.0035	0.0492	0.0057	995	24	**968**	**19**	969	110	1061	90	85	13.97	0.1644
AP-048 - 28	1.522	0.033	0.157	0.0029	0.07	0.002	0.0506	0.0062	938	13	**940**	**16**	990	130	929	56	64.2	5.41	0.0843
AP-048 - 29	2.101	0.031	0.1956	0.0031	0.07772	0.0011	0.0563	0.0046	1148.8	10	**1152**	**17**	1106	89	1142	26	255	87.8	0.3443
AP-048 - 30	1.557	0.045	0.1611	0.0028	0.0698	0.0023	0.0449	0.0049	952	18	**963**	**15**	886	95	935	66	37.7	7.76	0.2058
AP-048 - 31	1.474	0.041	0.1535	0.0025	0.069	0.0018	0.0479	0.0056	919	16	**920.6**	**14**	940	130	910	54	55.9	3.77	0.0674
AP-048 - 32	1.977	0.046	0.1868	0.003	0.077	0.0017	0.0563	0.0049	1112	16	**1104**	**16**	1107	94	1122	46	88.9	36	0.4049
AP-048 - 33	1.637	0.069	0.1701	0.0035	0.0699	0.0028	0.0507	0.0072	982	27	**1012**	**20**	1000	140	947	83	31.6	3.82	0.1209
AP-048 - 34	2.211	0.062	0.2052	0.0048	0.078	0.002	0.0586	0.0071	1184	20	**1203**	**26**	1171	130	1144	51	30.1	6.6	0.2193
AP-048 - 35	1.555	0.034	0.1616	0.0025	0.0703	0.0015	0.0476	0.0043	952	14	**965.6**	**14**	939	82	931	43	110.3	33.4	0.3028
AP-048 - 36	1.77	0.1	0.1746	0.0078	0.0724	0.0022	0.046	0.0058	1027	36	**1036**	**42**	907	110	995	60	47.9	5.94	0.1240
AP-048 - 37	2.165	0.073	0.2003	0.005	0.0784	0.0017	0.0572	0.0057	1167	23	**1177**	**27**	1124	110	1166	41

AP-048 - 97	1.615	0.068	0.1654	0.0038	0.0707	0.0025	0.0554	0.0067	972	26	**987**	**21**	1087	130	933	74	49	4.87	0.0994
AP-048 - 98	2.746	0.044	0.2324	0.0037	0.0865	0.0014	0.0651	0.0054	1342	13	**1347**	**20**	1274	100	1346	32	148.1	60.4	0.4078
AP-048 - 99	2.229	0.041	0.1987	0.0037	0.08095	0.0012	0.0587	0.0048	1190	13	**1168**	**20**	1152	92	1219	29	810	174.3	0.2152
AP-048 - 100	2.02	0.052	0.1913	0.0047	0.07708	0.0012	0.0561	0.0048	1126	16	**1128**	**25**	1102	91	1125	33	277	41.3	0.1491
AP-048 - 101	2.684	0.053	0.2311	0.0053	0.0845	0.0016	0.0628	0.0061	1324	15	**1340**	**27**	1230	120	1314	41	651	48	0.0737
AP-048 - 102	1.822	0.096	0.1794	0.0057	0.0739	0.002	0.0548	0.0054	1058	33	**1063**	**31**	1077	100	1030	57	55.1	9.9	0.1797
AP-048 - 103	2.233	0.055	0.2032	0.0039	0.0797	0.0013	0.0646	0.0058	1193	17	**1192**	**21**	1264	110	1192	34	260	37.6	0.1446
AP-048 - 104	1.486	0.037	0.1495	0.0032	0.0719	0.002	0.0449	0.0055	924	15	**898**	**18**	887	110	979	58	79.3	10.19	0.1285
AP-048 - 105	2.295	0.041	0.2038	0.005	0.0824	0.0013	0.059	0.005	1211	13	**1196**	**27**	1159	95	1255	30	499	193	0.3868
AP-048 - 106	2.188	0.07	0.1959	0.0049	0.0808	0.0021	0.0593	0.0054	1177	22	**1153**	**27**	1164	100	1214	51	297	117	0.3939
AP-048 - 107	2.076	0.053	0.1899	0.0042	0.0785	0.0019	0.065	0.0066	1140	18	**1121**	**23**	1273	130	1158	48	173	49	0.2832
AP-048 - 108	2.641	0.04	0.2245	0.0037	0.08528	0.0011	0.0664	0.0054	1311.6	11	**1306**	**19**	1299	100	1321	25	245	84.8	0.3461
AP-048 - 109	1.584	0.068	0.1529	0.0036	0.0763	0.0033	0.0544	0.0077	963	26	**917**	**20**	1070	150	1115	79	51.7	8.59	0.1662
AP-048 - 110	2.461	0.041	0.2165	0.0033	0.08293	0.0012	0.0626	0.0051	1260	12	**1263**	**18**	1227	98	1266	28	298.1	112.9	0.3787
AP-048 - 111	2.058	0.032	0.1908	0.0031	0.0786	0.0013	0.0572	0.005	1134.8	10	**1125**	**17**	1125	95	1160	33	333.5	41.8	0.1253
AP-048 - 112	2.155	0.066	0.2029	0.0042	0.0769	0.0025	0.0516	0.0069	1165	21	**1191**	**23**	1010	130	1120	67	37.2	4.42	0.1188
AP-048 - 113	1.61	0.029	0.1619	0.0026	0.07215	0.0011	0.0478	0.004	974	11	**967.2**	**15**	944	77	988	31	192	52.8	0.2750
AP-048 - 114	1.756	0.066	0.1745	0.0054	0.0725	0.0022	0.0526	0.006	1026	25	**1036**	**29**	1035	120	989	62	34	6.11	0.1797
AP-048 - 115	1.644	0.051	0.1688	0.0035	0.07	0.0025	0.0471	0.0072	986	19	**1005**	**20**	930	140	950	68	31.8	4.1	0.1289
AP-048 - 116	2.048	0.081	0.19	0.0053	0.0789	0.0027	0.0513	0.0079	1133	25	**1121**	**29**	1010	150	1189	62	27.2	2.256	0.0829
AP-048 - 117	2.289	0.066	0.209	0.0042	0.0796	0.0021	0.0641	0.0057	1214	20	**1223**	**22**	1255	110	1182	52	86.2	23.1	0.2680
AP-048 - 118	2.08	0.051	0.1958	0.0034	0.0763	0.0022	0.055	0.0056	1141	17	**1153**	**18**	1082	110	1093	58	43.7	9.39	0.2149
AP-048 - 119	2.002	0.084	0.1887	0.0058	0.077	0.002	0.0547	0.0054	1112	29	**1113**	**31**	1075	100	1114	52	64.3	14.9	0.2317
AP-048 - 120	2.079	0.057	0.1948	0.0052	0.0779	0.0021	0.0604	0.0087	1140	19	**1147**	**28**	1180	160	1145	55	34.1	3.28	0.0962
AP-048 - 121	1.592	0.051	0.1624	0.0031	0.0707	0.0024	0.0465	0.0062	965	20	**970**	**17**	915	120	933	70	50.1	5.61	0.1120
AP-048 - 122	2.129	0.045	0.1986	0.0039	0.0775	0.0015	0.0641	0.0075	1162	14	**1167**	**21**	1250	140	1131	38	127.4	8.56	0.0672
AP-048 - 123	2.44	0.054	0.2161	0.0038	0.0823	0.0015	0.0617	0.0053	1256	15	**1261**	**20**	1210	100	1250	36	159	40.1	0.2522
AP-048 - 124	2.16	0.049	0.1956	0.0041	0.0799	0.0024	0.0636	0.0075	1167	16	**1152**	**22**	1240	140	1185	60	42.5	10	0.2353
AP-048 - 125	2.006	0.046	0.189	0.003	0.0767	0.0019	0.0597	0.0054	1117	16	**1116**	**16**	1172	100	1112	51	90.9	14.32	0.1575
AP-048 - 126	1.463	0.053	0.1489	0.0033	0.0711	0.0027	0.051	0.0078	914	22	**895**	**19**	1000	150	987	79	32.7	3.97	0.1214
AP-048 - 127	2.151	0.058	0.1965	0.004	0.0792	0.0016	0.0582	0.005	1164	19	**1156**	**22**	1142	95	1174	40	140	44.6	0.3186
AP-048 - 128	2.025	0.033	0.1891	0.0031	0.0776	0.0013	0.057	0.0046	1123.6	11	**1116**	**17**	1120	89	1134	33	626	167.8	0.2681
AP-048 - 129	1.855	0.056	0.1804	0.0036	0.0745	0.0021	0.0555	0.0065	1063	20	**1069**	**19**	1106	120	1044	58	45.6	6.06	0.1329
AP-048 - 130	2.526	0.042	0.2176	0.0035	0.084	0.0014	0.0661	0.0054	1281	12	**1269**	**18**	1294	100	1291	33	223.4	79.6	0.3563
AP-048 - 131	1.959	0.054	0.1704	0.0046	0.0837	0.0019	0.0654	0.0063	1101	18	**1014**	**25**	1280	120	1283	46	185.3	54.3	0.2930
AP-048 - 132	2.231	0.064	0.2046	0.0038	0.0791	0.0025	0.0644	0.0065	1189	20	**1200**	**20**	1220	120	1164	61	49.2	8.29	0.1685
AP-048 - 133	2.392	0.04	0.2107	0.0032	0.0824	0.0013	0.0633	0.0051	1240	12	**1233**	**17**	1241	97	1258	30	303	138.9	0.4584
AP-048 - 134	2.252	0.076	0.2024	0.005	0.0812	0.0024	0.0517	0.0073	1194	24	**1188**	**27**	1030	140	1215	60	37.7	3.78	0.1003
AP-048 - 135	2.425	0.073	0.2145	0.0055	0.08183	0.0012	0.0614	0.0052	1248	22	**1252**	**29**	1204	98	1244	28	750	88	0.1173
AP-048 - 136	2.119	0.076	0.1974	0.005	0.0783	0.0019	0.0596	0.0061	1156	24	**1161**	**27**	1168	120	1164	43	44.2	9.3	0.2104
AP-048 - 137	1.708	0.045	0.168	0.0031	0.0741	0.0016	0.0502	0.005	1013	16	**1001**	**17**	988	96	1047	41	61.6	8.36	0.1357
AP-048 - 138	2.189	0.057	0.2016	0.0043	0.0782	0.0018	0.0571	0.0058	1179	17	**1184**	**23**	1122	110	1155	44	51.6	10.67	0.2068
AP-048 - 139	2.098	0.03	0.1939	0.0034	0.0788	0.0011	0.0582	0.0048	1147.7	9.9	**1142**	**18**	1144	92	1166	28	726	86.2	0.1187
AP-048 - 140	2.004	0.051	0.1903	0.0038	0.076	0.0016	0.0575	0.0054	1119	16	**1123**	**21**	1129	100	1098	43	55.9	13.81	0.2470
AP-048 - 141	2.156	0.045	0.2001	0.0039	0.0777	0.0017	0.0592	0.0072	1166	15	**1175**	**21**	1160	140	1134	43	67.7	5.78	0.0854
AP-048 - 142	2.212	0.096	0.2052	0.0057	0.079	0.0028	0.0618	0.01	1185	31	**1203**	**30**	1200	190	1157	71	29.7	2.39	0.0805
AP-048 - 143	1.828	0.057	0.1779	0.0033	0.0742	0.0021	0.0496	0.0048	1057	20	**1055**	**18**	978	93	1046	60	55.1	11.01	0.1998
AP-048 - 144	1.528	0.061	0.1617	0.0041	0.068	0.0026	0.0485	0.0074	943	23	**966**	**24**	950	140	875	78	30.7	4.14	0.1349
AP-048 - 145	2.578	0.053	0.2246	0.0045	0.08284	0.0012	0.0634	0.0052	1293	15	**1306**	**24**	1242	98	1264	27	610	90	0.1475
AP-048 - 146	2.032	0.057	0.1911	0.0037	0.0768	0.0023	0.0516	0.0055	1125	19	**1127**	**20**	1015	110	1113	63	44	6.29	0.1430
AP-048 - 147	1.525	0.063	0.1611	0.0034	0.0683	0.0025	0.0525	0.0081	938	25	**963**	**19**	1030	160	894	83	52.3	5.38	0.1029
AP-048 - 148	1.572	0.06	0.1574	0.0032	0.0718	0.0029	0.0511	0.0081	956	24	**942**	**18**	1000	160	973	84	27.2	3.1	0.1140
AP-048 - 149	2.523	0.04	0.2163	0.004	0.0846	0.0016	0.0675	0.0056	1278.6	11	**1262**	**21**	1321	110	1306	36	249.5	83.7	0.3355
AP-048 - 150	1.483	0.057	0.1577	0.0029	0.0677	0.0024	0.045	0.0058	922	23	**944**	**16**	887	110	862	76	47.6	8.45	0.1775
AP-048 - 151	2.608	0.053	0.2262	0.0051	0.0835	0.0014	0.0665	0.0057	1302	15	**1314**	**27**	1302	110	1285	31	589	106.8	0.1813
AP-048 - 152	2.049	0.053	0.1893	0.0042	0.0781	0.002	0.0554	0.0049	1131	18	**1118**	**23**	1089	93	1147	50	165.6	62.5	0.3774
AP-048 - 153	2.554	0.038	0.2197	0.0036	0.08408	0.0012	0.0655	0.0054	1287.2	11	**1280**	**19**	1283	100	1293	27	374	82.5	0.2206
AP-048 - 154	1.5	0.035	0.1533	0.0026	0.0706	0.0016	0.0481	0.0053	930	14	**919.1**	**14**	948	100	939	46	86.5	9.17	0.1060
AP-048 - 155	1.515	0.044	0.1533	0.0031	0.0714	0.0024	0.0454	0.0043	936	17	**919**	**17**	896	84	964	70	126.2	23.92	0.1895
AP-048 - 156	2.196	0.042	0.2001	0.0035	0.0789	0.0013	0.0553	0.0049	1179	13	**1176**	**19**	1087	95	1171	31	295.9	28.99	0.0980
AP-048 - 157	2.414	0.045	0.2139	0.0037	0.08233	0.001	0.0616	0.005	1246	13	**1249**	**20**	1208	94	1253	24	888	159.8	0.1800
AP-048 - 158	1.64	0.082	0.1597	0.0035	0.074	0.0039	0.0558	0.0097	983	31	**955**	**19**	1130	200	1050	110	37.7	5.1	0.1353
AP-048 - 159	2.241	0.055	0.2018	0.0037	0.08	0.0014	0.0603	0.005	1193	17	**1185**	**20**	1184	96	1199	36	305	103	0.3377
AP-048 - 160	1.963	0.038	0.1837	0.0034	0.0767	0.0015	0.0563	0.0048	1102	13	**1087**	**18**	1107	92	1117	42	86.9	36.9	0.4246
AP-048 - 161	1.929	0.083	0.1828	0.0045	0.0767	0.0024	0.0562	0.0064	1092	29	**1087**	**26**	1104	120	1101	63	43.5	8.23	0.1892
AP-048 - 162	1.482	0.071	0.1535	0.0031	0.0692	0.0033	0.0467	0.0061	919	29	**921**	**17**	937	110	890	100	30.5	5.45	0.1787
AP-048 - 163	1.519	0.061	0.1588	0.0046	0.0703	0.0026	0.0479	0.0079	942	22	**950**	**25**	940	150	928	77	48.7	4.75	0.0975
AP-048 - 164	2.216	0.054	0.2089	0.0043	0.0772	0.0013	0.0608	0.0056	1187	16	**1223**	**23**	1193	110	1125	33	200	23.6	0.1180
AP-048 - 165	1.541	0.046	0.1582	0.0029	0.0704	0.0022	0.0484	0.0067	948	18	**947**	**16**	950	130	938	65	60.4	3.8	0.0629
AP-048 - 166	1.64	0.049	0.1622	0.003	0.073	0.0021	0.0484	0.005	984	19	**969**	**17**	954	97	1014	53	34.6	6.8	0.1965
AP-048 - 167	2.415	0.085	0.2163	0.0041	0.0814	0.0024	0.0562	0.006	1252	27	**1262**	**22**	1104	110	1238	63	36.8	7.71	0.2095
AP-048 - 168	2.367	0.049	0.2094	0.0041	0.08229	0.0012	0.0615	0.0051	1234	14	**1226**	**22**	1206	96	1251	28	980	212	0.2163
AP-048 - 169	2.34	0.044	0.2039	0.0037	0.0831	0.0014	0.0596	0.0051	1224	14	**1196**	**20**	1171	96	1270	33	236	67	0.2839
AP-048 - 170	1.628	0.045	0.1643	0.0032	0.0712	0.002	0.0505	0.0045	983	18	**981**	**18**	995	86	963	59	56.9	13.81	0.2427
AP-048 - 171	2.065	0.047	0.1924	0.0032	0.0768	0.0014	0.0558	0.0049	1136	15	**1134**	**17**	1097	93	1125	37	125.1	31.8	0.2542
AP-048 - 172	2.08	0.062	0.1909	0.0037	0.0791	0.0022	0.0479	0.0083	1140	21	**1126**	**20**	940	160	1176	52	30.4	1.893	0.0623
AP-048 - 173	1.527	0.049	0.1547	0.0034	0.0711	0.0022	0.0492	0.007	939	19	**927**	**19**	980	130	964	58	33.6	5.26	0.1565
AP-048 - 174	2.072	0.044	0.1961	0.0033	0.0785	0.0015	0.0564	0.005	1139	14	**1122**	**18**	1109	95	1158	38	289	57.9	0.2003
AP-048 - 175	1.717	0.055	0.1648	0.005	0.0772	0.0028	0.0659	0.01	1014	21	**983**	**28**	1290	190	1118	74	56.05	6.48	0.1156
AP-048 - 176	2.44	0.046	0.215	0.0036	0.08264	0.0013	0.0657	0.0056	1258	13	**1255**	**19**	1286	110	1259	30	212.7	54	0.2539
AP-048 - 177	1.49	0.039	0.1552	0.0027	0.0703	0.0019	0.0459	0.0053	927	16	**930**	**15**	920	110	937	55	80.1	8.48	0.1059
AP-048 - 178	1.95	0.15	0.183	0.011	0.0762	0.0024	0.0612	0.0087	1083	52	**1081**	**57**	1220	160	1088	65	71.6	5.7	0.0796
AP-048 - 179	2.425	0.044	0.2115	0.0039	0.0832	0.0014	0.0582	0.0051	1250	13	**1237**	**21**	1143	97	1272	32	298.8	118.3	0.3959
AP-048 - 180	1.99	0.071	0.1909	0.0046	0.0745	0.0025	0.0699	0.011	1113	23	**1126**	**25**	1360	210	1053	65	26.8	1.478	0.0551
AP-048 - 181	1.733	0.054	0.1715	0.0033	0.073	0.0017	0.0529	0.006	1020	20	**1020**	**18**	1058	120	1011	47	104.4	8.85	0.0848
AP-048 - 182	2.586	0.058	0.2217	0.0044	0.0842	0.0014	0.0648	0.0056	1295	16	**1290**	**23**	1269	100	1296	34	138	36.1	0.2645
AP-048 - 183	2.187	0.06	0.1989	0.0043	0.0801	0.0017	0.0586	0.0067	1175	19	**1169**	**23**	1149	130	1194	41	56.8	4.36	0.0768
AP-048 - 184	2.06	0.042	0.1903	0.0039	0.0789	0.0016	0.0567	0.0048	1138	14	**1123**	**21**	1114	92	1168	40	367	68.3	0.1861
AP-048 - 185	2.624	0.037	0.2241	0.0036	0.08465	0.001	0.06539	0.0052	1307	10	**1304**	**19**	1280	99	1307	23	448	202	0.4509
AP-048 - 186	1.559	0.057	0.1575	0.0031	0.0717	0.0024	0.0462	0.0048	951	23	**943**	**17**	912	93	973	67	39.5	9.33	0.2362
AP-048 - 187	2.48	0.047	0.215	0.0039	0.0834	0.0015	0.0624	0.0052	1266	14	**1255**	**21**	1224	98	1275	36	146.2	53	0.3625
AP-048 - 188	1.55	0.028	0.1566	0.0027	0.0719	0.0011	0.04797	0.0039	949.9	11	**938**	**15**	947	75	981	31	385	124.4	0.3231
AP-048 - 189	1.6	0.047	0.164	0.0031	0.071	0.002	0.049	0.0052	968	18	**979**	**17**	966	99	946	59	51.6	11.53	0.2234
AP-048 - 190	2.195	0.037	0.2018	0.0034	0.0789	0.0014	0.0612	0.0052	1179	12	**1185**	**18**	1201	98	1168	34	183.3	37.4	0.2040
AP-048 - 191	1.504	0.051	0.1548	0.0033	0.0708	0.0024	0.0582	0.0055	930	21	**938**	**18**	850	100	937	70	33.4	6.14	0.1838
AP-048 - 192	1.889	0.076	0.1803	0.0036	0.0754	0.0022	0.0497	0.006	1074	27	**1068**	**20**	978	110	1100	61	56.4	6.72	0.1191
AP-048 - 193	1.603	0.063	0.1627	0.0038	0.0723	0.0028	0.0476	0.0079	976	25	**972**	**21**	960	150	973	80	42.4	2.191	0.0517
AP-048 - 194	2.194	0.055	0.199	0.0047	0.0803	0.002	0.0592	0.0055	1181	19	**1169**	**25**	1161	110	1198	48	79.4	11.4	0.1436
AP-048 - 195	2.332	0.052	0.2054	0.0041	0.0825	0.0019	0.0612	0.0052	1221	16	**1204**	**22**	1200	98	1255	45	168.9	72.9	0.4316
AP-048 - 196	2.027	0.058	0.1876	0.0035	0.0777	0.0017	0.0567	0.0051	1123	20	**1108**	**19**	1114	98	1144	45	274	59.8	0.2182
AP-048 - 197	1.649	0.054	0.1626	0.0033	0.0726	0.0023	0.0549	0.0061	987	21	**971**	**19**	1079	120	1001	64	63.3	7.45	0.1177
AP-048 - 198	2.235	0.096	0.1983	0.0054	0.0823	0.0037	0.06	0.012	1190	30	**1166**	**29**	1170	240	1242	91	37.6	3.33	0.0886
AP-048 - 199	2.394	0.067	0.2133	0.0057	0.08183	0.0013	0.0619	0.0051	1239	20	**1246**	**30**	1214	97	1240	30	158	63.4	0.4013
AP-048 - 200	2.727	0.049	0.2299	0.004	0.0861	0.0014	0.0674	0.0057	1335	13	**1334**	**21**	1318	110	1337	31	182.7	41.8	0.2288
AP-048 - 201	2.123	0.036	0.1954	0.0035	0.0783	0.0013	0.0589	0.0051	1156	12	**1151**	**19**	1157	97	1159	31	193	64.4	0.3337
AP-048 - 202	1.798	0.055	0.166	0.0036	0.0787	0.0025	0.064	0.0083	1044	20	**990**	**20**	1250	160	1157	64	57.8	5.82	0.1007
AP-048 - 203	1.552	0.056	0.1583	0.003	0.0714	0.0025	0.0434	0.0075	949	23	**947**	**17**	850	150	951	75	29	3.79	0.1307
AP-048 - 204	2.231	0.047	0.1987	0.0036	0.0817	0.0015	0.059	0.0054	1190	15	**1168**	**19**	1158	100	1237	35	498	103.5	0.2078
AP-048 - 205	1.943	0.044	0.1828	0.0037	0.0764	0.0015	0.0574	0.0051	1095	15	**1082**	**20**	1128	98	1108	41	364	72	0.1978
AP-048 - 206	1.941	0.043	0.1824	0.0031	0.0776	0.0019	0.0603	0.0056	1097	14	**1080**	**17**	1182	110	1130	51	129.5	22.52	0.1747
AP-048 - 207	2.137	0.057	0.199	0.0036	0.0777	0.0022	0.0554	0.0059	1159	19	**1170**	**19**	1089	110	1130	57	50	6.91	0.1382
AP-048 - 208	2.015	0.043	0.1917	0.0033	0.0765	0.0019	0.0547	0.0069	1125	16	**1131**	**18**	1070	130	1100	51	57.6	6.18	0.1073
AP-048 - 209	2.309	0.094	0.2021	0.0053	0.0823	0.0028	0.0586	0.0081	1212	29	**1186**	**28**	1150	150	1243	67	47.3	3.93	0.0831
AP-048 - 210	1.441	0.041	0.1505	0.0025	0.0696	0.0021	0.0491	0.009	910	17	**904**	**14**	960	170	923	62	59.4	2.87	0.0483
AP-048 - 211	1.962	0.052	0.1847	0.0041	0.0779	0.0013	0.0562	0.0047	1107	18	**1092**	**22**	1105	91	1141	33	244	78	0.3197
AP-048 - 212	2.377	0.047	0.2136	0.0043	0.0809	0.0015	0.063	0.0054	1235	14	**1251**	**22**	1234	100	1216	37	89.5	32.2	0.3598
AP-048 - 213	1.465	0.029	0.1527	0.0028	0.069	0.0015	0.0462	0.0041	917	12	**916**	**16**	912	79	905	43	139	40.2	0.2892
AP-048 - 214	1.798	0.083	0.1708	0.0051	0.0752	0.0023	0.0529	0.0059	1040	31	**1016**	**28**	1040	110	1072	63	97	21.7	0.2237
AP-048 - 215	2.496	0.047	0.2133	0.0041	0.08458	0.001	0.0639	0.0051	1270	14	**1246**	**22**	1161	97	1305	24	612	145.7	0.2381
AP-048 - 216	2.289	0.069	0.2097	0.004	0.0781	0.002	0.0582	0.0058	1207	22	**1227**	**21**	1142	110	1156	56	63.1	23.36	0.3702
AP-048 - 217	3.101	0.044	0.2479	0.004	0.09041	0.001	0.0703	0.0056	1432.6	11	**1427**	**21**	1373	110	1434	22	1397	306.3	0.2193
AP-048 - 218	1.907	0.059	0.1818	0.0042	0.0757	0.0026	0.0598	0.0074	1085	22	**1077**	**23**	1170	140	1070	71	32	3.78	0.181
AP-048 - 219	2.585	0.054	0.2273	0.0043	0.0822	0.0013	0.066	0.0055	1295	15	**1320**	**23**	1298	110	1249	32	206	58.1	0.2820
AP-048 - 220	2.03	0.066	0.1881	0.0042	0.0781	0.0023	0.0609	0.0064	1124	22	**1111**	**23**	1194	120	1152	56	43.8	7.15	0.1632
DAA-39																			
DAA-39 - 1	1.548	0.082	0.1571	0.0037	0.0703	0.0037	0.0464	0.0047	944	33	**940**	**21**	916	92	950	110	16.8	14.1	0.8393
DAA-39 - 2	1.409	0.039	0.1468	0.0023	0.0696	0.0021	0.0456	0.0046	891	17	**883**	**13**	901	90	906	61	64.7	11.57	0.1788
DAA-39 - 3	1.424	0.051	0.1496	0.003	0.0678	0.0023	0.0447	0.0048	900	20	**899**	**17**	882	93	873	74	40.1	6.39	0.1594
DAA-39 - 4	1.513	0.037	0.1553	0.0024	0.0705	0.0017	0.0482	0.0042	937	15	**930.7**	**13**	950	81	937	50	94.2	41.8	0.4437
DAA-39 - 5	1.225	0.061	0.1318	0.0026	0.0676	0.0034	0.042	0.0041	815	29	**798**	**15**	832	80	880	100	38.6	30.76	0.7969
DAA-39 - 6	1.471	0.042	0.1509	0.0026	0.0712	0.0019	0.0429	0.0037	917	17	**907**	**14**	849	73	961	58	81	47.7	0.5889
DAA-39 - 7	1.359	0.025	0.1433	0.0021	0.0685	0.0013	0.043	0.0037	873	11	**863.5**	**12**	851	72	887	42	168	41.3	0.2458
DAA-39 - 8	1.47	0.054	0.1523	0.0032	0.0701	0.0024	0.0457	0.0042	923	21	**917**	**19**	902	81	938	73	27.81	19.65	0.7066
DAA-39 - 9	1.997	0.036	0.1486	0.0026	0.0684	0.0016	0.0453	0.0042	886	15	**893**	**15**	895	82	873	49	95	16.49	0.1736
DAA-39 - 10	1.873	0.072	0.1809	0.0051	0.0748	0.002	0.055	0.0048	1068	25	**1071**	**28**	1082	92	1073	53	46.7	46.2	0

DAA-39 - 72	1.582	0.043	0.1609	0.0032	0.0713	0.0018	0.0491	0.0042	962	17	**961**	**18**	969	81	958	53	49.9	32.9	0.6593
DAA-39 - 73	1.526	0.069	0.1545	0.0032	0.0711	0.0029	0.0469	0.0049	942	27	**926**	**18**	926	95	952	90	22.12	13.4	0.6058
DAA-39 - 74	1.57	0.18	0.1649	0.0053	0.0677	0.008	0.0485	0.0096	930	73	**984**	**29**	950	180	770	250	4.7	1.484	0.3157
DAA-39 - 75	1.433	0.042	0.15	0.0027	0.0691	0.002	0.0452	0.0038	901	18	**901**	**15**	894	73	899	58	71.6	51.5	0.7193
DAA-39 - 76	1.338	0.022	0.1441	0.0024	0.0677	0.0016	0.04358	0.0035	861.9	9.7	**869.3**	**13**	862	68	861	49	126.1	199.4	1.5813
DAA-39 - 77	1.38	0.036	0.1429	0.0024	0.0703	0.0016	0.042	0.0036	882	16	**861**	**14**	832	71	938	45	108.4	40.1	0.3699
DAA-39 - 78	1.386	0.03	0.1448	0.0028	0.0699	0.0012	0.0416	0.0034	882	13	**872**	**16**	824	65	924	36	667	303	0.4543
DAA-39 - 79	1.6	0.12	0.1598	0.0043	0.0728	0.0051	0.058	0.013	965	44	**955**	**24**	1170	250	960	150	7.09	1.386	0.1955
DAA-39 - 80	1.638	0.043	0.1649	0.0029	0.0724	0.0021	0.0489	0.004	984	16	**984**	**16**	965	78	995	56	58.3	66.9	1.1475
DAA-39 - 81	1.463	0.039	0.1504	0.0027	0.0703	0.002	0.0454	0.0048	914	16	**903**	**15**	896	94	945	60	59.1	9.8	0.1658
DAA-39 - 82	1.527	0.037	0.1539	0.0036	0.07191	0.0012	0.04319	0.0035	940	15	**923**	**20**	855	67	984	35	200.5	383	1.9102
DAA-39 - 83	1.444	0.035	0.152	0.0027	0.0686	0.0018	0.0431	0.004	906	14	**912**	**15**	853	77	878	54	64.5	36.7	0.5690
DAA-39 - 84	1.437	0.067	0.1509	0.0032	0.0685	0.0033	0.0487	0.0058	901	28	**906**	**18**	973	110	890	100	21.67	8.08	0.3729
DAA-39 - 85	1.448	0.026	0.1511	0.0023	0.0697	0.0013	0.0466	0.0038	908.7	11	**906.8**	**13**	920	73	916	39	167.4	88.4	0.5281
DAA-39 - 86	1.399	0.038	0.1469	0.0026	0.0688	0.0018	0.0455	0.004	887	16	**884**	**15**	899	77	895	58	51.1	27.3	0.5342
DAA-39 - 87	1.495	0.055	0.1522	0.0026	0.0719	0.0027	0.0443	0.004	930	23	**913**	**15**	875	78	976	74	33.4	28.7	0.8593
DAA-39 - 88	1.901	0.061	0.1555	0.0034	0.0879	0.0026	0.0542	0.0044	1079	21	**932**	**19**	1066	84	1371	57	76.7	79.9	1.0417
DAA-39 - 89	1.41	0.031	0.1482	0.0024	0.0693	0.0017	0.04356	0.0035	892	13	**891**	**13**	862	69	900	50	92.9	70.4	0.7578
DAA-39 - 90	1.481	0.099	0.1528	0.0044	0.0688	0.0043	0.0437	0.0074	914	40	**916**	**25**	860	140	920	150	8.98	2.49	0.2773
DAA-39 - 91	1.514	0.04	0.1536	0.0028	0.0705	0.0018	0.046	0.004	935	16	**921**	**16**	909	77	937	51	69.1	35.33	0.5113
DAA-39 - 92	1.407	0.034	0.1474	0.0028	0.0695	0.0017	0.0448	0.0037	891	15	**886**	**16**	885	71	926	52	121.1	182.9	1.5103
DAA-39 - 93	1.402	0.052	0.1455	0.0031	0.0696	0.0025	0.0418	0.0042	887	22	**878**	**17**	828	82	910	74	43.8	12.4	0.2831
DAA-39 - 94	1.431	0.03	0.1496	0.0024	0.0694	0.0016	0.04476	0.0036	901	13	**898.4**	**13**	885	70	906	48	107.4	283	2.6350
DAA-39 - 95	1.552	0.086	0.1589	0.0034	0.0708	0.0043	0.0432	0.0052	951	36	**950**	**19**	853	100	940	140	17.33	5.39	0.3110
DAA-39 - 96	1.48	0.059	0.158	0.0034	0.067	0.0027	0.0456	0.0041	920	24	**945**	**19**	902	79	851	84	29.6	22.9	0.7736
DAA-39 - 97	1.52	0.041	0.1557	0.0025	0.0698	0.002	0.0436	0.0044	937	17	**932.8**	**14**	861	85	928	59	57.4	10.9	0.1899
DAA-39 - 98	1.45	0.075	0.1503	0.0034	0.0699	0.0036	0.0439	0.0039	907	32	**903**	**19**	869	75	910	110	41.2	38.3	0.9296
DAA-39 - 99	1.462	0.054	0.1547	0.0032	0.0682	0.0025	0.0481	0.0056	912	22	**927**	**18**	947	110	884	75	30.77	7.6	0.2470
DAA-39 - 100	0.284	0.015	0.03852	0.0008	0.0531	0.0031	0.025	0.01	253	12	**243.6**	**5**	490	200	340	120	53.7	0.922	0.0172
DAA-39 - 101	0.2547	0.0057	0.03701	0.00055	0.0501	0.0012	0.0116	0.0014	230.3	4.6	**234.3**	**3.4**	232	27	193	52	468	17.2	0.0368
DAA-39 - 102	1.437	0.049	0.1504	0.0023	0.0694	0.0025	0.0444	0.0039	902	21	**903.2**	**13**	877	76	903	79	58.4	44.4	0.7603
DAA-39 - 103	1.437	0.049	0.1506	0.003	0.0694	0.0026	0.0459	0.0042	902	20	**904**	**17**	907	82	917	81	31.9	27.5	0.8621
DAA-39 - 104	1.66	0.13	0.1619	0.0049	0.0735	0.0058	0.0503	0.0078	981	49	**967**	**27**	1010	160	1000	170	5.36	2.5	0.4664
DAA-39 - 105	1.477	0.079	0.1525	0.0032	0.0708	0.0038	0.0441	0.0055	915	33	**915**	**18**	870	110	910	110	19.8	7.39	0.3732
DAA-39 - 106	1.49	0.13	0.1553	0.0033	0.0698	0.0063	0.05	0.0073	929	51	**931**	**19**	980	140	890	180	13.85	6.13	0.4426
DAA-39 - 107	1.507	0.04	0.1553	0.0025	0.0705	0.0019	0.0453	0.0042	935	16	**930.5**	**14**	895	81	933	57	60.4	27.8	0.4603
DAA-39 - 108	1.756	0.058	0.1718	0.0036	0.0731	0.0023	0.0494	0.0042	1031	20	**1022**	**20**	974	81	1004	65	43.5	43.1	0.9908
DAA-39 - 109	1.736	0.067	0.1713	0.0036	0.0735	0.0027	0.0511	0.0047	1023	26	**1019**	**20**	1006	90	1024	76	22.3	20.2	0.9058
DAA-39 - 110	1.48	0.1	0.1531	0.0039	0.068	0.0045	0.043	0.0051	913	43	**918**	**20**	850	99	870	140	11.5	5.65	0.4913
DAA-39 - 111	1.448	0.041	0.1524	0.0028	0.0692	0.002	0.05	0.0044	911	16	**914**	**15**	986	85	894	61	54.6	13.7	0.2509
DAA-39 - 112	1.393	0.023	0.1457	0.0022	0.0685	0.0012	0.0442	0.0036	885.8	9.7	**877**	**12**	873	70	881	38	169.6	169.2	0.9976
DAA-39 - 113	1.393	0.043	0.1472	0.0029	0.0687	0.0019	0.0455	0.0039	884	18	**885**	**16**	899	76	881	58	70	31.31	0.4473
DAA-39 - 114	1.761	0.069	0.176	0.0054	0.0734	0.0019	0.0495	0.0044	1028	26	**1044**	**30**	976	85	1026	51	58.3	39.4	0.6758
DAA-39 - 115	1.428	0.052	0.1485	0.0028	0.0688	0.0028	0.0442	0.004	899	22	**892**	**16**	874	78	899	84	49.5	24.8	0.5010
DAA-39 - 116	1.456	0.027	0.1512	0.0023	0.0697	0.0014	0.0439	0.0036	912	11	**907.7**	**13**	868	70	926	42	119.3	57	0.4778
DAA-39 - 117	1.494	0.062	0.1559	0.0033	0.0706	0.0032	0.0435	0.0053	925	25	**934**	**18**	871	100	930	91	17.7	5.2	0.2938
DAA-39 - 118	1.504	0.035	0.1545	0.0024	0.0708	0.0015	0.0461	0.0038	931	14	**925.8**	**14**	911	73	946	45	143.6	99.7	0.6943
DAA-39 - 119	1.43	0.05	0.1519	0.0027	0.069	0.0024	0.0456	0.0047	899	21	**912**	**15**	900	91	907	70	34	15.51	0.4562
DAA-39 - 120	1.445	0.068	0.1517	0.0033	0.068	0.0033	0.0483	0.0054	914	28	**910**	**19**	953	110	875	95	21.03	6.25	0.2972
DAA-39 - 121	1.427	0.037	0.1483	0.0026	0.0698	0.0019	0.044	0.0038	899	15	**891**	**15**	869	74	914	56	84	40.4	0.4810
DAA-39 - 122	1.407	0.049	0.145	0.0023	0.0709	0.0025	0.0467	0.0044	890	21	**873**	**13**	923	84	962	72	48.8	20.3	0.4160
DAA-39 - 123	1.463	0.072	0.1566	0.0033	0.0681	0.0037	0.0527	0.0066	911	29	**937**	**18**	1050	130	870	100	13.3	4.4	0.3308
DAA-39 - 124	1.398	0.079	0.1521	0.0036	0.067	0.0041	0.0506	0.0073	884	34	**913**	**20**	990	140	800	130	19	5.92	0.3116
DAA-39 - 125	1.609	0.043	0.1617	0.0033	0.0714	0.0014	0.0506	0.0045	972	17	**966**	**18**	998	86	965	39	133.2	31.79	0.2387
DAA-39 - 126	1.401	0.025	0.1463	0.0025	0.0696	0.0013	0.04367	0.0035	888.9	11	**880**	**14**	864	69	914	37	294.2	153	0.5201
DAA-39 - 127	1.469	0.049	0.1497	0.0037	0.0718	0.0025	0.0465	0.0042	917	20	**899**	**21**	919	82	989	66	52.8	50.4	0.9545
DAA-39 - 128	1.435	0.047	0.1488	0.0027	0.0694	0.0022	0.0444	0.0039	902	19	**894**	**15**	878	76	908	68	39.5	20.9	0.5291
DAA-39 - 129	1.499	0.038	0.1571	0.0028	0.0704	0.0017	0.047	0.0041	935	16	**941**	**16**	928	79	934	50	95.7	50.3	0.5256
DAA-39 - 130	1.466	0.051	0.152	0.0029	0.0698	0.0027	0.0441	0.004	914	21	**912**	**16**	872	77	903	79	35.7	23.5	0.6583
DAA-39 - 131	1.503	0.048	0.1548	0.0025	0.0714	0.0024	0.0457	0.0039	933	19	**927.6**	**14**	903	75	964	71	44.8	22.3	0.4978
DAA-39 - 132	1.416	0.046	0.1496	0.003	0.0694	0.0022	0.046	0.0047	894	19	**898**	**17**	908	91	897	67	43.3	10.67	0.2464
DAA-39 - 133	1.35	0.043	0.1438	0.0027	0.0689	0.002	0.0425	0.0037	866	18	**866**	**15**	841	71	893	62	47.97	35.6	0.7421
DAA-39 - 134	1.74	0.045	0.1728	0.0032	0.074	0.0018	0.0507	0.0042	1022	17	**1027**	**18**	999	81	1033	50	63.9	49.73	0.7782
DAA-39 - 135	1.294	0.028	0.1378	0.0026	0.0683	0.0014	0.0421	0.0036	843	12	**832**	**15**	833	69	876	43	498	242	0.4859
DAA-39 - 136	1.422	0.069	0.1432	0.0052	0.0724	0.0046	0.0491	0.0071	906	24	**863**	**29**	970	140	980	130	23.52	6.74	0.2866
DAA-39 - 137	1.422	0.024	0.1493	0.0024	0.069	0.0011	0.04472	0.0036	897.8	10	**897.2**	**14**	884	70	900	33	442	261	0.5905
DAA-39 - 138	1.762	0.053	0.1745	0.0034	0.0726	0.0022	0.0494	0.0043	1030	20	**1036**	**19**	974	83	1001	59	55.2	45.3	0.8207
DAA-39 - 139	1.531	0.046	0.1555	0.003	0.0723	0.0025	0.0443	0.0048	944	20	**932**	**17**	874	93	978	71	33.3	7.32	0.2198
DAA-39 - 140	1.743	0.038	0.1704	0.0027	0.0738	0.0018	0.0486	0.004	1026	14	**1014.1**	**15**	959	78	1030	49	103.2	96.5	0.9351
DAA-39 - 141	1.487	0.035	0.1556	0.0029	0.0695	0.0015	0.0442	0.0039	924	14	**932**	**16**	875	75	909	45	60.2	42.8	0.7110
DAA-39 - 142	1.375	0.042	0.1448	0.0027	0.0685	0.0024	0.0481	0.0045	880	19	**872**	**15**	950	86	901	70	68.8	14.3	0.2078
DAA-39 - 143	1.552	0.069	0.1559	0.003	0.0712	0.0029	0.0419	0.0044	947	28	**934**	**17**	828	85	953	88	21.84	10.61	0.4858
DAA-39 - 144	1.572	0.096	0.1614	0.0053	0.0708	0.0042	0.0579	0.0078	955	38	**964**	**30**	1140	150	940	130	13.1	6.2	0.4733
DAA-39 - 145	1.625	0.042	0.1655	0.0033	0.0708	0.0014	0.0484	0.004	978	16	**987**	**18**	955	77	949	40	132.6	77.8	0.5867
DAA-39 - 146	1.407	0.052	0.1463	0.0029	0.0689	0.0023	0.0435	0.0044	893	22	**880**	**17**	861	85	892	72	28.3	13.7	0.4841
DAA-39 - 147	1.69	0.044	0.1662	0.0035	0.0741	0.0022	0.0466	0.0039	1004	17	**993**	**19**	920	75	1033	59	48	44.4	0.9250
DAA-39 - 148	1.59	0.11	0.1507	0.004	0.0759	0.0059	0.0544	0.0089	973	48	**905**	**23**	1070	170	1050	160	17.98	6.18	0.3437
DAA-39 - 149	1.453	0.037	0.1516	0.0026	0.0693	0.0017	0.0457	0.0043	910	15	**909.8**	**14**	902	83	908	51	93.8	17.8	0.1898
DAA-39 - 150	1.399	0.049	0.1471	0.0024	0.0697	0.0021	0.0458	0.0042	894	19	**884.9**	**14**	904	82	910	62	81.4	22.8	0.2801
DAA-39 - 151	1.412	0.028	0.1466	0.0031	0.0695	0.0013	0.04312	0.0035	894	12	**882**	**16**	857	68	913	38	316.2	129.9	0.4108
DAA-39 - 152	1.526	0.024	0.1556	0.0028	0.07063	0.00096	0.0464	0.0038	940.6	9.9	**932**	**16**	918	73	946	28	209	124.7	0.5967
DAA-39 - 153	1.453	0.061	0.155	0.0031	0.0677	0.0029	0.0467	0.0043	910	25	**929**	**17**	921	83	847	91	67.44	42.6	0.6317
DAA-39 - 154	1.562	0.074	0.155	0.0033	0.0735	0.0027	0.0457	0.0045	952	30	**939**	**18**	903	85	1027	79	26.6	13.66	0.5135
DAA-39 - 155	1.481	0.077	0.1517	0.0033	0.0711	0.0035	0.0469	0.004	927	32	**910**	**19**	925	77	959	96	19.2	56.1	2.9219
DAA-39 - 156	1.54	0.1	0.152	0.005	0.0752	0.0052	0.0479	0.0076	948	44	**912**	**28**	940	150	1030	150	9.36	3.18	0.3397
DAA-39 - 157	1.412	0.058	0.1493	0.0027	0.0674	0.0029	0.04	0.0053	899	23	**897**	**15**	804	99	854	83	38.2	6.5	0.1702
DAA-39 - 158	1.474	0.029	0.1517	0.0028	0.07043	0.0011	0.04516	0.0037	920	12	**910**	**16**	893	71	940	31	495	260	0.5253
DAA-39 - 159	2.42	0.11	0.161	0.0032	0.1079	0.0048	0.0716	0.0071	1242	33	**962**	**18**	1397	130	1767	83	21.32	12.13	0.5689
DAA-39 - 160	1.492	0.075	0.158	0.0039	0.0673	0.0034	0.0452	0.006	924	30	**946**	**22**	892	98	880	110	16.46	9.95	0.6045
DAA-39 - 161	1.624	0.033	0.1615	0.0027	0.0725	0.0015	0.0488	0.0041	979	14	**965**	**15**	963	79	996	44	96.1	58.8	0.6119
DAA-39 - 162	1.432	0.031	0.1487	0.0026	0.0699	0.0013	0.0441	0.0038	902	13	**894**	**15**	872	73	930	41	168.9	54	0.3197
DAA-39 - 163	1.483	0.044	0.1527	0.0032	0.0711	0.0018	0.046	0.0043	922	18	**916**	**18**	910	80	953	52	84	37.3	0.4440
DAA-39 - 164	1.52	0.16	0.1509	0.0043	0.0723	0.0075	0.04	0.012	937	62	**906**	**24**	790	240	940	210	5.63	1.082	0.1922
DAA-39 - 165	1.494	0.066	0.1503	0.0032	0.071	0.003	0.0427	0.0042	924	26	**903**	**18**	845	82	933	86	20.89	19.85	0.9502
DAA-39 - 166	1.535	0.069	0.1592	0.0038	0.0701	0.0033	0.0503	0.0061	941	28	**952**	**21**	990	120	898	100	17.13	6.35	0.3707
DAA-39 - 167	1.479	0.047	0.1537	0.0029	0.069	0.0021	0.0439	0.0053	923	18	**922**	**16**	882	110	898	61	37.04	6.59	0.1779
DAA-39 - 168	1.69	0.052	0.1656	0.0032	0.0748	0.0023	0.0508	0.0049	1007	21	**987**	**17**	1001	94	1054	64	41.9	22.75	0.5430
DAA-39 - 169	1.526	0.062	0.1519	0.004	0.0727	0.0035	0.0481	0.0056	939	25	**911**	**23**	949	110	986	100	21.1	8.4	0.3981
DAA-39 - 170	1.432	0.058	0.1509	0.0031	0.0679	0.0032	0.0477	0.0046	899	24	**908**	**18**	940	88	860	100	31.2	11.27	0.3612
DAA-39 - 171	1.424	0.065	0.1476	0.0025	0.0699	0.0032	0.0419	0.0048	896	27	**887.4**	**14**	829	93	918	100	40	13.06	0.3265
DAA-39 - 172	1.486	0.051	0.1554	0.0032	0.0689	0.0025	0.0465	0.005	926	20	**931**	**17**	917	97	939	73	30.2	10.9	0.3609
DAA-39 - 173	1.5	0.066	0.1548	0.0032	0.0715	0.003	0.0477	0.0056	937	27	**928**	**18**	940	110	1000	81	30.1	11.9	0.3953
DAA-39 - 174	1.864	0.085	0.1823	0.0043	0.0751	0.0032	0.0535	0.0048	1068	31	**1079**	**23**	1052	92	1047	86	30	27.8	0.9267
DAA-39 - 175	1.515	0.056	0.1568	0.0029	0.0706	0.0027	0.0453	0.0043	941	23	**939**	**16**	895	84	937	77	34.76	14.43	0.4151
DAA-39 - 176	1.475	0.072	0.1527	0.0034	0.0694	0.0028	0.0466	0.0051	921	30	**916**	**19**	920	98	889	82	16.6	6.94	0.4181
DAA-39 - 177	1.5	0.036	0.1571	0.0027	0.0694	0.0018	0.0466	0.0044	930	15	**941**	**15**	920	86	910	54	63.2	19.09	0.3021
DAA-39 - 178	0.564	0.509	0.1549	0.0041	0.0705	0.0027	0.0423	0.0049	932	26	**928**	**23**	836	95	930	77	28	16.56	0.5914
DAA-39 - 179	1.449	0.059	0.1485	0.0033	0.0718	0.0032	0.0438	0.0047	911	25	**892**	**18**	865	90	957	91	24.08	11.22	0.4659
DAA-39 - 180	1.366	0.03	0.1453	0.0025	0.0686	0.0014	0.0456	0.004	876	13	**874.4**	**14**	901	78	882	42	155.7	22.85	0.1468
DAA-39 - 181	1.415	0.039	0.1497	0.0023	0.0693	0.0021	0.0426	0.0036	894	17	**899.1**	**13**	834	70	894	67	53.4	46.7	0.8745
DAA-39 - 182	1.425	0.04	0.1498	0.0026	0.0688	0.0019	0.0448	0.0049	898	17	**900**	**15**	963	95	902	60	85.6	10.99	0.1284
DAA-39 - 183	1.471	0.036	0.1534	0.0028	0.0698	0.0019	0.0453	0.004	920	15	**920**	**16**	894	78	913	55	57.3	37.6	0.6562
DAA-39 - 184	1.924	0.068	0.184	0.0035	0.076	0.0026	0.0549	0.0047	1087	24	**1089**	**19**	1080	90	1080	69	45.7	26.8	0.5864
DAA-39 - 185	1.565	0.054	0.156	0.0034	0.0729	0.0027	0.0456	0.0039	960	20	**934**	**19**	902	76	1016	71	50.8	49.8	0.9803
DAA-39 - 186	1.441	0.036	0.1481	0.0023	0.0703	0.0018	0.0449	0.0041	905	15	**890**	**13**	886	79	927	54	88.6	25.6	0.2889
DAA-39 - 187	1.491	0.094	0.1513	0.0038	0.0713	0.0043	0.0405	0.0054	926	39	**917**	**21**	800	110	980	140	13.8	4.5	0.3261
DAA-39 - 188	1.423	0.047	0.1463	0.0027	0.0708	0.0024	0.0438	0.004	898	20	**880**	**15**	866	77	942	71	64.3	57.6	0.8958
DAA-39 - 189	1.452	0.087	0.1553	0.0035	0.0673	0.004	0.0338	0.0081	910	37	**931**	**20**	670	160	840	120	16.23	1.037	0.0639
DAA-39 - 190	1.494	0.052	0.1578	0.0028	0.0682	0.0022	0.046	0.0043	930	22	**944**	**16**	908	82	875	69	52.6	28.8	0.5475
DAA-39 - 191	1.626	0.085	0.162	0.0039	0.0733	0.0038	0.0441	0.0059	991	31	**968**	**22**	871	110	990	110	16.74	4.04	0.2413
DAA-39 - 192	1.368	0.029	0.1449	0.0023	0.068	0.0014	0.04095	0.0033	875	12	**872.1**	**13**	811	65	863	42	177	182	1.0282
DAA-39 - 193	1.505	0.043	0.1552	0.0025	0.0701	0.0021	0.0429	0.0046	931	17	**929.9**	**14**	848	88	921	60	45.2	9.95	0.2201
DAA-39 - 194	1.399	0.043	0.1504	0.0027	0.0683	0.0022	0.0433	0.0039	887	18	**903**	**15**	857	75	876	65	70.5	25.7	0.3645
DAA-39 - 195	1.423	0.071	0.1469	0.0037	0.0707	0.0036	0.0435	0.008	899	29	**883**	**21**	850	150	950	110	14.2	2.65	0.1866
DAA-39 - 196	1.404	0.031	0.148	0.0023	0.0686	0.0017	0.0413	0.0046	892	13	**891.2**	**14**	818	88	888	49	68.7	13.68	0.1991
DAA-39 - 197	1.577	0.063	0.1595	0.0033	0.0729	0.003	0.0465	0.0052	958	25	**954**	**19**	930	95	989	83	20.4	5.91	0.2897
MPR-33A																			
MPR_33A_1	0.314	0.013	0.04456	0.00081	0.0513	0.0017	0.01366	0.0011	276.9	9.7	**281**	**5**	274.3	21	245	74	392	264	0.6735
MPR_33A_2	0.295	0.01	0.0414	0.00097	0.05183	0.00082	0.01283	0.00093	262.3	7.8	**261.5**	**6**	257.7	19	274	36	1911	593	0.3103
MPR_33A_3	0.313	0.015	0.04372	0.00087	0.0519	0.0021	0.0138	0.0011	276	12	**275.8**	**5.4**	277	23	266	88	260.7	167.9	0.6440
MPR_33A_4	0.3035	0.0087	0.04258	0.00086	0.05188	0.00082	0.01283	0.00095	269	6.8	**268.8**	**5.3**	257.6	19	276	36	1293	371.9	0.2876
MPR_33A_5	0.3097	0.012	0.04304	0.00098	0.0524	0.0016	0.0141	0.0011	273.6	9.3	**271.6**	**6.1**	283	21	292	68	530	288	0.5434
MPR_33A_6	0.333	0.017	0.04546	0.0011	0.0534	0.0024	0.01434	0.0013	291	13	**286.5**	**6.9**	288	27	322	96	121.9	99.9	0.8195
MPR_33A_7	0.307	0.027	0.0445	0.0024	0.0504	0.0033	0.0133	0.0017	272	21	**280**	**15**	266	33	210	150	335	370	1.1045
MPR_33A_8	0.703	0.075	0.0888	0.003	0.0559	0.005	0.0273	0.0025	530	44	**549**	**18**	544	49	420	190	30	50.6	1.6867
MPR_33A_9	0.307	0.015	0.04377	0.00092	0.0511	0.0021	0.01414	0.0012	271	11	**276.1

MPR_33A_72	0.273	0.019	0.0307	0.0012	0.0648	0.0039	0.0112	0.0018	244	15	**194.8**	**7.5**	225	37	720	120	520	680	1.3077
MPR_33A_73	0.276	0.017	0.0378	0.0013	0.053	0.0024	0.01293	0.0011	247	14	**238.9**	**8**	260	22	321	99	310	481	1.5516
MPR_33A_74	0.305	0.018	0.04447	0.0011	0.0499	0.0027	0.01503	0.0013	269	14	**280.4**	**6.8**	301	26	180	110	178.3	162	0.9086
MPR_33A_75	0.3012	0.011	0.04229	0.00087	0.0519	0.0016	0.01219	0.00097	267.1	8.8	**267**	**5.4**	244.9	19	267	67	285.8	414	1.4486
MPR_33A_76	0.313	0.013	0.03998	0.001	0.057	0.0022	0.01503	0.0013	276	10	**252.7**	**6.3**	301	25	473	86	213	145.1	0.6812
MPR_33A_77	0.31	0.017	0.04337	0.00088	0.052	0.0027	0.01376	0.0012	273	13	**273.7**	**5.5**	276	24	270	110	203	214	1.0542
MPR_33A_78	0.346	0.015	0.0481	0.0013	0.0524	0.002	0.01383	0.0012	301	12	**302.6**	**8.1**	278	24	290	84	201.9	116.1	0.5750
MPR_33A_79	0.3001	0.0092	0.04238	0.00088	0.05155	0.00099	0.01257	0.00095	266.4	7.2	**267.5**	**5.4**	252.4	19	260	45	1460	691	0.4733
MPR_33A_80	0.328	0.014	0.04394	0.001	0.0545	0.0023	0.01426	0.0012	287.5	11	**277.2**	**6.4**	286	23	368	92	266	256	0.9624
MPR_33A_81	0.316	0.017	0.04439	0.001	0.0525	0.0027	0.01448	0.0012	278	13	**280**	**6.5**	291	24	280	110	171.9	144	0.8377
MPR_33A_82	0.31	0.015	0.04457	0.001	0.0507	0.0021	0.01297	0.001	274	12	**281.1**	**6.4**	260.4	20	216	89	318	431	1.3553
MPR_33A_83	0.328	0.016	0.0452	0.0012	0.053	0.0025	0.0135	0.0011	288	12	**284.8**	**7.6**	271	23	310	100	274	136.2	0.4971
MPR_33A_84	0.315	0.014	0.04387	0.00093	0.0523	0.002	0.014	0.0012	277.7	11	**276.8**	**5.7**	281	23	288	84	264	186.2	0.7053
MPR_33A_85	0.314	0.0083	0.04376	0.00088	0.05241	0.00076	0.01341	0.00098	277.2	6.4	**276.1**	**5.4**	269.3	19	300	34	2070	939	0.4536
MPR_33A_86	1.672	0.058	0.1645	0.0042	0.0736	0.0013	0.0485	0.0038	996	22	**981**	**23**	956	73	1025	36	254	91.1	0.3587
MPR_33A_87	0.2958	0.0094	0.04072	0.00093	0.0528	0.0014	0.01261	0.001	263	7.4	**257.3**	**5.8**	253	20	315	59	1368	512	0.3743
MPR_33A_88	0.305	0.011	0.04351	0.001	0.051	0.0012	0.0138	0.001	270.1	8.6	**274.6**	**6.4**	277	20	235	53	1211	1541	1.2725
MPR_33A_89	0.327	0.016	0.04607	0.0011	0.0517	0.0021	0.01353	0.0013	287	12	**290.3**	**6.6**	272	26	260	87	251	144.1	0.5741
MPR_33A_90	0.359	0.02	0.0492	0.0012	0.0528	0.0021	0.01453	0.0012	311	15	**309.8**	**7.6**	291	24	305	84	257	179.8	0.6996
MPR_33A_91	0.308	0.027	0.0436	0.0013	0.0516	0.0047	0.0138	0.0018	272	21	**275.3**	**8.2**	277	35	240	190	103.5	68.2	0.6589
MPR_33A_92	0.3188	0.012	0.04132	0.001	0.0559	0.002	0.01406	0.0012	280.7	9.2	**261**	**6.2**	282	24	433	77	328.2	151.2	0.4607
MPR_33A_93	0.308	0.018	0.0421	0.001	0.0534	0.003	0.01338	0.0012	272	14	**265.8**	**6.4**	269	23	320	120	128.9	102.1	0.7921
MPR_33A_94	0.473	0.024	0.0455	0.0015	0.0765	0.0032	0.02042	0.0017	392	17	**286.8**	**9.4**	408	34	1085	84	188	126.6	0.6734
MPR_33A_95	0.388	0.018	0.04329	0.0009	0.0642	0.0027	0.01616	0.0013	332	13	**273.2**	**5.6**	324	27	719	91	274	168	0.6131
MPR_33A_96	0.327	0.018	0.04416	0.001	0.0538	0.0023	0.01462	0.0012	287	14	**278.6**	**6.2**	293	24	349	97	245.1	192.4	0.7850
MPR_33A_97	0.3072	0.011	0.04366	0.00094	0.0512	0.0016	0.01335	0.001	271.8	8.9	**275.4**	**5.8**	268	20	244	68	449	429	0.9555
MPR_33A_98	0.321	0.014	0.04351	0.00095	0.0536	0.0019	0.01335	0.001	282	11	**274.6**	**5.8**	268	21	340	77	304	307.6	1.0118
MPR_33A_99	0.309	0.012	0.04354	0.00086	0.0516	0.0017	0.01362	0.0011	272.9	9.3	**274.7**	**5.3**	273.5	21	256	72	336	260	0.7738
MPR_33A_100	0.303	0.014	0.04295	0.00098	0.0512	0.0019	0.01365	0.0011	268.1	11	**271.1**	**6**	274	22	239	81	364	311	0.8544
MPR_33A_101	0.716	0.024	0.0879	0.0024	0.0592	0.0011	0.02907	0.0022	548	14	**543**	**14**	579	44	573	40	1270	226	0.1780
MPR_33A_102	0.31	0.011	0.04296	0.00093	0.0522	0.0012	0.01456	0.0011	274	8.1	**271.1**	**5.8**	292.2	21	288	53	524.7	421	0.8024
MPR_33A_103	0.3057	0.0097	0.04284	0.00083	0.0522	0.0012	0.01378	0.001	272.1	8.3	**270.4**	**5.1**	276.7	20	285	51	837	1046	1.2497
MPR_33A_104	0.3135	0.012	0.04344	0.00084	0.0524	0.0015	0.01417	0.0012	276.6	9.1	**274.1**	**5.2**	284	23	294	63	576	158.3	0.2748
MPR_33A_105	0.323	0.015	0.04414	0.001	0.0533	0.0024	0.01477	0.0012	284	12	**278.4**	**6.4**	296	24	323	95	227	142	0.6256
MPR_33A_106	0.384	0.02	0.0391	0.0012	0.0717	0.0041	0.01462	0.0013	329	15	**247.2**	**7.6**	293	26	950	110	305	260	0.8525
MPR_33A_107	0.2945	0.012	0.04066	0.00097	0.0526	0.0019	0.01243	0.00096	261.9	9.3	**256.9**	**6**	249.7	19	307	83	448	509	1.1362
MPR_33A_108	0.323	0.015	0.04452	0.0011	0.0527	0.0018	0.01338	0.0011	283.7	11	**280.8**	**6.6**	269	21	301	76	242	220	0.9091
GLV-11																			
GLV-11 - 1	4.54	0.11	0.3081	0.0065	0.1077	0.0017	0.0978	0.011	1743	22	**1731**	**32**	1885	210	1758	28	74.3	100.3	1.3499
GLV-11 - 2	4.77	0.19	0.3152	0.0049	0.1099	0.0039	0.0997	0.012	1776	34	**1774**	**19**	1919	220	1791	65	38.1	52.5	1.3780
GLV-11 - 3	0.762	0.015	0.0929	0.0012	0.0596	0.0011	0.03208	0.0037	575	8.9	**572.6**	**6.9**	638	73	584	39	472	380.6	0.8064
GLV-11 - 4	0.778	0.019	0.0949	0.0013	0.0596	0.0015	0.0331	0.0039	584	11	**584.6**	**7.7**	659	77	579	52	244	147.3	0.6037
GLV-11 - 5	1.922	0.054	0.1839	0.0035	0.0765	0.0021	0.0649	0.0081	1087	19	**1088**	**19**	1270	150	1098	53	99.5	50.6	0.5085
GLV-11 - 6	1.4	0.23	0.1616	0.0048	0.063	0.011	0.143	0.078	876	98	**965**	**26**	2.60E+03	1.30E+03	620	360	8.61	0.414	0.0481
GLV-11 - 7	8.45	0.31	0.415	0.013	0.1477	0.0047	0.145	0.039	2279	33	**2235**	**58**	2740	330	2316	54	68	60	0.8824
GLV-11 - 8	0.358	0.011	0.04811	0.0077	0.0542	0.0019	0.0232	0.0031	310.7	8.5	**302.9**	**4.8**	464	62	372	79	572	105.3	0.1841
GLV-11 - 9	2.105	0.043	0.1956	0.0026	0.0782	0.0015	0.063	0.0078	1149	14	**1151**	**14**	1234	150	1146	39	166.4	54.7	0.3287
GLV-11 - 10	2.142	0.04	0.1986	0.0024	0.078	0.0013	0.0624	0.0077	1162	13	**1148**	**13**	1222	150	1143	34	221.1	71.8	0.3244
GLV-11 - 11	0.697	0.026	0.0863	0.0016	0.0589	0.0025	0.0284	0.0037	536	16	**533.5**	**9.2**	566	73	534	91	113.2	63.7	0.5627
GLV-11 - 12	3.76	0.06	0.2735	0.0066	0.1002	0.0021	0.0824	0.011	1584	13	**1558**	**34**	1599	200	1625	40	541	218.4	0.4037
GLV-11 - 13	0.582	0.017	0.0745	0.0011	0.0567	0.0014	0.02679	0.0035	465	11	**463.3**	**6.4**	534	68	469	55	363	84.3	0.2322
GLV-11 - 14	0.9	0.025	0.1071	0.0016	0.0609	0.0018	0.03398	0.0043	651	13	**655.6**	**9.1**	675	85	620	64	235	180	0.7660
GLV-11 - 15	3.682	0.091	0.2694	0.0069	0.0993	0.0025	0.0825	0.011	1567	20	**1537**	**35**	1601	200	1609	47	207.5	193.4	0.9320
GLV-11 - 16	2.302	0.046	0.2051	0.0027	0.0814	0.0012	0.0635	0.0083	1212	14	**1203**	**14**	1245	160	1229	29	314	94.2	0.3000
GLV-11 - 17	1.453	0.051	0.1513	0.0029	0.0698	0.0025	0.0433	0.0062	909	21	**908**	**16**	857	120	905	72	50.4	14.82	0.2940
GLV-11 - 18	4.538	0.091	0.3058	0.0057	0.1075	0.002	0.0941	0.013	1738	17	**1720**	**28**	1817	230	1756	34	399	193	0.4837
GLV-11 - 19	4.02	0.079	0.2647	0.004	0.1098	0.0018	0.0864	0.011	1637	16	**1514**	**25**	1674	210	1792	31	133.4	82.9	0.6214
GLV-11 - 20	0.508	0.013	0.0632	0.0012	0.0585	0.0013	0.0191	0.0035	416.8	8.8	**395.3**	**7.6**	383	70	543	49	1825	25.11	0.0138
GLV-11 - 21	0.813	0.023	0.0848	0.0013	0.0696	0.0018	0.0417	0.0058	603	13	**524.9**	**7.6**	826	110	908	53	259.9	56.5	0.2174
GLV-11 - 22	0.693	0.023	0.0845	0.0014	0.0596	0.0016	0.0264	0.0039	534	14	**522.9**	**8.5**	527	77	579	59	315	51.3	0.1629
GLV-11 - 23	0.332	0.011	0.04504	0.00085	0.0534	0.0019	0.01429	0.002	290.6	8.2	**284**	**5.2**	287	40	363	93	337.9	284.8	0.8429
GLV-11 - 24	0.453	0.021	0.05522	0.00073	0.0596	0.003	0.01856	0.0027	378	15	**346.5**	**4.5**	372	53	550	110	114.5	78.3	0.6838
MG-063																			
MG-063 - 1	0.314	0.016	0.04371	0.00073	0.0521	0.0024	0.01392	0.0019	277	12	**275.8**	**4.5**	279	38	268	97	180.2	174.9	0.9706
MG-063 - 2	1.544	0.055	0.1563	0.0045	0.0718	0.0014	0.0491	0.007	946	22	**936**	**25**	968	140	976	40	406.3	85	0.2092
MG-063 - 3	1.711	0.046	0.1728	0.0048	0.0715	0.0018	0.0501	0.0068	1011	18	**1027**	**26**	988	130	963	54	320	156	0.4875
MG-063 - 4	1.467	0.071	0.1558	0.0033	0.0686	0.0035	0.0477	0.007	912	29	**933**	**18**	940	130	850	110	32.25	13.66	0.4236
MG-063 - 5	1.478	0.043	0.1533	0.0018	0.0698	0.0021	0.0481	0.0065	920	18	**919.5**	**10**	949	120	910	64	85.2	31.5	0.3697
MG-063 - 6	1.447	0.024	0.1515	0.0017	0.0694	0.0011	0.0471	0.0061	908.3	9.8	**909**	**9.6**	931	120	907	32	356	62.5	0.1756
MG-063 - 7	1.684	0.04	0.1678	0.0024	0.0728	0.0013	0.0544	0.007	1001	15	**1000**	**13**	1071	130	1004	38	176.3	83.9	0.4759
MG-063 - 8	1.519	0.043	0.1566	0.0025	0.0704	0.0017	0.0486	0.0065	937	17	**938**	**14**	959	130	931	51	73.9	34.3	0.4641
MG-063 - 9	1.517	0.043	0.1546	0.0021	0.0712	0.002	0.0488	0.0062	936	17	**927**	**12**	962	120	952	57	120.2	51	0.4243
MG-063 - 10	1.555	0.048	0.1567	0.0022	0.072	0.0021	0.0526	0.0068	950	19	**938**	**12**	1035	130	974	59	100.4	53	0.5279
MG-063 - 11	0.3152	0.0092	0.04318	0.00062	0.053	0.0016	0.01506	0.0018	277.9	7.2	**272.5**	**3.8**	302	36	318	68	300	235	0.7833
MG-063 - 12	1.533	0.04	0.1579	0.0021	0.0705	0.0016	0.0545	0.0065	942	16	**945**	**12**	1072	130	935	47	118.8	51.2	0.4310
MG-063 - 13	1.471	0.019	0.1522	0.0021	0.07018	0.00087	0.0512	0.0059	918	8	**913**	**12**	1008	110	931	26	521	252.8	0.4852
MG-063 - 14	1.53	0.05	0.1588	0.0026	0.07	0.0021	0.0547	0.0066	940	21	**950**	**14**	1075	130	912	65	76.1	34.2	0.4494
MG-063 - 15	2.622	0.063	0.2218	0.0037	0.0859	0.0022	0.0762	0.0089	1305	18	**1291**	**19**	1483	170	1330	49	134.5	51.26	0.3811
MG-063 - 16	1.437	0.039	0.1485	0.0024	0.0709	0.0023	0.0561	0.0064	903	16	**892**	**13**	1102	120	940	66	111	63.8	0.5748
MG-063 - 17	1.475	0.043	0.1503	0.0024	0.071	0.002	0.0552	0.0069	920	18	**903**	**14**	1086	130	955	55	489	85.6	0.1751
MG-063 - 18	1.535	0.043	0.1559	0.0021	0.0714	0.0018	0.0572	0.0063	943	17	**934**	**12**	1124	120	972	49	83.3	49.2	0.5906
MG-063 - 19	1.54	0.041	0.1558	0.0022	0.0713	0.0018	0.0578	0.0064	945	16	**934**	**12**	1135	120	969	54	89.6	54.9	0.6127
MG-063 - 20	1.467	0.074	0.1496	0.0036	0.0714	0.0037	0.0618	0.0078	915	31	**899**	**20**	1210	150	960	110	117.5	64.5	0.5489
MG-063 - 21	1.487	0.055	0.1534	0.0021	0.0701	0.0024	0.0594	0.0067	922	22	**920**	**12**	1165	130	912	72	80.6	28.6	0.3548
MG-063 - 22	0.3095	0.0063	0.0432	0.00032	0.05187	0.00099	0.01713	0.0017	279.7	4.9	**272.7**	**2**	343.4	35	273	44	1191	1245	1.0453
MG-063 - 23	2.884	0.065	0.24	0.0032	0.0872	0.0016	0.088	0.009	1376	17	**1386**	**17**	1704	170	1360	35	126	86.6	0.6873
MG-063 - 24	2.483	0.056	0.2149	0.0028	0.0839	0.0019	0.0802	0.0082	1266	16	**1255**	**15**	1558	160	1263	45	109.6	114	1.0401
MG-063 - 25	1.541	0.025	0.1533	0.002	0.07287	0.00086	0.0642	0.0067	946.4	9.9	**919**	**11**	1258	130	1009	24	908	54.1	0.0596
MG-063 - 26	1.494	0.048	0.1544	0.0027	0.0703	0.0018	0.0659	0.0071	926	19	**925**	**15**	1289	140	929	52	80.7	41.3	0.5118
MG-063 - 27	1.579	0.055	0.1578	0.0022	0.0726	0.0023	0.0626	0.007	960	21	**944**	**12**	1226	140	989	63	86	31.9	0.3709
MG-063 - 28	0.338	0.014	0.04203	0.00061	0.0584	0.0023	0.01833	0.0018	295	11	**265.4**	**3.7**	367	37	525	86	288	302	1.0486
MG-063 - 29	1.566	0.052	0.154	0.0025	0.0737	0.0023	0.0641	0.0074	956	20	**924**	**14**	1254	140	1025	64	81.2	46.3	0.5702
MG-063 - 30	1.691	0.05	0.1642	0.0037	0.0747	0.0017	0.0639	0.0064	1004	19	**980**	**20**	1226	140	1058	46	287	319.5	1.1132
MG-063 - 31	1.631	0.048	0.1674	0.0043	0.0706	0.0016	0.0648	0.0072	982	18	**998**	**24**	1269	140	942	46	338	74.9	0.2216
MG-063 - 32	1.455	0.03	0.15	0.0025	0.0705	0.0012	0.0618	0.0066	911	12	**901**	**14**	1212	130	937	36	150.7	48.5	0.3218
MG-063 - 33	1.543	0.063	0.1575	0.0029	0.0711	0.0026	0.06	0.0075	944	25	**943**	**16**	1176	140	938	79	40.8	19.66	0.4819
MG-063 - 34	2.27	0.049	0.2062	0.0037	0.0799	0.0011	0.0761	0.0082	1202	15	**1213**	**18**	1482	160	1191	28	363	106.2	0.2926
MG-063 - 35	1.805	0.041	0.1736	0.0034	0.0755	0.0014	0.061	0.0081	1047	15	**1032**	**18**	1196	150	1080	38	435	53.5	0.1230
MG-063 - 36	1.54	0.049	0.1558	0.0035	0.0719	0.0021	0.0469	0.0065	945	20	**933**	**20**	925	120	974	59	154.4	61.3	0.3970
MG-063 - 37	1.532	0.048	0.1546	0.0024	0.0719	0.0021	0.0449	0.0062	941	19	**926**	**14**	887	120	970	62	82.5	59.3	0.7188
MG-063 - 38	1.525	0.047	0.1558	0.0028	0.0711	0.0021	0.0449	0.0067	939	19	**933**	**16**	887	130	946	63	56	30.5	0.5446
MG-063 - 39	1.534	0.043	0.1553	0.002	0.0716	0.0017	0.0433	0.0061	943	17	**931**	**11**	857	120	967	48	114	136.6	1.1982
MG-063 - 40	1.509	0.037	0.1539	0.0018	0.0711	0.0017	0.0424	0.0062	933	15	**922.7**	**10**	839	120	953	48	102.3	46.1	0.4506
MG-063 - 41	1.626	0.059	0.1612	0.0026	0.0731	0.0024	0.0435	0.0068	977	23	**963**	**14**	860	130	1002	68	46.7	21.9	0.4690
MG-063 - 42	1.507	0.033	0.1539	0.0022	0.0711	0.0014	0.0414	0.0061	932	13	**923**	**13**	819	120	954	42	157.6	108.6	0.6891
MG-063 - 43	1.549	0.045	0.1567	0.0028	0.0711	0.0023	0.0419	0.0068	948	18	**938**	**16**	828	130	946	68	43.5	19.95	0.4586
MG-063 - 44	1.477	0.041	0.1511	0.0021	0.0709	0.0016	0.0409	0.0063	918	17	**907**	**12**	810	120	947	46	145.4	59.2	0.4072
MG-063 - 45	1.524	0.059	0.1603	0.0022	0.0696	0.0022	0.0418	0.0068	943	22	**959**	**12**	828	130	899	69	50.7	31.9	0.6292
MG-063 - 46	1.458	0.068	0.1467	0.0025	0.0715	0.0034	0.0411	0.0071	911	28	**882**	**14**	813	140	954	99	57.5	42.1	0.7322
MG-063 - 47	1.517	0.044	0.1539	0.0023	0.0719	0.0023	0.0417	0.0068	940	20	**923**	**13**	826	130	968	65	84.9	47.5	0.5595
MG-063 - 48	2.17	0.21	0.1018	0.0029	0.156	0.016	0.111	0.031	1146	68	**625**	**17**	2090	530	2290	180	46.6	16	0.3433
MG-063 - 49	1.691	0.045	0.1675	0.0023	0.073	0.0019	0.0452	0.007	1004	17	**998**	**13**	893	140	1005	51	137.5	121.4	0.8829
MG-063 - 50	1.522	0.046	0.1546	0.002	0.0714	0.0019	0.038	0.0061	937	18	**927**	**11**	754	120	957	56	91.4	60.74	0.6646
MG-063 - 51	1.503	0.031	0.1529	0.0021	0.0713	0.0014	0.0413	0.0066	931	13	**917**	**12**	817	130	961	41	135.7	69.9	0.5151
MG-063 - 52	0.671	0.01	0.0755	0.0012	0.06433	0.00054	0.01849	0.003	520.9	6.2	**468.9**	**7.1**	370	58	752	18	3160	228	0.0722
MG-063 - 53	2.584	0.061	0.2196	0.0034	0.0854	0.0017	0.0553	0.0087	1294	17	**1279**	**18**	1088	160	1318	39	93	95.6	1.0280
MG-063 - 54	1.437	0.028	0.1495	0.0017	0.0697	0.0012	0.0405	0.0066	904	12	**898.3**	**9.4**	802	130	914	37	197	47.4	0.2406
MG-063 - 55	1.489	0.041	0.152	0.002	0.0711	0.0019	0.0409	0.0064	924	17	**912**	**11**	810	120	949	57	93.1	72	0.7734
MG-063 - 56	1.574	0.07	0.1595	0.0034	0.0709	0.0027	0.0402	0.0073	956	27	**954**	**19**	796	140	949	86	27.2	13.77	0.5063
MG-063 - 57	1.007	0.052	0.107	0.0038	0.0682	0.0028	0.0374	0.0064	705	27	**655**	**22**	742	120	861	88	116.6	40.3	0.3456
MG-063 - 58	1.475	0.058	0.1534	0.0032	0.0699	0.0028	0.0412	0.0069	917	24	**920**	**18**	816	130	920	76	36.8	15.46	0.4201
MG-063 - 59	1.462	0.027	0.1509	0.0021	0.07004	0.00094	0.0395	0.0061	914	11	**906**	**12**	782	120	927	28	890	205	0.2303
MG-063 - 60	0.304	0.02	0.04383	0.00087	0.0502	0.0029	0.01524	0.0024	268	15	**276.5**	**5.4**	250	47	190	120	89.4	42.5	0.4754
MG-063 - 61	0.32	0.014	0.04312	0.00068	0.0538	0.0022	0.01173	0.0018	281	11	**272.1**	**4.2**	235.6	36	341	89	190.8	210	1.1006
MG-063 - 62	0.989	0.03	0.0984	0.0012	0.0732	0.002	0.0473	0.0076	697	16	**605.2**	**7.3**	933	150	1009	57	226.4	34.56	0.1527
MG-063 - 63	1.49	0.044	0.155	0.0022	0.0697	0.002	0.0404	0.0063	925	18	**929**	**12**	800	120	908	60	71.9	45	0.6258
MG-063 - 64	1.566	0.057	0.1555	0.003	0.0731	0.0028	0.0413	0.0065	955	23	**932**	**17**	818	130	1003	77	75	51.3	0.6840
MG-063 - 65	1.566	0.064	0.1557	0.0027	0.073	0.0029	0.0447	0.0076	955	25	**933**	**15**	882	150	997	83	44.3	26.3	0.5937
MG-063 - 66	1.505	0.058	0.1532	0.0023	0.0712	0.0025	0.0422	0.0063	929	23	**919**	**13**	835	120	946	72	71.3	54.2	0.7602
MG-063 - 67	1.506	0.054	0.1585	0.0029	0.069	0.0024	0.0432	0.0069	930	22	**948**	**16**	867	150	880	73	50.2	21.8	0.4343
MG-063 - 68	1.53	0.068	0.1582	0.0029	0.0708	0.0029	0.0468	0.0075	945	30	**946**	**16**	923	140	927	86	39.7	16.63	0.4189
MG-063 - 69	1.51	0.044	0.1545	0.0021	0.0709	0.002	0.0426	0.0063	933	18	**926**	**12**	815	120	944	57	85.9	59.9	0.6973
MG-063 - 70	1.56	0.11	0.1519	0.0027	0.0748	0.0055	0.0484	0.007	952	44	**912**	**15**	955	140	1040	160	68.6	39.7	0.5787
MG-063 - 71	1.484	0.035	0.1517	0.0032	0.0711	0.0013	0.0458	0.0061	923	14	**910**	**18**	904	120	957	38	292	173.2	0.5932
MG-063 - 72	1.453	0.021	0.1449	0.0022	0.07277	0.00072	0.0499	0.0066	910.9	8.8	**872**	**13**	984	130	1006	20	1144	105.6	0.0923
MG-063 - 73	0.304	0.013	0.04345	0.00065	0.0507	0.0022	0.01419	0.0019	269	10	**274.1**	**4**	285	38	217

MG-063 - 132	1.467	0.041	0.1496	0.0028	0.0713	0.0022	0.0413	0.0067	916	17	**899**	**16**	817	130	959	63	156.3	43.49	0.2782
MG-063 - 133	1.544	0.059	0.1597	0.0028	0.0701	0.0025	0.0447	0.0068	946	24	**955**	**16**	883	130	916	77	66.6	39.5	0.5931
MG-063 - 134	1.537	0.061	0.156	0.0023	0.0712	0.0028	0.0442	0.0072	942	24	**934**	**13**	873	140	940	81	57.7	23.21	0.4023
MG-063 - 135	1.739	0.032	0.1696	0.0018	0.0743	0.0013	0.0469	0.0069	1022	12	**1010**	**9.9**	926	130	1046	35	250	44.2	0.1768
MG-063 - 136	1.523	0.049	0.1544	0.0022	0.0713	0.0024	0.0458	0.0066	938	20	**926**	**12**	904	130	965	65	67.8	40.8	0.6018
MG-063 - 137	1.669	0.055	0.1567	0.0025	0.0794	0.0024	0.0524	0.0076	994	21	**910**	**14**	1032	150	1170	58	82.6	37.9	0.4588
MG-063 - 138	1.501	0.052	0.1531	0.0022	0.0709	0.0025	0.0434	0.0064	928	21	**918**	**12**	858	120	935	74	50.3	27.14	0.5396
MG-063 - 139	1.194	0.031	0.1159	0.0026	0.0747	0.0011	0.0487	0.0061	797	14	**707**	**15**	962	120	1057	28	570	96.8	0.1698
MG-063 - 140	0.322	0.017	0.04395	0.00062	0.0532	0.0028	0.0158	0.0021	283	13	**277.2**	**3.8**	317	42	310	110	150	77.8	0.5187
MG-063 - 141	1.558	0.027	0.1475	0.002	0.0767	0.0013	0.0586	0.0072	953	11	**887**	**11**	1150	140	1111	34	469	124.9	0.2663
MG-063 - 142	1.421	0.056	0.136	0.004	0.0755	0.0018	0.0785	0.011	897	24	**822**	**23**	1530	200	1079	45	882	145.1	0.1645
MG-063 - 143	0.3155	0.0095	0.04361	0.00076	0.0521	0.0013	0.0168	0.002	278.2	7.3	**277**	**4.7**	337	39	280	56	444	304	0.6847
MG-063 - 144	1.631	0.079	0.1592	0.003	0.0743	0.0031	0.0589	0.0072	980	30	**953**	**17**	1156	140	1039	86	175	60.9	0.3480
MG-063 - 145	1.675	0.049	0.1691	0.0024	0.0717	0.0018	0.0528	0.0062	997	18	**1007**	**13**	1040	120	969	51	79	56.5	0.7152
MG-063 - 146	1.52	0.051	0.1545	0.0029	0.072	0.0025	0.0539	0.0068	941	22	**926**	**16**	1099	130	968	69	61.7	33.7	0.5462
MG-063 - 147	2.235	0.082	0.199	0.0063	0.0816	0.002	0.0775	0.011	1191	26	**1170**	**34**	1510	200	1234	49	441	58.5	0.1327
MG-063 - 148	1.896	0.072	0.1781	0.003	0.0775	0.0032	0.089	0.014	1079	25	**1057**	**16**	1720	250	1130	82	594	15.6	0.0263
MG-063 - 149	2.64	0.11	0.2231	0.0057	0.086	0.0024	0.0763	0.0088	1311	30	**1298**	**30**	1485	170	1335	56	298.1	196	0.6575
MG-063 - 150	1.89	0.035	0.1833	0.0028	0.07473	0.00098	0.0633	0.0072	1077	12	**1085**	**15**	1241	140	1060	27	995	393	0.3950
MG-063 - 151	0.34	0.011	0.04698	0.00076	0.0524	0.0016	0.01878	0.0023	296.7	8.4	**296**	**4.7**	376	45	291	67	392.5	228.8	0.5829
MG-063 - 152	0.3	0.0046	0.04229	0.00056	0.0514	0.00087	0.01467	0.0017	266.4	3.6	**267**	**3.4**	294.4	33	255	38	1050	2150	2.0476
MG-063 - 153	1.555	0.037	0.1621	0.003	0.07	0.0018	0.0533	0.0066	951	15	**968**	**16**	1049	130	920	52	113.7	37.8	0.3325
MG-063 - 154	1.492	0.042	0.1524	0.002	0.0709	0.0018	0.0517	0.006	926	17	**914**	**11**	1018	120	946	52	129.7	187.7	1.4472
MG-063 - 155	0.333	0.025	0.04533	0.00071	0.0528	0.0039	0.0157	0.0021	290	19	**285.8**	**4.4**	315	42	290	150	94	29.5	0.3138
MG-063 - 156	1.506	0.088	0.1547	0.0032	0.0707	0.0041	0.053	0.0076	929	36	**927**	**18**	1043	150	920	120	24.22	20.29	0.8377
MG-063 - 157	0.3115	0.0092	0.04367	0.00049	0.0517	0.0016	0.01527	0.0019	275	7.2	**275.5**	**3**	306	39	262	68	332	180	0.5422
MG-063 - 158	0.323	0.012	0.04187	0.00077	0.0559	0.0019	0.01478	0.0018	283.7	9.3	**264.4**	**4.8**	296	37	435	76	471	243.4	0.5168
MG-063 - 159	1.54	0.1	0.1512	0.0041	0.0735	0.0044	0.052	0.0077	941	42	**907**	**23**	1023	150	1000	120	45.2	20.91	0.4626
MG-063 - 160	1.759	0.034	0.1708	0.0031	0.0746	0.0014	0.0564	0.007	1030	12	**1016**	**17**	1109	130	1054	36	241	137.6	0.5710
MG-063 - 161	0.3074	0.0089	0.04235	0.00094	0.0525	0.0013	0.01318	0.0016	272.1	6.9	**267.4**	**5.8**	264.6	33	302	57	1290	2820	2.1860
MG-063 - 162	1.513	0.038	0.1521	0.0036	0.0722	0.0015	0.0499	0.0064	935	16	**913**	**20**	984	120	990	42	287	177.2	0.6174
MG-063 - 163	1.406	0.042	0.1454	0.0025	0.0702	0.0021	0.0469	0.0062	890	18	**875**	**16**	926	120	919	64	87.6	48.1	0.5491
MG-063 - 164	1.639	0.054	0.1619	0.003	0.0742	0.0024	0.0523	0.0068	991	24	**967**	**16**	1030	130	1039	64	121	102	0.8430
MG-063 - 165	0.304	0.019	0.04351	0.00092	0.0499	0.0031	0.01459	0.002	268	15	**274.5**	**5.7**	293	41	210	130	124.4	57.4	0.4614
MG-063 - 166	1.531	0.059	0.156	0.0026	0.0711	0.0026	0.0501	0.0072	940	24	**934**	**14**	988	140	940	75	39.1	18.1	0.4629
MG-063 - 167	1.515	0.065	0.1534	0.0029	0.0717	0.0031	0.0479	0.0068	934	27	**920**	**16**	945	130	956	88	54.9	26.43	0.4814
MG-063 - 168	1.599	0.045	0.1602	0.0023	0.0715	0.0013	0.0522	0.007	969	18	**958**	**13**	1028	130	971	38	335	70.9	0.2116
MG-063 - 169	0.315	0.014	0.04281	0.00074	0.0532	0.0028	0.01357	0.0019	277	11	**270.2**	**4.6**	272	38	310	110	127.4	106	0.8320
MG-063 - 170	1.492	0.037	0.1526	0.0018	0.0709	0.0018	0.0463	0.0063	926	15	**915.6**	**10**	928	120	943	53	120.5	82.2	0.6822
MG-063 - 171	1.473	0.057	0.1534	0.0019	0.0694	0.0028	0.048	0.007	916	23	**920**	**11**	946	130	888	82	67.7	32.6	0.4815
MG-063 - 172	0.313	0.0097	0.04448	0.00069	0.0509	0.0014	0.01346	0.0018	276.2	7.5	**280.5**	**4.3**	270	37	232	59	446	226	0.5067
MG-063 - 173	0.323	0.012	0.04507	0.00066	0.0521	0.0021	0.0146	0.0022	284	8.9	**284.2**	**4.1**	292	44	269	87	120.7	57.3	0.4747
LRW-21																			
LRW_21_1	0.2579	0.0078	0.03694	0.00073	0.0507	0.0011	0.01123	0.00087	232.9	6.3	**233.8**	**4.5**	225.8	17	223	48	1325	305	0.2302
LRW_21_2	0.2631	0.0094	0.03677	0.00081	0.052	0.0015	0.01118	0.0012	237	7.6	**232.2**	**5**	225	23	276	61	500	85.5	0.1910
LRW_21_3	0.2561	0.01	0.03603	0.00074	0.0517	0.0018	0.01129	0.0011	231.3	8.4	**228.1**	**4.6**	227	22	258	75	448	103.8	0.2317
LRW_21_4	0.2622	0.01	0.037	0.00073	0.0514	0.0014	0.01157	0.0011	236.2	8.2	**234.2**	**4.6**	233	22	249	60	479	108.6	0.2267
LRW_21_5	0.2654	0.011	0.03687	0.00074	0.0523	0.0017	0.01209	0.001	238.7	8.8	**233.4**	**4.6**	243	21	281	74	463	88.8	0.2134
LRW_21_6	0.2577	0.0087	0.03626	0.00072	0.0514	0.0014	0.01182	0.0011	232.7	7	**229.6**	**4.5**	238	22	249	60	690	147	0.2130
LRW_21_7	0.2621	0.01	0.03698	0.00084	0.0514	0.0013	0.01126	0.0011	236.1	8.4	**234.1**	**5.2**	226	22	250	57	554	70.2	0.1267
LRW_21_8	0.2548	0.01	0.03661	0.00079	0.0506	0.0017	0.01164	0.001	230.2	8.2	**231.8**	**4.9**	234	23	211	71	329	62.1	0.1888
LRW_21_9	0.2531	0.01	0.0366	0.00073	0.0502	0.0017	0.01127	0.0011	228.8	8.4	**231.7**	**4.5**	226	22	193	70	325	49.4	0.1520
LRW_21_10	0.2551	0.011	0.03643	0.00074	0.0509	0.002	0.01154	0.00097	230.4	9	**230.6**	**4.6**	232	19	223	82	357	67.6	0.1894
LRW_21_11	0.2484	0.011	0.03647	0.00076	0.0495	0.0019	0.01185	0.0012	225	8.6	**230.9**	**4.7**	238	24	166	80	406	64.1	0.1579
LRW_21_13	0.258	0.012	0.03786	0.00099	0.0496	0.002	0.01144	0.0011	233.1	9.7	**239.5**	**6.1**	230	22	171	84	414	91.5	0.2210
LRW_21_15	0.2684	0.01	0.03752	0.00076	0.0518	0.0017	0.01187	0.0011	241.1	8.2	**237.4**	**4.7**	238	21	264	71	398	108.7	0.2731
LRW_21_17	0.265	0.012	0.03858	0.00098	0.05	0.0021	0.01301	0.0013	238.7	10	**244**	**6**	261	27	188	87	301.2	50.7	0.1683
LRW_21_18	0.258	0.015	0.0382	0.00096	0.049	0.0023	0.0125	0.0014	233	12	**241.7**	**6**	250	29	148	97	249.1	37.8	0.1517
LRW_21_19	0.277	0.02	0.03829	0.0011	0.0523	0.0035	0.0109	0.0013	247	16	**242.2**	**6.6**	219	25	270	140	70.2	33.93	0.4833
LRW_21_20	0.274	0.0092	0.03877	0.00088	0.0513	0.001	0.01151	0.00087	245.7	7.3	**245.2**	**5.5**	231.4	17	247	47	1596	420	0.2789
LRW_21_21	0.269	0.015	0.0376	0.0011	0.0519	0.0027	0.0117	0.0016	242	12	**238.1**	**7.1**	236	31	270	110	397	54.8	0.1380
LRW_21_22	0.278	0.012	0.03874	0.001	0.0521	0.0019	0.01164	0.0013	249	9.9	**245**	**6.5**	234	26	279	81	442	117.1	0.2649
LRW_21_23	0.2714	0.01	0.03842	0.00075	0.051	0.0014	0.01187	0.001	243.6	8.3	**243**	**4.6**	238	21	231	59	530	126.6	0.2389
LRW_21_24	0.277	0.012	0.03807	0.00085	0.0533	0.002	0.01171	0.0011	247.9	9.7	**240.8**	**5.3**	235	22	322	82	376	98.7	0.2625
LRW_21_25	0.2634	0.0092	0.03791	0.00081	0.0504	0.0014	0.01136	0.0011	237.3	7.4	**239.8**	**5**	228	23	208	60	636	97.4	0.1531
LRW_21_26	0.27	0.019	0.03767	0.00087	0.052	0.0035	0.013	0.0016	242	15	**238.3**	**5.4**	262	31	250	130	675	32.5	0.4815
LRW_21_27	0.2639	0.011	0.03763	0.0008	0.0509	0.0018	0.01218	0.0013	237.5	8.6	**238.1**	**5**	245	26	224	78	371	64.4	0.1736
LRW_21_28	0.267	0.012	0.03772	0.00085	0.0515	0.002	0.01159	0.0012	240.3	9.8	**238.6**	**5.3**	233	25	249	85	271	53.6	0.1978
LRW_21_29	0.263	0.012	0.03805	0.00079	0.0494	0.0021	0.01244	0.0012	236.6	9.8	**240.7**	**4.9**	250	25	182	94	284	62.8	0.2211
LRW_21_30	0.2712	0.011	0.03735	0.0009	0.0527	0.0017	0.01175	0.001	243.4	8.7	**236.4**	**5.6**	236	21	304	72	577	136.4	0.2364
LRW_21_31	0.2578	0.0084	0.03713	0.00087	0.0504	0.0013	0.01211	0.00096	232.8	6.8	**235**	**5.4**	243.2	19	209	56	557	150	0.2693
LRW_21_32	0.268	0.011	0.03741	0.00086	0.0519	0.0016	0.0121	0.0014	240.8	8.6	**236.7**	**5.3**	243	27	271	68	365	57.4	0.1573
LRW_21_33	0.2623	0.011	0.03641	0.00081	0.0517	0.0015	0.0127	0.0014	236.1	8.4	**230.6**	**5.1**	254	28	277	68	374	60.5	0.1618
LRW_21_34	0.264	0.014	0.03732	0.00081	0.0513	0.0023	0.0114	0.0014	237.7	11	**236.2**	**5.1**	229	27	242	96	321	50.7	0.1579
LRW_21_35	0.273	0.012	0.03776	0.00073	0.0524	0.0016	0.01279	0.0012	245.1	9.3	**239.7**	**4.5**	257	23	292	70	454	94.1	0.2073
LRW_21_36	0.2624	0.011	0.03709	0.00076	0.0513	0.0018	0.01257	0.0013	236.3	8.8	**234.7**	**4.7**	252	25	243	76	379	64.9	0.1712
LRW_21_37	0.2658	0.01	0.03734	0.00081	0.0516	0.0016	0.01129	0.00098	239.1	8	**236.3**	**5**	227	20	255	67	548	149	0.2719
LRW_21_38	0.263	0.015	0.03843	0.00091	0.0497	0.0027	0.0125	0.0018	237	12	**243.1**	**5.7**	251	36	170	110	144	31.8	0.2208
LRW_21_39	0.265	0.012	0.03763	0.00087	0.051	0.0018	0.01134	0.0012	238.2	9.3	**238.1**	**5.4**	228	24	231	78	311	63	0.2026
LRW_21_40	0.2614	0.0094	0.03684	0.00078	0.0511	0.0014	0.01144	0.00097	235.6	7.5	**233.2**	**4.9**	230	19	239	62	695	214.9	0.3092
LRW_21_41	0.2541	0.0086	0.03636	0.0007	0.0506	0.0012	0.01153	0.0011	229.7	7	**230.2**	**4.3**	232	21	214	52	818	135.9	0.1661
LRW_21_42	0.257	0.012	0.03661	0.0009	0.0508	0.002	0.01152	0.0012	231.6	9.4	**231.8**	**5.6**	232	24	224	84	347	59.5	0.1715
LRW_21_45	0.28	0.016	0.0383	0.00082	0.0528	0.0026	0.0126	0.0015	250	12	**242.3**	**5.1**	253	31	300	100	220.8	34	0.1540
LRW_21_46	0.2699	0.011	0.03774	0.00083	0.0518	0.0018	0.01243	0.0011	242.3	8.8	**238.8**	**5.1**	250	23	260	75	416	91.8	0.2207
LRW_21_47	0.2719	0.01	0.03851	0.00096	0.0511	0.0015	0.01232	0.001	244	8.3	**243.5**	**6**	248	20	237	64	565	150.4	0.2662
LRW_21_48	0.2645	0.0099	0.03727	0.00078	0.0514	0.0016	0.01133	0.001	238	7.9	**235.9**	**4.8**	228	20	247	67	656	132.9	0.2026
LRW_21_49	0.27	0.013	0.03762	0.00082	0.0519	0.0022	0.0121	0.0014	242	11	**238.1**	**5.1**	244	29	261	91	260.3	42.6	0.1637
LRW_21_50	0.2672	0.011	0.038	0.00088	0.051	0.0019	0.01243	0.0012	240.1	8.7	**240.4**	**5.4**	250	25	227	79	373	67.4	0.1807
LRW_21_51	0.2664	0.01	0.038	0.00089	0.0508	0.0015	0.01156	0.00099	239.6	8	**240.4**	**5.5**	232	20	218	64	571	97	0.1699
LRW_21_52	0.266	0.011	0.03747	0.0009	0.051	0.0013	0.01177	0.001	239.2	8.6	**237.1**	**5.6**	236	21	248	63	618	93.2	0.1508
LRW_21_53	0.265	0.012	0.03844	0.00097	0.0501	0.002	0.0124	0.0014	238.7	9.4	**243.1**	**6**	248	27	191	84	338	55.8	0.1651
LRW_21_54	0.2659	0.011	0.03733	0.00087	0.0519	0.0014	0.01193	0.00095	239.1	9.1	**236.2**	**5.4**	239.7	19	271	59	653	202.6	0.3103
LRW_21_55	0.276	0.014	0.03793	0.00088	0.0525	0.0022	0.01132	0.0012	246.7	11	**240**	**5.5**	227	23	293	91	183.3	46.8	0.2553
LRW_21_57	0.275	0.013	0.03853	0.00089	0.0512	0.0018	0.0127	0.0015	246	10	**243.7**	**5.5**	254	29	239	74	337	59.9	0.1777
LRW_21_58	0.2657	0.011	0.03714	0.00076	0.0515	0.0015	0.01154	0.0011	238.9	8.6	**235.1**	**4.7**	232	22	253	65	444	61.6	0.1387
LRW_21_59	0.2783	0.01	0.0384	0.00081	0.0525	0.0016	0.0117	0.0013	249.1	8.1	**242.9**	**5**	235	27	294	69	341	52.8	0.1548
LRW_21_60	0.278	0.013	0.03799	0.00098	0.0529	0.0023	0.0128	0.0013	248.6	10	**240.4**	**6.1**	257	26	310	96	407	70.8	0.1740
LRW_21_61	0.2588	0.01	0.03674	0.001	0.0516	0.0021	0.01156	0.0011	235.9	9.7	**232.6**	**6.3**	232	21	257	86	859	204.3	0.2378
LRW_21_62	0.259	0.024	0.03848	0.00083	0.0488	0.0047	0.0134	0.0016	233	20	**243.4**	**5.2**	269	32	140	200	395.9	88.1	0.2225
LRW_21_63	0.264	0.014	0.03792	0.00082	0.0506	0.0024	0.0114	0.0018	237.2	11	**239.9**	**5.1**	229	36	208	99	244	35.3	0.1447
LRW_21_66	0.273	0.014	0.03952	0.001	0.0499	0.002	0.0119	0.0014	244.8	11	**249.8**	**6.2**	240	27	186	86	240.2	53.3	0.2219
LRW_21_67	0.2731	0.0098	0.03819	0.00087	0.0517	0.0013	0.01157	0.0009	245	7.8	**241.6**	**5.4**	232.5	18	264	57	815	268	0.3288
LRW_21_68	0.2681	0.01	0.03771	0.00087	0.0514	0.0015	0.01227	0.0011	240.9	8.2	**238.6**	**5.4**	246	22	248	63	530	120.4	0.2272
LRW_21_69	0.2646	0.01	0.03776	0.00082	0.0506	0.0013	0.01154	0.0012	238.1	8.3	**238.9**	**5.1**	232	24	216	58	547	104.9	0.1918
LRW_21_70	0.267	0.012	0.0377	0.00084	0.0512	0.002	0.01172	0.0012	239.8	9.3	**238.6**	**5.2**	235	24	236	86	366	60	0.1639
LRW_21_71	0.258	0.011	0.03766	0.00084	0.0496	0.0018	0.01244	0.0013	232.8	8.5	**238.3**	**5.2**	250	26	169	78	406	88.2	0.2172
LRW_21_72	0.262	0.013	0.03787	0.00096	0.05	0.0022	0.01237	0.0013	235.6	11	**239.6**	**6**	248	26	186	90	347	54.2	0.1562
LRW_21_74	0.2575	0.009	0.0368	0.00071	0.0507	0.0013	0.01126	0.00093	232.5	7.3	**232.9**	**4.4**	226	19	220	57	977	294.1	0.3010
LRW_21_75	0.2603	0.0076	0.03705	0.00077	0.0508	0.0011	0.01163	0.0009	234.8	6.1	**234.5**	**4.8**	233.7	18	225	47	1030	338	0.3282
LRW_21_76	0.2654	0.0083	0.03754	0.00073	0.0511	0.0012	0.01177	0.0009	238.9	6.7	**237.6**	**4.5**	236.5	18	238	50	1193	240.8	0.2018
LRW_21_77	0.2691	0.011	0.03809	0.00093	0.051	0.0017	0.01225	0.0012	241.6	9	**241**	**5.8**	246	24	235	73	601	100.5	0.1672
LRW_21_80	0.274	0.019	0.03818	0.001	0.0519	0.0032	0.013	0.0019	245	15	**241.5**	**6.3**	261	38	260	130	114.9	24.4	0.2124
LRW_21_82	0.2682	0.011	0.0389	0.00077	0.0496	0.0016	0.01207	0.0012	241	9	**246**	**4.8**	242	24	171	70	382	77.9	0.2039
CVI-13108																			
108 - 1	0.284	0.012	0.03933	0.001	0.0517	0.0018	0.013	0.0014	253.9	9.4	**248.6**	**6.3**	261	28	260	77	328	46	0.1402
108 - 2	0.279	0.017	0.03946	0.001	0.051	0.003	0.0113	0.002	249	14	**249.5**	**6.5**	226	39	220	120	149.6	15.91	0.1064
108 - 3	0.2641	0.01	0.03703	0.0008	0.0515	0.0014	0.01189	0.0011	237.7	8.1	**234.4**	**5**	239	22	255	61	697	133.3	0.1912
108 - 4	1.674	0.055	0.1654	0.0043	0.0731	0.001	0.0554	0.0043	997	21	**986**	**24**	1089	83	1013	28	1160	150	0.1293
108 - 5	1.66	0.057	0.1659	0.0037	0.072	0.0019	0.0505	0.0055	992	22	**989**	**20**	994	110	975	54	121.5	17.05	0.1403
108 - 6	0.275	0.013	0.03883	0.00091	0.0512	0.0019	0.01118	0.0014	246.7	10	**245.6**	**5.6**	236	27	240	79	378	56.4	0.1492
108 - 7	0.271	0.012	0.03805	0.00085	0.0515	0.002	0.01113	0.0012	243.1	9.8	**240.7**	**5.2**	224	24	249	86	376	47.6	0.1266
108 - 8	0.263	0.021	0.0389	0.0012	0.0494	0.0043	0.013	0.0021	236	17	**246**	**7.2**	262	41	150	170	98.9	17.06	0.1725
108 - 9	0.264	0.019	0.03783	0.00093	0.05	0.0032	0.012	0.0021	236	15	**239.4**	**5.8**	241	41	180	130	104	18.19	0.1749
108 - 10	1.685	0.059	0.1665	0.0056	0.0731	0.0012	0.046	0.0046	1003	22	**992**	**31**	909	89	1016	34	935	145.4	0.1555
108 - 11	0.272	0.012	0.03821	0.0009	0.0514	0.0018	0.01222	0.0012	244	9.2	**241.7**	**5.6**	245	24	248	77	412	73.3	0.1779
108 - 12	0.271	0.02	0.03899	0.001	0.0501	0.0031	0.013	0.002	243	16	**246.6**	**6.2**	260	40	190	120	118.7	14.46	0.1218
108 - 13	0.264	0.013	0.03813	0.00089	0.0499	0.0021	0.0115	0.0014	237.3	11	**241.2**	**5.5**	230	28	184	87	324	35.5	0.1096
108 - 14	0.273	0.015	0.03855	0.00081	0.0511	0.0023	0.012	0.0015	245	12	**243.8**	**5.1**	241	29	224	95	340	38.4	0.1129
108 - 15	0.256	0.012	0.03607	0.0008	0.0513	0.0021	0.01193	0.0013	231.4	9.8	**228.4**	**5**	240	25	244	87	455	80.4	0.1767
108 - 16	0.2632	0.011	0.03801	0.00098	0.0507	0.0022	0.0118	0.0017	236.9	8.8	**240.5**	**6.1**	236	33	214	92	224	21.66	0.0967
108 - 18	0.264	0.012	0.03783	0.00094	0.0505	0.0018	0.0111	0.0013	237.9	9.4	**239.3**	**5.9**	223	26	210	77	335	45.7	0.1364
108 - 19	0.2651	0.0097	0.03778	0.00083	0.0507	0.0014	0.01144	0.001	238.6	7.8	**239**	**5.2**	230	21	219	59	1010	225	0.2228
108 - 21	0.264	0.012	0.03788	0.00085	0.0502	0.0019	0.01204	0.0012	237.2	9.7	**239.7**	**5.3**	242	24	199	80	527	78.7	0.1493
108 - 22	0.268	0.012	0.03714	0.00082	0.0522	0.0019	0.01176	0.0011	241.1	9.6	**235**	**5.1**	236	23	281	80	437	71.8	0.1643
108 - 23	0.273	0.012	0.0369	0.0012	0.0533	0.0023	0.0123	0.0017	244.6	9.5	**233.7**	**7.6**	248	34	333

108 - 83	1.666	0.064	0.1684	0.0038	0.0716	0.0022	0.0503	0.0045	994	24	**1003**	**21**	991	87	962	60	68.4	37.4	0.5468
108 - 84	1.939	0.063	0.1864	0.0044	0.0757	0.0015	0.0552	0.0042	1093	22	**1102**	**24**	1086	81	1082	40	218	123.3	0.5656
108 - 85	0.2612	0.0092	0.03682	0.00069	0.0513	0.0012	0.01213	0.0013	215.5	7.4	**233.1**	**4.3**	244	23	262	59	444	67.2	0.1514
108 - 86	0.2701	0.009	0.03835	0.00082	0.0512	0.001	0.01162	0.00097	242.7	7.2	**242.6**	**5.1**	233	19	234	51	1090	134.6	0.1235
108 - 87	0.2706	0.011	0.03798	0.00083	0.0511	0.0015	0.0122	0.0015	242.9	9	**240.3**	**5.1**	245	29	255	72	252	34.7	0.1377
108 - 88	0.264	0.015	0.03738	0.00088	0.0511	0.0026	0.0116	0.0016	237	12	**236.6**	**5.4**	233	31	230	110	189.2	21.39	0.1131
108 - 89	0.2534	0.01	0.03632	0.0008	0.0505	0.0016	0.01136	0.0012	229.1	8.1	**230**	**5**	228	24	208	67	409	49.1	0.1200
108 - 90	0.2652	0.0089	0.03774	0.00072	0.0508	0.001	0.01185	0.00099	238.7	7.1	**238.8**	**4.4**	238	20	227	46	1117	262	0.2346
108 - 91	0.2591	0.01	0.03703	0.00077	0.0507	0.0017	0.01137	0.0011	233.7	8.4	**234.4**	**4.8**	228	21	218	72	481.6	105.8	0.2197
108 - 92	0.267	0.018	0.03727	0.00075	0.0517	0.0031	0.0117	0.002	239	14	**235.9**	**4.7**	235	40	250	120	186.7	22	0.1178
108 - 93	0.27	0.025	0.037	0.0012	0.0544	0.0054	0.0123	0.0028	246	22	**234.3**	**7.5**	247	55	320	190	363.8	8.15	0.2215
108 - 94	0.242	0.014	0.0363	0.00082	0.0483	0.0027	0.0123	0.0017	219	12	**229.9**	**5.1**	246	34	120	110	186.9	32.4	0.1734
108 - 95	0.256	0.015	0.03647	0.00077	0.0508	0.0031	0.0093	0.0015	231	12	**230.9**	**4.8**	187	30	210	120	175.5	18.94	0.1079
108 - 96	1.684	0.045	0.1693	0.0034	0.0717	0.0012	0.047	0.0039	1002	17	**1008**	**19**	928	75	974	36	439	53.1	0.1210
108 - 97	0.2605	0.011	0.03652	0.00075	0.0514	0.0016	0.0114	0.0013	234.8	8.8	**231.2**	**4.6**	228	34	248	69	268	26.29	0.0981
108 - 98	0.2549	0.0094	0.03624	0.00073	0.051	0.0016	0.011	0.0013	230.4	7.6	**229.5**	**4.5**	222	26	232	68	376	43.5	0.1157
108 - 99	0.261	0.013	0.03761	0.00093	0.0504	0.0023	0.011	0.0013	235.3	10	**238**	**5.8**	220	26	202	94	271.4	37.7	0.1389
108 - 100	0.2599	0.011	0.03676	0.00082	0.0507	0.0015	0.01189	0.0012	234.3	9	**232.7**	**5.1**	239	25	220	65	441	76.8	0.1741
108 - 101	0.263	0.012	0.03752	0.00084	0.0509	0.0017	0.0108	0.0014	237.1	9.3	**237.4**	**5.2**	217	28	240	78	325	36.6	0.1126
108 - 102	0.263	0.012	0.03686	0.00074	0.0516	0.002	0.01156	0.0012	236.6	9.8	**233.4**	**4.6**	232	24	255	83	330	46.7	0.1415
108 - 103	0.262	0.015	0.03799	0.001	0.0495	0.0025	0.0128	0.0017	236	12	**240.4**	**6.3**	258	34	190	110	164	42.8	0.2610
108 - 104	0.895	0.041	0.0988	0.003	0.0655	0.0021	0.0475	0.0046	648	22	**608**	**17**	937	89	782	67	155.3	37	0.2382
108 - 105	0.2586	0.0098	0.03703	0.00077	0.051	0.0016	0.01198	0.0012	233.4	7.9	**234.4**	**4.8**	241	25	228	68	457	71.7	0.1569
108 - 106	1.652	0.05	0.1657	0.0033	0.0722	0.0015	0.0487	0.0037	989	19	**988**	**18**	960	71	985	42	276	91.9	0.3330
108 - 107	0.2655	0.0088	0.03687	0.00081	0.0522	0.0012	0.01183	0.00093	238.9	7.1	**233.4**	**5**	237.6	19	285	53	840	191.4	0.2279
108 - 108	0.2651	0.0094	0.037	0.00084	0.0519	0.0014	0.01138	0.0011	238.6	7.5	**234.2**	**5.2**	229	22	273	59	611	138	0.2259
108 - 111	0.2648	0.0093	0.03787	0.00075	0.0506	0.0012	0.01205	0.00097	238.4	7.5	**239.6**	**4.7**	242.1	19	217	53	1109	237.4	0.2141
108 - 113	0.28	0.012	0.03896	0.001	0.052	0.0015	0.01154	0.0011	250.1	9.7	**261.4**	**6.5**	232	23	273	64	525	87.9	0.1674
108 - 114	0.257	0.02	0.0384	0.0014	0.0489	0.0037	0.0124	0.0023	231	16	**242.7**	**8.5**	248	45	140	150	50.8	10.18	0.2004
108 - 115	0.255	0.024	0.0381	0.0013	0.0488	0.0047	0.0108	0.0023	229	19	**241.3**	**7.8**	218	46	120	180	96.3	10.03	0.1042
108 - 116	0.262	0.012	0.0377	0.0009	0.0505	0.0022	0.0105	0.0016	235.7	9.6	**238.6**	**5.6**	251	31	205	92	312	37.5	0.1202
108 - 117	0.318	0.021	0.04528	0.0012	0.0507	0.0032	0.0174	0.0028	279	16	**285.5**	**7.2**	349	55	240	140	75.8	13.04	0.1720
108 - 118	0.2716	0.01	0.03857	0.0008	0.0504	0.0012	0.01202	0.0011	243.8	8.3	**243.9**	**5**	241	21	224	56	1026	155	0.1511
108 - 119	0.271	0.011	0.03752	0.0009	0.0523	0.0017	0.01242	0.0013	243.2	8.8	**237.5**	**5.6**	248	26	287	70	392	64.7	0.1651
108 - 120	0.2554	0.0098	0.03614	0.00085	0.0514	0.0015	0.0115	0.0018	230.7	7.9	**228.8**	**5.3**	231	36	248	62	456	24.88	0.0546
108 - 121	0.262	0.013	0.0384	0.00081	0.0495	0.0019	0.0113	0.0016	236.3	10	**242.6**	**5**	227	27	165	83	415	51.7	0.1246
108 - 122	1.98	0.11	0.1871	0.005	0.0769	0.0036	0.0533	0.0058	1104	36	**1105**	**27**	1048	110	1090	90	21.82	21.15	0.9693
108 - 123	0.2676	0.011	0.03726	0.0008	0.0521	0.0017	0.0112	0.0013	240.5	8.5	**235.8**	**5**	225	25	278	73	494	79.4	0.1607
108 - 124	0.263	0.014	0.03749	0.00094	0.0508	0.0025	0.0108	0.0013	236	12	**237.2**	**5.8**	217	26	220	100	174.4	38.2	0.2190
ABH-27																			
ABH-27 - 1	0.474	0.045	0.0625	0.0058	0.0549	0.0012	0.0165	0.0034	392	32	**390**	**35**	331	67	405	49	4420	8.10E+03	1.8326
ABH-27 - 2	0.576	0.012	0.0733	0.0012	0.0571	0.001	0.0253	0.0032	461.4	7.6	**456**	**7**	505	64	498	36	650	645	0.9923
ABH-27 - 3	1.959	0.038	0.1837	0.0022	0.0775	0.0014	0.0561	0.0072	1104	14	**1087**	**12**	1102	140	1128	37	165	68.9	0.4176
ABH-27 - 4	0.586	0.014	0.07507	0.00075	0.0566	0.0014	0.02549	0.0033	467.6	9.2	**466.6**	**4.5**	509	64	465	52	329	149	0.4529
ABH-27 - 5	0.416	0.013	0.0557	0.0013	0.05426	0.0093	0.0192	0.0029	355.7	7.8	**349.5**	**8**	385	57	379	39	2200	246	0.1118
ABH-27 - 6	0.4838	0.0081	0.06309	0.00074	0.0558	0.0092	0.02268	0.0028	400.5	5.6	**394.4**	**4.5**	453	56	440	36	705	278	0.3943
ABH-27 - 7	0.569	0.017	0.0721	0.0012	0.0574	0.0017	0.0266	0.0043	457	11	**448.9**	**7.2**	529	84	497	65	193.6	18.33	0.0947
ABH-27 - 8	1.784	0.048	0.1761	0.0023	0.0736	0.0019	0.0555	0.0073	1038	17	**1046**	**13**	1091	140	1022	52	95	28.6	0.3011
ABH-27 - 9	0.544	0.017	0.0703	0.00099	0.0564	0.0019	0.0248	0.0036	441	11	**438**	**6**	494	71	449	77	172.1	19	0.1104
ABH-27 - 10	2.074	0.027	0.1897	0.0019	0.07943	0.00081	0.0596	0.0074	1139.9	9	**1119.6**	**10**	1170	140	1181	20	494	123.8	0.2506
ABH-27 - 11	0.471	0.016	0.0616	0.0014	0.0556	0.0019	0.0232	0.003	391	11	**385.4**	**8.7**	464	60	421	78	177.8	115.2	0.6479
ABH-27 - 12	0.549	0.015	0.0698	0.0012	0.0572	0.0016	0.0245	0.0031	444	10	**434.9**	**7.5**	490	62	489	61	221	160	0.7240
ABH-27 - 13	0.4013	0.0081	0.05387	0.0006	0.05408	0.00097	0.02109	0.0028	342.5	5.9	**338.2**	**3.7**	422	55	370	41	923	126.4	0.1369
ABH-27 - 14	0.2667	0.005	0.03842	0.00036	0.05059	0.00082	0.0126	0.0022	240	4	**243.1**	**2.2**	253	44	219	37	1841	22.91	0.0124
ABH-27 - 15	0.431	0.015	0.0577	0.0018	0.05422	0.00073	0.0215	0.0028	363	11	**362**	**11**	430	55	377	30	1390	191.6	0.1378
ABH-27 - 16	0.578	0.018	0.07452	0.00089	0.0563	0.0017	0.02376	0.0031	462	12	**463.3**	**5.3**	475	61	450	65	189.5	82.6	0.4359
ABH-27 - 17	0.533	0.01	0.06843	0.00076	0.0566	0.0011	0.02201	0.0028	433.4	6.7	**426.6**	**4.6**	440	56	470	40	645	201.9	0.3130
ABH-27 - 18	2.258	0.052	0.2026	0.0035	0.081	0.0013	0.0627	0.0086	1198	16	**1189**	**19**	1227	160	1219	32	134	41.69	0.3111
ABH-27 - 19	0.577	0.013	0.07375	0.00097	0.0569	0.0012	0.0243	0.0034	462	8.1	**458.7**	**5.8**	485	68	479	48	292	45.1	0.1545
ABH-27 - 20	0.552	0.02	0.0727	0.0011	0.0558	0.0023	0.02155	0.0029	449	14	**452.6**	**6.6**	431	57	418	88	138.9	134.5	0.9683
ABH-27 - 21	0.5749	0.0096	0.0741	0.0011	0.05645	0.0085	0.0225	0.0031	461	6.2	**460.6**	**6.8**	449	61	466	33	821	81.3	0.0990
ABH-27 - 22	1.582	0.062	0.1585	0.0034	0.0727	0.0024	0.0466	0.0064	962	24	**948**	**19**	920	120	998	65	205	50.5	0.2463
ABH-27 - 23	0.784	0.034	0.0585	0.0027	0.0977	0.0024	0.107	0.017	586	19	**367**	**16**	2050	310	1575	45	1508	140	0.0928
ABH-27 - 24	0.542	0.015	0.06955	0.00082	0.0566	0.0016	0.02	0.0034	439	9.9	**433.4**	**4.9**	399	66	465	63	187.7	15.04	0.0801
ABH-27 - 25	2.246	0.051	0.1895	0.0036	0.0862	0.0013	0.0669	0.009	1194	16	**1118**	**19**	1308	170	1339	30	228.7	63	0.2755
ABH-27 - 26	0.559	0.014	0.07224	0.00086	0.0562	0.0014	0.0203	0.0031	450.1	9.2	**449.6**	**5.2**	405	61	450	56	297	31.9	0.1074
ABH-27 - 27	0.588	0.023	0.07278	0.00093	0.0588	0.0026	0.0237	0.0043	469	15	**452.8**	**5.6**	473	86	539	97	154.1	14.46	0.0938
ABH-27 - 28	0.559	0.013	0.07193	0.00083	0.0565	0.0013	0.02144	0.0029	450.3	8.2	**447.7**	**5**	429	58	462	50	404	221.4	0.5480
ABH-27 - 29	0.565	0.013	0.0722	0.0011	0.0569	0.0012	0.02204	0.0031	454.3	8.6	**449.2**	**6.8**	441	61	481	46	381	137.3	0.3604
ABH-27 - 30	0.564	0.012	0.07275	0.00092	0.0562	0.001	0.0218	0.0034	453.7	7.9	**452.7**	**5.5**	436	67	453	40	354	26.8	0.0757
ABH-27 - 31	0.2626	0.006	0.03727	0.0005	0.0512	0.0011	0.0188	0.0034	236.6	4.8	**235.9**	**3.1**	376	67	244	47	847	24.9	0.0294
ABH-27 - 32	0.2461	0.0069	0.03471	0.00085	0.05196	0.00077	0.01122	0.0018	223.2	5.7	**219.9**	**5.3**	225	35	280	34	2190	53	0.0242
ABH-27 - 33	0.563	0.012	0.07232	0.00087	0.0565	0.0013	0.02194	0.003	453.4	7.9	**450.1**	**5.2**	438.7	59	463	50	486	440	0.9053
ABH-27 - 34	1.306	0.039	0.1373	0.0024	0.0699	0.0026	0.0396	0.0059	847	17	**829**	**14**	785	120	906	75	44.6	19.29	0.4325
ABH-27 - 35	0.2534	0.0062	0.03542	0.00065	0.052	0.0012	0.00776	0.0012	229.3	5	**224.4**	**4.1**	156	24	283	54	3390	118.3	0.0349
ABH-27 - 36	0.5494	0.0074	0.07151	0.00069	0.0568	0.0026	0.02109	0.0029	444.5	4.8	**445.2**	**4.2**	421.8	56	438	24	2230	1860	0.8341
ABH-27 - 37	1.66	0.033	0.1422	0.0019	0.0849	0.0015	0.0503	0.0069	993	13	**857**	**11**	991	130	1310	35	305	127	0.4164
ABH-27 - 38	0.521	0.011	0.0685	0.00085	0.0554	0.0012	0.0222	0.0033	425.8	7.1	**427.1**	**5.1**	444	65	419	47	323	28.7	0.0889
ABH-27 - 39	0.5875	0.0098	0.0758	0.001	0.0636	0.0085	0.02336	0.0031	469.1	6.3	**471**	**6.2**	467	62	463	34	1111	601	0.5404
ABH-27 - 40	0.5574	0.0069	0.07249	0.00068	0.05589	0.00066	0.02207	0.0029	449.7	4.5	**451.1**	**4.1**	441.1	58	446	26	1400	1520	1.0857
ABH-27 - 41	0.5587	0.0093	0.07133	0.00078	0.05696	0.00078	0.02178	0.003	450.4	6.1	**444.1**	**4.7**	435	58	487	30	583	624	1.0703
ABH-27 - 42	1.231	0.076	0.1033	0.0058	0.0866	0.0019	0.0672	0.0095	811	34	**633**	**34**	1314	180	1349	43	425	84.1	0.1979
ABH-27 - 43	0.499	0.015	0.0645	0.0013	0.0563	0.0013	0.02078	0.0029	411	10	**403.1**	**7.7**	416	57	454	51	417	105	0.2518
ABH-27 - 44	0.2562	0.0044	0.03647	0.0005	0.051	0.00067	0.0118	0.002	231.5	3.6	**230.9**	**3.1**	237	39	238	30	2260	32.9	0.0146
ABH-27 - 45	1.282	0.057	0.1349	0.0031	0.0693	0.003	0.044	0.0063	836	26	**816**	**18**	871	120	897	87	137	68.6	0.6467
ABH-27 - 46	0.2701	0.0052	0.03816	0.00056	0.05145	0.00067	0.0127	0.0022	242.7	4.2	**241.4**	**3.5**	255	44	258	30	2760	23.77	0.0086
ABH-27 - 47	1.064	0.031	0.1187	0.0015	0.0653	0.0012	0.0367	0.0052	735	15	**723**	**20**	727	100	780	40	667	208	0.3118
ABH-27 - 48	0.554	0.015	0.0723	0.0011	0.0554	0.0013	0.02211	0.003	447.4	9.6	**450.2**	**6.4**	442	59	431	58	230	218	0.9478
ABH-27 - 49	0.573	0.019	0.0749	0.0011	0.0556	0.002	0.0221	0.0035	459	12	**465.8**	**6.7**	441	69	418	78	141.4	26.6	0.1881
ABH-27 - 50	0.804	0.083	0.0697	0.0017	0.0826	0.0069	0.0287	0.0046	588	45	**434**	**10**	583	99	1170	160	748	695	0.9291
ABH-27 - 52	0.592	0.018	0.07429	0.001	0.0579	0.0015	0.02308	0.0032	471	12	**461.9**	**6.1**	461	63	514	56	257	113	0.4397
ABH-27 - 53	0.559	0.013	0.0722	0.001	0.0563	0.0013	0.0226	0.0033	450.3	8.7	**449.3**	**6.3**	451	64	455	54	301.8	47.4	0.1571
ABH-27 - 54	0.766	0.041	0.0912	0.0031	0.0608	0.0019	0.0314	0.0047	575	23	**563**	**18**	525	92	616	72	161	44.8	0.2783
ABH-27 - 55	0.515	0.013	0.05951	0.00089	0.063	0.0014	0.0328	0.0047	421.6	8.4	**372.6**	**5.4**	652	93	699	47	344	28.5	0.0828
ABH-27 - 56	1.852	0.045	0.171	0.0038	0.0799	0.0021	0.0549	0.0074	1063	16	**1017**	**21**	1079	130	1198	43	181	66.9	0.3696
ABH-27 - 57	0.297	0.0099	0.04273	0.00067	0.0505	0.0015	0.0184	0.0044	263.9	7.8	**269.7**	**4.1**	368	86	211	67	673	6.61	0.0098
ABH-27 - 58	0.546	0.031	0.0717	0.0014	0.0554	0.003	0.0244	0.0035	440	20	**446.2**	**8.7**	487	68	400	120	71.3	49.8	0.6985
ABH-27 - 60	40.8	4.7	0.371	0.042	0.805	0.031	21.7	6.6	3760	100	**2020**	**190**	6.03E+04	4.80E+03	4973	70	7.33	0.332	0.0453
CP-055																			
CP055_1	0.428	0.013	0.0582	0.0014	0.05348	0.00095	0.018	0.0021	361.1	9.3	**364.9**	**8.5**	360	42	334	39	128	175	1.3672
CP055_2	0.2631	0.008	0.03798	0.0009	0.05042	0.00092	0.0112	0.0015	236.9	6.4	**240.3**	**5.6**	224	30	206	40	234	35	0.1496
CP055_3	0.395	0.012	0.0542	0.0013	0.05306	0.00087	0.0159	0.0019	337.7	8.4	**340.2**	**7.8**	318	38	319	36	218	136	0.6239
CP055_4	0.2458	0.008	0.03465	0.00082	0.0518	0.0011	0.0112	0.0015	223	6.5	**219.6**	**5.1**	225	30	267	45	390	45	0.1154
CP055_5	0.395	0.013	0.0541	0.0013	0.0532	0.0011	0.0159	0.0019	337.4	9.1	**339.6**	**7.9**	319	38	316	46	110	77	0.7000
CP055_6	0.2565	0.0077	0.03671	0.00091	0.05099	0.00081	0.0103	0.0014	231.6	6.2	**232.4**	**5.6**	206	28	232	35	308	186	0.6039
CP055_7	0.2835	0.0083	0.0402	0.00095	0.0512	0.00082	0.0117	0.0014	253.2	6.5	**254.1**	**5.9**	236	27	246	36	274	274	1.1184
CP055_8	0.2847	0.0084	0.04006	0.00095	0.05169	0.00083	0.0109	0.0013	254.1	6.6	**253.2**	**5.9**	219	26	262	35	230	278	1.2087
CP055_9	0.311	0.022	0.0377	0.001	0.0603	0.003	0.0157	0.0045	275	15	**238.7**	**6.2**	314	87	597	78	325	128	0.3938
CP055_10	0.656	0.032	0.0816	0.0036	0.05852	0.0094	0.0246	0.0025	511	22	**505**	**22**	491	50	543	39	343	265	0.7726
CP055_11	0.2536	0.0071	0.0354	0.00084	0.0523	0.00086	0.0118	0.0015	229.4	5.8	**224.3**	**5.2**	236	30	292	36	518	104	0.2008
CP055_12	4.35	0.11	0.2923	0.0068	0.10859	0.0006	0.0813	0.0095	1702	20	**1653**	**34**	1580	180	1775	10	207	278	1.3430
CP055_13	0.2608	0.0079	0.0374	0.00089	0.05085	0.00085	0.0113	0.0016	235	6.3	**236.7**	**5.5**	226	32	225	36	288	25	0.0868
CP055_14	0.465	0.013	0.061	0.0015	0.05543	0.00071	0.0203	0.0029	386.9	9.4	**381.8**	**9.3**	406	57	420	29	239	19	0.0795
CP055_15	0.501	0.018	0.0644	0.0019	0.05668	0.00092	0.0209	0.0034	412	13	**402**	**12**	417	68	466	36	166	7	0.0422
CP055_16	0.376	0.011	0.0398	0.0011	0.0688	0.0012	0.0344	0.0042	323.5	8.7	**251.5**	**7**	684	82	889	35	465	56	0.1204
CP055_17	0.713	0.019	0.0884	0.0021	0.05878	0.00065	0.0275	0.0032	546	12	**546**	**12**	548	63	552	24	255	178	0.6980
CP055_18	0.2763	0.0087	0.0387	0.001	0.05167	0.00088	0.012	0.0023	247.4	6.9	**244.9**	**6.2**	239	46	273	38	282	7	0.0248
CP055_19	0.3185	0.0094	0.0445	0.0011	0.05213	0.00089	0.0139	0.0017	280.4	7.2	**280.4**	**6.6**	278	33	279	38	194	103	0.5309
CP055_20	0.2421	0.0075	0.03463	0.00085	0.05038	0.00095	0.0113	0.0017	219.9	6.1	**219.5**	**5.3**	227	34	212	39	315	33	0.1048
CP055_21	1.814	0.069	0.1785	0.0058	0.0741	0.0013	0.0475	0.0054	1048	29	**1059**	**33**	940	100	1038	37	44	45	1.0227
CP055_22	0.2738	0.0084	0.03524	0.00084	0.0568	0.0012	0.014	0.0019	245.5	6.6	**223.2**	**5.3**	282	38	467	45	462	78	0.1688
CP055_23	0.2704	0.007	0.03811	0.00092	0.05149	0.00052	0.0115	0.0014	242.9	5.6	**241.1**	**5.7**	231	27	259	23	916	469	0.5120
CP055_24	0.243	0.0092	0.0338	0.0011	0.0525	0.001	0.0135	0.0021	220.8	7.2	**214.1**	**6.8**	252	42	298	37	480	26	0.0542
CP055_25	1.718	0.097	0.1688	0.0086	0.0743	0.0015	0.0497	0.0047	1014	49	**1005**	**50**	981	92	1048	48	268	171	0.6381
CP055_26	0.3577	0.0098	0.0493	0.0012	0.05301	0.00065	0.0152	0.0017	310.3	7.4	**310.1**	**7.5**	305	35	323	28	361	182	0.5042
CP055_27	0.291	0.0087	0.03735	0.0009	0.0568	0.001	0.0123	0.0015	259.2	6.8	**256.4**	**5.6**	246	30	478	37	864	773	0.8947
CP055_28	0.254	0.013	0.03482	0.00088	0.0522	0.0021	0.0109	0.0059	229	10	**220.6**	**5.5**	220	32	322	71	265	61	0.2302
CP055_29	0.26	0.033	0.038	0.0011	0.0499	0.0036	0.0116	0.0069	235	19	**240.5**	**6.8**	230	130	186	97	267	48	0.1798
CP055_30	0.266	0.013	0.0364	0.0013	0.0537	0.0011	0.016	0.038	240.8	9.5	**230.7**	**7.1**	330	360	152	43	830	41	0.0494
CP055_31	0.949	0.042	0.0995	0.0036	0.0692	0.0011	0.0479	0.0058	675	20	**611**	**21**	950	110	899	31	113	32	0.2832
CP055_32	0.351	0.012	0.0495	0.0015	0.05165	0.00087	0.0158	0.0019	305	9	**311.5**	**9.3**	317	38	260	37	195	128	0.6564
CP055_33	0.239	0.0074	0.03373	0.00086	0.0518	0.0011	0.012	0.0017	218.1	6.6	**213.8**	**5.4**	240	34	266	47	416	29	0.0697
CP055_34	0.27	0.0081	0.03901	0.00094	0.05041	0.00097	0.0129	0.0017	242.5	6.5	**246.7**	**5.9**	258	35	212	41	245	42	0.1714
CP055_35	0.2557	0.0086	0.03633	0.00085	0.0512	0.0012	0.0112	0.0021	231	6.8	**230**	**5.3**	225	42	239	48	382	43	0.1126
CP055_36	0.435	0.019	0.0587	0.0015	0.0539	0.0019	0.017	0.0021	365	13	**367.6**	**8.8**	342	42	329	73	37	48

AK-01 - 8	0.211	0.025	0.02764	0.00098	0.055	0.0061	0.00904	0.0011	192	21	**175.7**	**6.1**	182	22	370	230	33.4	34.6	1.0359
AK-01 - 9	0.209	0.019	0.02929	0.00092	0.0518	0.0045	0.00964	0.0011	191	16	**186.1**	**5.8**	194	23	240	170	47.1	37.5	0.7962
AK-01 - 10	1.665	0.053	0.1655	0.0032	0.0728	0.0013	0.05	0.0042	994	20	**987**	**18**	985	80	1004	36	139.2	30.5	0.2191
AK-01 - 11	1.704	0.074	0.1709	0.0041	0.0725	0.0022	0.0509	0.0042	1007	27	**1017**	**22**	1003	81	986	100	56.1	40.7	0.7255
AK-01 - 12	0.192	0.018	0.02899	0.00076	0.0483	0.0045	0.0094	0.0014	177	15	**184.2**	**4.8**	188	27	90	170	56.4	30.8	0.5461
AK-01 - 13	0.203	0.016	0.02826	0.00076	0.0524	0.0039	0.00876	0.0011	187	13	**179.6**	**4.8**	176	22	260	150	65	50.9	0.7831
AK-01 - 14	0.203	0.023	0.03056	0.00095	0.049	0.0058	0.00932	0.0011	186	19	**194.1**	**5.9**	187	23	110	210	45.7	36.4	0.7965
AK-01 - 15	0.233	0.033	0.02996	0.00092	0.0563	0.0075	0.0104	0.0014	209	27	**190.3**	**5.7**	209	29	340	250	34.9	24.6	0.7049
AK-01 - 16	0.209	0.022	0.02944	0.00081	0.0519	0.0055	0.0092	0.0013	191	18	**187.1**	**5.1**	185	25	270	210	44.4	33.3	0.7509
AK-01 - 17	0.2	0.015	0.03011	0.00088	0.0485	0.0037	0.00915	0.00094	184	13	**191.2**	**5.5**	184	19	120	150	66.2	97.2	1.4683
AK-01 - 18	0.21	0.03	0.03044	0.00097	0.0501	0.007	0.0092	0.0014	192	26	**193.3**	**6.1**	185	28	180	270	90.2	91.7	1.0166
AK-01 - 19	1.554	0.059	0.1441	0.0051	0.0784	0.0016	0.0589	0.0046	951	24	**867**	**29**	1156	88	1155	40	627	116.4	0.1856
AK-01 - 20	2.221	0.074	0.2016	0.0048	0.0801	0.0017	0.0651	0.005	1186	23	**1183**	**26**	1274	95	1194	42	105.6	39.9	0.3778
AK-01 - 21	1.525	0.071	0.1536	0.0034	0.0719	0.0034	0.0462	0.0047	938	29	**921**	**19**	913	91	959	98	34.5	20.3	0.5884
AK-01 - 22	0.209	0.02	0.02943	0.00092	0.0519	0.0049	0.00881	0.00099	191	17	**186.9**	**5.7**	177	20	230	180	48.6	55	1.1317
AK-01 - 23	0.206	0.019	0.02932	0.00076	0.0512	0.0048	0.0093	0.001	189	16	**186.3**	**4.8**	187	20	200	170	55.8	42.6	0.7634
AK-01 - 24	0.199	0.016	0.02914	0.00075	0.0507	0.0042	0.00975	0.001	183	13	**185.2**	**4.7**	196	21	200	160	57	68.2	1.1965
AK-01 - 25	0.208	0.024	0.02938	0.00072	0.0511	0.0056	0.009	0.0012	190	20	**186.7**	**4.5**	181	24	190	200	42	37.6	0.8952
AK-01 - 26	0.207	0.02	0.0291	0.00092	0.0521	0.0051	0.0087	0.0012	189	17	**184.9**	**5.8**	175	24	240	190	36.2	24	0.6630
AK-01 - 27	0.21	0.023	0.02922	0.0011	0.0527	0.0056	0.00921	0.0011	192	19	**185.6**	**6.8**	185	21	240	200	37.5	34.9	0.9307
AK-01 - 28	0.209	0.027	0.0298	0.0013	0.0512	0.0059	0.0095	0.0014	192	23	**189.3**	**8.2**	191	28	230	230	45.4	44.1	0.9714
AK-01 - 29	2.62	0.092	0.2259	0.0062	0.0844	0.0015	0.0661	0.0053	1305	26	**1313**	**32**	1294	100	1299	34	394	94.6	0.2401
AK-01 - 30	1.708	0.061	0.1697	0.0032	0.073	0.0021	0.0487	0.0041	1010	23	**1010**	**18**	961	78	1016	52	95.9	40.5	0.4223
AK-01 - 31	0.198	0.034	0.0306	0.0011	0.0472	0.0079	0.0093	0.0015	181	29	**194**	**7**	188	30	50	300	36.41	31.4	0.8624
AK-01 - 32	0.195	0.015	0.02953	0.00081	0.0484	0.0037	0.00952	0.00092	180	12	**187.6**	**5**	192	18	150	160	55.5	66.9	1.2054
AK-01 - 33	1.683	0.085	0.1682	0.0039	0.0727	0.0032	0.0516	0.0045	998	32	**1002**	**21**	1015	86	979	90	39.79	22.61	0.5682
AK-01 - 34	0.317	0.022	0.02922	0.00089	0.0796	0.0062	0.01063	0.0011	278	17	**185.6**	**5.6**	214	22	1100	160	61.2	67.1	1.0964
AK-01 - 35	0.223	0.037	0.028	0.0011	0.0583	0.0097	0.0091	0.0011	202	30	**177.8**	**7.2**	183	22	420	300	59.9	67.9	1.1336
AK-01 - 36	0.183	0.019	0.02796	0.00074	0.0479	0.0052	0.0086	0.0013	169	17	**177.8**	**4.7**	173	26	130	210	52.3	24.58	0.4700
AK-01 - 37	0.188	0.018	0.02878	0.00092	0.048	0.0048	0.00892	0.0009	173	15	**182.9**	**5.7**	180	18	90	180	62.6	74.4	1.1885
AK-01 - 38	0.202	0.025	0.0294	0.0012	0.0506	0.0061	0.0098	0.0015	185	21	**186.8**	**7.4**	196	31	180	220	30.5	20.52	0.6728
AK-01 - 39	1.669	0.051	0.1678	0.0034	0.0723	0.0014	0.0494	0.0036	996	19	**1000**	**19**	974	70	990	40	225	91.7	0.4076
AK-01 - 40	0.191	0.021	0.0296	0.00089	0.0475	0.0052	0.0096	0.0013	176	18	**188**	**5.6**	193	26	110	210	38.8	34.8	0.8969
AK-01 - 41	0.222	0.027	0.0291	0.0012	0.056	0.007	0.0094	0.0014	202	22	**185**	**7.3**	188	27	350	240	36.4	27.2	0.7473
AK-01 - 42	0.191	0.017	0.02927	0.00079	0.0474	0.004	0.00963	0.001	176	14	**186**	**5**	194	20	70	150	59.6	67.1	1.1258
AK-01 - 43	1.616	0.045	0.1625	0.0033	0.07223	0.00085	0.0479	0.0034	976	17	**970**	**18**	946	66	990	24	544	270.8	0.4978
AK-01 - 44	0.219	0.023	0.02937	0.0011	0.0544	0.0055	0.0089	0.0012	200	19	**186.6**	**6.8**	179	24	320	200	47.3	42.2	0.8922
AK-01 - 45	1.818	0.059	0.1812	0.0048	0.0729	0.002	0.0527	0.0041	1051	21	**1073**	**26**	1039	79	1007	56	211.2	137.6	0.6515
AK-01 - 46	1.727	0.054	0.1703	0.0036	0.0738	0.0016	0.0482	0.0037	1018	20	**1013**	**21**	951	72	1028	43	136.5	62	0.4542
AK-01 - 47	2.425	0.095	0.2088	0.0072	0.0843	0.0035	0.0614	0.0043	1250	28	**1222**	**39**	1204	82	1298	80	300	124.8	0.4160
AK-01 - 48	0.221	0.024	0.02913	0.00091	0.0552	0.0056	0.01026	0.0011	201	20	**185.1**	**5.7**	206	21	340	200	47.6	52.1	1.0945
AK-01 - 49	0.218	0.026	0.02936	0.001	0.0543	0.0065	0.00872	0.001	198	22	**186.5**	**6.5**	175	21	310	230	38.5	30.7	0.7974
AK-01 - 50	0.213	0.02	0.02988	0.001	0.0524	0.0052	0.00841	0.001	194	16	**189.8**	**6.4**	169	20	190	300	40.5	37.9	0.9358
AK-01 - 51	1.655	0.061	0.1681	0.0035	0.0716	0.002	0.0487	0.004	989	23	**1001**	**19**	960	78	961	59	53	28	0.5283
AK-01 - 52	2.169	0.066	0.1909	0.0044	0.0825	0.0012	0.0587	0.0044	1170	21	**1126**	**24**	1152	84	1255	30	495	106.1	0.2143
AK-01 - 53	1.689	0.088	0.1647	0.0058	0.0744	0.0027	0.0534	0.0047	1003	34	**983**	**32**	1051	90	1046	73	128.1	50.4	0.3934
AK-01 - 54	0.186	0.02	0.0294	0.0012	0.0467	0.005	0.0097	0.0016	172	17	**186.5**	**7.3**	195	32	40	190	36	20	0.5556
AK-01 - 55	1.742	0.076	0.1708	0.0039	0.0741	0.0025	0.0516	0.0048	1021	28	**1016**	**22**	1017	93	1027	69	32.35	23.85	0.7372
AK-01 - 56	0.205	0.021	0.02978	0.00084	0.049	0.0046	0.00857	0.00097	188	18	**189.2**	**5.3**	173	20	160	180	54.09	42.2	0.7802
AK-01 - 57	0.205	0.025	0.02867	0.001	0.0521	0.0061	0.0087	0.0012	187	21	**182.2**	**6.4**	175	25	230	220	33.69	28.2	0.8370
AK-01 - 58	0.22	0.024	0.02928	0.00086	0.0544	0.0054	0.00836	0.00099	200	20	**186**	**5.4**	168	20	320	200	42.9	37.1	0.8648
AK-01 - 59	1.649	0.051	0.1665	0.0035	0.072	0.0014	0.05	0.0039	988	20	**993**	**19**	985	76	980	40	217.1	53.9	0.2483
AK-01 - 60	1.629	0.05	0.162	0.0034	0.0732	0.0017	0.0475	0.0035	981	19	**968**	**19**	937	68	1011	49	174.5	156.6	0.8974
AK-01 - 61	1.24	0.058	0.1184	0.0049	0.076	0.0014	0.0414	0.0051	818	27	**721**	**28**	819	99	1094	37	806	101.3	0.1257
AK-01 - 62	1.718	0.054	0.1719	0.0037	0.0727	0.0017	0.051	0.0041	1014	20	**1022**	**20**	1005	79	999	47	152	67	0.4408
AK-01 - 63	0.209	0.035	0.02826	0.00097	0.0534	0.0079	0.0088	0.0013	191	28	**179.6**	**6.1**	177	25	270	270	85.9	91	1.0594
AK-01 - 64	1.724	0.069	0.172	0.0036	0.0729	0.0026	0.0505	0.0045	1015	26	**1023**	**20**	995	85	993	74	98	48.1	0.4908
AK-01 - 65	0.219	0.031	0.02888	0.0011	0.0561	0.009	0.0099	0.0015	199	26	**183.5**	**6.7**	198	29	350	300	39.2	35.3	0.9005
AK-01 - 66	1.634	0.045	0.1631	0.0032	0.0729	0.0013	0.0495	0.0039	983	18	**974**	**18**	976	75	1006	36	158.1	56.9	0.3599
AK-01 - 67	2.353	0.076	0.2069	0.0049	0.0826	0.0016	0.0602	0.0045	1227	23	**1212**	**26**	1182	87	1256	38	245.8	68.2	0.2775
AK-01 - 68	0.225	0.024	0.02898	0.00089	0.0569	0.0064	0.0093	0.0013	205	20	**184.2**	**5.6**	188	27	410	230	44.5	47.3	1.0629
AK-01 - 69	1.95	0.17	0.1808	0.0063	0.0784	0.006	0.0567	0.0085	1094	59	**1071**	**34**	1110	160	1140	150	59.9	20.3	0.3389
AK-01 - 70	2.036	0.059	0.1894	0.0038	0.0781	0.0013	0.0578	0.0043	1127	20	**1118**	**21**	1135	82	1147	33	235.1	92.5	0.3934
AK-01 - 71	2.322	0.096	0.2034	0.0058	0.0831	0.0025	0.0571	0.0054	1218	29	**1194**	**31**	1122	100	1268	59	562	115.4	0.2053
AK-01 - 72	0.217	0.023	0.03014	0.00086	0.0527	0.0058	0.0091	0.0013	197	20	**191.4**	**5.4**	183	26	250	210	41.1	33.2	0.8078
AK-01 - 73	1.693	0.054	0.1714	0.0035	0.0718	0.0015	0.054	0.0044	1005	20	**1020**	**19**	1062	84	974	42	137.4	41.4	0.3013
AK-01 - 74	0.206	0.018	0.02954	0.00094	0.0509	0.0044	0.00965	0.0011	189	15	**187.7**	**5.9**	194	21	200	170	55.4	48.8	0.8809
AK-01 - 75	1.65	0.066	0.1674	0.0039	0.0718	0.0027	0.05	0.0042	987	25	**998**	**21**	985	81	960	78	52.3	41.4	0.7916
AK-01 - 76	0.185	0.02	0.02956	0.001	0.0463	0.0053	0.0098	0.0013	171	17	**187.7**	**6.4**	196	26	20	200	36.2	26.3	0.7265
AK-01 - 77	0.181	0.017	0.02881	0.0007	0.0456	0.0041	0.0095	0.0012	168	15	**183.1**	**4.4**	192	24	40	180	53.1	48.5	0.9134
AK-01 - 78	0.199	0.02	0.02963	0.0008	0.0492	0.0049	0.0096	0.0012	183	17	**188.2**	**5**	193	24	130	190	56	41.7	0.7446
AK-01 - 79	0.252	0.023	0.02912	0.00084	0.063	0.006	0.01061	0.001	226	19	**185**	**5.3**	213	20	600	200	69.5	59.2	0.8518
AK-01 - 80	0.204	0.016	0.02894	0.00078	0.0515	0.0041	0.00873	0.00098	188	14	**183.9**	**4.9**	176	20	240	160	74.3	72.9	0.9812
AK-01 - 81	0.187	0.019	0.02948	0.00092	0.0464	0.0047	0.00911	0.00098	173	16	**187.3**	**5.8**	183	20	30	180	60.2	68.3	1.1346
AK-01 - 82	2.614	0.074	0.2248	0.0042	0.0845	0.0011	0.0667	0.0049	1304	21	**1307**	**22**	1305	92	1301	26	346	101.6	0.2936
AK-01 - 83	2.364	0.071	0.2046	0.0038	0.0838	0.0013	0.0659	0.0049	1231	21	**1200**	**20**	1290	93	1287	30	265	99.8	0.3766
AK-01 - 84	1.474	0.066	0.1408	0.0046	0.076	0.0011	0.0442	0.0042	918	27	**849**	**26**	873	82	1094	28	1251	45.7	0.0365
AK-01 - 85	0.223	0.02	0.02982	0.00077	0.0545	0.0047	0.00891	0.00083	203	16	**189.4**	**4.8**	179	17	340	180	73.4	100.2	1.3651
AK-01 - 86	0.196	0.021	0.02849	0.00093	0.05	0.0053	0.00838	0.00093	180	17	**182.2**	**5.8**	169	19	150	190	51.1	46.9	0.9178
AK-01 - 87	3.232	0.098	0.195	0.0045	0.1204	0.0018	0.0579	0.0042	1464	24	**1148**	**24**	1137	80	1960	26	370	236	0.6378
AK-01 - 88	1.704	0.055	0.1714	0.0038	0.0723	0.0014	0.0497	0.0038	1009	20	**1019**	**21**	981	73	989	38	111.4	50.5	0.4533
AK-01 - 89	1.706	0.063	0.1726	0.0036	0.0715	0.002	0.0525	0.0049	1014	22	**1026**	**20**	1034	94	976	52	73.4	20.5	0.2793
AK-01 - 90	0.215	0.025	0.02246	0.00062	0.0464	0.0041	0.0075	0.0032	148	13	**156.6**	**3.9**	150	64	40	160	95	3.17	0.0334
AK-01 - 91	0.186	0.016	0.02897	0.00066	0.0466	0.0039	0.00956	0.0011	172	14	**184.1**	**4.1**	192	22	80	170	79.5	77.5	0.9748
AK-01 - 92	0.192	0.021	0.02859	0.0008	0.049	0.0053	0.00886	0.00089	177	18	**181.7**	**5**	178	18	120	200	57.2	64.5	1.1276
AK-01 - 93	0.201	0.019	0.02874	0.00085	0.0511	0.0048	0.00959	0.00099	185	16	**182.6**	**5.3**	193	20	210	180	56.1	61.8	1.1016
AK-01 - 94	1.696	0.058	0.1693	0.0034	0.0728	0.0017	0.0517	0.0039	1005	22	**1008**	**19**	1019	76	1011	45	150.9	65.1	0.4314
AK-01 - 95	0.216	0.022	0.02996	0.00088	0.0523	0.0053	0.00857	0.0011	197	18	**190.2**	**5.5**	172	22	250	190	39	38.4	0.9846
AK-01 - 96	1.348	0.054	0.1265	0.005	0.0775	0.001	0.0582	0.005	865	23	**768**	**29**	1143	95	1133	27	2118	125.3	0.0592
AK-01 - 97	1.871	0.069	0.1692	0.004	0.0803	0.0018	0.056	0.0044	1069	24	**1008**	**22**	1101	85	1201	44	135.4	73.6	0.5436
AK-01 - 98	1.603	0.065	0.1591	0.0049	0.0728	0.002	0.0474	0.004	969	25	**951**	**27**	935	77	1013	59	70	45.3	0.6471
AK-01 - 99	0.215	0.025	0.02985	0.00083	0.0523	0.0063	0.00907	0.001	194	21	**189.6**	**5.2**	182	20	220	220	57.2	56.21	0.9827
AK-01 - 100	2.714	0.083	0.2324	0.0051	0.085	0.0018	0.068	0.0056	1331	23	**1347**	**27**	1329	110	1309	42	118.2	35.8	0.3029
AK-01 - 101	1.994	0.094	0.1796	0.0049	0.0808	0.0027	0.0543	0.0044	1112	32	**1065**	**27**	1068	85	1212	67	312	239	0.7660
AK-01 - 102	2.173	0.061	0.1995	0.0042	0.0792	0.0095	0.0588	0.0043	1172	20	**1172**	**23**	1154	82	1175	24	547	79	0.1444
AK-01 - 103	0.206	0.02	0.02959	0.00088	0.0511	0.0053	0.00882	0.00098	189	17	**188**	**5.5**	177	20	190	190	55.2	67.2	1.2174
AK-01 - 104	0.273	0.024	0.03008	0.00096	0.0677	0.0066	0.00987	0.00098	243	19	**191**	**6**	198	20	740	200	50.2	58.5	1.1653
AK-01 - 105	0.201	0.021	0.02889	0.00078	0.0508	0.0053	0.00944	0.0012	184	18	**183.6**	**4.9**	190	24	200	210	40.2	33.7	0.8383
AK-01 - 106	0.198	0.02	0.02995	0.00089	0.0483	0.0047	0.00886	0.00079	182	17	**190.2**	**5.6**	178.4	16	100	180	69.1	94.1	1.3618
AK-01 - 107	0.209	0.017	0.02934	0.00086	0.051	0.0049	0.00954	0.00098	191	14	**186.4**	**5.4**	192	20	200	180	57.8	51	0.8824
AK-01 - 108	0.184	0.021	0.02769	0.00088	0.0485	0.0057	0.0087	0.0012	174	19	**176**	**5.5**	175	24	140	230	36.9	27.44	0.7436
AK-01 - 109	1.708	0.078	0.1728	0.0049	0.0718	0.0025	0.0537	0.005	1010	29	**1027**	**27**	1056	95	971	71	60	29.7	0.4950
AK-01 - 110	2.288	0.062	0.2096	0.0046	0.0794	0.0017	0.066	0.005	1208	19	**1227**	**25**	1291	96	1178	41	263	93.7	0.3563
AK-01 - 111	1.672	0.055	0.1663	0.0033	0.0731	0.0016	0.0481	0.0036	997	21	**992**	**18**	950	70	1009	43	202.6	53.7	0.2651
AK-01 - 112	1.676	0.052	0.1695	0.0036	0.072	0.0012	0.0481	0.0038	1002	22	**1009**	**20**	949	74	989	36	224	58.7	0.2621
AK-01 - 113	0.924	0.027	0.0964	0.0021	0.06926	0.00084	0.03404	0.0025	664.1	14	**593.1**	**13**	676	49	905	25	1030	391.9	0.3805
AK-01 - 114	1.806	0.064	0.1728	0.0037	0.0766	0.0023	0.0543	0.0047	1046	23	**1027**	**20**	1067	89	1099	60	78.7	28.7	0.3798
AK-01 - 115	0.218	0.018	0.02974	0.00084	0.0536	0.0046	0.00849	0.001	199	15	**188.9**	**5.3**	171	21	300	170	50.9	29.3	0.5756
AK-01 - 116	1.675	0.045	0.1681	0.0033	0.0725	0.001	0.04999	0.0035	998.4	17	**1001**	**18**	986	68	996	28	383	430	1.1227
AK-01 - 117	0.219	0.021	0.02923	0.00083	0.0546	0.005	0.00927	0.00096	200	17	**185.7**	**5.2**	187	19	330	180	57.6	59.6	1.0347
AK-01 - 118	1.723	0.06	0.1733	0.0038	0.0723	0.0017	0.0511	0.0039	1016	23	**1030**	**21**	1007	76	987	48	134	55.9	0.4172
AK-01 - 119	2.049	0.091	0.1764	0.0067	0.0846	0.0022	0.0626	0.0056	1131	30	**1047**	**37**	1227	110	1305	49	403	133.8	0.3320
AK-01 - 120	0.783	0.034	0.0791	0.0028	0.0721	0.0015	0.054	0.0047	587	19	**491**	**17**	1064	90	987	41	2250	96.3	0.0428
AK-01 - 121	0.202	0.018	0.02923	0.00091	0.0506	0.0045	0.00969	0.001	185	15	**185.7**	**5.7**	195	21	190	170	53.4	45.6	0.8539
AK-01 - 122	1.969	0.054	0.1823	0.0034	0.0785	0.0013	0.055	0.004	1104	19	**1080**	**19**	1081	77	1157	32	498	181.9	0.3653
AK-01 - 123	2.587	0.079	0.2219	0.0043	0.0845	0.0018	0.0684	0.0053	1296	22	**1292**	**23**	1337	100	1299	40	167.8	50.7	0.3021
AK-01 - 124	2.683	0.067	0.2251	0.005	0.0864	0.001	0.0653	0.0048	1323.5	19	**1309**	**26**	1278	91	1346	23	452	139.2	0.3080
AK-01 - 125	0.193	0.015	0.02935	0.00077	0.0489	0.004	0.00956	0.001	178	12	**186.4**	**4.8**	192	20	130	150	87.6	60.5	0.6906
AK-01 - 126	0.202	0.017	0.02822	0.00074	0.0522	0.0043	0.00851	0.0011	186	14	**179.4**	**4.6**	171	21	260	160	56.7	42.1	0.7425
AK-01 - 127	2.029	0.066	0.1897	0.0042	0.0779	0.0018	0.0571	0.0046	1124	22	**1120**	**23**	1122	88	1137	46	167.2	52	0.3110
AK-01 - 128	0.233	0.025	0.0304	0.0012	0.0559	0.0064	0.0101	0.0013	211	21	**193.3**	**7.5**	202	26	380	230	44.6	36.1	0.8094
AK-01 - 129	0.204	0.018	0.02938	0.00089	0.0507	0.0042	0.00876	0.00092	187	15	**186.7**	**5.6**	176	18	200	160	55.3	60.5	1.1040
AK-01 - 130	0.187	0.017	0.02905	0.00095	0.0472	0.0044	0.00889	0.001	173	14	**184.6**	**5.9**	179	21	60	170	57.5	64.5	1.1217
AK-01 - 131	0.19	0.024	0.02946	0.00085	0.0472	0.006	0.0094	0.0012	174	20	**187.2**	**5.3**	189	25	30	220	36.9	30.68	0.8314
AK-01 - 132	1.694	0.047	0.169	0.0033	0.0729	0.001	0.0509	0.0038	1006	18	**1006**	**18**	1003	72	1009	29	557	198	0.3555
AK-01 - 133	0.193	0.023	0.02904	0.00088	0.0486	0.0056	0.00879	0.0011	177	20	**184.5**	**5.5**	177	21	110	210	48.6	44.6	0.9177
AK-01 - 134	0.1966	0.0094	0.0288	0.00057	0.0497	0.0021	0.00854	0.00077	182	8	**183**	**3.6**	171.9	15	174	88	341	113.9	0.3340
AK-01 - 135	0.19	0.011	0.02838	0.00064	0.0487	0.0025	0.00906	0.0009	176.1	9.4	**180.4**	**4**	182	18	130	100	255	82	0.3489
AK-01 - 136	0.191	0.02	0.0292	0.00094	0.0481	0.0052	0.00883	0.0011	176	17	**185.5**	**5.9**	178	22	80	190	44.2	42.3	0.9570
AK-01 - 137	0.202	0.02	0.02941	0.00098	0.0494	0.0048	0.0093	0.0012	186	17	**186.9**	**6.1**	187	25	180	200	43.3	34.2	0.7898
AK-01 - 138	1.642	0.051	0.1623	0.0031	0.0734	0.0016	0.0472	0.0037	984	21	**969**	**17**	931	72	1019	44	180	68.9	0.3828
AK-01 - 139	1.732	0.066	0.1725	0.0035	0.0731	0.0023	0.0496	0.0041	1018	25	**1026**	**19**	979	78	1002	66	91.1	40.7	0.4468
AK-01 - 140	1.792	0.068	0.1727	0.0036	0.0767	0.0026	0.0531	0.0046	1041	25	**1027**	**20**	1045	88	1097	67	60.8	33.3	0.5477
AK-01 - 141	0.209	0.016	0.02923	0.00076	0.0522	0.0038	0.00955	0.0086	192	13	**185.7**	**4.8**	192	17

CVI-1344 - 54	0.0714	0.0049	0.01072	0.00026	0.0484	0.0037	0.00291	0.00057	69.9	4.6	**68.8**	**1.6**	59	11	110	140	227	36.8	0.1621
CVI-1344 - 55	0.0739	0.0047	0.01072	0.00021	0.0502	0.0033	0.00423	0.00059	72.3	4.5	**68.8**	**1.3**	85.3	12	190	130	496	116.3	0.2345
CVI-1344 - 56	0.0696	0.0027	0.01062	0.00014	0.0476	0.0018	0.0039	0.00047	68.3	2.6	**68.13**	**0.9**	78.7	9.4	84	74	948	287	0.3027
CVI-1344 - 57	0.0736	0.0057	0.01111	0.00027	0.0485	0.0041	0.00433	0.00084	71.9	5.4	**71.2**	**1.7**	87	17	110	160	218	31.5	0.1445
CVI-1344 - 58	0.0698	0.0036	0.011	0.00023	0.047	0.0028	0.00413	0.00069	68.4	3.4	**70.5**	**1.4**	83	14	60	110	302	57.9	0.1917
CVI-1367																			
CVI-1367 - 1	0.0731	0.0042	0.01104	0.00017	0.0481	0.003	0.00314	0.00063	71.6	3.9	**70.8**	**1.1**	63.4	13	100	120	310	60.3	0.1945
CVI-1367 - 2	0.0662	0.0046	0.01059	0.00019	0.0454	0.0032	0.00339	0.00062	65	4.4	**67.9**	**1.2**	68.5	12	-10	130	257.7	77	0.2988
CVI-1367 - 3	0.0533	0.0064	0.0086	0.00024	0.044	0.0052	0.00221	0.00051	52.6	6.1	**55.2**	**1.6**	44.5	10	-40	200	90.6	43.4	0.4790
CVI-1367 - 4	0.0551	0.0069	0.00843	0.00023	0.0478	0.0065	0.00214	0.00045	54.3	6.6	**54.1**	**1.5**	43.2	9	60	240	134.9	97.1	0.7198
CVI-1367 - 5	0.0624	0.0055	0.00898	0.00023	0.0508	0.0049	0.00247	0.00064	61.3	5.2	**57.7**	**1.5**	49.9	13	190	180	235	39.3	0.1672
CVI-1367 - 6	0.0642	0.0098	0.00861	0.00051	0.0539	0.0061	0.00252	0.00063	63.1	9.2	**55.3**	**3.2**	50.9	13	340	240	322	90.3	0.2804
CVI-1367 - 7	0.058	0.0027	0.00852	0.00011	0.0492	0.0021	0.00228	0.00039	57.2	2.6	**54.7**	**0.73**	45.9	7.9	152	88	1196	484	0.4047
CVI-1367 - 8	0.0602	0.002	0.00908	0.00017	0.0481	0.0017	0.00222	0.00038	59.4	1.9	**58.3**	**1.1**	44.9	7.8	108	75	1353	696	0.5144
CVI-1367 - 9	0.094	0.016	0.01446	0.00083	0.0465	0.0064	0.0045	0.0015	91	15	**92.5**	**5.3**	91	31	40	260	288	141	0.4896
CVI-1367 - 10	0.0512	0.0045	0.00803	0.00019	0.0464	0.0042	0.00188	0.00036	50.6	4.3	**51.6**	**1.2**	38	7.2	30	160	160	162	1.0125
CVI-1367 - 11	0.9	0.076	0.1039	0.003	0.0632	0.0058	0.0264	0.0052	646	43	**637**	**17**	527	100	660	210	24.3	22.9	0.9424
CVI-1367 - 12	0.0575	0.0032	0.00863	0.00017	0.0483	0.0026	0.00215	0.00053	56.7	3.1	**55.4**	**1.1**	43.4	11	110	110	421	91	0.2162
CVI-1367 - 13	0.0628	0.0047	0.00868	0.00019	0.0528	0.0042	0.00225	0.00083	61.8	4.5	**55.7**	**1.2**	45	17	290	160	242	43.5	0.1798
CVI-1367 - 14	0.453	0.028	0.0532	0.0027	0.0614	0.0016	0.018	0.0034	377	19	**334**	**16**	359	67	643	55	438	46.2	0.1055
CVI-1367 - 15	0.0686	0.0082	0.00903	0.00043	0.055	0.0046	0.00259	0.00064	67.3	7.7	**58**	**2.8**	52.4	13	390	180	1013	378	0.3731
CVI-1367 - 16	0.139	0.011	0.01943	0.001	0.0524	0.0017	0.00466	0.001	131.6	9.4	**124**	**6.3**	94	21	294	71	402.2	58	0.1442
CVI-1367 - 17	0.359	0.022	0.0485	0.001	0.0528	0.0025	0.01545	0.0026	310	16	**305.1**	**6.4**	310	52	330	110	146.7	75.3	0.5133
AP-038																			
AP-038 - 1	0.033	0.036	0.00899	0.00043	0.019	0.026	0.02	0.035	26	35	**57.7**	**2.8**	330	690	1630	410	2750	71.3	0.0259
AP-038 - 2	0.037	0.028	0.00994	0.00052	0.029	0.022	0.044	0.022	40	31	**63.8**	**3.3**	840	420	1260	280	7630	620	0.0813
AP-038 - 3	0.027	0.035	0.00962	0.00037	0.023	0.027	0.056	0.041	29	38	**61.7**	**2.3**	1030	770	1270	400	3500	76	0.0217
AP-038 - 4	0.0364	0.0093	0.00762	0.00013	0.0339	0.0085	-0.0045	0.0098	35.8	9.1	**48.96**	**0.86**	-90	200	800	220	5000	164.6	0.0329
AP-038 - 5	0.0526	0.0077	0.00829	0.00023	0.046	0.0065	0.0028	0.011	51.9	7.4	**53.2**	**1.5**	50	220	670	200	7870	212	0.0269
AP-038 - 6	0.0503	0.0043	0.00796	0.00012	0.0458	0.0038	0.0005	0.0035	49.7	4.2	**51.12**	**0.75**	9	71	400	110	6650	380	0.0571
AP-038 - 7	0.0507	0.0028	0.0078	0.00014	0.0472	0.0024	0.0027	0.0047	50.2	2.7	**50.06**	**0.88**	55	95	250	100	11470	243	0.0212
AP-038 - 8	0.0482	0.0035	0.007633	0.000075	0.0457	0.0033	0.0014	0.0034	47.7	3.4	**49.02**	**0.48**	27	68	410	110	9360	246	0.0263
AP-038 - 9	0.0496	0.0039	0.00799	0.0002	0.0449	0.0033	0	0.0038	49.1	3.8	**51.3**	**1.3**	0	76	360	120	9470	312	0.0329
AP-038 - 10	0.023	0.048	0.0108	0.0011	0.013	0.026	0.088	0.064	23	43	**69.1**	**7.1**	1430	1.10E+03	1290	410	4910	120.3	0.0245
AP-038 - 11	0.0435	0.0038	0.00796	0.00019	0.0398	0.0034	-0.0042	0.0062	43.2	3.7	**51.1**	**1.2**	-85	130	370	84	8800	208	0.0236
AP-038 - 12	0.0442	0.0049	0.00736	0.00013	0.0434	0.0044	0.0006	0.0042	43.8	4.8	**47.27**	**0.82**	12	85	300	100	11140	309	0.0277
AP-038 - 13	0.052	0.011	0.00822	0.00031	0.0452	0.0091	0.0027	0.006	51	11	**52.7**	**2**	53	120	660	270	7540	353	0.0468
AP-038 - 14	0.0498	0.0066	0.00789	0.00016	0.0457	0.0058	0.0015	0.01	49.2	6.4	**50.7**	**1**	30	210	510	180	5040	114	0.0226
AP-038 - 15	0.0426	0.0048	0.00675	0.00025	0.0447	0.0045	-0.0002	0.0048	42.3	4.7	**43.4**	**1.6**	-6	98	410	190	1.85E+04	970	0.0524
AP-038 - 16	0.0474	0.0057	0.00748	0.00016	0.0459	0.0052	0.0016	0.0088	47	5.6	**48**	**1**	30	180	280	110	6540	95.6	0.0146
AP-038 - 17	0.0471	0.0036	0.007705	0.000099	0.0437	0.0033	-0.0004	0.0049	46.7	3.5	**49.48**	**0.64**	-10	98	260	100	7690	171	0.0222
AP-038 - 18	0.0498	0.0033	0.0079	0.00013	0.0457	0.0028	0.0011	0.0054	49.3	3.1	**50.74**	**0.8**	21	110	282	77	8930	187	0.0209
AP-038 - 19	0.0439	0.0039	0.00745	0.00017	0.0427	0.0034	-0.0001	0.0025	43.6	3.8	**47.8**	**1.1**	-3	51	260	150	6930	242.9	0.0351
AP-038 - 20	0.0511	0.0023	0.00765	0.00012	0.0483	0.002	0.0039	0.0048	50.5	2.3	**49.12**	**0.77**	77	96	238	40	8830	134.7	0.0153
AP-038 - 21	0.0457	0.0051	0.00753	0.00026	0.044	0.0044	-0.0005	0.0052	45.2	4.9	**48.3**	**1.6**	-11	100	480	140	7440	369	0.0496
AP-038 - 22	0.0464	0.0059	0.00803	0.00022	0.0416	0.0049	-0.0037	0.016	45.9	5.7	**51.5**	**1.4**	-80	320	450	150	4920	94.7	0.0192
AP-038 - 23	1.715	0.073	0.1709	0.0022	0.0724	0.0027	0.0521	0.017	1010	28	**1017**	**12**	1024	340	976	81	281	82.6	0.2940
AP-038 - 24	1.683	0.024	0.1679	0.0023	0.0728	0.0011	0.04	0.021	1001.7	9.2	**1000**	**13**	790	400	1006	30	1355	64.1	0.0473
AP-038 - 25	0.049	0.0077	0.00783	0.00038	0.0463	0.0062	0.0148	0.0078	48.3	7.4	**50.3**	**2.5**	290	150	590	180	1.02E+04	327	0.0321
AP-038 - 26	0.295	0.048	0.04358	0.00077	0.0488	0.0076	0.01361	0.0034	258	40	**275**	**4.8**	273	69	610	110	529.1	630	1.1907
AP-038 - 27	0.296	0.067	0.0475	0.0013	0.0437	0.0097	0.0134	0.0044	247	56	**298.8**	**7.8**	269	87	750	200	295	374	1.2678
AP-038 - 28	0.29	0.023	0.0423	0.00063	0.0495	0.0037	0.01264	0.0028	257	19	**267.1**	**3.9**	253.8	56	468	98	853	1281	1.5018
AP-038 - 29	0.0533	0.0045	0.00802	0.0002	0.0479	0.0031	0.00165	0.00066	52.6	4.3	**51.5**	**1.3**	33	13	370	120	1.89E+04	1810	0.0958
AP-038 - 30	0.0511	0.0033	0.008	0.00012	0.0463	0.0028	0.0019	0.0076	50.5	3.2	**51.37**	**0.78**	36	150	318	67	7570	121	0.0160
AP-038 - 31	0.0484	0.0025	0.007802	0.0001	0.0448	0.0022	0	0.0032	47.9	2.4	**50.1**	**0.65**	-1	65	254	85	9160	201	0.0219
AP-038 - 32	0.0488	0.0042	0.0076	0.00011	0.0466	0.0038	0.0018	0.0066	48.3	4	**48.84**	**0.69**	36	130	411	85	6710	162.1	0.0242
AP-038 - 33	0.0487	0.0068	0.00763	0.00011	0.0461	0.0061	0.0013	0.013	48.1	6.6	**48.99**	**0.71**	20	260	690	120	5130	84.9	0.0165
AP-038 - 34	0.045	0.0066	0.0078	0.00023	0.0416	0.0054	0.0011	0.004	44.6	6.4	**50.1**	**1.5**	20	81	390	150	12380	366	0.0296
AP-038 - 35	0.0484	0.0027	0.007633	0.000091	0.0461	0.0025	0.0006	0.005	48	2.6	**49.02**	**0.58**	11	100	308	88	1.15E+04	266	0.0231
AP-038 - 36	0.0511	0.0031	0.00784	0.00012	0.0473	0.0028	0.002	0.0045	50.5	3	**50.31**	**0.74**	40	91	282	60	6950	111.2	0.0160
AP-038 - 37	0.0526	0.002	0.00788	0.000098	0.0484	0.0018	0.003	0.0023	52	2	**50.6**	**0.63**	61	46	249	57	10210	270.4	0.0265
AP-038 - 38	0.0438	0.0097	0.00787	0.00014	0.0401	0.0087	0.0002	0.0083	43	9.5	**50.53**	**0.9**	0	170	820	140	8160	332	0.0407
AP-038 - 39	0.0515	0.0059	0.00835	0.00017	0.0451	0.0051	0.0006	0.0029	50.8	5.8	**53.6**	**1.1**	12	59	520	150	7680	540	0.0703
AP-038 - 40	0.0475	0.0043	0.00768	0.00015	0.045	0.0038	-0.0004	0.0076	47.1	4.2	**49.32**	**0.93**	-10	160	171	55	8480	130.7	0.0154
AP-038 - 41	0.0506	0.0024	0.007874	0.0001	0.0465	0.0021	0.00158	0.0011	50.1	2.4	**50.56**	**0.64**	32	22	276	69	9250	491	0.0531
AP-038 - 42	2.154	0.076	0.199	0.0029	0.0784	0.0022	0.0573	0.015	1163	26	**1170**	**16**	1125	290	1146	59	340	180	0.5294
AP-038 - 43	1.707	0.045	0.1685	0.0022	0.0735	0.0014	0.0598	0.018	1010	17	**1004**	**12**	1172	340	1023	40	556	83	0.1493
AP-038 - 44	0.0549	0.0027	0.00812	0.00011	0.0491	0.0022	0.00286	0.00061	54.3	2.6	**52.15**	**0.71**	57.7	12	271	72	9010	714	0.0792
AP-038 - 45	0.0487	0.0025	0.007699	0.00009	0.0464	0.0019	0.00133	0.0016	48.2	2.4	**49.44**	**0.57**	27	32	217	52	1.84E+04	901	0.0490
AP-038 - 46	0.0476	0.0042	0.00777	0.00017	0.0445	0.0038	0.00243	0.0007	47.1	4.1	**49.9**	**1.1**	49	14	400	130	9040	1590	0.1759
AP-038 - 47	0.0458	0.0055	0.00744	0.00012	0.0444	0.005	-0.0004	0.0051	45.3	5.4	**47.77**	**0.78**	-10	100	480	160	5090	150	0.0295
AP-038 - 48	0.0492	0.0048	0.00788	0.00012	0.0451	0.0041	0.0025	0.003	48.7	4.6	**50.59**	**0.74**	51	61	420	100	3900	354	0.0908
AP-038 - 49	0.0458	0.0043	0.00762	0.00012	0.0435	0.0038	-0.0005	0.0044	45.4	4.2	**48.91**	**0.78**	-10	90	423	92	7320	210	0.0287
AP-038 - 50	0.0531	0.0026	0.0084	0.00019	0.046	0.002	0.0011	0.0021	52.5	2.5	**53.9**	**1.2**	22	42	216	68	1.22E+04	327	0.0268
AP-038 - 51	0.0524	0.003	0.007878	0.0001	0.0482	0.0027	0.0042	0.0056	51.8	2.9	**50.59**	**0.65**	84	110	333	80	4330	54.4	0.0126
AP-038 - 52	0.014	0.028	0.00735	0.00031	0.012	0.027	0.0006	0.0027	13	28	**47.2**	**2**	13	54	840	640	4610	1400	0.3037

TABLE A2. Trace elements in Zircon, and Ti-in Zr Thermometry

I.D.	target	$^{238}U/^{206}Pb$	Al	Ti	Y	Zr	Ba	La	Ce	Pr	Nd	Sm	Eu	Gd	Tb	Dy	Ho	Er	Tm	Yb	Lu	Hf	Th	U	Log Ti	Ti T°C
AP-009																										
AP_09_145	core	**51.1**	-1.4	1.98	1057	4.80E+05	0.03	0	7.4	0.005	0.29	1.06	0.81	10.1	4.5	68.1	31.6	174.9	49.3	563	114.1	10510	17.6	161.9	0.29666519	616.00
AP_09_16	core	**51.4**	-2.7	1.88	2280	5.45E+05	-0.003	-0.01155	11.71	0.05	1.64	4.41	2.83	35.2	12.26	174	68.9	364	94.1	1056	194	13090	49.4	361	0.27415785	612.51
AP_09_29	core	**51.7**	4.5	4.36	1220	4.94E+05	0.099	-0.00363	11.8	0.03	0.77	2.86	1.41	16.9	6.47	88.6	39.3	202.5	52	592	118.1	8440	30.1	107.7	0.63948649	672.76
AP_09_11	core	**52.12**	29	10.05	2620	5.19E+05	0.267	0.018	35.96	0.071	1.64	4.96	3.08	38.8	14.84	204.2	85.4	419.9	99.9	1036	208.5	9630	111.2	255.1	1.00216606	741.26
AP_09_105	core	**52.21**	-1.1	7.85	1539	4.64E+05	0.063	0.004	25.02	0.06	1.17	3.19	1.97	21.9	8.46	116.4	49.8	242.6	63.5	658	124.2	7500	63.6	194.3	0.89486966	719.98
AP_09_135	core	**53.7**	3.3	3.12	1115	5.58E+05	0.15	0	11	0.016	0.26	2	0.88	13.3	5.28	79.7	34.6	188	52.7	656	122.3	10390	26.2	155.5	0.49415459	647.83
AP_09_44	core	**54.3**	6.1	2.16	831	5.31E+05	0.099	0	4.98	0.006	0.22	0.66	0.38	6.3	3.14	50	26.75	150.2	41.6	502	103.4	12820	15.74	198.8	0.33445375	621.92
AP_09_138	core	**54.7**	18.8	3.29	1085	4.78E+05	0.206	0.018	9.24	0.0121	0.27	1.36	0.87	11.17	4.72	72.8	33.1	175.3	49.8	584	119.4	9500	26.64	152.2	0.5171959	651.70
AP_09_4	core	**173.9**	6	14.5	590	4.91E+05	0.042	0.0041	9.93	0.066	1.49	3.23	0.345	13.4	4.29	50.7	19.3	90.9	18.7	178.3	34.7	12910	53.5	114.4	1.161368	774.57
AP_09_51	core	**180.6**	13.5	9	1954	4.88E+05	0.074	0.087	17.2	0.34	6.3	9.1	1.38	42.9	14.9	182.4	69.4	309	63.5	586	105.7	9360	47.5	44.4	0.95422521	731.65
AP_09_143	core	**181.4**	6.2	16.21	654	4.75E+05	0.119	0.0133	14.78	0.071	1.47	2.98	0.407	14.22	5.44	59.6	22.43	93.9	21.49	194.1	32.5	10390	55.7	61	1.20978301	785.14
AP_09_126	core	**185.2**	-2.8	1.2	117.6	4.95E+05	0.011	0	1.68	0	0	0.06	0.009	1.19	0.38	7.69	3.41	20.22	6.1	70.7	15.5	12340	0.728	21.4	0.07918125	583.39
AP_09_42	core	**186.3**	25.2	19.5	749	4.94E+05	0.1	0.006	12.63	0.01	0.89	2.52	0.26	14.4	4.83	68.5	25.4	114.1	26.4	273	44.8	11480	28.4	51.6	1.29003461	803.13
AP_09_53	core	**195.1**	9.5	5.3	1490	5.02E+05	0.086	0	7.06	0	0.29	1.7	1.84	18.9	7.81	113	47.22	236.2	55.2	564	106.8	9910	6.12	76.3	0.72427587	687.93
AP_09_48	core	**244.4**	10.1	3.62	736	4.84E+05	0.065	0	9.87	0.04	1.54	3.08	1.32	15.4	5.09	61.9	24.61	117.5	26.7	265.9	54.1	10160	18.1	36.7	0.55870857	658.74
AP_09_88	core	**256**	1.2	3.09	889	4.75E+05	0.087	0	18.98	0.035	0.95	2.52	1.18	14.31	5.27	70.2	28.1	142.3	36.1	396.3	76.7	10160	29.8	107.2	0.48995848	647.13
AP_09_125	core	**393**	6.7	18.6	361.5	4.59E+05	0.012	0.022	2.13	0	0.2	0.1	0.103	2.12	1.13	18.23	9.86	63.6	20.72	280.7	61.2	11290	17.52	1483	1.26951294	798.47
AP_09_89	core	**645**	12.9	16.3	270.7	4.83E+05	0.018	0.025	9.91	0.058	1.31	2.6	0.51	10	2.66	28.2	9	32.1	7.84	72.6	12.06	10860	31.1	95.3	1.2121876	785.67
AP_09_97	core	**761**	216	69.7	454	4.98E+05	7.9	0.005	6.14	0.041	0.78	2.1	0.242	7.1	2.94	34.5	14.73	64.9	16.25	168.5	28.5	9680	1.27	9.66	1.84322078	946.02
AP_09_65	core	**768**	16.7	8.88	918	5.41E+05	0.104	0	16.61	0.061	1.43	3.4	0.356	18.4	7.04	82.2	29.5	130	27.9	255.5	38.8	11530	201.4	440	0.94841297	730.49
AP_09_15	core	**824**	101	5.47	692	4.90E+05	1.57	0	10.56	0.024	0.96	3.35	0.25	14.7	4.64	59.3	22.1	103.7	24.21	227.4	43.6	10720	171.4	356	0.73798733	690.43
AP_09_101	core	**831**	68	70	1144	4.91E+05	0.17	0.022	6.41	0.014	0.44	1.4	0.4	14.1	5.99	89.8	39.1	183.2	42.8	418	65.9	9740	74.2	233.4	1.84509804	946.57
AP_09_127	core	**833**	6.3	10.35	554	4.78E+05	0.039	0.026	20.2	0.053	1.21	2.31	0.33	13.5	4.06	46.3	18.4	86.6	20.3	192.5	38.7	11100	111.1	322.8	1.01494035	743.85
AP_09_63	core	**834**	30.3	11.3	150.3	4.88E+05	0.041	0.008	10.54	0.044	1.66	2.9	0.72	9.8	2.55	19.7	5.14	17.6	3.1	26.6	4.06	10870	62.6	189.3	1.05307844	751.68
AP_09_1	core	**838.5**	4760	827	318.9	5.08E+05	185.6	0.0037	5.96	0.044	0.57	1.36	0.325	6.89	2.49	27.6	10.1	43.8	10.13	95.2	18.86	9340	30.81	103.6	2.91750551	1369.54
AP_09_112	core	**859.5**	19.6	23	201	4.85E+05	0.104	0.009	17.9	0.107	1.51	1.39	0.69	4.74	1.4	15.3	6.07	31	7.84	87.6	16.91	9720	72.9	266	1.36172784	819.73
AP_09_110	core	**869**	9.2	2.55	427	4.62E+05	0.129	0	6.86	0.006	0.25	0.89	0.41	5.3	2.29	31	13.17	67.7	18.49	210	39.6	10170	76.9	288	0.40654018	633.43
AP_09_70	core	**872**	5.4	7.2	559	4.88E+05	0.005	0.084	13.39	0	1.21	3.32	0.27	13.1	4.32	52.7	19.4	82	18.88	179	30.4	10800	56.6	186.5	0.85733325	712.75
AP_09_128	core	**875**	5.2	12.7	874	4.98E+05	0.143	-0.00535	34	0.055	1.65	2.96	0.256	18.2	6.69	77.4	29.66	135.8	32.92	332.2	61.7	11040	45.1	75.1	1.10380372	762.28
AP_09_124	core	**878.9**	58	45.2	279	5.09E+05	0.174	-0.002622	34.3	0.136	2.4	2.54	0.713	10.01	2.78	26	9.37	36.7	8.31	80.8	16.5	10780	64.4	133.1	1.65513843	893.36
AP_09_78	core	**886**	92.2	37.2	303	4.86E+05	0.128	0.029	22.69	0.217	3.09	3.37	0.704	10.1	2.37	27	9.75	53.7	15.99	212.4	41.4	12350	33.1	228.8	1.57054294	871.13
AP_09_102	core	**889.9**	4.4	14.3	1540	4.68E+05	0.28	0.031	45	0.07	1.6	4.74	0.59	30.9	11.46	148.8	52.7	229.9	50.3	489	82.8	11150	267.6	846	1.15533604	773.27
AP_09_125	core	**894**	22.3	15.2	460	4.74E+05	0.65	0.02	12.53	0.063	0.47	1.68	0.14	10	3.66	40.7	15.8	70.8	15.8	142.2	28.1	10900	41.4	175	1.18184359	779.01
AP_09_136	core	**896**	26	8.3	247.5	4.59E+05	0.114	0.024	18.68	0.095	0.72	0.95	0.27	4.06	1.5	19.4	8.05	38	9.83	114.9	22.83	9940	71.9	271.4	0.91907809	724.70
AP_09_49	core	**901.7**	970	43	1185	4.84E+05	4	0.051	20.7	0.03	1.26	4	0.27	24.8	8.09	99.5	37.9	168.4	37.4	352.4	63.9	10030	537	776	1.63346846	887.59
AP_09_32	core	**912**	19.9	23.7	154	4.86E+05	0.006	0.0069	2.85	0.013	0.5	0.96	0.404	3.68	1.23	14	5.44	24.4	6.37	66.5	13.08	8800	7.77	55.7	1.37474835	822.80
AP_09_118	core	**914**	30.8	17	331.8	4.97E+05	0.036	0.0029	8.25	0.034	0.56	1.12	0.141	6.1	2.36	27.2	10.52	46.9	11.18	107.7	18.56	10980	2.643	14.68	1.23044892	789.71
AP_09_122	core	**919**	2.6	11.44	874.9	5.02E+05	0.105	0.0054	20.14	0.0172	0.62	1.75	0.765	12.09	4.93	64.4	27.43	137.1	32.75	336.4	66.13	10370	48.5	59.24	1.05842602	752.79
AP_09_20	core	**935**	126	17.3	702	4.83E+05	0.5	0.01	8.06	0.022	0.35	1.21	0.091	5.75	2.29	34.8	19.69	171.8	74.7	1124	250.4	11600	189.8	2409	1.2380461	791.40
AP_09_71	core	**936.4**	170	37.9	1049	4.89E+05	7.7	0.007	13.48	0.021	0.88	3.53	0.262	22.2	7.85	92.5	35.81	153.6	34.1	337	58.4	10900	246.8	595	1.57863921	873.22
AP_09_38	core	**946**	107	40.1	243.2	4.90E+05	1.4	0.027	15.04	0.12	2.7	4.58	0.67	17.07	4	34.7	8.26	28.67	4.95	43.8	6.84	10470	9.23	95.9	1.60314437	879.60
AP_09_92	core	**957**	46.5	29	373	5.08E+05	0.49	0	7.08	0.091	1.39	1.91	0.32	9.5	3.43	38.6	14.5	51.6	12	107.6	16.1	11520	1.18	26.3	1.462398	843.92
AP_09_8	core	**959.1**	33	21.2	1562	5.20E+05	0.341	0.035	10.9	0.051	0.71	1.79	0.351	13.59	6.21	104.3	50.5	277	74.2	813	165.9	16280	95.3	2560	1.32633586	811.47
AP_09_60	core	**961.3**	95	11.8	1661	5.37E+05	1.45	0.117	20.28	0.131	1.69	2.69	0.321	16.2	6.65	104.3	51.9	323.4	92.1	1091	228.9	12980	309.1	1924	1.07188201	755.58
AP_09_111	core	**967**	38.8	22	467.7	4.64E+05	0.034	0.0017	13.58	0.068	0.96	2.24	0.399	12.87	3.87	45.1	16.12	67.4	15.96	156.1	25.83	11000	36.13	135.4	1.34242268	815.21
AP_09_104	core	**981**	15.5	15.4	603	4.73E+05	0.03	0.0102	15.11	0.045	0.83	1.66	0.69	10.92	4.27	53.4	19.52	91.1	22.16	225.7	41.24	10960	35.24	213.3	1.18752072	780.25
AP_09_86	core	**982**	39.7	16.8	80.1	4.70E+05	-0.001	0.012	7.95	0.047	0.78	1.5	0.266	4.81	1.28	9.15	2.69	9.24	1.56	12.44	1.94	10050	12.7	50.94	1.22530928	788.57
AP_09_61	core	**986.9**	43.6	14.8	489	4.95E+05	0.6	0.0079	4.16	0.016	0.31	0.84	0.467	7.42	2.92	36.4	14.47	69.4	15.61	154.2	30.6	11870	23.76	1837	1.17026172	776.49
AP_09_5	core	**989**	68.3	17.34	57.9	5.29E+05	0.039	0.0049	9.05	0.103	1.54	2.53	0.406	6.28	1.35	8.71	1.88	5.47	0.833	5.52	0.887	11960	16.96	37.1	1.23904909	791.63
AP_09_132	core	**992**	84.8	27.46	950	4.82E+05	0.061	0.0068	12.91	0.148	2.7	5.76	1.072	31.9	10.3	104.2	30.94	110.7	21.52	180.3	26.73	11340	152.8	105.1	1.43870053	828.13
AP_09_57	core	**1000**	16.5	24.1	671	5.41E+05	0.154	0	35.6	0.102	2.66	11	0.348	51.1	11.44	89.1	23.24	73.9	13.37	101.2	16.3	15300	113.3	1278	1.38201704	824.52
AP_09_99	core	**1012.1**	178.5	44.1	140.1	4.87E+05	0.035	0.018	12.35	0.43	6.31	7.17	0.53	15.45	2.72	19.85	4.8	13.87	2.44	17.83	2.34	12430	537.3	247.9	1.64443859	890.50
AP_09_27	core	**1016**	17.6	25.4	902	4.95E+05	0.055	0.007	8.96	0.042	1.08	2.96	0.35	18.3	6.25	82.1	30.4	134.4	29.14	273.2	44.6	10650	91.3	329	1.40483372	829.96
AP_09_6	core	**1020.9**	6.3	34.4	777	5.22E+05	0.038	0	13.82	0.06	1.41	2.56	0.623	15.1	5.23	67.7	25.32	118.1	26.96	256.1	45.55	12340	14.93	68.6	1.53655844	862.44
AP_09_69	core	**1026**	57.5	25.5	133.9	4.86E+05	0.059	0.0111	10.04	0.104	1.58	2.01	0.589	8.09	2.03	16.5	4.66	15.7	2.69	22	3.41	11310	0.968	19.11	1.40656018	830.37
AP_09_93	core	**1031**	14.6	17.1	708	4.90E+05	0.037	0.017	2.36	0.0072	0.13	0.098	0.212	5.1	2.65	39.4	20.44	120.3	37	482	103.2	14280	11.93	2324	1.23299611	790.28
AP_09_45	core	**1034**	8.9	36.6	335.1	4.99E+05	0.024	0.002	5.17	0.036	0.9	2.22	0.415	11.71	3.55	36.2	11.18	43.8	8.02	68.4	10.49	11920	1.808	34.84	1.56348109	869.32
AP_09_2	core	**1046**	4.4	20.4	1745	5.27E+05	0.049	0.091	19.43	0.075	1.28	3.87	0.306	24.3	10.26	135.6	58.9	295.4	69.1	696	133.2	13010	543	2006	1.30963017	807.62
AP_09_107	core	**1060**	189.1	103.1	570	4.66E+05	0.001	0.028	3.6	0.355	4.52	5.42	0.212	18.3	5.43	61.2	19.67	69.2	12.33	95.9	13.5	11340	94.1	156.6	2.01325867	997.89
AP_09_18	core	**1065**	10.2	30.1	378.1	5.02E+05	0.078	0.0082	13.61	0.118	2.73	5.75	2.23	19.5	4.64	44.5	13.37	51.6	10.26	92.6	15.69	8740	30.4	55	1.4785665	847.91
AP_09_80	core	**1097**	2.8	41.4	431	4.90E+05	0.191	0.01	39.4	0.205	3.78	5.42	1.98	16.2	4.28	42.1	13.92	58.1	13.89	143	24.2	8680	78.3	139.7	1.61700034	883.24
AP_09_119	core	**1126**	6.5	62.2	3801	4.94E+05	0.174	0.055	50.8	0.433	9.34	22.7	1.97	107.3	35.1	381	129.9	527	108.8	920	148.9	11330	235.9	284	1.79379038	931.72
AP_09_115	core	**1128**	3.9	31.4	643	4.71E+05	0.025	0.0034	3.51	0.04	0.54	1.54	0.281	11.82	4.41	53.8	21.85	98.4	23.41	231.5	41.18	10450	5.09	40.99	1.49692965	852.47
AP_09_43	core	**1186**	4.7	16.7	1464	4.69E+05	0.062	0	8.23	0.023	0.93	3.21	0.558	24	9.13	125.8	51.5	241	51.4	506	85	10140	65.8	491	1.22271647	787.99
AP_09_82	core	**1209**	2.3	16.87	600	4.75E+05	0.013	-0.0004	5.37	0.05	1.01	2.32	0.327	12.3	4.69	55.7	20.89	91.9	20.95	198.1	32.55	10400	15.67	51.78	1.22711508	788.97
AP_09_74	core	**1221**	-1.1	19.36	720	4.89E+05	0.048	0.0053	10.63	0.009	0.43	1.8	0.075	11.09	4.46	61.7	24.14	116.8	27.96	270.9	44.96	11430	74.2	286.9	1.28690535	802.42
AP_09_30	core	**1237**	7.8	2.61	2573	4.87E+05	0.081	0.0082	20.21	0.166	3.75	8.7	0.293	57.6	20.51	250.5	93.8	402	83.9	753	116.2	10950	217	502	0.41664051	635.07
AP_09_21	core	**1256**	4.6	19.2	1421	4.94E+05	0.062	0.004	6.86	0.021	0.66	3.85	0.743	27.5	10.58	134.4	53.4	237.5	52.1	517	86.6	9750	77.3	338	1.28330128	801.60
AP_09_124	core	**1324**	-1.4	21.7	972	4.83E+05	0.015	0.0055	10.76	0.045	1.15	3.65	0.108	21.1	8.09	97.8	34.8	149.2	31.56	288.2	45.29	9830	32.99	130.6	1.33645973	813.82
AP_09_33	core	**1389**	-1.4	26	968	4.96E+05	0.057	0	11.53	0.03	1.66	4.25	0.98	21.9	7.76	95.4	34.54	156.1	33.8	343	55.4	10330	26.42	89.2	1.41497335	832.39
AP_09_96	rim	**49.25**	1.3	4.13	1582	4.71E+05	0.064	0	18.11	0.0134	0.5	2.39	1.38	18.36	8.02	111.3	48.3	255.8	67.7	778	151.3	11180	125.7	649	0.61595005	668.63
AP_09_114	rim	**49.66**	0.4	5.91	2460	4.83E+05	0.103	0	23.2	0.036	0.72	2.85	1.78	26.4	12.03	170.9	76.9	388	101.7	1090	215.8	10660	55.5	265	0.77158748	696.61
AP_09_73	rim	**49.73**	1.4	1.85	2173	4.74E+05	0.161	0	11.97	0	0.23	1.78	0.85	19.9	9.52	146	68.6	349.6	91.3	1008	204.3	15930	139.7	1836	0.26771177	611.43
AP_09_120	rim	**49.75**	-2.2	2.16	1186	4.85E+05	0.06	0	9.3	0.0033	0.12	1.03	0.81	12.15	5.5	78.6	35.54	189.6	49.8	572	118.8	12290	58.2	538	0.33445375	621.92
AP_09_76	rim	**50.26**	6.8	1.53	1065	4.66E+05	0.056	0.013	5.65	0.0048	0.087	0.89	0.457	9.43	4.44	69.7	33.3	177.7	47	538	110.9	13320	34.4	619	0.18469143	598.91
AP_09_90	rim	**50.35**	0.7	2.42	3568	4.72E+05	0.049	0.0044	13.65	0.0073	0.178	2.46	1.52	29.9	14.38	218.5	107.1	570	156.2	1787	356.3	14030	60	1107	0.38381537	629.77
AP_09_10	rim	**50.52**	-1	4.98	1854	5.42E+05	0.118	0.0039	35.99	0.027	1.18	4.35	2.3	29.5	11.19	142.3	59.5	295.1	72.9	778	159.6	11540	283.3	630.1	0.69723842	683.04
AP_09_54	rim	**50.52**	8.5	1.88	892	5.03E+05	0.019	0.0088	5.85	0.0177	0.169	0.62	0.559	8.78	3.76	56.7	26.9	148.7	39.3	447	96.9	12690	27	261	0.27415785	612.51
AP_09_9	rim	**50.55**	3.8	2.75	1697	5.23E+05	0.062	0	10.73	0.0023	0.307	1.62	1.093	16.34	7.24	111	52	288.7	78	882	192.2	13380	43.5	463	0.43933269	638.77
AP_09_22	rim	**50.6**	-4.3	7.06	2690	4.84E+05	0.122	0.0005	42.5	0.046	1.54	4.54	2.59	36	13.86	202.8	84.5	432	105.7	1118	208.6	9700	102.2	273	0.8488047	711.12
AP_09_133	rim	**50.83**	0.1	1.87	2010	4.79E+05	0.03	0.0094	6.84	0	0.04	0.97	0.605	15.13	8.36	132.6	63	337.3	92	1013	200.8	13590	20.02	541	0.27184161	612.15
AP_09_87	rim	**51.19**	-1.7	2.43	1986	4.69E+05	0.06	0.0048	16.05	0.015	0.41	1.61	1.19	20	9.29	136.6	62.6	329.5	86.4	944	185.2	12710	62.7	906	0.38560827	680.06
AP_09_62	rim	**51.2**	1.5	3.87	1978	5.20E+05	0.055	0	13.7	0.0105	0.29	1.71	1.2	16.16	8.13	122.6	58.8	324	84.8	977	213.2	12120	34.1	319	0.58771097	663.72
AP_09_140	rim	**51.2**	2.6	1.38	1412	4.77E+05	0.015	0	4.52	0.0025	0.046	0.74	0.523	10.52	5.51	87.7	42.6	241.8	67.6	798	166.6	13660	11.91	420	0.13987909	592.25
AP_09_129	rim	**51.32**	-0.1	4.71	5180	4.86E+05	0.185	0	65.3	0.023	1.03	6.4	3.24	63.5	27.25	396.7	172.4	816	195	1995	359.6	12510	154.1	1229	0.67302091	678.70
AP_09_52	rim	**51.34**	0.5	4.77	2422	5.04E+05	0.119	0.0022	26.6	0.031	0.84	3.43	2	26.1	10.84	151.7	72.3	389	102.7	1176	246.5	11910	97	499	0.67851838	679.68
AP_09_117	rim	**51.45**	-1.7	2.86	3731	4.82E+05	0.055	0	16.83	0.0059	0.196	2.09	1.28	32.3	16.49	250.6	117	606.3	151.8	1599	323.2	13970	66.9	1011	0.45636603	643.57
AP_09_108	rim	**51.63**	3.3	3.85	2142	4.72E+05	0.051	0.008	17.4	0.024	0.5	2.5	1.48	22.7	10.25	149.7	66.5	349	95.4	1044	215.8	11250	79.4	572	0.58546073	663.34
AP_09_77	rim	**51.68**	1530	10.5	2503	4.78E+05	0.97	0.055	36.29	0.065	1.78	5.31	3.24	36.9	13.9	192.6	80.3	395.6	100.1	1666	191.7	8370	92.9	275.7	1.0211893	745.13
AP_09_75	rim	**51.7**	2.8	3.57	1570	4.87E+05	0.03	0.0063	12.23	0.009	0.5	1.85	1.07	14.7	6.61	105	48.3	266.9	69.8	842	168.3	11450	30.4	237	0.55266822	657.71
AP_09_34	rim	**51.74**	3.1	2.9	940	4.90E+05	0.058	0	7.47	0.0124	0.218	1.17	0.85	10.03	5.24	84.7	40.87	225.7	62.5	729	147.3	11570	19.77	271.5	0.42813479	636.94
AP_09_59	rim	**51.78**	-0.6	6.26	2218	5.12E+05	0.063	-0.00739	16.06	0.025	0.7	2.8	1.7	23.3	10.33	152.7	68.53	365.5	91.8	998	210.6	10890	51.1	339.3	0.79657433	701.26
AP_09_31	rim	**51.8**	1.5	2.59	1853	5.18E+05	0.11	0.78	16.9	0.63	5	4.77	1.5	20.6	8.56	125.1	55.6	304	86.9	1007	191	12770	42.3	510	0.41329976	634.53
AP_09_55	rim	**51.84**	4.5	2.87	1404	5.03E+05	0.089	0.0061	10.45	0.0033	0.266	1.16	1.04	14.43	6.21	94.9	43.09	229.3	60.6	675	144.6	12680	42.2	299.9	0.45788619	641.82
AP_09_46	rim	**51.9**	1.6	3.03	1624	5.00E+05	0.017	0	10.68	0.0046	0.41	1.47	0.98	13.7	6.56	104.9	48.89	269.3	75.8	873	181.4	11500	25.91	310	0.68144265	675.72
AP_09_72	rim	**51.9**	1.3	2.44	1923	4.61E+05	0.091	0	10.37	0.013	0.39	0.97	0.82	16.4	8.49	142.4	62.9	326	81.4	847	160.6	12230	24	416	0.38738983	630.34
AP_09_116	rim	**51.9**	-1.8	1.05	2021	4.76E+05	-0.008	0	7.18	0.0044	0.086	1.09	0.631	16.1	8.64	135.8	63.7	338	90.3	995	200.7	14490	29.3	729	0.0211893	575.10
AP_09_126	rim	**51.95**	1.1	2.1	1680	4.94E+05	0	0.0031	6.99	0.0054	0.07	0.69	0.65	11.5	6.13	98.4	48	279	76	881	197	13540	17.75	406	0.32221929	619.99
AP_09_121	rim	**51.99**	-2.6	5.

AP_010_27	core	**828**	4.7	8.49	180.7	4.85E+05	0.073	0.014	7.86	0.068	1.31	3.06	0.88	11.74	2.8	21.8	5.92	18.57	3.23	26.34	4.14	10340	6.4	37.25	0.92890769	726.64
AP_010_37	rim	**945**	17.5	9.48	83.6	4.82E+05	0.026	0.0051	5.3	0.039	0.65	1.4	0.456	6.26	1.58	11.07	2.75	6.7	1.07	7.83	1.09	11950	2.643	26.22	0.97680834	736.15
AP_010_22	core	**919**	9.3	10.6	1230	4.81E+05	0.092	0.011	14.3	0.039	0.53	1.24	0.171	9.2	4.55	69	37.4	218	65.4	729	156.5	10660	377	1259	1.02530587	745.97
AP_010_6	rim	**1137**	13	11.2	177.7	4.72E+05	0.049	0.0021	8.6	0.028	0.48	1.13	0.429	6.31	1.98	18.92	6.07	22.2	4.06	33.7	5.61	11950	43.11	103.3	1.04921802	750.88
AP_010_42	rim	**680**	42.6	11.5	146.4	5.11E+05	0.057	-0.0088	4.44	0.026	0.28	0.68	0.2	5.1	1.75	14.1	4.49	19.8	4.2	41.9	9.43	11980	3.37	21.74	1.06069784	753.26
AP_010_81	core	**762**	13.3	12.6	150.8	4.66E+05	0.09	0.014	2.35	0	0.76	0.37	0.228	3.6	1.27	14.4	4.8	14.9	2.36	18	2.78	12310	18.3	429	1.10037055	761.55
AP_010_128	rim	**549**	10.7	12.6	136	5.12E+05	0.081	-0.00769	12.55	0.05	0.69	2.32	1.38	8.6	1.8	15.5	4.25	16.8	4.17	43.1	9.7	10610	11.8	131.7	1.10037055	761.55
AP_010_66	core	**1087**	1.7	13.6	879	4.98E+05	0.085	0.055	14.36	0.115	1.92	4.03	1.15	23.1	6.94	78.6	28.9	127.7	29.7	305	56.7	10360	168.4	405	1.13353891	768.59
AP_010_105	rim	**833**	12.3	13.7	552	5.08E+05	0.093	0	8.41	0.009	0.61	1.3	0.36	5.94	2.32	37.7	18.24	100.6	28.3	315.1	69.7	12080	29.87	136.7	1.13672057	769.27
AP_010_13	core	**1132**	1.5	14.1	1617	4.64E+05	0.034	0	10.24	0.087	2.51	6.4	0.55	38	13.8	160.4	58.9	237	49.8	416	70.9	10930	53.3	133.3	1.14921911	771.95
AP_010_90	core	**850**	22.2	14.2	18.2	4.86E+05	0.05	-0.00595	4.84	0.053	0.68	1.36	0.39	5.29	1.57	16.04	4.46	15.05	2.89	23	3.89	10920	2.15	19.28	1.15228834	772.61
AP_010_61	rim	**1095**	-0.7	14.9	481	4.92E+05	0.033	0	9.75	0.047	0.59	1.98	0.38	11.1	3.66	43.5	16.48	65.6	14.1	127.8	21.8	12100	38.17	58.4	1.17318627	777.13
AP_010_60	core	**829.6**	20.2	15.4	202.6	4.82E+05	0.172	0.0047	3.71	0.021	0.22	1.02	0.75	8.07	2.54	25.2	6.46	18.2	2.73	18.2	2.95	12530	15.9	637	1.18752072	780.25
AP_010_54	core	**930**	6.6	15.6	166.1	4.79E+05	0.29	-0.00569	5.65	0.065	1.02	2.85	0.97	13.82	3.27	23.9	5.32	14.17	2.05	13.4	1.9	10880	4.07	24.06	1.1931246	781.48
AP_010_26	core	**869**	26.3	15.7	175.4	4.86E+05	0.15	0.008	15.47	0.057	0.8	1.86	0.6	9.8	2.96	23.3	5.71	17.3	2.75	20.6	3.21	11400	273.8	390	1.19589965	782.08
AP_010_68	core	**922**	5.4	15.7	115.8	4.87E+05	0.088	0.033	3.44	0.009	0.39	0.87	0.53	6.1	1.73	14.98	3.63	9.09	1.41	10.58	1.61	13110	20.34	551	1.19589965	782.08
AP_010_53	core	**973**	5.9	16.2	399	4.88E+05	0.017	0.012	3.37	0.01	0.181	0.74	0.468	6.54	2.72	33.1	12.11	49.6	10.63	96.2	18.14	11990	21.7	753	1.20951501	785.08
AP_010_100	rim	**923**	51.4	16.67	157.2	5.02E+05	0.029	0	5.24	0.028	0.37	1.42	0.319	5.76	1.63	17.4	5.04	18.31	3.2	26.8	4.13	10510	2.1	18.49	1.2219356	787.82
AP_010_69	rim	**805**	29	16.9	181.9	4.59E+05	0.048	0.01	6.05	0.025	1	1.5	0.58	7.2	1.86	20.9	6.06	21.8	4.02	34.8	6.19	10110	7.41	26.6	1.2278867	789.14
AP_010_98	core	**761**	-0.2	16.9	281	5.03E+05	0.069	0.0037	9.09	0.015	0.91	1.87	0.55	8.84	2.89	29.1	9.13	36.3	7.35	62.4	10.9	10850	47.8	81.9	1.2278867	789.14
AP_010_41	core	**772**	38.7	17	143.2	4.58E+05	0.124	0.023	8.01	0.067	1.46	3.1	0.8	10.3	2.27	17.7	4.49	15.3	3.08	23.6	4.03	10230	25.3	81.2	1.23044892	789.71
AP_010_56	core	**1107**	6.7	17.4	228.8	4.94E+05	-0.002	0	10.85	0.038	0.54	2.18	0.77	10.4	2.82	27.1	7.86	22.3	3.67	28.5	4.32	11300	158.9	376	1.24054925	791.96
AP_010_70	rim	**1133**	5.1	17.5	232	4.83E+05	0.061	0.0092	4.4	0.011	0.28	0.75	0.42	5.5	1.95	23.2	7.07	26.4	5.01	40.4	6.35	12030	40.1	388	1.24303805	792.52
AP_010_92	rim	**866**	10.6	17.7	364	4.89E+05	0.034	0.013	6.15	0.029	0.46	1.46	0.333	7.05	2.32	30.5	11.81	57.2	13.77	144.1	28.45	10540	10.81	38.93	1.24797327	793.62
AP_010_35	core	**1003**	5.8	17.82	220.6	4.82E+05	0.055	0.0059	9.96	0.042	0.78	1.68	0.69	9.53	3.05	26.4	7.51	22.4	3.82	30.1	5.06	11370	148	362	1.2509077	794.28
AP_010_7	core	**1053**	15.1	18.1	381	5.03E+05	0.13	0	11.81	0.059	0.96	2.91	1.21	16.5	5.61	49.8	13.41	37.9	6.02	37.3	4.86	12390	353	666	1.25767857	795.80
AP_010_102	core	**909**	10.7	18.1	250.3	4.83E+05	0.09	0.024	15.7	0.156	2.7	5.37	0.77	18	4.35	33.3	7.92	23.65	4.12	31.9	4.74	11430	3.23	25.31	1.25767857	795.80
AP_010_34	core	**911**	7.6	18.2	288.3	4.95E+05	0.044	0.005	3.18	0.0026	0.3	0.95	0.545	6.87	2.51	28.3	8.85	29.6	4.62	33.1	4.7	12650	13.91	650	1.26007139	796.34
AP_010_119	core	**1040**	6.2	18.2	398	5.03E+05	0.07	0.018	7.31	0.011	0.41	1.19	0.556	9.4	3.26	36.9	12.3	49	9.31	78.9	13.29	12180	207.9	624	1.26007139	796.34
AP_010_46	rim	**922**	27.5	19	265	5.07E+05	0.078	0.014	6.07	0.049	0.55	1.49	0.47	5.7	2.14	21.8	8.98	38	8.73	89.6	17.6	10430	2.95	26	1.2787536	800.56
AP_010_51	core	**951**	55.8	19.1	233.5	4.80E+05	0.353	0.051	4.7	0.063	0.55	0.96	0.522	5.72	1.96	21.99	7.42	27.2	5.27	43.6	7.31	11270	10.33	382	1.28103337	801.08
AP_010_16	core	**969**	4	19.14	1588	4.97E+05	0.127	0.026	31.1	0.204	3.32	7.19	0.531	39.3	13.82	153.1	56.6	239.4	50.9	478	82.8	13450	79.7	366	1.28194193	801.29
AP_010_127	core	**1450**	2	19.3	424	4.81E+05	0.07	0.071	4.3	0.136	2.64	3.9	1.69	14.51	3.91	41.5	13.69	58.2	12.7	120.6	21.87	6660	30.4	73.9	1.28555731	802.11
AP_010_28	core	**981**	1.9	19.4	350	5.02E+05	0.072	0	2.59	0.0035	0.077	0.48	0.33	4.9	1.97	26	10.18	49	11	109.5	18.9	13080	13.5	846	1.28780173	802.62
AP_010_77	core	**919**	11.3	19.4	194.8	4.49E+05	0.11	0.021	5.38	0.009	0.66	0.87	0.65	4.2	1.86	18.8	6.08	23.4	4.67	42.7	8.3	11180	55.2	218	1.28780173	802.62
AP_010_20	core	**892**	44.7	19.7	91.9	4.76E+05	0.039	0	4.76	0.036	0.71	1.5	0.63	6.1	1.53	12.01	3.25	10.03	1.75	13.64	1.98	9850	11.65	57.1	1.29446623	804.14
AP_010_114	rim	**1035**	5.2	19.8	721	4.88E+05	0.095	0.019	23.62	0.074	1.67	3.79	0.218	18.6	6.23	67.8	24	106	22.5	214	36.7	12060	108	199	1.29666519	804.64
AP_010_130	core	**892**	15.1	19.9	212.1	4.95E+05	0.14	0.011	3.64	0.027	0.3	0.4	0.5	3.5	1.3	18.1	6.24	29.2	6.54	61.4	10.74	12900	31.5	427	1.29885308	805.14
AP_010_3	rim	**958**	54.2	20.2	107.5	4.74E+05	0.04	0.02	5.77	0.062	0.81	1.61	0.594	5.29	1.56	14.18	3.67	12.08	2.04	16.03	2.41	10020	2.42	15.52	1.30535137	806.63
AP_010_113	core	**968**	5.4	20.2	684	5.12E+05	0.16	0	25.3	0.092	1.9	3.6	0.096	17.1	5.76	65.3	24.1	102.5	23	218	34.3	12360	137.8	95.8	1.30535137	806.63
AP_010_43	core	**1075**	1	20.6	269.9	4.86E+05	0.09	0.016	11.94	0.037	1.17	2.66	0.86	13.4	4	33	8.88	28.5	4.6	39	6.07	10740	209	376	1.31386722	808.59
AP_010_87	core	**1175**	0.1	20.7	207	4.82E+05	0.076	0.0017	2.67	0.0063	0.143	0.64	0.524	3.61	1.3	16.03	5.94	26.59	5.55	51.7	8.57	11200	17.36	173.3	1.31597035	809.08
AP_010_36	rim	**1032**	192.6	21.1	330	4.81E+05	0.917	0.014	6.91	0.03	0.44	1.19	0.308	5.71	1.98	24.74	10.23	50.8	13.29	136.9	25.59	11650	19.44	123.2	1.32428246	811.00
AP_010_65	rim	**999**	21.2	21.3	113.9	4.77E+05	0.02	0.0148	6.88	0.05	0.71	1.21	0.341	4.99	1.37	12.1	3.9	14.1	2.88	25.1	4.09	9840	3	34.9	1.3283796	811.94
AP_010_109	core	**1055**	-1.4	21.3	567.6	4.87E+05	0.032	0	7.21	0.039	0.68	1.93	0.349	10.3	3.76	47	18.61	84.9	19.89	203.2	37.8	11000	40.04	101.5	1.3283796	811.94
AP_010_118	core	**1021**	2.8	21.3	492	4.90E+05	-0.002	-0.00561	7	0.039	0.65	1.31	0.34	8.8	3.35	40	15.75	73.3	17.22	174.8	31.3	10390	11.95	21.68	1.3283796	811.94
AP_010_28	core	**896**	80.7	21.4	130.8	4.84E+05	0.053	0.041	5.4	0.068	0.98	1.67	0.581	6.78	1.75	16.3	4.48	15.26	2.74	22.4	3.5	10240	13.86	130.4	1.33043377	812.42
AP_010_115	core	**1145**	-2	21.9	503	4.89E+05	0.051	0	12.38	0.054	0.92	2.28	0.67	14.9	4.85	50.4	16.8	64.3	13.09	113.5	19.31	10890	47	79.3	1.34044411	814.75
AP_010_23	rim	**972**	3	21.97	1202	4.89E+05	0.107	0.0033	22.1	0.046	0.57	2.25	0.452	14.3	6.54	94.5	40.1	197.8	49.7	522	98.3	12330	76.9	291.6	1.34183006	815.07
AP_010_4	core	**891**	37.2	22	108.3	4.56E+05	0.058	-0.0041	6.07	0.056	0.78	1.75	0.84	6.9	1.85	13.9	3.59	12.3	2.11	17.5	3.04	10010	8.26	48.3	1.34242268	815.21
AP_010_33	core	**918**	34	22.1	304	4.85E+05	-0.0009	0.0048	4.94	0.06	0.76	1.82	0.56	9.2	2.78	31	10.16	40.3	8.43	73.2	12.8	9890	6.8	53	1.34439227	815.67
AP_010_88	core	**602**	86.9	22.1	140.1	4.65E+05	0.4	0.018	5.9	0.151	1.28	2.75	1.41	7.8	1.74	16.4	4.81	15.4	3.03	26.8	4.53	9190	2.94	22.04	1.34439227	815.67
AP_010_39	core	**1006**	69.3	22.2	113.7	4.78E+05	0.027	0	5.5	0.07	1.12	1.9	0.67	7.87	1.84	14.9	4	12.12	2.05	14.5	2.36	9310	2.61	14.78	1.34635297	816.13
AP_010_50	rim	**950**	73.7	22.2	77.6	4.91E+05	0.123	0.018	6.05	0.058	0.84	1.41	0.63	5.35	1.2	10.24	2.43	8.12	1.43	11	1.6	9960	4.94	28.63	1.34635297	816.13
AP_010_63	rim	**1117**	-1.1	22.2	521	4.84E+05	0.069	0.0054	6.89	0.027	0.55	1.68	0.42	9.14	3.46	44.4	16.59	78.7	18.94	188.2	35.3	9460	3.96	13.3	1.34635297	816.13
AP_010_89	core	**983**	42.9	22.4	201.3	4.78E+05	0.007	0	4.21	0.026	0.52	1.32	0.425	6.9	2.01	21	6.71	24.3	4.7	41	6.26	9910	1.483	12.76	1.35024802	817.04
AP_010_112	core	**840**	13.1	22.5	239	4.95E+05	0.048	0.0053	6.33	0.03	0.42	1.02	0.45	6.07	1.88	21.8	7.56	33.3	7.52	75.5	14.6	11310	35.3	181	1.35218252	817.49
AP_010_93	core	**1220**	0.6	22.6	170	4.83E+05	0.028	0.0037	2.96	0.012	0.151	0.29	0.274	2.73	1.13	12.51	4.92	24.6	5.64	60	11.79	11830	25.9	245	1.35410844	817.94
AP_010_107	core	**1124**	1.3	22.7	434	4.83E+05	0.078	0	14.67	0.077	1.76	4.77	1.84	26.9	6.72	59.5	14.72	40.4	6.16	46	6.83	10610	403	475	1.35602586	818.39
AP_010_12	core	**1003**	20.9	22.8	192.3	4.79E+05	0.034	0.007	3.68	0.011	0.27	0.72	0.282	4.05	1.56	16.9	5.7	27.9	6.64	68.5	14.6	12540	23.3	513	1.35793485	818.84
AP_010_82	core	**949**	6.5	22.8	446	4.96E+05	0.031	0.023	6.33	0.109	1.9	3.48	1.2	18.5	4.91	48.9	14.65	56.2	10.91	88.9	14.99	9750	5.06	20.78	1.35793485	818.84
AP_010_106	rim	**989**	17.3	22.9	304.4	4.89E+05	0.026	0.0071	4.56	0.042	0.73	1.61	0.61	9.14	3.19	30.9	10.3	37.7	7.06	60.7	9.79	9820	1.67	13.53	1.35983548	819.28
AP_010_5	core	**1101**	3.6	23	414	5.13E+05	0.006	0.019	1.72	0.035	0.19	0.53	0.42	6.3	2.64	34.5	13.2	51.1	9.41	83	10.45	14850	6.11	781	1.36172784	819.73
AP_010_95	core	**1086**	5	23	419	5.16E+05	0.071	0.039	21.33	0.087	2.38	4.18	1.31	23.5	7.09	55.6	13.43	38	6.11	45.3	6.16	11600	468	545	1.36172784	819.73
AP_010_79	core	**896**	64.3	23.1	165.1	4.84E+05	0.059	0	4.8	0.05	0.9	1.22	0.573	7.1	1.91	19.5	5.56	20.08	3.78	33.4	5.87	9480	1.688	12.69	1.36361198	820.17
AP_010_116	rim	**956**	57.1	23.1	93.1	4.87E+05	-0.01	-0.006	4.78	0.044	0.83	1.48	0.589	5.63	1.26	10.88	3.18	11.19	2.16	18.7	3.37	9490	8.93	47.1	1.36361198	820.17
AP_010_11	rim	**884**	61.9	23.3	229.7	5.13E+05	0.026	0.005	5.39	0.045	0.83	1.57	0.33	8.1	2.48	23.7	8.28	31.5	6.75	58.6	9.93	11050	1.494	14.74	1.36735592	821.05
AP_010_122	core	**952**	68.2	23.6	130.9	4.65E+05	0.056	0.0058	4.21	0.032	0.6	1.35	0.407	5.18	1.51	13.96	4	14.11	2.56	20.83	3.19	8810	1.326	10.17	1.372912	822.37
AP_010_123	core	**1045**	6.7	23.6	298.8	4.78E+05	0.002	-0.0026	1.54	0.005	0.066	0.26	0.152	2.48	1.21	17.86	8.56	44.1	10.17	98.4	18.1	12140	10.48	267.5	1.372912	822.37
AP_010_74	core	**1097**	20	23.7	183	4.83E+05	0.058	0	6.25	0.043	0.7	1.54	0.51	6.95	1.85	18	5.83	22.8	4.8	44.1	8.56	10600	31.3	109	1.37474835	822.80
AP_010_29	core	**964**	71.5	23.9	217.4	4.92E+05	0.035	0	4.73	0.057	0.55	1.75	0.408	6.91	2.23	21.53	7.47	29	5.62	49.4	7.98	10010	1.517	12.35	1.3783979	823.66
AP_010_52	rim	**535**	138	23.9	186.3	4.49E+05	2.4	0.047	5.16	0.037	0.92	2.15	0.69	7.4	2.3	21.7	6.28	21.5	4.12	36	6.32	9240	4.05	23.1	1.3783979	823.66
AP_010_73	core	**963**	81.4	23.9	180.2	4.87E+05	0.003	0.0074	4.17	0.024	0.54	1.24	0.341	5.82	1.85	18.72	6.01	22.7	4.49	39.3	6.26	9670	1.22	11	1.3783979	823.66
AP_010_75	core	**967**	35.9	23.9	236.8	4.84E+05	0.023	0.0073	4.43	0.043	0.52	1.36	0.428	7.09	2.19	23.7	7.82	31.4	6.65	56.5	10	9610	1.217	11.37	1.3783979	823.66
AP_010_45	core	**1116**	2.1	24	155.6	5.11E+05	0.054	0.065	2.63	0.037	0.61	0.49	0.45	4.68	1.61	16.5	4.84	16.1	2.64	17.2	2.45	14230	7.78	472	1.38021124	824.09
AP_010_67	core	**971**	63.5	24	174.6	4.82E+05	0.045	0.0104	4.58	0.05	0.68	1.32	0.47	7.25	2.07	18.7	5.97	20	3.79	31.4	4.96	10350	1.644	11.75	1.38021124	824.09
AP_010_83	core	**976**	47.7	24.1	139.3	4.87E+05	0.054	0.0123	4.95	0.059	0.64	1.89	0.64	6.99	1.9	16.8	4.42	15.43	2.84	23.1	3.49	10300	2.59	15.9	1.38201704	824.52
AP_010_84	core	**954**	21.3	24.2	207.3	4.79E+05	0.023	0.0055	5	0.072	0.98	2.14	0.73	10.26	2.64	25	6.84	22.6	3.85	29.6	4.64	9990	2.43	14.82	1.38381537	824.95
AP_010_129	rim	**1056**	18.6	24.2	253	5.01E+05	0.025	0	6.72	0.05	0.65	1.07	0.38	7.12	2.12	23.9	8.05	34.2	7.27	70.7	11.84	11060	21.23	289	1.38381537	824.95
AP_010_30	core	**963**	47.6	24.5	204.8	4.93E+05	0.074	0.023	5.82	0.1	2.1	3.71	1.2	15	3.23	27.7	6.92	22.6	3.56	27.7	4.21	10390	3.55	18.02	1.38916608	826.22
AP_010_8	core	**955**	42.4	24.6	296.4	4.83E+05	0.038	0.0021	6.18	0.078	1.79	3.81	1.39	16.7	4.67	40.4	10.8	35	5.94	45.2	6.88	10260	3.08	18.1	1.39093511	826.64
AP_010_55	core	**949**	49.4	24.6	153.4	4.94E+05	0.046	0.001	4.57	0.071	0.69	1.65	0.494	7.22	1.91	17.83	5.14	16.65	3.23	25.3	4.05	9760	1.342	11.04	1.39093511	826.64
AP_010_78	rim	**888**	73.3	24.6	95.3	4.82E+05	0.081	0.06	5.21	0.081	1.23	1.76	0.76	5.78	1.44	12.04	3.15	10.08	1.79	12.04	2.41	9440	1.596	12.51	1.39093511	826.64
AP_010_9	core	**941**	69.9	24.7	180.9	4.80E+05	0.047	0.013	6.08	0.116	2.12	3.36	1.12	13	3.05	24.4	6.57	19.8	3.13	26.9	3.71	9830	2.54	16.54	1.39269695	827.06
AP_010_2	core	**1079**	5	24.8	454	4.55E+05	0.004	0	5.98	0.032	0.1	1.75	0.69	8.7	3.62	41.1	15.04	59.5	11.29	97.4	18.5	11920	45.8	814	1.39445168	827.48
AP_010_99	core	**1031**	11.7	24.8	282.8	4.87E+05	0.055	0	6.84	0.0138	0.27	1.06	0.353	5.22	1.76	22.8	9.21	43.4	10.33	105.2	20.54	11630	4.17	62.8	1.39445168	827.48
AP_010_31	core	**1017**	53.5	24.9	174.5	4.81E+05	0.046	0.0103	4.74	0.036	0.84	1.18	0.463	6.34	1.93	18.51	5.79	22.61	4.51	37	6.27	9570	2.2	12.21	1.39619935	827.89
AP_010_76	core	**1000**	98.6	25	185.7	4.84E+05	0.059	0	4.97	0.028	0.83	1.57	0.368	6.33	1.8	20	6.18	23.9	4.59	37.6	6.33	10130	1.901	13.06	1.39794001	828.31
AP_010_124	core	**994**	87.5	25	111.2	4.82E+05	-0.001	-0.01007	4.6	0.036	0.47	1.11	0.388	5.08	1.37	12.46	3.63	12.2	2.25	18.9	3.1	8940	1.351	11.3	1.39794001	828.31
AP_010_97	core	**969**	33	25.1	205.4	4.89E+05	0.063	0.0073	4.78	0.051	0.96	1.98	0.68	9.34	2.46	25.1	7.02	23.86	4.21	34.1	5.44	9810	2.16	13.54	1.39967372	828.72
AP_010_111	core	**1181**	35.5	25.3	634	5.03E+05	0.008	0.019	2.12	0.062	2.25	5.08	0.071	31.8	8.91	81.9	22.09	70.8	11.5	86	13.39	11730	91.8	198	1.40312052	829.55
AP_010_96	rim	**1035**	101.9	25.4	170.6	5.18E+05	0.052	0	5.37	0.023	0.64	1.38	0.52	8.5	2.07	18.8	6.06	21.8	4.03	32.6	4.71	10820	2.28	14.8	1.40483372	829.95
AP_010_1	rim	**968**	59.4	25.6	132.8	4.69E+05	0.01	0.0055	4.49	0.043	0.73	1.32	0.415	5.98	1.82	16.63	4.7	16.04	2.89	23	3.9	10100	1.237	10.94	1.40823997	830.78
AP_010_44	core	**839**	69	25.7	163.6	4.69E+05	2.09	0.005	5.35	0.081	1.18	2.32	0.81	9.6	2.29	20.2	5.13	16	2.87	22.7	3.7	10320	2.65	20.3	1.40993312	831.18
AP_010_49	core	**918**	69.5	25.7	104.5	4.93E+05	0.039	0.0035	7.48	0.076	0.92	1.86	0.56	6.14	1.61	13.22	3.31	10.72	1.75	14	2.18	10770	12.53	57.5	1.40993312	831.18
AP_010_18	core	**948**	36.1	25.8	166	4.85E+05	0.018	0.0087	5.38	0.017	0.58	1.27	0.395	5.1	1.54	15.3	5.56	24.9	5.94	61	13.1	11050	6	46.2	1.41161971	831.59
AP_010_108	rim	**983**	66.2	25.9	88.6	4.84E+05	0.027	0	5.92	0.073	0.71	1.62	0.455	4.79	1.259	10.89	2.85	9.63	1.68	14.3	2.19	10440	4.1	22.92	1.41329076	831.99
AP_010_80	core	**991**	32	26.2	382.6	4.86E+05	0.029	0.0019	5.97	0.038	0.75	1.53	0.417	7.27	2.55	30.6	12.17	57.6	13.17	130.3	23.99	11080	4.3	23.91	1.41830129	833.19
AP_010_57	rim	**1000**	65.9	26.4	164.4	4.88E+05	0.035	0.0068	4.89	0.046	0.91	1.44	0.513	7.44	2.1

AP_011_31	rim	**1002**	67.3	24.8	300.1	4.81E+05	0.023	0	15.07	0.08	1.52	2.99	0.63	12.3	3.59	35.4	10.18	36.5	7.01	58.7	8.91	10690	5.25	10.84	1.39445168	827.48
AP_011_32	core	**973**	32.4	26.5	511	4.85E+05	0.046	0	11.8	0.074	1.09	2.45	0.332	10.42	3.74	45.9	17.61	77.5	18.38	190.5	32.9	11050	1.94	9.08	1.42324587	834.39
AP_011_33	rim	**980**	9.7	18.85	651	4.74E+05	0.066	0.0075	12.71	0.076	1.5	3.07	0.594	15.55	5.01	59.8	21.49	91.7	20.13	186	30.53	10750	2.998	10.97	1.27531135	799.78
AP_011_34	core	**1017**	73.9	13.4	146.5	4.72E+05	0.038	0.0081	14.8	0.086	2.24	2.82	0.79	10.55	2.34	18.63	4.82	15.15	2.7	20.9	3.18	10630	18.7	49.3	1.1271048	767.22
AP_011_35	rim	**919**	28.6	15.9	607	4.88E+05	0.04	-0.00381	18.5	0.042	1.13	2.39	0.366	11.44	4.1	51.4	20.6	98	23.8	254	44.9	11240	27.4	49.5	1.20139712	783.29
AP_011_36	rim	**989**	27.2	21.63	761	4.78E+05	0.039	-0.00788	11.32	0.055	1.03	1.8	0.434	11.71	4.49	63.8	25.27	118.2	28.02	277	47.2	11110	4.75	15.24	1.33505652	813.49
AP_011_37	core	**940**	47.8	24.4	313	4.65E+05	0.026	0	16.26	0.113	2.24	3.77	0.83	16.5	3.99	37.1	10.31	35.5	6.63	54.8	8.16	10660	6.94	13.65	1.38738983	825.80
AP_011_38	core	**964**	32.1	25.35	476.1	4.78E+05	0.061	0.0031	13.31	0.085	1.24	2.31	0.434	11.38	3.98	44.2	16.18	68.7	15.24	143.1	25.34	11150	2.94	11.17	1.40397796	829.75
AP_011_39	core	**946**	11.4	10.4	774	4.84E+05	0.039	0.0011	16.91	0.049	1.14	3.11	0.396	14	5.25	63.8	25.7	120.4	28.6	283	50.1	11490	23.46	35	1.01703334	744.28
AP_011_40	core	**921**	6.1	12.3	1074	4.82E+05	0.023	0	17.72	0.036	0.94	2.75	0.237	15.8	6.18	84.6	35.02	176.5	43.8	437	81	11520	15.12	24.05	1.08990511	759.35
AP_011_41	core	**935**	9.9	10.96	1185	4.89E+05	0.084	0.0034	16.04	0.031	1.19	2.76	0.302	18.94	6.91	94.3	38.91	193.5	47.3	483	86.2	11300	12.05	18.08	1.03981053	748.94
AP_011_42	core	**992**	3.5	12.23	1141	4.81E+05	0.002	-0.002653	11.61	0.022	0.76	2.63	0.347	17	6.44	86.8	36.7	191.4	53.7	615	111.3	12980	71.7	745	1.08742646	758.83
AP_011_43	rim	**930.4**	37.3	11.05	506	4.81E+05	0.11	0.0033	11.02	0.049	0.97	1.92	0.495	9.81	3.26	38.6	15.5	87	23.8	283	54	11850	13.2	256	1.04336228	749.67
AP_011_44	core	**1004**	65.6	25.6	384	4.90E+05	0.032	0.0038	12.62	0.124	1.47	2.3	0.726	12.16	3.61	39.6	12.98	50.4	10.38	93.6	14.89	10230	3.97	9.29	1.40823997	830.78
AP_011_45	rim	**924.3**	50.5	9.37	244.9	4.85E+05	0.051	0.014	16.15	0.091	1.58	2.76	0.645	9.24	2.43	25.15	8.25	32.8	7.26	66.9	10.51	9800	22.03	40.2	0.97173959	735.13
AP_011_46	core	**906.5**	7.9	7	1227	4.96E+05	0.118	0.014	19.21	0.074	1.09	2.97	1.21	17.9	6.96	92.5	38.28	184.7	46	492.4	93.5	7010	259.8	409.3	0.84509804	710.41
AP_011_47	rim	**931**	14	9.9	491	4.71E+05	0.12	0	13.49	0.013	0.99	2.1	0.46	9.9	3.39	42	16.19	72.6	18.5	183.2	31	10650	25.5	40.4	0.99563519	739.94
AP_011_48	core	**1023.1**	83	9.11	1299	4.82E+05	0.067	0	10.07	0.0111	0.72	3.5	0.43	27.3	9.78	121.6	45.3	198.3	46.2	432.6	76.9	9930	130.8	472.6	0.95951838	732.69
AP_011_49	core	**1049**	9.9	16.17	841	4.83E+05	0.079	0.0093	21	0.045	1.26	2.08	0.205	13.67	4.94	67	28.2	139.3	36	365	65.6	11670	23	29.5	1.20871002	784.90
AP_011_50	rim	**976**	29.4	24.5	829	4.66E+05	-0.005	-0.00844	10.18	0.043	0.8	1.92	0.355	12.23	5.01	68.4	27.88	127	29.92	274.2	43.69	10950	2.58	9.05	1.38916608	826.22
AP_011_51	rim	**1007**	47.3	24.6	419	4.93E+05	0.033	0.018	12.89	0.08	1.77	2.35	0.457	11.74	3.37	36.8	13.64	57.7	13.47	132.7	22.9	10920	5.64	16.1	1.39093511	826.64
AP_011_52	rim	**985**	8.6	15.92	915	4.88E+05	0.081	0.003	25.52	0.072	1.28	2.5	0.207	13.63	5.07	72	29.91	149.8	38.34	387.4	68.5	11450	29.93	25.07	1.20194306	783.41
AP_011_53	core	**960**	17.4	11.86	665	4.85E+05	0.101	0.034	21.3	0.1	1.19	3.2	0.262	18.6	6.16	64	20.84	85.5	18.8	175	29.1	12320	58.9	136	1.07408469	756.04
AP_011_54	rim	**1011**	31	18.2	525	4.96E+05	0.055	0.008	18	0.066	1.26	2.45	0.55	10	3.61	46.9	18.38	81.4	19.93	201.7	33.6	11710	43.6	61.9	1.26007139	796.34
AP_011_55	core	**977**	4.6	14.54	1633	4.84E+05	0.093	0	21.89	0.074	1.35	3.66	0.186	20.7	8.95	127.6	55	274.4	68.1	679	115.4	11540	151.8	80.3	1.16256441	774.83
AP_011_56	rim	**935**	50.4	18.96	476.3	4.78E+05	0.057	0.0061	12.69	0.072	0.94	2.38	0.463	11.1	3.99	46	16.07	66.6	15.55	146.3	25.39	10860	2.344	9.99	1.27783833	800.36
AP_011_57	core	**955**	89.2	19	43.2	4.77E+05	0.071	-0.0046	24.11	0.095	1.41	1.29	0.581	1.97	0.407	4.1	1.32	6.22	1.45	15.3	2.86	10850	37.37	83.8	1.2787536	800.56
AP_011_58	core	**1154**	6.7	20	944	4.90E+05	0.127	-0.0009	22.15	0.064	1.28	3.01	0.255	16.13	6.19	79.5	31.91	146.7	35.33	352.2	59.4	11450	43.62	47.64	1.30103	805.64
AP_011_59	rim	**978**	31.8	15.03	454.1	4.99E+05	0.035	0.004	12.66	0.077	1.6	2.81	0.457	11.4	3.59	42.2	15.15	67.8	15.82	154.9	26.51	11070	2.166	9.18	1.17659898	777.95
AP_011_60	rim	**987**	26.4	28	818	4.96E+05	0.019	0.0019	11.15	0.07	1.03	2.29	0.341	14.6	5.26	70.7	27.45	119.5	27.74	257.9	44.5	11110	2.58	9.57	1.44715803	840.19
AP_011_61	core	**995**	15.8	18.21	1159	4.82E+05	0.079	0.0093	18.24	0.05	1.34	3.17	0.294	17.6	6.85	91.8	38.62	191.2	47.2	486	84.9	11440	10.34	18.23	1.26030995	796.39
AP_011_62	rim	**968**	51.2	16.93	244	4.75E+05	0.045	0.0115	16.86	0.073	1.38	2.26	0.481	8.91	2.51	25.5	8.34	31.9	7.02	64.9	10.83	10930	19	37.6	1.22865696	789.31
AP_011_63	rim	**945**	60.6	23.6	244.2	4.81E+05	0.058	0.0032	14.71	0.108	1.94	2.8	0.626	10.49	2.93	27	8.28	32.3	6.98	60.4	10.37	10820	8.73	24.11	1.372912	822.37
AP_011_64	core	**1031**	0.5	12.06	1753	4.85E+05	0.071	0.036	24.07	0.111	1.97	5.7	0.668	15.1	12.99	160.1	60.2	263.8	60.2	572	92.5	11230	59.5	62.3	1.08134731	757.56
AP_011_65	rim	**939.4**	14	9.72	449.5	4.94E+05	0.036	0.0094	12.76	0.046	1.06	4.41	0.91	22.3	6.78	58.4	14.18	44.9	7.71	61.3	8.38	13020	44.8	124.2	0.98766626	738.33
AP_011_66	core	**949**	7.9	8.27	935	4.85E+05	0.101	0	7.69	0.016	0.22	0.69	0.318	8.34	4.69	68	28.95	139.2	34.08	346.3	57.5	14600	26.1	1694	0.91750551	724.40
AP_011_67	rim	**1298**	5.1	12.24	682	4.99E+05	0.02	0	4.41	0.048	0.7	1.88	0.504	12.5	4.29	55.7	22.68	107.8	26.79	268	48.1	8220	39.1	145	1.08778142	758.90
AP_011_68	core	**993**	38.3	25.2	520	4.86E+05	0.038	0	12.3	0.077	1.44	2.59	0.481	13.33	4.21	46.7	17.05	73.4	17.35	170.2	28.98	10650	3.11	10.91	1.40140054	829.14
AP_011_69	core	**975**	56.5	21.1	299	4.86E+05	0.063	0	13.77	0.097	1.7	2.8	0.564	11.52	2.77	29.9	9.5	38.5	8.4	80	12.2	10490	5.9	16.8	1.32428246	811.00
AP_011_70	rim	**1255**	1.6	17.99	790	4.87E+05	0.067	0	17.1	0.034	0.86	2.42	0.305	13.2	5.22	68.1	26.54	123.8	29.51	299.9	51.4	11610	25.55	34.13	1.25503116	795.21
AP_011_71	rim	**976**	30.2	15.44	302	4.79E+05	0.055	0	19.12	0.079	1.35	2.29	0.549	8.84	2.59	27.2	9.64	43.2	10.33	109	20.1	11120	31.1	54.4	1.1886473	780.50
AP_011_72	core	**973**	68.7	19.41	233.8	4.78E+05	0.003	0.0077	12.1	0.076	1.26	2.38	0.645	10.29	2.73	26.7	7.97	27.44	5.54	45.3	6.97	10760	6.73	15.77	1.28802554	802.67
AP_011_73	core	**973**	63.9	25.4	252	4.83E+05	0.03	0.0031	15.08	0.099	1.53	3.08	0.625	11.53	2.81	28.8	8.82	32.7	6.86	61.7	10.26	11140	6.95	21.35	1.40483197	829.96
AP_011_74	core	**964**	21.4	16.09	586	4.81E+05	0.036	0.0028	12.17	0.079	1.57	2.77	0.468	12.68	4.17	50.4	19.69	87.2	20.66	205.3	36.52	11140	4.12	14.27	1.20655604	784.42
AP_011_75	core	**974.7**	-0.7	12.79	979	4.84E+05	0.076	0.003	17.47	0.039	1.01	2.89	0.344	16.93	6.22	82.2	32.75	151.5	35.27	347.3	59.9	11180	34.9	41.22	1.10687054	762.92
AP_011_76	core	**1021**	128.9	29.5	128.9	4.83E+05	0.013	0.0108	16.25	0.115	1.73	2.33	0.614	7.27	1.78	15.48	3.99	13.44	2.59	21	2.97	10070	15.57	37.4	1.46982202	845.75
AP_011_77	core	**1072**	6.7	19.85	1126	4.79E+05	0.07	-0.00279	18.84	0.056	1.16	2.64	0.217	16.03	6.56	90.6	37.21	185.6	46.07	462	83.1	11490	26.5	32.1	1.29776053	804.89
AP_011_78	core	**969**	2.5	9.85	1749	4.90E+05	0.103	0.0062	26.3	0.066	1.73	4.68	0.497	33.3	11.7	151	58.2	263.8	60.4	565	93	11220	91.6	71	0.99343623	739.50
AP_011_79	rim	**1087**	8.1	20.02	955	4.89E+05	0.076	0.0092	23.19	0.071	1.07	2.86	0.303	14.84	5.5	76.7	31.5	155	39.08	392.5	69.4	11830	38.1	30.7	1.30146407	805.74
AP_011_80	rim	**1005**	3.7	16.2	882	4.79E+05	0.095	0	20.53	0.033	1.05	2.47	0.314	15.6	5.42	76.2	28.7	133.8	32.3	325.7	52.9	11080	35.9	41.4	1.20951501	785.08
AP_011_81	rim	**1047**	20.8	18.39	383.2	4.77E+05	0.069	0.0044	14.71	0.06	1.55	5.15	0.599	21.7	5.2	45.5	12.69	45.4	9.7	81.9	12.9	11400	37.2	35.77	1.26458173	797.36
AP_011_82	core	**1285**	12.5	17.1	667	4.86E+05	0.025	0.002	13.45	0.057	1.7	5.77	1.12	32.9	9.32	83.1	21.9	63.9	11.66	94.6	12.41	14020	44.7	190.9	1.23298611	790.28
AP_011_83	rim	**998**	17.2	11.7	481	4.82E+05	0.009	0.0034	12.26	0.025	0.63	1.44	0.262	9.3	3.13	39.63	15.72	75.9	18.54	192.5	34.3	11600	19.96	53.3	1.06818586	754.81
AP_011_84	core	**1178**	0.3	18.8	1269	4.86E+05	0.056	0.0057	24.54	0.087	1.46	3.67	0.324	20.7	7.94	103.9	42.2	199.2	48.5	470.7	79.6	11280	58.24	57.7	1.27415785	799.52
AP_011_85	core	**1165**	0.7	15.12	1190	4.86E+05	0.042	-0.002872	20.53	0.051	1.34	3.36	0.452	20.95	7.73	101	39.93	180.8	43.75	422.8	72.1	11370	34.07	49.16	1.17955179	778.51
AP_011_86	rim	**1012**	25.7	19.1	481	4.85E+05	0.059	0.0033	18.36	0.042	1.08	1.65	0.479	8.44	3.09	41	16.6	75.9	19.3	196.4	34.2	11250	44.2	61.5	1.28103337	801.08
AP_011_87	core	**981**	11.6	14.95	537	4.88E+05	0.008	0	8.9	0.034	0.6	2.1	0.54	13.1	4.89	56.8	16.8	56.8	11.1	85	12.8	12940	29.8	397	1.17464119	777.44
AP_011_88	core	**1083**	0.8	17.22	1176	4.88E+05	0.049	-0.0085	20.26	0.043	1.19	3.09	0.416	21.4	7.64	99.4	39.51	177.2	40.8	397	66.2	11010	36.98	51.3	1.23603315	790.95
AP_011_89	core	**944**	7.1	9.74	1236	4.86E+05	0.045	0.022	13.05	0.04	0.71	1.64	0.323	12.74	5.4	84.8	38.06	212.8	64.6	782	145.8	12610	47.1	1752	0.98855896	738.51
AP_011_90	rim	**1030**	15.4	19.43	439	4.89E+05	0.042	0	21.5	0.064	1.04	3.79	0.521	20.4	5.84	51.8	14.57	49.1	9.7	85.1	12.52	11760	54.3	118.5	1.2884728	802.77
AP_011_91	core	**985**	4.1	14.2	1576	4.65E+05	0.012	0.019	7.66	0.022	0.27	1	0.228	13.05	5.83	102.5	48.4	281.2	86.9	1046	204.6	12800	39.8	2234	1.15228834	772.61
AP_011_92	core	**1004**	3.6	17.6	986	4.89E+05	0.08	0.0034	23.29	0.025	0.83	1.8	0.269	12.34	5.39	75.9	33.1	159.9	41	413	74.2	12160	43.3	129.7	1.24551267	793.07
AP_011_93	rim	**968**	82.8	21.58	199.1	4.72E+05	0.011	0.0074	12.85	0.073	1.41	2.28	0.531	8.62	2.29	23.53	6.52	21.97	4.17	35.1	4.96	10270	7.52	16.86	1.33405144	813.26
AP_011_94	core	**1018**	130	10.7	1086	4.61E+05	1	2.5	20.9	2.3	17.2	7.2	1.04	22.1	6.9	90.1	35.7	165	39.2	391	67.3	12160	105	912	1.02938378	746.80
AP_011_95	core	**968**	11.5	12.84	937	4.90E+05	0.065	0.0057	16.44	0.057	1.15	2.8	0.221	14.93	5.67	73.6	30.5	153.1	37.5	380	66.4	11510	11.31	18.66	1.10856502	763.28
AP_011_96	core	**958**	47.2	22.2	320.2	4.78E+05	0.045	0.006	16.5	0.117	2.3	3.69	0.9	15.78	4.12	40.3	11.06	36.7	6.68	55.3	8.14	11000	7.35	14.24	1.34635297	816.13
AP_011_97	core	**1077**	2.1	15.65	1265	4.83E+05	0.05	0	21.06	0.061	1.21	3.3	0.295	17.94	8.07	105.8	41.59	195.6	46.94	457.9	76.7	12410	150.1	263.3	1.19451434	781.78
AP_011_98	core	**933**	15.9	14.4	1033	4.87E+05	0.085	0.0097	18.5	0.047	0.97	2.7	0.231	16.48	6.08	84.2	34.74	168.7	41.89	427	73.3	11580	11.42	19.83	1.15836249	773.92
AP_011_99	rim	**975**	63	19.6	189.9	4.72E+05	0.085	0.0108	21.28	0.114	2.44	3.93	0.86	13.23	2.95	25.64	6.55	20.18	3.58	27.8	3.86	11070	14.85	22.01	1.29225607	803.64
AP_011_100	core	**1007**	8	15.01	986	4.84E+05	0.031	0.17	17.24	0.093	0.91	2.46	0.396	17.57	6.41	79.6	31.3	157.5	42.4	436	75.3	10080	70.6	507.1	1.17638069	777.82
AP_011_101	rim	**926.9**	29.2	11.28	361	4.84E+05	0.06	0.0027	16.6	0.042	1.21	3.18	0.628	12.84	3.36	35.7	11.96	50.1	11.32	111.4	19.8	11670	39.17	211	1.0523091	751.52
AP_011_102	rim	**1112**	36.3	21	1134	5.00E+05	0.073	0	18.99	0.092	1.19	3.38	0.43	19.2	7.26	95	38.8	183.5	46.24	480	78.8	11960	18.54	33.1	1.32221929	810.52
AP_011_103	core	**949**	43.5	18.04	493.6	4.84E+05	0.078	0	13.23	0.032	1	3.64	0.843	23.44	7.12	60.6	15.49	48	8.41	67.2	8.98	13050	35.58	132.8	1.25623653	759.48
AP_011_104	core	**976**	23.7	26.2	631	4.76E+05	0.044	0	12.04	0.085	1.47	2.89	0.478	13.02	4.41	56.5	20.96	95.1	22.64	228.1	38.75	10700	2.878	11.23	1.41830243	833.19
AP_011_105	rim	**980**	67.7	25.79	264	4.72E+05	0.046	0.0033	13.86	0.108	1.43	2.52	0.474	10.39	2.86	28.7	8.59	31	6.42	56.2	9.02	10570	4.28	14.24	1.41145134	831.55
AP_011_106	rim	**1077**	4.4	20.92	936	4.79E+05	0.086	0	22.3	0.087	1.43	2.9	0.227	15.4	5.74	76	31.18	152.4	38.42	393	67.7	11430	27.75	23.66	1.32056168	810.14
AP_011_107	rim	**1078**	61.8	20.3	430.5	5.00E+05	0.107	0.0019	13.23	0.044	1.35	1.97	0.441	11.28	3.63	41.2	14.42	60.6	12.77	117.1	19.96	11370	5	11.52	1.30749604	807.13
AP_011_108	core	**991**	7	16.5	1367	4.72E+05	0.1	0.31	17.84	0.072	1.38	3.56	0.41	21.4	8.26	109.9	47.4	253.8	71.6	794	152.7	12960	230	1357	1.21748394	786.84
AP_011_109	core	**1041**	6	12.3	953	4.94E+05	0.06	0.0043	8.76	0.026	0.47	2.01	0.453	15.8	5.86	81.6	31.9	149.3	35.5	355	61.6	10430	127	684	1.08990514	759.35
AP_011_110	rim	**1129**	5.4	15.1	767	4.76E+05	0.103	0	14.74	0.052	1.16	2.29	0.31	15.7	5.25	68.9	25.7	121.1	29.2	280	50.3	11510	19.3	31.39	1.17897695	778.39
AP_011_111	core	**935.3**	6.3	9.02	1286	4.88E+05	0.049	0.0041	9.56	0.025	0.68	1.59	0.273	11.16	5.23	88.1	42.16	246.4	72.7	861	161.1	13850	123.4	2005	0.95520654	731.84
AP_011_112	rim	**962**	59	17.9	291.8	4.88E+05	0.078	0.008	15.69	0.108	1.78	3.77	0.72	13.4	3.73	36.1	9.79	34.4	6.49	54.5	8.41	11130	6.44	13.96	1.25285303	794.72
AP_011_113	core	**944**	4.7	11.5	1011	4.76E+05	0.047	0	11.26	0.0044	0.73	1.49	0.3	15.7	6.58	79.7	31.5	148.5	37.3	377	66.2	12290	50.4	757	1.06069794	753.26
AP_011_114	core	**1125**	-0.3	19	1143	4.89E+05	0.055	0.0024	19.38	0.062	1.02	2.75	0.377	18	7.32	95.4	37.6	175.4	41.3	405	66.9	11530	41.86	46.6	1.2787536	800.56
AP_011_115	core	**957**	78.1	25.84	160.5	4.69E+05	0.065	0.0139	15.94	0.119	1.97	2.89	0.66	9.18	2.23	18.9	5.61	19.22	3.88	34.5	5.44	10870	18.1	39.84	1.41229251	831.75
AP_011_116	core	**1026**	38.8	28.2	493.8	4.79E+05	0.028	0	11.32	0.075	1.15	1.95	0.339	10.13	3.45	42.8	16.6	76.2	17.41	175.2	30.86	10890	3.47	13.51	1.45024911	840.95
AP_011_117	rim	**999**	2.2	14.04	961	4.79E+05	0.089	0.0059	21.43	0.062	1.17	2.57	0.252	13.56	4.98	74	32.4	166.6	42.39	441.9	81.8	12150	25.53	39.73	1.14736711	771.55
AP_011_118	core	**1093**	37.2	20.3	1291	4.74E+05	0.08	0	16.22	0.08	1.65	2.79	0.23	20.8	7.46	106.4	44.3	221	54	536	96	11260	8.53	13.53	1.30749604	827.13
AP_011_119	core	**1107**	-1.2	18.1	1016	4.82E+05	0.082	0.0041	26.54	0.073	1.41	2.97	0.178	18.14	6.59	84.9	34.3	165.1	39.2	389	69.5	12330	68.6	51.3	1.25767857	795.80
AP_011_120	core	**1372**	4.3	20.5	782	4.62E+05	0.048	0	15.02	0.069	0.8	2.46	0.266	13.4	4.97	64.4	25.35	123.9	28.8	287.4	53.4	11450	14.2	34.7	1.31175386	808.10
AP_011_121	rim	**944**	8.3	12.03	1373	4.74E+05	0.053	0.0151	17.46	0.096	1.37	3.46	0.292	19.9	8.1	108.1	44.99	226.2	55.3	570	100.4	11030	12.17	15	1.08026563	757.33
AP_011_122	core	**1166**	7.1	18.09	1194	4.74E+05	0.057	0.0028	17.71	0.051	1.44	3.16	0.292	19.18	7.01	95.8	39.71	192.1	47.79	480.5	85.4	11370	11.41	17.38	1.25743857	765.75
AP_011_123	rim	**975.5**	53.8	17.09	336	4.71E+05	0.069	0	19.81	0.064	1.39	2.27	0.556	9.69	2.76	30.6	11.96	50.3	11.71	118	20.7	11110	44.67	73.7	1.23274206	790.22
AP_011_124	core	**961**	50.8	14.01	190.5	4.71E+05	0.04	0.0101	18.96	0.099	1.59	2.83	0.712	10.13	2.43	22.56	6.72	23.43	4.39	39.1	5.81	11320	41.85	69.5	1.14643814	771.35
AP_011_125	core	**1115**	107.3	26	370.7	4.72E+05	0.051	0.006	13.07	0.101	1.53	2.69	0.72	13.13	3.82	39.8	12.34	46.9	9.43	83.1	13.33	10200	4.05	8.69	1.14197335	832.39
AP_011_126	core	**999**	18.9	13.46	554	4.75E+05	0.019	-0.00823	8.81	0.0069	0.57	2.21	0.487	14.9	5.31	59.5	18.2	65.4	12.9	112	16.2	11330	25.3	93	1.12904506	767.63
AP_011_127	core	**998.9**	37.4	18.8	616	4.84E+05	0.071	0.0097	15.55	0.091	1.93	5.04	0.545	23.7	6.59	68	20.85	78.7	15.97	139.7	22.8	10300	151.9	118.9	1.27415785	759.35
AP_011_128	rim	**915.5**	57	22.1	287	4.64E+05	0.053	0.093	14.86	0.091	1.51	2.35	0.589	9.36	2.55	28.2	9.18	41	8.92	90.4	15.34	11100	14.64	32.29	1.34439227	815.67
AP_011_129	rim	**954**	49.8	14.09	187.5	4.75E+05	0.075	0.0043	20.31	0.12	2.36	3.58	0.9	13.22	2.98	24.09

AP_011_189	core	**1090**	5.4	18.33	1317	4.94E+05	0.097	0	18.21	0.051	1.48	2.95	0.338	20.5	8.28	108.4	43.63	208.1	52.5	525	94.9	11840	14.66	29.29	1.26316246	797.04
AP_011_190	core	**1004**	2.3	17.7	671	4.88E+05	0.032	0	14.45	0.027	0.8	2.22	0.266	11.76	4.52	57.9	22.36	103.8	25.63	252	42.9	11360	16.96	29.73	1.24797327	793.62
AP_011_191	rim	**984**	44.8	19.48	773	4.94E+05	0.093	0.0087	11.68	0.063	0.88	1.8	0.365	12.62	4.76	63.5	25.93	120.1	29.11	283.5	49.61	11680	9.35	26.57	1.28958895	803.03
AP_011_192	rim	**946**	45.4	26.9	371.3	4.85E+05	0.068	0.008	13.36	0.116	1.37	2.97	0.525	12.37	3.66	37.33	11.99	49.6	10.53	96.9	15.7	10680	3.65	12.16	1.42975228	835.96
AP_011_193	rim	**1228**	3.9	17.59	1051	4.92E+05	0.042	0	22.53	0.053	0.87	2.74	0.39	19.62	7.12	90.6	35.33	159.8	38.07	369.1	64	11300	37.06	55.45	1.24526584	793.02
AP_011_194	core	**1060**	117.9	22.61	137.3	4.90E+05	0.073	0.0088	15.63	0.108	1.62	2.46	0.538	9.11	2.12	17.05	4.61	15.41	3.04	28.2	4.3	10860	14.17	34.7	1.35430056	817.99
AP_011_195	rim	**1023**	68.7	20.9	427.7	4.91E+05	0.043	0.0065	11.71	0.053	1.11	1.76	0.425	10.72	3.32	38.8	14.36	64.3	15.12	148	25.59	10870	2.139	8.9	1.32014629	810.04
AP_011_196	rim	**960.2**	378	11.9	745	4.76E+05	0.102	0	12.7	0.015	0.63	1.37	0.327	10.3	3.9	53.9	23.6	124	32.1	351	66	11830	42.1	670	1.07554696	756.35
AP_011_197	rim	**1008**	96.2	16.65	163.2	4.72E+05	0.03	0	14.89	0.117	1.76	2.41	0.482	9.34	2.4	19.72	5.63	18.58	3.7	30.7	4.63	10520	19.3	46.32	1.22141424	787.71
AP_011_198	rim	**981**	52.7	26.6	429.7	4.83E+05	0.039	0.0017	11.23	0.063	1.11	1.93	0.381	10.59	3.31	38.8	14.37	66	15.32	157.4	27.07	10900	2.73	11.11	1.42488164	834.78
AP_011_199	core	**985**	49.2	25.7	552	4.82E+05	0.053	0.0028	18.45	0.071	1.3	2.19	0.383	12.4	4.05	49	18.4	85	21.3	207	34.8	11830	28.1	47.3	1.40993312	831.18
AP_011_200	core	**1287**	4	18.24	820	4.85E+05	0.094	0.0025	26.26	0.177	4	14	3.23	71	17.71	125.8	26.6	70.4	10.64	75.6	9.55	11500	128.4	142.8	1.26102483	796.55
AP_011_201	core	**1130**	1.1	21.88	1099	4.88E+05	0.086	0.0102	20.32	0.042	1.32	3.06	0.284	19.8	6.9	92.5	36.1	168.3	40.05	399.9	68	11850	46.28	54.1	1.34004732	814.66
AP_011_202	core	**972**	5.1	10.15	1187	5.25E+05	0.119	0.011	9.09	0.052	0.92	3.74	0.93	22.6	8.31	100.5	39.4	189.6	45.7	501	85.7	9540	119.4	503	1.00646604	742.13
AP_011_203	rim	**922**	16.1	13.7	525	4.87E+05	0.1	0	24.7	0.015	0.83	3.95	0.35	20.6	5.34	62.4	16.54	61.82	11.95	105.3	16	13030	58.7	99.3	1.13672057	769.27
AP_011_204	core	**1062**	1.1	9.99	1224	5.00E+05	0.054	0	13.47	0.0068	0.51	1.95	0.206	20.5	7.98	105	41.21	191.8	48.83	465	78	10620	123.7	526	0.99566549	740.73
AP_011_205	core	**1008**	37.7	29.08	537.9	4.82E+05	0.057	0.018	12.13	0.067	1.52	2.24	0.406	11.64	4.09	47.6	18.17	81.4	19.66	193.9	33.41	10920	3.23	12.34	1.4635944	844.22
AP-048																										
AP_048_1	core	**1196**	0.6	8.9	1749	5.15E+05	0.071	0.0095	19.99	0.135	3.33	7.71	0.238	41.9	14.86	168.2	60.6	256.9	51.9	447	76.2	10660	139.3	333	0.94939001	730.68
AP_048_2	core	**1095.9**	4.3	8.14	594	5.13E+05	0.031	0.0087	8.17	0.012	0.48	0.76	0.099	7.46	3.15	44.3	17.92	92.8	24.87	258.3	50.4	13170	103.4	559	0.9106244	723.05
AP_048_3	rim	**1090**	-1.3	7.47	757	5.04E+05	0.011	0.0033	10.26	0.039	0.76	2.38	0.211	15.5	5.57	66.3	25.7	113.6	25.1	225	40.7	10420	44.4	144.1	0.87313206	715.82
AP_048_4	core	**979**	5.7	11.51	373	5.08E+05	0.031	0.0032	8.04	0.09	1.75	3.51	0.336	17.3	4.85	43.5	12.7	42.9	7.71	61.7	9.7	11840	8.89	77.5	1.06107532	753.34
AP_048_5	core	**1178**	1.5	11.25	506.6	5.11E+05	0.006	0.0041	7.58	0.0173	0.73	1.84	0.08	10.39	3.82	45.4	17.19	76.6	17.04	164.5	29.9	12780	11.04	60.5	1.05115252	751.28
AP_048_6	core	**1193**	0.8	7.54	1176	4.99E+05	0.028	0.0063	10.76	0.028	1.01	2.97	0.499	22.5	7.95	103.1	39.3	175.5	38.2	362	63.8	10390	69.4	211	0.87737135	716.60
AP_048_7	rim	**1007**	1.6	8.53	391	4.98E+05	0.033	-0.00425	8.74	0.038	1.08	2.62	0.25	12.3	3.52	39	12.73	53.5	10.94	102	16.8	11300	8.76	69	0.93094903	727.04
AP_048_8	core	**1009**	-0.5	5.51	1052	4.97E+05	0.009	0.0029	12.31	0.028	1.05	3.01	0.565	20.5	7.4	88.8	35.1	161	35.6	343	61.9	10030	80.5	256	0.74115516	691.01
AP_048_9	rim	**1165**	2590	40	375.7	4.77E+05	0.9	44.2	95.9	11.2	48.1	10.4	1.87	14.6	3.73	36.8	12.22	54.8	11.95	122.1	23.2	11050	26.6	198	1.60205999	879.32
AP_048_10	core	**987.4**	0.2	5.52	1678	4.89E+05	-0.019	0.025	3.38	0.032	0.54	1.79	0.088	20.6	10.09	144.3	53.6	243.2	53.5	513	86.7	15300	32.28	715	0.74193908	691.15
AP_048_11	rim	**1000**	9.5	10.81	163.1	4.89E+05	0.02	0	6.59	0.062	1.02	1.98	0.333	7.75	2.24	18.81	5.69	21.8	4.47	38.4	6.94	11010	4.46	68.2	1.03382569	747.71
AP_048_12	core	**1155**	0.5	7.37	1296	4.90E+05	0.012	0	21.04	0.053	1.55	4.26	0.193	26.9	10.2	123.7	44	196.4	40.9	369	64.8	11370	201	528	0.86746746	714.69
AP_048_13	core	**1245.6**	5.1	6.98	527.8	5.06E+05	0.078	0.177	8.4	0.05	0.64	1.1	0.06	7.92	3.16	43.2	17.36	85.5	21.11	216.5	41.21	12760	97	778	0.84385542	710.18
AP_048_14	rim	**1239.6**	0.7	11.31	478.8	4.85E+05	0.003	0	5.87	0.033	0.66	1.48	0.058	9.18	3.5	43.7	16.46	75.2	17.16	160.3	28.05	11640	6.1	59.4	1.0534626	751.76
AP_048_15	core	**1204**	4.7	10.54	1111	4.94E+05	0.086	0	8.35	0.028	0.77	2.56	0.084	19.61	7.6	98.2	37.72	168.6	37.71	349.3	61.1	11450	30.75	217.5	1.02284061	745.47
AP_048_16	rim	**1255**	0.7	10.71	628	5.03E+05	0.022	0.0009	9.25	0.049	1.12	2.46	0.173	15.52	5.12	60.8	21.37	91.8	19.4	178	30.85	11250	11.37	43.76	1.02978947	746.89
AP_048_17	core	**1222**	2.2	7.9	590	4.85E+05	0.014	0.008	7.36	0.07	0.94	1.85	0.1	14.6	4.59	56.1	20.05	89	19.8	182.6	31.4	10990	15.2	64.3	0.89762709	720.52
AP_048_18	rim	**1060**	210	15.6	625	4.92E+05	0.58	0.023	11.98	0.053	0.74	2.48	0.265	12.87	4.77	57.3	21.2	92.1	18.98	168.9	28.9	11360	58.6	344	1.1931246	781.48
AP_048_19	core	**1204**	2.3	15.5	1720	5.00E+05	0.053	0	13.56	0.061	1.53	4.89	0.61	33.5	12.04	155.3	56.7	250.5	53.4	487.1	86	10590	128	349.7	1.1903317	780.86
AP_048_20	core	**966**	1.1	6.7	536.7	5.06E+05	0.024	0.0091	8.26	0.046	0.75	1.65	0.067	10.15	3.97	47.3	18.14	81.6	18.15	167	29.3	12080	10.3	75.4	0.8260748	706.80
AP_048_21	core	**1034**	2.5	6.7	932	4.91E+05	0.055	0	11.51	0.064	0.98	0.15	1.23	0.153	8.1	3.28	48.4	19.68	97.6	22.1	211.4	38.4	11960	34.86	241.3	0.8260748	706.80
AP_048_22	rim	**1098**	1.2	7.72	479	5.05E+05	0.033	0.0046	7.01	0.029	0.84	1.41	0.083	9.5	3.4	42.7	15.9	72.7	16.52	157.9	28.74	11940	9.55	50.5	0.8876173	718.58
AP_048_23	core	**1232**	4.2	10.65	606	5.09E+05	0.033	0.0062	8.9	0.024	0.44	1.3	0.075	7.9	3.4	42.3	18.5	96.6	24.9	251	53.7	13440	104.2	980	1.02734961	746.39
AP_048_24	core	**979**	13.2	14.06	141	4.91E+05	0.003	0	6.59	0.072	1.19	1.85	0.375	6.92	1.77	15.7	4.82	17.3	3.8	31.5	5.32	10510	3.53	58.5	1.14798532	771.68
AP_048_25	core	**1145**	2.5	7.6	915	4.96E+05	0.041	-0.0056	8.49	0.048	0.84	2.29	0.279	16	6.34	77.9	30.58	144.4	32.8	312.1	57	10580	44.3	173.1	0.88081359	717.26
AP_048_26	core	**1088**	1.1	5.7	1203	4.96E+05	0.028	-0.02188	12.26	0.044	1.88	4.99	0.207	25.6	9.94	110.3	42.2	180.9	38	342	58.9	11130	89.5	288	0.75587486	693.71
AP_048_27	rim	**968**	0	10.8	638	5.08E+05	0.181	0.011	10.78	0.089	1.69	4.16	0.28	20.1	6.11	64.6	21.1	82.6	15.04	134.7	23.05	12260	16.56	100.6	1.03342376	747.63
AP_048_28	rim	**940**	11	11.1	191.2	5.00E+05	0.047	-0.0043	7.76	0.073	1.49	2.99	0.383	10.35	2.87	24.2	6.66	22.05	4.01	32.4	4.76	10970	6.03	70.1	1.04532298	750.08
AP_048_29	core	**1152**	0.4	7.17	332.5	4.98E+05	-0.018	0	8.95	0.029	0.65	1.54	0.84	10.71	3.64	36.1	10.82	38.8	6.83	51.4	7.88	12000	94	273.7	0.85551916	712.40
AP_048_30	core	**963**	15.2	11.89	187.3	4.86E+05	0.014	0.0055	9.15	0.095	1.43	2.91	0.305	11.14	3	23.8	6.44	19.2	3.4	27.7	3.9	11640	8.7	42.8	1.07518185	756.27
AP_048_31	rim	**920.6**	17.9	11.83	104.9	4.89E+05	0.05	0.0061	6.94	0.065	1.39	2.28	0.391	8.06	2.04	14.16	3.71	10.58	1.79	13.62	2.1	10530	4.23	62.4	1.07298474	755.81
AP_048_32	rim	**1104**	-0.6	6.23	466.2	4.77E+05	0.061	0.06	9.49	0.045	0.79	1.8	0.143	10.44	3.42	43.5	15.93	67	15.2	138.6	22.59	11020	39.3	97.9	0.79448805	700.87
AP_048_33	rim	**1012**	6.3	8.57	177.7	4.96E+05	0.041	0.0025	9.17	0.104	1.78	3.29	0.6	13.9	3.27	24.2	6.29	18.87	3	23.1	3.26	10750	4.01	33.8	0.93298082	727.44
AP_048_34	core	**1203**	-0.7	9.6	565	4.72E+05	-0.009	0	6.79	0.031	0.56	1.96	0.133	12.39	4.14	52.4	19.26	88.7	19.76	196.2	34.36	11000	7.92	36.75	0.98227123	737.25
AP_048_35	rim	**965.6**	-0.9	6.62	594	4.86E+05	0.124	0.005	8.75	0.039	0.77	1.83	0.208	11.72	4.15	54.7	20.4	89.9	20.45	194.5	33.2	10240	36.7	122	0.82085799	752.65
AP_048_36	rim	**1036**	1.6	9.87	289	4.84E+05	0.049	0	7.79	0.061	1.17	2.54	0.217	11.03	3.31	32.6	9.87	36.2	6.8	58.5	9.18	10740	6.65	54.3	0.99431715	739.67
AP_048_37	core	**1177**	3.2	9.83	73.2	4.83E+05	0.02	0	5.6	0.023	0.37	0.53	0.319	2.41	0.854	8.25	2.15	7.66	1.33	11.31	1.8	11250	13.26	86.2	0.99255352	739.32
AP_048_38	rim	**995**	0.7	9.2	362.4	4.76E+05	0.061	0.011	7.79	0.07	1.18	2.39	0.251	11.9	3.73	38.8	12.25	48.5	9.7	82.8	13.34	10730	8.51	61.2	0.96378783	733.55
AP_048_39	core	**1260**	1.2	8.23	720	4.79E+05	0.039	0.0029	11.06	0.031	1.05	2.31	0.135	14.6	5.46	68.6	25.82	109.1	25	240.3	41.08	11050	67.4	312	0.91539984	724.98
AP_048_40	core	**1172**	1.9	7.78	733	4.88E+05	0.027	0.142	10.49	0.092	1.04	2.22	0.345	15.14	5.52	70.8	25.73	113.9	24.88	235.9	39.91	10700	41.79	140.9	0.8909796	719.23
AP_048_41	rim	**939**	8.3	9.73	157.8	4.89E+05	0.008	-0.0007	9.1	0.09	2.09	3.8	0.478	13.38	2.81	22.24	5.46	15.79	2.61	20	3	11120	10.25	55.2	0.98811284	738.42
AP_048_42	core	**1141.6**	3.1	8.7	272	4.82E+05	0.025	0	8.56	0.0126	0.21	1.06	0.599	6.44	2.12	26.2	9.33	38.6	8.33	73.5	13.1	13350	29.8	254	0.93951925	728.73
AP_048_43	core	**1145**	75	6.89	1653	4.75E+05	0.166	0.031	20.1	0.039	0.87	2.51	0.131	22.2	9.4	129.1	52.5	256.2	61.9	595	103.5	12120	404	1678	0.83821922	709.10
AP_048_44	rim	**977**	21	13.25	126.7	4.87E+05	0.041	0.0027	8.76	0.07	1.72	2.56	0.41	8.69	2.5	19.2	4.37	13.09	2.2	16.06	2.52	10870	5.69	44.5	1.12221588	766.18
AP_048_45	core	**1110**	3	10.1	191	4.76E+05	0.017	0	5.39	0.011	0.39	0.92	0.234	4.62	1.73	18.6	6.08	24.7	5.44	47.6	8	11840	27.71	214.7	1.00432137	741.70
AP_048_46	core	**1014**	10.9	11.86	107.8	4.79E+05	0.02	0.0014	7.57	0.093	1.45	2.36	0.421	9.19	2.08	15.71	3.42	10.93	1.89	13.91	2.07	10600	4.83	69.3	1.07408469	756.04
AP_048_47	core	**1058**	0.1	8.31	458.6	4.76E+05	0.036	0	8.75	0.0246	0.66	1.86	0.1	10.52	3.64	43	15.6	67.5	14.76	138.2	22.4	11020	29.95	85.4	0.91960102	724.81
AP_048_48	core	**955**	16.7	11.78	133.9	4.67E+05	0.163	0.023	7.79	0.054	1.42	2.86	0.434	8.9	2.34	18.6	4.59	15	2.58	21.6	2.94	10460	5.92	38.2	1.07114529	755.43
AP_048_49	rim	**984**	2.2	9.59	366	4.83E+05	0.048	0	7.94	0.09	1.41	2.86	0.264	13.43	3.96	39.1	12.2	47.1	9.63	82.3	13.6	11060	8.4	76.7	0.98181861	737.16
AP_048_50	core	**1223**	1.5	8.87	131	4.88E+05	0.015	0	6.77	0.0084	0.314	0.93	0.39	4.15	1.31	13.8	4.18	15.4	2.79	24	3.93	11290	25.9	127	0.94792362	730.39
AP_048_51	rim	**994**	7.2	12.95	258.8	4.88E+05	0.113	0.0115	8.88	0.066	1.45	3.2	0.237	13.75	3.84	33.5	8.86	29.3	5.56	42.6	6.55	11080	7.62	41.78	1.11226977	764.07
AP_048_52	core	**1094**	-1.1	7.71	738	4.74E+05	0.014	0.0046	7.27	0.034	1.02	2.49	0.151	15.92	5.55	71.7	25.46	116.2	25.63	247.5	41.9	11150	7.83	55.57	0.88705438	718.47
AP_048_53	core	**1328**	0.3	9.57	510.2	4.81E+05	0.038	0.0054	9.35	0.04	0.59	1.59	0.083	11.17	4.16	47.2	17.21	74.6	15.59	146.2	24.39	11440	25.3	95.1	0.98091194	756.97
AP_048_54	rim	**948**	16.4	11.78	141.3	4.94E+05	0.035	0.0032	9.7	0.129	1.96	3.46	0.476	11.69	2.6	21	4.9	14.09	2.28	17.63	2.76	11550	9.84	52.51	1.07114529	755.43
AP_048_55	rim	**1091**	2.8	7.94	1121	4.81E+05	0.04	0.0016	19.38	0.039	1.37	4.03	0.221	25.06	8.93	109.3	39.54	171.4	36.25	326.7	54.84	10680	94.8	353	0.8998205	720.94
AP_048_56	core	**1193**	-2.6	11.16	706	4.86E+05	0.003	0.0045	7.42	0.04	0.9	2.55	0.179	14.71	5.21	62.9	24.04	107.2	23.91	225	39.72	11660	19.7	64.8	1.04766419	750.56
AP_048_57	rim	**991**	20.6	14.6	130.6	4.75E+05	0.048	0.008	8.4	0.09	1.25	2.77	0.352	8.99	2.53	18.07	4.31	13.14	2.4	16.34	2.49	10600	7.66	38.7	1.16435286	775.21
AP_048_58	core	**1200**	-0.5	9.72	550	4.93E+05	0.06	0	9.75	0.042	0.84	2.01	0.172	12.8	4.49	51.6	18.5	76.4	16.5	152	25.3	11590	41.65	159	0.98766626	738.33
AP_048_59	core	**1340**	1.1	9.7	877	4.92E+05	0.034	0	8.49	0.069	0.98	2.74	0.445	15.7	6.02	76.5	30.4	138.2	31.3	305	51.9	10210	43.7	165	0.98677173	738.15
AP_048_60	rim	**1145**	2.8	7.97	512	4.87E+05	0.41	0.0058	8.91	0.037	0.65	2.29	0.16	11.98	4.19	47.5	17.06	71.4	15.12	140.4	22.5	11320	30.03	92.8	0.90145832	721.26
AP_048_61	core	**1242**	224.4	10.1	1437	4.89E+05	0.279	0.093	16.11	0.08	1.28	3.34	0.415	23.5	9.88	124.3	49.9	230	51.3	490	84.1	11820	158.3	664	1.00432137	741.70
AP_048_62	rim	**1110**	52	6.28	1856	4.71E+05	0.188	0.12	18.02	0.227	3.23	7.03	0.317	39.4	13.95	174	53.1	272.8	57.5	495	79.2	8410	184	402	0.79795964	701.52
AP_048_63	rim	**956**	4.2	5.05	224	4.83E+05	0.015	0.0165	7.63	0.089	1.01	2.2	0.228	9.29	2.55	25.1	7.45	28	6	54	8.4	10130	11.1	60.3	0.70329138	684.13
AP_048_64	core	**932**	1.2	4.54	417.2	4.81E+05	0.012	0.073	7.93	0.05	0.83	1.66	0.131	8.1	2.95	38.1	14.41	63.6	14.63	140.2	24.17	10790	34.2	175.3	0.65705585	675.86
AP_048_65	core	**948**	12.7	11.08	262.2	4.75E+05	0	0	8.47	0.036	1.19	2.56	0.131	10.24	3.02	31.4	9.22	33.4	6.55	52.5	8.05	10940	10.96	55.6	1.04453976	749.92
AP_048_66	core	**1206**	1.6	11.36	350	4.74E+05	0.034	0	6.72	0.039	0.47	1.06	0.198	6.86	2.62	32.9	11.24	51.6	11.37	109.7	18.4	10900	17.02	89.9	1.05537823	752.16
AP_048_67	core	**1166**	-0.3	9.95	1041	4.79E+05	0.05	0.005	7.37	0.069	1.21	3.74	0.226	23.3	8.37	97.1	36.2	157.5	34.71	323.9	55	10910	21.28	61	0.99782308	740.38
AP_048_68	core	**1163**	3.7	8.34	992	4.94E+05	0.094	0.0055	16.99	0.041	1.17	3.69	0.156	20.6	8.02	95.2	34.8	149.2	32.94	297.2	48.2	10490	72.1	226.9	0.92116605	725.11
AP_048_69	rim	**957**	0	8.91	367.6	4.74E+05	0.043	0	9.15	0.037	0.67	1.32	0.181	8.91	3.06	36.5	12.49	52.5	10.48	100.4	16.37	11820	12.25	81	0.9498777	730.78
AP_048_70	core	**1221**	29	9.7	1164	4.82E+05	0.09	0	16.35	0.0152	0.75	3.24	0.224	21	8.44	102.6	39.2	183.5	41.3	399	67.8	11030	133.2	612	0.98677173	738.15
AP_048_71	rim	**941**	12.2	8.85	216	5.02E+05	0.022	0	8.61	0.041	0.7	1.72	0.213	8.05	2.35	23.3	7.27	27.5	5.36	54	8.16	11090	8.24	65.1	0.94694127	730.20
AP_048_72	core	**1118**	-0.3	7.47	868	4.72E+05	0.029	0	8.07	0.047	1.07	2.82	0.195	19.3	6.75	82.3	29.91	129.3	27.83	255.2	43.6	11120	5.68	42.02	0.8733206	715.82
AP_048_73	core	**1088**	-0.9	11.05	604	4.75E+05	0.008	0.0054	6.53	0.019	0.71	1.87	0.079	11.34	4.34	55.3	20.85	95.3	21.38	211.6	34.67	11070	2.704	44.55	1.04336228	749.67
AP_048_74	rim	**954**	6.1	9.51	206.4	4.73E+05	0.009	0	7.95	0.055	1.26	2.39	0.242	10.87	2.95	27.4	6.96	23.5	3.86	31.4	5.02	10500	5.94	65	0.97818052	736.43
AP_048_75	core	**1235**	3.1	7.55	1230	4.78E+05	0.012	0.013	8.53	0.095	1.63	4.28	0.538	27.3	9.46	114.4	43.1	187.5	41.2	369	61.4	10120	67.1	167	0.87794695	716.71
AP_048_76	rim	**1177**	0.7	8.88	1025	4.84E+05	0.024	0	8.69	0.043	1.01	3.28	0.183	21.3	7.86	95.5	34.62	152.1	33.25	300.6	49.86	11330	16.21	81.6	0.94841297	730.49
AP_048_77	core	**1186.2**	2.7	10.46	774	4.87E+05	0.083	0.001	14.73	0.054	1.55	3	0.358	19.8	6.48	75.8	25.7	100.2	19.7	174	26.7	11990	144	863	1.01953168	744.79
AP_048_78	rim	**1215**	1.8	11.48	602	4.75E+05	0.037	0	5.77	0.0203	0.65	1.61	0.114	11.24	4.06	53.9	20.72	93.9	22.07	213.8	35.5	10700	4.15	52.4	1.05994189	753.10
AP_048_79	rim	**926**	10.2	9.21	306.5	4.94E+05	0.143	0.0126	7.71	0.052	1.18	2.61	0.175	11.55	3.57	36	10.92	37.7	7.14	59.8	9.02	11270	7.3	64.6	0.96425963	733.64
AP_048_80	core	**943**	3.4	9.1	137.3	4.71E+05	0.052	0.0019	8.7	0.074	1.4	2.94	0.6	10.43	2.49	19.35	4.45	14.64	2.34	19.3	2.58	10530	4.2	31.93	0.95903549	732.60
AP_048_81	rim	**901.9**	6	8.02	282	4.76E+05	-0.013	0.023	9.27	0.044	1.1	1.93	0.228	9.26	2.64	27	9.33	40.8	8.51	79.1	14.6	10540	10.19	59.8	0.77959649	698.09
AP_048_82	core	**1270**	3.4	8.06	685	4.76

AP_048_141	core	**1175**	0.6	12.41	618.7	4.84E+05	-0.007	0.009	6.29	0.055	0.84	2.22	0.17	13.72	4.79	59.6	22.35	98.2	22.73	210.9	36.75	11890	6.34	75.8	1.09377178	760.16
AP_048_142	core	**1203**	-0.2	11.48	411.4	4.82E+05	0.042	-0.00576	5.18	0.01168	0.64	1.41	0.068	8.69	3.12	38.6	14.43	65.6	15.11	142.5	24.5	10580	2.7	33.37	1.05994189	753.10
AP_048_143	core	**1055**	3	8.98	1113	4.77E+05	0.036	0.0143	11.17	0.029	1.09	4.02	0.282	27.2	9.18	110.4	38.7	158.4	33.1	302.3	48.1	11010	12.13	62.3	0.95327634	751.45
AP_048_144	core	**966**	38.4	13.45	93.9	4.78E+05	0.029	0	8.59	0.075	1.12	2.03	0.304	7.59	1.77	13.19	3.16	9.78	1.724	12.32	1.72	10550	4.59	35.09	1.12872228	767.56
AP_048_145	core	**1306**	2.2	8.26	699	4.68E+05	0.097	0	10.8	0.0103	0.53	1.87	0.099	11.8	4.19	58.7	23.6	112.6	26.9	276	48	11400	89	630	0.91698005	724.29
AP_048_146	rim	**1127**	0.7	10.69	706	4.81E+05	0.025	0.0013	8.41	0.023	0.85	1.7	0.104	13.92	5.1	65.5	24.23	108.5	24.6	232.1	38.79	11180	6.94	49.6	1.02897771	746.72
AP_048_147	rim	**963**	14.2	10.65	214	4.88E+05	0.047	0	7.54	0.08	0.98	2.49	0.3	10.34	2.7	25.5	7.32	27	5.14	42.9	6.59	10780	5.55	54.7	1.02734961	746.39
AP_048_148	rim	**942**	17.7	11.02	122.5	4.78E+05	0.029	0.0081	8.81	0.07	1.25	2.5	0.382	9.9	2.19	17.61	4.36	12.33	2.26	16.9	2.4	10410	3.35	30.03	1.04218159	749.43
AP_048_149	core	**1262**	5.3	9.7	1379	4.71E+05	0.12	0.68	12.5	0.31	2.82	5.29	0.81	31.2	10.72	127.8	49.4	205.4	44.47	421	69.2	9670	90.4	274.6	0.98677173	738.15
AP_048_150	rim	**944**	11.3	12.39	194.5	4.73E+05	0.089	0.01	8.91	0.078	1.36	3.05	0.282	13.93	3.36	27.4	6.76	20.3	3.1	26.1	3.68	11560	9.65	55.36	1.09307131	760.02
AP_048_151	core	**1314**	17	7.17	1005	4.61E+05	0.066	0.01	12.02	0.7	2.39	0.132	15.6	6.26	84.4	33	149.2	36.9	349	63.5	10850	116.1	653	0.85551916	712.40
AP_048_152	rim	**1118**	1.1	7.19	1266	4.70E+05	0.045	0.015	8.89	0.053	2.13	5.13	0.237	29.2	10.06	125.4	46	183.7	39.8	366	59.5	9800	61.8	166.5	0.85672889	712.63
AP_048_153	rim	**1280**	-0.6	8.4	869	4.81E+05	0.14	0.0074	14.07	0.027	0.69	2.02	0.212	14.71	6.19	79.1	31.03	135.1	31.11	312.5	51.1	10920	87	404.3	0.92427929	725.73
AP_048_154	core	**919.1**	25.4	9.53	204.5	4.74E+05	-0.004	0	7.75	0.05	0.9	2.38	0.178	10.62	2.78	25.7	6.99	23.7	4.29	35	5.04	11140	9.89	92.9	0.9790929	736.61
AP_048_155	rim	**919**	484	6.62	307.6	4.58E+05	0.167	0.019	9.24	0.043	0.19	0.98	0.24	6.1	2.16	28	10.4	49.7	11.79	117.8	20.82	10470	28.02	152.5	0.82085799	705.82
AP_048_156	core	**1176**	5.4	8.13	1019	4.72E+05	0.023	0	2.59	0.025	0.55	2.19	0.146	16.3	6.2	87	34.85	161.8	38.6	376	66.2	12740	31.58	327.9	0.91009055	722.95
AP_048_157	core	**1249**	4.6	7.84	977	4.80E+05	0.058	0	15.39	0.011	0.49	2.02	0.067	14.96	5.9	80.4	32.46	153.9	38.8	384.4	68.5	12450	168.5	946	0.89431606	719.87
AP_048_158	rim	**955**	16.5	10.68	163	4.72E+05	0.062	0.008	8.45	0.048	1	2.7	0.232	8.28	2.39	20.5	5.38	18.8	3.46	30.9	4.36	10470	5.56	41.7	1.02857125	746.64
AP_048_159	core	**1185**	2.9	6.88	1280	4.78E+05	0.062	0.0032	15.5	0.116	2.84	5.9	0.21	30.7	11.1	132	47.8	190	40.9	360	58.3	10630	107	325	0.83758844	708.98
AP_048_160	core	**1087**	0.8	6.39	973	4.79E+05	0.003	0.0118	5.53	0.085	1.67	3.58	0.265	25.4	7.79	92.8	34.2	146.2	31.8	296	49.1	9450	41.5	98.2	0.80550086	702.93
AP_048_161	core	**1087**	-0.3	8.69	577.1	4.79E+05	0.018	0.0053	7.11	0.043	0.91	1.82	0.184	12.17	4.44	52.5	19.96	87.7	20.43	196.9	34.9	10940	9.18	49.9	0.93901978	728.63
AP_048_162	core	**921**	11.4	7.7	151.8	4.80E+05	0.004	0.035	8.4	0.058	1.26	2.13	0.308	9.33	2.49	20	5.53	17.11	2.8	22.5	3.5	10150	6.01	34.23	0.88649073	718.36
AP_048_163	rim	**950**	11.1	11.1	199.2	4.78E+05	0.04	0	7.43	0.046	1.09	2.17	0.256	9.55	2.82	25.1	6.83	25.3	4.7	40.6	6.1	11120	5.65	59.6	1.04532298	750.08
AP_048_164	core	**1223**	-1.2	6.93	200.4	4.88E+05	0.016	0.0074	6.53	0.0162	0.34	0.96	0.37	6.2	2.03	22.2	6.82	22.9	4.52	34.7	4.85	11580	25.1	215	0.84073323	709.58
AP_048_165	core	**947**	36.2	14.9	89.6	4.84E+05	-0.009	0.0036	8.08	0.086	1.23	2.33	0.435	7.7	1.87	12.85	2.93	8.66	1.41	11.47	1.54	10340	4.31	68.8	1.17318627	777.13
AP_048_166	core	**969**	16.2	14.94	173.4	4.87E+05	0.049	0	8.46	0.107	1.8	3.17	0.301	11.13	2.8	24.8	5.85	17.99	3.28	23.8	3.44	11120	7.65	40	1.1743506	777.38
AP_048_167	rim	**1262**	2.7	9.5	557	4.71E+05	0.024	0.0113	7.76	0.042	0.67	1.84	0.129	11.49	4.2	52.3	19.69	84.8	18.53	177.8	29.75	10730	8.65	41.9	0.97772361	736.33
AP_048_168	core	**1226**	8	8.42	980	4.74E+05	0.084	0.0041	12.37	0.0219	0.55	1.83	0.135	15	5.96	80.8	32.6	153.8	37.7	388	70.9	12390	221	1040	0.92531209	725.93
AP_048_169	core	**1196**	3.3	8.11	880	4.80E+05	0.041	0.0078	11.65	0.022	0.83	2.77	0.355	17.1	6.08	80.9	31.5	138.6	32.2	306	51.4	10140	68	247	0.90902085	722.74
AP_048_170	rim	**981**	-1.4	6.69	473.5	4.79E+05	0.041	0.0016	7.64	0.035	0.61	1.93	0.114	10.58	3.7	43.6	16.84	72	16.96	161.6	26.65	11020	15.7	64.1	0.82542612	706.68
AP_048_171	rim	**1134**	0	8.5	434.3	4.82E+05	0.017	0.002	7.12	0.021	0.68	1.32	0.092	8.86	3.1	38.8	14.54	67.4	15.92	161.8	27.72	11590	34.25	137.2	0.92941893	726.74
AP_048_172	core	**1126**	1.8	12.95	490.5	4.91E+05	-0.014	0	5.74	0.0128	0.51	1.23	0.091	9.39	3.51	45.3	17.57	78	17.76	173.6	30.14	11450	2.152	34.51	1.11226977	764.07
AP_048_173	core	**927**	51.4	13.09	92.3	4.80E+05	0.001	0.0083	9.34	0.062	1.33	2.17	0.361	9.04	1.91	13.69	3.17	9.61	1.598	11.01	1.61	10080	5.78	37.43	1.11693965	765.06
AP_048_174	core	**1122**	2	9.1	773	4.72E+05	0.071	0	11.49	0.247	1.03	2.77	0.21	17.3	6.26	77.7	28	116.8	25.2	227.3	35.3	11400	61.8	311.2	0.95902135	732.60
AP_048_175	rim	**983**	3.8	10.3	391	4.82E+05	0.105	-0.00665	8.09	0.093	0.97	3.17	0.309	15.7	4.71	48.1	13.64	46.8	8.39	63.4	10.21	11190	7.2	63.5	1.01283722	743.43
AP_048_176	core	**1255**	3.2	7.4	782	4.76E+05	-0.006	0.0017	11.63	0.044	0.72	2.1	0.063	14.8	5.7	68.4	26.8	123.1	27.4	264	44.7	10300	61.6	240.8	0.86923172	715.03
AP_048_177	rim	**930**	17	12.49	222.6	4.80E+05	0.042	0.0062	8.03	0.058	1.16	3.14	0.157	11.83	3.17	28	7.87	24.5	4.53	37.3	5.61	11310	9.16	88	1.09656244	760.75
AP_048_178	core	**1081**	20.3	8.83	343	4.71E+05	0.66	0	6.73	0.047	0.76	1.99	0.204	8.22	2.89	34.3	12.1	52	11.8	113	19.6	10690	6.6	81.6	0.94594607	730.00
AP_048_179	core	**1237**	2.6	10.34	1762	4.95E+05	0.059	0.014	16.42	0.228	4.74	7.92	0.369	51.3	16.41	187.2	66	257.3	55.7	472	72.4	9920	120.5	308.7	1.01452054	743.77
AP_048_180	core	**1126**	2.3	9.11	459.8	4.77E+05	0.016	0	5.18	0.019	0.56	1.39	0.06	8.06	3.09	42.5	16.33	75	17.5	170.3	28.75	11090	1.619	29.66	0.95951838	732.69
AP_048_181	core	**1020**	20.5	13.9	192	4.87E+05	-0.011	-0.00596	7.73	0.074	1.45	2.1	0.192	9.81	2.68	23.9	6.75	26.3	5.4	49.6	7.9	11870	9.04	107.5	1.1430148	770.62
AP_048_182	core	**1290**	0.5	9.07	713	4.72E+05	0.065	0	10.78	0.03	0.8	2.57	0.116	14.61	5.36	69.2	25.8	111	24.41	226.6	36.2	10870	39.8	151.6	0.95760729	732.31
AP_048_183	rim	**1169**	6	8.01	250	4.87E+05	0.008	0	6.12	0.032	0.57	1.22	0.2	6.41	2.11	24.9	8.76	37.2	8.43	80.2	13.38	11060	4.98	64.7	0.90362452	721.69
AP_048_184	core	**1123**	3.9	7.43	412.8	4.91E+05	0.099	0.0083	8.24	0.0063	0.32	0.71	0.034	6.28	2.34	32.4	13.61	68.7	17.55	197.9	34.4	12390	69.7	381	0.87098881	715.37
AP_048_185	core	**1304**	7.6	14.05	2400	4.81E+05	0.064	0.032	22.81	0.406	7.49	15.8	0.385	71.6	22.92	256	88.6	358	75.2	641	98.2	10820	218	489	1.14767632	771.62
AP_048_186	rim	**943**	21.5	13.68	198.8	4.80E+05	0.03	0	8.78	0.111	1.64	3.19	0.365	13.83	3.22	27.07	6.7	20	3.45	28.8	4.05	11080	10.42	44.7	1.1360861	769.13
AP_048_187	core	**1255**	0.4	8.41	964	4.77E+05	0.032	0	14.35	0.065	1.24	4.06	0.203	21	7.67	95.1	34.88	145.7	31.37	290.2	46.3	9860	57.8	161.7	0.9247796	725.83
AP_048_188	core	**938**	10.3	7.46	1098	4.85E+05	0.077	0.039	20.83	0.057	1.64	4.93	0.264	25.6	9.28	109.4	40.4	168.1	35.6	334	53.5	10740	134.9	428	0.87273883	715.70
AP_048_189	core	**979**	12.2	17.77	249.2	4.81E+05	0.022	0.0079	9.62	0.098	1.99	3.98	0.365	15.38	4.1	34.2	8.73	27.56	5	36.8	5.54	11390	12.71	57.6	1.24968743	794.01
AP_048_190	core	**1185**	1.5	10.64	171.7	4.84E+05	0.043	0	6.04	0.0167	0.67	1.29	0.928	8.29	2.14	19.91	5.3	16.55	3.03	22.3	3.13	11810	42.5	210.6	1.02694163	746.30
AP_048_191	rim	**928**	22.7	11.01	115.1	4.73E+05	0.009	-0.00456	7.93	0.071	1.19	2.37	0.354	8.87	2.13	16.6	3.93	11.85	2.03	16.2	2.28	10550	6.67	36.75	1.04178732	749.35
AP_048_192	rim	**1068**	1.7	8.89	505.5	4.82E+05	0.03	0.002	7.22	0.025	0.75	1.67	0.086	9.31	3.68	46.9	17.87	78	17.75	173	28.15	11200	7.6	64.6	0.94890176	730.58
AP_048_193	core	**972**	8	10.29	170	4.87E+05	0.038	0	6.83	0.07	0.98	2.07	0.346	9.04	2.57	22.2	6.15	21.6	4	34.2	5.2	10120	2.49	49	1.01241537	743.34
AP_048_194	core	**1169**	0.6	9.03	550	4.67E+05	0.031	0.0018	7.04	0.024	0.66	1.82	0.125	11.9	4.1	50.8	19.03	82.8	18.74	179.3	29.1	11060	13.1	94	0.95568775	731.93
AP_048_195	core	**1204**	0.8	8.6	1560	4.94E+05	0.055	0	13.15	0.076	1.62	6.24	0.357	39	13.59	158.4	55.5	225.5	46.1	413	64.2	10000	79.2	185.2	0.93449845	727.74
AP_048_196	core	**1108**	4.2	7.17	1160	4.83E+05	0.062	0	15.35	0.065	1.15	3.37	0.084	24.4	8.95	113.1	41.7	180.6	38	363	57.5	10440	65.2	305	0.85551916	712.40
AP_048_197	rim	**971**	3.8	9.2	312	4.82E+05	-0.007	0	7.64	0.046	0.84	2.12	0.182	9.55	3.24	33.8	10.69	41.6	8.61	78.9	12.85	10830	8.1	70	0.96378783	733.55
AP_048_198	core	**1166**	3.1	12.9	424	4.91E+05	0.018	0.01	6.48	0.012	0.56	1.4	0.077	10.5	3.27	41.4	15.25	66.8	15.85	155.1	25.9	11980	3.48	40.9	1.11058971	763.71
AP_048_199	core	**1246**	10.8	8.61	1370	4.91E+05	0.007	0.0115	12.9	0.185	3.55	8.5	0.442	36.6	13	147	50.5	200	40	359	57.3	9850	67.8	172	0.93500315	727.84
AP_048_200	core	**1334**	2.8	9.32	535.4	4.71E+05	0.042	0	7.97	0.0054	0.39	1.27	0.076	8.46	3.3	43.8	18.05	84.1	21.16	205.6	34.21	11790	45.8	201.8	0.96941591	734.67
AP_048_201	core	**1151**	1.1	7.09	827	4.84E+05	0.036	-0.0011	13.1	0.025	1	3.17	0.096	17.8	6.58	82	29.7	129	27.7	260	41.3	11130	65.1	204	0.85064624	711.47
AP_048_202	rim	**990**	5.9	7.61	325.1	4.85E+05	0.107	0.022	6.6	0.052	0.77	2.39	0.229	10.83	3.29	34.6	11.6	46.1	9.47	97.8	16.26	10870	5.66	59.6	0.88138466	717.37
AP_048_203	core	**947**	44.5	15.03	90.4	4.81E+05	0.048	0	8.58	0.073	1.43	1.87	0.273	7.07	1.53	12.17	3.19	8.72	1.482	11.06	1.6	10370	4.17	32.32	1.17695898	777.95
AP_048_204	core	**1168**	10.7	7.8	1103	4.74E+05	1.8	228	560	74	344	78	2.88	81	15.6	123.2	36.7	162.4	34.2	329	59.4	11740	131.5	642	0.8920946	719.44
AP_048_205	rim	**1082**	14	7.26	638	4.92E+05	0.171	0.013	8.52	0.033	0.93	1.78	0.136	11.2	4.23	56.4	21.6	100	23.2	230	39.2	10730	83	424	0.86093662	713.44
AP_048_206	core	**1080**	9.4	8.05	232	4.77E+05	0.137	0.078	6.8	0.051	0.45	1.04	0.257	4.84	1.66	20.4	8.09	33.9	8.12	76.3	12.8	11070	24.9	144.9	0.90579588	722.11
AP_048_207	rim	**1170**	-0.5	10.99	519.2	4.72E+05	0.024	0	7.46	0.027	0.62	1.5	0.123	10.45	3.84	49.4	17.33	80	17.56	173	27.53	11300	7.62	54.9	1.04099769	749.19
AP_048_208	core	**1131**	0.4	9.04	824	4.74E+05	0.04	0.02	7.39	0.046	0.85	2.75	0.158	17.7	6.43	74.7	28.06	121.7	27.49	260	44.12	11120	6.76	63.9	0.95616843	732.03
AP_048_209	core	**1186**	1.7	11.56	580	4.77E+05	0.033	0	6.07	0.048	0.74	2.04	0.161	11.6	4.34	54.3	20	91.7	20.9	200	32.3	10850	4.22	51	1.06295783	753.73
AP_048_210	rim	**904**	7.8	8.56	126.5	4.78E+05	0.036	0.003	7.26	0.056	1.11	2.06	0.357	7.71	1.92	16.44	4.12	14.08	2.33	19.7	2.75	9770	3.06	65.8	0.93247376	727.34
AP_048_211	core	**1092**	0.6	7.26	1030	4.78E+05	0.064	0	14.83	0.056	1.26	3.75	0.13	22.7	8.5	100	37.3	157	33.5	303	49	10510	81	262	0.86093662	713.44
AP_048_212	core	**1251**	0.2	7.35	838	4.75E+05	0.021	0	10.4	0.066	1.17	3.21	0.209	19.9	6.77	82.8	29.7	128.8	27.2	248	40.8	9100	34.4	97.6	0.86628734	714.46
AP_048_213	rim	**916**	2.3	4.46	595	4.63E+05	0.036	0	9.63	0.016	0.47	1.28	0.13	9.11	3.86	51.6	20.44	96.4	23	229.3	39.4	11530	42.6	150.1	0.64933486	674.49
AP_048_214	rim	**1016**	2.2	8.16	460	4.84E+05	0.046	0	8.21	0.056	1.55	2.88	0.391	14.8	4.57	49.5	16.7	67	13.7	126	19.5	9840	24.7	111	0.91160815	729.76
AP_048_215	core	**1246**	3.2	8.45	1151	4.74E+05	0.065	-0.00539	16.93	0.052	0.94	3.43	0.199	21.4	7.73	102.8	39.84	178	42.26	406	67.9	10930	156.1	667	0.92685671	726.23
AP_048_216	rim	**1227**	1.8	11.8	501.2	4.68E+05	0.043	0	9.49	0.024	0.95	2.08	0.142	12.1	4.17	49.7	17.2	75.5	16.74	154.4	26.19	11080	27.08	74.6	1.07188201	755.58
AP_048_217	core	**1427**	1090	51.8	2514	4.73E+05	1.1	1.03	24	0.32	2.6	4.82	0.72	32.5	14.49	208.4	88.1	425	100.5	988	170	11330	327.4	1543	1.71432976	909.44
AP_048_218	core	**1077**	0.3	7.48	558	4.75E+05	0.029	0.0055	10.89	0.025	0.67	1.63	0.106	10.95	4.23	50.1	18.77	82.1	17.92	170	28.14	10840	4.29	36.7	0.8739016	715.93
AP_048_219	core	**1320**	190	7.29	948	4.68E+05	0.63	0.035	9.99	0.061	1.12	2.45	0.383	18.8	6.94	84.3	32.67	146.1	32.31	304.9	50.7	9350	64.3	232.9	0.86272513	713.78
AP_048_220	rim	**1111**	930	10.26	369.1	4.82E+05	0.047	2.5	11.5	0.58	3	2.13	0.164	9.85	3.28	36	12.82	53.9	12.01	110.2	19.4	10680	7.55	47.47	1.01114736	743.08
DAA-039																										
DAA_39_1	core	**940**	18.6	37.7	224	4.87E+05	0.048	0.029	13.6	0.182	3.08	4.26	2.09	14	2.88	25.5	7.9	28.9	6.3	59	9.7	8570	16.7	19.8	1.57634135	872.63
DAA_39_2	core	**883**	48.8	26.3	57.6	4.84E+05	0.043	0.017	14.92	0.121	2.84	3.2	1.59	8.76	1.45	9.02	1.81	5.46	0.866	6.47	1.015	9160	13.32	72.3	1.41995575	833.59
DAA_39_3	core	**899**	45.5	37.9	57	4.83E+05	0.022	0.018	9.9	0.095	1.7	2.63	1.12	5.63	1.245	8.57	1.9	5.47	0.872	6.04	0.881	9150	7.31	45.5	1.57863922	873.22
DAA_39_4	rim	**930.7**	24.2	31.3	330.7	4.96E+05	0.115	0.0046	30.57	0.063	1.28	2.47	0.87	10.75	2.81	30.1	10.57	47.8	10.96	110.7	18.8	10040	48.8	109.1	1.49554434	882.12
DAA_39_5	core	**798**	11.7	23.4	457	4.79E+05	0.085	0.008	21.9	0.297	4.65	6.41	2.34	22.1	5.47	49.5	15.17	62.6	13.3	121.2	21.39	7990	38.1	47.1	1.36921586	821.49
DAA_39_6	core	**907**	10.1	33.1	581	4.88E+05	0.155	0.0017	45.9	0.149	2.56	5.7	1.43	22.5	5.77	60.8	20.05	83	17.92	175.6	29.8	9090	56.3	92.2	1.51982799	858.21
DAA_39_7	rim	**863.5**	94	50.1	159.2	4.86E+05	2.8	0.0014	14.22	0.066	1.6	2.2	1.17	9.01	2.08	18.89	5.14	18.1	3.36	27.3	4.37	9150	47	189.4	1.69983773	905.46
DAA_39_8	core	**917**	21.5	36.2	341.8	4.80E+05	0.066	0.0114	22	0.121	2.28	4	1.39	13.75	3.88	35.6	11.05	47.4	10.31	98.3	16.99	8090	23	31.7	1.55870857	868.09
DAA_39_9	rim	**893**	40.1	28.1	140.6	4.91E+05	0.043	0.0049	14.2	0.056	1.08	1.55	0.94	5.26	1.256	12.96	4.1	19.4	5.14	53.1	9.7	9030	18.81	106.3	1.44870632	840.57
DAA_39_10	core	**1071**	1776	45.7	750	4.71E+05	0.966	0.06	24.94	0.745	11.18	13.81	5.02	40.9	9.36	85.2	26.1	99.3	20.37	184.4	31.61	7810	52.8	52	1.6599162	894.54
DAA_39_11	core	**905.4**	15.8	27.2	1118	4.88E+05	0.206	0.104	25.75	0.555	9.49	13.14	5.47	53.5	13.51	126	38.62	149.8	31.23	280.7	47.5	7620	100.2	82.4	1.4345689	837.13
DAA_39_12	core	**912**	60	43.6	24	4.86E+05	0.028	0.015	10.11	0.085	1.57	1.94	0.106	3.83	0.67	4.85	0.808	2.08	0.397	1.92	0.221	8840	15.36	42.97	1.66948649	889.18
DAA_39_13	rim	**932**	69.5	37	36.9	4.73E+05	0.032	0.0034	6.7	0.044	1.01	1.66	0.759	4.03	0.838	5.64	1.195	3.01	0.462	4.38	0.639	7950	5.89	13.13	1.56820172	870.53
DAA_39_14	core	**1047**	4.5	34.03	809	4.86E+05	0.086	0.023	21.27	0.386	8.17	12.49	4.91	42.4	9.88	92.6	27.76	107.9	22.82	201.9	33.43	8180	38.14	36.66	1.53186195	861.25
DAA_39_15	core	**891**	80	29.3	504	4.78E+05	0.209	0.0089	22.96	0.115	2.82	4.87	1.83	19	5.14	50.4	16.77	70.1	15.57	142.4	24.81	8870	45.3	84.7	1.46686762	845.02
DAA_39_16	core	**921**	68.9	28.5	43.7	4.75E+05	0.007	0	11.86	0.073	1.53	1.43	0.81	4.76	0.943	6.56	1.4	4.09	0.73	5.65	0.89	8780	12.06	27.34	1.45484486	842.07
DAA_39_17	core	**911**	18.6	36.9	476	4.90E+05	0.084	0.0035	20.9	0.105	2.01	5.09	1.92	19.1	4.85	49.5	15.7	64.1	14	136	22.8	9640	47.6	88.7	1.56702637	870.23
DAA_39_18	core	**1027**	1.7	35.1	744	4.82E+05	0.091	0.176	22.2	0.954	13.6	14.43	5.14	40.9	9.29	85.7	24.81	98.7	20.5	186.5	31.44	7710	39.83	37.55	1.54530712	864.67
DAA_39_19	rim	**880**	39.3	33.8	88.5	4.89E+05	0.065	0.0015	16.91	0.161	2.74	3.89	1.72	10.58	1.79	12.44

DAA_39_78	core	**872**	21.7	24.3	1387	4.95E+05	0.181	0	41.3	0.161	4.32	7.9	2.24	40	12.55	136.4	48.5	205.8	46.4	459	75.2	10900	331	725	1.38560627	825.37
DAA_39_79	rim	**955**	69	39.7	82	4.83E+05	0.013	0.018	8	0.079	1.49	2.06	0.96	6.68	1.43	11.19	2.73	8.37	1.36	9.79	1.37	9230	1.63	8.4	1.59879051	878.46
DAA_39_80	rim	**984**	-0.7	27.7	1048	4.74E+05	0.156	0.108	43.1	1.16	17.7	19.8	5.92	58.8	13.35	124.2	38.1	147.8	29.8	265.5	44.3	7930	80.9	70.5	1.44247977	839.05
DAA_39_81	rim	**903**	33.3	40.4	71.3	4.72E+05	0.044	0	14.64	0.065	1.22	2.59	1.23	6.85	1.39	9.83	2.47	7.09	1.102	8.09	1.191	9320	11.33	68.9	1.60638137	880.45
DAA_39_82	core	**923**	28.7	32.5	364	4.74E+05	0.153	0.137	37.6	1.24	14.1	13.2	5.3	29.9	6.17	47.7	12.84	45.2	9.27	84.9	13.37	10450	456	238	1.51188336	856.21
DAA_39_83	core	**912**	49.4	29.9	68.8	4.76E+05	0.048	0.0066	17.96	0.122	2.31	3.67	0.97	8.21	1.51	10.2	2.18	6.44	0.949	7.32	1.074	10030	41.9	75.5	1.47567119	847.19
DAA_39_84	core	**906**	40.2	37.6	44.84	4.81E+05	0.023	0.0017	11.42	0.043	1.35	1.64	1.27	5.25	0.949	6.75	1.48	3.88	0.604	3.96	0.534	9660	9.72	26.1	1.57518784	872.33
DAA_39_85	rim	**906.8**	30.7	25	562	4.75E+05	0.139	0.0053	32.01	0.215	3.77	5.59	1.37	22.2	5.95	60.5	19.32	75.9	16.64	138	23.8	8950	103.1	196.3	1.39794001	828.31
DAA_39_86	core	**884**	48.8	36.5	21.1	4.73E+05	0.081	0.0086	10.89	0.095	1.1	1.43	0.91	2.51	0.483	2.97	0.707	2.1	0.392	3.65	0.613	9220	32.1	59.7	1.56229286	869.01
DAA_39_87	core	**913**	13.7	31.7	472	4.83E+05	0.056	0.027	19.91	0.409	6.57	7.36	2.93	23.3	5.51	52.7	16.66	65.8	13.31	125.7	23.07	8040	33	38.4	1.50105926	853.50
DAA_39_88	core	**932**	41.4	71.4	923	4.72E+05	0.06	0.047	58.1	0.862	14.38	16.6	4.7	50.3	11.6	107.5	31.8	124.4	25.36	232.5	38.1	8400	96.3	90.9	1.85369821	849.09
DAA_39_89	core	**891**	12.3	33.5	772	4.73E+05	0.07	0.0052	30.51	0.27	6.59	9.86	3.54	33.2	8.49	83.1	27.08	104.4	22.88	208.3	34.9	9210	80.9	106.7	1.52504481	859.53
DAA_39_90	core	**916**	55.7	34.5	76.6	4.82E+05	0.031	0.0016	8.81	0.08	0.96	1.7	0.836	6.13	1.433	10.6	2.75	7.96	1.34	10.15	1.47	8900	2.91	10.55	1.5378191	862.76
DAA_39_91	core	**921**	48.5	40.6	55.4	4.80E+05	0.024	0.013	12.13	0.098	1.69	1.95	0.77	5.17	1.039	7.59	1.85	5.52	0.859	6.39	0.987	8260	41.6	80.5	1.60852603	881.01
DAA_39_92	rim	**886**	52	29.5	1718	4.76E+05	0.55	0.194	36.1	0.57	9.8	19.6	8.61	87.1	20.71	195.2	60.2	229.6	44.7	397	67.3	7540	221	147.7	1.46982202	845.75
DAA_39_93	rim	**878**	46.4	18.66	128	4.69E+05	0.021	0.0068	10.81	0.081	1.44	2.21	0.949	7.59	1.81	15.3	4.23	16.2	3.22	29.5	5.3	9370	15.1	52.7	1.27091166	798.79
DAA_39_94	core	**898.4**	52.7	36.8	47.83	4.74E+05	0.092	0.02	26.76	0.148	2.12	2.38	0.45	5.89	1.088	7.52	1.522	3.96	0.575	4.91	0.704	10300	321	122	1.56584782	869.93
DAA_39_95	core	**950**	60.3	43.2	55.5	4.70E+05	0.029	0.0115	8.66	0.078	1.36	2.15	1.28	5.03	1.036	7.59	1.83	5.42	0.932	7.04	1.13	8240	6.36	20.49	1.63548375	888.12
DAA_39_96	core	**945**	28.3	27.8	466	4.86E+05	0.058	0.017	17.3	0.325	4.64	6.33	2.44	20.9	5.15	49.9	15.4	64.2	13.22	130	22.1	7940	26.1	34.5	1.44404448	839.43
DAA_39_97	core	**932.8**	51.9	38.9	91.8	4.72E+05	0.007	0	10.44	0.052	1.21	2	0.809	6.41	1.5	12.7	3.12	9.78	1.72	12	1.66	9400	12.65	66.5	1.58994496	876.16
DAA_39_98	rim	**903**	466	31.3	513	4.74E+05	0.635	0.055	25.58	0.492	7.53	8.82	3.44	25.7	6.39	57.3	17.43	69.6	13.8	132.5	22.37	7880	41.55	45.9	1.49554434	852.12
DAA_39_99	rim	**927**	40	37.1	80	4.68E+05	0.026	0.0077	9.86	0.063	1.61	2.26	0.957	7.47	1.57	10.8	2.63	8.2	1.63	13.5	2.41	9460	8.8	35.6	1.56937391	870.83
DAA_39_102	core	**903.2**	298.9	38.9	554.1	4.62E+05	0.306	0.021	27.57	0.23	4.34	7.94	2.84	27.6	6.53	62.7	19.3	75.6	16.26	149.7	25.56	8560	51.16	66.1	1.5899496	876.16
DAA_39_103	core	**904**	83.8	24.5	418.2	4.77E+05	0.14	0.033	18	0.221	4.37	5.79	2.58	20.2	4.86	47.3	14.87	57.9	12.04	113.3	19.03	8410	32	37.5	1.38916608	826.22
DAA_39_104	core	**967**	51.1	39.9	144.5	4.70E+05	0.017	0.0071	5.96	0.09	1.34	1.77	1.15	7.05	1.69	12.18	4.93	17.94	3.52	29.1	4.37	7940	2.95	6.33	1.6009729	879.03
DAA_39_105	core	**915**	66.5	37.8	59.8	4.76E+05	0.037	0.0016	12.21	0.112	1.66	2.27	0.99	6.72	1.408	8.96	2.07	5.53	0.999	7.04	1.12	8650	8.46	22.42	1.5774918	872.93
DAA_39_106	core	**931**	73.3	33.9	48.7	4.72E+05	-0.001	0	6.29	0.061	0.92	1.51	0.74	6.12	1.08	7.22	1.63	4.77	0.742	5.03	0.619	9780	15.49	15.44	1.53019997	860.83
DAA_39_107	core	**930.5**	46.4	43	108.8	4.88E+05	0.062	-0.003012	9.61	0.087	1.62	2.93	1.4	9.08	2.05	16.18	3.25	9.12	1.254	8.96	1.08	9090	33.44	71.6	1.63346846	887.59
DAA_39_108	core	**1022**	0.9	25.96	724	4.72E+05	0.086	0.027	24.8	0.468	9.53	13.2	4.82	41.4	9.32	82.2	24.95	94.9	19.79	180.9	31	8080	50	50	1.41436069	822.23
DAA_39_109	core	**1019**	-0.6	32.5	534	4.78E+05	0.046	0.0116	15.95	0.164	3.17	5.13	2.66	22.8	5.76	58.7	18.02	72.6	15.39	144.5	24.42	8060	24.3	26.54	1.51188336	856.21
DAA_39_110	core	**918**	44.8	33.3	40.4	4.69E+05	0.027	-0.002194	8.29	0.067	1.15	1.7	1.36	5.35	0.878	6.34	1.29	3.51	0.568	4.45	0.736	8050	6.74	13.8	1.52244423	858.87
DAA_39_111	rim	**914**	22.8	33.6	150	4.68E+05	0.012	0.0074	13.08	0.135	2.22	2.98	1.38	8.9	2.17	18.3	4.95	19	4.3	39.6	6.7	9490	16.3	64	1.52633928	859.85
DAA_39_112	core	**877**	33	26.4	1433	4.72E+05	0.283	0.026	65	0.763	13.72	20.1	5.94	69.9	16.99	159.6	49.53	191.8	39.95	357	57.6	8760	196.9	196.5	1.42160393	833.99
DAA_39_113	rim	**885**	50.7	29.7	87.6	4.64E+05	0.015	0.0016	9.89	0.08	1.23	2.06	1.227	8.05	1.9	13.31	2.75	7.15	1.074	7.38	1.02	8980	37.2	83.2	1.47275645	846.47
DAA_39_114	core	**1044**	0.5	38.9	495.5	4.66E+05	0.114	-0.0034	24.01	0.175	3.05	5.18	1.76	18.39	5.35	51.4	16.55	68.1	15.01	145.6	25.04	8440	45.5	66.9	1.5899496	876.16
DAA_39_115	core	**892**	28.5	32	309.2	4.68E+05	0.088	0.0059	25.69	0.093	1.64	2.33	0.73	10.11	2.83	31.1	10.8	46.7	10.63	110.1	19.73	10000	28.47	56	1.50514998	854.52
DAA_39_116	core	**907.7**	42.8	32.3	91	4.66E+05	0.065	0.018	19.07	0.162	2.94	4.68	1.41	10.62	1.95	13.67	2.93	8.15	1.321	10.27	1.49	8880	66.4	139.5	1.50902052	855.54
DAA_39_117	rim	**934**	61.9	34.1	46.2	4.72E+05	0.026	0.0036	7.2	0.054	1.05	1.63	0.78	4.79	0.94	7.02	1.52	4.64	0.793	5.25	0.635	8140	6.06	20.14	1.51279658	861.48
DAA_39_118	core	**925.8**	40	30	686	4.64E+05	0.79	0.023	81.2	0.386	6.69	9.4	2.09	29.7	7.26	72.8	23.66	94.7	20.96	202.4	36	8700	114.7	165.2	1.47712125	847.55
DAA_39_119	core	**912**	74.2	34.8	56	4.59E+05	0.049	0.0064	8.18	0.047	0.78	1.35	0.87	4.48	1.113	8.02	1.89	4.62	0.734	5.67	0.712	8080	17.97	39.19	1.54157924	863.72
DAA_39_120	rim	**910**	70.2	37.8	54.1	4.54E+05	0.032	0.0018	10.29	0.103	1.52	2.15	1.05	6.13	1.114	7.6	1.69	4.83	0.916	7.35	1.124	8470	7.3	24.31	1.5774918	872.93
DAA_39_121	core	**891**	19	23.7	506	4.74E+05	0.092	0.0067	20.2	0.262	5.04	6.89	2.64	20.6	5.41	52.9	16.4	66.4	15.11	137.6	24.39	9030	46.6	95	1.37474835	822.80
DAA_39_122	core	**873**	38.4	17.91	256	4.74E+05	0.093	0	15.3	0.075	1.34	2.45	0.84	9.39	2.42	24.7	8.22	34.2	8.16	80	14.15	8980	23.7	55	1.25302557	794.77
DAA_39_123	core	**937**	43.3	40	59.8	4.67E+05	0.055	0.0031	9.37	0.08	1.33	2.25	1.22	6.26	1.27	8.59	2.04	5.82	1.07	8.3	1.33	8410	5.09	15.31	1.60205999	879.32
DAA_39_124	rim	**913**	46.8	25.7	83.4	4.65E+05	0.041	0.0129	10.09	0.072	1.67	1.8	1.4	6.42	1.42	11.33	2.63	8.88	1.59	13.8	2.31	8500	6.75	20.9	1.40993312	831.18
DAA_39_125	rim	**966**	4	37.1	428	4.66E+05	0.057	-0.002157	17.66	0.034	0.61	1.51	0.64	7.51	2.76	34.2	13.71	63.2	15.4	151	26.5	9190	36.8	152.5	1.56937391	870.83
DAA_39_126	core	**880**	17.2	21.17	874	4.65E+05	0.261	0	63.1	0.114	2.4	5.38	0.95	25.4	7.41	85.5	29.12	124.5	27.57	250.1	41.2	10570	177.9	336	1.32572096	811.33
DAA_39_127	core	**899**	1530	108	630	4.61E+05	11	0.083	24	0.71	9.08	9.57	4.02	33.8	7.61	70.3	21.85	82.5	17.74	165.5	27.95	7720	55.5	57.4	2.03342376	1004.33
DAA_39_128	rim	**894**	69.1	40.8	109.7	4.64E+05	0.208	0.007	7.49	0.041	1.05	2.1	0.905	7.8	1.74	13.82	3.75	10.69	1.575	12.13	1.93	8540	24	45.8	1.61066016	881.57
DAA_39_129	rim	**941**	17.1	28.6	551	4.70E+05	0.09	0	27.51	0.109	2.85	5.31	1.84	18.7	5.15	53.8	18.75	78.3	17.57	171.1	30.81	8750	58.9	111.4	1.45636603	842.44
DAA_39_130	core	**912**	31.5	22.04	327.4	4.66E+05	0.098	0.0101	22.85	0.169	2.8	3.91	1.83	14.61	3.69	35.7	11.2	44.3	9.46	95	16.35	7960	26.65	40.6	1.34321159	815.39
DAA_39_131	core	**927.6**	54.3	41.2	323.7	4.62E+05	-0.016	0	11.22	0.071	1.03	1.29	0.595	3.58	0.753	4.45	1.006	2.94	0.527	3.38	0.56	8290	25.44	51.4	1.61489722	882.68
DAA_39_132	rim	**898**	28.3	38.3	64.9	4.53E+05	0.022	0	11.64	0.053	0.73	1.34	0.84	4.99	1	8.56	2.09	6.85	1.013	9.09	1.32	9400	11.54	47	1.58319877	874.41
DAA_39_133	core	**866**	32.9	24.5	316	4.68E+05	0.076	0.0106	21.71	0.087	1.81	2.2	1.03	9.48	2.53	28.4	10.62	46.5	10	99.8	17.9	8970	39.9	53.7	1.38916608	826.22
DAA_39_134	core	**1027**	2.3	29.6	678	4.58E+05	0.094	0.0175	22.33	0.489	7.4	8.61	3.39	30.2	7.39	73.8	22.34	90	19.08	177.4	30.34	8260	57.7	73.7	1.47129171	846.11
DAA_39_135	core	**832**	41	22.6	1382	4.85E+05	0.64	0.034	68.5	0.244	3.71	8.35	1.82	40.5	12.27	137.2	47.9	204.6	43.6	408	68.2	10720	254	515	1.35410844	817.94
DAA_39_136	rim	**863**	52.9	28.4	70.8	4.63E+05	0.079	0.088	9.33	0.082	1.47	2.19	1.06	6.14	1.3	10.05	2.38	6.88	1.15	10.11	1.7	9020	8.32	28.96	1.45331834	841.70
DAA_39_137	core	**897.2**	13.5	32	831	4.73E+05	0.147	0.0074	43.8	0.144	2.23	5.14	1.84	27.3	7.87	86	28.47	117.3	24.45	229.1	37.41	9150	289.2	491.9	1.50514998	854.52
DAA_39_138	core	**1036**	2.5	36.4	807	4.73E+05	0.083	0.0101	24.03	0.177	3.37	6.79	2.41	30.2	7.93	82	27.37	112.5	23.33	226.2	38.16	9110	50.6	61.4	1.56110138	868.71
DAA_39_139	rim	**932**	80.3	37.8	44.5	4.62E+05	0.038	0.0102	8.6	0.075	0.93	1.31	0.551	3.63	0.77	5.38	1.41	4.59	0.75	5.9	0.914	8440	8.22	36.8	1.5774918	872.93
DAA_39_140	core	**1014.1**	0.9	41.2	1103	4.74E+05	0.08	0.077	28.18	0.657	10.09	13.49	5.49	50.6	12.51	117.1	38.06	145	30.34	278.5	48.9	8370	110.2	117.5	1.61489722	882.68
DAA_39_141	core	**932**	3.6	37.8	462	4.69E+05	0.06	0	23.45	0.2	3.46	5.01	2.06	19.21	4.76	46.7	15.51	63.5	13.94	128.7	23.6	8370	48.79	67.4	1.5774918	872.93
DAA_39_142	rim	**872**	48.5	24.8	87.2	4.69E+05	0.048	0	16.35	0.176	2.53	3.93	1.63	9.93	1.69	12.66	3.04	9.59	1.77	14.3	2.73	9340	16.12	78.2	1.39445168	827.48
DAA_39_143	core	**934**	78.1	43.5	98.3	4.66E+05	0.019	0.0016	7.47	0.062	1.37	1.88	1.11	7.11	1.5	12.48	3.27	10.28	1.58	12.43	1.83	9050	12.29	25.19	1.63848926	888.92
DAA_39_144	rim	**964**	68.9	33.3	72.1	4.76E+05	0.039	0	8.7	0.111	1.42	2.05	0.658	6.15	1.36	9.88	2.42	8	1.27	9.83	1.36	9370	6.63	14.08	1.52244423	858.87
DAA_39_145	core	**987**	28.1	37.4	385.6	4.90E+05	0.125	0.033	29.26	0.553	8.28	11.58	4.74	32	6.12	46.9	12.16	39.6	6.5	49.3	7.56	8410	89.7	154	1.5728716	871.73
DAA_39_146	core	**880**	66.9	36.8	48.1	4.77E+05	0.029	0	9.55	0.068	1.08	1.59	0.538	3.96	0.928	6.29	1.56	4.95	0.768	6.48	1.007	8580	15.75	32.49	1.56584782	869.93
DAA_39_147	core	**993**	0.2	30.5	711	4.90E+05	0.1	0.048	29.73	0.531	9.24	11.5	3.85	36	8.35	78.2	24.6	94.4	19.59	175.6	32.5	8810	50.1	54.4	1.48429984	849.33
DAA_39_148	rim	**905**	78.6	34	54.2	4.49E+05	0.168	0.012	10.14	0.083	1.5	2.31	0.83	5.45	1	7.72	1.69	4.68	0.86	5.82	1	8740	7.77	22.6	1.53147892	861.15
DAA_39_149	core	**909.8**	44.7	40.4	57.4	4.70E+05	0.03	0	17.06	0.14	2.88	4.57	1.74	9.88	1.49	9.57	1.92	5.53	0.864	6.78	1.026	9170	20.36	106.8	1.60638137	880.45
DAA_39_150	core	**884.9**	76.1	35.4	197	4.58E+05	0.308	-0.00296	22.2	0.085	1.92	2.6	0.99	9.2	2.16	21.6	6.64	28.5	5.63	56.7	10.4	8980	27.8	96	1.54900326	865.61
DAA_39_151	core	**882**	17.6	29.5	933	4.92E+05	0.239	-0.00592	49.2	0.099	2.02	5.79	1.17	25	8.18	86.4	31.9	133	29.8	278.6	45.6	10930	135.2	333	1.46982202	845.75
DAA_39_152	core	**932**	10.2	29.2	943	4.68E+05	0.138	0.017	41.3	0.426	7.05	10.49	3.4	38	9.6	98	31.4	127.9	27.26	260.1	44.2	8990	143.1	240	1.46538285	844.66
DAA_39_153	core	**929**	6.9	31.1	476	4.64E+05	0.062	0.011	25.6	0.12	1.91	4.59	1.34	15.7	4.7	46.9	15.86	69.2	14.59	143.1	26.53	8520	47.9	77.6	1.49276093	851.43
DAA_39_154	core	**929**	67	39.1	52.5	4.63E+05	-0.007	0.017	9.82	0.063	0.91	1.56	0.51	5.27	0.907	6.92	1.8	5.45	0.9	6.74	1.13	7890	15.77	30.6	1.59217676	876.74
DAA_39_155	core	**910**	44	36.1	38.6	4.62E+05	0.072	0.0015	16.6	0.15	2.53	2.8	0.575	4.7	0.83	5.05	1.21	3.6	0.603	4.98	0.788	10130	62.4	21.6	1.5575072	867.78
DAA_39_156	rim	**912**	82.1	38.1	41	4.56E+05	0.064	-0.002904	6.27	0.06	0.87	1.28	0.66	4.43	0.816	5.21	1.41	3.9	0.552	4.39	0.754	8570	3.72	10.97	1.58092498	873.82
DAA_39_157	rim	**897**	55.3	44.1	68.5	4.68E+05	0.043	0.0076	9.99	0.095	1.96	1.5	7.82	1.58	10.35	2.47	6.35	0.983	8.11	1.11	9360	7.46	43.96	1.64443859	890.50
DAA_39_158	core	**910**	670	33.6	1470	4.56E+05	2.9	0.046	61.9	0.324	5.61	10.65	2.72	46.1	13.69	145.9	45.9	205	45.8	435	72.4	9860	316	592	1.52633928	859.85
DAA_39_159	core	**962**	688	37.8	54.6	4.60E+05	1.52	0.0092	7.67	0.076	0.94	1.27	0.498	4.47	0.933	6.62	1.81	6.33	1.132	8.79	1.42	10020	13.82	25.27	1.5774918	872.93
DAA_39_160	core	**946**	45.3	43.1	118.3	4.69E+05	0.021	0.0114	10.71	0.082	2.25	3.44	1.24	10.9	2.33	16.29	3.91	12.01	1.86	14.21	1.91	8970	10.96	18.37	1.63447727	887.85
DAA_39_161	core	**965**	2.4	25.4	644	4.77E+05	0.121	0.0149	35.8	0.188	3.6	5.79	1.8	23.4	6.07	65	21.41	91.6	19.64	201.2	34.6	8550	67.7	112.1	1.40483372	829.96
DAA_39_162	rim	**894**	30.1	36.7	85.1	4.81E+05	0.063	0.0113	15.42	0.152	2.32	3.96	1.55	10.58	1.99	13.48	3	8.19	1.286	9.34	1.3	9500	62.5	197	1.56466606	869.62
DAA_39_163	rim	**916**	43.1	34.2	82.1	4.72E+05	0.056	0.01	15.38	0.109	1.97	2.9	1.15	8.79	1.68	11.98	2.7	8.03	1.3	9.53	1.6	9240	44.2	100	1.53402611	861.80
DAA_39_164	core	**906**	56.7	21.5	63.3	4.60E+05	0.037	0.0022	12.09	0.086	1.39	2.5	0.979	6.37	1.336	9.27	1.95	5.68	0.997	7.06	0.935	8970	1.183	6.16	1.33243846	812.89
DAA_39_165	core	**903**	30	22.9	339.1	4.81E+05	0.064	0.024	19.89	0.182	2.89	4.5	1.91	16.8	3.89	35.7	11.37	46.1	9.4	90.5	15.6	8020	22.77	23.92	1.35983548	819.28
DAA_39_166	core	**952**	60	34.4	80.8	4.61E+05	0.029	0.0105	10.63	0.089	1.92	2.8	1.39	8.43	1.56	11.07	2.7	8.14	1.313	9.19	1.27	8550	7.2	19.62	1.53655844	862.44
DAA_39_167	core	**922**	20.8	40.5	119.1	4.64E+05	0.029	0.026	10.58	0.058	1.08	1.86	3.45	1.8	10.84	2.22	17.24	4.13	11.65	53	1.97	14.08	1.97	9560	7.62	43	1.60745502	880.73
DAA_39_168	core	**987**	-2.6	38.6	405.6	4.71E+05	0.018	0	17.72	0.137	2.16	3.28	1.54	13.07	3.66	40.1	13.34	55.3	12.48	126.6	21.83	8870	25.89	48.2	1.5865873	875.28
DAA_39_169	core	**911**	46.3	38.1	55	4.89E+05	0.033	0.0077	12.95	0.068	1.09	1.89	1.25	5.75	1.18	8.66	1.74	5.09	0.799	5.07	0.652	9100	9.02	22.97	1.58092498	873.82
DAA_39_170	rim	**908**	44.4	32.6	44.3	4.78E+05	0.024	0.0017	10.54	0.057	1.1	1.97	2.2	5.2	0.861	6.21	1.46	4.78	0.81	6.4	1.21	8330	13.21	37.18	1.5132176	856.55
DAA_39_171	rim	**887.4**	57	30.6	70.7	4.74E+05	0.039	0.0061	11.2	0.085	1.41	2.18	1.06	6.88	1.23	9.74	2.42	6.73	1.19	8.56	1.24	9100	14.66	44.9	1.48572145	849.68
DAA_39_172	core	**931**	29.1	39.8	85.8	4.69E+05	0.02	0.0121	9.64	0.074	1.21	1.74	1.35	6.5	1.41	10.19	2.71	8.68	1.4	9.69	1.24	9060	11.8	33.8	1.59988307	878.75
DAA_39_173	core	**928**	48.5	31.5	166	4.74E+05	0.062	0.0103	14.37	0.098	1.69	2.68	1.22	9.86	2.07	19.6	5.53	20	3.56	35.2	6.1	8840	14.1	36.8	1.49831055	852.81
DAA_39_174	core	**1079**	2.3	37.1	518	4.70E+05	0.048	0.014	19.67	0.214	4.48	7.71	3.3	25.4	6.11	58.9	17.51	68.3	14.07	132.1	22.66	8230	31.79	34.4	1.56937391	870.83
DAA_39_175	rim	**939**	46.4	36.3	86	4.69E+05	0.054	0.0049	16.19	0.143	2.46	3.55	1.66	9.53	1.79	12.72	2.74	8.59	1.344	10.4	1.45	8670	16.45	40.5	1.55990663	868.40
DAA_39_176	core	**916**	82.9	35.8	21.2	4.65E+05	0.038	0	8.74	0.035	0.66	0.92	0.82	2.36	0.389	2.94	0.664	1.72	0.292	1.95	0.275	8520	8.14	19.47	1.55388203	866.86
DAA_39_177	core	**941**	53.8	39.8	57.2	4.77E+05	0.043	0.0031	12.29	0.09	1.41	2.13	0.653	5.12

MPR_33A_67	core	**266.1**	15	4.15	1555	4.66E+05	0.25	0.013	23.8	0.117	2.51	5.09	1.24	30.8	10.94	131.9	51.5	249	57.2	573	111.9	9070	255.4	305	0.6180481	668.99
MPR_33A_5	core	**271.6**	9.6	4.39	1900	4.85E+05	0.096	0.046	21.7	0.13	1.9	5.26	1.27	29.7	11.58	153.6	62.7	307.2	72.8	754	143.9	9850	309	610	0.6424645	673.28
MPR_33A_7	core	**280**	1.4	4.4	1950	5.13E+05	0.15	0.051	23.25	0.42	7.8	10.7	3.28	46.4	15.97	193.6	65.2	309	72.2	711	137.8	8620	338	319	0.64345268	673.45
MPR_33A_71	rim	**302.1**	-1.6	4.43	528	4.82E+05	0.073	0	10.1	0.037	0.57	1.41	0.39	9.82	3.25	42.9	17.46	86.9	21.3	214.3	43	9090	84.6	127	0.64640373	673.98
MPR_33A_61	rim	**292.3**	4.7	4.45	737	4.80E+05	0.048	0.009	7.02	0.031	0.81	2.32	0.83	13.7	4.96	59.1	24.42	117.7	27.48	286.1	56.1	8280	65.5	136.7	0.64836001	674.32
MPR_33A_26	rim	**285.8**	3.3	4.52	1381	4.84E+05	0.191	0.012	38.6	0.102	1.85	4.97	1.5	28.8	9.81	124.2	47.5	218.1	50.9	500	94.5	9590	441.4	304.9	0.65513843	675.52
MPR_33A_40	core	**268.6**	-1.4	4.53	1934	4.84E+05	0.082	0.0088	25.1	0.099	1.95	4.57	1.17	33.2	12.66	162.1	65.6	311.9	71.4	713	133.4	9070	570	582	0.6560982	675.69
MPR_33A_34	core	**267.6**	3.5	4.55	1056	4.82E+05	0.056	0.016	10.63	0.1	1.72	3.23	0.94	18.5	6.55	85	35.5	174.2	44.5	475	93.6	10350	140.4	304	0.6580114	676.03
MPR_33A_105	core	**278.4**	6.6	4.6	1496	4.83E+05	0.31	8	22	1.9	12.8	9.3	1.41	34.4	11.29	137.3	51.4	241	54.8	538	99.9	8710	149.4	247.4	0.66275783	676.87
MPR_33A_107	core	**256.9**	4.5	4.64	1821	4.73E+05	0.28	0.014	23.8	0.098	1.75	4.04	0.92	31.2	11.91	154.2	63.3	284	66.6	631	123.9	9560	584	518	0.66651798	677.54
MPR_33A_89	rim	**290.3**	6.4	4.66	834	4.74E+05	0.131	0.006	18.18	0.047	0.66	1.92	0.381	12.7	5.03	65.1	26.8	131.2	32	331	63.2	9940	151.7	268.5	0.66838592	677.87
MPR_33A_25	core	**276.6**	17	4.68	4210	4.79E+05	0.075	0.026	12.55	0.149	2.18	7.11	0.87	56.5	23.84	339.7	139.7	665	155.3	1536	278.2	10270	651	1267	0.67024585	678.20
MPR_33A_99	core	**274.7**	0.7	4.91	1646	4.81E+05	0.104	0.069	29.7	0.114	1.93	3.82	0.94	26.3	9.87	129.4	53.1	266	64.5	662	129.1	9130	279	367	0.69108149	681.93
MPR_33A_93	core	**265.8**	45	5.2	1280	4.85E+05	0.173	0.051	10.01	0.277	5.23	7.51	2.3	35.5	10.5	121.4	43.2	197.7	43.3	418	77.6	8050	113.9	145.4	0.71600334	686.43
MPR_33A_22	rim	**245**	11.1	5.3	744	4.66E+05	0.14	0.08	14.46	0.005	0.52	1.73	0.56	12.2	4.2	58.3	24.7	120.4	29.5	291	58.2	9550	139.2	216	0.72427587	687.93
MPR_33A_41	core	**252.1**	12.5	5.3	2670	4.45E+05	0.58	0.019	59.9	0.177	2.53	7.02	0.49	48.9	19.1	237	93.1	430	99.8	923	169.7	12670	1590	1940	0.72427587	687.93
MPR_33A_96	rim	**278.6**	5.3	5.3	1041	4.82E+05	0.221	1.14	34.6	2.03	14.9	11.3	1.03	29.3	8.79	98.6	34.9	160.3	37	359	64.9	9150	204.3	262.9	0.72427587	687.93
MPR_33A_74	core	**280.4**	6.1	5.37	1256	5.06E+05	0.09	0.012	15.3	0.15	2.42	4.92	1.49	26	8.57	107.8	42.2	193	47.4	481	93.4	8640	172	194.1	0.72997429	688.97
MPR_33A_6	rim	**286.5**	15.3	5.5	592	4.85E+05	0.186	0.014	10.6	0.065	0.58	2.2	0.567	10.17	3.74	47.6	20.33	95.7	22.68	231.6	46.6	8740	109.7	138.2	0.74036269	690.86
MPR_33A_101	core	**543**	37	5.5	848	4.60E+05	0.26	0.02	10.37	0.046	0.84	1.82	0.099	12.5	5	68.6	27.8	136.4	34.4	346	66	14490	273	1540	0.74036269	690.86
MPR_33A_47	rim	**275.7**	10.8	5.56	2163	4.70E+05	0.117	0.179	16.24	0.493	8.28	13.1	3.5	63.9	19.91	214.9	77.4	331.2	72.2	641	120.1	8270	223.2	255.6	0.74507479	691.73
MPR_33A_37	core	**272.8**	178	5.81	4300	4.76E+05	1.15	0.094	39.2	0.89	16.4	28.3	3.79	131.1	40.3	443	156.5	644	131.6	1212	212.6	7680	665	635	0.76417613	695.24
MPR_33A_75	rim	**267**	1.3	5.89	1132	4.80E+05	0.135	0.002	26.84	0.097	1.96	3.68	1.42	23.5	7.93	98.4	37.3	176.3	41.5	408.8	81.1	8830	460	328.8	0.77011529	696.34
MPR_33A_30	rim	**277.8**	3.9	5.92	1197	4.76E+05	0.026	0	12.24	0.028	0.65	1.78	0.531	13.25	6.09	88.7	40	213	55.7	616	123.1	12030	161.5	536	0.77232171	696.75
MPR_33A_42	core	**263.9**	53	5.99	2580	4.77E+05	0.58	7.8	83	5.8	29	27	2.68	75	23.9	262	90	389	88.7	841	156	8560	553	307	0.77742682	697.69
MPR_33A_78	rim	**302.6**	4.3	6.02	1196	4.87E+05	0.086	-0.0027	15.52	0.083	1.25	2.96	0.83	18.5	7.01	94.6	39.46	198.1	48.6	504	100.6	8770	131.1	235	0.77959649	698.09
MPR_33A_100	core	**271.1**	31	6.14	2760	4.77E+05	2.2	0.049	19.5	0.365	6.74	13	2.91	70.9	23.3	273	98.4	430	91.6	857	154.1	8300	335	398	0.78816837	699.69
MPR_33A_46	rim	**265.8**	17	6.3	1326	4.81E+05	0.29	0.018	29.7	0.08	2.38	4.27	1.05	25.7	8.65	114.7	44.2	212.8	49.6	484	95.3	9460	488	436	0.79934055	701.77
MPR_33A_82	core	**281.1**	4	6.3	2607	5.01E+05	0.16	0.054	32.8	0.672	8.6	15.1	4.86	70	22.33	246	90.5	410	92.3	895	167.2	8690	473	356	0.79934055	701.77
MPR_33A_24	core	**290.4**	3.1	6.51	1259	4.78E+05	0.098	0.012	14.5	0.096	1.57	4.06	1.44	24.7	8.12	106.6	43.2	201	48.7	496	98.7	8160	154	181	0.81358099	704.45
MPR_33A_81	core	**280**	-0.9	6.61	1303	4.81E+05	0.072	0	16.9	0.083	1.77	3.23	1.12	22.5	7.91	103.4	43	212	51	522	103	8250	160	193	0.82020146	705.69
MPR_33A_84	core	**276.8**	2.1	6.75	1712	4.76E+05	0.076	0.0066	15.94	0.102	2.33	4.87	1.43	31.1	11.19	143.3	57.6	274	62.2	604	112	7970	202.9	293.4	0.82930377	707.41
MPR_33A_9	core	**276.1**	1.4	6.86	1990	4.77E+05	0.086	0.0046	28.5	0.151	2.72	5.9	1.57	35.3	13.2	168	67	322	76	770	154	7630	415	395	0.83632412	708.74
MPR_33A_77	core	**273.7**	-0.5	6.87	1517	4.45E+05	0.16	0.017	20.01	0.128	2.58	4.93	1.69	31	10.61	129	50.8	244.3	55.7	561	105.3	7820	235	229.8	0.83695074	708.86
MPR_33A_98	rim	**274.6**	60.8	6.94	1339	4.79E+05	0.284	0.032	22.27	0.063	1.84	3.37	1.11	22.3	8.3	109.3	43.72	209.5	50	497	96.4	8510	339.7	336.1	0.84135947	709.70
MPR_33A_31	core	**283.9**	30	7.1	2130	4.97E+05	0.5	0.025	37.6	0.217	4.72	8	2.43	44.4	14.3	181	72.4	338	84.9	898	167	9220	446	447	0.85125835	711.59
MPR_33A_36	core	**273.5**	26	7.1	2261	4.83E+05	1.51	135	310	35	152	40	2.68	71.7	19	211	76.3	346	79.3	748	144.1	10190	482	595	0.85125835	711.59
MPR_33A_19	core	**270.1**	27.6	7.11	2283	4.95E+05	0.257	0.204	24.57	0.697	9.05	13.9	3.42	54.9	18.14	216.7	77.5	355	82.6	831	150.7	8200	361	328.3	0.85186896	711.70
MPR_33A_103	core	**270.4**	12.6	7.28	3460	4.76E+05	0.241	0.076	61.1	0.499	8.29	16	3.68	77.6	24.5	295	113.7	531	124.6	1268	246.1	7910	1116	904	0.86213138	713.67
MPR_33A_97	core	**275.4**	20.1	7.36	2565	4.93E+05	0.215	0.047	28.5	0.211	3.24	7.49	2.2	51.3	18.2	233	90.1	412	91.6	857	156.5	8320	467	495	0.86687781	714.58
MPR_33A_65	core	**271.9**	15.2	7.5	2184	4.94E+05	0.19	0.031	27.4	0.111	2.59	6.28	1.68	38.2	14.93	181.5	73.2	347.1	81.2	799	151.1	8590	1122	951	0.87506126	716.15
MPR_33A_44	rim	**269.4**	29	7.6	1751	4.94E+05	0.149	0.013	21.2	0.074	1.5	3.88	1.11	25.7	9.59	133.6	57.2	290.5	69.5	718	143.5	9490	226	379.4	0.88081359	717.26
MPR_33A_11	core	**288.3**	1.3	7.68	1268	4.87E+05	0.018	0.033	13.73	0.101	2.14	4.36	1.42	24.3	8.33	104.8	42.6	203	48.5	504	103.2	7690	162	182.4	0.88536122	718.14
MPR_33A_13	core	**263**	4	8.27	1055	4.86E+05	0.121	0.056	22.28	0.122	2.15	4.11	1.23	20.9	7.28	91.3	35.74	166.4	38.2	387	73.4	8640	336.9	284.6	0.91750551	724.40
MPR_33A_28	core	**279.9**	2.5	8.29	1239	4.89E+05	0.075	0.0116	15.37	0.083	1.45	2.35	1.19	20	7.28	99.3	41.5	198	47.9	489	98.2	7650	120.2	146.3	0.91855453	724.60
MPR_33A_12	rim	**276**	-0.2	8.37	1812	4.78E+05	0.059	0	30.3	0.097	2.2	4.12	1.32	29.9	11.32	149.9	61.4	288.1	68.3	684	132.3	8570	362	367	0.92272546	725.42
MPR_33A_10	rim	**273.1**	0.1	8.4	1723	4.86E+05	0.096	0.0129	22.82	0.082	1.87	4.52	1.46	26.2	10.6	139.2	57.4	275.9	66.7	675	132.2	8440	263.7	309.4	0.92422929	725.73
MPR_33A_86	core	**981**	8.4	8.7	607	4.84E+05	0.084	0.027	8.79	0.058	0.92	2.43	0.144	12.1	4.62	55.5	21.4	93.2	21.1	205	35.9	11690	103	288	0.93951925	728.73
MPR_33A_57	core	**277.5**	-1.1	9.5	2168	4.96E+05	0.061	0.026	26.7	0.205	3.22	6.66	2.13	37.3	13.29	174.8	70.9	338.1	77.8	774	149.6	7790	295	303	0.97772361	736.33
MPR_33A_18	rim	**287.1**	4.7	9.6	2313	5.03E+05	0.118	0.012	38.6	0.113	2.54	5.26	1.81	39.8	14.6	190.1	77.6	364	85.4	925	162.4	8950	626	747	0.98227123	737.25
MPR_33A_108	core	**280.8**	0.7	9.8	1758	4.81E+05	0.1	0.02	24.48	0.115	2.16	4.71	1.65	29.5	10.61	144.6	57.5	278.5	65.8	669	133	8020	231.6	254	0.99122608	739.05
MPR_33A_88	core	**274.6**	34.2	10.4	4050	4.88E+05	0.317	0.035	61.8	0.274	4.36	10.7	5.45	65.9	22.9	316	128.5	617	149	1514	304	9130	1625	1299	1.01703334	744.28
MPR_33A_33	core	**280.6**	360	11.6	1551	4.69E+05	5.9	4.2	31.6	1.15	7.5	6	1.89	31.5	10.43	130.8	52.4	248.7	60.6	615	122.5	9440	240	265	1.06445799	754.04
MPR_33A_51	rim	**269.4**	433	17.7	1911	4.71E+05	3.51	0.063	19.07	0.185	3.69	7.8	1.34	40.9	14.48	171.3	65.4	290.4	64.4	607	109.4	8520	287.9	446	1.24797327	793.62
MPR_33A_8	core	**549**	37.4	29.5	1880	4.78E+05	0.054	0.027	14	0.204	3.8	7.49	2.54	48.2	15.8	185	67	292	65.2	676	102	9970	53.4	33.1	1.46982202	845.75
MPR_33A_60	rim	**263.4**	412	32.6	1902	4.72E+05	0.36	0.019	20.4	0.116	1.7	5.19	0.2884	34.6	12.64	163.8	65.8	303	70.7	681	123.2	11660	436	764	1.51321765	856.55
MPR_33A_52	core	**256.5**	1880	67	1701	4.40E+05	16	0.121	15.43	0.081	1.6	3.67	0.29	27	10.6	138.9	57	256.8	60.4	576	112.3	10430	342	685	1.8260748	941.02
MPR_33A_73	core	**238.9**	2360	74	1422	4.74E+05	14.6	0.023	32	0.118	2.54	4.4	1.83	26.5	9.52	121.9	47.1	218.3	52.8	505	100.5	8530	594	393	1.86923172	953.68
MPR_33A_70	core	**236**	4.18E+04	1480	1660	2.91E+05	170	0.4	44.8	0.93	9.9	14.7	1.69	54.9	15.3	163	55.7	242	53.1	485	97.1	6130	6.30E+03	2080	3.17026172	1515.75
MPR_33A_76	rim	**252.7**	9.99E+03	307	1082	4.17E+05	57.7	0.226	15.02	0.224	2.43	4.41	1.35	21	7.44	92.9	36.3	176.2	41.7	412	82.2	7750	170.6	256.2	2.48713838	1168.86
MPR_33A_92	rim	**261**	184	8.79	1508	4.72E+05	0.145	0.1	15.75	0.066	1.18	3.84	0.382	24.2	9.14	123.9	48.4	239.9	56.4	556	106.1	10420	171	377	0.94398688	729.61
MPR_33A_94	core	**286.8**	6680	29.1	1318	4.19E+05	96.9	0.129	9.83	0.125	2.21	4.79	1.24	27.2	9.28	113.8	43.8	210.4	46.4	465	89.2	6900	151.3	225	1.46389299	844.29
MPR_33A_95	rim	**273.2**	634	16	1125	4.77E+05	1.05	0.132	18.6	0.068	1.45	3.28	0.63	19.1	7.29	92.6	36.8	178.1	40.6	402	76.5	9540	194.6	320	1.20411998	783.89
MPR_33A_106	rim	**247.2**	812	18	909	4.77E+05	28.3	0.245	12.18	0.111	1.18	3.05	0.84	17.9	6.54	81.2	32.1	148.8	35.4	364	66.5	9250	257	303	1.25527251	795.26
MPR_33A_54	core	**262.7**	202	31.3	4120	4.68E+05	0.73	0.68	4.83	0.254	1.95	4.17	0.215	37	19.3	296	129	658	158	1630	304	12310	198	960	1.49556434	852.12
MPR_33A_62	core	**239**	7.2	5.42	1653	4.77E+05	0.193	0.088	13.11	0.499	8.28	11.81	3.84	50.9	14.64	160.1	57.2	259.1	56.1	543	104.4	7530	191	212.8	0.73399929	689.70
MPR_33A_59	rim	**237**	142	4.4	1538	4.99E+05	0.79	0.098	11.47	0.036	0.7	1.48	0.31	13.9	6.59	96.1	46	256	66.6	733	170.3	14030	156	716	0.64345268	673.45
MPR_33A_16	core	**228**	3750	15.6	5200	4.36E+05	16	8.9	25.6	3.8	22.6	13.9	1.67	61	26.7	394	168	830	202	2030	384	11750	690	1675	1.1931246	781.48
GLV-11																										
GLV_11_1	rim	**284**	63	14.7	752	4.85E+05	0.339		10.39	0.145		4.42	0.354	21.1	6.75	75	28.43	116.3	23.58	219.1	36.92	10740	104.8	84.3	1.16731733	775.86
GLV_11_2	core	**302.9**	17.9	21.1	638	5.12E+05	0.002		5.61	0.057		3.57	0.447	20.2	5.62	64.2	23.42	98.1	20.7	191.8	32.3	10370	49.8	39.1	1.32428246	831.00
GLV_11_3	core	**463.3**	16	8.45	3321	5.02E+05	0.129		20.77	0.565		19.2	0.111	108.5	35.1	375	126.5	480	88.4	719	107	8500	381	509.1	0.92685671	726.23
GLV_11_4	rim	**522.9**	9.4	6.56	1265	4.96E+05	0.09		17.31	0.145		6.85	0.051	38.8	12.61	138.8	47.8	188.8	37	311	47.2	8860	147.2	263.9	0.81690384	705.07
GLV_11_5	core	**524.9**	1.1	28.6	1191	4.94E+05	0.007		7.24	0.074		3.88	0.452	26.3	9.2	112.4	42.7	178.8	37.84	340.4	57.3	8590	49.5	105.1	1.45636603	842.44
GLV_11_6	rim	**533.5**	48.2	34	519	4.97E+05	0.052		3.62	0.029		3.4	1.32	15.3	4.68	54.4	18.5	78.6	17.5	166.9	27.6	8770	0.362	8.25	1.51147892	863.15
GLV_11_7	rim	**572.6**	45.8	7.5	843	4.65E+05	1.92		206	23.6		23.3	3.63	33.5	8.5	79.3	28.4	126	26.6	276	53.6	8970	77.7	95.3	0.87506126	716.15
GLV_11_8	core	**584.6**	38.6	9.3	1744	5.11E+05	0.29		6.36	0.065		3.81	0.9	33.6	12.55	157.1	59.3	281	64.2	630	112.5	11770	93.4	558	0.96848295	734.48
GLV_11_9	core	**655.6**	5.3	7.82	951	4.86E+05	-0.018		2.77	0.064		3.01	0.177	21.4	7.35	90.3	34.3	149	32.01	290.7	52.3	10110	52.8	176.4	0.89320675	719.66
GLV_11_10	rim	**908**	8.9	9.41	1065	4.89E+05	0.013		3.63	0.082		3.39	0.184	22.9	8.04	99.4	38.44	166.4	35.6	327.5	57.9	10460	68.7	234.1	0.97358962	735.50
GLV_11_11	rim	**965**	-3.1	3.64	461	4.82E+05	0.013		10.83	0.0118		1.17	0.231	6.03	2.65	35.3	15.17	75.7	19.1	194.6	38.93	11490	60.9	119.9	0.56110138	659.15
GLV_11_12	core	**1088**	-1	7	1520	5.03E+05	0.078		18.2	0.033		2.6	0.25	20.6	8.91	132	53	258	60.6	564	97.9	12860	186	510	0.84509804	710.41
GLV_11_13	rim	**1151**	25	4.49	2671	4.95E+05	0.076		5.86	0.0177		3	0.43	26.9	14.88	213.4	92.7	449.5	111.8	1082	196.6	13290	81.1	385.2	0.65224634	675.01
GLV_11_14	core	**1168**	16.9	6.43	812	4.94E+05	0.2		23.54	0.074		4.15	0.277	19.3	6.61	81.5	28.9	128.6	27.2	258	45.4	11050	172	249	0.80821097	703.44
GLV_11_15	rim	**1203**	6.1	5.9	1144	4.77E+05	0.29		44.6	0.077		2.9	0.43	21	7.6	100.1	40.6	189	42.5	425	77.6	11730	188.2	224.7	0.77085208	696.47
GLV_11_16	core	**1514**	1.1	15	891	4.86E+05	0.016		10.77	0.056		2.36	0.368	17.3	6.11	76.9	30.4	141.5	32.8	317	55.6	12280	89.8	329	1.17609126	777.76
GLV_11_17	rim	**1537**	70	36.2	174.3	4.89E+05	0.273		17.72	0.199		4.89	0.621	15.3	3.21	25.5	6.27	20.14	3.26	29.1	4.87	11590	14.55	55.1	1.55870857	868.09
GLV_11_18	rim	**1558**	713	15.7	1054	4.54E+05	2.83		19.6	0.149		3.28	0.4	20.2	7.3	93	36.5	165.3	36.9	325	57.9	10660	239	549	1.19589965	782.08
GLV_11_19	core	**1720**	291	11.4	767	4.69E+05	1.42		26	2.8		7	0.76	22.4	6.71	77.2	27	115.2	24.41	216.5	38.1	9090	80.7	144.2	1.05690485	752.47
GLV_11_21	rim	**1731**	142	19.4	1183	4.96E+05	1.18		4.81	0.139		4.13	0.75	27.1	9.4	112.2	42.7	191.9	42.3	412.9	77.6	10480	54.6	286	1.28780173	810.28
GLV_11_22	rim	**1774**	5.1	5.16	927	4.80E+05	0.049		19.83	0.024		1.39	0.142	12.92	5.64	80.2	32.42	158.5	37.58	372	71.7	13160	47.6	325.9	0.7126497	685.82
GLV_11_23	rim	**2235**	122	12.3	2933	5.16E+05	1.7		17.86	0.415		15.8	3.29	81	25.9	287.3	103	437	86.9	753	142.9	9980	331.5	441	1.08990511	759.35
GLV_11_20	core	**346.5**	124	14.3	371	4.84E+05	0.37		0.53	0.041		4.05	0.29	31	8.17	59.2	12.34	31.2	4.7	33.7	4.52	12810	21.79	1772	1.15533604	773.27
GLV_11_24	core	**395.3**	9.8	11.9	927	4.79E+05	0.165		9.68	0.114		3.88	1.33	24.1	7.92	89.6	33.24	144.3	30.44	279.9	51.3	8360	78.2	128.5	1.07554696	756.35
MG-063																										
MG_063_170	core	**270.2**	170	27	1444	4.84E+05	0.97		9.81	0.258		8.79	2.07	45.3	12.72	145.6	51.4	220.7	46.5	419	74.9	8550	115.8	147.4	1.43136376	836.35
MG_063_110	core	**262**	-1.4	2.86	726	4.66E+05	0.095		25.2	0.039		2.16	1.26	15.7	5.53	62	23.39	111.8	25.6	262	51.1	10020	486	710	0.45636603	641.57
MG_063_124	core	**263.2**	-0.6	6.88	1243	4.78E+05	0.061		10.74	0.124		4.52	1.34	28.4	9.57	114.1	42.7	199	42.7	426	78.2	8870	122.7	190.1	0.83758844	708.98
MG_063_159	rim	**264.4**	21.2	5.8	863	5.22E+05	0.48		18.99	0.031		2.62	0.87	16	5.13	64.7	28	137.7	33.5	340	70.5	10750	267.4	559	0.76342799	695.10
MG_063_28	rim	**265.4**	153.1	14.6	2695	4.96E+05	0.358		18.67	0.534		13.7	3.88	73.7	23.9	324.5	93.8	394	81.8	759	132.5	8420	287	294	1.16435284	775.21
MG_063_93	core	**266.9**	-0.5	10.2	2150	4.74E+05	0.137		22.2	1.06		10.8	2.74	58.5	18.39	209.4	76.3	331	69.4	646	113.8	8770	241	261.4	1.00860017	742.57
MG_063_153	core	**267**	-0.2	5.79	4342	4.78E+05	0.587		199	0.91		30.9	4.94	142.1	41.5	443	153.7	656	140.2	1273	224.7	7600	2150	1160	0.76267856	694.96
MG_063_162	rim	**267.4**	17.4	6.8	2484	4.59E+05	0.79		225.9	0.457		19.1	6.56	83.3	23	249.5	82.5	348	73.1	694	133.5	9550	3610	1800	0.83250891	708.02
MG_063_123	rim	**270.3**	-5.7	2.87	698	4.81E+05	0.079		18.94	0.032		1.75	0.8	12.4	4.61	55.6	22.69	110.4	26.46	287.4	57.3	10360	341	635	0.46578819	641.82
MG_063_111	rim	**272**	131	3.92	719	4.75E+05	1.79		20.5	0.0146		1.6	1.05	11.2	3.9	49.1	21.5	113

MG_063_106	rim	**911**	47.6	7.6	417	4.66E+05	0.274		7.76	0.023		1.75	0.145	8.7	3.42	38.1	15.17	66.4	14.81	147.3	25.51	11750	35.08	94.6	0.88081359	717.26
MG_063_55	core	**912**	1.1	5.17	1864	4.79E+05	0.051		11.36	1.16		22.4	1.77	82.7	22.43	230.3	72.4	271.5	53.8	444	72.2	9990	74.1	112.7	0.71349054	685.97
MG_063_70	rim	**912**	302	14.9	736	4.72E+05	8.9		9.62	0.196		5.4	0.69	27	8.12	82.3	27.2	106.5	21.4	197	31.9	10090	34.6	64.6	1.17318627	777.13
MG_063_13	core	**913**	6.1	2.38	1519	4.85E+05	0.107		21.29	0.186		8.93	0.36	44.6	14.29	164.1	56.9	233.6	50.9	455	75	12890	243.1	543	0.37657696	628.61
MG_063_163	core	**913**	307	5.84	2607	4.83E+05	1.18		16.7	0.77		20.9	1.35	99.3	30	311	104.9	409	80.2	667	110.4	10770	173.1	303	0.76641285	695.65
MG_063_155	rim	**914**	13.9	20.7	3381	4.88E+05	0.108		20.9	0.567		27.9	0.5	132.5	38.4	391	123	474	92.2	762	123	11430	203	151.1	1.31597035	809.08
MG_063_91	rim	**915**	1	19.7	530	4.83E+05	0.069		4.85	0.058		3.56	0.5	17.2	5.23	56.3	18.8	81.1	16.42	149.8	25.92	9830	19.37	37.3	1.29446623	804.14
MG_063_171	core	**915.6**	1.3	2.71	1848	4.90E+05	0.03		13.01	0.87		22.3	1.49	80.4	22.83	229.7	73	272.9	54.6	447.8	73.4	10390	88.7	137.7	0.43296929	637.73
MG_063_80	core	**916**	2.3	7.19	550	4.81E+05	0.041		8.53	0.075		3.01	0.191	16.7	5.13	59	20.21	80.8	17.16	153.9	26.36	10790	31.3	73.8	0.85672889	712.63
MG_063_88	rim	**916**	-0.6	9.88	504.7	4.83E+05	0.067		7.7	0.057		2.96	0.224	14.8	4.47	52.3	17.78	73.8	15.67	144.8	24.94	11090	27.69	72.2	0.99475694	739.76
MG_063_51	core	**917**	483	46	612	4.68E+05	0.63		15.5	0.055		3.07	0.181	17	5.61	60.7	21	84.3	17.02	146.8	23.97	12170	72.8	164.7	1.66275783	895.41
MG_063_78	core	**917**	-0.5	9.84	452.1	4.66E+05	-0.002		7	0.052		2.41	0.169	13.3	4.42	48.2	16.45	65.9	14.15	134	22.58	11110	24.63	64.3	0.9929951	739.41
MG_063_116	rim	**918**	11.8	11.87	441.6	4.90E+05	0.054		6.88	0.111		2.58	0.27	13.7	4.31	46	16.35	67.4	13.92	129.1	20.96	10660	23.56	55.7	1.07445072	756.12
MG_063_139	rim	**918**	11.3	13.8	680	4.98E+05	0.087		6.86	0.125		3.9	0.448	20.6	6.69	72.9	25.38	104.2	20.98	191	32.78	10250	27.48	56.3	1.13987909	769.95
MG_063_25	rim	**919**	20.5	6.17	910	4.80E+05	0.015		2.28	0.053		1.34	0.153	14.5	6.9	85.9	27.31	102.8	19.2	154.2	23.82	14020	53.3	955	0.79028516	700.08
MG_063_66	core	**919**	1.4	2.9	1304	4.70E+05	0.044		9.73	0.496		13.9	1.07	56.3	15.62	159.2	50.6	194.1	38.2	323	53	10160	56	85.9	0.462363	642.56
MG_063_5	core	**919.5**	1.3	7.3	374.7	4.89E+05	0.023		7.42	0.028		1.5	0.179	9.81	3.17	36.9	13.74	58.6	12.74	122	21.31	11660	30	88.8	0.86332286	713.89
MG_063_21	rim	**920**	1	7.74	447.7	4.80E+05	0.045		7.4	0.029		2.16	0.181	11.58	3.89	45.6	16.62	69.6	14.92	139	24.17	11690	27.6	84	0.88874096	718.79
MG_063_58	core	**920**	2.3	7.97	325.1	4.82E+05	0.06		5.48	0.05		1.84	0.185	9.38	2.85	33.1	11.97	51.5	10.98	98.3	17.36	10960	16.41	46.01	0.90145832	721.26
MG_063_168	rim	**920**	3.1	12.5	564	4.88E+05	0.009		7.57	0.089		3.62	0.253	17.1	5.55	61.3	20.64	87.5	18.17	158.7	28.23	10450	27.65	61.4	1.09691001	760.82
MG_063_172	rim	**920**	-1.6	5.11	245	4.83E+05	0.021		5.68	0.034		1.35	0.138	6.85	1.96	23.8	8.58	36.1	8.15	79	13.8	10980	34.73	76.8	0.7084209	685.06
MG_063_126	core	**921**	2.1	4.94	1686	4.94E+05	0.082		11.88	0.84		18.2	1.26	69.9	20	205.6	64.6	250.5	48.5	413	64.3	9990	80.3	125.5	0.69372695	682.41
MG_063_115	rim	**922**	1.8	5.89	422.7	4.82E+05	0.032		6.74	0.054		2.19	0.238	11.9	3.97	46.1	15.16	65.2	13.83	127.9	21.58	10870	24.09	61.6	0.77011529	696.34
MG_063_40	core	**922.7**	-3.1	8.47	747	4.87E+05	0.089		12.1	0.127		4.48	0.337	23.3	7.39	83.3	28.21	113.5	23.7	205.4	34.65	11220	47	116.5	0.92788341	726.43
MG_063_42	core	**923**	4.4	4.99	2333	4.89E+05	0.093		14.2	1.06		21.1	1.46	92.2	26.42	278	88.8	340	65.9	552	90.6	10200	111.1	181.7	0.69810655	683.19
MG_063_47	core	**923**	11.3	9.15	831	4.79E+05	0.97		200	24.8		27.5	1.53	44.3	10.38	99.9	31.16	125.5	25.42	216.5	36.1	10830	49.8	102.1	0.96142109	733.07
MG_063_101	rim	**923**	-5	7	911	4.90E+05	0.034		10.27	0.236		8.35	0.68	34.6	10.62	101.2	103.2	34.6	134.2	27	240	39.5	10320	52	91.1	0.84509804	710.41
MG_063_107	core	**923**	1.9	18.3	434	4.94E+05	0.04		4.37	0.059		2.39	0.328	13	4.01	44.3	15.67	65.6	13.41	124.4	21.29	10100	14.35	31.3	1.26245109	796.88
MG_063_118	core	**923**	-2.3	12.5	613	4.91E+05	0.054		6.28	0.102		3.87	0.51	20.9	6.21	67.4	22.41	93.2	18.95	170.1	28.32	10280	26.47	52.9	1.09691001	760.82
MG_063_29	core	**924**	1.8	7.2	910	4.79E+05	2.17		558	71		62.1	3.77	68	13.17	114	35.2	129.3	25.7	216.4	35.9	10560	50	94.4	0.8573325	712.75
MG_063_26	core	**925**	16	8.8	702	4.93E+05	0.52		10.4	0.19		5.78	0.455	22.9	7.32	77.8	26.4	103.4	21.17	191.9	31.2	10710	38.3	80.5	0.94448267	729.71
MG_063_37	core	**926**	2.6	5.2	1506	4.84E+05	0.039		12.1	0.95		15.7	1.27	64.9	18.19	180.2	56.4	214	42.3	359.4	57.6	10330	59.9	91.8	0.71600334	686.43
MG_063_69	rim	**926**	3.2	8.3	1194	4.80E+05	0.064		10.53	0.415		12.1	0.84	48.7	14.04	140	46.48	180.6	36	305.2	50	10170	61.8	101.6	0.91907809	724.70
MG_063_74	core	**926**	35	4.97	1754	4.94E+05	-0.152		11.82	0.88		20.5	1.52	80.2	21.21	214.9	67.1	246	47.9	413	67.2	10480	71.3	111.2	0.69635639	682.88
MG_063_99	rim	**926**	2.4	9.1	1390	4.83E+05	0.066		23.95	0.181		6.93	0.444	37.1	11.99	139	49.6	213.1	45.3	421	72.3	11650	159.9	248.3	0.95904139	732.60
MG_063_108	rim	**926**	-0.7	12.2	551	4.88E+05	0.009		7.31	0.06		3.06	0.284	18.2	5.47	60.4	20.36	84	17.24	156.9	25.37	10790	28.85	63.8	1.08635983	758.61
MG_063_137	core	**926**	3.1	7.68	760	4.99E+05	0.059		9.35	0.113		6.42	0.532	28.4	8.33	86.5	29.18	113.1	23.26	200.2	34	10070	41.7	78.3	0.88536122	718.14
MG_063_147	rim	**926**	-1.7	12.6	667	5.01E+05	0.008		8.19	0.07		4.44	0.453	19.9	6.61	72.7	24.99	99.8	20.63	177.4	31.4	10610	35.51	71.4	1.10039015	761.55
MG_063_9	core	**927**	-1.5	5.9	738	4.70E+05	0.046		11.55	0.105		5.03	0.343	24.9	7.61	81.3	28.12	114.2	23	209.7	34	11000	48.7	124.3	0.77085201	696.47
MG_063_50	core	**927**	-1.2	4.49	1445	4.76E+05	0.079		21.3	2.2		18.5	1.04	59.3	17.18	172.1	55	218	42.9	360	59.2	10420	64.3	112.9	0.65224634	675.01
MG_063_119	core	**927**	-1.5	7.63	623	4.78E+05	0.019		11.56	0.091		3.77	0.268	20.3	6.62	71.7	24.52	100.8	20.07	185.8	30.88	11520	45.5	119.3	0.88252454	717.59
MG_063_157	rim	**927**	2.8	22.3	1145	4.89E+05	0.057		6.01	0.455		13.1	2.83	54.8	13.7	137.8	42.4	157.9	31.1	267.3	43.6	9510	20.49	26.56	1.34830486	816.58
MG_063_90	core	**928**	3.5	22.5	1193	4.97E+05	-0.005		6.91	0.6		14.4	2.24	54.5	15.34	144.3	45.3	167.7	33.7	297	45.7	9560	27.3	35.4	1.35211825	817.49
MG_063_63	core	**929**	3.2	8.26	812	4.75E+05	0.044		10.13	0.136		7.51	0.52	28.9	8.54	94.1	30.79	124	24.92	216.9	35.9	10370	48.4	90.9	0.91698005	724.29
MG_063_75	rim	**930**	1.7	13.6	678	4.74E+05	0.015		7.42	0.149		4.94	0.46	23.9	6.84	74.5	24.6	95.9	20.4	179	30.5	9970	31.8	58.8	1.13353891	768.59
MG_063_39	rim	**931**	-2.7	19.5	1583	4.95E+05	0.075		17.28	0.197		9.59	0.394	50.7	15.32	166.8	57.1	220.1	45.6	399.9	67.1	11480	139.6	130.3	1.29003461	803.13
MG_063_74	core	**931**	3	11.7	781	4.79E+05	0.025		7.46	0.144		5.63	0.7	28.1	8.44	90.5	28.87	113.5	22.63	201.5	33.9	10140	37.93	62.8	1.06818586	754.81
MG_063_120	core	**931**	0.9	12.9	545	4.90E+05	0.023		7	0.057		3.25	0.329	16.8	5.34	56.3	20.34	82	16.97	152.3	25.59	10510	26.95	59.9	1.11058971	763.71
MG_063_127	core	**931**	1.6	7.29	513.3	4.90E+05	0.029		6.79	0.078		3.36	0.167	14.4	4.72	55	19.05	81.1	16.61	151.4	25.89	11010	23.58	56.6	0.86272753	713.78
MG_063_129	core	**931**	-2	12.08	480	4.82E+05	0.034		6.73	0.043		2.66	0.284	14.45	4.58	50.7	17.67	72.6	15.09	136.7	23.56	10220	23.42	55.3	1.08206693	757.71
MG_063_64	core	**932**	-1.7	5.8	1164	4.63E+05	0.026		9.59	0.48		11.3	0.81	44.7	13	137	43.5	174.8	34.4	290.5	48.1	9840	54.7	94.3	0.76342799	695.10
MG_063_112	core	**932**	1.5	15.9	700	4.85E+05	0.034		6.8	0.089		4.56	0.56	22.3	7.09	75.9	25.32	101.6	21.39	184.6	30.63	10180	32.33	56.2	1.20139712	783.29
MG_063_4	core	**933**	1.3	13.2	329	5.00E+05	0.033		4.66	0.046		2.18	0.203	9.5	3.07	34.7	12.06	50.2	11.02	98.6	16.86	10910	13.5	34.84	1.12057393	765.83
MG_063_36	core	**933**	18	17.6	824	4.86E+05	0.28		7.44	0.182		7.04	0.51	26	7.91	88.3	29.5	115.8	24.1	217	36.2	10300	59.3	166	1.24551267	793.07
MG_063_38	rim	**933**	5	6.71	548.3	4.79E+05	0.037		7.53	0.062		3.79	0.368	17.9	5.46	61.5	20.13	82.4	16.84	152.5	25.81	10230	30.25	61.8	0.82672252	706.92
MG_063_65	rim	**933**	-0.8	11.9	596	4.72E+05	0.052		6.39	0.061		4.21	0.35	17.6	5.69	63.5	21.95	90.9	18.61	164.4	28.44	10330	28.45	56.3	1.07554696	756.35
MG_063_18	core	**934**	2.9	9.39	833	4.84E+05	0.077		10.77	0.2		7.59	0.511	29.6	9.12	95.8	31.17	122.1	25.31	215.8	35.63	10490	49.23	90.4	0.97266559	735.32
MG_063_19	core	**934**	21	3.16	914	4.86E+05	0.19		21.2	1.79		10.2	0.69	34	10.3	106	34.3	136	27.3	238	37.9	10650	53.4	94.2	0.49668708	648.76
MG_063_135	rim	**934**	-0.6	8.8	423.9	4.89E+05	0.035		7.08	0.052		2.49	0.186	12.07	3.76	44.1	15.38	63.5	13.37	124.1	21.17	10890	24.12	66.91	0.94448267	729.71
MG_063_167	core	**934**	1.3	10.95	427.9	4.82E+05	0.052		5.5	0.074		2.15	0.269	13.3	4.16	45.7	15.73	65.8	13.88	122.9	21.55	10400	19.47	45	1.03941412	748.86
MG_063_2	core	**935**	11.1	6.04	615	4.89E+05	0.046		2.8	0.049		3.38	0.125	17.2	6.02	62.1	21.2	85.4	17.5	158.2	26.5	12010	76.5	405	0.78103694	698.36
MG_063_81	rim	**936**	1.4	6.35	325	4.83E+05	0.065		5.84	0.034		1.45	0.19	8.54	2.79	32.3	11.72	50	11.24	106	18.54	10750	25.9	58.5	0.80277373	702.42
MG_063_87	core	**937**	-0.6	13.1	495	4.88E+05	0.056		4.76	0.066		2.54	0.334	14.1	4.73	52.8	17.92	72.6	15.6	140.4	24.15	10610	16.91	37.79	1.1172713	765.13
MG_063_8	core	**938**	-2.9	8.77	515.5	4.92E+05	0.076		8.82	0.058		2.73	0.268	14.33	4.55	54.1	18.79	78.9	17.03	148.1	25.31	11460	33.65	80.1	0.94299959	729.42
MG_063_10	rim	**938**	-2.8	9.91	823	4.82E+05	0.012		11.25	0.185		6.44	0.414	30	9.17	92.3	31.45	125.8	25.3	226.8	36.86	10500	50.7	105.4	0.99607365	740.03
MG_063_43	rim	**938**	5.2	11.6	396.2	4.83E+05	0.189		5.98	0.055		2.24	0.177	12.37	3.83	41.9	14.44	59.5	12.64	116.7	19.76	10650	20.48	50.77	1.06445799	754.04
MG_063_100	core	**940**	-4.4	8.9	446	4.72E+05	0.041		9.83	0.057		2.1	0.206	10.97	4.08	44.2	15.73	70.9	15.44	149	26.35	11010	42.8	117.9	0.94939001	730.68
MG_063_33	core	**943**	0.5	13.38	566	4.85E+05	-0.009		5.68	0.103		3.35	0.313	16.2	5.19	57.4	20.4	84.4	17.85	164.9	27.63	10510	19.98	44.7	1.12645611	767.08
MG_063_27	rim	**944**	0	10.1	472	4.83E+05	0.083		7.41	0.053		2.74	0.207	12.6	4.33	49.2	17.14	72	15.59	141.6	24.27	11070	30.8	88.3	1.00432137	741.70
MG_063_92	rim	**944**	134.2	5.94	692	4.85E+05	0.36		10.75	0.096		5.29	0.371	23.6	7.22	77.1	25.6	103.9	21.45	195	31.9	10680	44.3	96.9	0.77378644	697.02
MG_063_12	core	**945**	-0.3	6.33	717	4.79E+05	0.148		10.52	0.155		5.15	0.384	24.8	7.26	80.6	27	110.3	22.9	200.4	33.57	10910	49.3	123.9	0.80140371	702.16
MG_063_131	rim	**945**	12.6	22.3	748	4.88E+05	0.058		7.24	0.202		11.11	0.218	46.5	11.22	93.6	26.7	98.4	18.2	154.2	25.92	10510	138.3	74.4	1.34830486	816.58
MG_063_68	rim	**946**	0.7	5.44	367.4	4.76E+05	0.182		5.48	0.068		1.95	0.198	10.42	3.49	39.4	13.77	57.8	12.2	113.9	20.09	11160	17.76	49.3	0.7355989	689.99
MG_063_67	rim	**948**	2.2	8.6	484.8	4.81E+05	0.019		6.5	0.039		2.63	0.327	12.9	4.55	53	18.04	76.1	16.14	149.3	25.39	11090	22.7	60.8	0.93449843	729.74
MG_063_104	rim	**949**	-0.1	10.4	413	4.77E+05	0.033		5.05	0.074		2.07	0.294	12.2	3.71	43.6	15.44	65.8	13.24	124.3	21.48	10500	17.08	42.9	1.01703334	744.28
MG_063_14	rim	**950**	1.5	6.35	518	4.82E+05	0.024		7.64	0.057		3.22	0.378	15.8	4.84	54.8	19.15	80.5	16.28	153.1	26.4	10920	32.9	79.2	0.80277373	702.42
MG_063_82	rim	**951**	-2.3	6.6	250.2	4.96E+05	0.05		4.59	0.006		0.66	0.306	4.37	1.58	21.1	8.02	36.3	8.21	85	15.74	11110	49.1	92.4	0.81954394	705.57
MG_063_145	core	**953**	14	7.9	774	4.88E+05	0.088		6.71	0.02		2.26	0.068	13	4.93	64.4	25.24	124.9	28.8	278	47.1	11110	56.4	177.8	0.89762709	720.52
MG_063_56	core	**954**	0.9	12.9	356	4.87E+05	0.041		4.19	0.06		1.79	0.185	10.44	3.35	38.2	13.37	54.7	11.51	106.2	18.09	10650	14.42	33.55	1.11058971	763.71
MG_063_134	core	**955**	12	5.5	907	4.98E+05	0.101		8.52	0.42		8.9	0.74	36.8	10.3	107.4	35.1	133.3	27	234	38.6	10410	40	75.2	0.74036269	690.86
MG_063_169	rim	**958**	2.2	7	812	4.75E+05	0.018		4.13	0.021		1.77	0.125	17.3	6.44	75.3	26.7	117.7	26.4	242.7	45.9	12460	84	423.5	0.84509804	710.41
MG_063_45	core	**959**	3.8	8.35	839	4.81E+05	-0.01		7.75	0.188		6.35	0.56	29.7	8.56	94.4	31.73	124.7	25.37	222	37.62	10380	32.97	59.7	0.92168648	725.22
MG_063_85	core	**959**	0.2	7.5	499	4.81E+05	0.048		9.25	0.068		2.15	0.201	14.1	4.43	51.7	17.99	75.2	15.82	150.3	25.27	11260	33.9	98.7	0.87506126	716.15
MG_063_41	core	**963**	1790	85	445.5	4.66E+05	3.65		5.95	0.063		2.78	0.218	12.6	4.25	47.7	16.42	64.7	13.93	131	22.7	10360	23.03	55.5	1.92941893	971.77
MG_063_165	core	**967**	5.5	6.9	696	4.83E+05	0.06		13.4	0.171		6	0.68	26.5	7.4	73.5	25	101.8	21.8	193	33.4	10640	102	131.3	0.83884909	709.22
MG_063_77	core	**968**	0.5	7.72	398.3	4.81E+05	0.017		6.79	0.022		1.98	0.153	10.8	3.52	40.7	14.28	59.8	13.12	121.3	21.42	11620	25.33	77.7	0.8876173	718.58
MG_063_154	rim	**968**	0.3	10.6	419	4.79E+05	0.033		5.79	0.063		2.39	0.325	11.8	3.98	42.9	15.06	63.6	13.79	127.3	22.81	10410	40.3	131.4	1.02530587	745.97
MG_063_30	core	**980**	2.5	9.2	1522	4.82E+05	0.085		20.5	0.605		19.1	1.25	65.2	17.6	172.5	54.8	211.9	42.3	378	64.1	10650	303.5	293.4	0.96378783	733.55
MG_063_117	rim	**989**	-3.4	9.77	298.9	4.98E+05	-0.001		5.02	0.041		1.61	0.136	8.6	3.03	31.2	10.89	46	9.87	89.9	15.81	11300	15.53	43.19	0.98989456	738.78
MG_063_31	rim	**998**	2.7	6.8	629	4.91E+05	0.075		11.21	0.033		1.98	0.23	9.5	4.47	55	21.4	96.4	21.1	202	37.2	11170	88.2	426	0.83250891	708.02
MG_063_49	core	**998**	6.3	11.2	694	4.78E+05	0.354		13.16	0.154		6.32	0.6	27.3	6.96	73.8	24.65	101.1	20.61	193.1	32.8	10580	127.9	167.6	1.04921802	750.88
MG_063_7	core	**1000**	3.4	7.68	594	4.90E+05	0.083		3.79	0.049		1.9	0.037	13.2	4.56	54.8	20.21	91.8	20.05	187.4	32.9	12400	81.4	186.4	0.88534232	718.14
MG_063_113	core	**1002**	3.5	7.3	1736	4.76E+05	0.058		11.89	0.076		4.98	0.213	31.4	13.3	160.4	58.9	260.1	56.8	517	89.6	11770	251.4	536	0.86332286	713.89
MG_063_130	core	**1006**	0.8	8.18	1802	4.85E+05	0.096		8.72	0.079		5	0.183	36.6	13.28	163.8	62.2	281.2	59.7	532	88.9	12780	279	536.3	0.9127533	723.47
MG_063_146	core	**1007**	0.3	10.4	1051	4.94E+05	0.111		13.52	0.131		5.14	0.204	29.5	9.34	103.8	37.7	156.9	33.5	297	52.2	11580	58.2	90.4	1.01703334	744.28
MG_063_98	rim	**1009**	-0.1	7.3	1089	4.76E+05	0.026		5.56	0.085		4.36	0.141	24.3	9.07	102.1	37.1	167.1	35.59	332.1	57.4	11830	181.1	342.5	0.86332286	713.89
MG_063_114	rim	**1009**	6.5	7.7	650	4.84E+05	0.016		12.21	0.096		3.86	0.382	21	6.39	67.7	22.6	96.8	20	183.7	32	10590	71	103.6	0.88649073	713.71
MG_063_136	rim	**1010**	310	9.5	223	4.89E+05	4.35		1.67	0.029		2.13	0.088	13.2	3.7	30.2	7.05	21.3	3.62	26.8	4.28	13060	45.6	288.4	0.97772361	736.33
MG_063_161	rim	**1016**	-2.6	8.2	1014	4.75E+05	0.025		5.52	0.066		3.69	0.105	23.5	8.14	96.9	34.5	156.8	32.67	300.4	53.7	11820	157.4	298.3	0.91381385	723.67
MG_063_3	core	**1027**	2.5	6.62	949	4.97E+05	0.031		5.03	0.112		4.08	0.131	24.9	8.03	89.5	32.8	139	29.5	274	46.1	12560	147	342	0.82085799	705.82
MG_063_35	core	**1032**	10.7	7.6	1179	4.89E+05	0.19		29.7	0.017		0.84	0.36	9.45	4.82	77.9	37.4	210.3	51.1	757	144.7	12210	50	439	0.58080135	717.26
MG_063_149	core	**1057**	90	7.3	1037	5.28E+05	0.48		2.42	0		1.1	0.28	8.9	5.03	80.6	34.7	197	58	656	124.8	14370	14	585	0.86332286	713.89
MG_063_151	core	**1085**	1750	10	1505	4.63E+05	2.42		14.81	0.331		12.4	0.64	58.3	17.41	168.2	54.4	205.3	40.1	342	58.1	9740	378	1051	1	740.82
MG_063_148	core	**1170**	82	19.2	355	4.70E+05	0.87		6.07	0.035		0.49	0.183	4.43	1.92	26.8	11.88	62.6	17.89	210.9	43.2	13230	50.5	418	1.28330123	801.60
MG_063_34	rim	**1213**	289	10.7	2405	4.86E+05	0.89		130.6	0.173		6.36	1.99	38.2	14.09	186.2	78.5	375	89.9	891	163.4	7810	106	390	1.02938378	746.80
MG_063_4	core	**1255**	6.8	9.81	1349	4.85E+05	0.078		19.8	0.212		5.22	1.4	31.4	10.09	121.3	45.5	199.1	45.7	442	78.3	9280	112.4	117	0.91660703	735.

LRW_21_35	core	**239.7**	10.2	13.9	153.4	4.74E+05	0.012	0.0021	3.99	0.09	2.28	6.18	0.676	19.3	3.74	25.7	5.61	15.7	2.52	16.8	2.03	11430	102.7	510.1	1.1430148	770.62
LRW_21_42	core	**231.8**	7.5	14.03	201.1	4.80E+05	0.054	0.0068	3.32	0.107	1.73	5.57	0.508	20.3	4.07	31.2	7.33	24.7	4.22	33.9	5.27	11340	66.6	402.7	1.14705767	771.49
LRW_21_57	core	**243.7**	6.1	14.2	191.7	4.58E+05	0.044	0.012	4.12	0.115	1.99	4.76	0.76	15.8	3.78	27.4	6.78	21.8	3.59	27.8	4.32	10700	68.6	411.9	1.15228834	772.61
LRW_21_49	core	**238.1**	26.4	14.4	80.4	4.61E+05	0.046	0.0074	2.95	0.057	0.86	2.09	0.391	8.83	1.69	12.54	2.71	8.16	1.101	9.18	1.37	10660	48.2	309.1	1.15836249	773.92
LRW_21_80	core	**241.5**	38	14.4	16.1	4.44E+05	0.037	0.01	0.87	0.0042	0.068	0.27	0.126	0.66	0.265	1.77	0.451	1.5	0.314	2.13	0.281	8170	27.61	140.9	1.15836249	773.92
LRW_21_54	rim	**236.2**	0.7	14.6	274.7	4.69E+05	0.062	-0.002	5.25	0.302	7.14	15.2	1.66	43.7	8.19	50.7	10.4	29.2	4.02	27.6	3.78	11440	228.6	786	1.16435286	775.21
LRW_21_4	core	**234.2**	32.5	14.9	171	4.85E+05	0.065	0	4.48	0.093	1.91	5.48	0.61	19.5	3.87	25.6	5.83	18.9	3.15	22.9	3.49	11070	116.6	520	1.17318627	777.13
LRW_21_27	core	**238.1**	7	15	229.6	4.74E+05	0.017	0.0043	3.67	0.12	1.89	4.39	0.65	17.4	3.66	30	7.72	26.5	5.02	40.8	6.46	10020	68.9	405	1.17609126	777.76
LRW_21_46	core	**238.8**	20.2	15.2	140.6	4.63E+05	0.003	0.007	4.22	0.094	1.81	4.58	0.78	16.9	3.44	22.6	5	13.14	1.8	12.29	1.91	9980	105.8	502	1.18184359	779.01
LRW_21_37	core	**236.3**	11.6	15.49	184	4.81E+05	0.052	0.015	4.96	0.141	2.7	8.3	1.16	29.5	5.58	35.2	6.79	17.2	2.57	17.9	2.44	11270	159	611	1.19005142	780.80
LRW_21_31	core	**235**	7.3	15.6	216.7	4.74E+05	0.042	0.018	5.72	0.305	5.72	13.2	1.57	34.2	6.11	38.4	7.8	20.11	2.88	19.66	2.73	10230	160.9	605	1.1931246	781.48
LRW_21_66	core	**249.8**	31.1	15.6	129.4	4.45E+05	0.029	0.013	3.08	0.079	2	4.21	0.59	16.2	3.24	20.3	4.71	12.16	2.02	15.3	2.16	10120	63	307.1	1.19312466	781.48
LRW_21_55	core	**240**	22.5	15.7	23.37	4.65E+05	0.016	0	1.5	0.016	0.35	0.52	0.34	1.89	0.36	3.09	0.73	1.71	0.339	2.12	0.32	9140	52.4	217.9	1.19589965	782.08
LRW_21_13	core	**239.5**	20.5	15.8	136.3	4.80E+05	0.016	0.021	4.75	0.141	2.56	5.31	0.84	20.1	3.63	23.7	4.28	11.77	1.46	10.29	1.39	9600	98.4	448	1.19865709	782.69
LRW_21_24	core	**240.8**	17.7	15.99	189	4.65E+05	0.066	-0.00251	5.1	0.2	4.23	7.92	0.93	24.4	4.37	29.8	6.62	18.3	3.12	21	3.33	8760	104.7	401	1.20384846	783.83
LRW_21_74	rim	**232.9**	2.5	16.2	201.2	4.72E+05	0.003	0.021	6.46	0.329	5.36	7.68	1.15	20.7	4.42	32.4	7.63	23.5	3.44	25.6	3.72	13550	323	1166	1.20951501	785.08
LRW_21_30	core	**236.4**	9.8	16.6	121.6	4.76E+05	0.04	0.0053	4.98	0.071	1.15	2.89	0.49	10	2.41	17	4.11	13.09	1.96	13.7	1.82	11590	139.9	599	1.22010809	787.42
LRW_21_40	core	**233.2**	6.4	16.8	249	4.83E+05	0.026	0.028	6.99	0.475	9.69	17.5	2.15	46.5	8.43	49.4	9.1	23.97	3.27	23.3	2.98	11140	234.9	786	1.22530928	788.57
LRW_21_22	rim	**245**	29	16.8	216.8	4.55E+05	0.021	0.017	4.23	0.139	2.39	6.75	0.96	26	4.81	31.6	7.32	23.7	3.92	31.7	4.98	9630	126.7	483	1.22530928	788.57
LRW_21_5	core	**233.4**	21.2	16.98	177.3	4.80E+05	0.06	0	4.78	0.166	2.5	5.97	0.84	20.8	4.19	28.5	6.41	18.1	2.94	19.5	2.75	10460	105.6	493.7	1.22993769	789.60
LRW_21_2	core	**232.8**	32.5	18.7	238.2	4.77E+05	0.044	0.0113	5.13	0.189	3.2	7.57	1.03	27.6	5.49	36.9	7.85	24.5	3.9	29.6	4.39	10520	101.4	533	1.27184161	799.00
LRW_21_75	rim	**234.5**	9.3	18.7	148.3	4.63E+05	0.036	0.009	8.15	0.119	2.16	4.83	0.82	17.4	3.55	24.6	5.87	16.41	2.33	16	2.26	11970	355.8	1178	1.27184161	799.00
LRW_21_33	core	**230.6**	588	211	146.2	4.77E+05	10.97	0.0067	2.93	0.057	1.26	3.6	0.78	13.6	2.91	20.4	5.05	15.5	2.55	19.9	3.2	10880	65.8	417.6	2.32428246	1105.14
LRW_21_62	core	**243.4**	19.4	2.08E+05	163.9	4.94E+05	0.9	0.05	3.64	0.199	2.72	5.3	0.59	16.9	4.02	28	5.41	17.5	3.14	22.3	3.51	11750	151.8	734	5.31806333	7068.56
CVI-13108																										
108b- -2	core	**234.5**	1.05	0.66	3.03	31160	0.0028	0.00068	0.151	0.0044	0.103	0.197	0.0411	0.704	0.116	0.575	0.104	0.242	0.0347	0.317	0.064	653	3.18	23.53	-0.1804561	547.47
108b- -7	core	**237.2**	0.52	0.702	2.647	30680	-0.00253	0.00066	0.08	0.00132	0.034	0.09	0.0307	0.259	0.0608	0.382	0.0743	0.206	0.0292	0.223	0.0363	596	1.091	9.61	-0.1536629	551.04
108- -124	core	**237.2**	0.34	0.725	3.371	31940	0.002	0.0003	0.0837	0.0044	0.035	0.079	0.0322	0.398	0.0645	0.479	0.099	0.27	0.0485	0.341	0.0576	791	2.58	12.93	-0.139662	552.91
108b- -1	core	**235.3**	0	0.731	3.081	30390	0.0015	0.00059	0.1075	0.0034	0.067	0.119	0.0327	0.478	0.0969	0.568	0.102	0.241	0.0291	0.194	0.0228	679	1.629	15.19	-0.1360826	553.39
108b- -5	core	**237.4**	35.1	0.945	11.35	31080	0.0019	0.0024	0.29	0.0319	0.504	0.612	0.128	1.91	0.353	2.15	0.39	1.012	0.133	0.922	0.1336	686	9.48	51.8	-0.0245682	568.67
108- -74	core	**240**	-1.3	4.39	103	4.76E+05	0.016	0	0.426	0	0.074	0.25	0.082	1.38	0.476	6.88	2.94	16.3	4.23	48.9	11.64	8700	8.25	20.97	0.64246452	673.28
108- -97	rim	**231.2**	30.4	5.01	142.9	4.88E+05	-0.0142	0	1.31	0.0117	0.44	1.96	0.237	12.3	3.25	24.1	4.78	11.66	1.84	14.4	2.2	13080	26.48	289	0.69983773	683.51
108- -95	core	**230.9**	27.2	6.2	91.3	5.02E+05	0.061	0	1.24	0.0095	0.27	0.69	0.148	3.54	1.2	8.91	2.89	11.01	1.96	15.8	2.99	10280	19.31	194.3	0.79239169	700.48
108- -60	core	**241.8**	8.3	6.56	54.2	4.74E+05	0.076	0.015	0.406	0	0.024	0.22	0.185	1.29	0.533	5.42	1.49	5.73	1.1	9.14	1.8	9440	7.86	21.39	0.81690384	705.07
108- -117	core	**285.5**	5.6	6.99	49.6	4.77E+05	-0.014	0	0.68	0.0127	0.164	0.45	0.209	2.34	0.503	4.79	1.55	5.73	1.02	8.6	1.5	8720	12.59	88.3	0.84447718	710.29
108- -53	core	**245.9**	5	7.08	85.2	4.71E+05	0.005	0.0067	0.61	0.0068	0.29	0.51	0.251	2.48	0.76	7.59	2.29	8.83	1.73	15.6	2.66	8420	9.04	72.1	0.85003326	711.35
108- -69	core	**239.2**	36.7	7.74	43.3	4.65E+05	0.066	0	2.05	0.0153	0.64	1.44	0.327	5.11	1.11	6.33	1.49	3.67	0.46	3.88	0.444	9620	42.9	379	0.88874096	718.79
108- -13	core	**241.2**	34.4	7.95	59.5	4.65E+05	-0.007	0.0027	2.13	0.055	0.5	1.5	0.363	5.2	1.31	9.1	2.12	5.97	0.908	8.97	1.64	10080	37.4	366	0.90036713	721.05
108- -30	core	**238.5**	0.9	8.1	178.4	4.75E+05	0.04	0.0099	0.95	0.031	0.55	1.15	0.49	5.38	1.65	15.94	5.35	21.9	4.31	36.7	6.46	8710	15.99	184.5	0.90848502	722.63
108- -92	core	**235.9**	29.4	8.27	21.15	4.97E+05	0.009	0.0047	1.2	0.0039	0.28	0.52	0.202	2.32	0.479	3.31	0.563	1.61	0.193	1.52	0.237	11760	21.95	203	0.91750551	724.40
108- -101	core	**237.4**	36.5	8.37	55.5	4.76E+05	0.021	0	2.13	0.023	0.7	1.63	0.267	6.59	1.29	8.23	2.07	5.05	0.74	5.61	0.7	10100	36.94	356.5	0.92272546	725.42
108- -93	core	**234.3**	11.2	8.49	17.12	4.92E+05	0.038	0	0.468	0.0039	0.18	0.16	0.193	0.79	0.237	1.86	0.482	1.82	0.26	2.44	0.407	11300	8.09	39.49	0.92890769	726.64
108- -34	rim	**236.5**	26.4	8.64	45.9	4.74E+05	0.062	0	4.23	0.054	0.93	2.62	0.283	9.18	1.72	9.19	1.45	3.22	0.31	1.87	0.224	14460	219.3	1529	0.93651374	728.13
108- -103	core	**240.4**	41.9	8.7	185	4.75E+05	0.069	0.013	1.85	0.086	1.4	3.9	0.56	15.6	3.27	23.2	5.84	22.3	5	54	11.8	11520	41.7	182	0.93951929	728.73
108- -120	core	**228.8**	6.4	8.74	344	4.62E+05	0.252	-0.00575	1.6	0.034	0.7	2.24	0.54	16	5.45	45.5	10.56	31.3	5.33	42.2	6.81	9380	26.01	525	0.94151143	729.12
108- -44	rim	**231.5**	42.1	8.85	25.8	4.78E+05	0.023	-0.00363	1.72	0.014	0.38	0.85	0.186	3.23	0.635	4.01	0.77	1.92	0.231	1.77	0.272	11270	31.65	233.9	0.94694327	730.20
108- -35	core	**235.3**	19.7	8.94	32.5	4.85E+05	0.013	0	1.96	0.014	0.47	1.38	0.261	4.8	0.96	5.57	0.96	2.24	0.283	1.83	0.227	11480	33.2	308.6	0.95133752	731.07
108- -114	core	**242.7**	28.4	9.15	14.19	4.61E+05	0.022	0.0052	0.423	0.0081	0.04	0.1	0.122	0.88	0.177	1.01	0.328	1	0.24	1.4	0.21	9030	10.51	57	0.96142109	733.07
108- -98	rim	**229.5**	47.3	9.18	32.8	5.06E+05	0.042	-0.00711	1.98	0.016	0.71	1.14	0.228	4.9	1.02	6.05	1.095	2.34	0.332	1.82	0.264	11940	44.3	415.4	0.96284268	733.36
108- -59	core	**232.6**	23.1	9.34	60.2	4.74E+05	0.015	0	1.87	0.0057	0.58	0.85	0.319	4.13	0.698	6.32	1.93	7.85	1.62	15.8	3.4	10600	45.2	290.4	0.97034688	734.86
108- -88	rim	**236.6**	27.9	9.38	27.47	4.92E+05	-0.021	0.0082	1.26	0.012	0.45	0.97	0.287	3.82	0.72	4.13	0.83	2.07	0.303	1.91	0.26	11020	21.68	207.6	0.97220284	735.23
108- -2	rim	**249.5**	6.5	9.42	24.24	4.42E+05	0.023	0.0072	1.01	0.0114	0.46	0.37	0.231	2.88	0.585	3.45	0.7	1.9	0.202	1.51	0.216	9810	18	179.6	0.9740509	735.60
108- -99	core	**238**	21.6	9.47	82.4	4.49E+05	0.009	0	2.23	0.039	0.85	1.98	0.401	8.92	1.63	11.5	2.9	8.46	1.62	11.8	2.06	10590	37.6	294.2	0.97634698	736.06
108- -113	core	**246.4**	13.5	9.48	88	4.58E+05	0.033	0.01	3.54	0.079	1.53	4.61	0.79	14.7	2.76	15.08	2.65	6.3	0.84	6.13	0.64	8730	90.5	586	0.97680834	736.15
108- -16	rim	**240.5**	24.1	9.6	33.8	4.72E+05	0.059	0	1.41	0.02	0.36	1.11	0.22	3.42	0.91	5.79	1.14	3.52	0.44	3.67	0.493	11020	23	253.1	0.98227123	737.25
108- -66	rim	**234.8**	47.8	9.63	55.4	4.77E+05	0.33	0.012	3.77	0.074	1.3	2.38	0.53	12.4	2.07	12.1	1.72	3.27	0.334	2.17	0.32	12370	192.3	1081	0.98362629	737.52
108- -28	core	**237.4**	22	9.7	77.6	4.49E+05	0.098	0.003	1.54	0.04	0.54	1.25	0.23	5.3	1.39	9.6	2.69	6.92	1.35	11.6	1.47	9300	29.1	312	0.98677173	738.15
108- -12	core	**246.6**	12.6	9.78	26.56	4.68E+05	0.023	0	1.16	0.028	0.42	0.77	0.446	3.47	0.675	4.08	0.85	2.04	0.355	2.29	0.348	10460	15.35	134.5	0.99033885	738.87
108- -64	rim	**244.2**	29.7	9.89	57.4	4.62E+05	0.034	0.023	2.27	0.041	0.74	2.03	0.367	7.52	1.52	9.22	1.76	4.14	0.534	3.57	0.447	9390	40.7	361.3	0.99519629	739.85
108- -87	core	**240.3**	12	9.9	89.8	4.91E+05	-0.003	0	1.67	0.062	1.12	1.73	0.4	6.42	1.63	10.57	2.89	10.31	2.09	16.8	3.23	10110	35.1	278	0.99563519	739.94
108- -9	core	**239.4**	2.9	9.94	31.7	4.68E+05	0.044	0.012	0.84	0.032	0.34	0.68	0.379	2.57	0.524	3.75	0.98	3.18	0.499	3.91	0.591	11130	19.98	122.9	0.99738638	740.29
108- -79	core	**235.4**	3.2	10	58	4.88E+05	-0.026	0.0028	1.16	0.028	0.8	1.68	0.7	5.29	1.04	6.59	1.66	5.57	1.049	10.52	1.96	10030	26.45	160.3	1	740.82
108- -8	core	**246**	0.8	10	29.93	4.63E+05	0.023	0.005	0.754	0.011	0.26	0.45	0.282	1.89	0.487	3.77	0.96	2.76	0.424	3.9	0.596	10910	18.6	116.4	1	740.82
108- -94	core	**229.9**	4.6	10.08	64.6	5.04E+05	0.042	0.0072	2.02	0.084	1.96	3.62	1.2	11.4	1.85	10.66	2.21	5.6	0.83	5.83	0.97	11130	33.41	210.4	1.00346053	741.52
108- -26	core	**239.3**	41.4	10.11	39	4.57E+05	0.045	0	5.42	0.07	1.79	3.88	0.71	12	1.74	8.53	1.154	2.61	0.374	1.88	0.256	13710	575	2831	1.00475116	741.78
108- -39	rim	**229.4**	27.2	10.17	73.2	4.89E+05	0.006	0.0023	3.09	0.057	1.16	2.97	0.59	10.36	2.04	12.79	2.36	5.71	0.749	4.5	0.64	10980	59.6	422.2	1.00732095	742.31
108- -70	core	**236.6**	3.7	10.28	94	4.66E+05	0.192	0.022	3.92	0.445	6.72	10.2	1.74	27.6	4.28	20.2	3.09	6.27	0.66	4.13	0.527	11030	176	811	1.01199311	743.26
108- -116	rim	**238.6**	30.4	10.28	25.9	4.64E+05	0.017	0	1.76	0.024	0.42	1.04	0.286	3.48	0.74	4.71	0.79	1.78	0.276	1.06	0.178	9640	37.9	342.8	1.01199311	743.26
108- -15	core	**228.4**	80	10.3	92.2	4.62E+05	0.134	0.282	3.38	0.322	4.1	6.45	1.27	16.4	3.37	18	3.44	7.39	0.966	5.45	0.75	10770	85	516	1.01283722	743.43
108- -33	rim	**240.7**	1.2	10.37	36.3	4.88E+05	0.028	0.005	0.94	0.032	0.38	0.74	0.5	3.42	0.688	4.98	1.12	2.94	0.549	4.11	0.65	10550	7.33	68.9	1.01577876	744.03
108- -42	rim	**235.1**	27.4	10.4	49.4	4.69E+05	0.045	0.007	3.32	0.032	1.08	2.73	0.46	10	1.84	10.05	1.8	3.31	0.478	2.15	0.361	12280	104.9	741	1.01703334	744.28
108- -46	core	**236.1**	34.5	10.4	28.3	4.80E+05	-0.011	0	1.89	0.021	0.29	0.75	0.36	4.47	0.81	5.41	0.91	2.45	0.354	2.13	0.237	10710	35.9	342	1.01703334	744.28
108- -115	rim	**241.3**	0.1	10.41	33.06	4.51E+05	-0.008	0.016	0.95	0.022	0.29	0.92	0.4	3.28	0.68	4.84	0.9	2.46	0.363	2.89	0.41	9880	10.5	109.5	1.01745073	744.37
108- -41	rim	**233.8**	42.5	10.42	71.4	4.78E+05	0.02	0.0025	2.42	0.031	0.72	1.93	0.295	6.3	1.62	11.36	2.51	7.16	1.23	9.48	1.39	11300	64.2	625	1.01786772	744.45
108- -14	core	**243.8**	2.2	10.55	108	4.59E+05	-0.039	0.0023	2.16	0.09	1.27	2.7	0.46	10.2	2.32	18.1	3.76	11.19	1.82	13.34	2.1	10520	39.82	377.3	1.02325246	745.55
108- -77	rim	**232.5**	30.2	10.56	86.4	4.81E+05	0.03	0.009	3.7	0.109	1.31	4.54	0.77	12.8	2.75	16.3	2.78	7.09	0.96	6.68	0.94	11320	173.2	905	1.02366392	745.63
108- -47	core	**226.2**	14.2	10.6	124.3	4.61E+05	0.05	0	4.04	0.339	4.4	6.7	0.98	24.8	4.46	24.2	4.3	10.97	1.33	7.9	1	12240	457	1398	1.02530587	745.97
108- -111	core	**239.6**	40.4	10.6	85.7	4.58E+05	0.006	0.005	2.19	0.021	0.45	1.41	0.282	5.46	1.38	10.87	2.83	9.53	1.89	16.3	2.72	13090	241.9	1231	1.02530587	745.97
108- -62	core	**239.8**	7.2	10.6	44	4.71E+05	0.026	0	1.65	0.032	0.88	1.82	0.74	6.96	1.33	8.04	1.45	3.29	0.454	2.98	0.384	9800	32.4	218	1.02530587	745.97
108- -23	core	**232.3**	8.9	10.62	44.4	4.61E+05	0.047	0.0073	2.21	0.08	1.59	2.54	0.78	7.76	1.39	8.33	1.51	3.19	0.403	2.49	0.33	10340	48.4	350.2	1.02612621	746.14
108- -51	core	**242.9**	0.2	10.63	75.3	4.50E+05	0.018	0.004	2.09	0.029	0.72	1.81	0.5	6.73	1.36	10.96	2.55	7.73	1.38	10.83	1.86	10110	48.5	272.1	1.02653326	746.22
108- -52	core	**237.9**	38.7	10.73	50.6	4.56E+05	-0.008	0.0071	2.08	0.023	0.61	1.14	0.305	4.97	1.044	6.92	1.65	4.5	0.69	5.25	0.89	9260	29.91	312	1.03059972	747.05
108- -89	core	**230**	39.1	10.8	67	4.87E+05	-0.007	0.008	2.39	0.042	0.8	1.75	0.469	7.4	1.55	10.23	2.36	6.34	0.86	6.24	0.828	10750	48.62	441.4	1.03342376	747.63
108- -102	rim	**233.4**	6.8	10.8	78.7	4.86E+05	0.014	0.0024	2.5	0.047	1.08	2.58	0.5	10.68	1.94	13.67	2.77	7.02	0.874	5.44	0.76	10620	47.3	360.2	1.03342376	747.63
108- -68	core	**240.3**	2.7	10.8	86.3	4.80E+05	0.008	0	2.45	0.029	1.28	2.11	0.89	7.5	2.01	13.53	2.75	7.6	1.3	10.76	1.55	11440	12.37	48.7	1.03342376	747.63
108- -11	core	**241.7**	13.6	10.8	78.6	4.50E+05	0.019	0.0048	3	0.166	2.81	4.43	1.25	15.2	2.93	16.4	2.7	5.49	0.745	4.77	0.498	11310	75.5	459	1.03342376	747.63
108- -67	core	**237.2**	6.9	10.87	71.4	4.66E+05	0.09	0.0093	2.88	0.063	2.12	4.32	0.4	15.3	2.75	14.7	2.38	4.46	0.489	3.18	0.339	12330	125.3	839	1.03622954	748.21
108- -105	core	**234.4**	2.4	11	103.9	4.87E+05	0.019	0	2.85	0.092	1.83	5.36	0.94	16.7	3.06	18.3	3.62	8.79	1.14	7.54	0.986	10650	69.9	491	1.04139269	749.27
108- -86	core	**242.6**	18.1	11.01	235	4.74E+05	-0.003	0.066	3.47	0.37	5.6	9.7	1.76	28.2	5.3	36.9	8.21	25.5	4.62	32.2	4.91	11050	137.6	1250	1.04178292	749.35
108- -75	core	**229.8**	14.7	11.04	197	4.71E+05	0.027	0.031	5.43	0.429	7.46	12.88	1.4	36.3	6.43	35.3	6.83	17.22	2.53	16.8	2.51	10390	165.6	871	1.04296907	749.59
108- -108	core	**234.2**	8.1	11.06	125.5	4.77E+05	0.042	0.05	4.21	0.462	7.13	9.5	1.75	26.5	4.2	25.4	4.43	10.22	1.49	9.49	1.33	10650	134.1	649	1.04375513	749.76
108- -18	core	**239.3**	5.9	11.25	93.2	4.52E+05	0.104	0.002	2.56	0.05	1.13	2.68	0.45	10.39	2.41	15	3.08	8.13	1.07	7.67	1.13	9420	48.4	378.8	1.05115252	751.28
108- -19	rim	**239**	9.6	11.3	81.1	4.54E+05	-0.01276	0.018	3.18	0.077	1.22	2.77	0.54	11.9	2.28	13.83	2.71	7.11	0.99	6.97	1.11	10080	225	1093	1.05307844	751.68
108- -21	core	**239.7**	9.8	11.3	49.4	4.65E+05	0.062	0.0046	2.95	0.075	1.5	3.31	0.84	12.3	2.17	11.27	1.74	3.155	0.413	2.36	0.311	10610	78.6	559	1.05307844	751.68
108- -29	core	**236.1**	4.9	11.4	157.5	4.69E+05	0.058	0.0093	4.02	0.3	5.8	10.8	2.17	31.3	4.95	29.6	5.47	13.67	1.83	10.97	1.67	9970	109.5	585	1.05690485	752.47
108- -24	core	**232.5**	18.5	11.5	19.01	4.67E+05	0.013	0	0.569	0.028	0.21	0.48	0.286	1.23	0.251	2.06	0.483	1.83	0.345	2.52	0.567	10190	11.82	61.3	1.06069784	753.26
108- -43	rim	**232.6**	19.6	11.5	66	4.79E+05	0.004	0.0099	2.5	0.043	0.83	1.92	0.385	7.16	1.36	10.42	2.3	6.36	1.21	8.68	1.57	11490	83.9	447	1.06069784	753.26
108- -61	core	**238.1**	14.1	11.54	88.1	4.77E+05	0.055	0.019	2.46	0.163	2.31	3.68	0.79	12.4	2.24	18.1	3.76	7.68	1.34	9.33	1.42	9690	54.1	380	1.06220581	753.57
108- -1	core	**248.6**	9.2

ABH_27_6	rim	**394.4**	36.8	3.66	825	4.78E+05	0.192		14.31	0.021		1.37	0.061	11.72	4.96	65.6	27.97	131.8	32.36	313.9	56.2	11750	283.1	774	0.56348109	659.56
ABH_27_43	rim	**403.1**	86.4	11.7	2648	5.02E+05	0.152		6.37	0.08		3.91	1.25	33.2	15.6	222.7	93.5	446	102.9	963	172.9	12820	106.5	463.6	0.06818586	754.81
ABH_27_17	rim	**426.6**	3.1	3.32	685	4.88E+05	0.022		12.69	0.0096		1.01	0.058	8.48	3.78	50.3	21.9	112.2	28.22	286.6	53.1	13740	203.9	719	0.52113808	652.36
ABH_27_38	core	**427.1**	783	87.3	1364	4.86E+05	3.03		1.58	0.067		3.41	0.308	26.8	11.42	138.5	46.9	186	37.56	334.7	61.5	10800	29.63	361.2	1.94101424	975.32
ABH_27_24	core	**433.4**	88	8.3	1571	4.81E+05	0.345		0.796	0.0059		1.41	0.158	12.44	7.17	115.8	53.6	281.2	74.5	770	144.3	13240	15.32	212.1	0.91907809	724.70
ABH_27_12	core	**434.9**	990	174	1014	4.83E+05	3.1		11.94	0.088		3.8	0.36	21.1	8.17	97.1	36.1	155	34	314	52.7	9670	159	243	2.24054925	1074.53
ABH_27_9	rim	**438**	14.1	4.78	1776	4.88E+05	0.022		1.49	0.011		1.37	0.18	14.8	8.25	130.1	62.6	306.4	75.9	751	133	12880	19.33	191.7	0.6794279	679.84
ABH_27_41	core	**444.1**	129	30.5	3760	4.98E+05	1.2		31.9	0.19		9	0.97	53	23.02	322.3	130	612	139.7	1311	225.6	12060	636	650	1.48429984	849.33
ABH_27_36	rim	**445.2**	133	15.5	4040	4.81E+05	1.29		52.8	2.16		15.4	0.54	72.5	26.75	341	132.5	600	140.2	1263	216.2	11110	1878	2499	1.1903317	780.86
ABH_27_58	core	**446.2**	7.9	4.23	804	4.94E+05	0.051		16.25	0.096		3.65	1.14	19	6.49	75.6	29.2	129.9	28.2	267	48.7	10100	48.4	74.5	0.62634037	670.45
ABH_27_28	rim	**447.7**	1.9	6.05	982	4.84E+05	0.056		19.77	0.029		2.51	0.066	16	6.52	84.9	33.77	155.5	35.87	339.6	58.7	11380	226.8	459.1	0.78175537	698.50
ABH_27_7	rim	**448.9**	1480	123	1536	4.69E+05	3.9		1.28	0.0076		1.28	0.114	12.54	7.21	114.4	53.3	268	71.3	743	133.6	12400	17.9	208	2.08990511	1022.74
ABH_27_29	core	**449.2**	9.2	4.6	699	4.82E+05	0.072		15.5	0.77		3.07	0.174	12.6	4.61	60.5	23.68	113.7	26.9	255.6	47.6	11010	138.8	428.7	0.66275783	676.87
ABH_27_53	rim	**449.3**	13.3	5.02	3420	5.02E+05	0.025		2.45	0.055		3.21	0.339	32.9	16.7	263	114.3	579	138.2	1329	239	12540	48.5	327	0.70070372	683.66
ABH_27_26	rim	**449.6**	12.9	4.26	2666	4.89E+05	0.008		1.82	0.032		2.5	0.228	21.7	12.71	202.8	93.5	462	119.3	1180	212.7	13170	32.35	332.2	0.6294096	670.98
ABH_27_33	core	**450.1**	7.9	6.22	2854	4.84E+05	0.106		22.5	0.183		8.39	0.66	53.5	21.02	263.4	102.3	460	103	949	165.5	11610	446	554	0.79379038	700.74
ABH_27_48	rim	**450.2**	0	6.44	1403	4.96E+05	0.13		34.7	0.059		4.05	1.24	25.2	9.87	125	49.5	224.3	49.7	480	85.5	11500	218	250	0.80888587	703.56
ABH_27_40	rim	**451.1**	12.2	6.32	2143	4.89E+05	0.194		48	0.173		6.49	0.305	40.3	15.3	188.2	72	326	71	644	107.4	11740	1528	1554	0.80071708	702.03
ABH_27_20	core	**452.6**	47	11.5	1956	4.90E+05	0.6		36.2	1.99		9.2	1.99	44.4	15.17	183	71.8	308	68.4	633	108.4	10550	136.9	156.7	1.06069784	753.26
ABH_27_30	rim	**452.7**	17.4	3.69	2624	4.82E+05	0.196		1.7	0.0113		2.22	0.235	21.8	12.85	196.8	90.2	457	120.3	1231	222.1	13600	27.32	401.9	0.56702637	660.16
ABH_27_27	rim	**452.8**	2300	28	1438	4.69E+05	1.11		1.36	0.031		1.08	0.218	13.45	7.22	108.8	47.9	235	57.8	573	104.7	12580	14.65	174.1	1.44715803	840.19
ABH_27_2	rim	**456**	179	7.55	1462	4.71E+05	1.47		72	5.3		11.1	0.55	36.3	12.1	142	52.3	225.7	49.1	446	73.9	10480	677	715	0.87794695	716.71
ABH_27_19	rim	**458.7**	400	49	3458	4.89E+05	1.2		2.8	0.069		4.18	0.363	33.1	17.39	264.7	115.4	569	140.5	1323	234	12350	45.5	326.6	1.69019608	902.83
ABH_27_21	rim	**460.6**	17.3	3.71	3794	4.83E+05	0.024		2.58	0.065		3.57	0.335	33.8	18.91	295.1	126.5	644	170	1743	310	13860	81.3	912	0.56937391	660.57
ABH_27_52	rim	**461.9**	17.8	7.82	2145	4.97E+05	0.204		11.2	0.101		3.49	0.541	25.9	12.12	169	75.4	372.4	87.6	865	152.2	11750	109.8	274.1	0.89320675	719.66
ABH_27_16	core	**463.3**	3.7	6.44	526.3	4.86E+05	0.036		11.08	0.032		0.84	0.073	7.69	3.19	43.9	18.16	85.5	19.72	197.7	34.31	11320	86.5	218.7	0.80888587	703.56
ABH_27_49	core	**465.8**	27.6	6.97	2232	4.97E+05	0.038		2.63	0.016		2.7	0.222	23.4	11.91	175.1	76.7	379	90.2	854	154	12000	26.99	156.5	0.84323278	710.06
ABH_27_4	rim	**466.6**	2.7	5.28	625	4.78E+05	0.007		11.48	0.031		1.23	0.107	8.91	3.77	49.2	21.88	100.2	23.52	225.4	38.46	11030	148.9	354	0.72263392	687.63
ABH_27_39	core	**471**	0.7	3.75	1290	4.84E+05	0.094		22.5	0.37		3.87	0.178	18.5	7.55	106.8	43	206.9	48.6	465	81	11580	589	1203	0.57403127	661.37
ABH_27_54	core	**563**	12.2	5.71	1282	4.97E+05	0.024		8.8	0.159		5	1.7	24.1	8.89	117.1	44.7	214	50.1	502	91.8	11670	43.8	168	0.75663611	693.85
ABH_27_47	core	**723**	530	48	1001	4.84E+05	3.06		13.56	0.029		2.35	0.37	13.3	5.89	83.2	34.2	172.8	40.8	412	79.9	13420	192	670	1.68124124	900.40
ABH_27_45	rim	**816**	84	8.3	2140	4.97E+05	0.3		10.5	0.72		13.4	2.17	64.1	20.5	223	76.4	314	65.6	594	95.9	8710	82.1	139	0.91907809	724.70
ABH_27_34	core	**829**	2.7	6.97	745	4.78E+05	0.071		6.21	0.1		3.38	0.465	16.9	6.17	71	26.8	114.5	25.5	230.5	41.4	9860	19.69	50.5	0.84323278	710.06
ABH_27_22	core	**948**	88	19.4	516	4.85E+05	1.47		10.39	0.028		0.76	0.179	7.19	2.63	38.3	17.37	81.1	21.5	209	35.7	11060	48.3	217	1.28780179	802.62
ABH_27_8	core	**1046**	-0.7	7.09	416	4.82E+05	0.056		4.81	0.055		3.52	0.28	13.4	4.13	41.9	14.7	57.6	12.38	111.6	18.7	9080	29.3	105	0.85064624	711.47
ABH_27_3	core	**1087**	7.3	7.33	885	4.85E+05	0.098		10.78	0.059		2.43	0.152	14.6	6.39	79.6	31.7	148.1	34.43	338.7	59.6	10110	71.7	187.2	0.86510397	714.24
ABH_27_10	core	**1119.6**	116.1	7.39	402.1	4.87E+05	0.204		13.83	0.038		0.8	0.198	3.82	1.92	24.7	11.43	63.1	17.87	225	47.7	11370	125.6	548	0.86864444	714.92
ABH_27_18	core	**1189**	-4.1	5.44	1252	4.87E+05	0.045		11.48	0.087		4.5	0.534	29.2	10.61	123.2	46.2	187.3	39.5	340.4	56.2	8680	41.27	145	0.7355989	689.99
ABH_27_23	rim	**367**	252	36.7	1052	4.81E+05	6.63		13.37	0.504		2.54	0.589	14.6	6.33	85.3	34.09	169	42.72	449	87.3	12780	139.7	1720	1.56466606	869.62
ABH_27_25	rim	**1118**	61	12.4	920	4.88E+05	0.217		6.7	0.066		2.29	0.279	13.7	5.34	75.1	31.1	152.3	37.6	385	75.7	10070	64.5	260.6	1.09342169	760.09
ABH_27_37	rim	**857**	10020	840	1070	4.30E+05	25.7		8.8	0.194		3.65	0.312	22.6	7.89	96.9	36.1	169.1	37.7	360	67.1	9520	126.5	336	2.92427929	1373.14
ABH_27_42	core	**633**	220	23.7	991	4.99E+05	0.67		7.6	0.076		3.1	0.149	16.9	6.56	87.1	34.4	166.9	39.1	382	72.5	10970	79.4	441	1.37474835	822.80
ABH_27_50	core	**434**	21.6	8.44	4440	5.01E+05	1.3		37.2	0.557		17.7	1.37	96.5	34.6	414	156	695	149	1353	231.9	10140	705	814	0.92634124	726.13
ABH_27_56	core	**1017**	53	12.7	1682	4.98E+05	0.5		11.82	0.079		4.44	0.355	28.3	11.6	151.6	59.2	277.2	59.3	564	96.5	10330	72.2	208.1	1.10380372	762.28
ABH_27_60		**2020**	7.77E+04	960	0.61	1.3	15.37		0.474	0.048		0.14	0.71	0.068	0.026	0.16	0.027	0.19	0	0.16	0	0	0.49	11.3	2.98227123	1404.68
AK-01																										
AK_01_1	core	**1172**	740	30.2	2850	4.55E+05	1.71	20	65.4	5.7	32.3	20.1	4.09	75.8	24.4	275	97.2	408	83.1	710	119.4	9360	390	964	1.48000694	848.26
AK_01_2	rim	**189.2**	4.9	11.68	571	4.87E+05	0.081	0	12.29	0.034	0.45	1.32	0.247	9.49	3.4	45.8	18.5	87.3	21.06	204.9	38.4	10680	30.44	44	1.06744284	754.66
AK_01_3	core	**1004**	39.5	16	1966	4.80E+05	0.076	0.0081	16.42	0.147	3.21	7.74	0.347	43.4	15.11	183.1	65.8	290.7	64.6	588	99.5	11030	112.4	281.2	1.20411998	783.89
AK_01_4	core	**190.1**	6.8	6.77	4240	4.95E+05	0.347	0.086	88.8	0.454	7.55	14.2	3.49	83.6	29.3	366	140.6	641	143.2	1350	244.3	8630	361	232.3	0.83058867	707.66
AK_01_5	rim	**1020**	-3	8.43	708	4.78E+05	0.05	0.0023	14.42	0.05	0.99	2.1	0.122	13.8	5.09	63	25.11	108.5	24.27	227.7	40.1	10970	74.7	269.2	0.92582757	726.03
AK_01_6	core	**191.6**	7.6	14.2	1444	4.80E+05	0.208	5.9	32.1	2.24	12.3	7.75	1.8	35.2	11.2	131.3	47.8	214.2	47.3	439.3	78.7	9170	61.9	57	1.15228834	772.61
AK_01_7	rim	**188**	-0.2	16.7	916	4.85E+05	0.092	0.01	15.28	0.075	1.93	3.28	0.75	18.8	6.51	80.7	30.93	138.5	31.45	295.2	53.1	9390	46.31	51.3	1.22271647	787.99
AK_01_8	core	**175.7**	3.7	12.16	2805	4.84E+05	0.214	0.036	31.3	0.563	9.31	15.2	8.7	72.3	22.71	258.8	95.4	424.8	92.8	883	165.8	7200	36.8	37.61	1.08493357	758.31
AK_01_9	rim	**186.1**	33.1	13.5	744	4.82E+05	0.45	0	15.72	0.037	0.83	2.05	0.341	13.04	4.7	61.4	24.44	115.4	27	263	48.7	10360	41.1	54.5	1.13033377	767.90
AK_01_11	core	**1017**	-0.4	7.43	1217	4.79E+05	0.01	0.036	17.73	0.263	4.3	7.9	2.17	40.2	11.81	126.6	42.9	174	37	331	55.9	8610	43.2	63.1	0.87098881	715.37
AK_01_12	rim	**184.2**	-2	8.11	510	4.87E+05	0.067	0.0074	14.24	0.015	0.46	1.03	0.135	7	3.03	39	16.03	81.2	19.61	202.4	38.1	11800	33.5	64.6	0.90902085	722.74
AK_01_13	rim	**179.6**	2.7	11.75	988	4.89E+05	0.085	0.032	14	0.146	2.3	3.8	0.68	22.4	7.07	86.4	33.7	154	35.2	326	61.3	10260	56	74.2	1.07003787	755.20
AK_01_14	rim	**194.1**	2.1	13.06	674	4.78E+05	0.045	0.0036	15.13	0.043	0.57	1.59	0.287	11.08	4.17	55.8	21.7	104.1	24.55	240	43.8	10400	39.3	52.2	1.11594318	764.84
AK_01_15	core	**190.3**	35	13.24	858	4.84E+05	0.08	0.0038	11.43	0.067	1	2.56	0.472	14.8	5.55	70.2	28.3	134.3	30.7	306	56.7	9970	26.85	40.2	1.12188799	766.11
AK_01_16	rim	**187.1**	2.6	11.18	722	4.89E+05	0.109	0.0076	14.95	0.027	0.45	1.59	0.23	11.53	4.23	57.1	23.5	112.3	26.9	264	49.7	10830	35.9	50.6	1.0484418	750.72
AK_01_17	core	**191.2**	2.4	13.19	2977	4.84E+05	0.143	0.2	29.5	0.498	7.85	15.63	6.45	84.2	26.95	310	108.8	460.9	94.1	831	143.5	8340	104.6	75.2	1.12022448	765.76
AK_01_18	rim	**193.3**	7	28.1	1484	5.10E+05	0.071	0.04	19.99	0.5	6.4	9.9	0.68	44	13.48	145.8	50.8	209.6	43.6	392	62.7	10310	94.9	98.8	1.44870632	840.57
AK_01_19	core	**867**	41.8	14.4	959	4.46E+05	0.22	0.027	9.27	0.112	1.33	2.82	0.37	17.2	6.52	81.9	32	153.9	35.1	343.8	66	9760	129.7	735	1.15836249	773.92
AK_01_20	rim	**1183**	1.5	15.7	650	4.94E+05	0.153	0.027	8.42	0.075	1.25	2.1	0.357	12.58	4.59	56.4	21.79	101.1	23.25	219.6	39.5	10650	43.3	120.2	1.19589965	782.08
AK_01_21	core	**921**	43	17.62	751	4.84E+05	0.28	4.4	27	13	6.4	6.4	1.47	21.8	6.69	74	26.5	112.3	26	233	41.3	9470	21.89	39.4	1.2460059	793.18
AK_01_22	core	**186.9**	28.9	10.67	1334	4.87E+05	0.63	0	16.71	0.081	1.84	5.01	0.82	29.7	9.69	119.9	45	200.5	43.5	412	71.9	10040	60.9	56.6	1.02816442	746.55
AK_01_23	core	**186.3**	0.8	10.73	726	4.88E+05	0.023	0.002	17.12	0.04	0.68	1.71	0.318	12.25	4.62	60.8	23.59	114.1	26.47	259.8	48.8	10910	46.41	64	1.03059972	747.05
AK_01_24	core	**185.2**	-2.2	14.1	1575	4.86E+05	0.133	3.2	26.1	0.98	8.9	9.51	1.59	44.1	13.38	154.6	54.6	232.2	50.5	461	81	9590	74.6	65.7	1.14921911	771.95
AK_01_25	rim	**186.7**	3.1	15.88	811	4.79E+05	0.046	0.0041	15.18	0.05	0.98	2.51	0.511	16.2	5.61	70.8	26.44	124.1	27.98	270.2	49.8	9530	40.76	47.9	1.2008505	783.17
AK_01_26	core	**184.9**	245	13.78	797	4.81E+05	1.84	0	11.21	0.039	0.72	2.36	0.326	13.9	4.67	62.7	25.71	123.8	28.74	286.1	54.2	10440	25.67	40.6	1.13924922	769.81
AK_01_27	core	**185.6**	1.7	18.2	840	4.86E+05	0.076	0.0092	13.85	0.049	1.41	2.75	0.468	18.3	5.8	72.7	28.8	130.1	29.8	278.2	52.5	9160	37.6	42.5	1.26007139	796.34
AK_01_28	core	**189.3**	0.8	12.4	1034	5.09E+05	0.089	0.0037	13.93	0.054	1.13	3.07	0.56	20.6	6.89	88.9	34.9	158.3	35.7	340	60	10370	44.5	48.2	1.09342169	760.09
AK_01_29	core	**1313**	7.3	10.5	2070	4.86E+05	0.15	10	33	4.2	23	9.5	0.29	37.6	14.48	187.3	72.4	317	71.4	650	109.3	12100	90.7	392	1.0211893	745.13
AK_01_30	rim	**1010**	-1.4	13.2	872	4.85E+05	0.075	2.1	13.6	0.49	5.7	4.9	0.64	24.9	7.57	96.6	30.8	130.5	27.6	250	43	9610	42.7	104.3	1.12057393	755.83
AK_01_31	rim	**194**	1.6	14	766	4.93E+05	0.113	bdl	11.49	0.08	1.15	2.95	0.46	15.4	5.54	67.4	25.5	118.7	27.2	260	47.3	9920	32.6	39.5	1.14612804	771.29
AK_01_32	core	**187.6**	-0.2	16.1	1593	4.87E+05	0.07	0.0054	17.49	0.204	3.86	7.92	1.47	41.6	13.13	150.1	54.9	237.5	52	469	82.8	9790	72.6	63.4	1.20682588	784.48
AK_01_33	rim	**1002**	8.9	21.5	876	4.84E+05	0.063	0.012	15.4	0.082	1.42	3.79	1.27	20.8	7.14	82.8	30.34	132.4	29.2	266.3	46.7	9520	24.29	45	1.33243846	812.89
AK_01_34	rim	**185.6**	253.4	641	1545	4.87E+05	2.21	0.043	16.59	0.209	3.68	6.78	1.04	35.7	11.18	137.8	51.2	232	50.4	486	84.8	9540	74.5	70.5	2.80685803	1312.79
AK_01_35	rim	**177.8**	104	23.6	1449	4.99E+05	0.87	0.047	17.8	0.133	3.4	7.4	1.27	35.3	11.05	136	49.4	215	48.7	454	77.8	9920	68.3	63.1	1.372132	822.37
AK_01_36	core	**177.8**	4.2	7.89	428.6	4.83E+05	0.177	0	11.33	0.013	0.261	0.98	0.116	5.76	2.38	32.2	13.45	69.7	17.11	176.7	34.52	11630	26.86	59	0.897077	720.41
AK_01_37	core	**182.9**	1.7	12.43	1610	4.92E+05	0.087	0.016	19.44	0.185	3.84	7.93	1.32	41.7	13.29	152.2	54.6	238	52.3	471	83.6	10070	80.5	70.6	1.09447113	760.31
AK_01_38	core	**186.8**	12.9	13.9	705	4.84E+05	0.18	-0.0007	10.42	0.043	0.77	1.92	0.409	12.7	4.4	58.1	22.92	113.1	26.39	252.1	47.3	10250	22.84	35.29	1.1430148	770.62
AK_01_39	rim	**1000**	41.4	16.4	1000	4.85E+05	0.023	0.029	4.39	0.092	2.25	4.86	0.087	28	9.6	101.3	34.29	139.4	29.83	271.2	44.5	10260	98.4	251.2	1.2148485	786.25
AK_01_40	rim	**188**	-0.3	13.2	813	4.85E+05	0.074	0.0063	14.71	0.026	0.75	2.23	0.307	14.5	5.32	69.2	26.68	127.1	29.3	279	51.7	9690	38.83	45.2	1.12057393	765.83
AK_01_41	core	**185**	4.9	10.1	780	4.92E+05	0.068	0.0026	16.9	0.034	0.57	2.16	0.39	13.1	4.98	65	28	126	28.2	276	52.6	10310	30.1	41.9	1.00432137	741.70
AK_01_42	core	**186**	-0.8	11.21	1554	4.79E+05	0.134	2.2	23.7	1.01	9.1	9.17	1.57	42.4	12.82	146.6	53	231.2	50.5	452	81.1	9290	73.9	68	1.04960561	750.96
AK_01_43	core	**970**	-1.5	12.64	2710	4.85E+05	0.049	0.0074	10.31	0.204	4.12	10.15	0.161	61.6	21.96	262.1	90.5	388.8	82.7	725	121.2	12260	281.6	588	1.10174707	761.84
AK_01_44	core	**186.6**	-0.1	13.6	875	4.90E+05	0.086	0.0019	15.6	0.069	0.95	2.55	0.444	17.5	6.09	73.3	29	135.6	33.93	303.2	55.2	10130	44.88	52.2	1.13353893	768.59
AK_01_45	core	**1073**	7.8	10.5	392.8	4.83E+05	0.045	0.007	12.6	0.017	0.61	1.03	0.43	7.8	2.6	35.7	13.86	61.7	14.06	138.7	26.1	10130	148.4	235.2	1.0211893	745.13
AK_01_46	rim	**1013**	5.4	13.57	841	4.76E+05	0.188	0.007	24.72	0.063	1.13	2.62	0.58	17.2	6.21	77.7	28.93	134.9	29.8	290	52.1	10970	64.3	145.5	1.13257985	768.38
AK_01_47	core	**1222**	87	22.8	1508	4.81E+05	0.88	0.016	9.58	0.21	4.2	6	0.85	35.6	11.29	143	51	228	50	447	76.8	9570	122	302	1.35793485	818.84
AK_01_48	core	**185.1**	12.7	27.8	1192	4.88E+05	4.4	16.3	49.5	5.2	28.3	13.1	1.07	39.8	10.86	118.3	41.2	171	37.1	358	312.7	53.6	9580	55.3	51.7	1.4440448	839.43
AK_01_49	rim	**186.5**	2.6	13.6	617	4.83E+05	0.081	0.009	13.68	0.045	0.56	1.78	0.367	11	4.17	50.5	20.17	95.6	22.28	214.6	39.8	10080	33.35	42.82	1.13353891	768.59
AK_01_50	core	**189.8**	1.5	16.7	882	4.92E+05	0.114	0.01	14.02	0.074	1.41	2.92	0.54	18.6	6.16	76.1	28.98	133.4	30.64	287.1	53.7	9570	41.36	45.44	1.22271647	787.99
AK_01_51	rim	**1001**	0	12.5	476.8	4.90E+05	0.14	0.004	17.43	0.025	0.76	1.38	0.335	7.62	3.13	40.1	15.6	75.3	18.2	189.5	35.38	10940	29.96	58.2	1.09691001	760.82
AK_01_52	core	**1126**	6.6	5.14	1872	4.91E+05	0.109	0.193	12	0.109	1.96	4.74	0.85	31.9	12.51	165.1	66.2	302.7	66.2	617	111.1	10060	111	534	0.71096312	685.51
AK_01_53	rim	**983**	3.1	5.4	947	4.75E+05	0.22	0.014	27.4	0.034	0.52	1.5	0.073	13.2	5.99	81.4	32.5	156.2	35	327	59.2	13450	58.5	152.5	0.71233076	684.41
AK_01_54	core	**186.5**	3.1	9.21	418	4.88E+05	0.074	0	10.39	0.0115	0.39	1	0.19	5.89	2.58	33.8	13.92	66.6	16.06	162.4	31.22	11670	21.72	40.1	0.96425963	733.64
AK_01_55	core	**1016**	1.3	20.7	989	4.80E+05	0.08	0.015	15.46	0.164	2.63	5.04	1.77	28.5	8.72	99.5	35	145.9	31.7	283	49	9510	25.9	35.18	1.31597035	809.08
AK_01_56	core	**189.2**	7	10	959	4.80E+05	0.17	0	12.66	0.063	1.37	3.2	0.56	18.9	6.62	85	33.4	149.9	33.1	315.6	57.7	9860	45.3	59.7	1	740.82
AK_01_57	rim	**182.2**	12.1	14.75	919	4.84E+05	0.103	0.006	11.25	0.062	1.07	2.81	0.521	18.6	6.33	76.6	30.18	142.8	31.47	305.9	56.2	9950	31	37.28	1.16879202	776.17
AK_01_58	core	**186**	-0.8	13.81	813	4.89E+05	0.097	-0.0052	14.77	0.067	0.96	2.42	0.447	16.2	5.41	69.4	26.86	123.7	29	275.7	52.2	10020	40.5	48	1.14019368	770.01
AK_01_59	rim	**993**	9

AK_01_113	core	**593.1**	2140	25	1200	4.41E+05	8.19	0.543	19.5	0.293	2.86	4.75	0.407	25	8.23	105	41.7	199.1	48.6	494	94.9	10280	438	1167	1.39794001	828.31
AK_01_114	core	**1027**	470	16.7	678	4.71E+05	2.5	0.34	10.15	0.159	1.69	2.96	0.7	15.9	5.6	66.5	23.36	103.8	22.1	208.3	37.1	9640	29.8	81.3	1.22271647	787.99
AK_01_115	core	**188.9**	-1.2	8.92	499	4.85E+05	0.162	0.0066	13.38	0.0082	0.47	1.39	0.219	6.89	2.85	40.3	16.78	81.1	19.52	194.9	37.4	12050	31.72	57	0.95036485	730.87
AK_01_116	core	**1001**	81	6.41	2820	4.86E+05	0.87	0.108	14.71	0.417	7.58	16.1	3.75	97.4	29.4	310	101.8	404	78.4	663	110.7	9290	435	403	0.80685803	703.18
AK_01_117	core	**185.7**	-0.9	15.4	1107	4.85E+05	0.056	0.073	16.39	0.187	2.73	4.62	0.87	23.6	7.96	102.3	38.7	171.2	38.6	361	65.3	9760	64.1	64.2	1.18752072	780.25
AK_01_118	core	**1030**	1.9	10.71	757	4.81E+05	0.107	0.0085	24.2	0.043	0.66	2.08	0.526	13.7	5.26	68	25.6	117.6	27.3	270	48.3	11790	57.7	143.2	1.02978947	746.89
AK_01_119	rim	**1047**	19.5	12.2	1266	5.19E+05	2.8	0.068	16.2	0.22	1.92	3.9	0.19	20	8.02	106.5	43.7	219.3	53.8	576	95.3	14190	132.9	416	1.08635983	758.61
AK_01_120	core	**491**	37.8	16	798	4.50E+05	1.48	0.62	7.4	0.75	6.3	4.24	1.05	16.4	4.74	60.9	26.4	143.2	38.4	449	94.5	15410	84.7	2045	1.20411998	783.89
AK_01_121	core	**185.7**	0.4	13.28	827	4.84E+05	0.073	-0.0006	17.43	0.045	1.06	3.05	0.52	15.2	5.9	70.3	27.49	129.5	29.25	279.6	51.4	10410	50.1	60.3	1.12319808	766.38
AK_01_122	core	**1080**	22.8	11.9	1283	4.77E+05	0.153	0.027	15.64	0.072	1.43	3.41	0.186	24	9.13	117.1	45.4	201.8	44.3	409.3	71.9	11240	193	548	1.07554696	756.35
AK_01_123	core	**1292**	160	24.3	622	4.76E+05	0.152	0.0036	8.64	0.039	0.63	1.8	0.197	11.8	4.21	56.1	21.54	99.8	22.37	218.2	38.95	10790	52.5	179.1	1.38560627	825.37
AK_01_124	rim	**1309**	6.2	11.95	1110	4.83E+05	0.193	8	36.7	3.3	14.4	6.3	0.241	23.5	7.94	98.4	39.6	179.2	39.3	380	67.1	11470	136.5	456	1.07736791	756.73
AK_01_125	rim	**186.4**	5.4	4.66	1124	4.90E+05	0.258	0.0054	35.35	0.037	1.11	2.97	0.52	17.4	6.98	95.9	38.56	182.6	42.8	415.6	77.1	11520	64.9	97.1	0.66838592	677.87
AK_01_126	core	**179.4**	0.3	9.44	950	4.80E+05	0.105	0	26.84	0.036	0.92	2.39	0.5	16.2	6.03	81.2	32.25	152.5	35.3	345.1	64.1	10960	45.2	63.4	0.97497199	735.78
AK_01_127	rim	**1120**	8	11.06	673	4.78E+05	0.058	5	17.6	1.34	5.7	2.65	0.205	12.08	4.74	60.8	23.12	109.1	24.51	229.5	40.9	11130	53.6	178.5	1.04375513	749.76
AK_01_128	rim	**193.3**	51.4	14.5	982	4.88E+05	0.32	0	12.99	0.085	1.86	3.21	0.64	19.3	6.81	85	33.4	151.5	35.2	339.4	63	10250	35.5	45.5	1.1613 68	774.57
AK_01_129	core	**186.7**	0.4	9.04	1225	4.88E+05	0.038	0	16.77	0.045	1.17	3.43	0.64	23.7	8.59	106.7	42.1	187.2	40.9	391.5	69.3	10520	65.1	61.8	0.95616843	732.03
AK_01_130	core	**184.6**	0.1	14.49	1412	4.82E+05	0.057	0.015	16.91	0.218	4.25	7.66	1.34	34.5	11.33	132.6	48.2	210.8	46.1	431	75.7	9790	66.9	61.9	1.16106839	774.50
AK_01_131	core	**187.2**	13.5	14.2	885	4.76E+05	0.045	0	11.92	0.067	1.05	3.03	0.5	16.8	6.03	75.8	29.7	136.4	30.7	294.5	54.7	9780	32.79	40.6	1.15228834	772.61
AK_01_132	core	**1006**	3.2	11.31	1598	4.74E+05	0.192	0.176	28.81	0.144	1.76	4.15	0.429	27.2	10.77	139.4	54.7	246.9	56.5	525	93.2	12150	202.3	591	1.05344626	761.76
AK_01_133	core	**184.5**	-0.5	16.5	835	4.83E+05	0.05	0	15.69	0.088	1.32	3.16	0.54	17.3	5.89	74.6	28.26	127.2	29.4	278.8	51.7	9850	46.76	52.9	1.21748394	786.84
AK_01_134	rim	**183**	-2.7	1.96	2690	4.87E+05	0.146	3.78	37	1.52	9.1	5.05	0.54	31.2	13.17	195	88.2	446	112.4	1169	223	12560	123.4	382.8	0.29225607	615.31
AK_01_135	core	**180.4**	1.6	1.08	1937	4.84E+05	0.065	0.31	13.8	0.23	1.63	3.45	0.59	25.1	10.28	151.2	63.1	321	78.8	784	152.7	11520	86.7	257	0.03342376	576.83
AK_01_136	core	**185.5**	-1.7	15.4	978	4.79E+05	0.071	0.0088	14.05	0.123	1.75	4.34	0.81	22	7.02	86.4	33.21	150.9	33.34	321.1	59.3	9430	45.1	48.7	1.18752072	780.25
AK_01_137	core	**186.9**	1.8	11.4	750	4.89E+05	0.363	0	14.75	0.044	0.6	1.83	0.388	12.6	4.43	60.1	24.24	115.8	27.25	270.8	51	11330	37.73	49.5	1.06690485	752.47
AK_01_138	rim	**969**	4.4	11.37	821	4.82E+05	0.135	0.312	22.53	0.161	1.19	2.71	0.61	16.6	5.54	72.2	28.2	131.4	30.2	292.6	55.8	12530	73.4	198	1.05576046	752.23
AK_01_139	core	**1026**	209	8.87	1214	4.82E+05	0.73	0.105	13.3	0.086	1.63	4	0.75	25.7	8.84	111.9	42	188.2	40.4	383	69.2	10700	43.4	99.6	0.94792362	730.39
AK_01_140	core	**1027**	490	29	884	4.73E+05	4.04	0.043	18.99	0.105	1.54	3.48	0.83	19.8	6.82	83	31.1	132.3	29.3	277	49.5	10060	35.2	66.7	1.462398	843.92
AK_01_141	rim	**185.7**	2	10.02	2470	4.79E+05	0.236	0.92	37.9	1.14	12.6	14.9	4.45	66.2	20.9	242	88.5	383	81.3	738	135.4	10310	112.4	86.9	1.00086772	741.00
AK_01_142	core	**155**	1980	105	1431	4.89E+05	15.2	5.7	31.5	2.2	16.2	10.3	1.89	36.1	11.39	135.3	48.8	215.9	46	428	79.1	10200	68.1	62.8	2.0211893	1000.41
AK_01_143	core	**1318**	6	12.8	2740	4.99E+05	0.1	0.0015	8.41	0.205	5.13	12.3	0.62	72.7	23	268	95.3	396	78.6	697	119.8	11400	161	349	1.10720997	762.99
AK_01_144	rim	**194**	10.7	1.55	1400	5.12E+05	0.17	3.7	21.5	1.99	13.3	4.9	0.68	19.7	6.83	98.3	45.3	240.6	60.5	680	140.5	14310	53.3	210.4	0.1903317	599.75
AK_01_145	rim	**187.1**	-1.3	13.1	827	4.96E+05	0.074	0.0087	16.8	0.042	0.9	2.48	0.379	14.16	5.16	70.3	27.38	129	29.19	282.2	54	11010	45.6	55.6	1.1172713	765.13
AK_01_146	rim	**1001**	22.6	16.5	1656	4.79E+05	0.11	0.108	6.32	0.127	2.05	5.11	0.187	32.2	11.98	147.3	55.7	248.1	56.1	527	91	13450	161.6	488	1.21748394	786.84
AK_01_147	core	**1007**	-1.7	15.52	683	4.89E+05	0.034	0.0045	9.85	0.043	0.94	2.14	0.307	14.8	5.11	62.2	23.69	103.8	22.96	214.8	37.7	10640	38.1	107.7	1.19089172	780.99
AK_01_148	rim	**608**	-5.9	9.97	1130	5.09E+05	0.084	0.0086	14.71	0.03	0.87	2.29	0.455	17	6.89	93.8	38.61	186	44.1	439.8	83.2	11560	20.99	64.9	0.99869516	740.56
AK_01_149	rim	**189.8**	0.1	16	772	4.97E+05	0.145	4.5	26.7	1.77	8.5	4.5	0.82	16.8	5.75	66.7	25.85	119	26.53	261.3	47.9	10020	39.82	47.8	1.20411998	783.89
AK_01_150	core	**973**	-2.5	12.3	762	4.93E+05	0.057	0.0086	14.64	0.085	1.14	3.62	1.15	19.5	6.01	72	27.7	117.8	25.64	236.8	43	10340	22.17	40.8	1.08990511	759.35
CVI-1344																										
CVI_1344_46	core	**66.1**	10	9.3	1022	4.96E+05	0.172		1.41	0.043		1.74	0.5	14.2	5.67	76.8	32.94	160.1	38.88	423	84.6	8210	83.9	429	0.96848295	734.48
CVI_1344_48	core	**66.3**	7.3	9.3	990	4.87E+05	0.021		1.17	0.042		1.97	0.47	15.1	5.49	75.1	32.5	160.7	37.7	397	81.5	7660	76.9	330	0.96848295	734.48
CVI_1344_4	core	**67.2**	46	4.82	1422	4.84E+05	0.061		2.67	0.069		2.5	0.57	20.8	8.06	110.3	47.2	237.3	56.9	595	122.4	9300	145.8	651	1.06304704	680.49
CVI_1344_36	core	**67.3**	6.8	11.57	1094	4.92E+05	0.01		1.31	0.031		1.66	0.51	14.6	5.97	80.2	35	173.3	41.82	440.9	89.6	7720	89.4	402.1	1.06333336	753.80
CVI_1344_8	core	**67.6**	7.5	11.3	1167	4.74E+05	0.054		0.83	0.084		2.63	0.9	19.9	7.03	95.6	38.26	181.1	42	440	89.5	6640	76	327.9	1.05307844	751.68
CVI_1344_20	rim	**67.7**	3.4	9.24	961	4.81E+05	-0.009		1.248	0.028		1.35	0.394	11.7	4.76	70.5	30.92	156.3	37.92	401.1	82.1	8180	76.5	397.7	0.96567197	733.92
CVI_1344_35	rim	**68**	210	7.4	1268	4.76E+05	0.77		2.76	0.058		2.08	0.5	17	6.61	96	40.27	196.7	47.4	484	100.4	10250	138.7	672	0.86923172	715.03
CVI_1344_38	core	**68**	40	23.1	6000	5.01E+05	0.166		11.98	1.01		39.2	8.91	204	59.1	591	186	695	138.7	1204	202.1	7200	1250	1768	1.36361198	820.17
CVI_1344_50	core	**68.1**	-0.1	6	1285	4.88E+05	0.044		2.18	0.031		3.2	0.52	20.6	8.17	106.1	43.7	210.8	48.9	513	98.7	10080	128.2	613	0.77815125	697.83
CVI_1344_56	rim	**68.13**	7.2	6.48	1781	4.83E+05	0.105		4.18	0.045		3.34	0.54	30.2	11.16	146.7	61.7	284	65	659	124.4	11580	293	1019	0.81157501	704.07
CVI_1344_22	rim	**68.2**	2.4	12.5	1662	4.85E+05	0		2.18	0.052		2.57	0.59	24.7	9.97	129.4	54.4	255.3	61.5	615	123.7	7940	181.3	646	1.09691001	760.82
CVI_1344_41	rim	**68.2**	5.2	6.92	1050	4.91E+05	0.051		1.83	0.029		2.43	0.375	17.1	6.85	87.9	36.1	163.6	38.6	378	74.1	8740	168.3	538	0.84010609	709.46
CVI_1344_15	core	**68.3**	9.1	5.39	755	4.88E+05	0.09		1.05	0.024		1.33	0.336	10.3	4.35	58.6	25	124.6	31.3	340	72.1	9380	59.9	321	0.73158877	689.26
CVI_1344_16	rim	**68.32**	1.7	7.19	1897	4.75E+05	-0.02		3.2	0.03		3.41	0.64	30.4	11.49	159.2	65	303	68.3	688	135.4	9660	185.9	755	0.85672889	712.63
CVI_1344_2	core	**68.39**	7.8	15.6	4318	4.78E+05	0.118		18.03	2.32		44.1	11.66	161.9	44.4	451.1	142.8	586	122.9	1176	209.6	7170	640	1017	1.1931246	781.48
CVI_1344_47	rim	**68.6**	35	6.62	1090	4.83E+05	0.126		2.51	0.249		4.11	0.85	21.2	7.4	89.1	36.6	169	40.6	416	82.9	8140	93	361	0.82085799	705.82
CVI_1344_54	core	**68.8**	10.7	4.28	613	4.92E+05	0.048		0.75	0.018		1.21	0.307	8.02	3.17	43.2	19.6	100	26.6	300	65.1	8260	37	247	0.63144377	671.34
CVI_1344_55	rim	**68.8**	3.80E+03	7.81	999	4.76E+05	-1.49		1.58	0.05		1.56	0.47	13.6	5.55	76.8	32.9	157.8	38.6	411	80.9	8410	118	534	0.89265103	719.55
CVI_1344_14	core	**68.9**	8.5	8.99	897	4.84E+05	-0.008		1	0.035		1.92	0.53	13.8	4.9	70.3	30	144.4	35.9	384	77.1	7890	59.6	302	0.95375969	731.55
CVI_1344_23	core	**69**	20	9.2	947	4.84E+05	0.103		1.31	0.047		1.87	0.501	14.7	5.26	71.6	30.3	147.9	36.3	380	79.8	7410	81.6	320	0.96378783	733.55
CVI_1344_6	core	**69.1**	230	6.5	1187	4.85E+05	0.118		1.37	0.115		4.1	0.76	25	8.55	107.5	41.5	185.6	42.8	431	81	8410	77.4	312	0.81291336	704.32
CVI_1344_32	rim	**69.1**	2.2	7.28	1305	4.83E+05	0.033		2.96	0.039		3.16	0.481	22.4	8.64	106.1	43.3	202	46.5	476	89.9	9300	234.6	781	0.86213138	713.67
CVI_1344_44	rim	**69.1**	-1.7	6.3	944	4.90E+05	0.043		1.99	0.045		1.62	0.323	12.8	4.79	66.2	30.3	153.4	37.7	402	85	9540	123	564	0.79934055	701.77
CVI_1344_9	core	**69.2**	4.7	13.3	1498	4.78E+05	0.02		1.97	0.06		2.21	0.514	21.3	8.41	115	49	238.5	56.6	593	119.4	7730	131.3	578	1.12385164	766.52
CVI_1344_13	rim	**69.2**	8.8	8.79	961	4.78E+05	0.028		1.125	0.037		1.5	0.344	13.2	5.37	74.2	31.75	154.3	37.6	393	80.7	8250	70.1	358	0.94398888	729.61
CVI_1344_3	rim	**69.3**	18	9.68	1422	4.79E+05	0.17		1.82	0.054		2.81	0.79	24.3	9.08	118.9	48.5	224.6	50.9	512	100.6	7930	190	555	0.98587536	737.97
CVI_1344_24	rim	**69.3**	28	6.72	1589	4.88E+05	0.076		2.75	0.045		2.9	0.288	22.8	9.46	128.9	53.7	250	57.5	554	106.2	9530	140.4	598	0.82736927	707.05
CVI_1344_45	rim	**69.4**	4.3	8.31	968	4.92E+05	0.029		1.37	0.032		2.74	0.392	16.02	6	76	31.98	153.3	35.61	364.3	72.4	8200	129.5	422	0.91960102	724.81
CVI_1344_18	rim	**69.49**	-0.8	6.45	1552	4.72E+05	0.053		4.45	0.054		5.08	0.84	40.3	13.12	149.9	52.8	221.1	46.8	432	75.4	10380	532	1616	0.80955971	703.69
CVI_1344_1	rim	**69.5**	4.4	8.16	1322	4.76E+05	0.015		2.77	0.064		3.46	0.54	24.4	8.82	112	46.2	205.6	47.1	456.9	86.9	8860	252.9	711	0.91169016	723.26
CVI_1344_11	rim	**69.5**	23.8	19.9	2531	4.84E+05	0.032		1.47	0.132		6.06	0.344	43.4	16.34	220.6	89.7	423.4	96.4	924	169.9	10030	73.3	284.9	1.29885308	805.14
CVI_1344_27	rim	**69.5**	6.4	5.84	1189	4.84E+05	0.035		2.16	0.022		2.14	0.238	18	6.99	94.7	39.1	189	44.3	433	85	9840	104.1	466	0.76641285	695.65
CVI_1344_40	core	**69.5**	1.4	5.68	1108	5.01E+05	0.052		1.22	0.079		3.31	0.5	21.1	7.49	92.1	38.7	176.6	42	408	79.1	8220	66.9	291.1	0.75434834	693.43
CVI_1344_7	rim	**69.8**	7.3	8.08	790	4.72E+05	0.03		2.08	0.027		2.53	0.593	17.6	5.54	68.6	26.72	122	27.79	277.3	53.9	8540	272.1	702	0.90741136	722.42
CVI_1344_25	core	**69.8**	0.1	6.63	1199	4.77E+05	0.04		1.3	0.046		2.4	0.409	18	6.97	97	40.3	190.6	45.1	459	88.8	8230	65.3	336	0.82151353	705.94
CVI_1344_31	rim	**69.8**	160	4.63	636	4.84E+05	0.059		1.5	0.172		2.78	0.64	13.3	4.74	53	20.9	94.8	23.4	249	51	8820	81.6	338	0.66550899	677.37
CVI_1344_28	core	**69.9**	10.6	8.24	908	4.92E+05	0.024		1.62	0.121		2.46	0.57	14.2	5.24	70.1	28.67	144	35.2	364	77.9	7780	69	308.2	0.91592721	724.09
CVI_1344_39	rim	**69.9**	0.4	9.2	1492	4.91E+05	0.01		2.21	0.097		3.19	0.72	21.5	8.97	114.9	48.5	226.1	55.2	553	110.8	8550	143.4	629	0.96378783	733.55
CVI_1344_29	rim	**70**	27.3	9.27	1267	4.94E+05	0.272		1.87	0.106		2.65	0.44	20.8	7.27	98.3	41.6	200.8	46.9	471	95.6	9290	116.2	511	0.96707973	734.20
CVI_1344_37	core	**70**	16.8	6.6	1321	4.83E+05	0.207		1.86	0.029		2.26	0.331	18.9	7.47	100.3	42.3	213.1	49.2	497	98.1	9370	105.9	547	0.81954394	705.57
CVI_1344_42	core	**70.09**	0.4	9.64	1546	4.80E+05	-0.008		1.5	0.043		2.45	0.388	21.2	8.94	119.1	51.7	246.8	57.1	565	113.2	8440	118	579	0.98407403	737.61
CVI_1344_19	core	**70.1**	48.1	7.03	1301	4.86E+05	0.43		3.1	0.196		8.17	1.66	63.2	18.66	165.5	38.5	97.8	14.46	103.8	14.57	9280	243.2	975	0.84695533	710.77
CVI_1344_30	rim	**70.2**	9	9.62	792	4.87E+05	0.041		1.19	0.027		1.1	0.404	11.61	4.62	57.9	25.97	124.4	31.23	316.7	63.2	7910	101.8	377.8	0.98317507	737.43
CVI_1344_5	rim	**70.3**	-1.5	5.26	1493	4.78E+05	0.002		3.56	0.163		2.7	0.414	20.9	8.87	122.4	51.3	243.5	57.3	566	110.7	10550	110.6	622	0.72098574	687.33
CVI_1344_26	core	**70.5**	10	5.96	1010	4.86E+05	0.06		1.27	0.068		2.83	0.42	18.5	6.65	83	32.8	155	37	368	75.4	8430	78	303	0.97524628	697.29
CVI_1344_58	rim	**70.5**	7.5	9	910	4.91E+05	0.038		1.19	0.031		1.59	0.313	11.9	4.53	66.5	30.35	149.4	37.4	393.2	83	7990	58.3	327.3	0.95424251	731.65
CVI_1344_34	core	**70.8**	313	10.7	1807	4.67E+05	5.1		2.46	0.122		5.41	1.2	33.8	12.45	146.4	58.5	270	63.9	637	126.5	7340	200	600	1.02938378	746.80
CVI_1344_43	core	**71.2**	7.9	6.59	637	5.03E+05	0.017		0.71	0.0136		1.49	0.275	9	3.32	46.6	20.3	103.5	26.9	285	61	8220	34.7	204	0.81888541	705.45
CVI_1344_57	rim	**71.2**	5.9	6.73	623	4.97E+05	0.031		0.881	0.022		1.17	0.247	7.67	3.17	44.2	20.2	102	25.4	275	57.5	8820	31.7	237	0.82801506	707.17
CVI_1344_24	core	**71.3**	8	8.42	955	4.90E+05	0.056		1.11	0.054		2.07	0.59	14	5.49	71.8	30.3	152.3	36.9	391	83	7490	62.8	303	0.92531209	725.93
CVI_1344_53	rim	**72.93**	-2.5	7.66	1340	4.93E+05	0.045		2.77	0.031		2.2	0.41	22	8.02	108.1	45.9	212.4	48.2	472	91.3	9450	198.6	598	0.88422877	717.92
CVI_1344_17	core	**73.6**	44	6.49	635	4.82E+05	0.32		0.77	0.05		1.89	0.396	10.7	3.58	48.7	20.51	102.2	25.43	269.6	58.3	7830	43.1	206.6	0.8122447	704.19
CVI_1344_10	core	**87.7**	35.1	22.7	1844	4.88E+05	0.172		3.08	0.084		4.3	0.376	29.9	11.38	153.9	64.2	299.8	69.1	697	127.7	9400	113	410	1.35602586	818.39
CVI_1344_33	core	**90.9**	6	10.8	1195	5.24E+05	0.062		1.9	0.044		1.6	0.6	17.3	6.61	89.9	38.1	193.6	48.4	488	95.3	8850	98.1	458	1.01432376	777.63
CVI_1344_49	rim	**268.9**	16.3	9.55	2462	4.83E+05	0.136		29.7	0.144		5.4	1.72	41.7	14.9	195	81.9	394	95.7	983	183.5	10310	399	695	0.98000337	736.79
CVI_1344_12	core	**no value**	-400	80	-20	1.20E+03	21		0	0		0	0	9	0	0	0	0	0	-10	0	-10	0	0.28	1.90308999	963.79
CVI_1344_51	core	**70.7**	113	11.09	872	5.28E+05	0.283		0.97	0.073		2.02	0.45	13.9	5.03	64.6	28.64	139.3	32.94	358.1	78.3	8980	61	286.1	1.04493155	750.00
CVI_1344_52	rim	**68.8**	19.7	10	973	5.01E+05	0.177		1.37	0.026		1.68	0.444	13.7	5.48	73.4	31.54	156.4	37.8	392.3	82.4	8510	98.3	415	1	740.82
CVI-1367																										
CVI_1367_1	rim	**70.8**	9.4	7.45	1114	5.11E+05	0.081		1.57	0.031		1.8	0.337	12.67	5.06	76.5	34.48	190.4	47.5	509	106.9	10030	60.61	342.2	0.87215627	715.59
CVI_1367_2	core	**67.9**	20.3	8.51	1468	5.07E+05	0.03		1.46	0.108		4.59	0.66	26.9	9.46	120.6	48.2	231.9	55.1	548	107.3	8730	77.8	289.4	0.92992956	726.84
CVI_1367_3	rim	**55.2**	2.8	7.93	448.5	5.11E+05	0.026		8.54	0.0085		0.9	0.302	6.87	2.56	34.7	14.08	69.4	16.46	166.3	32.76	11140	43.75	101.3	0.89927319	720.84
CVI_1367_4	core	**54.1**	0.8	8.4	1049	5.06E+05	0.068		11.85	0.08		3.85	1.28	23.9	7.58	93.6	35.2	159.9	34.7	332	63.9	10640	102.6	157.7	0.92427929	725.73
CVI_1367_5	core	**57.7**	-1.8	10.8	1826	5.15E+05	0.007		3.81	0.031		2.02	1.83	17.1	7.78	116.1	56.3	305	77.9	856	189.2	7580	40.4	268	1.03423776	763.61
CVI_1367_6	core	**55.3**	4.4	4.1	749	5.62E+05	0.14		9.72	0.037		0.88	1.19	11	4.14	55.2	23.2	120.9	31.4	357	72.6	11490	87.8	346	0.61278386	668.08
CVI_1367_7	rim	**54.7**	12.5	8.8	1810	5.41E+05	0.54		22.8	0.061		4.51	2.83	28.9	11.46	142.6	56.1	270.9	59.7	586

AP_038_1	rim	**57.7**	270	132	1330	4.33E+05	5.07	4.44	0.69	5.77	0.9	26.2	11.7	125	34.4	137	32.7	335	53.6	2.68E+04	74.2	3270	2.12057393	1032.96
AP_038_3	core	**61.7**	2.31E+04	29.8	2970	3.95E+05	8.6	3.45	0.369	4.64	0.75	40.6	20.7	260	85	374	103	1120	204	22260	93	4730	1.47421626	846.83
AP_038_2	core	**63.8**	2590	90	8830	4.83E+05	12.4	36	4.36	43	7.6	179	71.1	820	268	1216	305	3260	595	21330	670	9680	1.95424251	979.39
AP_038_10	core	**69.1**	2920	28.2	2440	4.32E+05	15.9	8.9	1.44	15.8	1.98	71.7	27.2	254	60	206.8	47.2	482	66.8	34250	127.8	5740	1.45024911	840.95
AP_038_28	core	**267.1**	132	11.3	2123	4.72E+05	0.614	104.4	0.59	11.32	2.68	58	17.61	205.5	75.3	323.9	69.1	639	114.6	9310	1358	903	1.05307844	751.68
AP_038_26	core	**275**	64	15.3	1709	4.76E+05	0.301	61.1	0.292	8.17	2.56	41	13.28	156.2	59.8	255	57.8	554	97.8	7950	629	530	1.18469143	779.63
AP_038_27	rim	**298.8**	-0.1	10.75	936	4.73E+05	0.138	35.7	0.12	4.16	1.99	22.1	7.44	85.7	32.54	144.9	33.3	335	61.7	7280	392	310	1.03140846	747.22
AP_038_24	core	**1000**	17.4	29.4	1577	4.74E+05	0.045	4.8	0.51	2.06	0.233	18.2	8.76	122.8	51.3	247.9	63.2	666	118.3	13840	64.9	1408	1.46834733	845.39
AP_038_43	rim	**1004**	16.6	38.4	1479	4.74E+05	0.001	3.07	0.064	3.3	0.161	23.4	9.47	125.2	49.7	213.7	47.3	413	70.2	12890	85.4	594	1.58433122	874.70
AP_038_23	rim	**1017**	12.6	30.8	1347	4.82E+05	0.029	2.38	0.065	3.06	0.074	24.8	9.88	121.7	44.5	186.4	38.9	352	58.9	12890	85.8	297.2	1.48855072	850.38
AP_038_42	core	**1170**	3.2	36.3	1810	4.72E+05	0.037	18.66	0.133	5.14	1.04	34	12.48	158.4	62.9	289.5	66	641	116.9	9630	188	357	1.55990663	868.40

TABLE A3. Representative electron microprobe analysis of garnet, biotite, and plagioclase in the La Secreta garnet-bearing mylonite samples.

CVI-1388 Amphibolite

Hornblende

No Spot.	13	14	15	16	17	18	19	21	22	23	24	50	51	52	53	Average
SiO2	40.83	40.69	40.88	40.30	40.46	40.24	41.07	40.77	40.65	40.98	40.50	41.29	40.71	41.85	42.09	40.89
TiO2	0.34	0.51	0.86	0.45	0.40	0.51	0.44	0.51	0.50	0.50	0.52	0.30	0.36	1.47	1.21	0.59
Al2O3	17.39	17.59	17.22	18.40	18.06	18.57	17.75	18.38	18.05	18.32	18.00	16.89	18.05	14.25	14.79	17.45
FeO	18.35	18.20	18.07	18.61	18.19	18.63	18.76	18.68	18.30	18.60	18.30	18.26	18.70	18.28	17.96	18.39
MnO	0.06	0.08	0.04	0.07	0.09	0.10	0.11	0.10	0.07	0.07	0.15	0.07	0.12	0.10	0.08	0.09
MgO	6.46	6.15	6.52	5.71	6.08	5.95	6.06	5.91	6.05	5.98	6.06	6.46	6.04	7.40	7.39	6.28
CaO	11.57	11.54	11.48	11.50	11.52	11.51	11.50	11.61	11.60	11.63	11.63	11.56	11.58	11.43	11.48	11.54
Na2O	1.37	1.34	1.38	1.32	1.36	1.38	1.46	1.34	1.32	1.32	1.35	1.41	1.31	1.19	1.29	1.34
K2O	0.63	0.75	0.80	0.82	0.78	0.84	0.71	0.82	0.76	0.82	0.76	0.65	0.81	1.00	0.76	0.78
Cr2O3	0.00	0.01	0.01	0.00	0.01	0.02	0.04	0.00	0.02	0.00	0.01	0.01	0.01	0.00	0.02	0.01
Total	97.00	96.85	97.26	97.17	96.95	97.74	97.90	98.12	97.31	98.21	97.27	96.92	97.68	96.96	97.07	97.36
X	3.7358	3.4265	2.0987	1.3472	5.497	5.0935	-2.062	9.6249	9.359	9.6249	9.359	5.7633	5.5853	5.8701	5.7539	
Y	12.1451	12.3738	24.2658	24.3123	0.3253	1.0513	15.149	18.1043	17.8883	18.1043	17.8883	11.0842	11.1491	5.6276	5.5939	
Z	10.771	10.771	10.771	10.771	10.771	10.767	10.788	10.786	10.787	10.786	10.787	10.786	10.775	10.775	10.775	

Plagioclase

No Spot.	54	55	56	58	59	60	61	Average
SiO2	59.22	59.07	60.13	60.23	58.17	58.78	58.46	59.15
TiO2	0.02	0.00	0.02	0.02	0.00	0.00	0.00	0.01
Al2O3	25.21	25.77	24.87	25.09	26.01	26.17	25.90	25.58
FeO	0.05	0.02	0.03	0.06	0.31	0.07	0.27	0.12
MnO	0.03	0.02	0.01	0.01	0.02	0.01	0.02	0.02
MgO	0.00	0.00	0.00	0.00	0.00	0.00	0.00	0.00
CaO	7.01	7.28	6.50	6.64	7.98	7.65	7.72	7.25
Na2O	7.80	7.67	8.08	8.15	7.12	7.41	7.36	7.66
K2O	0.06	0.04	0.06	0.06	0.07	0.05	0.07	0.06
Cr2O3	0.00	0.01	0.00	0.00	0.00	0.02	0.00	0.01
Total	99.41	99.89	99.70	100.24	99.68	100.16	99.81	99.84
X	-3.2063	-3.4838	-2.7598	-0.8973	-1.1577	-6.3201	-6.438	
Y	14.5321	14.5321	5.2804	-0.2922	-0.4422	25.6195	25.7962	
Z	10.765	10.765	10.763	10.7625	10.763	10.7655	10.765	

Garnet

Profile 1

No Spot.	104	105	106	107	108	109	110	111	112	113	114	115	116	117	118	119	120	121	122	123
SiO2	36.90	36.78	36.96	36.88	36.92	36.88	36.97	37.04	36.80	36.76	36.91	36.90	36.87	36.76	36.74	36.84	36.68	36.54	36.36	36.14
TiO2	0.11	0.12	0.08	0.10	0.10	0.09	0.11	0.10	0.09	0.09	0.10	0.11	0.10	0.09	0.08	0.10	0.09	0.06	0.10	0.02
Al2O3	20.25	20.25	20.32	20.29	20.31	20.31	20.17	20.31	20.28	20.31	20.30	20.34	20.29	20.19	20.19	20.30	20.22	20.28	20.54	20.37
FeO	26.36	26.28	26.19	26.23	26.03	26.06	26.44	26.45	26.62	26.45	26.67	26.62	26.99	27.19	27.12	27.04	27.81	28.21	29.00	29.58
MnO	0.61	0.65	0.60	0.61	0.62	0.55	0.62	0.64	0.63	0.59	0.66	0.68	0.71	0.74	0.71	0.69	0.81	1.92	1.84	2.06
MgO	3.04	3.07	3.10	3.09	3.02	3.15	3.13	3.14	3.18	3.16	3.12	3.13	3.11	3.09	3.06	2.98	2.83	1.88	1.65	1.52
CaO	11.18	11.02	11.23	11.20	11.11	11.14	10.92	10.76	10.70	10.64	10.76	10.52	10.46	10.22	10.32	10.18	9.95	9.44	8.81	8.62
Na2O	0.02	0.00	0.01	0.01	0.01	0.02	0.00	0.01	0.02	0.00	0.02	0.01	0.00	0.01	0.00	0.01	0.01	0.01	0.02	0.00
K2O	0.00	0.00	0.00	0.01	0.00	0.00	0.00	0.00	0.00	0.00	0.01	0.00	0.01	0.00	0.00	0.00	0.00	0.00	0.00	0.00
Cr2O3	0.00	0.00	0.00	0.01	0.01	0.00	0.01	0.02	0.00	0.01	0.00	0.01	0.00	0.00	0.00	0.02	0.01	0.01	0.01	0.00
Total	98.44	98.18	98.49	98.42	98.13	98.21	98.38	98.47	98.32	98.01	98.55	98.33	98.54	98.30	98.24	98.15	98.40	98.35	98.33	98.30
X	3.7051	3.685	3.6701	3.6601	3.6521	3.6379	3.6232	3.6148	3.6071	3.591	3.5786	3.5624	3.5455	3.53	3.5116	3.5002	3.4787	3.4615	3.4523	3.4471
Y	12.1627	12.1778	12.1896	12.1977	12.2051	12.2166	12.2267	12.227	12.2375	12.2499	12.25	12.259	12.2725	12.2885	12.3	12.3135	12.325	12.349	12.3575	12.364
Z	10.771	10.771	10.771	10.771	10.771	10.771	10.771	10.771	10.771	10.771	10.771	10.771	10.771	10.771	10.771	10.771	10.771	10.771	10.771	10.771

Profile 2

No Spot.	124	125	126	127	128	129	130	131	132	133	134	135	136	137	138	139	140
SiO2	36.71	36.55	36.79	36.85	36.92	36.62	36.77	36.91	36.92	36.92	37.05	36.85	36.90	36.76	37.00	36.86	36.67
TiO2	0.03	0.02	0.07	0.09	0.10	0.13	0.11	0.09	0.09	0.10	0.11	0.08	0.09	0.09	0.11	0.10	0.11
Al2O3	20.73	20.56	20.39	20.21	20.29	20.21	20.09	20.37	20.41	20.38	20.29	20.38	20.37	20.21	20.17	20.31	20.16
FeO	28.80	28.40	27.80	26.91	26.73	26.76	26.75	26.33	26.56	26.18	26.38	27.95	27.62	28.03	27.43	27.94	28.82
MnO	1.53	2.15	1.05	0.71	0.63	0.66	0.66	0.59	0.59	0.53	0.56	0.77	0.75	1.18	0.70	0.82	1.24
MgO	1.74	1.66	2.65	3.17	3.22	3.17	3.17	3.20	3.27	3.27	3.20	2.80	2.84	2.31	3.04	2.70	1.80
CaO	9.32	9.04	9.58	10.24	10.49	10.50	10.53	10.95	10.64	10.99	10.84	9.89	10.06	9.92	9.97	9.94	9.98
Na2O	0.01	0.01	0.00	0.00	0.00	0.00	0.00	0.01	0.01	0.00	0.01	0.00	0.00	0.02	0.00	0.01	0.00
K2O	0.00	0.00	0.00	0.00	0.00	0.00	0.00	0.00	0.00	0.00	0.00	0.01	0.00	0.01	0.00	0.01	0.00
Cr2O3	0.00	0.02	0.00	0.01	0.00	0.00	0.00	0.00	0.02	0.00	0.00	0.00	0.00	0.00	0.00	0.00	0.00
Total	98.89	98.40	98.33	98.19	98.39	98.05	98.07	98.44	98.53	98.37	98.44	98.73	98.63	98.52	98.42	98.69	98.78
X	2.0655	2.0456	2.0274	1.9743	1.9228	1.8681	1.815	1.7838	1.7546	1.6942	1.6289	1.5442	1.5061	1.4769	1.4518	1.4254	1.4076
Y	24.2877	24.2893	24.2885	24.2917	24.2949	24.2973	24.2953	24.2961	24.2941	24.2904	24.3168	24.335	24.337	24.3358	24.3082	24.2936	24.2851
Z	10.771	10.771	10.771	10.771	10.771	10.771	10.771	10.771	10.771	10.771	10.771	10.771	10.771	10.771	10.771	10.771	10.771

Profile 3

No Spot.	144	145	146	147	148	149	150	151	152	153	154	155	156	157	158	159	160	161	162	163
SiO2	37.16	37.34	37.44	37.44	37.40	37.37	37.50	37.39	35.57	37.48	37.24	37.38	37.29	37.38	37.51	37.38	37.46	37.57	37.50	37.45
TiO2	0.09	0.06	0.05	0.06	0.08	0.09	0.09	0.09	0.09	0.10	0.09	0.09	0.04	0.09	0.07	0.10	0.09	0.07	0.11	0.04
Al2O3	20.67	20.75	20.61	20.65	20.67	20.61	20.60	20.69	19.52	20.49	20.42	20.69	20.53	20.54	20.52	20.60	20.91	20.84	20.89	20.84
FeO	28.29	28.02	27.81	27.85	27.81	27.68	27.49	27.25	26.98	27.48	28.07	28.39	27.55	27.48	27.17	27.26	26.97	27.12	27.10	27.48
MnO	1.08	1.01	0.87	0.83	0.87	0.70	0.69	0.72	0.78	0.70	0.87	1.37	0.77	0.99	0.69	0.71	0.69	0.72	0.77	0.69
MgO	2.42	2.62	2.89	2.90	2.93	3.01	3.08	3.11	2.78	3.15	2.65	2.04	2.89	2.71	3.01	3.19	3.25	3.24	3.23	3.22
CaO	9.58	9.55	9.60	9.61	9.56	9.65	9.82	9.98	9.77	9.89	9.86	9.53	9.84	10.12	10.41	9.99	9.87	9.83	9.64	9.31
Na2O	0.03	0.00	0.00	0.00	0.00	0.02	0.00	0.00	0.00	0.02	0.00	0.00	0.00	0.01	0.01	0.01	0.01	0.01	0.02	0.02
K2O	0.00	0.01	0.00	0.01	0.00	0.00	0.01	0.00	0.00	0.00	0.00	0.00	0.00	0.00	0.00	0.00	0.01	0.00	0.00	0.00
Cr2O3	0.00	0.00	0.00	0.00	0.00	0.01	0.00	0.01	0.01	0.02	0.00	0.01	0.02	0.00	0.00	0.00	0.00	0.01	0.01	0.01
Total	99.32	99.36	99.28	99.33	99.32	99.12	99.29	99.23	95.50	99.31	99.23	99.44	98.95	99.33	99.42	99.24	99.25	99.43	99.21	99.08
X	5.4499	5.4385	5.4378	5.4224	5.4085	5.3928	5.3722	5.3662	5.3491	5.32	5.2965	5.2725	5.2699	5.2415	5.2383	5.2009	5.1744	5.1571	5.1352	5.0974
Y	0.3672	0.3845	0.395	0.4079	0.4481	0.4859	0.521	0.5538	0.554	0.6262	0.6665	0.709	0.7496	0.7939	0.8479	0.8881	0.9192	0.9508	0.9783	1.006
Z	10.771	10.771	10.771	10.771	10.771	10.771	10.771	10.771	10.771	10.771	10.771	10.771	10.771	10.771	10.771	10.771	10.771	10.771	10.771	10.771

X-ray Map 1 Profile 4

No Spot.	164	165	166	167	168	169	170	171	172	173	174	175	176	177	178	179	180	181	182	183	184	185	186	187	188	189	190	191	192
SiO2	37.23	37.30	37.51	37.67	37.62	37.51	37.55	37.56	37.70	37.59	37.30	37.61	37.45	37.65	37.73	37.71	37.56	37.33	37.47	37.64	37.50	37.74	37.52	37.66	37.59	37.50	37.28	37.49	37.23
TiO2	0.02	0.06	0.05	0.12	0.10	0.09	0.09	0.09	0.07	0.09	0.09	0.09	0.07	0.07	0.08	0.06	0.07	0.06	0.09	0.09	0.08	0.09	0.10	0.07	0.03	0.01	0.09	0.06	0.00
Al2O3	20.98	20.83	20.82	20.44	20.61	20.55	20.60	20.74	20.71	20.65	20.52	20.59	20.72	20.79	20.69	20.75	20.82	20.61	20.69	20.53	20.69	20.63	20.63	20.75	20.97	20.94	20.43	20.94	20.87
FeO	29.46	29.72	28.44	27.50	27.13	26.68	26.50	26.77	27.09	26.99	28.04	27.11	27.50	27.19	26.76	27.11	27.32	28.45	27.64	27.58	27.12	27.06	27.06	27.62	28.00	28.81	29.18	28.15	29.36
MnO	1.54	1.71	1.25	0.72	0.65	0.64	0.64	0.64	0.70	0.59	1.20	0.69	0.88	0.60	0.64	0.61	0.70	1.16	0.78	0.93	0.70	0.64	0.81	0.76	0.76	1.04	1.08	0.86	1.59
MgO	1.75	1.84	2.33	3.03	3.14	3.07	3.01	2.99	2.88	2.99	1.98	2.74	2.42	3.03	3.08	3.09	3.08	2.14	2.53	2.58	3.05	2.99	2.75	2.98	2.92	2.20	2.19	2.57	1.75
CaO	8.77	8.25	9.38	10.01	10.13	10.87	10.75	10.67	10.38	10.60	10.26	10.42	10.32	10.32	10.22	10.18	10.11	10.00	10.24	10.34	10.42	10.24	10.31	9.65	9.47	9.42	9.56	9.54	8.80
Na2O	0.02	0.00	0.01	0.00	0.01	0.00	0.01	0.00	0.01	0.00	0.00	0.01	0.02	0.00	0.00	0.00	0.01	0.00	0.00	0.00	0.00	0.01	0.01	0.00	0.00	0.01	0.00	0.01	0.01
K2O	0.01	0.00	0.00	0.00	0.00	0.00	0.00	0.00	0.00	0.00	0.00	0.01	0.01	0.00	0.00	0.00	0.00	0.00	0.00	0.00	0.00	0.00	0.00	0.00	0.00	0.00	0.00	0.00	0.00
Cr2O3	0.01	0.02	0.00	0.00	0.00	0.00	0.00	0.01	0.00	0.00	0.00	0.00	0.00	0.00	0.00	0.00	0.00	0.00	0.00	0.00	0.00	0.00	0.00	0.00	0.00	0.01	0.00	0.00	0.00
Total	99.79	99.72	99.81	99.49	99.58	99.41	99.15	99.47	99.56	99.50	99.41	99.27	99.38	99.64	99.20	99.52	99.67	99.76	99.44	99.69	99.58	99.43	99.37	99.51	99.75	99.93	99.80	99.62	99.60
X	-2.078	-2.0885	-2.1	-2.135	-2.1725	-2.2265	-2.2565	-2.2835	-2.3105	-2.3415	-2.379	-2.416	-2.436	-2.466	-2.485	-2.5275	-2.5635	-2.587	-2.645	-2.69	-2.7275	-2.782	-2.8045	-2.8455	-2.8715	-2.8965	-2.916	-2.932	-2.9393
Y	15.1335	15.133	15.128	15.117	15.1105	15.076	15.0495	15.025	15.0075	14.987	14.9615	14.944	14.936	14.918	14.906	14.8835	14.8685	14.848	14.8375	14.8155	14.794	14.7755	14.747	14.728	14.7165	14.6975	14.6855	14.6705	14.6602
Z	10.767	10.767	10.7675	10.767	10.7665	10.766	10.7675	10.7675	10.767	10.7675	10.767	10.7675	10.771	10.771	10.771	10.771	10.7665	10.767	10.7675	10.7675	10.767	10.7665	10.7665	10.7665	10.7665	10.766	10.7655	10.766	10.7665	10.7655

Profile 5

No Spot.	196	197	198	199	200	201	202	203	204	205	206	207	208	209	210	211	212	213	214
SiO2	37.48	37.20	37.54	37.71	37.47	37.58	37.61	37.61	37.50	37.64	37.60	37.41	37.51	37.49	37.30	37.24	37.23	37.16	37.13
TiO2	0.04	0.09	0.11	0.10	0.07	0.10	0.08	0.08	0.08	0.06	0.08	0.10	0.08	0.07	0.05	0.06	0.06	0.08	0.08
Al2O3	20.92	20.30	20.62	20.60	20.51	20.55	20.56	20.89	20.86	20.95	20.90	20.58	20.86	20.74	20.94	20.86	20.70	20.77	20.77
FeO	28.48	28.90	27.25	27.23	27.33	27.27	27.05	26.70	26.76	27.05	27.13	27.29	27.12	27.74	29.16	29.63	29.23	29.15	29.20
MnO	1.81	1.95	0.70	0.71	0.81	0.70	0.67	0.68	0.68	0.67	0.72	0.66	0.70	1.10	2.07	1.94	1.87	1.89	1.87
MgO	1.54	1.41	3.18	3.11	3.00	3.08	3.21	3.26	3.30	3.29	3.31	3.27	3.30	2.56	1.78	1.76	1.73	1.73	1.76
CaO	9.77	9.88	10.15	10.12	10.09	10.24	10.30	10.38	10.24	9.96	9.84	9.81	9.72	9.66	8.48	8.50	8.55	8.84	8.59
Na2O	0.00	0.01	0.00	0.00	0.01	0.00	0.01	0.01	0.00	0.00	0.00	0.00	0.03	0.00	0.02	0.01	0.00	0.00	0.00
K2O	0.01	0.01	0.00	0.00	0.00	0.00	0.01	0.00	0.00	0.00	0.00	0.00	0.00	0.00	0.00	0.00	0.00	0.00	0.00
Cr2O3	0.00	0.02	0.02	0.01	0.00	0.00	0.00	0.01	0.01	0.00	0.00	0.00	0.02	0.01	0.00	0.02	0.00	0.01	0.02
Total	100.03	99.76	99.57	99.59	99.29	99.52	99.49	99.62	99.43	99.62	99.59	99.14	99.34	99.38	99.81	100.02	99.36	99.74	99.42
X	9.6172	9.6109	9.5894	9.5711	9.5534	9.5411	9.5283	9.5144	9.4997	9.4866	9.473	9.4572	9.4433	9.4305	9.4239	9.4043	9.3898	9.3768	9.3793
Y	18.0904	18.0848	18.0637	18.0509	18.0416	18.0271	18.0167	18.0039	17.9897	17.9788	17.9676	17.9572	17.9496	17.9436	17.936	17.9344	17.9295	17.9082	17.9019
Z	10.7875	10.788	10.7875	10.787	10.7875	10.7875	10.787	10.7875	10.787	10.7875	10.7875	10.787	10.7875	10.7875	10.787	10.7875	10.787	10.787	10.7875

CVI-13108 Bt+Grt Schist

Biotite

No Spot.	9	46	7	8	11	12	31	32	33	36	38	39	41	Average
SiO2	33.1798	37.43	36.8772	38.1058	37.07	36.77	36.80	38.05	37.81	37.51	36.18	37.89	37.29	37.00
TiO2	1.1235	1.49	1.4872	1.588	1.24	1.41	1.30	1.48	1.53	1.47	1.54	1.39	1.49	1.43
Al2O3	19.1173	18.14	17.7005	18.0123	17.55	19.00	18.50	17.73	18.58	18.27	17.35	18.49	18.13	18.20
FeO	18.6754	14.97	15.497	15.0192	15.09	14.68	15.45	15.09	14.07	14.99	14.35	14.56	14.96	15.18
MnO	0.0882	0.05	0.0487	0.052	0.07	0.03	0.03	0.04	0.05	0.04	0.04	0.06	0.05	
MgO	15.1145	14.56	14.3424	14.5891	15.03	14.03	15.28	13.85	14.28	13.68	14.51	14.25	14.23	14.44
CaO	0.1732	0.03	0.0244	0.0868	0.02	0.03	0.03	0.03	0.00	0.01	0.07	0.03	0.00	0.04
Na2O	0.1466	0.25	0.2373	0.3397	0.26	0.30	0.27	0.25	0.30	0.27	0.29	0.32	0.29	0.27
K2O	4.5882	8.30	8.0523	8.0008	8.17	7.74	6.98	8.17	7.94	8.04	7.98	7.97	8.35	7.71
Cr2O3	0.118	0.09	0.1175	0.0782	0.04	0.15	0.04	0.06	0.05	0.07	0.08	0.09	0.09	0.08
Total	92.3248	95.30	94.3846	95.872	94.54	94.13	94.69	94.75	94.61	94.35	92.38	95.03	94.88	94.40
X	-31.9516	-33.0963	-26.7946	-24.228	-20.7804	-19.2198	-23.4645	-23.4965	-20.3974	-20.6778	-20.2616	-21.3716	-34.3899	
Y	5.0561	3.9513	13.0525	11.4772	2.6234	4.4832	10.0241	10.0391	5.8018	19.7915	20.1137	19.54	21.0375	
Z	10.7405	10.743	10.7485	10.744	10.7565	10.7485	10.743	10.743	10.743	10.743	10.743	10.743	10.743	

Plagioclase

No Spot.	47	10	34	32	Average
SiO2	53.05	55.12	55.32	46.37	52.46
TiO2	0.05	0.02	0.01	0.00	0.02
Al2O3	23.65	28.26	28.18	31.75	27.96
FeO	0.93	0.32	0.33	0.13	0.43
MnO	0.01	0.00	0.02	0.00	0.01
MgO	1.10	0.00	0.00	0.00	0.27
CaO	6.88	10.59	10.49	16.63	11.15
Na2O	9.50	5.75	5.88	2.10	5.81
K2O	0.52	0.04	0.03	0.04	0.16
Cr2O3	0.01	0.00	0.00	0.03	0.01
Total	95.70	100.11	100.27	97.05	98.28
X	-33.1825	-33.0857	-20.5961	-22.3335	
Y	4.0151	5.1175	5.801	9.8544	
Z	10.743	10.741	10.758	10.7515	

Garnet

Grt composition scatter

No Spot.	4	5	6	7	8	9	10	11	12	13	14	15	16	17	18	20	21	22
SiO2	38.59	37.77	38.73	38.63	38.54	37.89	38.41	38.71	38.67	38.48	38.53	38.41	38.52	38.60	38.76	38.81	37.63	38.61
TiO2	0.16	0.07	0.16	0.18	0.20	0.17	0.24	0.09	0.10	0.09	0.16	0.24	0.10	0.10	0.09	0.09	0.07	0.08
Al2O3	21.52	21.30	21.55	21.49	21.34	21.26	21.40	21.72	21.71	21.73	21.46	21.43	21.51	21.64	21.63	21.60	21.15	21.67
FeO	22.45	28.98	22.65	23.07	23.00	26.22	22.89	23.43	23.22	23.17	22.88	22.81	23.21	23.44	23.74	23.89	29.03	24.15
MnO	1.05	3.52	0.97	1.14	1.24	1.75	1.20	0.96	0.86	0.98	1.08	1.15	1.13	0.89	0.69	0.50	2.71	0.45
MgO	6.74	3.24	6.94	6.59	6.24	4.66	6.22	7.09	7.19	6.98	6.71	6.36	6.54	6.89	7.62	8.23	3.95	8.33
CaO	9.35	6.13	9.30	9.10	9.49	8.38	9.44	8.33	8.29	8.54	8.91	9.47	8.91	8.52	7.50	6.80	6.00	6.52
Na2O	0.00	0.00	0.00	0.01	0.03	0.00	0.01	0.00	0.01	0.01	0.00	0.03	0.00	0.00	0.00	0.00	0.00	0.00
K2O	0.00	0.01	0.00	0.00	0.00	0.01	0.00	0.00	0.00	0.00	0.00	0.00	0.00	0.01	0.00	0.00	0.00	0.00
Cr2O3	0.01	0.05	0.05	0.03	0.03	0.00	0.04	0.01	0.02	0.01	0.01	0.00	0.01	0.02	0.07	0.05	0.04	0.06
Total	99.88	101.08	100.35	100.23	100.11	100.34	99.84	100.33

X-ray Map 2 Profile 3

No Spot.	59	60	61	62	63	64	65	66	67	68	69	70	71	72	73	74	75	76	77	78	79	80
SiO2	37.86	37.53	37.38	37.29	37.33	37.36	37.32	37.41	37.60	37.89	38.03	38.47	38.83	38.76	38.92	38.79	38.99	37.96	37.34	37.19	37.33	37.08
TiO2	0.11	0.07	0.05	0.02	0.00	0.00	0.00	0.01	0.01	0.05	0.06	0.05	0.10	0.08	0.07	0.11	0.09	0.06	0.02	0.04	0.02	0.06
Al2O3	21.35	21.10	21.10	20.98	21.02	20.90	20.99	21.09	20.96	20.99	21.17	21.59	21.50	21.67	21.50	21.55	21.52	21.31	21.06	21.02	21.16	20.90
FeO	28.03	30.65	30.47	30.85	30.43	30.10	30.05	30.22	29.44	28.88	27.52	25.25	22.50	22.32	22.33	22.52	22.61	26.61	30.07	30.87	29.61	29.39
MnO	2.41	3.25	3.52	3.79	4.26	4.22	4.22	4.21	3.14	2.29	2.13	1.04	0.64	0.65	0.73	0.75	0.68	1.71	3.65	3.21	2.47	2.31
MgO	2.83	3.06	3.19	3.38	3.30	3.37	3.36	3.48	4.06	4.64	4.96	6.68	8.02	8.11	8.03	8.07	8.01	5.16	3.34	3.23	2.95	3.12
CaO	7.29	4.57	4.50	3.71	3.90	4.17	4.26	3.96	4.99	5.41	6.19	6.85	7.90	8.00	8.17	7.92	7.90	7.11	4.59	4.42	6.29	6.37
Na2O	0.00	0.02	0.03	0.02	0.00	0.00	0.00	0.00	0.00	0.02	0.01	0.00	0.02	0.00	0.00	0.01	0.00	0.00	0.00	0.00	0.00	0.00
K2O	0.01	0.00	0.02	0.00	0.00	0.01	0.00	0.00	0.00	0.00	0.00	0.00	0.00	0.01	0.00	0.00	0.00	0.00	0.00	0.00	0.00	0.01
Cr2O3	0.04	0.05	0.04	0.05	0.07	0.05	0.05	0.06	0.07	0.04	0.04	0.04	0.02	0.02	0.06	0.05	0.05	0.02	0.04	0.07	0.02	0.05
Total	100.44	100.32	100.30	100.10	100.31	100.18	100.25	100.46	100.29	100.22	100.11	99.98	99.52	99.62	99.81	99.78	99.86	99.95	100.10	100.05	99.87	99.28
X	-31.9705	-31.9975	-32.0289	-32.0667	-32.1399	-32.184	-32.2205	-32.2461	-32.3264	-32.3942	-32.4816	-32.5374	-32.6013	-32.6558	-32.7264	-32.785	-32.8166	-32.8646	-32.9301	-32.9767	-33.0425	-33.0633
Y	5.0607	5.0662	5.0706	5.0812	5.095	5.0973	5.1021	5.1014	5.1014	5.1046	5.1138	5.1133	5.1177	5.1135	5.117	5.1168	5.1168	5.1145	5.1145	5.114	5.1135	5.1117
Z	10.7405	10.7425	10.744	10.7445	10.7485	10.744	10.7435	10.7485	10.744	10.7445	10.744	10.7485	10.7435	10.744	10.743	10.743	10.743	10.7485	10.743	10.7435	10.743	10.7425

Profile 4

No Spot.	84	85	86	87	88	89	90	92	93	94	95	96	97	98	99	100
SiO2	37.60	38.96	38.96	38.91	38.92	39.13	39.10	39.11	39.11	39.18	39.21	39.15	39.21	38.50	37.94	37.71
TiO2	0.02	0.10	0.10	0.12	0.10	0.03	0.09	0.09	0.09	0.07	0.09	0.08	0.08	0.09	0.08	0.01
Al2O3	21.20	21.61	21.68	21.64	21.63	21.79	21.63	21.83	21.74	21.78	21.79	21.75	21.79	21.31	21.13	21.15
FeO	30.39	22.80	23.00	22.77	23.08	23.51	23.46	23.75	23.48	23.35	23.35	23.50	23.58	27.19	28.84	30.36
MnO	3.58	0.58	0.61	0.58	0.59	0.50	0.50	0.47	0.43	0.43	0.44	0.44	0.43	0.86	2.70	3.87
MgO	3.38	8.07	8.20	8.10	8.30	8.54	8.63	8.93	8.96	9.08	9.07	9.14	9.11	6.39	4.13	3.21
CaO	4.66	7.80	7.69	7.60	7.19	6.83	6.84	6.46	6.44	6.32	6.22	6.22	6.25	6.10	5.97	4.57
Na2O	0.00	0.00	0.00	0.00	0.01	0.02	0.01	0.01	0.00	0.02	0.00	0.03	0.00	0.00	0.00	0.00
K2O	0.01	0.00	0.00	0.01	0.00	0.01	0.00	0.00	0.00	0.00	0.00	0.00	0.00	0.01	0.00	0.00
Cr2O3	0.04	0.07	0.04	0.03	0.06	0.04	0.05	0.03	0.07	0.05	0.08	0.07	0.05	0.05	0.06	0.05
Total	100.88	99.99	100.29	99.75	99.88	100.40	100.31	100.69	100.31	100.27	100.26	100.38	100.50	100.49	100.86	100.93
X	-20.7463	-20.644	-20.5554	-20.4054	-20.2363	-20.0317	-19.8722	-19.5968	-19.5109	-19.3432	-19.3105	-19.2655	-19.2372	-19.2139	-19.1656	-19.2031
Y	2.7366	2.8021	2.8757	2.9834	3.1034	3.2616	3.3666	3.6735	3.758	3.9189	3.9816	4.1248	4.2023	4.2365	4.2973	4.3857
Z	10.76	10.76	10.761	10.761	10.761	10.761	10.761	10.7615	10.761	10.762	10.7615	10.7615	10.7615	10.761	10.7615	10.7615

CVI-1385 Bt+Ms+Grt Schist

	Biotite					Plagioclase
No Spot.	25	26	27	28	29	30
SiO2	35.19	26.81	26.88	36.05	37.72	98.61
TiO2	1.61	0.08	0.07	1.52	0.80	0.01
Al2O3	18.62	21.27	20.67	17.36	19.21	0.03
FeO	17.96	21.88	23.71	19.32	17.36	0.23
MnO	0.07	0.11	0.19	0.16	0.10	0.01
MgO	11.35	16.37	16.25	10.31	11.91	0.00
CaO	0.15	0.18	0.09	0.04	0.08	0.00
Na2O	0.17	0.03	0.00	0.09	0.15	0.00
K2O	8.74	0.02	0.06	9.01	8.92	0.02
Cr2O3	0.03	0.02	0.01	0.04	0.00	0.03
Total	93.90	86.76	87.92	93.91	96.26	98.94
X	37.4839	37.3558	29.8817	29.5245	31.2525	30.222
Y	18.2219	18.5457	17.6441	18.1685	19.2434	19.1264
Z	10.7715	10.772	10.7805	10.7805	10.7805	10.7805

X-ray Map 1 Profile 1

No Spot.	238	239	240	241	242	243	244	245	246	247	248	249	250	251	252	253	254	255	256	257	258	259	260	261	262	263	264
SiO2	37.17	37.07	37.21	30.75	36.53	36.35	36.79	36.76	36.63	36.68	36.67	36.62	36.77	33.24	36.40	36.42	36.86	36.71	36.68	36.54	36.83	36.78	36.67	36.63	36.79	36.73	37.22
TiO2	0.03	0.05	0.07	0.05	0.06	0.04	0.01	0.02	0.00	0.00	0.00	0.02	0.01	0.00	0.01	0.01	0.00	0.00	0.00	0.01	0.01	0.01	0.01	0.00	0.02	0.00	0.01
Al2O3	20.98	20.84	20.88	16.43	20.52	20.42	20.75	20.76	20.61	20.82	20.77	20.73	20.57	18.71	20.70	20.62	20.76	20.80	20.71	20.72	20.71	20.66	20.71	20.73	20.79	20.87	21.08
FeO	31.96	31.11	31.42	30.12	30.97	30.71	32.55	32.19	32.03	31.36	30.67	30.57	30.69	30.09	30.74	30.53	30.47	30.67	30.50	30.24	30.14	30.60	30.78	30.94	31.03	31.55	31.71
MnO	1.81	1.76	1.97	2.26	2.47	2.99	4.57	5.13	5.38	5.89	6.10	6.29	6.45	6.15	6.39	6.41	6.44	6.31	6.41	6.45	6.46	6.48	6.54	6.24	6.23	5.99	5.34
MgO	3.20	3.02	2.96	1.73	2.67	2.81	2.96	2.98	2.92	2.84	2.76	2.74	2.76	2.57	2.71	2.78	2.83	2.85	2.88	2.77	2.79	2.77	2.79	2.81	2.87	2.94	2.87
CaO	4.47	5.40	5.07	4.69	5.48	5.22	2.15	1.80	1.64	2.11	2.49	2.39	2.22	1.97	2.04	1.98	2.27	2.33	2.31	2.52	2.49	2.37	2.11	1.96	1.77	1.65	1.59
Na2O	0.00	0.04	0.01	0.01	0.00	0.03	0.01	0.00	0.01	0.00	0.01	0.00	0.02	0.03	0.00	0.02	0.01	0.00	0.01	0.01	0.00	0.00	0.04	0.00	0.02	0.02	0.00
K2O	0.00	0.01	0.00	0.01	0.01	0.00	0.00	0.00	0.00	0.00	0.00	0.00	0.00	0.00	0.00	0.00	0.00	0.00	0.00	0.00	0.00	0.00	0.00	0.00	0.00	0.00	0.02
Cr2O3	0.01	0.01	0.01	0.02	0.00	0.03	0.00	0.00	0.01	0.03	0.01	0.00	0.01	0.01	0.00	0.02	0.02	0.02	0.03	0.02	0.00	0.02	0.04	0.02	0.02	0.01	0.01
Total	99.63	99.31	99.58	86.07	98.70	98.60	99.78	99.65	99.24	99.74	99.50	99.35	99.49	92.77	98.99	98.78	99.65	99.70	99.54	99.27	99.43	99.68	99.68	99.33	99.54	99.77	99.87
X	29.8643	29.8525	29.846	29.8355	29.8379	29.8274	29.8124	29.8006	29.7843	29.7702	29.7569	29.744	29.7281	29.7178	29.7011	29.6827	29.6718	29.6527	29.6397	29.6288	29.6186	29.6084	29.5968	29.5811	29.5695	29.5504	29.5361
Y	17.6636	17.6737	17.6855	17.705	17.712	17.7242	17.7457	17.7733	17.7866	17.8089	17.8265	17.827	17.868	17.8834	17.9155	17.9394	17.9735	18.0008	18.018	18.0403	18.0573	18.0778	18.0962	18.1214	18.133	18.1453	18.1542
Z	10.7805	10.7805	10.7805	10.7805	10.7805	10.7805	10.7805	10.7805	10.7805	10.7805	10.7805	10.7805	10.7805	10.7805	10.7805	10.7805	10.7805	10.7805	10.7805	10.7805	10.7805	10.7805	10.7805	10.7805	10.7805	10.7805	10.7805

Profile 2

No Spot.	265	266	267	268	269	270	271	272	273	274	275	276	277	278	279	280	281	282	283	284	285	286	287	288	289	290	291	292
SiO2	37.44	37.20	37.09	37.13	37.02	36.80	36.94	36.18	37.03	37.03	37.01	36.99	36.89	36.97	37.00	36.88	36.71	36.80	36.78	36.68	36.74	36.69	36.73	36.78	36.76	36.76	37.17	95.41
TiO2	0.01	0.00	0.02	0.02	0.02	0.02	0.01	0.11	0.02	0.05	0.04	0.03	0.02	0.00	0.00	0.02	0.00	0.01	0.00	0.00	0.00	0.00	0.00	0.01	0.00	0.00	0.00	0.00
Al2O3	21.13	20.98	21.00	21.02	20.94	20.86	20.94	20.11	20.87	20.92	20.81	20.93	20.91	20.88	20.75	20.76	20.70	20.70	20.84	20.70	20.65	20.69	20.87	20.78	20.77	20.71	20.98	0.08
FeO	33.37	32.83	30.88	32.14	32.56	32.60	32.13	29.48	31.79	32.58	32.20	32.15	32.23	32.74	31.87	32.06	31.64	30.81	31.27	31.54	31.44	31.86	32.14	33.02	33.58	33.04	33.66	0.45
MnO	2.12	2.00	2.75	3.99	4.25	4.25	4.02	3.28	2.80	2.12	2.17	2.52	4.34	4.86	5.36	5.82	6.08	6.24	6.45	6.33	6.17	5.75	5.13	4.25	3.11	3.02	2.35	0.00
MgO	3.03	2.87	2.83	2.81	2.82	2.89	2.79	2.57	2.76	3.01	2.96	2.91	3.01	3.06	2.98	3.01	2.94	2.85	2.91	2.86	2.89	3.01	3.14	3.31	3.49	3.40	3.37	0.00
CaO	2.85	3.95	5.25	3.02	2.55	2.43	3.07	5.70	4.57	4.38	4.48	4.29	2.52	1.65	1.83	1.58	1.79	1.91	1.73	1.63	1.72	1.63	1.60	1.65	1.79	2.17	2.42	0.01
Na2O	0.01	0.00	0.01	0.00	0.00	0.00	0.01	0.02	0.01	0.01	0.01	0.01	0.01	0.03	0.00	0.02	0.00	0.03	0.03	0.00	0.00	0.00	0.01	0.00	0.00	0.01	0.00	0.00
K2O	0.01	0.00	0.00	0.00	0.00	0.00	0.00	0.04	0.00	0.00	0.00	0.00	0.00	0.00	0.00	0.00	0.01	0.00	0.00	0.01	0.00	0.00	0.00	0.00	0.00	0.01	0.00	0.00
Cr2O3	0.00	0.00	0.00	0.03	0.01	0.00	0.00	0.02	0.00	0.01	0.03	0.03	0.01	0.02	0.02	0.01	0.03	0.02	0.02	0.00	0.02	0.00	0.02	0.01	0.02	0.01	0.00	0.02
Total	99.98	99.83	99.83	100.17	100.16	99.85	99.90	97.54	99.86	100.12	99.71	99.88	99.95	100.21	99.82	100.15	99.90	99.37	100.02	99.75	99.64	99.65	99.65	99.79	99.52	99.13	99.97	95.97
X	31.2405	31.2198	31.1931	31.1613	31.1322	31.0758	31.0374	30.9948	30.9438	30.8838	30.8511	30.8217	30.7719	30.7443	30.7026	30.6453	30.5736	30.5001	30.4668	30.4413	30.3987	30.3546	30.3348	30.3135	30.2943	30.2664	30.2454	30.2355
Y	19.2479	19.2452	19.2431	19.2404	19.2347	19.2347	19.2293	19.2236	19.2176	19.2176	19.2182	19.2185	19.22	19.2113	19.2032	19.2032	19.1957	19.1834	19.1762	19.1792	19.1864	19.1879	19.1885	19.1804	19.172	19.1498	19.1435	19.1372
Z	10.7805	10.7805	10.7805	10.7805	10.7805	10.7805	10.7805	10.7805	10.7805	10.7805	10.7805	10.7805	10.7805	10.7805	10.7805	10.7805	10.7805	10.7805	10.7805	10.7805	10.7805	10.7805	10.7805	10.7805	10.7805	10.7805	10.7805	10.7805

TABLE A4. Whole rock geochemistry used in this study

SAMPLE	AP-038	AP-010	AP-009	CJJ-91	CVI-1367	MPR-33	CVI-1388	CVI-13108	LRW-21
Ba	833	472	1005	365	937	288	90.2	852	519
Ce	18.4	38.6	29.3	6.4	28.3	98.2	180	40.4	94.1
Cr	20	30	0	0	150	30	40	160	210
Cs	1.17	0.56	0.29	0.13	2.81	0.97	0.16	1.43	1.45
Dy	2.47	6.69	1.32	0.3	2.57	5.97	19.9	5.06	9.48
Er	1.94	3.94	0.94	0.19	1.3	2.86	12.75	2.39	4.79
Eu	0.42	2.01	0.74	0.59	0.85	2.71	5.93	1.29	2.18
Ga	17.2	21.4	18.7	22.6	17.7	27	21.1	26.7	31.4
Gd	2.21	7.04	1.79	0.25	2.5	7.69	19.1	6.08	11.85
Hf	1.6	3.7	3.1	0.4	2.8	6.9	30.7	1.5	2.3
Ho	0.59	1.35	0.3	0.08	0.53	1.08	4.35	0.94	1.91
La	9.2	17.1	14.5	3.6	14.1	47.5	81.4	16.8	38
Lu	0.33	0.53	0.16	0.02	0.2	0.36	1.79	0.27	0.62
Nb	4.5	7	7.1	1.3	3	9.9	20.1	13.4	23.2
Nd	8.8	25.4	13.8	1.9	13.2	42.4	99.1	24.2	52.5
Pr	2.2	5.66	3.53	0.62	3.46	11.3	23.9	5.53	12.35
Rb	109	16.3	38.4	4.6	47.1	27.3	4.8	114	118.5
Sm	2.11	6.85	2.36	0.27	2.56	8.63	18.9	5.7	12.75
Sn	1	2	1	1	1	3	1	1	2
Sr	207	452	500	1550	303	931	404	196	319
Ta	0.5	0.3	0.4	0.1	0.2	0.7	0.9	0.6	1
Tb	0.41	1.06	0.23	0.05	0.36	1.12	3.13	0.99	1.79
Th	4.34	0.06	1.95	0.35	4.26	11.65	5.73	1.16	3.01
Tm	0.28	0.59	0.15	0.02	0.21	0.36	1.85	0.3	0.68
U	2.94	0.09	0.86	0.12	1.87	3.95	1.32	1.26	1.7
V	12	133	41	21	153	214	164	238	238
W	1	1	1	3	1	1	1	2	1
Y	16.9	35.9	8.7	1.7	13.2	32	119	25.9	49.7
Yb	2.35	3.68	1.08	0.15	1.35	2.51	11.65	2.13	4.29
Zr	38	124	110	10	98	276	1400	57	76
SiO2	74.7	59.7	70.3	59.8	54.9	52.9	40.2	55.1	45.5
Al2O3	14.2	15.3	16.05	25.1	15	15.85	19.1	17.1	19.15
Fe2O3t	1.21	9.27	2.61	0.91	5.55	9.47	22.1	9.19	16.1
CaO	1.03	5.76	3.03	7.87	6.43	8.8	11.4	5.7	6.22
MgO	0.07	2.45	0.66	0.19	4.24	4.45	3.18	5.44	4.1
Na2O	3.92	4.26	4.21	6.31	3.99	4.02	1.44	0.96	2.43
K2O	4.56	1	2.05	0.35	1.48	1.28	0.39	3.11	2.31
Cr2O3	0	0	0	0	0.02	0.01	0.01	0.02	0.03
TiO2	0.03	1.25	0.23	0.04	0.61	0.87	1.71	1.42	2.58
MnO	0.1	0.17	0.1	0.02	0.11	0.2	0.49	0.13	0.32
P2O5	0.02	0.46	0.09	0.01	0.21	0.39	1.14	0.65	0.9
SrO	0.03	0.06	0.07	0.19	0.04	0.11	0.06	0.03	0.04
BaO	0.1	0.06	0.11	0.04	0.11	0.03	0.01	0.1	0.06
LOI	0.41	1.15	1.72	0.54	7.27	1.57	-0.88	1.34	0.3
Total	100.38	100.89	101.23	101.37	99.96	99.95	100.35	100.29	100.04
Ag	0	0	0	0	0	0	0	0	0
As	0	0	6	0	0	0	5	0	0
Cd	0	0	0	0	0	0	0.9	0	0
Co	1	17	3	1	17	22	23	27	41
Cu	1	33	3	2	40	586	22	5	43
Li	0	10	10	0	30	10	0	10	30
Mo	1	1	0	1	0	1	3	0	0
Ni	1	9	1	1	27	23	15	57	68
Pb	29	4	6	8	8	16	5	11	5
Sc	2	22	3	1	18	13	40	23	34
Tl	0	0	0	0	0	0	0	0	0
Zn	16	92	63	18	78	110	174	168	248
FeO	0.9254443	7.0899741	1.9962063	0.6959953	4.2448065	7.2429401	16.902743	7.0287877	12.313763
Fe2O3	0.1815	1.3905	0.3915	0.1365	0.8325	1.4205	3.315	1.3785	2.415
mg	0.05947605	0.22414398	0.2165563	0.18581993	0.45506714	0.3393465	0.13591054	0.39285672	0.21775196

TABLE A5. ANACOMP Database Results, geochemical analysis from major Oxides, the First 6 samples are control from the database
This table includes NORMAL wt. % and LOG wt. % comparisons

*** Output of program and database A N A C O M P from C. Roehr, version Mar. 1991 ***

Date: 5.11.2016. Analyses read from file EXAMPLE.DAT (recalculated to 100%). The database holds 3591 analyses for comparison.
Abs. diff. of wt.% for most similiar: 3.36. Comparison using NORMAL wt.% oxides. No oxides ommited from comparison.

No.	dif.	name of rock	location	source	SiO2	TiO2	Al2O3	FeOt	MnO	MgO	CaO	Na2O	K2O	P2O5
		Metagabbro, KTB VB			48.8	1.80	15.7	12.0	.17	8.1	9.5	2.5	.9	.45
1	100	basalt. scoria lava	Lahn-Dill, Germany	Schmincke+Sunkel_87_	48.4	1.52	15.9	11.3	.19	8.0	9.7	3.7	1.0	.22
2	132	basalt	kenya rift	Wilson,M._(1989)____	48.5	1.98	15.6	12.3	.21	6.6	11.3	2.3	.8	.43
3	134	Amphibolite	Arquia Complex	Villagomez_2011_____	48.8	1.94	14.7	12.3	.20	8.0	10.5	3.3	.2	.17
4	139	Basalt	Columbia River Province	Wilson,M._(1989)____	49.8	1.62	16.0	11.3	.18	7.3	10.2	2.8	.5	.25
5	143	Latit-Basalt	Siebengebirge	Wimmenauer_(1985)___	49.0	1.93	15.0	10.4	.15	9.2	9.9	2.6	1.5	.35
6	146	altered pillow lava	Hokkaido, Japan	Amstutz_(ed)_(1974)_	48.9	3.06	16.4	11.4	.15	7.9	8.1	2.8	.8	.53
7	151	Arquia	Serpentinite	Cochrane_2014a______	49.1	1.63	14.9	11.8	.21	8.6	11.2	2.2	.2	.11
8	154	basalt	(average)	Best_82/LeMaitre_76_	50.1	1.88	16.0	10.8	.20	6.9	9.7	3.0	1.1	.36
9	160	Amph	Monte Ol.	Cochrane_2014_______	50.7	1.22	15.1	12.2	.15	8.4	9.0	2.8	.3	.08
10	161	basalt. scoria lava	Lahn-Dill, Germany	Schmincke+Sunkel_87_	48.2	2.03	16.4	11.3	.17	7.2	9.2	3.7	1.5	.33

Date: 5.11.2016. Analyses read from file EXAMPLE.DAT (recalculated to 100%). The database holds 3591 analyses for comparison.
Abs. diff. of wt.% for most similiar: 2.12. Comparison using NORMAL wt.% oxides. No oxides ommited from comparison.

No.	dif.	name of rock	location	source	SiO2	TiO2	Al2O3	FeOt	MnO	MgO	CaO	Na2O	K2O	P2O5
		Paragneis 33a, Nordrach, Schwarzwald			70.4	.74	14.0	4.9	.12	2.5	2.4	2.7	2.2	.07
1	100	graywacke, Proterozoic	NW Barrandium, CSFR	Chab_and_Pelc_1973__	70.1	.59								

```
  14.0  4.5  .09  2.3  2.5  3.5  2.2  .13
  2  154 La Bocana                migmatite                 Riel_2013___________ 71.4  .82
  14.1  4.9  .07  1.8  1.8  2.5  2.7  .
  3  176 Amphibolic Gneiss        JL-5036-RA                Lopez_2012__________ 69.2  .65
  14.5  5.2  .06  2.1  2.9  3.2  2.0  .15
  4  186 graywacke, Proterozoic   NW Barrandium, CSFR       Chab_and_Pelc_1973__ 69.3  .65
  14.0  4.7  .12  2.5  3.5  3.4  1.7  .12
  5  190 graywacke, Proterozoic   NW Barrandium, CSFR       Chab_and_Pelc_1973__ 69.7  .47
  14.7  4.3  .07  2.1  2.5  3.5  2.5  .14
  6  190 graywacke, Proterozoic   NW Barrandium, CSFR       Chab_and_Pelc_1973__ 69.2  .49
  14.5  4.6  .07  2.7  2.2  3.8  2.2  .23
  7  191 graywacke, Proterozoic   NW Barrandium, CSFR       Chab_and_Pelc_1973__ 70.1  .69
  13.6  5.0  .08  1.4  2.4  4.5  2.0  .13
  8  194 arkose                   Santa Ynes Mt.,California v.d.Kamp_et_al_1976_ 71.1  .67
  14.5  4.8  .06  2.1  1.4  3.5  1.6  .10
  9  194 arkose                   Santa Ynes Mt.,California v.d.Kamp_et_al_1976_ 71.1  .54
  13.6  4.6  .07  1.9  1.8  2.9  3.2  .12
 10  195 granitoid                CICUCO 2A                 Cardona_2010c_______ 69.8  .53
 15.2  4.9  .07  1.6  2.2  2.8  2.9  .17


Date: 5.11.2016. Analyses read from file EXAMPLE.DAT (recalculated to 100%). The database
holds 3591 analyses for comparison.
Abs. diff. of wt.% for most similiar: 1.32. Comparison using NORMAL wt.% oxides. No oxides
ommited from comparison.

 No. dif. name of rock             location                  source                SiO2 TiO2
 Al2O3 FeOt MnO MgO  CaO  Na2O  K2O P2O5
-------------------------------------------------------------------------------------------------
-------------------------------------
         Biotit-reicher Leptinit 182, Nordrach                                      75.4  .10
         13.6  1.8  .04   .4   .9  3.4  4.4  .03
-------------------------------------------------------------------------------------------------
-------------------------------------
  1  100 CdL                       granite                   Bock_et_al.,_2000___ 75.2  .13
  13.5  1.7  .05   .5  1.4  3.3  4.3  .04
  2  128 Puquio                    rhyolite                  Mamani_et_al.,_2008_ 75.4  .23
  13.4  1.7  .07   .3   .9  4.0  4.0  .03
  3  134 Precordillera             rhyolite                  Haschke_2002________ 75.1  .19
  13.5  1.5  .02   .4  1.2  3.8  4.3  .01
  4  139 Caquena                   rhyolite                  Davidson_1990_______ 75.4  .22
  13.2  1.3  .04   .4   .8  3.8  4.8  .04
  5  148 Yura                      rhyolite                  Paquereau_2008______ 75.1  .20
  13.6  1.3  .08   .2  1.0  3.8  4.6  .04
  6  152 Precordillera             rhyolite                  Haschke_2002________ 75.8  .21
  13.3  1.7  .04   .5  1.3  3.3  3.8  .05
  7  170 Yura                      rhyolite                  Paquereau_2008______ 74.7  .23
  13.6  1.4  .08   .4  1.3  3.5  4.7  .06
  8  171 Vitor                     rhyolite                  Paquereau_2008______ 75.1  .19
  13.6  1.2  .07   .3  1.0  4.3  4.4  .04
  9  177 Chili                     rhyolite                  Paquereau_2008______ 75.1  .19
  13.7  1.2  .07   .3  1.1  4.1  4.3  .04
 10  186 Yura                      rhyolite                  Paquereau_2008______ 74.9  .19
 13.8  1.2  .08   .3  1.1  4.0  4.5  .04


Date: 5.11.2016. Analyses read from file EXAMPLE.DAT (recalculated to 100%). The database
```

holds 3591 analyses for comparison.
Abs. diff. of wt.% for most similiar: 3.14. Comparison using NORMAL wt.% oxides. No oxides ommited from comparison.

No.	dif.	name of rock	location	source	SiO2	TiO2	Al2O3	FeOt	MnO	MgO	CaO	Na2O	K2O	P2O5
		Silikatmarmor, Val Strona			7.0	.02	1.5	1.7	.54	1.1	88.0	.1	.1	.02
1	100	limestone	Rhein.Schiefergeb.Germany	Schulz-Dobrick(1975)	6.9	.07	1.9	.6	.34	.9	88.7	.3	.3	.02
2	178	limestone	Rhein.Schiefergeb.Germany	Schulz-Dobrick(1975)	6.1	.14	3.2	1.1	.07	.9	87.4	.0	1.0	.02
3	187	limestone	Rhein.Schiefergeb.Germany	Schulz-Dobrick(1975)	8.1	.02	.3	.5	.10	1.0	89.8	.0	.1	.07
4	257	lake chalk (Seekreide)	Gross Drewitz,Germany	Niggli,_P._(1952)___	7.7	.	1.5	4.7	.36	.5	85.1	.	.	.
5	267	limestone	Rhein.Schiefergeb.Germany	Schulz-Dobrick(1975)	8.4	.03	.5	2.5	1.78	1.5	84.9	.2	.0	.27
6	288	limestone	Rhein.Schiefergeb.Germany	Schulz-Dobrick(1975)	11.3	.05	.8	.8	.13	1.0	85.5	.1	.2	.03
7	296	limestone	Rhein.Schiefergeb.Germany	Schulz-Dobrick(1975)	11.0	.05	1.2	.6	.22	1.4	85.1	.1	.2	.15
8	351	limestone	Rhein.Schiefergeb.Germany	Schulz-Dobrick(1975)	3.7	.03	.7	1.0	.23	.7	93.4	.1	.1	.05
9	385	limestone	Rhein.Schiefergeb.Germany	Schulz-Dobrick(1975)	11.3	.13	2.5	1.1	.46	.8	82.9	.5	.3	.07
10	419	limestone	Rhein.Schiefergeb.Germany	Schulz-Dobrick(1975)	3.0	.05	1.2	.5	.07	.5	94.2	.0	.4	.

Date: 5.11.2016. Analyses read from file EXAMPLE.DAT (recalculated to 100%). The database holds 3591 analyses for comparison.
Abs. diff. of wt.% for most similiar: 3.04. Comparison using NORMAL wt.% oxides. No oxides ommited from comparison.

No.	dif.	name of rock	location	source	SiO2	TiO2	Al2O3	FeOt	MnO	MgO	CaO	Na2O	K2O	P2O5
		Serpentinit, Foehrenbuehl, EGZ			46.8	.33	3.5	9.1	.11	37.6	2.1	.2	.2	.06
1	100	Lherzolith	Ivrea-Zone,Italien	Wimmenauer_(1985)___	46.5	.09	3.2	8.7	.16	37.9	3.2	.2	.0	.
2	175	Spinell-Lherzolith	S. de Ronda,Spanien	Wimmenauer_(1985)___	48.8	.06	2.7	7.9	.13	37.5	2.8	.1	.	.
3	176	Raspas Complex	peridotite	John_2010_____	47.2	.05	2.1	8.7	.12	40.0	1.9	.0	.	.
4	203	Rio Panupili Mafic	Harzburgite	Bosch_2002_____	44.5	.09	3.2	9.0	.12	39.8	2.6	.5	.0	.08
5	250	El Toro Unit UM	Serpentinite	Bosch_2002_____	44.1	.10	3.1	9.1	.11	40.7	2.8	.1	.0	.01

```
  6  270 serpentinite              Peräpohja, Finnland       Amstutz_(ed)_(1974)_ 45.8  .39
  2.3 12.6  .18 38.1   .5   .1   .   .02
  7  292 Granat-Peridotit          Böhmen,CSFR               Wimmenauer_(1985)___ 44.0  .14
  2.5  9.2  .16 42.0  2.0   .    .   .
  8  295 Komatiit                  Munro Township,Kanada     Wimmenauer_(1985)___ 44.2  .19
  6.6  7.4  .11 38.1  2.9   .2   .1  .03
  9  299 Al-spinel lherzolite                                Wilson,M._(1989)____ 44.6  .18
  1.8  8.9  .14 41.9  2.3   .1   .0  .01
 10  307 Arquia                    Serpentinite              Cochrane_2014a______ 46.4  .05
 1.7  8.3  .10 42.4  1.0   .    .   .01


Date: 5.11.2016. Analyses read from file EXAMPLE.DAT (recalculated to 100%). The database
holds 3591 analyses for comparison.
Abs. diff. of wt.% for most similiar: 32.30. Comparison using NORMAL wt.% oxides. No oxides
ommited from comparison.

 No. dif. name of rock             location                  source               SiO2 TiO2
 Al2O3 FeOt MnO MgO  CaO  Na2O  K2O P2O5
-------------------------------------------------------------------------------------------
-------------------------------------
         Chloritschiefer Stbr. Marienstollen, EGZ                                 32.1 2.13
         20.1 12.1  .39 32.7   .4   .1   .0  .03
-------------------------------------------------------------------------------------------
-------------------------------------
  1  100 harzburgite (serpentin.)  Harzburg massif, Germany  Vinx,_R._(1982)_____ 43.1  .15
  6.9 11.3  .19 35.1  2.8   .2   .2  .02
  2  104 mela-olivinegabbronorite  Harzburg massif, Germany  Vinx,_R._(1982)_____ 42.2  .17
  7.2 10.3  .19 34.6  4.5   .7   .0  .05
  3  104 feldspar peridotite       Lahn-Dill, Germany        Amstutz_(ed)_(1974)_ 43.2  .66
  5.5 15.2  .19 32.2  2.7   .2   .1  .
  4  105 Kimberlit                 Iron Mountain,Wyoming     Wimmenauer_(1985)___ 39.2 3.50
  3.3 12.5  .21 33.2  6.0   .1  1.6  .41
  5  108 mela-olivinenorite        Harzburg massif, Germany  Vinx,_R._(1982)_____ 44.3  .36
  7.2 10.3  .17 31.8  5.1   .4   .2  .05
  6  112 picrite                   Rhein.Schiefergeb.Germany Schulz-Dobrick(1975) 41.8  .79
  6.0 15.7  .23 30.2  4.1   .8   .3  .05
  7  114 Komatiit                  Munro Township,Kanada     Wimmenauer_(1985)___ 44.2  .23
  6.0 10.0  .14 34.5  4.5   .3   .1  .01
  8  116 perodotite                (average)                 Best_82/LeMaitre_76_ 44.7  .67
  4.5 10.4  .43 33.0  5.3   .5   .4  .11
  9  118 Peridotit                 Skaergaard,Grönland       Wimmenauer_(1985)___ 41.6  .07
  8.8 13.1  .16 27.3  6.6   .7   .1 1.55
 10  120 kimberlite                                          Wilson,M._(1989)____ 38.1 2.37
 3.1  9.8  .24 33.8  9.7   .2  1.3 1.31

Date: 5.11.2016. Analyses read from file EXAMPLE.DAT (recalculated to 100%). The database
holds 3591 analyses for comparison.
Abs. diff. of wt.% for most similiar: 3.64. Comparison using NORMAL wt.% oxides. No oxides
ommited from comparison.

 No. dif. name of rock             location                  source               SiO2 TiO2
 Al2O3 FeOt MnO MgO  CaO  Na2O  K2O P2O5
-------------------------------------------------------------------------------------------
-------------------------------------
         AP-010                                                                   59.9 1.25
         15.4  9.3  .17  2.5  5.8  4.3  1.0  .46
```

```
------------------------------------------------------------------------------------------------------------
-------------------------------------
  1  100 Andesit                    San Salvador              Wimmenauer_(1985)___ 58.7 1.19
 15.5  9.4  .20  2.5  6.2  4.0  2.1  .19
  2  128 Andesite, calc-alk.series South Sandwich arc        Wilson,M._(1989)____ 60.4 1.12
 14.2 10.6  .22  2.1  6.1  3.8  1.2  .26
  3  143 spilite                    Schirmeck, Vosges, France Amstutz_(ed)_(1974)_ 61.4 1.30
 14.4 10.2  .16  2.3  5.6  3.4  1.3  .
  4  146 acid andesite,med-K,TH     New Britain               Gill,_J.B._(1981)___ 58.9  .89
 15.5  8.7  .18  3.2  7.0  3.8  1.5  .25
  5  152 Andesit                    Thingmuli,Island          Wimmenauer_(1985)___ 61.9 1.28
 15.4  8.0  .19  1.8  5.1  4.4  1.6  .44
  6  153 Clemesi                    andesite                  Mamani_et_al.,_2008_ 59.3 1.03
 16.3  8.6  .15  2.7  6.3  3.4  2.0  .23
  7  176 Pyroxen-Bio.-Qrz.-Andesit Saar-Nahe                 Wimmenauer_(1985)___ 59.7 1.79
 16.2  7.5  .09  3.2  6.2  3.3  1.7  .35
  8  178 Andesite,tholeiit. series South Sandwich arc        Wilson,M._(1989)____ 62.8 1.01
 14.2  8.8  .18  2.1  6.2  4.1   .4  .17
  9  179 spilit.tuffite (Schalst.) Schirmeck, Vosges, France Amstutz_(ed)_(1974)_ 60.2 1.12
 14.5 10.7  .16  3.9  3.9  4.5   .9  .
 10  185 Misti                      andesite                  Mamani_et_al.,_2008_ 58.9  .90
 16.9  7.5  .12  3.2  6.0  4.3  1.8  .29


Date: 5.11.2016. Analyses read from file EXAMPLE.DAT (recalculated to 100%). The database
holds 3591 analyses for comparison.
Abs. diff. of wt.% for most similiar: 2.85. Comparison using NORMAL wt.% oxides. No oxides
ommited from comparison.

 No. dif. name of rock             location                  source                SiO2 TiO2
 Al2O3 FeOt MnO MgO  CaO  Na2O  K2O P2O5
------------------------------------------------------------------------------------------------------------
-------------------------------------
         CVI-1367                                                                    59.3  .66
         16.2  6.0  .12  4.6  6.9  4.3  1.6  .23
------------------------------------------------------------------------------------------------------------
-------------------------------------
  1  100 Lascar                     andesite                  Mamani_et_al.,_2008_ 59.0  .76
 16.4  7.0  .12  4.4  6.9  3.5  1.8  .19
  2  114 Lascar                     andesite                  Mamani_et_al.,_2009_ 58.8  .75
 16.1  7.3  .12  4.7  7.0  3.3  1.7  .19
  3  115 Lascar                     andesite                  Mamani_et_al.,_2009_ 58.7  .75
 16.4  7.1  .12  4.7  7.1  3.4  1.7  .19
  4  117 Precordillera              andesite                  Haschke_2002________ 59.5  .81
 16.6  5.9  .11  3.6  6.9  3.8  2.5  .31
  5  119 Andesite                   South-west Pacific        Wilson,M._(1989)____ 59.3  .73
 16.9  6.7  .13  3.8  7.1  3.4  1.7  .23
  6  128 Negrillar                  andesite                  Mamani_et_al.,_2009_ 58.5 1.08
 16.5  6.6  .09  4.1  6.6  4.1  2.0  .39
  7  136 Lascar                     andesite                  Mamani_et_al.,_2009_ 58.4  .76
 16.4  7.2  .12  4.8  7.2  3.4  1.6  .19
  8  136 Las Cuevas                 andesite                  Worner_1992_________ 59.3  .95
 16.8  6.5  .09  3.8  5.9  4.4  2.0  .26
  9  138 Base Misti                 andesite                  Mamani_et_al.,_2008_ 58.7  .84
 16.6  7.1  .11  4.3  6.5  3.6  1.9  .22
 10  143 acid andesite,med-K, CA    Fiji                      Gill,_J.B._(1981)___ 60.1  .69
 17.2  6.0  .14  3.3  7.2  3.9  1.3  .20
```

Date: 5.11.2016. Analyses read from file EXAMPLE.DAT (recalculated to 100%). The database holds 3591 analyses for comparison.
Abs. diff. of wt.% for most similiar: 3.96. Comparison using NORMAL wt.% oxides. No oxides ommited from comparison.

No.	dif.	name of rock	location	source	SiO2	TiO2	Al2O3	FeOt	MnO	MgO	CaO	Na2O	K2O	P2O5
		MPR-33			53.8	.89	16.1	9.6	.20	4.5	9.0	4.1	1.3	.40
1	100	Kalk-Alkali-Basalt	San Salvador	Wimmenauer_(1985)___	53.3	1.23	17.3	9.9	.20	4.0	9.1	3.3	1.4	.20
2	103	Leon Muerto	basalt	Trumbull__1999_____	54.1	1.26	17.2	10.0	.17	3.8	8.2	3.7	1.4	.32
3	111	Kalk-Alkali-Basalt	San Salvador	Wimmenauer_(1985)___	53.0	.97	17.1	10.1	.19	4.5	9.7	3.0	1.3	.20
4	111	Kalk-Alkali-Basalt	San Salvador	Wimmenauer_(1985)___	53.0	.97	17.1	10.1	.19	4.5	9.7	3.0	1.3	.20
5	111	Antofagasta	gabbro	Mamani_et_al.,_2008_	53.7	1.37	15.8	11.2	.16	4.6	8.4	3.2	1.4	.22
6	117	Nicholson	basaltic andesite	Delacour__2007_____	52.7	1.47	16.6	9.5	.12	5.4	8.4	3.7	1.7	.36
7	119	Las Cuevas	basalt	Worner_1992_____	52.9	1.42	17.1	9.2	.11	5.2	8.7	3.6	1.5	.27
8	119	Rhyolite	Riolita de Golero	Colmenares_2009_____	54.2	1.27	16.1	9.9	.17	5.8	8.5	2.6	1.1	.34
9	119	Santa Marta	Qz-Andesite	Quandt_2013_____	54.2	1.27	16.1	9.9	.17	5.8	8.5	2.6	1.1	.34
10	120	Nicholson	basalt	Mamani_et_al.,_2008_	52.5	1.47	16.5	9.6	.14	5.5	8.5	3.7	1.8	.35

Date: 5.11.2016. Analyses read from file EXAMPLE.DAT (recalculated to 100%). The database holds 3591 analyses for comparison.
Abs. diff. of wt.% for most similiar: 14.32. Comparison using NORMAL wt.% oxides. No oxides ommited from comparison.

No.	dif.	name of rock	location	source	SiO2	TiO2	Al2O3	FeOt	MnO	MgO	CaO	Na2O	K2O	P2O5
		CVI-1388			39.7	1.69	18.9	21.9	.48	3.1	11.3	1.4	.4	1.13
1	100	volcaniclastic rock	E Iceland, drill hole	Schmincke_et_al.1982	41.1	4.22	17.9	20.6	.18	3.5	7.3	1.5	3.2	.44
2	105	olivinegabbro	Harzburg massif, Germany	Vinx,_R._(1982)_____	45.7	1.84	16.8	21.9	.51	1.2	8.1	2.5	.6	.73
3	122	volcaniclastic rock	E Iceland, drill hole	Schmincke_et_al.1982	45.2	3.19	19.5	16.1	.18	4.3	11.0	.2	.1	.27
4	132	olivinegabbronorite	Harzburg massif, Germany	Vinx,_R._(1982)_____	42.9	3.70								

```
  12.3 22.7  .41  5.1  8.4  1.8  1.0 1.71
  5  135 spilite                  Cornwall-Devonshire, UK   Amstutz_(ed)_(1974)_ 34.9 4.82
  20.6 18.5  .35  4.8 12.6  1.1  2.3  .
  6  138 spilit.tuffite (Schalst.) Lahn-Dill, Germany       Amstutz_(ed)_(1974)_ 38.6 3.95
  19.7 14.6  .13  6.6 11.7  1.3  3.4  .
  7  142 basaltic pyroclastic rock Devonian,Weilburg,Germany Flick_and_Nesbor_88_ 42.6 3.25
  17.4 16.6  .09  6.6  9.6   .9  2.7  .34
  8  143 Diabas                   Lahn-Dill, Germany        Hentschel_(1970)____ 45.4 2.84
  18.5 14.0  .    5.4 10.4  2.3   .8  .32
  9  146 spilite                  Cornwall-Devonshire, UK   Amstutz_(ed)_(1974)_ 42.3 3.36
  17.4 16.3  .20  6.9  9.2  4.0   .4  .
 10  149 spilitic pillow lava     Lahn-Dill, Germany        Amstutz_(ed)_(1974)_ 40.1 2.27
 17.4 14.0  .20  8.2 13.8  3.7   .4  .


Date: 5.11.2016. Analyses read from file EXAMPLE.DAT (recalculated to 100%). The database
holds 3591 analyses for comparison.
Abs. diff. of wt.% for most similiar: 6.73. Comparison using NORMAL wt.% oxides. No oxides
ommited from comparison.

 No. dif. name of rock            location                  source               SiO2 TiO2
 Al2O3 FeOt MnO MgO  CaO  Na2O  K2O P2O5
-------------------------------------------------------------------------------------------
-------------------------------------
         CVI-13108                                                                 55.8 1.44
         17.3  9.3  .13  5.5  5.8  1.0  3.2  .66
-------------------------------------------------------------------------------------------
-------------------------------------
  1  100 tuffite, Upper Devonian   Rhein.Schiefergeb.Germany Schulz-Dobrick(1975) 55.6 1.25
  16.3 10.5  .12  4.9  4.9  3.0  3.3  .24
  2  100 Oruro                     basalt                    Aitcheson__1995_____ 55.6 1.20
  15.7  8.3  .12  6.0  6.3  3.3  3.0  .50
  3  109 claystone                 Rhein.Schiefergeb.Germany Schulz-Dobrick(1975) 57.0  .90
  17.9  8.7  .10  4.0  6.0   .6  4.8  .10
  4  112 Sandstones and Mudstones  Formación Los Indios      Colmenares_2009_____ 54.9 1.29
  16.7  9.9  .17  4.1  6.4  3.5  2.7  .42
  5  114 Ignimbrite                Ignimbrita de los Clavos  Colmenares_2009_____ 54.4 1.60
  17.1  9.9  .17  4.0  5.7  3.7  2.5  .93
  6  116 Hornblende-Biotit-Diorit  Grafenstein,Oberfranken   Wimmenauer_(1985)___ 55.4 1.19
  18.4  6.9  .13  5.4  6.5  3.0  2.6  .48
  7  119 APVC                      andesite                  Kay_et_al.,__1994___ 55.7 1.36
  16.0  7.4  .14  6.1  7.2  2.9  2.7  .42
  8  119 spilite                   Himachal Pradesh, India   Amstutz_(ed)_(1974)_ 54.7 1.57
  15.3 11.0  .28  5.9  5.4  2.6  3.2  .
  9  120 Santa Marta               Qz-Andesite               Quandt_2013_________ 57.9 1.08
  16.5  8.0  .19  4.2  6.0  2.4  3.3  .38
 10  120 Basalts and tuffs         Formacion Corual          Colmenares_2009_____ 57.9 1.08
 16.5  8.0  .19  4.2  6.0  2.4  3.3  .38


Date: 5.11.2016. Analyses read from file EXAMPLE.DAT (recalculated to 100%). The database
holds 3591 analyses for comparison.
Abs. diff. of wt.% for most similiar: 7.59. Comparison using NORMAL wt.% oxides. No oxides
ommited from comparison.

 No. dif. name of rock            location                  source               SiO2 TiO2
 Al2O3 FeOt MnO MgO  CaO  Na2O  K2O P2O5
```

```
---------------------------------------------------------------------------------------------------
-------------------------------------
          LRW-21                                                                    45.7 2.59
          19.2 16.2  .32  4.1  6.2  2.4  2.3  .90
---------------------------------------------------------------------------------------------------
-------------------------------------
  1  100 pillow lava              Lahn-Dill, Germany        Schmincke+Sunkel_87_ 46.7 3.72
  18.6 14.5  .15  4.6  4.9  3.4  2.6  .92
  2  106 volcaniclastic rock      E Iceland, drill hole     Schmincke_et_al.1982 47.3 3.39
  20.0 17.0  .27  3.5  3.9  2.1  2.3  .19
  3  125 pillow lava              Lahn-Dill, Germany        Schmincke+Sunkel_87_ 46.7 4.06
  19.2 13.4  .12  4.3  5.0  2.1  4.4  .73
  4  134 volcaniclastic rock      E Iceland, drill hole     Schmincke_et_al.1982 45.2 4.77
  17.8 18.4  .41  3.0  5.8  1.3  2.9  .33
  5  145 volcaniclastic rock      E Iceland, drill hole     Schmincke_et_al.1982 47.2 2.86
  16.4 14.6  .31  6.5  6.5  2.0  3.4  .26
  6  145 spilite                  Rhein.Schiefergeb.Germany Schulz-Dobrick(1975) 45.2 3.46
  15.5 17.5  .24  5.7  7.1  3.2  1.6  .45
  7  146 Diabas                   Lahn-Dill, Germany        Hentschel_(1970)____ 45.4 2.84
  18.5 14.0  .    5.4 10.4  2.3   .8  .32
  8  147 volcaniclastic rock      E Iceland, drill hole     Schmincke_et_al.1982 48.1 3.54
  16.0 16.5  .32  5.6  6.6  1.8  1.2  .33
  9  151 basalt. volcaniclastic   Lahn-Dill, Germany        Schmincke+Sunkel_87_ 47.9 3.51
  19.9 14.1  .10  3.3  3.8  2.7  4.0  .69
 10  152 albitized basalt         Deccan, Bombay, India     Amstutz_(ed)_(1974)_ 47.9 2.32
 15.1 16.1  .    5.9  7.5  3.2  2.0  .


Date: 5.11.2016. Analyses read from file EXAMPLE.DAT (recalculated to 100%). The database
holds 3591 analyses for comparison.
Abs. diff. of wt.% for most similiar: 1.09. Comparison using NORMAL wt.% oxides. No oxides
ommited from comparison.

 No. dif. name of rock             location                  source               SiO2 TiO2
 Al2O3 FeOt MnO MgO  CaO  Na2O  K2O P2O5
---------------------------------------------------------------------------------------------------
-------------------------------------
           AP-038                                                                    74.8
           .03 14.2  1.2  .10   .1  1.0  3.9  4.6  .02
---------------------------------------------------------------------------------------------------
-------------------------------------
  1  100 Yura                     rhyolite                  Paquereau_2008______ 74.9  .19
  13.8  1.2  .08   .3  1.1  4.0  4.5  .04
  2  111 Chili                    rhyolite                  Paquereau_2008______ 74.7  .20
  13.9  1.3  .08   .3  1.0  4.0  4.5  .05
  3  143 Vitor                    rhyolite                  Paquereau_2008______ 74.8  .20
  13.8  1.2  .08   .2  1.0  4.4  4.3  .04
  4  150 Yura                     rhyolite                  Paquereau_2008______ 75.1  .20
  13.6  1.3  .08   .2  1.0  3.8  4.6  .04
  5  152 Chili                    rhyolite                  Paquereau_2008______ 75.1  .19
  13.7  1.2  .07   .3  1.1  4.1  4.3  .04
  6  153 Guallatiri               rhyolite                  Worner_1992_________ 74.3  .19
  14.0  1.1  .06   .3  1.1  4.3  4.6  .02
  7  164 Yura                     rhyolite                  Paquereau_2008______ 74.4  .23
  13.9  1.5  .08   .3  1.1  4.1  4.4  .04
  8  164 Vitor                    rhyolite                  Paquereau_2008______ 75.0  .19
  13.7  1.2  .07   .2  1.0  4.3  4.3  .04
```

```
  9  167 Chachani                  rhyolite                  Mamani_et_al.,_2008_ 74.5  .19
 13.7  1.3  .07   .3  1.0  4.0  5.0  .05
 10  169 Chili                     rhyolite                  Paquereau_2008______ 74.5  .14
 14.2  1.1  .09   .3  1.2  3.4  5.0  .05

Date: 5.11.2016. Analyses read from file EXAMPLE.DAT (recalculated to 100%). The database
holds 3591 analyses for comparison.
Abs. diff. of wt.% for most similiar: 3.19. Comparison using NORMAL wt.% oxides. No oxides
ommited from comparison.

 No. dif. name of rock             location                  source               SiO2 TiO2
 Al2O3 FeOt MnO MgO  CaO  Na2O  K2O P2O5
-------------------------------------------------------------------------------------------
-------------------------------------
            AP-009                                                                  70.8
            .23 16.2  2.6  .10   .7  3.0  4.2  2.1  .09
-------------------------------------------------------------------------------------------
-------------------------------------
  1  100 Santa Marta               Granodiorite              Quandt_2013_________ 70.9  .37
 15.4  2.6  .06  1.3  2.3  4.3  2.7  .13
  2  104 Mylonites                 Santa Marta P-Triassic    Cardona_2010c_______ 70.8  .19
 16.4  1.9  .09   .3  2.5  4.9  2.8  .06
  3  107 Santa Marta               Granodiorite              Quandt_2013_________ 69.9  .22
 17.0  2.0  .04   .6  3.6  4.6  1.9  .09
  4  113 dacite                    Saint-Bel-Sourcieux,Rhone Davoine,_P._(1968)__ 70.4  .25
 16.2  2.2  .08  1.3  4.0  3.2  2.2  .13
  5  124 Granodiorit               Sierra Nevada,USA         Wimmenauer_(1985)___ 70.3  .38
 15.5  2.1  .06   .7  2.7  4.3  3.7  .14
  6  124 Mylonites                 Santa Marta P-Triassic    Cardona_2010c_______ 71.2  .23
 15.7  3.1  .03   .4  2.9  5.4  1.0  .07
  7  134 Sara Sara                 rhyolite                  Mamani_et_al.,_2008_ 70.3  .37
 15.5  2.5  .05   .6  2.3  4.5  3.7  .15
  8  145 Pichu Pichu               rhyolite                  Mamani_et_al.,_2009_ 70.8  .30
 15.1  2.4  .05   .8  2.3  4.1  4.2  .10
  9  145 Huanynaputina             dacite                    Mamani_et_al.,_2008_ 69.1  .40
 15.7  3.0  .06  1.0  2.8  4.5  3.2  .14
 10  145 Santa Marta               Granodiorite              Quandt_2013_________ 69.2  .46
 15.6  3.1  .06  1.2  3.0  4.1  3.1  .15


Date: 5.11.2016. Analyses read from file EXAMPLE.DAT (recalculated to 100%). The database
holds 3591 analyses for comparison.
Abs. diff. of wt.% for most similiar: 11.01. Comparison using NORMAL wt.% oxides. No oxides
ommited from comparison.

 No. dif. name of rock             location                  source               SiO2 TiO2
 Al2O3 FeOt MnO MgO  CaO  Na2O  K2O P2O5
-------------------------------------------------------------------------------------------
-------------------------------------
            CJJ-91                                                                  59.4
            .04 25.0   .9  .02   .2  7.8  6.3   .4  .01
-------------------------------------------------------------------------------------------
-------------------------------------
  1  100 Anorthosit                Adirondack,New York       Wimmenauer_(1985)___ 55.4  .87
 24.0  2.4  .01  1.4  9.1  5.8  1.0  .
  2  124 Anorthosit                Labrador                  Wimmenauer_(1985)___ 57.0  .79
 22.2  4.6  .06  1.4  7.1  5.4  1.4  .12
```

```
  3  152 Cancrinit-Syenit          Lueshe, Zaire            Wimmenauer_(1985)___ 57.9  .05
 20.9   .7  .06   .2  5.3  9.5  5.2  .31
  4  154 Tuti                      andesite                 Mamani_et_al.,_2008_ 60.0  .72
 18.1  4.8  .17  1.5  6.8  5.6  2.0  .23
  5  155 Phonolith                 Kaiserstuhl              Wimmenauer_(1985)___ 58.3  .51
 21.3  3.5  .10  1.3  4.8  5.6  4.7  .03
  6  162 Pyroxen-Andesit           Saar-Nahe                Wimmenauer_(1985)___ 54.6  .09
 22.1  5.1  .09  3.3  7.7  5.1  1.7  .14
  7  168 lava (variolite)          NE Bothnia, Finnland     Amstutz_(ed)_(1974)_ 64.0  .68
 18.5   .9  .10   .2  5.1  9.8   .7  .07
  8  170 dacite                    after Johannsen (1952)   Davoine,_P._(1968)__ 59.2  .
 18.6  6.1  .    3.1  7.7  4.0  1.4  .
  9  173 Precordillera             andesite                 Haschke_2002________ 59.1 1.06
 19.5  5.9  .11  2.0  6.7  3.8  1.7  .21
 10  175 Pampa Negra               gabbro                   Ruprecht__2007______ 59.5  .97
 19.4   .1  .17  5.9  9.9  3.0   .9  .10
```

Date: 5.11.2016. Analyses read from file EXAMPLE.DAT (recalculated to 100%). The database holds 3591 analyses for comparison.
Abs. diff. of wt.% for most similiar: 4.63. Comparison using NORMAL wt.% oxides. No oxides ommited from comparison.

```
 No. dif. name of rock             location                 source               SiO2 TiO2
 Al2O3 FeOt MnO MgO  CaO  Na2O  K2O P2O5
-------------------------------------------------------------------------------------------
-------------------------------------
         GC-061                                                                   67.0  .38
         16.1  4.1  .07  1.4  4.6  5.7   .6  .11
-------------------------------------------------------------------------------------------
-------------------------------------
  1  100 Ilo                       granodiorite             Mamani_et_al.,_2008_ 67.0  .45
 16.1  4.5  .07  2.0  4.4  3.6  1.7  .13
  2  110 dacite                    after Johannsen (1952)   Davoine,_P._(1968)__ 67.4  .
 17.0  4.3  .    1.5  4.5  3.7  1.6  .
  3  114 Ocoña                     granodiorite             Mamani_et_al.,_2009_ 66.7  .37
 16.7  4.0  .15  1.2  5.3  3.6  1.9  .15
  4  115 graywacke, Proterozoic    NW Barrandium, CSFR      Chab_and_Pelc_1973__ 67.5  .88
 16.1  4.6  .11  2.0  2.3  5.3  1.0  .15
  5  116 Punta de Bombon           granodiorite             Mamani_et_al.,_2008_ 67.2  .39
 15.9  4.0  .06  1.7  4.6  3.3  2.8  .12
  6  121 dacite                    Carpathian Mt., Romania  Davoine,_P._(1968)__ 66.7  .49
 16.7  4.2  .14  1.8  4.6  3.2  2.1  .11
  7  122 granodiorite              (average)                Best_82/LeMaitre_76_ 67.0  .55
 15.9  4.0  .08  1.8  3.9  3.8  2.8  .18
  8  124 dacite                    (average)                Best_82/LeMaitre_76_ 66.1  .59
 16.2  4.6  .09  1.8  4.4  3.9  2.2  .15
  9  125 LLullaillaco              dacite                   Mamani_et_al.,_2008_ 66.3  .72
 15.9  3.9  .06  1.6  3.8  4.6  2.8  .26
 10  127 LLullaillaco              dacite                   Mamani_et_al.,_2008_ 66.5  .70
 15.8  3.9  .06  1.6  3.8  4.5  2.9  .24
```

Date: 5.11.2016. Analyses read from file EXAMPLE.DAT (recalculated to 100%). The database holds 3591 analyses for comparison.
Abs. diff. of wt.% for most similiar: 2.63. Comparison using NORMAL wt.% oxides. No oxides ommited from comparison.

```
 No. dif. name of rock             location                  source               SiO2 TiO2
 Al2O3 FeOt MnO MgO  CaO  Na2O  K2O P2O5
-------------------------------------------------------------------------------------------
-------------------------------------
         EMP-001                                                                   70.5  .30
         14.7  3.3  .11  1.1  3.0  3.9  3.0  .11
-------------------------------------------------------------------------------------------
-------------------------------------
  1  100 graywacke                  Franciscan, California    Pettijohn,_F.J._1963 70.6  .26
  14.9  3.1  .    2.0  2.3  4.0  2.8  .15
  2  100 Holocene feldspar sand     Salton Basin, California  v.d.Kamp_et_al_1976_ 71.1  .42
  14.3  3.1  .06  1.4  2.9  3.3  3.4  .05
  3  117 arkose                     Santa Ynes Mt.,California v.d.Kamp_et_al_1976_ 70.5  .38
  14.5  3.7  .06  1.8  1.8  4.0  3.3  .08
  4  121 Santa Marta                Granodiorite              Quandt_2013_________ 69.2  .46
  15.6  3.1  .06  1.2  3.0  4.1  3.1  .15
  5  125 Holocene feldspar sand     Salton Basin, California  v.d.Kamp_et_al_1976_ 71.1  .37
  14.9  2.5  .05  1.2  3.1  3.1  3.6  .03
  6  129 Salar de la Isla           rhyolite                  Siebel_et_al.,_2001_ 70.5  .45
  14.6  2.7  .05   .7  2.9  3.4  4.5  .12
  7  129 Ibague                     Granite                   Cochrane_2014a______ 71.5  .35
  14.8  2.7  .05  1.1  2.4  3.5  3.5  .09
  8  132 Santa Marta                Dacite                    Quandt_2013_________ 70.6  .42
  15.3  2.9  .08   .8  2.1  3.7  3.9  .12
  9  133 Santa Marta                Granodiorite              Quandt_2013_________ 70.9  .37
  15.4  2.6  .06  1.3  2.3  4.3  2.7  .13
 10  133 Santa Marta                Granite                   Quandt_2013_________ 69.1  .47
 15.6  3.2  .06  1.2  3.4  4.0  2.8  .19
```

Date: 5.11.2016. Analyses read from file EXAMPLE.DAT (recalculated to 100%). The database holds 3591 analyses for comparison.
Abs. diff. of wt.% for most similiar: 1.88. Comparison using NORMAL wt.% oxides. No oxides ommited from comparison.

```
 No. dif. name of rock             location                  source               SiO2 TiO2
 Al2O3 FeOt MnO MgO  CaO  Na2O  K2O P2O5
-------------------------------------------------------------------------------------------
-------------------------------------
         EMP-270                                                                   74.2  .07
         14.8  1.4  .03   .1  1.2  4.5  3.8  .01
-------------------------------------------------------------------------------------------
-------------------------------------
  1  100 Arequipa                   rhyolite                  Paquereau_2008______ 74.1  .22
  14.0  1.5  .08   .3  1.2  4.5  4.0  .06
  2  106 Ignimbrite                 Ignimbrita de los Clavos  Colmenares_2009_____ 73.4  .29
  14.7  1.6  .04   .5  1.0  4.5  3.9  .08
  3  107 Aritinca Salar de Surire   dacite                    Mamani_et_al.,_2008_ 73.8  .24
  14.2  1.4  .07   .4  1.1  4.5  4.2  .04
  4  115 Chucal                     rhyolite                  Mamani_et_al.,_2009_ 74.7  .21
  14.0  1.2  .05   .3  1.0  4.7  3.8  .06
  5  119 Chucal                     rhyolite                  Mamani_et_al.,_2009_ 74.8  .22
  14.0  1.2  .05   .2  1.0  4.7  3.8  .06
  6  123 Santa Marta                Granite                   Quandt_2013_________ 74.3  .14
  14.7  1.4  .05   .3  1.9  4.3  2.9  .06
  7  130 Caraveli                   rhyolite                  Mamani_et_al.,_2009_ 74.0  .24
```

```
  13.8  1.7  .09   .3  1.2  4.4  4.2  .07
  8  139 Abitagua                Monzogranite            Cochrane_2014a_____ 74.8  .17
  14.3  1.5  .04   .2  1.5  3.7  3.8  .05
  9  143 Guallatiri               rhyolite                Worner_1992_________ 74.3  .19
  14.0  1.1  .06   .3  1.1  4.3  4.6  .02
 10  148 Oberer Oxaya             rhyolite                Mamani_et_al.,_2009_ 74.2  .18
 14.0  1.4  .07   .6  1.8  3.9  3.8  .04


Date: 5.11.2016. Analyses read from file EXAMPLE.DAT (recalculated to 100%). The database
holds 3591 analyses for comparison.
Abs. diff. of wt.% for most similiar: 4.58. Comparison using NORMAL wt.% oxides. No oxides
ommited from comparison.

 No. dif. name of rock            location                source              SiO2 TiO2
 Al2O3 FeOt MnO MgO  CaO  Na2O  K2O P2O5
-------------------------------------------------------------------------------------------
-------------------------------------
            16-JDMA-028-028                                                    50.9
            .86 17.7 11.5  .15  6.0  7.3  4.1  1.3  .25
-------------------------------------------------------------------------------------------
-------------------------------------
  1  100 spilite                  Rhein.Schiefergeb.Germany Schulz-Dobrick(1975) 51.2 1.49
  17.3 12.0  .14  4.3  8.2  4.0  1.2  .23
  2  116 La Chilca Unit mafic     Eclogite metabasalt      Bosch_2002_________ 51.5 2.50
  17.3  9.6  .18  6.1  7.2  4.2   .9  .52
  3  117 spilite, Jurassic-Cretac. Sakhalin, USSR          Amstutz_(ed)_(1974)_ 53.1  .78
  16.3 11.3  .18  6.1  6.3  4.2  1.6  .10
  4  120 Spilit                   Kellerwald               Wimmenauer_(1985)___ 49.3 1.82
  17.3 11.9  .17  6.9  7.4  4.4   .5  .28
  5  127 Punta de Bombon          andesite                 Mamani_et_al.,_2008_ 51.4  .81
  17.9 10.8  .09  5.9  8.4  2.2  2.3  .17
  6  128 Diabas                   Lahn-Dill, Germany       Hentschel_(1970)____ 50.4 1.56
  16.8 11.1  .16  7.0  7.7  5.0   .2  .21
  7  131 Spilite, Av.92                                    Amstutz_(ed)_(1974)_ 52.5 1.66
  16.9 10.1  .16  5.4  7.0  4.5  1.4  .28
  8  134 Spilite                  Nundle, New South Wales  Amstutz_(ed)_(1974)_ 51.5 2.04
  15.6 12.4  .19  5.9  7.5  3.9   .6  .37
  9  140 Basalt,High-K-calc-alk.  Sunda arc                Wilson,M._(1989)____ 50.3 1.13
  18.1  9.8  .18  5.6  9.7  3.7  1.2  .25
 10  142 spilite, Jurassic-Cretac. Sakhalin, USSR          Amstutz_(ed)_(1974)_ 52.8  .90
 16.5  9.8  .22  6.5  7.1  4.9  1.3  .10


 ----------------------------------------------------------LOG
 COMPARISON-----------------------------------------------------------------

 -------------------------------------------------------------------------------------------
 -------------------------------------

 Date: 5.11.2016. Analyses read from file EXAMPLE.DAT (recalculated to 100%). The database
 holds 3591 analyses for comparison.
Comparison using LOG wt.-% oxides. No oxides ommited from comparison.

 No. dif. name of rock            location                source              SiO2 TiO2
 Al2O3 FeOt MnO MgO  CaO  Na2O  K2O P2O5
-------------------------------------------------------------------------------------------
```

```
-------------------------------------
         AP-010                                                                  59.9 1.25
         15.4  9.3  .17  2.5  5.8  4.3  1.0  .46
-------------------------------------------------------------------------------------------------
-------------------------------------
  1  100 Andesit                  Thingmuli,Island          Wimmenauer_(1985)___ 61.9 1.28
  15.4  8.0  .19  1.8  5.1  4.4  1.6  .44
  2  123 Andesite, calc-alk.series South Sandwich arc        Wilson,M._(1989)____ 60.4 1.12
  14.2 10.6  .22  2.1  6.1  3.8  1.2  .26
  3  126 spilite                  Schirmeck, Vosges, France Amstutz_(ed)_(1974)_ 61.4 1.30
  14.4 10.2  .16  2.3  5.6  3.4  1.3  .
  4  143 Santa Marta              Granodiorite              Quandt_2013_________ 56.3 1.01
  17.7  8.8  .16  3.5  5.6  4.4  1.8  .65
  5  143 Santa Marta              Andesite                  Quandt_2013_________ 56.3 1.01
  17.7  8.8  .16  3.5  5.6  4.4  1.8  .65
  6  144 CdL                      andesite                  Bock_et_al.,_2000___ 56.6 1.20
  18.2  8.1  .12  3.9  6.3  4.4   .8  .33
  7  145 Leon Muerto              basalt                    Trumbull__1999______ 54.1 1.26
  17.2 10.0  .17  3.8  8.2  3.7  1.4  .32
  8  145 Quarz-Andesit, Mean      Chile                     Wimmenauer_(1985)___ 57.3  .94
  17.5  7.4  .16  4.6  6.8  3.9  1.1  .37
  9  147 Basaltic andesites       Andes,southern volc. zone Wilson,M._(1989)____ 55.5 1.35
  16.7 10.1  .19  3.3  7.3  4.5   .9  .21
 10  151 Andesit                  San Salvador              Wimmenauer_(1985)___ 58.7 1.19
 15.5  9.4  .20  2.5  6.2  4.0  2.1  .19


Date: 5.11.2016. Analyses read from file EXAMPLE.DAT (recalculated to 100%). The database
holds 3591 analyses for comparison.
Comparison using LOG wt.-% oxides. No oxides ommited from comparison.

 No. dif. name of rock             location                  source               SiO2 TiO2
 Al2O3 FeOt MnO MgO  CaO  Na2O  K2O P2O5
-------------------------------------------------------------------------------------------------
-------------------------------------
         CVI-1367                                                                59.3  .66
         16.2  6.0  .12  4.6  6.9  4.3  1.6  .23
-------------------------------------------------------------------------------------------------
-------------------------------------
  1  100 Lascar                   andesite                  Mamani_et_al.,_2009_ 58.7  .75
  16.4  7.1  .12  4.7  7.1  3.4  1.7  .19
  2  103 Andesite                 South-west Pacific        Wilson,M._(1989)____ 59.3  .73
  16.9  6.7  .13  3.8  7.1  3.4  1.7  .23
  3  104 Lascar                   andesite                  Mamani_et_al.,_2008_ 59.0  .76
  16.4  7.0  .12  4.4  6.9  3.5  1.8  .19
  4  104 Lascar                   andesite                  Mamani_et_al.,_2009_ 58.4  .76
  16.4  7.2  .12  4.8  7.2  3.4  1.6  .19
  5  107 Lascar                   andesite                  Mamani_et_al.,_2009_ 58.8  .75
  16.1  7.3  .12  4.7  7.0  3.3  1.7  .19
  6  108 Lascar                   andesite                  Mamani_et_al.,_2009_ 58.0  .86
  16.8  7.1  .11  4.8  7.0  3.7  1.5  .24
  7  111 Lascar                   andesite                  Mamani_et_al.,_2009_ 58.2  .76
  16.4  7.2  .12  4.9  7.3  3.4  1.6  .19
  8  118 Base Misti               andesite                  Mamani_et_al.,_2008_ 58.7  .84
  16.6  7.1  .11  4.3  6.5  3.6  1.9  .22
  9  126 Lascar                   andesite                  Mamani_et_al.,_2009_ 60.2  .73
  17.0  6.5  .11  3.6  6.1  3.6  1.9  .22
```

```
 10  130 Lascar                    andesite                  Mamani_et_al.,_2009_ 57.2  .95
 17.1  7.9  .12  4.3  6.9  3.6  1.5  .24


Date: 5.11.2016. Analyses read from file EXAMPLE.DAT (recalculated to 100%). The database
holds 3591 analyses for comparison.
Comparison using LOG wt.-% oxides. No oxides ommited from comparison.

 No. dif. name of rock             location                  source               SiO2 TiO2
 Al2O3 FeOt MnO MgO  CaO  Na2O  K2O P2O5
-------------------------------------------------------------------------------------------
-------------------------------------
         MPR-33                                                                   53.8  .89
         16.1  9.6  .20  4.5  9.0  4.1  1.3  .40
-------------------------------------------------------------------------------------------
-------------------------------------
  1  100 Basalt                    Andes                     Wilson,M._(1989)____ 51.2 1.14
  18.6  8.6  .16  5.6  8.9  4.0  1.4  .38
  2  108 Quarz-Andesit, Mean       Chile                     Wimmenauer_(1985)___ 57.3  .94
  17.5  7.4  .16  4.6  6.8  3.9  1.1  .37
  3  109 basic andesite,med-K, TH  Bagana volc.,Bougainville Gill,_J.B._(1981)___ 55.8  .81
  17.8  8.0  .18  3.4  8.0  4.0  1.6  .35
  4  112 Leon Muerto               basalt                    Trumbull__1999______ 54.1 1.26
  17.2 10.0  .17  3.8  8.2  3.7  1.4  .32
  5  118 Kalk-Alkali-Basalt        San Salvador              Wimmenauer_(1985)___ 53.0  .97
  17.1 10.1  .19  4.5  9.7  3.0  1.3  .20
  6  118 Kalk-Alkali-Basalt        San Salvador              Wimmenauer_(1985)___ 53.0  .97
  17.1 10.1  .19  4.5  9.7  3.0  1.3  .20
  7  121 Basaltic andesite         South-west Pacific        Wilson,M._(1989)____ 54.4  .83
  17.1  8.6  .16  5.3  9.1  2.9  1.3  .26
  8  129 Basalt,High-K-calc-alk.   Sunda arc                 Wilson,M._(1989)____ 50.3 1.13
  18.1  9.8  .18  5.6  9.7  3.7  1.2  .25
  9  130 Kalk-Alkali-Basalt        San Salvador              Wimmenauer_(1985)___ 53.3 1.23
  17.3  9.9  .20  4.0  9.1  3.3  1.4  .20
 10  136 basalt, Late Cretaceous   Kurile islands, USSR      Amstutz_(ed)_(1974)_ 53.7 1.10
 18.9  7.8  .19  3.8  8.6  4.6  1.1  .27


Date: 5.11.2016. Analyses read from file EXAMPLE.DAT (recalculated to 100%). The database
holds 3591 analyses for comparison.
Comparison using LOG wt.-% oxides. No oxides ommited from comparison.

 No. dif. name of rock             location                  source               SiO2 TiO2
 Al2O3 FeOt MnO MgO  CaO  Na2O  K2O P2O5
-------------------------------------------------------------------------------------------
-------------------------------------
         CVI-1388                                                                 39.7 1.69
         18.9 21.9  .48  3.1 11.3  1.4   .4 1.13
-------------------------------------------------------------------------------------------
-------------------------------------
  1  100 olivinegabbro             Harzburg massif, Germany  Vinx,_R._(1982)_____ 45.7 1.84
  16.8 21.9  .51  1.2  8.1  2.5   .6  .73
  2  121 olivinegabbronorite       Harzburg massif, Germany  Vinx,_R._(1982)_____ 42.9 3.70
  12.3 22.7  .41  5.1  8.4  1.8  1.0 1.71
  3  130 Glimmerdiabas             Lahn-Dill, Germany        Hentschel_(1970)____ 45.5 1.62
  21.5 12.1  .    4.6 12.1  1.5   .8  .36
  4  132 spilite, average                                    Amstutz_(ed)_(1974)_ 49.8 2.39
```

```
  16.5 10.7  .36  4.5  9.4  5.4   .4  .66
  5  135 Ferro-Diorit             Skaergard,Grönland       Wimmenauer_(1985)___ 49.3 2.86
  12.1 21.0  .34  1.5  8.3  3.2   .6  .82
  6  135 Glimmerdiabas            Lahn-Dill, Germany       Hentschel_(1970)____ 46.3 1.91
  16.0 12.5  .    8.8  9.6  1.9   .4 2.37
  7  140 Amphibolic Gneiss        SK-5026RA                Lopez_2012__________ 52.8 2.84
  17.2 10.9  .14  3.6 10.3  1.3   .5  .40
  8  141 Tholeiit-Basalt          Thingmuli,Island         Wimmenauer_(1985)___ 50.6 3.38
  12.6 15.1  .30  4.4  8.7  3.1   .8 1.00
  9  141 gabbronorite             Harzburg massif, Germany Vinx,_R._(1982)_____ 50.3 1.25
  16.3 11.7  .27  6.8 10.6  1.7   .6  .41
 10  148 Augusta Victoria Fm.     basalt                   Ruprecht__2007______ 51.8 1.44
 18.1  9.6  .25  5.8  9.6  2.6   .5  .39


Date: 5.11.2016. Analyses read from file EXAMPLE.DAT (recalculated to 100%). The database
holds 3591 analyses for comparison.
Comparison using LOG wt.-% oxides. No oxides ommited from comparison.

 No. dif. name of rock            location                 source               SiO2 TiO2
 Al2O3 FeOt MnO MgO  CaO  Na2O  K2O P2O5
-------------------------------------------------------------------------------------------
-------------------------------------
         CVI-13108                                                              55.8 1.44
         17.3  9.3  .13  5.5  5.8  1.0  3.2  .66
-------------------------------------------------------------------------------------------
-------------------------------------
  1  100 Oruro                    basalt                   Aitcheson__1995_____ 53.4 1.39
  15.4  9.4  .13  6.6  7.2  3.3  2.6  .59
  2  102 Oruro                    basalt                   Aitcheson__1995_____ 55.6 1.20
  15.7  8.3  .12  6.0  6.3  3.3  3.0  .50
  3  106 basalt. volcanicalstic   Lahn-Dill, Germany       Schmincke+Sunkel_87_ 50.7 1.89
  18.3 10.4  .11  6.8  5.8  2.1  3.4  .40
  4  109 Diabas                   Lahn-Dill, Germany       Hentschel_(1970)____ 48.0 2.01
  19.6 10.3  .17  6.0  7.9  2.4  2.9  .66
  5  109 Hornblende-Biotit-Diorit Grafenstein,Oberfranken  Wimmenauer_(1985)___ 55.4 1.19
  18.4  6.9  .13  5.4  6.5  3.0  2.6  .48
  6  113 APVC                     andesite                 Kay_et_al.,__1994___ 55.7 1.36
  16.0  7.4  .14  6.1  7.2  2.9  2.7  .42
  7  115 Quinzachatas             trachyandesite           Mamani_et_al.,_2008_ 57.5 1.29
  15.2  6.7  .09  5.6  5.7  2.9  4.5  .62
  8  117 co jajoloma              trachybasalt             Mamani_et_al.,_2004_ 50.1 1.12
  16.8  9.9  .15  6.2  9.3  2.8  2.9  .55
  9  118 C° auquiza               trachybasalt             Mamani_et_al.,_2009_ 53.4 1.38
  16.5  9.8  .13  5.4  7.9  3.0  2.0  .43
 10  118 Rhyolite                 Riolita de los Tábanos   Colmenares_2009_____ 58.6 1.31
 16.8  7.9  .13  3.4  4.4  3.0  3.9  .60


Date: 5.11.2016. Analyses read from file EXAMPLE.DAT (recalculated to 100%). The database
holds 3591 analyses for comparison.
Comparison using LOG wt.-% oxides. No oxides ommited from comparison.

 No. dif. name of rock            location                 source               SiO2 TiO2
 Al2O3 FeOt MnO MgO  CaO  Na2O  K2O P2O5
-------------------------------------------------------------------------------------------
-------------------------------------
```

```
          LRW-21                                                                    45.7 2.59
          19.2 16.2  .32  4.1  6.2  2.4  2.3  .90
-------------------------------------------------------------------------------------------------
-------------------------------------
  1  100 Basalt                    Columbia River Province   Wilson,M._(1989)____ 54.6 2.91
  13.6 12.9  .24  2.8  6.2  3.3  2.6  .88
  2  104 pillow lava               Lahn-Dill, Germany        Schmincke+Sunkel_87_ 46.7 3.72
  18.6 14.5  .15  4.6  4.9  3.4  2.6  .92
  3  114 Tholeiit-Basalt           Washington,USA            Wimmenauer_(1985)___ 54.0 3.03
  13.4 13.0  .18  3.0  6.5  3.4  2.6  .91
  4  124 High P2O5-TiO2 Volcanite  Parana                   Wilson,M._(1989)____ 54.0 2.93
  13.9 12.7  .19  3.0  7.6  3.0  2.0  .74
  5  128 Ignimbrite                Ignimbrita de los Clavos  Colmenares_2009_____ 54.4 1.60
  17.1  9.9  .17  4.0  5.7  3.7  2.5  .93
  6  130 Diabas                    Lahn-Dill, Germany        Hentschel_(1970)____ 48.0 2.01
  19.6 10.3  .17  6.0  7.9  2.4  2.9  .66
  7  130 Basalt                    Ascension Island Atlantic Wilson,M._(1989)____ 48.3 3.15
  16.3 11.7  .19  5.1  8.4  4.0  1.9 1.02
  8  130 Basalt                    Columbia River Province   Wilson,M._(1989)____ 51.2 3.21
  13.5 14.2  .22  4.5  8.4  2.9  1.3  .68
  9  133 Basalt                    Columbia River Province   Wilson,M._(1989)____ 51.0 3.56
  12.9 15.0  .22  4.4  8.5  2.5  1.4  .57
 10  134 spilite                   Rhein.Schiefergeb.Germany Schulz-Dobrick(1975) 45.2 3.46
 15.5 17.5  .24  5.7  7.1  3.2  1.6  .45


Date: 5.11.2016. Analyses read from file EXAMPLE.DAT (recalculated to 100%). The database
holds 3591 analyses for comparison.
Comparison using LOG wt.-% oxides. No oxides ommited from comparison.

 No. dif. name of rock             location                  source               SiO2 TiO2
 Al2O3 FeOt MnO MgO  CaO  Na2O  K2O P2O5
-------------------------------------------------------------------------------------------------
-------------------------------------
            AP-038                                                                  74.8
            .03 14.2  1.2  .10   .1  1.0  3.9  4.6  .02
-------------------------------------------------------------------------------------------------
-------------------------------------
  1  100 Azafran                   Granodiorite              Cochrane_2014a______ 76.0  .07
  13.6  1.0  .09   .0   .6  4.1  4.4  .02
  2  118 Azafran                   Monzogranite              Cochrane_2014a______ 76.7  .12
  13.2   .8  .06   .1   .8  3.6  4.7  .03
  3  118 Salar de la Isla          rhyolite                  Siebel_et_al.,_2001_ 76.1  .10
  13.6   .8  .07   .1  1.1  3.5  4.5  .04
  4  118 Yura                      rhyolite                  Mamani_et_al.,_2008_ 75.9  .15
  13.1  1.1  .07   .2  1.0  4.1  4.4  .03
  5  119 C° Villacollo             rhyolite                  Mamani_et_al.,_2009_ 75.1  .12
  13.8   .9  .07   .2  1.0  3.7  5.0  .02
  6  119 Yura                      rhyolite                  Paquereau_2008______ 75.9  .16
  13.3  1.1  .08   .2   .8  3.9  4.6  .03
  7  122 Salar de Antofalla        rhyolite                  Siebel_et_al.,_2001_ 75.7  .11
  13.0   .8  .08   .1  1.6  3.0  5.6  .03
  8  123 calcalkaline rhyolite     after Johannsen (1952)    Davoine,_P._(1968)__ 74.1  .18
  14.7  1.0  .     .1  1.0  3.0  5.9  .03
  9  124 Yura                      rhyolite                  Paquereau_2008______ 75.7  .16
  13.3  1.0  .07   .2  1.1  4.1  4.4  .03
 10  129 Lauca_Pérez               rhyolite                  Mamani_et_al.,_2008_ 76.4  .12
```

```
 12.8   .9  .09   .2   .6  3.5  5.4  .03


Date: 5.11.2016. Analyses read from file EXAMPLE.DAT (recalculated to 100%). The database
holds 3591 analyses for comparison.
Comparison using LOG wt.-% oxides. No oxides ommited from comparison.

 No. dif. name of rock             location                  source               SiO2 TiO2
 Al2O3 FeOt MnO MgO  CaO  Na2O  K2O P2O5
-------------------------------------------------------------------------------------------
-------------------------------------
           AP-010                                                                   59.9
           1.25 15.4  9.3  .17  2.5  5.8  4.3  1.0  .46
-------------------------------------------------------------------------------------------
-------------------------------------
  1  100 Andesit                    Thingmuli,Island          Wimmenauer_(1985)___ 61.9 1.28
  15.4  8.0  .19  1.8  5.1  4.4  1.6  .44
  2  123 Andesite, calc-alk.series South Sandwich arc        Wilson,M._(1989)____ 60.4 1.12
  14.2 10.6  .22  2.1  6.1  3.8  1.2  .26
  3  126 spilite                    Schirmeck, Vosges, France Amstutz_(ed)_(1974)_ 61.4 1.30
  14.4 10.2  .16  2.3  5.6  3.4  1.3  .
  4  143 Santa Marta                Granodiorite              Quandt_2013_________ 56.3 1.01
  17.7  8.8  .16  3.5  5.6  4.4  1.8  .65
  5  143 Santa Marta                Andesite                  Quandt_2013_________ 56.3 1.01
  17.7  8.8  .16  3.5  5.6  4.4  1.8  .65
  6  144 CdL                        andesite                  Bock_et_al.,_2000___ 56.6 1.20
  18.2  8.1  .12  3.9  6.3  4.4   .8  .33
  7  145 Leon Muerto                basalt                    Trumbull__1999______ 54.1 1.26
  17.2 10.0  .17  3.8  8.2  3.7  1.4  .32
  8  145 Quarz-Andesit, Mean        Chile                     Wimmenauer_(1985)___ 57.3  .94
  17.5  7.4  .16  4.6  6.8  3.9  1.1  .37
  9  147 Basaltic andesites         Andes,southern volc. zone Wilson,M._(1989)____ 55.5 1.35
  16.7 10.1  .19  3.3  7.3  4.5   .9  .21
 10  151 Andesit                    San Salvador              Wimmenauer_(1985)___ 58.7 1.19
 15.5  9.4  .20  2.5  6.2  4.0  2.1  .19


Date: 5.11.2016. Analyses read from file EXAMPLE.DAT (recalculated to 100%). The database
holds 3591 analyses for comparison.
Comparison using LOG wt.-% oxides. No oxides ommited from comparison.

 No. dif. name of rock             location                  source               SiO2 TiO2
 Al2O3 FeOt MnO MgO  CaO  Na2O  K2O P2O5
-------------------------------------------------------------------------------------------
-------------------------------------
           AP-009                                                                   70.8
           .23 16.2  2.6  .10   .7  3.0  4.2  2.1  .09
-------------------------------------------------------------------------------------------
-------------------------------------
  1  100 Ocoña                      granite                   Mamani_et_al.,_2008_ 72.5  .24
  14.2  2.9  .07   .8  3.0  3.6  2.7  .08
  2  127 Pausa                      rhyolite                  Mamani_et_al.,_2008_ 71.6  .35
  14.4  2.7  .08   .7  2.4  4.1  3.6  .10
  3  127 Santa Marta                Granodiorite              Quandt_2013_________ 69.9  .22
  17.0  2.0  .04   .6  3.6  4.6  1.9  .09
  4  155 Abitagua                   Granodiorite              Cochrane_2014a______ 63.8  .20
  19.8  3.2  .13   .5  2.8  5.5  3.9  .09
```

```
  5  156 dacite                    Saint-Bel-Sourcieux,Rhone Davoine,_P._(1968)__ 70.4  .25
 16.2  2.2  .08  1.3  4.0  3.2  2.2  .13
  6  168 Caraveli                  rhyolite                  Mamani_et_al.,_2009_ 73.4  .26
 12.4  2.3  .11   .4  2.3  4.3  4.4  .10
  7  172 Ubinas                    dacite                    Thouret_et_al.,_2005 69.6  .38
 15.9  2.6  .07   .7  2.4  4.0  4.2  .13
  8  174 Ubinas                    dacite                    Thouret_et_al.,_2005 69.7  .38
 15.7  2.6  .07   .7  2.4  4.0  4.3  .14
  9  176 Mylonites                 Santa Marta P-Triassic    Cardona_2010c_______ 70.8  .19
 16.4  1.9  .09   .3  2.5  4.9  2.8  .06
 10  177 Pichu Pichu               rhyolite                  Mamani_et_al.,_2009_ 70.8  .30
 15.1  2.4  .05   .8  2.3  4.1  4.2  .10


Date: 5.11.2016. Analyses read from file EXAMPLE.DAT (recalculated to 100%). The database
holds 3591 analyses for comparison.
Comparison using LOG wt.-% oxides. No oxides ommited from comparison.

 No. dif. name of rock             location                  source               SiO2 TiO2
 Al2O3 FeOt MnO MgO  CaO  Na2O  K2O P2O5
-------------------------------------------------------------------------------------------
-------------------------------------
            CJJ-91                                                                  59.4
            .04 25.0   .9  .02   .2  7.8  6.3   .4  .01
-------------------------------------------------------------------------------------------
-------------------------------------
  1  100 Ibague                    Leucogranite              Cochrane_2014a______ 69.5  .03
 18.7  1.4  .     .1  4.8  5.1   .4  .02
  2  112 Mylonites                 Santa Marta P-Triassic    Cardona_2010c_______ 73.3  .18
 15.8  1.5  .02   .3  2.7  5.4   .8  .03
  3  116 Quarzkeratophyr           Lahn-Dill, Germany        Hentschel_(1970)____ 67.9  .30
 14.6  1.5  .03   .   6.9  8.6   .1  .08
  4  119 Quartzfeldsphatic Gneiss  MM-5IID-34-17             Lopez_2012__________ 75.4  .04
 15.9   .7  .02   .2   .8  5.2  1.8  .02
  5  128 Quartzfeldsphatic Gneiss  MP-5IIIC-38               Lopez_2012__________ 78.2  .13
 12.2  2.2  .05   .4  2.0  4.5   .4  .02
  6  139 lava (variolite)          NE Bothnia, Finnland      Amstutz_(ed)_(1974)_ 64.0  .68
 18.5   .9  .10   .2  5.1  9.8   .7  .07
  7  144 Anorthosit                Südafrika                 Wimmenauer_(1985)___ 48.0  .17
 32.5   .8  .03   .6 15.2  2.0   .8  .12
  8  146 Caraveli                  andesite                  Mamani_et_al.,_2009_ 62.7  .11
 11.1   .8  .05   .8  8.4 12.0  4.1  .03
  9  148 Cancrinit-Syenit          Lueshe, Zaire             Wimmenauer_(1985)___ 57.9  .05
 20.9   .7  .06   .2  5.3  9.5  5.2  .31
 10  150 Mylonites                 Santa Marta P-Triassic    Cardona_2010c_______ 71.2  .23
 15.7  3.1  .03   .4  2.9  5.4  1.0  .07


Date: 5.11.2016. Analyses read from file EXAMPLE.DAT (recalculated to 100%). The database
holds 3591 analyses for comparison.
Comparison using LOG wt.-% oxides. No oxides ommited from comparison.

 No. dif. name of rock             location                  source               SiO2 TiO2
 Al2O3 FeOt MnO MgO  CaO  Na2O  K2O P2O5
-------------------------------------------------------------------------------------------
-------------------------------------
         GC-061                                                                 67.0  .38
```

```
         16.1  4.1  .07  1.4  4.6  5.7   .6  .11
-------------------------------------------------------------------------------------------------
-------------------------------------
  1  100 Amphibolic Gneiss          SK-5003-RA               Lopez_2012__________ 70.2  .38
  13.5  4.9  .08  2.0  4.8  3.4   .6  .09
  2  144 Ilo                       granodiorite             Mamani_et_al.,_2008_ 67.0  .45
  16.1  4.5  .07  2.0  4.4  3.6  1.7  .13
  3  154 Punta de Bombon           granodiorite             Mamani_et_al.,_2008_ 67.2  .39
  15.9  4.0  .06  1.7  4.6  3.3  2.8  .12
  4  157 dacite                    after Johannsen (1952)   Davoine,_P._(1968)__ 64.6  .38
  17.3  4.1  .09  2.3  5.0  4.1  2.0  .10
  5  159 Granodiorite              Cordoba Pluton           Villagomez_2011_____ 62.3  .67
  17.5  5.7  .09  1.7  5.8  5.2   .7  .20
  6  165 Zamora                    Granodiorite             Cochrane_2014a______ 66.1  .35
  17.5  4.1  .10  1.4  4.4  3.5  2.5  .09
  7  172 Ocoña dike                amphibolite              Mamani_et_al.,_2009_ 65.3  .41
  17.9  3.8  .12  1.9  4.9  3.8  1.7  .14
  8  174 Amphibolic Gneiss         DRR-6-052A               Lopez_2012__________ 69.0  .27
  14.1  5.5  .07  1.5  4.9  4.3   .3  .04
  9  174 El Abra                   monzonite                Ruprecht__2007______ 65.5  .49
  17.1  3.7  .06  1.3  4.2  4.9  2.5  .19
 10  176 Anorthosit                Labrador                 Wimmenauer_(1985)___ 57.0  .79
 22.2  4.6  .06  1.4  7.1  5.4  1.4  .12


Date: 5.11.2016. Analyses read from file EXAMPLE.DAT (recalculated to 100%). The database
holds 3591 analyses for comparison.
Comparison using LOG wt.-% oxides. No oxides ommited from comparison.

 No. dif. name of rock             location                 source               SiO2 TiO2
 Al2O3 FeOt MnO MgO  CaO  Na2O  K2O P2O5
-------------------------------------------------------------------------------------------------
-------------------------------------
         EMP-001                                                                  70.5  .30
         14.7  3.3  .11  1.1  3.0  3.9  3.0  .11
-------------------------------------------------------------------------------------------------
-------------------------------------
  1  100 Salar de la Isla          dacite                   Siebel_et_al.,_2001_ 69.1  .46
  15.7  3.2  .11  1.3  3.0  3.1  3.8  .14
  2  102 Segovia                   Monzogranite             Cochrane_2014a______ 69.1  .51
  15.2  3.9  .13  1.2  3.4  3.7  2.7  .13
  3  114 Granodiorite              Coastal Batholith of Peru Wilson,M._(1989)____ 69.5  .42
  15.1  3.0  .07  1.2  2.9  3.5  4.1  .10
  4  117 Huanynaputina             dacite                   Mamani_et_al.,_2008_ 69.1  .40
  15.7  3.0  .06  1.0  2.8  4.5  3.2  .14
  5  118 Rhyolite                  Saldaña Fm.              Villagomez_2011_____ 66.1  .47
  16.6  3.8  .09  1.3  3.0  4.4  4.1  .12
  6  120 Pausa                     rhyolite                 Mamani_et_al.,_2008_ 71.6  .35
  14.4  2.7  .08   .7  2.4  4.1  3.6  .10
  7  120 Misti                     dacite                   Mamani_et_al.,_2009_ 68.1  .43
  15.9  3.5  .07  1.3  3.4  3.9  3.4  .15
  8  121 Santa Marta               Granodiorite             Quandt_2013_________ 69.2  .46
  15.6  3.1  .06  1.2  3.0  4.1  3.1  .15
  9  123 Ocoña                     granite                  Mamani_et_al.,_2008_ 72.5  .24
  14.2  2.9  .07   .8  3.0  3.6  2.7  .08
 10  126 Zamora                    Granodiorite             Cochrane_2014a______ 66.1  .35
 17.5  4.1  .10  1.4  4.4  3.5  2.5  .09
```

Date: 5.11.2016. Analyses read from file EXAMPLE.DAT (recalculated to 100%). The database holds 3591 analyses for comparison.
Comparison using LOG wt.-% oxides. No oxides ommited from comparison.

No.	dif.	name of rock	location	source	SiO2	TiO2	Al2O3	FeOt	MnO	MgO	CaO	Na2O	K2O	P2O5
		EMP-270			74.2	.07	14.8	1.4	.03	.1	1.2	4.5	3.8	.01
1	100	Saldana fm.	Qtz porphyry	Cochrane_2014a_____	76.6	.19	13.2	1.5	.03	.2	1.0	4.0	3.3	.04
2	108	Lauca/Pérez-Ignimbrit	rhyolite	Mamani_et_al.,_2009_	76.2	.13	12.4	.8	.03	.1	.8	4.5	4.9	.02
3	111	Abitagua	Monzogranite	Cochrane_2014a_____	74.8	.17	14.3	1.5	.04	.2	1.5	3.7	3.8	.05
4	116	Salar de la Isla	rhyolite	Siebel_et_al.,_2001_	76.1	.10	13.6	.8	.07	.1	1.1	3.5	4.5	.04
5	119	Azafran	Monzogranite	Cochrane_2014a_____	76.7	.12	13.2	.8	.06	.1	.8	3.6	4.7	.03
6	123	Yura	rhyolite	Mamani_et_al.,_2008_	75.9	.15	13.1	1.1	.07	.2	1.0	4.1	4.4	.03
7	124	Arequipa	rhyolite	Paquereau_2008_____	75.7	.16	12.9	1.0	.05	.1	.8	4.3	4.8	.02
8	124	Salar de Antofalla	rhyolite	Siebel_et_al.,_2001_	76.5	.15	12.7	.9	.06	.2	.8	4.0	4.6	.03
9	125	Salar de Antofalla	rhyolite	Siebel_et_al.,_2001_	76.0	.10	13.2	.7	.05	.1	1.4	3.5	5.0	.02
10	126	Yura	rhyolite	Paquereau_2008_____	75.7	.16	13.3	1.0	.07	.2	1.1	4.1	4.4	.03

Date: 5.11.2016. Analyses read from file EXAMPLE.DAT (recalculated to 100%). The database holds 3591 analyses for comparison.
Comparison using LOG wt.-% oxides. No oxides ommited from comparison.

No.	dif.	name of rock	location	source	SiO2	TiO2	Al2O3	FeOt	MnO	MgO	CaO	Na2O	K2O	P2O5
		16-JDMA-028-028			50.9		.86	17.7	11.5	.15	6.0	7.3	4.1	1.3	.25
1	100	Basalt,High-K-calc-alk.	Sunda arc	Wilson,M._(1989)____	50.3	1.13	18.1	9.8	.18	5.6	9.7	3.7	1.2	.25
2	101	Lascar	andesite	Mamani_et_al.,_2009_	56.0	.84	16.9	8.1	.13	5.4	7.9	3.5	1.2	.23
3	101	Lascar	andesite	Mamani_et_al.,_2009_	56.2	.85	17.2	7.8	.13	4.9	7.8	3.6	1.3	.24
4	109	Basaltic andesite	South-west Pacific	Wilson,M._(1989)____	54.4	.83	17.1	8.6	.16	5.3	9.1	2.9	1.3	.26
5	118	Spilite, Av.92		Amstutz_(ed)_(1974)_	52.5	1.66								

```
 16.9 10.1  .16  5.4  7.0  4.5  1.4  .28
 6  119 spilite                  Rhein.Schiefergeb.Germany Schulz-Dobrick(1975) 51.2 1.49
 17.3 12.0  .14  4.3  8.2  4.0  1.2  .23
 7  123 Linga Yarabamba          gabbro                    Mamani_et_al.,_2009_ 56.3  .86
 17.1  8.2  .14  4.4  7.1  4.1  1.6  .19
 8  124 Basaltic andesites       Andes NVZ                 Wilson,M._(1989)____ 56.1  .90
 17.0  7.9  .10  5.2  7.6  3.9  1.1  .23
 9  127 Andesit, Mean            Chile                     Wimmenauer_(1985)___ 53.2 1.07
 18.4  8.6  .14  5.3  8.2  4.1   .8  .26
10  128 amygdaloidal spilite     Schirmeck, Vosges, France Amstutz_(ed)_(1974)_ 52.1 1.05
16.7 10.3  .22  7.7  6.2  4.5  1.3  .
```

TABLE 6. LOCATION, DESCRIPTION, OF SAMPLES ANALYZED BY U-Pb LA-ICP-MS

Sample Code	Coordinates		Elevation (m)	Lithology	Stratigraphic division	Unit
	Lat (ºN)	Long (ºW)				
CVI13-108	10.93455475	-74.1374652	545	Grt-Bt Mylonite	Triassic	La Secreta Mylonites
MPR-33A	11.07315844	-74.0739827	1000	Hbl+Plg+Qtz, Orthogneiss	Permian	El Encanto Orthogneiss
GLV-11	11.02193134	-74.1710838	112	Ms+Bt+Grt schist	Permian	Gaira Schists
MG-063	11.24749859	-73.7426375	25	Bt+Qtz schist	Permian	Gaira Schists
LRW-21	10.91291052	-74.1444955	141	Plg+Grt+Qtz gneiss	Triassic	La Secreta Mylonites
CP-055	11.31664991	-74.0792714	6	Psephite	Upper Cretaceous	Cinto Formation
ABH-27	11.16934363	-74.031142	1320	Bt+Ms schist	Jurassic	Lower San Lorenzo Schists

AP-009	10.80251034	-74.0296855	779	Granodiorite	Eocene	Sevilla Stock
CVI1367	11.30005034	-74.1891957	69	Meta-andesite	Paleogene	Concha Formation
CVI1344	11.31848483	-74.0688197	160	Dioritic dike	Paleogene	Concha Formation
AK-01	10.88033347	-74.1140673	487	Metapelite	Jurassic	Lower San Lorenzo Schists
AP-038	11.19673862	-73.8712134	110	Leucosome	Eocene	Guachaca Migmatites
AP-011	10.87057863	-74.0463749	663	Gneiss	Neoproterozoic	Lower San Lorenzo Schists
DAA-039	11.16191682	-73.7866815	168	Gneiss	Neoproterozoic	Lower San Lorenzo Schists
AP-010	10.81871073	-74.0283751	923	Migmatite	Neoproterozoic	Lower San Lorenzo Schists
AP-048	11.26295572	-73.5921871	9	Gneiss	Neoproterozoic	Lower San Lorenzo Schists

APPENDIX CHAPTER 2

TABLE A1. ZFT Analytical data from the Sierra Nevada de Santa Marta

Sample	Lithology	ratigraphic Ag	Elevation(m)	Lat	Long	Grains	RhoS Track/cm2	RhoI Track/cm2	RhoD Track/cm2	U(ppm)	P(x2) Binomfit	Pooled fission Track Age (Ma)	± 2σ	Central fission Track Age (Ma)	± 2σ
CVI13-108	Gr-Bio Filonite	Triassic	545	-74.1375	10.9346	20	4.28E+06	2.67E+06	3.094E+05	431	0	34.9	2.1	34.7	1.9
AP-009	Tonalite	Eocene	779	-74.0297	10.8025	20	3.07E+06	1.84E+06	3.097E+05	297	1.2	36.3	2.2	36.1	1.3
MPR-33A	Ortogneiss	Permian	1000	-74.0740	11.0732	22	3.61E+06	2.16E+06	3.094E+05	349	61.8	36.3	2.9	36.3	1
MPR-34A	Schist	Permian	1054	-74.0777	11.0699	21	3.65E+06	2.17E+06	3.094E+05	351	5.7	36.6	3.7	36.6	1.8
CP-055	Psephite	per Cretaceo	6	-74.0793	11.3166	20	8.67E+05	7.41E+06	3.095E+05	85	63.7	42.3	3.4	42.4	1.3
AP-042	Tonalite	Eocene	89	-73.7238	11.2029	23	1.05E+06	5.07E+05	3.097E+05	82	58.3	44.9	4.5	45	2
AP-010	Migmatite	leoproterozoi	923	-74.0284	10.8187	25	1.02E+06	4.92E+05	3.097E+05	79	61.1	45.3	4.5	45.3	1.9
AP-048	Gneiss	leoproterozoi	9	-73.5922	11.2630	24	2.14E+06	1.01E+06	3.096E+05	163	0	46.1	3.7	45.8	3.8
CVI13-120	Mylonite	Jurassic	426	-74.1076	10.9860	24	1.36E+06	6.23E+05	3.095E+05	101	0	47.3	3.8	47.5	2.8
AP-011	Gneiss	Neoproterozo	663	-74.0464	10.8706	24	5.29E+05	2.34E+05	3.097E+05	38	78.9	49.1	5.9	49.1	2.9
DAA-039	Gneiss	leoproterozoi	168	-73.7867	11.1619	25	1.16E+06	4.99E+05	3.095E+05	81	0	50.6	5.1	49.3	3
MG-063	Schist	Permian	25	-73.7426	11.2475	20	2.12E+06	8.94E+05	3.094E+05	145	8	51.6	5.2	53.8	3.1

TABLE A2. AFT Analytical data from the Sierra Nevada de Santa Marta

Sample	Lithology	ratigraphic Ag	Elevation(m)	Lat	Long	Grains	RhoS Track/cm2	RhoI Track/cm2	RhoD Track/cm2	U(ppm)	P(x2) Binomfit	Pooled fission Track Age (Ma)	± 2σ	Central fission Track Age (Ma)	± 2σ
CVI13-108	Gr-Bio Filonite	Triassic	545	-74.1375	10.9346	20	2.32E+05	2.79E+06	1.335E+06	31	93.2	15	2	14.96	0.9
LRW-21	Gneiss Hbn-Gr	Triassic	141	-74.1445	10.9129	25	9.33E+04	1.22E+06	1.330E+06	14	100	13.69	2.45	13.7	1.2
MPR-33A	Ortogneiss	Permian	1000	-74.0740	11.0732	22	2.43E+05	2.53E+06	1.326E+06	29	97.3	17.17	2.33	17.2	1.1
GLV-11	Musc-Gr-Schis	Permian	112	-74.1711	11.0219	20	2.77E+05	3.50E+06	1.322E+06	40	99.8	14.11	2.1	14.11	0.97
CVI13-120	Mylonite	Jurassic	426	-74.1076	10.9860	21	1.32E+05	1.46E+06	1.318E+06	17	54	16.2	3.25	16.2	1.6
CVI13-67	Meta tuff	Paleogene	69	-74.1892	11.3001	22	1.31E+05	5.74E+05	1.313E+06	7	14.7	40.21	7.08	40.5	3.7
CVI13-44	Phillite	Paleogene	160	-74.0688	11.3185	19	2.30E+05	1.90E+06	1.309E+06	22	69.9	21.35	3.25	21.3	1.5
CP-055	Psephite	per Cretaceo	6	-74.0793	11.3166	20	8.67E+05	7.41E+06	1.301E+06	85	63.7	20.6	1.77	20.6	0.66
AP-048	Gneiss	leoproterozoi	9	-73.5922	11.2630	25	1.96E+05	9.19E+05	1.297E+06	11	75.7	37.25	5.15	37.2	2.3
AP-042	Tonalite	Eocene	89	-73.7238	11.2029	22	3.11E+05	1.31E+06	1.292E+06	15	80.3	41.3	5.12	41.3	2.3
AP-009	Tonalite	Eocene	779	-74.0297	10.8025	24	1.31E+05	6.10E+05	1.284E+06	7	48.8	37.17	6.15	37.4	3.1

TABLE A3. (U-Th-Sm)/He analytical data from the Sierra Nevada de Santa Marta

Sample	Coordinates Lat	Long	z	Grain ID	He fmol	238U fmol	U ppm	232Th fmol	Th ppm	147Sm fmol	Sm ppm	Mass microng	eU ppm	RAW AGE Ma	Ft EU	Ft EL	Ft CY	SHAPE	CORR.AGE Ma	age error Ma (1σ)	AVG Age Ma	error Ma (1σ)	replicate #	U blk %	Th blk %	Rs EU microNm	Rs EL microNm	Rs CY microNm
AP-010			923	ap010a1	0.17	8.18	1.46	6.37	1.10	156.09	113.71	1.35	1.72	12.57	0.86	0.87	0.92	CY	13.61	0.96	**13.61**	**0.96**	**1**	29.79	28.89	38.76	42.01	68.97
				ap010a2	0.16	12.28	0.43	1.54	0.05	472.73	67.12	6.90	0.44	8.36	0.93	0.93	0.96	CY	8.70	0.43				19.84	119.65	66.66	67.06	119.67
				ap010a3	0.03	61.17	9.04	6.29	0.90	118.15	71.38	1.62	9.25	0.38	0.81	0.82	0.89	CY	0.42	0.18				3.98	29.29	41.00	44.26	73.75
				ap010a4	0.01	0.93	0.19	24.62	4.99	60.20	51.51	1.15	1.37	1.62	0.78	0.80	0.88	EU	2.08	1.10				263.85	7.46	36.03	39.54	65.54
				ap010a5	0.07	5.78	0.65	0.24	0.03	199.20	91.89	2.12	0.66	7.50	0.89	0.90	0.94	EU	8.43	0.99				42.21	3090.88	42.44	48.58	78.96
AP-042			89	ap42a1	1.36	174.77	9.49	314.84	16.54	244.65	54.29	4.42	13.37	4.25	0.79	0.81	0.89	EU	5.35	0.11	**6.84**	**0.89**	**5**	1.40	1.95	57.09	61.78	102.94
				ap42a2	4.82	294.11	11.73	658.06	25.41	514.57	83.93	6.01	17.71	8.34	0.81	0.82	0.90	EU	10.28	0.07				0.83	0.93	61.84	64.78	113.79
				ap42a3	1.50	153.82	9.23	310.73	18.05	229.32	56.26	3.99	13.47	5.12	0.79	0.80	0.88	EU	6.52	0.12				1.60	1.98	55.18	60.04	99.36
				ap42a4	1.44	149.79	8.01	311.16	16.11	227.10	49.67	4.48	11.80	5.02	0.79	0.79	0.88	EU	6.39	0.03				1.03	1.73	56.01	58.36	103.18
				ap42a5	0.38	47.00	2.97	82.04	5.02	62.99	16.28	3.79	4.15	4.40	0.78	0.78	0.88	EU	5.67	0.07				3.29	6.58	53.25	54.34	97.81
AP-048			9	ap48a1	12.65	320.21	12.07	1111.04	40.55	4418.92	681.16	6.36	21.60	16.37	0.89	0.90	0.94	EL	18.22	0.07	**18.30**	**1.69**	**5**	0.77	0.55	63.08	72.33	114.85
				ap48a2	13.56	411.29	15.48	325.54	11.86	3463.27	532.83	6.37	18.27	20.81	0.90	0.91	0.95	CY	22.00	0.09				0.60	1.89	63.92	67.88	116.52
				ap48a3	6.29	296.35	16.14	198.54	10.46	2744.09	610.85	4.40	18.60	13.67	0.89	0.90	0.94	CY	14.52	0.10				0.83	3.10	56.77	60.93	102.61
				ap48a4	8.18	194.17	10.59	388.35	20.50	3736.36	833.14	4.40	15.41	20.91	0.89	0.90	0.94	CY	22.20	0.11				1.26	1.58	56.60	57.60	102.70
				ap48a5	4.53	200.27	10.73	181.98	9.44	2526.00	553.23	4.47	12.95	13.76	0.90	0.90	0.94	CY	14.58	0.14				1.23	3.38	58.23	61.03	103.55
CVI13-108			545	cvi13108a1	0.99	102.83	11.81	-1.15	-0.13	49.91	23.43	2.09	11.78	7.42	0.75	0.78	0.87	EL	9.56	0.37	**8.30**	**0.85**	**5**	2.39	-552.51	42.98	48.51	79.01
				cvi13108a2	1.39	147.70	15.28	-1.26	-0.13	92.68	39.18	2.32	15.25	7.27	0.78	0.79	0.88	CY	8.28	0.25				1.66	-490.75	45.79	49.18	82.73
				cvi13108a3	0.32	48.69	3.36	-3.73	-0.25	51.21	14.46	3.47	3.30	5.18	0.83	0.84	0.91	CY	5.71	0.50				5.04	-164.94	52.24	55.35	95.17
				cvi13108a4	0.30	40.48	6.55	0.00	0.00	36.23	23.98	1.48	6.55	5.67	0.76	0.77	0.87	EL	7.39	0.10				3.82	-195.33	39.20	40.73	71.56
				cvi13108a5	0.21	18.47	2.89	0.00	0.00	39.10	25.04	1.53	2.89	8.75	0.82	0.83	0.90	EL	10.57	0.37				8.37	-176.60	40.40	43.73	72.16
CVI13-120			426	cvi13120a1	12.29	480.31	8.81	951.71	16.89	352.28	26.40	13.08	12.77	13.57	0.83	0.84	0.91	EU	16.27	0.06	**11.73**	**3.08**	**3**	0.51	0.65	80.86	87.24	147.06
				cvi13120a2	7.39	438.07	11.53	886.58	22.58	772.50	83.10	9.11	16.83	8.85	0.84	0.84	0.91	CY	9.71	0.06				0.56	0.69	71.88	73.75	130.90
				cvi13120a3	1.78	150.44	2.00	37.96	0.49	134.07	7.30	17.99	2.12	8.64	0.89	0.89	0.94	CY	9.21	0.22				1.63	16.20	91.10	93.15	164.70
DAA-039			168	DAA03a1	0.16	24.42	1.19	2.30	0.11	115.06	22.87	4.93	1.21	4.84	0.89	0.90	0.94	EL	5.36	0.25				19.83	163.34	57.99	64.94	105.60
				DAA03a2	0.04	14.51	0.59	-0.09	0.00	134.80	22.24	5.94	0.58	1.88	0.92	0.92	0.95	EL	2.04	0.36				33.37	-5273.12	63.46	68.52	113.57
				DAA03a3	0.13	11.62	0.65	16.72	0.91	36.84	8.48	4.26	0.87	6.28	0.83	0.83	0.91	CY	6.90	0.48				41.66	22.36	54.39	56.02	101.34
				DAA03a4	0.17	45.98	3.72	54.65	4.27	51.09	16.88	2.97	4.72	2.24	0.77	0.77	0.87	CY	2.57	0.09				3.36	9.87	49.44	51.75	90.30
LRW-21			141	irw21a1	7.75	664.58	10.72	393.50	6.14	2160.00	142.42	14.86	12.16	7.83	0.91	0.91	0.95	CY	8.25	0.03	**8.27**	**0.40**	**5**	0.37	0.47	84.77	85.43	154.51
				irw21a2	1.74	194.47	10.17	31.14	1.58	476.27	101.82	4.58	10.54	6.59	0.87	0.87	0.93	EL	7.54	0.05				1.25	5.90	58.19	60.72	104.40
				irw21a3	3.45	301.23	4.79	63.03	0.97	571.20	37.16	15.07	5.02	8.38	0.90	0.91	0.95	EL	9.21	0.04				0.81	2.91	83.95	93.46	153.30
				lrw21a4	9.50	770.27	7.77	343.64	3.36	3280.71	135.32	23.76	8.56	8.49	0.93	0.93	0.96	EL	9.11	0.03				0.20	1.57	100.89	105.61	180.49
				lrw21a5	2.66	269.14	6.73	108.80	2.63	1113.72	113.79	9.59	7.35	6.87	0.90	0.91	0.95	CY	7.26	0.03				0.57	4.96	73.75	76.88	133.54
MPR-33A			1000	mpr33a1	0.84	65.28	4.83	69.72	4.99	48.02	14.51	3.24	6.00	7.99	0.76	0.78	0.87	EU	10.51	0.12	**10.51**	**0.25**	**5**	3.73	2.63	50.91	56.40	92.07
				mpr33a2	3.67	270.14	25.59	320.03	29.34	137.33	53.17	2.53	32.48	8.24	0.72	0.74	0.85	EU	11.40	0.04				0.90	0.57	47.07	52.31	85.16
				mpr33a3	2.75	233.72	28.24	260.60	30.48	112.59	55.61	1.98	35.40	7.24	0.69	0.70	0.83	EU	10.45	0.06				1.04	0.70	42.70	44.88	78.82
				mpr33a4	7.58	561.40	34.10	422.29	24.82	111.34	27.65	3.95	39.93	8.90	0.75	0.75	0.86	CY	10.34	0.04				0.43	0.43	55.57	57.08	99.21
				mpr33a5	5.19	435.19	20.69	383.08	17.63	174.28	33.87	5.04	24.83	7.67	0.78	0.78	0.88	EU	9.85	0.04				0.56	0.48	59.51	61.26	107.79

APPENDIX CHAPTER 3

TABLE A1. U, Pb AND Th ISOTOPIC DATA OBTAINED USING THE LA-ICP-MS METHOD

I.D.	Isotopic Ratios								Isotopic Ages								Parts per million (ppm)			Best Age		Best Age threshold (Spencer et al. 2015)
	$^{207}Pb/^{235}U$	±2σ	$^{206}Pb/^{238}U$	±2σ	Pb^{207}/Pb^{206}	±2σ	$^{208}Pb/^{232}U$	±2σ	$^{235}U/^{207}Pb$	±2σ	$^{238}U/^{206}Pb$	±2σ	$^{232}U/^{208}Pb$	±2σ	Pb^{207}/Pb^{206}	±2σ	^{238}U	^{232}Th	Th/U	(Ma)	±2σ	
AP-045																						
AP_45_1	1.68	0.17	0.1647	0.0061	0.0746	0.0077	0.032	0.032	980	65	982	34	530	610	930	210	5.25	0.176	0.0335	982	34	1500
AP_45_2	1.646	0.056	0.1686	0.0036	0.071	0.0027	0.051	0.0063	986	22	1004	20	1000	120	937	77	20.5	6.77	0.3302	1004	20	
AP_45_3	2.08	0.052	0.183	0.0034	0.0825	0.0019	0.058	0.0041	1082	17	1083	18	1140	78	1250	45	126	54	0.4286	1083	18	
AP_45_4	2.024	0.054	0.1912	0.0032	0.0767	0.0015	0.0582	0.0041	1122	18	1128	17	1143	78	1109	40	107.4	116.8	1.0875	1128	17	
AP_45_5	1.64	0.058	0.1697	0.0036	0.0702	0.0026	0.0543	0.0073	983	22	1010	20	1060	140	915	77	38.6	4.4	0.1140	1010	20	
AP_45_6	1.64	0.12	0.1656	0.0058	0.0743	0.0067	0.054	0.0069	996	54	987	32	1060	130	990	180	15.4	5.97	0.3877	987	32	
AP_45_7	1.645	0.047	0.1654	0.003	0.072	0.0017	0.0492	0.0037	989	18	986	17	970	72	980	48	112.9	69	0.6112	986	17	
AP_45_8	1.661	0.054	0.1668	0.0028	0.0722	0.0023	0.0516	0.004	992	21	994	16	1017	77	977	69	57.8	29	0.5017	994	16	
AP_45_9	1.67	0.13	0.1683	0.0052	0.0721	0.0054	0.0429	0.01	985	50	1002	28	840	190	920	160	10.7	1.16	0.1084	1002	28	
AP_45_10	1.72	0.15	0.161	0.0053	0.0777	0.0068	0.061	0.02	1004	56	962	29	1160	370	1060	180	7.57	0.932	0.1231	962	29	
AP_45_11	1.52	0.12	0.1615	0.0048	0.0685	0.0052	0.0515	0.0094	928	48	965	27	1010	180	800	160	9.02	1.596	0.1769	965	27	
AP_45_12	1.853	0.058	0.176	0.0028	0.0765	0.0025	0.0556	0.004	1062	21	1045	16	1094	77	1094	62	51.3	63.8	1.2437	1045	16	
AP_45_13	1.656	0.039	0.1636	0.003	0.0734	0.0015	0.0518	0.0041	991	15	976	17	1020	78	1030	38	117.7	34.2	0.2906	976	17	
AP_45_14	1.637	0.06	0.1654	0.003	0.0717	0.0024	0.0496	0.0041	982	23	987	17	977	79	964	66	44.7	31.9	0.7136	987	17	
AP_45_15	1.67	0.075	0.1653	0.0031	0.0734	0.0034	0.0541	0.0055	993	28	986	17	1064	100	996	92	30.1	15.46	0.5136	986	17	
AP_45_16	1.806	0.074	0.1784	0.0044	0.0736	0.0026	0.0534	0.0043	1044	26	1058	24	1051	83	1013	73	40	38.2	0.9550	1056	24	
AP_45_17	1.8	0.21	0.1706	0.0071	0.0766	0.0088	0.051	0.011	1023	79	1014	39	1010	210	1000	250	4.79	2.32	0.4843	1014	39	
AP_45_18	1.91	0.062	0.1812	0.0037	0.0765	0.0023	0.0546	0.0041	1082	22	1073	20	1075	79	1096	59	42.7	38.1	0.8923	1073	20	
AP_45_19	1.76	0.11	0.1718	0.0047	0.0745	0.0047	0.0558	0.0093	1021	40	1021	26	1090	180	1000	130	11.6	3.35	0.2888	1021	26	
AP_45_20	1.643	0.038	0.1661	0.0027	0.0717	0.0014	0.0493	0.0037	986	14	991	15	973	72	972	41	149.2	67.1	0.4497	991	15	
AP_45_21	2.029	0.035	0.1865	0.0028	0.07887	0.001	0.0569	0.004	1125	12	1102	15	1118	77	1167	26	297	121	0.4074	1102	15	
AP_45_22	2.063	0.043	0.1916	0.0029	0.0777	0.0011	0.0659	0.0053	1136	14	1130	17	1289	100	1137	28	1130	391	0.3461	1130	17	
AP_45_23	1.691	0.07	0.1673	0.0033	0.0734	0.003	0.0511	0.0057	1002	26	997	18	1004	120	1001	84	35.9	7.24	0.2017	997	18	
AP_45_24	0.264	0.032	0.0395	0.0021	0.0486	0.0067	0.013	0.016	236	30	250	13	130	140	130	270	30.5	5.77	0.1892	250	13	
AP_45_25	1.679	0.076	0.1707	0.0038	0.0716	0.0035	0.0542	0.0093	996	29	1015	21	1060	180	1040	100	25.2	1.891	0.0750	1015	21	
AP_45_26	1.681	0.06	0.1676	0.0027	0.0729	0.0029	0.0507	0.0049	999	23	999	15	998	94	989	80	58.3	11.7	0.2007	999	15	
AP_45_27	1.68	0.05	0.166	0.0028	0.0734	0.002	0.0523	0.0046	999	19	990	16	1030	89	1014	57	94.3	17.6	0.1866	990	16	
AP_45_28	1.51	0.1	0.1493	0.0036	0.0735	0.0046	0.0438	0.0066	929	40	897	20	860	130	900	130	28.97	4.7	0.1622	897	20	
AP_45_29	0.2282	0.004	0.03668	0.00074	0.0516	0.0042	0.013	0.002	251	19	232.8	4.6	261	40	240	160	61.8	12.07	0.1953	250.8	4.6	
AP_45_30	1.684	0.039	0.1695	0.0029	0.072	0.0013	0.0518	0.0037	1002	15	1009	16	1021	72	982	37	158.3	90.1	0.5765	1009	16	
AP_45_31	2.325	0.052	0.2124	0.0092	0.0792	0.0021	0.0628	0.0063	1217	25	1241	28	1229	120	1170	53	49.5	24	0.4848	1241	28	
AP_45_32	1.783	0.047	0.1724	0.0033	0.075	0.0017	0.0519	0.0042	1042	16	1025	18	1022	81	1062	46	61.2	29.9	0.4886	1025	18	
AP_45_33	1.689	0.069	0.1664	0.0031	0.0736	0.0032	0.0489	0.0041	1001	26	995	17	964	93	1004	87	34.6	16.51	0.4772	995	17	
AP_45_34	1.653	0.047	0.1661	0.0027	0.0721	0.0016	0.0518	0.0072	989	18	990	15	1020	140	982	45	114.4	5.19	0.0454	990	15	
AP_45_35	1.714	0.071	0.1731	0.0027	0.0723	0.0014	0.054	0.0057	1013	15	1018	15	1062	110	997	45	238	11.1	0.0466	1018	15	
AP_45_36	1.54	0.12	0.1655	0.0059	0.0682	0.0057	0.079	0.029	934	52	986	33	1480	580	780	190	5.81	0.325	0.0559	986	33	
AP_45_37	1.623	0.072	0.1693	0.0032	0.0695	0.003	0.0488	0.0048	976	17	964	92	890	87	26.8	10.6	0.3681	1008	17			
AP_45_38	1.626	0.083	0.1632	0.0036	0.0722	0.0035	0.0481	0.0055	975	32	974	20	947	110	961	98	23.57	8.98	0.3810	974	20	
AP_45_39	2.123	0.088	0.1897	0.0049	0.0809	0.0023	0.058	0.0053	1153	28	1119	23	1139	91	1213	58	126	41.8	0.3317	1119	23	
AP_45_40	1.619	0.045	0.1647	0.0024	0.0713	0.002	0.0493	0.0038	976	18	983	13	973	74	955	57	76.8	44.9	0.5846	983	13	
AP_45_41	1.607	0.066	0.1645	0.0035	0.071	0.0029	0.0528	0.0067	969	26	981	19	1040	130	932	67	28.7	3.47	0.1209	981	19	
AP_45_42	1.694	0.058	0.1694	0.0031	0.0774	0.0023	0.0518	0.0063	1008	21	1008	17	1020	160	1120	59	54.1	4.08	0.0754	1008	17	
AP_45_43	2.09	0.059	0.1884	0.0031	0.0805	0.0016	0.0572	0.0046	1144	19	1112	17	1124	87	1205	41	120.3	49.8	0.4140	1112	17	
AP_45_44	1.567	0.075	0.1619	0.0036	0.0731	0.0039	0.0419	0.0079	960	33	967	20	830	150	854	87	18.7	2.05	0.1096	967	20	
AP_45_45	1.702	0.089	0.1656	0.0034	0.0746	0.0037	0.054	0.012	1004	33	987	19	1060	220	1020	100	12.33	1.265	0.1042	987	19	
AP_45_46	1.629	0.063	0.1633	0.0031	0.0731	0.0026	0.0495	0.004	979	25	964	17	976	76	1004	76	80.3	42.7	0.5318	964	17	
AP_45_47	1.614	0.044	0.1623	0.0039	0.0725	0.0026	0.0467	0.0043	975	17	969	22	923	83	994	74	113	36.8	0.3257	969	22	
AP_45_48	1.586	0.051	0.1623	0.0031	0.0709	0.002	0.0474	0.0043	963	20	969	17	930	120	947	58	54.7	6.77	0.1238	969	17	
AP_45_49	2.091	0.048	0.1924	0.0032	0.0789	0.0018	0.0565	0.0043	1145	16	1134	18	1111	82	1162	46	115.1	48.5	0.4214	1134	18	
AP_45_50	2.076	0.04	0.193	0.0025	0.0779	0.0013	0.0561	0.004	1140	13	1137	13	1103	76	1142	33	317.6	248	0.7809	1137	13	
AP_45_51	2.109	0.054	0.1956	0.0033	0.0782	0.0018	0.057	0.0042	1150	18	1152	18	1120	81	1144	48	87.5	54.9	0.6274	1152	18	
AP_45_52	1.635	0.05	0.167	0.0028	0.0721	0.0021	0.0485	0.0032	982	19	996	16	953	72	945	61	67.5	31	0.4593	996	16	
AP_45_53	1.706	0.07	0.1693	0.0034	0.073	0.0026	0.0527	0.0056	1007	26	1008	19	1036	110	996	73	41.5	12.22	0.2945	1008	19	
AP_45_54	1.61	0.064	0.165	0.0034	0.0716	0.0029	0.0513	0.0071	971	27	984	23	1040	140	953	79	26	2.19	0.0842	984	23	
AP_45_55	0.275	0.027	0.03893	0.0009	0.0517	0.0053	0.0111	0.0013	244	21	246.1	5.6	222	26	200	190	33.9	25.7	0.7581	246.1	5.6	
AP_45_56	0.297	0.021	0.04	0.0011	0.0541	0.004	0.0123	0.0043	263	16	253.1	6.6	240	33	320	150	48.9	13.99	0.2861	253.1	6.6	
AP_45_57	1.65	0.11	0.1659	0.0047	0.0723	0.0043	0.057	0.016	982	40	989	26	1090	300	940	120	10.94	0.643	0.0588	989	26	
AP_45_58	0.282	0.014	0.03995	0.00098	0.0513	0.0027	0.0118	0.0015	251	11	252.5	6.1	237	29	240	110	75.6	22.1	0.2923	252.5	6.1	
AP_45_59	0.28	0.019	0.03943	0.00096	0.0517	0.0036	0.018	0.0012	250	15	249.3	6.5	241	24	340	140	38.7	32.8	0.8475	249.3	6	
AP_45_60	2.159	0.065	0.1957	0.0043	0.0798	0.0018	0.0589	0.0051	1167	21	1152	23	1156	98	1190	45	134.2	48.3	0.3599	1152	23	
AP_45_61	1.566	0.073	0.16	0.0046	0.0709	0.0027	0.0515	0.0053	952	29	956	26	1013	100	934	82	33.7	7.53	0.2234	956	26	
AP_45_62	1.608	0.073	0.1651	0.0038	0.0707	0.0027	0.054	0.011	972	28	985	21	1060	210	943	74	53	4.43	0.0836	985	21	
AP_45_63	1.656	0.069	0.1656	0.003	0.0725	0.0028	0.0519	0.0079	989	26	988	17	1030	200	984	79	44.2	2.57	0.0581	988	17	
AP_45_64	0.048	0.055	0.1939	0.0038	0.0766	0.0017	0.0558	0.0047	1131	18	1142	20	1097	90	1108	43	153	56.5	0.3693	1142	20	
AP_45_65	1.643	0.048	0.1657	0.0028	0.0717	0.0022	0.0505	0.0042	985	18	988	15	995	80	965	61	62.3	20.78	0.3335	988	15	
AP_45_66	1.659	0.056	0.1697	0.0035	0.0711	0.0027	0.0518	0.0055	991	22	1010	19	1020	100	940	78	37.26	8.87	0.2381	1010	19	
AP_45_67	1.647	0.059	0.1623	0.0031	0.0709	0.0025	0.0483	0.0058	986	22	972	14	952	110	1008	71	42.7	8.87	0.2030	972	14	
AP_45_68	1.604	0.08	0.1676	0.0034	0.0687	0.0031	0.0561	0.0056	967	31	999	19	1102	110	880	100	17.1	8.28	0.4842	999	19	
AP_45_69	1.613	0.041	0.1602	0.0029	0.0736	0.0021	0.0433	0.0054	974	16	958	16	855	110	1019	56	51.8	5.02	0.0969	958	16	
AP_45_70	1.66	0.16	0.1624	0.0065	0.0751	0.0079	0.0559	0.0065	973	63	969	36	1097	120	930	220	4.76	5.35	1.1239	969	36	
AP_45_71	1.568	0.041	0.162	0.003	0.0703	0.0021	0.0485	0.0044	956	17	968	17	956	85	926	61	52.1	16.05	0.3081	968	17	
AP_45_72	1.622	0.078	0.1672	0.0034	0.0703	0.0032	0.0498	0.0082	974	31	997	19	986	160	908	96	24.3	2.64	0.1086	997	19	
AP_45_73	1.904	0.059	0.1809	0.0031	0.0763	0.0018	0.0563	0.0049	1081	21	1072	17	1105	94	1095	47	157.4	13.09	0.0832	1072	17	
AP_45_74	1.699	0.065	0.1674	0.0039	0.0737	0.0029	0.0487	0.006	995	24	998	22	960	150	1015	77	24.42	2.56	0.1048	998	22	
AP_45_75	1.625	0.026	0.1643	0.002	0.07172	0.00099	0.0487	0.0036	979.7	10	980.3	11	961	69	976	29	510	74.3	0.1457	980.3	11	
AP_45_76	1.752	0.047	0.1747	0.0039	0.0713	0.0023	0.0494	0.0036	1026	17	1038	21	1049	69	1036	35	289	108	0.3737	1021	21	
AP_45_77	1.704	0.07	0.1691	0.0032	0.0731	0.0029	0.0518	0.0042	1007	26	1007	18	1020	80	996	80	29.85	44.3	1.4841	1007	18	
AP_45_78	1.649	0.041	0.1641	0.0028	0.0772	0.0013	0.0552	0.0041	1011	13	1089	15	1085	83	1131	31	220.7	54.1	0.2451	1089	15	
AP_45_79	1.769	0.06	0.1713	0.0045	0.0749	0.0017	0.0483	0.0044	1032	22	1019	25	952	76	1058	47	126	33.3	0.2643	1019	25	
AP_45_80	1.709	0.078	0.1685	0.0034	0.0734	0.0028	0.0527	0.0057	1007	30	1004	19	1039	120	1003	81	37.9	5.93	0.1565	1004	19	
AP_45_81	1.71	0.11	0.1626	0.0036	0.0755	0.0046	0.0542	0.0099	1002	42	971	20	1060	190	1030	130	10.68	2.31	0.2163	971	20	
AP_45_82	1.601	0.056	0.163	0.0028	0.0712	0.0023	0.0507	0.004	968	22	973	15	1000	77	950	65	57.8	41.5	0.7180	973	15	
AP_45_83	1.751	0.073	0.1696	0.0034	0.0752	0.0033	0.0495	0.0066	1031	29	1010	19	970	130	1049	90	28.4	3.53	0.1243	1010	19	
AP_45_84	1.824	0.062	0.174	0.0035	0.0757	0.0023	0.0538	0.0052	1034	22	1034	20	1058	92	1076	62	98	10.6	0.1082	1034	20	
AP_45_85	1.915	0.034	0.1832	0.0028	0.07577	0.00094	0.0499	0.0043	1086	12	1084	15	984	83	1088	25	1311	41.8	0.0319	1084	15	
AP_45_86	1.71	0.031	0.1683	0.002	0.0755	0.0017	0.0475	0.0036	805	14	709	12	937	69	1075	46	202	85.7	0.4243	709	12	
AP_45_87	1.966	0.049	0.1867	0.0042	0.0776	0.0015	0.0609	0.0056	1103	17	1103	23	1193	110	1140	34	192	50.4	0.2625	1103	23	
AP_45_88	1.921	0.084	0.1848	0.0047	0.0753	0.0023	0.0547	0.004	1085	30	1093	26	1076	76	1067	62	87.8	73.4	0.8360	1093	26	
AP_45_89	0.235	0.019	0.03007	0.00074	0.0565	0.0042	0.00879	0.00082	213	16	191	4.7	177	16	420	160	60.1	63.2	1.0516	191	4.7	
AP_45_90	0.2078	0.0049	0.0301	0.00051	0.0501	0.0011	0.0096	0.000669	191.6	4.1	191.2	3.2	193	14	197	51	1050	760	0.7238	191.2	3.2	
AP_45_91	0.271	0.031	0.0401	0.0013	0.0476	0.0053	0.0121	0.002	247	27	265.8	8	242	40	70	200	35.5	14.47	0.4076	265.8	8	
AP_45_92	2.138	0.072	0.2003	0.0052	0.0774	0.0021	0.0559	0.0041	1160	23	1177	28	1100	79	1127	52	126.9	101.2	0.7975	1177	28	
AP_45_93	1.664	0.036	0.1663	0.0028	0.0726	0.0013	0.0512	0.0037	994	14	992	16	1010	71	998	36	216.8	197.7	0.9119	992	16	
AP_45_94	1.662	0.082	0.1657	0.0041	0.0728	0.0034	0.0496	0.0058	1033	31	988	23	984	92	985	96	33.5	26.1	0.7791	988	23	
AP_45_95	1.66	0.042	0.1679	0.0027	0.0713	0.0013	0.0515	0.0038	992	16	1000	15	1015	74	971	42	144.3	65.8	0.4560	1000	15	
AP_45_96	1.669	0.044	0.1671	0.0035	0.0725	0.0021	0.0499	0.0039	995	17	996	19	984	76	991	57	78.7	36.1	0.4587	996	19	
AP_45_97	1.654	0.054	0.1661	0.0033	0.0722	0.0021	0.0499	0.0048	989	21	990	17	983	81	994	56	56.9	27.99	0.4919	990	17	
AP_45_98	1.676	0.035	0.1674	0.0026	0.0726	0.0012	0.0496	0.0044	999	13	998	14	975	85	999	35	248.6	32.27	0.1298	998	14	
AP_45_99	1.838	0.056	0.1805	0.004	0.0739	0.0019	0.0573	0.0057	1057	20	1069	22	1120	140	1030	52	102	9.3	0.0912	1069	22	
AP_45_100	1.635	0.037	0.1631	0.0031	0.0727	0.0013	0.0489	0.004	983	14	974	17	965	77	1001	38	310	44.1	0.1423	974	17	
AP_45_101	0.194	0.019	0.02978	0.00095	0.0463	0.0041	0.0081	0.0014	179	16	189.2	5.9	175	29	70	170	53.2	19.4	0.3647	189.2	5.9	
AP_45_102	0.273	0.012	0.03865	0.00077	0.0513	0.002	0.0117	0.0021	244.8	9.6	244.4	4.8	234	42	246	93	136.5	12.7	0.0930	244.4	4.8	
AP_45_103	0.306	0.027	0.04093	0.00092	0.0544	0.0046	0.0208	0.0047	269	21	258.6	5.7	410	93	330	180	53.8	4.91	0.0913	258.6	5.7	
AP_45_104	1.631	0.042	0.1626	0.0026	0.0724	0.0015	0.0486	0.0036	981	16	971	14	959	70	991	42	131.4	91.2	0.6941	971	14	
AP_45_105	1.679	0.032	0.1626	0.0026	0.0746	0.0013	0.0516	0.0038	1000	12	971	14	1017	73	1064	35	382	91.1	0.2385	971	14	
AP_45_106	1.568	0.046	0.1641	0.0069	0.0729	0.0029	0.0528	0.0056	955	26	984	23	1030	180	878	91	36.8	4.92	0.1337	984	23	
AP_45_107	0.266	0.029	0.0401	0.0011	0.0483	0.0053	0.01167	0.0013	237	23	253.3	6.6	234	25	90	200	41.5	32.4	0.7807	253.3	6.6	
AP_45_108	0.29	0.021	0.0401	0.001	0.0526	0.005	0.0112	0.0014	256	21	253.6	6.5	225	28	290	190	35.8	19	0.5307	253.6	6.5	
AP_45_109	1.771	0.052	0.1734	0.0039	0.0736	0.0016	0.0494	0.0046	1033	19	1031	21	975	88	1036	49	127	25	0.1969	1031	21	
AP_45_110	1.647	0.066	0.1633	0.0033	0.0732	0.0029	0.0496	0.0062	992	23	975	17	999	100	1019	75	50.7	8.18	0.1613	975	17	
AP_45_111	1.7	0.073	0.1647	0.0033	0.075	0.0037	0.049	0.012	1004	29	982	18	950	220	1036	95	21	1.6	0.0762	982	18	
AP_45_112	1.69	0.092	0.1649	0.0038	0.0744	0.0041	0.0505	0.0097	999	34	984	21	990	180	1010	110	17.23	3.46	0.2008	984	21	
AP_45_113	1.592	0.066	0.1612	0.0029	0.0709	0.0032	0.049	0.0035	984	26	963	16	966	67	925	98	36.2	181	5.0000	963	16	
AP_45_114	0.313	0.035	0.04083	0.00089	0.0556	0.0043	0.0119	0.0015	275	25	257.9	5.5	239	31	380	160	58.5	21.8	0.3726	257.9	5.5	
AP_45_115	1.749	0.046	0.1747	0.0035	0.0726	0.0015	0.0517	0.0041	1026	17	1038	19	1019	79	997	42	114	46	0.4035	1038	19	
AP_45_116	1.621	0.028	0.1609	0.0025	0.07334	0.00098	0.0505	0.0041	980	12	961	14	1003	79	1021	27	516	36.2	0.0702	961	14	
AP_45_117	1.666	0.057	0.1696	0.0034	0.0798	0.0017	0.059	0.0063	1169	18	1154	18	1157	120	1186	43	115.7	13.62	0.1177	1154	18	
AP_45_118	1.578	0.035	0.1618	0.0029	0.0712	0.0014	0.047	0.004	961	14	966	16	928	77	959	41	121.2	38.6	0.3185	966	16	
AP_45_119	1.872	0.045	0.18	0.003	0.0755	0.0015	0.0532	0.0049	1070	16	1067	16	1046	94	1075	38	162.8	17.02	0.1045	1067	16	
AP_45_120	1.6	0.17	0.1669	0.006	0.0706	0.0084	0.035	0.06	964	62	994	33	1000	860	220	6.54	0.181	0.0277	994	33		
AP_45_121	1.631	0.047	0.1631	0.0038	0.0718	0.0016	0.0509	0.0039	981	15	982	17	996	75	975	46	108.7	46.5	0.4278	982	17	
AP_45_122	1.66	0.05	0.1662	0.0033	0.0724	0.0019	0.0481	0.0043	992	19	991	18	949	92	989	55	84.7	25.84	0.3051	991	18	
AP_45_123	1.97	0.15	0.1857	0.0091	0.0764	0.0036	0.0625	0.0092	1098	49	1096	49	1220	170	1078	90	38	8.6	0.2263	1096	49	
AP_45_124	1.69	0.057	0.17	0.0031	0.0721	0.0021	0.0497	0.0037	1003	22	1012	17	980

EMP_16_70	2.809	0.082	0.2316	0.0052	0.088	0.0019	0.0715	0.0056	1356	22	1342	27	1395	110	1377	41	415	116.7	0.2812	1342	27
EMP_16_71	2.518	0.045	0.2076	0.003	0.088	0.0015	0.0669	0.0049	1276	13	1216	16	1309	100	1379	32	1034	329	0.3182	1216	16
EMP_16_72	3.158	0.096	0.247	0.0071	0.0927	0.0019	0.07	0.005	1446	23	1423	36	1368	94	1480	40	856	520	0.6075	1423	36
EMP_16_73	1.736	0.05	0.1752	0.0031	0.0719	0.002	0.052	0.0045	1020	19	1040	17	1023	86	974	56	206	83	0.4029	1040	17
EMP_16_74	1.807	0.066	0.1749	0.0034	0.0748	0.0023	0.0528	0.0047	1046	24	1039	19	1041	91	1053	63	331	114	0.3444	1039	19
EMP_16_75	1.65	0.061	0.1617	0.0034	0.0741	0.0025	0.0478	0.0036	987	23	966	19	943	70	1030	65	162.5	110.9	0.6825	966	19
EMP_16_76	1.719	0.057	0.1715	0.0032	0.0727	0.0024	0.0513	0.0041	1013	21	1020	18	1010	79	993	65	193	76.7	0.3974	1020	18
EMP_16_77	1.701	0.064	0.1703	0.0035	0.0725	0.0026	0.0522	0.0046	1006	24	1014	20	1027	89	981	75	142.4	43.6	0.3062	1014	20
EMP_16_78	1.68	0.065	0.1635	0.0039	0.0739	0.0026	0.0537	0.0046	998	24	984	22	1056	88	1023	72	134.8	67.9	0.5037	984	22
EMP_16_79	2.427	0.078	0.2126	0.005	0.0826	0.0018	0.0655	0.0057	1249	24	1242	27	1283	110	1256	43	770	218	0.2831	1242	27
EMP_16_80	2.69	0.18	0.225	0.013	0.0867	0.0026	0.0687	0.0063	1321	49	1305	69	1340	120	1350	58	340	120	0.3529	1305	69
EMP_16_81	1.689	0.052	0.1658	0.0032	0.074	0.0024	0.0485	0.0043	1003	19	989	18	957	83	1031	65	209.7	67.6	0.3224	989	18
EMP_16_82	1.83	0.14	0.1667	0.0068	0.0793	0.0033	0.0553	0.0052	1052	51	993	53	1096	99	1172	65	324	124.2	0.3833	993	53
EMP_16_83	1.694	0.034	0.166	0.0033	0.0737	0.0014	0.0489	0.0039	1015	13	990	18	965	75	1029	39	425	120.4	0.2833	990	18
EMP_16_84	1.674	0.035	0.1664	0.0032	0.0731	0.0013	0.0495	0.0037	998	13	992	18	976	72	1015	36	1219	337	0.2765	992	18
EMP_16_85	1.695	0.037	0.168	0.0031	0.0731	0.0014	0.0517	0.0038	1006	14	1001	14	1018	74	1013	40	308	124.8	0.4052	1001	14
EMP_16_86	1.917	0.065	0.1694	0.0049	0.082	0.0013	0.0588	0.0045	1084	22	1008	27	1154	86	1243	30	1328	170.7	0.1285	1008	27
EMP_16_87	2.505	0.078	0.2193	0.0049	0.0834	0.0024	0.0647	0.0051	1271	23	1281	26	1265	110	1267	57	147	56	0.3810	1281	26
EMP_16_88	1.651	0.057	0.1631	0.0044	0.0733	0.0023	0.0526	0.0044	989	22	974	24	1036	85	1019	63	987	339	0.3435	974	24
EMP_16_89	1.689	0.039	0.1666	0.0025	0.0735	0.0015	0.0514	0.0038	1003	15	993	14	1014	72	1023	40	238	125.9	0.5290	993	14
EMP_16_90	1.454	0.046	0.1193	0.0024	0.0885	0.0028	0.0724	0.0072	910	19	727	14	1410	140	1387	59	118.6	23.2	0.1956	727	14
EMP_16_91	2.562	0.074	0.2208	0.0038	0.0841	0.0021	0.0642	0.0054	1288	21	1286	24	1256	100	1288	49	121	44	0.3636	1286	24
EMP_16_92	2.12	0.13	0.1914	0.0064	0.08	0.0036	0.0629	0.0076	1152	40	1129	34	1220	140	1187	89	85.7	18.44	0.2152	1129	34
EMP_16_93	1.643	0.024	0.1637	0.0022	0.0705	0.0011	0.0517	0.0038	986.6	9	977	12	1019	72	1013	29	377	183.9	0.4878	977	12
EMP_16_94	1.952	0.038	0.1844	0.0029	0.0768	0.0012	0.0572	0.004	1098	13	1091	16	1124	77	1112	33	439	217.1	0.4945	1091	16
EMP_16_95	1.917	0.051	0.1811	0.0033	0.0767	0.0021	0.0543	0.0044	1087	18	1073	18	1068	84	1109	54	549	161.7	0.2945	1073	18
EMP_16_96	2.052	0.045	0.1904	0.0032	0.0787	0.0019	0.0577	0.0042	1132	15	1123	17	1133	81	1158	47	139.3	111.2	0.7983	1123	17
EMP_16_97	1.764	0.17	0.1612	0.0074	0.0744	0.0016	0.0516	0.0037	1031	21	1012	17	998	71	1058	50	120.8	74.6	0.6175	1012	17
EMP_16_98	1.698	0.042	0.1676	0.0024	0.0736	0.0021	0.0515	0.0043	1007	16	999	13	1014	83	1020	56	53.3	24.5	0.4597	999	13
EMP_16_99	1.606	0.033	0.1613	0.0025	0.0726	0.0013	0.0536	0.0037	975	14	964	14	998	72	999	35	424	50.4	0.1189	964	14
EMP_16_100	1.702	0.034	0.1691	0.0024	0.073	0.0014	0.0536	0.004	1009	14	1007	13	1055	76	1010	40	156.3	46.3	0.2962	1007	13
EMP_16_101	2.211	0.044	0.1996	0.0031	0.0803	0.0015	0.0572	0.0042	1184	14	1173	17	1124	79	1201	38	415.6	270	0.6497	1173	17
EMP_16_102	2.048	0.054	0.1927	0.0041	0.0771	0.0023	0.0548	0.0045	1130	18	1136	22	1149	85	1120	34	301	41.9	0.1392	1136	22
EMP_16_103	1.781	0.046	0.1769	0.0033	0.0729	0.0018	0.0521	0.004	1038	17	1050	18	1026	77	1020	44	107.6	72.1	0.6701	1050	18
EMP_16_104	1.711	0.032	0.1691	0.0024	0.0737	0.0011	0.0526	0.0038	1012	12	1007	13	996	72	1030	31	220	72.9	0.3314	1007	13
EMP_16_105	1.64	0.046	0.1616	0.0046	0.0738	0.0017	0.0522	0.0039	985	18	965	26	1028	76	1032	48	198.6	58.2	0.2830	965	26
EMP_16_106	1.713	0.049	0.1676	0.0028	0.0741	0.0019	0.0573	0.0042	1019	19	1026	18	1126	95	1036	52	61	17.94	0.2941	999	18
EMP_16_107	1.758	0.032	0.1709	0.0028	0.0746	0.0012	0.0544	0.0039	1030	12	1029	17	1070	75	1056	32	222	68.05	0.2960	1017	15
EMP_16_108	2.51	0.11	0.2182	0.009	0.0831	0.002	0.0648	0.0049	1269	36	1271	37	1269	110	1263	48	106.7	43.7	0.4096	1271	37
EMP_16_109	1.129	0.058	0.1042	0.0043	0.0783	0.0014	0.0404	0.0033	764	28	638	25	801	64	1151	36	471	110.7	0.2350	638	25
EMP_16_110	1.699	0.072	0.1684	0.0028	0.0729	0.0032	0.053	0.0055	1005	29	1003	19	1042	100	986	89	17.34	9.48	0.5467	1003	19
EMP_16_111	2.18	0.16	0.174	0.011	0.0904	0.0015	0.0529	0.0049	1162	48	1030	59	1041	94	1431	32	505	413	0.8178	1030	59
EMP_16_112	1.671	0.036	0.1662	0.003	0.0729	0.0012	0.05	0.0036	1000	14	991	17	986	69	1008	35	299	82.2	0.2764	991	17
EMP_16_113	1.737	0.072	0.1711	0.0034	0.073	0.0028	0.0492	0.0049	1019	27	1018	19	969	93	1010	89	25.5	8.2	0.3216	1018	19
EMP_16_114	1.748	0.069	0.1698	0.0034	0.0747	0.0026	0.0558	0.0055	1023	25	1031	19	1092	100	1061	66	22.6	15.42	0.6823	1031	19
EMP_16_115	1.58	0.055	0.16	0.0039	0.0716	0.002	0.05	0.0043	960	21	956	19	986	83	964	58	52.6	27.3	0.5190	956	19
EMP_16_116	1.67	0.03	0.1667	0.0024	0.0727	0.0012	0.0517	0.0038	997	11	994	13	1018	74	1002	34	246	62.5	0.2541	994	13
EMP_16_117	0.1325	0.0061	0.02659	0.0035	0.0489	0.0021	0.0892	0.00079	178.5	6.9	181.7	2.2	179	16	140	89	2006	83.9	0.4073	181.7	2.2
EMP_16_118	0.212	0.012	0.02899	0.0005	0.0528	0.0032	0.0101	195	10	184.2	3.2	211	22	300	130	204	77.8	0.3814	184.2	3.2
EMP_16_119	1.7	0.1	0.1617	0.0055	0.0764	0.0046	0.0479	0.0057	1003	38	968	30	944	110	1080	120	26.7	14.85	0.5562	968	30
EMP_16_120	1.652	0.051	0.1635	0.003	0.0734	0.0023	0.0512	0.004	988	19	976	17	1009	78	1012	64	59.8	23.72	0.3967	976	17
EMP_16_121	0.205	0.023	0.02902	0.00085	0.0514	0.0058	0.0099	0.0013	187	20	184.4	5.3	198	30	200	210	22.97	11.3	0.4919	184.4	5.3
EMP_16_122	0.216	0.03	0.02824	0.00098	0.0558	0.0076	0.0095	0.0015	196	25	179.5	6.1	191	30	350	260	26.11	19.93	0.7633	179.5	6.1
EMP_16_123	2.621	0.063	0.2249	0.0038	0.0845	0.0015	0.0673	0.0053	1305	18	1307	19	1316	91	1301	34	210	82.4	0.3924	1307	19
EMP_16_124	2.783	0.055	0.232	0.0037	0.087	0.0014	0.0704	0.0051	1350	15	1345	20	1375	96	1358	31	253	119.3	0.4715	1345	20
EMP_16_125	2.156	0.139	0.1884	0.0035	0.0788	0.0011	0.0612	0.0046	1166	13	1167	19	1166	81	1166	29	474	217	0.4578	1167	19
EMP_16_126	1.699	0.045	0.1682	0.0034	0.0732	0.0016	0.0525	0.004	1007	17	1002	19	1035	77	1014	46	172.5	65.5	0.3797	1002	19
EMP_16_127	1.739	0.04	0.1619	0.0042	0.0776	0.0011	0.0498	0.0036	1022	16	967	23	983	70	1133	29	107	248	0.2463	967	23
EMP_16_128	2.131	0.041	0.1953	0.0034	0.0791	0.0011	0.0614	0.0043	1158	13	1150	18	1204	82	1173	26	722	150.8	0.2089	1150	18
EMP_16_129	1.804	0.053	0.1692	0.0039	0.0777	0.0014	0.0594	0.0047	1046	19	1047	19	1147	130	1138	36	559	63.9	0.1143	1008	21
EMP_16_130	2.563	0.045	0.2187	0.0045	0.0852	0.0014	0.062	0.0043	1289	15	1275	24	1216	81	1317	32	444	288	0.6036	1275	24
EMP_16_131	1.728	0.039	0.1692	0.0024	0.0738	0.0015	0.0483	0.0034	1018	14	1008	13	953	66	1032	41	214	83.1	0.3883	1008	13
EMP_16_132	1.651	0.064	0.1624	0.005	0.0736	0.0021	0.0518	0.0053	989	31	970	28	1021	110	1028	56	298	77.6	0.2604	970	28
EMP_16_133	0.204	0.017	0.02855	0.00072	0.0524	0.0051	0.00974	0.00095	187	15	181.5	4.5	196	19	260	190	62.9	48.3	0.7679	181.5	4.5
EMP_16_134	0.185	0.012	0.02835	0.00063	0.0477	0.0032	0.00872	0.00077	172	10	180.2	3.9	176	15	120	140	137.2	147.4	1.0743	180.2	3.9
EMP_16_135	1.854	0.064	0.1719	0.0051	0.0781	0.0012	0.0607	0.0051	1062	23	1022	28	1191	98	1146	31	488	47.2	0.0967	1022	28
EMP_16_136	1.154	0.055	0.1073	0.004	0.0713	0.0018	0.0398	0.0033	776	17	657	21	731	63	1140	31	712	279	0.3919	657	25
EMP_16_137	1.687	0.033	0.1694	0.0024	0.0723	0.0014	0.0517	0.0038	1003	13	1019	13	993	90	1019	73	990	39	155.6	72.3	0.4647	1008	13
EMP_16_138	0.846	0.051	0.0827	0.0043	0.0739	0.0013	0.046	0.0044	618	28	512	25	908	80	1036	36	1580	94.5	0.0598	512	25
EMP_16_139	1.425	0.031	0.1379	0.0027	0.075	0.0013	0.0527	0.0038	898	13	833	15	1038	73	1064	35	402	130	0.3234	833	15
EMP_16_140	2.522	0.059	0.2169	0.0042	0.0832	0.0015	0.0656	0.0052	1277	17	1281	22	1282	110	1270	36	160	59.1	0.3694	1281	22
EMP_16_141	2.681	0.061	0.2267	0.0045	0.0858	0.0012	0.0687	0.0053	1322	17	1317	24	1343	100	1331	28	167	146.7	0.2233	1317	24
EMP_16_142	1.817	0.067	0.1687	0.004	0.0784	0.003	0.0548	0.0041	1048	21	1066	91	1152	74	1086	91	75.8	75.8	0.3690	1005	24
EMP_16_143	1.923	0.072	0.1873	0.0039	0.0744	0.0023	0.053	0.0046	1086	25	1106	21	1042	89	1039	63	65.7	29.3	0.4460	1106	21
EMP_16_144	1.927	0.051	0.1827	0.003	0.0766	0.0021	0.0573	0.0048	1089	18	1081	16	1126	92	1101	55	85.1	45.7	0.5370	1081	18
EMP_16_145	1.659	0.043	0.1674	0.0033	0.0719	0.0016	0.051	0.0041	992	16	1006	78	977	46	211	86	0.4076	997	16		
EMP_16_146	1.654	0.035	0.1643	0.0026	0.073	0.0011	0.0497	0.0037	990	13	980	14	980	72	1012	32	364	116.5	0.3201	980	14
EMP_16_147	2.574	0.083	0.2168	0.0047	0.0866	0.0025	0.0657	0.0064	1292	24	1265	25	1249	84	1347	57	265	455	1.7170	1265	25
EMP_16_148	1.708	0.04	0.1704	0.0028	0.0727	0.0017	0.0526	0.0039	1010	15	1014	16	1036	75	1000	47	153.4	69.3	0.4518	1014	16
EMP_16_149	2.83	0.062	0.2358	0.0041	0.087	0.0015	0.0706	0.0062	1362	16	1365	22	1378	99	1358	35	239	68.7	0.2791	1365	22
EMP_16_150	2.432	0.057	0.2114	0.0033	0.0835	0.0017	0.0635	0.0046	1251	17	1236	17	1244	87	1277	38	409	124	0.3032	1236	17
EMP_16_151	2.365	0.058	0.2072	0.0052	0.0828	0.0022	0.0645	0.0057	1231	18	1213	28	1263	110	1259	53	250	58.8	0.2352	1213	28

EMP-49A

EMP_49A_1	1.733	0.044	0.1718	0.0031	0.0732	0.0015	0.0534	0.0041	1020	16	1022	17	1051	78	1013	41	317	177	0.5584	1022	17
EMP_49A_2	1.676	0.051	0.1671	0.0025	0.0728	0.0021	0.0515	0.0042	998	19	996	14	1014	81	996	60	138.3	40.9	0.2957	996	14
EMP_49A_3	1.672	0.028	0.1672	0.0028	0.0727	0.002	0.0505	0.0039	1001	20	997	16	995	74	997	54	148.5	45.1	0.3037	997	16
EMP_49A_4	1.607	0.034	0.1607	0.0021	0.0725	0.0015	0.0482	0.0037	972	13	961	12	951	71	1005	39	248	70.8	0.2855	961	12
EMP_49A_5	1.684	0.068	0.1676	0.0032	0.0729	0.0027	0.0526	0.0043	999	26	999	19	1036	82	1013	68	92	38.6	0.4196	999	19
EMP_49A_6	1.731	0.048	0.1731	0.0048	0.0732	0.0016	0.0542	0.0046	1019	18	1029	26	1066	88	1013	44	211	54.4	0.2578	1029	26
EMP_49A_7	1.616	0.046	0.1617	0.0035	0.0727	0.0023	0.0502	0.0042	975	21	969	18	989	88	992	64	116	38.6	0.3155	966	19
EMP_49A_8	1.202	0.04	0.1222	0.0043	0.0713	0.0016	0.0471	0.0041	801	18	743	25	930	79	964	46	813	114.6	0.1410	743	25
EMP_49A_9	1.747	0.043	0.1719	0.0032	0.0737	0.0012	0.0588	0.0054	1025	16	1022	18	1150	100	1030	33	626	97	0.1552	1022	18
EMP_49A_10	1.617	0.044	0.1635	0.0026	0.0713	0.0018	0.05	0.0041	976	15	976	14	986	79	957	52	246	83.1	0.3378	976	14
EMP_49A_11	1.675	0.053	0.1672	0.0029	0.0727	0.0022	0.049	0.0047	997	20	970	17	966	91	994	61	78.7	15.09	0.1914	997	16
EMP_49A_12	1.653	0.076	0.1624	0.003	0.0738	0.0031	0.0482	0.006	987	29	970	17	949	110	1012	87	42.2	10.3	0.2441	970	17
EMP_49A_13	1.94	0.15	0.192	0.01	0.0735	0.0046	0.0484	0.0053	1091	59	1131	56	954	100	1010	120	50.4	39.28	0.7790	1131	56
EMP_49A_14	1.685	0.058	0.1679	0.0031	0.0728	0.0023	0.0504	0.0041	1001	22	1000	17	993	78	995	69	92.5	34.2	0.3697	1000	17
EMP_49A_15	1.701	0.046	0.1705	0.0031	0.0723	0.0016	0.0521	0.004	1007	18	1015	17	1026	77	989	46	119.1	51.6	0.4332	1015	17
EMP_49A_16	1.661	0.091	0.1614	0.0032	0.0747	0.004	0.0481	0.0079	999	35	965	18	950	150	1030	110	40.5	3.06	0.0756	965	18
EMP_49A_17	1.714	0.094	0.1726	0.0046	0.0712	0.0035	0.055	0.012	1007	35	1026	25	1070	220	950	100	16.1	1.79	0.1112	1026	25
EMP_49A_18	1.594	0.096	0.1605	0.0041	0.0695	0.0041	0.0517	0.0057	957	38	988	22	1010	130	860	120	25.32	5.72	0.2259	988	22
EMP_49A_19	1.68	0.066	0.167	0.003	0.073	0.0026	0.0502	0.0075	1004	24	995	17	990	140	997	71	57.2	5.89	0.1030	995	17
EMP_49A_20	1.695	0.05	0.1672	0.0038	0.0736	0.002	0.0502	0.004	1005	19	999	18	1019	77	1019	58	78.7	38.4	0.4879	996	16
EMP_49A_21	1.666	0.062	0.1652	0.0032	0.0733	0.0028	0.0512	0.0056	993	24	986	18	1008	110	1001	79	46.5	10.42	0.2241	986	18
EMP_49A_22	1.7	0.12	0.1706	0.0047	0.0722	0.0047	0.05	0.008	998	44	1015	26	1030	190	930	130	19.1	3.44	0.1801	1015	26
EMP_49A_23	2.079	0.066	0.193	0.0038	0.0782	0.0021	0.0563	0.0044	1140	22	1137	21	1106	84	1141	57	90.4	66.4	0.7345	1137	21
EMP_49A_24	1.77	0.19	0.1797	0.0081	0.0726	0.0084	0.066	0.018	1067	64	1064	44	1350	370	850	230	5.7	1.26	0.2211	1064	44
EMP_49A_25	1.69	0.055	0.1688	0.0028	0.0727	0.0023	0.0518	0.0043	1003	21	1006	15	1020	83	990	66	102	39.9	0.3912	1006	15
EMP_49A_26	1.733	0.069	0.1692	0.0032	0.0744	0.003	0.0512	0.0062	1017	26	1008	18	1007	120	1050	74	34.9	14.44	0.4138	1008	18
EMP_49A_27	1.737	0.07	0.1693	0.0037	0.0744	0.0027	0.0519	0.0044	1019	26	1008	21	1023	85	1035	76	43.7	27.1	0.6201	1008	21
EMP_49A_28	1.644	0.048	0.1668	0.0031	0.0716	0.002	0.0528	0.0042	985	18	994	17	1038	80	962	59	91.5	34.7	0.3792	994	17
EMP_49A_29	1.57	0.042	0.159	0.0028	0.0719	0.0019	0.0481	0.0036	961	18	951	16	950	69	973	54	150.2	79.8	0.5313	951	16
EMP_49A_30	1.609	0.059	0.1664	0.0038	0.0702	0.0021	0.0519	0.0042	971	23	992	21	1022	81	938	67	64.6	27.9	0.4319	992	21
EMP_49A_31	2.513	0.073	0.2157	0.0049	0.0844	0.0019	0.0629	0.0056	1275	21	1259	26	1233	110	1299	44	220.3	55.4	0.2515	1259	26
EMP_49A_32	1.681	0.043	0.1677	0.0025	0.0727	0.0015	0.0503	0.0039	1000	16	999	14	992	74	999	42	184.1	111.3	0.6046	999	14
EMP_49A_33	1.69	0.052	0.1673	0.0031	0.0732	0.002	0.0502	0.004	1003	18	999	17	990	77	1010	58	120	32.4	0.2783	999	17
EMP_49A_34	1.648	0.046	0.1662	0.003	0.0719	0.0014	0.0506	0.0039	987	18	991	17	997	75	977	40	208.8	88.9	0.4258	991	17
EMP_49A_35	1.697	0.067	0.1644	0.0039	0.0751	0.002	0.05	0.0044	1017	33	981	22	985	85	1066	56	163.1	46	0.2820	981	22
EMP_49A_36	1.7	0.043	0.1688	0.0032	0.0736	0.0016	0.0516	0.004	1007	16	1015	16	1016	77	1024	45	96.4	41.1	0.4263	1005	18
EMP_49A_37	1.715	0.078	0.1712	0.004	0.0729	0.0034	0.053	0.0058	1010	29	1018	22	1042	110	979	34	34	12.4	0.3647	1018	22
EMP_49A_38	1.686	0.043	0.1683	0.0029	0.0727	0.0017	0.0509	0.0041	1002	16	1003	18	1003	79	999	47	201	58.5	0.2910	1003	16
EMP_49A_39	1.589	0.037	0.1599	0.0025	0.0722	0.0014	0.0517	0.0045	955	16	956	14	1018	88	988	39	195.5	42.4	0.2169	956	14
EMP_49A_40	1.714	0.042	0.1685	0.003	0.0738	0.0016	0.05	0.0039	1013	16	1004	17	985	75	1029	47	183.7	51.6	0.2809	1004	17
EMP_49A_41	1.703	0.041	0.1708	0.0031	0.0724	0.0014	0.0522	0.0038	1008	15	1016	17	1028	76	991	41	253	104	0.4111	1016	17
EMP_49A_42	1.648	0.056	0.1677	0.0029	0.0714	0.0025	0.0506	0.0039	986	21	999	16	998	75	951	71	83.3	58	0.6963	999	16
EMP_49A_43	1.691	0.049	0.1648	0.0032	0.0739	0.0023	0.0498	0.0041	1004	22	989	18	982	78	1015	63	132.1	40.4	0.3058	989	18
EMP_49A_44	1.675	0.039	0.1666	0.0024	0.0734	0.0017	0.0513	0.004	1002	16	993	13	1011	76	1018	45

M1_CP088_2	1.381	0.059	0.1336	0.0045	0.0732	0.0017	0.0358	0.0073	878	22	808	25	710	140	1014	47	22	3	0.1364	808	25			
M1_CP088_3	2.606	0.071	0.2242	0.0057	0.08432	0.00038	0.0665	0.0083	1301	20	1305	30	1300	160	1300.2	8.8	602	61	0.1013	1305	30			
M1_CP088_4	2.532	0.067	0.2188	0.0052	0.08385	0.00068	0.0662	0.0079	1290	19	1275	28	1290	150	1286	16	137	87	0.6350	1275	28			
M1_CP088_5	2.213	0.057	0.1985	0.0049	0.08085	0.00041	0.0669	0.0081	1184	19	1167	27	1310	150	1217	10	360	71	0.1972	1167	27			
M1_CP088_6	2.958	0.075	0.2422	0.0057	0.08869	0.00069	0.0777	0.0094	1396	19	1398	30	1510	180	1395	15	171	64	0.3743	1398	30			
M1_CP088_7	2.722	0.067	0.2294	0.0054	0.08596	0.00046	0.0684	0.0082	1334	18	1331	28	1340	150	1336	10	441	139	0.3152	1331	28			
M1_CP088_8	2.213	0.056	0.2016	0.0047	0.07941	0.00064	0.0595	0.0071	1184	18	1184	26	1170	140	1181	16	249	169	0.8895	1184	26			
M1_CP088_9	2.002	0.06	0.1935	0.005	0.0761	0.001	0.0581	0.0066	1121	21	1140	27	1140	130	1089	26	53	45	0.8491	1140	27			
M1_CP088_10	2.255	0.057	0.1981	0.0047	0.08238	0.00085	0.0593	0.0071	1198	18	1165	25	1140	140	1251	16	162	90	0.5556	1165	25			
M1_CP088_11	2.076	0.053	0.1922	0.0046	0.07831	0.00067	0.0534	0.0065	1140	18	1133	25	1050	120	1151	17	236	73	0.3093	1133	25			
M1_CP088_12	1.977	0.054	0.1857	0.0046	0.07608	0.00064	0.057	0.0068	1106	19	1109	24	1120	130	1093	24	76	43	0.5658	1109	24			
M1_CP088_13	2.354	0.063	0.2099	0.005	0.08106	0.00096	0.0613	0.0073	1227	19	1228	26	1200	140	1216	24	76	114	1.5060	1228	26			
M1_CP088_14	2.076	0.055	0.1925	0.0046	0.07801	0.00096	0.0571	0.0071	1140	18	1135	25	1120	130	1144	24	67	40	0.4598	1135	25			
M1_CP088_15	2.68	0.073	0.2274	0.0054	0.0852	0.0011	0.0623	0.0078	1321	20	1321	28	1220	150	1312	25	62	30	0.4839	1321	28			
M1_CP088_16	1.784	0.047	0.177	0.0041	0.0728	0.00092	0.053	0.0065	1038	17	1050	23	1040	120	1007	25	87	34	0.3908	1050	23			
M1_CP088_17	1.72	0.044	0.1692	0.0039	0.07335	0.00076	0.0488	0.0059	1015	17	1007	22	990	120	1019	21	134	77	0.5746	1007	22			
M1_CP088_18	3.042	0.082	0.1874	0.0055	0.1179	0.0028	0.1	0.01	1416	22	1107	29	1930	190	1915	52	49	34	0.6939	1107	29			
M1_CP088_19	0.151	0.019	0.02185	0.00081	0.0486	0.0046	0.007	0.0014	140	16	139.4	5.1	141	29	60	160	18	22	1.2222	139.4	5.1			
M1_CP088_20	1.856	0.059	0.1732	0.0052	0.07717	0.00046	0.0566	0.0063	1060	22	1028	28	1110	120	1124	12	1382	399	0.2887	1028	28			
M1_CP088_21	0.151	0.017	0.02186	0.0008	0.0497	0.0043	0.007	0.0014	142	15	139.4	5.5	110	28	110	150	18	12	0.6667	139.4	5.5			
M1_CP088_22	1.742	0.044	0.1702	0.004	0.07395	0.00058	0.0505	0.0062	1023	16	1013	22	1000	120	1037	16	299	133	0.4448	1013	22			
M1_CP088_23	1.328	0.035	0.1223	0.0041	0.0779	0.00063	0.0553	0.0075	857	18	743	23	1280	150	1142	14	341	31	0.0909	743	23			
M1_CP088_24	2.38	0.069	0.2035	0.0048	0.084	0.002	0.0655	0.0094	1233	22	1194	25	1280	180	1276	44	29	16	0.5517	1194	25			
M1_CP088_25	2.691	0.067	0.2261	0.0053	0.08583	0.00052	0.0669	0.008	1336	18	1314	28	1310	150	1333	13	209	105	0.5024	1314	28			
M1_CP088_26	0.208	0.014	0.03114	0.00081	0.0489	0.0033	0.0084	0.0015	193	12	197.6	5.1	168	30	120	120	30	15	0.5000	197.6	5.1			
M1_CP088_27	1.709	0.054	0.1671	0.0043	0.0738	0.001	0.0498	0.0062	1010	19	996	23	980	100	1033	27	108	63	0.5833	996	23			
M1_CP088_28	2.434	0.062	0.2095	0.0049	0.08378	0.00082	0.0634	0.0078	1253	19	1226	26	1240	150	1285	20	200	102	0.5100	1226	26			
M1_CP088_29	0.209	0.012	0.02972	0.0018	0.0511	0.0029	0.0087	0.0015	192	11	186.8	4.9	175	29	190	100	43	26	0.6512	186.8	4.9			
M1_CP088_30	3.82	0.16	0.2076	0.0048	0.1318	0.0058	0.095	0.0091	1576	49	1215	26	1830	170	2040	110	18	22	1.2222	1215	26			
M1_CP088_31	1.799	0.049	0.1754	0.0042	0.07404	0.00094	0.0524	0.0065	1045	18	1042	23	1030	120	1038	26	87	42	0.4828	1042	23			
M1_CP088_32	0.2054	0.0098	0.03083	0.00075	0.0497	0.0021	0.009	0.0012	188.7	8.3	189.5	4.7	180	25	163	84	64	70	1.0938	189.5	4.7			
M1_CP088_33	2.35	0.058	0.2087	0.0049	0.08101	0.00053	0.0636	0.0076	1227	18	1222	26	1250	140	1224	13	422	128	0.3033	1222	26			
M1_CP088_34	1.975	0.054	0.1956	0.0048	0.07303	0.00081	0.0515	0.0064	1090	19	1151	26	1010	120	1010	22	102	68	0.6557	1151	26			
M1_CP088_35	2.644	0.068	0.2234	0.0053	0.08515	0.00086	0.0646	0.0079	1312	19	1299	28	1270	150	1314	20	111	50	0.4505	1299	28			
M1_CP088_36	1.518	0.034	0.1505	0.0038	0.07288	0.00044	0.0492	0.0059	937	17	904	22	970	110	1010	12	820	118	0.1439	904	22			
M1_CP088_37	0.167	0.019	0.02318	0.00088	0.0521	0.0048	0.0068	0.0014	156	16	147.7	5.5	139	28	180	160	17	19	1.1176	147.7	5.5			
M1_CP088_38	1.745	0.046	0.169	0.004	0.07501	0.00081	0.0508	0.0065	1025	17	1000	120	1064	22	140	111	0.7609	1000	22					
M1_CP088_39	1.764	0.044	0.1683	0.0041	0.07532	0.00046	0.0553	0.0067	1032	16	1003	22	1090	130	1077	12	580	187	0.3224	1003	22			
M1_CP088_40	2.363	0.061	0.2155	0.005	0.07878	0.00083	0.0625	0.0074	1230	19	1258	27	1230	140	1161	21	96	84	0.8750	1258	27			
M1_CP088_41	1.721	0.043	0.1698	0.004	0.07306	0.00053	0.0513	0.0062	1016	16	1011	22	1010	120	1013	15	314	137	0.4363	1011	22			
M1_CP088_42	1.868	0.061	0.1884	0.0044	0.0716	0.0019	0.0529	0.0064	1053	24	1112	25	1040	130	951	53	23	30	1.3043	1112	25			
M1_CP088_43	2.645	0.067	0.2223	0.0052	0.08569	0.0007	0.0656	0.008	1312	19	1294	28	1280	150	1328	16	149	66	0.4430	1294	28			
M1_CP088_44	1.716	0.068	0.1681	0.0046	0.07379	0.00097	0.0518	0.0073	1013	21	1001	27	1040	120	1016	21	91	91	0.3263	1001	27			
M1_CP088_45	1.727	0.044	0.1706	0.0041	0.07282	0.00043	0.0532	0.0062	1018	17	1016	23	1050	120	1007	12	445	297	0.6674	1016	23			
M1_CP088_46	2.273	0.066	0.2052	0.0056	0.0799	0.00067	0.0694	0.0089	1201	21	1203	30	1350	170	1194	17	278	43	0.1547	1203	30			
M1_CP088_47	1.721	0.055	0.17	0.0052	0.07324	0.00055	0.05	0.006	1016	23	1012	30	990	110	1018	15	293	151	0.5154	1012	30			
M1_CP088_48	2.409	0.06	0.2101	0.005	0.08302	0.00049	0.0629	0.0076	1245	18	1229	26	1230	140	1268	12	544	214	0.3934	1229	26			
M1_CP088_49	1.731	0.044	0.1715	0.004	0.07285	0.00062	0.052	0.0065	1019	16	1020	22	1020	120	1006	17	180	133	0.7389	1020	22			
M1_CP088_50	1.74	0.047	0.1731	0.0041	0.0727	0.001	0.0519	0.0065	1023	18	1029	23	1020	120	996	28	68	39	0.5735	1029	23			
M1_CP088_51	1.197	0.05	0.116	0.0037	0.0742	0.0016	0.0538	0.0057	797	21	707	21	1060	140	1040	38	112	49	0.4375	707	21			
M1_CP088_52	1.742	0.044	0.171	0.004	0.07354	0.00066	0.0534	0.0064	1023	17	1018	22	1050	130	1025	18	191	100	0.5236	1018	22			
M1_CP088_53	2.151	0.063	0.1967	0.0046	0.07934	0.00052	0.0588	0.0071	1165	17	1157	25	1160	140	1179	13	433	246	0.5688	1157	25			
M1_CP088_54	1.69	0.043	0.1685	0.004	0.07255	0.0007	0.0522	0.0064	1004	16	1004	22	1030	120	997	19	178	51	0.2865	1004	22			
M1_CP088_55	1.732	0.045	0.1706	0.004	0.07327	0.00077	0.053	0.0064	1019	17	1015	22	1040	120	1016	21	147	86	0.5850	1015	22			
M1_CP088_56	2.762	0.072	0.2323	0.0055	0.08594	0.00083	0.0677	0.0083	1344	20	1346	29	1320	160	1332	19	99	41	0.4141	1346	29			
M1_CP088_57	1.674	0.046	0.167	0.004	0.0727	0.001	0.0498	0.0061	998	16	1000	22	1000	120	1007	28	68	58	0.8529	998	22			
M1_CP088_58	2.486	0.063	0.2167	0.0052	0.08319	0.00046	0.0681	0.0081	1268	19	1264	28	1330	150	1272	11	482	116	0.2407	1264	28			
M1_CP088_59	1.691	0.043	0.1682	0.0039	0.07296	0.00066	0.0512	0.0062	1004	16	1002	22	1020	120	1009	18	250	94	0.3760	1002	22			
M1_CP088_60	2.616	0.067	0.2224	0.0054	0.08483	0.00047	0.0692	0.0083	1305	19	1294	28	1350	160	1310	11	368	164	0.4457	1294	28			
M1_CP088_61	1.517	0.064	0.1367	0.0047	0.0787	0.0016	0.0461	0.007	934	22	826	26	910	130	1146	40	34	19	0.5588	826	26			
M1_CP088_62	1.988	0.058	0.1886	0.0054	0.07619	0.00051	0.0605	0.0072	1110	21	1113	30	1190	140	1098	14	465	99	0.2129	1113	30			
M1_CP088_63	0.141	0.016	0.02004	0.00084	0.0505	0.004	0.0067	0.0016	132	13	127.9	5.3	135	32	160	140	20	13	0.6500	127.9	5.3			
M1_CP088_64	2.648	0.075	0.228	0.0062	0.08396	0.00047	0.0734	0.0087	1311	21	1323	33	1430	160	1292	11	405	218	0.5383	1323	33			
M1_CP088_65	0.207	0.01	0.02932	0.00075	0.0507	0.0023	0.0095	0.0013	190	8.7	186.3	4.7	191	25	216	90	61	49	0.8033	186.3	4.7			
M1_CP088_66	1.641	0.037	0.1634	0.0039	0.07289	0.00043	0.0494	0.0068	985	18	977	22	950	130	1008	25	184	88	0.4783	977	22			
M1_CP088_67	1.193	0.055	0.1144	0.0041	0.074	0.0017	0.0392	0.0069	796	21	698	23	770	130	1031	47	24	5	0.2083	698	23			
M1_CP088_68	0.1895	0.0059	0.02789	0.00067	0.0494	0.001	0.0082	0.0016	176	5	177.3	4.2	165	33	161	43	253	14	0.0553	177.3	4.2			
M1_CP088_69	1.64	0.24	0.134	0.011	0.0875	0.0068	0.03	0.11	945	69	809	55	-300	1200	1130	170	2	0	0.0000	809	55			
M1_CP088_70	1.625	0.046	0.156	0.0039	0.0755	0.001	0.052	0.0062	974	18	934	22	1020	140	1080	27	115	11	0.6957	934	22			
M1_CP088_71	2.29	0.059	0.2052	0.0049	0.08077	0.00075	0.0621	0.0075	1208	18	1203	26	1220	140	1212	18	152	70	0.4605	1203	26			
M1_CP088_72	1.676	0.043	0.1667	0.0039	0.07372	0.00053	0.0513	0.0063	993	16	994	22	1010	120	1013	20	198	55	0.2778	994	22			
M1_CP088_73	47.2	5.2	0.587	0.046	0.575	0.03	0.62	0.17	3900	160	2970	190	9.60E+03	1.70E+03	4440	120	520	1045	2.0096	4440	120			
M1_CP088_74	2.03	0.063	0.187	0.0044	0.07967	0.00079	0.0598	0.0071	1124	18	1105	24	1170	140	1160	20	131	51	0.3893	1105	24			
M1_CP088_75	1.726	0.046	0.172	0.0043	0.07316	0.00049	0.0515	0.0065	1018	17	1023	24	1020	120	1016	14	435	148	0.3402	1023	24			
M1_CP088_76	1.686	0.044	0.1684	0.004	0.07272	0.00072	0.0523	0.0063	1002	16	1003	22	1030	120	1001	20	177	87	0.4915	1003	22			
M1_CP088_77	0.574	0.02	0.0626	0.0019	0.06675	0.0015	0.0219	0.0028	461	12	392	12	438	56	827	16	990	436	0.4404	392	12			
M1_CP088_78	1.646	0.046	0.1634	0.0039	0.0734	0.001	0.05	0.0063	987	18	975	22	980	120	1021	30	85	25	0.2941	975	22			
M1_CP088_79	2.429	0.083	0.2154	0.0058	0.0824	0.0013	0.0659	0.0077	1250	24	1257	31	1190	150	1246	30	55	24	0.4364	1257	31			
M1_CP088_80	1.662	0.041	0.1657	0.0039	0.0729	0.00034	0.0508	0.0063	994	16	988	22	1000	120	1010	9.8	734	222	0.3025	988	22			
M1_CP088_81	2.711	0.07	0.2225	0.0052	0.0887	0.001	0.0711	0.009	1393	20	1295	27	1390	170	1394	22	128	51	0.3884	1295	27			
M1_CP088_82	2.452	0.064	0.2139	0.0051	0.08352	0.00076	0.0616	0.0077	1257	19	1249	27	1210	150	1278	18	165	76	0.4606	1249	27			
M1_CP088_83	2.658	0.075	0.2294	0.0055	0.0842	0.0013	0.0659	0.0085	1314	22	1331	29	1270	150	1287	29	48	26	0.5417	1331	29			
M1_CP088_84	0.145	0.017	0.02081	0.00089	0.0502	0.004	0.0061	0.0015	136	14	132.8	5.6	124	29	140	140	21	18	0.8571	132.8	5.6			
M1_CP088_85	1.617	0.07	0.1386	0.0064	0.0824	0.001	0.0558	0.0071	976	21	837	29	1000	140	1030	27	107	34	0.3178	837	29			
M1_CP088_86	1.717	0.047	0.1713	0.0041	0.073	0.001	0.0513	0.0062	1014	18	1019	22	1010	120	1007	28	97	72	0.7423	1019	22			
M1_CP088_87	1.609	0.04	0.1707	0.0041	0.07341	0.00065	0.0524	0.0065	973	15	955	22	1030	120	1015	13	274	152	0.5547	955	22			
M1_CP088_88	1.61	0.042	0.1533	0.0039	0.07665	0.00044	0.046	0.0051	974	17	919	22	908	98	1111	11	782	265	0.3389	919	22			
M1_CP088_89	1.194	0.035	0.1156	0.0039	0.07393	0.00094	0.0408	0.0063	797	16	705	17	910	100	1038	17	326	105	0.5982	705	17			
M1_CP088_90	1.718	0.048	0.1723	0.004	0.0726	0.0012	0.0523	0.0069	1013	19	1026	22	1030	130	986	33	48	13	0.2708	1026	22			
M1_CP088_91	0.1989	0.0056	0.02893	0.00068	0.04998	0.00073	0.0094	0.0013	184	4.9	183.8	4.3	189	25	188	32	565	89	0.1575	183.8	4.3			
M1_CP088_92	1.928	0.077	0.1681	0.0053	0.0823	0.0015	0.0533	0.008	987	22	1002	29	1050	150	1237	36	25	20	0.8000	1002	29			
M1_CP088_93	1.847	0.061	0.1824	0.0047	0.0736	0.0013	0.0523	0.0068	1059	22	1080	25	1030	130	1013	36	40	29	0.7250	1080	25			
M1_CP088_94	1.673	0.053	0.1662	0.004	0.07447	0.00094	0.0519	0.0063	996	16	991	22	1020	120	1042	23	392	406	1.0357	991	22			
M1_CP088_95	1.754	0.046	0.1741	0.0041	0.07339	0.00087	0.0517	0.0063	1027	17	1036	22	1020	120	1021	24	103	94	0.9126	1036	22			
M1_CP088_96	0.2083	0.009	0.03022	0.00073	0.0501	0.0019	0.009	0.0013	191.5	7.7	191.9	4.6	181	25	186	74	74	80	1.0811	191.9	4.6			
M1_CP088_97	1.976	0.052	0.1881	0.0047	0.07666	0.0005	0.0534	0.0066	1106	18	1111	26	1050	130	1110	13	360	98	0.2722	1111	26			
M1_CP088_98	1.721	0.044	0.1707	0.004	0.07341	0.00065	0.0524	0.0065	1016	16	1016	22	1030	120	1022	18	213	84	0.3944	1016	22			
M1_CP088_99	2.76	0.1	0.2347	0.0072	0.0856	0.001	0.0739	0.0088	1347	25	1359	37	1440	160	1321	22	86	46	0.5349	1359	37			
M1_CP088_100	0.1445	0.0092	0.02079	0.00074	0.0495	0.0019	0.0075	0.0011	136.5	7.7	132.7	4.6	151	29	178	78	73	144	1.0726	132.7	4.6			
M1_CP088_101	1.285	0.062	0.1209	0.0044	0.0753	0.0019	0.0413	0.0068	835	23	736	24	820	130	1042	53	22	16	0.7273	736	24			
M1_CP088_102	2.316	0.094	0.2011	0.0064	0.08409	0.0065	0.0677	0.0088	1216	24	1181	34	1330	170	1293	14	304	67	0.2206	1181	34			
M1_CP088_103	1.655	0.045	0.166	0.004	0.07253	0.00069	0.0516	0.0063	991	17	990	22	1020	120	997	19	123	138	0.6244	990	22			
M1_CP088_104	2.716	0.069	0.2301	0.0054	0.08615	0.00052	0.0702	0.0085	1332	18	1335	28	1370	160	1341	12	281	93	0.3310	1335	28			
M1_CP088_105	1.869	0.05	0.1805	0.0042	0.0757	0.001	0.0569	0.0071	1070	18	1069	23	1120	130	1083	27	98	47	0.4796	1069	23			
M1_CP088_106	1.729	0.045	0.1721	0.004	0.07325	0.00075	0.0516	0.0063	1019	16	1024	22	1020	120	1016	21	138	74	0.5362	1024	22			
M1_CP088_107	1.973	0.062	0.1966	0.0044	0.0734	0.0018	0.0516	0.007	1200	23	1156	24	1010	130	969	53	19	14	0.7368	1156	24			
M1_CP088_108	1.66	0.043	0.1669	0.0039	0.0725	0.00066	0.0515	0.0062	993	16	995	22	1020	120	998	19	246	227	0.9228	995	22			
M1_CP088_109	2.342	0.054	0.2155	0.0049	0.079	0.0013	0.0612	0.0076	1222	20	1258	27	1200	150	1159	32	42	19	0.4524	1258	27			
M1_CP088_110	1.378	0.059	0.1391	0.0043	0.0709	0.0019	0.041	0.0075	874	23	839	24	810	130	916	54	19	8	0.4211	839	24			
M1_CP088_111	1.694	0.06	0.1703	0.004	0.0725	0.0012	0.0547	0.0075	1004	20	1014	22	1070	140	992	32	69	15	0.2174	1014	22			
M1_CP088_112	1.841	0.047	0.1775	0.0042	0.07591	0.00047	0.0578	0.0073	1060	16	1053	23	1140	140	1091	54	429	148	0.3450	1053	23			
M1_CP088_113	2.211	0.064	0.2211	0.0054	0.08546	0.00052	0.0679	0.0081	1298	19	1287	27	1330	170	1328	12	336	185	0.5506	1287	27			
M1_CP088_114	1.822	0.057	0.1798	0.0049	0.0741	0.0011	0.0513	0.0064	1050	20	1066	27	1010	120	1043	29	57	74	1.2982	1066	27			
M1_CP088_115	0.213	0.01	0.02948	0.00079	0.0519	0.0022	0.009	0.0013	195.3	8.4	187.3	4.6	180	27	193	94	69	34	0.4928	187.3	4.6			
M1_CP088_116	2.68	0.087	0.2283	0.0054	0.08575	0.00086	0.0667	0.0082	1323	19	1325	28	1310	150	1328	20	116	74	0.6379	1325	28			
M1_CP088_117	1.666	0.043	0.165	0.0039	0.07349	0.00065	0.0532	0.0062	995	16	984	22	1050	120	1028	17	211	211	1.0000	984	22			
M1_CP088_118	1.667	0.043	0.1672	0.0039	0.07277	0.00079	0.0496	0.0061	995	17	997	22	980	130	1005	22	137	75	0.1095	997	22			
M1_CP088_119	2.7	0.067	0.2279	0.0054	0.08649	0.00041	0.0712	0.0085	1328	18	1324	28	1390	160	1348.1	9	461	136	0.2950	1324	28			
M1_CP088_120	2.387	0.061	0.2105	0.005	0.08274	0.0006	0.0639	0.0077	1238	19	1231	27	1240	150	1261	14	214	84	0.3925	1231	27			
M1_CP088_121	1.927	0.052	0.1823	0.0044	0.07719	0.0008	0.0552	0.0067	1090	18	1080	24	1090	130	1122	20	186	88	0.4731	1080	24			
M1_CP088_122	1.88	0.052	0.1906	0.0048	0.07222	0.00073	0.0561	0.0068	1072	19	1124	27	1010	130	985	10	110	31	0.2818	1124	27			
M1_CP088_123	2.622	0.069	0.2265	0.0055	0.08398	0.00048	0.0717	0.0082	1306	20	1318	29	1400	150	1291	11	389	231	0.5938	1318	29			
M1_CP088_124	2.687	0.07	0.2295	0.0056	0.08531	0.00066	0.0705	0.0084	1332	19	1332	29	1380	170	1320	15	142	54	0.3803	1332	29			
M1_CP088_125	1.732	0.046	0.1729	0.004	0.07324	0.00078	0.0521	0.0064	1019	17	1028	22	1030	120	1015	22	103	44	0.4272	1028	22			
M1_CP088_126	1.774	0.048

M2_CV1302_9	1.688	0.044	0.1685	0.004	0.0727	0.00084	0.0499	0.006	1003	18	1003	22	980	110	1000	23	103	78	0.7573	1003	22
M2_CV1302_10	2.686	0.069	0.2269	0.0054	0.08566	0.00068	0.0666	0.0078	1323	19	1318	28	1300	150	1328	15	181	84	0.4641	1318	28
M2_CV1302_11	1.743	0.047	0.1716	0.0041	0.0736	0.001	0.0488	0.0059	1023	18	1021	22	960	110	1020	29	81	41	0.5062	1021	22
M2_CV1302_12	2.59	0.066	0.2224	0.0052	0.08431	0.00066	0.0646	0.0077	1297	19	1294	27	1260	150	1297	15	151	55	0.3642	1294	27
M2_CV1302_13	1.704	0.046	0.1706	0.004	0.07219	0.00097	0.0494	0.0059	1009	17	1015	22	950	110	987	28	77	59	0.7682	1015	22
M2_CV1302_14	2.27	0.056	0.2015	0.0048	0.08131	0.0005	0.0649	0.0072	1202	18	1183	26	1270	140	1227	12	266	130	0.4887	1183	26
M2_CV1302_15	1.756	0.047	0.1726	0.0041	0.07364	0.00095	0.0517	0.0062	1028	17	1026	23	1020	120	1025	26	89	59	0.6629	1026	23
M2_CV1302_16	2.202	0.071	0.2009	0.0059	0.07904	0.00072	0.0572	0.0066	1180	25	1180	33	1120	130	1169	19	123	47	0.3821	1180	33
M2_CV1302_17	2.164	0.053	0.1962	0.0046	0.07953	0.00045	0.0612	0.007	1170	17	1155	25	1200	130	1186	12	376	190	0.5053	1155	25
M2_CV1302_18	2.568	0.064	0.2224	0.0052	0.08358	0.00047	0.0698	0.0081	1291	18	1295	27	1360	150	1283	11	275	103	0.3745	1295	27
M2_CV1302_19	1.912	0.056	0.1848	0.0042	0.0747	0.0014	0.0525	0.0064	1081	20	1093	23	1030	120	1045	36	46	29	0.6304	1093	23
M2_CV1302_20	1.719	0.047	0.1694	0.004	0.0737	0.001	0.0488	0.0059	1017	18	1009	22	970	110	1026	29	97	43	0.4433	1009	22
M2_CV1302_21	1.696	0.044	0.1669	0.004	0.07345	0.00052	0.0548	0.0063	1006	17	995	22	1080	130	1024	14	302	181	0.5993	995	22
M2_CV1302_22	1.735	0.046	0.1743	0.0041	0.07219	0.00098	0.0476	0.0059	1020	18	1035	23	940	110	983	27	86	71	0.8256	1035	23
M2_CV1302_23	1.941	0.057	0.1774	0.0048	0.07948	0.00051	0.054	0.0068	1095	19	1053	26	1060	130	1183	13	418	170	0.4067	1053	26
M2_CV1302_24	1.733	0.045	0.1748	0.004	0.07199	0.00082	0.0496	0.0058	1021	17	1038	22	980	110	979	23	87	73	0.8391	1038	22
M2_CV1302_25	2.519	0.066	0.2206	0.0053	0.08248	0.00059	0.0669	0.0077	1277	20	1285	28	1310	150	1254	14	148	63	0.4257	1285	28
M2_CV1302_26	2.572	0.066	0.2239	0.0054	0.083	0.00055	0.0665	0.0077	1292	19	1302	29	1300	150	1267	12	227	91	0.4009	1302	29
M2_CV1302_27	1.704	0.044	0.1706	0.0039	0.07217	0.00079	0.0498	0.006	1009	16	1015	21	980	120	985	23	105	67	0.6381	1015	21
M2_CV1302_28	2.145	0.056	0.2009	0.0046	0.07697	0.00098	0.0534	0.0064	1162	19	1180	25	1050	120	1112	26	51	31	0.6078	1180	25
M2_CV1302_29	1.051	0.028	0.1058	0.0028	0.07196	0.00036	0.0387	0.0044	728	14	648	16	767	86	984	10	1070	157	0.1467	648	16
M2_CV1302_30	2.036	0.057	0.1825	0.0043	0.08086	0.00098	0.0581	0.0076	1127	19	1081	24	1140	150	1215	23	128	46	0.3594	1081	24
M2_CV1302_31	2.701	0.095	0.2259	0.0065	0.086	0.0012	0.083	0.012	1327	29	1313	35	1620	210	1334	25	155	34	0.2194	1313	35
M2_CV1302_32	1.49	0.041	0.1381	0.0037	0.07783	0.00041	0.044	0.0051	926	17	834	21	870	100	1141	11	530	231	0.4358	834	21
M2_CV1302_33	1.754	0.045	0.1747	0.004	0.07246	0.0009	0.0518	0.0062	1028	17	1038	22	1020	120	995	24	86	69	0.8923	1038	22
M2_CV1302_34	1.76	0.046	0.1741	0.004	0.07319	0.00099	0.0506	0.0062	1031	17	1035	22	1000	120	1011	28	82	59	0.7195	1035	22
M2_CV1302_35	1.753	0.046	0.1733	0.004	0.07309	0.00082	0.052	0.0064	1028	17	1030	22	1020	120	1010	23	114	47	0.4123	1030	22
M2_CV1302_36	1.74	0.047	0.1744	0.004	0.0718	0.00098	0.0506	0.0062	1021	18	1036	22	1000	130	970	28	72	57	0.7917	1036	22
M2_CV1302_37	1.774	0.047	0.1757	0.0041	0.07278	0.00091	0.0533	0.0064	1034	17	1043	22	1050	120	999	26	90	48	0.5333	1043	22
M2_CV1302_38	2.185	0.055	0.2002	0.0046	0.07851	0.00086	0.0598	0.0071	1175	18	1176	25	1170	140	1154	22	98	49	0.5000	1176	25
M2_CV1302_39	2.786	0.072	0.2526	0.0059	0.08641	0.0007	0.0716	0.0085	1351	19	1349	29	1400	160	1345	16	181	84	0.4641	1349	29
M2_CV1302_40	1.664	0.042	0.1677	0.0038	0.07184	0.00078	0.0489	0.0056	994	17	999	21	960	110	976	22	134	84	0.6269	999	21
M2_CV1302_41	2.538	0.08	0.2234	0.0063	0.08237	0.00073	0.0689	0.008	1262	26	1299	34	1350	150	1252	18	243	72	0.2963	1299	34
M2_CV1302_42	1.744	0.053	0.1718	0.0048	0.07306	0.00067	0.0528	0.0063	1022	20	1021	26	1040	120	1012	18	143	66	0.4615	1021	26
M2_CV1302_43	2.744	0.068	0.2365	0.0055	0.08328	0.00069	0.0671	0.0079	1340	18	1355	29	1310	150	1273	16	139	33	0.2374	1368	29
M2_CV1302_44	2.303	0.066	0.189	0.0051	0.0876	0.00057	0.0685	0.0079	1212	20	1116	27	1340	150	1371	13	355	135	0.3803	1116	27
M2_CV1302_45	2.529	0.064	0.2207	0.0052	0.08238	0.00051	0.0674	0.008	1280	18	1285	28	1320	150	1253	12	173	79	0.4566	1285	28
M2_CV1302_46	1.759	0.046	0.1732	0.004	0.07301	0.00098	0.0497	0.006	1029	18	1030	22	980	120	1005	28	78	53	0.6795	1030	22
M2_CV1302_47	0.669	0.021	0.0694	0.0021	0.06958	0.00053	0.0262	523	523	14	432	13	523	55	913	16	1027	470	0.4578	432	13
M2_CV1302_48	1.661	0.041	0.1656	0.0039	0.07255	0.00051	0.0511	0.0059	993	16	988	21	1010	110	999	15	387	162	0.4186	988	21
M2_CV1302_49	2.579	0.064	0.2205	0.0051	0.08386	0.00055	0.0675	0.0078	1294	18	1284	27	1320	150	1287	13	177	98	0.5537	1284	27
M2_CV1302_50	2.604	0.065	0.2207	0.0051	0.0847	0.00063	0.066	0.0079	1301	18	1285	27	1290	150	1306	14	140	63	0.4500	1285	27
M2_CV1302_51	2.092	0.052	0.1886	0.0046	0.07964	0.00045	0.0537	0.0069	1146	17	1114	24	1150	130	1187	11	385	140	0.3636	1114	24
M2_CV1302_52	1.669	0.041	0.165	0.0039	0.07272	0.00041	0.0508	0.0059	996	16	984	21	1000	110	1005	12	449	319	0.7105	984	21
M2_CV1302_53	2.688	0.07	0.2265	0.0055	0.08508	0.0005	0.0677	0.0078	1324	20	1316	29	1320	150	1315	11	251	101	0.4024	1316	29
M2_CV1302_54	2.912	0.072	0.2438	0.0057	0.08579	0.00052	0.0748	0.0086	1384	19	1406	30	1460	160	1335	12	197	77	0.3909	1406	30
M2_CV1302_55	1.742	0.049	0.175	0.004	0.0717	0.0012	0.0492	0.0059	1024	18	1040	22	970	110	969	36	41	73	1.7805	1040	22
M2_CV1302_56	2.264	0.078	0.1981	0.006	0.0825	0.0014	0.0786	0.0084	1290	25	1165	33	1530	160	1259	31	322	180	0.5590	1165	33
M2_CV1302_57	1.711	0.045	0.1688	0.004	0.07306	0.00092	0.0506	0.0061	1012	18	1006	22	1000	120	1013	26	93	69	0.7419	1006	22
M2_CV1302_58	2.922	0.073	0.2455	0.0057	0.08541	0.00054	0.0769	0.0087	1387	19	1415	30	1500	160	1323	12	162	67	0.4136	1415	30
M2_CV1302_59	1.6	0.11	0.169	0.0085	0.0685	0.0021	0.0453	0.0075	967	40	1006	47	890	140	867	63	30	17	0.5667	1006	47
M2_CV1302_60	1.714	0.047	0.1739	0.0041	0.071	0.0012	0.0546	0.0072	1014	18	1033	22	1070	140	956	32	42	12	0.2857	1033	22
M2_CV1302_61	1.711	0.047	0.1694	0.004	0.073	0.001	0.0505	0.0061	1011	18	1009	22	1000	120	1002	30	69	43	0.6232	1009	22
M2_CV1302_62	1.688	0.046	0.1675	0.004	0.07262	0.00087	0.0503	0.0061	1004	17	998	22	990	120	1001	25	109	83	0.7615	998	22
M2_CV1302_63	2.742	0.078	0.2266	0.0063	0.08722	0.00052	0.0724	0.0082	1338	23	1316	33	1410	150	1364	12	398	198	0.4975	1316	33
M2_CV1302_64	0.934	0.031	0.0867	0.0028	0.07732	0.00066	0.0345	0.0042	669	17	536	15	685	82	1128	17	683	198	0.2899	536	15
M2_CV1302_65	2.551	0.064	0.2184	0.0051	0.08428	0.00072	0.0684	0.0084	1286	19	1273	27	1340	160	1295	17	166	57	0.3434	1273	27
M2_CV1302_66	1.946	0.052	0.1785	0.0046	0.07863	0.00074	0.0574	0.0072	1098	18	1059	24	1130	140	1159	19	151	53	0.3510	1059	24
M2_CV1302_67	1.714	0.048	0.1709	0.0041	0.0723	0.0011	0.0499	0.006	1012	18	1017	22	980	120	991	30	63	45	0.7143	1017	22
M2_CV1302_68	1.673	0.042	0.166	0.0039	0.07251	0.00043	0.0519	0.0061	998	16	990	21	1020	120	998	12	408	368	0.9020	990	21
M2_CV1302_69	1.935	0.054	0.1778	0.0051	0.07891	0.00075	0.06	0.0071	1095	20	1055	29	1180	140	1168	18	435	135	0.3103	1055	29
M2_CV1302_70	1.324	0.069	0.1265	0.0044	0.0743	0.0024	0.0411	0.0064	850	26	768	24	810	120	1003	68	17	27	1.5882	768	24
M2_CV1302_71	2.943	0.077	0.2492	0.0062	0.08503	0.00052	0.0777	0.0087	1392	20	1434	32	1510	160	1315	12	245	96	0.3918	1434	32
M2_CV1302_72	1.695	0.046	0.1684	0.004	0.07272	0.00098	0.0501	0.0061	1005	18	1003	22	990	120	1002	27	92	76	0.8261	1003	22
M2_CV1302_73	2.026	0.054	0.1888	0.0047	0.07736	0.00061	0.0549	0.0063	1124	19	1115	26	1080	120	1123	12	162	67	0.4136	1115	26
M2_CV1302_74	2.685	0.068	0.226	0.0054	0.08595	0.00065	0.0664	0.0079	1323	18	1313	28	1300	150	1335	15	203	106	0.5222	1313	28
M2_CV1302_75	1.753	0.051	0.1741	0.0041	0.0727	0.0012	0.0522	0.0063	1026	19	1035	23	1030	120	997	34	78	48	0.6154	1035	23
M2_CV1302_76	2.559	0.065	0.2182	0.0052	0.08472	0.00052	0.0658	0.0078	1289	18	1272	27	1290	150	1307	12	300	118	0.3933	1272	27
M2_CV1302_77	0.739	0.032	0.0672	0.0028	0.07942	0.00061	0.0283	0.0036	562	18	419	17	564	70	1180	15	674	296	0.4392	419	17
M2_CV1302_78	1.65	0.047	0.1679	0.0041	0.0712	0.001	0.0517	0.0064	990	18	1000	23	1020	120	952	29	87	40	0.4598	1000	23
M2_CV1302_79	2.76	0.068	0.2317	0.0054	0.08609	0.00047	0.0701	0.0083	1344	18	1343	28	1370	160	1339	11	353	192	0.5439	1343	28
M2_CV1302_80	1.75	0.049	0.1724	0.0042	0.07347	0.00094	0.0519	0.0063	1025	18	1025	23	1020	120	1019	26	92	55	0.5978	1025	23
M2_CV1302_81	1.652	0.042	0.1591	0.0038	0.07533	0.00048	0.0496	0.0055	990	17	952	22	980	110	1076	13	478	181	0.3787	952	22
M2_CV1302_82	1.732	0.047	0.172	0.004	0.07294	0.00098	0.0524	0.0063	1019	18	1023	22	1030	120	1004	27	78	57	0.7308	1023	22
M2_CV1302_83	1.721	0.044	0.1714	0.0041	0.07277	0.00047	0.0542	0.0064	1016	17	1020	22	1070	120	1006	13	440	159	0.3614	1020	22
M2_CV1302_84	1.428	0.049	0.1433	0.0046	0.07247	0.00051	0.0496	0.005	900	23	863	27	982	98	998	15	749	183	0.2443	863	27
M2_CV1302_85	0.93	0.032	0.095	0.0032	0.07107	0.00046	0.0388	0.0047	667	16	585	19	769	92	957	13	610	132	0.2164	585	19
M2_CV1302_86	0.592	0.024	0.0656	0.002	0.06575	0.00089	0.0398	0.0046	472	15	409	12	730	89	795	26	1471	142	0.0965	409	12
M2_CV1302_87	1.659	0.042	0.1652	0.0038	0.07276	0.00055	0.05	0.0059	992	16	985	21	990	110	1005	15	250	131	0.5240	985	21
M2_CV1302_88	1.294	0.059	0.1327	0.0056	0.07087	0.00069	0.0454	0.0043	841	31	803	33	897	84	952	22	1419	103	0.0726	803	33
M2_CV1302_89	2.214	0.061	0.2003	0.005	0.08004	0.00074	0.0606	0.0073	1184	19	1177	27	1190	140	1194	19	167	67	0.4012	1177	27
M2_CV1302_90	1.874	0.07	0.171	0.006	0.07925	0.00051	0.0534	0.0066	1071	23	1017	33	1050	130	1176	12	407	189	0.4644	1017	33
M2_CV1302_91	1.72	0.045	0.1719	0.004	0.07254	0.00094	0.0508	0.0061	1015	17	1022	22	1000	120	993	27	73	55	0.7534	1022	22
M2_CV1302_92	2.577	0.065	0.2203	0.0053	0.08477	0.00048	0.0694	0.0081	1293	19	1283	28	1350	150	1309	11	349	149	0.4269	1283	28
M2_CV1302_93	2.789	0.071	0.2338	0.0055	0.08649	0.00058	0.0704	0.0084	1352	19	1354	29	1380	160	1347	13	219	76	0.3470	1354	29
M2_CV1302_94	1.975	0.082	0.1728	0.0094	0.0827	0.001	0.047	0.0069	1107	33	1027	36	928	95	1262	25	91	46	0.5055	1027	36
M2_CV1302_95	1.835	0.054	0.1807	0.0041	0.0733	0.0016	0.0519	0.0064	1054	20	1071	23	1020	120	1000	45	27	17	0.6296	1071	23
M2_CV1302_96	1.247	0.047	0.1187	0.0033	0.07617	0.00044	0.0417	0.005	823	16	723	19	825	97	1098	11	609	313	0.5140	723	19
M2_CV1302_97	1.654	0.042	0.1657	0.0039	0.07236	0.00051	0.0506	0.006	991	16	988	22	1000	110	994	14	301	113	0.3754	988	22
M2_CV1302_98	0.883	0.031	0.0829	0.0025	0.07677	0.0008	0.0309	0.0033	642	18	514	15	614	64	1111	22	407	174	0.4275	514	15
M2_CV1302_99	3.36	0.11	0.2456	0.0098	0.0981	0.0026	0.0847	0.0099	1479	25	1415	30	1630	180	1579	45	47	24	0.5106	1415	30
M2_CV1302_100	2.269	0.06	0.205	0.005	0.08	0.00071	0.07	0.0082	1201	19	1202	27	1370	160	1193	18	91	38	0.4176	1202	27
M2_CV1302_101	1.749	0.049	0.1731	0.004	0.0733	0.0012	0.0514	0.0061	1024	19	1029	22	1010	120	1014	33	68	143	2.1029	1029	22
M2_CV1302_102	1.921	0.05	0.1848	0.0043	0.07562	0.00087	0.0556	0.0067	1087	18	1093	24	1090	130	1082	24	84	61	0.7262	1093	24
M2_CV1302_103	3.05	0.077	0.239	0.0056	0.09268	0.00071	0.09	0.01	1419	20	1381	29	1740	200	1479	15	159	53	0.3333	1381	29
M2_CV1302_104	1.728	0.069	0.1719	0.0049	0.07336	0.00096	0.0521	0.0067	1018	23	1022	27	1030	130	1022	24	505	235	0.4653	1022	27
M2_CV1302_105	2.343	0.067	0.2044	0.0054	0.08348	0.00061	0.0681	0.0083	1224	21	1198	29	1330	160	1283	14	457	151	0.3304	1198	29
M2_CV1302_106	1.724	0.047	0.1728	0.004	0.0728	0.001	0.0516	0.0062	1016	18	1027	22	1020	120	1000	28	79	58	0.7342	1027	22
M2_CV1302_107	2.061	0.057	0.1746	0.0041	0.0859	0.0014	0.0609	0.0073	1133	20	1037	23	1190	140	1325	32	63	51	0.8095	1037	23
M2_CV1302_108	0.956	0.027	0.0889	0.0028	0.07847	0.00083	0.0352	0.004	681	14	549	15	698	77	1156	20	711	331	0.4655	549	15
M2_CV1302_109	1.959	0.065	0.1866	0.0043	0.0762	0.0017	0.0546	0.0069	1098	23	1103	23	1070	130	1083	45	34	28	0.8235	1103	23
M2_CV1302_110	1.693	0.047	0.172	0.004	0.0717	0.001	0.0494	0.0061	1004	18	1023	22	970	120	970	29	80	61	0.7625	1023	22
M2_CV1302_111	2.691	0.067	0.2098	0.0054	0.08573	0.00048	0.0694	0.0082	1325	18	1327	28	1360	160	1331	11	295	165	0.5593	1327	28
M2_CV1302_112	0.719	0.03	0.0634	0.0019	0.0806	0.0019	0.0335	0.004	542	17	396	11	664	78	1192	45	1824	702	0.3849	396	11
M2_CV1302_113	2.794	0.086	0.2246	0.0058	0.09005	0.00096	0.0895	0.0094	1350	24	1308	31	1710	180	1418	21	243	97	0.3992	1306	31
M2_CV1302_114	2.725	0.084	0.2293	0.0054	0.08616	0.0007	0.069	0.0082	1334	24	1330	34	1350	160	1338	16	133	55	0.4135	1330	34
M2_CV1302_115	1.749	0.045	0.1737	0.004	0.07353	0.00083	0.052	0.0063	1027	17	1032	23	1020	120	1026	22	97	61	0.6289	1032	23
M2_CV1302_116	2.408	0.063	0.2114	0.005	0.08308	0.00082	0.0622	0.0075	1245	19	1236	27	1220	140	1269	18	126	58	0.4603	1236	27
M2_CV1302_117	2.166	0.054	0.192	0.0046	0.08212	0.0004	0.0573	0.0068	1170	17	1132	25	1130	130	1247.4	9.5	588	183	0.3112	1132	25
M2_CV1302_118	1.739	0.047	0.1767	0.004	0.0716	0.0012	0.0488	0.006	1021	18	1049	22	960	110	966	32	60	45	0.7500	1049	22
M2_CV1302_119	1.242	0.039	0.1184	0.0035	0.07463	0.00058	0.0475	0.0054	817	18	721	20	940	110	1060	16	377	196	0.5199	721	20
M2_CV1302_120	2.07	0.051	0.1973	0.0046	0.07584	0.00077	0.0635	0.0072	1138	17	1160	25	1240	140	1085	20	103	63	0.6117	1160	25
M2_CV1302_121	2.425	0.064	0.2113	0.0052	0.08345	0.00059	0.0631	0.0068	1249	20	1236	28	1240	130	1278	14	317	198	0.6246	1236	28
M2_CV1302_122	2.612	0.076	0.2251	0.0059	0.08429	0.00087	0.0678	0.0086	1303	21	1308	31	1320	160	1295	20	88	36	0.4091	1308	31
M2_CV1302_123	2.605	0.071	0.2237	0.0054	0.08476	0.00077	0.0642	0.008	1301	20	1301	28	1260	150	1307	17	191	85	0.4450	1301	28
M2_CV1302_124	1.99	0.073	0.1785	0.0094	0.08123	0.00083	0.0533	0.0069	1110	25	1059	34	1040	130	1222	20	71	60	0.8451	1059	35
M2_CV1302_125	1.696	0.055	0.1597	0.0049	0.07733	0.00045	0.0504	0.0052	1006	23	955	28	990	100	1129	12	652	187	0.2868	955	28
M2_CV1302_126	1.478	0.046	0.1479	0.0046	0.07258	0.00077	0.0536	0.0066	920	19	889	25	1050	120	996	21	109	71	0.6514	889	25
M2_CV1302_127	1.684	0.042	0.1685	0.004	0.07257	0.00057	0.0509	0.0061	1002	16	1004	22	1000	120	999	16	239	84	0.3515	1004	22
M2_CV1302_128	2.203	0.057	0.2032	0.0047	0.07846	0.00093	0.0597	0.007	1180	19	1192	25	1170	130	1153	24	67	47	0.7015	1192	25
M2_CV1302_129	2.896	0.075	0.2431	0.0056	0.08655	0.00088	0.0646	0.008	1379	20	1403	29	1260	150	1349	19	67	39	0.5821	1403	29
M2_CV1302_130	1.965	0.049	0.1823	0.0044	0.07858	0.00046	0.0548	0.0068	1103	17	1079	24	1080	130	1160	12	397	154	0.3879	1079	24
M2_CV1302_131	1.755	0.048	0.1628	0.0042	0.07812	0.00054	0.049	0.0058	1038	19	972	24	970	110	1147	14	323	162	0.5015	972	24
M2_CV1302_132	2.687	0.067	0.2253	0.0053	0.08657	0.00064	0.0672	0.0079	1324	19	1310	28	1310	150	1349	15	171	72	0.4211	1310	28
M2_CV1302_133	1.748	0.048	0.1752	0.0041	0.0724	0.001	0.0516	0.0063	1024	18	1041	23	1020	120	987	28	82	54	0.6585	1041	23
M2_CV1302_134	1.314	0.047	0.1232	0.0041	0.07596	0.00069	0.043	0.0045	850	23	749	24	850	88	1090	19	214	57	0.2664	749	24
M2_CV1302_135	1.745	0.046	0.1745	0.004	0.07268	0.00095	0.0504	0.0061	1024	18	1037	22	990	120	998	26	89	68	0.7640	1037	22
M2_CV1302_136	1.

TABLE A2. ZIRCON AND APATITE FISSION TRACK DATA, FROM THE SEDIMENTARY ROCKS OF THE ARACATACA AND PALOMINO BASINS

Zircon Fission Track data

Sample	Lithology	Stratigraphic age	Elevation (m)	Latitude	Longitude	U (ppm)	2σ	Grains *n*	Ns	Ni	Counted squares	ζ estimate (Ma.cm^2)	se(ζ) std error on ζ estimate (Ma.cm^2)	P1	2σ se(t) (Frac)	P2	2σ se(t) (Frac)	P3	2σ se(t) (Frac)	P4	2σ se(t) (Frac)
CP-088	Coarse Sandstone	Miocene	180	10º31'33"	74º03'13"	216	8	96	20034	5105	4606	141.03	2.32	32.9	± 15 (2%)	64.9	± 5 (37.4%)	103.6	± 6.9 (60.7%)		
CVI-1302	Conglomerate	Miocene	150	10º35'18"	74º05'06"	226	10	68	11865	2566	2249	141.03	2.32	29.2	± 3 (6.4%)	52	± 8 (18.9%)	103.8	± 6.6 (74.7%)		
EMP-16	Conglomerate	Lower Miocene	176	10º32'21"	74º03'50"	180	8	98	13572	2457	3441	128.02	1.87			56.8	± 11 (11.8%)	95.9	± 10 (72.5%)	140.9	± 29 (15.7%)
EMP-49A	Conglomerate	Lower Miocene	55	11º12'33"	73º30'17"	180	8	97	17574	3314	3996	128.02	1.87			74.4	± 7 (37.1%)	107.4	± 14 (52.8%)	158.4	± 52 (10.1%)
AP-045	Conglomerate	Miocene	55	11º13'12"	73º28'39"	89	4	101	17531	2781	6886	128.02	1.87	41	± 13.1(1.4%	89.6	± 9.4 (38.6%)	131.6	± 11.6 (60 %)		
AP-046	Conglomerate	Miocene	65	11º13' 7.99"	73º28' 41.4"	97	5	158	13884	2172	4417	126.82	2.05	32.9	± 6.3 (5.1%)	79.6	± 15.2 (9%)	129.4	±12.1 (74.1%)	250.6	± 68.7 (11.7%)
AP-050	Conglomerate	Miocene	14	11º15' 29.78"	73º36' 47.4"	225	8	93	17166	5347	4696	126.82	2.05	38.9	± 4.5 (14.6%	54.8	± 3.7 (47.3%)	94	± 14.6 (20.1%)	154.8	± 27.5 (18%)
EMP-35b	Conglomerate	Miocene	0	11º15' 34.31"	73º29' 53.1"	129	6	99	15535	2288	3856	128.02	1.87			55.6	± 14.5 (1.8%)	104.9	± 7 (56.4)	170.5	± 21 (41.7%)
											Detrital Apatite										

Apatite Fission Track data

Sample	Lithology	Stratigraphic age	Elevation (m)	Latitude	Longitude	U (ppm)	2σ	Grains *n*	Ns	Ni	Counted squares	ζ estimate (Ma.cm^2)	se(ζ) std error on ζ estimate (Ma.cm^2)	P1	2σ se(t) (Frac)	P2	2σ se(t) (Frac)	P3	2σ se(t) (Frac)
CVI-1302	Conglomerate	Miocene	150	10º35'18"	74º05'06"	41	1	35	1382	7662	3350	270.07	6.38	19.2	± 4.2 (17.3%	29.8	± 4.8 (48.8%)	42	± 5.7 (33.9%)
EMP-16	Conglomerate	Lower Miocene	176	10º32'21"	74º03'50"	14	1	38	557	2169	3570	284.52	5.65			21.8	± 4 (41%)	59.9	± 9.3 (59%)
AP-045	Conglomerate	Miocene	55	11º13'12"	73º28'39"	10	0	72	685	2369	5478	284.52	5.65			26.8	± 6.5 (31.3%)	52.3	± 6.3 (68.7%)
EMP-49A	Conglomerate	Miocene	55	11º12'33"	73º30'17"	12	1	8	143	494	780	270.07	6.38			33.4	± 10.6 (72.6%)	59.2	± 36 (27.4%)

Note: *n* = total number of grains counted; binomial peak- fit ages are given 2SE.The percentage of grains in a specíćc peak is also given.

All samples were counted at 1250 dry (100 objective, 1.25 tube factor, 10 oculars). Apatite samples by by A. Piraquive ζ (CN-1) of 284.52 5.65 (1SE). Samples CVI-1302, EMP-16, AP-045, EMP-49A

Zircon Samples EMP-16, EMP-49A, AP-45, AP-46, AP-50 and EMP-35b were counted by E. Pinzón (CN-1 zeta 128.02 1.87).

Zircon Samples CP-088 and CVI-1302 were counted by A. Piraquive (CN-1 zeta 141.03 2.32). Depositional ages after Tschanz (1969)

Chi-squared test: values greater than 5% are considered to pass the test and represent a single age population.

Merged dataset:
C:\BH2\Edna\6-2015\AP-046\AP_046-2.FTZ
C:\BH2\Edna\6-2015\AP-046\AP_046-1.ftz

NEW PARAMETERS - ZETA METHOD

EFFECTIVE TRACK DENSITY FOR FLUENCE MONITOR (tracks/cm^2): 3,06E+05
RELATIVE ERROR (%): 1,16
EFFECTIVE URANIUM CONTENT OF MONITOR (ppm): 50,00
ZETA FACTOR AND STANDARD ERROR (yr cm^2): 126,82 2,05
SIZE OF COUNTER SQUARE (cm^2): 8,30E-07

GRAIN AGES IN ORIGINAL ORDER

Grain no.	RhoS (cm^-2)	(Ns)	RhoI (cm^-2)	(Ni)	Squares	U+/-2s		Grain Age (Ma) Age	--95% CI--	
1	1,33E+06	(33)	1,20E+05	(3)	30	20	21	200.3	66.5	1004.1
2	8,66E+06	(115)	2,26E+05	(3)	16	37	40	670.3	243.2	2896.0
3	4,02E+06	(70)	2,98E+06	(52)	21	488	135	26.0	17.9	38.0
4	2,85E+06	(71)	3,61E+05	(9)	30	59	38	148.8	75.7	339.0
5	4,50E+06	(56)	4,82E+05	(6)	15	79	62	174.2	77.6	494.5
6	4,22E+06	(84)	1,05E+06	(21)	24	172	75	76.6	47.4	130.4
7	6,43E+06	(320)	1,06E+06	(53)	60	174	48	114.9	86.0	153.4
8	7,04E+06	(146)	9,64E+05	(20)	25	158	70	139.0	87.7	234.3
9	2,83E+06	(47)	6,02E+05	(10)	20	99	61	89.3	45.2	199.1
10	1,53E+06	(61)	2,01E+05	(8)	48	33	23	143.6	70.0	348.2
11	5,02E+06	(150)	4,35E+05	(13)	36	71	39	217.3	125.6	416.2
12	2,98E+06	(89)	3,68E+05	(11)	36	60	36	152.9	83.0	317.6
13	3,50E+06	(93)	4,14E+05	(11)	32	68	40	159.7	86.8	331.0
14	1,73E+06	(86)	3,82E+05	(19)	60	62	28	86.5	52.7	151.0
15	7,11E+06	(354)	2,11E+06	(105)	60	345	68	64.7	51.9	80.6
16	1,03E+07	(256)	1,65E+06	(41)	30	269	84	119.5	86.1	170.5
17	1,79E+06	(89)	1,61E+05	(8)	60	26	18	208.3	103.9	495.4
18	3,31E+06	(275)	3,25E+05	(27)	100	53	20	193.4	131.3	298.2
19	3,61E+06	(54)	1,00E+06	(15)	18	164	84	68.9	38.7	131.8
20	1,76E+06	(146)	1,69E+05	(14)	100	28	15	196.9	115.6	368.3
21	6,53E+06	(130)	7,53E+05	(15)	24	123	63	164.2	97.4	301.7
22	9,17E+06	(426)	6,45E+05	(30)	56	106	38	268.1	187.0	400.5
23	1,48E+06	(60)	1,97E+05	(8)	49	32	22	141.3	68.8	342.8
24	1,72E+06	(143)	1,93E+05	(16)	100	32	16	169.4	102.2	304.1
25	3,66E+06	(76)	7,23E+05	(15)	25	118	60	96.6	55.7	181.5
26	6,27E+06	(104)	1,02E+06	(17)	20	168	80	116.5	70.2	208.0
27	9,98E+05	(58)	1,20E+05	(7)	70	20	14	155.5	72.7	404.2
28	7,68E+06	(153)	1,36E+06	(27)	24	222	85	108.4	72.1	169.9
29	5,83E+06	(121)	1,01E+06	(21)	25	166	72	110.0	69.4	184.4
30	3,64E+06	(151)	4,82E+05	(20)	50	79	35	143.7	90.8	241.9
31	3,66E+06	(146)	6,02E+05	(24)	48	99	40	116.2	75.7	187.3
32	1,90E+06	(158)	1,93E+05	(16)	100	32	16	186.9	113.2	334.4
33	5,78E+06	(288)	8,43E+05	(42)	60	138	42	131.1	95.1	185.8
34	1,12E+07	(84)	2,81E+06	(21)	9	460	199	76.6	47.4	130.4
35	4,88E+06	(385)	5,83E+05	(46)	95	95	28	159.7	118.1	221.6
36	5,71E+06	(166)	4,82E+05	(14)	35	79	41	223.4	131.7	416.0
37	3,04E+06	(53)	4,02E+05	(7)	21	66	48	142.2	66.1	371.8
38	1,08E+06	(44)	1,23E+05	(5)	49	20	17	163.7	67.4	528.9
39	2,11E+06	(70)	4,82E+05	(16)	40	79	39	83.6	48.5	154.6
40	7,48E+06	(621)	1,19E+06	(99)	100	195	39	119.8	96.8	148.3
41	8,49E+06	(296)	1,20E+06	(42)	42	197	61	134.7	97.8	190.8
42	4,63E+06	(73)	5,07E+05	(8)	19	83	57	171.4	84.6	411.7
43	2,70E+06	(179)	3,92E+05	(26)	80	64	25	131.4	87.5	206.6
44	3,23E+06	(268)	6,63E+05	(55)	100	108	29	92.9	69.5	124.1
45	2,98E+06	(99)	4,52E+05	(15)	40	74	38	125.5	73.5	233.0
46	2,25E+06	(140)	1,77E+05	(11)	75	29	17	238.8	132.3	486.8
47	6,25E+06	(363)	3,96E+05	(23)	70	65	27	296.9	197.5	471.3
48	3,83E+06	(127)	3,61E+05	(12)	40	59	33	199.5	112.4	395.2
49	1,89E+06	(47)	5,22E+05	(13)	30	85	47	69.1	37.2	139.7
50	1,03E+06	(77)	1,61E+05	(12)	90	26	15	121.8	66.9	246.4
51	4,78E+06	(119)	1,61E+05	(4)	30	26	25	532.4	215.6	1856.3
52	3,49E+06	(290)	4,22E+05	(35)	100	69	23	158.0	111.8	231.0

Merged dataset:
C:\BH2\Edna\6-2015\AP-046\AP_046-2.FTZ
C:\BH2\Edna\6-2015\AP-046\AP_046-1.ftz

Grain no.	RhoS (cm^-2)	(Ns)	RhoI (cm^-2)	(Ni)	Squares	U+/-2s	Grain Age (Ma) Age	--95% CI--	
53	3,33E+06	(276)	4,94E+05	(41)	100	81 25	128.7	93.0	183.3
54	9,24E+05	(46)	1,41E+05	(7)	60	23 17	123.7	56.8	326.0
55	3,99E+06	(53)	6,78E+05	(9)	16	111 72	111.5	55.5	258.0
56	2,61E+06	(26)	2,01E+05	(2)	12	33 42	231.0	62.7	1885.8
57	5,18E+06	(86)	1,14E+06	(19)	20	187 85	86.5	52.7	151.0
58	2,51E+06	(75)	2,01E+05	(6)	36	33 26	232.1	105.3	647.6

Merged dataset:
C:\BH2\Edna\6-2015\AP-046\AP_046-2.FTZ
C:\BH2\Edna\6-2015\AP-046\AP_046-1.ftz

NEW PARAMETERS - ZETA METHOD

EFFECTIVE TRACK DENSITY FOR FLUENCE MONITOR (tracks/cm^2): 3,06E+05
RELATIVE ERROR (%): 1,17
EFFECTIVE URANIUM CONTENT OF MONITOR (ppm): 50,00
ZETA FACTOR AND STANDARD ERROR (yr cm^2): 126,82 2,05
SIZE OF COUNTER SQUARE (cm^2): 8,30E-07

Grain no.	RhoS (cm^-2)	(Ns)	RhoI (cm^-2)	(Ni)	Squares	U+/-2s	Grain Age (Ma) Age	--95% CI--	
59	6,02E+06	(250)	8,19E+05	(34)	50	134 46	140.5	98.6	207.4
60	4,06E+06	(101)	3,61E+05	(9)	30	59 38	210.7	109.3	472.4
61	2,53E+06	(147)	3,96E+05	(23)	70	65 27	122.1	79.0	198.8
62	6,69E+06	(50)	9,37E+05	(7)	9	153 112	134.5	62.2	352.6
63	1,97E+06	(80)	1,72E+05	(7)	49	28 21	213.6	101.9	545.7
64	6,02E+06	(100)	1,45E+06	(24)	20	236 96	79.9	51.1	130.8
65	6,61E+06	(351)	1,45E+06	(77)	64	237 54	87.3	68.2	111.8
66	9,29E+05	(27)	2,41E+05	(7)	35	39 29	73.2	31.7	200.5
67	4,76E+06	(79)	7,83E+05	(13)	20	128 70	115.6	64.8	227.2
68	3,27E+06	(114)	5,45E+05	(19)	42	89 40	114.6	70.8	197.5
69	3,10E+06	(108)	5,45E+05	(19)	42	89 40	108.6	66.9	187.6
70	3,07E+06	(252)	4,75E+05	(39)	99	78 25	123.7	88.5	178.2
71	4,70E+06	(195)	7,23E+05	(30)	50	118 43	124.3	84.9	189.3
72	1,14E+06	(57)	2,41E+05	(12)	60	39 22	90.5	48.7	186.1
73	1,08E+06	(27)	2,81E+05	(7)	30	46 34	73.2	31.7	200.5
74	6,27E+06	(156)	1,04E+06	(26)	30	171 66	114.8	76.0	181.3
75	7,92E+06	(322)	1,20E+06	(49)	49	197 56	125.9	93.4	173.7
76	5,16E+06	(60)	1,12E+06	(13)	14	183 100	88.1	48.4	175.5
77	1,45E+06	(42)	7,23E+05	(21)	35	118 51	38.5	22.4	68.7
78	6,20E+06	(72)	1,46E+06	(17)	14	239 114	81.1	47.7	147.1
79	1,42E+06	(59)	1,69E+05	(7)	50	28 20	158.3	74.1	411.2
80	4,31E+06	(143)	3,92E+05	(13)	40	64 35	207.6	119.7	398.3
81	3,15E+06	(94)	3,68E+05	(11)	36	60 36	161.6	87.9	334.8
82	1,05E+06	(21)	4,02E+05	(8)	24	66 45	50.1	21.6	131.7
83	5,16E+06	(210)	8,85E+05	(36)	49	145 48	111.8	78.6	164.0
84	2,28E+06	(34)	2,68E+05	(4)	18	44 41	157.4	58.5	610.2
85	1,41E+06	(35)	3,61E+05	(9)	30	59 38	74.0	35.4	176.1
86	3,51E+06	(70)	7,03E+05	(14)	24	115 60	95.4	53.9	184.0
87	3,21E+06	(24)	1,34E+05	(1)	9	22 36	396.5	75.5	8889.8
88	7,03E+06	(70)	1,10E+06	(11)	12	180 107	120.8	64.6	253.7
89	3,66E+06	(73)	6,02E+05	(12)	24	98 56	115.7	63.3	234.6
90	3,60E+06	(209)	4,30E+05	(25)	70	70 28	159.3	105.9	251.6
91	7,23E+06	(108)	1,27E+06	(19)	18	208 94	108.6	66.9	187.6
92	8,78E+05	(51)	4,99E+05	(29)	70	82 30	34.0	21.2	55.6
93	6,57E+06	(229)	8,89E+05	(31)	42	145 52	141.1	97.4	212.5
94	2,74E+06	(91)	1,57E+06	(52)	40	256 71	33.8	23.8	48.6
95	1,78E+06	(59)	9,34E+05	(31)	40	153 54	36.7	23.5	58.8
96	4,95E+06	(411)	6,75E+05	(56)	100	110 29	139.6	105.7	184.3
97	7,88E+06	(157)	6,53E+05	(13)	24	107 58	227.6	131.7	435.1
98	4,47E+06	(89)	9,54E+05	(19)	24	156 71	89.6	54.7	156.2
99	1,87E+06	(31)	2,41E+05	(4)	20	39 37	143.7	52.9	561.3
100	7,11E+06	(354)	1,20E+06	(60)	60	197 51	112.6	85.6	147.8
POOLED	3,79E+06	(13884)	5,92E+05	(2172)	4417	97 5	122.7	115.6	130.2

CHI^2 PROBABILITY (%): 0.0

POOLED AGE W/ 68% CONF. INTERVAL(Ma): 122.7, 119.0 -- 126.4 (-3.6 +3.8)
95% CONF. INTERVAL(Ma): 115.6 -- 130.2 (-7.0 +7.5)

CENTRAL AGE W/ 68% CONF. INTERVAL(Ma): 117.6, 111.0 -- 124.5 (-6.6 +6.9)
95% CONF. INTERVAL(Ma): 105.1 -- 131.6 (-12.5 +14.0)
AGE DISPERSION (%): 47.2

Merged dataset:
C:\BH2\Edna\6-2015\AP-046\AP_046-2.FTZ
C:\BH2\Edna\6-2015\AP-046\AP_046-1.ftz

FIT OPTION: Best-fit peaks using the binomial model of Galbraith and Green

INITIAL GUESS FOR MODEL PARAMETERS (number of peaks to fit = 4)

Peak #.	Peak Age	Theta	Fraction(%)	Count
1.	64.80	0.771	9.6	9.65
2.	86.80	0.819	20.8	20.82
3.	122.60	0.865	41.5	41.48
4.	202.50	0.914	16.2	16.21

Total range for grain ages:	26,0 to 609,7 Ma
Number of active grains (Num. used for fit):	100
Number of removed grains:	0
Degrees of freedom for fit:	93
Average of the SE(Z)'s for the grains:	0,31
Estimated width of peaks in PD plot in Z units:	0,36

PARAMETERS FOR BEST-FIT PEAKS

* *Standard error for peak age includes group error*
* *Peak width is for PD plot assuming a kernel factor = 0.60*

#.	Peak Age(Ma)	68%CI	95%CI	W(Z)	Frac(%)	SE,%	Count
1.	32.9	-3,0 ...+3,3	-5,7 ...+6,9	0.25	5.1	2.3	5.1
2.	79.6	-7,3 ...+8,1	-13,7 ...+16,5	0.22	9.0	6.1	9.0
3.	129.4	-6,0 ...+6,3	-11,6 ...+12,7	0.27	74.1	8.0	74.1
4.	250.6	-30,8 ...+35,1	-56,9 ...+73,3	0.34	11.7	6.2	11.7

Log-likelihood for best fit:	-324,328
Chi-squared value for best fit:	93,580
Reduced chi-squared value:	1,006
Probability for F test:	4%
Condition number for COVAR matrix:	51,79
Number of iterations:	17

Merged dataset:
C:\BH2\Edna\6-2015\AP-046\AP_046-2.FTZ
C:\BH2\Edna\6-2015\AP-046\AP_046-1.ftz

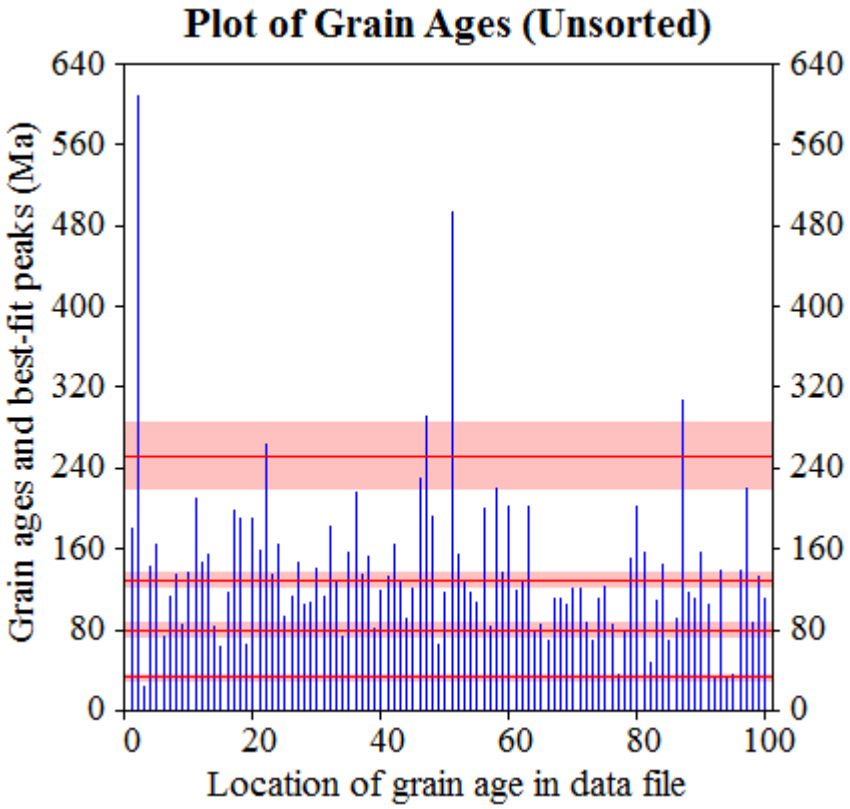

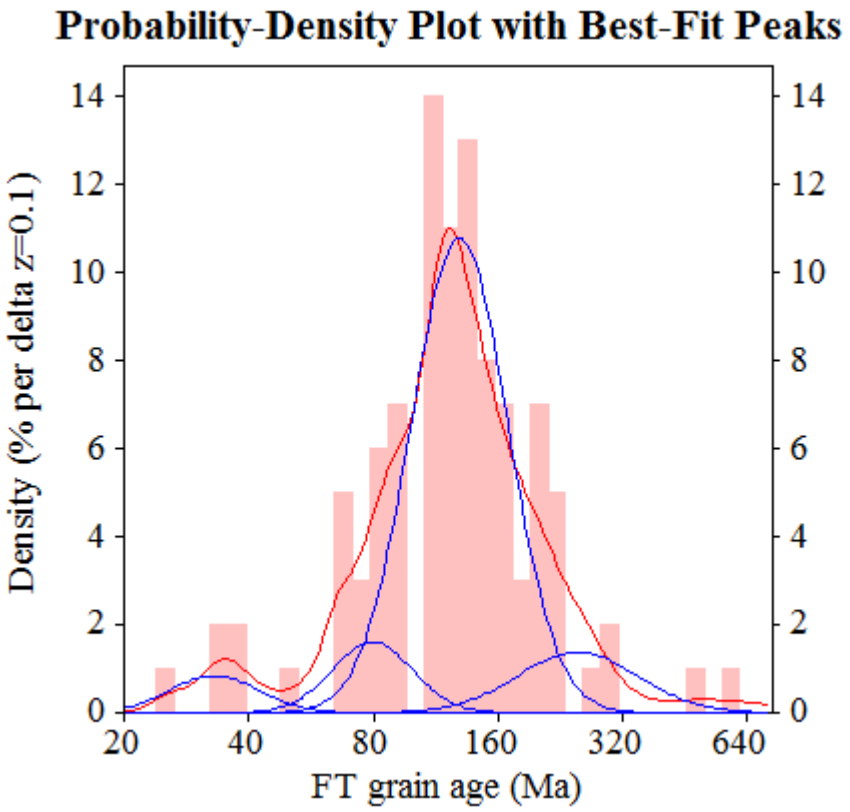

Merged dataset:
C:\BH2\Edna\6-2015\AP-046\AP_046-2.FTZ
C:\BH2\Edna\6-2015\AP-046\AP_046-1.ftz

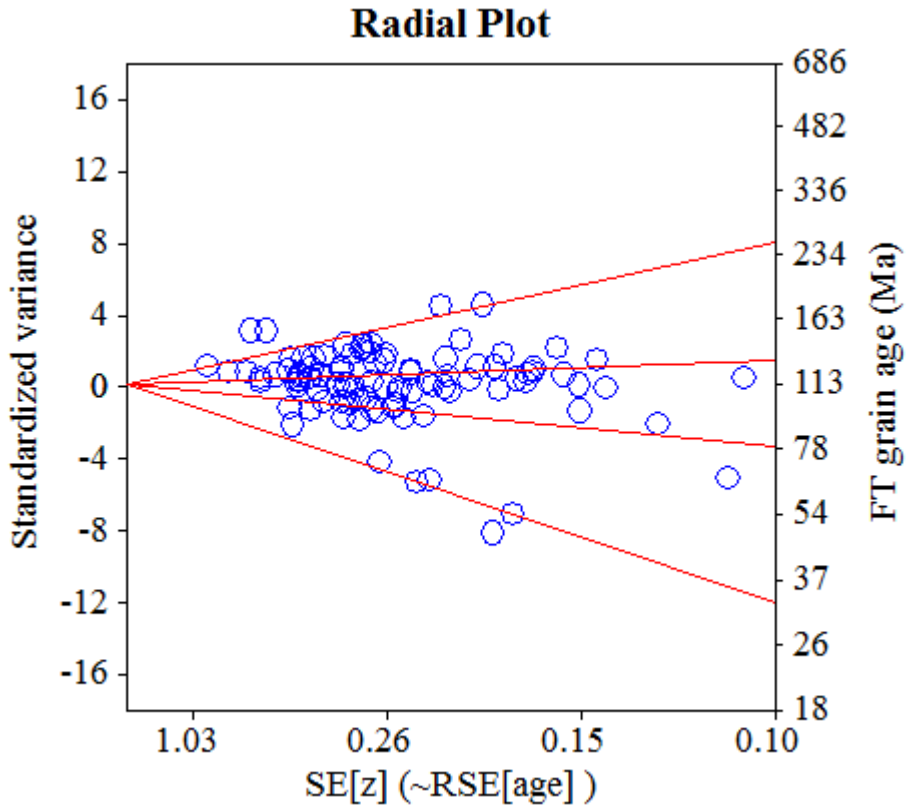

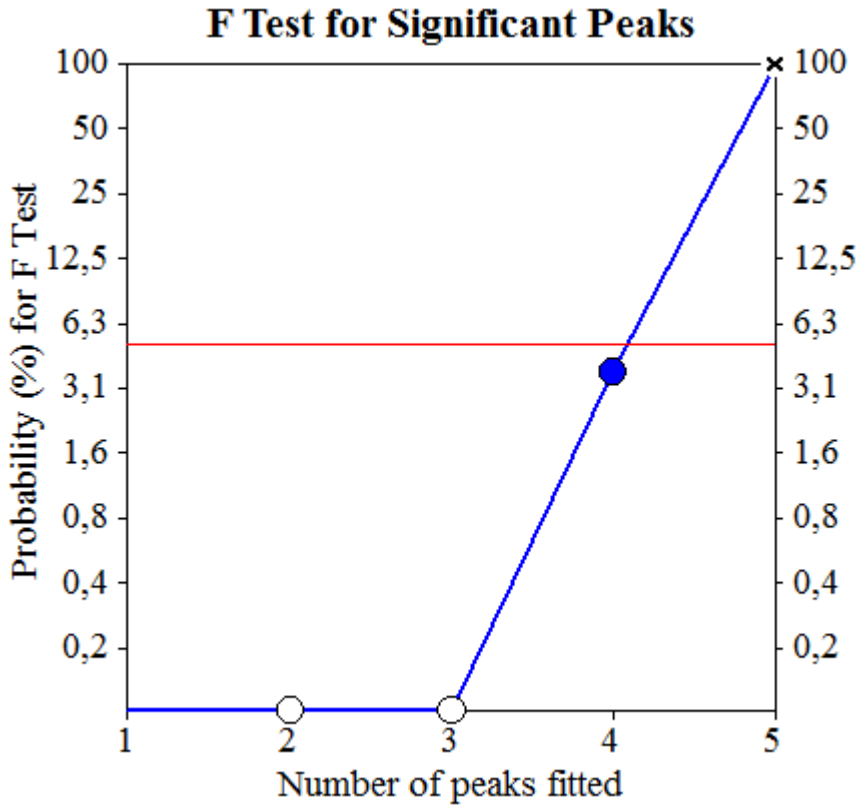

Merged dataset:
C:\BH2\Edna\6-2015\AP-050\AP_050-2.ftz
C:\BH2\Edna\6-2015\AP-050\AP_050-1.ftz

NEW PARAMETERS - ZETA METHOD

EFFECTIVE TRACK DENSITY FOR FLUENCE MONITOR (tracks/cm^2): 3,04E+05
RELATIVE ERROR (%): 1,14
EFFECTIVE URANIUM CONTENT OF MONITOR (ppm): 50,00
ZETA FACTOR AND STANDARD ERROR (yr cm^2): 126,82 2,05
SIZE OF COUNTER SQUARE (cm^2): 8,30E-07

GRAIN AGES IN ORIGINAL ORDER

Grain no.	RhoS (cm^-2)	(Ns)	RhoI (cm^-2)	(Ni)	Squares	U+/-2s	Grain Age (Ma) Age	--95% CI--	
1	4,13E+06	(144)	2,01E+05	(7)	42	33 24	377.2	185.1	934.5
2	3,84E+06	(255)	1,93E+06	(128)	80	317 56	38.2	30.8	47.3
3	9,94E+06	(165)	2,23E+06	(37)	20	366 120	85.2	59.6	125.4
4	4,53E+06	(263)	1,45E+06	(84)	70	237 52	59.8	46.7	76.5
5	6,66E+06	(221)	1,08E+06	(36)	40	178 59	117.0	82.4	171.4
6	6,49E+06	(264)	6,64E+05	(27)	49	109 42	185.0	125.5	285.6
7	2,14E+06	(71)	2,71E+05	(9)	40	45 29	148.2	75.4	337.7
8	5,12E+06	(153)	1,41E+06	(42)	36	231 71	69.7	49.5	100.7
9	5,66E+06	(94)	3,01E+05	(5)	20	49 42	342.8	148.3	1053.0
10	4,82E+06	(120)	1,85E+06	(46)	30	303 89	50.1	35.4	72.0
11	1,70E+06	(113)	2,11E+05	(14)	80	35 18	152.4	88.5	287.7
12	5,71E+06	(166)	7,23E+05	(21)	35	119 51	149.8	95.8	248.3
13	4,72E+06	(47)	1,00E+06	(10)	12	165 102	89.0	45.1	198.4
14	4,80E+06	(319)	5,87E+05	(39)	80	96 31	155.4	111.9	222.5
15	3,17E+06	(158)	1,51E+06	(75)	60	247 57	40.3	30.6	53.1
16	6,55E+06	(136)	1,30E+06	(27)	25	214 82	96.0	63.6	151.2
17	2,86E+06	(190)	5,57E+05	(37)	80	92 30	98.0	69.0	143.6
18	3,41E+06	(198)	1,70E+06	(99)	70	280 56	38.3	30.0	48.8
19	5,69E+06	(85)	1,54E+06	(23)	18	253 104	70.6	44.4	117.5
20	4,39E+06	(91)	1,54E+06	(32)	25	253 89	54.5	36.2	84.4
21	4,42E+06	(33)	6,69E+05	(5)	9	110 94	122.8	49.2	405.1
22	3,98E+06	(132)	1,69E+06	(56)	40	277 74	45.3	32.9	63.1
23	4,60E+06	(382)	1,57E+06	(130)	100	257 45	56.3	46.0	68.8
24	8,43E+06	(84)	1,71E+06	(17)	12	280 134	94.0	55.9	169.2
25	2,33E+06	(31)	7,53E+05	(10)	16	124 76	58.9	28.5	135.4
26	5,01E+06	(208)	1,37E+06	(57)	50	226 60	69.9	52.1	95.5
27	4,46E+06	(148)	1,96E+06	(65)	40	322 80	43.5	32.5	58.2
28	7,99E+06	(232)	1,20E+06	(35)	35	198 67	126.2	88.7	185.6
29	4,81E+06	(399)	9,76E+05	(81)	100	160 36	93.8	73.8	119.2
30	6,44E+06	(171)	7,91E+05	(21)	32	130 56	154.2	98.8	255.5
31	5,20E+06	(108)	1,73E+06	(36)	25	285 95	57.5	39.2	86.4
32	8,19E+06	(408)	2,53E+06	(126)	60	416 75	62.0	50.6	75.8
33	3,41E+06	(198)	6,88E+05	(40)	70	113 36	94.5	67.3	136.5
34	4,99E+06	(145)	5,51E+05	(16)	35	90 45	171.1	103.3	306.9
35	5,16E+06	(214)	1,13E+06	(47)	50	186 54	87.1	63.5	122.2
36	3,04E+06	(252)	1,00E+06	(83)	100	164 36	58.0	45.2	74.4
37	4,55E+06	(378)	1,49E+06	(124)	100	245 44	58.3	47.5	71.6
38	5,62E+06	(112)	1,46E+06	(29)	24	239 88	73.8	49.0	115.4
39	1,87E+06	(124)	3,31E+05	(22)	80	54 23	107.2	68.3	177.5
40	2,54E+06	(76)	6,36E+05	(19)	36	104 47	76.3	46.0	133.9
41	8,73E+06	(87)	1,51E+06	(15)	12	247 126	110.0	63.9	205.4
42	5,09E+06	(296)	2,08E+06	(121)	70	342 63	46.9	37.8	58.0
43	5,31E+06	(141)	2,90E+06	(77)	32	476 109	35.0	26.5	46.3
44	4,61E+06	(268)	1,03E+06	(60)	70	170 44	85.0	64.2	112.4
45	4,50E+06	(56)	1,61E+06	(20)	15	264 117	53.5	31.8	94.4
46	5,50E+06	(219)	8,53E+05	(34)	48	140 48	122.7	85.7	181.7
47	5,83E+06	(121)	9,64E+05	(20)	25	158 70	115.0	71.9	195.1
48	6,02E+06	(80)	2,33E+06	(31)	16	383 137	49.5	32.4	77.6
49	4,75E+06	(197)	2,55E+06	(106)	50	420 82	35.6	28.1	45.2
50	6,78E+06	(563)	2,22E+06	(184)	100	364 54	58.6	49.5	69.5
51	3,54E+06	(294)	1,30E+06	(108)	100	214 41	52.1	41.7	65.1
52	5,83E+06	(237)	2,26E+06	(92)	49	372 78	49.3	38.7	62.8

Merged dataset:
C:\BH2\Edna\6-2015\AP-050\AP_050-2A.FTZ
C:\BH2\Edna\6-2015\AP-050\AP_050-1.ftz

Grain no.	RhoS (cm^-2)	(Ns)	RhoI (cm^-2)	(Ni)	Squares	U+/-2s	Grain Age (Ma) Age	--95% CI--	
53	4,75E+06	(197)	1,54E+06	(64)	50	253 63	58.7	44.2	77.8
54	4,67E+06	(388)	1,42E+06	(118)	100	234 43	62.9	51.1	77.5
55	4,55E+06	(151)	1,75E+06	(58)	40	287 75	50.0	36.8	68.9
56	5,42E+06	(135)	1,73E+06	(43)	30	284 86	60.2	42.5	87.0
57	4,92E+06	(204)	1,88E+06	(78)	50	309 70	50.0	38.5	64.9
58	4,71E+06	(313)	1,70E+06	(113)	80	280 53	53.0	42.7	65.9
59	3,52E+06	(292)	1,61E+06	(134)	100	265 46	41.8	34.0	51.4
60	3,10E+06	(90)	1,10E+06	(32)	35	181 64	53.9	35.8	83.5
61	1,19E+07	(158)	1,43E+06	(19)	16	235 107	157.4	98.6	268.2
62	1,05E+07	(174)	4,28E+06	(71)	20	703 167	46.8	35.5	61.7
63	5,07E+06	(202)	2,11E+06	(84)	48	346 76	46.0	35.6	59.4
64	5,64E+06	(117)	7,23E+05	(15)	25	119 60	147.4	87.0	271.9
65	6,02E+06	(300)	2,41E+06	(120)	60	396 73	47.9	38.7	59.3
66	4,54E+06	(226)	1,65E+06	(82)	60	270 60	52.7	40.9	67.9
67	4,42E+06	(55)	8,03E+05	(10)	15	132 81	103.9	53.4	229.6
68	4,72E+06	(274)	1,22E+06	(71)	70	201 48	73.6	56.6	95.5
69	2,65E+06	(77)	1,96E+06	(57)	35	322 85	26.0	18.2	37.3
70	4,08E+06	(339)	2,14E+06	(178)	100	352 53	36.6	30.4	44.0
71	3,95E+06	(164)	2,19E+06	(91)	50	360 76	34.5	26.7	44.7
72	4,82E+06	(240)	1,79E+06	(89)	60	294 62	51.6	40.4	65.9
73	5,06E+06	(126)	7,23E+05	(18)	30	119 55	132.7	81.5	231.3
74	2,41E+06	(40)	2,41E+05	(4)	20	40 37	183.7	69.4	703.2
75	4,73E+06	(110)	4,73E+05	(11)	28	78 46	187.7	102.9	386.3
76	4,04E+06	(67)	2,17E+06	(36)	20	356 118	35.8	23.6	55.3
77	4,30E+06	(125)	7,23E+05	(21)	35	119 51	113.2	71.6	189.4

Merged dataset:
C:\BH2\Edna\6-2015\AP-050\AP_050-2A.FTZ
C:\BH2\Edna\6-2015\AP-050\AP_050-1.ftz

NEW PARAMETERS - ZETA METHOD

EFFECTIVE TRACK DENSITY FOR FLUENCE MONITOR (tracks/cm^2): 3,05E+05
RELATIVE ERROR (%): 1,14
EFFECTIVE URANIUM CONTENT OF MONITOR (ppm): 50,00
ZETA FACTOR AND STANDARD ERROR (yr cm^2): 126,82 2,05
SIZE OF COUNTER SQUARE (cm^2): 8,30E-07

Grain no.	RhoS (cm^-2)	(Ns)	RhoI (cm^-2)	(Ni)	Squares	U+/-2s	Grain Age (Ma) Age	--95% CI--	
78	5,27E+06	(328)	1,70E+06	(106)	75	279 55	59.3	47.5	73.9
79	3,57E+06	(296)	1,19E+06	(99)	100	196 39	57.3	45.5	72.0
80	3,19E+06	(238)	6,56E+05	(49)	90	108 31	93.0	68.4	129.2
81	3,23E+06	(268)	1,36E+06	(113)	100	223 42	45.5	36.4	56.8
82	3,60E+06	(239)	1,17E+06	(78)	80	193 44	58.6	45.3	75.7
83	4,56E+06	(159)	2,18E+06	(76)	42	358 82	40.1	30.4	52.7
84	3,98E+06	(330)	1,51E+06	(125)	100	247 44	50.6	41.1	62.3
85	3,96E+06	(263)	1,45E+06	(96)	80	237 49	52.5	41.5	66.4
86	1,39E+06	(115)	3,37E+05	(28)	100	55 21	78.6	51.9	123.6
87	5,46E+06	(136)	2,17E+06	(54)	30	356 97	48.4	35.1	67.7
88	2,74E+06	(91)	6,93E+05	(23)	40	114 47	75.6	47.8	125.5
89	6,58E+06	(131)	2,61E+06	(52)	24	428 119	48.4	34.9	68.2
90	2,60E+06	(54)	1,20E+06	(25)	25	198 78	41.5	25.5	69.7
91	1,36E+06	(54)	4,52E+05	(18)	48	74 35	57.4	33.4	104.3
92	3,92E+06	(130)	1,54E+06	(51)	40	252 70	49.0	35.3	69.2
93	4,63E+06	(123)	2,00E+06	(53)	32	327 90	44.6	32.1	62.9
POOLED	4,40E+06	(17166)	1,37E+06	(5347)	4696	225 8	61.7	58.7	64.8

CHI^2 PROBABILITY (%): 0.0

POOLED AGE W/ 68% CONF. INTERVAL(Ma): 61.7, 60.1 -- 63.2 (-1.5 +1.6)
95% CONF. INTERVAL(Ma): 58.7 -- 64.8 (-3.0 +3.1)

CENTRAL AGE W/ 68% CONF. INTERVAL(Ma): 65.6, 62.4 -- 69.0 (-3.2 +3.4)
95% CONF. INTERVAL(Ma): 59.5 -- 72.4 (-6.2 +6.8)
AGE DISPERSION (%): 41.2

Merged dataset:
C:\BH2\Edna\6-2015\AP-050\AP_050-2A.FTZ
C:\BH2\Edna\6-2015\AP-050\AP_050-1.ftz

FIT OPTION: Best-fit peaks using the binomial model of Galbraith and Green

INITIAL GUESS FOR MODEL PARAMETERS (number of peaks to fit = 4)

Peak #.	Peak Age	Theta	Fraction(%)	Count
1.	36.60	0.655	17.4	16.17
2.	48.90	0.718	41.5	38.57
3.	61.70	0.762	32.4	30.10
4.	361.60	0.951	1.3	1.21

Total range for grain ages:	26,0 to 361,6 Ma
Number of active grains (Num. used for fit):	93
Number of removed grains:	0
Degrees of freedom for fit:	86
Average of the SE(Z)'s for the grains:	0,21
Estimated width of peaks in PD plot in Z units:	0,24

PARAMETERS FOR BEST-FIT PEAKS

* *Standard error for peak age includes group error*
* *Peak width is for PD plot assuming a kernel factor = 0.60*

#.	Peak Age(Ma)	68%CI	95%CI	W(Z)	Frac(%)	SE,%	Count
1.	38.9	-2,2 ...+2,3	-4,2 ...+4,7	0.15	14.6	5.5	13.6
2.	54.8	-1,8 ...+1,9	-3,5 ...+3,8	0.16	47.3	6.9	44.0
3.	94.0	-7,2 ...+7,7	-13,5 ...+15,8	0.22	20.1	6.4	18.7
4.	154.8	-13,5 ...+14,7	-25,3 ...+30,1	0.29	18.0	6.2	16.7

Log-likelihood for best fit:	-380,676
Chi-squared value for best fit:	93,978
Reduced chi-squared value:	1,093
Probability for F test:	0%
Condition number for COVAR matrix:	20,75
Number of iterations:	14

Merged dataset:
C:\BH2\Edna\6-2015\AP-050\AP_050-2A.FTZ
C:\BH2\Edna\6-2015\AP-050\AP_050-1.ftz

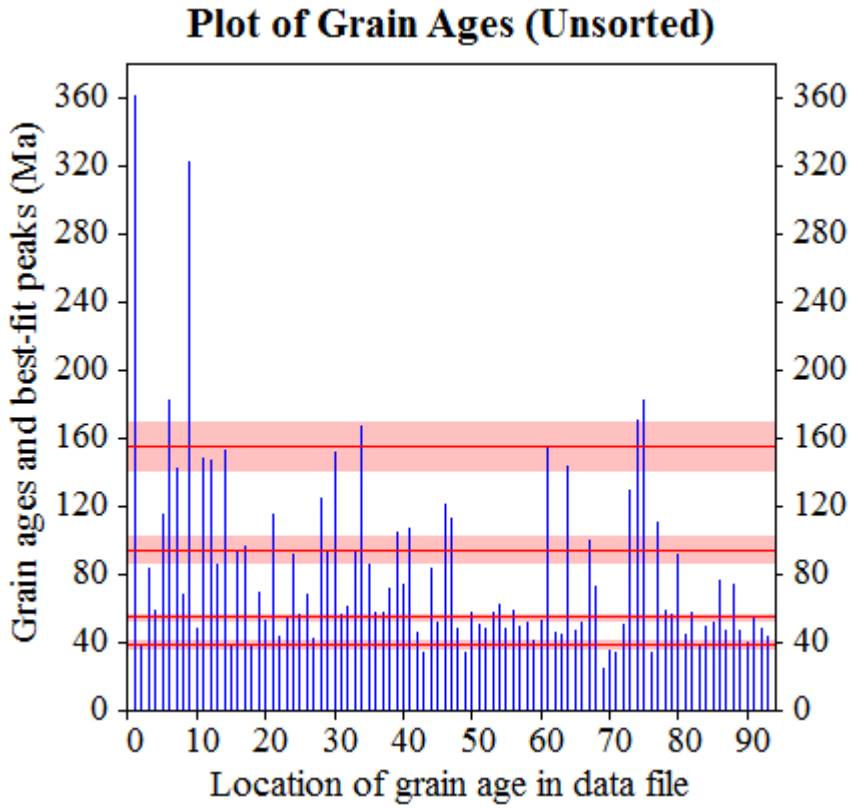

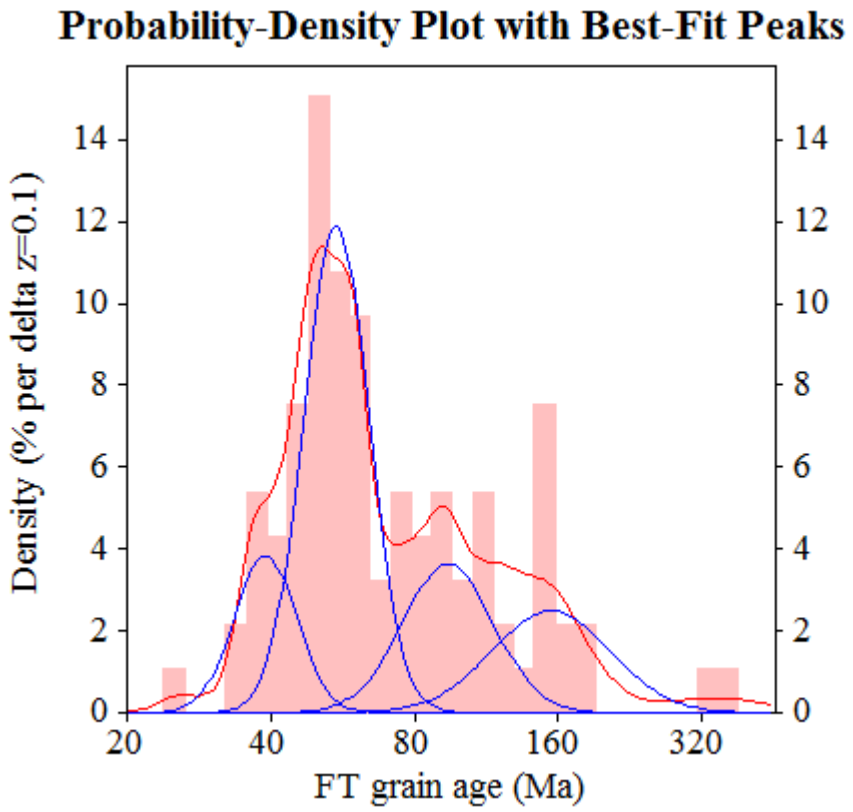

Merged dataset:
C:\BH2\Edna\6-2015\AP-050\AP_050-2A.FTZ
C:\BH2\Edna\6-2015\AP-050\AP_050-1.ftz

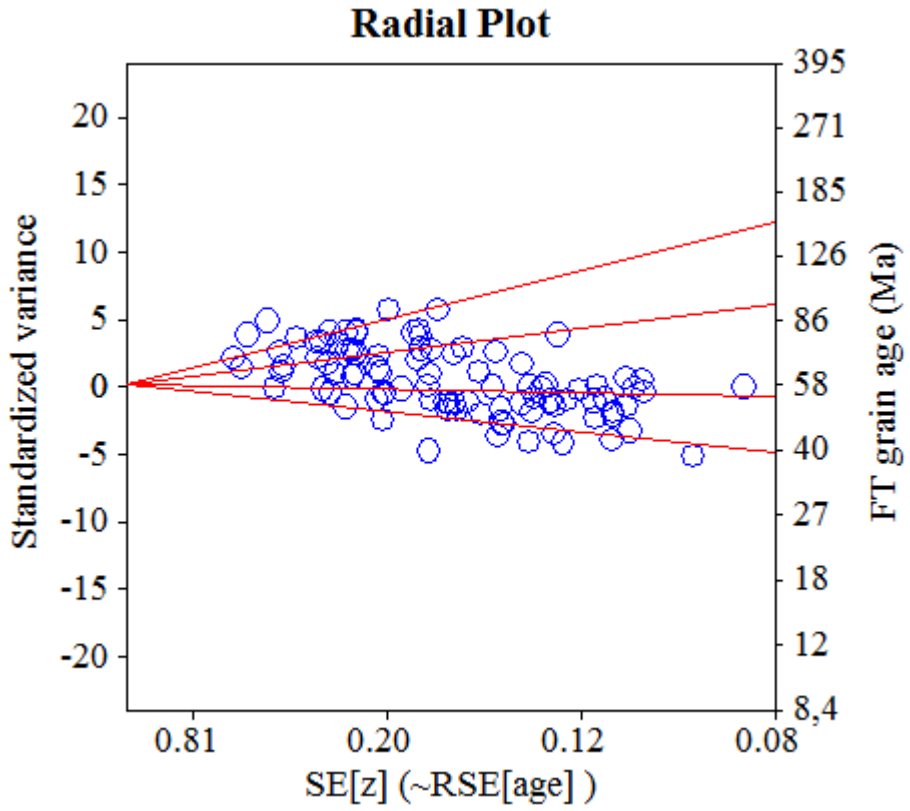

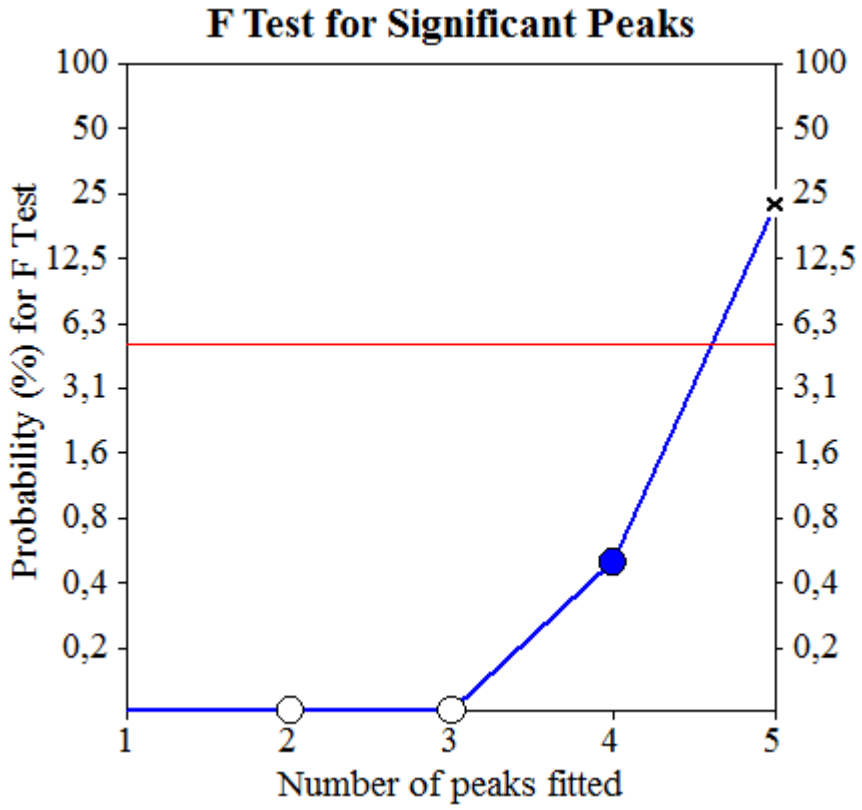

Datafile: C:\BH2\Edna\12-2015\AP-045\AP_45_12_2015-19.ftz
Title: Sample No. AP-45 Irr 12-2015-19

NEW PARAMETERS - ZETA METHOD

EFFECTIVE TRACK DENSITY FOR FLUENCE MONITOR (tracks/cm^2): 2,74E+05
RELATIVE ERROR (%): 1,20
EFFECTIVE URANIUM CONTENT OF MONITOR (ppm): 50,00
ZETA FACTOR AND STANDARD ERROR (yr cm^2): 128,02 1,87
SIZE OF COUNTER SQUARE (cm^2): 8,30E-07

GRAIN AGES IN ORIGINAL ORDER

Grain	RhoS	(Ns)	RhoI	(Ni)	Squares	U+/-2s		Grain Age (Ma)		
no.	(cm^-2)		(cm^-2)					Age	--95% CI--	
1	7,95E+05	(66)	1,08E+05	(9)	100	20	13	125.2	63.3	286.7
2	3,71E+06	(148)	5,77E+05	(23)	48	106	44	111.0	71.8	180.8
3	3,49E+06	(87)	3,21E+05	(8)	30	59	40	184.3	91.8	439.7
4	2,09E+06	(97)	3,44E+05	(16)	56	63	31	104.4	61.8	190.3
5	2,23E+06	(185)	3,01E+05	(25)	100	55	22	127.5	84.4	202.3
6	4,43E+06	(92)	4,34E+05	(9)	25	79	51	173.7	89.6	391.7
7	3,22E+06	(267)	3,86E+05	(32)	100	70	25	143.8	100.1	214.5
8	1,36E+06	(113)	2,29E+05	(19)	100	42	19	102.5	63.3	177.0
9	9,29E+05	(27)	2,07E+05	(6)	35	38	30	76.7	31.8	229.3
10	1,31E+06	(109)	1,45E+05	(12)	100	26	15	155.2	86.8	309.8
11	4,19E+06	(87)	9,64E+05	(20)	25	176	78	75.2	46.2	129.5
12	4,60E+06	(191)	5,30E+05	(22)	50	97	41	149.2	96.7	243.8
13	5,07E+06	(202)	1,15E+06	(46)	48	211	62	76.2	55.3	107.5
14	2,75E+06	(137)	5,02E+05	(25)	60	92	36	94.7	62.0	151.7
15	2,80E+06	(232)	4,22E+05	(35)	100	77	26	114.6	80.5	168.6
16	1,05E+06	(87)	8,43E+04	(7)	100	15	11	209.6	100.4	534.6
17	1,13E+06	(94)	1,45E+05	(12)	100	26	15	134.1	74.4	269.3
18	2,24E+06	(67)	2,68E+05	(8)	36	49	34	142.4	69.9	344.2
19	3,81E+06	(316)	5,06E+05	(42)	100	93	28	129.9	94.5	183.9
20	2,97E+06	(74)	2,81E+05	(7)	30	51	38	178.7	84.9	459.6
21	5,22E+06	(52)	9,04E+05	(9)	12	165	107	98.9	49.2	229.4
22	2,77E+06	(92)	3,61E+05	(12)	40	66	37	131.3	72.8	263.8
23	4,18E+06	(104)	7,23E+05	(18)	30	132	62	99.6	60.6	175.0
24	2,01E+06	(100)	1,81E+05	(9)	60	33	21	188.6	97.7	423.7
25	2,74E+06	(205)	3,21E+05	(24)	90	59	24	146.9	96.9	234.6
26	3,06E+06	(203)	7,08E+05	(47)	80	129	38	75.0	54.5	105.4
27	6,36E+06	(132)	1,06E+06	(22)	25	194	82	103.5	66.2	171.1
28	3,94E+06	(327)	6,14E+05	(51)	100	112	31	111.0	82.7	152.2
29	4,56E+06	(227)	5,02E+05	(25)	60	92	36	156.1	104.0	246.2
30	2,18E+06	(152)	5,88E+05	(41)	84	108	33	64.4	45.5	93.4
31	9,11E+06	(121)	1,66E+06	(22)	16	303	128	95.0	60.5	157.5
32	3,92E+06	(130)	2,41E+05	(8)	40	44	30	273.2	138.6	640.2
33	3,78E+06	(314)	4,94E+05	(41)	100	90	28	132.2	95.8	187.9
34	1,83E+06	(152)	1,93E+05	(16)	100	35	17	162.7	98.3	291.8
35	9,64E+05	(80)	9,64E+04	(8)	100	18	12	169.6	84.1	406.5
36	2,37E+06	(197)	2,05E+05	(17)	100	37	18	198.0	122.3	346.0
37	4,47E+06	(371)	5,54E+05	(46)	100	101	30	139.2	102.8	193.5
38	2,09E+06	(111)	4,89E+05	(26)	64	89	35	74.0	48.2	118.4
39	1,98E+06	(164)	2,41E+05	(20)	100	44	19	141.0	89.3	236.9
40	2,68E+06	(80)	4,69E+05	(14)	36	86	45	98.3	56.0	188.5
41	7,63E+06	(95)	1,12E+06	(14)	15	206	108	116.6	67.0	221.8
42	3,86E+06	(96)	7,63E+05	(19)	30	139	63	87.2	53.4	151.6
43	3,11E+06	(258)	6,75E+05	(56)	100	123	33	79.5	59.5	106.0
44	6,21E+05	(33)	5,65E+04	(3)	64	10	11	181.2	60.1	913.6
45	1,55E+06	(129)	2,89E+05	(24)	100	53	21	92.9	60.2	150.5
46	1,99E+06	(165)	2,89E+05	(24)	100	53	21	118.6	77.6	190.5
47	2,60E+06	(216)	5,42E+05	(45)	100	99	29	83.2	60.4	117.6
48	3,29E+06	(134)	2,21E+05	(9)	49	40	26	251.3	131.8	557.8
49	1,80E+06	(149)	3,98E+05	(33)	100	73	25	78.3	53.6	118.0
50	3,52E+06	(146)	7,95E+05	(33)	50	145	50	76.7	52.5	115.8
51	7,57E+06	(157)	1,35E+06	(28)	25	247	93	97.0	65.0	150.8
52	4,24E+06	(88)	1,06E+06	(22)	25	194	82	69.3	43.3	116.4
53	5,28E+06	(438)	1,01E+06	(84)	100	185	40	90.1	71.3	113.9

Datafile: C:\BH2\Edna\12-2015\AP-045\AP_45_12_2015-19.ftz
Title: Sample No. AP-45 Irr 12-2015-19

Grain no.	RhoS (cm^-2)	(Ns)	RhoI (cm^-2)	(Ni)	Squares	U+/-2s		Grain Age (Ma) Age	--95% CI--	
54	6,84E+06	(142)	1,20E+06	(25)	25	220	87	98.1	64.3	157.0
55	2,43E+06	(202)	3,98E+05	(33)	100	73	25	105.8	73.4	158.1
56	1,95E+06	(162)	3,01E+05	(25)	100	55	22	111.8	73.7	178.1
57	2,25E+06	(56)	2,41E+05	(6)	30	44	35	157.6	70.1	448.3
58	4,26E+06	(99)	6,02E+05	(14)	28	110	58	121.4	70.0	230.6
59	4,59E+06	(137)	1,94E+06	(58)	36	355	93	41.2	30.1	57.0
60	3,94E+06	(229)	9,98E+05	(58)	70	183	48	68.2	51.1	90.9
61	3,42E+06	(284)	4,46E+05	(37)	100	81	27	132.5	94.4	192.0
62	4,85E+06	(322)	1,02E+06	(68)	80	187	45	81.8	62.9	106.2
63	1,10E+06	(91)	1,33E+05	(11)	100	24	14	141.4	76.7	293.7
64	2,46E+06	(204)	3,86E+05	(32)	100	70	25	110.2	76.1	165.5
65	2,91E+06	(145)	5,02E+05	(25)	60	92	36	100.2	65.7	160.2
66	1,93E+06	(160)	3,49E+05	(29)	100	64	24	95.4	64.4	147.3
67	4,26E+06	(212)	6,02E+05	(30)	60	110	40	122.0	83.5	185.3
68	3,33E+06	(276)	6,75E+05	(56)	100	123	33	85.0	63.8	113.1
69	4,54E+06	(377)	4,58E+05	(38)	100	84	27	170.7	122.9	244.8
70	7,33E+06	(219)	9,71E+05	(29)	36	177	65	130.2	88.8	199.1
71	4,58E+06	(380)	5,30E+05	(44)	100	97	29	149.0	109.4	208.4
72	2,95E+06	(88)	4,02E+05	(12)	36	73	42	125.6	69.5	253.0
73	1,77E+06	(88)	3,01E+05	(15)	60	55	28	101.0	58.7	188.6
74	5,45E+06	(226)	8,43E+05	(35)	50	154	52	111.6	78.4	164.4
75	3,73E+06	(310)	7,35E+05	(61)	100	134	34	87.7	66.6	115.3
76	3,69E+06	(230)	4,66E+05	(29)	75	85	31	136.7	93.4	208.7
77	6,52E+06	(379)	1,22E+06	(71)	70	223	53	92.1	71.5	118.7
78	2,43E+06	(97)	4,02E+05	(16)	48	73	36	104.4	61.8	190.3
79	4,92E+06	(204)	7,47E+05	(31)	50	137	49	113.7	78.1	171.8
80	3,86E+06	(192)	4,42E+05	(22)	60	81	34	150.0	97.2	245.0
81	1,27E+06	(21)	6,63E+05	(11)	20	121	72	33.1	15.4	76.3
82	4,10E+06	(340)	5,06E+05	(42)	100	93	28	139.7	101.7	197.4
83	1,54E+06	(51)	3,31E+05	(11)	40	61	36	79.7	41.6	170.5
84	4,64E+06	(385)	8,07E+05	(67)	100	148	36	99.1	76.5	128.4
85	8,31E+06	(69)	9,64E+05	(8)	10	176	121	146.6	72.1	353.8
86	2,57E+06	(213)	5,66E+05	(47)	100	104	30	78.6	57.3	110.4
87	3,71E+06	(154)	5,54E+05	(23)	50	101	42	115.5	74.8	187.8
88	2,67E+06	(222)	3,49E+05	(29)	100	64	24	132.0	90.0	201.7
89	4,47E+06	(297)	7,38E+05	(49)	80	135	38	105.0	77.7	145.1
90	2,92E+06	(242)	3,61E+05	(30)	100	66	24	139.0	95.6	210.5
91	1,66E+06	(138)	2,65E+05	(22)	100	48	20	108.2	69.3	178.5
92	3,69E+06	(306)	5,42E+05	(45)	100	99	29	117.6	86.2	164.7
93	2,79E+06	(139)	7,43E+05	(37)	60	136	44	65.2	45.3	96.6
94	1,74E+06	(52)	4,02E+05	(12)	36	73	42	74.6	39.8	154.3
95	5,85E+06	(238)	8,61E+05	(35)	49	157	53	117.5	82.6	172.8
96	2,98E+06	(247)	3,37E+05	(28)	100	62	23	151.8	103.3	233.1
97	4,62E+06	(230)	8,23E+05	(41)	60	151	47	97.1	69.8	139.1
98	4,28E+06	(213)	4,62E+05	(23)	60	84	35	159.1	104.3	256.3
99	2,00E+06	(166)	3,49E+05	(29)	100	64	24	99.0	66.8	152.6
100	1,88E+06	(156)	3,13E+05	(26)	100	57	22	103.6	68.6	163.8
101	6,02E+06	(45)	4,02E+05	(3)	9	73	79	245.5	83.7	1201.9
POOLED	3,07E+06	(17531)	4,87E+05	(2781)	6886	89	4	109.4	103.6	115.5

CHI^2 PROBABILITY (%): 0.0

POOLED AGE W/ 68% CONF. INTERVAL(Ma): 109.4, 106.4 -- 112.5 (-3.0 +3.1)
95% CONF. INTERVAL(Ma): 103.6 -- 115.5 (-5.8 +6.1)

CENTRAL AGE W/ 68% CONF. INTERVAL(Ma): 109.7, 105.7 -- 113.8 (-4.0 +4.1)
95% CONF. INTERVAL(Ma): 102.1 -- 117.9 (-7.6 +8.2)
AGE DISPERSION (%): 23.4

FIT OPTION: Best-fit peaks using the binomial model of Galbraith and Green

INITIAL GUESS FOR MODEL PARAMETERS (number of peaks to fit = 3)

Peak #.	Peak Age	Theta	Fraction(%)	Count
1.	40.90	0.701	2.0	2.06
2.	109.40	0.863	43.1	43.56
3.	263.30	0.939	2.9	2.96

Total range for grain ages:	32,6 to 263,3 Ma
Number of active grains (Num. used for fit):	101
Number of removed grains:	0
Degrees of freedom for fit:	96
Average of the SE(Z)'s for the grains:	0,25
Estimated width of peaks in PD plot in Z units:	0,29

PARAMETERS FOR BEST-FIT PEAKS

* *Standard error for peak age includes group error*
* *Peak width is for PD plot assuming a kernel factor = 0.60*

#.	Peak Age(Ma)	68%CI	95%CI	W(Z)	Frac(%)	SE,%	Count
1.	41.0	-6,1 ...+7,1	-11,0 ...+15,1	0.21	1.4	1.3	1.4
2.	89.6	-4,7 ...+4,9	-8,9 ...+9,9	0.22	38.6	10.2	39.0
3.	131.6	-5,8 ...+6,0	-11,1 ...+12,1	0.26	60.0	10.2	60.6

Log-likelihood for best fit:	-326,691
Chi-squared value for best fit:	98,578
Reduced chi-squared value:	1,027
Probability for F test:	0%
Condition number for COVAR matrix:	152,47
Number of iterations:	34

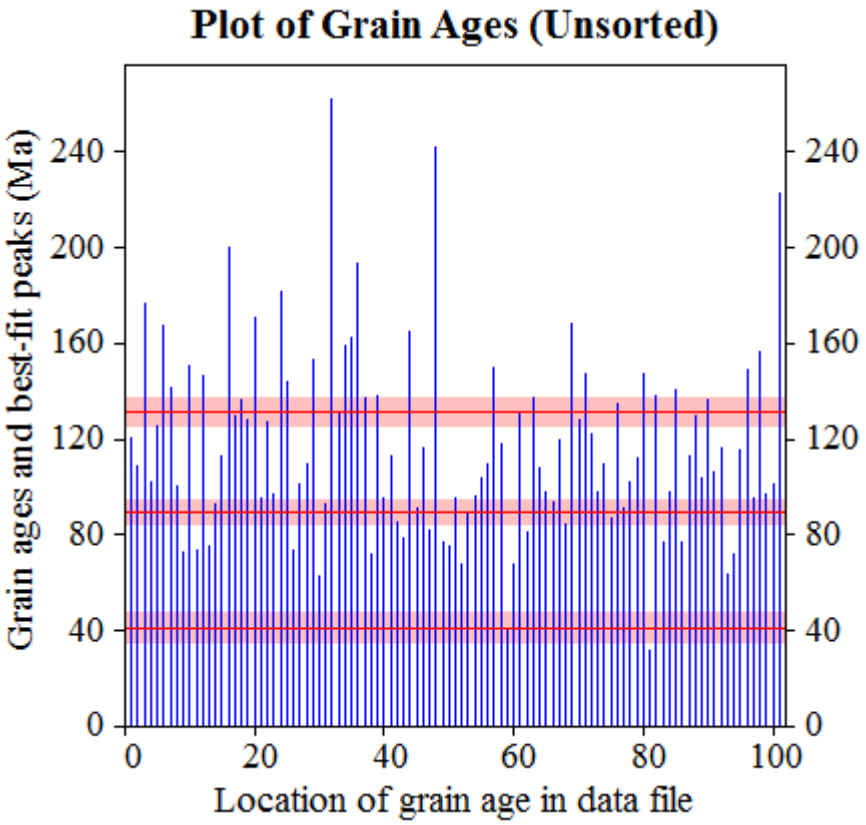
Plot of Grain Ages (Unsorted)
Grain ages and best-fit peaks (Ma)
0
40
80
120
160
200
240
0
20
40
60
80
100
Location of grain age in data file

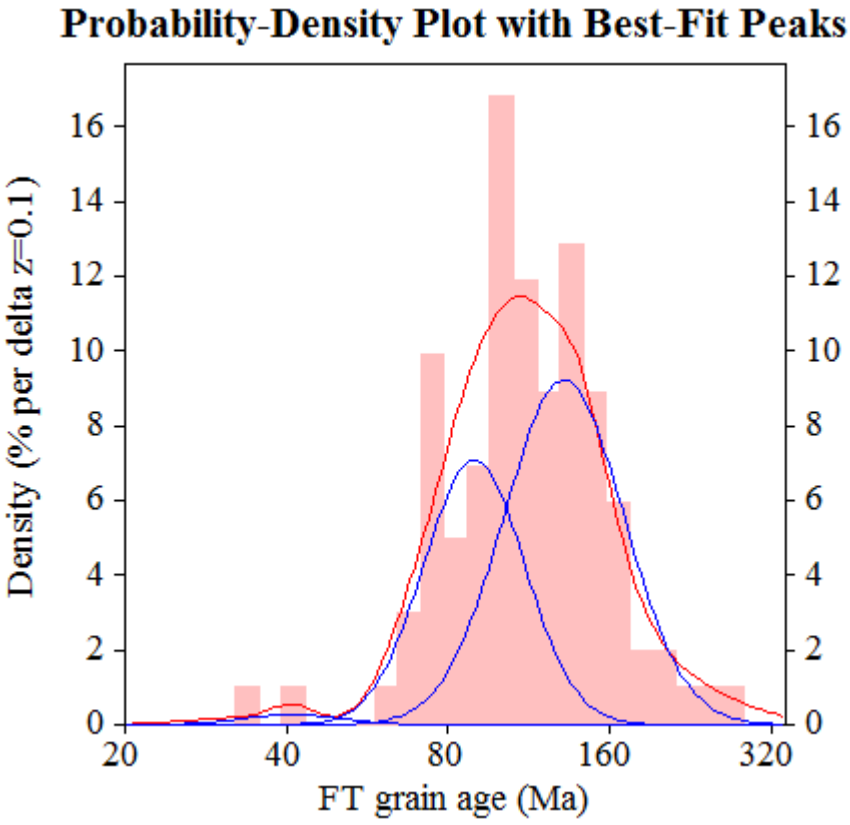
Probability-Density Plot with Best-Fit Peaks
Density (% per delta z=0.1)
0
2
4
6
8
10
12
14
16
20
40
80
160
320
FT grain age (Ma)

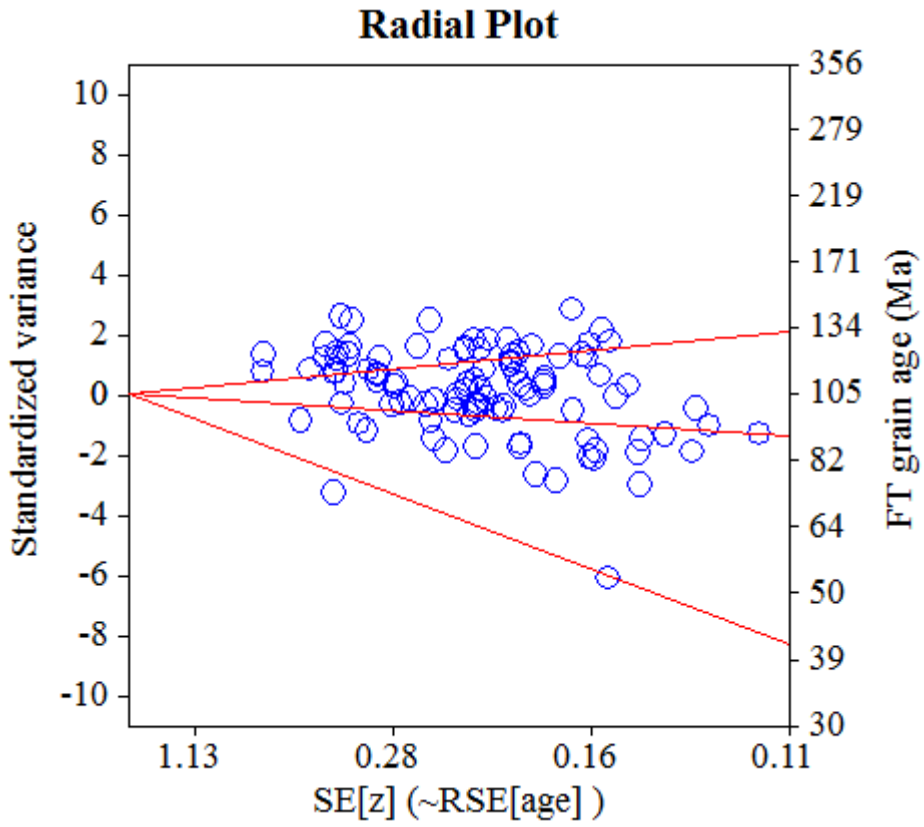
Radial Plot
Standardized variance
10
8
6
4
2
0
-2
-4
-6
-8
-10
356
279
219
171
134
105
82
64
50
39
30
FT grain age (Ma)
1.13
0.28
0.16
0.11
SE[z] (~RSE[age])

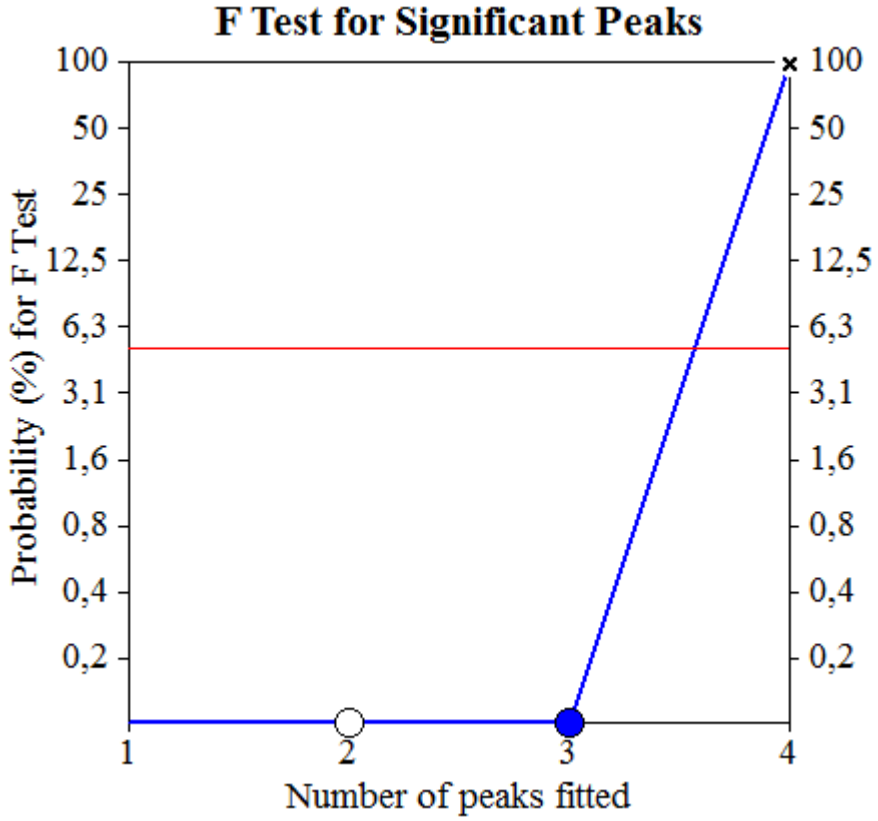
F Test for Significant Peaks
Probability (%) for F Test
100
50
25
12,5
6,3
3,1
1,6
0,8
0,4
0,2
1
2
3
4
Number of peaks fitted

Datafile: C:\BH2\Alejandro\6-2015_zircon\CP_088b\CP_088b.ftz
Title: Sample No. CP-088b Irr 6-2015-30

NEW PARAMETERS - ZETA METHOD

EFFECTIVE TRACK DENSITY FOR FLUENCE MONITOR (tracks/cm^2): 3,10E+05
RELATIVE ERROR (%): 1,12
EFFECTIVE URANIUM CONTENT OF MONITOR (ppm): 50,00
ZETA FACTOR AND STANDARD ERROR (yr cm^2): 141,03 2,32
SIZE OF COUNTER SQUARE (cm^2): 8,30E-07

GRAIN AGES IN ORIGINAL ORDER

Grain no.	RhoS (cm^-2)	(Ns)	RhoI (cm^-2)	(Ni)	Squares	U+/-2s	Grain Age (Ma) Age	--95% CI--	
1	7,72E+06	(205)	2,37E+06	(63)	32	383 97	70.1	52.8	93.0
2	6,31E+06	(110)	2,24E+06	(39)	21	361 115	61.1	42.2	90.6
3	1,02E+07	(676)	2,00E+06	(133)	80	324 56	109.6	90.8	132.2
4	5,75E+06	(229)	2,54E+06	(101)	48	410 82	49.1	38.7	62.1
5	6,10E+06	(253)	1,78E+06	(74)	50	288 67	73.7	56.8	95.5
6	7,73E+06	(77)	2,21E+06	(22)	12	357 151	75.5	46.8	127.7
7	5,61E+06	(466)	1,18E+06	(98)	100	191 39	102.4	82.3	127.5
8	5,72E+06	(57)	1,10E+06	(11)	12	178 105	110.8	58.4	234.9
9	4,21E+06	(339)	1,08E+06	(87)	97	175 38	84.0	66.3	106.4
10	6,53E+06	(65)	1,41E+06	(14)	12	227 119	99.6	56.0	192.7
11	4,63E+06	(384)	1,37E+06	(114)	100	222 42	72.8	58.9	89.9
12	6,43E+06	(48)	4,42E+06	(33)	9	714 247	31.6	19.9	50.9
13	1,69E+07	(126)	3,75E+06	(28)	9	606 227	97.0	64.4	152.0
14	7,07E+06	(176)	1,77E+06	(44)	30	285 86	86.5	62.1	123.3
15	8,97E+06	(521)	4,06E+06	(236)	70	656 87	47.9	40.9	56.1
16	9,04E+06	(225)	2,37E+06	(59)	30	383 100	82.0	61.6	109.2
17	8,67E+06	(180)	1,59E+06	(33)	25	257 89	117.5	81.2	175.9
18	7,19E+06	(179)	1,24E+06	(31)	30	201 72	124.3	85.1	188.3
19	8,35E+06	(104)	1,12E+06	(14)	15	182 96	158.5	91.7	299.9
20	1,32E+07	(219)	4,40E+06	(73)	20	710 166	64.7	49.6	84.4
21	5,69E+06	(236)	1,18E+06	(49)	50	191 54	104.0	76.5	144.6
22	7,49E+06	(261)	1,86E+06	(65)	42	301 75	86.4	65.8	113.4
23	5,34E+06	(124)	1,12E+06	(26)	28	181 70	102.7	67.4	163.6
24	4,73E+06	(393)	1,06E+06	(88)	100	171 37	96.2	76.3	121.3
25	9,37E+06	(389)	3,23E+06	(134)	50	522 91	62.8	51.5	76.6
26	8,19E+06	(340)	2,63E+06	(109)	50	424 82	67.4	54.2	83.8
27	1,65E+06	(41)	2,01E+05	(5)	30	32 28	171.7	70.4	555.8
28	4,53E+06	(376)	9,28E+05	(77)	100	150 34	105.0	82.1	134.2
29	6,37E+06	(148)	1,42E+06	(33)	28	229 79	96.8	66.4	145.9
30	5,22E+06	(303)	1,48E+06	(86)	70	239 52	76.0	59.7	96.7
31	6,39E+06	(371)	1,41E+06	(82)	70	228 50	97.4	76.6	123.8
32	6,99E+06	(58)	3,49E+06	(29)	10	564 208	43.4	27.4	70.4
33	5,35E+06	(311)	1,67E+06	(97)	70	270 55	69.3	55.0	87.1
34	6,39E+06	(191)	1,10E+06	(33)	36	178 62	124.6	86.3	186.2
35	4,54E+06	(264)	1,02E+06	(59)	70	164 43	96.1	72.5	127.4
36	7,59E+06	(126)	2,35E+06	(39)	20	380 121	69.9	48.7	103.0
37	9,64E+06	(200)	2,46E+06	(51)	25	397 111	84.8	62.3	117.8
38	7,90E+06	(236)	1,37E+06	(41)	36	222 69	124.0	89.2	177.3
39	6,31E+06	(220)	1,66E+06	(58)	42	269 71	81.6	61.1	108.9
40	4,40E+06	(219)	1,02E+06	(51)	60	165 46	92.8	68.4	128.6
41	4,37E+06	(58)	1,13E+06	(15)	16	182 93	83.2	47.0	158.4
42	6,12E+06	(61)	2,81E+06	(28)	12	454 170	47.2	29.8	76.8
43	6,59E+06	(164)	1,49E+06	(37)	30	240 79	95.7	67.0	140.8
44	6,48E+06	(113)	2,07E+06	(36)	21	334 111	67.9	46.5	101.9
45	3,01E+05	(25)	2,17E+05	(18)	100	35 16	30.2	15.9	58.7
46	2,92E+06	(242)	6,75E+05	(56)	100	109 29	92.8	69.4	124.0
47	4,10E+06	(170)	1,23E+06	(51)	50	199 56	72.2	52.7	100.8
48	4,87E+06	(101)	1,64E+06	(34)	25	265 90	64.3	43.4	98.0
49	5,27E+06	(70)	1,43E+06	(19)	16	231 105	79.4	47.7	140.0
50	5,16E+06	(107)	6,75E+05	(14)	25	109 57	163.0	94.4	308.1
51	5,72E+06	(285)	1,91E+06	(95)	60	308 63	64.8	51.3	81.9
52	5,66E+06	(169)	1,81E+06	(54)	36	292 79	67.8	49.8	94.0
53	8,39E+06	(174)	2,46E+06	(51)	25	397 111	73.9	53.9	103.1

Datafile: C:\BH2\Alejandro\6-2015_zircon\CP_088b\CP_088b.ftz
Title: Sample No. CP-088b Irr 6-2015-30

Grain no.	RhoS (cm^-2)	(Ns)	RhoI (cm^-2)	(Ni)	Squares	U+/-2s	Grain Age (Ma) Age	--95% CI--	
54	3,75E+06	(28)	2,54E+06	(19)	9	411 186	32.0	17.3	60.7
55	4,22E+06	(70)	1,02E+06	(17)	20	165 79	88.6	52.1	161.0
56	1,08E+06	(90)	2,41E+05	(20)	100	39 17	96.9	59.7	166.3
57	3,45E+06	(258)	9,91E+05	(74)	90	160 37	75.2	58.0	97.4
58	5,27E+06	(437)	1,17E+06	(97)	100	189 38	97.1	77.8	121.1
59	7,83E+06	(156)	1,61E+06	(32)	24	260 91	105.1	71.9	159.0
60	4,01E+06	(266)	1,36E+06	(90)	80	219 46	63.8	50.2	81.2
61	4,98E+06	(413)	1,57E+06	(130)	100	253 45	68.7	56.3	83.9
62	1,65E+06	(137)	4,58E+05	(38)	100	74 24	78.0	54.3	114.9
63	4,82E+06	(40)	1,81E+06	(15)	10	292 148	57.5	31.4	112.5
64	4,74E+06	(118)	9,64E+05	(24)	30	156 63	105.8	68.3	171.9
65	5,98E+06	(124)	9,64E+05	(20)	25	156 69	133.0	83.4	225.3
66	7,11E+06	(590)	1,11E+06	(92)	100	179 37	137.7	110.5	171.6
67	9,80E+06	(813)	1,64E+06	(136)	100	265 46	128.7	107.1	154.6
68	5,82E+06	(116)	1,36E+06	(27)	24	219 84	92.7	60.9	146.7
69	7,52E+06	(131)	2,01E+06	(35)	21	324 109	80.9	55.6	121.2
70	3,73E+06	(155)	1,11E+06	(46)	50	179 53	72.9	52.4	103.8
71	5,82E+06	(464)	1,23E+06	(98)	96	199 40	102.0	81.9	127.0
72	1,33E+06	(55)	2,65E+05	(11)	50	43 25	106.9	56.2	227.3
73	7,41E+06	(369)	1,87E+06	(93)	60	302 63	85.6	68.1	107.5
74	5,37E+06	(446)	1,13E+06	(94)	100	183 38	102.2	81.7	127.8
75	4,52E+06	(375)	9,76E+05	(81)	100	158 35	99.7	78.3	126.8
76	1,30E+06	(54)	2,41E+05	(10)	50	39 24	115.3	59.1	254.6
77	2,94E+06	(122)	5,30E+05	(22)	50	86 36	119.2	75.9	197.3
78	4,96E+06	(103)	1,73E+06	(36)	25	280 93	62.0	42.2	93.4
79	6,25E+06	(83)	2,33E+06	(31)	16	377 135	58.0	38.1	90.8
80	4,56E+06	(121)	1,69E+06	(45)	32	274 81	58.3	41.2	84.1
81	6,02E+06	(45)	1,20E+06	(9)	9	195 126	106.7	52.4	249.1
82	2,17E+06	(63)	3,10E+05	(9)	35	50 32	148.7	75.1	340.4
83	6,67E+06	(277)	1,04E+06	(43)	50	167 51	138.6	100.8	195.8
84	4,39E+06	(182)	5,54E+05	(23)	50	90 37	169.4	110.6	273.6
85	4,51E+06	(262)	1,26E+06	(73)	70	203 48	77.3	59.6	100.3
86	4,37E+06	(254)	9,64E+05	(56)	70	156 42	97.4	73.0	129.9
87	3,45E+06	(172)	8,63E+05	(43)	60	139 42	86.5	61.8	123.9
88	4,49E+06	(261)	2,05E+06	(119)	70	331 61	47.5	38.2	59.1
89	5,49E+06	(164)	2,04E+06	(61)	36	330 84	58.3	43.3	79.7
90	4,48E+06	(186)	6,02E+05	(25)	50	97 39	159.5	105.7	252.5
91	2,11E+06	(105)	5,02E+05	(25)	60	81 32	90.6	58.5	146.4
92	3,82E+06	(57)	7,36E+05	(11)	18	119 70	110.8	58.4	234.9
93	6,29E+06	(47)	1,61E+06	(12)	9	260 147	84.1	44.5	174.7
94	8,19E+06	(68)	1,33E+06	(11)	10	214 126	131.9	70.4	277.0
95	5,49E+06	(456)	1,36E+06	(113)	100	220 42	87.1	70.7	107.2
96	3,33E+06	(116)	3,44E+05	(12)	42	56 31	205.1	115.2	407.1
POOLED	5,24E+06	(20034)	1,34E+06	(5105)	4606	216 8	85.1	81.0	89.4

CHI^2 PROBABILITY (%): 0.0

POOLED AGE W/	68% CONF. INTERVAL(Ma):	85.1,	83.0 --	87.2	(-2.1 +2.2)
	95% CONF. INTERVAL(Ma):		81.0 --	89.4	(-4.1 +4.3)
CENTRAL AGE W/	68% CONF. INTERVAL(Ma):	84.3,	81.1 --	87.6	(-3.2 +3.3)
	95% CONF. INTERVAL(Ma):		78.2 --	90.9	(-6.1 +6.6)
	AGE DISPERSION (%):	27.0			

FIT OPTION: Best-fit peaks using the binomial model of Galbraith and Green

INITIAL GUESS FOR MODEL PARAMETERS (number of peaks to fit = 3)

Peak #.	Peak Age	Theta	Fraction(%)	Count
1.	30.80	0.586	2.9	2.80
2.	47.90	0.688	11.6	11.16
3.	85.10	0.797	42.1	40.45

Total range for grain ages:	30,0 to 200,3 Ma
Number of active grains (Num. used for fit):	96
Number of removed grains:	0
Degrees of freedom for fit:	91
Average of the SE(Z)'s for the grains:	0,2
Estimated width of peaks in PD plot in Z units:	0,24

PARAMETERS FOR BEST-FIT PEAKS

* *Standard error for peak age includes group error*
* *Peak width is for PD plot assuming a kernel factor = 0.60*

#.	Peak Age(Ma)	68%CI	95%CI	W(Z)	Frac(%)	SE,%	Count
1.	32.9	-8,5 ...+11,4	-14,5 ...+26,0	0.29	2.0	1.9	1.9
2.	64.9	-2,5 ...+2,6	-4,7 ...+5,1	0.17	37.4	6.7	35.9
3.	103.6	-3,4 ...+3,5	-6,5 ...+6,9	0.19	60.7	6.7	58.3

Log-likelihood for best fit:	-377,072
Chi-squared value for best fit:	98,995
Reduced chi-squared value:	1,088
Probability for F test:	0%
Condition number for COVAR matrix:	282,89
Number of iterations:	14

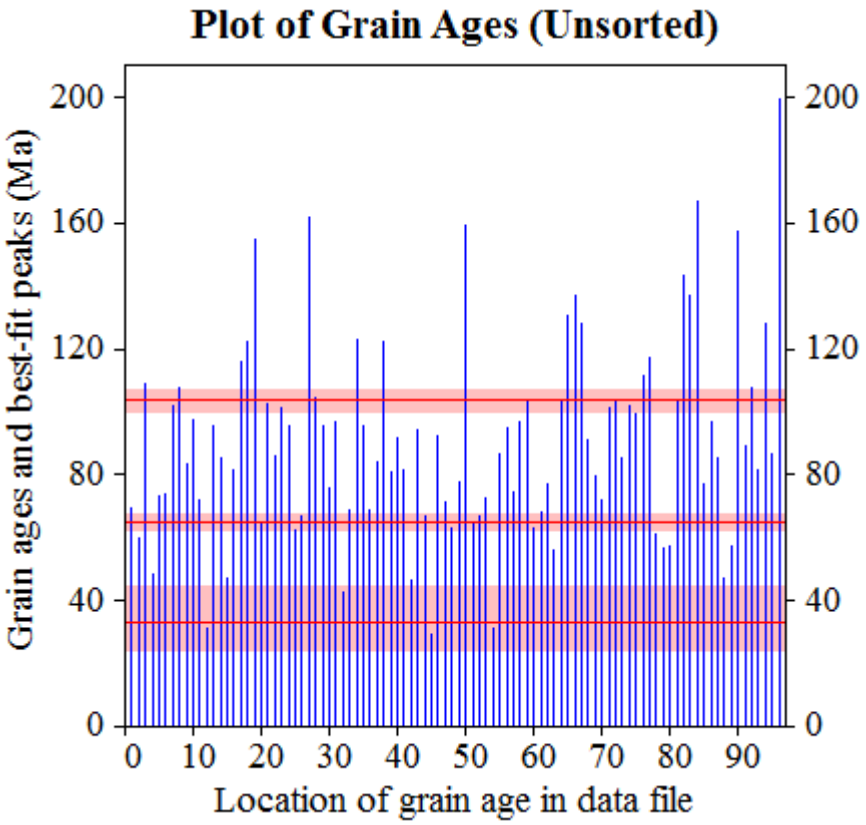
Plot of Grain Ages (Unsorted)
Grain ages and best-fit peaks (Ma)
0
40
80
120
160
200
0 10 20 30 40 50 60 70 80 90
Location of grain age in data file

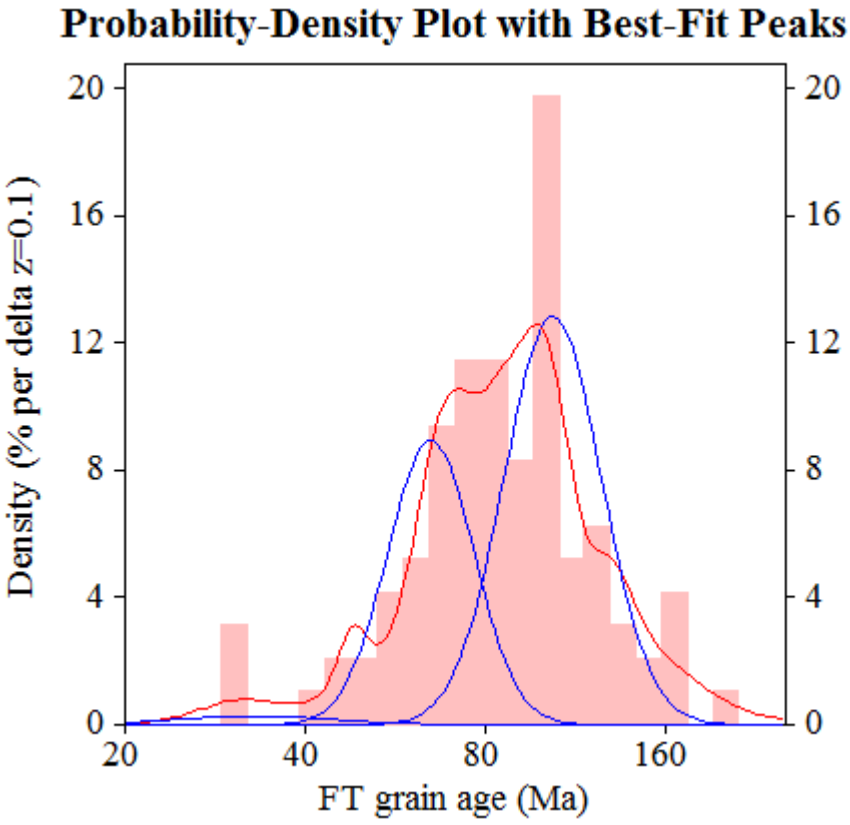
Probability-Density Plot with Best-Fit Peaks
Density (% per delta z=0.1)
0
4
8
12
16
20
20 40 80 160
FT grain age (Ma)

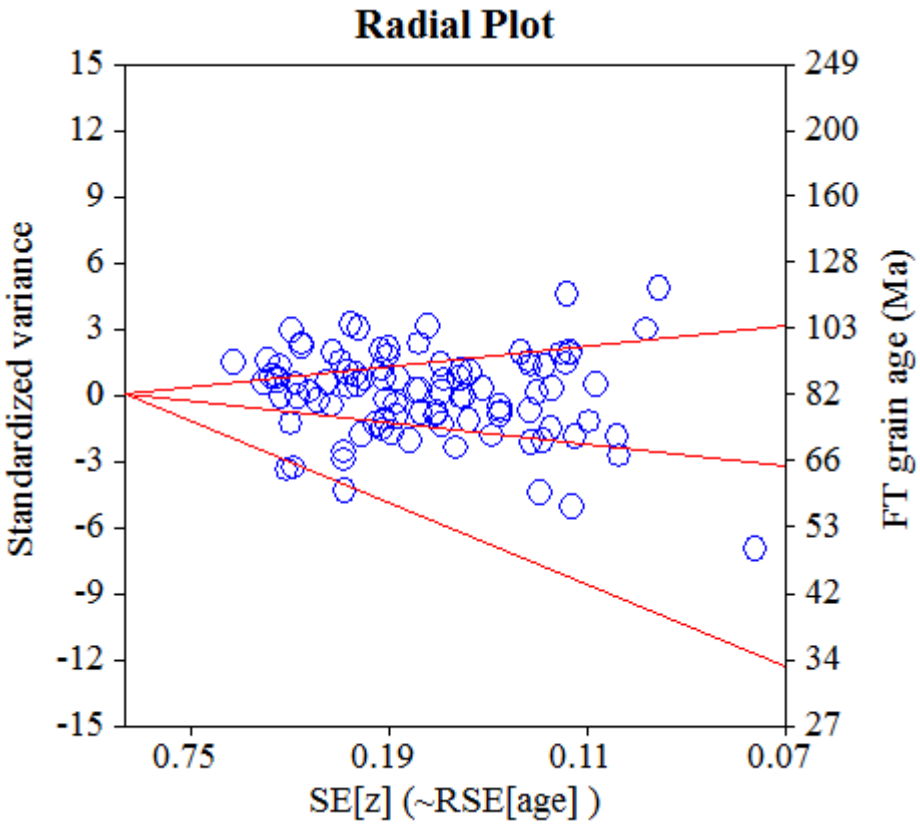
Radial Plot
Standardized variance
FT grain age (Ma)
SE[z] (~RSE[age])
15
12
9
6
3
0
-3
-6
-9
-12
-15
249
200
160
128
103
82
66
53
42
34
27
0.75
0.19
0.11
0.07

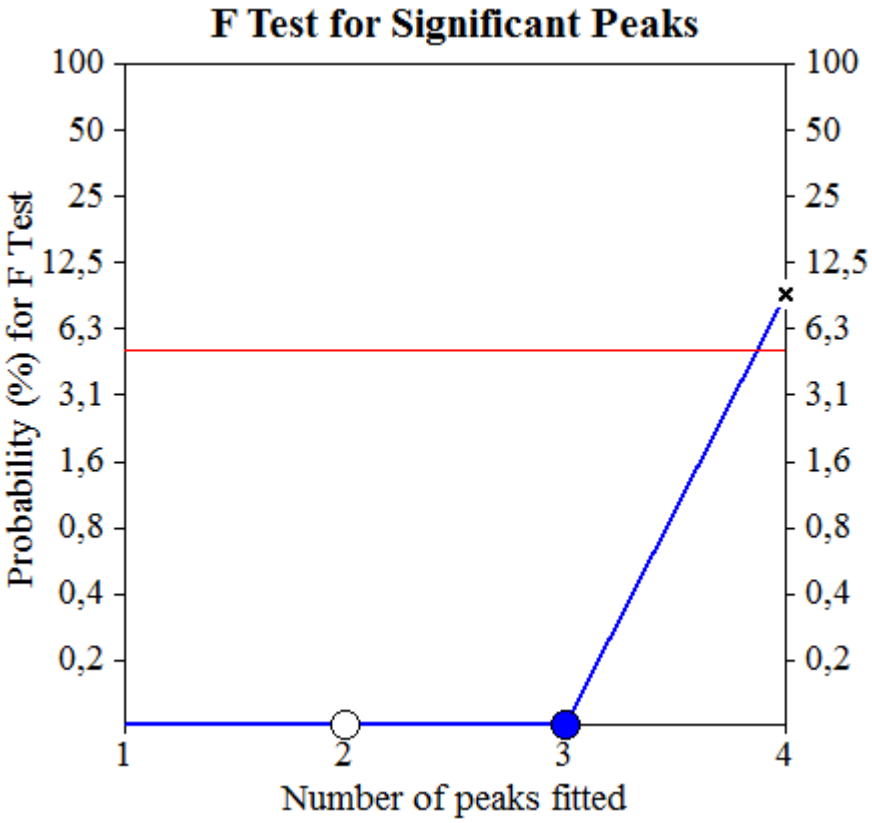
F Test for Significant Peaks
Probability (%) for F Test
Number of peaks fitted
100
50
25
12,5
6,3
3,1
1,6
0,8
0,4
0,2
1
2
3
4

Datafile: C:\BH2\Edna\6-2015\CVI-1302\CVI_1302_6-2015-26A.FTZ.txt
Title: Sample No. CVI_1302 Irr 6-2015-26

NEW PARAMETERS - ZETA METHOD

EFFECTIVE TRACK DENSITY FOR FLUENCE MONITOR (tracks/cm^2): 3,04E+05
RELATIVE ERROR (%): 1,13
EFFECTIVE URANIUM CONTENT OF MONITOR (ppm): 50,00
ZETA FACTOR AND STANDARD ERROR (yr cm^2): 126,82 2,05
SIZE OF COUNTER SQUARE (cm^2): 8,30E-07

GRAIN AGES IN ORIGINAL ORDER

Grain no.	RhoS (cm^-2)	(Ns)	RhoI (cm^-2)	(Ni)	Squares	U+/-2s	Grain Age (Ma) Age	--95% CI--	
1	6,75E+06	(112)	1,14E+06	(19)	20	188 85	111.8	69.1	192.9
2	4,82E+06	(64)	9,79E+05	(13)	16	161 88	93.3	51.5	185.2
3	2,41E+06	(100)	4,34E+05	(18)	50	71 33	105.4	64.1	185.4
4	5,30E+06	(176)	9,64E+05	(32)	40	159 56	104.7	72.0	157.9
5	7,83E+06	(78)	1,61E+06	(16)	12	264 130	92.5	54.1	170.3
6	6,10E+06	(253)	1,49E+06	(62)	50	246 62	77.6	58.7	102.4
7	5,76E+06	(287)	1,02E+06	(51)	60	168 47	107.3	79.7	147.6
8	6,20E+06	(144)	2,32E+06	(54)	28	382 104	51.1	37.2	71.3
9	8,13E+06	(81)	2,11E+06	(21)	12	347 150	73.5	45.4	125.4
10	4,55E+06	(34)	2,41E+06	(18)	9	396 185	36.2	20.0	68.1
11	8,48E+06	(352)	1,61E+06	(67)	50	266 65	99.8	76.8	129.5
12	8,67E+06	(144)	2,83E+06	(47)	20	466 136	58.7	42.0	83.5
13	4,69E+06	(35)	1,47E+06	(11)	9	242 143	60.4	30.4	132.6
14	7,93E+06	(79)	1,61E+06	(16)	12	264 130	93.7	54.9	172.3
15	6,48E+06	(86)	1,66E+06	(22)	16	272 115	74.5	46.5	125.3
16	8,96E+06	(119)	1,66E+06	(22)	16	272 115	102.8	65.4	170.5
17	8,98E+06	(149)	2,23E+06	(37)	20	367 120	76.9	53.6	113.6
18	6,69E+06	(333)	1,20E+06	(60)	60	198 51	105.3	80.0	138.4
19	6,25E+06	(83)	9,79E+05	(13)	16	161 88	120.6	67.8	236.5
20	6,82E+06	(283)	1,28E+06	(53)	50	210 58	101.9	76.0	139.4
21	8,04E+06	(667)	1,55E+06	(129)	100	256 45	98.5	81.4	119.2
22	5,54E+06	(69)	1,93E+06	(24)	15	317 128	54.9	34.3	91.6
23	5,60E+06	(372)	1,11E+06	(74)	80	183 43	95.6	74.4	122.6
24	2,96E+06	(59)	1,61E+06	(32)	24	264 93	35.4	22.7	56.3
25	5,25E+06	(122)	1,33E+06	(31)	28	219 78	75.1	50.6	115.5
26	4,59E+06	(61)	1,20E+06	(16)	16	198 98	72.5	41.7	135.2
27	9,13E+06	(379)	1,30E+06	(54)	50	214 58	132.7	99.9	176.1
28	5,30E+06	(132)	7,63E+05	(19)	30	126 57	131.6	81.9	225.6
29	7,63E+06	(57)	3,48E+06	(26)	9	572 223	42.0	26.1	69.7
30	3,25E+06	(135)	2,17E+06	(90)	50	357 75	28.7	21.9	37.5
31	6,33E+06	(105)	1,27E+06	(21)	20	208 90	95.1	59.6	160.3
32	5,28E+06	(92)	1,95E+06	(34)	21	321 109	51.8	34.7	79.3
33	6,46E+06	(134)	1,40E+06	(29)	25	230 85	88.1	59.0	136.7
34	5,29E+06	(123)	1,68E+06	(39)	28	276 88	60.3	41.9	89.0
35	5,42E+06	(72)	1,13E+06	(15)	16	186 94	91.1	52.3	171.6
36	4,96E+06	(103)	8,67E+05	(18)	25	143 66	108.6	66.1	190.7
37	5,54E+06	(216)	1,05E+06	(41)	47	173 54	100.4	72.0	144.0
38	2,61E+06	(26)	1,00E+05	(1)	12	17 27	425.6	81.8	9232.3
39	6,08E+06	(106)	2,29E+06	(40)	21	377 119	50.8	35.1	75.1
40	3,68E+06	(55)	1,54E+06	(23)	18	253 105	45.7	27.8	78.2
41	4,92E+06	(49)	3,21E+06	(32)	12	528 186	29.4	18.5	47.5
42	6,28E+06	(198)	1,33E+06	(42)	38	219 67	90.0	64.5	128.8
43	9,23E+06	(268)	1,62E+06	(47)	35	266 77	108.7	79.8	151.6
44	8,28E+06	(165)	8,53E+05	(17)	24	140 67	182.9	112.3	321.0
45	4,39E+06	(153)	1,15E+06	(40)	42	189 59	73.1	51.5	106.4
46	4,42E+06	(33)	2,41E+06	(18)	9	396 185	35.1	19.3	66.3
47	8,96E+06	(223)	2,01E+06	(50)	30	330 93	85.2	62.7	118.3
48	8,82E+06	(183)	3,33E+06	(69)	25	547 132	50.6	38.3	66.7
49	8,89E+06	(118)	1,73E+06	(23)	16	285 118	97.6	62.5	160.1
50	4,88E+06	(81)	2,05E+06	(34)	20	337 115	45.6	30.3	70.4
51	7,86E+06	(652)	1,33E+06	(110)	100	218 42	112.8	92.0	138.2
52	5,77E+06	(115)	9,04E+05	(18)	24	149 69	121.1	74.1	211.7
53	6,02E+06	(250)	9,88E+05	(41)	50	162 51	116.1	83.6	165.8

Datafile: C:\BH2\Edna\6-2015\CVI-1302\CVI_1302_6-2015-26A.FTZ.txt
Title: Sample No. CVI_1302 Irr 6-2015-26

Grain no.	RhoS (cm^-2)	(Ns)	RhoI (cm^-2)	(Ni)	Squares	U+/-2s	Grain Age (Ma) Age	--95% CI--	
54	7,20E+06	(251)	8,61E+05	(30)	42	142 51	158.5	109.2	239.7
55	9,69E+06	(201)	1,30E+06	(27)	25	214 82	141.2	95.0	219.5
56	8,28E+06	(110)	3,01E+05	(4)	16	50 47	491.1	198.1	1727.0
57	3,88E+06	(116)	8,70E+05	(26)	36	143 56	85.0	55.6	135.8
58	3,40E+06	(79)	2,62E+06	(61)	28	432 111	24.9	17.6	35.4
59	7,23E+06	(150)	1,16E+06	(24)	25	190 77	118.7	77.4	191.2
60	7,57E+06	(628)	1,22E+06	(101)	100	200 40	118.2	95.7	146.0
61	5,87E+06	(78)	9,79E+05	(13)	16	161 88	113.4	63.5	223.0
62	5,48E+06	(364)	1,31E+06	(87)	80	216 46	79.7	63.0	100.8
63	5,98E+06	(124)	9,64E+05	(20)	25	159 70	117.6	73.7	199.4
64	5,98E+06	(248)	1,23E+06	(51)	50	202 57	92.8	68.7	128.2
65	7,13E+06	(355)	1,20E+06	(60)	60	198 51	112.1	85.3	147.3
66	5,36E+06	(267)	9,64E+05	(48)	60	159 46	106.0	78.1	147.4
67	5,62E+06	(56)	1,20E+06	(12)	12	198 112	88.4	47.5	181.9
68	6,85E+06	(273)	1,33E+06	(53)	48	219 60	98.3	73.3	134.6
POOLED	6,36E+06	(11865)	1,37E+06	(2566)	2249	226 10	88.5	83.6	93.7

CHI^2 PROBABILITY (%): 0.0

POOLED AGE W/ 68% CONF. INTERVAL(Ma): 88.5, 86.0 -- 91.1 (-2.5 +2.6)
95% CONF. INTERVAL(Ma): 83.6 -- 93.7 (-4.9 +5.2)

CENTRAL AGE W/ 68% CONF. INTERVAL(Ma): 80.9, 76.1 -- 85.9 (-4.8 +5.1)
95% CONF. INTERVAL(Ma): 71.8 -- 91.1 (-9.1 +10.3)
AGE DISPERSION (%): 43.2

FIT OPTION: Best-fit peaks using the binomial model of Galbraith and Green

INITIAL GUESS FOR MODEL PARAMETERS (number of peaks to fit = 3)

Peak #.	Peak Age	Theta	Fraction(%)	Count
1.	24.90	0.564	3.9	2.62
2.	88.50	0.822	37.4	25.45
3.	99.10	0.838	51.6	35.10

Total range for grain ages:	24,9 to 456,8 Ma
Number of active grains (Num. used for fit):	68
Number of removed grains:	0
Degrees of freedom for fit:	63
Average of the SE(Z)'s for the grains:	0,24
Estimated width of peaks in PD plot in Z units:	0,28

PARAMETERS FOR BEST-FIT PEAKS

* *Standard error for peak age includes group error*
* *Peak width is for PD plot assuming a kernel factor = 0.60*

#.	Peak Age(Ma)	68%CI	95%CI	W(Z)	Frac(%)	SE,%	Count
1.	29.2	-2,9 ...+3,2	-5,4 ...+6,6	0.21	6.4	3.7	4.3
2.	52.0	-3,9 ...+4,2	-7,3 ...+8,5	0.23	18.9	5.6	12.9
3.	103.8	-3,3 ...+3,4	-6,4 ...+6,8	0.21	74.7	5.8	50.8

Log-likelihood for best fit:	-252,314
Chi-squared value for best fit:	67,569
Reduced chi-squared value:	1,073
Probability for F test:	0%
Condition number for COVAR matrix:	17,08
Number of iterations:	18

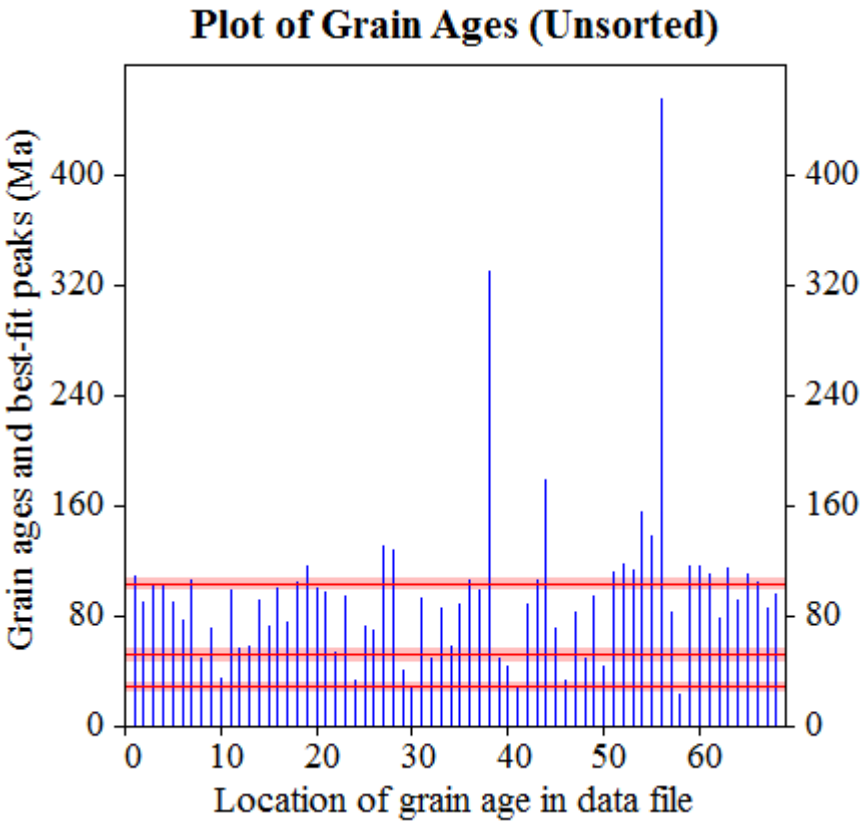
Plot of Grain Ages (Unsorted)
Grain ages and best-fit peaks (Ma)
0
80
160
240
320
400
0
10
20
30
40
50
60
Location of grain age in data file

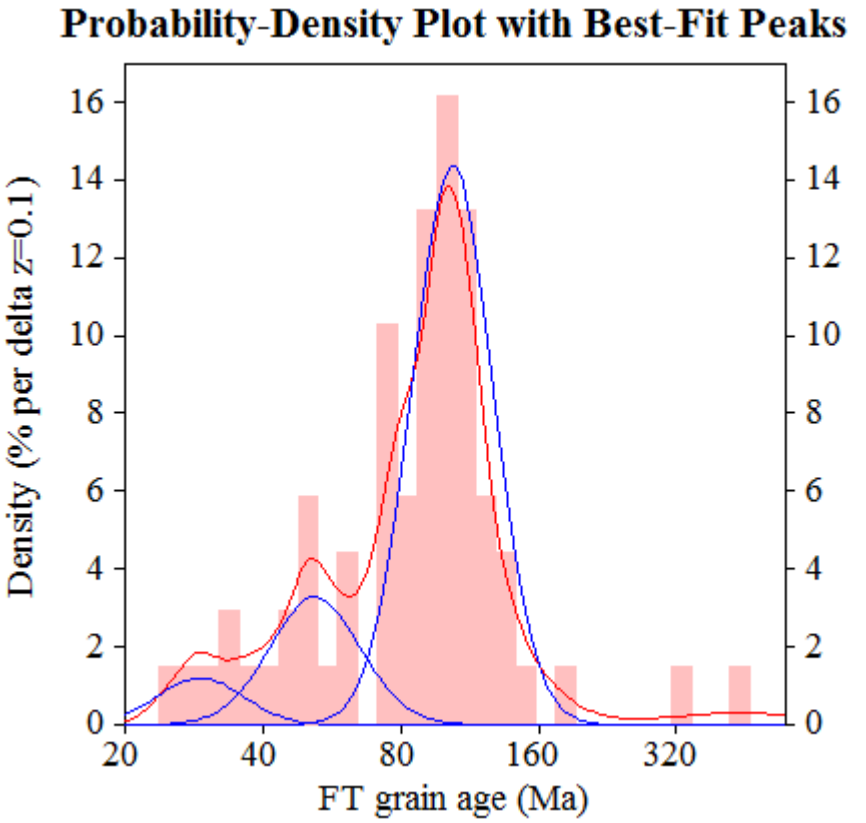
Probability-Density Plot with Best-Fit Peaks
Density (% per delta z=0.1)
0
2
4
6
8
10
12
14
16
20
40
80
160
320
FT grain age (Ma)

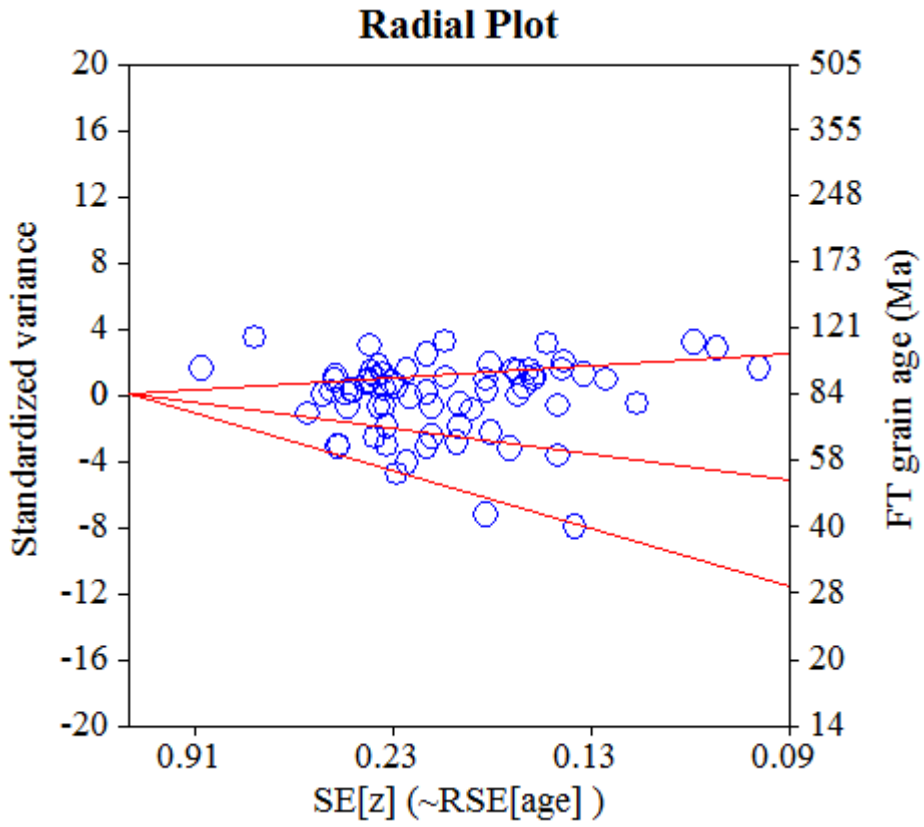
Radial Plot
Standardized variance
20
16
12
8
4
0
-4
-8
-12
-16
-20
505
355
248
173
121
84
58
40
28
20
14
FT grain age (Ma)
0.91
0.23
0.13
0.09
SE[z] (~RSE[age])

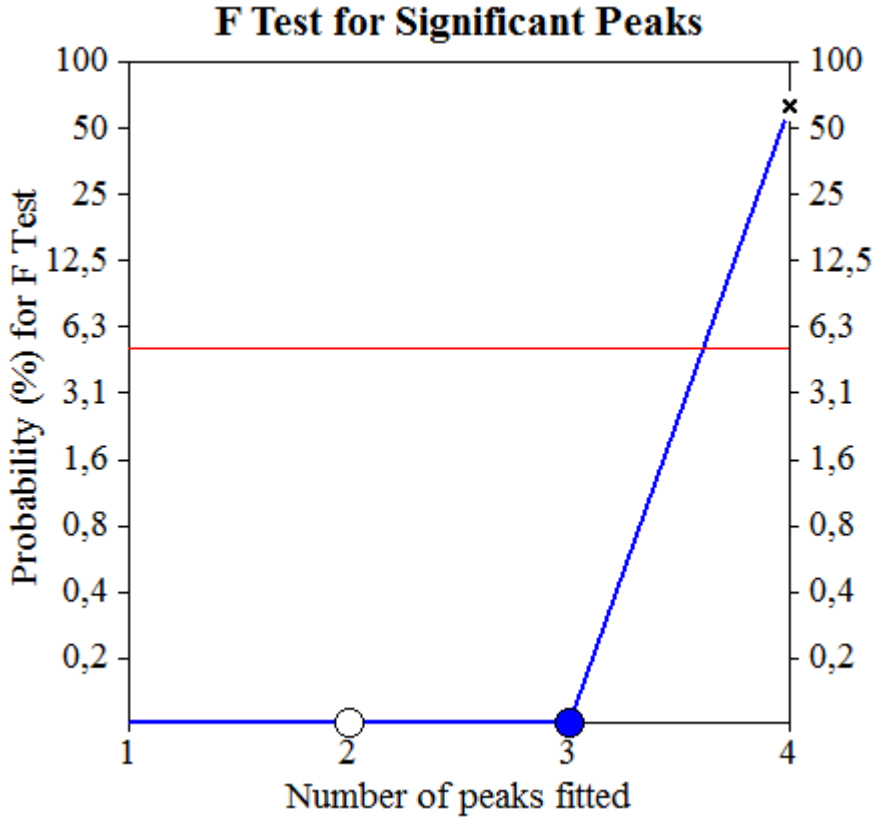
F Test for Significant Peaks
Probability (%) for F Test
100
50
25
12,5
6,3
3,1
1,6
0,8
0,4
0,2
1
2
3
4
Number of peaks fitted

Datafile: C:\BH2\Edna\12-2015\EMP_49\EMP_16_12_2015_20.ftz
Title: Sample No. EMP_49 Irr 12-2015-22

NEW PARAMETERS - ZETA METHOD

EFFECTIVE TRACK DENSITY FOR FLUENCE MONITOR (tracks/cm^2): 2,77E+05
RELATIVE ERROR (%): 1,23
EFFECTIVE URANIUM CONTENT OF MONITOR (ppm): 50,00
ZETA FACTOR AND STANDARD ERROR (yr cm^2): 128,02 1,87
SIZE OF COUNTER SQUARE (cm^2): 8,30E-07

GRAIN AGES IN ORIGINAL ORDER

Grain	RhoS	(Ns)	RhoI	(Ni)	Squares	U+/-2s		Grain Age (Ma)		
no.	(cm^-2)		(cm^-2)					Age	--95% CI--	
1	7,28E+06	(302)	1,20E+06	(50)	50	217	61	106.1	78.7	146.2
2	6,60E+06	(274)	1,37E+06	(57)	50	248	66	84.1	63.2	111.8
3	5,76E+06	(478)	1,48E+06	(123)	100	267	49	68.4	56.0	83.5
4	3,80E+06	(63)	6,02E+05	(10)	20	109	67	109.4	56.7	240.1
5	6,07E+06	(247)	9,34E+05	(38)	49	168	54	114.0	81.2	165.0
6	4,73E+06	(165)	4,02E+05	(14)	42	72	38	203.8	120.0	380.0
7	4,03E+06	(164)	4,92E+05	(20)	49	89	39	143.0	90.6	240.3
8	9,04E+06	(225)	1,37E+06	(34)	30	246	84	116.0	81.1	171.7
9	6,55E+06	(87)	9,04E+05	(12)	16	163	92	126.0	69.7	253.8
10	5,54E+06	(230)	6,02E+05	(25)	50	109	43	160.4	106.9	252.9
11	5,24E+06	(87)	7,23E+05	(12)	20	130	74	126.0	69.7	253.8
12	8,07E+06	(134)	1,81E+06	(30)	20	326	118	78.5	52.8	121.1
13	7,67E+06	(191)	1,53E+06	(38)	30	275	89	88.3	62.4	128.8
14	5,75E+06	(191)	7,53E+05	(25)	40	136	54	133.5	88.5	211.6
15	7,23E+06	(210)	1,65E+06	(48)	35	298	86	77.0	56.2	107.8
16	8,29E+06	(344)	1,40E+06	(58)	50	252	66	103.6	78.5	136.7
17	2,37E+06	(59)	2,41E+05	(6)	30	43	34	168.3	75.1	477.0
18	6,60E+06	(219)	1,42E+06	(47)	40	255	74	82.0	59.8	115.0
19	2,74E+06	(91)	4,22E+05	(14)	40	76	40	113.3	65.0	215.9
20	8,06E+06	(107)	1,43E+06	(19)	16	258	117	98.5	60.7	170.4
21	7,95E+06	(66)	8,43E+05	(7)	10	152	111	162.0	76.4	418.9
22	5,73E+06	(476)	1,08E+06	(90)	100	195	41	92.7	73.9	116.2
23	4,56E+06	(265)	1,41E+06	(82)	70	254	56	56.8	44.3	72.8
24	3,93E+06	(261)	8,58E+05	(57)	80	155	41	80.1	60.2	106.6
25	7,11E+06	(118)	1,39E+06	(23)	20	250	103	89.9	57.6	147.7
26	3,32E+06	(248)	4,28E+05	(32)	90	77	27	135.6	94.2	202.6
27	4,82E+06	(168)	1,15E+06	(40)	42	207	65	73.9	52.3	107.3
28	8,76E+06	(109)	2,01E+06	(25)	15	362	144	76.6	49.5	123.7
29	7,20E+06	(299)	1,57E+06	(65)	50	282	70	80.6	61.6	105.3
30	7,44E+06	(247)	1,99E+06	(66)	40	358	88	65.6	50.0	86.1
31	4,22E+06	(210)	4,42E+05	(22)	60	80	34	166.2	108.0	270.7
32	6,40E+06	(85)	1,20E+06	(16)	16	217	107	92.9	54.6	170.3
33	6,69E+06	(50)	1,47E+06	(11)	9	265	157	79.3	41.3	169.8
34	8,55E+06	(213)	1,57E+06	(39)	30	282	90	95.9	68.3	138.8
35	6,90E+06	(573)	1,06E+06	(88)	100	191	41	114.0	91.0	142.7
36	7,04E+06	(146)	1,73E+06	(36)	25	313	104	71.4	49.5	106.0
37	4,50E+06	(112)	2,81E+05	(7)	30	51	37	272.2	132.0	685.4
38	5,93E+06	(246)	9,64E+05	(40)	50	174	55	107.9	77.4	154.9
39	6,51E+06	(216)	1,51E+06	(50)	40	271	77	76.1	55.9	105.8
40	5,92E+06	(59)	1,51E+06	(15)	12	271	138	68.9	39.0	131.3
41	3,06E+06	(142)	5,38E+05	(25)	56	97	38	99.5	65.2	159.2
42	9,12E+06	(227)	1,37E+06	(34)	30	246	84	117.0	81.8	173.2
43	4,05E+06	(84)	6,75E+05	(14)	25	122	64	104.7	59.8	200.2
44	5,53E+06	(225)	1,25E+06	(51)	49	226	63	77.7	57.3	107.6
45	6,14E+06	(255)	1,57E+06	(65)	50	282	70	68.8	52.4	90.3
46	4,13E+06	(137)	1,48E+06	(49)	40	266	76	49.4	35.5	70.0
47	2,30E+06	(153)	4,82E+05	(32)	80	87	31	84.0	57.4	127.3
48	3,34E+06	(222)	4,22E+05	(28)	80	76	29	138.6	94.0	213.3
49	6,10E+06	(76)	1,12E+06	(14)	15	203	107	94.8	53.8	182.1
50	7,13E+06	(142)	1,26E+06	(25)	24	226	90	99.5	65.2	159.2
51	2,82E+06	(187)	3,92E+05	(26)	80	71	27	125.8	83.8	197.7
52	8,03E+06	(80)	1,20E+06	(12)	12	217	123	116.0	63.8	234.5
53	8,76E+06	(218)	1,20E+06	(30)	30	217	79	127.2	87.2	193.1

Datafile: C:\BH2\Edna\12-2015\EMP_49\EMP_16_12_2015_20.ftz
Title: Sample No. EMP_49 Irr 12-2015-22

Grain no.	RhoS (cm^-2)	(Ns)	RhoI (cm^-2)	(Ni)	Squares	U+/-2s		Grain Age (Ma) Age	--95% CI--	
54	1,54E+06	(46)	1,67E+05	(5)	36	30	26	156.9	64.8	506.6
55	3,33E+06	(69)	3,37E+05	(7)	25	61	44	169.2	80.0	436.6
56	2,71E+06	(90)	4,52E+05	(15)	40	81	41	104.7	61.0	195.3
57	4,82E+06	(64)	8,28E+05	(11)	16	149	88	101.3	53.8	213.8
58	2,31E+06	(94)	4,43E+05	(18)	49	80	37	91.4	55.3	161.3
59	3,33E+06	(83)	4,82E+05	(12)	30	87	49	120.3	66.3	242.7
60	3,13E+06	(78)	7,63E+05	(19)	30	138	62	72.0	43.5	126.3
61	2,81E+06	(28)	9,04E+05	(9)	12	163	106	54.3	25.3	131.8
62	7,98E+06	(265)	1,48E+06	(49)	40	266	76	95.1	70.1	131.8
63	3,10E+06	(103)	5,12E+05	(17)	40	92	44	105.9	63.7	189.1
64	3,34E+06	(111)	6,63E+05	(22)	40	119	50	88.4	56.0	147.1
65	7,15E+06	(178)	1,24E+06	(31)	30	224	80	100.7	68.9	152.8
66	6,48E+06	(538)	1,05E+06	(87)	100	189	41	108.3	86.3	135.8
67	3,31E+06	(44)	1,51E+05	(2)	16	27	34	353.9	101.1	2682.8
68	5,37E+06	(312)	1,27E+06	(74)	70	230	53	73.9	57.4	95.3
69	7,15E+06	(178)	1,24E+06	(31)	30	224	80	100.7	68.9	152.8
70	6,48E+06	(538)	1,05E+06	(87)	100	189	41	108.3	86.3	135.8
71	3,31E+06	(44)	1,51E+05	(2)	16	27	34	353.9	101.1	2682.8
72	5,37E+06	(312)	1,27E+06	(74)	70	230	53	73.9	57.4	95.3
73	5,11E+06	(178)	1,15E+06	(40)	42	207	65	78.3	55.5	113.4
74	5,37E+06	(223)	5,30E+05	(22)	50	96	40	176.3	114.8	286.8
75	5,54E+06	(138)	9,64E+05	(24)	30	174	70	100.7	65.5	162.8
76	5,14E+06	(128)	8,03E+05	(20)	30	145	64	111.9	70.2	189.6
77	5,54E+06	(184)	1,11E+06	(37)	40	201	66	87.4	61.4	128.2
78	7,35E+06	(305)	1,01E+06	(42)	50	182	56	127.3	92.4	180.2
79	1,69E+06	(42)	3,61E+05	(9)	30	65	42	81.2	39.6	190.8
80	2,83E+06	(188)	6,02E+05	(40)	80	109	34	82.7	58.7	119.5
81	4,92E+06	(143)	8,26E+05	(24)	35	149	60	104.4	67.9	168.4
82	2,21E+06	(33)	1,34E+05	(2)	18	24	31	267.5	74.5	2127.5
83	7,08E+06	(94)	8,28E+05	(11)	16	149	88	148.1	80.5	307.1
84	5,35E+06	(71)	9,04E+05	(12)	16	163	92	103.1	56.3	209.5
85	9,49E+06	(126)	2,64E+06	(35)	16	475	160	63.4	43.5	95.2
86	8,18E+06	(285)	2,67E+06	(93)	42	481	100	53.9	42.6	68.2
87	7,68E+06	(255)	1,72E+06	(57)	40	309	82	78.3	58.8	104.3
88	2,94E+06	(171)	2,58E+05	(15)	70	47	24	197.4	118.2	359.6
89	7,93E+06	(79)	1,81E+06	(18)	12	326	152	76.9	46.1	136.8
90	6,35E+06	(369)	1,36E+06	(79)	70	245	55	81.9	64.2	104.5
91	2,82E+06	(164)	4,48E+05	(26)	70	81	31	110.5	73.3	174.3
92	3,90E+06	(97)	4,82E+05	(12)	30	87	49	140.3	78.0	281.3
93	5,79E+06	(202)	1,69E+06	(59)	42	305	79	60.0	44.9	80.2
94	8,19E+06	(204)	2,17E+06	(54)	30	391	106	66.6	49.2	91.8
95	6,53E+06	(271)	1,42E+06	(59)	50	256	67	80.4	60.7	106.5
96	5,23E+06	(152)	9,64E+05	(28)	35	174	65	95.2	63.7	148.3
97	5,49E+06	(114)	1,35E+06	(28)	25	243	91	71.6	47.3	112.7
POOLED	5,30E+06	(17574)	9,99E+05	(3314)	3996	180	8	93.5	88.7	98.5

CHI^2 PROBABILITY (%): 0.0

POOLED AGE W/ 68% CONF. INTERVAL(Ma): 93.5, 91.0 -- 96.0 (-2.5 +2.5)
95% CONF. INTERVAL(Ma): 88.7 -- 98.5 (-4.8 +5.0)

CENTRAL AGE W/ 68% CONF. INTERVAL(Ma): 95.7, 92.2 -- 99.3 (-3.4 +3.6)
95% CONF. INTERVAL(Ma): 89.1 -- 102.8 (-6.6 +7.1)
AGE DISPERSION (%): 23.2

FIT OPTION: Best-fit peaks using the binomial model of Galbraith and Green

INITIAL GUESS FOR MODEL PARAMETERS (number of peaks to fit = 3)

Peak #.	Peak Age	Theta	Fraction(%)	Count
1.	93.50	0.841	41.1	39.89
2.	109.40	0.861	41.8	40.50
3.	139.60	0.888	18.9	18.33

Total range for grain ages:	49,1 to 308,6 Ma
Number of active grains (Num. used for fit):	97
Number of removed grains:	0
Degrees of freedom for fit:	92
Average of the SE(Z)'s for the grains:	0,25
Estimated width of peaks in PD plot in Z units:	0,3

PARAMETERS FOR BEST-FIT PEAKS

* *Standard error for peak age includes group error*
* *Peak width is for PD plot assuming a kernel factor = 0.60*

#.	Peak Age(Ma)	68%CI	95%CI	W(Z)	Frac(%)	SE,%	Count
1.	74.4	-3,5 ...+3,7	-6,7 ...+7,4	0.19	37.1	10.7	35.9
2.	107.4	-7,2 ...+7,7	-13,6 ...+15,6	0.23	52.8	11.5	51.3
3.	158.4	-25,8 ...+30,7	-46,6 ...+65,6	0.31	10.1	9.0	9.8

Log-likelihood for best fit:	-331,339
Chi-squared value for best fit:	97,246
Reduced chi-squared value:	1,057
Probability for F test:	0%
Condition number for COVAR matrix:	41,65
Number of iterations:	22

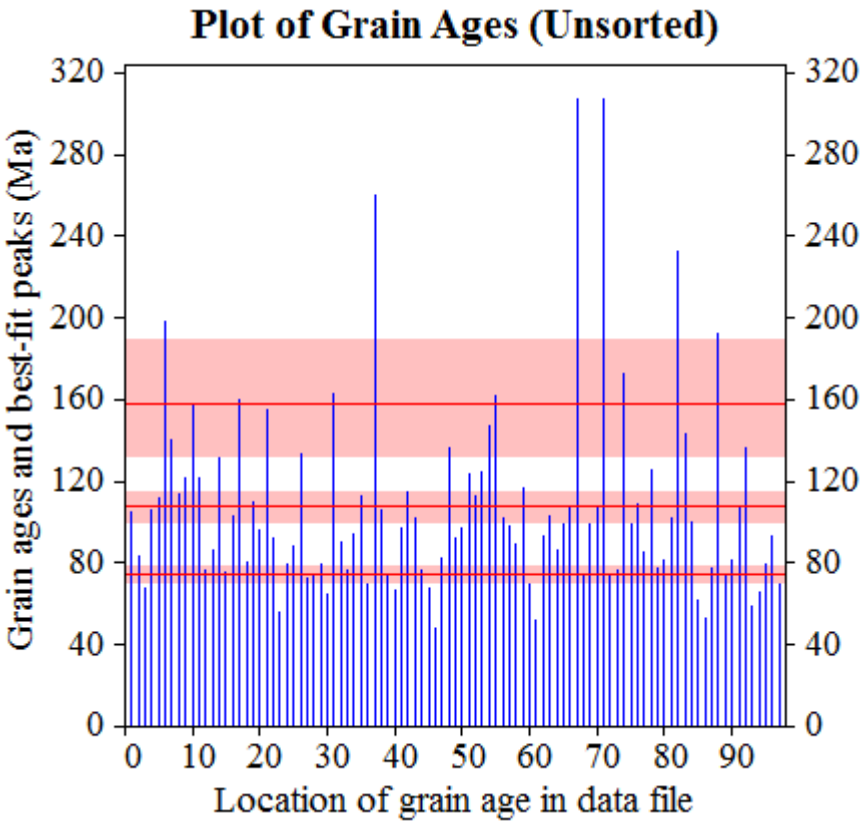
Plot of Grain Ages (Unsorted)
Grain ages and best-fit peaks (Ma)
320
280
240
200
160
120
80
40
0
0 10 20 30 40 50 60 70 80 90
Location of grain age in data file

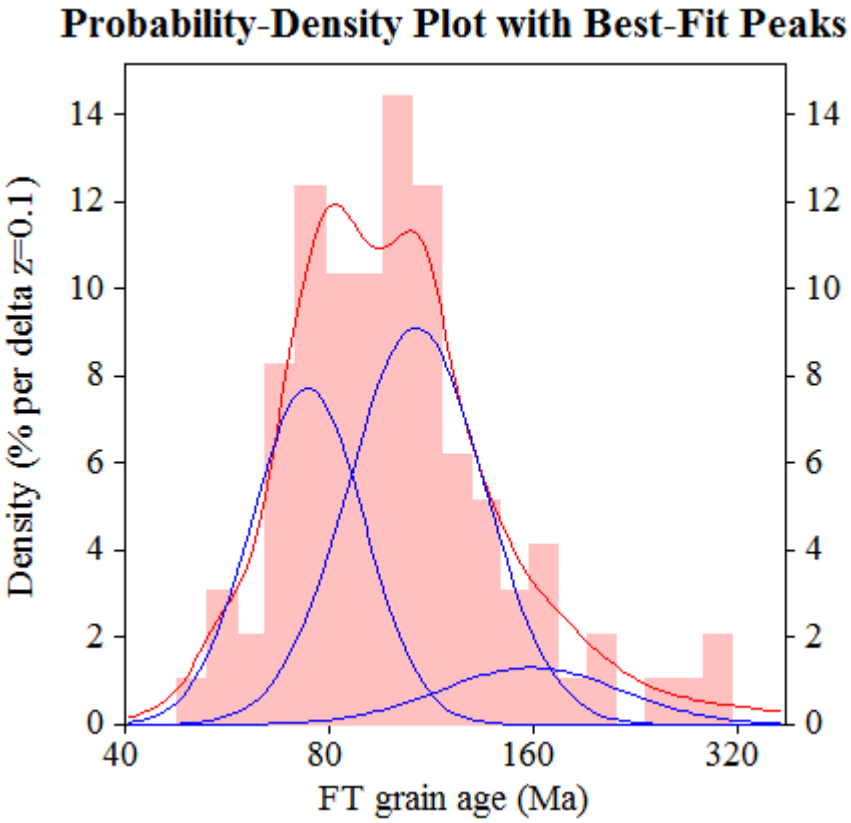
Probability-Density Plot with Best-Fit Peaks
Density (% per delta z=0.1)
14
12
10
8
6
4
2
0
40 80 160 320
FT grain age (Ma)

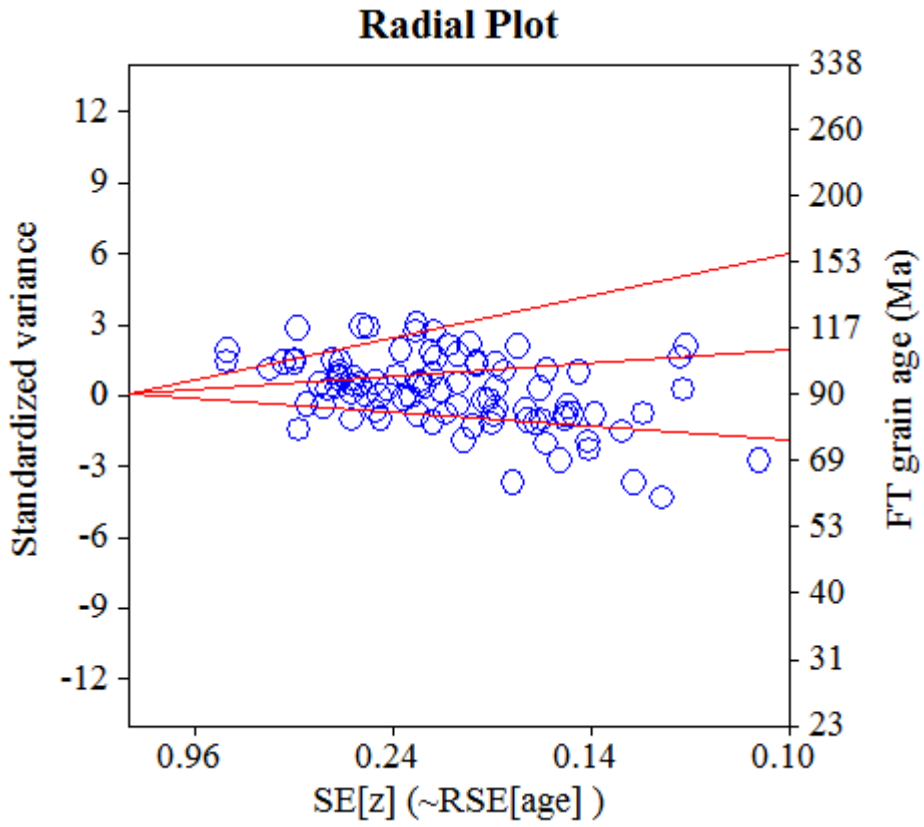
Radial Plot
Standardized variance
12
9
6
3
0
-3
-6
-9
-12
338
260
200
153
117
90
69
53
40
31
23
FT grain age (Ma)
0.96
0.24
0.14
0.10
SE[z] (~RSE[age])

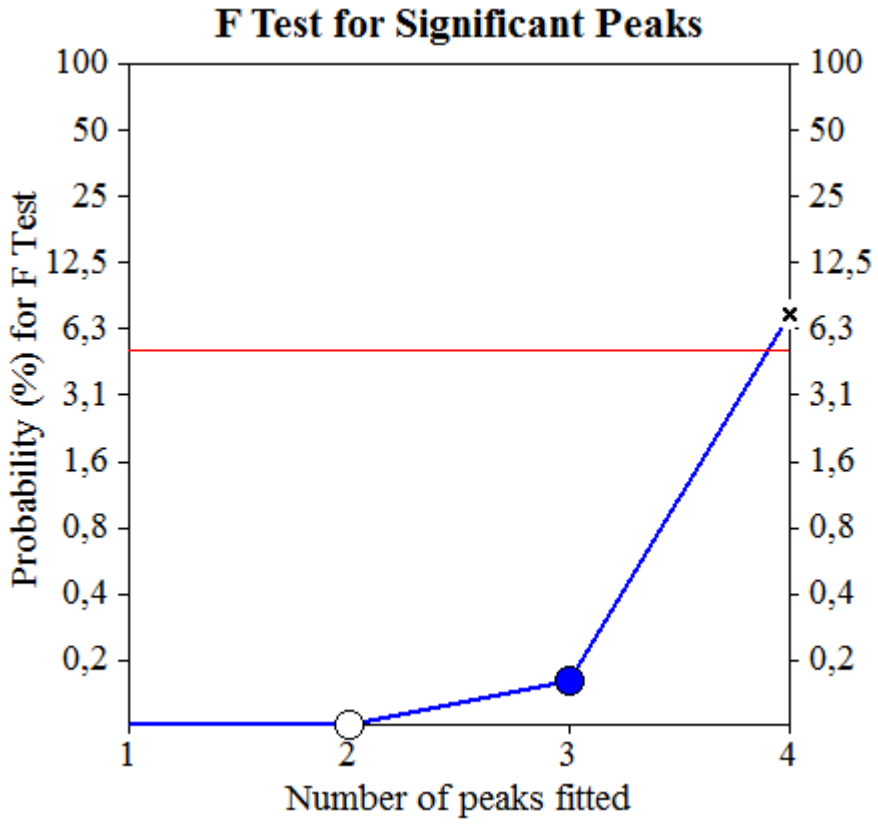
F Test for Significant Peaks
Probability (%) for F Test
100
50
25
12,5
6,3
3,1
1,6
0,8
0,4
0,2
1
2
3
4
Number of peaks fitted

Datafile: C:\Users\Administrador\Documents\PhD\Termocronologia resultados\Z\12-2015\EMP_35b\EMP_35b_12_2015_21.ftz
Title: Sample No. EMP_35b Irr 12-2015-21

NEW PARAMETERS - ZETA METHOD

EFFECTIVE TRACK DENSITY FOR FLUENCE MONITOR (tracks/cm^2): 2.76E+05
RELATIVE ERROR (%): 1.22
EFFECTIVE URANIUM CONTENT OF MONITOR (ppm): 50.00
ZETA FACTOR AND STANDARD ERROR (yr cm^2): 128.02 1.87
SIZE OF COUNTER SQUARE (cm^2): 8.30E-07

GRAIN AGES IN ORIGINAL ORDER

Grain no.	RhoS (cm^-2)	(Ns)	RhoI (cm^-2)	(Ni)	Squares	U+/-2s		Grain Age (Ma) Age	--95% CI--	
1	2.61E+06	(26)	2.01E+05	(2)	12	36	46	211.0	57.3	1740.3
2	3.64E+06	(121)	1.51E+05	(5)	40	27	23	402.0	175.8	1218.6
3	5.70E+06	(142)	3.21E+05	(8)	30	58	40	300.7	153.0	701.5
4	5.22E+06	(39)	2.68E+05	(2)	9	48	61	313.3	88.6	2426.9
5	5.78E+06	(96)	5.42E+05	(9)	20	98	64	182.9	94.5	411.5
6	5.76E+06	(43)	1.20E+06	(9)	9	218	142	82.7	40.5	194.1
7	6.96E+06	(52)	1.20E+06	(9)	9	218	142	99.8	49.6	231.6
8	3.77E+06	(50)	4.52E+05	(6)	16	82	64	142.3	62.8	407.4
9	4.46E+06	(37)	3.61E+05	(3)	10	65	70	204.6	68.6	1020.2
10	7.71E+06	(192)	1.29E+06	(32)	30	233	82	104.7	72.2	157.6
11	6.96E+06	(52)	9.37E+05	(7)	9	170	124	127.4	59.1	333.9
12	5.34E+06	(93)	9.75E+05	(17)	21	177	85	95.2	57.0	170.8
13	3.09E+06	(77)	4.42E+05	(11)	30	80	47	121.0	65.1	253.2
14	6.27E+06	(156)	7.63E+05	(19)	30	138	63	142.4	89.2	243.0
15	4.96E+06	(247)	5.02E+05	(25)	60	91	36	171.3	114.4	269.6
16	6.57E+06	(229)	1.41E+06	(49)	42	255	73	81.9	60.1	114.0
17	5.22E+06	(52)	1.10E+06	(11)	12	200	118	82.1	42.9	175.3
18	3.09E+06	(77)	4.42E+05	(11)	30	80	47	121.0	65.1	253.2
19	5.14E+06	(427)	8.43E+05	(70)	100	153	37	106.2	82.5	136.6
20	3.42E+06	(142)	3.37E+05	(14)	50	61	32	175.0	102.5	328.0
21	8.70E+06	(65)	5.35E+05	(4)	9	97	91	271.0	106.0	1003.6
22	2.69E+06	(67)	6.83E+05	(17)	30	124	59	68.8	40.3	125.4
23	4.12E+06	(171)	4.34E+05	(18)	50	79	37	164.4	102.2	283.9
24	3.84E+06	(134)	4.88E+05	(17)	42	88	42	136.7	83.2	241.8
25	2.80E+06	(58)	6.27E+05	(13)	25	113	62	77.6	42.5	155.1
26	7.63E+06	(57)	1.07E+06	(8)	9	194	133	122.6	59.5	298.7
27	5.87E+06	(78)	1.28E+06	(17)	16	232	111	80.0	47.3	144.7
28	2.91E+06	(58)	2.01E+05	(4)	24	36	34	242.4	94.1	905.7
29	4.29E+06	(57)	8.28E+05	(11)	16	150	89	89.9	47.3	190.9
30	1.61E+06	(40)	1.61E+05	(4)	30	29	27	168.4	63.6	646.8
31	2.09E+06	(26)	1.61E+05	(2)	15	29	37	211.0	57.3	1740.3
32	2.13E+06	(53)	1.61E+05	(4)	30	29	27	222.0	85.7	834.8
33	5.85E+06	(102)	1.09E+06	(19)	21	197	90	93.5	57.5	162.1
34	8.99E+06	(179)	1.56E+06	(31)	24	282	101	100.8	69.0	153.0
35	5.92E+06	(59)	5.02E+05	(5)	12	91	78	199.5	83.9	633.9
36	2.77E+06	(46)	6.02E+05	(10)	20	109	67	79.8	40.3	178.3
37	5.66E+06	(169)	1.04E+06	(31)	36	188	67	95.2	65.0	144.7
38	4.30E+06	(107)	3.61E+05	(9)	30	65	43	203.4	105.7	455.7
39	7.53E+06	(75)	1.31E+06	(13)	12	236	129	100.1	55.9	197.4
40	4.15E+06	(62)	2.68E+05	(4)	18	48	46	258.8	100.9	961.8
41	3.82E+06	(57)	3.35E+05	(5)	18	61	52	192.8	80.9	614.2
42	4.19E+06	(327)	4.74E+05	(37)	94	86	28	153.7	109.9	222.1
43	1.93E+06	(32)	3.01E+05	(5)	20	55	47	109.2	43.6	361.6
44	1.00E+07	(75)	2.01E+06	(15)	9	364	185	87.0	50.1	163.7
45	2.71E+06	(36)	3.77E+05	(5)	16	68	58	122.6	49.6	402.7
46	2.29E+06	(95)	1.93E+05	(8)	50	35	24	202.8	101.4	481.9
47	5.16E+06	(214)	7.95E+05	(33)	50	144	50	113.1	78.6	168.7
48	3.77E+06	(50)	1.51E+05	(2)	16	27	35	398.7	115.0	2955.6
49	6.93E+06	(115)	4.22E+05	(7)	20	76	56	278.1	135.0	699.3
50	4.42E+06	(33)	1.34E+05	(1)	9	24	40	492.1	96.9	9950.2
51	3.68E+06	(110)	4.35E+05	(13)	36	79	43	146.2	83.3	283.6
52	2.33E+06	(116)	1.81E+05	(9)	60	33	21	220.2	114.8	491.7
53	8.51E+06	(113)	9.04E+05	(12)	16	164	93	162.4	90.9	323.6

Datafile: C:\Users\Administrador\Documents\PhD\Termocronologia resultados\Z\12-2015\EMP_35b\EMP_35b_12_2015_21.ftz
Title: Sample No. EMP_35b Irr 12-2015-21

Grain no.	RhoS (cm^-2)	(Ns)	RhoI (cm^-2)	(Ni)	Squares	U+/-2s	Grain Age (Ma) Age	--95% CI--	
54	3.35E+06	(25)	1.47E+06	(11)	9	267 157	39.7	19.0	89.9
55	1.81E+06	(60)	2.41E+05	(8)	40	44 30	129.0	62.8	313.4
56	5.06E+06	(294)	4.82E+05	(28)	70	87 33	182.0	124.4	278.3
57	7.52E+06	(624)	1.28E+06	(106)	100	231 45	102.7	83.5	126.4
58	9.42E+06	(391)	1.40E+06	(58)	50	253 66	117.1	88.9	154.0
59	7.36E+06	(55)	6.69E+05	(5)	9	121 103	186.2	77.9	594.3
60	5.66E+06	(188)	7.23E+05	(24)	40	131 53	136.2	89.6	217.9
61	3.68E+06	(214)	6.37E+05	(37)	70	115 38	101.1	71.4	147.5
62	5.31E+06	(216)	7.62E+05	(31)	49	138 49	121.4	83.6	183.2
63	8.63E+06	(86)	1.10E+06	(11)	12	200 118	135.0	73.0	281.0
64	2.73E+06	(181)	5.42E+05	(36)	80	98 33	87.9	61.5	129.7
65	8.16E+06	(271)	7.83E+05	(26)	40	142 55	180.6	121.7	281.1
66	4.28E+06	(284)	3.61E+05	(24)	80	65 26	204.6	136.2	323.8
67	4.18E+06	(52)	5.62E+05	(7)	15	102 74	127.4	59.1	333.9
68	2.69E+06	(134)	3.41E+05	(17)	60	62 30	136.7	83.2	241.8
69	2.41E+06	(50)	1.45E+05	(3)	25	26 28	274.7	94.4	1329.8
70	7.53E+06	(250)	1.27E+06	(42)	40	229 71	104.0	75.1	148.0
71	3.73E+06	(93)	4.02E+05	(10)	30	73 45	160.0	84.9	344.8
72	4.02E+06	(30)	8.03E+05	(6)	9	145 114	85.9	36.1	254.7
73	4.82E+06	(280)	4.65E+05	(27)	70	84 32	179.8	122.0	277.3
74	4.63E+06	(192)	5.30E+05	(22)	50	96 41	151.4	98.2	247.3
75	3.03E+06	(151)	3.61E+05	(18)	60	65 30	145.4	90.0	252.1
76	4.93E+06	(368)	5.49E+05	(41)	90	99 31	156.2	113.6	221.1
77	3.18E+06	(264)	1.02E+06	(85)	100	185 40	54.4	42.5	69.5
78	4.88E+06	(405)	8.80E+05	(73)	100	159 37	96.7	75.3	124.0
79	7.92E+06	(657)	1.27E+06	(105)	100	229 45	109.1	88.7	134.2
80	6.46E+06	(193)	6.36E+05	(19)	36	115 52	175.7	110.8	297.9
81	6.70E+06	(139)	1.01E+06	(21)	25	183 79	115.2	73.1	192.2
82	3.37E+06	(28)	1.20E+06	(10)	10	218 135	48.8	23.3	113.2
83	6.31E+06	(262)	9.64E+05	(40)	50	175 55	114.3	82.2	163.8
84	2.37E+06	(63)	4.52E+05	(12)	32	82 46	91.1	49.4	186.4
85	6.59E+06	(547)	1.41E+06	(117)	100	255 48	81.8	66.8	100.0
86	3.13E+06	(260)	4.70E+05	(39)	100	85 27	116.4	83.3	167.5
87	3.04E+06	(252)	6.39E+05	(53)	100	116 32	83.3	61.9	114.4
88	5.30E+06	(220)	1.16E+06	(48)	50	209 60	80.3	58.7	112.3
89	7.08E+06	(147)	1.73E+06	(36)	25	314 104	71.5	49.6	106.2
90	5.35E+06	(160)	6.69E+05	(20)	36	121 54	138.9	87.9	233.6
91	6.18E+06	(154)	6.02E+05	(15)	30	109 55	177.2	105.7	324.0
92	6.67E+06	(554)	1.02E+06	(85)	100	185 40	113.5	90.3	142.7
93	3.36E+06	(209)	4.18E+05	(26)	75	76 29	139.8	93.5	219.0
94	6.73E+06	(335)	1.08E+06	(54)	60	196 53	107.7	80.9	143.4
95	5.88E+06	(244)	8.67E+05	(36)	50	157 52	118.2	83.6	172.9
96	3.15E+06	(157)	3.61E+05	(18)	60	65 30	151.1	93.7	261.7
97	7.43E+06	(259)	1.12E+06	(39)	42	203 65	115.9	83.0	166.8
98	7.45E+06	(99)	1.20E+06	(16)	16	218 108	107.5	63.8	195.9
99	6.96E+06	(52)	1.47E+06	(11)	9	267 157	82.1	42.9	175.3
POOLED	4.85E+06	(15535)	7.15E+05	(2288)	3856	129 6	118.9	112.3	125.8

CHI^2 PROBABILITY (%): 0.0

POOLED AGE W/ 68% CONF. INTERVAL(Ma): 118.9, 115.5 -- 122.4 (-3.4 +3.5)
95% CONF. INTERVAL(Ma): 112.3 -- 125.8 (-6.6 +7.0)

CENTRAL AGE W/ 68% CONF. INTERVAL(Ma): 123.5, 118.4 -- 128.9 (-5.1 +5.3)
95% CONF. INTERVAL(Ma): 113.7 -- 134.2 (-9.8 +10.7)
AGE DISPERSION (%): 27.3

FIT OPTION: Best-fit peaks using the binomial model of Galbraith and Green

INITIAL GUESS FOR MODEL PARAMETERS (number of peaks to fit = 3)

Peak #.	Peak Age	Theta	Fraction(%)	Count
1.	39.10	0.690	1.2	1.18
2.	118.90	0.872	35.8	35.43
3.	311.20	0.947	5.2	5.12

Total range for grain ages: 39.1 to 383.1 Ma
Number of active grains (Num. used for fit): 99
Number of removed grains: 0
Degrees of freedom for fit: 94
Average of the SE(Z)'s for the grains: 0.33
Estimated width of peaks in PD plot in Z units: 0.39

PARAMETERS FOR BEST-FIT PEAKS

* *Standard error for peak age includes group error*
* *Peak width is for PD plot assuming a kernel factor = 0.60*

#.	Peak Age(Ma)	68%CI	95%CI	W(Z)	Frac(%)	SE,%	Count
1.	55.6	-7.1 ...+8.1	-13.0 ...+16.9	0.18	1.8	1.8	1.8
2.	104.9	-4.0 ...+4.2	-7.7 ...+8.3	0.23	56.4	8.4	55.8
3.	170.5	-10.3 ...+10.9	-19.6 ...+22.1	0.33	41.7	8.3	41.3

Log-likelihood for best fit: -306.293
Chi-squared value for best fit: 103.646
Reduced chi-squared value: 1.103
Probability for F test: 0%
Condition number for COVAR matrix: 64.72
Number of iterations: 18

Datafile: C:\Users\Administrador\Documents\PhD\Termocronologia resultados\Z\12-2015\EMP_35b\EMP_35b_12_2015_21.ftz
Title: Sample No. EMP_35b Irr 12-2015-21

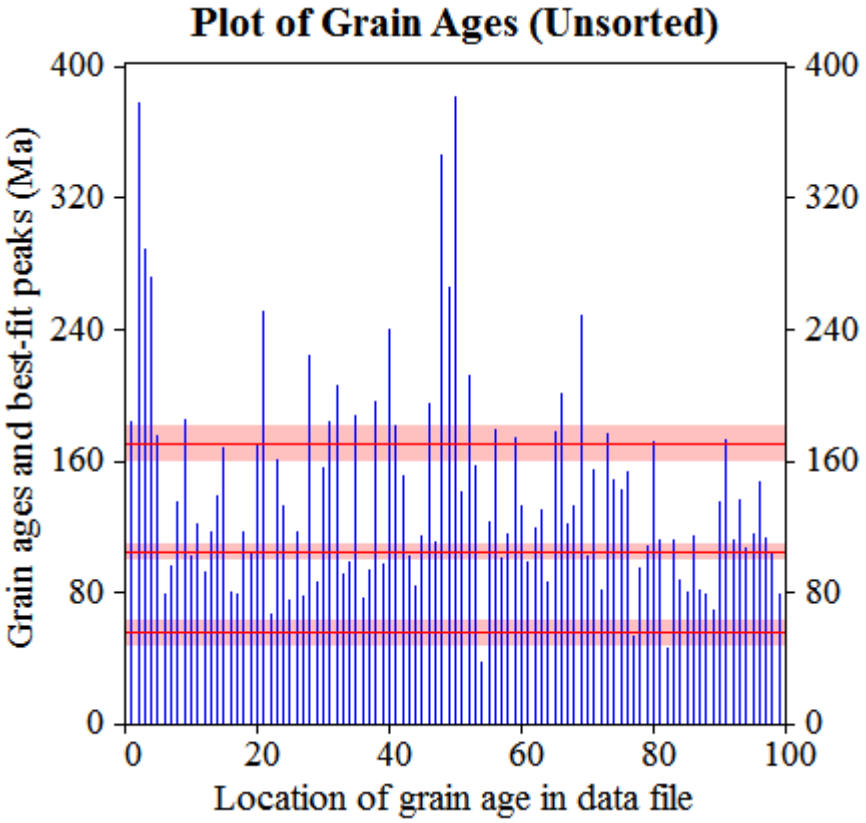

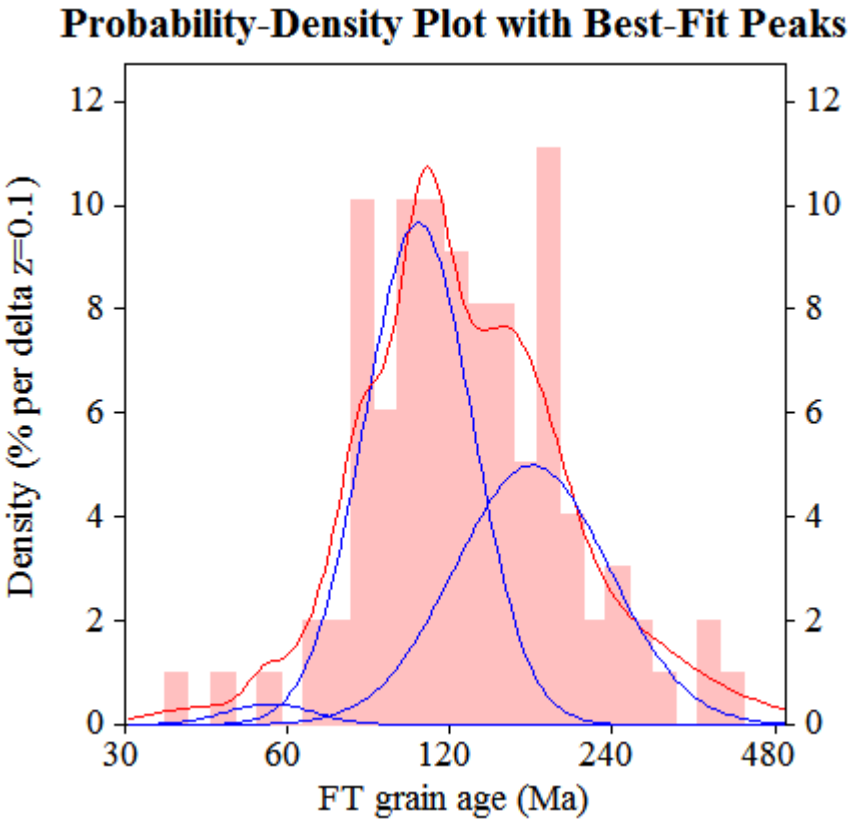

Datafile: C:\Users\Administrador\Documents\PhD\Termocronologia resultados\Z\12-2015\EMP_35b\EMP_35b_12_2015_21.ftz
Title: Sample No. EMP_35b Irr 12-2015-21

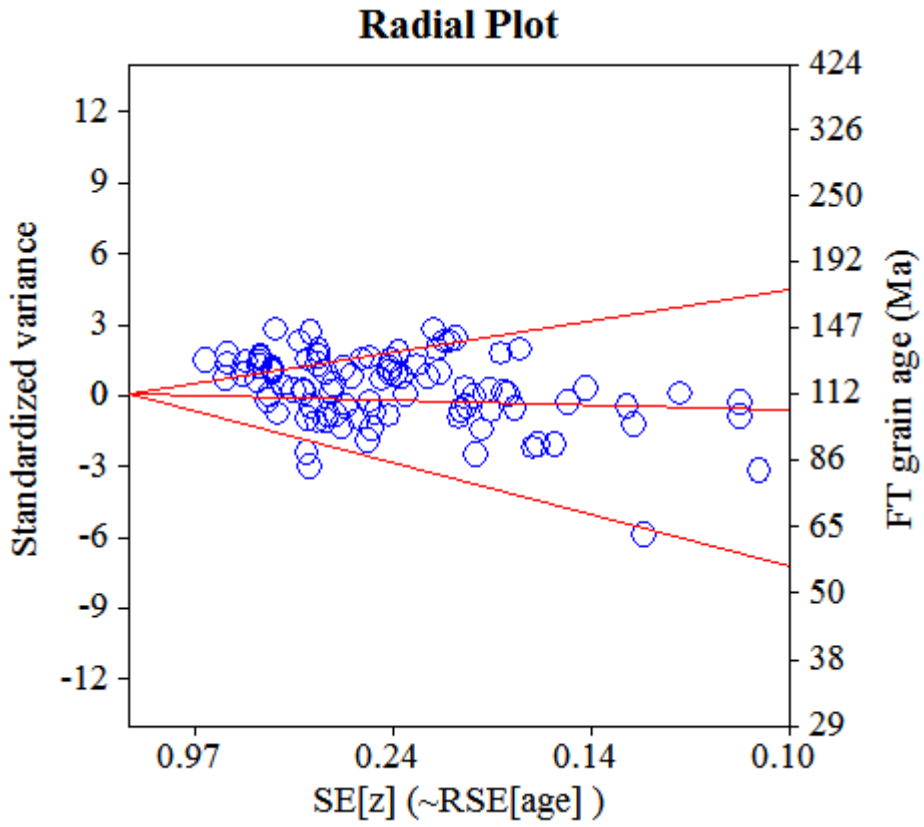

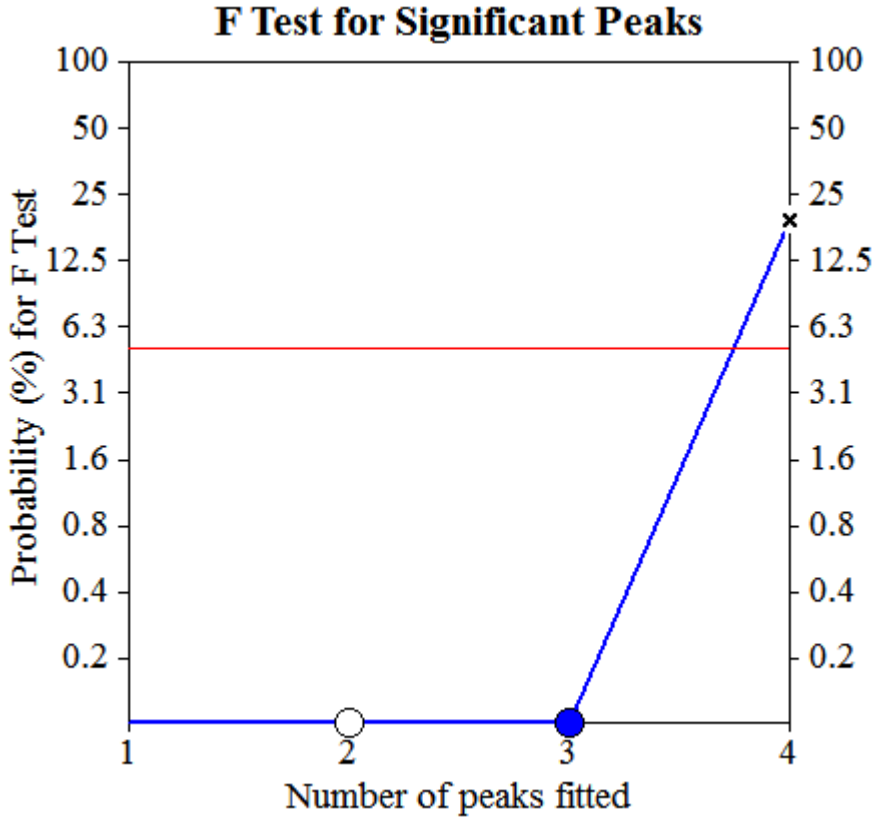

Datafile: C:\BH2\Edna\12-2015\EMP_49\EMP_49_12_2015_22.ftz
Title: Sample No. EMP_49 Irr 12-2015-22

NEW PARAMETERS - ZETA METHOD

EFFECTIVE TRACK DENSITY FOR FLUENCE MONITOR (tracks/cm^2): 2,77E+05
RELATIVE ERROR (%): 1,23
EFFECTIVE URANIUM CONTENT OF MONITOR (ppm): 50,00
ZETA FACTOR AND STANDARD ERROR (yr cm^2): 128,02 1,87
SIZE OF COUNTER SQUARE (cm^2): 8,30E-07

GRAIN AGES IN ORIGINAL ORDER

Grain	RhoS	(Ns)	RhoI	(Ni)	Squares	U+/-2s		Grain Age (Ma)		
no.	(cm^-2)		(cm^-2)					Age	--95% CI--	
1	7,28E+06	(302)	1,20E+06	(50)	50	217	61	106.1	78.7	146.2
2	6,60E+06	(274)	1,37E+06	(57)	50	248	66	84.1	63.2	111.8
3	5,76E+06	(478)	1,48E+06	(123)	100	267	49	68.4	56.0	83.5
4	3,80E+06	(63)	6,02E+05	(10)	20	109	67	109.4	56.7	240.1
5	6,07E+06	(247)	9,34E+05	(38)	49	168	54	114.0	81.2	165.0
6	4,73E+06	(165)	4,02E+05	(14)	42	72	38	203.8	120.0	380.0
7	4,03E+06	(164)	4,92E+05	(20)	49	89	39	143.0	90.6	240.3
8	9,04E+06	(225)	1,37E+06	(34)	30	246	84	116.0	81.1	171.7
9	6,55E+06	(87)	9,04E+05	(12)	16	163	92	126.0	69.7	253.8
10	5,54E+06	(230)	6,02E+05	(25)	50	109	43	160.4	106.9	252.9
11	5,24E+06	(87)	7,23E+05	(12)	20	130	74	126.0	69.7	253.8
12	8,07E+06	(134)	1,81E+06	(30)	20	326	118	78.5	52.8	121.1
13	7,67E+06	(191)	1,53E+06	(38)	30	275	89	88.3	62.4	128.8
14	5,75E+06	(191)	7,53E+05	(25)	40	136	54	133.5	88.5	211.6
15	7,23E+06	(210)	1,65E+06	(48)	35	298	86	77.0	56.2	107.8
16	8,29E+06	(344)	1,40E+06	(58)	50	252	66	103.6	78.5	136.7
17	2,37E+06	(59)	2,41E+05	(6)	30	43	34	168.3	75.1	477.0
18	6,60E+06	(219)	1,42E+06	(47)	40	255	74	82.0	59.8	115.0
19	2,74E+06	(91)	4,22E+05	(14)	40	76	40	113.3	65.0	215.9
20	8,06E+06	(107)	1,43E+06	(19)	16	258	117	98.5	60.7	170.4
21	7,95E+06	(66)	8,43E+05	(7)	10	152	111	162.0	76.4	418.9
22	5,73E+06	(476)	1,08E+06	(90)	100	195	41	92.7	73.9	116.2
23	4,56E+06	(265)	1,41E+06	(82)	70	254	56	56.8	44.3	72.8
24	3,93E+06	(261)	8,58E+05	(57)	80	155	41	80.1	60.2	106.6
25	7,11E+06	(118)	1,39E+06	(23)	20	250	103	89.9	57.6	147.7
26	3,32E+06	(248)	4,28E+05	(32)	90	77	27	135.6	94.2	202.6
27	4,82E+06	(168)	1,15E+06	(40)	42	207	65	73.9	52.3	107.3
28	8,76E+06	(109)	2,01E+06	(25)	15	362	144	76.6	49.5	123.7
29	7,20E+06	(299)	1,57E+06	(65)	50	282	70	80.6	61.6	105.3
30	7,44E+06	(247)	1,99E+06	(66)	40	358	88	65.6	50.0	86.1
31	4,22E+06	(210)	4,42E+05	(22)	60	80	34	166.2	108.0	270.7
32	6,40E+06	(85)	1,20E+06	(16)	16	217	107	92.9	54.6	170.3
33	6,69E+06	(50)	1,47E+06	(11)	9	265	157	79.3	41.3	169.8
34	8,55E+06	(213)	1,57E+06	(39)	30	282	90	95.9	68.3	138.8
35	6,90E+06	(573)	1,06E+06	(88)	100	191	41	114.0	91.0	142.7
36	7,04E+06	(146)	1,73E+06	(36)	25	313	104	71.4	49.5	106.0
37	4,50E+06	(112)	2,81E+05	(7)	30	51	37	272.2	132.0	685.4
38	5,93E+06	(246)	9,64E+05	(40)	50	174	55	107.9	77.4	154.9
39	6,51E+06	(216)	1,51E+06	(50)	40	271	77	76.1	55.9	105.8
40	5,92E+06	(59)	1,51E+06	(15)	12	271	138	68.9	39.0	131.3
41	3,06E+06	(142)	5,38E+05	(25)	56	97	38	99.5	65.2	159.2
42	9,12E+06	(227)	1,37E+06	(34)	30	246	84	117.0	81.8	173.2
43	4,05E+06	(84)	6,75E+05	(14)	25	122	64	104.7	59.8	200.2
44	5,53E+06	(225)	1,25E+06	(51)	49	226	63	77.7	57.3	107.6
45	6,14E+06	(255)	1,57E+06	(65)	50	282	70	68.8	52.4	90.3
46	4,13E+06	(137)	1,48E+06	(49)	40	266	76	49.4	35.5	70.0
47	2,30E+06	(153)	4,82E+05	(32)	80	87	31	84.0	57.4	127.3
48	3,34E+06	(222)	4,22E+05	(28)	80	76	29	138.6	94.0	213.3
49	6,10E+06	(76)	1,12E+06	(14)	15	203	107	94.8	53.8	182.1
50	7,13E+06	(142)	1,26E+06	(25)	24	226	90	99.5	65.2	159.2
51	2,82E+06	(187)	3,92E+05	(26)	80	71	27	125.8	83.8	197.7
52	8,03E+06	(80)	1,20E+06	(12)	12	217	123	116.0	63.8	234.5
53	8,76E+06	(218)	1,20E+06	(30)	30	217	79	127.2	87.2	193.1

Datafile: C:\BH2\Edna\12-2015\EMP_49\EMP_49_12_2015_22.ftz
Title: Sample No. EMP_49 Irr 12-2015-22

Grain no.	RhoS (cm^-2)	(Ns)	RhoI (cm^-2)	(Ni)	Squares	U+/-2s		Grain Age (Ma) Age	--95% CI--	
54	1,54E+06	(46)	1,67E+05	(5)	36	30	26	156.9	64.8	506.6
55	3,33E+06	(69)	3,37E+05	(7)	25	61	44	169.2	80.0	436.6
56	2,71E+06	(90)	4,52E+05	(15)	40	81	41	104.7	61.0	195.3
57	4,82E+06	(64)	8,28E+05	(11)	16	149	88	101.3	53.8	213.8
58	2,31E+06	(94)	4,43E+05	(18)	49	80	37	91.4	55.3	161.3
59	3,33E+06	(83)	4,82E+05	(12)	30	87	49	120.3	66.3	242.7
60	3,13E+06	(78)	7,63E+05	(19)	30	138	62	72.0	43.5	126.3
61	2,81E+06	(28)	9,04E+05	(9)	12	163	106	54.3	25.3	131.8
62	7,98E+06	(265)	1,48E+06	(49)	40	266	76	95.1	70.1	131.8
63	3,10E+06	(103)	5,12E+05	(17)	40	92	44	105.9	63.7	189.1
64	3,34E+06	(111)	6,63E+05	(22)	40	119	50	88.4	56.0	147.1
65	7,15E+06	(178)	1,24E+06	(31)	30	224	80	100.7	68.9	152.8
66	6,48E+06	(538)	1,05E+06	(87)	100	189	41	108.3	86.3	135.8
67	3,31E+06	(44)	1,51E+05	(2)	16	27	34	353.9	101.1	2682.8
68	5,37E+06	(312)	1,27E+06	(74)	70	230	53	73.9	57.4	95.3
69	7,15E+06	(178)	1,24E+06	(31)	30	224	80	100.7	68.9	152.8
70	6,48E+06	(538)	1,05E+06	(87)	100	189	41	108.3	86.3	135.8
71	3,31E+06	(44)	1,51E+05	(2)	16	27	34	353.9	101.1	2682.8
72	5,37E+06	(312)	1,27E+06	(74)	70	230	53	73.9	57.4	95.3
73	5,11E+06	(178)	1,15E+06	(40)	42	207	65	78.3	55.5	113.4
74	5,37E+06	(223)	5,30E+05	(22)	50	96	40	176.3	114.8	286.8
75	5,54E+06	(138)	9,64E+05	(24)	30	174	70	100.7	65.5	162.8
76	5,14E+06	(128)	8,03E+05	(20)	30	145	64	111.9	70.2	189.6
77	5,54E+06	(184)	1,11E+06	(37)	40	201	66	87.4	61.4	128.2
78	7,35E+06	(305)	1,01E+06	(42)	50	182	56	127.3	92.4	180.2
79	1,69E+06	(42)	3,61E+05	(9)	30	65	42	81.2	39.6	190.8
80	2,83E+06	(188)	6,02E+05	(40)	80	109	34	82.7	58.7	119.5
81	4,92E+06	(143)	8,26E+05	(24)	35	149	60	104.4	67.9	168.4
82	2,21E+06	(33)	1,34E+05	(2)	18	24	31	267.5	74.5	2127.5
83	7,08E+06	(94)	8,28E+05	(11)	16	149	88	148.1	80.5	307.1
84	5,35E+06	(71)	9,04E+05	(12)	16	163	92	103.1	56.3	209.5
85	9,49E+06	(126)	2,64E+06	(35)	16	475	160	63.4	43.5	95.2
86	8,18E+06	(285)	2,67E+06	(93)	42	481	100	53.9	42.6	68.2
87	7,68E+06	(255)	1,72E+06	(57)	40	309	82	78.3	58.8	104.3
88	2,94E+06	(171)	2,58E+05	(15)	70	47	24	197.4	118.2	359.6
89	7,93E+06	(79)	1,81E+06	(18)	12	326	152	76.9	46.1	136.8
90	6,35E+06	(369)	1,36E+06	(79)	70	245	55	81.9	64.2	104.5
91	2,82E+06	(164)	4,48E+05	(26)	70	81	31	110.5	73.3	174.3
92	3,90E+06	(97)	4,82E+05	(12)	30	87	49	140.3	78.0	281.3
93	5,79E+06	(202)	1,69E+06	(59)	42	305	79	60.0	44.9	80.2
94	8,19E+06	(204)	2,17E+06	(54)	30	391	106	66.6	49.2	91.8
95	6,53E+06	(271)	1,42E+06	(59)	50	256	67	80.4	60.7	106.5
96	5,23E+06	(152)	9,64E+05	(28)	35	174	65	95.2	63.7	148.3
97	5,49E+06	(114)	1,35E+06	(28)	25	243	91	71.6	47.3	112.7
POOLED	5,30E+06	(17574)	9,99E+05	(3314)	3996	180	8	93.5	88.7	98.5

CHI^2 PROBABILITY (%): 0.0

POOLED AGE W/ 68% CONF. INTERVAL(Ma): 93.5, 91.0 -- 96.0 (-2.5 +2.5)
95% CONF. INTERVAL(Ma): 88.7 -- 98.5 (-4.8 +5.0)

CENTRAL AGE W/ 68% CONF. INTERVAL(Ma): 95.7, 92.2 -- 99.3 (-3.4 +3.6)
95% CONF. INTERVAL(Ma): 89.1 -- 102.8 (-6.6 +7.1)
AGE DISPERSION (%): 23.2

FIT OPTION: Best-fit peaks using the binomial model of Galbraith and Green

INITIAL GUESS FOR MODEL PARAMETERS (number of peaks to fit = 3)

Peak #.	Peak Age	Theta	Fraction(%)	Count
1.	93.50	0.841	41.1	39.89
2.	109.40	0.861	41.8	40.50
3.	139.60	0.888	18.9	18.33

Total range for grain ages:	49,1 to 308,6 Ma
Number of active grains (Num. used for fit):	97
Number of removed grains:	0
Degrees of freedom for fit:	92
Average of the SE(Z)'s for the grains:	0,25
Estimated width of peaks in PD plot in Z units:	0,3

PARAMETERS FOR BEST-FIT PEAKS

* *Standard error for peak age includes group error*
* *Peak width is for PD plot assuming a kernel factor = 0.60*

#.	Peak Age(Ma)	68%CI	95%CI	W(Z)	Frac(%)	SE,%	Count
1.	74.4	-3,5 ...+3,7	-6,7 ...+7,4	0.19	37.1	10.7	35.9
2.	107.4	-7,2 ...+7,7	-13,6 ...+15,6	0.23	52.8	11.5	51.3
3.	158.4	-25,8 ...+30,7	-46,6 ...+65,6	0.31	10.1	9.0	9.8

Log-likelihood for best fit:	-331,339
Chi-squared value for best fit:	97,246
Reduced chi-squared value:	1,057
Probability for F test:	0%
Condition number for COVAR matrix:	41,65
Number of iterations:	22

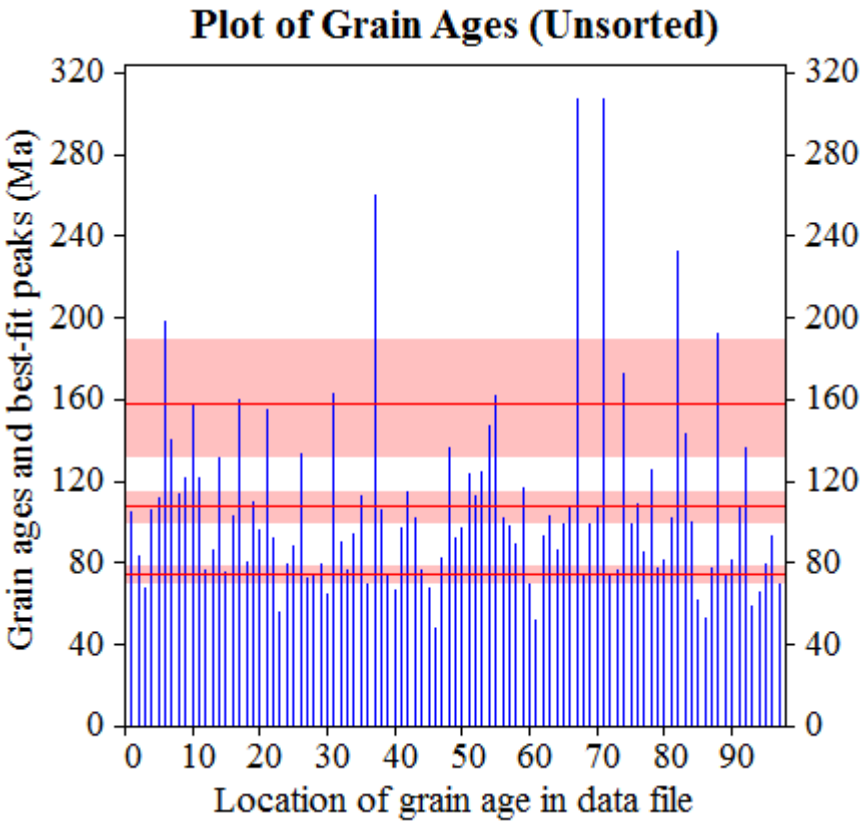
Plot of Grain Ages (Unsorted)
Grain ages and best-fit peaks (Ma)
320
280
240
200
160
120
80
40
0
0 10 20 30 40 50 60 70 80 90
Location of grain age in data file

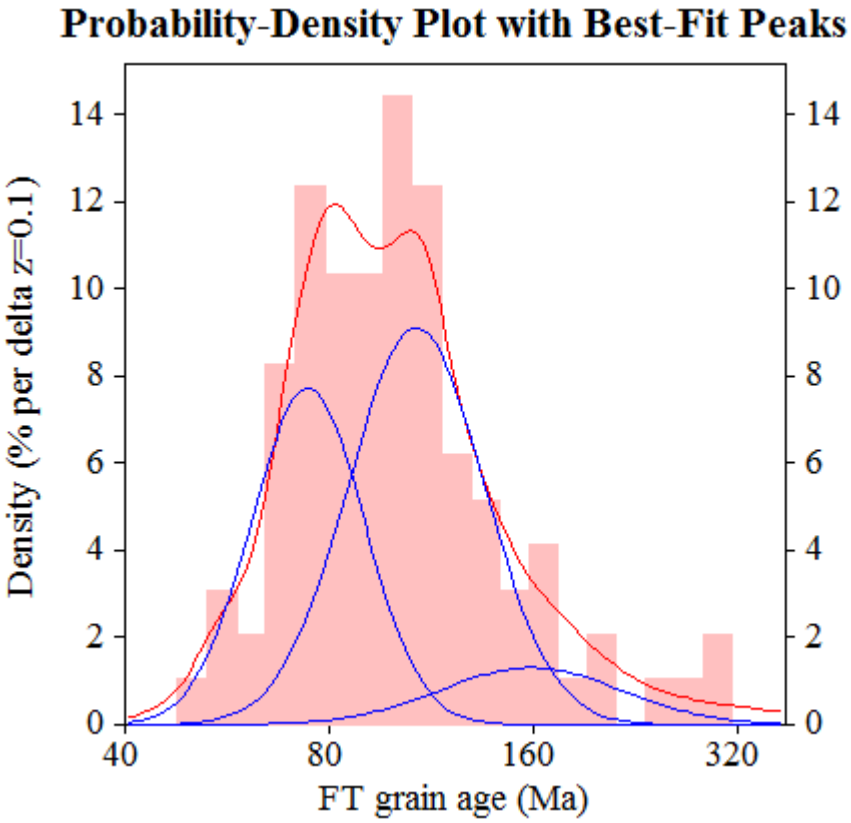
Probability-Density Plot with Best-Fit Peaks
Density (% per delta z=0.1)
14
12
10
8
6
4
2
0
40 80 160 320
FT grain age (Ma)

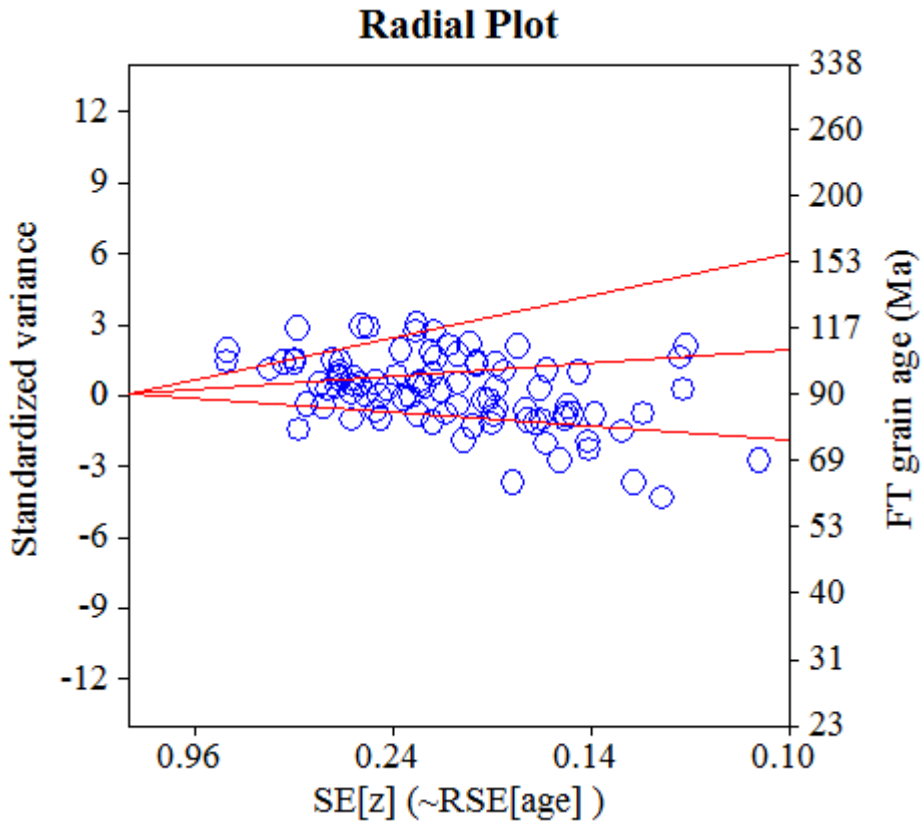
Radial Plot
Standardized variance
12
9
6
3
0
-3
-6
-9
-12
338
260
200
153
117
90
69
53
40
31
23
FT grain age (Ma)
0.96
0.24
0.14
0.10
SE[z] (~RSE[age])

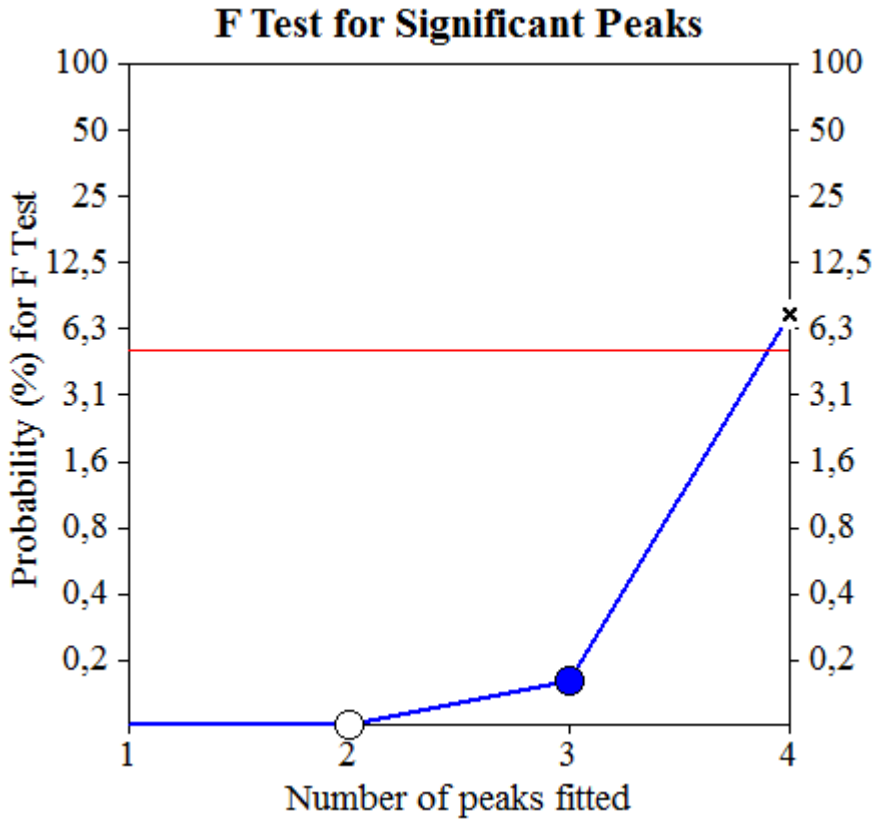
F Test for Significant Peaks
Probability (%) for F Test
100
50
25
12,5
6,3
3,1
1,6
0,8
0,4
0,2
1
2
3
4
Number of peaks fitted

NEW PARAMETERS - ZETA METHOD

EFFECTIVE TRACK DENSITY FOR FLUENCE MONITOR (tracks/cm^2): 1,01E+06
RELATIVE ERROR (%): 1,16
EFFECTIVE URANIUM CONTENT OF MONITOR (ppm): 15,00
ZETA FACTOR AND STANDARD ERROR (yr cm^2): 284,52 5,65
SIZE OF COUNTER SQUARE (cm^2): 6,39E-07

GRAIN AGES IN ORIGINAL ORDER

Grain no.	RhoS (cm^-2)	(Ns)	RhoI (cm^-2)	(Ni)	Squares	U+/-2s		Grain Age (Ma) Age	--95% CI--	
1	1,56E+05	(6)	3,13E+05	(12)	60	5	3	72.3	22.0	203.3
2	9,39E+04	(3)	2,19E+05	(7)	50	3	2	63.0	10.2	263.8
3	1,88E+05	(12)	5,01E+05	(32)	100	7	3	54.0	25.2	106.4
4	2,35E+05	(15)	7,36E+05	(47)	100	11	3	45.9	23.7	82.8
5	1,25E+05	(4)	1,56E+05	(5)	50	2	2	114.6	22.7	512.3
6	1,17E+05	(6)	2,15E+05	(11)	80	3	2	78.7	23.7	226.8
7	7,82E+04	(3)	2,09E+05	(8)	60	3	2	55.3	9.2	220.3
8	3,35E+05	(15)	1,12E+06	(50)	70	17	5	43.2	22.4	77.4
9	1,96E+05	(10)	3,52E+05	(18)	80	5	2	79.8	32.8	179.6
10	2,19E+05	(7)	5,63E+05	(18)	50	8	4	56.3	19.7	138.5
11	6,96E+05	(16)	2,22E+06	(51)	36	33	9	45.2	23.9	79.7
12	1,10E+05	(7)	2,50E+05	(16)	100	4	2	63.2	21.8	159.3
13	2,90E+05	(10)	8,40E+05	(29)	54	13	5	49.8	21.5	103.6
14	1,88E+05	(12)	4,54E+05	(29)	100	7	2	59.5	27.5	118.9
15	1,88E+05	(12)	4,69E+05	(30)	100	7	3	57.6	26.7	114.4
16	4,69E+04	(3)	9,39E+04	(6)	100	1	1	73.1	11.6	327.4
17	9,39E+04	(6)	2,82E+05	(18)	100	4	2	48.5	15.5	124.6
18	1,56E+04	(1)	4,69E+04	(3)	100	1	1	51.9	0.9	569.6
19	1,56E+05	(4)	4,69E+05	(12)	40	7	4	48.9	11.2	155.9
20	8,94E+04	(4)	2,46E+05	(11)	70	4	2	53.2	12.1	173.7
21	9,78E+04	(5)	6,85E+05	(35)	80	10	3	21.0	6.3	52.3
22	1,37E+05	(7)	4,30E+05	(22)	80	6	3	46.2	16.4	109.7
23	1,72E+05	(11)	5,01E+05	(32)	100	7	3	49.6	22.4	99.6
24	5,63E+05	(18)	1,82E+06	(58)	50	27	7	44.6	24.6	76.2
25	1,17E+05	(6)	5,48E+05	(28)	80	8	3	31.3	10.4	75.2
26	3,76E+05	(24)	1,82E+06	(116)	100	27	5	29.8	18.2	46.2
27	6,26E+04	(2)	1,56E+05	(5)	50	2	2	59.6	5.5	341.3
28	3,76E+05	(12)	7,82E+05	(25)	50	12	5	69.0	31.4	140.7
29	9,39E+04	(3)	1,88E+05	(6)	50	3	2	73.1	11.6	327.4
30	1,17E+05	(6)	3,91E+05	(20)	80	6	3	43.7	14.1	110.2
31	2,19E+05	(14)	7,82E+05	(50)	100	12	3	40.4	20.5	73.4
32	1,30E+05	(5)	3,39E+05	(13)	60	5	3	56.0	15.4	162.9
33	6,26E+04	(4)	3,44E+05	(22)	100	5	2	26.9	6.5	76.4
34	1,04E+05	(4)	4,69E+05	(18)	60	7	3	32.8	7.8	96.1
35	2,61E+05	(6)	9,13E+05	(21)	36	14	6	41.6	13.5	104.2
36	1,41E+05	(9)	5,16E+05	(33)	100	8	3	39.5	16.4	83.1
37	2,03E+05	(13)	1,22E+06	(78)	100	18	4	24.1	12.2	43.2
38	9,39E+05	(54)	2,07E+06	(119)	90	31	6	64.9	46.1	89.9
39	4,69E+04	(3)	2,82E+05	(18)	100	4	2	24.9	4.5	81.4
40	4,07E+05	(13)	1,44E+06	(46)	50	21	6	40.8	20.0	75.9
41	6,52E+05	(15)	3,65E+06	(84)	36	54	12	25.8	13.7	44.6
42	9,39E+04	(6)	5,63E+05	(36)	100	8	3	24.4	8.2	57.0
43	4,69E+04	(3)	1,41E+05	(9)	100	2	1	49.3	8.3	188.8
44	3,13E+04	(2)	3,44E+05	(22)	100	5	2	13.9	1.5	52.8
45	4,47E+04	(2)	3,13E+05	(14)	70	5	2	21.8	2.3	88.6
46	4,56E+05	(14)	2,18E+06	(67)	48	33	8	30.2	15.5	53.7
47	1,41E+05	(9)	2,97E+05	(19)	100	4	2	68.2	27.0	155.7
48	1,25E+05	(8)	4,07E+05	(26)	100	6	2	44.6	17.2	99.6
49	8,94E+04	(4)	8,72E+05	(39)	70	13	4	15.2	3.8	40.7
50	1,10E+05	(7)	2,97E+05	(19)	100	4	2	53.4	18.7	130.0
51	4,54E+05	(29)	2,43E+06	(155)	100	36	6	26.9	17.4	40.0
52	8,94E+04	(4)	1,56E+05	(7)	70	2	2	82.8	17.6	314.6
53	1,56E+05	(9)	4,35E+05	(25)	90	6	3	52.0	21.2	113.4
54	4,69E+04	(3)	5,63E+05	(36)	100	8	3	12.5	2.4	37.7

Grain no.	RhoS (cm^-2)	(Ns)	RhoI (cm^-2)	(Ni)	Squares	U+/-2s		Grain Age (Ma) Age	--95% CI--	
55	3,13E+04	(1)	5,01E+05	(16)	50	7	4	10.2	0.2	57.5
56	2,09E+05	(8)	2,87E+05	(11)	60	4	3	104.0	36.3	278.7
57	7,82E+04	(5)	1,22E+06	(78)	100	18	4	9.5	2.9	22.4
58	1,96E+05	(6)	3,59E+05	(11)	48	5	3	78.7	23.7	226.8
59	9,78E+04	(5)	2,35E+05	(12)	80	3	2	60.6	16.5	179.8
60	2,66E+05	(17)	1,36E+06	(87)	100	20	4	28.2	15.6	47.3
61	1,30E+05	(5)	3,13E+05	(12)	60	5	3	60.6	16.5	179.8
62	1,25E+05	(8)	2,50E+05	(16)	100	4	2	72.0	26.5	175.2
63	5,01E+05	(16)	8,14E+05	(26)	50	12	5	88.0	44.1	168.7
64	1,03E+06	(46)	2,73E+06	(122)	70	41	7	54.0	37.5	76.1
65	3,13E+05	(6)	5,22E+05	(10)	30	8	5	86.4	25.6	256.2
66	1,88E+05	(6)	4,38E+05	(14)	50	7	3	62.1	19.3	168.1
67	5,16E+05	(33)	1,35E+06	(86)	100	20	4	55.0	35.6	82.6
68	1,10E+05	(7)	6,10E+05	(39)	100	9	3	26.2	9.7	58.0
69	6,26E+04	(2)	1,25E+05	(4)	50	2	2	73.9	6.5	482.0
70	2,50E+05	(16)	8,14E+05	(52)	100	12	3	44.3	23.5	78.1
71	5,87E+04	(3)	5,48E+05	(28)	80	8	3	16.1	3.0	49.6
72	1,56E+05	(5)	2,82E+05	(9)	50	4	3	80.3	20.9	259.5
POOLED	1,96E+05	(685)	6,77E+05	(2369)	5478	10	0	41.3	37.5	45.5

CHI^2 PROBABILITY (%): 0.3
>>> Beware: possible upward bias in Chi^2 probability due to low counts <<<

POOLED AGE W/ 68% CONF. INTERVAL(Ma): 41.3, 39.4 -- 43.4 (-2.0 +2.1)
95% CONF. INTERVAL(Ma): 37.5 -- 45.5 (-3.8 +4.2)

CENTRAL AGE W/ 68% CONF. INTERVAL(Ma): 42.6, 40.0 -- 45.3 (-2.6 +2.7)
95% CONF. INTERVAL(Ma): 37.7 -- 48.1 (-4.9 +5.5)
AGE DISPERSION (%): 27.1

FIT OPTION: Best-fit peaks using the binomial model of Galbraith and Green

INITIAL GUESS FOR MODEL PARAMETERS (number of peaks to fit = 2)

Peak #.	Peak Age	Theta	Fraction(%)	Count
1.	41.30	0.224	23.4	16.81
2.	63.80	0.309	27.3	19.63

Total range for grain ages: 10,0 to 116,3 Ma
Number of active grains (Num. used for fit): 72
Number of removed grains: 0
Degrees of freedom for fit: 69
Average of the SE(Z)'s for the grains: 0,48
Estimated width of peaks in PD plot in Z units: 0,56

PARAMETERS FOR BEST-FIT PEAKS

* *Standard error for peak age includes group error*
* *Peak width is for PD plot assuming a kernel factor = 0.60*

#.	Peak Age(Ma)	68%CI	95%CI	W(Z)	Frac(%)	SE,%	Count
1.	26.8	-3,0 ...+3,4	-5,6 ...+7,1	0.44	31.3	10.5	22.5
2.	52.3	-3,6 ...+3,9	-6,8 ...+7,8	0.43	68.7	10.5	49.5

Log-likelihood for best fit: -173,701
Chi-squared value for best fit: 61,407
Reduced chi-squared value: 0,890
Probability for F test: 0%
Condition number for COVAR matrix: 6,12
Number of iterations: 21

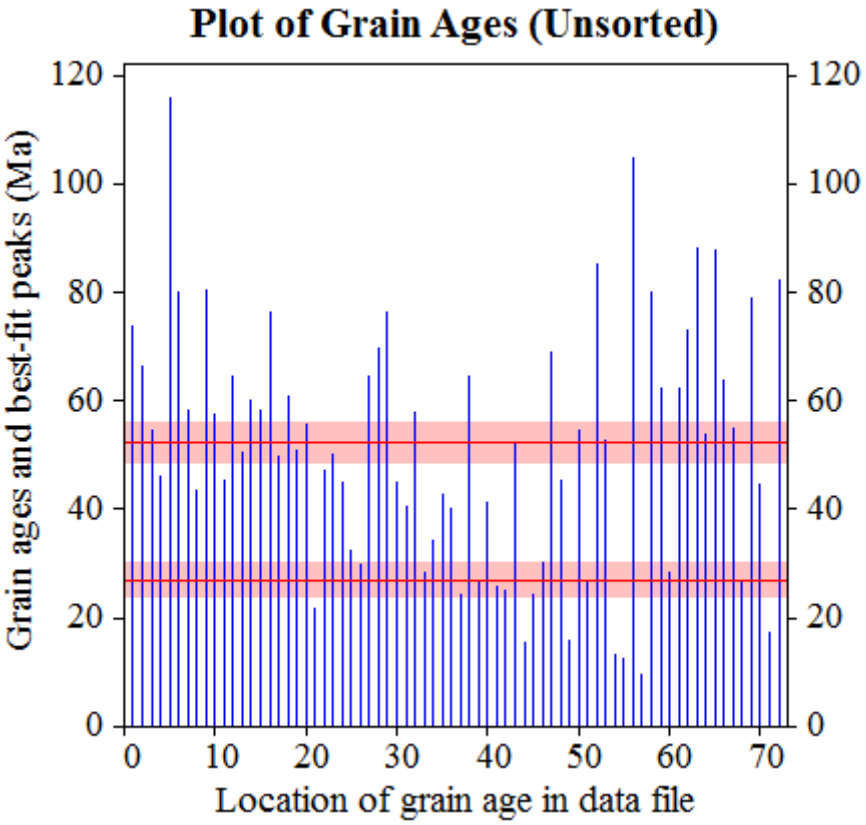
Plot of Grain Ages (Unsorted)
Grain ages and best-fit peaks (Ma)
Location of grain age in data file
0
20
40
60
80
100
120
0
10
20
30
40
50
60
70

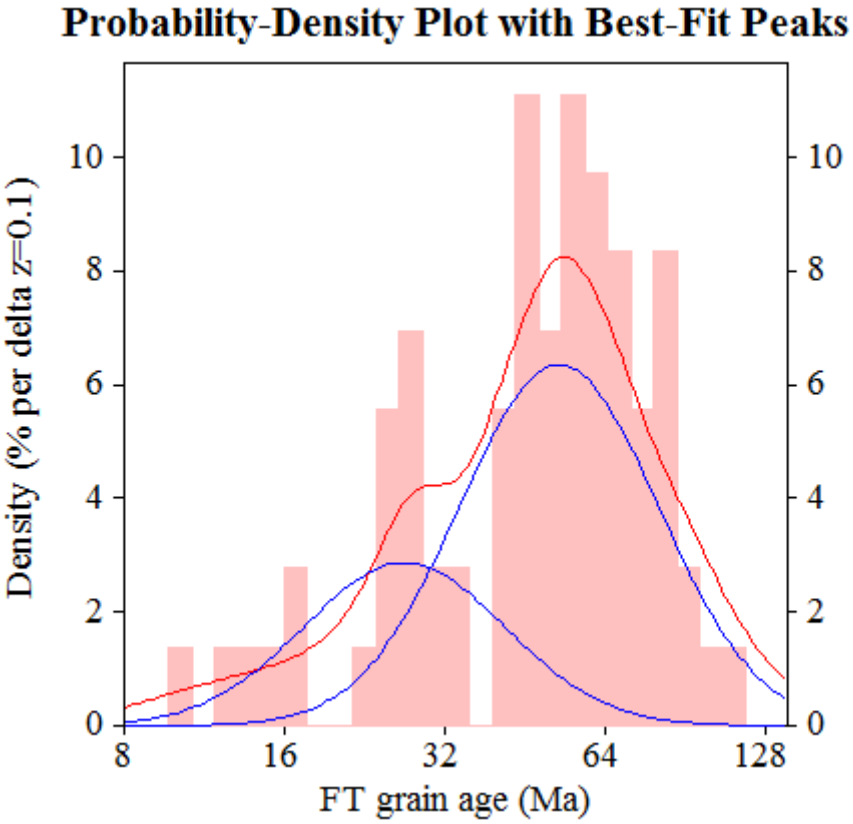
Probability-Density Plot with Best-Fit Peaks
Density (% per delta z=0.1)
FT grain age (Ma)
0
2
4
6
8
10
8
16
32
64
128

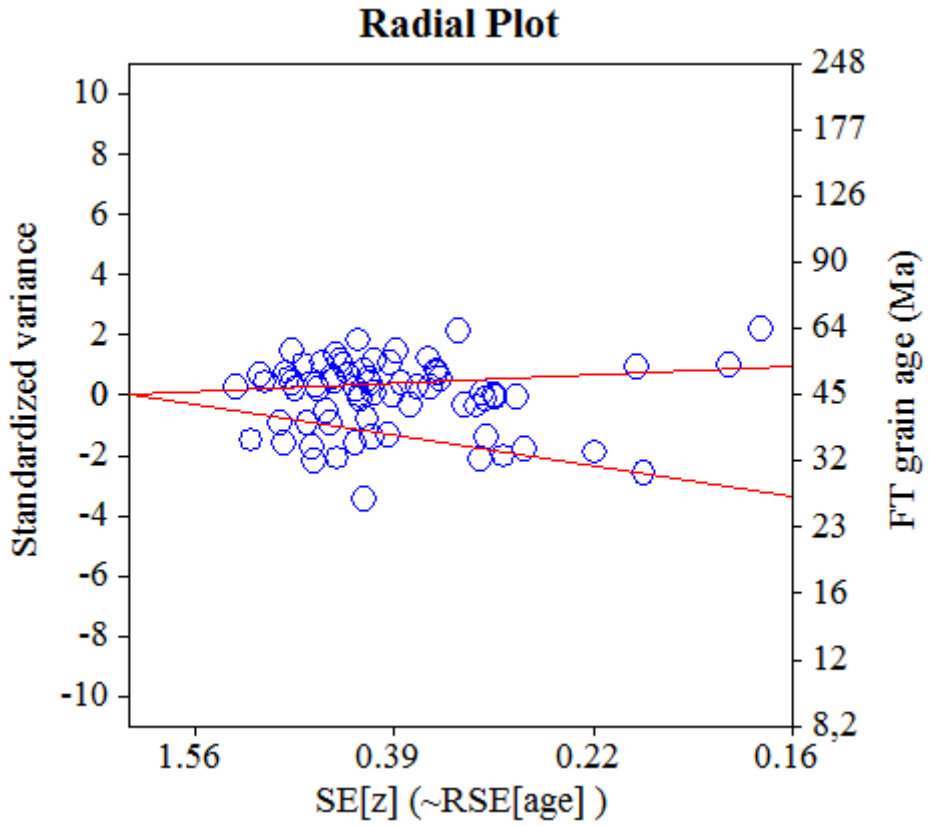
Radial Plot
Standardized variance
10
8
6
4
2
0
-2
-4
-6
-8
-10
248
177
126
90
64
45
32
23
16
12
8,2
FT grain age (Ma)
1.56
0.39
0.22
0.16
SE[z] (~RSE[age])

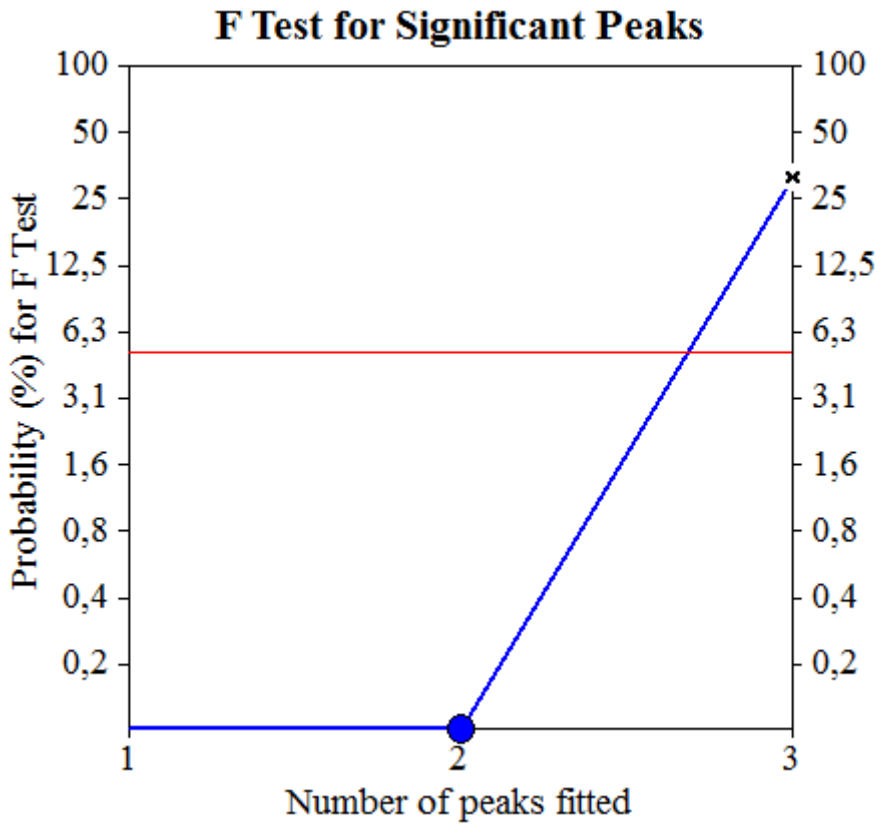
F Test for Significant Peaks
Probability (%) for F Test
100
50
25
12,5
6,3
3,1
1,6
0,8
0,4
0,2
1
2
3
Number of peaks fitted

Datafile: C:\BH2\Alejandro\AFT\5-2015\CVI_1302\CVI_1302.ftz
Title: CVI_1302 Irr 5-2015-14

NEW PARAMETERS - ZETA METHOD

EFFECTIVE TRACK DENSITY FOR FLUENCE MONITOR (tracks/cm^2): 1,31E+06
RELATIVE ERROR (%): 1,11
EFFECTIVE URANIUM CONTENT OF MONITOR (ppm): 15,00
ZETA FACTOR AND STANDARD ERROR (yr cm^2): 270,07 6,38
SIZE OF COUNTER SQUARE (cm^2): 6,39E-07

GRAIN AGES IN ORIGINAL ORDER

Grain no.	RhoS (cm^-2)	(Ns)	RhoI (cm^-2)	(Ni)	Squares	U+/-2s		Grain Age (Ma) Age	--95% CI--	
1	6,26E+05	(40)	3,80E+06	(243)	100	44	6	29.0	20.2	40.6
2	4,23E+05	(27)	2,27E+06	(145)	100	26	4	32.9	20.9	49.6
3	5,48E+05	(35)	3,68E+06	(235)	100	42	6	26.3	17.8	37.5
4	3,60E+05	(23)	1,92E+06	(123)	100	22	4	33.1	20.1	51.6
5	3,76E+05	(24)	3,19E+06	(204)	100	37	5	20.8	13.0	31.7
6	6,57E+05	(42)	3,99E+06	(255)	100	46	6	29.1	20.4	40.3
7	1,33E+06	(85)	5,90E+06	(377)	100	68	7	39.6	31.1	50.3
8	1,75E+06	(112)	7,59E+06	(485)	100	87	8	40.5	32.8	50.0
9	5,48E+05	(35)	2,57E+06	(164)	100	30	5	37.6	25.3	54.3
10	4,07E+05	(26)	3,76E+06	(240)	100	43	6	19.2	12.2	28.6
11	1,03E+06	(66)	5,93E+06	(379)	100	68	7	30.6	23.5	39.9
12	5,95E+05	(38)	2,97E+06	(190)	100	34	5	35.3	24.1	50.0
13	5,63E+05	(36)	3,87E+06	(247)	100	44	6	25.7	17.5	36.5
14	2,35E+05	(15)	1,38E+06	(88)	100	16	3	30.2	16.1	52.1
15	1,72E+05	(11)	8,92E+05	(57)	100	10	3	34.3	16.1	65.2
16	4,38E+05	(28)	2,55E+06	(163)	100	29	5	30.3	19.5	45.3
17	7,51E+05	(48)	2,82E+06	(180)	100	32	5	46.9	33.3	64.7
18	4,23E+05	(27)	3,62E+06	(231)	100	42	6	20.7	13.3	30.7
19	9,55E+05	(61)	3,90E+06	(249)	100	45	6	43.0	32.4	57.0
20	3,91E+05	(25)	3,51E+06	(224)	100	40	5	19.8	12.4	29.8
21	8,14E+05	(52)	4,10E+06	(262)	100	47	6	35.0	25.4	47.1
22	6,57E+05	(42)	3,47E+06	(222)	100	40	5	33.4	23.3	46.4
23	5,16E+05	(33)	3,43E+06	(219)	100	39	5	26.6	17.8	38.3
24	7,20E+05	(46)	7,75E+06	(495)	100	89	8	16.4	11.8	22.2
25	5,01E+05	(16)	2,88E+06	(92)	50	33	7	30.8	16.8	52.3
26	7,82E+05	(50)	2,54E+06	(162)	100	29	5	54.3	38.6	74.7
27	2,97E+05	(19)	2,49E+06	(159)	100	29	5	21.2	12.3	33.9
28	3,60E+05	(23)	3,63E+06	(232)	100	42	6	17.6	10.8	26.8
29	1,10E+06	(42)	3,50E+06	(134)	60	40	7	55.1	38.0	78.2
30	5,39E+05	(31)	3,55E+06	(204)	90	41	6	26.8	17.7	39.1
31	1,03E+06	(66)	5,77E+06	(369)	100	66	7	31.4	24.1	41.0
32	7,04E+05	(45)	3,13E+06	(200)	100	36	5	39.6	28.0	54.8
33	1,27E+06	(81)	4,74E+06	(303)	100	55	6	46.9	36.6	60.1
34	5,32E+05	(17)	2,50E+06	(80)	50	29	6	37.6	20.8	63.5
35	2,35E+05	(15)	7,82E+05	(50)	100	9	3	53.1	27.5	95.0
POOLED	6,46E+05	(1382)	3,58E+06	(7662)	3350	41	1	31.7	29.4	34.2

CHI^2 PROBABILITY (%): 0.0

POOLED AGE W/ 68% CONF. INTERVAL(Ma): 31.7, 30.5 -- 33.0 (-1.2 +1.3)
95% CONF. INTERVAL(Ma): 29.4 -- 34.2 (-2.3 +2.5)

CENTRAL AGE W/ 68% CONF. INTERVAL(Ma): 31.9, 30.1 -- 33.9 (-1.8 +1.9)
95% CONF. INTERVAL(Ma): 28.4 -- 35.8 (-3.5 +3.9)
AGE DISPERSION (%): 25.3

FIT OPTION: Best-fit peaks using the binomial model of Galbraith and Green

INITIAL GUESS FOR MODEL PARAMETERS (number of peaks to fit = 3)

Peak #.	Peak Age	Theta	Fraction(%)	Count
1.	31.70	0.153	48.8	17.09
2.	48.60	0.217	20.3	7.11
3.	55.40	0.240	12.9	4.52

Total range for grain ages:	16,5 to 55,4 Ma
Number of active grains (Num. used for fit):	35
Number of removed grains:	0
Degrees of freedom for fit:	30
Average of the SE(Z)'s for the grains:	0,2
Estimated width of peaks in PD plot in Z units:	0,23

PARAMETERS FOR BEST-FIT PEAKS

* *Standard error for peak age includes group error*
* *Peak width is for PD plot assuming a kernel factor = 0.60*

#.	Peak Age(Ma)	68%CI	95%CI	W(Z)	Frac(%)	SE,%	Count
1.	19.2	-2,0 ...+2,3	-3,8 ...+4,7	0.23	17.3	10.1	6.1
2.	29.8	-2,3 ...+2,5	-4,4 ...+5,1	0.21	48.8	14.5	17.1
3.	42.0	-2,8 ...+3,0	-5,4 ...+6,1	0.18	33.9	13.0	11.9

Log-likelihood for best fit:	-126,208
Chi-squared value for best fit:	33,775
Reduced chi-squared value:	1,126
Probability for F test:	5%
Condition number for COVAR matrix:	11,08
Number of iterations:	48

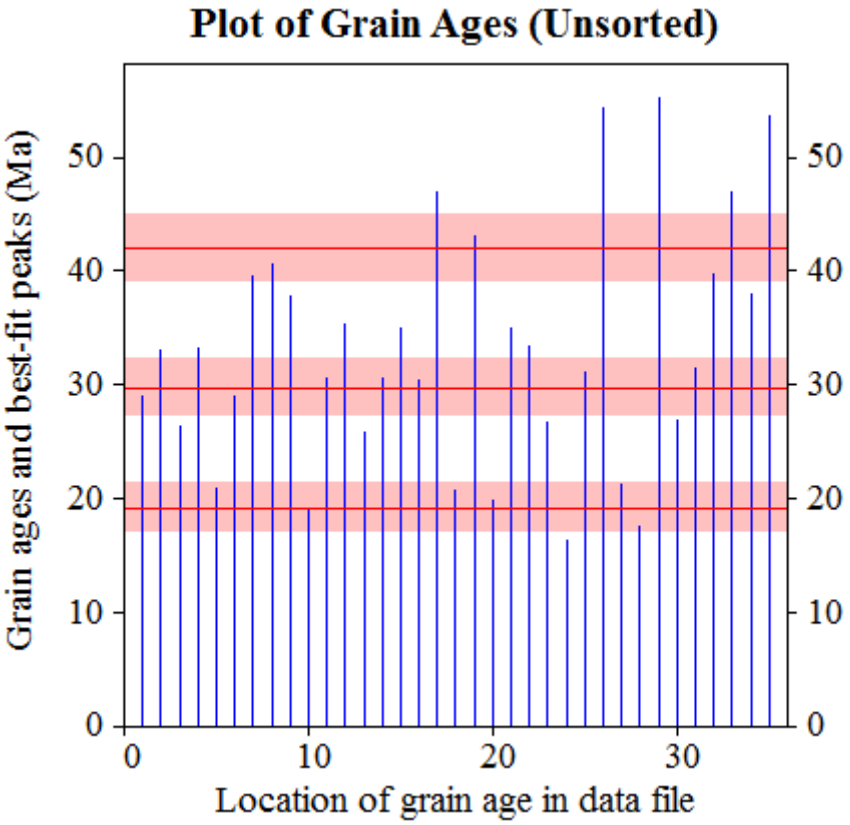
Plot of Grain Ages (Unsorted)
Grain ages and best-fit peaks (Ma)
0
10
20
30
40
50
Location of grain age in data file

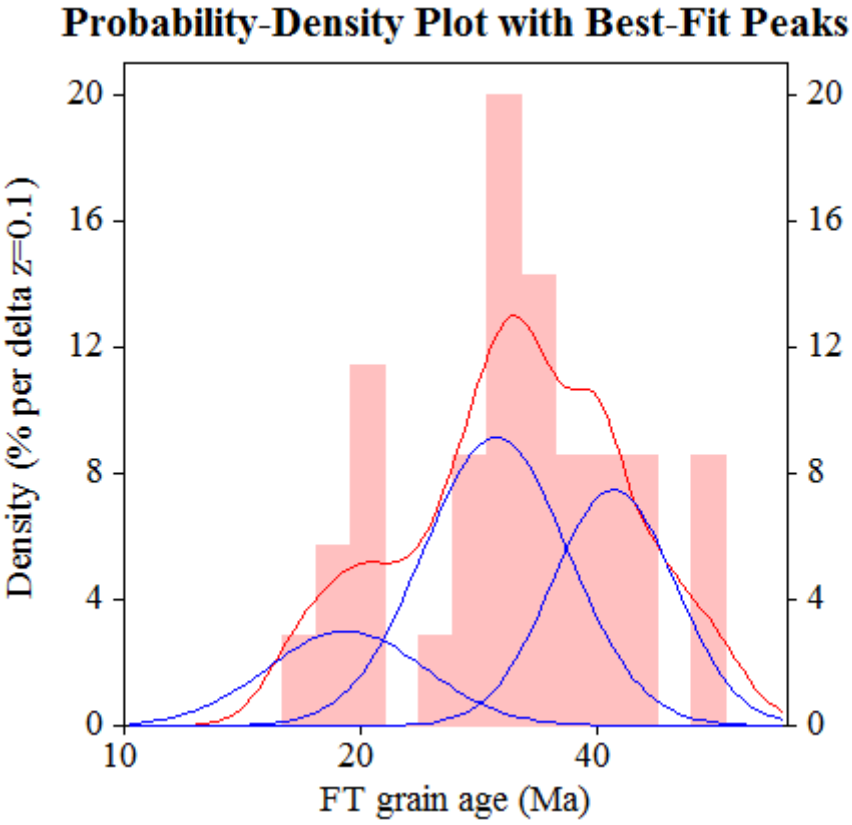
Probability-Density Plot with Best-Fit Peaks
Density (% per delta z=0.1)
0
4
8
12
16
20
10
20
40
FT grain age (Ma)

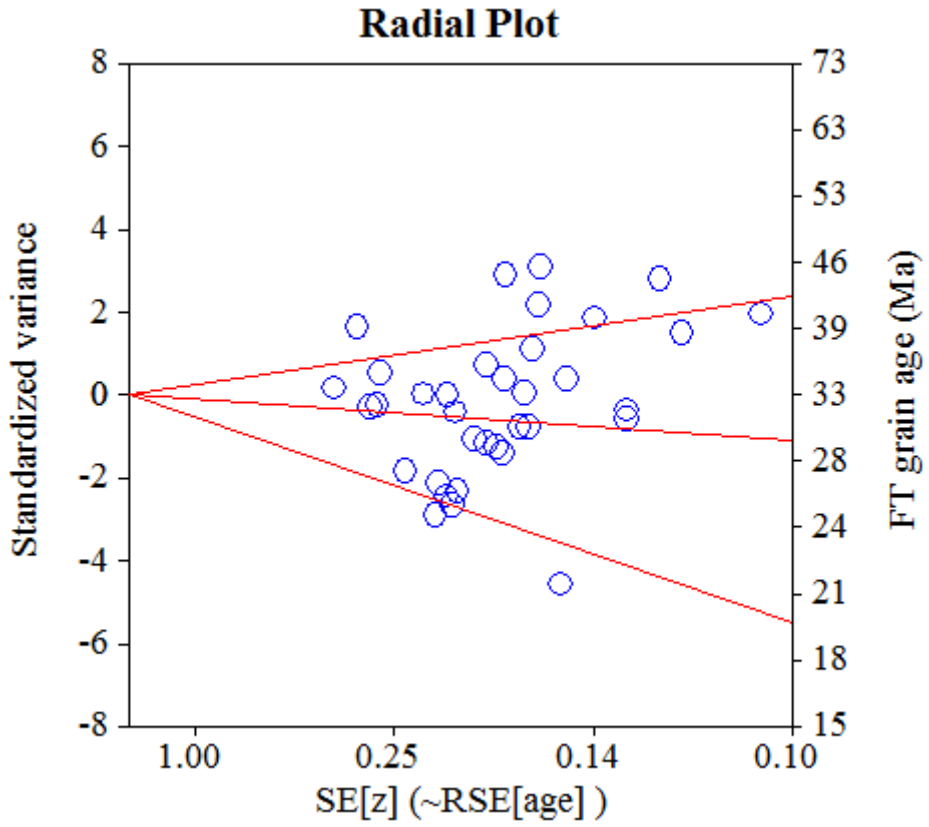
Radial Plot
Standardized variance
8
6
4
2
0
-2
-4
-6
-8
FT grain age (Ma)
73
63
53
46
39
33
28
24
21
18
15
1.00
0.25
0.14
0.10
SE[z] (~RSE[age])

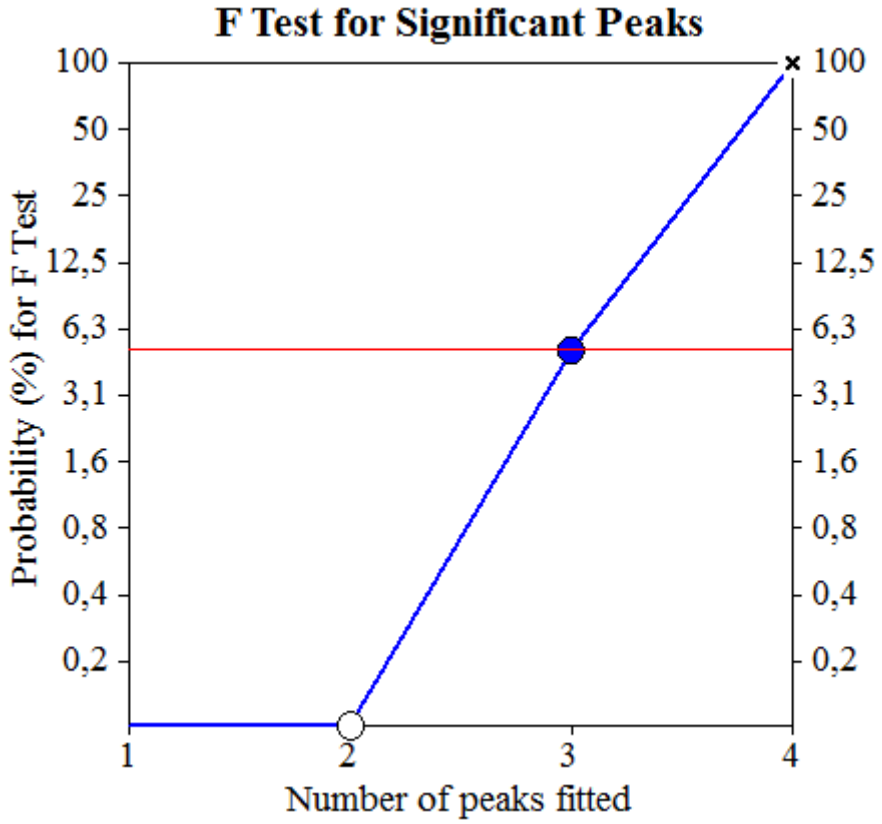
F Test for Significant Peaks
Probability (%) for F Test
100
50
25
12,5
6,3
3,1
1,6
0,8
0,4
0,2
1
2
3
4
Number of peaks fitted

Datafile: C:\BH2\Alejandro\AFT\11-2015\EMP_16\EMP_16.ftz
Title: EMP_16 Irr 11-2015-10

NEW PARAMETERS - ZETA METHOD

EFFECTIVE TRACK DENSITY FOR FLUENCE MONITOR (tracks/cm^2): 1,02E+06
RELATIVE ERROR (%): 1,24
EFFECTIVE URANIUM CONTENT OF MONITOR (ppm): 15,00
ZETA FACTOR AND STANDARD ERROR (yr cm^2): 284,52 5,65
SIZE OF COUNTER SQUARE (cm^2): 6,39E-07

GRAIN AGES IN ORIGINAL ORDER

Grain no.	RhoS (cm^-2)	(Ns)	RhoI (cm^-2)	(Ni)	Squares	U+/-2s		Grain Age (Ma) Age	--95% CI--	
1	3,29E+05	(21)	5,32E+05	(34)	100	8	3	89.2	49.2	157.0
2	1,96E+05	(10)	1,33E+06	(68)	80	20	5	21.6	9.8	41.5
3	2,03E+05	(13)	4,69E+05	(30)	100	7	3	63.0	30.0	123.0
4	6,26E+04	(4)	1,88E+05	(12)	100	3	2	49.4	11.3	157.6
5	1,56E+05	(10)	7,36E+05	(47)	100	11	3	31.2	13.9	61.6
6	2,82E+05	(18)	4,23E+05	(27)	100	6	2	96.2	49.9	179.6
7	2,97E+05	(19)	6,73E+05	(43)	100	10	3	64.1	35.1	111.4
8	4,69E+04	(3)	2,97E+05	(19)	100	4	2	23.9	4.3	77.3
9	2,35E+05	(9)	4,43E+05	(17)	60	7	3	76.9	30.1	179.6
10	4,69E+04	(3)	2,35E+05	(15)	100	3	2	30.1	5.4	101.7
11	1,41E+05	(9)	1,00E+06	(64)	100	15	4	20.7	8.9	41.1
12	2,03E+05	(13)	5,01E+05	(32)	100	7	3	59.1	28.3	114.4
13	2,03E+05	(13)	3,60E+05	(23)	100	5	2	81.9	38.0	166.6
14	3,80E+05	(17)	7,82E+05	(35)	70	12	4	70.4	36.9	127.9
15	1,25E+05	(8)	7,51E+05	(48)	100	11	3	24.5	9.9	51.4
16	2,24E+05	(10)	4,92E+05	(22)	70	7	3	66.1	27.8	143.5
17	6,71E+04	(3)	6,04E+05	(27)	70	9	3	16.8	3.1	52.2
18	7,82E+04	(5)	5,32E+05	(34)	100	8	3	21.9	6.5	54.6
19	6,26E+04	(4)	3,13E+05	(20)	100	5	2	29.9	7.2	86.0
20	4,38E+05	(28)	3,16E+06	(202)	100	47	7	20.2	13.0	29.9
21	2,66E+05	(17)	7,98E+05	(51)	100	12	3	48.5	26.1	84.6
22	5,48E+05	(35)	9,23E+05	(59)	100	14	4	85.6	54.7	131.6
23	3,13E+05	(12)	1,98E+06	(76)	60	29	7	23.1	11.3	42.2
24	8,76E+05	(56)	7,10E+06	(454)	100	105	10	17.9	13.5	23.6
25	2,19E+05	(14)	4,23E+05	(27)	100	6	2	75.2	36.3	146.9
26	2,82E+05	(18)	9,08E+05	(58)	100	13	4	45.1	24.9	77.1
27	5,09E+05	(26)	7,63E+05	(39)	80	11	4	96.1	56.2	160.9
28	1,56E+05	(10)	5,16E+05	(33)	100	8	3	44.3	19.3	90.7
29	1,25E+05	(8)	7,67E+05	(49)	100	11	3	24.0	9.7	50.2
30	4,54E+05	(29)	1,35E+06	(86)	100	20	4	48.9	30.8	74.9
31	2,66E+05	(17)	1,13E+06	(72)	100	17	4	34.4	18.9	58.5
32	1,56E+05	(8)	1,21E+06	(62)	80	18	5	19.0	7.7	39.1
33	3,13E+05	(20)	1,03E+06	(66)	100	15	4	44.0	25.2	73.0
34	1,72E+05	(11)	8,92E+05	(57)	100	13	3	28.3	13.2	53.7
35	1,41E+05	(9)	5,95E+05	(38)	100	9	3	34.7	14.6	71.9
36	1,56E+05	(10)	5,48E+05	(35)	100	8	3	41.8	18.3	85.0
37	2,97E+05	(19)	8,14E+05	(52)	100	12	3	53.0	29.5	90.5
38	2,82E+05	(18)	5,63E+05	(36)	100	8	3	72.4	38.6	129.8
POOLED	2,44E+05	(557)	9,51E+05	(2169)	3570	14	1	37.1	33.5	41.2

CHI^2 PROBABILITY (%): 0.0
>>> Beware: possible upward bias in Chi^2 probability due to low counts <<<

POOLED AGE W/ 68% CONF. INTERVAL(Ma): 37.1, 35.2 -- 39.1 (-1.9 +2.0)
95% CONF. INTERVAL(Ma): 33.5 -- 41.2 (-3.6 +4.0)

CENTRAL AGE W/ 68% CONF. INTERVAL(Ma): 43.3, 39.5 -- 47.4 (-3.7 +4.1)
95% CONF. INTERVAL(Ma): 36.2 -- 51.6 (-7.0 +8.4)
AGE DISPERSION (%): 43.3

FIT OPTION: Best-fit peaks using the binomial model of Galbraith and Green

INITIAL GUESS FOR MODEL PARAMETERS (number of peaks to fit = 2)

Peak #.	Peak Age	Theta	Fraction(%)	Count
1.	22.50	0.135	19.4	7.37
2.	37.10	0.204	17.7	6.71

Total range for grain ages:	18,0 to 96,8 Ma
Number of active grains (Num. used for fit):	38
Number of removed grains:	0
Degrees of freedom for fit:	35
Average of the SE(Z)'s for the grains:	0,36
Estimated width of peaks in PD plot in Z units:	0,42

PARAMETERS FOR BEST-FIT PEAKS

* *Standard error for peak age includes group error*
* *Peak width is for PD plot assuming a kernel factor = 0.60*

#.	Peak Age(Ma)	68%CI	95%CI	W(Z)	Frac(%)	SE,%	Count
1.	21.8	-1,9 ...+2,1	-3,6 ...+4,3	0.35	41.0	9.9	15.6
2.	59.9	-4,6 ...+5,0	-8,6 ...+10,1	0.35	59.0	9.9	22.4

Log-likelihood for best fit:	-113,730
Chi-squared value for best fit:	34,537
Reduced chi-squared value:	0,987
Probability for F test:	0%
Condition number for COVAR matrix:	2,68
Number of iterations:	9

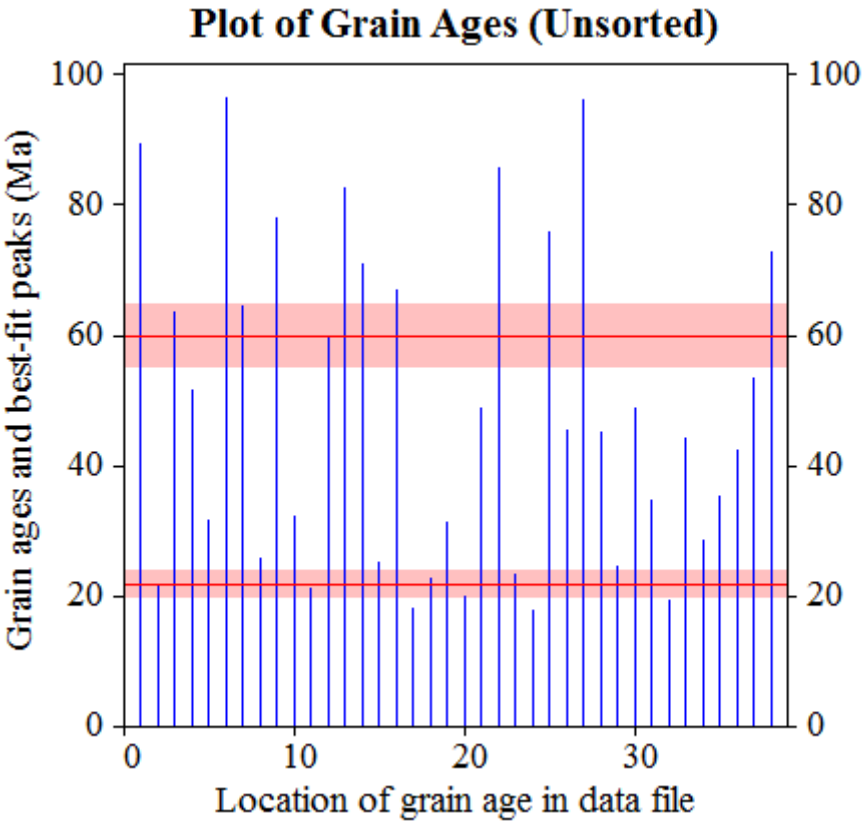
Plot of Grain Ages (Unsorted)
Grain ages and best-fit peaks (Ma)
Location of grain age in data file
0
10
20
30
0
20
40
60
80
100

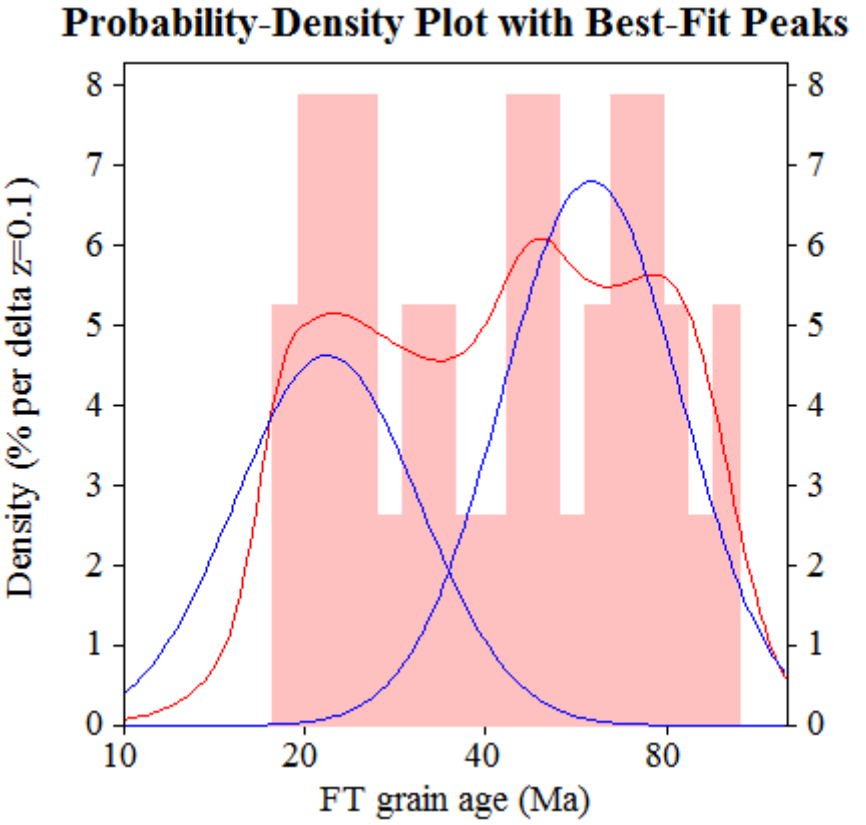
Probability-Density Plot with Best-Fit Peaks
Density (% per delta z=0.1)
FT grain age (Ma)
10
20
40
80
0
1
2
3
4
5
6
7
8

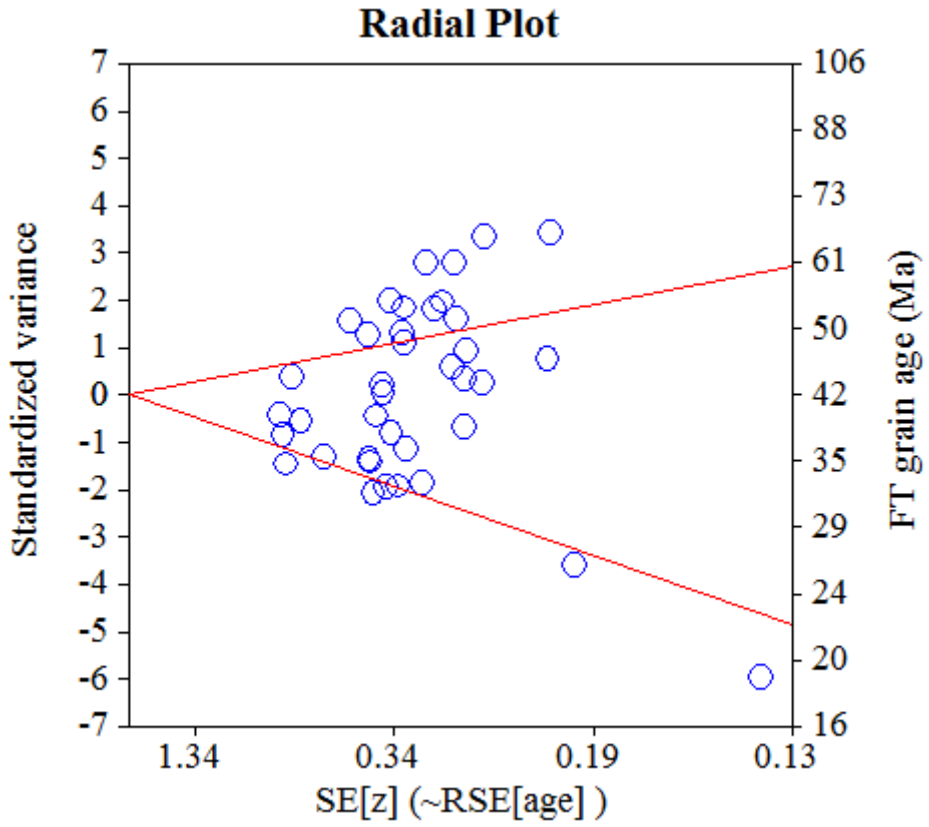
Radial Plot
Standardized variance
7
6
5
4
3
2
1
0
-1
-2
-3
-4
-5
-6
-7
106
88
73
61
50
42
35
29
24
20
16
FT grain age (Ma)
1.34
0.34
0.19
0.13
SE[z] (~RSE[age])

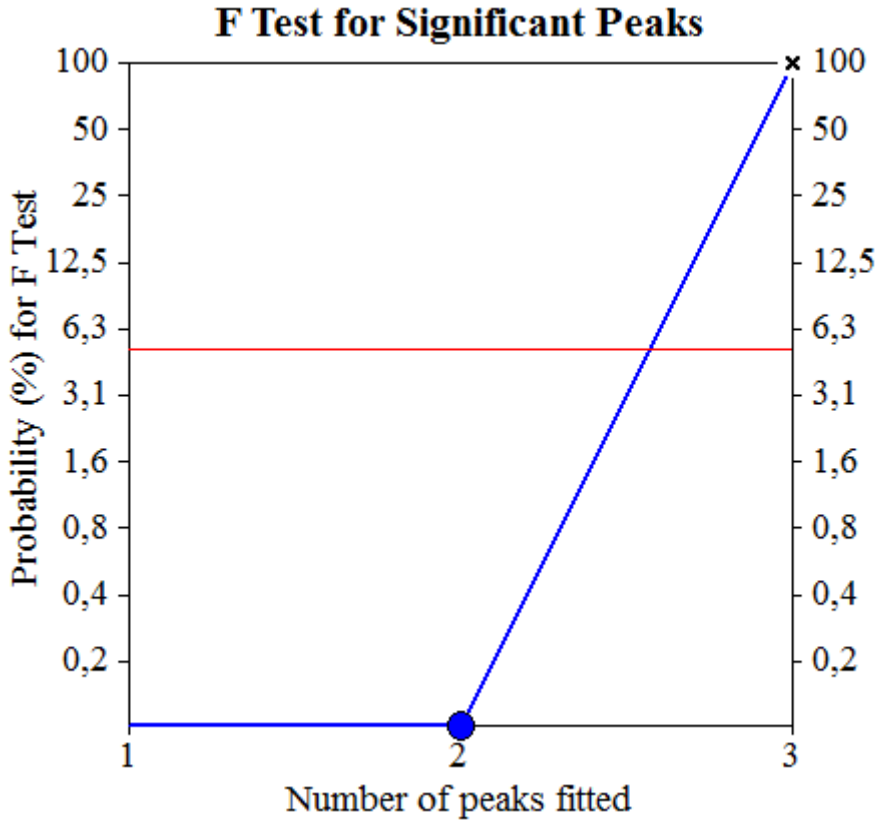
F Test for Significant Peaks
Probability (%) for F Test
100
50
25
12,5
6,3
3,1
1,6
0,8
0,4
0,2
1
2
3
Number of peaks fitted

Datafile: C:\BX51\Cristhian\EMP_49-11-2015-11\EMP_49_2015_11C.txt
Title: EMP_49A Irr 11-2015-11

NEW PARAMETERS - ZETA METHOD

EFFECTIVE TRACK DENSITY FOR FLUENCE MONITOR (tracks/cm^2): 1,26E+06
RELATIVE ERROR (%): 1,15
EFFECTIVE URANIUM CONTENT OF MONITOR (ppm): 15,00
ZETA FACTOR AND STANDARD ERROR (yr cm^2): 288,88 16,55
SIZE OF COUNTER SQUARE (cm^2): 6,39E-07

GRAIN AGES IN ORIGINAL ORDER

Grain no.	RhoS (cm^-2)	(Ns)	RhoI (cm^-2)	(Ni)	Squares	U+/-2s		Grain Age (Ma) Age	--95% CI--	
1	2,35E+05	(15)	6,26E+05	(40)	100	7	2	68.2	34.8	124.8
2	1,56E+05	(8)	8,22E+05	(42)	80	10	3	35.1	14.0	74.2
3	3,13E+05	(20)	1,50E+06	(96)	100	18	4	38.0	22.1	61.4
4	5,95E+05	(38)	1,22E+06	(78)	100	15	3	88.0	58.1	130.7
5	2,50E+05	(16)	9,23E+05	(59)	100	11	3	49.4	26.4	86.2
6	4,23E+05	(27)	1,36E+06	(87)	100	16	3	56.3	35.0	87.1
7	1,72E+05	(11)	1,11E+06	(71)	100	13	3	28.4	13.4	53.2
8	1,25E+05	(8)	3,29E+05	(21)	100	4	2	69.7	26.4	160.6
POOLED	2,87E+05	(143)	9,91E+05	(494)	780	12	1	52.3	42.1	65.0

CHI^2 PROBABILITY (%): 3.3

POOLED AGE W/ 68% CONF. INTERVAL(Ma): 52.3, 46.8 -- 58.4 (-5.5 +6.1)
95% CONF. INTERVAL(Ma): 42.1 -- 65.0 (-10.2 +12.7)

CENTRAL AGE W/ 68% CONF. INTERVAL(Ma): 51.9, 44.9 -- 60.1 (-7.1 +8.2)
95% CONF. INTERVAL(Ma): 39.0 -- 69.2 (-13.0 +17.3)
AGE DISPERSION (%): 26.2

FIT OPTION: Best-fit peaks using the binomial model of Galbraith and Green

INITIAL GUESS FOR MODEL PARAMETERS (number of peaks to fit = 2)

Peak #.	Peak Age	Theta	Fraction(%)	Count
1.	29.10	0.139	17.2	1.38
2.	52.30	0.224	32.7	2.61

Total range for grain ages: 29,1 to 88,4 Ma
Number of active grains (Num. used for fit): 8
Number of removed grains: 0
Degrees of freedom for fit: 5
Average of the SE(Z)'s for the grains: 0,3
Estimated width of peaks in PD plot in Z units: 0,35

PARAMETERS FOR BEST-FIT PEAKS

* *Standard error for peak age includes group error*
* *Peak width is for PD plot assuming a kernel factor = 0.60*

#.	Peak Age(Ma)	68%CI	95%CI	W(Z)	Frac(%)	SE,%	Count
1.	43.6	-6,7 ...+7,9	-12,2 ...+16,9	0.33	72.6	31.3	5.8
2.	77.2	-19,0 ...+25,2	-32,9 ...+57,1	0.28	27.4	31.3	2.2

Log-likelihood for best fit: -23,278
Chi-squared value for best fit: 7,077
Reduced chi-squared value: 1,415
Probability for F test: 5%
Condition number for COVAR matrix: 9,94
Number of iterations: 32

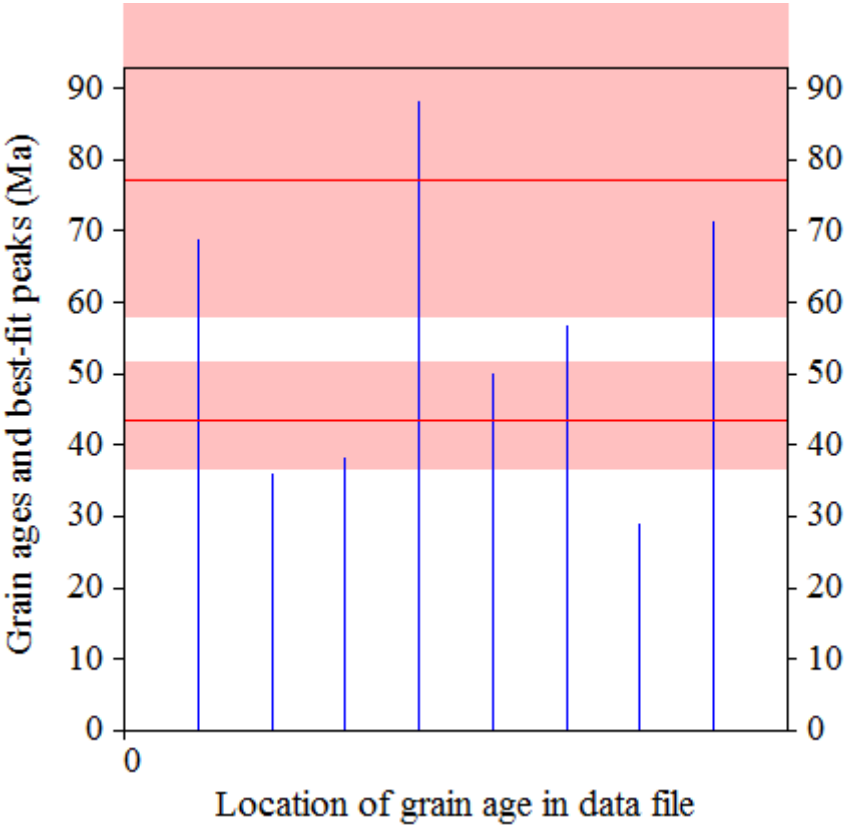
Grain ages and best-fit peaks (Ma)
90
80
70
60
50
40
30
20
10
0
0
Location of grain age in data file

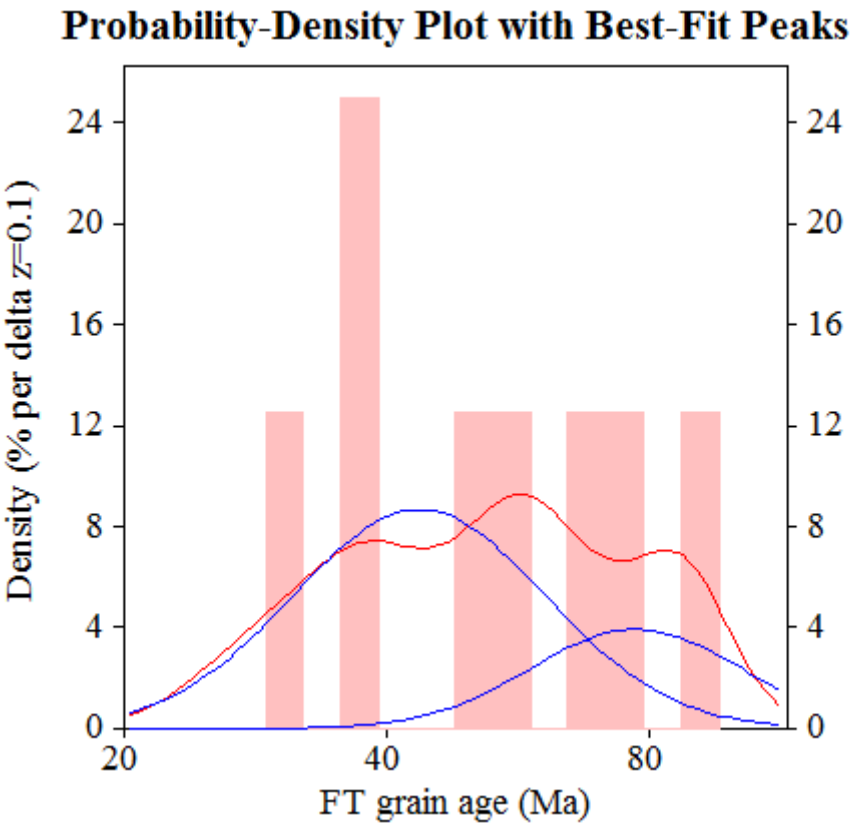
Probability-Density Plot with Best-Fit Peaks
Density (% per delta z=0.1)
24
20
16
12
8
4
0
20
40
80
FT grain age (Ma)

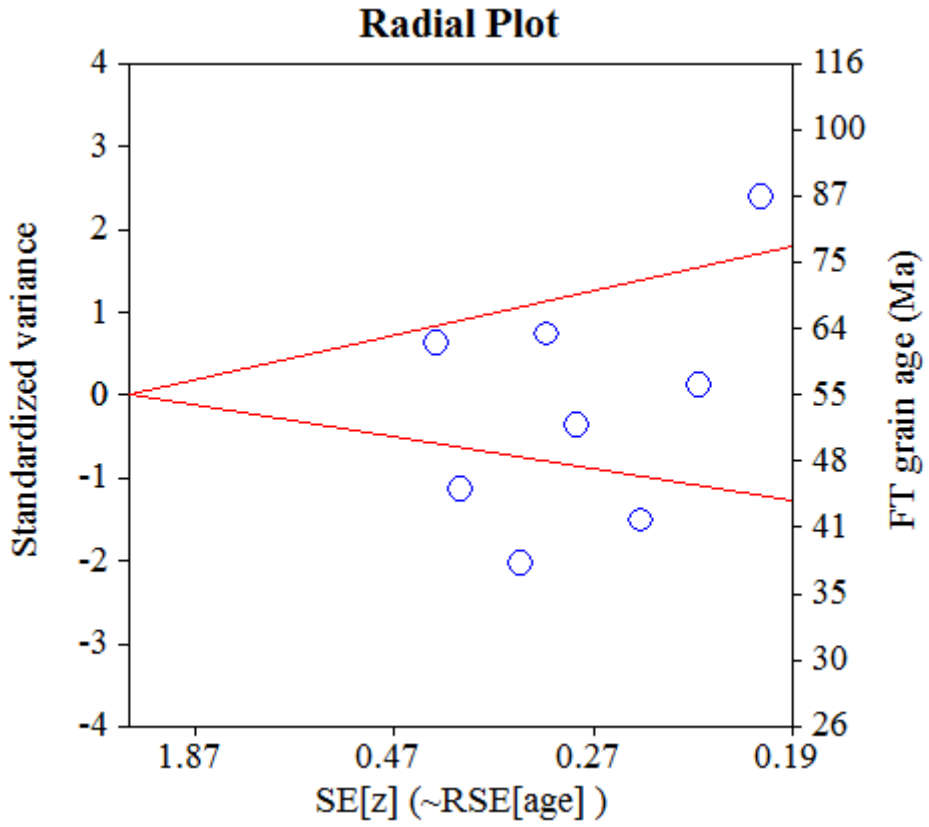
Radial Plot
Standardized variance
FT grain age (Ma)
SE[z] (~RSE[age])
4
3
2
1
0
-1
-2
-3
-4
116
100
87
75
64
55
48
41
35
30
26
1.87
0.47
0.27
0.19

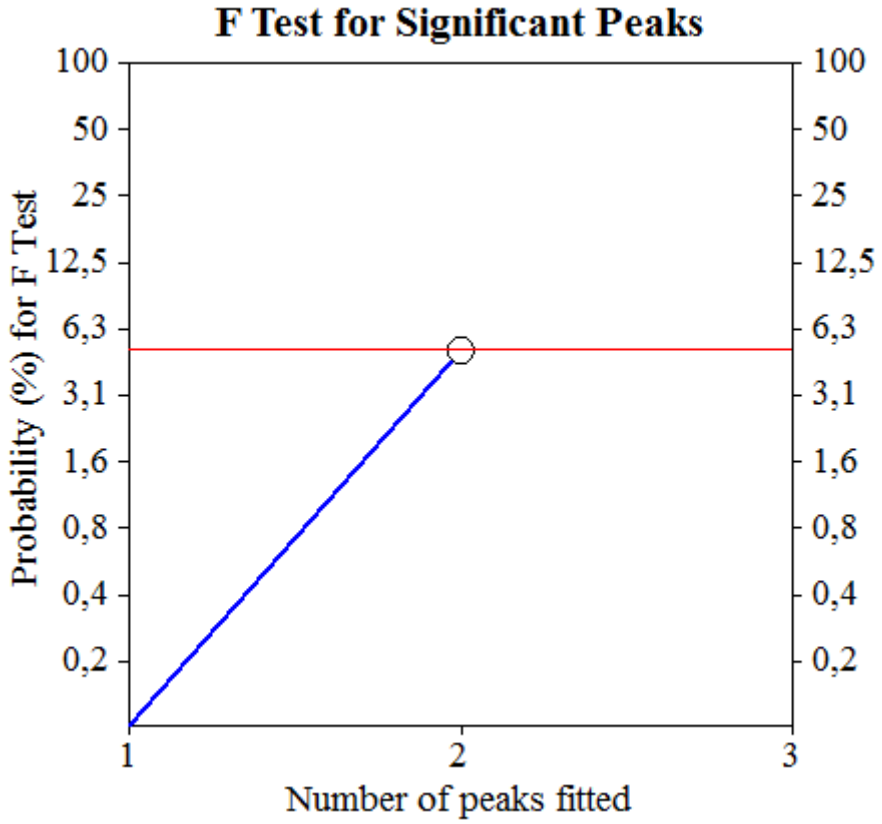
F Test for Significant Peaks
Probability (%) for F Test
Number of peaks fitted
100
50
25
12,5
6,3
3,1
1,6
0,8
0,4
0,2
1
2
3

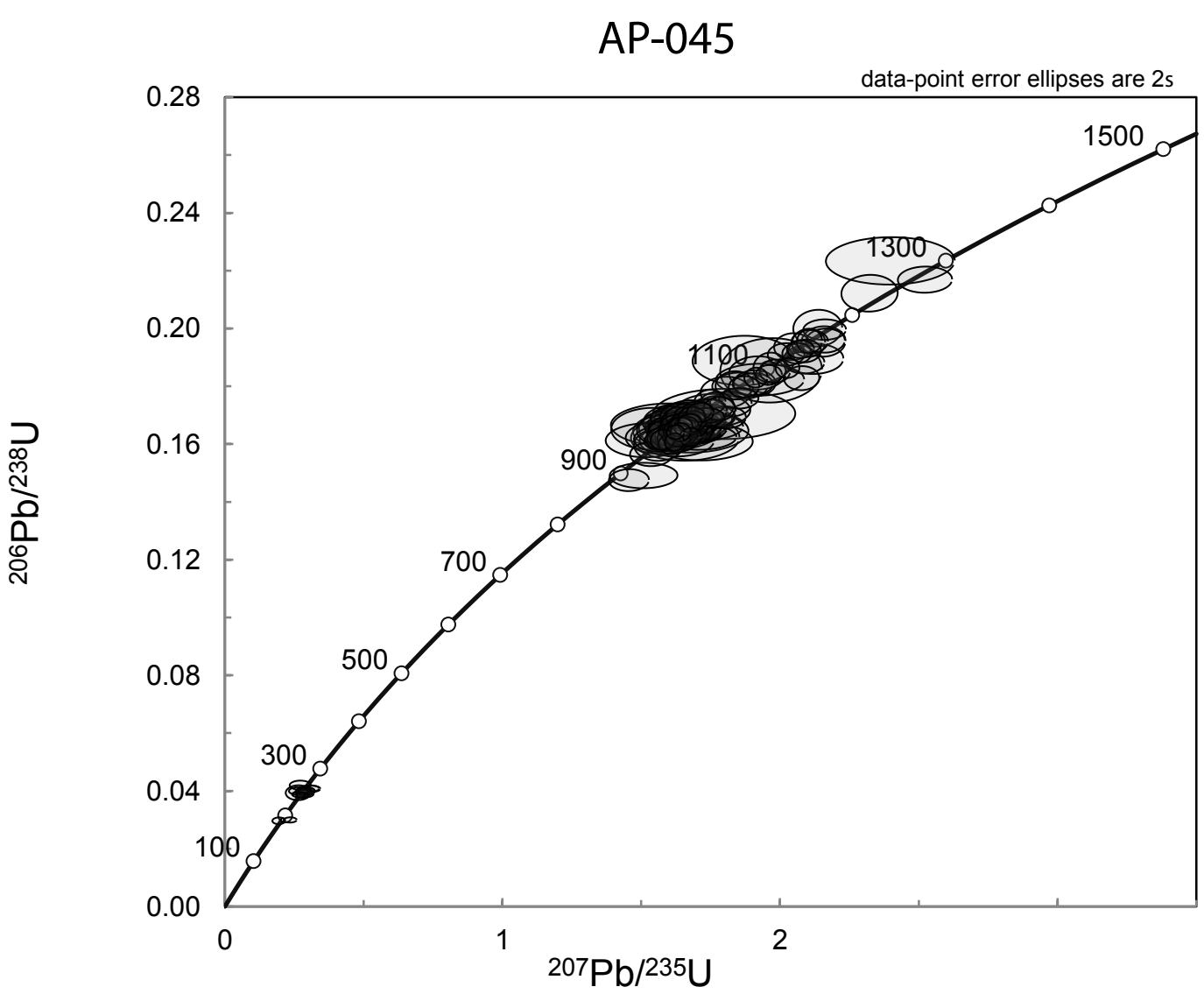
AP-045
data-point error ellipses are 2s
0.28
0.24
0.20
0.16
0.12
0.08
0.04
0.00
0
1
2
206Pb/238U
207Pb/235U
100
300
500
700
900
1100
1300
1500

CP-088

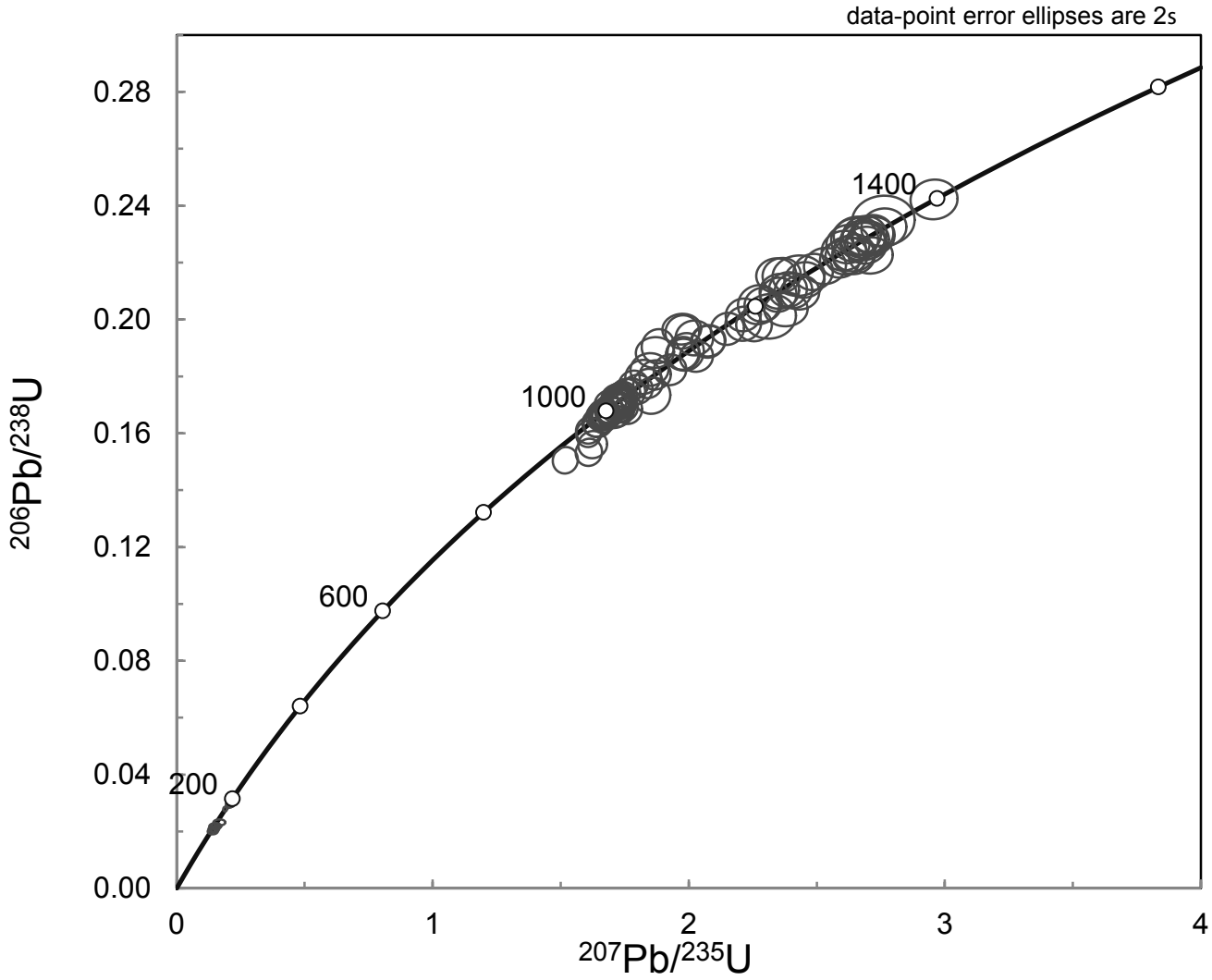
data-point error ellipses are 2s
0.28
0.24
0.20
0.16
0.12
0.08
0.04
0.00
206Pb/238U
0
1
2
3
4
207Pb/235U
200
600
1000
1400

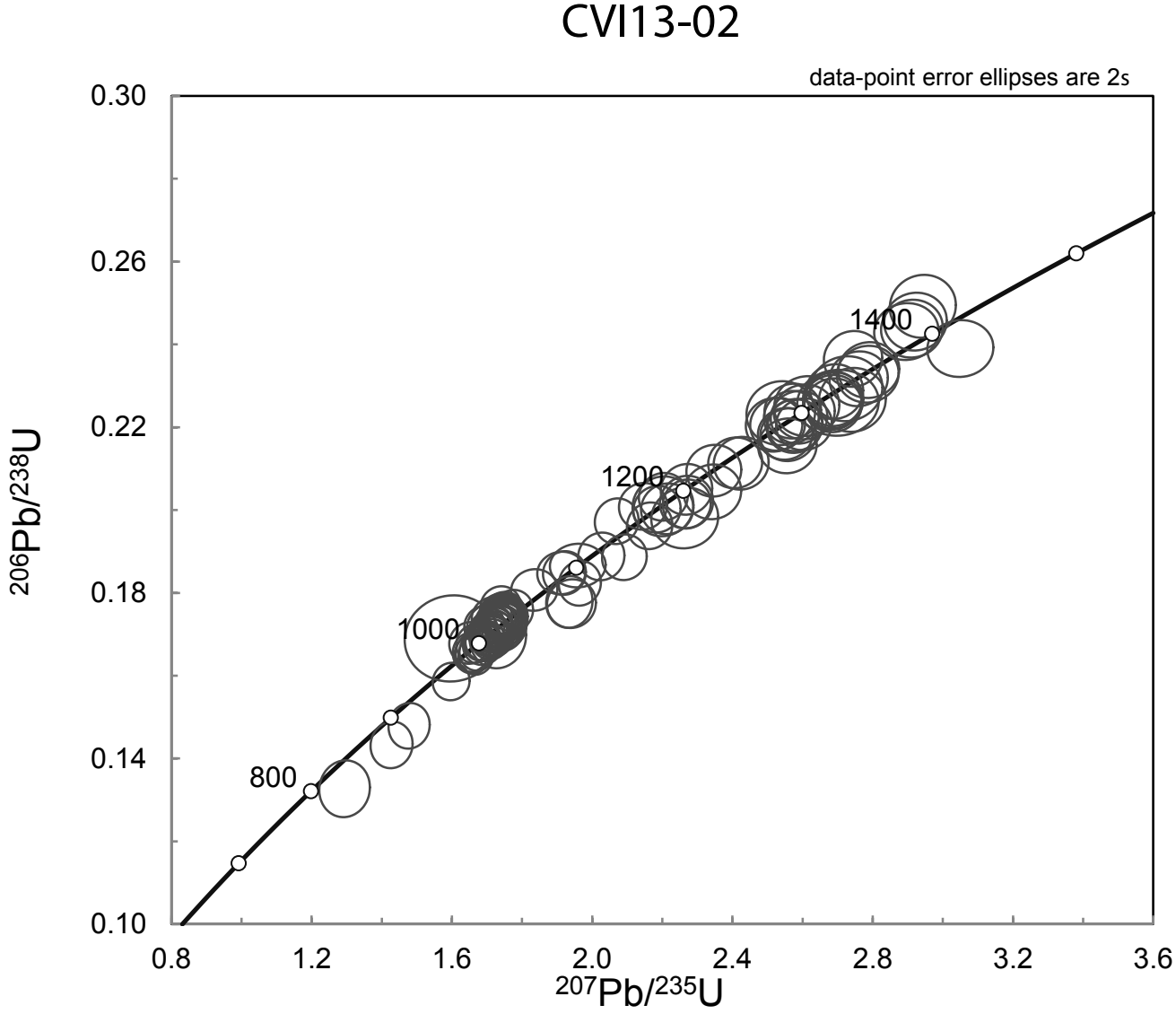
CVI13-02
data-point error ellipses are 2s
0.30
0.26
0.22
0.18
0.14
0.10
206Pb/238U
0.8
1.2
1.6
2.0
2.4
2.8
3.2
3.6
207Pb/235U
800
1000
1200
1400

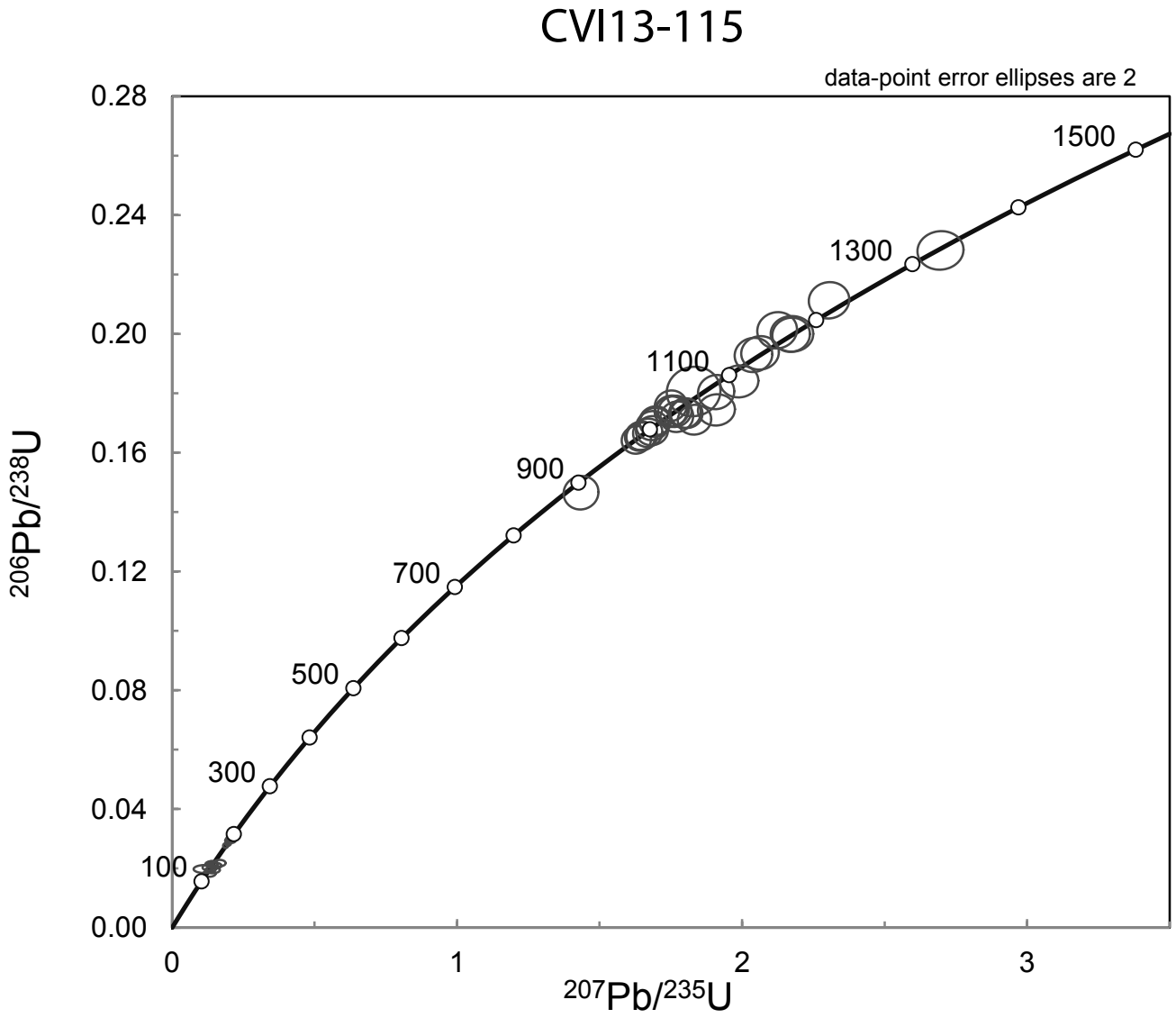
CVI13-115
data-point error ellipses are 2
0.28
0.24
0.20
0.16
0.12
0.08
0.04
0.00
0
1
2
3
100
300
500
700
900
1100
1300
1500
206Pb/238U
207Pb/235U

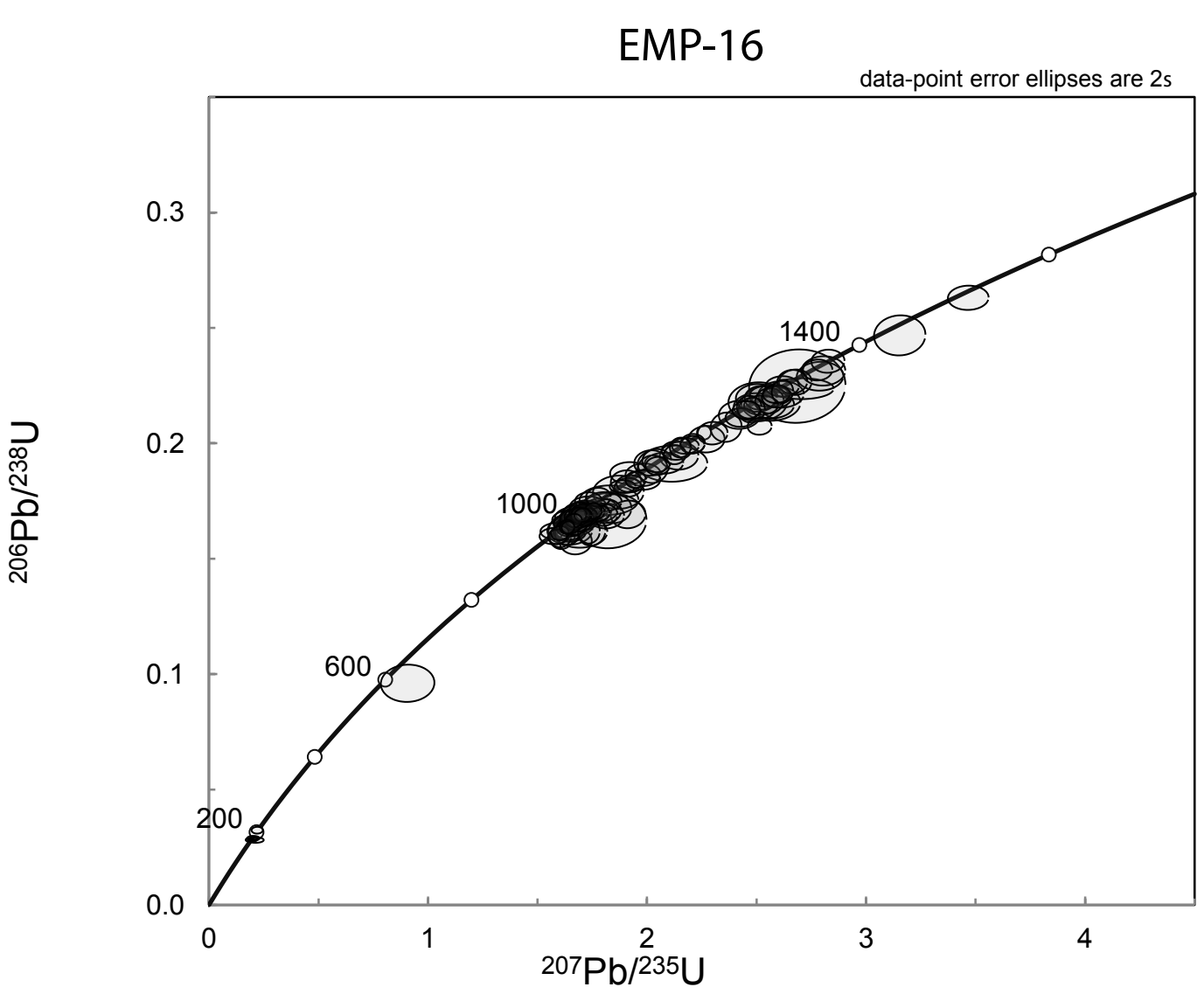
EMP-16
data-point error ellipses are 2s
0.3
0.2
0.1
0.0
206Pb/238U
1400
1000
600
200
0
1
2
3
4
207Pb/235U

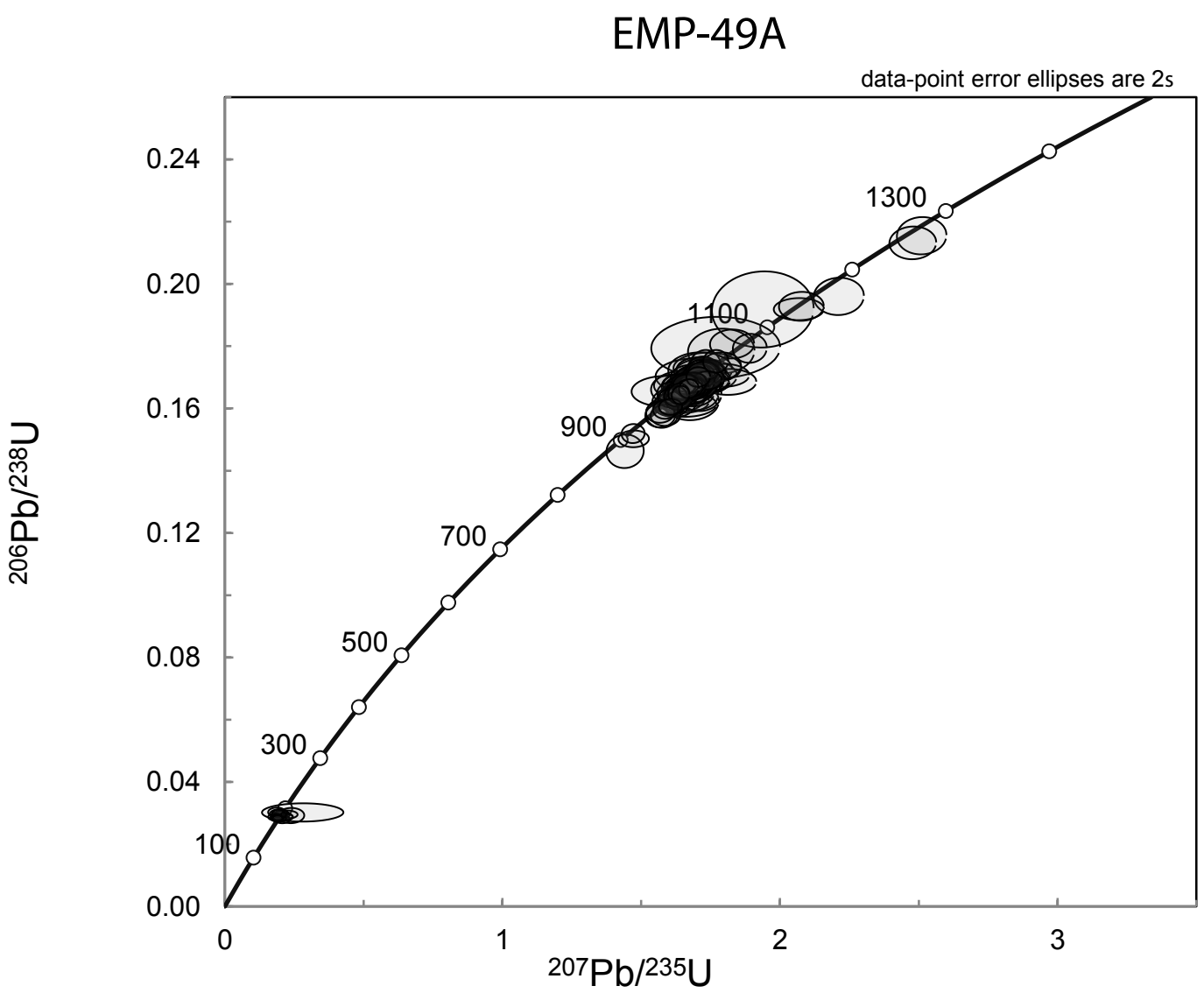
EMP-49A
data-point error ellipses are 2s
0.24
0.20
0.16
0.12
0.08
0.04
0.00
0
1
2
3
100
300
500
700
900
1100
1300
206Pb/238U
207Pb/235U